

2021-22

Low-stress Mechanical Properties and Fabric Hand of Soybean & Polyester Fiber Blended Plain Woven Dyed Fabrics

Ashish Bhardwaj & Ajit Kumar Pattanayak*

Department of Textile Technology, The Technological Institute of Textile & Sciences, Bhiwani, Haryana, India

Abstract:

This study is focused to explore the potential uses of soybean fibers for apparels. The soybean fibers are sustainable fibers as they are manufactured from the by-product of soybean cakes. The compatibility of the blends of soybean fibers and polyester fiber is considered for this study as polyester fibers adds excellent mechanical properties to the blended fabrics whereas the soybean fibers are eco-friendly fibers. In this study, 5 different single yarns were spun of 100% soybean, 100% polyester, 65%–35% soybean/polyester, 50%–50% soybean/polyester and 35%–65% soybean/polyester in conventional ring spinning system. These single yarns are converted into 2 ply yarns using two for one twister machine and these 2 ply yarns are woven into five plain-woven fabrics with similar areal density values. These fabrics are further dyed with 1:2 metal complex dyes after suitable pre-treatment process. Finally, the low stress mechanical properties are measured using KES-FB tester and the THV (Total Hand Value) are estimated for these dyed samples. The results indicate that soybean rich blended fabrics show better THV than the polyester rich fabrics for the use in winter. Therefore, soybean has a great commercial potential in apparels as it exhibits decent low stress mechanical properties, good total hand values for the apparel grade fabrics.

Keywords: Fabric hand, Low Stress Mechanical Properties, Metal Complex Dyes, Soybean fibers, Total Hand Value

Citation: Ashish Bhardwaj & Ajit Kumar Pattanayak*, "Low-stress Mechanical Properties and Fabric Hand of Soybean & Polyester Fiber Blended Plain Woven Dyed Fabrics", *Journal of the Textile Association*, **82/5** (300-304), (Jan-Feb'2022), <https://doi.org/10.17605/OSF.IO/WIIE2Y>

Article Received: 19-08-21, Revised: 18-02-22, Accepted: 18-02-22

1. Introduction :

The global garment consumption is increasing consistently with the rise of population as well as the disposable income which makes the textile industry is one of the leading polluting industries on this earth [1]. The manufacturing process, usage and disposal of these garments cause the pollution. It is stated that the textile industry produced 1715 million tons of carbon dioxide and consumed 79 billion cubic meters of fresh water in the year 2018 [1]. The recent focus on the environmental impacts of textiles is largely due to a surge in public interest in plastic pollution of which a significant proportion is thought to come from textile microfibres, a form of microplastic [2, 3]. It is found that the Polyester fibers controls around 52% of the textile fibers which are manufactured from the petroleum base and 24% of the market is controlled by cotton fibers [4]. The polyester fibers are manufactured from the petroleum base hence has great impact on the environment. The cotton fibers are natural fibers but consume lots of water and pesticides during the cultivation. Because of these cited challenges, there is increasing interest to reduce the use of synthetic fibers in the textile products as well as to include sustainable fibers like soybean for the reduction of environmental pollution level. The soybean fibers are produced from the residual cake after extraction of soybean oil. The soybean protein fibre has decent mechanical properties and environmentally friendly [5].

The fabric quality can be accessed from design, aesthetic, comfort and fit. The evaluation of fabric quality is mostly subjective, but fabric hand is an objective measurement technique developed by Kawabata and Niwa [6]. The fabric hand is one of the most important parameter of fabric marketing and is based upon the end uses. The fabric hand is affected by many parameters such as fiber characteristics, yarn type, fabric structure and the wet processing methods [7]. The low stress mechanical properties are typically more useful for the study, the daily use garments and it affects on many other properties like fabric drape [8]. These properties are used for the evaluation of fabric total hand values (THV). Many researchers studied the low stress mechanical properties of different fabrics, but no published documents found the study of the blended fabrics produced from eco-friendly soybean fibers and polyester which is the mostly used synthetic fiber for apparels. Hence, an attempt is made to study the effect of different blend ratio of soybean and polyester fibers on the low stress mechanical properties and to evaluate the total hand value of these fabrics. The blending of soybean fibers with polyester fibers will improve the softness, smoothness and moisture content of the blended fabric. The addition of the soybean fibers will reduce the polyester content in the fabric and the resultant fabric will become more sustainable. Hence, the optimum percentage of the soybean fibers to be determined in the polyester and soybean blended fabrics with respect to fabric handle.

*Corresponding Author :

Dr. Ajit Kumar Pattanayak
Assistant Professor, Department of Textile Technology
The Technological Institute of Textile & Sciences, Bhiwani,
Haryana-127 021
E-mail: ajitpattanayak@titsbhiwani.ac.in

2. Materials and Methods

2.1 Materials

The polyester and soybean fibres were sourced from the industry and the specifications of these fibers are shown in

Table 2.1. The polyester and the soybean fibers are mixed at the blow-room stage for the satisfactory blending and five different single yarns are spun by using traditional ring spinning technique. The turns per meter (TPM) of all samples are kept alike. Then, these single yarns are transformed in to 5 different 2-ply yarns with the two for one twister machine (TFO). These 2 ply yarns then converted into 1/1 Plain fabrics by a sample rapier loom. The areal densities (grams/meter²) of all the five fabrics were kept alike for easy comparison as mentioned in Table 2.2.

Table 2.1 Fiber Properties of Soybean and Polyester

Fiber Properties	Polyester	Soybean
Fineness, denier	1.4	1.5
Length, mm (2.5% span length)	44	40
Elongation at Break, %	17.12	19.5
Tenacity, cN/tex	60.2	40.7

Table 2.2 Fabric Constructional Properties

Fabric Type	Warp Ne*	Weft Ne*	EPI**	PPI**	Areal Density, gm/m ²
Polyester (100%)	30/2	30/2	60	54	194
Polyester / Soybean (65/35)	30/2	30/2	60	54	190
Polyester / Soybean (50/50)	30/2	30/2	62	56	192
Polyester / Soybean (35/65)	30/2	30/2	60	54	193
Soybean (100%)	30/2	30/2	60	56	193

*Ne is English Count, **EPI & PPI are Ends per inch and Picks per inch

These five fabrics were pre-treated with standard conditions and then the ready for dyeing (RFD) fabric samples were prepared. Then these RFD fabric samples were dyed with 1:2 metal complex dyes of Lanaset Blue 2R (commercial dye sourced from Huntsman co-operation). The dyeing was carried out in a roto-dyer. The dye bath of the roto-dyer was set to 400 C and MLR (material to liquor ration with mass) was kept at 1:40. Then fabric was treated with 4% ammonium sulphate and 1% levelling agent (Uniperol SE, BASF) for 10 minutes then required amount of acetic acid was added to get pH a 4.5-5. After that dye was added and dye bath was heated to 900 C and held at this temperature up to 60 minutes. The dyed samples were soaped mildly with non-ionic detergent (2 grams per liter) and then washed with cold water and dried [9].

2.2 Methods

The sixteen low stress mechanical properties of these dyed

fabric samples were measured for the five woven fabric samples by using KES-FB (Kawabata Evaluation System) tester [10]. The values of the low stress mechanical properties are tabulated in Table 3.1. This system has the capability to measure Tensile, Shear, Bending, Compression and Surface properties with a sample size of 20×20 cm. The average value of each low stress mechanical properties is estimated from four test results. All the samples are tested at the standard testing conditions of 20±20C and 65%±2% Relative Humidity (RH%). The objective assessment of the five fabrics was evaluated after the estimation of the Koshi (stiffness), Fukurami (Resilience) and Numeri (softness). These called the Primary Hand Values (PHVs) and normally rated on a scale from 0 (weak) to 10 (strong). The Total Hand Value (THV) of these five fabric samples were obtained automatically with KES-FB tester by using the Primary Hand Values. The THV is rated on a scale from 0 (not useful) to 5 (excellent) [11].

3 Result & Discussion

The results of low stress mechanical properties of the five fabric samples measured by Kawabata Evaluation System are shown in Table 3.1.

3.1 Tensile Properties

The low stress tensile properties measured by KES-FB1 are shown in Table 3.1. Four different low stress tensile properties such as extensibility (EMT), tensile linearity (LT), tensile energy (WT) and tensile resiliency (RT) have been measured. The LT value of fabric represent the linearity of the stress-strain curve and the higher LT values indicate the better fabric extension behaviour during the initial extension range [12]. It is observed that the fabrics with 100% Polyester shows higher LT values than the fabrics with the 100 % soybean fibers. The LT values of the blended fabrics decreases proportionally with the gradual increase of soybean fibers as shown in Table 3.1.

The value of EMT% (tensile strain) represents the decrimping of yarns during tensile loading. Higher EMT% is better for the fabric comfort. It is observed that the EMT values of the sample fabrics increases proportionally with the increase of soybean fiber content in the blended fabric. Hence, soybean rich fabrics scores better than the polyester rich fabrics in terms of extensibility. This may be attributed to the higher bending rigidity and higher initial modulus of the polyester fibers as compared to the soybean fibers.

The WT values show a decreasing trend with the increase of soybean fiber content in the fabric blend. The higher values of WT indicate the better performance of breakage for polyester rich fabrics than the soybean rich fabrics as the polyester fibers are possess higher values of elongation at break as well as the tenacity as per Table 1.

The RT value indicates the ability of the fabric to recover after the tensile deformation. It is observed that the RT values decreases with the increase of the soybean fiber content in the fabric. This may be attributed to the higher RT value of the polyester fiber as compared to the soybean fibres.

3.2 Shear Properties

Three low stress shear properties such as G (Shear Rigidity), HB (the shear hysteresis of the shear force at 0.50) and 2HB5 (the shear hysteresis of the shear force at 50) measured by KES-FB1. The results of these low stress properties are shown in Table 3.1.

It is observed that the G value decreases with the increase of the soybean fiber content in the blended fabric samples. This may be attributed to the higher flexural rigidity and the coefficient of friction of the polyester fiber as compared to the soybean fibers. The lower value of shear rigidity (G) provides more comfort to the wearer as well as exhibits better drapability and tailorability of the garments. The lower value of the shear rigidity (G) observed for the soybean rich fabrics due to the lesser resistance to the shear forces and with less wrap angle between the warp and weft [13]. It is also observed that the values of HB and 2HB5 decreases with the increase of soybean content in the blended fabrics as shown in Table 3.1. The soybean rich fabrics are thicker than the polyester rich fabrics. The thicker fabric structures allow the yarn to recover more efficiently after the disengagement of load than the compact structures.

3.3 Bending Properties

The pure bending properties are tested by KES-FB2. The B (bending rigidity) and 2HB (Hysteresis to bending moment) values of the fabric samples are shown in Table 3.1. It is observed that the fabric made up with 100% soybean fibers shows lowest B value in comparison to blended fabrics and the 100% polyester fabrics and the bending rigidity value gradually increases with the increase of polyester fiber percentage in the blended fabric. The bending rigidity (B) depends upon the bending rigidity of the constituent yarns of the fabrics and the interlacement points of warp and weft in the fabric structure. The interlacement points govern the mobility of warp and weft in the fabric structure [12]. The 100% soybean yarn has lower bending rigidity than the 100% polyester yarns which lead the fabric made up with 100% soybean yarns will exhibit lowest bending rigidity value.

The other bending parameter of low stress mechanical properties is the bending hysteresis of the bending moment

and is represented by the 2HB. 2HB value indicates the recovery from the induced bending deformation. It is observed that the 2HB value decreases with the increase of soybean fiber content in the blended fabric. The fabric made up with 100% soybean yarns shows lowest value of B and 2HB due to lower yarn rigidity.

3.4 Compression Properties

The compression properties of the sample fabrics are measured by KES FB-3. The Linearity of the compression, compressional energy (WC), compressional resiliency (RC), fabric thickness at pressure 0.5gf/cm² (T₀) and fabric thickness at pressure 50gf/cm² (T_m) are the low stress compression properties measured for this study and the respective values are shown in Table 3.1. It is observed that the LC value are similar for all types of fabrics but the WC value of 100 % soybean fabric is lowest and this value increases with the decrease of the soybean fiber content in the fabric blend. The low compressibility energy of the fabric made up with 100% soybean fiber is due to the lower rigidity and higher fiber to fiber friction of soybean fibers than the polyester fibers. Higher coefficient fiber to fiber friction leads to the less energy consumption for the compression.

It is also observed that that the RC value is lowest for the 100 % soybean fabric and RC value increases proportionally with the decrease of the soybean fiber content or increase with the polyester fiber content. This trend can be attributed to the lower resilience and higher fiber to fiber friction of soybean fibers than the polyester fibers.

3.5 Surface Properties

The surface properties namely MIU (coefficient of friction), MMD (mean deviation coefficient of friction) and SMD (geometric roughness) of the sample fabrics are measured by KES-FB4. The values of these surface parameters are shown in Table 3.1. It is observed that the MIU and SMD value decreases with the increase of the soybean content as the 100% polyester yarns are relatively bulkier than the 100% soybean yarns. The MIU value mostly increase with increase of the cross-section area of the constituent yarn. MMD values of the fabric samples do not show any significant variation with change of any fiber content.

Table 3.1 Low Stress Mechanical Properties of the Fabric Samples

Property	Polyester (100%)	Polyester/Soyabean (65/35)	Polyester/Soyabean (50/50)	Polyester/Soyabean (35/65)	Soybean (100%)
Tensile					
LT	0.765	0.722	0.703	0.686	0.654
EMT, %	6.979	7.284	8.83	9.828	11.48
WT, gf/cm ²	17.315	14.98	12.01	10.27	8.312
RT, %	60.727	56.738	50.727	42.054	38.183
Shear					
G, gf/cm	1.226	1.201	1.186	1.128	1.046
2HG, gf/cm	6.866	6.427	6.042	5.754	5.351

Table 3.1 (Cont.) : Low Stress Mechanical Properties of the Fabric Samples

Property	Polyester (100%)	Polyester/Soyabean (65/35)	Polyester/Soybean (50/50)	Polyester/Soybean (35/65)	Soybean (100%)
2HG5, gf/cm	5.842	5.395	5.021	4.851	4.325
Bending					
B, gf.cm ² /cm	0.047	0.038	0.031	0.028	0.022
2HB, gf.cm/cm	0.058	0.047	0.042	0.037	0.034
Compression					
LC, %	0.643	0.606	0.571	0.432	0.401
WC, gf.cm/cm ²	0.068	0.059	0.052	0.044	0.041
RC, %	77.98	70.85	66.03	53.73	47.67
Weight					
W, mg/cm ²	19.4	19.1	19.2	19.3	19.3
Thickness					
To, mm	0.98	0.94	0.95	0.93	0.94
Tm, mm	0.72	0.75	0.76	0.74	0.75

3.6 Fabric Hand Value

Koshi (Stiffness), Fukurami (Fullness and Softness) and Numeri (Smoothness) are the three primary hand values (PHV) considered for the fabric samples as these fabric samples are suitable for the winter garments. The Koshi (Stiffness), Fukurami (Fullness and Softness) and Numeri (Smoothness) are the values are tabulated in Table 3.2.

Table 3.2 Hand Values of the Fabric Samples

	Polyester (100%)	Polyester / Soyabean (65/35)	Polyester / Soybean (50/50)	Polyester / Soybean (35/65)	Soybean (100%)
Koshi	8.99	8.62	8.55	8.44	8.4
Fukurami	4.69	4.82	4.83	4.85	5.74
Numeri	3.46	3.75	4.21	4.64	5.69
THV	3.22	3.33	3.33	3.44	3.54

It is observed that the Koshi, Fukurami and Numeri value decreases with increase of the soybean content in the fabric samples. The lower value of Koshi for soybean rich fabrics can be attributed to the lower value of bending rigidity, shear rigidity (G) and the tensile resilience (RT) of the constituent soybean rich yarns in the blended fabrics. The decreasing trend of the Fukurami value for the soybean rich fabrics can be attributed to the lower value of hysteresis of shear force

References:

- [1] Desore A., Narula S.A., An overview on corporate response towards sustainability issues in textile industry. Environ. Dev. Sustain. 20, 1439–1459,(2018)
- [2] Pirc U., Vidmar M., Mozer A., Krz'an A., Emissions of microplastic fibers from microfibre fleece during domestic washing. Environ. Sci. Pollut. Res. 23, 22206–22211,(2016)
- [3] Henry B., Laitala K., Klepp I.G., Microfibres from apparel and home textiles: prospects for including microplastics in environmental sustainability assessment. Sci. Total Environ. 652, 483–494,(2019)
- [4] Preferred Fiber & Materials Market Report 2020 https://textileexchange.org/wp-content/uploads/2020/06/Textile-Exchange_PREFERRED-Fiber-Material-Market-Report_2020.pdf 46–47,(2004)
- [5] Kawabata, S., Niwa, M., 'Objective Measurement of Fabric Mechanical Property and Quality, its Application to Textile and

(2HG) and relatively higher value of compressional resiliency (RC). The downward curve of the Numeri value for the soybean rich fabrics is due to the increase of compressional energy (WC).

The THV (Total Hand Value) of the developed fabric samples are calculated from the inherent Kawabata system of equations [14]. The THV of the developed fabric samples are found to be in the range of 3.33-3.54. The soybean rich fabrics show slightly better THV than the polyester rich fabrics.

4 Conclusion

The investigated fabric with higher soybean fiber content exhibits decent low stress mechanical properties for the use of apparels. The soybean fiber rich blended fabrics show good values of Koshi (Stiffness), Fukurami (Fullness and Softness) and Numeri (Smoothness). It is also observed from the experimental data that the soybean rich fabric blended with polyester fibers shows THV in the range of 3.33 to 3.54. Hence, the investigated fabrics can be used for the apparels especially for the winter garments as per the THV. Hence, it can be concluded that the fabrics blended with higher content of soybean than the polyester fibers have the potential for the applications in sustainable textiles.

- Clothing Manufacture', Int. J. of Clothing Sci. and Tech, 1, 7-18,(1991)
- [6] Guruprasad R., Prasad Krishna G., Prabhu V.T.G., Raj Sheela., Patil G.P., Low-stress mechanical properties and fabric hand of cotton., Indian Journal of Fibre & Textile Research 43 (September), 381-38,(2018)
- [7] Pattanayak A.K., Luximon A., Khandual A. Prediction of drape profile of cotton woven fabrics using artificial neural network and multiple regression method. Textile Research Journal, 81(6), 559-566,(2011)
- [8] Bharadwaj A., Patra A. K., Pattanayak A. K., Thermal Comfort Properties of Soybean, Soybean & Polyester and Soybean & Wool Blended Plain-Woven Fabrics Dyed with 1:2 Metal Complex Dyes, Journal of the Textile Association, 81(5): 274-279,(2021)
- [9] Kawabata, S. 'Standardisation and Analysis of Hand Evaluation', Textile Machinery Society of Japan, Osaka, 2nd Edn.31 (1980).
- [10] Behery H (2006) "Effect of Mechanical and Physical Properties on Fabric Hand" Woodhead Publishing, 100-255
- [11] Nayak R.K., Comfort properties of suiting fabrics, Indian Journal of Fibre & Textile Research, (34) (2)122-128, (2009)
- [12] Subramaniam V, Sivakumar M, Srinivasan V, Sasikala M., Determining Factors That Affect Fabric Shear Behavior with the Twist Method. Textile Research Journal, 60(6):368-370,(1990)
- [13] Kawabata S., Niwa M., Yamashita Y., Recent developments in the evaluation technology of fiber and textiles: Toward the engineered design of textile performance. Journal of Applied Polymer Science, 83, 687-702. (2002) ■ ■ ■

APPEAL TO TAI MEMBERS

Dear Members,

You are requested to update your contact details to enable us to update the mailing list.

1. Full Name (Surname, First Name & Middle Name)
2. TAI Unit Name (you are registered)
3. Membership Registration No.
4. Date of Registered
5. Corresponding Full Address (with Pin code No. & State)
6. Contact No. (Landline & Mobile No.)
7. E-mail ID

Please furnish above details to your respective Units at your earliest.

Or sent it to
taicnt@gmail.com



To Book your 'Ads' in Print Journal & 'Ad Banners' on e-newsletter
Contact: J. B. SOMA
Tel.: +91-22-2446 1145, Mob.: +91-9819801922
E-mail: taicnt@gmail.com, jb.soma@gmail.com

4. Conclusions

In this study, the comfort properties of plain woven dyed fabrics with 100 % Soybean and two different blends of soybean such 65%-35% Soybean and Polyester and 65%-35% Soybean and Wool were investigated and the following observations are noted.

From thermal comfort point of view Soybean fabric shows the lowest air permeability and water vapor transmission rate due to more yarn hairiness as hairs provide hindrance to air flow while Polyester Wool fabric shows highest value of air permeability and water vapour transmission rate due to less yarn hairiness.

Polyester wool fabric shows highest value of thermal resistance due to higher thickness and Polyester Soybean fabric exhibits lowest thermal resistance due to lowest thickness while 100% Soybean shows value in between them.

Soybean shows highest vertical wicking in both warp and weft direction due to highest yarn hairiness. At higher hairiness, the yarn diameter is more and there are more capillary spaces hence more wicking. Polyester/Wool fabric shows lowest wicking while Polyester/Soybean fabric shows intermediate values.

To an extent, soybean fiber has slightly higher K_S value than wool fiber because acidic amino acids (glutamic and aspartic acid) are in much higher amounts in soybean than in wool that increases number of dye fiber interaction points which may attribute to slightly darker shade in Polyester/Soybean blended fabric.

In FTIR no significant changes in peaks were observed for these dyed samples except a little variation in peak intensities at places.

References

1. AM Mindpower, *Global Apparel and Textile Industry*. AM Mindpower Solutions. <https://www.prlog.org/11020734-global-apparel-textile-industry-womenswear-leading-the-global-demand-by-am-mindpower-solutions.html> (2010)
2. Lu S., *FASH1455 Global Apparel & Textile Trade and Sourcing*. Market Size of the Global Textile and Apparel Industry-2016-to-2021-2022. <https://shengluofashion.com/2018/12/18/market-size-of-the-global-textile-and-apparel-industry-2016-to-2021-2022>
3. Gugnani, A. and A. Mishra, *Textile & Apparel Compendium 2012*, Technopak, (2012)
4. Kirchman R., Olivetti E., Miller T-R., Greene S (2015) *Sustainable apparel materials*, <http://msl.mit.edu/publications/SustainableApparelMaterials.pdf>. (2015)
5. Zhang, Y., Ghasemzadeh, S., Kotliar, A. M., Kumar, S., Presnell, S. and Williams, L. D., Fibers from soybean protein and polyvinylalcohol, *Journal of Applied Polymer Science*, **71**(1), 11, (1999)
6. Reddy, N. and Yang, Y., Novel Protein Fibers from Wheat Gluten, *Biomacromolecules*, **8**(2), 638, (2007)
7. Li, Y-y., The Soybean Protein Fiber-A Healthy and Comfortable Fiber for the 21st Century, *Fibers & Textile in Eastern Europe*, **12**(2), 46, (2004)
8. Saville, B. P., *Physical testing of textiles*, Woodhead Publishing Limited, Cambridge, UK, **1**, (1999)
9. Onofrei E., Rocha A.M. and Catarino A., The influence of knitted fabrics' structure on the thermal and moisture management properties, *Journal of Engineering of Fibers Fabrics*, **4**(4), 10, (2011)
10. Patra A.K. and Astha, *Comparative Study of Dyeing performance of Soybean fibre and wool in Fibers and Textiles*, XXIV International Congress IFATCC, Czech Republic, **3**, (2016).
11. Mohapatra N.N., Processing Soybean fiber in Textile Industries, *Colourage*, **55** (3), 68-76, (2008).
12. ASTM D1776 / D1776M-16, *Standard Practice for Conditioning and Testing Textiles*, ASTM International, West Conshohocken, PA, (2016)
13. Tyagi G. K., *Advances in Yarn Spinning Technology*, Woodhead Publishing, Cambridge, UK, **1**, (2010)
14. ASTM D737-96, *Test Method for Air Permeability of Textile Fabrics*, ASTM International, West Conshohocken, PA, (1996)
15. ASTM E96 / E96M-16, *Standard Test Methods for Water Vapor Transmission of Materials*, ASTM International, West Conshohocken, PA, (2016)
16. AATCC TM195-2012, *Liquid Moisture Management Properties of Textile Fabrics*, AATCC Technical Manual, (2012)
17. Ozdil N., Marmarali A. and Kretzschmar S.D., Effect of yarn properties on thermal comfort of knitted fabrics, *International Journal of Thermal Science*, **46** (12), 1318, 2007
18. ASTM D5548-13, *Standard Guide for Evaluating Color Transfer or Color Loss of Dyed Fabrics in Laundering (Not Suitable for Detergent or Washing Machine Rankings)*, ASTM International, West Conshohocken, PA, (2013)



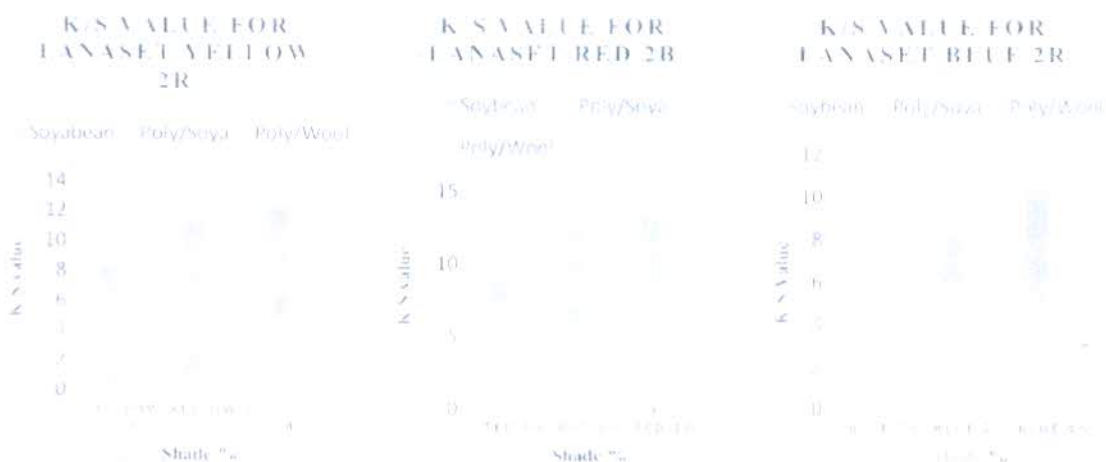


Figure 3.5: K/S value experimental fabrics dyed with (a) Lanaset Yellow 2R (b) Lanaset Red 2B and (c) Lanaset Blue 2R

3.2.2 Wash Fastness

The wash fastness of each sample dyed with the 1:2 metal complex dyes was assessed, and the results are Table 3.2. The staining of adjacent multifibres by the soybean blended fabrics was found to be of grade 4 or better. This cross-

staining indicate that the metal complex dyes have more dye affinity for protein fibers. Soybean fabric exhibits good washing fastness properties because of strong coordinate bond formation between the fiber and metal complex dye molecules.

Table 3.2: Comparative assessment of the washing fastness of the experimental fabrics

Fabrics	Lanaset Yellow 2R			Lanaset Red 2B			Lanaset Blue 2R		
	1%	2%	4%	1%	2%	4%	1%	2%	4%
100% Soybean	4	4	4.5	4.5	4.5	4	4	4	4
65-35% Polyester/Soybean	3-4	3-4	3	3-4	3	3	3	3	3
65-35% Polyester Wool	3	3	3	3	3	3	3	3	2.5

3.2.3 FTIR (Fourier Transform Infra Red)

The Soybean, Polyester-Soybean and Polyester-Wool blended fabric were tested for IR spectra. The spectra obtained (Figure 3.6) for three fabric similar from 4000 to 1800cm⁻¹ while subsequently their peaks significantly differ. This is indicative of the variation in structure and composition between regenerated protein and natural protein fiber blended with synthetic fiber. All three union fabrics

were dyed with 1:2 metal complex dyes in 4% shade and tested for IR spectra. However, no significant changes in peaks were observed for these dyed samples except a little variation in peak intensities at places (Figure 3.7). This indicates that no major change in functional group or strength properties have occurred in the fabrics after the preparatory process and subsequent coloration carried out



Figure 3.6: FTIR of Untreated Samples



Figure 3.7: FTIR of Dyed Samples

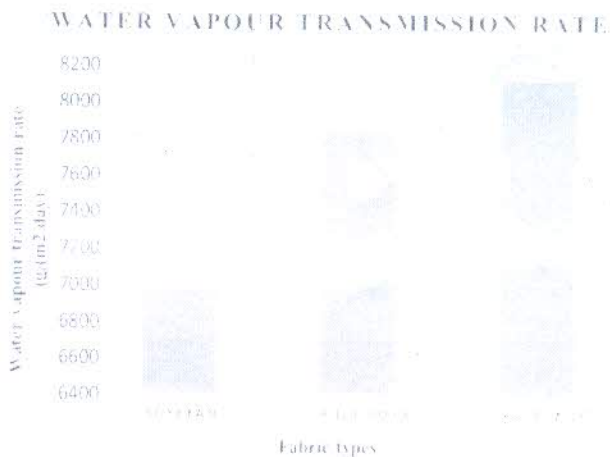


Figure 3.2: Comparative analysis of Water Vapor Transmission Rate of experimental fabrics

3.1.3 Thermal Resistance

Thermal resistance is an important measure for analyzing the effect of material properties on heat transfer. Thermal resistance is a measure of a materials ability to prevent heat from flowing through it. It is a very important parameter and is greatly influenced by fiber type and fabric thickness. Figure 3.3 depicts that Polyester/wool fabric exhibits highest value of thermal resistance while Polyester/soybean fabric shows lowest value of thermal resistance and Soybean fabric exhibits value of thermal resistance in between them. Increase in the fabric thickness will result in increase in thermal resistance. Because of crimp and felting property wool fiber makes the fabric bulky and lofty so Polyester/wool fabric has highest thickness among the three fabrics hence shows highest thermal resistance.

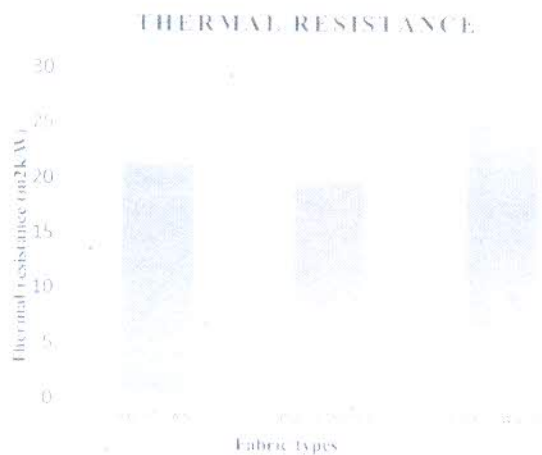


Figure 3.3 – Comparative analysis of Thermal resistance of experimental fabrics

3.1.4 Wicking Behavior

Wicking is the spontaneous flow of a liquid in a porous substrate, driven by capillary forces. It is an important factor in determining the comfort of clothing for active wear. High wickability facilitates quick drying and fast cooling in hot

environments. The wickability results of the tested fabric samples are given in Figure 3.4. It is observed that the 100% soybean fabric exhibits highest wicking height in warp & weft direction while Polyester/Wool fabric exhibits lowest wicking height in warp way and weft way. Polyester/Soybean fabric exhibits in between wicking height in warp & weft direction. It is found that the wicking height depends upon yarn hairness as the higher hairness causes higher yarn diameter therefore provides more capillary spaces which helps to achieve more wicking. The adjacent protruding fibers are also participating as the inclined capillary. As the hairness decreases the yarn become compact and hence there are fewer capillaries for wicking which causes less wicking height.



Figure 3.4 – Comparative analysis of Wickability of experimental fabrics

3.2 Dyeing Behaviour

3.2.1 Color Strength (K/S)

K/S value of 1:2 metal complex dyed fabrics with three different colors in different shade depths is shown in Figure 3.5. The result indicates that K/S value of Soybean fabric is highest and for Polyester/Wool K/S value is lowest. Polyester/Soybean fabric exhibits in between value of K/S. To an extent, soybean fiber has slightly higher K/S value than wool fiber because acidic amino acids (glutamic and aspartic acid) are in much higher amounts in soybean than in wool that increases number of dye fiber interaction points which may attribute to slightly darker shade in Polyester/Soybean blended fabric. Due to the presence of scales on wool surface results in difficulties in dyeing on the other hand soybean has smooth surface may be another reason for slightly higher K/S value in Polyester/Soybean. K/S value of 1:2 metal complex dyes increased as dye concentration increased. Lanaset Red 2B dye gave maximum K/S values in most cases which could be due to better dye absorption and penetration of dye in the fiber surface.

transmission rate of fabric was measured on W3 060 according to ASTM standard E96 [15]. Thermal insulation of fabric was measure on Alambeta tester which measures transient thermal characteristics of textile fabrics and the thermal resistance value is expressed in m² K/W. The vertical wicking test of the fabric was carried out according to the AATCC TM195-2012 standard [16]. The conditioned sample of 20cm x 2.5cm was cut both along the direction of warp and weft. A setup was installed which had a ring holder were in the fabric was hanged vertically. A beaker having colored solution of 2gpl cold brand reactive dye was taken. Each specimen was marked with a line 3cm away from its edge along its length. The specimen was then dipped inside the solution till the mark and wicking height was noted down after an interval of 5min, 10min, 15min and 30min. In addition to this, the porosity [17] of these fabrics is determined as per Equation 1

$$\text{Porosity Equation} = \left(1 - \frac{m}{p \cdot h}\right) \times 100 \text{ -----(1)}$$

where P is the porosity in percentage, m is the fabric areal density, p is the fiber density in g/cm³ and h is the fabric thickness in mm. The fiber density value in the equation is calculated by taking the individual fiber densities and blend ratios into consideration. The calculated values of the fabric porosity are shown in Table 2.1

The K/S values were determined by using a spectrophotometer (Premier Colorscan SS 5100A). The wash fastness was measured by using a Launderometer with a standard multifiber strip as per ASTM D5548 [18]. The samples were also tested for FTIR (Fourier Transform Infra-Red) spectroscopy using Bruker tabletop model based on ATR principle. The peaks were obtained by Attenuated Total Reflection (ATR)

3. Results and Discussion

The results of thermal comfort parameters such as air permeability, water vapor transmission rate, thermal resistance and vertical wicking values are shown in Table 3.1.

Table 3.1: Thermal comfort parameters of the experimental fabrics

Fabric Types	Air permeability (m ³ /m ² min.)	Thermal resistance (m ² k/W)	Water vapor transmission rate (g/m ² .day)	Wicking Height (cm)	
				Warp	Weft
100% Soybean	91.68	21.2	6978	16.8	16.3
65-35% Polyester Soybean	133.36	19.6	7834	16.4	15.8
65-35% Polyester Wool	158.37	26	8112	14.5	13.5

3.1 Thermal Comfort Properties

3.1.1 Air Permeability

Air permeability is an important comfort property which indicates the amount of air passed through the fabric unit

area. This is a very important thermal comfort parameter as it helps to balance the flow of air from environment to human body and vice versa. The air permeability depends on fabric porosity, which affected by the number of pores in the textile fabric, yarn linear density i.e., yarn diameter, yarn hairiness, fiber cross-section and shape. The pores in the fabric are affected by the hairs as the hairs significantly blocks these pores affecting the air permeability. The results showed that the air permeability of Polyester Wool blend exhibits highest value of air permeability while Soybean shows lowest value whereas the Polyester Soybean exhibits intermediate values. The 100% soybean fabric shows lowest value of air permeability due to more yarn hairiness, lower porosity values as shown in Figure 3.1. The lower value of porosity causes lower air passage and vice-versa. Air permeability also decreases with more protruding hairs as it hinders the passage of air through the fabric pores.



Figure 3.1 – Comparative analysis of air Permeability values of different types of fabrics

3.1.2 Water Vapor Transmission Rate

The water vapor transmission rate is another important parameter of thermal comfort which helps to transport the sweat from the skin for the comfortable feeling. Water vapor transmission rate is a measure of the passage of water vapor through the material. It is the mass of water vapor transmitted through a unit area in a unit time under specified conditions of temperature and humidity. The water vapor permeability depends on the several factors like fabric constructional parameters, fabric pores and type of constituent fiber. It is observed from the Figure 3.2 that the Polyester wool fabric exhibits highest water vapor transmission rate while Soybean fabric shows lowest water vapor transmission rate and Polyester Soybean fabric exhibits values in between them. Soybean fabric shows lowest water vapor transmission which may be due to more yarn hairiness and higher value of cloth cover. The higher hairiness value of the constituent yarn of the fabric provides hindrance to water vapor to pass through the fabric due to which water vapor transmission rate decreases at higher hairiness. Polyester Wool exhibits highest value of water vapor transmission rate due to structure of wool. The outer sheath i.e. epicuticle of the wool has tiny microscopic pores, through which water vapor may penetrate into the internal structure of the fiber. The outer sheath helps wool fabric to absorb water vapor & release into air.

2020-21

Thermal Comfort Properties of Soybean, Soybean & Polyester and Soybean & Wool Blended Plain-woven Fabrics Dyed with 1:2 Metal Complex Dyes

Mr. Ashish Bhardwaj¹, Dr. Arun Kumar Patra² & Dr. Ajit Kumar Pattanayak^{1*}

¹Department of Textile Technology, The Technological Institute of Textile & Sciences, Bhiwani

²Department of Textile Chemistry, Uttar Pradesh Textile Technology Institute, Kanpur

Abstract

Textile industry is one of the oldest manufacturing industries and also one of the most polluting industries on the earth today. This industry produced 150 billion garments in 2015 out of which 60% of garments are synthetically derived like polyester. Hence, effort should be made to use more natural fibers and reduce the use of synthetic fibers for the sustainability of this industry. Therefore, this study is focused to use more sustainable fibers like soybean wool with some polyester. The objective of this study is to develop more eco-friendly dyed fabrics produced from the different blend proportions of Soybean, Polyester and Wool fiber and to study their mechanical and comfort properties. In this study, two ply yarns were spun using spinning system with 100% Soybean, 65% / 35% Soybean-polyester and 65% / 35% Soybean wool. Then plain-woven fabrics were produced from these yarns and further dyed with 1:2 metal complex dyes. Finally, the thermal comfort parameters were measured for these dyed samples. The results indicated that soybean possess low air permeability, water vapor permeability with their counterparts but moderate thermal insulation and excellent wicking behavior. The moderate comfort behavior and good dyeability with 1:2 metal complex dyes of soybean fibers and its blends has a great commercial potential in apparels.

Keywords: Soybean, air permeability, thermal insulation, metal complex dyes, K_s value

1. Introduction

Clothing is not merely the necessity of humankind but defines the personality of the wearer. The improvement of the economic status drives the demand to produce 150 billion garments in 2010 [1]. This projection of the production of apparels in terms of value will touch to \$961.0 in 2021 with an increase of 28.5% since 2016 [2]. Gugnami and Mishra 2012 [3] estimated that 400 billion square meters of fabric produced in 2015 and 100 million tons of fibers were used to produce this huge volume of fabrics. The share of synthetic fibers (polyester, nylon) to produce this huge amount of garments was around 60%. The synthetic fibers mostly derived from the petroleum sources. Hence, this huge production of fabrics with synthetic fibers becomes a major contributor of Green House Gases. This huge quantity of fabric production also required a large amount of fresh water for processing [4]. Therefore, a more sustainable approach is required in every step of Textile and Apparel value chain. The first step to attain sustainability is to reduce the dependence on the synthetic fibers as well as to reduce the production level. The other challenge for the textile and apparel industry is also to produce long durable garments with better comfort. The key aspect of the clothing has been greatly influenced by the comfort characteristics of the constituent fabric of the garment. The fabric characteristics of the clothing are greatly influenced by the constituent fibers. The natural fibers like cotton, linen, wool and silk are the most used for the garments as well as the synthetic fibers like polyester, nylon, acrylic etc. The introduction of specific properties in

synthetic fibers makes them more functional and can be used in varying seasons. The rising demand of synthetic fibers makes the textile and apparel industry unsustainable. Hence, efforts have been carried to use more modified natural fibers which are environmentally friendly as well as more functional [5]. The natural protein fibers are extensively used for garments and have decent physical properties. Garments made of protein fibers are expensive due to low availability and higher processing stages [6]. The soybean fibres are typical plant protein fibres and spun by the wet method spinning process from the natural soybean cake after extraction of oil from the soybean. The auxiliaries and agents used to produce soybean is non-toxic and complies the environmental standards. Moreover, the production process causes least waste generation [7]. The natural protein fibres also offer difficulty for processing as non-uniform profile and limited fineness. The dyeing of wool is also difficult due to the presence of the scales in wool. Therefore, soybean can become a potential replacement of the wool and silk as it can be drawn with unlimited fineness. Soybean fibers are inherently softer, lustrous and drapable. The soybean fibers are also offering decent amount of UV resistant, antibacterial, transmission property as well as good dyeability [8]. It also possesses many advantages over the other fibers like moderate breaking strength, modulus, and low shrinkage in boiling water. The effective blending of soybean fibers with other fibers (polyester, wool, silk) will help to achieve various functionalities, yarn properties and to reduce the cost. The good quality garments must have decent aesthetic value, physical and mechanical properties as well as thermal comfort. Thermal comfort is the basic ability of the garment for the transmission of air, moisture, and heat. The transmission rate varies with the external environment as well as with the activity level [9]. Onofrei E. et al. [10] reported that the comfort parameters such as air permeability, thermal resistance and thermal absorptivity properties of

* All the correspondences shall be addressed to,

Dr. Ajit Kumar Pattanayak

Department of Textile Technology,

The Technological Institute of Textile & Sciences,

Bhiwani

Email: ajitpattanayak@titsbhiwani.ac.in

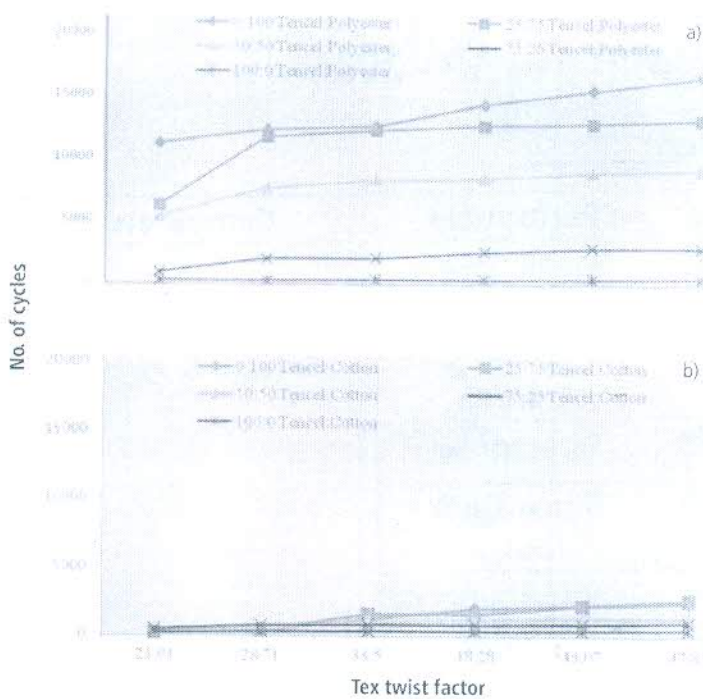


Fig. 2
Abrasion resistance at different twist factors
(a) Tencel/PET, (b) Tencel/CO

This is because of the better ability of the PET fiber to withstand repeated distortion as compared to CO and Tencel fibers [5]. Further, CO fiber yarn has better abrasion resistance than Tencel fiber yarns, probably due to wax on cuticle outer layers on the fiber acting as lubricating agent during the abrasion, and possess better abrasion resistance [4].

Effect of twist

Fig. 2 shows the abrasion resistance of ring spun Tencel, PET and CO fiber yarns spun at twist level ranges from 23.93-47.85. From the Anova analysis (Table 2), it is observed that twist affects the abrasion resistance of the yarns significantly. As expected, with the increase in the twist level, the abrasion resistance of Tencel, PET and CO yarns increase for all the ring spun yarns. This is because with increase in twist level there will be more complete binding of fibers in the yarn structure and during abrasion the disintegration of the yarn structure will delay, and hence higher

abrasion resistance of the yarns are observed. Fig. 2 also shows the abrasion resistance of Tencel/PET and Tencel/CO blended yarns at different twist factor. It can be easily observed from the data that the abrasion resistance of all the blended yarns increases with the increase in twist level irrespective of the blend type or blend ratio [6, 7].

Process variables	Abrasion resistance
A	S
B	S
C	S
D	S
A*B	S
B*C	S
B*D	S
C*D	S

S: significant at 95 % confidence level
A: fiber type, B: tex-twist factor, C: blend type, D: blend ratio

Table 2
Anova test results for abrasion resistance

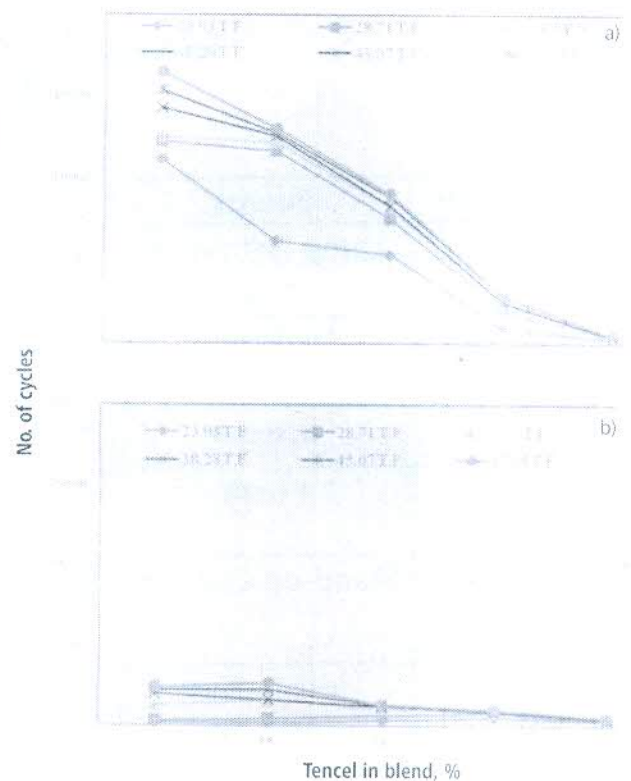


Fig. 3
Variation in abrasion resistance with blend proportions at different twist factors
(a) Tencel/PET, (b) Tencel/CO

Effect of blend ratio

Fig. 3 shows the abrasion resistance of Tencel/PET and Tencel/CO blended yarns at different proportion of Tencel in the blend. As expected, the Tencel-polyester blended yarns have much higher abrasion resistance as compared to Tencel/CO counterparts. This is because of higher abrasion resistance of PET fiber as compared to CO and Tencel fibers [5, 8]. Further, with the increase in the percentage of Tencel reduces the abrasion resistance of both Tencel/PET and Tencel/CO blended yarns.

Conclusions

From the results, it can be concluded that:

- PET fiber yarn has significantly higher abrasion resistance for all type of yarns and twist factors followed by CO and Tencel fiber yarns.
- The twist also influences the abrasion resistance significantly and with increase in twist, abrasion resistance increases for all types of yarn samples.
- Abrasion resistance of Tencel fiber yarn increases as content of PET and CO increases in blended yarns.

References

- [1] Abdullatif, I.; Blackburn, R.S.; Russell, S.J.; Taylor, J. *J. Polym. Sci. Part A: Polym. Chem.* 1991, 29, 1391-1398.
- [2] Kadir, S.; Quality Assurance for Textiles and Apparel (ISBN: 1-8517-1111-1/2007), Fairchild Publication.
- [3] Yazdi, A.; Hopfinger, G.R. *Fibers & Textiles in East Asia*, 1990, 22(1), 146-157.
- [4] Barella, A.; Mancini, A. *Text. Res. J.* 86 (1984) 314-319.
- [5] Ceven, E.K.; Ozdemir, O. *Text. Res. J.* 76 (1974) 315-322.
- [6] Chattopadhyay, R.; Tyagi, G.K.; Goyal, A. *J. Text. Inst.* 104 (2013) 339-343.
- [7] New, G.F. *J. Text. Inst.* 51 (1927) T595-T605.
- [8] Barella, A. *Good. J. J. Text. Inst.* 3 (1972) 496-498.

as strength, but it also affects the appearance of the fabric. Abrasion resistance is affected by the fiber type, yarn type, blend type and twist. Yarn abrasion is another important subject that should be considered during processing.

Yazdi et al. [3] investigated yarn abrasion resistance which is affected by the twist factor in the same way as the effect of twist on the yarn strength i.e. yarn on yarn abrasion resistance first increases up to a certain degree and then as the twist increases, the yarn on yarn abrasion resistance decreases.

Barella and Manich [4] studied the relation between twist and abrasion resistance of PET/CO (50/50), and PET/VI (50/50) blend yarns. They observed that abrasion resistance increases with yarn twist, first slowly and then rapidly, and from a certain twist multiplier onwards, the increase in abrasion resistance slows down. 40 tex yarns and for higher twists, cotton yarn shows a better abrasion resistance than polyester yarns. They observed that for the same linear density and high twist multipliers, the abrasion resistance of blended spun yarns is lower than the average, corresponding to the resistance of yarns spun from component fibers.

Kenan and Ozdemir [5] studied the abrasion behavior of chenille yarn produced from wool and wool-blend piles by a computerized image analysis method. They observed that using PET fiber in the blends, wool fibers with appropriate fineness and siro-spun pile yarn type in the production will help to produce chenille yarns with high abrasion resistance.

Chattopadhyay et al. [6] studied the abrasion resistance of Tencel blended ring yarns. Abrasion resistance of all the yarn samples calculated in terms of percentage loss in breaking load after abrading 200 cycles. For all the 3 types of structure, the strength loss is highest for Tencel and lowest for cotton. It was observed that with increase in Tencel content, abrasion resistance decreases.

New G.F. [7] investigated the abrasion resistance of flax yarns to wear by rubbing stationary yarn specimens carrying tension pieces with hardened steel surfaces of cylindrical cross-section. It was found that an increase in fiber quality as estimated in the trade, in yarn twist, or in preparing treatment within ordinary limits, gives a yarn with a higher resistance to wear. Boiling a yarn decreases its wear resistance while sizing increases it very greatly.

Barella et al. [8] studied the abrasion resistance of 8 yarns, of which 4 were conventional and 4 open-end spun yarns. Each pair of yarns was spun from the same raw material. They concluded that one cannot generalize as to whether open-end-spun yarns are resistant to abrasion than conventional yarns. This depends on the conditions under which the test is being done and on the nature and amount of the factors acting jointly with the abrasive effect.

Materials and methods

Fibers

Tencel, polyester and cotton fibers were used in this study. The cotton fiber (DCH 32) was obtained in form of combed sliver from an industry. The specifications of Tencel, PET and CO fibers are given in Table 1.

Preparation of yarn samples

Yarns of 29.5 tex were spun from Tencel and its blend with PET and CO fibers using different blend ratios (0:100, 25:75, 50:50, 75:25, 100:0) and 6 different tex twist factors ranging from 23.93, 28.71, 33.50, 38.28, 43.07 and 47.85 were prepared. For blending Tencel and PET fibers, each of the 2 components was opened manually and sandwiched well to produce a homoge-

neous blend. However, for Tencel/CO blended yarns, the combed cotton sliver was blended with Tencel fiber in the opening room. A predetermined quantity of fibers to be blended was mixed and processed in a Lakshmi Reiter's blow room line. The conversion to drawn sliver was carried out by using a MMC carding machine and Lakshmi Reiter's drawframe DO/2S. 2 drawing passages were given to the card sliver, the linear density of finisher sliver being adjusted to 3.69 ktex. The finisher sliver was converted into 492 tex roving on an OKK fly frame, which was used to produce 29.5 tex yarn on Lakshmi Reiter's G5/1 ring frame using a spindle speed of 12,000 rpm.

Measurement of yarn abrasion resistance

Abrasion resistance of all the yarn samples was determined by CSI universal abrasion tester. By winding a yarn sheet on wrap reel, specimen was prepared for flexing and abrasion. The number of ends in the specimen has been calculated according to ASTM standards D 1379-55T. Total 61 yarns were taken per specimen. Flex weight and spigot weight was 2.0 lbs and 0.5 lbs respectively. The end point specified in this procedure is based on the number of cycles required to abrade the specimen sufficiently to cause rupture under the specified tension. 10 readings were taken for each yarn sample.

Results and discussions

The influence of fiber type, yarn type, twist factor, blend type, blend ratio on the abrasion resistance has been tested for significance using Anova at 95 % level of significance (Table 2)

Effect of fiber type

Fig. 1 shows the abrasion resistance of Tencel, PET and CO fiber yarns spun on ring spinning system with different twist factors. It can be easily observed from the figure that PET fiber yarns have highest abrasion resistance followed by CO, and Tencel has the lowest value of abrasion resistance irrespective of the twist level.

Fiber	Length [mm]	Linear density [dtex]	Tenacity [cN/tex]	Breaking elongation [%]	Modulus [cN/tex]
Tencel	38	1.40	31.3	7.2	731.3
Polyester	38	1.33	56.2	10.8	638.9
Cotton	33.1*	1.18	24.9	6.5	525.5

*Span length 2.5 %

Table 1
Specifications of Tencel, PET and CO fibers

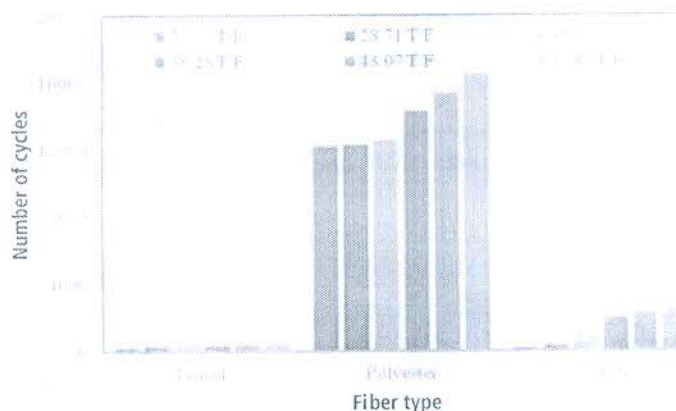


Fig. 1
Abrasion resistance of Tencel, polyester and cotton ring yarns

Abrasion resistance of Tencel blended ring spun yarns

Ashvani Goyal, Ritu Sharma

The Technological Institute of Textile & Sciences, Bhiwani/India

This paper investigated the effect of twist factor and blend ratio on abrasion resistance of Tencel-polyester and Tencel-cotton blended ring spun yarns. Anova (analysis of variance test) results of the experimental study show that blend ratio, tex-twist factors and type of fiber have a significant effect on abrasion resistance. Further, polyester (PET) fiber yarn always has higher abrasion resistance as compared to cotton (CO) and Tencel, and abrasion resistance of CO and Tencel improves as the content of PET increases.

Abrasion is the physical destruction of fibers, yarns, and fabrics, resulting from the rubbing of a textile surface over another surface [1]. Textile materials can be unserviceable because of several different factors and one of the most important causes is abra-

sion. Abrasion occurs during wearing, using, cleaning or washing process and this may distort the fabric, cause fibers or yarns [2] to be pulled out or remove fiber ends from the surface. Abrasion ultimately results in the loss of performance characteristics, such



Thermo-physiological comfort is one of the most important aspects of textiles and this property can be improved by improving moisture management of textiles. Wetting and wicking are two important properties which affect the moisture management of textiles. The ability of textiles to absorb and draw off liquid by help of capillary action is known as wicking. If wicking of a textile is good, it can be used for various applications e.g. in sportswear, medical products, footwear, and exercise garments. Lord¹ observed that wicking height is likely to be a function of twist multiple.

The influence of twist factor and blend ratio on wickability of tencel-polyester and tencel-cotton blended ring spun yarns have been investigated.

type of fiber, type of yarn structure & packing as well as migration. Chattopadhyay and Chauhan² studied the wicking behaviour of ring and compact spun yarns and observed that ring yarns wicked faster than compact yarns & coarser yarns wicked faster than finer ones. Sengupta and Murthy³ analysed that

However, there is no extensive study on wickability of tencel blended ring spun yarns. The present study aims at investigating the wickability of tencel-polyester and tencel-cotton blended yarns at different twist levels.

Material and methods

Fibres

The properties of tencel, polyester and cotton fibres used in this study are given in *Table 1*. The DCH 32 cotton was obtained in form of combed sliver which is used in this study.

Preparation of yarn samples

Yarns of 29.5 tex were spun from tencel and its blend with polyester and

Wickability of tencel blended ring spun yarns

Ashvani Goyal and Ritu Sharma

The Technological Institute of Textile & Sciences, Bhiwani 127 021, India
ashvanigoyal@titsbhiwani.ac.in, ashvanigoyal@gmail.com

for the ring spun yarns, the wicking time increases steeply as twist increases whereas for the open-end spun yarns the increase is gradual.

Tencel fibre can be used as a substitute of cotton fibre. Synthesis of tencel involves a solvent that can be recycled easily. Blending is a common practice for improving the properties of a textile material. There are various studies dealing with mechanical and physical properties of tencel blended yarns^{4,5}.

cotton fibres using different blend ratios (0:100, 25:75, 50:50, 75:25, 100:0) and six different tex twist factors (23.93, 28.71, 33.50, 38.28, 43.07 & 47.85). For blending tencel and polyester fibres, each of the two components was opened manually and sandwiched well to produce a homogeneous blend. However, for tencel-cotton blended yarns, the combed cotton sliver was blended with tencel fibre in the opening room. A predetermined quantity of fibres to be blended was mixed and

Table 1 : Properties of tencel, polyester and cotton fibre

Fibre	Length (mm)	Linear density (dtex)	Tenacity (cN/tex)	Breaking elongation (%)
Tencel	38	1.40	31.3	7.2
Polyester	38	1.33	56.2	10.8
Cotton	33.1*	1.18	24.9	6.5

*Span length, 2.5%

processed in a Lakshmi Rieter's blow room line. The conversion to drawn sliver was carried out by using a MMC carding machine and Lakshmi Rieter's drawframe DO 2S. Two drawing passages were given to the card sliver, the linear density of finisher sliver being adjusted to 3.69 ktex. The finisher sliver was converted into 492 tex roving on an OKK fly frame, which was used to produce 29.5 tex yarn on Lakshmi Rieter's G5 1 ring frame using a spindle speed of 12,000 rpm.

Tests

Yarn wicking

Vertical wicking height was measured by the method used by Sengupta and Murthy⁵. A 30 cm length of yarn was taken. One end of yarn was tied into clip, and other end, to a hook of a small weight (2.90 g). The yarn was hung on the notch of a nail fixed to a wooden plank held by an iron stand. Yarn was slowly lowered down into the measuring jar containing 3% reactive red dye M8B till the weight just touched the dye

Cotton has lowest wicking height as compared to polyester and tencel fibre yarns.

solution. The yarn was further lowered down into the measuring jar in such a way that the lower end, of about 1 cm was below the liquid surface. Simultaneously stopwatch was pressed and the rise of dye solution from the fluid surface in the yarn was continuously watched through the eyepiece. Wicking height was measured in 5 min at intervals of 1 min. Ten readings were taken for each sample. Wicking rate was calculated by ratio of wicking height and wicking time.

Results and discussion

The influence of fibre type, twist factor, blend type and blend ratio on the wickability has been checked for significance using ANOVA at 95% level of significance. The ANOVA results, which are shown in Table 2, confirm

Process variable	Wicking height	Wicking rate
A	s	s
B	s	s
C	s	s
D	s	s
A * B	s	s
A * C	s	s
B * C	ns	s
B * D	s	s
C * D	ns	s

s - Significant at 95% confidence level; ns - Non significant at 95% confidence level
A - Fibre type; B - Text twist factor; C - Time; D - Blend type

that all the factors significantly affect the wicking height and wicking rate.

Effect of fibre type

The wicking height and wicking rate of tencel, polyester and cotton fibre yarns spun on ring spinning system at twist factors ranging from 28.71 to 47.85 can be observed from Figs 1 & 2. Tencel fibre yarn has significantly higher wicking height and wicking rate as compared to polyester and cotton fibre yarns and cotton has the lowest value. The highest wicking height of tencel fibre yarns are due to its pore nano-structure which consists of countless, very hydrophilic, crystalline nano-fibrils, arranged in a very regular manner. The fibrils themselves do not absorb water, but water absorption only takes place in the capillaries between the fibrils⁸⁻⁹. Polyester fibre yarn is very smooth in appearance and have perfectly round

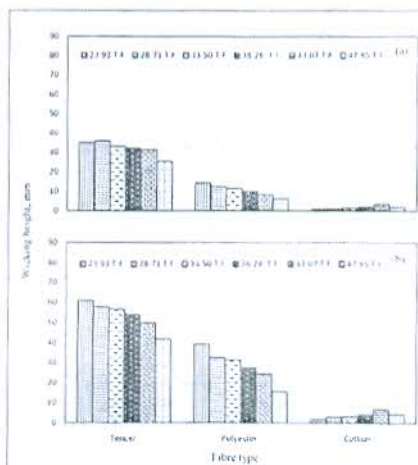


Fig 1 : Wicking Height of Tencel, Polyester and Cotton Ring Spun Yarns [(a) 1 min and (b) 5 min]

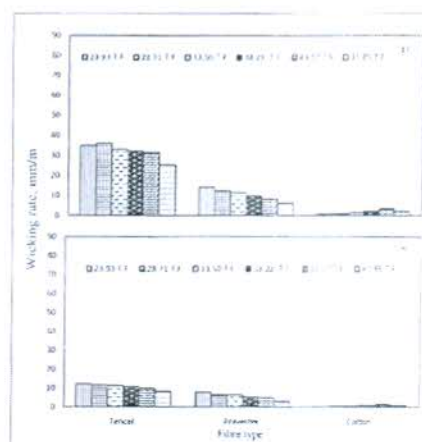


Fig 2 : Wicking Rate of Tencel, Polyester and Cotton Ring Spun Yarn [(a) 1 min and (b) 5 min]

cross-section with regular capillaries and it does not get swell when coming into contact with water hence water movements take place only on the surface of fiber that gives higher wicking height of polyester as compared to cotton yarns¹⁰⁻¹¹. Though cotton is also a cellulosic fiber and its moisture absorption is very high, yet it has lowest wicking height as compared to polyester and tencel fibre yarns. This is because cotton is a natural fiber and has irregular capillaries due to fiber roughness, cross-sectional shape and length which inhibit the fluid flow. Also cotton collects moisture inspite of flowing it out and swells¹² when coming into contact with water.

Effect of blend ratio

Figs 3-6 show the wicking height and wicking rate of tencel-polyester and tencel-cotton blended yarn at different twist factor in time intervals from 1 to 5

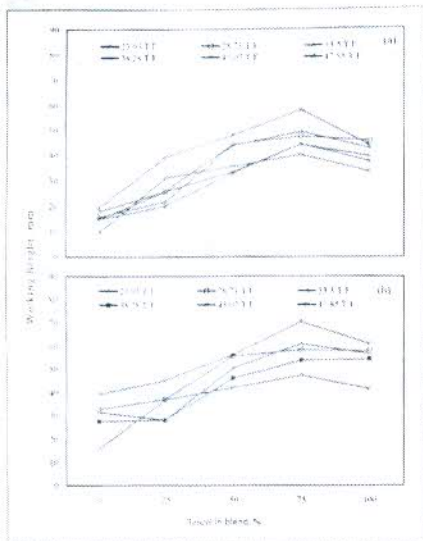


Fig 3 : Wicking Height of Tencel-Polyester Blended Yarn at Different Tencel Proportions [(a) 1 min and (b) 5 min]

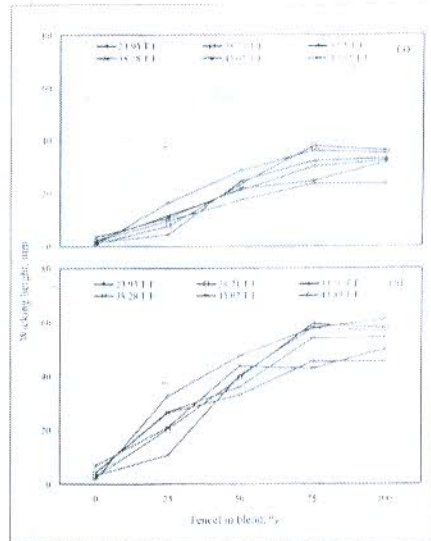


Fig 5 : Wicking Height of Tencel-Cotton Blended Yarns at Different Tencel Proportion [(a) 1 min and (b) 5 min]

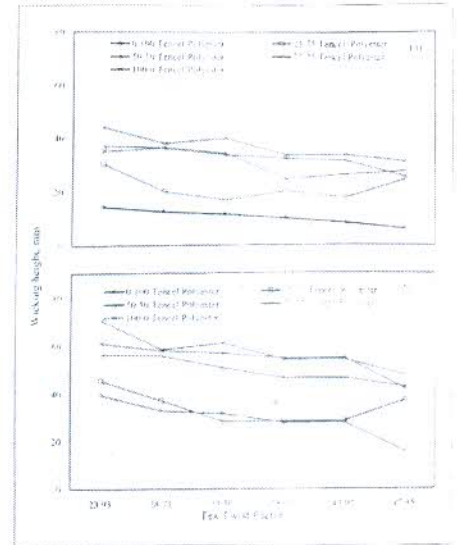


Fig 7 : Wicking Height of Tencel-Polyester Ring Spun Yarns at Different Twist Factor [(a) 1 min and (b) 5 min]

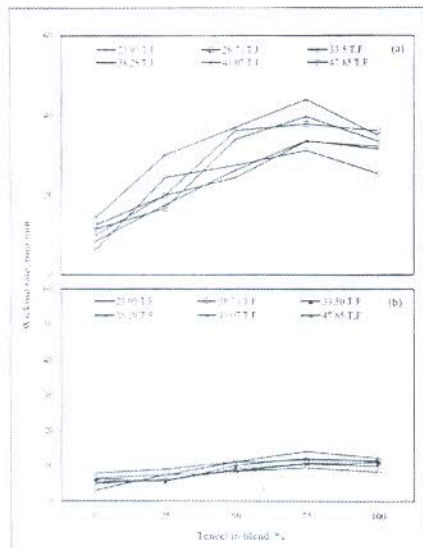


Fig 4 : Wicking Rate of Tencel-Polyester Blended Yarns at Different Tencel Proportions [(a) 1 min and (b) 5 min]

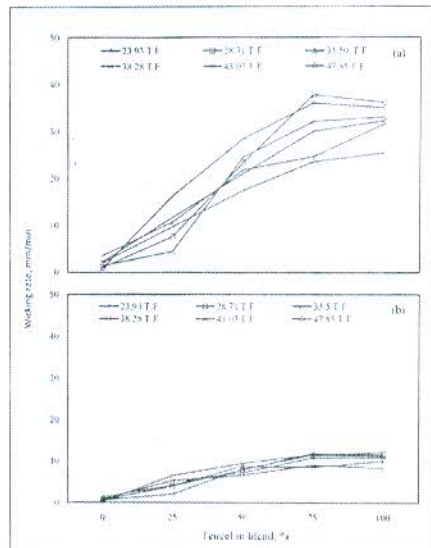


Fig 6 : Wicking Rate of Tencel-Cotton Blended Yarns at Different Tencel Proportions [(a) 1 min and (b) 5 min]

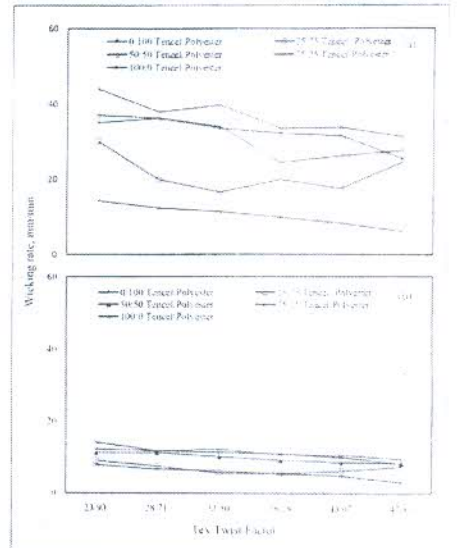


Fig 8 : Wicking Rate of Tencel-Polyester Ring Spun Yarns at Different Twist Factors [(a) 1 min and (b) 5 min]

min. It can be clearly observed from the results that tencel-polyester blended yarns have higher wicking height and wicking rate as compared to tencel-cotton blended yarn irrespective of the twist factor and wicking time. This is because of better wickability of polyester fibre as compared to cotton fibre¹³. Further, the wicking height and wicking rate improves in both the tencel fibre blend when proportion of tencel is increased either with polyester or cotton fibre in the mix and maximum wicking height was generally observed in case of 75:25 tencel-polyester or tencel-cotton blend.

The improvement in wicking height with increase in tencel proportion is due to higher hydrophilicity of tencel, which governs liquid transport through capillary interstices in yarns and due to the nano-fibrillary structure of tencel fibers.

Effect of twist

The influence of twist factors on ring spun tencel-polyester and tencel-cotton blended yarns are shown in Figs 7-10. It is observed that the twist influences the wicking height and wicking rate significantly and the influence of twist factor on wicking height and wicking

rate is similar for all tencel blended yarns except pure cotton yarns. In case of tencel-polyester and tencel-cotton blended yarns, the wicking height continuously decreases with increase in twist factor whereas in case of 100% cotton yarns the wicking height increases upto twist factor 38.28 and thereafter it decreases. With increase in twist factor in tencel blended yarns, the decrease in wicking height and wicking rate can be attributed to decrease in size of capillary channel between the fibers and increase in tortuosity that results to wick a longer path for a constant wicking

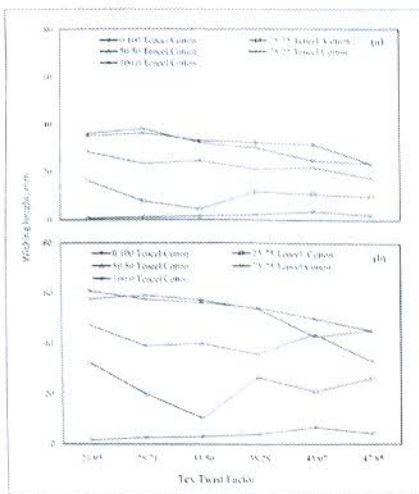


Fig 9 : Wicking Height of Tencel-Cotton Ring Spun Yarns at Different Twist Factors [a) 1 min and (b) 5 min]

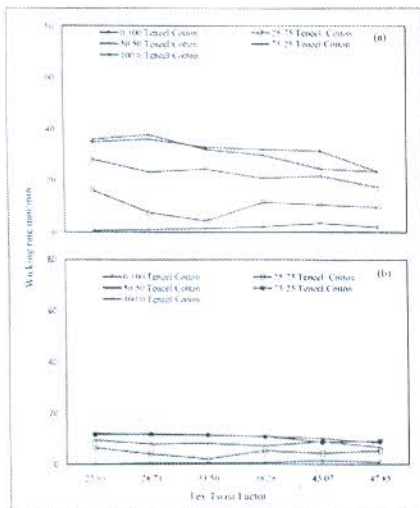


Fig 10 : Wicking Rate of Tencel-Cotton Ring Spun Yarns at Different Twist Factors [a) 1 min and (b) 5 min]

height and hence lower wicking height is observed. But in case of pure cotton yarns, wicking height increases with increase of twist factor at low levels and reaches the maximum at twist factor of 38.28 and thereafter it decreases. This behaviour is because at lower twist level the yarn is loosely packed and when additional twist is inserted into the yarn, constituent fibers tend to move inward and the becomes more compact¹¹. This appears to reduce the effective radii of inter fiber capillaries and enhance the wicking. The wicking reaches the maximum when the yarn is nearly closely packed. Further increase in twist results decrease in wicking height and wicking rate because of reduction in size of

capillary between the fibers and increase in tortuosity.

Effect of time

The ANOVA results in Table 2 and Figs 1-10 show that there is significant effect of time on wicking height and wicking rate. Wicking height continuously increases with increase in wicking time whereas wicking rate decreases continuously with the time. The decrease in wicking rate¹⁵ with increase in time for any given yarn can be attributed to the gravity of water column within capillary which acts against the capillary pressure.

Conclusion

- Tencel fibre yarn has maximum wicking height and wicking rate as compared to polyester and cotton fibre yarns and cotton has the lowest value.
- Tencel-polyester blended yarns have significantly higher wicking height and wicking rate as compared to tencel-cotton blended yarn and both properties improve with the addition of tencel fibre in the blend either with polyester or cotton fibre. Also, the maximum wicking height was found for 75: 25 tencel-polyester or tencel-cotton blend.
- Wicking height and wicking rate continuously decreases with increase in twist factor for tencel-polyester and tencel-cotton blended yarns except 100% cotton yarns where wicking height and wicking rate increases upto twist factor 38.28 and thereafter it decreases.
- Wicking height continuously increases with increase in wicking time whereas wicking rate decreases continuously with increase in wicking time.

References

1. Lord P R, A Comparison of the performance of Open-end and Ring Spun Yarns in Terry Toweling, Text Res J, 1974, Vol 44, No 16, 516-522
2. Chattopadhyay R and Chauhan A, Wicking Behaviour of Compact and Ring Spun Yarns and Fabrics, in One Day Seminar on Comfort in Textiles, Dept. of Textile Technology, IIT Delhi, India, Oct, 2004, Vol 16, No 3, 20-25
3. Sengupta A K and Muthy H V S, Wicking in Ring Spun Versus Rotor Spun Yarns, Indian J. Text. Res. 1985, Vol 10,

No 4, 155-157

4. Tyagi G K, Goyal A, Chattopadhyay R, Low-stress and recovery characteristics of tencel blended ring, rotor and MP yarns, Indian J Fibre Text Res, 2013, 38, 341-349
5. Chattopadhyay R, Tyagi Gk, Goyal A, Studies of the hybrid effect on mechanical properties of tencel blended ring, rotor and air-jet spun yarns, Journal of The Textile Institute, 2013, 104(B), 339-349
6. Tyagi GK, Goyal A, Chattopadhyay R, Influence of twist and blend ratio on characteristics of ring spun tencel blended yarns, Indian J Fibre Text Res, 2013, 38, 138-143
7. Tyagi G K, Goyal A, Chattopadhyay R, Physical characteristics of tencel-polyester and tencel-cotton yarns produced on ring, rotor and air-jet spinning machines, Indian J Fibre Text Res, 2013, 38, 230-236
8. Männer Johann, Schuster K C, Suchomel Friedrich, Gürtler Andreas, and Firgo, High Performance with Natural Intelligence, Lenzinger Berichte, 2004, Vol 83, 99-110
9. Firgo H, Schuster K C, Suchomel F, Männer J, Burrow I, Abu-Rous M, The Functional Properties of Tencel-A Current Update, Lenzinger Berichte, 2006, Vol 85, 22-23
10. Burton C, Critical Evaluation of Wicking in Performance Fabrics, Master Thesis, China, Dec, 2004, 1-93
11. Swani N M, Hari P K, & Anandjiwala R, Performance Properties of Terry Towels Made from Open-end and Ring- Spun Yarns, Indian J. Text. Res, Sept, 1984, Vol 9, 90-94
12. Kucukali, Ozturk M K, Nergis B and Cevza, Wicking Properties of Cotton-Acrylic Rotor Yarns and Knitted Fabrics, Text Res J, 2011, Vol 8, No 3, 324-328
13. K A Ramasamy, G Nalankilli & O L Shanmugasundaram, Properties of cotton, tencel and cotton/tencel blended ring-spun yarns Indian J Fibre Text Res, 2011, Vol 39, September, pp 322-325
14. Tao L, Coupled Mechanical and Liquid Moisture Transfer Behaviour of Textile Materials, Thesis for the Degree of Philosophy, Hong Kong, Jan, 2008, 1-60
15. Subramanian S N, Venkatachalam A and Subramanian V, Wicking Behaviour of Regular Ring, Jet Ring Spun and Other Type of Compact Yarns, Indian J. Fibre Text Res, June 2007, Vol 32, 158-162

Wickability of Tencel, Polyester and Cotton Fibre Yarns Spun on Ring and Rotor Spinning Systems

Ashvani Goyal* & Ritu Sharma

Department of Textile Technology, The Technological Institute of Textile & Sciences, Bhiwani

Abstract

This paper investigated the effect of twist factor and wicking time on wickability of tencel, polyester and cotton fibres yarns spun on ring and rotor spinning systems. The ANOVA results of the experimental study shows all these factors have a significant effect on both properties. Tencel fiber yarn always has higher wickability and wicking rate as compared to cotton and polyester. Rotor yarn always has higher wicking height as compared to their ring spun counterparts.

Keywords: Polyester yarn, Ring yarn, Rotor yarn, Tencel yarn, Yarn wicking

1 Introduction

The behaviour of a textile when come into the contact with water is one of the important properties of textiles. This property of textile is known as wicking. If wicking of a textile is good it can be used for various number of applications like sportswear, medical products, footwear and exercise garments. Numerous studies have been done on wickability of spun yarn. According to Harnett and Mehta¹, wicking is the spontaneous flow of water driven into a porous system by capillary forces. Norman² analyzed that speed of water in the capillaries reduced by the random arrangement of fibres in the yarn. Lord³ observed that wicking height is likely to be a function of twist multiple, type of fiber, type of yarn structure and packing as well as migration. Kucukali *et al*⁴ studied the wicking properties of cotton-acrylic rotor yarns and knitted fabrics. They observed that wicking height of the yarn tended to increase with increase of acrylic ratio and had a significant impact on wicking performance of single jersey knitted fabrics. Perwueiz *et al*⁵ studied the capillary flow in PET, PA yarns and glass fibers using a technique based on the analysis of CCD images taken during the capillary rise of colored liquid in yarns. Chattopadhyay and Chauhan⁶ studied the wicking behaviour of ring and compact spun yarns and observed that ring yarns wicked faster than compact yarns and coarser yarns wicked faster than finer ones. Sengupta and Murthy⁷ analyzed that for the ring spun yarns, the wicking time increase steeply as twist increase whereas for the open-end spun yarns the increase is gradual.

2. Material and Methods

2.1 Fibres

The tencel, polyester and cotton fibres were used in the present study. The cotton fibre (DCH 32) was obtained in form of combed sliver from an industry. The specifications of tencel, polyester and cotton fibres are given in Table 2.1.

2.2 Preparation of ring yarn samples

Yarns of 29.5 tex were spun from Tencel, polyester and cotton fibres using five different tex twist factors ranging from 28.71, 33.50, 38.28, 43.07 & 47.85 were prepared.

*All the correspondences shall be addressed to,
Dr Ashvani Goyal,
Assistant Professor & Head, Department of Textile Technology,
The Technological Institute of Textile & Sciences,
Bhiwani 127 021, India
E-mail: ashvanigoyal@titsbhiwani.ac.in

Table 2.1 Specifications of Tencel, Polyester and Cotton Fibre

Fibre	Length mm	Linear density, dtex	Tenacity, cN/tex	Breaking elongation %	Modulus, cN/tex
Tencel	38	1.40	31.3	7.2	731.3
Polyester	38	1.33	56.2	10.8	698.9
Cotton	33.1 ^a	1.18	24.9	6.5	525.5

^aSpan length, 2.5%

Combed cotton sliver was used for making cotton yarns. A predetermined quantity of fibres was processed in a Lakshmi Reiter's blow room line. The conversion to drawn sliver was carried out by using a MMC carding machine and Lakshmi Rieter's drawframe DO/2S. Two drawing passages were given to the card sliver; the linear density of finisher sliver being adjusted to 3.69 ktex. The finisher sliver was converted into 492 tex roving on an OKK fly frame, which was used to produce 29.5 tex yarn on Lakshmi Rieters'G5/1 ring frame using a spindle speed of 12,000 rpm.

2.3 Preparation of Rotor yarns

29.5 tex yarns were spun from tencel, polyester and cotton fibres on rotor spinning machines at twist factors ranging from 28.71 to 47.85. For all fibres, two passages of drawing were given for rotor-spun yarns. The linear density of finisher sliver being adjusted to 3.69 ktex. The yarns were spun on TRITEX miniature OE rotor spinning machine. The rotor spinning parameters involved a 43 mm rotor rotating at 45,000rpm and an opening roller speed of 8,000 rpm.

3. Tests

3.1.1 Yarn wicking

Vertical wicking height was measured by the method used by Sengupta and Murthy⁷. A 30 cm length of yarn was taken. One end of yarn was tied into clip, and other end, to a hook of a small weight (2.90g). The yarn was hung on the notch of a nail fixed to a wooden plank held by an iron stand. Yarn was slowly lowered down into the measuring jar containing 3% Reactive Red dye M8B till the weight just touched the dye solution. The yarn was further lowered down into the measuring jar in such a way that the lower end, of about 1cm was below the liquid surface. Simultaneously stopwatch was pressed and the rise of dye solution from the fluid surface in

the yarn was continuously watched through the eyepiece. Wicking height was measured in 5 min at intervals of 1 min. Ten readings were taken for each sample. Wicking rate was calculated by ratio of wicking height and wicking time.

4. Results and Discussion

The influence of fibre type, yarn type, twist factor, on the wickability has been tested for significance using ANOVA at 95% level of significance. The ANOVA results are shown in Table 4.1. As can be observed from results that all the factors significantly affect the wicking height and wicking rate.

Table 4.1-ANOVA Results for Wicking and Abrasion Properties

Process variable	Wicking height	Wicking rate
A	s	s
B	s	s
C	s	s
D	s	s
A*B	s	s
A*C	s	s
A*D	s	s
B*C	ns	ns
B*D	ns	s
C*D	ns	s

s- Significant at 95% confidence level; ns-Non significant at 95% confidence level
A-Fibre type; B-Tex twist factor; C-Yarn type; D-Time

4.1 Effect of Fibre Type

Figs. 4.1-4.2 shows the wicking height and wicking rate of tencel, polyester and cotton fibre yarns spun on ring and rotor spinning system at twist factors ranging from 28.71 to 47.85. It can be observed from the results that both wicking height and wicking rate is significantly different for different fibres yarns spun on ring and rotor spinning system at all twist factors. Tencel fibre yarn has maximum wicking height and wicking rate as compared to polyester and cotton fibre yarns and cotton has the lowest. Tencel fibre yarns have highest wicking height due to its pore nano-structure which consists of countless, hydrophilic, crystalline nano-fibrils which are arranged in a very regular manner. The fibrils themselves do not absorb water but water absorption only takes place in the capillaries between the fibrils. The space between these micro fibrils acts like capillaries giving rise to enhanced capillary effect. Swelling occurs in the non-crystalline regions and capillaries between the micro fibrils and nano-fibrils so tencel has greatest wicking height as compared to polyester and cotton^{8,9}. Though cotton is also a cellulosic fiber and its moisture absorption is very high, yet it has lowest wicking height as compared to polyester and Tencel fibres yarns. This is because the cotton is a natural fiber and has

irregular capillaries due to fiber roughness, cross-sectional shape and length which inhibit the fluid flow. With an increase in the non-roundness of a fibre, the specific area increases, thus increasing the proportion of capillary wall that drags the liquid. Also cotton collects moisture despite flowing it out and swells⁴ when come into contact with water. Polyester fibres yarn is very smooth in appearance and have perfectly round cross-section with regular capillaries and it does not get swell when come into contact with water hence water movements takes place only on the surface of fiber that gives higher wicking height of polyester as compared to cotton yarns¹⁰⁻¹¹.

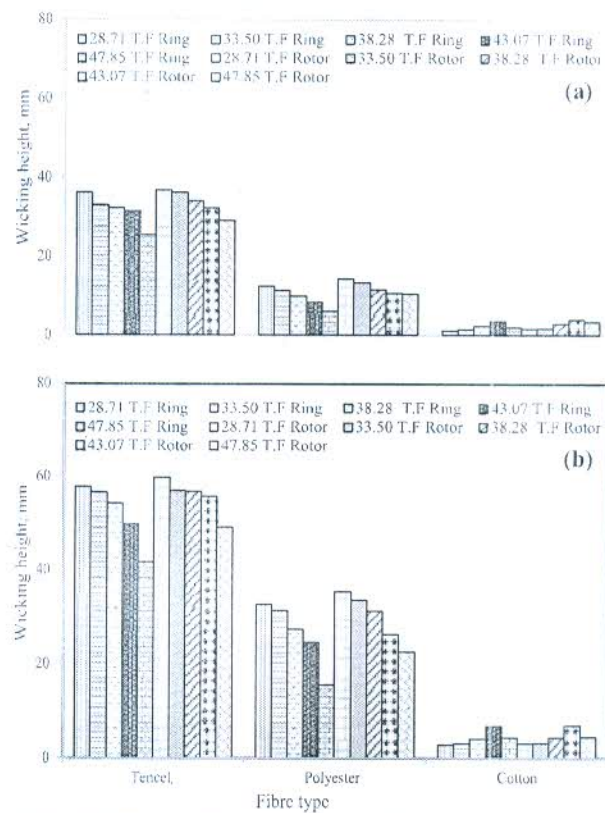


Fig. 4.1-Wicking Height of Tencel, Polyester and Cotton Ring and Rotor Spun Yarns[(a) 1 min and (b) 5 min]

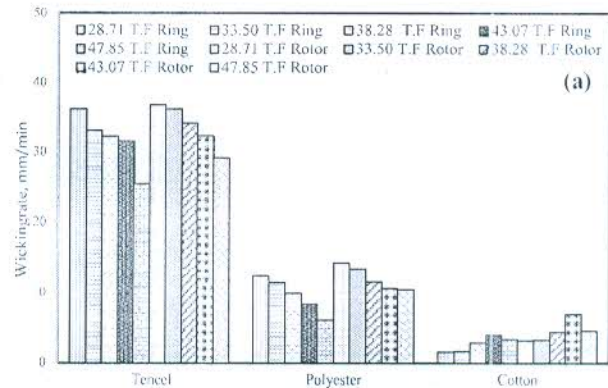


Fig. 4.2-Wicking Rate of Tencel, Polyester and Cotton Ring and Rotor Spun Yarn [(a) 1 min]

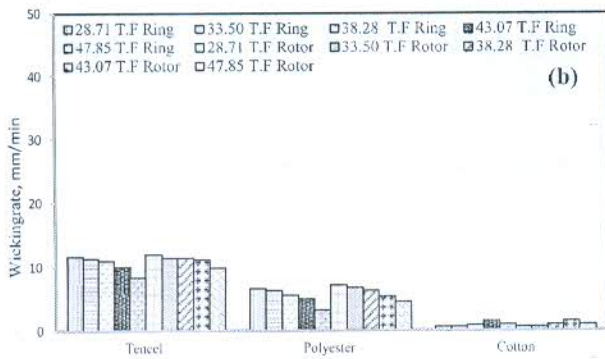


Fig. 4.2- Wicking Rate of Tencel, Polyester and Cotton Ring and Rotor Spun Yarn (b) 5 min]

4.2 Effect of yarn type

Figs.4.3-4.6 shows that wicking height and wicking rate of ring and rotor spun tencel, polyester and cotton yarns at different twist factors. It can be observed from results that for all the yarn samples rotor yarns have significantly higher wicking height and wicking rate when compared with their ring spun counterparts. The higher wicking height and wicking rate of rotor spun yarn is due to lower packing factor and softer skin of the yarns which makes the fibers in these yarns to be wet and wicks more quickly as compared to ring spun yarns. As ring spun^{4,7,11-12} yarns are more aligned towards the yarn axis and more compact than rotors. So wicking height of ring spun yarn is lower than rotor spun yarn.

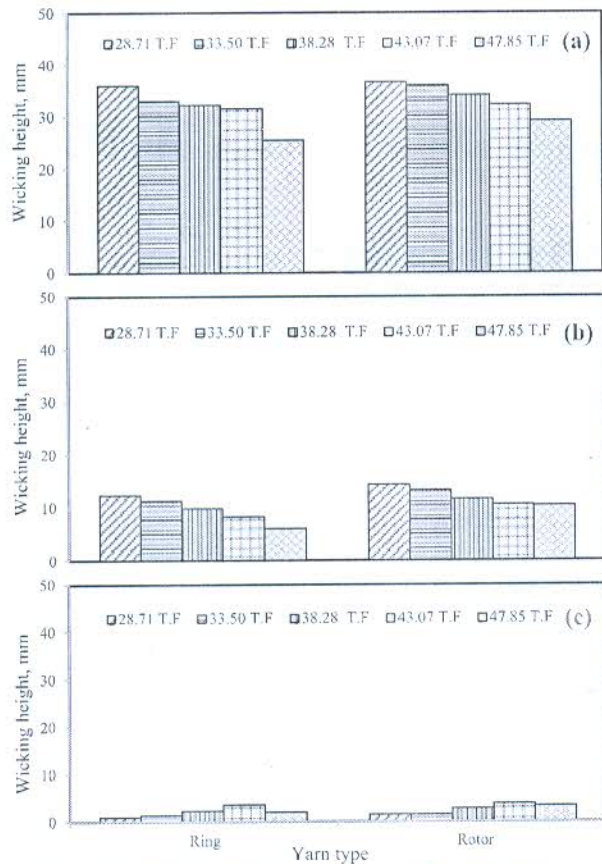


Fig. 4.3- Wicking Height of Ring and Rotor Yarns in 1 min[(a) Tencel,

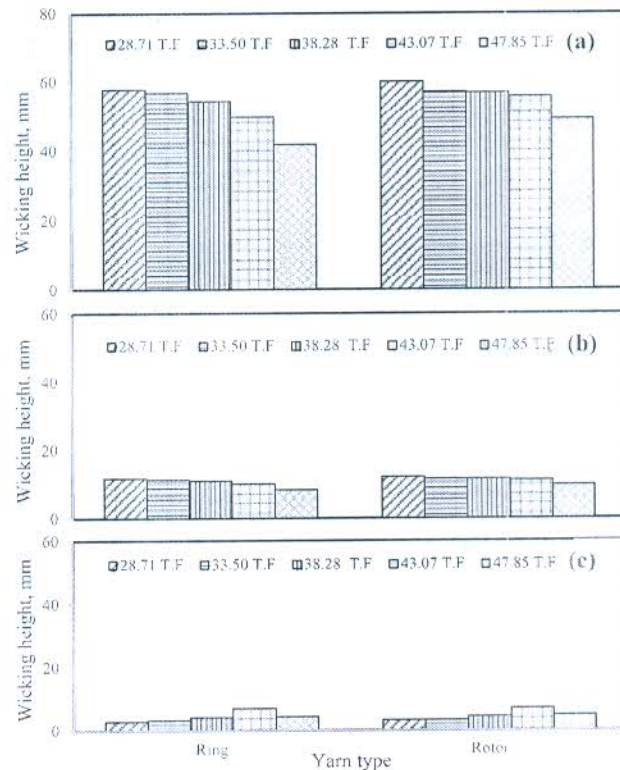


Fig. 4.4- Wicking Height of Ring and Rotor Yarn in 5 min[(a) Tencel,

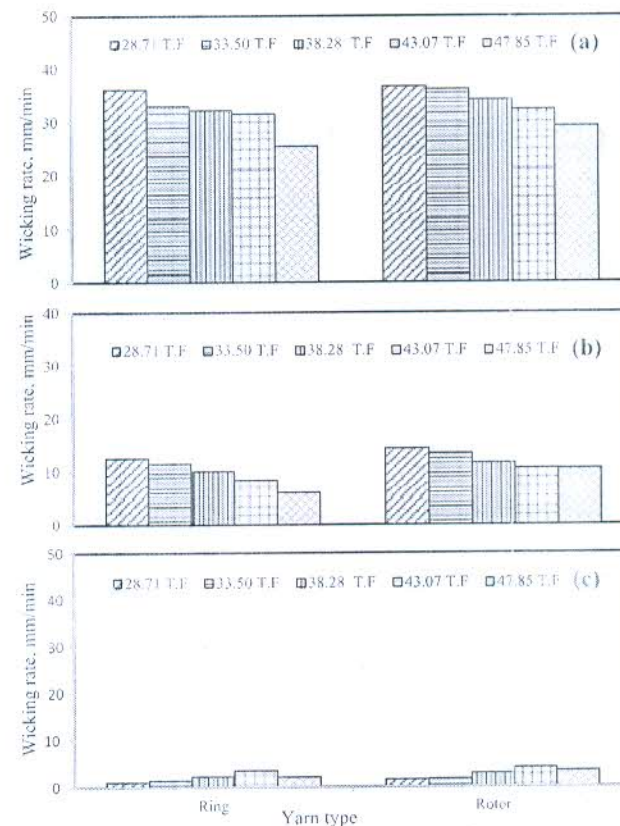


Fig. 4.5- Wicking Rate of Ring and Rotor Yarn in 1 min[(a) Tencel, (b) Polyester, and (c) Cotton]

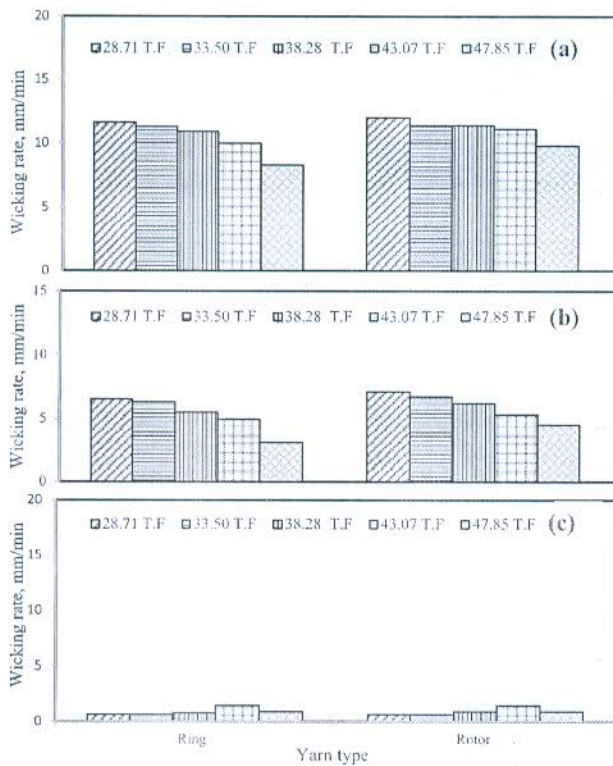


Fig. 4.6- Wicking Rate of Ring and Rotor Yarn in 5 min [(a) Tencel, (b) Polyester, and (c) Cotton]

4.3 Effect of twist

Fig. 4.7- 4.8 shows the influence of twist factors on ring and rotor spun tencel, polyester and cotton fibers yarn. From the ANOVA Table 3.1, it is observed that the twist influences the wicking height and wicking rate significantly and the influence of twist factor on wicking height and wicking rate is different for tencel, polyester and cotton yarns. In case of tencel and polyester yarns the wicking height continuously decreases with increase in twist factor for both ring and rotor spun yarn whereas in case of cotton yarns the wicking height increases upto twist factor 38.28 and thereafter it decreases for both yarn types. With the increase in twist factor for tencel and polyester yarns, the decrease in wicking height and wicking rate can be attributed to decrease in size of capillary channel between the fibers and increase in tortuosity that results to wick a longer path for a constant wicking height and hence lower wicking height is observed. But in case of cotton yarns, wicking height increases with increase of twist factor at low levels and reaches the maximum at twist factor of 38.28 and thereafter it decreases. This behaviour is due to that at lower twist level the yarn is loosely packed and when additional twist is inserted into the yarn, constituent fibers tend to move inward and the becomes more compact¹³. This appears to reduce the effective radii of inter fiber capillaries and enhance the wicking. The wicking reaches the maximum when the yarn is nearly closely packed. After that with the introduction of additional twist into the yarn the decrease in wicking height and wicking rate can be attributed to decrease in size of capillary channel between the fibers and increase in tortuosity.

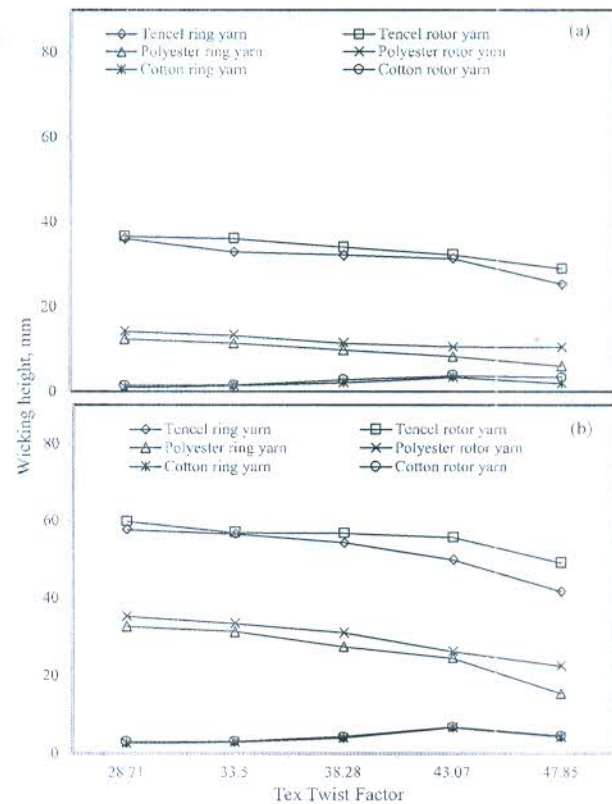


Fig. 4.7- Wicking Height of Tencel, Polyester and Cotton Ring and Rotor Spun Yarn at Different Twist Factors [(a) 1 min and (b) 5 min]

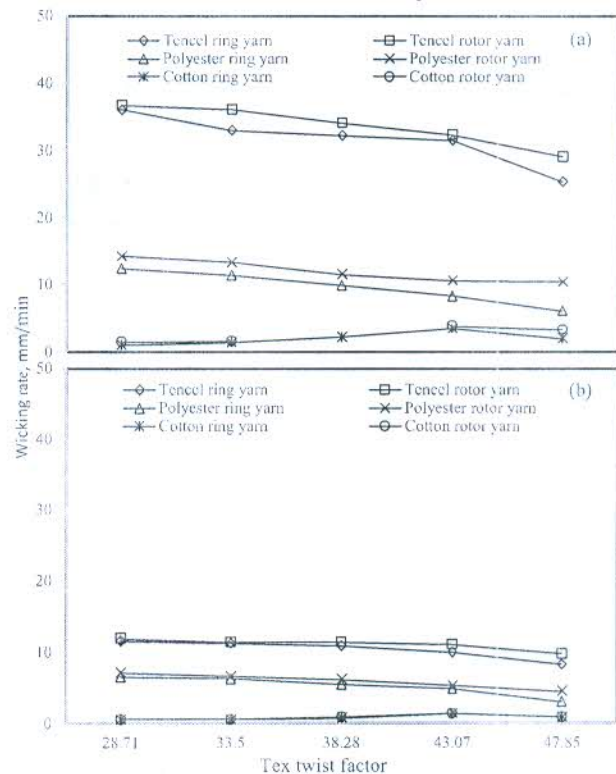


Fig. 4.8- Wicking Rate of Tencel, Polyester and Cotton Ring and Rotor Spun Yarns at Different Twist Factors [(a) 1 min and (b) 5 min]

4.4 Effect of time

Figs. 4.9-4.10 show that there is significant effect of time on wicking height and wicking rate. Wicking height continuously increases with increase in wicking time whereas wicking rate decreases continuously with the time. The decrease in wicking rate¹⁴ with increase in time for any given yarn can be attributed to the gravity of water column within capillary which acts against the capillary pressure.

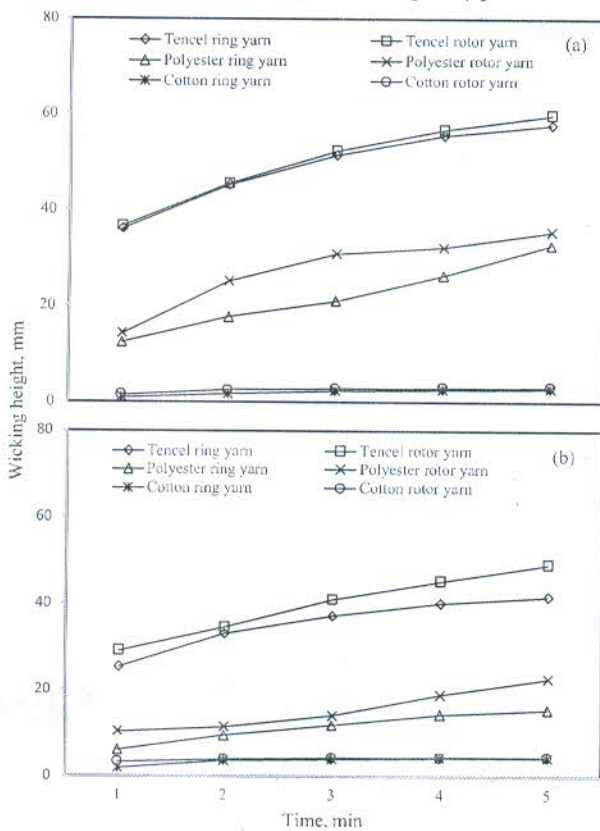


Fig. 4.9- Wicking Height of Tencel, Polyester and Cotton Ring and Rotor Spun Yarns at Different Time [(a) 28.71 T.F and (b) 47.85 T.F]

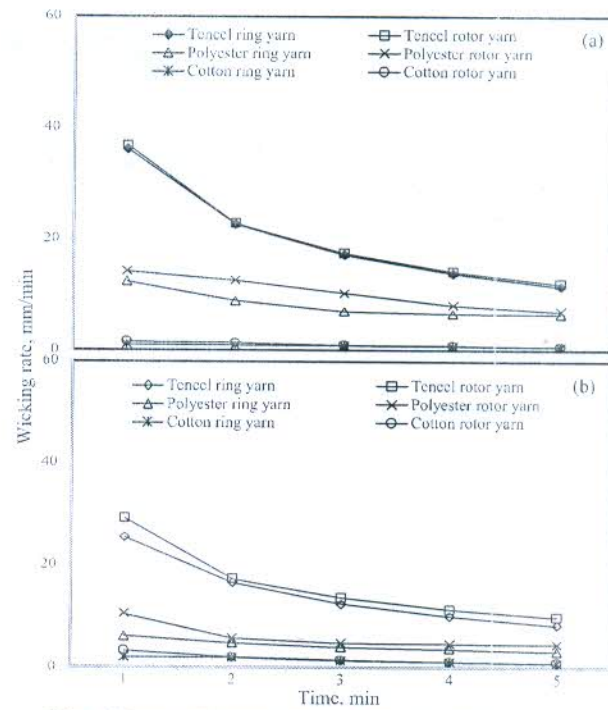


Fig. 4.10 (a) -Wicking Rate of Tencel, Polyester and Cotton Ring and Rotor Spun Yarns at Different Time [(a) 28.71 T.F and (b) 47.85 T.F]

5. Conclusions

- 5.1 Tencel fibre yarn has maximum wicking height and wicking rate as compared to polyester and cotton fibre yarns and cotton has the lowest value.
- 5.2 For all the yarn sample, rotor yarns have significantly higher wicking height and wicking rate as compared to their ring spun counterparts.
- 5.3 The influence of twist factor on wicking height and wicking rate is different for tencel, polyester and cotton yarns. For tencel and polyester yarns, the wicking height continuously decreases with increase in twist factor for both ring and rotor spun yarns whereas in case of cotton yarns the wicking height increases up to twist factor 38.28 and thereafter it decreases for both yarn types.
- 5.4 Wicking height continuously increases with increase in wicking time whereas wicking rate decreases continuously with increase in wicking time.


REFERENCES

- [1] Harnett, P. R., and Mehta, P. N., A Survey and Comparison of Laboratory Test Methods for Measuring Wicking, *Text. Res. J.*, 1984, Vol. 54, No.10, 471-478
- [2] Hollies N R.S, Kaessinger M, Watson B S and Bogaty Y, Water Transport Mechanisms in Textile Materials, *Text. Res. J.*, 1957, Vol.12, No.1, 8-13
- [3] Lord P.R, A Comparison of the performance of Open- end and Ring Spun Yarns in Terry Toweling, *Text. Res. J.*, 1974, Vol. 44, No. 16, 516-522
- [4] Kucukali, Ozturk M K, Nergis B and Cevza, Wicking Properties of Cotton- Acrylic Rotor Yarns and Knitted Fabrics, *Text. Res. J.*, 2011, Vol.8, No.3, 324-328
- [5] Perwueiz Anne, Mondon Pascal and Caze Claude, Experimental Study of Capillary Flow in Yarns, *Text. Res. J.*, 2000, Vol. 70, No.4, 333-339
- [6] Chattopadhyay R. and Chauhan A, Wicking Behaviour of Compact and Ring Spun Yarns and Fabrics, in One Day Seminar on Comfort in Textiles, Dept. of Textile Technology, IIT Delhi, India, Oct, 2004, Vol.16, No.3, 20-25

- [7] Sengupta A.K and Murthy H.V.S., Wicking in Ring Spun Vis-a Vis Rotor Spun Yarns, *Indian J.Text.Res.*, 1985, Vol. 10, No.4, 155-157.
- [8] Männer Johann, Schuster K. C, Suchomel Friedrich, Gürtler Andreas, and Firgo, High Performance with Natural Intelligence, *LenzingerBerichte*, 2004, Vol. 83, 99-110
- [9] Firgo H, Schuster K.C, Suchomel F, Männer J, Burrow T, Abu-Rous M, The Functional Properties of Tencel-A Current Update, *LenzingerBerichte*, 2006, Vol.85, 22-23
- [10] Burton C, Critical Evaluation of Wicking in Performance Fabrics, *Master Thesis, China*, Dec, 2004, 1-93
- [11] Swani NM, Hari PK, & Anandjiwala R, Performance Properties of Terry Towels Made from Open-end and Ring- Spun Yarns, *Indian J. Text. Res.*, Sept, 1984, Vol.9, 90-94
- [12] Das A, Zimniewska M and Mal R.D, Studies on Cotton- Acrylic Bulked Yarns Produced From Different Spinning Technology, *J.TexInst*, July 2000, Vol.100, No.5 420-429
- [13] Tao L, Coupled Mechanical and Liquid Moisture Transfer Behaviour of Textile Materials, *Thesis for the Degree of Philosophy, Hong Kong*, Jan, 2008, 1-60
- [14] Subramanian S.N, Venkatachalam A and Subramaniam V, Wicking Behaviour of Regular Ring, Jet Ring-Spun and Other Type of Compact Yarns, *Indian J. Fibre Text. Res.*, June 2007, Vol.32, 158-162



To Book your 'Ads' in Print Journal & 'Ad Banners' on e-newsletter
Contact: J. B. SOMA
Tel.: +91-22-2446 1145, Mob.: +91-9819801922
E-mail: talcnt@gmail.com, jb.soma@gmail.com




Nothing speaks of success like the fine fabric of your suit




Our Product Mix

- Polyester / Viscose Suiting & Shirting
- Polyester / Cotton Suiting & Shirting
- Polyester / Viscose Worsted Suiting
- Polyester / Viscose Denim
- Polyester / Cotton Denim

S.Kumars Limited, 3-A, Industrial Area No. 2, A. B. Road, Dewas 485001 (M.P.) Tel : +91 7272-258 025 / 26 Fax +91 7272-258 217
 Email : info@skumars.co, www.skumars.co

Follow us on S.Kumars.India You S.Kumars



Microencapsulation and its application in production of functional textiles

Nagender Singh & Javed Sheikh^a

Department of Textile and Fibre Engineering, Indian Institute of Technology Delhi, New Delhi 110 016, India

Received 28 February 2020; revised received and accepted 28 April 2020

Currently, the textile sector is moving towards the development of value-added functional textile products based on customer demand. Therefore, several new finishing techniques have been evolved so far to functionalize the textile substrates. In this context, the microencapsulation technique is one of the advanced technologies which has been used to impart functional properties such as antibacterial activity, aroma, mosquito repellency, UV protection, and thermoregulation to textiles. In microencapsulation, the volatile and non-volatile components can be encapsulated within a thin polymeric layer which causes a slow release of the compound, resulting in long-lasting functional effect. Various active materials, like essential oils, enzymes, drugs, pesticides and vitamins, have been successfully entrapped inside microcapsules made from a variety of polymeric materials. There are interesting reports available in the literature dealing with functionalization of textiles using microencapsulated materials. This review paper covers the fundamentals of microencapsulation, its major techniques, materials involved in microencapsulation and the important research reported in this area. The major essential oils used in microencapsulation and the subsequent functional effects are also reviewed. The present and futuristic research trends in this important area of chemical processing of textiles are presented.

Keywords: Controlled release, Essential oils, Functional textiles, Microencapsulation, Polymers

1 Introduction

The utilization of microencapsulated functional materials for functionalization of textiles has facilitated the evolution of value-added textile products with new and improved properties, such as fragrance¹, thermoregulation², flame retardancy³, UV protection⁴, antibacterial⁵, photochromic effects⁶, antioxidant⁷, or multifunctional ones by combining two or more functional elements^{8,9}. Microencapsulation involves the deposition of thin polymeric layers on the microdroplets of liquids or small particles of solids. It is a packaging technology which packs the substances at a micro-level. Primarily, this technique was introduced in the paper industry as the basis of the carbonless copy paper and is currently explored in other industries, such as agricultural, pharmaceutical, chemical, cosmetics, toiletries, and food processing. Various types of microcapsules loaded with varieties of functional materials are available in the market^{10,11}. This technique shows excellent possibilities for improving product and process performance. The improved performance, in terms of efficacy and durability, is offered by excellent stability of the volatile component against oxidation and a resultant controlled release mechanism.

The application of microencapsulated materials in the textile industry has been limited in the initial period because of lack of awareness regarding the scope of this technique and possible value-additions. Even though value-added textiles were prepared and reports regarding this are available in the literature, the practical difficulties faced during scaling-up has made it challenging to commercialize most of the microencapsulated materials. Apart from this, the high costs of processing is another limiting factor¹². Since the last two decades, the application of microencapsulated materials on textile is gaining momentum; however, the application is restricted to common substrates used in interior textiles and clothing¹³. The vast possibilities of microencapsulation technology have not been entirely exploited, and hence the scope for investigation still exists.

Functionalities can be imparted to textiles by the application of a variety of encapsulated materials, including both natural and synthetic ones. The use of sustainable natural materials for functionalization of textiles is the growing interest and rising demand from modern consumers. In this case, the use of essential oils (EOs) as an encapsulated material can serve the requirements of sustainable chemical finishing of textiles. Apart from the advantage of being natural products, EOs offer high value-added properties because of their interesting

^aCorresponding author.
E-mail: jnsheikh@iitd.ac.in

physicochemical characteristics¹⁴. EOs have a broad spectrum of antimicrobial and biological activities because of their complex chemical composition, resulting in the presence of several functional properties like antiviral, antifungal, insect and mosquito repellents, antibacterial and pest control¹⁵⁻¹⁷. In the textile industry, microencapsulated material can be applied on fibres, yarn, and fabrics as a finishing agent using finishing techniques such as pad-dry-cure, exhaustion, screen-printing, impregnation, and spraying¹⁸.

This paper reviews the important aspects of microencapsulation, including the fundamentals of microencapsulation, materials involved, and techniques of preparation. The reported literature dealing with functionalization of textiles using various microcapsules are thoroughly reviewed. Existing technology and futuristic trends are also discussed.

2 Microencapsulation Technology and its Application in Textiles

2.1 Microencapsulation Trends in the Textile Industry

The spray drying technique introduced the concept of microencapsulation and is known from the 1930s. In 1990s, the possibilities of microcapsules in finishing and colouration of textiles were explored, and that was the first application of microencapsulation in the textile industry^{19,21}.

The commercial use of microencapsulation in the textile industry was there from the beginning of the 21st century, specifically in Japan, Western Europe, and America. The technique was being used to introduce new and interesting properties in textiles, including antibacterial, flame retardant, and medicinal properties²². Nowadays, because of the success of microencapsulation in the textiles sector, the manufacturers are very much excited to capture the market opportunities by fulfilling the potential consumer demand^{23,24}.

2.2 Fundamentals of Microencapsulation

2.2.1 Microencapsulation Process

It is a technique to entrap the core materials (gas compound, solid particles, and liquid droplets) in wall materials (polymers) as shown in Fig. 1. The core compounds are fully covered with a thin film of wall material or embedded in a polymer matrix that forms a micro-size capsule with various important properties^{13,25}. The content of microcapsules is described as an internal phase, core, filler or active, and the entrapping material of capsules is known as shell, coating, membrane, wall, or carrier²⁰⁻²². Spears²⁶ have patented an invention based on encapsulation of

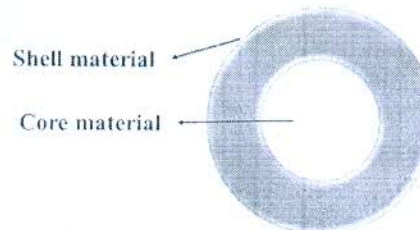


Fig.1 — Description of a microcapsule¹³.

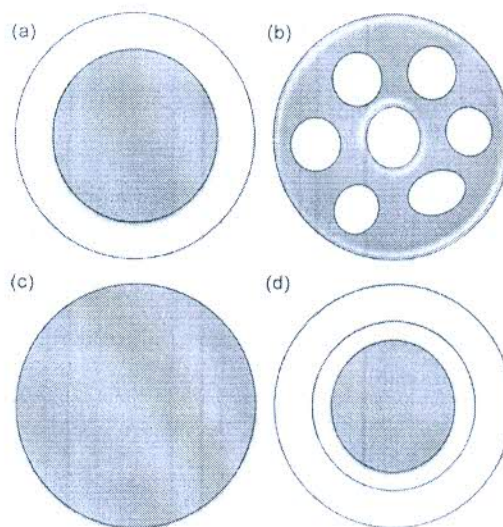


Fig. 2 — Microcapsules morphologies (a) reservoir, (b) polynucleated, (c) matrix and (d) multi-shell^{29,30}.

hyperbaric gas using sonication method. The prepared microcapsules containing hyperbaric gas were used for providing systemic oxygenation of tissues and in the treatment of infections, atherosclerosis and neoplasms.

Various materials can be encapsulated within macro-package that protect them from the external environment¹³. Various synthetic and natural polymers can be utilized as a shell material. The choice of shell material depends on the physicochemical characteristics of the core material. The hydrophilic core needs a hydrophobic shell, and a lipophilic core is required for hydrophilic shells. The natural polymers, including cellulosic materials, starch, Arabic gum, dextrin, chitosan, alginate, gelatine, and natural gum, have high possibilities of the use as an encapsulating agent^{27,28}.

2.2.2 Morphology of Microcapsules

The morphology of microcapsules can be classified into four major microcapsules structures, viz reservoir, polynucleated, matrix, and multi-shell structures, as shown in Fig. 2. Morphology of microcapsules is

typically recognized through shape, core material, size, size distribution, and the delivery mechanism³¹. The shape of the microcapsules depends on the type of core material. If the core material is in crystal or solid form, then the resultant microcapsules would be of irregular shape. The liquid core may provide spherical microcapsules. In a matrix structure, many fine core materials are uniformly distributed in the shell material. Moreover, the microcapsules can be formed in the form of multi-core or multi-shell^{27,32}.

2.2.3 Release Mechanisms

The diffusion rate across the polymer layer depends on the specific characteristics of the polymer network, such as flexibility, plasticization extent, absorbency, chain length, ion extent, or possible interactions between active agent and polymer, and therefore the active agent release³³. Figure 3 represents the EO-release through the polymeric layer of the microcapsule.

Martin del Valle *et al.*³⁴ suggested that the controlled release device can be formed when essential oil diffuses from the polymer layer of microcapsule. Generally, the release of core material from microcapsules is based on four mechanisms, viz. mechanical stimuli (during the application of mechanical force in processing), chemical stimuli (the core material slowly dissolves in shell membrane), thermal stimuli (heat), and diffusion^{24,35}.

2.3 Microencapsulation Techniques

Several techniques have been proposed for the production of microcapsules. The selection of the method depends on the core release rate, shell permeability, thickness, solubility, and physical properties. The microencapsulation techniques are divided into two categories, namely physical and chemical methods. The physical methods are further subdivided into physico-mechanical and physico-chemical methods. However, only commonly used techniques

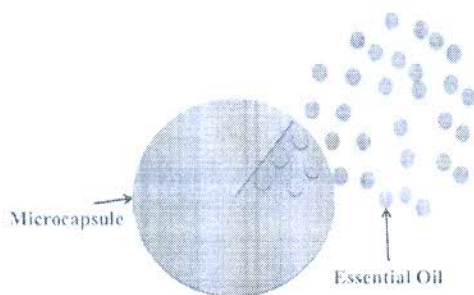


Fig. 3 — Representation of essential oil release from the microcapsule³⁶

from each category have been described. The standard microencapsulation techniques, are shown in Table 1. Table 2 shows the advantages and disadvantages of commonly used microencapsulation techniques.

2.3.1 Spray Drying

Spray drying technique is based on spraying the emulsion of shell and core material into a heating chamber with highly optimized atomization, where rapid evaporation of solvent occurs, thereby producing the capsules. The process flow chart and spray drying equipment are shown in Figs 4 and 5 respectively. The microencapsulation process consists of the following steps:

- Spraying the emulsion into small droplets at a constant feed rate using an atomizer.
- Drying the previously spread droplets by hot gas.
- Collecting and separating the capsules using cyclones and filters.

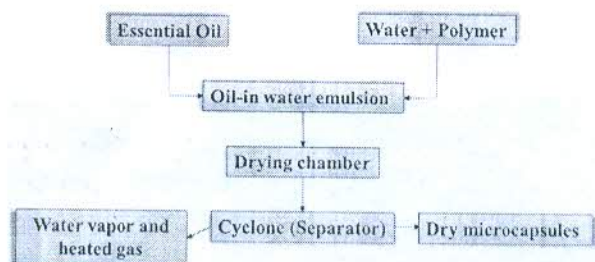
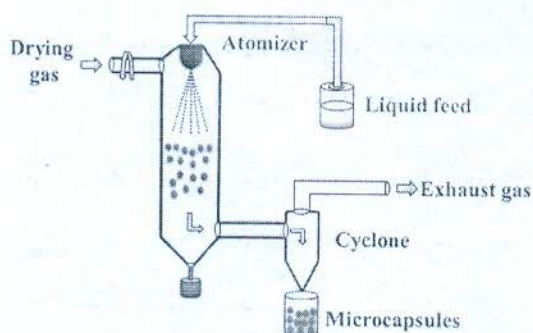
Generally, the morphology of microcapsules prepared by spray drying is a matrix or polynuclear type¹³. Li *et al.*⁴⁹ prepared the chitosan microcapsules loaded with orange oil using spray drying technique and analyzed their stability towards washing with different detergents. They investigated the retention of oils in the microcapsules applied to cotton after certain days. De Oliveira *et al.*⁵⁰ attempted to develop a blend of biopolymer for the encapsulation of EO and prepared nanoparticles of alginate/cashew gum using spray-drying. The TGA/DSC and X-ray showed sufficient miscibility of both the polymers. Moreover, a release profile was achieved for over 30 h. Carvalho *et al.*⁵¹ prepared green coffee loaded microcapsules via spray drying technique. The microcapsules displayed enhanced oxidative stability, excellent encapsulation efficiency, and SPF similar to the free green coffee oil.

Table 1 — Important microencapsulation techniques^{22,30,37-42}

Physical methods		Chemical methods
Physico-mechanical	Physico-chemical	
Pan coating	Ionic gelation	<i>In-situ</i> polymerization
Extrusion	Coacervation	Interfacial polymerization
Air-suspension coating	Sol-gel	Polymer-polymer incompatibility
Ultrasonic atomizer	Supercritical Fluids	Polycondensation
Spray drying	Solvent evaporation	Emulsification
Microwave processing	Polyelectrolyte Multilayer	Liposome formation

Table 2 — Advantages and disadvantages of commonly used microencapsulation techniques

Techniques	Advantages	Disadvantages	References
Spray drying	Quicker, scalable, affordable, offers desired size of microcapsules, spherical and small particles with homogeneous distribution, stable microcapsules	Microcapsules agglomeration, uncoated core material, works on moderate viscosity of the emulsion	43,44
Coacervation	High encapsulation efficiency, Easy and affordable	Limited stability of microcapsules in a limited ionic strength and range of pH, works on limited polymer materials and microcapsules agglomeration	45
Extrusion	Better stability of oils against oxidation, low surface oil, prolonged shelf-life of essential oils and reduce evaporation rate of essential oils	Expensive process, large particles size	46
<i>In-situ</i> polymerization	Spherical and smooth microcapsules, offers good chemical, storage, and thermal stability and provides high encapsulation efficiency	Sensitive microcapsules to pressure due to transparent wall	47
Emulsification	Relatively easy and low cost	Physical instability (pH, heating, drying, and high mineral concentrations) particles and offers limited control release of essential oil	46

Fig. 4 — Typical process flow of spray drying encapsulation technique⁴⁸Fig. 5 — Schematic diagram of spray drying equipment⁴³

2.3.2 Coacervation

The coacervation process can be either simple or complex. The interaction between the dissolved polymer and the low molecular compound results in the simple coacervation. When the two opposite

charges of polymers interact with each other, the process results in the complex coacervation⁵². Figure 6 shows the process flow of complex coacervation technique. Han *et al.*⁴⁵ used complex coacervation for encapsulating the patchouli oil. The volatility of the oil was reduced, which stabilized the strong smell of oil and also prevented its oxidation.

2.3.3 *In situ* Polymerization

In this technique, the polymerization process is responsible for the formation of a capsule shell where a specific pre-polymers or monomers are suspended into a stable emulsion of the immiscible core material and a continuous solution. In this chemical technique, the formation of microcapsules does not require reagents.

The capsules loaded with perfume, carbonless paper inks and other components are extensively produced by *in situ* polymerization technique⁵³. The melamine-formaldehyde and urea-formaldehyde encapsulation systems for phase change materials are perfect examples of this method^{47,54-56}. Chung *et al.*⁵⁷ utilized *in situ* polymerization technique for the development of microcapsules loaded with thyme oil (Fig. 7). The thyme oil loaded microparticles displayed excellent repellency (90%) against *Plodia interpunctella* for 30 days.

2.4 Materials Involved in Microencapsulation

2.4.1 Shell Materials

The selection of shell materials is crucial as it affects the stability of microcapsules, encapsulation

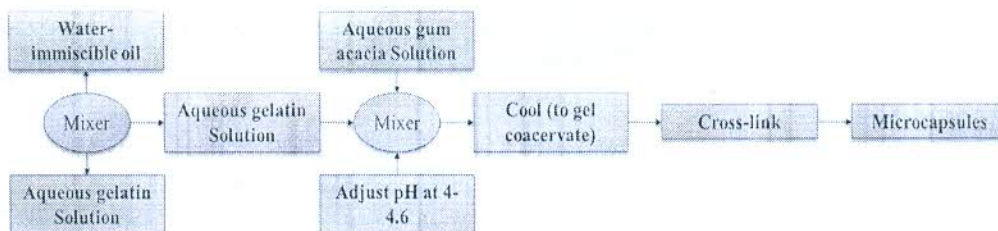
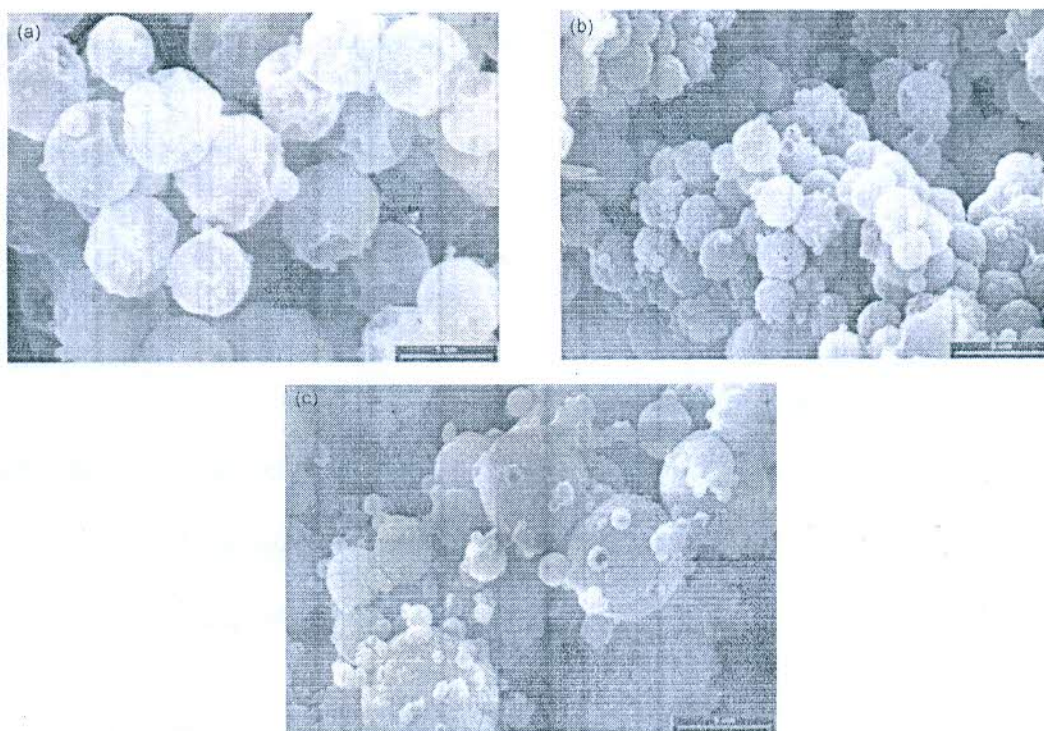


Fig. 6 — Typical process flow of complex coacervation technique

Fig. 7 — SEM images of microcapsules with different emulsifiers (bar is 5 μ m): (a) Sodium lauryl sulphate. (b) Tween 80 and (c) Pluronic F-127⁵⁷

efficiency, loading capacity, retention rate, and delivery system. The selection criteria for shell material depend on the physic-chemical characteristics of the core material such as solubility and porosity, the properties of the shell material such as mechanical properties, the viscosity of the emulsion/suspension, the compatibility of core-shell materials and the economic factors^{58,59}. Sometimes, the compatibility between the two materials becomes crucial because one shell material alone may not have all the required properties. Therefore, two or more polymers can be used to achieve the desired properties⁶⁰. The shell materials can be selected from a broad range of synthetic and natural polymers.

Some commonly used natural polymers (vegetable, animal or bacterial sources) are alginate, pectin,

chitosan, carrageenan, Arabic gum, cellulose derivative, starch, gelatine, milk protein, and gellan gum^{61,62}. Synthetic polymers that could be used are polyvinyl alcohol (PVA), polyethylene glycol, polycaprolactone, poly(lactic-co-glycolic acid), isocyanate, polyamide, polyurea, polyurethane, and melamine formaldehyde⁶³. The most commonly used biopolymers and their advantages/limitations are presented in Table 3.

Traditionally, Arabic gum is considered as one of the most common polymers used as a shell material. However, limited availability is the main issue for this polymer. Alginate is also an excellent polymer to entrap EOs, but it suffers from some problems related to porosity and high processing cost in the industry.

Gelatine can be potential polymer for the encapsulation of EOs for the application on textiles,

Table 3 — Commonly used natural polymers as shell material of microcapsules for textile application^{25,59,64,65}

Polymers	Advantages	Limitations
Acetophthalate cellulose	Cellulosic and biodegradable	Slows the absorption of drugs, dissolves only above pH 6, and synthetic polymer
Alginate	Natural product and easy to work on in the laboratory	Very permeable and porous membranes, challenging to scale-up, and costly on an industrial scale
Arabic Gum	Low viscosity, adequate solubility, smooth paste, and gives good emulsifying properties	Costly and availability problems
Chitosan	Derived from chitin, non-toxic, biodegradable, easy to scale-up, affordable and biocompatible, non-allergic and pH-sensitive	NA
Ethyl-cellulose	Insoluble in aqueous medium and derived from glucose	Low mechanical resistance and insoluble in the gastrointestinal system
Gelatine	Biodegradable, non-toxic and low price	Soluble in aqueous systems
k-carrageenan	Natural product	Soluble at temperatures (60–80 °C) for 2–5% concentration
Malto-dextrin	Low viscosity at high concentrations	
Starch	Abundant, biodegradable, and non-toxic	High viscosity

offering some advantages over other polymers such as biodegradability, availability at a low price, and non-toxicity. Also, it has some limitations like high solubility in an aqueous medium^{66,67}. Therefore, such polymers need to be modified or used in combination with other polymers.

Chitosan is a naturally occurring cationic polymer prepared from the alkaline deacetylation of chitin (N-acetylglucosamine polymer). Chitosan is used in many applications because of its excellent chemical properties, biodegradability, and polymer compatibility⁶⁸. In recent years, chitosan showed a great promise for its use in microencapsulation.

Various synthetic polymers have also been utilized to prepare microparticles. Since the last years, aliphatic polyesters, like polylactic acid and glycolic acids and lactic copolymers, have been used as biodegradable wall materials for controlled release devices⁶⁹. Nevertheless, modified celluloses such as hydroxypropyl cellulose and the semi-synthetic cellulose acetate, and butyrate are commonly utilized for the microencapsulation of EOS⁷⁰.

2.4.2 Core Materials

EOs are the aromatic materials, usually have a complex composition, acquired from specific plant raw materials, or extracted by a mechanical method. EOs are generally separated from the aqueous phase by a physical method without affecting their original chemical composition⁷¹. EOs are obtained from various defined plant organs such as fruits (star anise, anis), flowers (rose, jasmine, lavender and violet),

leaves (Eucalyptus, salvia, thyme), buds (clove), bark (cinnamon), seeds (cardamom), zest (citrus), roots (ginger) and wood (ginger). These are lipophilic, soluble in organic solvents and insoluble in water due to their hydrophobic nature, and lower density⁷².

The application of encapsulated PCMs for functional sportswear and technical garments has become popular among the textile and apparel industries. The microencapsulated PCMs can offer heat and cold absorbing ability which could be utilized to developed thermal regulating textile products. The working principle of PCMs is that it absorbs and release heat when the material changes from solid to liquid and vice versa. Therefore, the microencapsulated PCMs system helps to store the thermal energy efficiently. These materials change their physical state within a specific range of temperature and are different from one another in their heat storage capacity and phase change temperature²¹. Presently, varieties of PCMs are available such as n-hexadecane⁷³, n-nonadecane, n-eicosane, n-octadecane⁷⁴, and n-alkane. Various materials have been continuously used as an active core material for the application of functional textile products. These materials include vitamins, minerals, additives, oxides, aldehydes, thermochromic and photochromic materials, phase change materials and gasses^{24,75}.

2.5 Methods for Application of Microcapsules on Textiles

Various techniques can be used for stabilization of microcapsules on the fabric are padding, coating,

immersion, spraying and printing. In the padding method, the fabric is transported through the dispersion of microcapsules and then passed through the padding rollers to remove the excess liquor. The immersion method is the same as the padding method, except the fabric is not passed through the squeeze rolls. In the printing method, the printing paste is formed by mixing microcapsules with a binder and applied on the fabric⁷⁶. In the coating method, the uniform layer of microcapsules is deposited on the textiles. In spraying method, the microcapsules are sprayed on the fabric via spray nozzle in a closed chamber, and further curing is carried out to stabilize the microcapsules on the fabric by thermal treatment at a high temperature (130–170 °C). However, at high temperature, quick evaporation of liquor is taking place, which leads to instability of microcapsules. Therefore, ultra-violet and microwave curing could be the alternative to the high-temperature curing process. In microwave curing, the microwave vibrates and polarises liquor molecules which result in heat generation and stabilization of microcapsules on the fabric. The fabric is exposed to UV light, which polymerizes the resin to form continuous film and stabilizes the microcapsules on the fabric. The benefits of UV curing include lower time consumption, high production efficiency, energy-saving, low-temperature requirement, and lower pollution load. This avoids rupture of microcapsules and evaporation of the core element, which also improves the durability^{77,78}. The

durability of the finish on the fabric cured with UV was found to be more than 50 washing cycles, which was better than that of thermal curing (25 washes)⁷⁹.

2.6 Application of Microcapsules for the Development of Functional Textiles

2.6.1 Aroma/Fragrant Textiles

The aromatherapy textiles offer fragrance of EOs derived from plant-based raw materials, which could boost the emotional and physical scene of the body^{20,80,81}. During the second world war, Dr Jean Valnet used EOs for the surgeries and verified that they have more significant antiseptic properties than phenol⁸². Microcapsules loaded with EOs showed various applications in the textile and apparel sector⁸³. The mechanical pressure on the capsules during actual wear leads to the rupture of microcapsules which results in the release of active component^{84,85}. Several research studies have been conducted to develop aroma textiles, as shown in Table 4.

Sharkawy *et al.*¹⁸ utilized the complex coacervation method to prepare chitosan/Arabic gum loaded with limonene and vanillin microcapsules using tannic acid as a solidifying agent. The results showed a sustained release pattern where the cumulative release pattern after seven days at 37 ± 1 °C was 19.4%, 52%, and 75% for the polynuclear vanillin microcapsules, the mononuclear limonene microcapsules and the polynuclear limonene microcapsules, respectively.

Table 4 — Research studies on aroma/fragrant textiles

Core material	Shell material	Method	Fabric	Application method	Results obtained	Reference
Lemon fragrance	NA	NA	Cotton	Pad-dry-cure	UV-curing Durable up to 50 washes	79
Lemon fragrance	NA	NA	Cotton	Pad-dry-cure	Conventional curing Durable up to 25 washes	78
Rose fragrance	Polybutyleanoacrylate (PBCA)	Anionic polymerization	Cotton	Immersion	Durable up to 20 washes EE was 65.83%	86
Lavender fragrance	Melamine-formaldehyde	NA	Cotton	Pad-dry/ Exhaustion	Padding was found better than exhaustion	87
Lemon oil and rosemary oil	Methylmethacrylate-styrene	Mini-emulsion polymerization	Cotton	Immersion	6.8% cologne maintained after 15 washes EE was 85.4%	88
Jasmine oil	Acrylic-based	Two-stage emulsion polymerization	Cotton	Pad-dry-bake	25.3% residual rate of essential oil after 15 washes EE was 78.76%	89

Li *et al.*⁷⁹ utilized UV curing to stabilize the microcapsules on the cotton fabric. The fabric was suspended in a finished bath followed by padding and drying at 100 °C for 1.5 min. The finished fabric was then introduced under different UV lights, such as iron, xenon, and mercury lights, which showed different interaction of resin with the fabric. The excellent durability of finish was achieved when the finished fabric was cured with iron or mercury light.

Li *et al.*⁷⁸ applied the microcapsules loaded with lemon fragrance on the cotton fabrics by using an acrylic binder, polyurethane binder, and DMDHEU as a fixing agent. The acrylic binder was found more effective as compared to other fixing agents, as it showed excellent durability up to 25 washing cycles.

Hu *et al.*⁸⁶ synthesized the rose fragrance nanocapsules with poly butyl cyanoacrylate (PBCA) via anionic polymerization. The encapsulation efficiency was 65.83% with 0.8% butyl cyanoacrylate (BCA), 0.5% rose fragrance, 2.6% emulsifier (Tween-20) and a pH greater than 2. Nanoencapsulation of the fragrance by PBCA using anionic polymerization is found a suitable method for encapsulation, providing a sustained release pattern.

Bonet *et al.*⁸⁷ used exhaustion and padding methods for the application of microcapsules on the fabric surface. The fabric finished with padding methods, displayed more microcapsules on the fabric. Moreover, padding was found better than exhaustion because of the requirement of more chemical to fix the microcapsules on the fabric during exhaustion.

Liu *et al.*⁸⁸ used mini-emulsion polymerization to synthesize methylmethacrylate-styrene nanocapsules loaded with cologne EOs, and the synthesized nanocapsules were applied on cotton fabric via the immersion method (Fig. 8). The finished fabric displayed the uniform coating of capsules on the fabric and also showed good washing durability up to 15 washing cycle. Liu *et al.*⁸⁹ fabricated aromatic nanocapsules via two-stage emulsion polymerization

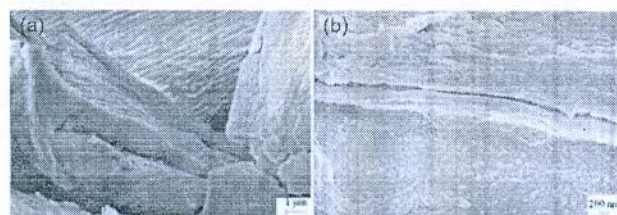


Fig. 8 — SEM photographs of cotton fabric (a) untreated ($\times 1\mu\text{m}$) and (b, c) treated with aromatic nanocapsules ($\times 200\text{nm}$)⁸⁸ (reproduced with permission)

method. The styrene/methyl methacrylate copolymer was used as a core material and modified poly(butyl acrylate) as a shell material which was modified by octamethylcyclotetrasiloxane. The nanocapsules showed excellent washing durability by providing around 25.3% residual content of essential oil after 15 washes.

Rodrigues *et al.*⁹⁰ prepared the polyurethane-urea microcapsules loaded with limonene oil through the interfacial polymerization method and utilized it for finishing of the fabric using the padding method. The GC-FID-headspace and SEM analysis confirmed the availability of limonene oil on the fabric. The results showed that the loss of limonene after the first and fifth dry cleaning was 4% and 97% respectively. The loss of limonene during abrasion after 3000 and 9000 cycles was 40% and 60% respectively.

Panisello *et al.*⁹¹ prepared the polysulfone microcapsules containing vanillin. The results showed that microcapsules were stable in the temperature range between 20 and 100 °C, and inhibits the bacterial growth during one week. The results showed moderate washing durability up to 5 washing cycle.

2.6.2 Antimicrobial Textiles

Various antimicrobial compounds such as quaternary ammonium salts, nanosilver and triclosan are available for imparting antimicrobial property to the textiles. However, because of the limitation of such agents like their limited availability, high cost, high toxicity and synthetic nature, manufacturers are moving towards the use of eco-friendly, low-cost antimicrobial chemicals for textile finishing³⁵.

Natural extracts are widely researched for the possible applications as antimicrobial finish; however, the efficacy of such finishes and the durability always remain a severe limitation. Most of the available EOs show antimicrobial activity and can be utilized for antimicrobial finishing of textiles. The limitations of EOs, especially the volatility can be overcome by encapsulating these in suitable polymer-shells. The various reports regarding the use of microcapsules containing EOs for antimicrobial finishing are available in the literature, as shown in Table 5.

Thilagavathi *et al.*⁹² prepared the microcapsules loaded with Mexican daisy and neem extracts using acacia gum as a shell material and applied on the cotton fabric. The finished fabric showed more antimicrobial properties against *S. aureus* as compared to *E. coli*, which were retained even after 15 washing cycles.

Table 5 — Research studies on antimicrobial textiles

Core material	Shell material	Method	Fabric	Application method	Results obtained	Reference
Neem oil + Mexican daisy leaves oil	Gum acacia	Simple coacervation	Cotton	Pad-dry-cure	Antibacterial properties even after 15 washes against <i>E. coli</i> and <i>S. aureus</i>	92
A mixture of turmeric, tulsi, and neem extracts	Fresh yeast	Plain diffusion method	Cotton and silk	Pad-dry-cure	A very active antimicrobial activity against <i>Pseudomonas</i>	93
Ozonated red pepper seed oil	Gelatine and Arabic Gum	Complex coacervation	PP non-woven	Padding	Good antimicrobial activity against <i>E. coli</i> , <i>S. aureus</i> , and <i>C. albicans</i> . Agar-gelatine microcapsules showed antimicrobial activity even after 20 washes against <i>S. aureus</i>	94
Berberine	Chitosan and agar-gelatine	NA	Cotton	Pad-dry-cure	Excellent antibacterial activities against <i>E. coli</i> , and <i>S. aureus</i> EE was 50.69%	95
Eucalyptus and sandalwood oils	Chitosan	Emulsion	Cotton	Pad-dry-cure	Antibacterial activity (65%) against <i>S. aureus</i> and <i>E. coli</i> even after 25 washes	96
Patchouli oil	Chitosan-gelatine	Complex coacervation	Cotton	Pad-dry-bake	Excellent antibacterial effect (99%) against <i>S. aureus</i>	97
Poly-(n-butyl acrylate)	Chitosan	Surfactant-free emulsion copolymerization (Microcapsules)	Cotton	Pad-dry-cure	The antibacterial activity > 99% and retained to 90% even after 50 laundering cycles against <i>S. aureus</i>	98
Poly(n-butyl acrylate)	Chitosan	Surfactant-free emulsion copolymerization (Nanosized particles)	Cotton	Pad-dry-cure	Strong antibacterial properties against <i>E. coli</i> and <i>S. aureus</i>	99
Poly(methyl methacrylate) (PMMA)	Chitosan, polyethyleneimine, and chitosan-polyethyleneimine	Emulsifier-free emulsion polymerization	NA	NA	EE was of 66.06% ± 2.53% Excellent inhibition rate against <i>S. aureus</i> (89%, and <i>E. coli</i> (87%) even after storage for 30 days	100
Tea tree oil	Sodium alginate and a quaternary ammonium salt of chitosan	Complex coacervation	NA	NA		101

Saraswathi *et al.*⁹³ developed the microcapsules loaded with a mixture of turmeric, tulsi, and neem, via plain diffusion method. The prepared microcapsules were applied on silk and cotton fabrics using a commercial binder at pH 5.5–6 and the treated fabrics were cured at 120 °C for 2 min. The treated fabrics showed active antimicrobial properties against the selected bacteria. Ozyildiz *et al.*⁹⁴ utilized the complex coacervation method to fabricate the microcapsules containing gelatine and Arabic gum as

a shell material and ozonated red pepper seed oil as a core, and then applied on 100% polypropylene non-woven fabric. The finished fabric exhibited antimicrobial activities against *E. coli*, *C. albicans*, and *S. aureus*. Lam *et al.*⁹⁵ prepared agar-gelatine and chitosan microcapsules loaded with berberine and applied on cotton fabric using acrylic binder to develop the antibacterial fabric. The presence of microcapsules on finished fabrics after 20 washes was confirmed by SEM images. The presence of a few

microcapsules was also reported after 50 washes. The antibacterial activity (against *S. aureus*) of the fabric treated with agar-gelatine microcapsules after 20 washes were better than that of the fabric treated using chitosan microcapsules.

Javid *et al.*⁹⁶ prepared the microcapsules loaded with sandalwood oils, and eucalyptus via emulsion method. The modified dihydroxy ethylene urea was used to graft the microcapsules on the cotton fabric. The antibacterial property of the finished fabric was evaluated against *S. aureus* and *E. coli* using the turbidity method, which shows higher antibacterial properties with the presence of the higher amount of chitosan and essential oils.

Liu *et al.*⁹⁷ developed chitosan-gelatin microcapsules loaded with patchouli oil using a complex coacervation method. The prepared microcapsules showed encapsulation efficiency of 50.69% and loading capacity of 30.31%. The treated fabric displayed good antibacterial activity (65%) against *E. coli* and *S. aureus*, which was durable even after 25 washing cycle. The results were encouraging, and the treated fabrics were projected for the possible applications in the fields like health-care clothes, bacteriostatic sheet, and antibacterial mask. Ye *et al.*⁹⁸ fabricated chitosan microcapsules loaded with poly-(n-butyl acrylate) through surfactant-free emulsion copolymerization methods. The cotton fabrics finished with such microcapsules displayed antibacterial property (99%) against *S. aureus*, and the unique core-shell structure showed antibacterial durability over repeated washing. Ye *et al.*⁹⁹ used surfactant-free emulsion copolymerization to prepared nanosized particles in aqueous chitosan. The fabric treated using such capsules displayed an excellent antibacterial property (> 99%), and the 90% antibacterial activity was retained even after 50 washes. Inphonlek *et al.*¹⁰⁰ fabricated nanoparticles loaded with poly(methyl methacrylate) using with chitosan, polyethyleneimine, and chitosan-polyethyleneimine as shell materials through emulsifier-free emulsion polymerization. The nanoparticles displayed excellent antibacterial properties against *S. aureus*, and *E. coli*. Chen *et al.*¹⁰¹ prepared the microcapsules containing tea tree oil (TTO) using sodium alginate and a quaternary ammonium salt of chitosan as a wall material. The prepared microcapsules displayed significant encapsulation efficiency (66.06% ± 2.53%). The microcapsules showed excellent antibacterial activities, (98.66%) against *E. Coli* and 100% activities against *S. aureus* after storage for five days. The TTO-loaded microcapsules also demonstrated

an excellent inhibition rate against *E. coli* (87%) and *S. aureus* (89%) even after storage for 30 days. Lee *et al.*¹⁰² prepared the melamine-formaldehyde microcapsules loaded with *C. unshiu* fruit extract via *in situ* polymerization and applied it on the cotton fabric using an acrylic binder. The SEM confirmed the presence of microcapsules on the fabric. Qi *et al.*¹⁰³ utilized the ionic gelation method to prepare nanoparticles of chitosan containing tripolyphosphate anions. The nanoparticles showed higher antibacterial activity against *E. coli*, *S. choleraesuis*, *S. aureus*, and *S. typhimurium* as compared to that using chitosan alone because the nanoparticles easily led to a disruption of cell membranes and the leakage of bacteria cytoplasm.

2.6.3 Insect/Mosquito Repellent Textiles

The textile product which offers mosquito repellency has been recently invented, and the method of preparation involves the application of mosquito repellent agents on to the textile materials. The N, N-diethyl-3 methyl benzamide (DEET) is the most commonly used insect/mosquito repellent. While providing effectiveness against most of the insects, DEET presents some limitations such as higher toxicity along with allergic and synthetic nature. Thus, recent research on mosquito repellent textiles focuses on the use of EOs, which is a safer and more effective way of achieving insect repellency¹⁰⁴. The examples of such EOs include cedar, pine, thyme, peppermint, citronella, geranium, cinnamon, garlic, and basil. Several research studies have been conducted to develop mosquito repellent textiles, as shown in Table. 6.

Kim and Sharma¹⁰⁵ prepared the gelatine microcapsules containing thyme and clove bud oil via coacervation process. The prepared microcapsules were applied on 100% acrylic fabric through vacuum drying. The finished fabrics acaricidal activities were investigated using AATCC test method 194-2007. The fabrics treated with microcapsules containing clove bud oil showed higher antioxidant and acaricidal activities against *Dermatophagoides farina* as compared to red thyme oil which might be because of the higher number of hydroxyls presence in clove bud oil. Ramya and Maheshwari¹⁰⁶ synthesized andrographolide loaded sodium alginate microcapsules via ionic gelation method, and the microcapsules were applied on the bamboo/cotton fabric by exhaustion method. The microcapsule-finished fabrics displayed 94% mosquito repellency as compared to 96% repellency in case of directly finished fabrics. The repellency was gradually decreased to 52% for

Table 6 — Research studies on insect/mosquito repellent textiles

Core material	Shell material	Microencapsulation method	Fabric	Application method	Results obtained	Reference
Thyme and clove bud oil	Gelatine	Coacervation	Acrylic	Pad-Vacuum drying	The antioxidant and acaricidal activities of clove bud against <i>Dermatophagoides farina</i> were higher than that of red thyme oil	105
Andrographolide	Sodium alginate	Ionic gelation	Bamboo/cotton blend	Exhaustion	Displayed 94% mosquito repellency and gradually decreased to 52% after 30 washes	106
Vitex negundo leaf extract	Alginate	Ionic gelation	Cotton	Pad-dry-cure	Showed 100% mosquito repellency and retained 70 % repellency till 15 washes	107
A mixture of grapefruit oil, cypress oil, and thyme oil	Acacia arabica, sodium alginate, and <i>Moringa oleifera</i> gum	Ionic gelation	Bamboo/Tencel blend	Exhaustion	<i>Moringa oleifera</i> gum microcapsules retained 60% mosquito repellency even after 30 washes	108

microcapsule-finished fabrics and 40% for directly finished fabrics after 30 washes. Ramasamy *et al.*¹⁰⁷ synthesized nanoparticle-containing *V. negundo* leaf extract through ionic gelation method to impart mosquito repellency to textile materials. The finished fabrics showed 100% mosquito repellency and retained 70 % repellency after 15 washes.

Geethadevi and Maheshwari¹⁰⁸ prepared mosquito repellent microcapsules by ionic gelation method using three wall materials such as acacia arabica, sodium alginate, and *Moringa oleifera* gum and the combination of three core materials namely grapefruit oil, cypress oil, and thyme oil. The microcapsules prepared using *Moringa oleifera* gum retained 60% mosquito repellency even after 30 washing cycles. Specos *et al.*¹⁰⁹ used a complex coacervation method to fabricate the microcapsules loaded with citronella essential oil. The gelatine and Arabic gum were used as a wall polymer, and glutardialdehyde was used as a hardening agent. The cotton fabrics finished using such microcapsules showed more than 90% repellent activity for three weeks.

2.6.4 Medical Textiles

The medical textiles are covering a wide range of application such as first aid, clinical, medicinal and hygienic purpose. Medical textiles are ranging from bandages wound dressing, gauzes and tissue-culturing to body implants like a skin, artificial heart, blood

vessel, and heart valve. These types of textiles have been developed by following various approaches. However, microencapsulation of EOs into a non-toxic, biocompatible, biodegradable polymers, and applying on the textile can be a possible approach to introduce an alternative of synthetic chemicals¹¹⁰.

Gouveia¹¹¹ investigated the development of microspheres using a combination of n-dodecane, bovine serum albumin (BSA), and L-Cysteine (L-Cys) and applied these microspheres as a coating on the fibrous material. The coated fibrous material showed excellent antibacterial activity along with high stability. The results suggest that the new coating could be an alternative to develop fibrous bioactive delivery systems. Gong *et al.*¹¹² utilized solid dispersion method to encapsulate the curcumin into poly(ethylene glycol)-poly(ϵ -caprolactone) copolymer and loaded it with a thermosensitive hydrogel composite namely poly(ethylene glycol)-poly(ϵ -caprolactone)-poly(ethylene glycol). The prepared wound dressing showed strong tissue-adhesiveness with an extended time of curcumin release, which results in suitable granulation, high collagen content, and excellent wound healing ability. Liakos *et al.*¹¹³ encapsulated different EOs such as chamomile blue, tea tree, lavender, lemongrass, peppermint, elicriso italic, lemon oils, cinnamon, and eucalyptus oils in a film of sodium alginate and glycerol as a plasticizer. The composite wound dressing film showed that

most of the EOs prevent the growth of *C. albicans*. However, peppermint oils, lemongrass, and cinnamon oils displayed antibacterial properties against *E. coli*.

2.6.5 Cosmetic Textiles

The microencapsulation is also used to prepare cosmetic textiles by applying cosmetic agents such as anti-ageing agents, essential oils, skin cooling agents, vitamins, and skin moisturizing agents. The microcapsules and their application should be based on the principles of good manufacturing practices. Moreover, the combination of cosmetic and textile materials offers an advance and unique cosmetic textile product. These kinds of product can offer other properties like antioxidant, odour-reducing, antimicrobial and mosquito repellence²¹. The durability of a cosmetic ingredient on the textile is essential. Several researchers have studied various techniques for enhancing the durability of functional properties offered by microcapsules; however, this is comparatively the most challenging work in the production of cosmetic textiles²². Cheng *et al.*²⁴ developed a vitamin C loaded gelatin microcapsules using emulsion hardening technique. The gelatin microcapsules were found to be non-cytotoxic based on the toxicity studies conducted on human liver. The prepared microcapsules were successfully grafted into textile materials.

2.6.6 Multifunctional Textiles

Multifunctional textiles offer two or more functional properties. The functional properties are derived from the functional shell and active core materials of microcapsules. In addition to the main

functional property, these microcapsules possess one or more functional properties like antibacterial activity, antifungal activity, flame retardancy, thermochromic performance, electrical conduction, photoluminescence and thermal stability^{21,85,114}.

Wang *et al.*¹¹⁵ developed multifunctional cotton with efficient ultraviolet protection, thermal insulation and superhydrophobic and aromatic performance using an aluminum-doped zinc oxide -embedded lemon microcapsule and SiO₂ dual-layer coating. Janarthanan and Kumar¹¹⁶ synthesized microcapsules containing brown algae extracts. The finished fabric with microencapsulated material showed excellent antioxidant and antimicrobial properties. Scacchetti *et al.*¹¹⁷ prepared multifunctional microcapsules using monochlorotriazinyl- β -cyclodextrin conjugated with thyme oil. The microcapsules provided antibacterial, antifungal and thermoregulation properties. Li *et al.*⁷⁵ prepared microcapsules with a high latent heat and a high thermal reliability using CuO-doped polyurea as a shell and an n-eicosane as a core through a one-step interfacial polymerization. Cotton fabric coated with the prepared microcapsules showed high phase change enthalpy of 36.8 J/g, an effective thermoregulation capability, and a large contact angle.

3 Recent Patents on Application of Microencapsulated Materials on Textiles

Recently, textile industry is exploring the potential of microencapsulation for developing innovative functional clothing/apparel. Patents on the functionalization of textiles using microcapsules are reported Table 7.

Table 7 — Summary of recent patents on application of microcapsules on textiles

Title	Year	References
Anti-mosquito finishing process of textile fabric	2012	118
Isatis root oil microcapsule and functional fabric finishing agent	2012	119
Double-layer aromatic phase change microcapsule textile finishing liquor as well as preparation method and application thereof	2015	120
Tea tree oil microcapsule antibacterial healthcare fiber and preparation method thereof	2015	121
Preparation and application of modified melamine resin essence microcapsule finishing agent	2015	122
Intelligent temperature adjustment textile and making method thereof	2016	123
Non-woven fabric, finishing method and application of non-woven fabric	2017	124
Durable flame-retardant finish method for cotton fabric based on ultraviolet light curing reaction	2017	125
Preparation for pinus koraiensis phytoncide finishing agent, fabric finished by same and finishing method thereof	2018	126
Preparation method and application of finishing agent containing rose essential oil microcapsules	2018	127
<i>In situ</i> microencapsulation treatment using a coacervated polymer system of asbestos fibres and other hazardous materials	2018	128
Aroma-loaded microcapsules with antibacterial activity for eco-friendly applications	2018	129
The preparation method of microcapsule coated insecticide-controlled release textile	2019	130
Ultra-thin glass, the method for ultra-thin ceramic and its manufactured goods and application are manufactured with fibre assist formation	2019	131
Encapsulation system for prolonged release of active agents	2019	132

The current trends in the development of functional textiles using microencapsulation techniques are mainly focused on the development of mosquito repellent, multifunctional, thermally sensitive, temperature adjusting and flame-retardant textile materials. The summarized patents cover the introduction of innovative microencapsulation techniques, functional polymers, novel EOs and additives. Moreover, the durability of finish and development of sustainable process are the prime concerns among the researchers.

4 Conclusion

The textile industry is currently experiencing many challenges due to the varied demands of modern customers. Functionalization of textile products is among the top requirements of the present market. Since the last two decades, microencapsulation technology is the most appreciated technology to functionalize the textile products. The beauty of this technique lies in the combination of two materials, both of which can be functional, which can synergistically enhance the functional properties. Microencapsulation could be one of the most promising techniques for functionalization of textile materials, especially with the use of volatile essential oils. The technical limitations like the need of fixing agents, limited durability, especially towards repeated washing and the changes in physical properties of textiles after application of microcapsules will remain the quest of research for the future. There is a broad scope in functionalization of textiles using microencapsulated materials, and it is expected that the development of multifunctional textiles will continue to grow and open up the new opportunity shortly. The limitation, however, must be countered through continuous research in this important area of chemical science. In future, innovative technologies and modern manufacturing techniques for microencapsulation and application on textiles will be required. The development of sustainable textile products using microencapsulation will be an interesting challenge for research in the near future.

References

- Miró Specos M M, Escobar G, Marino P, Puggia C, Defain Tesoriero M V & Hermida L, *J Ind Text*, 40 (2010) 13.
- Nejman A, Cieślak M, Gajdzicki B, Goetzendorf-Grabowska B & Karaszewska A, *Thermochim Acta*, 589 (2014) 158.
- Butstraen C, Salaün F, Devaux E, Giraud S Vroman P, *Polymers*, 8 (2016) 267.
- Vilchez-Maldonado S, Calderó G, Esquena J & Molina R, *Cellulose*, 21 (2014) 2133–2145.
- Miró Specos M M, Garcia J J, Gutierrez A C & Hermida L G, *J Text Inst*, 108 (2017) 1454.
- Feczko T, Samu K, Wenzel K, Neral B & Voncina B, *Color Technol*, 129 (2013) 18.
- Van Tran V, Loi Nguyen T, Moon J-Y & Lee Y-C, *Chem Eng J*, 368 (2019) 88.
- Mossotti R, Ferri A, Innocenti R, Zelenková T, Dotti F, Marchisio D L & Barresi A A, *J Microencapsul*, 32 (2015) 650.
- Drapeau J, Rossano M, Touraud D, Obermayr U, Geier M, Rose A & Kunz W, *Comptes Rendus Chim*, 14 (2011) 629.
- Lacasse K & Baumann W *Textile Chemicals: Environmental Data and Facts* (Springer), 2004.
- Nelson G, *Rev Prog Color Relat Top*, 31 (2008) 57.
- Sun-Waterhouse D, Wadhwa S S & Water house G I N, *Food Bioprocess Technol*, 6 (2013) 2376.
- Ghosh S K, *Functional Coatings: by Polymer Microencapsulation* (Wiley-VCH), 2006.
- Muthaiyan A, Limayem A & Ricke S C, *Prog Energy Combust Sci*, 37 (2011) 351.
- Burt S, *Int J Food Microbiol*, 94 (2004) 223.
- Tiwari B K, Valdramidis V P, O' Donnell C P, Muthukumarappan K, Bourke P & Cullen P J, *J Agric Food Chem*, 57 (2009) 5987.
- Yip J & Luk M Y A, in *Antimicrob Text* (Woodhead Publishing) 2016, 19.
- Sharkawy A, Fernandes I P, Barreiro M F, Rodrigues A E & Shoeib T, *Ind Eng Chem Res*, 56.(2017) 5516.
- Benita S, *Microencapsulation: Methods and Industrial Applications* (Taylor & Francis), 2006.
- Nelson G, *Rev Prog Color Relat Top*, 21 (2008) 72.
- Petrulis D & Petruyte S, *J Appl Polym Sci*, 136 (2019) 47066.
- Cheng S Y, Yuen C W M, Kan C W & Cheuk K K L, *Res J Text Appar*, 12 (2008) 41.
- Rajendran S & Anand C, *Indian J Fibre Text Res*, 31(1) (2006), 215.
- Cheng S Y, Yuen M C W, Kan C W, Cheuk K K L, Chui C H & Lam K H, *Int J Mol Med*, 24 (2009) 411.
- Estevinho B N, Rocha F, Santos L & Alves A, *Trends Food Sci Technol*, 31 (2013) 138.
- Spears J R, *U S Pat* 5086620(A), Wayne State University, Detroit, Mich., 1992.
- Bishop J R P, Nelson G & Lamb J, *J Microencapsul*, 15 (1998) 761.
- Ghayempour S & Mortazavi S M, *J Appl Polym Sci*, 132 (2015).
- Silva C, Ribeiro A, Ferreira D & Veiga F, *Rev Bras Ciências Farm*, 39 (2003) 1.
- Jamekhorshid A, Sadrameli S M & Farid M, *Renew Sustain Energy Rev*, 31 (2014) 531.
- Fanger G O, *Microencapsulation* (Springer Boston, MA USA), 1974, 1.
- Ubbink J, *Kirk-Othmer Encyclopedia of Chemical Technology*, (John Wiley & Sons, Inc.: Hoboken, NJ, USA), 2013, 1.
- Wischke C & Schwendeman S P, *Int J Pharm*, 364 (2008) 298.
- Martín del Valle E M, Galán M A & Carbonell R G, *Ind Eng Chem Res*, 48 (2009) 2475.
- Abdul Aziz F R, Jai J, Raslan R & Subuki I, *Adv Mater Res*, 1113 (2015) 346.

- 36 Martins I M, Barreiro M F, Coelho M & Rodrigues A E, *Chem Eng J*, 245 (2014) 191.
- 37 Dastjerdi R & Montazer M, *Colloids Surf B*, 79 (2010) 5.
- 38 Levine R M, Pearce T R, Adil M & Kokkoli E, *Langmuir*, 29 (2013) 9208.
- 39 Schell D & Beermann C, *Food Res Int*, 62 (2014) 308.
- 40 Cascone S, Lamberti G, Titomanlio G, Barba A A & d'Amore M, *Drug Dev Ind Pharm*, 38 (2012) 1486.
- 41 Ghayempour S & Montazer M, *J Microencapsul*, 33 (2016) 497.
- 42 Krokida M, *Thermal and Nonthermal Encapsulation Methods*; in Series: *Advances in Drying Science & Technology* (CRC Press; Boca Raton: CRC Press, Taylor & Francis Group), 2017.
- 43 Borreguero A M, Valverde J L, Rodriguez J F, Barber A H, Cabillo J J & Carmona M, *Chem Eng J*, 166 (2011) 384.
- 44 Chen Q, Zhong F, Wen J, McGillivray D & Quek S Y, *Dry Technol*, 31 (2013) 707.
- 45 Han G T, Yang Z M, Peng Z, Wang G, Zhou M, Pang Y X & Li P W, *Adv Mater Res*, 641-642 (2013) 935.
- 46 Bakry A M, Abbas S, Ali B, Majeed H, Abouelwafa M Y, Mousa A & Liang L, *Compr Rev Food Sci Food Saf*, 15 (2016) 143.
- 47 Nguon O, Lagugn -Labarthe F, Brandys F A, Li J & Gillies E R, *Polym Rev*, 58 (2018) 326.
- 48 Thies C, *Encyclopedia of Polymer Science and Technology*; (John Wiley & Sons, Inc.: Hoboken, NJ, USA), 2004.
- 49 Li Y, Ai L, Yokoyama W, Shoemaker C F, Wei D, Ma J & Zhong F, *J Agric Food Chem*, 61 (2013) 3311.
- 50 de Oliveira E F, Paula H C B & Paula R C M de, *Colloids Surf, B*, 113 (2014) 146.
- 51 Carvalho A G S, Silva V M & Hubinger M D, *Food Res Int*, 61 (2014) 236.
- 52 Jyothi N V N, Prasanna P M, Sakarkar S N, Prabha K S, Ramaiah P S & Srawan G Y, *J Microencapsul*, 27 (2010) 187.
- 53 Zuo M, Liu T, Han J, Tang Y, Yao F, Yuan Y & Qian Z, *Chem Eng J*, 249 (2014) 27.
- 54 Brown E N, Kessler M R, Sottos N R & White S R, *J Microencapsul*, 20 (2003) 719.
- 55 Arshady R, *Polym Eng Sci*, 29 (1989) 1746.
- 56 Lee H Y, Lee S J, Cheong I W & Kim J H, *J Microencapsul*, 19 (2002) 5599.
- 57 Chung S K, Seo J Y, Lim J H, Park H H, Yea M J & Park H J, *J Food Sci*, 78 (2013) E709.
- 58 Freiberg S & Zhu X X, *Int J Pharm*, 282 (2004) 1.
- 59 Gharsallaoui A, Roudaut G, Chambin O, Voilley A & Saurel R, *Food Res Int*, 40 (2007) 1107.
- 60 Dash M, Chiellini F, Ottenbrite R M & Chiellini E, *Prog Polym Sci*, 36 (2011) 981.
- 61 Aghbashlo M, Mobli H, Rafiee S & Madadlou A, *Biosyst Eng*, 111 (2012) 229.
- 62 Zhang Y, Jiang Z, Zhang Z, Ding Y, Yu Q & Li Y, *Chem Eng J*, 359 (2019) 1234.
- 63 Yin Q, Zhu Z, Li W, Guo M, Wang Y, Wang J & Zhang X, *Polymers*, 10 (2018) 726.
- 64 Anal A K & Singh H, *Trends Food Sci Technol*, 18 (2007) 240.
- 65 Jyothi Sri S, Seethadevi A, Suria Prabha K, Muthuprasanna P & Pavitra P, *Int J Pharma Bio Sci*, 3(1)(2012) 509.
- 66 Cortesi R, Nastruzzi C & Davis S S, *Biomaterials*, 19 (1998) 1641.
- 67 Favaro-Trindade C S, Santana A S, Monterrey-Quintero E S, Trindade M A & Netto F M, *Food Hydrocoll*, 24 (2010) 336.
- 68 Aranaz I, Mengibar M, Harris R, Panos I, Miralles B, Acosta N, Galed G & Heras A, *Curr Chem Biol*, 3 (2009) 203.
- 69 Freitas S, Merkle H P & Gander B, *J Control Release*, 102 (2005) 313.
- 70 Lam P L & Gambari R, *J Control Release*, 178 (2014) 25.
- 71 Asbahani A El, Miladi K, Badri W, Sala M, Addi E H A, Casabianca H, Mousadik A El, Hartmann D, Jilale A, Renaud F N R & Elaissari A, *Int J Pharm*, 483 (2015) 220.
- 72 Svoboda K & Greenaway R I, *Int J Aromather*, 13 (2003) 196.
- 73 Alay S, G de F & Alkan C, *J Appl Polym Sci*, 120 (2011) 2821.
- 74 Alay Aksoy S, Alkan C, T z m M S, Demirba  S, Altun Anayurt R & Ulcay Y, *J Text Inst*, 108 (2017) 30.
- 75 Li J, Zhu X, Wang H, Lin P, Jia L, Li L & Chen Y, *J Mater Sci*, 56 (3) (2021) 2176.
- 76 Salaun F, Vroman I & Elmajid I, *Chem Eng J*, 213 (2012) 78.
- 77 Calamari T A & Harper R J, *Kirk-Othmer Encyclopedia of Chemical Technology* (John Wiley & Sons, Inc.: Hoboken, NJ, USA), 2000.
- 78 Li S, Lewis J E, Stewart N M, Qian L & Boyter H, *J Text Inst*, 99 (2008) 177.
- 79 Li S, Boyter H & Qian L, *J Text Inst*, 96 (2005) 407.
- 80 Rodrigues S N, Martins I M, Fernandes I P, Gomes P B, Mata V G, Barreiro M F & Rodrigues A E, *Chem Eng J*, 149 (2009) 463.
- 81 Rodrigues Teixeira C S N, Martins I M D, Mata V L G, Barreiro M F F & Rodrigues A E, *J Text Inst*, (2011) 1.
- 82 Rhind J, *Essential Oils: A Handbook for Aromatherapy Practice* (Singing Dragon), 2012.
- 83 Teixeira M A, Rodriguez O, Rodrigues S, Martins I & Rodrigues A E, *AIChE J*, 58 (2012) 1939.
- 84 Boh B & Knez E, *Indian J Fibre Text Res*, 31 (2006) 72.
- 85 Huang X, Chen X, Li A, Atinafu D, Gao H, Dong W & Wang G, *Chem Eng J*, 356 (2019) 641.
- 86 Hu J, Xiao Z, Zhou R, Li Z, Wang M & Ma S, *Flavour Fragr J*, 26 (2011) 162.
- 87 Bonet M A, Capablanca L, Monllor P, Diaz P & Montava I, *J Text Inst*, 103 (2012) 629.
- 88 Liu C, Liang B, Shi G, Li Z, Zheng X, Huang Y & Lin L, *Flavour Fragr J*, 30 (2015) 295.
- 89 Liu C, Liang B, Wang Y, Li Y & Shi G, *J Appl Polym Sci*, 135 (2018) 45695.
- 90 Rodrigues S N, Fernandes I, Martins I M, Mata V G, Barreiro F & Rodrigues A E, *Ind Eng Chem Res*, 47 (2008) 4142.
- 91 Panisello C, Pe a B, Gilabert Oriol G, Constanti M, Gumi T & Garcia-Valls R, *Ind Eng Chem Res*, 52 (2013) 9995.
- 92 Thilagavathi G & Bala S K, *Indian J Fibre Text Res*, 32(3) (2007) 351.
- 93 Saraswathi R, Krishnan P & Dilip C, *Asian Pac J Trop Med*, 3 (2010) 128.
- 94  zyildiz F, Karag nl  S, Basal G, Uzel A & Bayraktar O, *Let Appl Microbiol*, 56 (2013) 168.
- 95 Lam P L, Li L, Yuen C W M, Gambari R, Wong R S M, Chui C H & Lam K H, *J Microencapsul*, 30 (2013) 143.
- 96 Javid A, Raza Z A, Hussain T & Rehman A, *J Microencapsul*, 31 (2014) 461.
- 97 Liu J, Liu C, Liu Y, Chen M, Hu Y & Yang Z, *Colloids Surf, B*, 109 (2013) 103.
- 98 Ye W, Leung M F, Xin J, Kwong T L, Lee D K L & Li P, *Polymer*, 46 (2005) 10538.

- 99 Ye W, Xin J H, Li P, Lee K-L D & Kwong T-L, *J Appl Polym Sci*, 102 (2006) 1787.
- 100 Inphonlek S, Pimpha N & Sunintaboon P, *Colloids Surf, B*, 77 (2010) 219.
- 101 Chen M, Hu Y, Zhou J, Xie Y, Wu H, Yuan T & Yang Z, *RSC Adv*, 6 (2016) 13032.
- 102 Lee A R, Han C H & Yi E, *Fibers Polym*, 15 (2014) 35.
- 103 Qi L, Xu Z, Jiang X, Hu C & Zou X, *Carbohydr Res*, 339 (2004) 2693.
- 104 Anitha R, Ramachandran T, Rajendran R & Mahalakshmi M, *Elixir Bio Phys*, 40 (2011) 5196.
- 105 Kim J R & Sharma S, *J Microencapsul*, 28 (2011) 82.
- 106 Ramya. K & Maheshwari V, *Int J Pharm Pharm Sci*, 6 (2014) 115.
- 107 Ramasamy R, Rajan R & Velmurugan R, *Malaya J Biosci*, 2014 (2013) 19.
- 108 Geethadevi R & Maheshwari V, *Indian J Fibre Text Res*, 40 (2015) 175.
- 109 Specos M M M, Garcia J J, Tornesello J, Marino P, Vecchia M Della, Tesoriero M V D & Herinida L G, *Trans R Soc Trop Med Hyg*, 104 (2010) 653.
- 110 Baykasoğlu A, Dereli T & Yilankirkan N, *Am J Infect Control*, 37 (2009) 215.
- 111 Gouveia I C, *Polym Adv Technol*, 23 (2012) 350.
- 112 Gong C, Wu Q, Wang Y, Zhang D, Luo F, Zhao X, Wei Y & Qian Z, *Biomaterials*, 34 (2013) 6377.
- 113 Liakos I, Rizzello L, Scurr D J, Pompa P P, Bayer I S & Athanassiou A, *Int J Pharm*, 463 (2014) 137.
- 114 Lu Y, Xiao X, Fu J, Huan C, Qi S, Zhan Y, Zhu Y & Xu G, *Chem Eng J*, 355 (2019) 532.
- 115 Wang W, Liang Y, Yang Z, Zhang W & Wang S, *Text Res J*, 89(18)(2019) 3860.
- 116 Janarthanan M & Senthil Kumar M, *Int J Cloth Sci Technol*, 29 (2017) 200-214.
- 117 Scacchetti F A P, Pinto E & Soares G M B, *Prog Org Coat*, 107 (2017) 64.
- 118 Yi X, Bingsheng G, Junfeng Z, Xu Y, Gao B & Zhang J, *CN Pat* 102154841(B Fujian Zhonghe Co Ltd, 2012.
- 119 Zhuohong Y, Yang H, Ze Y, Genquan L & Hong W, *CN Pat* 102405941(A), Univ South China Agricult, 2012.
- 120 Song X & Liu Q, *CN Pat* 103451939 (B), 2015.
- 121 Ling L, Zhao D, Tang P, Hu H & Chen Y, *CN Pat* 103147311(B), Jiangsu Yueda Textile Group Co Ltd, 2015.
- 122 Fei X, Zhang B, Fu Y, Zhao H & Yu M, *CN Pat* 103233368(B), 2015.
- 123 Ding A, Xiao L, Gao J, Gao J, Gao P & Gao W, *CN Pat* 104153203 (B), 2016.
- 124 Wang J, *CN Pat* 106480743 (A), 2017.
- 125 Xu L, Yu D & Wang W, *CN Pat* 106637960 (A), 2017.
- 126 Yan X & Wang H, *CN Pat* 107326685 (B), 2018.
- 127 Feng T, Wang H, Zhuang H, Zhao Y, Zeng X, Wang J, Wu Y, Zhang S, Xia Y, Li X, Shui M, Chen Z, Wang W, Wang X & Tong Y, *CN Pat* 107904928 (A), 2018.
- 128 Burns L, *WO Pat* 2018160201 (A1), 2018.
- 129 Sharkawy A, Shoeib T, Rodrigues A, Barreiro M & Fernandes I, *WO Pat* 2018183150 (A1), 2018.
- 130 Li C, Yin Q, Yu W & Zhang Y, *CN Pat* 109497056 (A), 2019.
- 131 Zhang Y, Zhu L, Yu Q, Liu T, Ma P, Jiang X, Xu J, Chi Z & Liu S, *CN Pat* 109694256 (A), 2019.
- 132 Jean-Francois G, , *WO Pat* 2019053689 (A1), 2019.



Cleaner Production of Dyed and Functional Polyester Using Natural Dyes vis-a-vis Exploration of Secondary Shades

S. Tambi, A. Mangal, N. Singh, J. Sheikh*

Department of Textile and Fibre Engineering, Indian Institute of Technology, P.O. Box: 110016, Hauz Khas, New Delhi, India

ARTICLE INFO

Article history:

Received: 24 Mar 2020

Final Revised: 19 Jul 2020

Accepted: 21 Jul 2020

Available online: 15 Sept 2020

Keywords:

Polyester

Natural dyeing

Functional properties

Secondary shades.

ABSTRACT

Natural dyes are known for their added benefits over synthetic dyes in terms of health and ecology. They are considered to present a limited range of shades, which limits their use in high-end value-added products. Thus, to explore natural dyes on large scales, it is essential to generate a wide range of shades like synthetic dyes. Therefore, it is important to explore the secondary shades of natural dyes especially those which can act as primary colors in the recipe (red, yellow and blue). In the present work, three natural dyes, namely indigo, pomegranate peels and kumkum were used to dye the polyester fabric. Along with color strength at different dye concentrations, functional properties such as antioxidant, antibacterial, and UV protection were also evaluated. The dyed polyester showed good color values ($K/S > 1.7$) and also displayed satisfactory color fastness to light, washing and rubbing. The polyester fabric dyed with pomegranate and kumkum in self-shades displayed a variety of functional properties including a bacterial reduction of more than 90%, radical scavenging activity of greater than 90% and also displayed excellent UPF values ($UPF > 270$). Indigo-dyed samples displayed antibacterial activity and UV-protection; however, their antioxidant activity was poor. The secondary shades of these dyes were produced on polyester fabric. Prog. Color Colorants Coat. 14 (2021), 121-128 © Institute for Color Science and Technology.

1. Introduction

Textile coloration using natural dyes is gaining momentum due to revival in the interest regarding sustainable chemical processing and awareness regarding toxic effects associated with some of azo dyes, especially those based on banned amines. This has led to increased exploration of natural resources for the coloration of textiles. Most of the studies in this area were done on cotton, wool, silk, nylon, jute, linen etc. Utilization of natural dyes for dyeing and functional finishing of textiles is widely reported in the literature [1-10].

Punica Granatum, which is commonly known as pomegranate, belongs to the Punicaceae family. It is a traditional medicine for diarrhoea and respiratory pathologies [11,12]. Its basic components are gallic acid, delphinidin, cyanidin, gallic acid, ellagic acid, pelargonidin and sitosterol [13]. Pomegranate and its chemical components offer many useful properties, including antibacterial activity [14], anti-inflammatory activity, antioxidant activity [15], anti-angiogenesis, and anti-cancer properties [13]. *Mallotus philippensis*, commonly known as Kumkum or Kapila, is a traditional drug used in India for the treatment of

*Corresponding author: jnsheikh@iitd.ac.in

tymphoid and stomach disorders [16, 17]. The basic component present in the dye is Rottlerin (1-[6-[(3-acetyl-2,4,6-trihydroxy-5-methyl phenyl) methyl]-5,7-dihydroxy -2,2-dimethyl -2H-1-benzopyran -8 -yl] -3-phenyl - 2 propen- 1 -one). It also contains different compounds, such as diterpenoids, phenols, flavonoids, steroids, coumarins, and triterpenoids [16]. Interesting biological activities of kumkum such as anti-oxidant activity, anti-microbial activity, cytotoxicity, antiviral activity, immunoregulatory activity, and anti-inflammatory activity were reported [17, 18]. *Indigofera Tinctoria*, also known as indigo blue, is a traditional dye associated with denim clothes and blue jeans [19]. The basic components present in *Indigofera tinctoria* leaf extract are tannins, phenols, saponins, terpenes, flavonoids, anthroquinonesence and steroidal. These chemical compounds possess various pharmacological properties such as anti-oxidant activity, anti-bacterial activity and cytotoxicity activity [20].

Polyester, being a synthetic fiber, is a less expensive option and has many advantages over other fibers like wrinkle-resistance, quick-drying and better resistance to microbial attack. Polyester fiber is widely used in apparels and technical textiles and the functional coloration of such substrate using natural dyes would be interesting. Sen et al. attempted dyeing of various polyester fibres like poly-trimethylene terephthalate (PTT) and poly-lactic acid (PLA), and poly-ethylene terephthalate (PET) with lac dye in presence of catechu as a bio-mordant [21]. Elnagar et al. dyed the polyester and nylon fabrics with curcumin and saffron natural dyes using UV/ozone pretreatment to activate fiber and improve the dyeability of the fabrics [22]. Bhuiyan et al. dyed the polyester fiber with henna as a natural dye without using metallic mordants [23]. Arain et al. provided an eco-friendly dyeing process for dyeing of polyester fabric with henna dye using microwave-assisted technology [24]. Abate et al. used supercritical CO₂ for bio-activation and coloration of polyester fabric with curcumin without mordant and achieved an excellent color strength and fastness properties [25]. Shahidi et al. modified the polyester fabric by dielectric barrier discharge and the dyeability of modified fabric with natural dyes was studied [26]. Zohdy used gamma radiations to improve the dyeability of polyester [27]. Some researchers have also used various novel techniques for natural dyeing of natural and synthetic

fibers [28–32].

Even though natural dyeing of textiles is reported widely, the reports regarding simultaneous dyeing and functional finishing of polyester are reported to a limited extent. The mixing of natural dyes to obtain a variety of shades on polyester to overcome the limitation of natural dye in terms of availability of limited shades is not reported. In the present work, three natural dyes namely indigo, kumkum and pomegranate were utilized for simultaneous dyeing and functionalization of polyester. The coloration and functional properties imparted to polyester using an application of such natural dyes were explored. Secondary shades of these dyes were also produced on polyester fabric to explore different shades.

2. Experimental

2.1. Materials

Polyester fabric was obtained from Toyota Water Jet machine with specifications 3937 ends/m and 2520 picks/m. The fabric was scoured using 2gpl detergent and 1gpl soda ash and further used for dyeing. Three natural dyes used were indigo (*Indigofera Tinctoria*), pomegranate peel (*Punica Granatum*) and kumkum (*Mallotus philippensis*). All were purchased in powder form from an Oriental drug store. The natural dye extraction was carried out in ethanol using soxhlet extraction for 12h. The dye powder was obtained by evaporating ethanol from the extract.

2.2. Methods

2.2.1. Dyeing of polyester fabric using natural dyes

The dyeing process was carried out via high-temperature high pressure (HTHP) method at 130 °C for 45 min in the Infrared Dyeing Machine. The polyester samples were dyed using different natural dyes (in various shade %) in acidic pH (4.5). The material to liquor ratio was kept as 1:10 and dispersing agent (1%) was used to prepare the dispersion of natural dye powder. Secondary shades were produced by mixing the natural dyes in weight proportions and maintaining the total shade percent as 1, 5 and 10%.

2.2.2. Measurement of color values

The color strength of dyed samples was compared by measuring K/S values [33] which were evaluated on

Gretag Macbeth Color Eye 7000A Spectrophotometer. The K/S values were assessed using the Kubelka-Munk equation (Eq. 1):

$$K/S = \frac{(1-R)^2}{2R} \quad (1)$$

where R is the observed reflectance, K is the absorption coefficient, and S is the light scattering coefficient.

2.2.3. Estimation of color fastness

Color fastness of the dyed fabrics to washing, rubbing and light was evaluated using ISO105-C06, ISO-105X12, and ISO105B02 test methods, respectively [34].

2.2.4. Evaluation of functional properties

The dyed polyester fabrics were analyzed for antioxidant activity as per the method reported in the literature [7], UV-protection as per AS/NZS 4399:1996 standard [35], and antibacterial activity against *S. aureus* as per AATCC-100 test method [36].

3. Results and Discussion

3.1. Color fastness of dyed polyester

Fastness to light, rubbing and washing (color change and staining) were evaluated for all the dyed samples (Table 1). As shown in Table 1, all the dyed samples showed significant light fastness, with ratings of 5 and more. It shows a good resistance of dye on dyed polyester against fading in the presence of light. All the dyed samples showed excellent washing fastness in terms of both color change and staining, as indicated by ratings of 4 to 5. The rubbing fastness was also

found in the range "good" to "very good". The results show satisfactory color fastness to light, washing and rubbing which might be attributed to the mechanism of dyeing of polyester using HTHP dyeing process. The dyes were applied on polyester through dispersion using HTHP method of dyeing. HTHP method utilizes high temperature to open the fibre structure which allows the dye to penetrate inside the core of the fibre. After dyeing, the bath is cooled which ensures the dye getting entrapped inside the fibre. This is very much similar to solid solution dyeing in case of disperse dyeing of polyester. The surface dye was removed by reduction clearance process after dyeing. This provides excellent resistance to color-bleeding in the presence of washing liquor, abrasive rubbing and light.

3.2. Functional properties of the dyed polyester

The polyester dyed with kumkum and pomegranate dyes showed excellent antioxidant activities, as shown in Table 2. The antioxidant activity of DPPH is based on the stability of the material. The odd electron of DPPH is responsible for a strong absorption at 517 nm. DPPH can accept electron donated by an antioxidant compound which further decolorizes the DPPH. The change in absorbance of decolorized DPPH can be quantitatively measured at 517 nm using UV-Visible spectrophotometer [37]. The dyed polyester, especially dyed with kumkum and pomegranate, exhibited excellent antioxidant property which might be because of the presence various compounds in natural dyes which are able to stabilize DPPH. They are electron-rich resonating centers which tend to avoid further oxidation and change the dye color. Indigo-dyed polyester showed significantly lower antioxidant activity as compared to other dyed samples.

Table 1: Color fastness of fabric samples dyed with indigo, kumkum and pomegranate dyes (5% shade).

S. No	Samples	Light Fastness	Rubbing Fastness	Washing Fastness	
				Staining	Color change
1	Kumkum	5	3-4	4	5
2	Indigo	5-6	3-4	4	4
3	Pomegranate	5	4	4	4

Table 2: Functional properties of polyester dyed with indigo, kumkum and pomegranate dyes (5% shade).

S. No	Samples	Radical scavenging activity (%)	UPF	Antibacterial activity (%)
1	Control	Negligible	42.97	-
2	Kumkum	91.44	322.07	85.87
3	Pomegranate	93.97	277.30	90.55
4	Indigo	43.82	198.40	83.82

The UV-protection properties of dyed fabrics were evaluated by measuring the UV-protection factor (UPF). UPF of the polyester fabric increased after dyeing with the three dyes, as shown in Table 2. As opposed to the UPF value of 42.97 for undyed fabric, dyed fabrics showed significant improvement in the UV-protection property. This behavior might be related to the introduction of dyes inside the fiber structure which produce hindrance in the ease of transmittance of UV radiation. UPF value of undyed polyester was also obtained which clearly indicates the dependence of UPF on the fiber properties. The presence of aromatic ring in the backbone of the polymer and the additive, which are added during fiber manufacturing, impart good UV-protection to the polyester. The antibacterial property of all the dyed samples was determined using the AATCC 100 method.

Table 2 shows the reduction of bacterial colonies by each dyed sample. All the dyed samples showed considerable antibacterial properties with the bacterial colony reduction of higher than 83%. The site and the number of hydroxyl groups on the phenolic components of dyes may increase the toxicity against the microorganisms. The phenolic groups in the dyes interfere with bacterial metabolism and inhibit their growth [17, 38]. Hence, all the dyed samples displayed a satisfactory antibacterial activity.

3.3. Primary and secondary shades of natural dyes on polyester

3.3.1. Color strength

Table 3 summarizes the L^* , a^* , b^* and K/S values of

dyed samples at 5% shade. Here, L^* is lightness (0 = Black; 100 = White), a^* is redness-greenness and b^* is yellowness-blueness.

In the secondary mixture of kumkum and indigo, the increase in kumkum concentration at the expense of indigo resulted in a decrease in L^* value indicating the increase in darkness of shade. This also resulted in a decrease in b^* indicating the increase in the blueness of shade. All the mixed shades of kumkum and indigo showed a negative value of a^* indicating the greenness of the obtained shades. The mixing of dyes resulted in beautiful shades with varying colour values. In most of the secondary shades, the dye present in a higher proportion showed the color dominance of the dyed fabric. The variation in dye concentration in binary mixture resulted in variations of tones and the lightness of shade (Table 3).

As shown in Table 1, the K/S values varied with varying the dye concentrations in the mixtures. The secondary mixture of pomegranate and kumkum showed higher K/S values as compared to other mixtures. In general, it can be concluded that the various dyes used for obtaining secondary shades showed good compatibility which resulted in a variety of shades on polyester fabric. Hence the suitability of these dyes for dyeing polyester in primary and secondary shades is confirmed.

3.4. Shade card formation

Nine mixtures were prepared with given dye proportions [(25% K, 75% I), (50% K, 50%I), (75% K, 25% I), (25% K, 75% P), (50% K, 50% P), (75% K,

25% P), (25% P, 75% I), (50% P, 50% I), (75% P, 25% I)]. All these dye mixtures were used to dye the polyester fabrics at different shade percentages, i.e. 1, 5 and 10%. Consequently, several different colors were observed in shade cards. Table 4 (a, b, c, and d) shows the shade cards for secondary shades, where the color of the fabric is gradually changing with a change in dye concentration. These colors and compositions are important for obtaining various desired shades. As shown in Table 4, the color changes into more bluish as indigo concentration increases; and it changes into brownish when the concentration of pomegranate dominates. Similar results were obtained for other combinations, and consequent shade

cards with various shades were prepared with various shades.

Moreover, it was observed that the mixing of these dyes showed uniform and homogenized colors and shades without getting any patches, dark and dull places. Thus, it can be concluded that using a mixture of natural dyes at different concentrations and proportions may generate a huge number of colors, shades and tones. Mixing of primary colors to get a variety of shades is a general practice in the textile industry. Natural dyes were used as primary colors to produce a variety of shades. This is particularly encouraging as various natural dyes can be mixed to get a wide spectrum of shades on textile materials.

Table 3: Color values and colour strengths of dyed samples at 5% shade.

S. No	Dye concentrations	L*	a*	b*	K/S
1	(100% I)	57.79	-6.15	-5.19	1.75
2	(100% K)	70.81	1.71	25.84	8.80
3	(100% P)	57.04	4.79	15.94	4.40
4	(25% K, 75% I)	70.05	-8.87	-5.04	1.78
5	(50% K, 50% I)	60.47	-12.13	-0.31	1.71
6	(75% K, 25% I)	54.89	-5.94	2.32	1.81
7	(25% P, 75% I)	57.37	-6.57	-5.13	1.75
8	(50% P, 50% I)	55.75	-5.95	1.17	1.80
9	(75%P, 25% I)	50.34	-4.02	4.14	2.26
10	(25% P, 75% K)	63.39	2.99	21.03	8.01
11	(50% P, 50% K)	61.00	2.75	16.97	5.05
12	(75% P, 25% K)	65.94	1.98	20.50	6.80

I: Indigo, K: Kumkum, P: Pomegranate

Table 4: Shade Cards for secondary shades
 a): Primary and secondary shade with 1% owf dye concentration

S. No	Dye Mixture	(100, 0)	(75, 25)	(50, 50)	(25,75)	(0, 100)
1	Indigo + Pomegranate					
2	Indigo + Kumkum					
3	Kumkum + Pomegranate					

b): Primary and secondary shade with 5% owf dye concentration

S. No	Dye Mixture	(100, 0)	(75, 25)	(50, 50)	(25,75)	(0, 100)
1	Indigo + Pomegranate					
2	Indigo + Kumkum					
3	Kumkum + Pomegranate					

c): Primary and secondary shade with 10% owf dye concentration

S. No	Dye Mixture	(100, 0)	(75, 25)	(50, 50)	(25,75)	(0, 100)
1	Indigo + Pomegranate					
2	Indigo + Kumkum					
3	Kumkum + Pomegranate					

4. Conclusions

The polyester fabrics were successfully dyed with natural dyes. The results showed that the natural dyes showed excellent compatibility with polyester fibers. The polyester fabrics dyed with kumkum and pomegranate dyes showed significant antioxidant properties (radical scavenging >90%), UV-protection (UPF>270), and also exhibited appropriate antibacterial activity against *S. aureus* (bacterial colony reduction >85%). The polyester dyed with indigo dye also displayed significant UV-protection and antibacterial properties; however, it showed inferior antioxidant

properties compared to polyester dyed with kumkum and pomegranate dyes. The polyester fabrics dyed with indigo, kumkum, and pomegranate dyes demonstrated good washing (rating 4 and above), rubbing (ratings 3-4 and above) and light (rating 5 and above) fastnesses. At a higher level, these dyes can be used with their sustainable nature, unique shade character and functionalities, which are also compatible with strong, wrinkle-resistant and economically feasible polyester. A variety of colors can be obtained by changing the percentages and proportions of the dyes.

5. References

1. F. Rehman, N. Sanbhal, T. Naveed, A. Farooq, Y. Wang, W. Wei, Antibacterial performance of tencel fabric dyed with pomegranate peel extracted via ultrasonic method, *Cellulose*. 25(2018), 4251–4260.
2. B. Patel, P. Kanade, Sustainable dyeing and printing with natural colours vis-à-vis preparation of hygienic viscose rayon fabric, *Sustain. Mater. Technol.* 22(2019), e00116.
3. Y. Zhou, J. Zhang, R. C. Tang, J. Zhang, Simultaneous dyeing and functionalization of silk with three natural yellow dyes, *Ind. Crops Prod.* 64(2015), 224–232.
4. X. Hou, F. Fang, X. Guo, J. Wizi, B. Ma, Y. Tao, Y. Yang, Potential of sorghum husk extracts as a natural functional dye for wool fabrics, *ACS Sustain. Chem. Eng.* 5(2017), 4589–4597.
5. M. Shabbir, L. J. Rather, F. Mohammad, Economically viable UV-protective and antioxidant finishing of wool fabric dyed with *Tagetes erecta* flower extract: Valorization of marigold, *Ind. Crops Prod.* 119(2018), 277–282.
6. J. Sheikh, N. Singh, D. Pinjari, Sustainable functional coloration of linen fabric using *kigelia africana* flower colorant, *J. Nat. Fibers.* (2019), 1–10.
7. J. Sheikh, N. Singh, M. Srivastava, Functional dyeing of cellulose-based (Linen) fabric using *bombax ceiba* (Kapok) flower extract, *Fibers Polym.* 20(2019), 312–319.
8. J. Sheikh, A. Agrawal, H. Garg, A. Agarwal, P. Mathur, Functionalization of wool fabric using pineapple peel extract (PPE) as a natural dye, *AATCC J. Res.* 6(2019), 16–20.
9. A. Sharma, S. Kadam, P. Mathur, Shahid-ul-Islam, J. Sheikh, Re-using henna natural dyeing wastewater for coloration and multifunctional finishing of linen fabric, *Sustain. Chem. Pharm.* 11(2019), 17–22.
10. M. Hosseinezhad, K. Gharanjig, R. Jafari, H. Imani, Green dyeing of woolen yarns with weld and Madder natural dyes in the presences of biomordant, *Prog. Color Colorant Coat.* 14(2021), 35–45.
11. J. G. Choi, O. H. Kang, Y. S. Lee, H. S. Chae, Y. C. Oh, O. O. Brice, M. S. Kim, D. H. Sohn, H. S. Kim, H. Park, D. W. Shin, J. R. Rho, D. Y. Kwon, In vitro and in vivo antibacterial activity of punica granatum peel ethanol extract against salmonella., *Evid. Based. Complement. Alternat. Med.* 2011(2011), 690518.
12. R. P. Singh, K. N. Chidambara Murthy, G. K. Jayaprakasha, Studies on the antioxidant activity of pomegranate (*Punica granatum*) peel and seed extracts using in vitro models, *J. Agric. Food Chem.*, 50(2002), 81–86.
13. E. P. Lansky, R. A. Newman, Punica granatum (pomegranate) and its potential for prevention and treatment of inflammation and cancer, *J. Ethnopharmacol.* 109(2007), 177–206.
14. L. C. Braga, J. W. Shupp, C. Cummings, M. Jett, J. A. Takahashi, L.S. Carmo, E. Chartone-Souza, A.M.A. Nascimento, Pomegranate extract inhibits staphylococcus aureus growth and subsequent enterotoxin production, *J. Ethnopharmacol.* 96(2005), 335–339.
15. D. Heber, N. P. Sceram, H. Wyatt, S. M. Henning, Y. Zhang, L. G. Ogden, M. Dreher, J. O. Hill, Safety and antioxidant activity of a pomegranate ellagitannin-enriched polyphenol dietary supplement in overweight individuals with increased waist size, *J. Agric. Food Chem.* 55(2007), 10050–10054.
16. M. Gangwar, R. K. Goel, G. Nath, *Mallotus philippinensis* muell. arg (euphorbiaceae): ethnopharmacology and phytochemistry review., *Biomed Res. Int.* 2014(2014), 213973.
17. V. P. Kumar, N. S. Chauhan, H. Padh, M. Rajani, Search for antibacterial and antifungal agents from selected Indian medicinal plants, *J. Ethnopharmacol.* 107(2006), 182–188.
18. A. A. Mostafa, A. A. Al-Askar, K. S. Almaary, T. M. Dawoud, E. N. Sholkamy, M. M. Bakri, Antimicrobial activity of some plant extracts against bacterial strains

- causing food poisoning diseases, *Saudi J. Biol. Sci.* 25(2018), 361–366.
19. W. O. Oduro, F. Addo-Yobo, Enhancing the value of indigo-blue dyes from *Lonchocarpus cyanescens* leaves, *Inter. J. Appl. Sci. Technol.* 3(2013), 78-86.
 20. S. Wahyuningsih, A. H. Ramelan, D. K. Wardani, F. N. Aini, P. L. Sari, B. P. N. Tamtama, Y. R. Kristiawan, Indigo dye derived from *Indigofera tinctoria* as natural food colorant, *IOP Conf. Ser. Mater. Sci. Eng.* 193(2017), 012048.
 21. A. Sen, A. Bhowal, S. Datta, Comparison of dyeing of polyester fibers with natural dye and bio-Mordant, *Prog. Color Colorant Coat.* 11(2018), 165–172.
 22. K. Elnagar, T. Abou Elmaaty, S. Raouf, Dyeing of polyester and polyamide synthetic fabrics with natural dyes using ecofriendly technique, *J. Text.* 2014(2014), 1–8.
 23. M. A. Rahman Bhuiyan, A. Ali, A. Islam, M. A. Hannan, S. M. Fijul Kabir, M. N. Islam, Coloration of polyester fiber with natural dye henna (*Lawsonia inermis* L.) without using mordant: a new approach towards a cleaner production, *Fash. Text.* 5(2018), 2–11.
 24. R. A. Arain, F. Ahmad, Z. khatri, M.H. Peerzada, Microwave assisted henna organic dyeing of polyester fabric: a green, economical and energy proficient substitute, *Nat. Prod. Res.* (2019), 1–4.
 25. M. T. Abate, A. Ferri, J. Guan, G. Chen, V. Nierstrasz, Colouration and bio-activation of polyester fabric with curcumin in supercritical CO₂: Part I - Investigating colouration properties, *J. Supercrit. Fluids.* 152(2019), 104548.
 26. S. Shahidi, M. Ghoranneviss, J. Wiener, Improving synthetic and natural dyeability of polyester fabrics by dielectric barrier discharge, *J. Plast. Film Sheeting.* 31(2015), 286–308.
 27. M. H. Zohdy, Cationization and gamma irradiation effects on the dyeability of polyester fabric towards disperse dyes, *Radiat. Phys. Chem.* 73(2005), 101–110.
 28. A. Haji, Dyeing of cotton fabric with natural dyes improved by mordants and plasma treatment, *Prog. Color Colorant Coat.* 12(2019), 191–201.
 29. M. Sadeghi-Kiakhani, S. Safapour, Y. Golpazir-Sorkheh, Impact of chitosan-poly(amidoamine) dendrimer hybrid treatment on dyeing and color fastness properties of wool yarn with madder natural dye, *Prog. Color Colorant Coat.* 12(2019), 241–250.
 30. A. Kerkeni, D. Gupta, A. Perwuelz, N. Behary, Chemical grafting of curcumin at polyethylene terephthalate woven fabric surface using a prior surface activation with ultraviolet excimer lamp, *J. Appl. Polym. Sci.* 120(2011), 1583–1590.
 31. S. Adeel, S. Shahid, S. G. Khan, F. Rehman, M. Muneer, M. Zuber, N. Akhtar, Eco-Friendly disperse dyeing of ultraviolet-treated polyester fabric using disperse yellow 211, *Polish J. Environ. Stud.* 27(2018), 1935–1939.
 32. S. Adeel, T. Gulzar, M. Azeem, Fazal-ur-Rehman, M. Saeed, I. Hanif, N. Iqbal, Appraisal of marigold flower based lutein as natural colourant for textile dyeing under the influence of gamma radiations, *Radiat. Phys. Chem.* 130(2017), 35–39.
 33. E. Yi, J.Y. Cho, Color analysis of natural colorant-dyed fabrics, *Color Res. Appl.* 33(2008), 148–157.
 34. ISO Technical Manual, Geneva, Switzerland, 2006.
 35. AS/NZS. AS/NZS 4399, Sun protective clothing - Evaluation and classification, (1996).
 36. AATCC Technical Manual; Res. Triangle Park. NC, USA. (2007).
 37. U. S. Sharma, A. Kumar, In vitro antioxidant activity of *Rubus ellipticus* fruits, *J. Adv. Pharm. Technol. Res.* 2(2011), 47–50.
 38. S. Naz, R. Siddiqi, S. Ahmad, S.A. Rasool, S.A. Sayeed, Antibacterial activity directed isolation of compounds from *punica granatum*, *J. Food Sci.* 72(2007), M341–M345.

How to cite this article:

S. Tambi, A. Mangal, N. Singh, J. Sheikh, Cleaner Production of Dyed and Functional Polyester Using Natural dyes vis-a-vis Exploration of Secondary Shades., *Prog. Color Colorants Coat.*, 14 (2021), 121-128.



DURABLE MULTIFUNCTIONAL FINISHING OF COTTON
USING β -CYCLODEXTRIN-GRAFTED CHITOSAN AND LEMONGRASS
(*CYMBOPOGON CITRATUS*) OIL

NAGENDER SINGH,* SAMINATHAN RATNAPANDIAN** and JAVED SHEIKH*

*Department of Textile Technology, Indian Institute of Technology, New Delhi, India

**Ethiopian Institute of Textile and Fashion Technology (EiTEX), Bahir Dar University, Ethiopia

✉ Corresponding author: N. Singh, jangra.nagender@gmail.com

Received June 29, 2020

Multifunctional finishing of textiles enhances the value of products by adding desired biological and functional properties. The purpose of this study was to extract essential oil from lemongrass and apply the extracted oil to traditional cotton fabric as finishing. Lemongrass oleoresin was obtained by extracting fresh blades of lemongrass for 16 h using a Soxhlet extractor, employing n-hexane as solvent, by the AATCC Method 30-25. The pad-dry technique was applied to impart fragrance to cotton fabric by using a finishing formulation containing lemongrass oil and β -cyclodextrin-grafted chitosan. The ester bond formation between β -cyclodextrin-grafted chitosan and cellulose was confirmed by FTIR spectroscopy (FTIR). After finishing, the fragrance release rate was evaluated by UV-visible spectroscopy. The fragrance release rate of the finished fabric was found to be durable up to 18 washing cycles and the fabric presented excellent antibacterial property and antioxidant activity. Standard test methods were used to evaluate the physical properties of the treated fabric.

Keywords: cotton fabric, lemongrass oil, fragrance, antibacterial property, β -cyclodextrin

INTRODUCTION

The surface modification of constituent fibres can modify the properties of fabrics and impart various desirable functionalities. Among all the available finishes, the application of fragrance or aroma is highly beneficial to enhance the aesthetic and hygienic value of textile materials. Various methods have been reported to impart such functional properties effectively and to control fragrance release during the use, achieving improved durability towards repeated washing.¹⁻³

Lemongrass (*Cymbopogon citratus*) is a tall perennial aromatic grass that contains essential oil with subtle lemon flavour. It is a genus of almost 55 species of grasses, grown in subtropical and tropical countries, being native to warm temperature regions.⁴ Citral is a biologically active agent of lemongrass, found in contents of 75% by weight in lemongrass essential oil.⁵ Lemongrass serves primarily for decorating houses, but is also used in indigenous medicine. Lemongrass tea helps to cure the central nervous system and is widely consumed in India.⁶ Also,

the essential oil of lemongrass has been used to treat several diseases, and health conditions, such as oily skin, acne, flatulence, scabies, excess perspiration, as well as an antimicrobial, antiviral, antifungal and aroma agents.⁷ Additionally, people have utilized it to impart temporary perfume to their clothes.⁸ Netella fabric is an open structure of 100% cotton fabric used in the form of a scarf by Ethiopian men and women during auspicious occasions.^{9,10} Cotton as a cellulosic material is more susceptible to the attack of bacterial colonies, which may cause an unpleasant smell in the cotton fabric. Therefore, it would be interesting to investigate the possibility of eliminating the above-mentioned issue by finishing the cotton fabric with suitable functional agents.

β -Cyclodextrins (β -CDs) are cyclic oligosaccharides consisting of 7 glucose units, which are linked by a subunit of α -(1,4) glucopyranose, having a hydrophobic inner ring and a hydrophilic outer ring. Inclusion complexes

with CDs can significantly increase the aqueous solubility of poorly soluble compound drugs, and thus improve the stability of fragile compounds, as well as aid in controlled release.¹¹ The cyclodextrins have various applications in the textile industry, starting from finishing to filtration, and other applications, such as UV protection, fragrance finishing, insecticide delivery, and antibacterial finishes.¹² Chitosan is a natural polysaccharide of N-acetyl-D-glucosamine and is prepared by N-deacetylation of chitin. It is biocompatible, non-toxic, mucoadhesive and antimicrobial, hence it has several applications in the pharmaceutical sector.¹³ According to Singh *et al.*, different techniques can be employed for fragrance finishing of textiles with the help of β -CDs. The β -CD-grafted chitosan finished cotton is a more desirable substitute for typical finishing.¹⁴ Several research works have reported the microencapsulation of lemongrass into β -cyclodextrins, with phenomenal results.¹⁵⁻¹⁸ Phunpee *et al.* studied the influence of spray drying on encapsulation of lemongrass into β -cyclodextrins. They identified the controlled release activity of the capsules.¹⁹ Scacchetti *et al.* developed cotton fabrics with antimicrobial activity and thermoregulation by the encapsulation of mPCM and thyme oil in MCT- β -CD. The obtained cotton fabric offers protection against dermatophytosis and prevention to various infections.²⁰

In the present work, essential oil was extracted from lemongrass by utilizing a Soxhlet extractor. The extracted oil was loaded onto β -cyclodextrin-grafted chitosan to finish cotton fabric by the pad-dry-cure method. The effect of such finishing on the physical properties of cotton fabric was also studied. The novelty of this work consists in obtaining multifunctional cotton fabric. The durability of the finish was attained by the use of β -cyclodextrins. All the chemicals used in this research were eco-friendly, non-toxic and biocompatible.

EXPERIMENTAL

Materials and methods

100% cotton fabric was procured from a local market in Bahir Dar, Ethiopia. The specifications of the fabric are listed in Table 1. β -Cyclodextrin and chitosan were obtained from SDFCL Fine-Chem Limited Mumbai, India. All the laboratory-grade chemicals, such as acetic acid, citric acid, ethanol,

methanol and n-hexane, were purchased from Addis Ababa, Ethiopia.

Essential oil extraction

Sample preparation

Lemongrass (*Cymbopogon citratus*) stems were collected from Lake Tana, which is the source of the Blue Nile and is the largest lake in Ethiopia. Before extraction, the lemongrass stems were cut to 2 mm and dried at 40 °C temperature for 12 h. After drying, the sample was placed in an air-tight bag.

Oil extraction

A Soxhlet extractor was used to extract the essential oil from dried lemongrass by utilizing n-hexane as solvent, for 16 h, by following the AATCC Method 30-25 (AATCC International, 2000).²¹

β -Cyclodextrin grafting to chitosan

The β -cyclodextrin-grafted chitosan was prepared according to the process explained by El-Tahlawy *et al.*²² β -CD citrate with a concentration of 0.54 g was added to a chitosan solution with a concentration of 0.6 g dissolved in formic acid (0.4 mL/1 g chitosan) using a M:L of 1:15. The reaction was performed at 100 °C for 3 h under magnetic stirring. Finally, 100 mL of NaOH solution (0.2 N) was added to the precipitated reaction product. The unreacted β -CD citrate was removed from the sample by washing with distilled water. The β -cyclodextrin-grafted chitosan was characterized using FTIR spectroscopy.

Calibration and optimization of lemongrass oil

A UV-visible spectrophotometer was utilized to calibrate the lemongrass oil for fragrance analysis by measuring the absorbance of various concentrations (1-10%) in 100% ethanol at $\lambda_{\text{max}} = 272$ nm. A plotted calibration curve was used to detect the unknown fragrance concentration in the solution. The optimization of oil concentration was done by measuring the absorbance of removed lemongrass oil from the finished cotton sample at different time ranging from 2 h to 24 h.

Fabric treatment

The fabric sample was immersed in a bath solution with 9% (w/w) β -cyclodextrin-grafted chitosan, followed by padding to obtain a wet pickup of 80%, then drying for 2 min at 80 °C and curing at 150 °C for 3 min. The unreacted β -cyclodextrin-grafted chitosan was washed out from the cured cotton fabric, and the fabric was further dried at room temperature.²³

The fabric sample finished with β -cyclodextrin-grafted chitosan was immersed into a 7% lemongrass concentrated solution in 80% ethanol and dried at 80 °C for 5 min. Then, the fragrance retention rate on the finished sample was examined by using a UV-visible spectrophotometer.

Testing methods

A Perkin-Elmer Lambda 25 UV-Visible Spectrophotometer (EiTEX Laboratory, Bahir Dar University, Ethiopia) was used to ascertain the absorbency index of lemongrass oil and the fragrance release rates quantitatively. A Spectrum Two FTIR Spectrometer by Perkin-Elmer (EiTEX Laboratory, Bahir Dar University, Ethiopia) was used to

characterize the β -CD citrate and β -cyclodextrin-grafted chitosan. The agar plate method (AATCC 100-2004) was used for determining the antimicrobial activity of the finished cotton fabric.²⁴ The antioxidant activity of the finished fabric was evaluated using 2,2,1-diphenyl-1-picrylhydrazyl (DPPH) radical with methanol as solvent.²⁵

Table 1
Cotton fabric specifications

S. I.	Features	Details
1	Grams, m ²	41
2	Warp count	40s Ne
3	Weft count	30s Ne
4	Ends/inch	36
5	Picks/inch	30

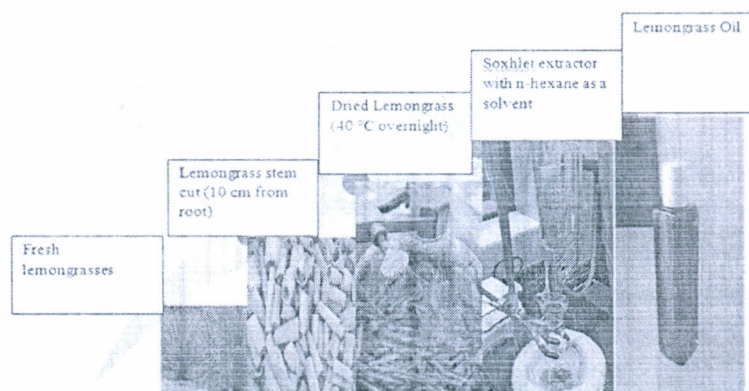


Figure 1: Lemongrass oil extraction process

The durability to laundering was assessed according to ISO 105-C01:1989. Tensile strength testing was evaluated using a Mesdan Lab strength tester as per ISO 13934/1-EN, and drape was measured as per BS 5058:1973. Air permeability testing was carried out using an SDL Atlas M021A Air Permeability Tester following standard ASTM D 3574. Fabric padding was done using padder lab 3399 horizontal padders, with 80% expression and drying at 80 °C for 2 min.

RESULTS AND DISCUSSION

Extraction of lemongrass oil

A Soxhlet extractor was employed to extract oil from fresh lemongrass stems by the AATCC Method 30-25, as shown in Figure 1. The plant material was separated from the extract by encasing it in a paper 'thimble'. When full, the solvent in the thimble siphons off into the main vessel containing the extract, and the process

continues. The amount of oil obtained using the Soxhlet extractor was 10 g per 500 g of dry lemongrass; this gives about a 2% yield of oil per 500 g of dry lemongrass.

Characterization of β -cyclodextrin-grafted chitosan

The β -cyclodextrin-grafted chitosan was characterized using FTIR spectroscopy, and the FTIR spectrum of the synthesized chemical is presented in Figure 2. The observed band at 1715 cm⁻¹ was due to the stretching of the C=O bond of the citrate moieties and the band for N-H stretching was observed at 1657 cm⁻¹ absorption, which confirmed the presence of the acetylated amino groups of chitosan, showing that the sample is not entirely deacetylated.²⁶

FTIR analysis is an appropriate technique to investigate the esterification between β -CD-

grafted chitosan and cotton. The presence of β -CD-grafted chitosan on the finished cotton is illustrated in Figure 3, wherein an additional peak is observed at 1723 cm^{-1} and can be attributed to carbonyl stretching.

The FTIR spectrum of β -CD-grafted chitosan shows the amide bands at $1600\text{--}1700\text{ cm}^{-1}$, which suggests the grafting of β -CD to chitosan by the amidation reaction. These results indicate the evolution of the ester and amide linkage between β -cyclodextrin-grafted chitosan and cotton fabric.

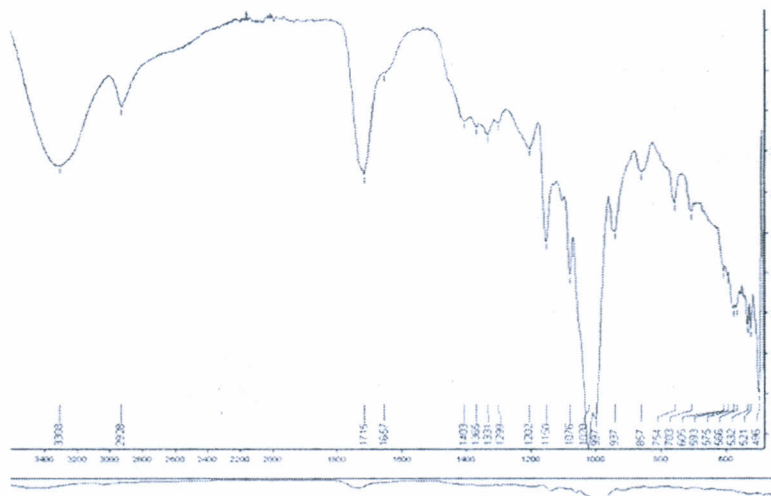


Figure 2: FTIR spectrum of synthesized β -CD-grafted chitosan compound

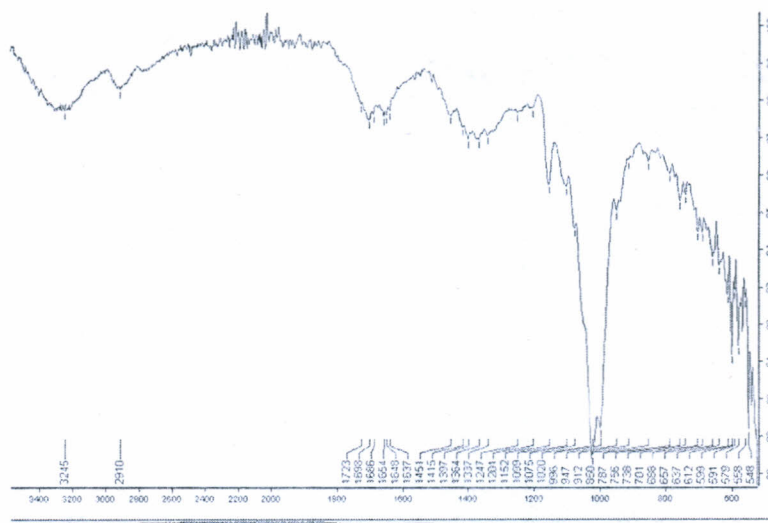


Figure 3: FTIR spectrum of cotton fabric finished with β -CD-grafted chitosan

Lemongrass oil calibration and optimization

The absorbance of different concentrations (1–10%) of lemongrass oil was evaluated against a

blank sample at 272 nm . The concentration versus the absorbance curve showed a straight-line equation (1) as shown in Figure 4.

The slope of the line interpreted from Equation (1) was used to measure the unknown concentration of lemongrass oil in cotton fabric finished with β -CD-grafted chitosan:

$$y = mx + b \quad (1)$$

$$\text{Absorbance} = (\text{Slope} \times \text{Concentration}) + 0 = 0.088 \times \text{Concentration} \quad (2)$$

The optimization of the lemongrass oil concentration was carried out by finishing the cotton fabrics with different concentrations (1-

10%) of the oil alone. Each finished fabric was cut to 2 mm and immersed in 10 mL of 80% ethanol solution to remove the oil from the finished fabrics. After that, the absorbance of the oil ethanol solution was measured using a UV-Visible Spectrophotometer at $\lambda_{\text{max}} = 272$ nm. The same procedure was followed for different times ranging from 0 h to 2 h. The result obtained confirmed the maximum absorbance, after 72 h, for the sample finished with 7% oil (Fig. 5).

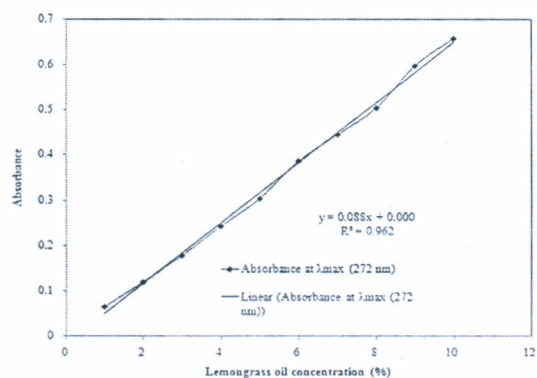


Figure 4: Calibration curve of lemongrass oil

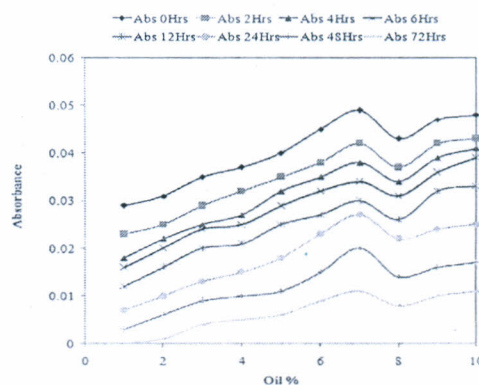


Figure 5: Lemongrass oil concentration optimization curves

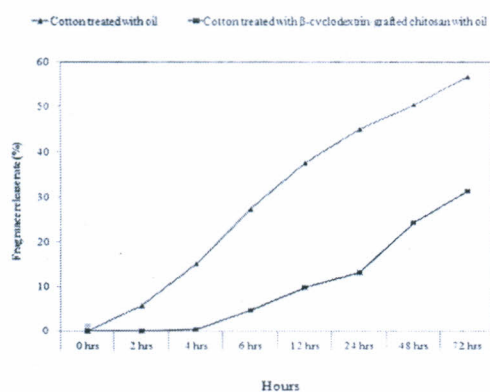


Figure 6: Fragrance release rate

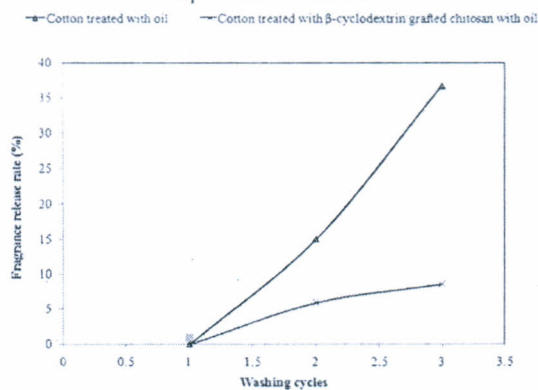


Figure 7: Durability to laundering

Table 2
Functional properties of the fabric finished with β -cyclodextrin-grafted chitosan

Samples	Antibacterial property		Antioxidant property
	Bacterial colony reduction (%)		(%)
	<i>E. coli</i>	<i>S. aureus</i>	
Finished sample	95	98	93

The slope of the line interpreted from Equation (1) was used to measure the unknown concentration of lemongrass oil in cotton fabric finished with β -CD-grafted chitosan:

$$y = mx + b \quad (1)$$

$$\text{Absorbance} = (\text{Slope} \times \text{Concentration}) + 0 = 0.088 \times \text{Concentration} \quad (2)$$

The optimization of the lemongrass oil concentration was carried out by finishing the cotton fabrics with different concentrations (1-

10%) of the oil alone. Each finished fabric was cut to 2 mm and immersed in 10 mL of 80% ethanol solution to remove the oil from the finished fabrics. After that, the absorbance of the oil ethanol solution was measured using a UV-Visible Spectrophotometer at $\lambda_{\text{max}} = 272 \text{ nm}$. The same procedure was followed for different times ranging from 0 h to 2 h. The result obtained confirmed the maximum absorbance, after 72 h, for the sample finished with 7% oil (Fig. 5).

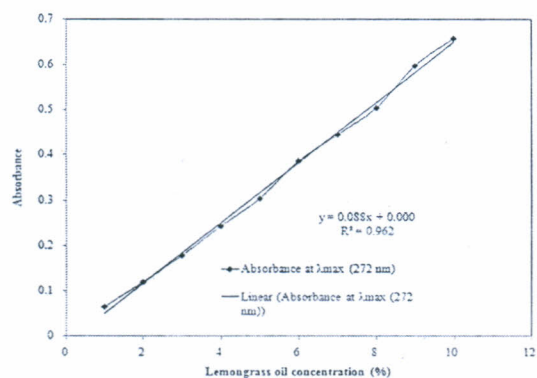


Figure 4: Calibration curve of lemongrass oil

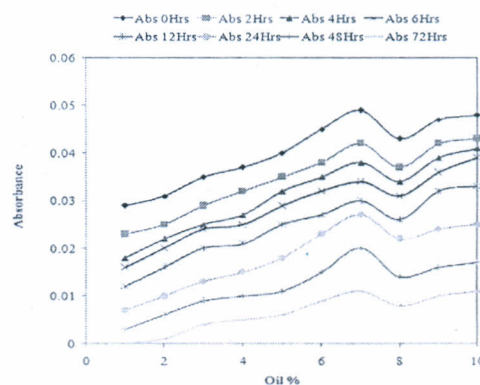


Figure 5: Lemongrass oil concentration optimization curves

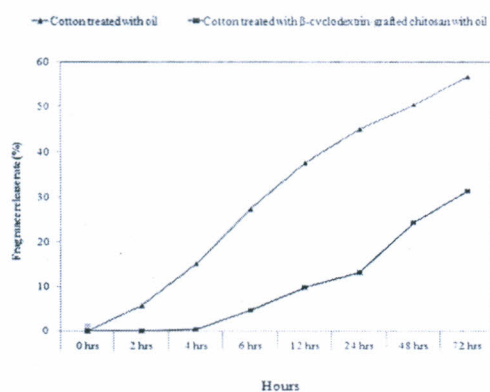


Figure 6: Fragrance release rate

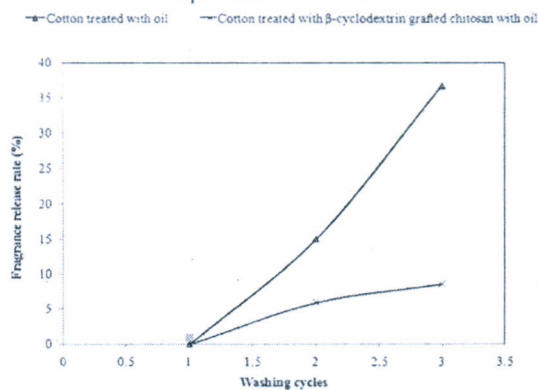


Figure 7: Durability to laundering

Table 2
Functional properties of the fabric finished with β -cyclodextrin-grafted chitosan

Samples	Antibacterial property		Antioxidant property
	Bacterial colony reduction (%)		(%)
	<i>E. coli</i>	<i>S. aureus</i>	
Finished sample	95	98	93

Functional properties of finished fabric

A UV-visible spectrophotometer was used to investigate the fragrance release rate. The cotton fabric finished with β -cyclodextrin-grafted chitosan showed a significant release rate even after 72 h, as compared to that of the fabric treated with oil alone. This long-lasting fragrance release performance may be due to the availability of β -CD cavities, which form an inclusion complex with the oil and are capable of holding oil fragrance for a more extended period. The ester linkages between the fabric and the β -CD might be another reason for the slow release rate, as shown in Figure 6.²⁷

The durability of the fragrance finishing was examined by subjecting the finished cotton to subsequent washing using 5 g/L of detergent solution for 30 min at 60 °C. After each washing cycle, the unknown concentration of oil from the fabric was determined by measuring the absorbance by using the UV-visible spectrophotometer. A significant amount of fragrance was still retained on the fabric, as shown in Figure 7.

The fabric finished with lemongrass oil was also investigated in terms of its antibacterial activity against *E. coli* and *S. aureus*, and the achieved results are tabulated in Table 2. The data in Table 2 indicate an excellent bacterial property of the finished fabric. It was found that *S. aureus* was more sensitive to lemongrass oil than *E. coli*.

The presence of 75% of citral by weight in lemongrass essential oil leads to excellent antibacterial activity against a broad spectrum of bacteria.²⁸ The phenolic constituents of lemongrass interact with the bacterial cell membrane, degrading the membrane and affecting its permeability.²⁹ The presence of chitosan also inhibits the growth of bacteria. Being a cationic polymer, it can be attached to the negative charge of the bacterial cell membrane, which results in leakage of the membrane.³⁰ The finished fabric also showed excellent antioxidant properties. This might be due to the presence of phenolic groups in lemongrass oil. The phenolic content present in lemongrass oil helps in free-radical scavenging.

Fabric performance

Tensile strength

The results of the tensile strength tests are illustrated in Figure 8, demonstrating that the fabric finished with β -cyclodextrin-grafted chitosan exhibits improved tensile strength.

It is interesting to note that the finishing treatments, in general, have detrimental effects on the tensile mechanical properties of cotton fabric. The improvement in strength is modest, but still, it is a significant advantage for the finished fabric. Singh *et al.* have reported similar results; the enhanced strength might be attributed to the plasticizing effect of β -CD citrate on fabric.¹⁴

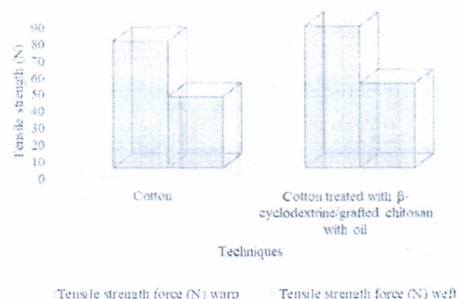


Figure 8: Effect of fragrance finishing treatment on tensile strength of fabric

holding the fragrance on fabric.

Drape

The cotton fabric finished with β -cyclodextrin-grafted chitosan showed a higher drape coefficient, as compared to the unfinished fabric, as shown in Figure 9. This could be explained by the ester linkage formed between the fabric and the β -CD-grafted chitosan component, and probably due to the modified host as a binder for

Air permeability

The air permeability of 4 layers of fabric was examined before and after the finishing treatment. It was found that the air permeability of the fabric decreased slightly after the treatment with β -cyclodextrin-grafted chitosan (Fig. 10). The reason may be attributed to swelling of cotton, which modifies the fabric interstices, its thickness and porosity, leading to a reduction in air

Functional properties of finished fabric

A UV-visible spectrophotometer was used to investigate the fragrance release rate. The cotton fabric finished with β -cyclodextrin-grafted chitosan showed a significant release rate even after 72 h, as compared to that of the fabric treated with oil alone. This long-lasting fragrance release performance may be due to the availability of β -CD cavities, which form an inclusion complex with the oil and are capable of holding oil fragrance for a more extended period. The ester linkages between the fabric and the β -CD might be another reason for the slow release rate, as shown in Figure 6.²⁷

The durability of the fragrance finishing was examined by subjecting the finished cotton to subsequent washing using 5 g/L of detergent solution for 30 min at 60 °C. After each washing cycle, the unknown concentration of oil from the fabric was determined by measuring the absorbance by using the UV-visible spectrophotometer. A significant amount of fragrance was still retained on the fabric, as shown in Figure 7.

The fabric finished with lemongrass oil was also investigated in terms of its antibacterial activity against *E. coli* and *S. aureus*, and the achieved results are tabulated in Table 2. The data in Table 2 indicate an excellent bacterial property of the finished fabric. It was found that *S. aureus* was more sensitive to lemongrass oil than *E. coli*.

The presence of 75% of citral by weight in lemongrass essential oil leads to excellent antibacterial activity against a broad spectrum of bacteria.²⁸ The phenolic constituents of lemongrass interact with the bacterial cell membrane, degrading the membrane and affecting its permeability.²⁹ The presence of chitosan also inhibits the growth of bacteria. Being a cationic polymer, it can be attached to the negative charge of the bacterial cell membrane, which results in leakage of the membrane.³⁰ The finished fabric also showed excellent antioxidant properties. This might be due to the presence of phenolic groups in lemongrass oil. The phenolic content present in lemongrass oil helps in free-radical scavenging.

Fabric performance

Tensile strength

The results of the tensile strength tests are illustrated in Figure 8, demonstrating that the fabric finished with β -cyclodextrin-grafted chitosan exhibits improved tensile strength.

It is interesting to note that the finishing treatments, in general, have detrimental effects on the tensile mechanical properties of cotton fabric. The improvement in strength is modest, but still, it is a significant advantage for the finished fabric. Singh *et al.* have reported similar results; the enhanced strength might be attributed to the plasticizing effect of β -CD citrate on fabric.¹⁴

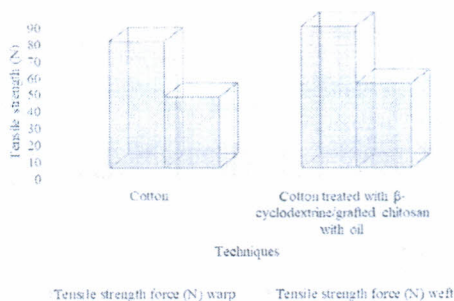


Figure 8: Effect of fragrance finishing treatment on tensile strength of fabric

holding the fragrance on fabric.

Drape

The cotton fabric finished with β -cyclodextrin-grafted chitosan showed a higher drape coefficient, as compared to the unfinished fabric, as shown in Figure 9. This could be explained by the ester linkage formed between the fabric and the β -CD-grafted chitosan component, and probably due to the modified host as a binder for

Air permeability

The air permeability of 4 layers of fabric was examined before and after the finishing treatment. It was found that the air permeability of the fabric decreased slightly after the treatment with β -cyclodextrin-grafted chitosan (Fig. 10). The reason may be attributed to swelling of cotton, which modifies the fabric interstices, its thickness and porosity, leading to a reduction in air

permeability of the cotton fabric.³¹

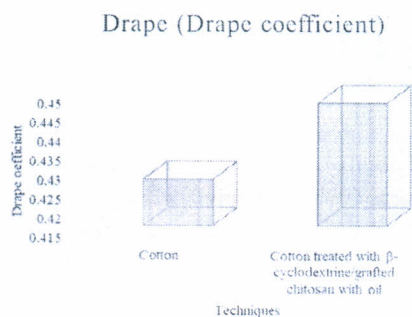


Figure 9: Drape coefficient of control and finished cotton fabric

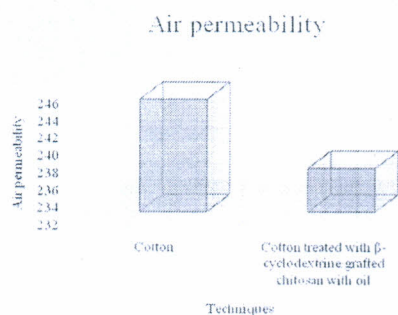


Figure 10: Air permeability of control and finished cotton fabric ($\text{cm}^3/\text{cm}^2/\text{s}$)

CONCLUSION

The novel application of β -CD-grafted chitosan on textile fabric for achieving slow release of volatile oil was successfully performed and investigated. The optimum yield of lemongrass oil obtained was $3.8 \pm 1\%$, by using a Soxhlet extractor, which is a quite significant aspect to explore in a further study. The optimized lemongrass oil concentration for achieving the maximum fragrance from the finished fabric was 7% in 80% ethanol. The results confirmed the significant role of β -CD cavities in the durability of the finish, and also established the ability of β -CDs to store the volatile compound and release it in a controlled manner. Also, the finished fabric exhibited excellent antibacterial activity due to the presence of citral in lemongrass oil and the availability of cationic chitosan. The β -CD-grafted chitosan finished fabric presented improved tensile strength, higher drape coefficient and slightly reduced air permeability, which was not significantly hampering the physical properties of the fabric. It can be concluded that lemongrass oil could be used as part of a finishing treatment to impart fragrance to traditional clothing. Also, the application of β -CD-grafted chitosan in finishing home furnishing textiles and apparel opens up new horizons for unique textile products.

REFERENCES

- H. J. Buschmann, D. Knittel and E. Schollmeyer, *J. Incl. Phenom.*, **40**, 169 (2001), <https://doi.org/10.1023/A:1011892600388>
- F. A. P. Scacchetti and G. M. B. Soares, *Cellulose Chem. Technol.*, **53**, 363 (2019), <https://doi.org/10.35812/CelluloseChemTechnol.2019.53.37>
- S. Sousa, C. Gaiolas, A. P. Costa, C. Baptista and M. E. Amaral, *Cellulose Chem. Technol.*, **50**, 711 (2016), [https://cellulosechemtechnol.ro/pdf/CCT5-6\(2016\)/p.711-719.pdf](https://cellulosechemtechnol.ro/pdf/CCT5-6(2016)/p.711-719.pdf)
- J. Cheel, C. Theoduloz, J. Rodríguez and G. Schmeda-Hirschmann, *J. Agric. Food Chem.*, **53**, 2511 (2005), <https://doi.org/10.1021/jf0479766>
- H. K. P. Ha, J. Maridable, P. Gaspillo, M. Hasika, R. Malaluan *et al.*, formerly *Philippine Agriculturist*, **91**, 36 (2008), <https://agris.fao.org/agris-search/search.do?recordID=PH2009000163>
- B. T. Schaneberg and I. A. Khan, *J. Agric. Food Chem.*, **50**, 1345 (2002), <https://doi.org/10.1021/jf011078h>
- N. Perry and E. Perry, *CNS Drugs*, **20**, 257 (2006), <https://doi.org/10.2165/00023210-200620040-00001>
- B. Taye, M. Giday, A. Anmut and J. Seid, *Asian Pac. J. Trop. Biomed.*, **1**, 370 (2011), [https://doi.org/10.1016/S2221-1691\(11\)60082-8](https://doi.org/10.1016/S2221-1691(11)60082-8)
- M. D. Balakumaran, R. Ramachandran, S. Jagadeeswari and P. T. Kalaichelvan, *Int. Biodeter. Biodegrad.*, **107**, 48 (2016), <https://doi.org/10.1016/j.ibiod.2015.11.011>
- Y. L. Lam, C. W. Kan and C. W. M. Yuen, *Text. Prog.*, **44**, 175 (2012), <https://doi.org/10.1080/00405167.2012.735517>
- J. Szejtli, *Pure Appl. Chem.*, **76**, 1825 (2004), <https://doi.org/10.1351/pac200476101825>
- N. Singh and O. Sahu, in "The Impact and Prospects of Green Chemistry for Textile Technology", edited by Shahid-ul-Islam and B. S. Butola, Elsevier, 2019, p. 83, <https://doi.org/10.1016/B978-0-08-102491-1.00004-6>
- M. F. I. Sharkawy, T. Shoeib, A. E. Rodrigues and M. F. F. Barreiro, Patent WO2018183150 (A1) (2018), <https://patents.google.com/patent/US20200315168A1/en>
- N. Singh, M. Yadav, S. Khanna and O. Sahu, *Sustain. Chem. Pharm.*, **5**, 22 (2017), <https://doi.org/10.1016/j.scp.2017.01.003>
- W. Krasaekoopt and A. Jongyin, *Br. Food J.*, **119**, 2240 (2017), <https://doi.org/10.1108/BFJ-10-2016->

0510

- ¹⁶ F. Maestá Bezerra, Ó. García Carmona, C. García Carmona, A. M. Souza Plath, and M. Lis, *Process Biochem.*, **77**, 151 (2019), <https://doi.org/10.1016/j.procbio.2018.11.018>
- ¹⁷ I. Mourtzinou, F. Salta, K. Yannakopoulou, A. Chiou and V. T. Karathanos, *J. Agric. Food Chem.*, **55**, 8088 (2007), <https://doi.org/10.1021/jf0709698>
- ¹⁸ J. Castro-Rosas, C. R. Ferreira-Grosso, C. A. Gómez-Aldapa, E. Rangel-Vargas, M. L. Rodríguez-Marín *et al.*, *Food Res. Int.*, **102**, 575 (2017), <https://doi.org/10.1016/j.foodres.2017.09.054>
- ¹⁹ S. Phunpee, U. R. Ruktanonchai, H. Yoshii, S. Assabumrungrat and A. Soottitantawat, *Biosci. Biotechnol. Biochem.*, **81**, 718 (2017), <https://doi.org/10.1080/09168451.2016.1277942>
- ²⁰ F. A. P. Scacchetti, E. Pinto and G. M. B. Soares, *Prog. Org. Coatings*, **107**, 64 (2017), <https://doi.org/10.1016/j.PORGCOAT.2017.03.015>
- ²¹ C. G. Lopresto, F. Petrillo, A. A. Casazza, B. Aliakbarian, P. Perego *et al.*, *Sep. Purif. Technol.*, **137**, 13 (2014), <https://doi.org/10.1016/j.seppur.2014.09.015>
- ²² K. El-Tahlawy, M. A. Gaffar and S. El-Rafie, *Carbohydr. Polym.*, **63**, 385 (2006), <https://doi.org/10.1016/j.carbpol.2005.08.057>
- ²³ W. Sricharussin, C. Sopajaree, T. Maneerung and N. Sangsuriya, *J. Text. Inst.*, **100**, 682 (2009), <https://doi.org/10.1080/00405000802158999>
- ²⁴ S. Saini, A. Gupta, N. Singh and J. Sheikh, *J. Ind. Eng. Chem.*, **82**, 138 (2020), <https://doi.org/10.1016/j.jiec.2019.10.005>
- ²⁵ S. Bhushan, A. Kumar, N. Singh and J. Sheikh, *Int. J. Biol. Macromol.*, **142**, 559 (2020), <https://doi.org/10.1016/j.ijbiomac.2019.09.130>
- ²⁶ M. Song, L. Li, Y. Zhang, K. Chen, H. Wang *et al.*, *React. Funct. Polym.*, **117**, 10 (2017), <https://doi.org/10.1016/j.reactfunctpolym.2017.05.008>
- ²⁷ X. Sun, S. Sui, C. Ference, Y. Zhang, S. Sun *et al.*, *J. Agric. Food Chem.*, **62**, 8914 (2014), <https://doi.org/10.1021/jf5027873>
- ²⁸ B. C. J. De Silva, W.-G. Jung, S. Hossain, S. H. M. P. Wimalasena, H. N. K. S. Pathirana *et al.*, *Lab. Anim. Res.*, **33**, 84 (2017), <https://doi.org/10.5625/lar.2017.33.2.84>
- ²⁹ D. Altiok, E. Altiok and F. Tihminlioglu, *J. Mater. Sci. Mater. Med.*, **21**, 2227 (2010), <https://doi.org/10.1007/s10856-010-4065-x>
- ³⁰ M. Kong, X. G. Chen, K. Xing and H. J. Park, *Int. J. Food Microbiol.*, **144**, 51 (2010), <https://doi.org/10.1016/J.IJFOODMICRO.2010.09.012>
- ³¹ A. Afzal, T. Hussain, M. H. Malik and Z. Javed, *J. Text. Inst.*, **105**, 214 (2014), <https://doi.org/10.1080/00405000.2013.834576>

Not in
List

MICROENCAPSULATION OF DEET & CITRIODIOL OIL BY UTILIZING FUNCTIONAL BIOPOLYMERS: A SUSTAINABLE APPROACH FOR MULTIFUNCTIONAL TEXTILES

Singh N., Sheikh J.

Dept. of Textile Technology, Indian Institute of Technology (I.I.T.) Delhi, New Delhi, India
jangra.nagender@gmail.com

ABSTRACT

The growth in technical textiles resulted in an increased demand for multifunctional textiles. Finishing using microencapsulated products can serve as the vital technique for imparting multiple functionalities to textile materials. The microencapsulation of essential oils in core-shell structure has been investigated for protection by evaporation, odor masking, and controlled release. The N,N-diethyl-meta-toluamide (DEET) and citriodiol oil (CO) have been reported to possess excellent mosquito repellent, antibacterial property. However, the rapid volatility is the limitation of CO and DEET exhibit high level of skin penetration, causing allergic to the skin or toxic encephalopathy in children. As a result, the consumers are demanding an alternative to DEET that contains natural ingredients. Therefore, the objective of this study was to investigate the sustainable approach for developing multifunctional textiles.

The DEET - CO microcapsules were prepared by using chitosan and gelatine as a shell material utilizing the highly sophisticated spray-drying technique. The optimum conditions were 0.75% chitosan in 0.5% acetic acid, 0.75% gelatine, 0.5% each DEET and CO with 0.7% tween 80 emulsifiers in distilled water. The surface morphology of microcapsules was analyzed by scanning electron microscopy (SEM) which confirmed the presence of spherical microcapsules with the diameter in the range of 1 and 5µm. The encapsulation efficiency (EE) and retention determination (RD) of the microcapsules were calculated as > 90% and >70% respectively. The microcapsules were applied on to cotton fabrics by a pad-dry-cure method. The SEM images of finished fabric showed that the microcapsules were not only tightly fixed on the fabric surface but also inserted in the fibers spacing. The mosquito repellency was analyzed by a screen cage test, which showed 90% inhibition of mosquitoes. The finished fabric also displayed an excellent antibacterial property along with superior antioxidant activity. All the functional properties were retained in the satisfactory level after 5 washes. The superior mosquito repellency achieved using DEET - CO microcapsules finish was likely due to the combined effect provided by the different working mechanisms of the two chemicals i.e. blocking of the receptors on the mosquitos' body by DEET and masking the odor of the human body by CO.



Sustainable development of mosquito-repellent, flame-retardant, antibacterial, fragrant and antioxidant linen using microcapsules containing *Thymus vulgaris* oil in in-situ generated chitosan-phosphate

Nagender Singh · Javed Sheikh

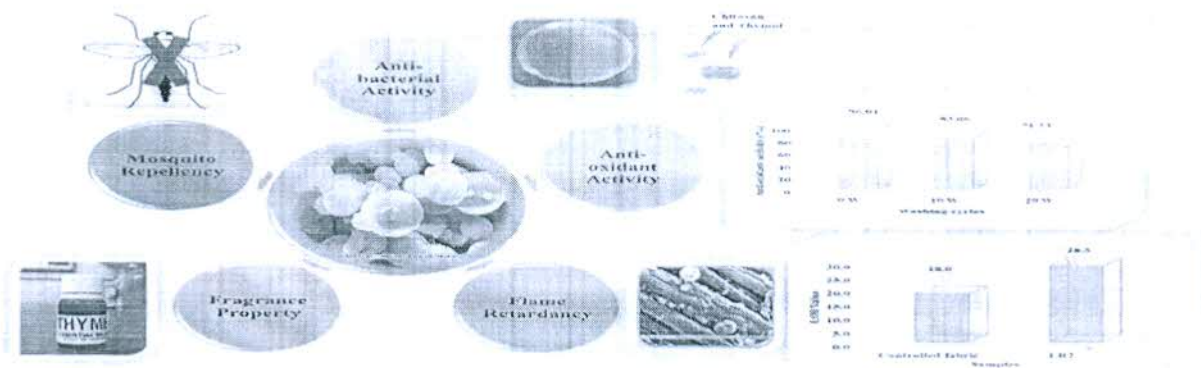
Received: 6 July 2020 / Accepted: 12 December 2020 / Published online: 26 January 2021
© The Author(s), under exclusive licence to Springer Nature B.V. part of Springer Nature 2021

Abstract In the present work, thyme oil embedded functional microcapsules were prepared using in-situ synthesized chitosan phosphate as a shell material through spray drying technique. The encapsulation efficiency (EE %) of microcapsules was determined to investigate the amount of oil entrapped inside the core-shell structure. The prepared microcapsules and finished fabric were characterized using FTIR, EDX, TGA and SEM analysis. The multifunctional properties of finished fabric were investigated using standard

test methods. The finished fabric showed excellent antibacterial property (> 98%), antioxidant activity (96%), flame retardancy (LOI > 28), mosquito repellency (100%) and an excellent fragrance. The functional properties were found durable until at least 20 washes. The structure-property relationship was also confirmed through various characterization techniques.

N. Singh · J. Sheikh (✉)
Department of Textile and Fibre Engineering, Indian
Institute of Technology (I.I.T.), Delhi, India
e-mail: jnsheikh@iitd.ac.in

Graphic abstract



Multifunctional properties of fabric finished with thyme oil loaded microcapsules

Keywords Chitosan · Microencapsulation · Multifunctional linen · Mosquito-repellent · Flame-retardant · Antioxidant

Introduction

In recent time, the textile industry is accelerating towards the development of innovative products, which is bridging the gap between customer demand and supply (Hassan and Sunderland 2015). Functional finishing is one of the most important unit operations in textile processing to develop innovative value-added products (Liu et al. 2019). Since the last decade, textile researcher fraternity is giving more emphasis on the development of multifunctional textile products (Joshi and Bhattacharyya 2011; Li et al. 2017). Multifunctional textile products can offer two or more functional properties such as fragrance, UV protection, antibacterial property, antioxidant activity, mosquito repellency, flame retardancy, anti-static, and thermal regulation property (Miró Specos et al. 2010; Vélchez-Maldonado et al. 2014; Nejman et al. 2014; Miro Specos et al. 2017; Van Tran et al. 2019).

In this context, microencapsulation technology is one of the potential techniques, which can offer controlled release system to the active ingredients. Microencapsulation technology involves the entrapment of active ingredient (core materials) into a thin layer of one or more polymers (shell materials) (Ghosh 2006; Nelson 2008). Several studies reported the development of multifunctional textiles using microencapsulation techniques (Tong 2016;

Janarthanan and Senthil Kumar 2017; Scacchetti et al. 2017). The current research trends show the effectiveness of essential oils as a core component for the functional finishing of textiles (Muthaiyan et al. 2011). The concept of cleaner production in the textile industry includes the utilization of deterrent environmental approaches for the products, processes and services. The adoption of cleaner production in the textile industry introduced the sustainable development of textile using natural resources (Pisitsak et al. 2018; de Oliveira Neto et al. 2019). The eco-friendly functional materials such as essential oils and chitosan can be utilized in the cleaner production of functional textiles. Essential oils are complex mixtures of aromatic components derived from herbaceous plants and their substitutes. Essential oils have a broad antimicrobial and biological activity spectrum because of its complex chemical composition (Burt 2004; Tiwari et al. 2009; Yip and Luk 2016). However, direct application of essential oils on textiles may impart non-durable functional properties because of their volatile nature. The chemical composition of essential oils can change because of volatilization, chemical interaction and oxidation. (Bakry et al. 2016; Sonam Chouhan 2017). Therefore, encapsulation of essential oil is beneficial, which can delay the degradation during storage/processing and manage the delivery system of capsules (Beirão-da-Costa et al. 2013; Bakry et al. 2016).

Thyme (*Thymus vulgaris*) is a known source of essential oils, and it is commonly used as a phyto-genic feed additive. Thyme oil is used extensively in the food and flavour industries as well as fragrance and beauty care products. The presence of thymol,

cinnamaldehyde, carvacrol, eugenol, and geraniol is primarily responsible for its antimicrobial and antioxidant properties (Šipailienė et al. 2006; Navarrete et al. 2010). Carvacrol and thymol are utilized as pharmaceutical compounds in creams, soaps and mouthwashes (Šipailienė et al. 2006). Burt et al. confirmed the presence of thymol and carvacrol, λ -terpinene and p-cymene in thyme oil; however, only thymol and carvacrol showed required bactericidal and bacteriostatic characteristics (Altiok et al. 2010; Burt et al. 2005). Thymol could have important impacts in regulating the inflammatory process in diseases, which are needed for adequate wound healing (Braga et al. 2006).

Chitosan is an important biopolymer and proved to be biodegradable, non-toxic, and biocompatible and antimicrobial. It is a cationic polymer prepared from the alkaline deacetylation of chitin (N-acetylglucosamine polymer) and possesses antimicrobial activity against various bacteria and fungi (Verlee et al. 2017; Ali Raza et al. 2019). Chitosan and its derivatives are used in many industrial applications due to their outstanding physicochemical characteristics and excellent compatibility (Pranoto et al. 2005; Aranaz et al. 2009; Aslam et al. 2020). The film forming property of chitosan along with its slow biodegradation and mechanical strength made it suitable for various applications in pharmaceutical systems and tissue engineering (Le Tien et al. 2003; Raza et al. 2019b; Munim et al. 2020; Ayub et al. 2020). The applications of chitosan in the encapsulation of essential oils have been reported in various studies (Trifković et al. 2014; Hadidi et al. 2020; Raza et al. 2020). Hadidi et al. encapsulated the clove essential oil (CEO) into chitosan nanoparticles and evaluated antioxidant and antibacterial activities of the resultant nanocapsules. An improved antioxidant and antibacterial activities of CEO-loaded chitosan nanoparticles as compared to free CEO were confirmed (Hadidi et al. 2020). Trifković et al. prepared chitosan microbeads by emulsion techniques and simultaneously loaded them with thyme polyphenols by diffusion from an external *thymus serpyllum* L. aqueous solution (Trifković et al. 2014). Different additives have been utilized to impart specific functional properties to textiles. The flame-retardant property can be achieved by using functional additives with chitosan (Wang et al. 2015; Cheng et al. 2019; Li et al. 2020). El-Tahlawy et al. developed an eco-friendly flame-

retardant cotton fabric via application of chitosan phosphate. The phosphorylation of chitosan with diammonium phosphate at higher temperature produces chitosan phosphate, which improves the flame retardancy of cotton fabric through P–N synergy (El-Tahlawy 2008). Li et al. prepared flame-retardant cotton fabric using a bio-based coating of chitosan (CS) and ammonium phytate (AP). The coating was found to impart antibacterial property to the cotton fabric along with an enhancement in its tensile strength (Li et al. 2020).

In this study, the multifunctional linen fabric is developed using *in situ* generated chitosan phosphate microcapsules loaded with thyme oil. The prepared microcapsules and finished linen fabrics were characterized, and the functional properties of finished linen were evaluated. The durability of functional properties against laundering treatments was also analysed. A novel route for durable, multifunctional finishing of linen was studied.

Materials and methods

Materials

The woven 100% linen fabric (EPI-72, PPI-68, and GSM-135) was used in this research. Thyme oil (TO) was supplied by Jain Super Store, New Delhi, India. Chitosan (5–20 mPa.s and Low molecular weight with 85% degree of deacetylation) and all other laboratory grade chemicals were brought from Merck Specialties Pvt. Ltd. (India).

Methods

Microencapsulation process

Optimization of emulsion concentration: Box-Behnken design of experiment was used to optimize the chitosan, TO, and DAP concentrations to achieve maximum microencapsulation yield and encapsulation efficiency. Table 1 shows the Box-Behnken design variables (Chitosan, TO, DAP and Tween 80).

The emulsion was prepared by dissolving chitosan (shell material) in 1% acetic acid and stirring at 60 °C with 800 rpm speed, followed by the addition of Thyme oil (core material), Tween 80 and

Table 1 Box-Behnken design variables with emulsion viscosity

Run	Chitosan (%)	TO (%)	DAP (%)	Tween 80 (%)	Viscosity (cP)
1	0.5	0.5	10	0.25	12
2	1	0.5	6.25	0.25	16
3	1	0.5	6.25	0.25	16
4	0.5	0.25	6.25	0.25	12
5	1.5	0.5	10	0.25	20
6	1	0.25	10	0.25	16
7	1	0.5	6.25	0.25	16
8	1	0.25	2.5	0.25	16
9	1	0.5	6.25	0.25	16
10	0.5	0.75	6.25	0.25	12
11	1	0.5	6.25	0.25	16
12	1	0.75	10	0.25	16
13	1.5	0.5	2.5	0.25	20
14	1.5	0.75	6.25	0.25	20
15	1.5	0.25	6.25	0.25	20
16	0.5	0.5	2.5	0.25	12
17	1	0.75	2.5	0.25	16

diammonium phosphate to the chitosan solution. The emulsion was homogenized at 1200 rpm for 10 min. The viscosity of emulsion was measured using a viscometer (Brookfield DV-II+Pro Viscometer, Canada) using spindle speed of 100 rpm (spindle number 3) to ensure the desirable viscosity (lower viscosity for spray-drying) (Li et al. 2013). A highly accurate spray dryer (Technosearch Instruments, India) was used for the preparation of microcapsules (Fig. 1).

The process parameters were as follows: air outlet-temperature of 140 °C; air inlet-temperature of 170 °C and an atmospheric pressure of 1.40 kg/cm². The emulsion feed rate was deliberately kept low, i.e., 3 ml/min to ensure the formation of spherical and smaller microcapsules. The dry microcapsules were collected from the cyclone units of the spray dryer and stored in airtight sealed packages at room temperature.

Encapsulation efficiency The amount of oil entrapped inside the chitosan shell was determined

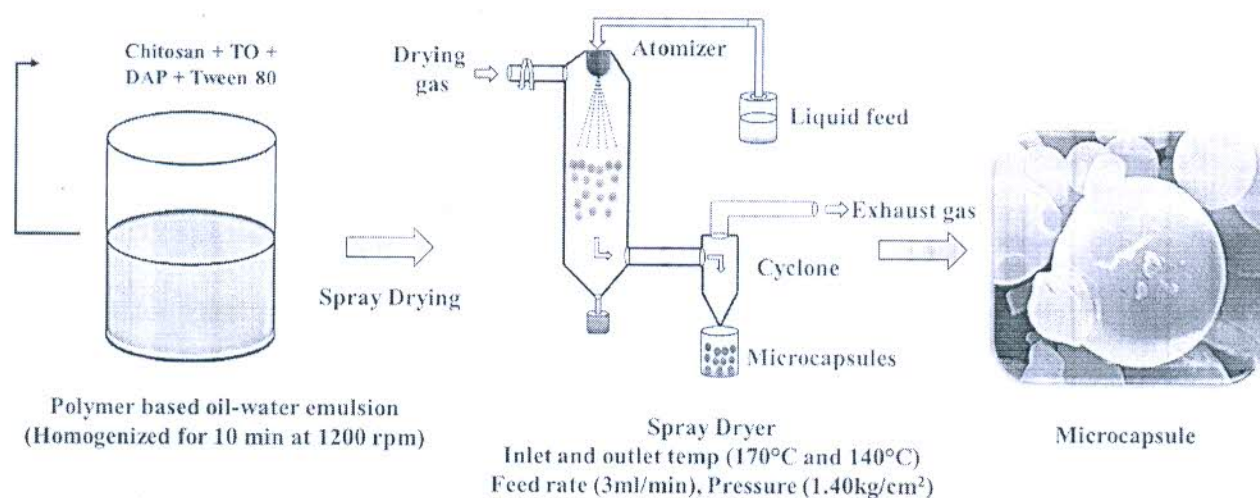


Fig. 1 Schematic diagram of the microencapsulation process

as encapsulation efficiency (EE) and was calculated by using the equation:

$$EE(\%) = \frac{\text{Total oil content} - \text{Surface oil content}}{\text{Total oil content}} \times 100$$

The microcapsules (1 g) were dissolved in 10 ml of aq. acetic acid (1%) in a 50 ml centrifuge tube by stirring at 600 rpm. The 50 ml of n-hexane was used to extract the thyme oil (TO) from the solution. The total amount of TO in the extract was determined by measuring the absorbance at 289.5 nm using UV spectrophotometer (UV-2450 Shimadzu, Japan). The microcapsules (1 g) were suspended in ethanol for 5 min. Then, the absorbance of ethanol was measured at 287 nm using a UV spectrophotometer (UV-2450 Shimadzu, Japan) to determine the surface oil content.

Finishing treatment

The finishing dispersion was prepared by adding microcapsules (100gpl), and acrylic binder (30gpl), which was stirred at 800 rpm for 5 min. The prepared dispersion was then used to finish the linen fabrics (LR2, LR4, LR5, LR14) by the pad (Pressure 1.5 kg/m², 75±2% expression)-dry (80 °C for 5 min) method (Fig. 2).

Characterization of microcapsules and finished fabrics

The morphology of microcapsules was studied using ultramicrotome instrument and SEM analysis (Zeiss EVO 18 Special, Germany). The microscopic images of the finished and burnt samples were recorded by SEM. The elemental analysis of microcapsules and

finished samples was carried out by EDX analysis (Bruker QuanTax 200, Germany). The functional groups of microcapsules on finished linen were identified using ATR-FTIR Spectrometer with 15 scans in the wavelength range 400–4000 cm⁻¹ at 4 cm⁻¹ resolution (Thermo Scientific Nicolet iS50, USA). The thermal stability of the finished sample was studied by thermogravimetric analysis (TGA). The weight loss (%) of controlled and finished fabric was measured while the samples being heated at a uniform rate of 20 °C/min in a nitrogen environment (Perkin Elmer TGA 4000, USA).

Evaluation of functional properties of finished fabrics

The agar plate method was used for determining the antibacterial activity of the finished linen (AATCC TM100-2004). Three judges evaluated the fragrance of finished fabric by sniffing the fabric after scratching an 'x' on the specimen with a plastic stick. The presence of the perfume on the fabric was measured on a "yes and no" scale (Li et al. 2005).

The finished sample's antioxidant property was evaluated using 1, 1-diphenyl-2-picrylhydrazyl (DPPH) as per the procedure available in the literature (Bhushan et al. 2020). Mosquito repellency of the finished fabric against Anopheles mosquitoes was investigated by a cage test method (Barnard et al. 2006). The average of three determinations was calculated and tabulated. The flame retardancy of the finished samples (LR2, LR4, LR5, LR14) was examined by measuring the LOI values as per ASTM D2863 standard. The durability of multifunctional properties of finished fabric towards repeated laundering was tested using standard laundering method (AATCC TM 61-2007).

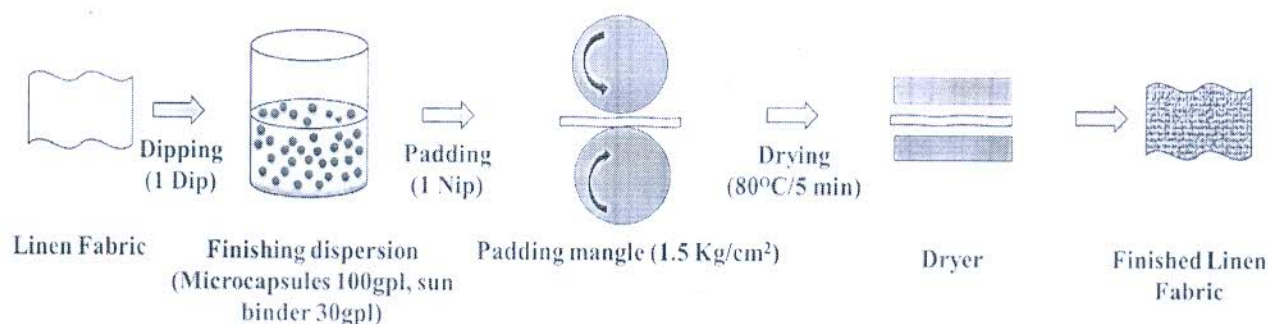


Fig. 2 Schematic diagram of the textile treatment process

Table 2 The EE of microcapsules based on total and surface oil content

Run	Yield (%)	Total oil content (Hexane)		Surface oil content (Ethanol)		EE (%)
		Absorbance at $\lambda 289.5$	Concentration ($\mu\text{l/ml}$)	Absorbance at $\lambda 287$ (5min)	Concentration ($\mu\text{l/ml}$)	
1	51.13	0.425	0.204	0.210	0.058	71.51
2	56.63	0.510	0.338	0.250	0.090	73.47
3	57.45	0.510	0.338	0.250	0.090	73.47
4	53.08	0.424	0.202	0.205	0.054	73.21
5	54.94	0.435	0.220	0.215	0.062	71.76
6	50.52	0.320	0.038	0.150	0.010	72.12
7	59.53	0.510	0.338	0.250	0.090	73.47
8	62.25	0.345	0.077	0.165	0.022	71.00
9	56.25	0.510	0.338	0.250	0.090	73.47
10	56.03	0.520	0.354	0.265	0.102	71.29
11	59.20	0.510	0.338	0.250	0.090	73.47
12	56.92	0.545	0.394	0.270	0.106	73.17
13	60.00	0.485	0.299	0.245	0.086	71.28
14	56.57	0.424	0.203	0.205	0.054	73.27
15	55.64	0.320	0.038	0.150	0.010	72.12
16	60.00	0.410	0.180	0.200	0.050	72.16
17	61.11	0.560	0.417	0.280	0.114	72.80

Results and discussion

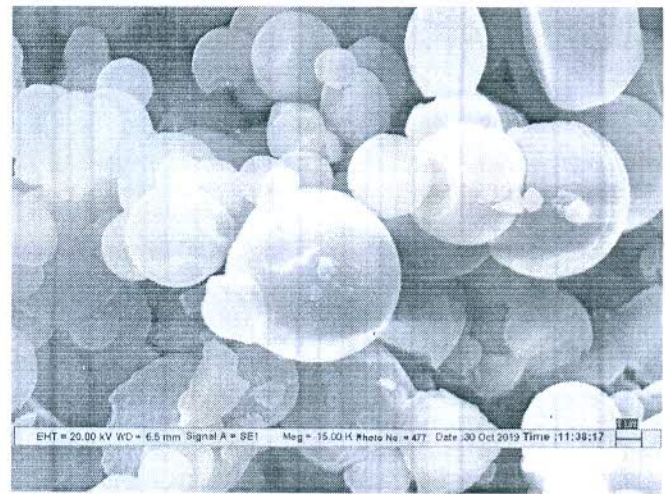
The multifunctional microcapsules were prepared using functional polymer (chitosan), thyme oil and DAP as an additive along with emulsifier. Thyme oil was expected to contribute towards the fragrance, mosquito repellency, antioxidant activity and antibacterial activity. The presence of DAP caused phosphorylation of chitosan, and the resultant chitosan phosphate was expected to provide antibacterial activity and flame retardancy. The resultant microcapsules were thus studied for their efficacy towards the multifunctional finishing of linen. The presence of microcapsules and controlled release of thyme oil from the microcapsules are responsible for the efficient functionalities and the durability of functional effects on the fabric. The durable and efficient multifunctional properties thus confirmed the hypothesis.

Encapsulation efficiency (EE)

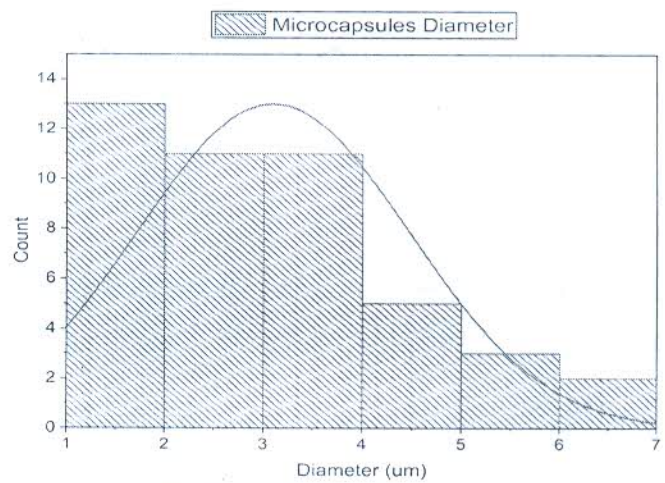
The encapsulation efficiency of microcapsules was measured for all the runs and the results are tabulated in Table 2.

The encapsulation efficiency of microcapsules was more than 71% for all the runs. As shown in Table 2, there were five common runs (2, 3, 7, 9 and 11), which displays the same and maximum encapsulation efficiency (73.47%) as compared to other runs. The reason might be the better compatibility of polymer, oil and additive at this ratio of concentrations. The encapsulation efficiency got reduced when the concentration ratio was varied from a particular (optimum) value. The encapsulation efficiency is dependent on the process parameters, polymer types, additives and the physicochemical properties of EOs and polymers. Therefore, the run numbers 2, 4, 5 and 14 were selected for the further experimental studies.

Fig. 3 a SEM images of TO loaded microcapsules. b The size distribution of microcapsules



(a) SEM images of TO loaded microcapsules



(b) The size distribution of microcapsules

Table 3 The statistical analysis of diameter of microcapsules

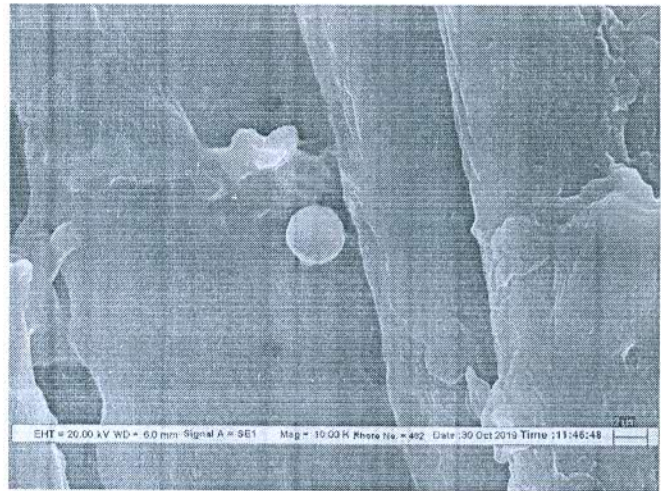
	N total	Mean	SD	Sum	Minimum	Median	Maximum
Diameter (μm)	45	3.09731	1.37157	139.379	1.464	2.824	6.848

Characterization of microcapsules and finished fabric

The microcapsules containing thyme oil and finished fabric (LR2) were characterized by using SEM analysis. The image of microcapsules and their size distribution are shown in Fig. 3a, b. Table 3 represents the statistical analysis of diameters of microcapsules. Figure 4 represents the SEM images of the finished fabric.

As shown in Fig. 3(a), the microcapsules loaded with thyme oil were stable and spherical in shape without agglomeration. The spherical microcapsules were composed of the rough outer surface. The size distribution graph shows that most of the microcapsules fall in a size range from 1 μm to 3 μm (Fig. 3b and Table 3). The above results suggest that the microcapsules prepared using optimized parameters were around 3 μm in size. Figure 4 confirmed the

Fig. 4 The SEM photographs of finished fabric (LR2)



presence of microcapsule on the fabric (LR2). The microcapsules were deposited on the surface of fibres along with the gap between the individual fibres. Thus, this confirms the presence of microcapsules on the fibre surface.

The resin-microcapsules composite was prepared and then chopped in microlayers through ultramicrotome instrument. The chopped microlayers were characterized in SEM analysis to studied the morphology of microcapsules.

As shown in Fig. 5, the microcapsules seem to be porous with a heterogeneous matrix structure.

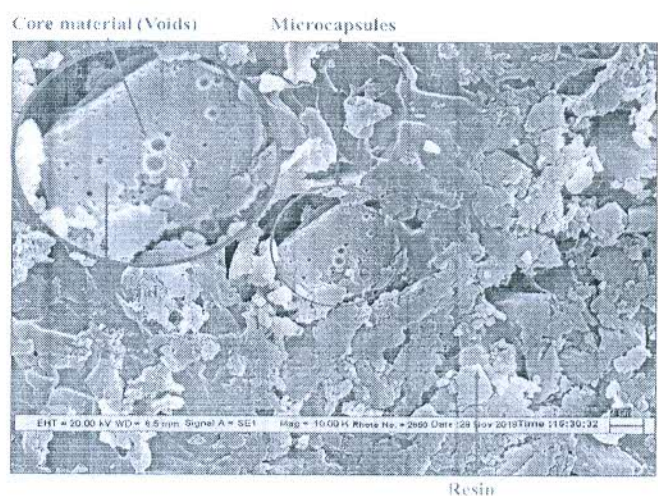
The matrix structure of the microcapsules is dependent on microencapsulation techniques. Here, the microcapsules were prepared by using a spray drying technique. Various research confirmed the matrix structure of microcapsules prepared by spray drying technique (Rosenberg Talmon and Kopelman

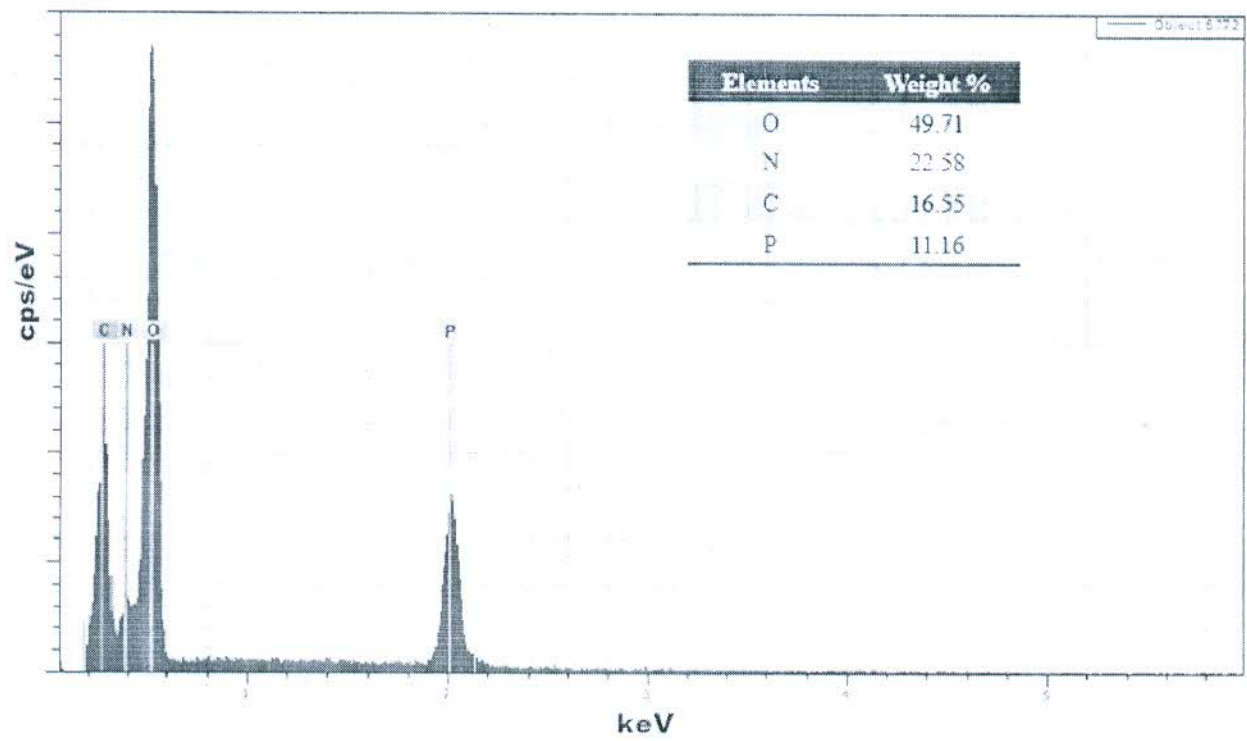
1988; Da Costa et al. 2013). The microcapsules are composed of shell and core materials, which represents the matrix structure. The presence of voids in the chopped microcapsules suggests the presence of cavities in the microcapsules to entrap the oil in the matrix structure.

EDX results of microcapsules loaded with TO and finished fabric are shown in Fig. 6.

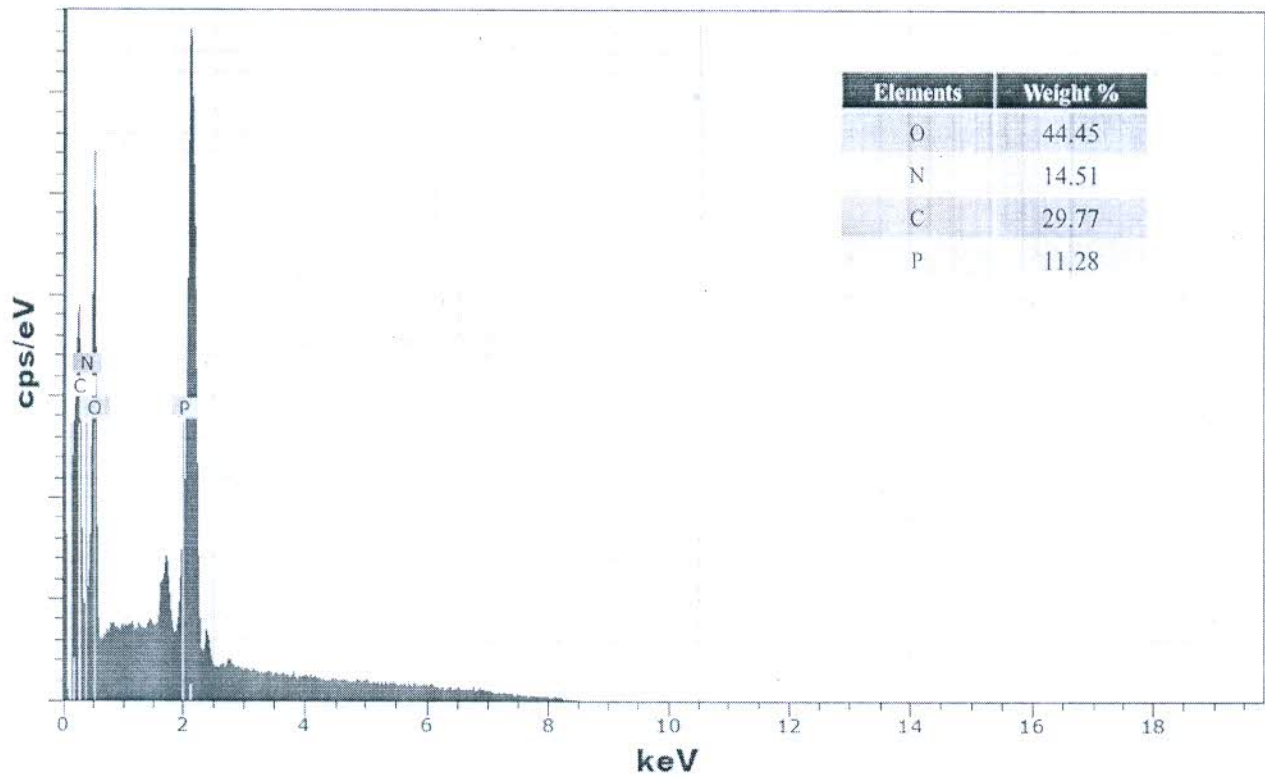
As shown in Fig. 6a, EDX images confirm the presence of phosphorus (11.16%) in the microcapsules. The phosphorylation of chitosan could be the reason behind the presence of phosphorus in the microcapsules. At high temperature (160 °C), phosphoric acid is liberated from diammonium phosphate, which was expected to react with the chitosan that results in the formation of chitosan phosphate (El-Tahlawy 2008). EDX graph shows the availability of nitrogen (22.58%) in the microcapsules, which is due

Fig. 5 The morphology of microcapsules embedded into resin





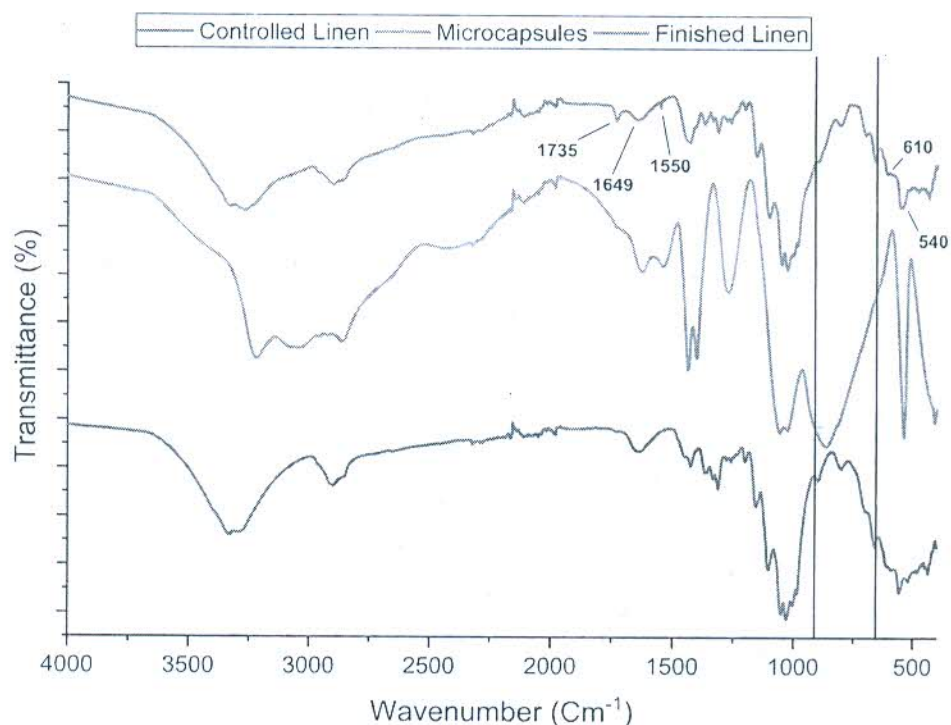
(a) EDX analysis of microcapsules



(b) EDX analysis of finished fabric (LR2)

Fig. 6 a EDX analysis of microcapsules. b EDX analysis of finished fabric (LR2)

Fig. 7 FTIR spectra of the controlled and finished fabric



to the presence of nitrogen-rich chitosan. The presence of phosphorus (11.28%) and nitrogen (14.52%) is also confirmed on finished fabric LR2 (Fig. 6b).

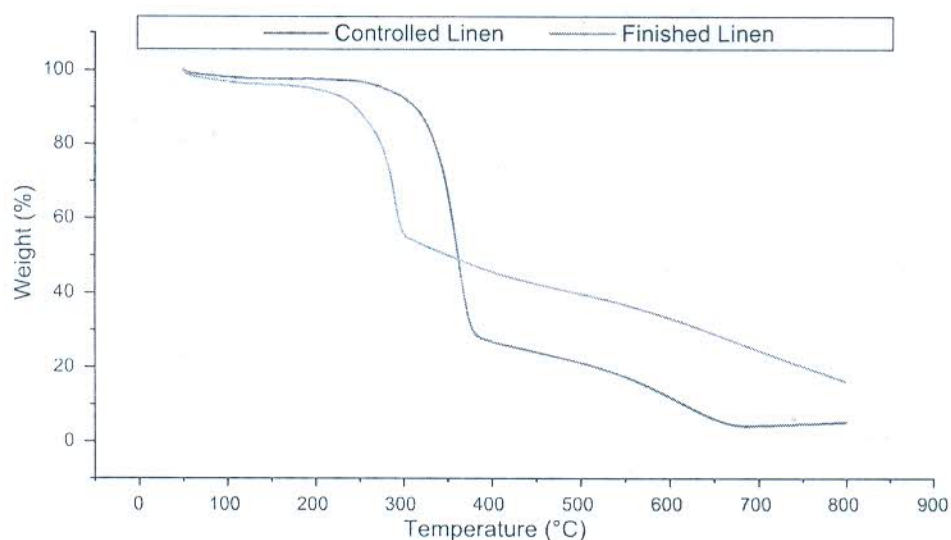
The FTIR spectra of controlled linen, microcapsules and finished fabric (LR2) are shown in Fig. 7.

As illustrated, the FTIR spectrum of the finished fabric showed the introduction of new peaks along with a slight shift in the existing peaks of controlled fabric. The spectrum displayed a moderate shift in transmittance of finished fabric as compared to the controlled fabric. Since microcapsules were chitosan-based, the FTIR spectrum a finished fabric displayed C = O stretching at 1735 cm^{-1} , and the peak at 1649 cm^{-1} suggests the formation of Schiff base between amide I group of chitosan and carbonyl group of bleached linen. The bands at 2800 cm^{-1} to 3350 cm^{-1} suggest the stretching vibration of O–H and N–H bonds. Such peaks may be due to the interactions between molecules of chitosan and TO without the formation of covalent bonds, e.g. electrostatic interactions, hydrogen bonds, and hydrophobic forces. The FTIR spectra of the microcapsule and finished fabric showed a similar peak at 1550 cm^{-1} , which could be attributed to amide II (N–H bending). The peaks at $1030\text{--}1160\text{ cm}^{-1}$ are allocated to the C–O bonds. The FTIR spectrum shows one mode of vibration due to

PO_4^{3-} groups and two weak bands are also detected at 610 cm^{-1} and 545 cm^{-1} , respectively. The broad stretching at $750\text{--}850\text{ cm}^{-1}$ is due to aromatic C–H bending, which represents the presence of thymol and carvacrol in the microcapsules.

Thermal analysis of the controlled and finished fabric (LR2) was carried out to understand the thermal behaviour of fabrics. The TGA thermograms of controlled and finished linen are shown in Fig. 8.

As shown in Fig. 8, the finished fabric shows an initial weight loss from 100 to $150\text{ }^\circ\text{C}$ due to the removal of volatile components. The finished fabric displayed a weight loss (8–12%) from 200 to $260\text{ }^\circ\text{C}$, and then 50% of weight loss has been observed at $300\text{ }^\circ\text{C}$. The finished fabric showed 11% more solid residual char as compared to controlled fabric at $800\text{ }^\circ\text{C}$. The finished fabric displayed the early start of pyrolysis; however, it shows high char formation. The char formation is due to the presence of phosphorus on the finished fabric (Levchik and Weil 2008). The finished fabric contains phosphorus and nitrogen components. Both the components mainly work in condensed phase and can act as intumescent flame retardants, which results in the formation of a char layer (Gao et al. 2006). The TGA analysis also

Fig. 8 TGA graph of controlled and finished linen fabric (LR2)**Table 4** Antibacterial activity, antioxidant activity and fragrance of finished fabric (LR2)

Statistics	Antibacterial property (BCR %)			Antioxidant activity (%)			Fragrance		Mosquito repellency (%)			
	0W	10W	20W	0W	10W	20W	0W	20W	0W	5W	10W	20W
<i>Unfinished fabric</i>												
Average	Nil	Nil	Nil	Nil	Nil	Nil	No	No	Nil	Nil	Nil	Nil
<i>Finished Fabric</i>												
Average	98.93	93.17	81.28	96.01	83.06	71.23	Yes	Yes	100	100	100	90
SD	0.27	0.28	0.25	0.24	0.23	0.23	–	–	0.00	0.00	0.00	0.00
Variance	0.07	0.08	0.06	0.06	0.05	0.05	–	–	0.00	0.00	0.00	0.00
Standard Error	0.15	0.16	0.14	0.14	0.13	0.13	–	–	0.00	0.00	0.00	0.00

*W-wash

*The average of three determinations

confirms the flame-retardant behaviour of finished linen.

Functional properties of finished fabrics

The functional properties, i.e. antibacterial activity against *E. coli*, antioxidant activity and fragrance ratings of finished fabric (LR2) are tabulated in Table 4. Table 4 also shows the mosquito repellency of finished fabric (LR2) against *Anopheles* mosquito. The flame-retardant property of the finished fabric, as indicated by LOI values, is summarized in Table 5.

The results in Table 4 indicate the excellent antibacterial property of the finished fabric. The antibacterial activity is a combined effect of the

presence of thyme oil and chitosan present in the microcapsules. The presence of thymol (32.55%) is responsible for excellent antibacterial properties of thyme oil against a broad range of the bacterial spectrum (Braga et al. 2006; Nagoor Meeran et al. 2017). The hydrophobic phenolic constituents of TO interact with the bacterial cell membrane, which would degrade the membrane and affect its permeability (Altiok et al. 2010). The presence of chitosan is also responsible for the inhibition of the growth of bacteria because of its cationic nature. It can attach to the negative charge of the bacterial cell, which results in leakage of the cell membrane (Kong et al. 2010; Raza et al. 2019a).

Table 5 Flame retardancy of the finished fabric samples

Sample	LOI value			
	Average	SD	Variance	Standard error
Controlled fabric	18.00	0.000	0.000	0.000
LR2	28.50	0.035	0.001	0.020
LR4	28.00	0.055	0.003	0.032
LR5	28.30	0.045	0.002	0.026
LR14	28.25	0.050	0.003	0.029

*Average values of three determinations

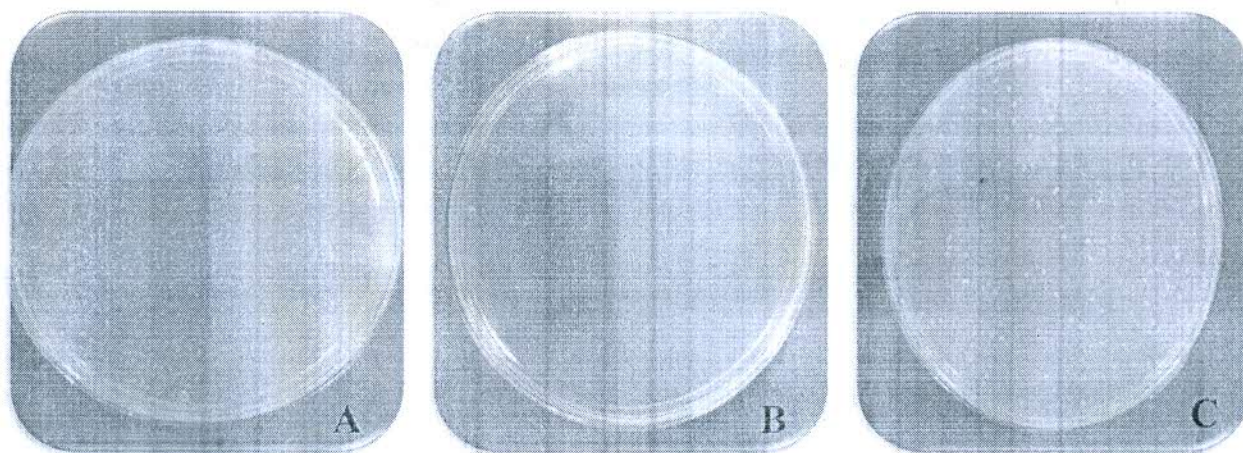


Fig. 9 Pictorial representation of antibacterial properties of finished fabric: **a** Controlled fabric, **b** finished fabric, **c** finished fabric after 10 washes

The finished fabric retained an excellent antibacterial property even after repeated washing (Fig. 9).

This indicates a wash-fast attachment of microcapsules with the linen fabric. The retention of thyme oil in the microcapsules can also be concluded as the samples retained the fragrance of thyme oil after repeated washing treatments.

The finished fabric also showed an excellent antioxidant activity because of the presence of phenolic compounds, mainly thymol and carvacrol, in the thyme oil (Ahtiok et al. 2010). The finished fabric showed potent antioxidant activity even after repeated washing treatments. Various research works confirmed the antioxidant activities of thymol and carvacrol (Schwarz et al. 1996; Lacroix et al. 1997; Talón et al. 2017).

The finished fabric also showed pleasant aroma along with the excellent durability up to 20 washing cycle. There are two probable reasons for the durability of the fragrance. The slow-release mechanism

offered by the matrix structure of microcapsules is the most important reason behind the retention of thyme oil in the microcapsules. The microcapsules loaded with TO can act as a reservoir, which could slowly release the TO through the diffusion process. The use of binder, which forms a film entrapping the microcapsules ensures the retention of microcapsules on linen fabric. The finished fabric also showed pleasant aroma even after prolonged storage.

As shown in Table 4, the finished fabric exhibited an excellent mosquito repellency against *Anopheles* mosquito. The reason could be the presence of TO in the microcapsule. The phenolic constituents of TO attack the nervous system of mosquitoes by reacting with the receptors. That may inhibit their growth and can also lead to the death of the mosquito. Thymol can also block the octopamine receptors of mosquitoes that play an important role in the transmission of signals to the nervous system (Rattan 2010). The attractants for female mosquitoes include carbon

dioxide and lactic acid present in sweat, and the resulting odour is recognized by chemoreceptors present in their antenna (Kröber et al. 2010). However, thyme oils block the lactic acid smell causing inhibition of mosquitoes. The monoterpenes such as thymol, carvacrol, α -terpinene, linalool, and *p*-cymene derived from the TO were proven to be excellent mosquito repellents (Park et al. 2005). The mosquito repellency of the finished fabric was retained in the excellent range even after repeated washing treatments. Thyme oil is the sole contributor to the mosquito repellency of finished fabric, and the durability of mosquito repellency proves the retention of thyme oil due to slow-release, as well as lower oxidation rates of the microencapsulated oil as compared to free oil due to protective shell material. Such a trend was also reported in the literature (Lehn et al. 2018).

The flame retardancy of the finished fabric samples (LR2, LR4, LR5, LR14) was measured using the LOI testing and the results are summarized in Table 5.

The fabrics with LOI > 27 are generally considered as the flame retardant. The finished fabric showed significantly higher LOI values as compared to the controlled sample. The formation of chitosan phosphate during the spray drying at a higher temperature could be the reason for flame retardancy. During heating, diammonium phosphate decomposes into phosphoric acid and ammonia. The ammonia gas was eliminated through the exhaust of spray dryer, while the reaction between chitosan and phosphoric acid results in the formation of chitosan phosphate shell material. As a natural nitrogen source, chitosan acts synergistically with the phosphorus components, which results in P–N synergy and condensed phased mechanism of flame retardancy (Nunthanid et al. 2001). Figure 10 shows the SEM images of controlled and finished linen fabric after burning

As shown in Fig. 10b, the finished fabric finished showed structure-integrity even after burning. However, the controlled fabric showed complete decomposition and did not maintain its structural integrity after burning. Also, the formation of char during burning was visible on the finished fabric. The microcapsules were also seen to retain their structures, which can act as a barrier in the propagation of flame. The results thus confirm the flame-retardant modification of linen using flame-retardant microcapsules.

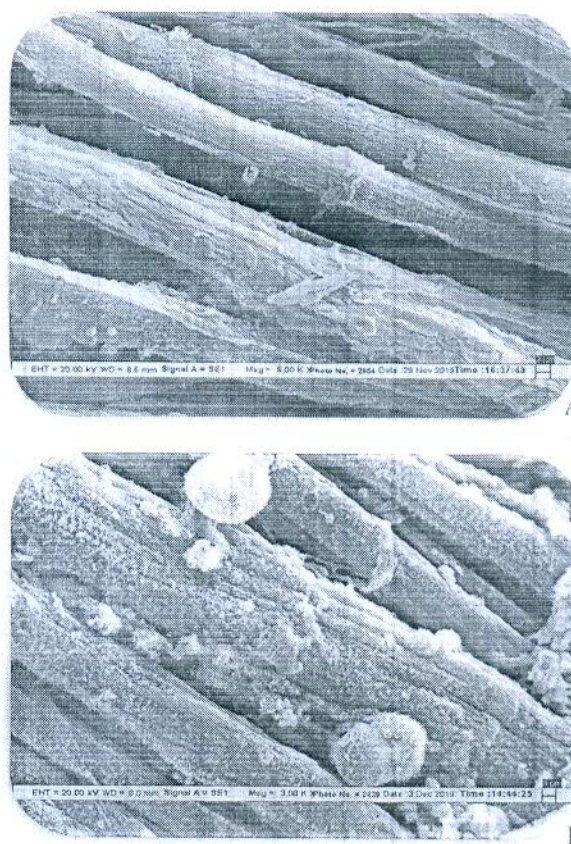


Fig. 10 The SEM images of **a** controlled and **b** finished fabric after burning

Conclusions

The sustainable multifunctional linen was successfully developed by using thyme oil loaded microcapsules. The SEM images confirmed the spherical morphology of the microcapsules. The EDX analysis of microcapsules showed the availability of phosphorus (11.16%) and nitrogen (22.58%), which confirmed the formation of chitosan phosphate during spray drying. The FTIR analysis confirmed the presence of functional groups of chitosan phosphate and thyme oil on the finished fabric. The finished fabric exhibited excellent antibacterial activity against *E. coli* because of the presence of phenolic content of TO and chitosan in microcapsules. Additionally, the finished fabric showed excellent antioxidant activities along with moderate flame retardancy. Furthermore, the finished fabric showed excellent mosquito repellency durable up to 20 washes. The finished fabric also displayed a pleasant aroma durable up to 20 washes. The advanced

protective fabric was thus prepared using sustainable chemicals.

Acknowledgments Authors gratefully acknowledge the research funding received from Science and Engineering Research Board (SERB, file no. ECR/2017/001041), Government of India.

Compliance with ethical standards

Conflict of interest The authors reported no potential conflict of interest.

References

- AATCC TM 61-2007 Test Method for Colorfastness to Laundering: Accelerated. American Association of Textile Chemists Colorists, USA
- AATCC TM100-2004 Test Method for Antibacterial Finishes on Textile Materials. American Association of Textile Chemists Colorists, USA
- Ali Raza Z, Anwar F, Hussain I et al (2019) Fabrication of PLA incorporated chitosan nanoparticles to create enhanced functional properties of cotton fabric. *Pigment Resin Technol* 48:169–177. <https://doi.org/10.1108/PRT-11-2017-0088>
- Altiock D, Altiock E, Tihminlioglu F (2010) Physical, antibacterial and antioxidant properties of chitosan films incorporated with thyme oil for potential wound healing applications. *J Mater Sci Mater Med* 21:2227–2236. <https://doi.org/10.1007/s10856-010-4065-x>
- Aranaz I, Mengibar M, Harris R et al (2009) Functional characterization of chitin and chitosan. *Curr Chem Biol* 3:203–230. <https://doi.org/10.2174/187231309788166415>
- Aslam M, Raza ZA, Siddique A (2020) Fabrication and chemophysical characterization of CuO/chitosan nanocomposite-mediated tricomponent PVA films. *Polym Bull* 77:1–11. <https://doi.org/10.1007/s00289-020-03194-4>
- Ayub A, Raza ZA, Majeed MI et al (2020) Development of sustainable magnetic chitosan biosorbent beads for kinetic remediation of arsenic contaminated water. *Int J Biol Macromol* 163:603–617. <https://doi.org/10.1016/j.ijbiomac.2020.06.287>
- Bakry AM, Abbas S, Ali B et al (2016) Microencapsulation of oils: a comprehensive review of benefits, techniques, and applications. *Compr Rev Food Sci Food Saf* 15:143–182. <https://doi.org/10.1111/1541-4337.12179>
- Barnard D, Bernier U, Xue R, Debboun M (2006) Standard methods for testing mosquito repellents. In: *Insect repellents*. CRC Press, Boca Raton, pp 103–110
- Beirão-da-Costa S, Duarte C, Bourbon AI et al (2013) Inulin potential for encapsulation and controlled delivery of Oregano essential oil. *Food Hydrocoll* 33:199–206. <https://doi.org/10.1016/j.FOODHYD.2013.03.009>
- Bhushan S, Kumar A, Singh N, Sheikh J (2020) Functionalization of wool fabric using lignin biomolecules extracted from groundnut shells. *Int J Biol Macromol* 142:559–563. <https://doi.org/10.1016/j.ijbiomac.2019.09.130>
- Braga PC, Dal Sasso M, Culici M et al (2006) Anti-inflammatory activity of thymol: inhibitory effect on the release of human neutrophil elastase. *Pharmacology* 77:130–136. <https://doi.org/10.1159/000093790>
- Burt S (2004) Essential oils: their antibacterial properties and potential applications in foods—A review. *Int J Food Microbiol* 94:223–253. <https://doi.org/10.1016/J.IJFOODMICRO.2004.03.022>
- Burt SA, Vlieland R, Haagsman HP, Veldhuizen EJA (2005) Increase in activity of essential oil components carvacrol and thymol against *Escherichia coli* O157:H7 by addition of food stabilizers. *J Food Prot* 68:919–926. <https://doi.org/10.4315/0362-028X-68.5.919>
- Cheng XW, Guan JP, Yang XH et al (2019) A bio-resourced phytic acid/chitosan polyelectrolyte complex for the flame retardant treatment of wool fabric. *J Clean Prod* 223:342–349. <https://doi.org/10.1016/j.jclepro.2019.03.157>
- Da Costa JMG, Borges SV, Hijo AACT et al (2013) Matrix structure selection in the microparticles of essential oil oregano produced by spray dryer. *J Microencapsul* 30:717–727. <https://doi.org/10.3109/02652048.2013.778909>
- de Oliveira Neto GC, Ferreira Correia JM, Silva PC et al (2019) Cleaner Production in the textile industry and its relationship to sustainable development goals. *J Clean Prod* 228:1514–1525. <https://doi.org/10.1016/j.jclepro.2019.04.334>
- El-Tahlawy K (2008) Chitosan phosphate: a new way for production of eco-friendly flame-retardant cotton textiles. *J Text Inst* 99:185–191. <https://doi.org/10.1080/00405000701584311>
- Gao F, Tong L, Fang Z (2006) Effect of a novel phosphorous-nitrogen containing intumescent flame retardant on the fire retardancy and the thermal behaviour of poly(butylene terephthalate). *Polym Degrad Stab* 91:1295–1299. <https://doi.org/10.1016/j.polymdegradstab.2005.08.013>
- Ghosh SK (2006) *Functional coatings: by polymer microencapsulation*. Wiley-VCH
- Hadidi M, Pouramin S, Adinepour F et al (2020) Chitosan nanoparticles loaded with clove essential oil: characterization, antioxidant and antibacterial activities. *Carbohydr Polym* 236:116075. <https://doi.org/10.1016/j.carbpol.2020.116075>
- Hassan MM, Sunderland M (2015) Antimicrobial and insect-resist wool fabrics by coating with microencapsulated antimicrobial and insect-resist agents. *Prog Org Coatings* 85:221–229. <https://doi.org/10.1016/J.PORGCOAT.2015.04.016>
- Janarthanan M, Senthil Kumar M (2017) Novel improvement of bioactive microencapsulated textile products using brown seaweed for healthcare applications. *Int J Cloth Sci Technol* 29:200–214. <https://doi.org/10.1108/IJCST-03-2016-0023>
- Joshi M, Bhattacharyya A (2011) Nanotechnology—A new route to high-performance functional textiles. *Text Prog* 43:155–233. <https://doi.org/10.1080/00405167.2011.570027>
- Kong M, Chen XG, Xing K, Park HJ (2010) Antimicrobial properties of chitosan and mode of action: a state of the art

- review. *Int J Food Microbiol* 144:51–63. <https://doi.org/10.1016/j.ijfoodmicro.2010.09.012>
- Kröber T, Kessler S, Frei J et al (2010) An in vitro assay for testing mosquito repellents employing a warm body and carbon dioxide as a behavioral activator. *J Am Mosq Control Assoc* 26:381–386. <https://doi.org/10.2987/10-6044.1>
- Lacroix M, Smoragiewicz W, Pazdernik L et al (1997) Prevention of lipid radiolysis by natural antioxidants from rosemary (*Rosmarinus officinalis* L.) and thyme (*Thymus vulgaris* L.). *Food Res Int* 30:457–462. [https://doi.org/10.1016/S0963-9969\(98\)00002-7](https://doi.org/10.1016/S0963-9969(98)00002-7)
- Le Tien C, Lacroix M, Ispas-Szabo P, Mateescu M-A (2003) N-acylated chitosan: hydrophobic matrices for controlled drug release. *J Control Release* 93:1–13. [https://doi.org/10.1016/S0168-3659\(03\)00327-4](https://doi.org/10.1016/S0168-3659(03)00327-4)
- Lehn DN, Esquerdo VM, Dahlem Júnior MA et al (2018) Microencapsulation of different oils rich in unsaturated fatty acids using dairy industry waste. *J Clean Prod* 196:665–673. <https://doi.org/10.1016/j.jclepro.2018.06.127>
- Levchik SV, Weil ED (2008) Developments in phosphorus flame retardants. In: *Advances in Fire retardant materials*. Elsevier Ltd, Amsterdam, pp 41–66
- Li P, Wang B, Liu YY et al (2020) Fully bio-based coating from chitosan and phytate for fire-safety and antibacterial cotton fabrics. *Carbohydr Polym* 237:116173. <https://doi.org/10.1016/j.carbpol.2020.116173>
- Li S, Boyter H, Qian L (2005) UV curing for encapsulated aroma finish on cotton. *J Text Inst* 96:407–411. <https://doi.org/10.1533/joti.2005.0116>
- Li S, Huang J, Chen Z et al (2017) A review on special wettability textiles: theoretical models, fabrication technologies and multifunctional applications. *J Mater Chem A* 5:31–55. <https://doi.org/10.1039/C6TA07984A>
- Li Y, Ai L, Yokoyama W et al (2013) Properties of chitosan-microencapsulated orange oil prepared by spray-drying and its stability to detergents. *J Agric Food Chem* 61:3311–3319. <https://doi.org/10.1021/jf305074q>
- Liu W, Wang M, Xu L et al (2019) Radiation technology application in high-performance fibers and functional textiles. In: *Radiation technology for advanced materials: from basic to modern applications*. Academic Press, London, pp 13–73
- Miró Specos MM, Escobar G, Marino P et al (2010) Aroma finishing of cotton fabrics by means of microencapsulation techniques. *J Ind Text* 40:13–32. <https://doi.org/10.1177/1528083709350184>
- Miró Specos MM, Garcia JJ, Gutierrez AC, Hermida LG (2017) Application of microencapsulated biopesticides to improve repellent finishing of cotton fabrics. *J Text Inst* 108:1454–1460. <https://doi.org/10.1080/00405000.2016.1257345>
- Munim SA, Saddique MT, Raza ZA, Majeed MI (2020) Fabrication of cellulose-mediated chitosan adsorbent beads and their surface chemical characterization. *Polym Bull* 77:183–196. <https://doi.org/10.1007/s00289-019-02711-4>
- Muthaiyan A, Limayem A, Ricke SC (2011) Antimicrobial strategies for limiting bacterial contaminants in fuel bioethanol fermentations. *Prog Energy Combust Sci* 37:351–370. <https://doi.org/10.1016/j.pecs.2010.06.005>
- Nagoor Meeran MF, Javed H, Tae H, Al et al (2017) Pharmacological properties and molecular mechanisms of thymol: prospects for its therapeutic potential and pharmaceutical development. *Front Pharmacol* 8:1–34. <https://doi.org/10.3389/fphar.2017.00380>
- Navarrete P, Toledo I, Mardones P et al (2010) Effect of *Thymus vulgaris* essential oil on intestinal bacterial microbiota of rainbow trout, *Oncorhynchus mykiss* (Walbaum) and bacterial isolates. *Aquac Res* 41:e667–e678. <https://doi.org/10.1111/j.1365-2109.2010.02590.x>
- Nejman A, Cieślak M, Gajdzicki B et al (2014) Methods of PCM microcapsules application and the thermal properties of modified knitted fabric. *Thermochim Acta* 589:158–163. <https://doi.org/10.1016/J.TCA.2014.05.037>
- Nelson G (2008) Microencapsulation in textile finishing. *Rev Prog Color Relat Top* 31:57–64. <https://doi.org/10.1111/j.1478-4408.2001.tb00138.x>
- Nunthanid J, Puttipatkhachorn S, Yamamoto K, Peck GE (2001) Physical properties and molecular behavior of chitosan films. *Drug Dev Ind Pharm* 27:143–157. <https://doi.org/10.1081/DDC-100000481>
- Park B-S, Choi W-S, Kim J-H et al (2005) Monoterpenes from thyme (*Thymus vulgaris*) as potential mosquito repellents. *J Am Mosq Control Assoc* 21:80–83. [https://doi.org/10.2987/8756-971x\(2005\)21\[80:mftva\]2.0.co;2](https://doi.org/10.2987/8756-971x(2005)21[80:mftva]2.0.co;2)
- Pisitsak P, Tungsombatvisit N, Singhanu K (2018) Utilization of waste protein from Antarctic krill oil production and natural dye to impart durable UV-properties to cotton textiles. *J Clean Prod* 174:1215–1223. <https://doi.org/10.1016/j.jclepro.2017.11.010>
- Pranoto Y, Rakshit SK, Salokhe VM (2005) Enhancing antimicrobial activity of chitosan films by incorporating garlic oil, potassium sorbate and nisin. *LWT - Food Sci Technol* 38:859–865. <https://doi.org/10.1016/J.LWT.2004.09.014>
- Rattan RS (2010) Mechanism of action of insecticidal secondary metabolites of plant origin. *Crop Prot* 29:913–920. <https://doi.org/10.1016/J.CROPRO.2010.05.008>
- Raza ZA, Anwar F, Abid S (2019a) Multi-response optimization in impregnation of chitosan nanoparticles on polyester fabric. *Polym Bull* 76:3039–3058. <https://doi.org/10.1007/s00289-018-2523-7>
- Raza ZA, Bilal U, Noreen U et al (2019b) Chitosan mediated formation and impregnation of silver nanoparticles on viscose fabric in single bath for antibacterial performance. *Fibers Polym* 20:1360–1367. <https://doi.org/10.1007/s12221-019-1018-y>
- Raza ZA, Khalil S, Ayub A, Banat IM (2020) Recent developments in chitosan encapsulation of various active ingredients for multifunctional applications. *Carbohydr Res* 492:1–15. <https://doi.org/10.1016/j.carres.2020.108004>
- Rosenberg Talmon JJ, Kopelman MY (1988) The microstructure of spray-dried microcapsules. *Food Struct* 7:15–23
- Scacchetti FAP, Pinto E, Soares GMB (2017) Functionalization and characterization of cotton with phase change materials and thyme oil encapsulated in beta-cyclodextrins. *Prog Org Coatings* 107:64–74. <https://doi.org/10.1016/J.PORGCOAT.2017.03.015>
- Schwarz K, Ernst H, Ternes W (1996) Evaluation of antioxidative constituents from thyme. *J Sci Food Agric*

- 70:217–223. [https://doi.org/10.1002/\(SICI\)1097-0010\(199602\)70:2<217::AID-JSFA488>3.0.CO;2-Y](https://doi.org/10.1002/(SICI)1097-0010(199602)70:2<217::AID-JSFA488>3.0.CO;2-Y)
- Šipailienė A, Venskutonis PR, Baranauskienė R, Šarkinas A (2006) Antimicrobial activity of commercial samples of thyme and marjoram oils. *J Essent Oil Res* 18:698–703. <https://doi.org/10.1080/10412905.2006.9699210>
- Sonam Chouhan KS and SG (2017) Antimicrobial activity of some essential oils—Present status and future perspectives. *Medicines* 4:1–21. <https://doi.org/10.3390/medicines4030058>
- Talón E, Trifković KT, Vargas M et al (2017) Release of polyphenols from starch-chitosan based films containing thyme extract. *Carbohydr Polym* 175:122–130. <https://doi.org/10.1016/j.carbpol.2017.07.067>
- Tiwari BK, Valdramidis VP, O' Donnell CP et al (2009) Application of natural antimicrobials for food preservation. *J Agric Food Chem* 57:5987–6000. <https://doi.org/10.1021/jf900668n>
- Tong W (2016) Formulation of nano and micro-encapsulated phase change materials with a solar-absorbing metamaterial shell. *J Nanoelectron Optoelectron* 11:756–761. <https://doi.org/10.1166/jno.2016.1962>
- Trifković KT, Milašinović NZ, Djordjević VB et al (2014) Chitosan microbeads for encapsulation of thyme (*Thymus serpyllum* L.) polyphenols. *Carbohydr Polym* 111:901–907. <https://doi.org/10.1016/j.carbpol.2014.05.053>
- Van Tran V, Loi Nguyen T, Moon J-Y, Lee Y-C (2019) Core-shell materials, lipid particles and nanoemulsions, for delivery of active anti-oxidants in cosmetics applications: challenges and development strategies. *Chem Eng J* 368:88–114. <https://doi.org/10.1016/J.CEJ.2019.02.168>
- Verlee A, Mincke S, Stevens CV (2017) Recent developments in antibacterial and antifungal chitosan and its derivatives. *Carbohydr Polym* 164:268–283
- Vilchez-Maldonado S, Calderó G, Esquena J, Molina R (2014) UV protective textiles by the deposition of functional ethylcellulose nanoparticles. *Cellulose* 21:2133–2145. <https://doi.org/10.1007/s10570-014-0217-3>
- Wang B, Sheng H, Shi Y et al (2015) Recent advances for microencapsulation of flame retardant. *Polym Degrad Stab* 113:96–109. <https://doi.org/10.1016/j.polymdegradstab.2015.01.008>
- Yip J, Luk MYA (2016) Microencapsulation technologies for antimicrobial textiles. *Antimicrob Text* 19–46. <https://doi.org/10.1016/B978-0-08-100576-7.00003-1>

Publisher's Note Springer Nature remains neutral with regard to jurisdictional claims in published maps and institutional affiliations



Multifunctional Linen Fabric Obtained through Finishing with Chitosan-gelatin Microcapsules Loaded with Cinnamon Oil

Nagender Singh & Javed Sheikh

To cite this article: Nagender Singh & Javed Sheikh (2021): Multifunctional Linen Fabric Obtained through Finishing with Chitosan-gelatin Microcapsules Loaded with Cinnamon Oil, Journal of Natural Fibers, DOI: [10.1080/15440478.2020.1870625](https://doi.org/10.1080/15440478.2020.1870625)

To link to this article: <https://doi.org/10.1080/15440478.2020.1870625>



Published online: 17 Feb 2021.



Submit your article to this journal [↗](#)



Article views: 202



View related articles [↗](#)



View Crossmark data [↗](#)



Citing articles: 1 View citing articles [↗](#)

Multifunctional Linen Fabric Obtained through Finishing with Chitosan-gelatin Microcapsules Loaded with Cinnamon Oil

Nagender Singh and Javed Sheikh

Dept. Of Textile and Fibre Engineering, Indian Institute of Technology (I.I.T.), Delhi, India

ABSTRACT

In the 21st century, the occurrences of deadly viruses, mosquito-borne and pathogenic diseases have increased significantly. To avoid the spread of these diseases, one of the best strategies is to use protective textile products such as functional (antibacterial, antioxidant, antiviral, mosquito repellent) mask, scarf, gowns, curtains, bedsheets, etc. The present work deals with the preparation of chitosan-gelatin microcapsules loaded with cinnamon bark oil and the application of prepared microcapsules to the linen to develop multifunctional protective linen fabric. The scanning electron microscopy (SEM), energy-dispersive X-ray (EDX) and Fourier transform infrared (ATR-FTIR) spectroscopy were utilized to characterize the prepared microcapsules and the finished fabric. The encapsulation efficiency of microcapsules was also calculated to optimize the concentration of polymers and oil. The chitosan-gelatin shell on cinnamon bark oil core provided a controlled-release system, which delivers excellent washing durability to the functionalities of the finished linen. The finished linen with an excellent antibacterial property against *E. coli* and *S. aureus* bacteria and outstanding mosquito repellency (up to 100%) durable up to 20 washes was obtained. The finished fabric also showed durable and efficient antioxidant property and a fragrance. The use of bio-materials for the functional finishing of linen was reported.

KEYWORDS



Chitosan; gelatin; microcapsules; cinnamon bark oil; multifunctional textile

摘要

进入21世纪,致命病毒、蚊媒传染病和致病性疾病的发生显著增加。为了避免这些疾病的传播,最好的策略之一就是使用防护性纺织品,如功能性(抗菌、抗氧化、抗病毒、驱蚊)面膜、围巾、长袍、窗帘、床单等。研究了以肉桂油为载体的壳聚糖-明胶微胶囊的制备及其在亚麻织物中的应用,以开发多功能亚麻防护织物。利用扫描电子显微镜(SEM)、能量色散X射线(EDX)和傅立叶变换红外光谱(ATR-FTIR)对制备的微胶囊和织物进行了表征。计算了微胶囊的包封率,优化了聚合物和油的浓度。壳聚糖-明胶壳在肉桂皮油芯上提供了一种控释系统,该系统对成品亚麻的功能提供了极好的耐洗性。整理后的亚麻具有优良的抗菌性能,对大肠杆菌和金黄色葡萄球菌的细菌和出色的驱蚊(高达100%)持久长达20洗。整理后的织物还显示出持久有效的抗氧化性能和香味。介绍了生物材料在亚麻功能整理中的应用。

Introduction

The essential oils have grown their importance, and several uses such as aromatherapy, cosmetics, therapeutic and medicinal applications are explored. Essential oils are a mixture of phenols, alcohols, hydrocarbons, ethers, esters, aldehydes, terpenes and ketones, which may yield distinct smells. The aromatic components present in essential oils can make the neighboring area free from viruses, bacteria, insects and fungi. These physicochemical characteristics are because of their complex

*CONTACT Javed Sheikh  jnsheikh@iitd.ac.in  Dept. Of Textile and Fibre Engineering, Indian Institute of Technology (I.I.T.), Delhi, India.

chemical composition, which offers antibacterial, antifungal, antiviral, anti-inflammatory and insect-repellent properties (Ali et al. 2015; Asbahani et al. 2015; Bakkali et al. 2008; Baratta et al. 1998a, 1998b). However, their volatile nature and sensitivity toward light and oxygen decline essential oil's stability on storage, which hamper their economic and functional effectiveness. Therefore, it is important to overcome these limitations by encapsulation of essential oils (active agent) in the polymer (encapsulating agent), which may control the release rate of essential oil and improve the physical, oxidative and storage stability of active agent (Razavi et al. 2020; Reineccius 2019). The encapsulated essential oils have various applications in pharmaceutical, cosmetic (Tang et al. 2020), food, flavor, agriculture and textile industries (Ammayappan et al. 2020; Pargai and Jahan 2020; Vehapi, Yilmaz, and Özçimen 2020).

Cinnamon (*Cinnamomum zeylanicum*) bark oil is obtained from the inner bark of trees belonging to *Cinnamomum* genus of Lauraceae family. It has been reported to cure various disorders and is known to have biological properties such as antioxidant activity, antifungal activity, antibacterial activity, antiviral activity, anticancer activity, anti-inflammatory action, anti-diabetic property and insecticidal activity (Cheng et al. 2009; Mathew and Abraham 2006; Melo et al. 2015; Nolkemper et al. 2006; Wang, Chen, and Chang 2005). These properties are mainly due to its phytochemical components such as cinnamaldehyde, cinnamic acid, eugenol, cinnamyl acetate, L-borneol, camphor, caryophyllene oxide, benzaldehyde and terpineol (Tung et al. 2010; Vangalapati et al. 2012; Vasconcelos, Croda, and Simionatto 2018).

Proteins have functional properties that are advantageous for the effective spray-drying procedures, and they can also serve as excellent emulsifiers. In spray drying, the primary step is to make an oil-water emulsion, where the emulsifier can stabilize the emulsion and distribute the bioactive ingredient in the encapsulating agent during drying (Reineccius 2019). Gelatin is a derivative of collagen and has received widespread attention in spray drying because of its excellent emulsifying and stabilizing properties, which forms dense networks during the drying process (Rostami et al. 2019). Chitosan is a cationic biopolymer obtained from the deacetylation of chitin (Yeddes et al. 2020). The mixture of polymers can be an alternative solution to enhance the overall performance of ultimate encapsulation complexes.

Moreover, mixtures of gelatin and chitosan are mainly exciting as both biopolymers are biodegradable, biocompatible and renewable (Atay et al. 2018; Roy et al. 2018). Additionally, gelatin and chitosan are known to interact via electrostatic interactions and hydrogen bonding, thus forming a compatible mixture (Kan et al. 2019). Whereas, encapsulation matrix from gelatin and chitosan mixture has already been reported using various techniques (Kim et al. 2006; Prata and Grosso 2015; Morelli, Holdich, and Dragosavac 2017). Kim et al. prepared and characterized the chitosan-gelatin microcapsules loaded with triclosan. The results showed that the microcapsules were spherical and had core/shell morphology (Kim et al. 2006). Prata et al. developed chitosan microcapsules via complexation with gelatin, where the core material was limonene oil. The obtained microcapsules were applied to the fabric to impart antimicrobial activity (Prata and Grosso 2015). Maji and Hussain prepared the microcapsules of chitosan-gelatin containing *Zanthoxylum limonella* oil for mosquito repellent application (Maji and Hussain 2008). Several attempts have been made to effectively utilize the chitosan-gelatin combination for encapsulating essential oils for various applications in food, pharmaceutical, cosmetic and agriculture industries (Gómez-Estaca et al. 2010; Gonçalves et al. 2018; Li et al. 2017). However, limited research has been reported in the area of use of multifunctional microcapsules based on a mixture of biopolymers and CBO for functional finishing of textiles. Thus, it is important to investigate the functional effects imparted to textiles by the use of cinnamon oil-based microcapsules.

In this research study, the cinnamon bark oil (CBO) was encapsulated in a gelatin-chitosan complex via optimized spray-drying technology, which provides spherical, solid and micro-sized capsules. The effect of polymers-to-oil ratio on the morphology, size and encapsulation efficiency of microcapsules was analyzed. The prepared microcapsules were characterized and applied on the linen fabric using the pad-dry method. Finally, the objective of this work was to investigate the finished

fabric's functional properties such as antioxidant activity, antibacterial activity, fragrance and mosquito repellent property. The effect of laundering on the functional properties of finished linen fabric was also studied.

Materials and methods

Materials

Merck Specialties Pvt. Ltd. (India) supplied the gelatin, low molecular weight chitosan (5–20 mPa.s) with 85% degree of deacetylation, acetic acid, ethanol, and n-hexane. Cinnamon bark oil (CBO) was purchased from Jain Super Store, New Delhi (India). A low-temperature curable binder (Solid content 40%, nonionic) was procured from Pidilite Industries Ltd. (India). In this study, linen fabric (Fiber composition: Flax fiber, Fabric type: 100% linen/ready-for-dyeing, Fabric structure: Plain weave (EPI-72, PPI-68, GSM-135)) was utilized.

Methods

Preparation of microcapsules and their optimization

In step 1, an emulsion of gelatin, CBO and Tween 80 was prepared by dissolving gelatin in de-ionized water at 50°C for 30 min and stirred at 800 rpm followed by cooling of gelatin solution and addition of CBO and Tween 80. Then, the above mixture was emulsified by mixing at 2000 rpm using a magnetic stirrer. In step 2, chitosan was dissolved in acetic acid (1% w/w) at 60°C for 1 hr using a magnetic stirrer at 800rpm. After that, the chitosan solution (100 ml) was added to the Gelatin-CBO emulsion (300 ml) and homogenized for 10 min at 1200 rpm. As shown in Table 1, the quantity of the gelatin was three times the quantity of chitosan because it is reported that it increases the elongation at the break of the gelatin-chitosan film (Roy et al. 2018). The viscosity of the prepared emulsion was measured by a viscometer (Brookfield DV- II +Pro Viscometer, Canada) using spindle number (3) and spindle speed (100rpm) (Yip and Luk 2016).

The microcapsules were prepared by feeding the above emulsion into a spray dryer (TechnoSearch Instruments, India). The following optimized spray dryer parameters were used: feed rate 2 ml/min; atmospheric pressure 1.20 kg/cm²; aspirator 80%; air inlet-temperature 160°C; air outlet-temperature 140°C. Finally, the stable microcapsules were collected from the spray dryer's cyclone assembly and stored in an airtight package. The encapsulation efficiency (EE) of the prepared microcapsule was measured to optimize the final composition (polymers ratios) of the microcapsule. The microcapsules (1 g) were dissolved in 10 ml aqueous acetic acid (1%). Then, 50 ml n-hexane was added to separate CBO from the solution using a separating funnel. After that, the total oil content was measured at $\lambda_{\max}(273.5\text{nm})$ with the help of UV-visible spectrophotometer (UV-2450 Shimadzu, Japan). For surface oil content, the microcapsules were suspended in ethanol for 5 min and then the absorbance of the solution was measured at $\lambda_{\max}(288\text{nm})$ by UV-visible spectrophotometer (UV-2450 Shimadzu, Japan). The EE (%) of microcapsules was determined by using the following equation:

$$EE (\%) = \frac{\text{Total oil content} - \text{Surface oil content}}{\text{Total oil content}} \times 100$$

Table 1. Effect of Polymer, oil and emulsifier concentrations on emulsion viscosity and microcapsule's encapsulation efficiency.

Run	Gelatin (% in 300 ml)	Chitosan (% in 100 ml)	CBO (% of gelatin solution)	Tween 80 (% of gelatin solution)	Viscosity (cP)	EE (%)
1	0.75	0.50	1	0.25	12	72.38
2	0.75	0.75	1	0.25	14	78.67
3	0.75	1	1	0.25	16	74.61

As shown in Table 1, Run 2 exhibited the maximum encapsulation efficiency (78.67%) of microcapsules. The reason could be better compatibility of polymers at that concentration. This suggests that the microcapsules obtained using Run 2 have more amount of oil present into them as compared to other Runs. The microcapsules prepared using Run 2 were selected for fabric finishing.

Fabric treatment

Initially, the dispersion of microcapsules (100gpl) and binder (30gpl) was prepared, then linen fabric was immersed in the dispersion. Finally, the fabric was passed through the padding mangle with 75 ±2% wet pick up, followed by drying at 80°C for 5 min and cooling at room temperature.

Characterization of microcapsules and finished fabric

The morphology, size distribution and presence of microcapsules on the finished fabric were analyzed by SEM (Zeiss EVO 18 Special, Germany) with a different resolution at an accelerating voltage of 20 kV. The elemental analysis of microcapsules and the finished fabric was carried out by EDX (Bruker QuanTax 200, Germany). The functional group analysis of controlled, microcapsules and the finished fabric was done to investigate functional groups using ATR-FTIR Spectrometer (Thermo Scientific Nicolet iS50, USA).

Functional properties of finished fabric

The antioxidant activity of the finished fabric was assessed by following the reported method using 1,1-diphenyl-2-picrylhydrazyl (DPPH) (Bhushan *et al.* 2020). Arm in the cage method was used to evaluate the mosquito repellent property of finished fabric against *Anopheles* mosquitoes (Barnard *et al.* 2006). The AATCC 100–2012 test method was utilized to examine the antibacterial property of finished fabric against *E. coli* and *S. aureus* bacteria (AATCC TM 100–2012). The aroma of essential oil on the finished fabric was assessed using the scratch-sniff test method (Li, Boyter, and Qian 2005). The durability of multifunctional properties of finished fabrics toward repeated laundering was tested using AATCC 61 1A test methods. The laundering was carried out at 40°C for 45 min with 10 steel balls as per the conditions provided in the standard AATCC TM 61–2007. Further rinsing was done in de-ionized water at 40°C for 1 min followed by drying in an air circulating oven at 60°C for 3 min.

Results and discussion

Microcapsules size distribution, morphology and their application on fabric

As shown in Figure 1, the gelatin-chitosan microcapsules containing CBO demonstrated the oval and sphere-shaped with an irregular surface, which is usually seen for microcapsules prepared using the spray-drying technique.

The SEM images show the varied size of microcapsules and their non-porous surface. The microcapsules displayed the reservoir and matrix morphology, as shown in Figure 1. It is reported that the microcapsules obtained by the spray-drying technique exhibit matrix structure (Zhang *et al.* 2017). The stable emulsion plays a vital role in the formation of both reservoir and matrix-structured microcapsules. Here, gelatin and chitosan formed a continuous layer on the CBO because of electrostatic interactions between the polymers. Thus, it offers a stable oil-in-water emulsion (Liu *et al.* 2013). During spray-drying, continuous layer on the CBO phase will be dried out and gives a reservoir type of microcapsules.

The gelatin-chitosan microcapsules containing CBO presented a narrow size distribution with an average size of 3.04 µm, as shown in Figure 2. The size of microcapsules depends upon the feed rate, pressure, aspirator and diameter of the nozzle tip. Varying of these parameters may affect the size of microcapsules.

As shown in Figure 3, microcapsules were present on the fibers and in the interstices between the fibers. The SEM images showed the existence of microcapsules on the fibers with good shape without

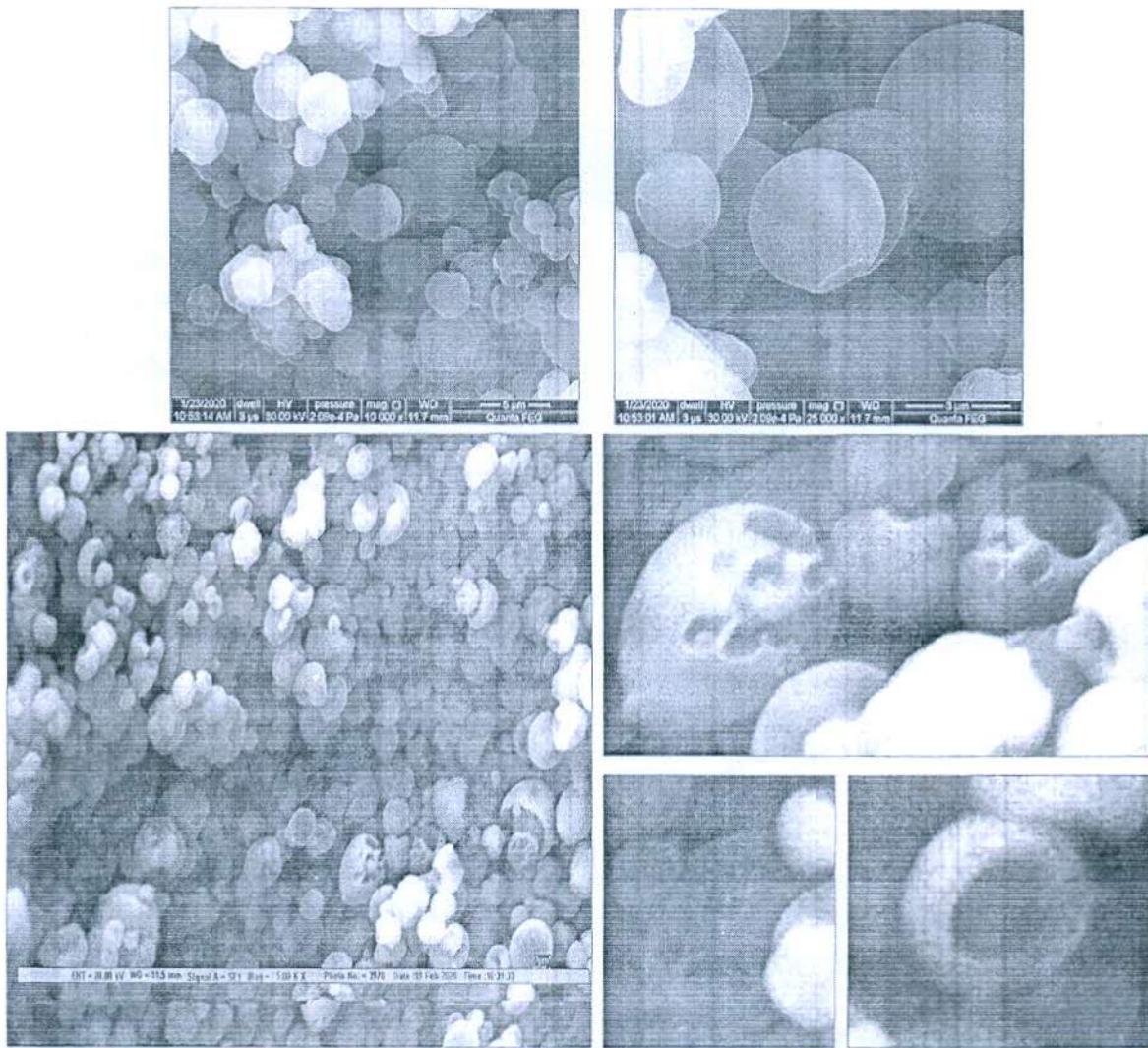


Figure 1. Morphology of microcapsules.

leakage. It is expected that the microcapsules were attached to fibers by the ionic interaction between chitosan and fibers and by the film of acrylic binder. Therefore, both ionic interaction and acrylic binder provide efficient washing durability to the finishing.

EDX analysis of microcapsules and finished fabric

Elemental analysis of gelatin-chitosan microcapsules containing CBO and the finished fabric was done to examine the elemental content of microcapsules and to assess the existence of microcapsules on the finished fabric.

The EDX graphs of microcapsules demonstrate the presence of nitrogen (22.88%) that suggests the microcapsules are composed of nitrogen-rich polymers (gelatin and chitosan) as shown in Figure 4 (A). As shown in Figure 4 (B), the EDX analysis of finished fabric also showed the existence of nitrogen, which shows the presence of microcapsules on the finished fabric. The results confirm the availability of gelatin and chitosan in the microcapsules as well as on the finished fabric.

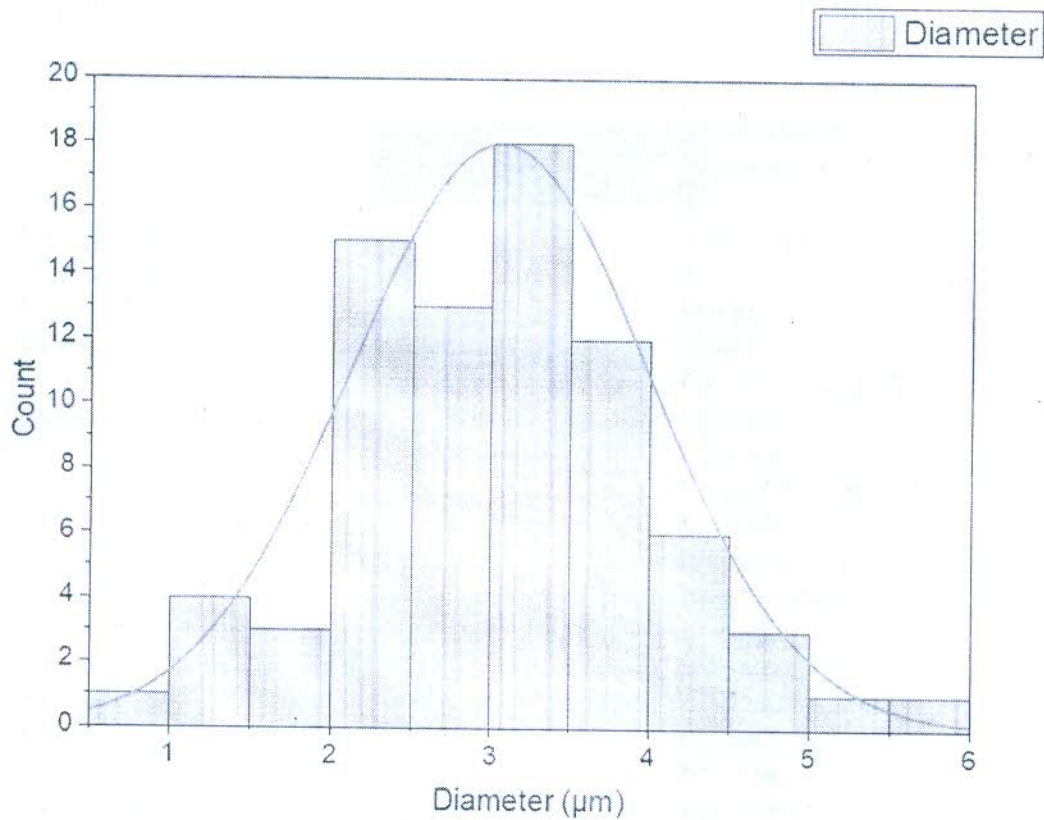


Figure 2. Size distribution of microcapsules.

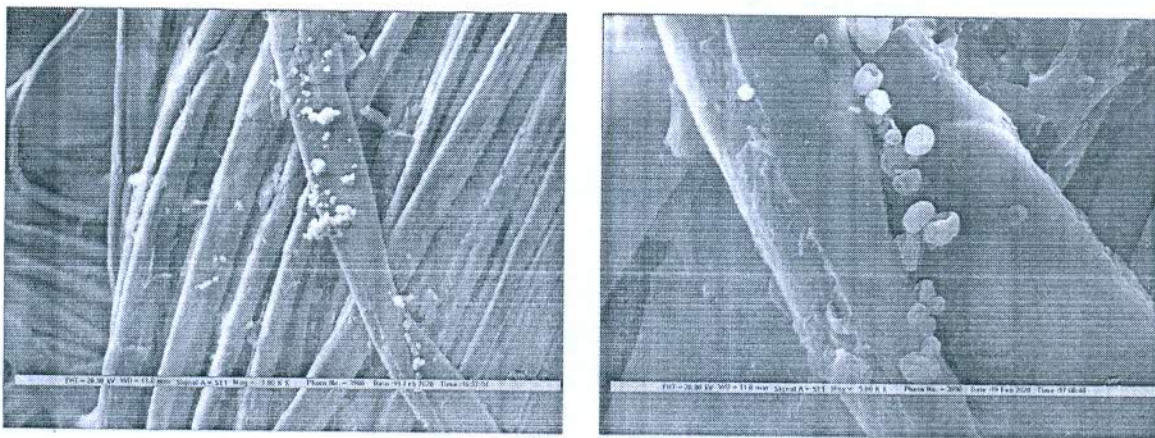


Figure 3. SEM micrograph of the finished fabric.

ATR-FTIR analysis

Figure 5 shows the FTIR spectra of controlled fabric, microcapsules and finished fabric. The FTIR spectrum of finished fabric displayed the peaks associated with gelatin, chitosan and CBO. The finished fabric spectrum shows the variation in the intensity of peaks as compared to controlled fabric. The $C=O$ stretching at 1735 cm^{-1} may be attributed to carbonyl groups of chitosan. The absorption peaks at 1654 cm^{-1} and 1560 cm^{-1} are related to amide I and amide II. Amide I is primarily allied with the $C=O$ stretching vibration, and amide II results from the N-H bending vibration and from the C-N stretching vibration, which shows the presence of chitosan and gelatin polymers in microcapsules

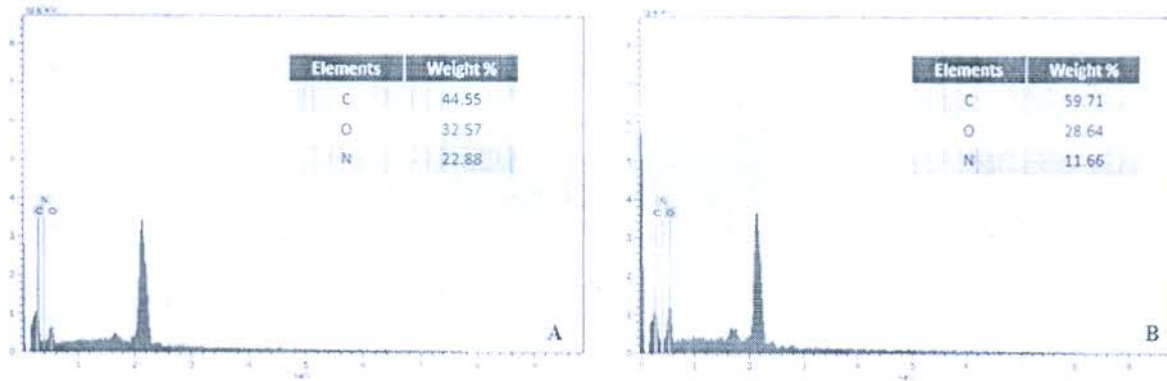


Figure 4. (A). Elemental analysis of microcapsules and (B). finished fabric.

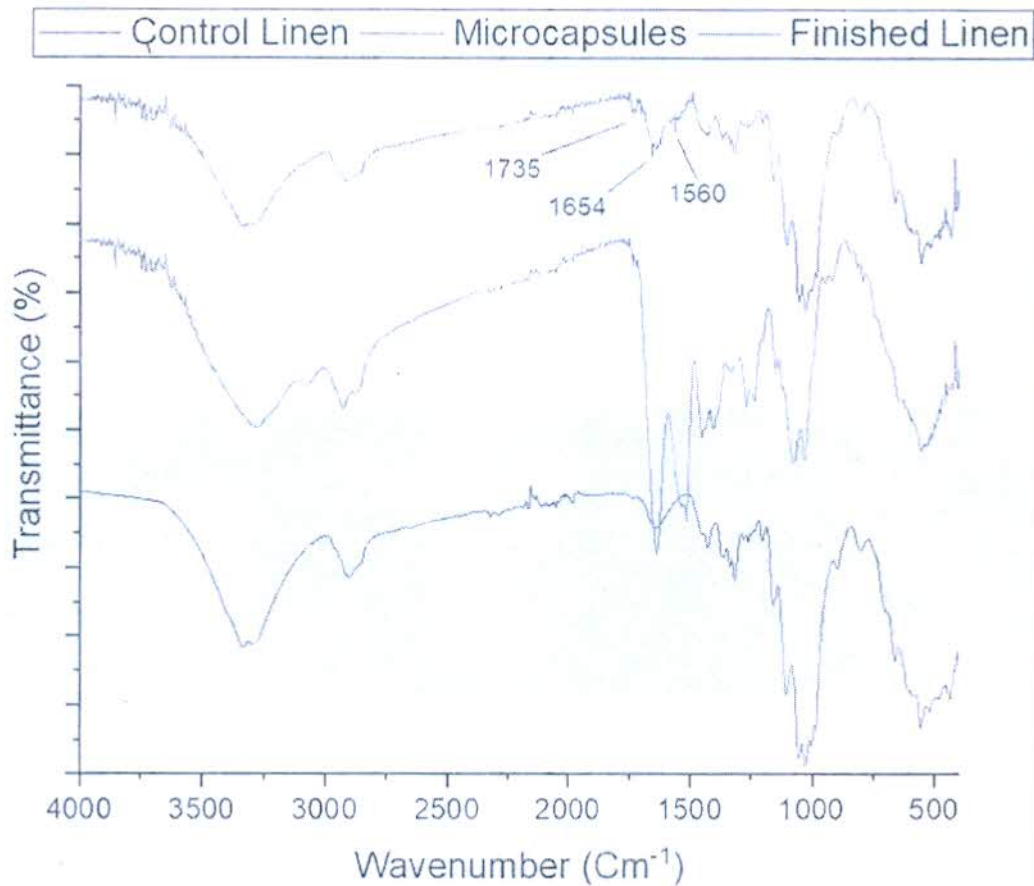


Figure 5. ATR-FTIR spectra of control fabric, microcapsules and finished fabric.

and on the finished fabric. The broad peak between 3900 and 3600 cm^{-1} indicates the hydroxyl functional group of CBOs. The peaks between 1200 and 1050 cm^{-1} are attributed to the stretching vibrations of C-O. The peaks at 913 and 816 cm^{-1} are ascribed to the aromatic ring, while the peaks between 750 and 600 cm^{-1} are because of the benzene ring = CH vibrations.

Table 2. Multifunctional properties of fabric finished with gelatin-chitosan microcapsules containing CBO.

Sample No	Mosquito repellency [§] (%)				Antibacterial activity [§] (BCR %)				Antioxidant activity [§] (%)		Aroma	
	0 wash	5 wash	10 wash	20 wash	<i>S. aureus</i>		<i>E. Coli</i>		0 wash	10 wash	0 wash	20 wash
					0 wash	10 wash	0 wash	10 wash				
Controlled	—	—	—	—	Nil	Nil	Nil	Nil	Nil	Nil	No	No
Finished fabric	100	100	100	100	98.00	93.91	96.33	91.11	97.01	93.03	Yes	Yes

§-

Average value of three determinations

Multifunctional properties of finished fabric

Table 2 shows the multifunctional properties such as mosquito repellency, antibacterial property, antioxidant activity, and aroma of the finished fabric. As shown in Table 2, the finished fabric showed an excellent mosquito repellency (100%) against *Anopheles* mosquitoes, which might be due to the presence of CBO in the gelatin-chitosan microcapsules. Since CBO contains cinnamaldehyde, cinnamyl acetate, eugenol, and anethole components and all are reported to possess a mosquito larvicidal activity (Cheng et al. 2009, 2004). However, CBO contains a higher amount of cinnamaldehyde which also shows strong mosquito repellency. It is also observed that the finished fabric showed excellent mosquito repellent activity even after 20 washes. The reason could be the effective encapsulation of CBO in gelatin-chitosan complex, providing an excellent controlled-release property. The essential oil present in the microcapsules diffused slowly through the wall due to suppressed volatility. Additionally, essential oils can mask the lactic acid and CO₂ smell of a human body, which may confuse the female mosquito.

The finished fabric showed significant antioxidant property (97%), as shown in Table 2. The presence of phenolic antioxidants and flavonoids in CBO is mainly responsible for antioxidant property (Jayaprakasha et al. 2007). DPPH is a stable free-radical and can accept a hydrogen atom or electron from phenolic components of CBO and become a stable molecule (Bouyahya et al. 2017). Eugenol and cinnamaldehyde components of CBO exhibited antioxidant activity. However, it is reported that the eugenol exhibited stronger antioxidant activity compared to cinnamaldehyde (Mathew and Abraham 2006). Moreover, it is also reported that the chitosan and gelatin polymers also possess some antioxidant properties due to the presence of radical-free amino group (Dou et al. 2018; Park, Je, and Kim 2004). Therefore, gelatin-chitosan microcapsules loaded with CBO showed excellent antioxidant activity. The finished fabric showed significant antioxidant activity even after 10 washes because of the presence of stable microcapsules on the fabric, which could offer the controlled-release effect to the active molecules.

The finished fabric displayed excellent antibacterial activity against *S. aureus* and *E. Coli*, as shown in Table 2. Cinnamaldehyde, eugenol and other phenolic components of CBO are reported to have an antimicrobial effect. Cinnamaldehyde has been the best antimicrobial compound of CBO, that showed antibacterial properties against *S. aureus* and *E. Coli*. Cinnamaldehyde can enter into microorganisms through the cell wall and may cause cellular damage (Muhammad and Dewettinck 2017; Ribeiro-Santos et al. 2017). Chitosan has been reported to provide excellent antibacterial activity. It can interact with the cell wall of the microorganisms that may block and leak the cell membrane of the microorganism (Kong et al. 2010). Therefore, chitosan and CBO in the microcapsules work synergistically and offer prominent antibacterial properties against several bacterial. Additionally, encapsulation of CBO in gelatin-chitosan film provides slow-release mechanism, which could increase the self-life of essential oil by suppressing its volatility.

As shown in Table 2, the finished fabric exhibited pleasant aroma before and after the wash. The main flavor component of CBO is cinnamaldehyde. Cinnamaldehyde is reported to be responsible for the sweet smell of cinnamon (Ribeiro-Santos et al. 2017; Thomas and Kuruvilla 2012). The other aromatic parts of CBO may also give a pleasant aroma. The results are impressive, since, in encapsulation, the CBO is entrapped into a polymeric film. This system offers a long-lasting aroma effect even after repeated washes.

Conclusions

In the present work, the cinnamon bark oil was successfully encapsulated in gelatin-chitosan complex film. The obtained microcapsules offered significant encapsulation efficiency (78.67%). The SEM images showed spherical shape with irregular surfaces of microcapsules and also displayed the reservoir and matrix type of morphology. The elemental study and IR analysis advocate the presence of gelatin-chitosan microcapsules loaded with CBO on the linen fabric. The combination of cinnamon bark oil, gelatin and chitosan worked synergistically, which imparted excellent antibacterial and antioxidant properties to the finished fabric. Furthermore, the finished fabric showed excellent mosquito repellent and aroma properties. The stable microcapsules were expected to cause slow-release of CBO by either diffusion or rupture due to pressure, temperature or alkaline conditions. Such finished fabric can be utilized as a protective textile, which can provide protection against various biological agencies.

Disclosure statement

There are no conflicts of interest to declare.

References

- AATCC TM 100-2012 Test Method for Antibacterial Finishes on Textile Materials. *American Association of Textile Chemists Colorists*, USA.
- AATCC TM 61-2007 Test Method for Colorfastness to Laundering: Accelerated. *American Association of Textile Chemists Colorists*, USA.
- Ali, B., N. A. Al-Wabel, S. Shams, A. Ahamad, S. A. Khan, and F. Anwar. 2015. Essential oils used in aromatherapy: A systemic review. *Asian Pacific Journal of Tropical Biomedicine* 5 (8):601–11. doi:10.1016/j.apjtb.2015.05.007.
- Ammayappan, L., N. C. Pan, S. Chakraborty, and A. Khan. 2020. A Study on Durability of a Fragrance Finishing on Jute Fabric. *Journal of Natural Fibers* 17 (11):1630–39. doi:10.1080/15440478.2019.1588186.
- Asbahani, A. E., K. Miladi, W. Badri, M. Sala, E. H. A. Addi, H. Casabianca, A. El Mousadiket et al. 2015. Essential oils: From extraction to encapsulation. *International Journal of Pharmaceutics*. 483(1–2):220–43. doi:10.1016/j.ijpharm.2014.12.069.
- Atay, E., M. J. Fabra, M. Martínez-Sanz, L. G. Gomez-Mascaraque, A. Altan, and A. Lopez-Rubio. 2018. Development and characterization of chitosan/gelatin electrosprayed microparticles as food grade delivery vehicles for anthocyanin extracts. *Food Hydrocolloids* 77:699–710. doi:10.1016/j.foodhyd.2017.11.011.
- Bakkali, F., S. Averbeck, D. Averbeck, and M. Idaomar. 2008. Biological effects of essential oils – A review. *Food and Chemical Toxicology* 46 (2):446–75. doi:10.1016/j.fct.2007.09.106.
- Baratta, M. T., H. J. Damien, S. G. Deans, D. M. Biondi, and G. Ruberto. 1998a. Chemical composition, antimicrobial and antioxidative activity of laurel, sage, rosemary, oregano and coriander essential oils. *Journal of Essential Oil Research* 10 (6):618–27. doi:10.1080/10412905.1998.9700989.
- Baratta, M. T., H. J. Dorman, S. G. Deans, A. C. Figueiredo, J. G. Barroso, and G. Ruberto. 1998b. Antimicrobial and antioxidant properties of some commercial essential oils. *Flavour and Fragrance Journal* 13 (4):235–44. doi:10.1002/(SICI)1099-1026(1998070)13:4<235::AID-FFJ733>3.0.CO;2-T.
- Barnard, D., U. Bernier, R. Xue, and M. Debboun. 2006. Standard Methods for Testing Mosquito Repellents. In *Insect Repellents: Principles, Methods, and Uses*. edited by M. Debboun, S. P. Frances, and D. Strickman, 103–110. Boca Raton, FL: CRC Press.
- Bhushan, S., A. Kumar, N. Singh, and J. Sheikh. 2020. Functionalization of wool fabric using lignin biomolecules extracted from groundnut shells. *International Journal of Biological Macromolecules* 142:559–63. doi:10.1016/j.ijbiomac.2019.09.130.

- Bouyahya, A., A. Et-Touys, Y. Bakri, A. Talbaui, H. Fellah, J. Abrini, and N. Dakka. 2017. Chemical composition of *Mentha pulegium* and *Rosmarinus officinalis* essential oils and their antileishmanial, antibacterial and antioxidant activities. *Microbial Pathogenesis* 111:41–49. doi:10.1016/j.micpath.2017.08.015.
- Cheng, S.-S., J.-Y. Liu, C.-G. Huang, Y.-R. Hsui, W.-J. Chen, and S.-T. Chang. 2009. Insecticidal activities of leaf essential oils from *Cinnamomum osmophloeum* against three mosquito species. *Bioresource Technology* 100 (1):457–64. doi:10.1016/j.biortech.2008.02.030.
- Cheng, S.-S., J.-Y. Liu, K.-H. Tsai, W.-J. Chen, and S.-T. Chang. 2004. Chemical Composition and Mosquito Larvicidal Activity of Essential Oils from Leaves of Different *Cinnamomum osmophloeum* Provenances. *Journal of Agricultural and Food Chemistry* 52 (14):4395–400. doi:10.1021/jf0497152.
- Dou, L., B. Li, K. Zhang, X. Chu, and H. Hou. 2018. Physical properties and antioxidant activity of gelatin-sodium alginate edible films with tea polyphenols. *International Journal of Biological Macromolecules* 118:1377–83. doi:10.1016/j.ijbiomac.2018.06.121.
- Gómez-Estaca, J., A. López de Lacey, M. E. López-Caballero, M. C. Gómez-Guillén, and P. Montero. 2010. Biodegradable gelatin-chitosan films incorporated with essential oils as antimicrobial agents for fish preservation. *Food Microbiology* 27 (7):889–96. doi:10.1016/j.fm.2010.05.012.
- Gonçalves, N. D., C. R. F. Grosso, R. S. Rabelo, M. D. Hubinger, and A. S. Prata. 2018. Comparison of microparticles produced with combinations of gelatin, chitosan and gum Arabic. *Carbohydrate Polymers* 196:427–32. doi:10.1016/j.carbpol.2018.05.027.
- Jayaprakasha, G. K., P. S. Negi, B. S. Jena, and L. Jagan Mohan Rao. 2007. Antioxidant and antimutagenic activities of *Cinnamomum zeylanicum* fruit extracts. *Journal of Food Composition and Analysis* 20 (3–4):330–36. doi:10.1016/j.jfca.2006.07.006.
- Kan, J., J. Liu, H. Yong, Y. Liu, Y. Qin, and J. Liu. 2019. Development of active packaging based on chitosan-gelatin blend films functionalized with Chinese hawthorn (*Crataegus pinnatifida*) fruit extract. *International Journal of Biological Macromolecules* 140:384–92. doi:10.1016/j.ijbiomac.2019.08.155.
- Kim, J.-C., H. Y. Lee, M. H. Kim, H.-J. Lee, H.-Y. Kang, and S. M. Kim. 2006. Preparation and characterization of chitosan/gelatin microcapsules containing triclosan. *Colloids and Surfaces. B, Biointerfaces* 52 (1):52–56. doi:10.1016/j.colsurfb.2006.07.001.
- Kong, M., X. G. Chen, K. Xing, and H. J. Park. 2010. Antimicrobial properties of chitosan and mode of action: A state of the art review. *International Journal of Food Microbiology* 144 (1):51–63. doi:10.1016/j.ijfoodmicro.2010.09.012.
- Li, Q., L.-J. Sun, X.-F. Gong, Y. Wang, and X.-L. Zhao. 2017. Simultaneous Optimization of Multiple Response Variables for the Gelatin-chitosan Microcapsules Containing Angelica Essential Oil. *Iranian Journal of Pharmaceutical Research* 16 (1):50–62.
- Li, S., H. Boyter, and L. Qian. 2005. UV curing for encapsulated aroma finish on cotton. *Journal of the Textile Institute* 96 (6):407–11. doi:10.1533/joti.2005.0116.
- Liu, J., C. Liu, Y. Liu, M. Chen, Y. Hu, and Z. Yang. 2013. Study on the grafting of chitosan-gelatin microcapsules onto cotton fabrics and its antibacterial effect. *Colloids and Surfaces. B, Biointerfaces* 109:103–08. doi:10.1016/j.colsurfb.2013.03.040.
- Maji, T. K., and M. R. Hussain. 2008. Microencapsulation of *Zanthoxylum limonella* oil (ZLO) in genipin crosslinked chitosan-gelatin complex for mosquito repellent application. *Journal of Applied Polymer Science* 111 (2):779–85.
- Mathew, S., and T. E. Abraham. 2006. Studies on the antioxidant activities of cinnamon (*Cinnamomum verum*) bark extracts, through various in vitro models. *Food Chemistry* 94 (4):520–28. doi:10.1016/j.foodchem.2004.11.043.
- Melo, A. D. B., A. F. Amaral, G. Schaefer, F. B. Luciano, C. de Andrade, L. B. Costa, and M. H. Rostagno. 2015. Antimicrobial effect against different bacterial strains and bacterial adaptation to essential oils used as feed additives. *Canadian Journal of Veterinary Research* 79 (4):285–89.
- Morelli, S., R. G. Holdich, and M. M. Dragosavac. 2017. Microparticles for cell encapsulation and colonic delivery produced by membrane emulsification. *Journal of Membrane Science* 524:377–88. doi:10.1016/j.memsci.2016.11.058.
- Muhammad, D. R. A., and K. Dewettinck. 2017. Cinnamon and its derivatives as potential ingredient in functional food—A review. *International Journal of Food Properties* 20:1–27. doi:10.1080/10942912.2017.1369102.
- Nolkemper, S., J. Reichling, F. C. Stintzing, R. Carle, and P. Schnitzler. 2006. Antiviral Effect of Aqueous Extracts from Species of the Lamiaceae Family against Herpes simplex Virus Type 1 and Type 2 in vitro. *Planta medica* 72 (15):1378–82. doi:10.1055/s-2006-951719.
- Pargai, D., and S. Jahan. 2020. Application of *Vitis vinifera* Microcapsules on Cotton Fabric: A Potential to Prevent UV-Induced Skin Problems. *Journal of Natural Fibers* 17 (3):412–26. doi:10.1080/15440478.2018.1500334.
- Park, P.-J., J.-Y. Je, and S.-K. Kim. 2004. Free radical scavenging activities of differently deacetylated chitosans using an ESR spectrometer. *Carbohydrate Polymers* 55 (1):17–22. doi:10.1016/j.carbpol.2003.05.002.
- Prata, A. S., and C. R. F. Grosso. 2015. Production of microparticles with gelatin and chitosan. *Carbohydrate Polymers* 116:292–99. doi:10.1016/j.carbpol.2014.03.056.
- Razavi, M. S., A. Golmohammadi, A. Nematollahzadeh, F. Fiori, C. Rovera, and S. Farris. 2020. Preparation of cinnamon essential oil emulsion by bacterial cellulose nanocrystals and fish gelatin. *Food Hydrocolloids* 109:106–11. doi:10.1016/j.foodhyd.2020.106111.

- Reineccius, G. 2019. Use of proteins for the delivery of flavours and other bioactive compounds. *Food Hydrocolloids* 86:62–69. doi:10.1016/j.foodhyd.2018.01.039.
- Ribeiro-Santos, R., M. Andrade, D. Madella, A. P. Martinazzo, L. de Aquino Garcia Moura, N. R. de Melo, and A. Sanches-Silva. 2017. Revisiting an ancient spice with medicinal purposes: Cinnamon. *Trends in Food Science and Technology* 62:154–69. doi:10.1016/j.tifs.2017.02.011.
- Rostami, M. R., M. Yousefi, A. Khezerlou, M. Aman Mohammadi, and S. M. Jafari. 2019. Application of different biopolymers for nanoencapsulation of antioxidants via electrohydrodynamic processes. *Food Hydrocolloids* 97:105170. doi:10.1016/j.foodhyd.2019.06.015.
- Roy, J. C., S. Giraud, A. Ferri, R. Mossotti, J. Guan, and F. Salaün. 2018. Influence of process parameters on microcapsule formation from chitosan—Type B gelatin complex coacervates. *Carbohydrate Polymers* 198:281–93. doi:10.1016/j.carbpol.2018.06.087.
- Tang, Y., S. Yang, W. He, L. Liu, and Z. Zhang. 2020. Stabilization of Chinese Gallnut (*Galla Chinensis*) Tannins by Spray-Drying Microencapsulation for Natural Hair Coloring. *Fibers and Polymers* 21 (6):1283–92. doi:10.1007/s12221-020-9634-0.
- Thomas, J., and K. M. Kuruvilla. 2012. Cinnamon. In *Handbook of Herbs and Spices*, Second ed. 182–96. Cambridge, England: Woodhead Publishing.
- Tung, Y.-T., P.-L. Yen, C.-Y. Lin, and S.-T. Chang. 2010. Anti-inflammatory activities of essential oils and their constituents from different provenances of indigenous cinnamon (*Cinnamomum osmophloeum*) leaves. *Pharmaceutical Biology* 48 (10):1130–36. doi:10.3109/13880200903527728.
- Vangalapati, M., N. Sree Satya, D. V. Surya Prakash, and S. Avanigadda. 2012. A review on pharmacological activities and clinical effects of Cinnamon species. *Research Journal of Pharmaceutical, Biological and Chemical Sciences* 3 (1):653–63.
- Vasconcelos, N. G., J. Croda, and S. Simionatto. 2018. Antibacterial mechanisms of cinnamon and its constituents: A review. *Microbial Pathogenesis* 120:198–203. doi:10.1016/j.micpath.2018.04.036.
- Vehapi, M., A. Yilmaz, and D. Özçimen. 2020. Fabrication of Oregano-Olive Oil Loaded PVA/Chitosan Nanoparticles via Electrospraying Method. *Journal of Natural Fibers* 1–15. doi:10.1080/15440478.2020.1774463.
- Wang, S.-Y., P.-F. Chen, and S.-T. Chang. 2005. Antifungal activities of essential oils and their constituents from indigenous cinnamon (*Cinnamomum osmophloeum*) leaves against wood decay fungi. *Bioresource Technology* 96 (7):813–18. doi:10.1016/j.biortech.2004.07.010.
- Yeddes, W., K. Djebali, W. Aidi Wannes, K. Horchani-Naifer, M. Hammami, I. Younes, and M. Saidani Tounsi. 2020. Gelatin-chitosan-pectin films incorporated with rosemary essential oil: Optimized formulation using mixture design and response surface methodology. *International Journal of Biological Macromolecules* 154:92–103. doi:10.1016/j.ijbiomac.2020.03.092.
- Yip, J., and M. Y. A. Luk. 2016. Microencapsulation technologies for antimicrobial textiles. In *Woodhead Publishing Series in Textiles, Antimicrobial Textiles*, edited by G. Sun, 19–46. Duxford, UK: Woodhead Publishing.
- Zhang, S., J. Chen, X. Yin, X. Wang, B. Qiu, L. Zhu, and Q. Lin. 2017. Microencapsulation of tea tree oil by spray-drying with methyl cellulose as the emulsifier and wall material together with chitosan/alginate. *Journal of Applied Polymer Science* 134 (1310.1002/app,44813).

Smart Sportswear -The Activity Trackers & Physiological Parameter Monitors for Sports Enthusiasts

*Achala Jaglan & Yamini Jhanji Dhir**

Department of Fashion and Apparel Engineering, The Technological Institute of Textiles & Sciences, Bhiwani

Abstract:

The ever-increasing indulgence of general masses in fitness and leisure activities such as yoga, gyming, cycling, and other indoor-outdoor activities has led to massive expansion of the sports segment with manufacturers focusing on developing sportswear to cater to the requirements of consumers. The consumers primarily seek performance, health, hygiene, comfort and safety aspects in their sports attire. However, apart from these aspects, tech savvy, fitness freak consumers also prefer technology laced smart wear that can be connected to their smart phone, play music, serve as global positioning systems and can keep a track on their workout schedule. Accordingly, a range of smart sports apparels and accessories are gaining popularity among fitness connoisseurs. Smartness can be engineered in sportswear by incorporation of external sensors and other components that can sense respond and adapt. Alternatively, the incorporation of smart materials like conductive fibres, yarns, shape memory polymers, phase change materials and profiled fibres can further impart smart functionality to clothing. The smart sportswear can serve as a personal coach for sportsperson monitoring their vital physiological parameters like heart rate, oxygen saturation along with performance and endurance related aspects like position, motion impact, workout patterns, calories burnt etc to enhance health, wellness and performance of athletes. This paper reviews the state-of-the-art smart sportswear that serve as activity trackers and physiological parameter monitors for sports enthusiasts with emphasis on working principle, application areas and recent developments in smart sportswear.

Keywords: *Comfort, Interactive, Physiological Parameters, Response, Sportswear, Smart, Sensor, Stimuli, Tracker*

Citation: Achala Jaglan & Yamini Jhanji Dhir "Smart Sportswear -The Activity Trackers & Physiological Parameter Monitors for Sports Enthusiasts", *Journal of the Textile Association*, **82/2** (150-154), (Sept-Oct '2021)

1. Introduction

Sportswear is one of the most promising and fastest growing segments of technical textiles. A considerable amount of research and innovation is involved in design and development of sportswear owing to a range of functional and performance requirements which sports person seek in their attire. Furthermore, the requirements vary as per the sportsperson's level of physical activity, ambient conditions and specific sport. Accordingly, the sportswear can be categorized into performance, basic, leisurewear and fashion clothing. Performance wear is technology driven sportswear category that enhances the functional attributes associated with clothing. The clothing category is intended for sportsperson involved in rigorous physical activity and is generally custom made in smaller quantities which accounts for their exorbitant prices. Contrastingly, the basic sportswear is designed with prime focus on aesthetics and silhouette rather than performance, caters to demands of mass public and are available at lower price points. Sports leisurewear, a cheaper replica of performance sportswear is preferred by millennials who indulge in leisure or light physical activities indoors [1]. Undoubtedly, the varied categories of sportswear clothing should exhibit the primary requirement of being light weight, comfortable, breathability and providing ease of movement for wearer. Thermo-physiological comfort involving consideration of heat, moisture vapour and liquid moisture transmission is of utmost importance while designing sportswear for particular sports.

*Corresponding Author :

Dr. Yamini Jhanji
Assistant Professor,
Department of Fashion & Apparel Engineering TIT&S,
Bhiwani - 127 021 Haryana
E-mail: yjhanji@gmail.com

The agility to wearer, light weight, durability, anti-odour, antimicrobial and antistatic properties are some other crucial aspects considered while designing sportswear. The design and development of sportswear with optimum, desirable, sport specific property thus involves considerable brain storming and research as far as selection of appropriate raw materials, ergonomics, sizing and incorporation of smart features to monitor physiological parameters of sportspersons are concerned. A myriad of innovative fibres, yarns and fabric structures are thus being explored for engineering sports textiles. The trend of wearables around arms or legs worn by sportsperson to monitor their fitness and other health parameters is bygone with inception of smart sportswear that behave intelligently and can monitor sportsperson's physiological parameters owing to high performance, smart fibres and yarns like optical fibres, conductive yarns, thermo-chromic materials, shape memory materials, that impart smart functionality to fabric [5]. Furthermore, introducing some salient smart features like GPS, music playing, phone charging, monitoring sportsperson's physiological parameters, stress relaxation and intensity of activity or workout are hailed and readily accepted by sportsperson who prefer performance clothing laced with technology.

Sportswear is not just crucial for athletes and sports person but this clothing segment has become an integral and inseparable part of users' routine activities like morning walk, jogging, yoga, stretching exercises and daily fitness activities owing to comfort, easy care properties and enticing aesthetic appeal of sports clothing [2, 3]. Smart materials possess the capability of responding to external stimulus such as change in the ambient conditions from mechanical, thermal, chemical, electrical or magnetic sources.

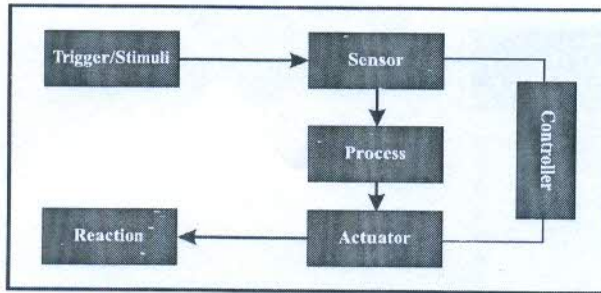


Fig. 1. Different components of smart clothing & the mode of responding to external stimulus

Figure 1 shows the different components of smart clothing like sensors, actuators, controlling unit and the mode of responding to external stimulus.

Sensors: are used to sense the stimulation in external environment and send it further for reaction.

Actuators: collect the sensed signal directly or from a central control unit; together with the sensors.

Controlling Unit: is analogous to human brain with cognition, reasoning and activating capacities [4].

2. Smart raw material procurements & innovative approaches for Smart Sportswear Designing

A major challenge in designing smart sportswear is engineering smartness without compromising the inherent

textile characteristics like handle, softness, light weight, washability, easy care properties, durability and comfort. Therefore, the conventional approach of designing the smart sportswear by integration of external sensors, light emitting elements, electronic circuitry and batteries have gradually undergone transformation with inclusion of high performance and smart fibres, yarns, fabric structures and innovative printing and finishing technologies. Figure 2 shows the innovative fibres, yarns and fabric structures used for sportswear development. The technological innovations at the fibre, yarn, fabric and finishing stage are discussed in the following section.

Hygra is a preferred choice for designing active sportswear owing to its superior antistatic properties and exceptionally high-water absorbing ability that is crucial to maintain dry microclimate for the sports person. The water absorbing ability of the fibre is attributed to the core-sheath filament composed of fibre made of water absorbing polymer and nylon. The water absorbing polymer can absorb 35 times its own weight of water and provide rapid dry ability of sports clothing while strength and dimensional stability is ensured by the core composed of nylon fibre.

Dryarn, a recyclable microfiber results in light weight, antibacterial, comfortable, soft handle and quick drying fabric with excellent thermal regulation and thus is suitable for smart sportswear [5,6]

Killat N is suitable for active and performance wear owing to

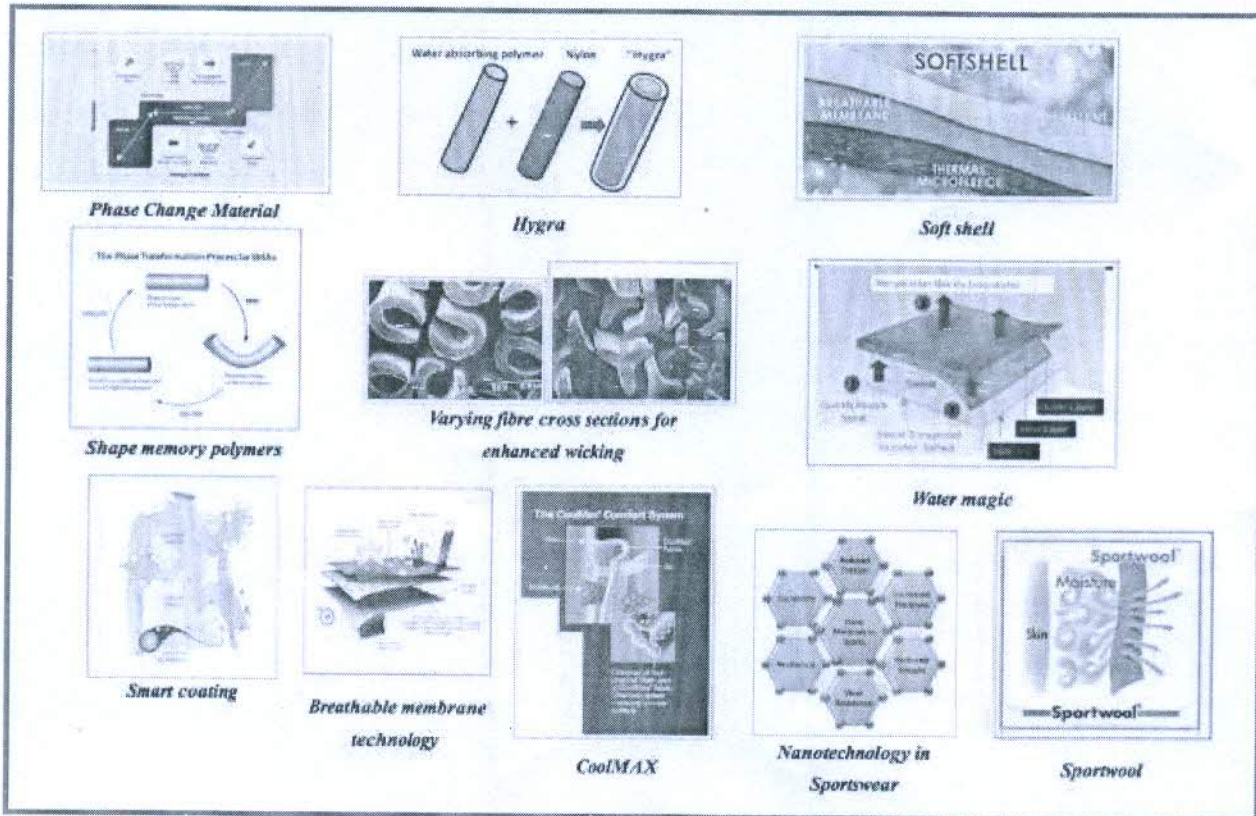


Fig. 2 – Innovative Sportswear fibres, yarns and fabrics

its rapid liquid transmission property by capillary wicking. The bi-component filament yarn is composed of soluble polyester copolymer core and nylon sheath. The water absorbency and heat retention characteristics are provided by nylon in sheath while capillary action for liquid transmission and creation of air pocket is due to hollow core produced by alkali dissolving of polyester copolymer core [6,7].

Triactor features Y shaped cross section thereby increasing the channels for capillary wicking and thus the fabric composed of this polyester variant exhibits faster release of perspiration.

Coolmax is another popular fibre generally used for sportswear owing to improved wicking capability and moisture vapour permeability that the double scalloped fibre exhibits.

Soft shell fabric features three layers namely the upper, middle and innermost layer. The upper layer is water repellent polyester, middle layer, the breathable membrane and innermost layer of micro fleece that provides good thermal insulation. The fabric is designed to impart wind and weather resistance, good breathability and freedom of movement along with maximum wearer comfort in different environmental conditions [8,9].

Naiva fabric is another specialty fabric suitable for mountaineering and active sportswear exhibiting good moisture permeability, light weight and soft feel. The fabric is composed of 55% Eval and 45% nylon, with Eval being copolymer resin of ethylene vinyl-alcohol [8,9].

Field Sensor is a high-performance multilayered fabric composed of coarser denier yarn in outer layer and inner layer of fine denier hydrophobic polyester. The variation of yarn coarseness in inner and outer layer of fabric results in quick sweat evaporation from fabric surface [8,9].

Phase change materials also referred to as latent heat storage materials find application in sportswear and cold weather clothing owing to their salient characteristic of changing their phase in response to external ambient conditions of variable temperature. The PCM can be applied to textile substrates as microcapsules that liquify and store heat energy at elevated temperatures whereas the paraffin solidifies and releases the stored heat as the temperature drops down [10].

Shape memory polymers in response to external ambient conditions like temperature, pH and chemical can respond and adapt by changing their shape and memorizing the previous shape. The materials find application in smart sportswear and winter wear for achieving enhanced thermal insulation [11, 12].

Membrane technology utilizes a thin polymeric membrane films of thickness of the order of 10 microns that can be coated on a textile substrate to render it waterproof, windproof and breathable. Micro porous and hydrophilic membrane are generally utilized for imparting water proofing and breathability in smart sportswear.

Smart coatings are effective in reducing the air drag to which cyclists, sprinters and swimmers are exposed to as they indulge in high-speed performance sports. The state of art biometric swimsuit Fastskin® is inspired from shark's skin which features specially articulated scales on its surface intended to reduce the drag through water [13].

Nano materials for smart sportswear Nano materials namely carbon nano fibres, nano clay, silver nano particles, nano nickel and carbon nanoparticles are increasingly finding application in smart sportswear as the nano finished textiles exhibit several salient features like UV, wind and water resistance, self-cleaning and antimicrobial properties [14-16]. One such state-of-the-art swim wear modified with nanoparticles is capable of reducing the absorption by 2% of fabric weight [17].

Water magic, a three-layered knitted fabric composed of 67% polyester and 33% nylon ultra-fine microfibre features innumerable random and minute pores that quickly transport perspiration from the wearer's skin to outer layer and thus provide dry, comfortable feel to the sportsperson [16,17].

Sportwool® by Woolmark is composed lightweight, machine washable fine merino wool and polyester exterior. The exceptionally high thermal insulation, UV protection and rapid sweat dissipation makes the fabric suitable for cold weather clothing and sportswear.

3. Smart sportswear for health & well-being monitoring

Fig. 3 shows smart sportswear to monitor sports person's physiological parameters.

The unique and smart features offered by smart sportswear make them suitable for a range of performance and functional based applications as enlisted below:

Performance and data analysis

An important aspect of sportswear encompasses maximizing human performance, improving and monitoring sports person's performance. Watches or strap bands equipped with sensors are capable of recording a range of wearer's physiological data such as distance covered, steps taken, calories burnt, speed of the activity and body temperature etc. The integrated sensors in the wearer's clothing are capable of monitoring health related parameters and in turn recording temperature, sweat and muscle movement and even the athlete's emotional response. The real time data recorded can be viewed or even retrieved for later use to track a sportsperson's performance. The data can be systematically analyzed to guide the sportsperson to improve and work on their technique, fitness level and even to avoid injuries [6].

Health monitoring

The smart sportswear ensemble is increasingly being incorporated with sensors exhibiting the capability of measuring body functions and biomechanics such as heart rate, breathing, lung capacity and perspiration or the muscle and joint movement. Smart sportswear so designed with

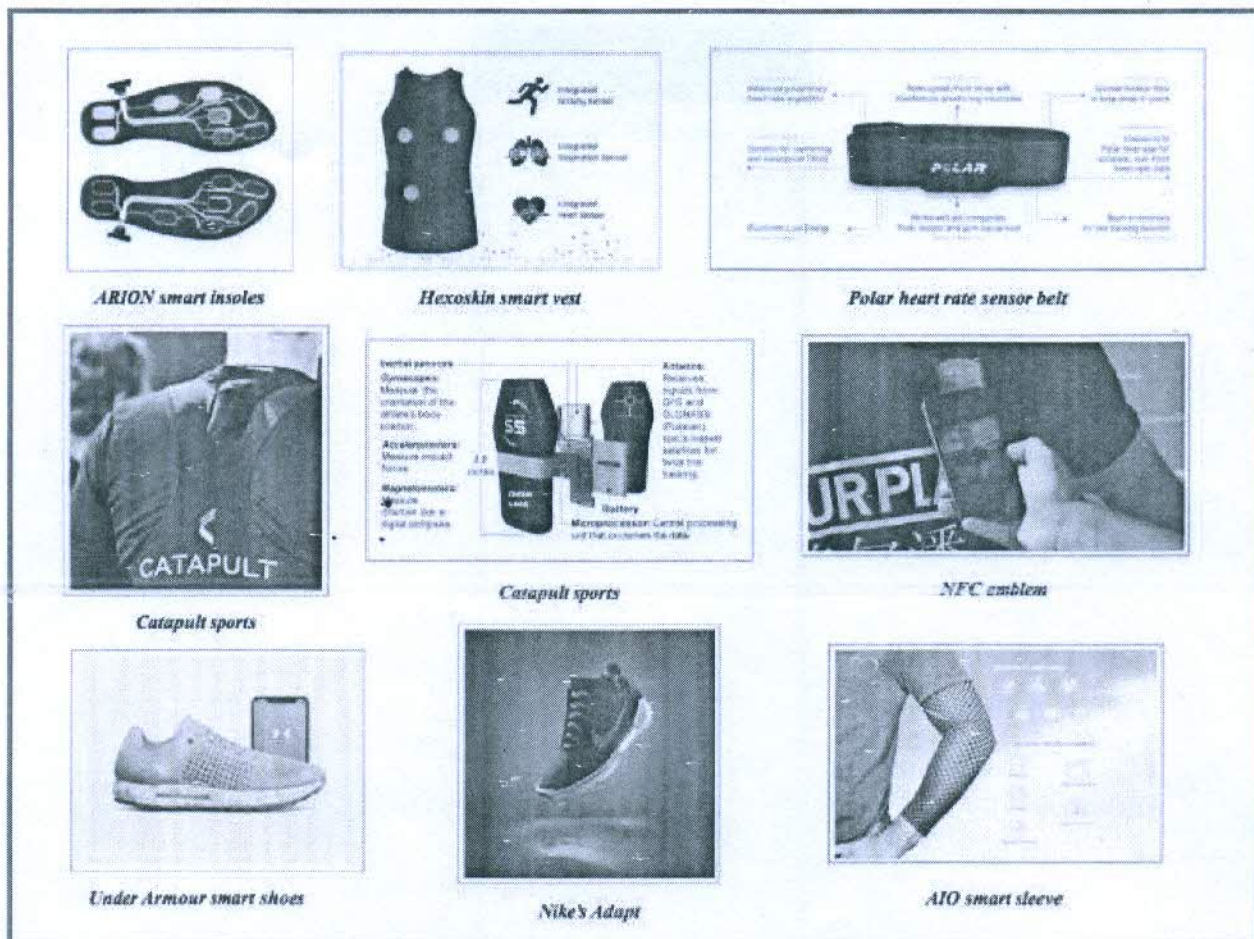


Fig. 3 – Smart Sportswear to monitor sports person's physiological parameters

integrated sensors can portray several salient and smart features like timely monitoring of any health ailment, reduction or elimination of injuries and prediction of injuries before hands as a result of Artificial Intelligence based analytics [6,7]. athletes and coaches in order to improve the performance of the athlete.

Several sportswear brands are offering technology laced, wearable sensors that cannot just monitor sportsperson's health related parameters but can serve as their personal coaches by providing data pertaining to workout patterns, intensity and speed of activity so that athletes can improvise based on the obtained data. The following section discusses some innovative smart sportswear that serve as a boon for sports person owing to multitude of functionalities they offer.

Nike's Adapt: Nike has been trailblazer in designing smart sports footwear that can electronically adjust according to the shape of wearer's feet [10].

Under Armour's smart shoe: uses record Sensor TM technology to connect to the smartphone app, MapMyRun. The app tracks the the course of a run by runner and reports data related to cadence, stride length, and distance travelled by the runner [9].

Polar heart rate sensor: Polar H10 heart rate sensor integrated in soft textile strap can effectively measure heart rate and connect heart rate to a wide variety of training devices via Bluetooth [7].

Intelligent heat ski jacket offers thermo regulation by sensing and responding to temperature variations. The sensors embedded in the jacket can measure the temperature difference of wearer and ideal temperature for wearer to be in thermal balance. As the ambient temperature drops down, the battery powered jacket will get heated up to provide warmth to wearer [6]

ARION smart insoles equipped with eight pressure sensitive sensors can measure the interaction between wearer's feet and the ground thereby assisting the runner to optimize running performance, reduce injury risk and increase the overall efficiency [7].

Hexoskin smart garments can track activity, sleep patterns and other physiological parameters of the sports person.[7]

Catapult sportswear is designing to monitor player's performance in terms of speed, distance covered, stress and fitness in real time thus improving athlete's performance and

reducing injuries by detection of stress on wearer's body during physical activity.

NFC emblems: NFC chip is integrated into the emblem to impart intelligence and functionality. The chips contain a UID which is connected to a customized ID and can be directly stitched to the textile [8, 11].

4. Conclusion

The sports segment of technical textiles is one of the most promising and innovative avenues that serves as food for the thought for researchers, sportswear designers and manufacturers. The inclination of common masses towards fitness and leisure activities prompts them to buy functional yet aesthetic athleisure. The consumers primarily seek performance, health, hygiene, comfort and safety aspects in their sports attire. Furthermore, smart features incorporated in sports person's clothing can enhance their performance by monitoring their physiological parameters and keep them updated on their workout patterns.

The quest for technology laced, sensor integrated smart sportswear is gaining momentum with the advent of

technology and smart apps to monitor's wearer's health and wellbeing. Consequently, not just sportsperson indulging in performance sports but tech savvy, fitness freak consumers also prefer a technologically evolved clothing that can be connected to their smart phone, play music, serve as global positioning systems and can keep a track on their workout schedule. Accordingly, a range of smart sports apparels and accessories are gaining popularity among fitness connoisseurs. Smartness can be engineered in sportswear by incorporation of external sensors and other components that can sense, respond and adapt. Alternatively, the incorporation of high performance and specialty material can further impart smart functionality to clothing. The smart sportswear can serve as a personal trainer for sportsperson monitoring their vital physiological parameters like heart rate, oxygen saturation along with performance and endurance related aspects like position, motion impact, workout patterns and calories burnt to enhance health, wellness and performance of athletes. The future thus belongs to smart sportswear as the field offers enormous potential for further technological innovations and developments.

References

- [1] <http://www.uptti.ac.in/classroom-content/data/high%20active%20sportswear%201.pd>
- [2] http://site.iugaza.edu.ps/aabuzarifa/files/Advanced-Materials-20151_Ch5.pdf
- [3] <https://core.ac.uk/download/pdf/270262935.pdf>
- [4] <https://www.slideshare.net/saifulalam16/smart-textile-55695496>
- [5] <https://www.bbntimes.com/technology/applications-and-challenges-of-smart-clothing>
- [6] <https://sporttomorrow.com/4-awesome-reasons-why-smart-textiles-improve-athlete-performance/>
- [7] <https://butlertechologies.com/performance-sportswear-smart-textiles/>
- [8] <https://www.smart-tec.com/en/business-sectors/textile-industry>
- [9] <https://www.roadrunnersports.com/blog/smart-shoes/>
- [10] <https://www.nike.com/in/adapt>
- [11] <https://komodoitec.com>
- [12] <https://www.ijert.org/research/recent-development-in-textile-for-sportswear-application-IJERTV3IS051844.pdf>
- [13] <http://www.mltj.online/wp-content/uploads/2020/06/Scataglini.pdf>
- [14] <http://www.sasmira.org/sportswear.pdf>
- [15] <https://blog.castbolzonella.com/2019/12/05/softshell-fabric-what-is-it-and-what-are-its-3-characteristics/>
- [16] <https://www.nanoshel.com/Nanotechnology-in-Sports>
- [17] <https://www.nanoshel.com/Nanotechnology-in-Sports-Equipment>
- [18] <https://static.fibre2fashion.com/articleresources/PdfFiles/57/5626.pdf>

Journal of the Textile Association


We are constantly working on ways to make each successive journal more relevant, internationally look and applicable to you and your business. With guidance and feedback from discerning readers such as you, we can add more value to future issues of JTA.

Your opinion is important to us. Please give us your feedback at
taicnt@gmail.com; jb.soma@gmail.com

Please visit us at
www.textileassociationindia.org

Recreation of Traditional Textile's Splendor in Contemporary Female Knitted Casualwear

Jhanji Y*

*Department of Fashion & Apparel Engineering, The Technological Institute of Textiles & Sciences, India****Corresponding author:** Jhanji Y, Department of Fashion & Apparel Engineering, The Technological Institute of Textiles & Sciences, IndiaReceived:  May 15, 2021Published:  May 28, 2021

Abstract

India is a country with rich culture and heritage which is reflected in the expression of folk art. Unity in diversity is apt not just in the dialect, lifestyle, and cuisines of different states but also in the dress up and traditional art, craft and folk culture. Due to diversified talents, interests and inspiration, each state has special identity for its unique traditional and hand-crafted textiles. The art of madhubani painting is the traditional style developed in the surrounding villages of madhubani in Mithila region, Bihar. The skill primarily accomplished for home decor has gradually evolved, being handed down through generations, and extensively employed for textile applications owing to the galore of traditional designs & patterns the technique offers. Most of the traditional techniques are performed on handloom fabrics; however, a range of raw materials can be experimented with to bring out the magnificence of traditional art forms on textiles. The apparel and accessory designers take inspiration from the lively, mythological and colorful motifs of these beautiful art forms and have been extensively using these motifs for design and development of a gamut of high-end artifacts, apparels, home textiles and accessories using a range of textile raw materials apart from conventionally used handlooms fabrics. The present study was undertaken to identify the preferential traditional techniques which entice consumers and thus designing cost effective contemporary apparel and accessory styles experimenting with base fabric and replacing handloom with knitted fabrics as the later ensures comfort, dexterity stretch ability and can be easily converted into complex silhouettes. The target consumer group was female millennials who prefer a casual look in office wear, seeking traditional appeal with a modern twist but shy away due to exorbitant prices of authentic handcrafted pieces of workmanship. Further, the respondents preferred complimenting the attires with quirky fashion jewelry and handbags. The designed collection named "Tradmod" symbolized fusion of traditional and modern features in female wear. The clothing was designed taking inspiration from structured and unstructured interview schedules, field visits to local markets selling traditional textiles and promotional hubs for artisans works like Suraj Kund Crafts Mela, Hunar Hatt, Delhi Hatt. Moreover, firsthand data collection by one-to-one communication with artisans in Haryana, Rajasthan and Bihar was accomplished with an indent to select the traditional motifs for surface ornamentation and thus recreation of traditional look in contemporary design collection.

Keywords: Artisans; contemporary craft; hand painting; madhubani; motifs; revival; shibori, stencils; traditional

Introduction

India is a country with rich culture and heritage which is reflected in the expression of folk art. Unity in diversity is apt not just in the dialect, lifestyle and cuisines of different states but also in the dress up and traditional art, craft and folk culture. Due to diversified talents, interests and inspirations, each state has distinctive identity for its unique traditional and hand-crafted textiles. A myriad of traditional techniques namely hand painting, dyeing and printing techniques are extensively utilized for surface ornamentation of textiles. The techniques are specific to particular region of country and accomplished by artisans as part of their rich legacy and also as a means of livelihood. The need of the hour is the massive promulgation of workmanship by artisans in

a holistic manner so that they are not forced to opt for alternative income generating sources due to waning of traditional arts with automation and mechanization in all spheres of textiles. Per se the designers have been working in close association with artisans not just to augment their earnings but also to come up with design collections intended for the consumers deeply connected to roots and having penchant for hand crafted, traditional artifacts. A range of traditional painting, embroidery, dyeing and printing techniques namely madhubani, kalamkari, phulkari, kaantha, shibori, tie and dye, block printing etc have been designers' source of inspiration for designing contemporary apparel and accessories with a tinge of traditional appeal. Designers work closely with artisans to

incorporate the design elements inspired from traditional motifs and colors frequently used by artisans in their creations. The design inspiration is drawn from the vibrant color hues and lively, mythological and colorful motifs of these beautiful art forms for design and development of a gamut of high-end artifacts, apparels, home textiles and accessories using a range of textile raw materials.

Most of the traditional techniques are performed on handloom fabrics; however, a range of raw materials can be experimented with to bring out the magnificence of traditional art forms on textiles. Madhubani painting is a traditional folk art of Bihar. Madhubani is synonym to Forest of Honey, a place near Durbhanga district in North Bihar. The places are well known for their beautiful traditional folk art- Madhubani painting. The wall paintings are not merely an aesthetic entity but express much deeper connotations, themes and narratives in the form of stories that are narrated in a series of panels. Apart from their decorative purpose, the paintings provide an aid for visual education like picture books depicting the rich heritage of Bihar [1-3]. The madhubani wall and floor painting are the most exclusive and popular art forms in Mithila region. The wall-paintings referred to as Mural, Mithila or Madhubani paintings can be seen in all household in and around this region. Indubitably, the paintings have been gaining widespread popularity in modern era's home decor for consumers having inclinations towards traditional textiles and art forms. The paintings can be accomplished on paper, canvas and cloth for commercial usage. The locals and artisans in countryside and nearby regions of Mithila practices the art form as part of their religious belief of staying connected to their Lords and have been diligently involved in decorating the pooja room, ritual area and bridal room, during processions, festivals, rituals and ceremonial activities with these paintings [4,5]. The symbols utilized in painting connote specific meanings such as fish symbolize fertility, procreation and good luck, peacocks symbolizes love and religion, and serpents are indicative of divine protectors. Animal, human and Flora and mythological motifs of Gods, Goddesses are an integral part of wall, floor and textile madhubani paintings. The skill primarily accomplished for home decor has gradually evolved, being handed down through generations, and extensively employed for textile applications owing to the galore of traditional designs & patterns the technique offers [6].

Shibori is a Japanese resist dyeing technique characterized by soft and blurry-edge pattern unlike the sharp-edged resist achievable with stencil, paste and wax. Although the technique finds its origin in Japan, nonetheless the craft has been enjoying worldwide popularity with Middle East, Indian subcontinent, South China, West Africa, Indonesia and Himalayan region exploring the art and incorporating the technique in regional design collections. The technique is no doubt labor intensive however the splendid patterns obtained by the resist dyeing technique has led to fashionable interpretations of shibori in global arena from local ramp shows to runways in Paris [7]. The shibori technique involves binding portions of fabric with thread to create a myriad of patterns on textile substrates for surface ornamentation. The prerequisite to

obtain shibori patterns is rendering a three-dimensional form to the fabric either by folding, crumpling, plaiting or twisting unlike other surface ornamentation techniques like stenciling that treats the fabric as a two-dimensional entity. A variety of contraptions like string, rubber bands, clamps and wooden blocks ensure that twisted, bound, folded or stitched fabric area is prevented from dye uptake whereas untied fabric area readily picks up the color thereby creating unique patterns and contrasting shades in corresponding dyed and undyed regions of fabric. The commonly employed shibori techniques for apparels and accessories include Kanoko, Muira, Kumo, Nui, Arashi and Itajime shibori [8,9]. Kanoko also referred to as tie-dye is accomplished by binding few sections of the base fabric in order to achieve the circular patterns. Muira shibori or looped binding involves plucking fabric regions via hooked needle and subsequently looping thread around each plucked section at least twice to create magnificent water like effect. The technique is devoid of any knots and thus enables convenient binding and unbinding of fabric. Kumo shibori utilizes fabric manipulation technique namely pleating to create elegant spider-web-like circular patterns as the fabric is subjected to pleated and binding.

Nui shibori also referred to as stitched is accomplished by application of running stitch and gathering it by pulling tightly so as to achieve undyed effect owing to resistance offered by stitches. However, the technique demands precision as securing of thread by knotting prior to dyeing is crucial to avoid the stitching getting undone. Arashi or pole-wrapping shibori symbolizes the driving rain of a heavy storm owing to diagonal pattern obtained on the treated fabric. It is one of the extensively used shibori technique owing to the simplicity and minimal skill requirement to perform the process. The technique involves diagonally wrapping the fabric around a pole. The tight binding of fabric by wrapping thread up and down the pole followed by fabric scrunching on the pole results in creation of pleated cloth with a diagonal design. Itajime shibori also known as shape resist shibori involves resisting dye penetration in certain fabric regions by sandwiching the fabric between two wooden pieces held in place with strings. The technique produces a distinctive grid like pattern owing to dye exposure to edges of the fold secured by wooden blocks [9]. Apart from conventional process of creating shibori effects on woven fabrics, the technique has undergone transformation as far as raw materials and process parameters are concerned. The clothing designed from knitted fabrics can also be embellished using the shibori technique. Furthermore, circular or flat knitting machines can be employed to obtain the resist dye patterning by imitating the distinguishing feature of three-dimensional forms of traditional shibori by varying process parameters like float length, course spacing, and distribution of tuck and float stitches of gathering threads [8,9].

Knitted fabrics owing to their stretch and comfort properties are widely being used for apparel and accessories development. Single jersey, rib and interlock knit structures vary widely in their physical and comfort properties and generally used for design and development of a range of apparels and accessories. Knitted fabrics

owing to their stretch ability and comfort properties are finding application in development of varying styles of female upper and lower torso garments namely crop tops, shift dress, sheath dress, slip dress, a line dress, flared skirt, pencil skirt, palazzo trousers, palazzo pants/ jeggings, layered palazzos, trouser style palazzos, pleated palazzos and side slit palazzo. Apart from apparels, knit structures are also increasingly utilized for accessory designing. Accessories are additional items worn along with apparels to complement and enhance the look of apparels. Accessories are categorized based on raw material usage, functionality, application area and styles. Handbags, hats, and scarves are considered to be functional accessories, however, ornaments, jewelry are merely decorative and status symbol in nature. Designing the surface of the garment to render it beautiful and attractive appeal is referred to as surface ornamentation or embellishment. Embroidery, beading, ribbon embroidery, hand painting, macrame, applique, crocheting resist dyeing and block printing are the different ornamentation techniques employed for surface embellishment of apparels and accessories. The market survey and field visits to local markets highlighted that although there is gamut of madhubani painted, foil printed and shibori dyed woven and handloom ethnic wear available in various price points. However, there was dearth of contemporary and customized range of knitted apparels and accessories embellished with aforesaid techniques. The present study therefore aims to address this pitfall and identify the preferential traditional techniques, styles and silhouettes which entice consumers and thus designing cost effective, contemporary apparel and accessory styles experimenting with base fabric and replacing handloom with knitted fabrics as the latter ensures comfort, dexterity, stretch ability and can be easily converted into complex silhouettes. The target consumer group for the study was female millennials who prefer a casual look in office wear, seeking traditional appeal with a modern twist but shy away due to exorbitant prices of authentic handcrafted pieces of workmanship.

Materials and Methods

Materials

Cotton knitted fabrics in three different structures namely single jersey, rib and interlock were procured from Richa Global, Gurugram. The fasteners such as zippers, velcro, magnetic closures, chain links and other essential supplies used for clothing construction and embellishment namely sewing thread, acrylic colors, indigo powder and washing soda were procured from local market in Bhiwani. The customized stencils were prepared by free hand sketching on cardboard and cutting along edges of required motifs.

Methods

Knitted samples were tested for their physical and mechanical properties. Aerial density of fabrics was determined on electronic weighing balance as per ASTM standard D3776. Courses and wales per inch of test samples were measured using pick glass. The fabric thickness was measured with Essdiel thickness tester.

Drape coefficient of test fabrics was determined on Cusick drape ability tester as per ISO 9073-9 standard. Knitted fabrics evaluated for their physical and mechanical properties were converted into wearable, functional apparels and accessories to render casual and relaxing look to workaholic professional women.

Design initiation & conceptualization

The design process initiated with garnering inspiration pertaining to colors, motifs, silhouette and design elements from structured and unstructured interview schedules, field visits to local markets selling traditional textiles and promotional hubs for artisans works like Suraj Kund Crafts Mela, Hunar Hatt and Delhi Hatt. Moreover, firsthand data collection by one-to-one communication with artisans in Haryana, Rajasthan and Bihar was accomplished with an intent to select the traditional motifs for surface ornamentation and thus recreation of traditional look in contemporary design collection. The selection of knit structures for varied styles and silhouettes was based on their test parameters and analysis of respondent's ratings. The styles of upper and lower torso garments to be designed were chosen based on expert ratings and subjective evaluation by respondents. The target respondents were professional female millennials with sedentary profile whose daily routine included commuting to workplace and spending long working hours on laptops. Consequently, the respondents preferred comfortable yet form fitting attire to suit their apple shaped body profiles. The respondents were females aged 25- 35 years working in corporate sector in Delhi, Gurgaon and Noida. The experts were free-lancing designers and faculty of Fashion Institutes in Delhi and Haryana. The responses by the respondents assisted in style selection of upper and lower torso garments namely cold shoulder, crop top, tank top and fit and flare dress, jeggings, harem pants and skirts. The design process initiated with hand drawn flat sketches for styles approved by expert panel and respondents. The sketches included all the design details pertaining to surface embellishment technique and motif placement on end products as shown in Figure 2.

Pattern making & assembling

The two-dimensional pattern making technique of drafting was utilized to prepare the patterns for each individual garment style using the standard size charts for aforesaid age groups. The sewing of garments was accomplished on Juki's single needle lock stitch machine; model DU-1181N with maximum sewing speed of 2,000st/min, SPI of 12. Class 4 flat seam was used for assembling the garment components.

Surface embellishment techniques

The field trials and questionnaires filled by female respondents suggested that females prefer complimenting the attires with quirky fashion jewelry and handbags. Accordingly, complimentary functional and aesthetic fashion accessories were designed to complete the contemporary look. The designed accessories included clutch and sling bag and fashion jewelry. Surface embellishment of

designed apparels and accessories was accomplished by kanoko shibori resist dyeing and hand painting to simulate the madhubani and foil printed effect. The dye solution for kanoko shibori was prepared by dissolving 4.5 tsp washing soda in 3-6 tbsp boiling water and allowing cooling slightly. Six level tsp indigo powder was added to the solution and mixed well into a smooth paste for nearly ten minutes. Approximately twelve litres of water were added to make the vat into a stainless-steel dye pot and heated up to 50 ° C followed by addition of twenty five g/1oz of hydros. The solution was stirred gently minimizing formation of air bubbles. The vat was allowed to stand for 30-45 minutes, covering the pot with lid and maintaining constant temperature. The damp fabric after being tied at random positions was dipped into the vat squeezing out any excess water already present in fabric. The dyed fabric after removal from vat was dipped in cold water ensuring that any undissolved grainy particles of indigo dye powder could get dissolved to avoid blotches on the fabric.

Motif selection

The motifs for simulating madhubani and foil printed effect on knitted fabrics via hand painting were chosen meticulously after brainstorming and exhaustive exploratory studies of madhubani and foil printed motifs extensively utilized in home decor, stoles, dupattas and sarees showcased in Delhi Hatt, Hunar Hatt, Fab India, online websites such as Tijori, Itokri and from traditional textiles sold in local markets in National Capital Region. A close dialogue with artisans of NCR, Bihar and Haryana region also depicted the motifs generally used by artisans for home decor or painting on textiles. Accordingly, 10 commonly used motifs depicting the flora and fauna were selected in totality for the present study. The ranking of motifs by expert evaluation indicated that the six motifs were among the highest ranked ones (Table 1). Thus, the six highest ranking motifs were used for simulating the madhubani art form and foil printing on the apparels and accessories. The motifs and their ranking are presented in Figure 1.

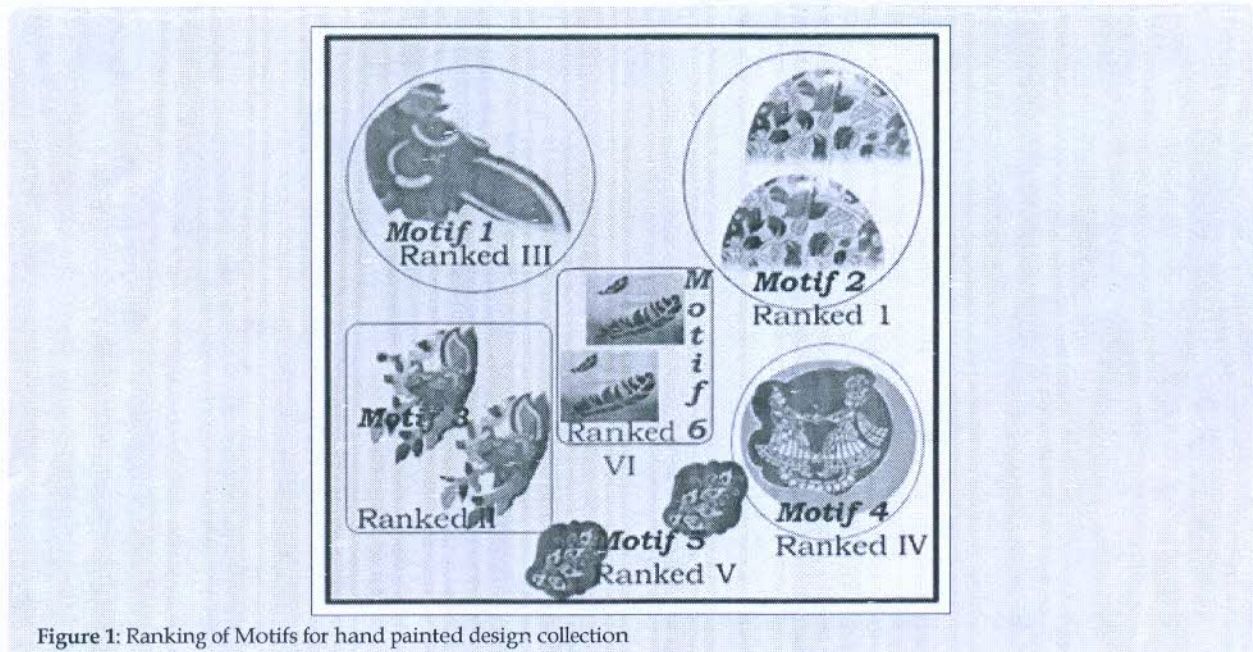


Figure 1: Ranking of Motifs for hand painted design collection

Table 1: Ranking, motif selection & placement for design collection.

Motif No.	Expert Ranking	Designed Article	Motif Placement
1	III	Sling bag	All over print
2	I	Clutch bag	All over print
3	II	Fit & flare dress	Left placement on dress's yoke
4	IV	Sling bag	Centrally placed
5	V	Sando top	Diagonal placement along hemline
6	VI	Crop top	Centrally placed

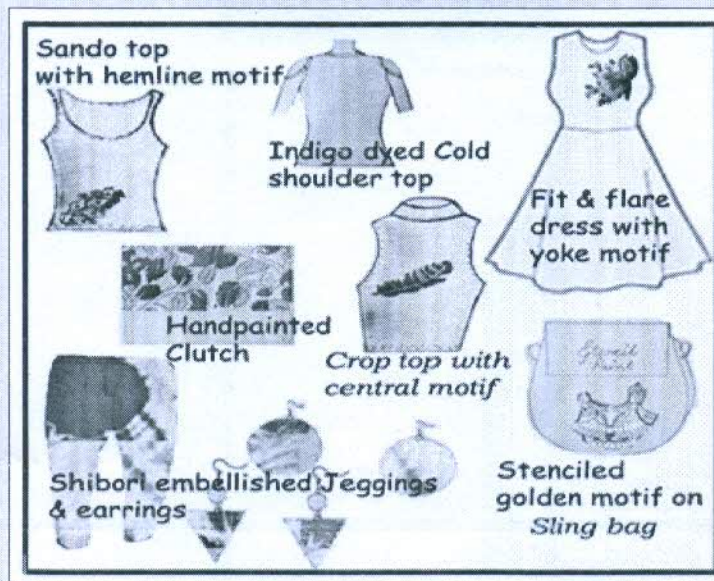


Figure 2: Flat Sketches depicting the embellishment technique & motifs

Color palettes for motifs

The filling of motifs for hand painting was accomplished by expert ratings and respondents color preferences as they were asked to choose from color palettes with an intent to coordinate the color of motifs with that of the base fabric being utilized for apparels and accessories. The final motif placement on apparels and accessories was decided based on expert ratings and respondents' preferences who were expected to express their likelihood of buying the attires embellished with same motif but variable placement on designed end articles.

Results & Discussion

The procured knitted fabrics were tested for their physical and mechanical properties. Results are presented in Table 2. Fabric thickness was observed to be highest for interlock structures and lowest for single jersey fabrics. The same trend was observed for

aerial density of fabrics. Comparison of knit structures revealed that single jersey fabrics showed the lowest value of drape coefficient. The structure was suitable for design and development of apparels owing to good drapability. However, the fabric exhibited curling at edges. Fabric chosen for apparel construction was based on their aerial density, drapability properties. Moreover, subjective evaluation also supported the objective evaluation with respondents giving precedence to single jersey fabrics for summer wear and clothing designed to exhibit larger amount of flare. Accordingly, single jersey fabric was utilized for harem pants which were designed to exhibit flare along the side seam. The rib structures owing to good drapability properties were used for construction of upper and lower torso garments. Interlock fabrics exhibited optimum drape ability to be used as heavier upper and lower torso garments. Hence fit and flare dress, tank top and skirt which required minimal flare compared to rib full sleeve top was developed using interlock fabrics.

Table 2: Physical & Mechanical Properties of knitted fabrics.

Fabric Sample Code	Aerial Density (g/m ²)	Bending Length (mm)	CPI	WPI	Thickness (mm)	Drape Coefficient
S	151	1.2	37	48	0.82	0.02
R	198	1.25	52	50	0.98	0.36
I	249	1.34	25	45	1.15	0.41

Crop top was designed as skin hugging entity constructed from rib knit structure rather than using interlock fabric owing to higher aerial density of the latter which may not be comfortable when worn next to skin. The subjective evaluation by respondents provided a foundation for selection of design elements, stylization and embellishment techniques for the design collection. The

respondents were working females aged 25- 35 years. The analysis of subjective evaluation suggested that 40% respondents preferred apparels composed of knitted fabrics over woven and non-woven counterparts (Figure 3a) while 60% preferred knitted accessories in contrast to woven and non-textiles accessories (Figure 3b). 50% respondents expressed liking for knitted earrings compared to

other knitted accessories as shown in Figure 3c. The style of upper torso garment most preferred by females was crop top with 50% respondents giving precedence to the former compared to tank and tube tops (Figure 3d). When asked about selection criteria for garments, 40% respondents confessed to make purchases considering the design aspects while nearly close percentage of 30% respondents gave precedence to comfort while buying a garment (Figure 3e). The subjects in response to the most preferred surface ornamentation techniques they seek in their apparels and accessories, had mixed reactions with 40% respondents expressing interest in hand painting, 30% in shibori dyed textiles, 20% in digital printing and only 10% preferred machine embroidery for surface embellishment as shown in Figure 3f. As far as the most

preferred style of lower torso garment was concerned, 40% respondents preferred jeggings while 30% of the respondents chose palazzo over other two styles and yet another 30% considered harem pants the ideal lower torso garment for themselves (Figure 3g). The analysis of subjective evaluation with 50% respondents choosing fit and flare dresses over other dress styles suggested that working females prefer fit and flare dresses compared to bodycon, shirt or asymmetrical dresses (Figure 3h). The handbag style most popular among female millennials emerge out to be sling bag with 50% females preferring sling bag in contrast to 30% preferring drawstring bag pack. However, females were hesitant to carry tote bag to offices as suggested by their poll as merely 10% chose tote as preferred office wear handbag style (Figure 3i).

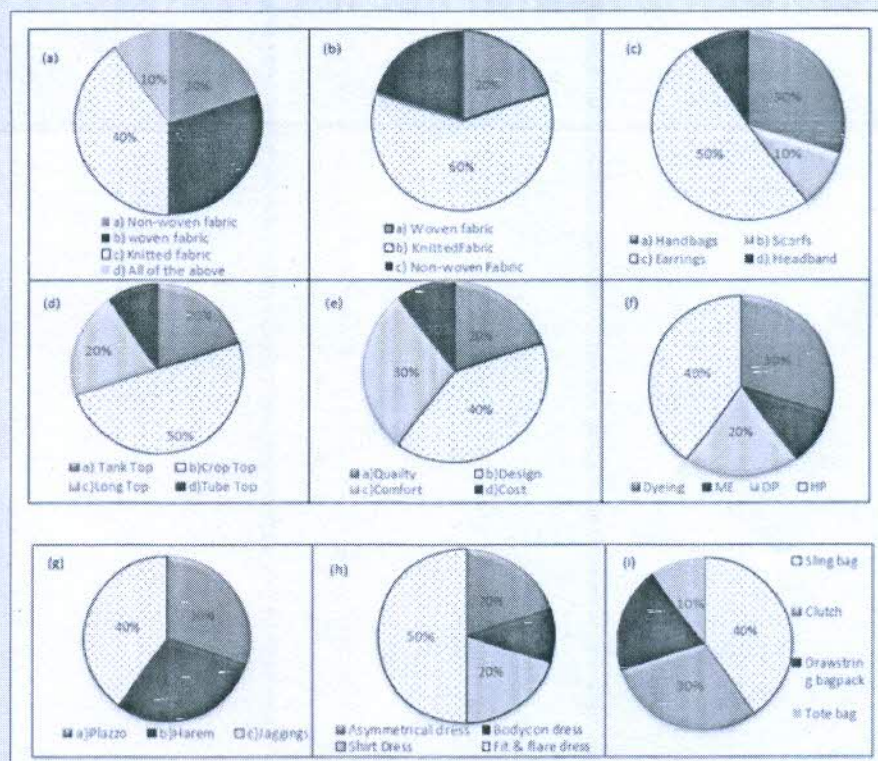


Figure 3 (a-i): Determination of style and embellishment techniques by subjective evaluation

The subjective evaluation served as a crucial and decisive aid for selection of the styles and embellishment techniques for apparels and accessories to be designed. Accordingly, based on respondent's responses, the chosen styles for design collection comprised of jeggings and harem pants for lower torso garments, fit and flare dress, crop top, sando top and cold shoulder top for upper torso garments. Likewise, the accessory styles chosen for the design collection included sling bag, clutch and drawstring bag pack. As far as surface embellishment techniques were concerned; hand painting, shibori dyed textiles and stencil painting were given precedence by respondents. Thus, based on subjective trial, the aforesaid embellishment techniques for apparels and accessories

were chosen to render traditional yet contemporary appeal to the design collection. The selection of styles and embellishment techniques was followed by motif selection and placement on apparels and accessories. Accordingly, the six highest rated motifs on the basis of expert ranking were chosen to simulate the madhubani and foil printed effect on developed end articles. Experts and respondents suggested an array of vibrant colors for motifs 1, 2 and 3 to recreate the madhubani look while they suggested otherwise for motif 4, 5 and 6 giving precedence to monochromes like silver, golden tones for simulating the foil printed effect on proposed design collection.

The vibrant color palettes used for motifs 1, 2 and 3 assisted in recreation of madhubani effect on hand painted end products while selection of monochromatic colors like golden and silver rendered a foil printed simulated effect using motifs 4, 5 and 6. The final motif placement on apparels and accessories was decided based on expert ratings and respondents' preferences who were expected to express their likelihood of buying the attires embellished with same motif but variable placement on designed end articles. Accordingly, motif 2, the highest ranked among all the motifs was preferred as all over print on accessories while respondents preferred motif 3 to be strategically positioned along the yoke of dress. Likewise, motif 1 depicting an intricate amalgamation of flora and fauna was preferred as overall print on designed accessories. However, motif 4 depicting the dancing deities was preferred along the centre front of the designed article. The respondents' rating suggested that motifs 5 and 6 would be more appealing to consumers as they are placed in offset position along the left or right panel of the garment. Figure 4 (a-c) shows the hand painted motifs and their placement

on the designed apparels and accessories. The designed collection named "Tradmod" (Figure 5) symbolizing the fusion of traditional and contemporary features in female work wear was developed utilizing the results and analysis of objective and subjective evaluation. The design collection comprised of three complete looks:

- Look I:** Solid dyed cold shoulder top and shibori leggings complimented with shibori dyed drawstring bag pack.
- Look II:** Fit and flare dress with hand painted madhubani motif complimented with hand painted sling bag
- Look III:** Stencil painted sando top and harem pant complimented with stencil painted sling bag

Figure 6 shows the designed female knitted casual wear recreating the appeal of traditional textiles.

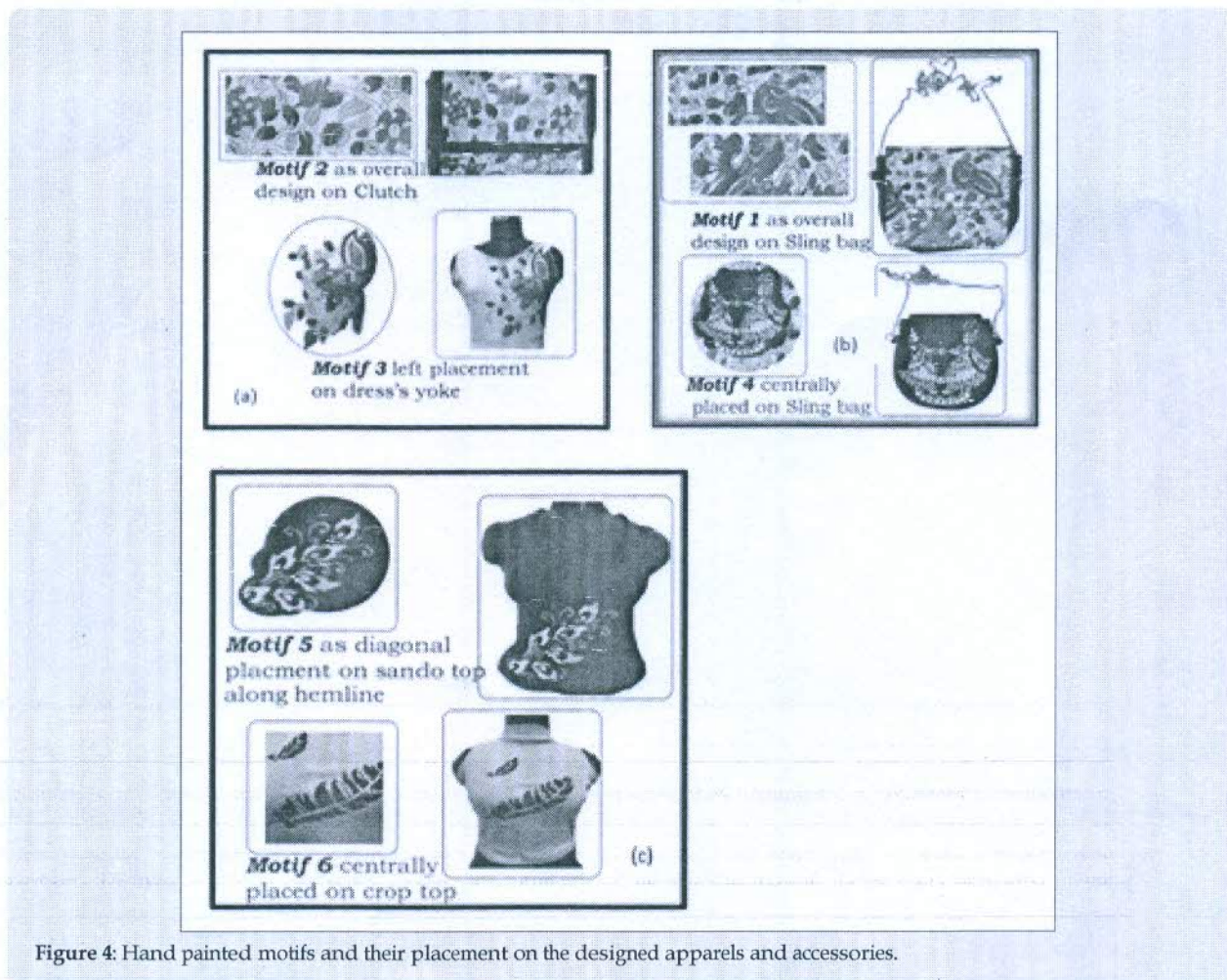


Figure 4: Hand painted motifs and their placement on the designed apparels and accessories.



Figure 5: Tradmod- The design collection.



Figure 6: Contemporary apparels & accessories (I, II & III clothing set with complementing accessories) created by recreation of traditional textiles.

The designed and developed apparels and accessories were evaluated subjectively and through wear trials to rate them on the basis of functionality, aesthetic appeal, and economic consideration. Figure 7 (a-h) shows the results of subjective evaluation of design collection by respondents. Sando top was the most preferred top style with 40% respondents voting for the mentioned top style while 30% females preferred crop top. However, kaftan top and cold shoulder top each were preferred by only 10% females. 40% subjects preferred to wear jeggings while skirts and harem pants each were selected by 30% respondents. 50% female respondents preferred madhubani painted design collection, 30% had soft corner for stencil painted designs while dyed dresses were preferred by 20% females as surface embellishment technique. The similar trend was observed for embellishment techniques for accessories. The styles of handbags evaluated subjectively highlighted that respondents gave precedence to sling bag style with 40% respondents rated the style their first choice while clutch

and draw string bags were equally likeable as each was chosen by 30% of the respondents. Stencil painted and shibori dyed lower torso garments were equally likeable with each preferred by 40% respondents while only 20% females preferred lowers dyed in solid colors. Eventually, the respondents were asked to provide overall rating to three looks comprising the design collection, 50% female respondents gave precedence to look II (fit and flare dress designed recreating the madhubani effect complemented with madhubani motif embellished sling bag) while 30% females preferred to look I (cold shoulder top and shibori dyed jeggings complimented with drawstring bag pack. Although, the percentage of respondents (20%) preferring look III (stencil painted crop top and harem pants complimented with sling bag) was less compared to other two looks, the concept was appreciated by females and suggested to replace the harem pants with palazzos or culottes for better dexterity and ease of travelling.

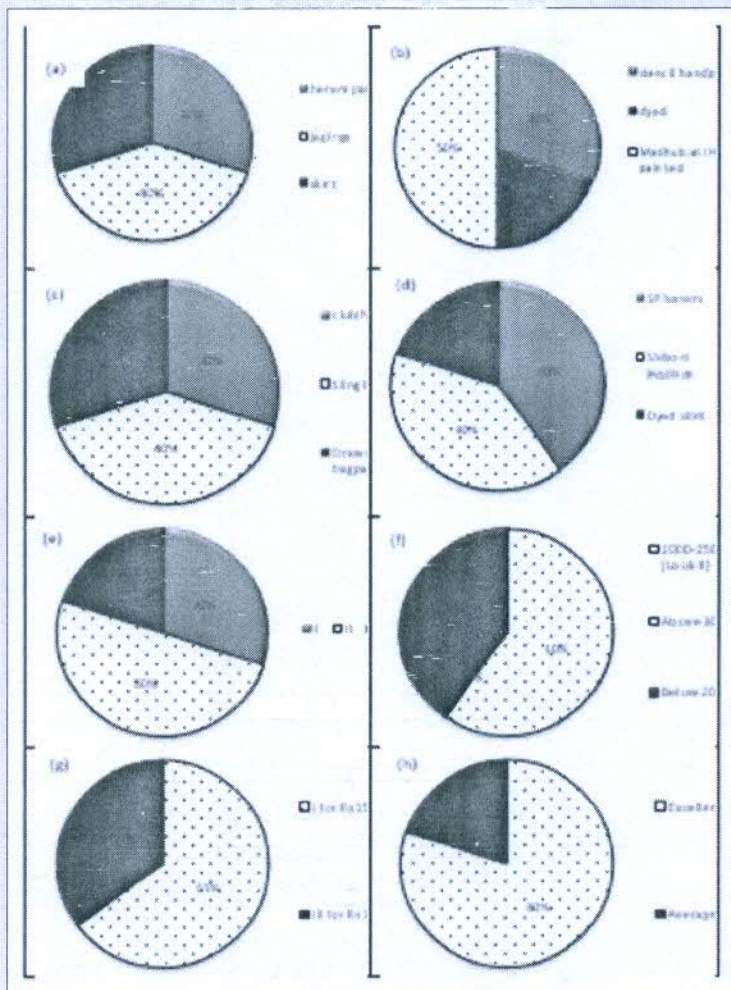


Figure 7: Rating of Design Collection based on subjective evaluation.

The cost evaluation analysis of three looks obtained from respondents suggested that 60% females would readily purchase the clothing and accessory set of look II in price range of Rs 2000-2500 while 40% expressed mixed opinion and would rather prefer the look if available below Rs 2000. As far as cost evaluation of look I and III was concerned, 65% female respondents expressed their promptness to buy the shibori dyed clothing set with complimenting bag pack in price range of Rs 1500-2000 while 35% females preferred look III over its counterpart. As the respondents were asked to provide overall rating of the design collection Tradmod, 80% respondents considered the collection excellent in terms of utility, comfort and aesthetic appeal while 20% considered the collection average. Thus, based on subjective evaluation, it was inferred that the most preferred contemporary style among female millennials was look II featuring fit and flare dress with sling bag both embellished with madhubani inspired hand painted motifs. The design collection was appreciated, and the respondents marked their acceptance by expressing willingness to purchase the attire at a price range of Rs 2000-2500. The feedback and wear trial by respondents suggested that the dress was comfortable, stretchable and aesthetically appealing. Furthermore, the respondents that accompanying sling bag not only beautified the dress but had functional aspect as well. The respondents after wear trials suggested that look I featuring a cold shoulder solid dyed top along with shibori dyed jeggings and bag pack were ideal combination while on move as the combo offered comfort and a quirky look to the wearer. The wear trial of look III by respondents suggested that although the silhouette and embellishment technique was likeable, but the harem pants were comparatively bulky and interfered with unrestricted wearer's movement. However, the female subjects explicitly appreciated the deity motif stenciled sling bag and showed promptness to buy the bag. Consequently, it can be recapitulated that today's professional, yet fashion conscious female seeks ethnic look with minimal attachments, particularly having a soft corner for handlooms traditional motifs like madhubani and shibori prints which was explored and presented to them via design collection "Tradmod".

Conclusions

The present study was undertaken to identify the preferential traditional techniques which entice consumers and thus designing cost effective contemporary apparel and accessory styles experimenting with base fabric, styles and surface embellishment techniques. The target consumer group was female millennials who prefer to titivate casual office wear and have penchant for traditional textiles. The designed collection named "Tradmod" symbolized fusion of traditional and contemporary features in female wear. The varied styles of apparels and accessories were designed and developed from different knit structures based on objective and subjective evaluation. It was inferred from subjective

evaluation that young women generally prefer knitted fabrics over woven and non-textiles for casual wear apparels and accessories. As far as surface embellishment techniques are concerned; today's professional yet fashion conscious female seeks ethnic look with minimal attachments, particularly possessing a soft corner for handlooms, traditional motifs, prints and textiles like madhubani and shibori prints. The design collection comprising of three looks was subjected to wear trials and ratings. The most preferred contemporary style among female millennials as a result of wear trials was look II featuring fit and flare dress with sling bag both embellished with madhubani inspired hand painted motifs. The respondents suggested that the dress was comfortable, stretchable and aesthetically appealing. Furthermore, the respondents opined that accompanying sling bag not only beautified the dress but had functional aspect as well. The respondents after wear trials suggested that look I featuring a cold shoulder solid dyed top along with shibori dyed jeggings and bag pack were ideal combination while on move as the combo offered comfort and a quirky look to the wearer. The wear trial of look III featuring sando, harem pants and sling bag embellished with customized stencils suggested that although the silhouette and embellishment technique was likeable, but the harem pants were comparatively bulky and interfered with unrestricted wearer's movement. However, the female subjects explicitly appreciated the deity motif stenciled sling bag and showed promptness to buy the bag. Consequently, it can be recapitulated that today's professional, yet fashion conscious female seeks ethnic look with minimal attachments, particularly having predilection for handlooms traditional motifs like madhubani and shibori prints which was explored and presented to them via design collection "Tradmod".

References

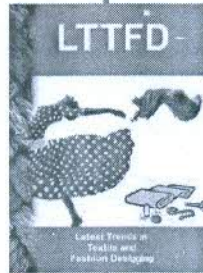
1. Yamini J (2020) Revival of Madhubani Painted Textiles.
2. Yamini J (2020) CAD intervention for Revival, Stylization & Adaptation of Madhubani Traditional Textiles, *Int J Mod Trend Sci Tech* 6(8S): 145-148.
3. <http://www.madhubanipaintings.com>
4. Thakur U (1982) Madhubani Painting, Abhinava Publication, New Delhi, India p.158.
5. Ram Prasad H, Arundhuti D, Shweta P (2018) A details study on Madhubani art of Mithila, Bihar, *J Emerg Techn Innov Res* 5(1): 1-5.
6. Mohini G, Swati G (2016) Adaptation of designs for textile products inspired from madhubani painting, *Int J Res Granthaalayah* 4(5): 1-3.
7. MacQuarrie L (2015) Modern shibori: beyond handcrafted tradition. University of New Brunswick, Canada p. 19-25.
8. Priyanka P, Aksiya A (2018) Application of Shibori Tie Dyeing Using Natural Dyes on Cotton Fabric, *Int J Manag, Tech Eng* 8(10): 2734- 2739.
9. William B, Kamwine S, Charles F (2015) Exploration of Innovative Techniques in Printed Textile Design, *Int J Innov Res Develop* 4(10): 1-3.



This work is licensed under Creative Commons Attribution 4.0 License

To Submit Your Article Click Here: [Submit Article](#)

DOI: 10.32474/LTTFD.2021.04.000178



Latest Trends in Textile and Fashion Designing

Assets of Publishing with us

- Global archiving of articles
- Immediate, unrestricted online access
- Rigorous Peer Review Process
- Authors Retain Copyrights
- Unique DOI for all articles



Moisture management properties of ring vis a vis rotor yarn plated knit structures

Y Jhanji^{1,a}, Deepti Gupta² & V K Kothari²

¹Department of Fashion & Apparel Engineering, The Technological Institute of Textiles & Sciences, Bhiwani 127 021, India

²Department of Textile Technology, Indian Institute of Technology Delhi, New Delhi 110 016, India

Received 11 June 2019; revised received and accepted 31 March 2020

The present investigation aims at studying the moisture management properties of polyester-cotton plated fabrics of ring vis a vis rotor yarns. Ring yarn fabrics exhibit higher moisture vapour transmission rate, trans planar wicking, lower wetting time and higher one way transport capacity as compared to rotor yarn fabrics, making the former suitable where body needs to dissipate sweat both in vapour and liquid forms. with respect to fabrics using combination of rotor-spun cotton yarns, which show higher absorbent capacity and would be slow drying with poor one way transport capacity. The study helps us to conclude that yarn spinning system plays an important role in influencing moisture management properties of fabrics intended for next to skin applications.

Keywords: Cotton, Fabric comfort, Moisture management, Plated fabric, Polyester, Ring yarn, Rotor yarn

1 Introduction

Clothing serves as a second skin enabling heat and mass transmission from human body to environment or vice-versa. Thermo-physiological properties of textiles are related to the thermal properties, air permeability and moisture management properties along with the drying ability of the textiles. Several fibre, yarn and fabric constructional variables determine the moisture management properties of textiles. Plated knit structures are characterized by distinct yet integrated inner and outer layers.

The flexibility in selection of contrastingly different fibre and yarn constituents in the two layers of plated fabrics make them suitable and versatile for applications, like intimate wears, sportswear, active wear, etc. The main elements of two-layered plated knitted structures are:

- Inner (next to skin) layer — This layer is in direct skin contact and consists of conductive and diffusive hydrophobic component which helps in removal and transportation of sweat to the outer layer.
- Outer (exposed to environment) layer — This layer is in contact with the environment and consists of absorptive hydrophilic components which provide large area for sweat absorption and evaporation to the outside environment¹⁻³.

Fibre parameters, process parameters and yarn production technologies are reported to change the yarn structure and the associated fabric properties. Ring-spun and rotor-spun yarns vary widely in their structures which contribute to the entirely different properties of the two yarns. Ring-spun yarn has an ideal cylindrical helical structure with same number of turns per unit length in each helix, uniform specific volume and maximum packing density in the outermost zone of the yarn cross-section. Rotor-spun yarn has a bipartite structure with an inner core which forms the bulk of the yarn and an outer zone of wrapper fibres occurring irregularly along the core length. Rotor yarn shows maximum packing density in first zone from core. Core part of rotor yarn relatively has dense structure; sheath part has less dense structure with belly-bands⁴⁻⁶.

Several researchers have studied the influence of various yarn variables like yarn types, yarn spinning systems and fibre variables like fibre fineness, fibre cross-sectional shapes on comfort properties of woven and knitted fabrics. Behera *et al*⁷ compared the comfort properties of ring-, rotor- and friction-spun yarn fabrics and suggested that rotor-spun yarn would be superior to ring-spun yarns in the absence of perspiration.

Lord⁸ investigated the relative moisture uptake characteristics of ring and open-end yarns and reported that open end yarn wicked better and more evenly but for a given yarn count, it is elevated to the

^aCorresponding author.
E-mail: yjhanji@gmail.com

same volume of water as ring yarn. Erdumlu and Saricam⁹ studied the wicking and drying properties of vortex spun yarns and knitted fabrics in comparison with ring-spun yarns and fabrics, and concluded that fabrics knitted from ring-spun yarns wicked and absorbed water more evenly than fabrics knitted from vortex spun yarns.

Manshahia and Das¹⁰ studied the effect of filament shape factor of inner and outer side of fabric on moisture management properties and concluded that the fabric, having filament of higher shape factor, exhibited better moisture management properties, viz larger wetting radius, higher one way transport capacity and quick absorption rate.

Smita *et al.*¹¹ investigated the effect of fibre composition on moisture management properties and peak heat flux (q_{max}) values of 100% polyester, 100% cotton, 100% modal, and cotton-polyester, modal-polyester blended fabrics. They observed that blending polyester fibre with cotton and modal resulted in improved moisture management properties of the fabrics in comparison to 100% polyester fabric.

Suganthi and Senthilkumar¹² studied the moisture management properties of bi layered knitted fabrics composed of varying fibre types in the inner and outer layers. They observed that the fabric composed of micro-fibre polyester in inner layer and modal in outer layer are suitable as active sportswear, owing to better moisture management property exhibited by the aforesaid fabrics in terms of high wetting radius, absorption rate and spreading speed.

However, literature survey shows that there is lack of systematic study on the influence of yarn spinning systems on thermo-physiological properties of plated knit structures. Yarns made on different spinning systems vary in their structure and packing, which may influence moisture vapour and liquid moisture transmission through fabrics. Therefore, the selected variable is crucial in influencing moisture management properties of fabrics. The present work, therefore, aims at studying the moisture management properties of ring vis a vis rotor yarn plated knit structures.

2 Materials and Methods

2.1 Materials

Cotton and polyester fibres were used for the production of the yarn samples. Cotton carded roving of 0.9 hank was used to spin 24 Ne single ring-spun yarn on blow room. Cotton carded sliver of 0.12 hank was used for the production of 24 Ne single rotor yarn

on Trytex rotor spinning machine. Polyester fibre of 1.1 & 3.3 decitex and with circular profile was used to spin 24Ne single ring-spun polyester yarns on 6/S LMW pilot plant ring frame. The three yarn samples in totality were used for the preparation of four single jersey plated fabrics. All the samples were prepared in plating relationship with ring and rotor cotton yarn in the outer and polyester fibres in the inner layer. The fabric samples were prepared on hand operated flatbed knitting machine (Elex, China) with machine gauge of 14, needle bed of 42 inches and 588 needles in each bed. Table 1 summarizes the plated fabric details.

2.2 Methods

The thickness of fabrics was measured on Essdie thickness gauge at a pressure of 20gf/cm². Aerial density of samples was determined according to ASTM D-1059. Fabric porosity was determined using the following equation:

$$\text{Porosity} = \frac{(\rho_o - \rho)}{\rho_o} \times 100\% \quad \dots (1)$$

where ρ_o is the fibre density (kg/m³); and ρ , the fabric density (kg/m³).

Moisture vapour transmission rate of the fabrics was tested on moisture vapour transmission cell (MVTR cell) (Grace, Cryov ac division). Absorbent capacity and trans planar wicking of test samples were determined by Gravimetric Absorbency Tester (GATS). Moisture management tester (MMT) (SDL Atlas, Hong Kong) (AATCC Test method 195-2009) was used for testing the liquid moisture transfer properties of the test fabrics. The sensor structure and measuring rings of MMT are shown in Figs 1(a) & (b).

3 Results and Discussion

3.1 Moisture Vapor Transmission Rate

Ring yarn fabrics exhibit higher rate of moisture vapour transmission (7.25 - 9.46 g/m²/24h) as compared to the rotor yarn fabric samples (6.31 - 8.81 g/m²/24h), which may be attributed to high porosity

Table 1 — Details of developed plated fabrics

Sample code	PET fibre linear density, dtex	Yarn spinning system
PCR _{1,1}	1.1	Ring
PCRO _{1,1}	1.1	Rotor
PCR _{3,3}	3.3	Ring
PCRO _{3,3}	3.3	Rotor

[Outer layer - C (cotton), Inner layer - P (polyester), R - ring, RO- rotor, and 1.1 & 3.3 - polyester fibre dtex].

of ring yarn fabrics (Table 2). Free open spaces in the fabric facilitate easy passage of moisture vapour, owing to diffusion of moisture vapour through air. As diffusion through fibrous material is restricted by fibre diffusivity, the ring yarn fabrics with higher air volume fraction were found to be more permeable to moisture vapour transmission.

3.2 Trans Planar Wicking

Trans planar wicking of ring yarn fabrics is found to be higher as compared to their rotor yarn counterparts. This may be attributed to the difference in yarn structure of two yarns used in the study. Better fibre alignment, higher degree of compactness due to high packing density might have favoured the formation of large number of continuous and small diameter capillaries in ring yarn fabrics. Rotor yarn on the contrary displays randomness in the internal structure with dense core, less dense sheath and belly bands.

The continuity of capillaries may be disturbed by tight wrappings along yarn length. In the light of above facts, it can be argued that randomness and tight wrapping along yarn length and more open structure as compared to their ring yarn counterpart may disrupt the continuity of capillaries, thereby inhibiting the liquid movement through capillary wicking in rotor yarn fabrics.

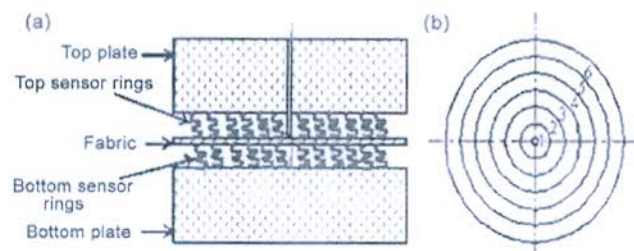


Fig. 1 — Sketch of MMT sensors (a) sensor structure and (b) measuring rings

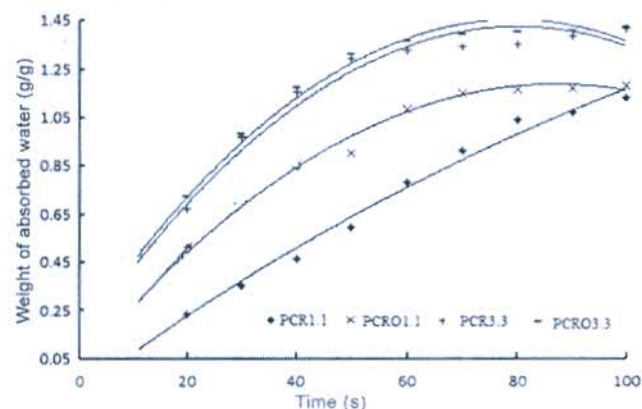


Fig. 2 — Absorbent capacity of plated knitted fabrics

3.3 Absorbent Capacity

Water absorption of the textile fabrics is a crucial property in wearer comfort as it determines the liquid sweat holding capacity of the fabrics. Rotor yarn fabrics show higher absorbent capacity as compared to ring yarn fabrics over a test period of 100 s as shown in Fig. 2. The observed trend may be attributed to high thickness, aerial density and bulk density and hence more water absorption by rotor yarn fabrics as compared to their ring yarn counterparts.

3.4 Moisture Management Properties

Table 3 shows the moisture management indices of test samples. It is observed that top (inner layer) and bottom (outer layer) wetting time are higher for rotor yarn fabrics as compared to their ring yarn counterparts, suggesting that the former would take longer to get wet on initial exposure to test liquid. Figures 3 (a) & (b) show the water content curves for ring and rotor yarn fabrics.

Spreading speed and one way transport capacity, which indicate effectiveness of fabric in liquid spreading and transporting from inner to outer layer, are higher for ring yarn fabrics as compared to those for rotor yarn fabrics. It can, therefore, be concluded that ring yarn fabrics would result in better spreading of test liquid in both inner and outer layers (higher SSt & SSb) and would be more effective in liquid transfer from top (inner/ next to skin layer) to bottom (outer) layer as suggested by higher one way transport capacity.

Table 2 — Physical properties and moisture vapour transmission rate of plated knitted fabrics

Sample code	Thickness mm	Aerial density, g/m ²	Porosity %	Moisture vapour transmission rate g/m ² /24h
PCR _{1.1}	0.927	248	81.68	7.25
PCRO _{1.1}	0.951	255	81.63	6.31
PCR _{3.3}	0.974	238	83.46	9.46
PCRO _{3.3}	0.985	250	82.56	8.81

Table 3 — Moisture management indices of plated knitted fabrics

Sample code	WTt, s	WTb, s	SSt, mm/s	SSb, mm/s	OWTC
PCR _{1.1}	2.91	2.06	2.38	3.44	622.57
PCRO _{1.1}	6.75	2.25	1.47	2.56	483.75
PCR _{3.3}	3.66	5.16	2.22	2.10	573.32
PCRO _{3.3}	7.45	6.23	1.25	1.83	428.62

WTt— Top wetting time, WTb — Bottom wetting time, SSt— Top spreading speed, SSb — Bottom spreading speed, and OWTC— One way transport capacity.

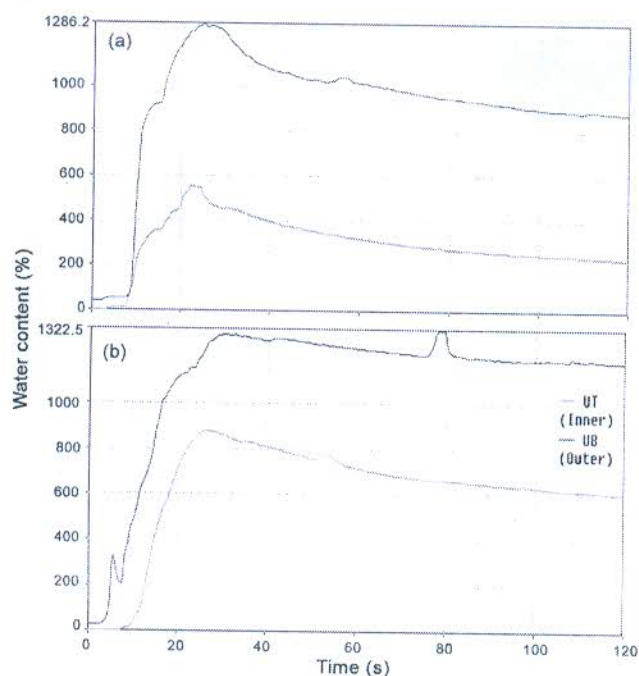


Fig. 3 — Water content vs time curve for inner (top) & outer (bottom) layers of (a) ring yarn fabrics and (b) rotor yarn fabrics

4 Conclusion

The study proposes development of plated knit structures with outer layer composed of two different yarn structures and the comparison of developed fabrics for their moisture management properties. Ring yarn fabrics exhibit higher moisture vapour transmission rate, trans planar wicking, lower wetting time, higher spreading speed and one way transport

capacity as against their rotor counterparts, thereby suggesting that ring yarn fabrics would result in better spreading of test liquid in both inner and outer layers. The former would be more effective in liquid transfer from top (inner/ next to skin layer) to bottom (outer) layer. The findings of the study help us to conclude that plated knit structures with ring yarn in the outer layer are suitable choice where body needs to dissipate sweat both in vapour and liquid form with respect to fabrics using rotor-spun cotton yarn in the outer layer, as the latter shows higher absorbent capacity, poor one way transport capacity and would be slow drying fabrics.

References

- 1 Geraldes M, Lubos H, Araujo M, Belino N J R & Nunes M F, *Autex Res J*, 8 (2008) 30.
- 2 Bivainyte A & Mikucioniene D, *Fibres Text East Eur*, 19 (2011) 64.
- 3 Vishal K & Rajesh D, *Trends Text Eng Fashion Tech*. DOI: 0.31031/TTEFT.2019.05.000606.
- 4 Kumar R C, Kumar A P, Senthilnathan P, Jeevith R & Anbumani N, *Autex Res J*, 8 (2008) 100.
- 5 Ozturk M J, Nergis B & Candan C, *Text Res J*, 81 (2011) 324.
- 6 Basu A, *Indian J Fibre Text Res*, 34 (2009) 287.
- 7 Behera B K, Ishtiaque S M & Chand S, *J Text Inst*, 1 (1997) 255.
- 8 Lord P R, *Text Res J*, 44 (1974) 516.
- 9 Erdumlu N & Saricam C, *J Text Inst*, 104 (2013) 1284.
- 10 Manshahia M & Das A, *Fibers Polym*, 15 (2014) 1221.
- 11 Smita Honade B, Neeraj S, Jagadananda B, Vijay R, Amit D & Ganesh J, *Indian J Fibre Text Res J*, 44 (2019) 24.
- 12 Suganthi T & Senthilkumar P, *J Ind Text*, 47 (2017) 1447.

Proceedings of the National Conference on Futuristic Trends in Textiles
organised by Center for Textile Functions, NMIMS, Shirpur on 26-27 March 2021

Evaluation and designing of mosquito repellent home textiles produced from cotton blended fabrics

Dr. Shelly Khanna¹, Dr. Amandeep Kaur²
¹Assistant Professor, ITI & S, Bhiwani, Haryana

Introduction

AMONG the increasing number of arthropod borne diseases as, Chikungunya, Malaria, Yellow fever, Dengue, only few are preventable by vaccines. There are no effective vaccines against Malaria, the only way to avoid it remains avoiding mosquito bites. For this reason, personal protective measures against biting arthropod & arthropod borne diseases constitute the first line of defense. A major advancement in the protection of high risk personnel (e.g. outdoor workers, travelers & soldiers) is the development of insects' repellent clothing, tents, netting and other secondary articles. Curtain fabrics are considered as one of the most important furnishing fabrics. Curtains are also used to impart aesthetic fashion by contributing to the interiors of the personal as well as public places as homes, offices, hotels, auditoriums, retail stores etc. The value addition of the textiles by chemical finishing is one of the commonly practiced process even for functional textiles. The importance of the mosquito repellency for home textiles lies in the fact that most of the mosquitoes enters from doors or windows. So, to protect the entry of mosquitoes, the mosquito repellent home textiles like curtains, bed sheets, wall hangings etc. can be the solutions of the problem. Mosquito repellent textiles are one of the revolutionary ways to advance the textile field by providing the much-needed features of driving away mosquitoes, in all the geographical regions. It protects the human beings from the bite of mosquitoes and thereby, promising safety from the mosquito-borne diseases, such as malaria, dengue fever (DF), Nile fever, chikungunya and filariasis, are serious public health problems. These diseases are transmitted to human beings through mosquito bites only. Since, there is no effective vaccine available for the control of all these diseases, prevention of mosquito bites is one of the main strategies to control or minimize the effects of these diseases. To overcome these problems mosquito repellence for home textiles plays vital a role to control the fatal ailments to human body and skin, either by contact (as clothing mainly garments, gloves, sleeves) or non-contact surrounding textiles (as home-textile items mainly curtains, Beddings).

Correspondence to: author.colourage@gmail.com

Techniques of imparting mosquito repellence

There are many techniques to impart the mosquito repellent effects for the human skin

- I. **Direct application:** In this type of method, mosquito repellent or even oils are applied directly onto the skin in the form of creams like Odomos body creams & onto the fabrics in the form of sprays like non aerosol permethrin spray.
- II. **Microencapsulation process:** Concentration microencapsulation technique is commonly used in the pharmaceutical, cosmetic and fragrance fields. This method requires a core material for encapsulation such as liquid or solid that must be water-insoluble. Usually, oil phase is encapsulated by mechanically dispersing it in a form of droplets in the aqueous phase resulting in a colloid as an oil-in-water (O/W) emulsion. The microcapsules are micron-sized capsules/micro-containers that encloses the mosquito repellents oils with a hard sheath. These micro containers can be applied to the textile surface with the aid of binding agents with long lasting finishing effects. These don't have any affinity for any form of textiles materials. But few limitations of this technique are the activation of these need some kind of external stimuli as light, abrasion heat, and dissolution. The microcapsules are sealed oil containers and always give monotonous fragrances.
- III. **Use of host-guest complexation techniques:** Cyclodextrin can act as host and form inclusion compounds with very small aromatic molecules. Such complexes can be formed in solutions, in a solid state as well as when cyclodextrins are linked to various surfaces where they can act permanent or temporary hosts for small molecules that provide certain desirable attributes.

Classification of mosquito repellents

The mosquito repellents can be categorized into two classes broadly as natural and synthetic repellents. These are listed in the Table 1.

Table 1: Types of mosquito repellents

Natural Mosquito repellents	Synthetic Mosquito repellents
Castor Oil	DEET
Lemongrass Oil	Pyrethroids
Citronella Oil	Niprolactone
Orange Oil	Permethrin
Eucalypt Oil	Resmethrin

Drawbacks of synthetic mosquito repellents

- Cause rashes, swelling, eye irritation and worse problems, though they are minimal including brain swelling in children, anaphylactic shock, low blood pressure, and one report of death.
- DEET must be used with caution, especially with children.
- It has been known to cause dizziness and can severely irritate the skin.
- DEET may even cause cancer and can produce defects in child birth.

For these reasons, many people choose to use a natural mosquito repellent like a Citronella spray, Clove Spray, Lemongrass oil & many more. Lemongrass & clove oil has active ingredients that repel mosquitoes and for some, the ginger smell is very appealing. It is fine to use a natural repellent which can make be unattractive in the eyes of mosquitoes. Dermatologist advise some plant oils such as Citronella Oil, Eucalyptus Oil and Lavender Oil which can effectively repel the mosquitoes.

Advantages of Natural Mosquito Repellents

- Insects are repulsed by the presence of the botanical extract and do not build up a resistance to these mosquito control treatments.
- Natural mosquito repellents can be applied to many sensitive areas, shrubs and turf that traditional treatments would harm.
- The natural extract in the mosquito control treatments does not affect insects that are beneficial to suburban landscapes.
- West Nile Virus-carrying mosquitoes are eliminated or repelled, helping to minimize the risk of bites and keep your family safe.

Mechanism of mosquito repellence of Essential oils

Repellents are substances that act locally or at a distance, deterring an arthropod from flying to, landing on or biting human or animal skin. Usually, insect repellents work by providing a vapour barrier detecting the arthropod from coming into contact with the surface. Among them, essential oils, complex mixtures of volatile compounds isolated from a large number of plants, have been found to have these properties against various haematophagous arthropods, some of them being the basis of commercial repellent formulations.

There are two mechanisms of mosquito repellence.

- **Based upon olfactory senses:** By sensing the temperature of human body, mosquitoes find the suitable places to bite. By applying mosquito repellents on textiles, the contact senses of mosquitoes get inactivated and get retarded.
 - **Based on Tactile senses:** By applying the mosquito repellents on fabric, the mosquitoes are affected at nervous system. This results in confused insects & helps in retarding them.
- Therefore, the aim of this work is to develop & characterize a fabric having long lasting mosquito repellent properties. The main objective of the project is the application of mosquito repellent finishes to polyester/cotton based home textiles to provide a safeguard against mosquito borne diseases either in the homes or offices. The use of natural oils as mosquito repellents will be able to open new horizons for eco-friendly & a safer approach towards the mankind.

Hence, objectives of the present work:

1. Comparative analysis of performance of natural mosquito repellents on textiles.
2. Production of mosquito repellent curtains from the optimized results.
3. To find an alternative to the synthetic mosquito repellents on textiles.

Material & methods

Materials

Fabric

40/60 Polyester/cotton blend fabric is procured from Bhawanji Textile Mills, Bhiwani. The fabric structural details are mentioned in Table 2.

Table 2: Fabric structural details

Fabric structure	
Blend	P/C (40/60)
GSM	247 g/sq.m
Count	80D (warp) 50D (weft)
EPI	64
PPI	52
Weave	Plain weave

The properties of 40/60 based polyester/cotton blended fabric are listed below in Table 3.

Chemicals Used

- Mosquito repellent (guests) : Lemongrass oil (LgO) & clove (CO)
- Host compound : β -Cyclodextrin (β -CD)

• Clove & Lemongrass reagents, NaOH, Phenolphthalein, Ethanol

Table 3: Fabric properties

Properties	
Tensile Strength	Warp - 25.36 kg Weft - 19.7 kg
Drape coefficient	2.18
Crease Recovery	Warp - 1.3683 Weft - 1.1298
Elongation	Warp - 2.01 Weft - 2.35
Air permeability	61.72 m ³ /m ² /min
Wooling Length	Warp - 2.7 cm Weft - 2.3 cm
Flexural Rigidity	170.14 kg/cm

Experimental

Initial Testing of fabric

Initial testing of control untreated fabric for physical and mechanical properties i.e. Tensile strength, Crease recovery, Drape test, Drapes and Air permeability has been carried out.

Calibration of mosquito repellent essential oils

Mosquito repellent essential oils was diluted into 100% ethanol i.e. 0.01 ml oil is added in 99.99 ml ethanol, stir it well and keep it for 5 minutes. After that 5 ml from the diluted solution was taken & placed in UV-Vis spectrophotometer for the spectral option & get the maximum wavelength through the highest peak of the graph. The process was repeated for both oils in the similar manner, the other concentrations of the oil are prepared for calibrating the oils.

Optimization of Mosquito repellent oils

Oil is applied on fabric (Polyester/cotton) at different concentrations through padding technique followed by drying at room temperature. Oil treated fabric was then cut in to 1x1cm sample and dipped in ethanol for 1 hour. The fabric was then removed and the solution is tested for the fragrance retention in the terms of absorbance values with UV-Vis spectrophotometer.

Optimization of β -CD

β -CD is applied on fabric (P/C) at different concentrations through padding technique. The assessment of quantity of β -CD on the fabric is determined in terms of weight gain (%) and absorbance of phenolphthalein solution with which the fabrics treated with β -Cyclodextrin are shaken through UV/Vis spectroscopy.

a) Weight gain percentage

The fabric sample was weighed before and after the padding treatment with β -CD to find the weight gain per coverage which was calculated as:

$$\text{Weight gain} = \frac{\text{Final weight} - \text{Initial weight}}{\text{Initial weight}} \times 100$$

b) UV-Visible spectroscopy

For plotting a calibration curve of phenolphthalein on UV-Vis spectrophotometer:

1% phenolphthalein solution is prepared in 50% ethanol i.e. 1 ml of phenolphthalein is dissolved in 100 ml of 50% ethanol. The pH of the solution is adjusted to the 10.5 using 0.5M NaOH hydroxide. The phenolphthalein solution prepared was then diluted to five concentrations as 0.1%, 0.2%, 0.3%, 0.4%, 0.5%. Concentration versus absorbance curve was plotted on UV-Visible spectrophotometer against blank sample at λ_{max} 556. A calibration curve was thus obtained and it was used for the detection of absorbance of unknown sample. The β -CD treated fabric was then cut to 1x1cm. The fabric sample was immersed in 30ml phenolphthalein solution is prepared above and shaken at 25°C for 1 hour. The fabric was then removed and absorbance of phenolphthalein solution was measured.

Treatment of fabric with Clove & Lemongrass oils alone

Fabric is directly treated with clove oil alone and lemongrass oil (separately) without any host compound. The clove oil solution is prepared in ethanol at the concentration of 7% & lemongrass oil solution at 6% according to the optimization. Fabrics were immersed in the oil-ethanol solutions for 2 minutes and padded at a pressure of 25 kg/cm² to the wet pick up of 100%. This process is repeated again as 2 dip-2 mg process. This was followed by drying at room temperature.

The calibration curve of clove oil in ethanol was taken as standard (λ_{max} 382nm) & Lemongrass oil (λ_{max} 466nm) to find the release rate of oils from the fabrics.

Process Variables:

- Clove oil = 7%
- Lemongrass oil = 6%

Treatment of fabric with IC of CO & β -CD and IgO & β -CD

Fabrics are treated in the two stages.

In the first stage, fabric is treated with the β -CD which acts as host compound for essential oils. β -CD solution is prepared at the concentration of 80g/l β -CD and 0.5% NaOH. Fabrics are immersed in the solution for 2 minutes and padded at a pressure of 25 kg/cm². After padding, drying is done at room temperature.

In the second stage, solutions of IgO & CO are prepared at the concentration of 6% and 7% respectively. Then, the fabrics that are treated in the first stage are immersed in the oil solutions for 2 minutes and again padded at the pressure of 25 kg/cm². This was followed by drying at room temperature.

Comparative analysis of functional properties (with and without wash)

Washing of untreated and treated fabrics was carried out twice with water containing 100 ppm sodium carbonate and 700 mg/l of soda ash at 40°C for 15 days for one wash. For Mosquito repellence, four sets of specimens were used for comparing the efficacy of the mosquito repellence of both essential oils. The mosquito repellence of oil treated fabrics, fabric treated with clove oil and lemon grass oil has been recorded. The test was conducted by placing direct light in open dish held in the left hand, which is taken as control. A total of three variables are recorded with oil alone. These are repellency rate, knockdown rate and mortality rate. The effect of these repellents against mosquitoes is expressed as the number of mosquitoes landed for the repellent test, the number of mosquitoes knocked down for knockdown test, and the number of mosquitoes died for mortality test. The numbers of repellent and knockdown mosquitoes were recorded at fixed intervals, i.e. every 10 minutes for 60 minutes. For mosquito mortality was observed after 1-24 hours.

After the control oil testing the untreated fabric was taken in the left hand and the fabric treated with clove oil was placed in the right hand. The comparative results are shown in the similar manner. Lemon grass treated fabric was used in the right hand and the untreated fabric was placed in the left hand for the comparison.

Designing and production of oleo products

The end products are designed

and produced with the best interpreted results from the previous work.

Results & discussions

Calibration of CC1 & IgG

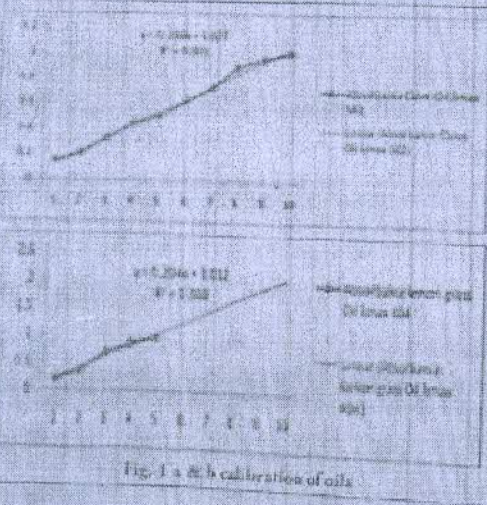
The calibration of both the oils are done at their respective contact and shown in *Figure 1 a & b*.

Optimization of β -CD

The amount of β -CD on fabrics is optimized with the use of weight gain technique and also inclusion compound formation with the help of phenolphthalein. The application of the β -CD on to the fabrics show substantial amount of weight gain in the fabrics that further indicates the presence of the cavities at the molecular level of the fabrics. At 80gpl of β -CD concentration had shown the maximum % weight gain, followed by the saturation of the fabric. The results show that 80 gpl β -CD gives the minimum absorbance

Table 4: Mosquito repellence evaluation of control and oil treated fabrics

Substrate	No. of mosq. landed	No. of mosq. repelled	No. of mosq. knocked down	No. of mosq. died	% R	% KD	% M
Control	10	26	02	02	57	7	7
Untreated fabric	50	31	0	0	75	0	0
Fabric treated with clove oil	25	11	3	1	84	12	4
Fabric treated with lemon grass oil	24	15	9	0	65	37	0



value of phenolphthalein in the solution. This is a further indication of the fact that lesser the amount of phenolphthalein in the solution, more is the amount that has gone into the cavities of β -CD. This depicts more concentration of β -CD on the fabrics in the form of cavities for inclusion compound formation. Thus, 4% and 7% lemon grass oil and clove oil are used for fabric finishing with 80 gpl β -CD for inclusion complex formation.

Comparative analysis of functional properties of treated fabrics

The results have been investigated for duration of 60 minutes to examine the Repellency rate (% R), Knockdown rate (% KD) and Mortality rate (% M) of the oils as shown in (the Table 4).

It can be inferred from the table that the oils used are more of mosquito repellents than the mosquito killers as mortality rate is 0% for both the oils. Also, clove oil is a better repellent than the lemon grass oil.

Conclusions

With the increase in the concentration of BCLD, the weight of the fabric increases. The overall immediate fragrance concentration is also less for both the fabrics due to the fabric composition having polyester as its main component of the blend. The cyclodextrin gets attached in the cotton part of the fabric through with the hydrogen bonds. This has resulted in a lower uptake and utilization of the host compound from the fabric. The oil is 3% less effective mosquito repellent than the control fabric due to its composition having 10 mg/ml as its main component, about 22-90% (5). On the other, the formulation of this composition based upon the citrus constituents. The combination of β -Cyclodextrin and clove oil is the best combination as the outcome of our study and it will be termed as fabric for the designing and production of the diapers, as shown in Figure 2a & b.

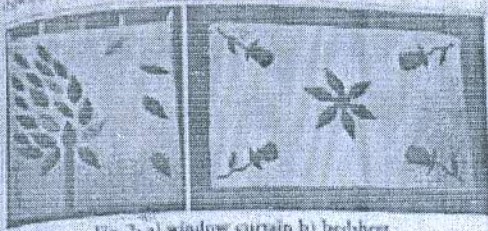


Fig. 2- a) window curtain b) bedsheet

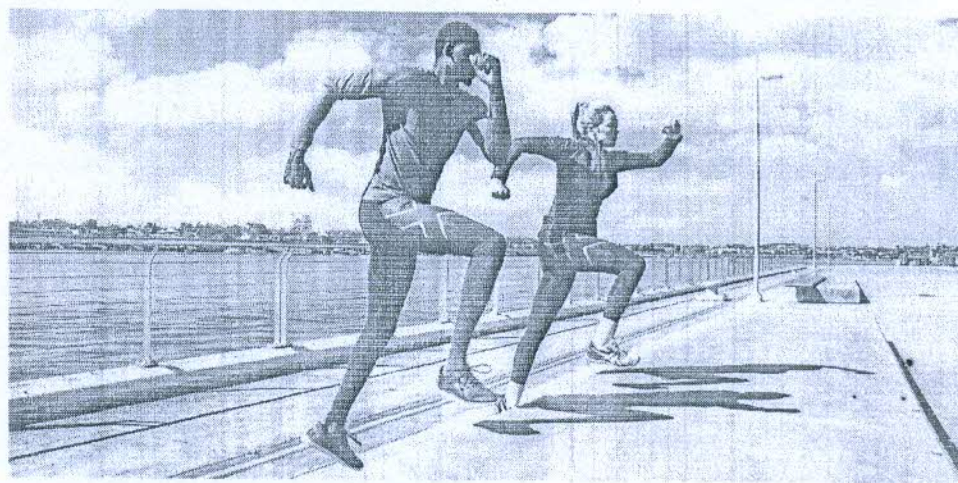
References

1. Abdel-Moady F A, Fouad Moustafa M G F, Rehan M F and Ali A S (2017). Repellency of controlled-release treated cotton fabric loaded with permethrin and Deltamethrin against mosquitoes. *J. Tex. Inst.* 106, 8:695-701.
2. Abdel-Moady F A, Fouad Moustafa M G, Rehan M F and Ali A S (2018). Repellency of controlled-release treated cotton fabric loaded with cypermethrin and prallethrin. *Carbohydrate Polymers* 73, 1, 92-97.
3. Sakchi A, Sankar E L, Quadraço, and Casanovi C. (2000). Evaluation of the sensitivity of *Aedes aegypti* and *Anopheles gambiae* complex mosquitoes to two insect repellents DEET and IZAR 2025. *Theoretical Medicine and International Health* 5, 3, 380-384.
4. Sarata Cruz, Angelo C, Alexandra D, Francesca G, Lima P (2010). Essential oil composition and larvicidal activity of six mediterranean aromatic plants against the mosquito *Aedes*

5. *Journal of Applied Science* 10, 1, 1-5.
6. Choudhary A, Sharma P, Mishra S, Sanyal D K, and Singh B (2011). Chemical Composition and Larvicidal Activities of the Plant *Clitoria crotolaria* (L.) DC. and Its Fractions Against the Mosquito *Aedes triseriatus* (Henderson). *J. Entomol.* 11, 1, 1-11.
7. Costa C, Jones JH (in English). *Plant* 5, (1999). Chemical and biological properties. *Agrochimica Technica*, 10, 1, 1-10.
8. Das S, Ghosh S, Das S, Das S, Das S, Das S (2001). Evaluation of the larvicidal activity against mosquitoes. *J. Vector Borne Dis.* 18, 1, 31-34.
9. Dey S, Das S, Das S, Das S, Das S, Das S (2000). Natural products as mosquito repellents. *Bio-organic & Medicinal Chemistry* 17, 4873-4874.
10. Ghosh S, Das S, Das S, Das S, Das S, Das S (2004). Effect of essential oils on the larvicidal activity of *Aedes triseriatus* (Henderson). *Indian J. Med Res.* 119, 375-381.
11. Khanna S & Chakravarty S. N. (2011). Mosquito repellent activity of essential oils loaded with inclusion complex of β -cyclodextrin. *Strat. and essential oils* 5, 9. <https://doi.org/10.1186/2075-0177-01234-2-18>
12. Khanna S & Saini A. (2011). Study on essential oils using various insecticides based home remedies. *Global International University Journal of Science and Technology* 10, 1-2, 31-36.
13. Medicine (2011). Clove (*Eugenia aromaticum*) and clove oil. <http://www.nhm.nih.gov/medlineplus/medlineplus/plants/plants/clove.html>
14. Sharma Anshu M, Senthil B, Boudhan S, Karthikeyan M (2015). Development of mosquito repellent finished cotton fabric using eco-friendly cyanoacrylate resin. *International Journal of Science, Technology & Management* 4, 2, 96-101.
15. Thiruvaiyaru V, Tawasin A, Chotrasamee J, Suwankird W, Chantong U and Anurachakinsakul P (2011). Laboratory and field evaluation of the insect repellent 3535 (ethyl butylacrylate/ethylacrylate) and DEET against mosquito vectors in Thailand. *J. Am. Mosq. Control Assoc.* 17, 3, 190-195.
16. Tripathi Y, Chinn G, Rongkavon V (2005). Efficacy of repellent products against aged and free flying *Anopheles stephensi* mosquitoes. *Southeast Asian J Trop Med Public Health* 36, 1823-31.

Information on your new products, equipments and processes

You are invited to submit information about new products, equipments, and processes, developed and offered by you to the Indian market. Such writeups are entertained for publication without any cost. Don't miss this opportunity to promote your new products.



WEARABLE BIOINSTRUMENTATION

Next generation medical responsive textiles

Shelly Khanna¹, Amandeep Kaur¹ and J N Chakraborty²

¹Dept of Fashion & Apparel Engineering, The Technological Institute of Textiles and Sciences, Bhiwani - 127021

²Department of Textile Technology, NIT, Jalandhar - 144 011

E-mail : chakrabortyn@gmail.com

This paper aims at the analysis of recent contributions of bioinstrumentation of medical usage owing to their diversified functions in different areas.

Bioinstrumentation is the application of electronic, measurement principles and techniques to develop devices used in diagnosis and treatment of diseases. Computers are becoming increasingly imperative in bioinstrumentation, with the dedicated microprocessor that does a variety of small tasks in a single purpose instrument to the extensive computing power needed to process the large amount of data in a medical imaging system. The biomedical instrument

uses a transducer or a sensor to convert a signal created by the body into the suitable and processable electrical signals. The extensive use of instruments for the recording or transmission of physiological information, such as breathing rate or heart rate has found tremendous applications in the diversified areas.

Bioinstrumentation also refers to the measurement, recording and transmission of data obtained on bodily functions. Intelligent medical clothing and textiles have the

potential to substantially change the provision of health & health care services for large population groups e.g. those suffering from chronic diseases (such as cardiovascular, diabetes, respiratory and neurological disorders) and the elderly population segment with specific physiological needs.

Need of the wearable bioinstrumentation

The health care and medical sector offers the utmost scope for developing the most sophisticated high value textiles and idealistic garments. The incorporation of the technology of 'smart- intelligent textile- garmenting' in the medical monitoring and medicine, opens up the newest arenas. Wearable sensors and systems have evolved to the point that they can be considered



geared up for clinical applications¹. Wearable systems and ambient intelligence are two important aspects of the wearable bioinstrumentation. The incorporation of interfaces and sensors into textiles and apparels is a highly attractive option for medical monitoring and treatment applications as it facilitates the automatic sensorisation of the bodily activity. Wearable Health Devices (WHDs) are increasingly helping people to better monitor their health status both at an activity/fitness

level for self-health tracking and at a medical level providing more data to clinicians with a potential for earlier diagnostic and guidance of treatment².

Developed technologies are truly able to reduce the overall costs for prevention and monitoring. This is possible by constantly monitoring health indicators in various areas, and in particular, wearable devices are considered to carry this task out. These wearable devices and mobile apps now have been integrated with tele-medicine and tele-health efficiently, to structure the medical Internet of Things (IOT)³.

The process of wearing the medical devices is casted off by the user as many of them stress upon the existence of pathologies or other medical problems. But, if the devices are integrated in the apparels, the problem of porting the cumbersome device is eliminated too. Advancements in packaging and fabrication technologies have enabled embedding various micro & nano-electronic and micromechanical sensors, such as gyroscopes, accelerometers, and image sensors, into a small area on a rigid or flexible substrate with high sensitivity at a low cost^{4,5}.

The merits of intelligent textiles for medical ventures are dual folded. These are in contact with the skin and these can easily follow the user's actions⁶. This duality makes it possible to effectively sense the physiological and biomechanical parameters of the subject's body. But, unfortunately, there is no one single 'intelligent textile' or 'wearable device' commercialized till the time, which has been able to gather and process all the signals generated by the human body as needed. Each application needs to acquire different physical parameters or to act on different parts/organs of the body. Also, the extent of integration of the device into the textile, cost effectiveness, desired complexity and application varies from wearable medical entity to the other.

Wearable Technology: Intelligent textiles

Wearable systems and technology amalgamate information and

communication features in apparels. Ambient intelligence is a way of making interfaces between humans and computers to disappear. Ambient implies an intelligent environment, in which computers disappear or become transparent.

Within ambient intelligence, intelligent textiles can be considered as a transparent interface incorporated in textile substrates or as sensors for recording the subject's activities. Both the approaches are highly suitable for medical and monitoring applications. The user's requirements for intelligent textiles include a number of aspects: reliability, robustness, durability, aesthetics, communication, minimum maintenance and above all, customization^{7,8}.

Intelligent textiles as sensors

Smart textiles are incorporated with sensors-actuators/sensors communicators' or 'sensors/ data storage' features. Various body signs can be acquired by means of the specific properties of smart materials capable of being embedded into the textile structures.

Wearable biosensors

The use of Wearable Monitoring Devices (WMDS) that allow continuous or intermittent monitoring of physiological signals is vital for the advanced diagnosis as well as disease management. Above this, the wearable systems are totally non-obtrusive devices that allow physicians to overcome the limitations of ambulatory technology and provide a response to the need for monitoring individuals over a stipulated time period. They typically rely on the embedment of wireless miniature sensors, enclosed in patches or in items that can be worn, such as band, ring or even as a complete garment shirt.

The data sets recorded using these systems are then processed to detect events predictive of possible worsening of the patient's clinical situations or they are explored to access the impact of clinical interventions. This technology represents a quantum leap in healthcare monitoring, producing accurate and real-time results.

A customized garment can have numerous functions as a computerized

gadget with the use of optical and conductive fibers. The incorporation of the sensors into the design of clothing could monitor the wearer's heart rate, respiration, temperature and a multitude of vital functions, alerting the wearer or physician, if there is the risk of a fatal problem. The various physiological information gathered by the wearable biosensors include heart rhythm, breathing rate, skin pH, body temperature, Interface pressure and foot pressure. The latest applications of biosensors hold considerable promise due to their high specificity, speed, portability, low cost and low power requirements. The innovative biosensor platforms for noninvasive chemical analysis of bio-fluids, such as sweat ears, saliva or interstitial fluid are gaining attention too⁹.

Applications of wearable sensors for the measurement of bodily functions

Monitoring of heart rhythm

The 'smart shirt'- wearable motherboard, given by Georgia Tech, can be used in patients having known disorders, permits a constant monitoring of their physical condition by medical personnel in a non-invasive manner¹⁰. The shirt includes many special optical sensors and interconnections to monitor and record individual's vital body signals to provide a systematic way of controlling the vital signs of humans in the most simplified manner.

Patients suffering from mental ailments need to be monitored on a regular basis to gain a better understanding of the relationship between their vital signs and behavioral patterns so that their treatments can be suitably modified. Such medical monitoring of individuals is critical for the successful practice of telemedicine. 'Lifeshirt' (@Vivometrics, Southern California-based health information and monitoring company¹¹) is a commercial service that collects, analyses and reports on the subject's pulmonary, cardiac and posture data (Fig 1). It also correlates data gathered by optional peripheral devices that measures blood



Fig 1 : VivoMetric's remote LifeShirt¹⁴

pressures, blood oxygen saturation, EEG, periodic leg movement, core body temperature, skin temperature and end-tidal CO₂. This system is an extensible data acquisition and processing platform consisting of a garment, a data recorder, and PC-based analysis software. The signals are displayed and stored on a handheld computer (Visor) and then, analyzed offline, extracting more than 40 clinical parameters relating to cardio-respiratory functions. It also serves as an electronic diary of symptoms, moods, and activities of the user^{12,13}.

Measurement of breathing rate

Respibelt (@Progressive Sports Technologies; Loughborough University, England), is a fabricated textile sensor made of a stainless steel yarn, knitted in a lycra belt, providing an adjustable stretch to the rib cage and lower chest area. By wrapping Respibelt around the abdomen or thorax, changes in the circumference and length of the Respibelt caused by wearer's breathing brings out variations in both inductance and resistance by the creation of the load on the application area. It, thus serves as the base for the

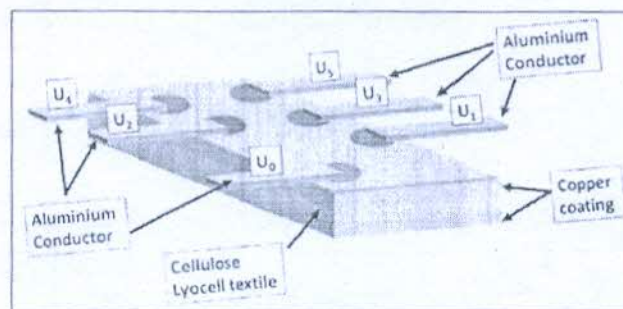


Fig 2 : Textile thermocouple embedment as conductor matrix¹⁷

breathing rate measurement of athletes, cyclists and other field events^{15,16}.

Body temperature monitoring

Body temperature can be measured by textile-embedded thermocouples or thermistor-based sensors as shown in Fig 2.

Temperature-sensitive polymers offer a change of phase at a tunable temperature. Textile thermocouples detect changes in temperature and consist of an indispensable conductive textile matrix with a textile character. Textile thermocouples should combine the flexibility and light weight of textiles with the conductive property of the conductor material, which can be defined as a truly textile thermocouple.

Skin pH analysis

Skin pH analysis can provide an in-depth sight into the person's well being. Changes in the pH of the skin are reported to play a role in the pathogenesis of skin

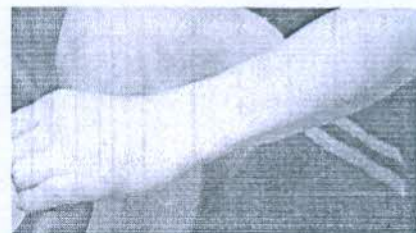


Fig 3 : Chemical sensor for sweat analysis¹⁹

diseases like irritant contact dermatitis and acne and also, showed that inducing metabolic alkalosis through the ingestion of sodium bicarbonate may lead to increased blood and sweat pH as shown in Fig 3¹⁸. In addition, it has been reported that sweat pH rises in response to an increased sweat rate. It can be determined

from the sweat analysis of the wearer using wearable textile-based sensors that can provide real-time information regarding sweat activity. It can be accomplished either by means of embedded pH responsive polymer fibres or a pH sensitive

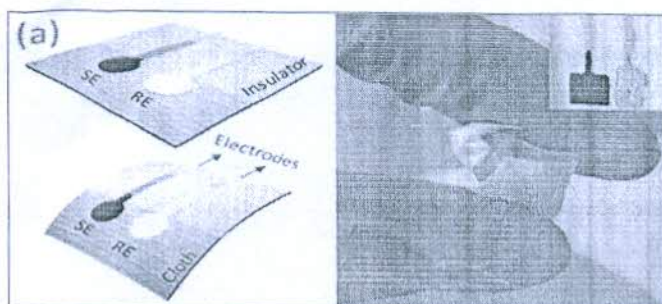


Fig 4 : (a) Line diagram representation of flexible potentiometric pH sensor interpreted on fabric (b) flexible and crumpled pH sensor (inset shows the image of the electrodes)

dye (bromophenol blue, bromocresol green, bromocresol purple and bromothymol blue) incorporated into a fabric fluidic system to determine sweat pH. The sensors are integrated into a waistband and controlled by a central unit with wireless connectivity. The use of such sensors for sweat analysis may provide valuable physiological information for applications in sports performance and also in healthcare too¹⁹ (Fig 3). The use of indicator dyes onto the textile could be used for monitoring the pH from 0 to 14 in intervals of one pH unit.

Another attractive strategy immobilized the cotton yarns with carbon nanotube ink and it was used as a potentiometric sensor for detection of pH to fabricate a novel pH-sensitive bandage as shown in Fig 4²⁰.

Maintenance of interface pressure

Pressure values between body and an interface have been utilized to reduce the pain or sores in elderly patients. The pressure sensitive mats consisting of a spacer fabric with embroidered electrically conductive patch arrays on both sides are employed. Each opposing patch pair in the arrays forms a plate capacitor whose capacity changes with the compression force on the spacer fabric.

Foot plantar pressure management

The measurement of foot plantar pressure has the prospective to be an important instrument in many areas such as enhancing sports performance, diagnosing diseases and rehabilitation in

patients with diabetes foot ulceration and foot pathologies. These plantar pressure sensors should have the robustness, durability and high repeatability, as it should measure the pressure due to body weight. An elastomeric sensor is made up of stainless steel, a crack-based sensor and a 3D-printed frame. Insoles are made of elastomer with which is used as part of the sensor to distribute the load to the sensor. The 3D-printed frame & stainless steel prevent the breakage of the crack-based sensor and enable elastic behavior²¹. The key feature of this sensor based foot plantar is the ease of customization as can be seen in Fig 5.

In another approach, wearable piezoelectric insoles have been developed

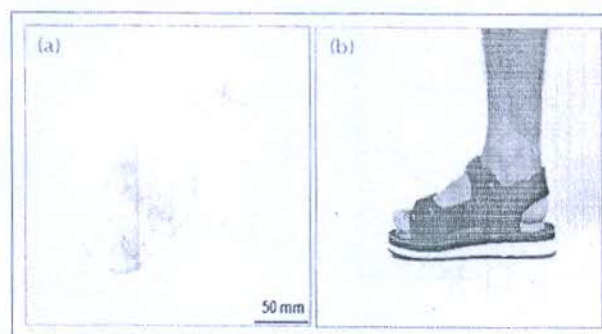


Fig 5 : Schematic and image of foot plantar pressure measurement system: (a) conceptual photograph of crack-based sensor-based insole plantar pressure sensor (b) conceptual photograph of a shoe with the insole inserted in it'

in order to reduce plantar pressure. PVDF (Polyvinylidene fluoride) is the most common and reliable material because it is flexible, thin and deformable^{22,23}.

Biofeedback system

Biofeedback is a therapeutic technique in which an individual learns to consciously control the involuntary responses such as heart rate, brain waves, or muscle contractions²⁴. It is a treatment method designed to facilitate self-regulation of bodily processes. In biofeedback, some aspect of individual's

physiological functioning is systematically monitored using electronic instruments and fed back to that individual, typically in the form of an auditory, a visual signal or tactile signals, so that the patient learns to modify that physiological function or process in some possible way. The sensor picks up the physiological function as an electrical activity, which is amplified and sent to a device that emits a signal which may be binary or analogue. These responses are electronically monitored and noted through beeps, graphs or on a computer screen for future reference. The wearer is taught the complete procedure and the working principles of biofeedback treatment with the recognition of the different modes of feedback of the physiological functions. There are numerous feedback systems employed in medical practice as Electromyographic (EMG) Biofeedback (for muscle activity), thermal Biofeedback (analysis of skin temperature to control blood flow), Electrodermal (EDR) Biofeedback (mea-

sure of skin conductance), Electroencephalographic (EEG) Biofeedback (measure of electrical activity of brain^{25,26}). The human biofeedback system is able to serve diversified clinical applications as muscle contraction headaches; cardiovascular disorders inclusive of hypertension, cardiac arrhythmias; neuromuscular

rehabilitation as chronic pain; gastrointestinal disorders; epilepsy, bronchial asthma and insomnia.

Wearable health assistants

Wearable technologies have become a standard part of life for consumers. Personalized data generated from wearable technology is empowering health care providers to make more informed care decisions with new insights that extend far beyond a patient's level of physical activity. The latest wearable tools can monitor everything from a patient's blood pressure to his or her oxygen

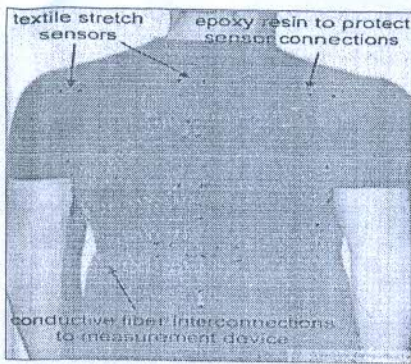


Fig 6 : Diagrammatic representation of Wearable Back Manager for the posture correction of the health care seeker²⁶

saturation, offering health care professionals, numerous unique ways of keeping tabs on their patients, who are distant apart²⁷. The portable and mobile health monitoring systems have changed the whole scenario of medical health assistance and possess the potential of replacing the conventional clinical environments. The wearable health assistants help to fight diseases by a preventive lifestyle and early diagnosis of the fatal ailments. Users are able to take control of their own health status and adapt a healthier lifestyle. The main features of wearable health assistants are: monitoring of the physiological parameters, detection of the operator's context and providing feedback to the user. The various physiological



Fig 7 : Systematic architecture of a personal health care assistant²¹

parameters comprise heart rate, ECG, respiration, EMG, blood pressure and temperature²⁸. Wearable back manager (WBM) and wearable heart manager (WHM) provides the data communication with the family doctor, hospital or Medical Care Centre (MCC) enabling the individual to lead a healthier lifestyle (Fig 6). Smart healthcare uses a new generation of information technologies, such as the 'Internet Of Things' (IOT), big data, cloud computing and artificial intelligence, to transform the traditional medical system in an all-round way, making healthcare more efficient, more convenient, and more personalized²⁹. These services consist of multiple participants such as doctors and patients, hospitals and research institutions (Fig 7).

Intelligent garments in pre-hospital emergency care


Pre-hospital emergency care is an essential part in the cases of trauma and other acute diseases^{29,32}. It is related to the period before arrival at the hospital and includes all diagnostic procedures carried out by the ambulance/emergency care team. Emergency Medical Services (EMS) providers are the first link to a trauma care system and trauma triage provided by EMS personnel is also a crucial factor in fruitful outcome of trauma patients. The assessment of patient and the treatment offered by the pre-hospital emergency care crew can levy a huge impact on the clinical evaluation.

Use of monitoring sensors integrated into textiles, in the form of shirt or a thorax surrounding belt, cables and provision of tele-consultation solves a number of problems in the pre-hospital emergency situations.

References

- 1 Wearable Sensors/Systems and their impact on biomedical engineering. Paolo Bonato IEEE Engineering in Medicine and Biology Magazine (2003), 22(3), 18-20. DOI: 10.1109/MEMB.2003.1213622
- 2 Dias D and Cunha J.P S, Wearable Health Devices-Vital sign monitoring, systems and Technologies. Sensors (2018), 18(8), 2414
- 3 Haghj M, Thurrow K, Habil I and Stoll R, Habil

- M. Wearable Devices in Medical Internet of Things: Scientific Research and Commercially Available Devices, Health Inform Res. (2017) 23(1), 4-15
- 4 Koydemir H C and Ozcan A, Wearable and Implantable Sensors for Biomedical Applications, Annual Review of Analytical Chemistry (2018) AC11CH06_Ozcan ARI, 11(17), 6.1-6.20
- 5 Ajami S and Teimouri F, Features and application of wearable biosensors in medical care, J Res Med Sci. (2015), 20(12), 1208-1215
- 6 Mattila H R, Intelligent textiles and clothing- a part of our Intelligence ambience, Intelligent textiles and clothing, Woodhead publishers in Textiles, Cambridge, England, 2006
- 7 Rajendran S, Advanced textiles for wound care (1st edition), Woodhead publishing in Textiles, Cambridge, England, 2009
- 8 Rajendran S, 'Advanced textiles for wound care' (2nd Edition), Woodhead publishing in Textiles, Cambridge, England, 2018
- 9 Kim J, Campbell A S, Esteban-Fernández de Avila B and Wang J, Wearable biosensors for healthcare monitoring, Nature Biotechnology (2019), 37(4), 389-406. doi: 10.1038/s41587-019-0045-y
- 10 www.gtvm.gatech.edu
- 11 Grossman P, The LifeShirt: a multi-function ambulatory system monitoring health, disease and medical intervention in the real world, Stud Health Technol Inform (2004), 108, 133-41
- 12 Wilhelm F H, Roth W and Sackner M, The LifeShirt An Advanced system for ambulatory measurement of respiratory and cardiac function, Behavior Modification (2003), 27(5), 671-691
- 13 Halin N, Junnilla M, Loula P and Aarnio P, The LifeShirt system for wireless patient monitoring in the operating room, Journal of Telemedicine and Telecare (2005) 11(2) 41-43
- 14 McAdams E, A Krupaviciute, C Gehin, A Dittmar, Delhomme, G Rubel P, J Fayn and J McLaughlin, Wearable electronic systems: Applications to Medical Diagnostics/ Monitoring, <https://vittorio-ferrari.unibs.it>, 2011, Wearable Monitoring Systems. 179-203. SpringerLink, Bostan, Online ISBN 978-1-4419-7384-9
- 15 Langenhove V L, Smart Textiles for Medicine and Healthcare: Materials, Systems and Applications, CRC press, Woodhead Publishing Limited, Cambridge, England, 2007

- 16 Song G and Wang F, Firefighters' Clothing and Equipment: Performance, Protection, and Comfort, 2018, CRC press, ISBN 9780367570682
- 17 Root W, Bechtold T and Pham T, Textile-Integrated thermocouples for temperature measurement, *Materials* (2020), 13(3), 626, doi.org/10.3390/ma13030626
- 18 Hatamie S, Angizi S, Kumar S, Pandey C M, Simchi A, Willander M and Malhotra B D, Textile based chemical and physical sensors for healthcare monitoring, *Journal of the Electrochemical Society* (2020), 167
- 19 Coyle S, Textile sensors to measure sweat pH and sweat-rate during exercise, 3rd International Conference on Pervasive Computing Technologies for Healthcare, Pervasive Health (2009), DOI: 10.4108/ICST.PERVASIVEHEALTH2009.5957
- 20 Manjakkal L, Dang W, Yogeswaran N and Dahiya R, Textile-Based potentiometric electrochemical pH sensor for wearable applications, *Biosensors* (2019), 9, 14, doi:10.3390/bios901001
- 21 Park J, Kim M, Hong I, Kim T, Lee E, Kim E, Ryu J, Jo Y J, Koo J, Han S, Koh J and Kang D, Foot plantar pressure measurement system using highly sensitive crack-based sensor, *Sensors* (2019), 19, 5504, DOI:10.3390/s19245504
- 22 Razak A H A, Begg A and Wahab Y, Foot Plantar Pressure Measurement System: A Review, *Sensors* (2012), 12, 9884-9912; DOI:10.3390/s120709884
- 23 Zhao J, Guo Y, Wang L, An Insole plantar pressure measurement system based on 3D forces piezoelectric sensor, *Sensors and Transducers*, (2012), 160 (12), 49-54
- 24 Sattar PS and Vaidya PS, 'Biofeedback in medical practice', *Med J Armed Forces India* (1999), 55(1), 51-54
- 25 Liu G, Huang B and Wang L, A wearable respiratory biofeedback system based on generalized body sensor network, *Telemed J E Health* (2011), 17(5), 348-357, DOI: 10.1089/tmj.2010.0182
- 26 Saljoughian M, Biofeedback Therapy: An Overview, *US Pharm.* (2018), 43(8), HS13-HS16
- 27 Steger A, Weighing the Pros and Cons of Wearable Health Technology, *HealthTech magazine* (2020)
- 28 Jegatheesh C, Kathiresan M, Raj M M, Janarthanan S and Srikanth S, Patient health monitoring with health assistant, *International Research Journal of Engineering and Technology (IRJET)* e-ISSN: 2395-0056 (2019), 06, 10
- 29 Tian S, Yang W, Grange J M L, Wang P, Huang W and Ye Z, Smart healthcare: making medical care more intelligent, *Global Health Journal* (2019) 3, 3, 62-65
- 30 Roggen D, Arnrich B and Troster G, Wearable health and life-style assistants Technology in support of well being, *Eurescom mess@ge*, 2007, 1, 10-11
- 31 Roggen D, Arnrich B and Troster G, Life Style management using Wearable computers, *International Conference on Ubiquitous Computing for Pervasive Healthcare Applications wearable.ethz.ch*, January, 2006
- 32 Popa T O, Cimpoesu D C and Nedelea P L, Pre-hospital emergency care in acute trauma conditions, *Emergency Medicine and Trauma* (2019), www.intechopen.com DOI: 10.5772/intechopen.86776. 

Tufropes installs new nonwovens manufacturing line

Rope and netting manufacturer Tufropes is installing a new nonwovens manufacturing line from Truetzschler Nonwovens and Voith to target the growing Indian market for wipes.

The line is based on patent pending 'pentamerous technology' which will allow the Gujarat-based company to produce five types of different eco-friendly wipes substrates and is based on Truetzschler/Voith core components for wet-laying, carding and hydroentangling.

Truetzschler/Voith's carded/pulp (CP) technology combines a cost-effective, wet-laid pulp layer and a carded web layer from cellulosic fibres.

Proprietary refinements will allow Tufropes to produce any possible hydroentangled nonwoven material, including biodegradable, natural fibre, eco-friendly high-performance nonwovens.

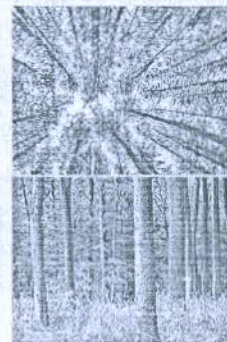
This will be a first industrial-scale pentamerous technology-based nonwoven project and is expected to be commissioned next year.

Founded in 1992, Tufropes' rope and netting solutions are used in a wide array of industries such as aquaculture, marine, safety, sports, shipping and defense.

The management team at Tufropes opted for Truetzschler Nonwovens and Voith for good reason to supply machinery and be the technology partners in this new project.

'The team of Truetzschler and Voith has extensive experience with the wet-laid/hydroentangled nonwoven technology,' said

Tufropes director Madhav Goel. 'Several wet-laying/spunlacing plants and their CP line at a European customer are running at full capacity. We wanted to invest in a unique and progressive technology and we are pleased to have found the best partners to realise our first step into this new business field.'



Truetzschler/Voith's carded/pulp (CP) technology combines a cost-effective, wet-laid pulp layer and a carded web layer from cellulosic fibres.

'The NCT high-speed card delivers a carded web into the manufacturing process and offers additional flexibility in web forming and end products,' added Christian Maennich, area sales manager at Truetzschler Nonwovens.

www.truetzschler.com

'A special advantage of our CP nonwovens technology is the very consistent distribution of stock suspension for highly flat profiles,' said Oliver Crasser, sales manager for inclined wire solutions at Voith Paper.

Magic Fashion Mirror: A New Approach for Fashion Wardrobe makeover through Rejuvenated Brick-n-Mortar Fashion Retail

Shelly Khanna* & Amandeep Kaur

Department of Fashion & Apparel Engineering, The Technological Institute of Textiles & Sciences, Bhiwani, Haryana, India

Abstract:

The Virtual Fashion Mirror uses the latest technology to provide fashion shoppers with a fascinating and interactive retail experience that fits the modern day retailer's multi-channel retailing strategy - selling via stores, websites, face-to-face selling, electronic kiosks and other tools at the disposal of the retailers. The fashion mirror is anticipated to be projected as a powerful tool to create interest and conviction for transforming the window fashion shoppers into the potential shoppers of the brands and fashion houses. In addition, the technology also inspires the consumers to shop for the related as well as complementary product ranges for the enhancement of the aesthetics of the required shopped entities. This paper aims at discovering the unrevealed state-of-the-art technology with the utilization of the advents of the modern day electronic information savvy techniques to persuade and convert the 'just passersby' into clients.

Keywords: aesthetics, Electronic kiosks, fashion shoppers, face-to-face selling, interactive retail experience.

Citation: Shelly Khanna & Amandeep Kaur, "Magic Fashion Mirror: A New Approach for Fashion Wardrobe makeover through Rejuvenated Brick-n-Mortar Fashion Retail Approach", *Journal of the Textile Association*, 82/3 (126-128), (Sep-Oct'2021)

1. Introduction

Fast fashion is the term used to indicate the strategies adopted by fashion retailers to reflect current and emerging fashion trends quickly and effectively in current merchandise assortments [1].

People use mirrors everyday to see how they look and choose outfits they will put on for a day before leaving their homes either for work or for some special occasions. Also, in clothing stores, many mirrors are provided to facilitate the shoppers that help in their decision to buy garments fitting well and looking appropriate. But the garment tried in one color scheme may be wished to be tried in other available color schemes and sizes too for the shopper's satisfaction. (Fig. 1a & 1b). The only way to figure out this requirement is the retrieval of the garments again and again till the final satisfactory selection. The accessories like footwear, jewelry, hats and handbags, may also require the similar sets of trials and retrials to make suitable complements with the chosen apparels. The extent of boredom that prevails during retrials of apparels is proving to be a killer for the shopper's interest in product selection and their acquisition.

The necessity of the fashion mirrors is the remedy to declining visitor numbers in the onsite- shopping centres due to a number of reasons. On the onset, the consumers have to juggle with their handbags, selected garments and their hangers to the dressing or trial rooms for repeated doffing and donning of garments and related accessories [2]. This results in the sweated and tired consumers under flashing lights. In addition, the consumers find it highly inconvenient to

measure their body measurements with the measuring tapes for the custom made garments. The pronounced use of hidden spy cameras in the most intimate locations of the physical dressing rooms have also raised an eyebrow over the confidentiality as well as the privacy of the consumers during changing clothes for trials. Moreover, from the retailer's perspective, the repeated donning and doffing of the garments, which finally do not become a part of anyone's shopping cart, results in the distressed look and increased handling. These garments might require some additional repressing or reshelving after every trial cycle thereby increasing the extent of effort, time and additional costs. A lot of floor space can be saved by showcasing the entire collection of the apparels in the store through dedicated software and can be made accessible in physicality on demand of the shoppers after final selections are made (Fig. 2) Lastly, the stores need not to plan for the dressing rooms and the supporting lanes for those who are waiting outside in queues for cubicles.



Fig. 1a & b Trials of outfits in variable color schemes

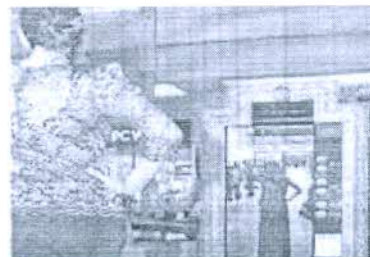


Fig. 2 Use of dedicated software for self trial of garments

*Corresponding Author:

Dr. Shelly Khanna
Department of Fashion & Apparel Engineering,
The Technological Institute of Textiles & Sciences,
Bhiwani - 127 021 (Haryana)
E-mail: sh_khanna2002@yahoo.com

2. Technology of fashion mirrors

The Virtual Fashion Mirror creates an 'augmented reality' retail experience [3], for both customers and retailers, that enables the convergence of 'on-line' and in-store shopping in the retail environment by bringing together the key ingredients of contented, intelligent video analytics, interactive experience, social media and digital innovation (Fig. 3) fashion mirror employs the use of the techniques involving simulation and digital graphics modeling. The mirror's memory consists of various templates of the anthropometric information related to the potential shoppers and probable shoppers to allow best fitted model in association with the captured details of the shoppers. This results in the generation of the modified model of the consumer by the incorporation of the body database. After this, the garment and background information is added to the reconstructed model with the selective concern and choice of the consumer [4]. The Garment Database includes all the merchandise offerings in the store along with the related and probable accessories to choose from. The apparels are chosen with the help of the touch sensitive screens installed with the radio frequency identification system (RFID). The background database can be optional information added to the reconstructed model (Fig 4). This takes account of the special kinds of environments in which the shoppers want to see themselves while draped in the chosen merchandise



Fig. 3 Display of fashion mirror in the store (www.proscreensltd.com)

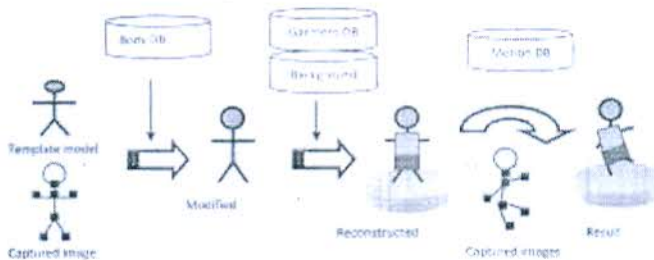


Fig. 4 Process of Image generation in virtual fashion mirror

The 'fashion mirror' is a sophisticated computer screen with in-built sensors and cameras that allow shoppers to stand in front of the mirror followed by the consumer body scanning to determine their exact dimensions for sizing garments [5] as seen in Fig 5. The use of interactive 46- 58" plasma screen equipped with a depth-sensing camera in a standalone unit with an internal cooling entity that facilitates the consumers to simply stand on the platform and use the touch- screen machine to superimpose an outfit on their body with the mere wave of their hands [6] as shown in Fig. 6. The range of menus is accessible for the selective purpose from the brand's

fashion assortment. It is also capable of projecting several merchandise items over the shopper's anatomy at the same time, to show how a complete outfit might look with shoes and other accessories [6]. The virtual technology is supported by a houseful of options based on silhouettes, colors, design patterns and sizes from which consumers can seek numerous variety of selection option (Fig. 7). Moreover, electronic gadgets as handy cams, iPad and others can be attached to the virtual technology to perform browsing through the virtual clothes even before the blink of the eyes of the shopper. The resizing of the reflection model of the shopper can also be easily undertaken with the aid of the interactive touch screen panel to fit into it. The potential consumers can have the opportunities to seek appointments with the expert stylists at the dress style station [7].

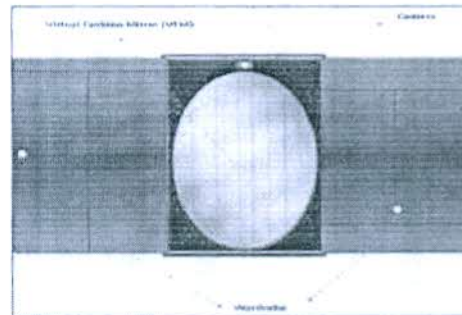


Fig. 5 Setup of Fashion magic mirror with wardrobes, cameras & mirror

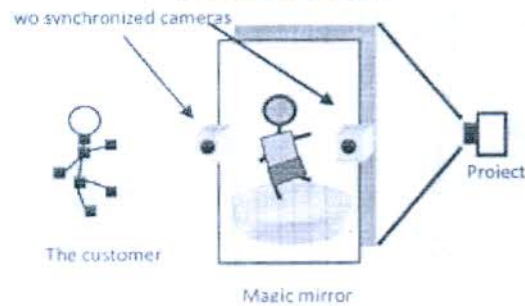


Fig. 6 Image build- up with unit of projector and cameras (gorgeoussdnbhd.blogspot.in/2010/06/virtual-fashion-mirrorvfm.html)



Fig. 7 Merchandise wardrobe showcasing fashion assortment

3. Commercially viable fashion mirrors

Fashion brands like John Lewis, Crowthorne and Furutani Industries Inc. have won accolades in the apparel retail business with the dissemination of the attributes of this revolutionary technology even at the evolution stage. The

Italian fashion company, Prada, enhances the aura of the retail outlets with a plasma screen invisibly built into the large mirror surface that allows consumers to see themselves both from the front and the back at the same time along with the integrated time delay that can even capture and replay movements. The consumers can also have an access to the garment closet of the merchandise that has been brought to the dressing room's privacy. Thus, the use of virtual closet in the trial rooms fully supports the fashion mirrors in the achievement of satisfied and persuaded consumers during heavy on site-shoppers traffic. In addition, Bloomingdale, owned by American multinational company Macy's Inc. has introduced the concept of virtual fitting rooms as "swivel" with the facility of intelligent product recommendation engine that serves the products to a shopper based on not only their personal preferences, but their behavior in the virtual fitting room like what kind of products have been looked upon, what has been tried on, how long the articles have been worn, the number of times re-trials on items have been done. Other big players as ZARA, H&M, Lacoste, Ralph Lauren and Burberry are making the use of virtual mirror technology.

4. Limitations of the virtual changing mirrors

The shoppers may be reluctant for acquainting to the cutting-edge technology due to the fear of everyone looking at them during the garment trials. The retail prices of the apparel products may rise up due to the inclusion of the facility of the fashion mirror in the shopping experience. Moreover, the trained professionals might be required for assisting the shoppers in their selections as well as for other functionalities. The mirror may need a special store location for its installation as well as easy accessibility to the consumers. The complete dependence on the virtual fashion mirrors can result in the return of unsatisfied consumers and unsold articles without trials in case the technological errors evoke in the operations of the mirror. The use of the mirror can't prove to be a salvation to the garment trials for many

shoppers as their suitability in the walking and sitting postures remain a fancy till these are physically tried.

5. Other application streams

In addition to apparels, the fashion mirror can find its applications in virtual cosmetics or make over tools. This tool allows the user to try various cosmetic product ranges like eyewear inclusive of eye shadow palettes, eye pencils, eye lens, lipsticks and liners to go with the skin color, skin textures and selected apparels. Lancôme Magic Mirror for virtual make up allows users to try the full cosmetic range on their still photographs. The accessories can also be added to the virtual try-on as handbags [8], footwear and jewelry [9] to mention a few.

6. Scope of advancements

The incorporation of virtual style and selection assistance can be provided as an enhanced interactive tool to the fashion mirror [10]. The mirrors can be further supported by the garment alteration technology if the consumer wants to see himself in the altered apparels of his personalized measurements. Various types of backgrounds like ramp environment, special public and personal gatherings can be made accessible to showcase the selected dresses before their actual draw on [11-12].

7. Conclusions

The Fashion mirrors can prove to be an exciting tool for the apparel retail to revive the old age tradition of on-site shopping culture by attracting more consumer traffic in the stores instead of the use of e-retail technology alone from homes and offices. But the practical implementation of the infant technology requires the prices charged for the technology, to be made affordable for a large number of retailers, may be based upon the number and types of products along with the promotions carried out by the retailer's team by using the advent of this magic mirror.

References

- [1] Madhani Pankaj M. (2011). RFID Deployment, Fast Fashion Retailing. SCMS Journal of Indian Management, April – June, 40-51.
- [2] DPA news agency (2008, September 21). Berlin Premieres Magic Dressing Room Mirror, Retrieved July 29, 2014, from <http://dw.de/p/FKrv>.
- [3] Curtis Sophie (2013, January 21). Tesco trials magic mirrors and digital mannequins to entice shoppers, Techworld. Retrieved on July 29, 2014 from <http://news.techworld.com/networking/3421851>.
- [4] Yeo Young In (2005). Magic Mirror: A Virtual Dressing Room. Retrieved May 28, 2013 from <http://www.cise.ufl.edu/~yiyeeo>.
- [5] Steiner Rupert (2011, July 23). The REAL magic mirror: Try a new outfit without taking off the old one. Retrieved 29 July, 2014, from <http://www.dailymail.co.uk>.
- [6] McMackin Kalyn (2012, March 14). 3D camera, 'magic mirror' let women shop in virtual changing rooms, The Daily caller. Retrieved January 28, 2013 from [magic mirror/3D camera, 'magic mirror' let women shop in virtual changing rooms _ The Daily Caller.htm](http://magic-mirror/3d-camera-'magic-mirror'-let-women-shop-in-virtual-changing-rooms_The-Daily-Caller.htm).
- [7] Wright Lucy (2012, September 27). Is this the future of shopping? Magic mirror launches in Chapelfield, Retrieved January 28, 2013 from <http://www.eveningnews24.co.uk/news>.
- [8] Wang, L., Villamil, R., Samarasekera, S. & Kumar R. (2012). Magic Mirror: A virtual handbag shopping system. Computer vision and pattern recognition workshops (CVPRW), IEEE computer Society conference, 16-21 June. 19-24.
- [9] Worthington Paul (2011, March 15). Mirror, mirror Total Immersion adds AR to iPad 2. Retrieved January 28, 2013 from [PMA Newsline.htm](http://PMA-Newsline.htm).
- [10] www.proscreensltd.com
- [11] www.inurfacemedia.co.uk
- [12] Gorgeous sdn bhd (2010, June 22). Virtual Fashion Mirror (VFM). Reterived September 5, 2014, from [tp://gorgeoussdnbhd.blogspot.in/2010/06/virtual-fashion-mirrorvfm.html](http://gorgeoussdnbhd.blogspot.in/2010/06/virtual-fashion-mirrorvfm.html)

Page Proof Instructions and Queries

Please respond to and approve your proof through the "Edit" tab, using this PDF to review figure and table formatting and placement. This PDF can also be downloaded for your records. We strongly encourage you to provide any edits through the "Edit" tab, should you wish to provide corrections via PDF, please see the instructions below and email this PDF to your Production Editor.

Journal Title: Proceedings of the Institution of Mechanical Engineers, Part E: Journal of Process Mechanical Engineering
Article Number: 1063099

Thank you for choosing to publish with us. This is your final opportunity to ensure your article will be accurate at publication. Please review your proof carefully and respond to the queries using the circled tools in the image below, which are available in Adobe Reader DC* by clicking **Tools** from the top menu, then clicking **Comment**.

Please use *only* the tools circled in the image, as edits via other tools/methods can be lost during file conversion. For comments, questions, or formatting requests, please use **T**. Please do *not* use comment bubbles/sticky notes.




*If you do not see these tools, please ensure you have opened this file with **Adobe Reader DC**, available for free at get.adobe.com/reader or by going to **Help > Check for Updates** within other versions of Reader. For more detailed instructions, please see us.sagepub.com/ReaderXProofs.

No.	Query
GQ1	Please confirm that all author information, including names, affiliations, sequence, and contact details, is correct.
GQ2	Please review the entire document for typographical errors, mathematical errors, and any other necessary corrections; check headings, tables, and figures.
GQ3	Please confirm that the Funding and Conflict of Interest statements are accurate.
GQ4	Please ensure that you have obtained and enclosed all necessary permissions for the reproduction of artistic works, (e.g. illustrations, photographs, charts, maps, other visual material, etc.) not owned by yourself. Please refer to your publishing agreement for further information. <input type="text" value="All are accurate"/>
GQ5	Please note that this proof represents your final opportunity to review your article prior to publication, so please do send all of your changes now.
GQ6	Please note, only ORCID iDs validated prior to acceptance will be authorized for publication; we are unable to add or amend ORCID iDs at this stage. <input type="text" value="ORCID iDs are accurate"/>
AQ1	Please provide page range in Refs. [2, 7, 15].
AQ2	Please provide the complete publication details (if missing) for all other-type references those are not having URL links
AQ3	Please provide article title in Ref. [33].
AQ4	Reference [33] is listed in the reference list but not cited in the text. Please cite in the text, else delete from the list.
AQ5	Reference [34] is listed in the reference list but not cited in the text. Please cite in the text, else delete from the list.

Metallurgical, mechanical and tribological behavior of Reinforced magnesium-based composite developed Via Friction stir processing

Proc IMechE Part E:
J Process Mechanical Engineering
1–12
© IMechE 2021
Article reuse guidelines:
sagepub.com/journals-permissions
DOI: 10.1177/09544089211063099
journals.sagepub.com/home/pie



GQ1 Prem Sagar¹ , Amit Handa¹ and Gitesh Kumar² 

Yes, author information,
including names, affiliations,
sequence, and contact details,
is correct.

GQ2 Abstract

GQ4 Reinforced magnesium metal matrix nanocomposites (MMMNCs) have piqued the interest of scientific community in
GQ5 recent years. Friction stir processing (FSP) is a known process to achieve the highest level of secondary phase nanocomposites distribution in the base monolithic matrix. In this study, an attempt has been made to synthesize magnesium base AZ61A/n-TiC nanocomposites using FSP and the influence of tool rotational speed on the metallurgical, mechanical, and tribological behavior of the developed composites has been studied. Microstructural examination shows that as tool rotational speed increases, high plastic deformation occurs and heat is generated along with the concomitant shattering impact of rotation, which consequently develops larger grains in the stir zone. However, this also provides thrusts resulting in uniform distribution of the nanoparticles in the base matrix. Microhardness and ultimate tensile strength of the developed nanocomposite were found to be significantly improved when contrasted with the base metal. Lower wear rate was observed for the composite developed at 800 rpm along with the abrasive type of wear mechanism.

Keywords

Friction stir processing, AZ61A magnesium alloy, Micro-hardness, Tensile strength, wear

Date received: 29 July 2021; accepted: 9 November 2021

Introduction

Researchers have Reported that in addition to improvement of the aerodynamic properties, up-gradation of the accessories, optimization of drive efficiency, improvement of tire rolling resistance, one way to control carbon dioxide emissions are reducing the vehicle weight (Cui 2008). For manufacturing lightweight vehicles to reduce GHG emissions, the demand for the development of lightweight materials in the past few decades has accelerated to an enormous degree. In addition to above, these novel materials are required to have high strength-to-weight ratios and low density for maximum use. Therefore, accentuation has now been on the creation of lightweight and reasonable strength materials to cater to a consistently developing industrial interest Recent studies show that magnesium's use in the automotive industry has increased by 10–15% each year over the last 15 years, please refer to Supplementary Figure 1.



However, to enhance the mechanical and tribological properties, numerous elements like aluminum and zinc, etc. are added in monolithic magnesium alloys. Although conferring improvements in certain applications, these magnesium alloys possess insufficient hardness, low tensile strength, ductility, wear-resistance, and

high corrosion rate which constraints their extensive use in structural applications.^{1,2} Numerous investigations have reported that these properties could be proficiently and viably improved by the incorporation of stiffer reinforcement particulates in various base alloys.^{3,4} Adding Nano/reinforce particulates is a promising approach as detailed by.⁵ For the homogeneous dispersion of the reinforcements and uniform distribution of the particulates, Friction stir processing (FSP) is considered to be the far head of other technologies. FSP is based on the principle of friction stir welding, which has been effectively used by numerous researchers to join lightweight materials.^{6–8} The detailed study of FSP is presented elsewhere.⁹ Due to uncommon attributes such as high temperature and strain, FSP develops composites with uniform

¹Department of Mechanical Engineering, I.K. Gujral Punjab Technical University, Kapurthala, India

²Department of Mechanical Engineering, Guru Jambheshwar University of Science and Technology, Hisar, India

Corresponding author:

Prem Sagar,  Amit Handa  Mechanical Engineering, I.K. Gujral Punjab Technical University, Kapurthala, India.
Email: jasujaprem@gmail.com ; handaamit2002@gmail.com

grains and morphology,¹⁰ crystallographic texture,¹¹ and perfect orientation.

Ahmadkhaniha et al.¹² analyzed wear resistance on AZ91/ Al₂O₃ as produced by FSP adopting groove filling approach with a circular tool. They further considered different tool rotation speeds, transverse speed, and a fixed tool tilt angle of 3° to investigate mechanical and metallurgical properties. Finally, the outcome of the study suggested that tool rotation speed of 800 rpm and transverse speed of 40 mm/min gave optimum results for grain refinement and wear behavior. Balakrishnan et al.¹³ studied the effect of adding different volume fractions of n-TiC particulates in base AZ31 magnesium with the aid of FSP. They drew the conclusions that n-TiC was properly distributed with no chemical reaction. Dinaharan et al.¹⁴ investigated how magnesium alloy AZ31 could be effectively reinforced with 10% FA (Fly Ash) particles using two different processing methods, namely, standard stirring and friction stirring (FSP). They looked into the microstructural characteristics of the composite and its sliding wear behavior. They reported that the stirred composite had a rough grain structure with a few FA particles crumbled and countered by the matrix alloy, as well as randomly oriented particle dispersion. Dynamic recrystallization of the FSP composite, on the other hand, resulted in a homogeneous distribution of reinforcement particles, as well as small, equiaxed grains. As opposed to the base matrix, the FSP composite had increased strength and resistance to wear. In contrast to stir casting process, the study reported that FSP was the best tool for incorporating reinforcements into the AZ31Mg base matrix.¹⁵ used the FSP technique to strengthen MWCNTs in an AZ31 Mg matrix. The tribological behavior of the AZ31/MWCNTs was investigated. Due to the self-lubricating nature of carbon, increasing the MWCNT volume percent resulted in a significant decrease in friction coefficient along with wear rate. Wear examination of the worn surfaces revealed abrasion, oxidation, and delamination forms of wear processes, as well as minor plastic deformation. The study established the inclusion of MWCNT in the AZ31 Mg base matrix through FSP. This research also showed that the existence of carbonaceous reinforcement improved wear properties by lowering the coefficient of friction.

The current research aims to generate a magnesium-based composite via FSP. The impact of FSP process parameters especially tool rotation speed on the metallurgical, mechanical, and tribological behavior of a newly produced AZ61A/TiC magnesium-based composite was also analyzed.

Experimental detail and materials used

Material used

Plates of magnesium alloy AZ61A of size 200 mm × 100 mm × 6 mm were used in the experimentation. The chemical composition of AZ61A magnesium alloy is given in Supplementary Table 1. Blind holes of dimension 2 × 4

mm were drilled on the top surface of AZ61A magnesium plates (please see Supplementary Figure 2).

Reinforcements and Processing method

Titanium carbide (TiC) is a ceramic substance with many unique properties, including high hardness, chemical stability, and corrosion and oxidation resistance. Therefore, nano TiC (n-TiC) powder was used as reinforcement particulate in this study. Technical properties of n-TiC reinforcement particulates used in this study is presented in Supplementary Table 2.

Before the final experiments, three types i.e., circular pin profile, taper cylindrical pin profile, and triangular pin profile of tool geometries were considered for the experimentation. In Supplementary Figure 3, all four types of tool geometries considered for the trial run experimentation are presented. A pilot study was carried out to determine the optimal operating range of various parameters. To rule out the occurrence of any material flaw, each trial specimen was evaluated for a seamless cross-section and crown appearance, as illustrated in Supplementary Figure 4.

After trial experiments, the tool with a triangular pin profile was selected. This selection was made due to the fact that the crown appearance of the specimens prepared from these tools showed no defects which was not the case for other tools. Dimensions of this tool were, shoulder diameter 21 mm, pin length 4 mm and pin making diameter 6 mm. Based upon extensive trial runs and literature survey, the final experimentation was planned varying tool rotation speed in a range of 800–1200 rpm with a step of 200 rpm and fixing all other parameters such as the number of passes, tool tilt angle, and transverse speed.

Microstructural characterization

After FSP was performed and the nanocomposite was manufactured, the standard metallographic procedures were followed. Microstructure characterization was done using optical microscopy. The distribution of the second phase particles in the base metal matrix, grain size, interface bonding among secondary phase particles and base metal, etc. were visualized under Field Emission Scanning Electron Microscope (FESEM) equipped with EDX JSM-6610LV by JEOL USA.

Mechanical testing

For Tensile test examination, all the specimens were prepared strictly according to ASTM E-8 M standards. Specimens were extracted from the stir zones of each nanocomposite along with a sample from base magnesium alloy. For the examination of the tensile test samples of size 100 × 40 × 5 mm were extracted from each nanocomposites using a wire electric discharge machine (WEDM) as shown in Figure 1.

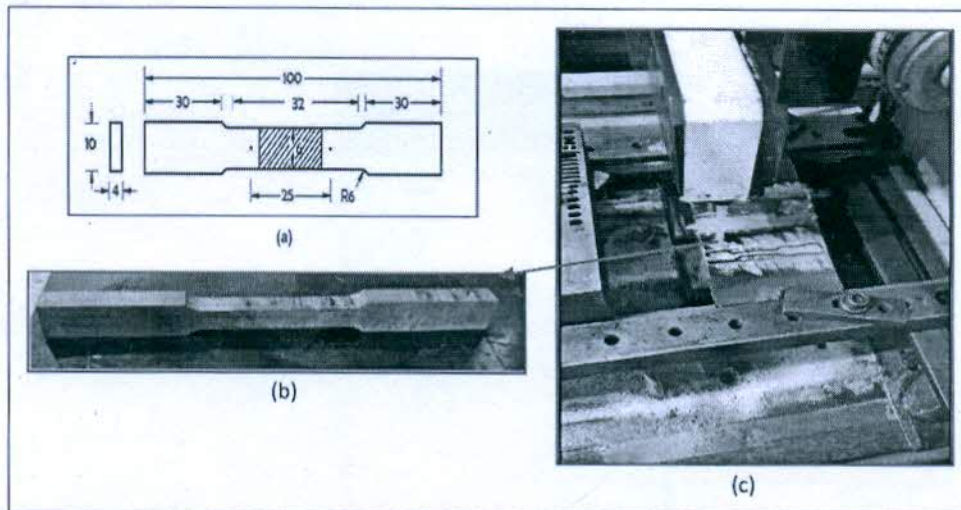


Figure 1. a) tensile specimen sample with detail geometry; b) extracting specimen from stir zone using WEDM; c) actual photograph of the tensile test specimen.

Experimentation was done on a Tinius Olsen UTM having load capacity of 50KN with an initial strain rate of $1 \times 10^{-4} \text{ s}^{-1}$. The fractured specimens were also investigated for crack propagation sites and final breaking by FESEM equipped with EDX JSM-6610LV Scanning Electron Microscope by JEOL USA. As per ASTM requirements, micro-hardness was determined using the Vickers indentation method. 500 gm of load was applied for 15 s dwell time. Indentation was done at equal intervals of 0.5 mm. Three values were taken at each indentation position, and the mean value was used.

Tribological properties Tests

Pins of dimension 3×30 mm were created from base metal and composites using wire cut electric discharge machining to investigate wear and friction properties. All the experiments followed ASTM G99 guidelines and were evaluated with a pin-on-disc tribotester (DUCOM TR-20 LE). All wear experiments were performed using a sliding distance of 500 m, a time of 600 s, a disc rpm of 400, and a fixed load of 20N. The volumetric loss was calculated by multiplying the height loss by the cross-sectional area of the pin. Further, the volumetric loss as a function of the sliding distance was used to quantify the wear rate. Scanning electron microscopy was used to examine worn surfaces and the underlying wear mechanism (JEOL, JSM-F100).

Results & Discussions (metallurgical)

Microstructure of AZ61A/n-TiC composite

In supplementary Figure 5, nanocomposites produced via the FSP route are presented. The FSP tool stirring is visible on the top surface of the nanocomposites. Also, the surface depicts very smooth quality with particular rings along with no prominences and defect (voids and

cracks) free zones. The obtained microstructures of monolithic AZ61A magnesium base alloy are shown in Figure 2 (a). The typical microstructure of AZ61A alloy is characterized by coarse β -Mg17-Al12 and α -Mg compound with a discontinuous network at the grain boundary. It was observed that unrefined coarse grains were distributed in the metal matrix. Additionally, clusters of small crystals were observed alongside segregated large crystals.

The base metal had an average grain size of $75 \mu\text{m}$. In Figure 2 (b) and Figure 2 (c), energy dispersive X-ray analysis (EDX) image and the spectrograph for the base metal are presented. The EDX scan shows the existence of pure magnesium, as well as zinc and other components, but no carbon atoms. This is because magnesium and its alloys are carbon-free at all levels.

In Figure 3, optical micrographs of the magnesium metal composite developed at 800, 1000 and 1200 rpm with four FSP passes is shown. These figures comprise of a typical cross-sectional view of FSPed AZ61A/n-TiC nanocomposite showing friction stir zone (SZ). The investigation of the stir zone shows the concept of dynamic recrystallization as a dominant phenomenon. The specimens demonstrate that coarse magnesium grains were not able to handle the rigorous action of the tool and broke up into tiny grains. The stir zone (SZ) of specimens developed at TRS-800 and four FSP exhibited finer grains and coarse grains, resulting in mixed microstructural features. The degree of grain refinement was found to be significantly higher in areas where the material had undergone intense plastic deformation. Dynamic recrystallization and heat generation during FSP results in evolving of fine grains, which is in agreement with several other studies.^{16,17}

In addition, the refined microstructure is due to grain boundary pinning with reinforced particles. Clustering of reinforcement particles is a major problem in composite fabrication in FSP, as it reduces the composite

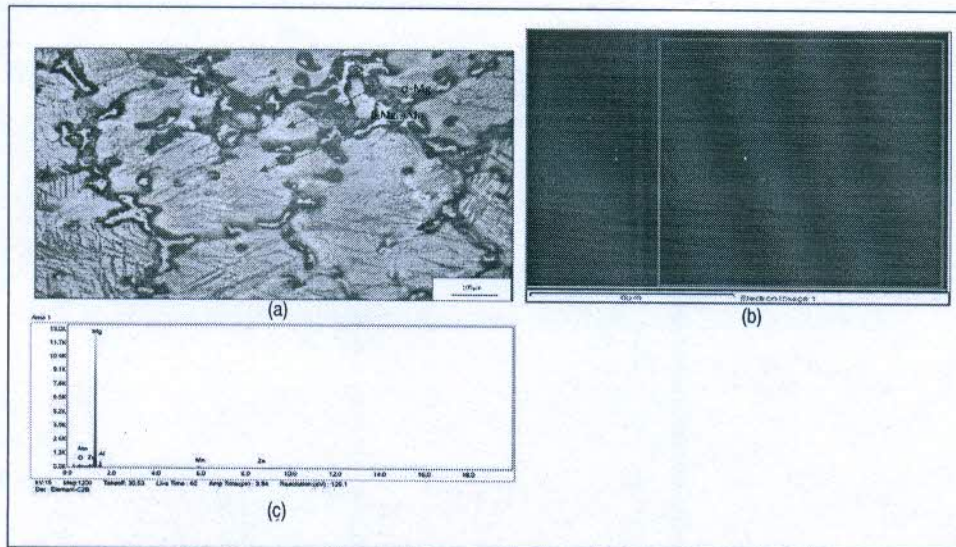


Figure 2 (a). optical micrograph of monolithic AZ61A base metal (at 200X).

strength. Refer to Figure 3 (a) for the formation of clusters or agglomeration of secondary phase particulates in the stir zone. This might be due to low tool rotation speed. As the FSP parameters changes, i.e. at the tool rotation speed of 800 rpm and FSP pass number 4, clusters of very small size of n-TiC particles were observed as shown in Figure 3 (a). In this Figure, the dark region in SZ is due to the agglomerated n-TiC particles. The advancing and rotating tool drove some of the preplaced particles away from the work piece surface. And the rest of the nanoparticles on the base metal surface were agglomerated and stirred into the base metal. As a result, nanoparticles dispersed poorly and gathered in large numbers in the SZ. Which further results that some degree of local clustering is inevitable, and not all nanoparticles can prevent grain boundary migration. Also, coarsening of the microstructure in the stir zone is more noticeable because of the higher amount of heat generated when the tool rotation speed is increased. A rotating speed of 800 rpm, lower heat flow and deformation developed to generate a sufficient distribution of n-TiC particles in the magnesium matrix substrate.

From Figure 3 (b), it can be deduced that as the tool rotation speed increases, the clusters gradually start to disappear which is in tune with Thangasuru. et al. (2014). It

was observed that grain size and agglomeration of n-TiC particles was slightly decreased at 1200 rpm and 4 FSP passes in contrast to 800 rpm and 4 FSP passes. In addition to this, as shown in Figure 3 (b), the reinforcement particles dispersed in the SZ in a scattered and homogeneous manner and also the n-TiC particles pinned the grain boundary. The grain structures in the SZ were observed to be uniform. The recrystallization resulted in equiaxed grains, whereas the distributions of nano-sized n-TiC particles differed because they received a unique stirring action. It is clear that for breaking up the clusters and uniform distribution of the nanoparticles, higher rotational speed is required. However, high heat input and too high rotational speed affects grain refinement.¹⁸

As the tool rotation speed reaches 1200 rpm, more material flow in the stir zone was noticed along with the homogenous distribution of the nanoparticles. Figure 3 (c), shows the optical micrographs of the developed composite at 1200 rpm and 4 FSP passes. The evolution of fine grains is vital in case of gaining improved mechanical properties. The flow of material in SZ improved with an increase in tool rotational speed. As a result, the cluster size of the particulates decreases in the AZ61A/ n-TiC composites which are in tune with¹⁹ As tool rotation speed increased to 1200 rpm, the microstructure images reveal that as heat input increased, the grain growth occurred and consequently larger grains were noticed at this parameter compared to 800 and 1000 rpm. However, too high tool rotational speed develops high heat, which further results in large size grains. In addition, this high tool rotation speed develops a shattering effect which results in uniform distribution of nano-particles of titanium carbide. Also, the more appropriate viscosity in the base AZ61A matrix could be due to high tool rotation speed with low tool transverse speed.

For all fabricated composites utilizing four FSP passes, higher grain boundaries developed. In addition, four-pass

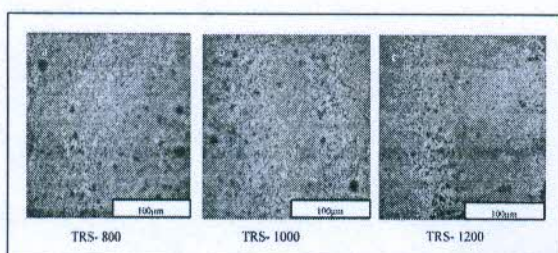


Figure 2 (b). EDX of base metal AZ61AMg (200X).

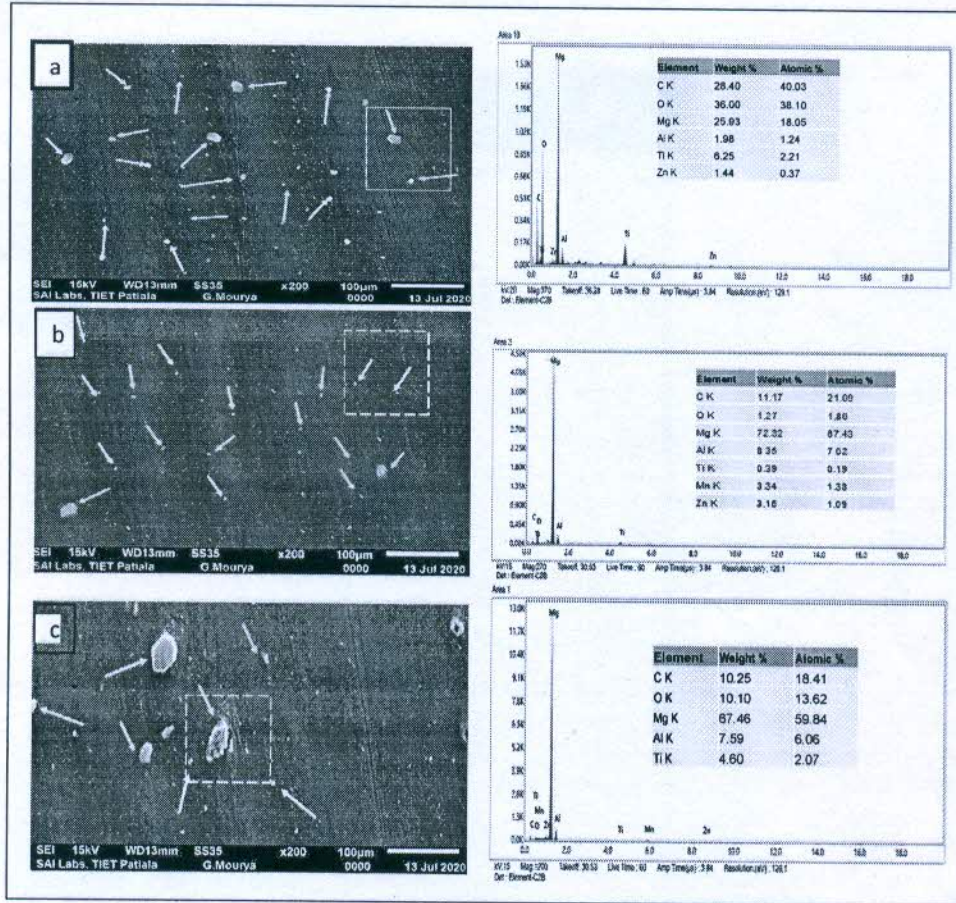


Figure 2 (c). spectrograph of base metal AZ61Mg (200X).

FSP develops dislocations in the grains, and due to high stacking fault and resulting energy generation produces dynamic recovery of low angle sub-grain boundaries. In addition, for all specimens' tool shape and sharp corner of the triangle, the tool develops rigorous stirring which develops a low percentage of clusters.

In all specimens during the solidification process, n-TiC particulates act as nuclei and limit grain size enlargement. Moreover, refinement of grains in the base matrix is due to the capacity of n-TiC to nucleate magnesium grains during recrystallization and the existence of the n-TiC particulates hampered the formation of recrystallized magnesium grains. Investigations strongly indicated that no interfacial interaction exists between carbide particles and the surrounding matrix because no intermetallic compound production occurs. This could be due to the FSP's lack of melting. Friction stirring generates the requisite heat in a short amount of time, which may result in high carbide particle adherence and bonding to the α -solid matrix solution. The FESEM images captured from SZ of the developed composites are presented in Figure 4 along with the EDX spectrum of the same.

For FSP processes, agglomeration and clustering of nano particulates is a prime issue and needs to be resolved as it adversely influences the strength of composites. As the FSP parameters changes i.e., at the tool rotation

speed of 800 rpm and FSP pass number 4 as shown in Figure 4 (c), clusters of very small sized n-TiC particles were observed which was in accord with Asadi et al.,¹⁹ and Khayyamin, et al.²⁰ In almost all the specimens, stir zone (SZ) exhibited finer grains, which may be attributed to dynamic recrystallization, and heat generation, which is in agreement with several other studies. High friction heat develops in the stir zone due to high tool rotation, which consequently produces coarsening of grain. The formation of clusters of n-TiC particles was noticed at 800 rpm due to inadequate heat generation at a low tool rotation speed. The existence of agglomeration slowly gets minimized as the tool rotational speed increases. Along with the generation of heat, tool rotational speed performs two more functions i.e., a) stirs the plasticized materials b) initiates material flow across FSP SZ. The amount of material flow increases with an increase in tool rotation speed which is in agreement with published research.²¹

Table 1 summarizes the values of grain sizes of all specimens obtained from SZ. Furthermore, spectrum analysis of the samples is displayed in Figure 4 (a, b, and c), which validate the presence of the carbon element dispersion in the zone. The figure shows the EDS result of the developed composites at various parameters. Peaks of titanium and carbon clearly show the presence of nanoparticles in the

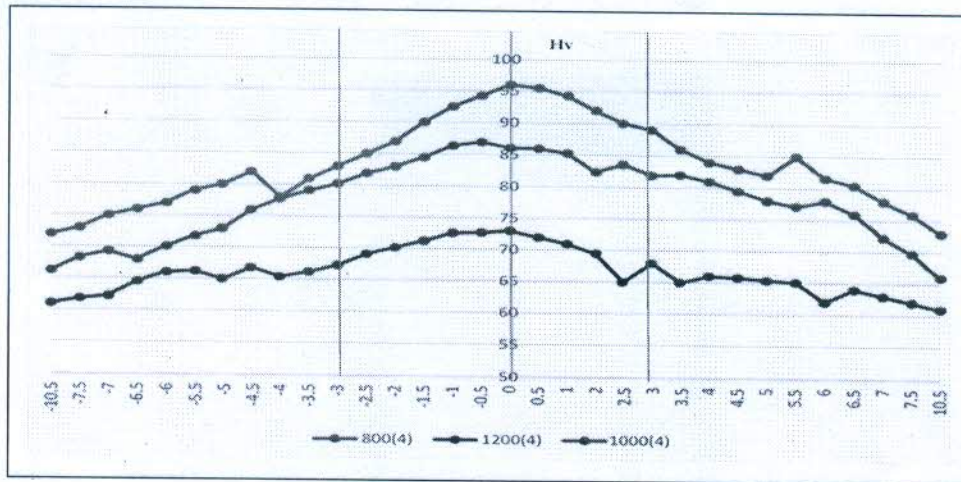


Figure 3. Optical micrographs images (at 100 μm and 200X) from stir zone (SZ) of the developed composites at various TRS and four FSP passes.

stir zone (SZ). These carbon elements are nothing more than reinforcements such as n-TiC, which can be seen duly bonded with the base matrix. The above analysis of the microstructures, SEM and EDS, clearly demonstrates that the best refinement of crystals and dispersion of the reinforcements were displayed by the nanocomposites. In contrast, grain refinement was much superior in all composites. Because of the activation of various strengthening mechanisms, the refinement of grains and grain boundary strengthening contributes to the enhancement of the strength of the formed nanocomposites and the generation of improved mechanical properties.

Mechanical properties (Microhardness testing)

Hardness values of the developed composites were examined and it was found that the average hardness of the

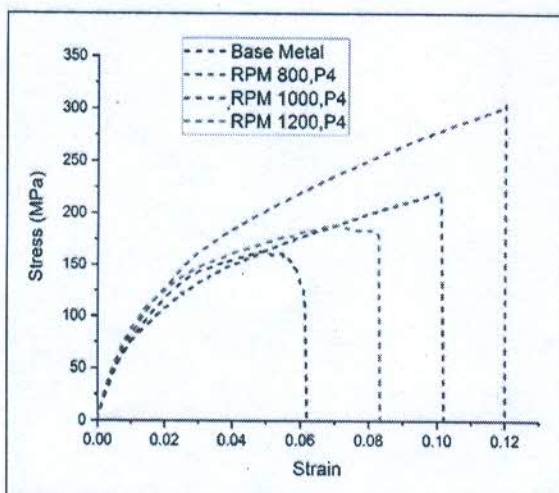


Figure 4. SEM and EDX images a) composite developed at tool rotation speed 1200 rpm and FSP pass number- 4: B) developed at tool rotation speed 1000 rpm and FSP pass number- 4: C) developed at tool rotation speed 800 rpm and FSP pass number- 4.

AZ61A magnesium metal was about 60 Hv. Table 1, summarizes the observed values, which are plotted as a graph in Figure 5.

As can be seen in Table 1 and Figure 5, all the developed FSPed specimens show an increased value of microhardness as compared to the base magnesium, which demonstrates the effect of FSP in developing composites. The hardness of the stir zone for all FSPed samples was considerably higher in contrast to the base magnesium alloy. This may be attributed to refining and small-sized grains at the stir zone due to the dynamic crystallization of FSP. Due to low heat input, rotational speed at 800 rpm, and thus less grain growth occurred but at the same time four FSP passes breaks the clusters hence these samples have the highest hardness (96 Hv), similar results were reported by 6. As a consequence, enhanced microhardness is mainly due to the following two mechanisms i.e., a) grain boundary strengthening which follows the Hall-Petch equation, and b) restricted grain boundary movement by nano-sized reinforcements as per the Zener pinning effect.²² According to Hall-Petch equation, the grain size bears an inverse relationship with hardness, so hardness increases with a decrease in the size of grains. Additionally, four FSP passes decreases the area of surface composite which further decreases inter-particle spacing in the SZ, thus there was an increase in the microhardness value.

In addition, researchers have reported that microhardness holds an inverse relation with interparticle spacing

Table 1. Grain size and microhardness values for the fabricated specimens.

Run	A:TRS (rpm)	B:Number of pass (N)	Grain size (μm)	(Hv)
1	800	4	2.9	96
2	1000	4	4.1	87
3	1200	4	4.9	73

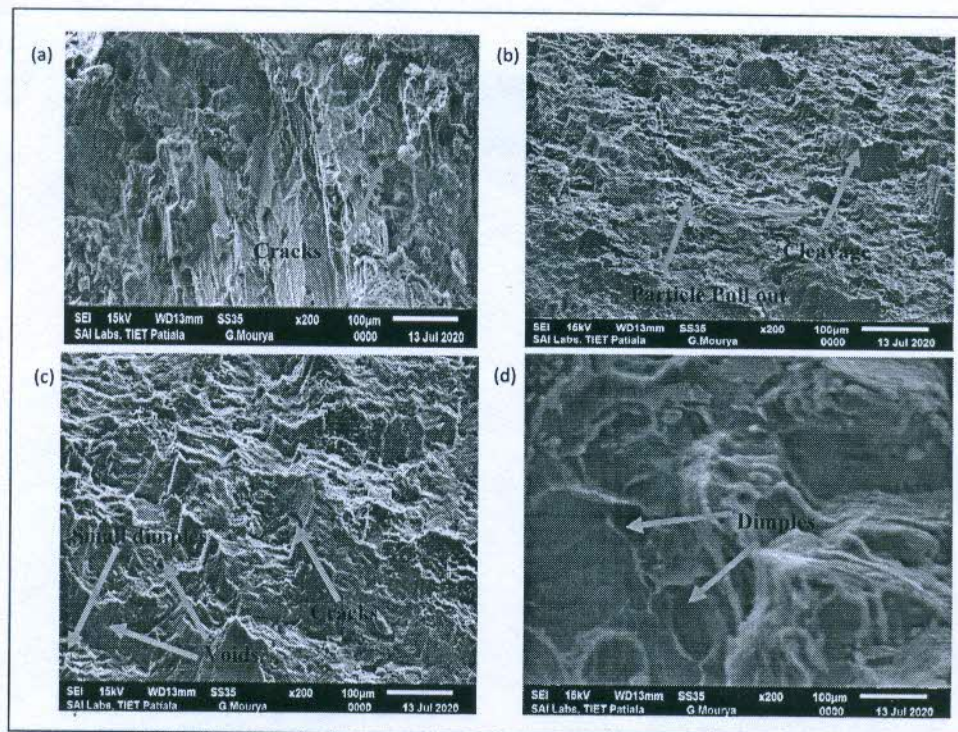


Figure 5. Microhardness distribution of the developed MMC at various FSP parameters.

(Thangarasu, A et. al., 2014). But as tool rotational speed is increased, the surface area and inter-particle spacing also increases. Thus, an increase in area and spacing decreases the amount of actual volume fraction of n-TiC particulates over the entire substrate. Therefore, the microhardness of the 1200 rpm composite drops. In the 1200 rpm samples, high heat generation occurred which led to grain growth and formation of large size grains, which resulted in lowest sample hardness compared to the others. At higher rotational speed of 1200 rpm, heat input increases, and grain growth occur that consequently results in low hardness, as detailed by Azizieh et al.¹⁸ Hence as tool rotational speed increases, the microhardness of the composite decreases, these findings are in confirmation with the findings of Sathiskumar, et al.,²¹ Sathiskumar et al.²³ The hardness value for the 1200 rpm processed sample was observed to be 73 HV, which was the lowest compared to 87 HV at 1000 rpm and 96 HV at 800 rpm. It is an indicator of finer grain evolution and precipitation in the microstructure. This also confirms the distribution of reinforcement particles in the area of stirring. This improved uniformity in the distribution of reinforcements in the SZ guarantees an improvement in mechanical properties. The availability of large grain boundaries, or simply grain size reduction, results in less dislocation movement and increased restriction for slip movement, thus increasing the hardness of FSPed samples which has been reported by Joshi S, et al. (2020).

Tensile Testing

For Tensile test examination, all the specimens were prepared strictly according to ASTM E-8 M standards.

Specimens were extracted from the stir zones of each nanocomposite along with a sample from base magnesium alloy. For the examination of the tensile test, samples of size 100×40×5 mm were prepared as shown in Supplementary Figure 6. All the MMCs showed higher strength and ductility values in contrast to base metal (Table 2) which is in confirmation with Abbasi et al.²⁴ As is summarized in Table 2, compared to the base magnesium alloy, almost all specimens attained higher ultimate tensile strength. Furthermore, in all MMCs, four FSP pass number resulted in uniform particle distribution which consequently resulted in an improvement in ultimate tensile strength of the samples compared to the base monolithic magnesium alloy. Also, FSP dissolved the hard precipitates of $Mg_{17}Al_{12}$ in the grain boundaries which are the sites prone to the formation of cracks. It was found that incorporation of nano-sized reinforcement particles improved the elastic modulus, yield strength (YS), and UTS of the composites significantly when compared to the base AZ61AMg matrix, which is also in conjunction with Liang J et al. 2017.

The tensile test results showed that the strength values for the 1200 rpm samples were lower than the 800 and 1000 rpm FSPed specimens. It was mainly due to large grains, low hardness and nucleation, and growth of cracks at these sites for tensile test, this was in tune with earlier findings.²⁵ In addition, low tensile values are due to large grains which were not able to provide adequate hardness. As shown in Table 2, the specimen fabricated at 800 rpm and four FSP passes had the highest increments in ultimate tensile strength (UTS)

Table 2. Tensile tests results.

Run	A:TRS(rpm)	B:Number ofpass (N)	E(GPa)	0.2%YS(MPa)	UTS(MPa)	(Hv)
1	800	4	11.54 ± 0.2	79.37 ± 2.5	304.64 ± 3.2	96
2	1000	4	8.16 ± 0.1	81.68 ± 3.2	226.66 ± 4.2	87
3	1200	4	8.06 ± 0.3	107.32 ± 2.2	186.18 ± 4.3	73
Base AZ61A	—	—	11.06 ± 0.3	65.3 ± 2.2	161.25 ± 3.7	60

and yield strength (YS) in contrast to the base alloy AZ61A. This could be due to dynamic recrystallization of the grain and appropriate development of heat due to tool rotation and FSP passes. In addition, microstructural changes such as grain refinement due to processing, good bonding between n-TiC particulates, and dispersion of dislocations in the matrix results in enhanced tensile properties.²⁶ Also, the low value of tensile strength in the 1200 rpm specimen was due to the evolution of large grains developed due to high heat produced by higher tool-rotational speeds. High tool rotation also causes uncontrollable turbulence of the plasticized materials in the FSP zone, which leads to the formation of joints. As a result, it can be concluded that increasing the rotational speed of the FSP tool leads to progressively diminishing strength values, which is consistent with that reported by.²⁷ In addition, delay in the formation of micro-cracks and their propagation is an outcome of uniformity of microstructure which allows dislocation slips to occur easily.²⁸ Also, FSP caused anisotropy in tensile properties with a higher level of anisotropy in multiple passes. In addition, the evolution of texture during FSP causes the $\{10\bar{1}0\}$ prismatic planes to be aligned for easy slip during tests in the transverse direction which leads to a good combination of ductility and strength.

The stress-strain curve for specimens developed at different tool rotation speeds (800, 1000, and 1200 rpm) and four FSP passes (two, three, and four) is shown in Figure 6. The ideal location for crack formation is the sites having presence of hard particulates of $Mg_{17}Al_{12}$ in grain boundaries and they were observed to be

completely dissolved by FSP. Also, FSP was found to have vanished the voids and porosities, if there were any present in the base metal or MMCs.

Fractographic analysis

SEM Fractography was done to examine and locate crack initiation and fracture mechanism of MMC's and base AZ61A alloy. The fracture mechanism of tensile fractured surfaces was investigated under monotonic loads. Figure 7 (a) depicts a typical tensile fracture surface of base AZ61A magnesium alloy. It shows the evolution of micro-cracks in the base AZ61A magnesium alloy. The presence of micro-cracks act to concentrate stress to their lips and the crack may come out of the collection of dislocation which indicated that the failure was brittle. This could have attributed to the crack propagation from weaker interfaces during tensile testing. This is well explained by Griffith's theory of failure.

Figure 7 (b) shows the specimens prepared at different tool rotation speed of 800 rpm. Specimens prepared at these parameters showed particle agglomeration which was already confirmed by SEM examination of the FSPed specimens. Machining-induced defects, such as sharp valleys, and particle agglomerations, act as stress concentrators, causing cracks to form. Also, void formation due to debonding matrix cracking and particle pull out were observed as shown in Figure 7 (b) and this can be attributed to overloading. Indeed, the presence of voids directly influenced the elongations of the specimen during tensile testing. In addition, increases in the flatness

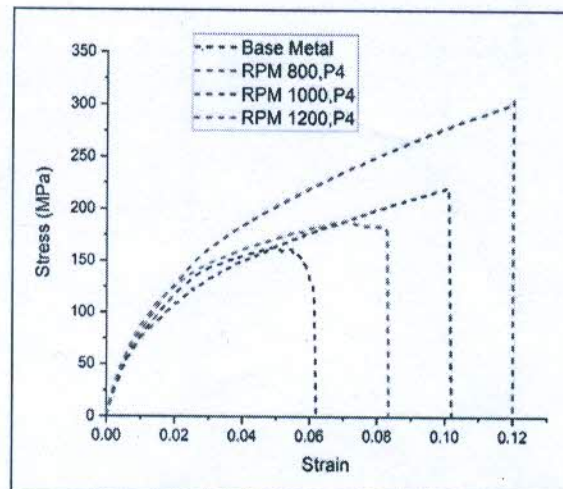


Figure 6. Stress-Strain graphs of various FSPed composites developed at 800 rpm, 1000 rpm, and 4 FSP passes with the base metal.

of the surface indicated that fracture mode gradually approaches the brittle mode which was again found to be in tune with Thangarasu A et al. (2015). Also, the incorporation of n-TiC particulates advanced the flatness in the fracture surface, which occurred due to lesser material flow caused by improved strengthening. In connection to above, most of the n-TiC particles were found to be embedded in the matrix and voids represented the pulling of particles from the matrix as shown in Figure 7 (b).

Figure 7 (c & d) show the specimens prepared at tool rotation speeds of 1000 rpm and 1200 rpm. It was observed that dimples formation took place on the fracture surface of friction stir processed magnesium-based composite. The presence of the fine dimples above the fracture surface could be attributed to the highly refined microstructure of the composite. This kind of presence of fine dimples over the surface demonstrated that the fracture mode was ductile and was in agreement with (Thangarasu A et al. 2015). Ductile fracture is introduced by significant plastic deformation. In addition, it was observed that the rate of deformation of material contained n-TiC (hard inclusions) not the same as compared to base matrix, however in MMCs specimens, to bridge the incongruity nucleation of voids were reported. This nucleation further led to the separating of particle and metal interface sites and fracture of n-TiC particulates. The nucleation may bring fracture of the inclusion at the inclusion-matrix interface. n-TiC reinforcement particles were founded to be embedded in the base matrix and cause the ductile failure of the composites. Also, the fractured surface indicated ductile failure which could be due to adequate heat generated by the combined effect of increasing FSP pass number and appropriate tool rotation speed.

Wear analysis

The Resultant wear rate was determined with the sliding distance. In addition, in Table 3 the overall wear rate results for the MMCs and the base alloy are tabulated. From Supplementary Figure 7, when contrasted to the composite formed at 1000 rpm, 1200 rpm, and the base metal, the specimen developed at 800 rpm displayed a reduced value of height loss concerning sliding distance. This could be due to lower tool rotational speed, which results in smaller grains, and higher hardness, which in turn resulted in reduced wear which was in tune with Asadi.¹⁹ Despite the low hardness value for FSPed, the sample produced at 1200 rpm showed a reduced wear rate and lower height loss because of more homogeneous nanoparticle distribution, in agreement with Azizieh et al.²⁹ Please see Supplementary Figure 7, when the sliding distance increased, the height loss for both base metal and produced composites increased, which was consistent with Archard's wear equation. The findings of wear rate comparison between AZ61A base metal and FSPed processed composites investigated at various FSP parameters and plotted in Supplementary Figure 8. Compared to the produced composites, the magnesium

base AZ61A metal wear rate was high, as shown in Supplementary Figure 8. However, the wear rate for the base metal increased dramatically, as seen in Supplementary Figure 8, indicating mild to severe surface delamination. The harder surface in FSP samples resulted due to refined grains and uniformly distributed secondary phase particles, as observed by numerous other researchers. This low wear rate was due to (a) the addition of second phase particles, which increased the hardness of the FSP composite, (b) the additive n-TiC particulate content, which not only reduced the contact area between the composite and the counter surface, but also effectively opposed the counter face's cutting activity and c) mechanisms of grain boundary and secondary phase i.e., the Hall-pitch mechanism which aids in the development of composite hardness and strength, resulting in an increased load-bearing capability.

Coefficient of Friction. Please see Supplementary Figure 9 which summarizes the amplitude of friction coefficient as a function of time for base metal and composites samples. The initial time frame's friction coefficient variations were observed to be unusually high, which could be related to the new disc surface being introduced to the pin. Before each run, the steel disc was cleaned to acquire precise values and to eliminate the material held on the plate. Higher variances are obtained for all specimens, as shown in Supplementary Figure 9. However, for base metal, there was a lot of variation in friction coefficient with large amplitudes, but these progressions for FSPed composites weren't as wide. The main cause of these oscillations was due to the pin's adherence to the counter-side. Furthermore, SEM pictures revealed that abrasive wear occurs. As a result, the adhesive wear mechanism was dominant, resulting in greater friction coefficient values for the base metal as compared to the produced composites. In successive samples, the n-TiC particle distribution worked as a thin film, resulting in selective material removal and a decrease in mean friction coefficient. The actuation shear stress on the sliding surface reduced as the friction coefficient lowered, resulting in wear resistance. Despite low hardness levels, homogeneous particle dispersion leads to homogeneity in FSPed composites produced at 1200 rpm, which prevented considerable variations in friction coefficient. In addition, compared to the base metal, mean friction coefficient of all FSPed composites dropped. This could be due to the enormous thermal energy that was produced, which softened the materials. Furthermore, mixing secondary phase particles reduced the direct contact area and direct contact load for FSPed specimens, resulting in a drop in the friction coefficient. Hardness might also be attributed to this tendency.

Wear mechanism. Worn Surface morphology was analyzed via SEM examination. SEM images of worn surfaces of base AZ61A and all specimens processed at different FSP machine parameter are presented in Supplementary Figure 10.

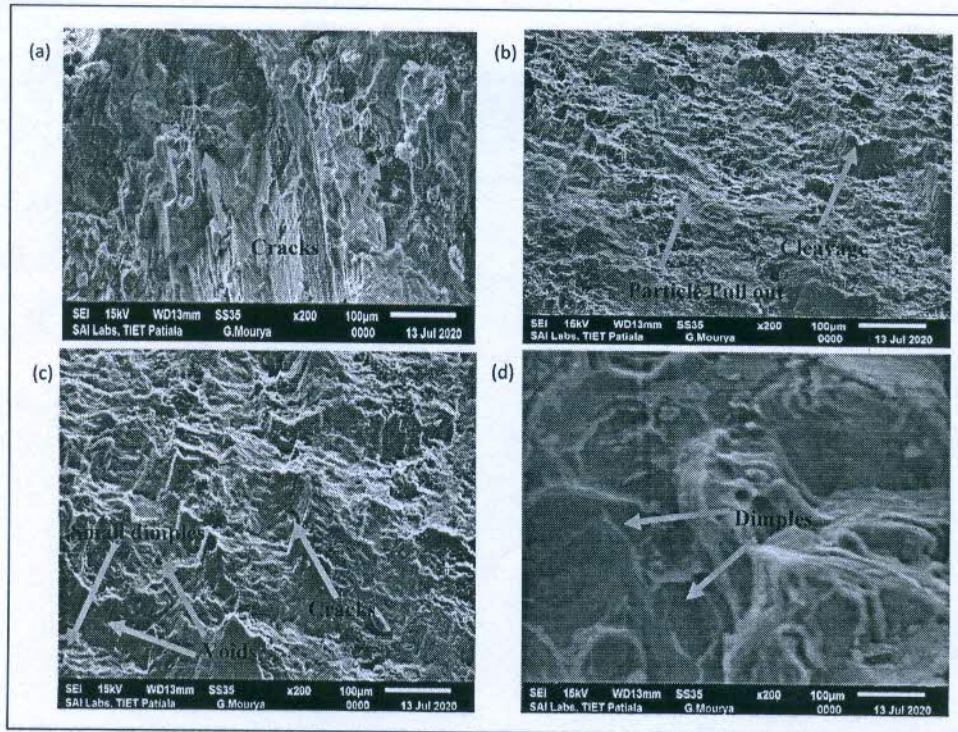


Figure 7. (A) SEM analysis of the fracture surface for the base AZ61A alloy (b) SEM image for composite developed at 800 rpm with 4 FSP passes (c) SEM image for composite developed at 1000 rpm with 4 FSP passes (d) SEM image for composite developed at 1000 rpm with 4 FSP passes.

As per the SEM micrographs of base AZ61A, it was observed that the texture of base material AZ61A comprised of straight deep ploughs/grooves. This could be due to frictional heat breaking into the initial magnesium network, such as $\beta\text{-Mg}_{17}\text{Al}_{12}$. This brittle and coarse phase demonstrated its inability to effectively operate as a wear barrier, resulting in material softening. The dominance of the abrasive wear mechanism was primarily responsible for the appearance of these deep grooves. Which consequently led to the formation of wear debris over the texture of the base metal. Furthermore, worn surface's morphology indicated significant plastic deformation and detached material from the base magnesium alloy. This could be also due to the development of high frictional heating, This significant plastic deformation and detached material from the base magnesium alloy further suggested the existence of adhesive and delamination wear mechanism for this sample. This could be attributed to the low softness of the sample compared to the FSPed composites. A variety of adhesive and

abrasive wear was found on base metal, which is consistent with Madhusudhan Reddy et al.³⁰

However, the wear component observed in the composites was distinct from the base metal. Wear resistance was impacted by uniform grains and homogeneous dispersion of n-TiC particles. In addition, the insertion of n-TiC particulates a) reduced metal-to-metal contact area and b) reduced direct load, resulting in a shift from severe to mild wear. On the other hand, the presence of shallow grooves and less pits along the wear tracks in the specimen processed at 800 rpm showed the dominance of mild abrasive wear mechanism. The wear morphology in MMC at 800 rpm may be due to ploughing, and preceded by a digging out of the TiC particles from the magnesium alloy composite which was in consensus with Aruri et. al.³¹ Presence of loose debris particles over the entire surface of all most all fabricated composites suggested that the abrasive wear mechanism was the dominating mechanism. These loose debris particles appear mostly as a result of oxidizing MMCs and n-TiC

Table 3. Wear results of composites and base metal.

RPM	Initial height (IH)	Final Height (FH)	Change in height ($\Delta h = \text{IH}-\text{FH}$)	Volumetric loss ($\text{VL} = \pi r^2 \Delta h (\text{mm}^3)$)	Wear rate = $\text{VL}/\text{S.D.} (\text{mm}^3/\text{m})$
800	30	29.41506	0.58494	4.1326011	0.00823398
1000	30	29.28874	0.71126	5.0250519	0.010020113
1200	30	29.34855	0.65145	4.60249425	0.009177505
AZ61A	30	29.057265	0.94273	6.66372234	0.013327445

tugging during sliding. Also, the change in wear morphology of the worn surface from scratches to grooves was mainly due to the development of continuous friction.

For the specimen processed at 1000 rpm, formation of wear debris and occurrence of delamination wear mechanism was noticed along with mild abrasive. This delamination wear mechanism could be mainly attributed to shear plastic deformation which produced nucleation and propagation of cracks beneath the surface, and these cracks eventually connected together, resulting in layered area separation which was in agreement with Sarmadi et al.³² In particular, the creation of pores in the subsurface area are caused by the buildup of dislocations under the surface. As there were no chemical interactions between n-TiC and magnesium alloy, pores could form at the interface between n-TiC particles and magnesium. The joining of these pores causes cracks to emerge, which then grow during the wear process, resulting in wear debris.

For specimen prepared at 1200 rpm, owing to good nanoparticle distribution of n-TiC particulates, the surface had fewer micro-cracks. In addition, this uniform distribution lowered the immediate contact load and prevented delamination. It was worth noting that specimen processed at 1000 rpm had delamination of the MMC layers at some spots. However, for 1200 rpm MMC, the case was different and less delamination was reported.

Conclusions

- 1) The n-TiC Particles are effectively absorbed in the base AZ61AMg metal matrix and significantly contribute to the enhancement of the mechanical properties. This significant improvement of the properties clearly demonstrates the tremendous potential of the FSP process within solid-state formability limits.
- 2) The presence of secondary phase n-TiC particles and grain refinement directly influenced the metallurgical, mechanical and tribological behavior of the developed composites. Large grains were observed at 1200 rpm due to heat development. However, as the tool rotation speed increased, homogenous distribution of the n-TiC particulates was noticed.
- 3) In contrast to base metal, 60% increase in hardness was observed in the sample processed at 800 rpm. Brittle mode of tensile failure occurred in AZ61A base magnesium metal. Enhanced tensile strength values were achieved for composite fabricated at 800 rpm which was nearly 88% higher than the hardness of AZ61A base metal.
- 4) Worn surface morphology was greatly influenced by tool rotational speeds. Due to the higher hardness as well as uniform particle distribution of the specimens prepared at 800 rpm and 1200 rpm, nearly 38% and 31% lesser wear rates were achieved when compared to the monolithic base metal. The worn surface appeared to be smooth with few shallow grooves.

Declaration of conflicting interests

The author(s) declared no potential conflicts of interest with respect to the research, authorship, and/or publication of this article.

the Funding and Conflict of Interest statements are accurate


Funding

The author(s) received no financial support for the research, authorship and/or publication of this article.

ORCID iDs

Prem Sagar  <https://orcid.org/0000-0003-2804-9458>

GQ6

Gitesh Kumar  <https://orcid.org/0000-0003-3988-6227>

Supplemental material

Supplemental material for this article is available online.

References

1. Esmaily M, Svensson JE, Fajardo S, et al. Fundamentals and advances in magnesium alloy corrosion. *Prog Mater Sci [Internet]* 2017; 89: 92–193.
2. Peron M, Torgersen J and Berto F. Mg and its alloys for biomedical applications: exploring corrosion and its interplay with mechanical failure. *Metals (Basel)* 2017; 7: 1–10.
3. Mallick A. Improvement of mechanical properties of weight Mg-based materials. *Procedia Eng* 2013; 77: 283–287.
the page range is not available till date as per DOI <https://doi.org/10.3390/met7070252>
4. Xie Y, Meng X, Wang F, et al. Insight on corrosion behavior of friction stir welded AA2219/AA2195 joints in astronautical engineering. *Corros Sci [Internet]*. 2021^a;192:109800.
5. Qin Z, Xie Y, Meng X, et al. Oriented attachment strategy toward enhancing ionic conductivity in garnet-type electrolytes for solid-state lithium batteries. *ACS Appl Mater Interfaces* 2021; 13: 34385–34396.
6. Handa A and Chawla V. Investigation of mechanical properties of friction-welded AISI 304 with AISI 1021 dissimilar steels. *Int J Adv Manuf Technol* 2014; 75: 1493–1500.
7. Meng X, Huang Y, Cao J, et al. Recent progress on control strategies for inherent issues in friction stir welding. *Prog Mater Sci [Internet]* 2020; 100706.
8. Xie Y, Meng X, Li Y, et al. Insight into the corrosion behavior of aluminum matrix composites via friction stir metallurgy. *Compos Commun [Internet]*. 2020; 101616.
the page range is not available till date as per <https://doi.org/10.1016/j.pmat.2020.100706>
9. Sagar P and Handa A. A comprehensive review of recent progress in fabrication of magnesium base composites by friction stir processing technique—A review. *AIMS Mater Sci* 2020; 7: 684–704.
10. Prangnell PB and Heason CP. ‘Grain structure formation during friction stir welding observed by the ‘stop action technique’’. *Acta Mater* 2005; 53: 3179–3192.
11. McNelley TR, Swaminathan S and Su JQ. Recrystallization mechanisms during friction stir welding/processing of aluminum alloys. *Scr Mater* 2008; 58: 349–354.
12. Ahmadkhanlida D, Heydarzadeh Sohi M, Salehi A, et al. Formations of AZ91/Al₂O₃ nano-composite layer by friction stir processing. *J Magnes Alloy [Internet]* 2016; 4: 314–318.
13. Balakrishnan M, Dinaharan I, Palanivel R, et al. Synthesize of AZ31/TiC magnesium matrix composites using friction stir processing. *J Magnes Alloy [Internet]* 2015; 3: 76–78.

14. Dinaharan I, Vettivel SC, Balakrishnan M, et al. Influence of processing route on microstructure and wear resistance of fly ash reinforced AZ31 magnesium matrix composites. *J Magnes Alloy [Internet]* 2019; 7: 155–165.
15. Abbas A, Huang SJ, Ballóková B, et al. Tribological effects of carbon nanotubes on magnesium alloy AZ31 and analyzing aging effects on CNTs/AZ31 composites fabricated by stir casting process. *Tribol Int* 2020; 142, (September 2019).
16. Huang Y, Wang Y, Meng X, et al. Dynamic recrystallization and mechanical properties of friction stir processed Mg-Zn-Y-Zr alloys. *J Mater Process Technol* 2017; 249: 331–338.
17. Li Y. "Dynamic Recrystallization of a Mg alloy during Friction Stir Processing: Grain Size Refinement and Texture Evolution." PhD diss., University of Tennessee, 2019. https://trace.tennessee.edu/utk_graddiss/5788. 2019. AQ2
18. Azizieh M, Kokabi AH and Abachi P. Effect of rotational speed and probe profile on microstructure and hardness of AZ31/Al₂O₃ nanocomposites fabricated by friction stir processing. *Mater Des [Internet]* 2011; 32: 2034–2041. Available from: <https://doi.org/10.1016/j.triboint.2019.105982>
19. Asadi P, Besharati Givi MK and Faraji G. Producing ultrafine-grained AZ91 from as-cast AZ91 by FSP. *Mater Manuf Process* 2010; 25: 1219–1226.
20. Khayyamin D, Mostafapour A and Keshmiri R. The effect of process parameters on microstructural characteristics of AZ91/SiO₂ composite fabricated by FSP. *Mater Sci Eng A [Internet]* 2013; 559: 217–221.
21. Sathiskumar R, Murugan N, Dinaharan I, et al. Prediction of mechanical and wear properties of copper surface composites fabricated using friction stir processing. *Mater Des [Internet]* 2014; 55: 224–234.
22. Morisada Y, Fujii H, Nagaoka T, et al. Effect of friction stir processing with SiC particles on microstructure and hardness of AZ31. *Mater Sci Eng A* 2006; 433: 50–54.
23. Sathiskumar R, Dinaharan I, Murugan N, et al. Influence of tool rotational speed on microstructure and sliding wear behavior of Cu/B₄C surface composite synthesized by friction stir processing. *Trans Nonferrous Met Soc China (English Ed.)* 2015; 25: 95–102.
24. Abbasi M, Bagheri B, Dadaei M, et al. The effect of FSP on mechanical, tribological, and corrosion behavior of composite layer developed on magnesium AZ91 alloy surface. *Int J Adv Manuf Technol* 2015; 77: 2051–2058.
25. Callister WD. *Materials science and engineering: an introduction*. USA: Wiley, 2007.
26. Park SHC, Sato YS and Kokawa H. Basal plane texture and flow pattern in friction stir weld of a magnesium alloy. *Metall Mater Sci Technol* 2003; 34, (September 2003). <https://doi.org/10.1016/j.triboint.2019.105982>
27. Besh C. Role of tool rotational speed in influencing microstructural evolution, residual-stress formation and tensile properties of friction-stir welded AZ80A Mg alloy. *Mater Tehnol* 2018; 52: 607–614.
28. Sharma SR, Ma ZY and Mishra RS. Effect of friction stir processing on microstructure and wear behavior of A356 alloy. *Scr Mater* 2004; 51: 237–241. the url is working fine
29. Azizieh M, Larki AN, Tahmasebi M, et al. Wear behavior of AZ31/Al₂O₃ magnesium matrix surface nanocomposite fabricated via friction stir processing. *J of Materials Engineering and Performance* 2018; 27: 2010–2017.
30. Madhusudhan Reddy G, Sambasiva Rao A and Srinivasa Rao K. Friction stir processing for enhancement of wear resistance of ZM21 magnesium alloy. *Trans Indian Inst Met* 2013; 66: 13–24.
31. Aruri D, Adepu K, Adepu K, et al. Wear and mechanical properties of 6061-T6 aluminum alloy surface hybrid composites [(SiC + Gr) and (SiC + Al₂O₃)] fabricated by friction stir processing. *J Mater Res Technol [Internet]* 2013; 2: 362–369.
32. Sarmadi H, Kokabi AH and Seyed Reihani SM. Friction and wear performance of copper-graphite surface composites fabricated by friction stir processing (FSP). *Wear [Internet]* 2013; 304: 1–12.
33. Lin C, Huang W and Liu C. *Structural analysis and optimization of bicycle frame designs* 2017; 9: 1–10. AQ3
34. Markets ME and Sheet MD. *Weblinks: Magnesium Applications-Weblinks: Magnesium Applications*. n.d. AQ4

Prediction of wear resistance model for magnesium metal composite by response surface methodology using central composite design

Prem Sagar and Amit Handa

Department of Mechanical Engineering, IK Gujral Punjab Technical University, Jalandhar, India

Abstract

Purpose – In recent days, friction stir processing (FSP) has emerged as a pioneering approach for the manufacture of composites with enhanced mechanical and tribological properties. The present study aims to examine the impact of process parameters such as tool rotation speed and number of FSP pass on the AZ61A/TiC magnesium metal composite for responses such as hardness and wear resistance.

Design/methodology/approach – To minimize number of experimental runs, design of experiment was configured according to the response surface methodology using central composite design. Analysis of variance has been conducted to develop mathematical and empirical model for studying relationship between tool rotation and number of pass for responses such as microhardness and wear resistance. Microhardness was checked on vickers microhardness testing machine, and tribological behavior were examined on pin-on-disc using tribotester. Wear morphology was analyzed via scanning electron microscopy.

Findings – The responses were predicted using validated mathematical model, and contour plots were generated to study the interaction and influence of process parameters. Wear observations suggest that for the base magnesium alloy adhesive wear mechanism was dominating and for the developed

Prediction of wear resistance model

Prem Sagar and Amit Handa

Dinakaran *et al.* (2019); developed a titanium particulate AZ31 magnesium-based composite and studied the effects of transverse speed and number of FSP passes. They reported that an increase in transverse speed gave rise to a clustered zone because of reduced frictional heat and an increase in FSP pass number at fixed traverse speed produced an enhanced tensile behavior in the developed composite. Furthermore, Dinakaran *et al.* (2020) studied the effects of volume fraction on tensile behavior of developed titanium particulate AZ31 magnesium-based composite. It was reported that the addition of Ti particles can lead to an improvement in UTS from 226.00 MPa (0 Vol.%) to 283.00 MPa (21.00 Vol.%). Very Recently, Sardar *et al.*, 2019; manufactured Al-Zn-Mg-Cu matrix composites reinforced with Al₂O₃ (0–20 Wt.%) and studied the effects of four independent variables on wear behavior of the developed composites using response surface-based analysis of variance (ANOVA) technique. They identified the optimum amount of reinforcement for obtaining the lowest values of wear rate and coefficient of friction. In addition, they proposed a promising mathematical model using RSM approach for optimizing the wear performances. In another work, Sardar *et al.* (2019); examined the tribo-performances of alumina reinforced Al-Zn-Mg-Cu composites for wear rate, coefficient of friction and abraded surface roughness considering varying abrasive size, load and sliding distance. Firstly, they converted all three tribo-responses into a single response of grey relational grade (GRG). Afterwards, response surface-based central composite design was adopted to improve tribo performances of the composites through optimal factor setting. They concluded that the contribution of abrasive size was the greatest at 56.60% followed by that of the particle quantity, evaluated only to be around 13.10%. The optimal GRG value as obtained from GRA was initially 0.78, and desirability-based optimization reached the level of 0.77.

World Journal of Engineering

Volume 18 · Number 2 · 2021 · 316–327

Literature survey revealed that researchers always strive for better performance in terms of mechanical and microstructural properties. However, because of the stochastic nature of FSP and large number of input and output parameters involved, its full potential is yet to be realized. It was observed from the literature review that the most significant FSP parameters for enhancing microstructural and mechanical properties of the base metal are tool rotation speed, penetration depth, tool tilt angle, axial force and number of FSP passes (Sharma *et al.*, 2018; Sunil *et al.*, 2016; Kumar *et al.*, 2020; Zohoor *et al.*, 2012; Jabbari *et al.*, 2015).

In this exploratory work, an endeavor was made to highlight the inter-relationship of input parameters (tool rotation speed and number of pass) to the response parameters such as microhardness and wear resistance. Additionally, using statistical tools such as design of experiments and analysis of variance, a scientific model has been developed to predict the multiple response characteristics of MMC.

2. Materials and methodology

2.1 Materials

The FSP was used on the selected substrate metal AZ61A magnesium alloy to develop composite mixed with reinforced TiC powder of particle size 80 nm. The complete chemical composition of the base AZ61A is presented in Table 1. The idea behind selecting AZ61A was because of its increasing use in manufacturing bicycle pedals and military equipment, wherein at certain places it needs to encounter friction (Monteiro *et al.*, 1998; Lin *et al.*, 2017; Markets and Sheet, 2020). The test samples were rectangular shaped plates of dimension 200 mm × 100 mm × 6 mm. Along the length of the plates, zig-zag holes of about 2 mm diameter and 4 mm depth were engraved as shown in Figure 1(a) and then filled with the TiC

powder. Initially, setting up of the powder was done using a pin less tool, after that the FSP process was executed by a second triangular tool, comprising of a pin and shoulder as presented in Figure 1(b).

2.2 Experimental design parameters and matrix

Upon extensive literature, it was found that rotating FSP tool developed high amount of heat because of friction between the tool and the work-piece. This interaction of rotating tool with work-piece generated plastic deformation and heat input in the stir zones influenced the material flow. This gave rise to microstructure evolution, which directly affected mechanical and tribological properties. Also, clustering of secondary phase particles in developed composite is an issue of prime importance which further affects the strength of the resulting composite. Increasing number of FSP passes not only reduced the size of cluster, it also provided uniform distribution of reinforcement particles which subsequently decreased the grain size of matrix, and gave additional strength to composite (Zohoor *et al.*, 2012; Jabbari *et al.*, 2015). Hence, final experimentation was done considering these two important FSP parameters (tool rotation speed and no. of FSP passes) as

a variable parameters and other variables such as tool transverse speed (40 mm/min) and tool tilt angle (2 degrees) were kept constant. A preliminary experiment was done for obtaining the best possible working range of the variable parameters. Each trial specimen was examined for seamless cross section and crown appearance, to rule out the appearance of any material defect. Final selected parameters, along with their ranges are presented in Table 2. A full factorial face centered central composite design with one center point and one alpha value from Design-Expert 11 software was employed for the design of experiments. Vertical milling center machine was used to conduct the final experimentation with the parameters selected according to design matrix shown in Table 2. The finally produced FSPed specimens are presented in Figure 2 (a) and 2(b). However, the few FSPed samples which were produced beyond the suitable selected combination of parameters are presented in Figure 2(c). Figure 2(c) could be characterized by visual defects, surface galling and insufficient metal flow was seen in this sample. Hence, the process parameters used to produce these welds were considered inappropriate in this case.

2.3 Microhardness

The measurement of microhardness was done by Vickers indentation method by applying a total load of 500 g for a dwell time of 15 s as per ASTM specifications. Hardness values were examined along a horizontal line underneath 1.50 mm from the top surface at equal intervals of 0.50 mm between adjacent points. At every indentation point, three values were taken and their mean value was considered for calculations. The value of microhardness for the base AZ61A was calculated to be 60.00 Hv and the respective values for all other processed specimens are presented in Table 3.

2.4 Wear morphology

For examining wear and friction characteristics, pins of size Ø3 mm × 30 mm were prepared using wire cut electric

Figure 2 FSPed composites surfaces

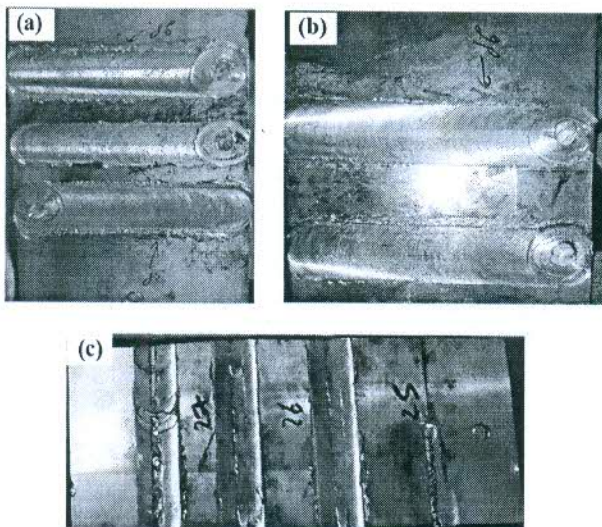


Table 2 FSP Parameters matrix along with their ranges

S. No.	Parameters	Unit	Levels		
			-1	0	1
1	Tool rotation speed (TRS)	rpm	800	1000	1200
2	Number of pass (N)	-	2	3	4

Table 3 Design matrix with its experimental wear resistance and micro hardness results

Run	Coded Value	Coded Value	Real value	Real value	ΔM	Wear rate	Hardness	Wear Resistance
	Factor 1	Factor 2	Factor 1	Factor 2				
	A:TRS (rpm)	B:Number of pass (N)	A:TRS (rpm)	B:No. of pass (N)	mg	(mg/N.m)	(HV)	(N.m/mg)
1	1	0	1200	3	11.70	0.00117	72	854.70
2	0	0	1000	3	16.66	0.00166	84	600.00
3	1	-1	1200	2	12.57	0.00125	64	795.27
4	-1	-1	800	2	9.50	0.00095	87	1052.63
5	-1	1	800	4	6.91	0.00069	96	1445.40
6	-1	0	800	3	7.50	0.00075	95	1333.30
7	0	-1	1000	2	17.64	0.00176	82	566.66
8	1	1	1200	4	11.11	0.00111	73	900.00
9	0	1	1000	4	13.00	0.00130	87	769.23

discharge machining from the base metal as well as the MMCs. All the experiments were done as per ASTM G99 standard and were examined on pin-on-disc tribotester. Steel disc (EN31) of hardness of 60 HRC was used as a counter surface and prepared by silicon carbide papers of grit size 800 and 1000 preceded by acetone cleaning. Wear analysis was conducted for a sliding distance of 500 m, time of 600 s, disc speed of 400 rpm, and a fixed load of 20 N. The wear rate and resistance of the specimens were determined utilizing equations (1) and (2) separately:

$$\text{Wear rate} = \frac{\Delta M}{F \times L} \quad (1)$$

$$\text{Wear resistance} = \frac{1}{\text{wear rate}} \quad (2)$$

Where ΔM was the loss of mass (mg) in specimen measured after wear test and calculated up to 0.001, F was applied force (N) and L was the sliding distance (m). In all specimens, the asperities of the disc deform the first layer of the specimen, trailed by defragmentation and evacuation of the furthest oxide layer. Wear rate and wear resistance for all processed specimen was calculated and presented in tabular form in Table 3. Worn surfaces and underlying wear mechanism were analyzed by scanning electron microscopy. The value of wear resistance for the base AZ61A was calculated to be 520.02 N.m/mg and the respective values for all other processed specimens are presented in Table 3.

Table 4 Fit statistics model analysis response for microhardness

SD	2.04	R^2	0.9865
Mean	82.22	Adjusted R^2	0.9641
C.V. %	2.48	Predicted R^2	0.8723
		Adeq Precision	18.4410

Table 5 Fit statistics model analysis response for wear resistance

SD	53.04	R^2	0.9885
Mean	924.14	Adjusted R^2	0.9694
C.V. %	5.74	Predicted R^2	0.8971
		Adeq Precision	21.6414

Table 6 Response 1: Microhardness

Source	Sum of Squares	df	Mean Square	F-value	p-value	
Model	911.11	5	182.22	43.93	0.0052	Significant
A-trs	793.50	1	793.50	191.29	0.0008	
B-no of pass	88.17	1	88.17	21.25	0.0192	
AB	0.0000	1	0.0000	0.0000	1.0000	
A ²	20.06	1	20.06	4.83	0.1153	
B ²	9.39	1	9.39	2.26	0.2295	
Residual	12.44	3	4.15			
Cor Total	923.56	8				

2.5 Creation of empirical correlations

The response parameters defining micro hardness and wear resistance are the functions of tool rotation speed and FSP pass number. The coefficients were determined utilizing the product Design software 11. After the coefficients were calculated, the empirical relationships were established. Both coefficients were tested at a confidence point of 95% for their meaning. Consideration was given to both the relevant coefficients for building the conclusive empirical relations. The final empirical relationships developed for both responses, i.e. microhardness and wear resistance are given below in equation (3) and (4):

$$\begin{aligned} \text{Microhardness} = & 33.1111 + 0.100833 \times \text{TRS} + 16.8333 \times N \\ & - 6.4113e - 17 \times \text{TRS} \times N - 7.91667e - 05 \\ & \times \text{TRS}^2 - 2.16667 \times N^2 \end{aligned} \quad (3)$$

$$\begin{aligned} \text{Wear resistance} = & 10674.3 - 20.9006 \times \text{TRS} + 523.598 \times N \\ & - 0.36005 \times \text{TRS} \times N + 0.0104565 \text{TRS}^2 \\ & - 7.81167N^2 \end{aligned} \quad (4)$$

2.6 Validating the sufficiency of the empirical relationship model

Table 3 presents the full factorial design and the analysis carried out using the statistical software tool design expert 11. Further analysis of variance (ANOVA) for the selected process parameters and their results pertaining to microhardness and wear resistance is presented in Table 4 and 5. Table 4 presents the fit statistics model analysis response for microhardness obtained from ANOVA analysis. It shows that for the microhardness experiments, predicted R^2 and adjusted R^2 with values of 0.8723 and 0.9641 were found to be in good agreement as the difference was less than 0.2. Signal to noise ratio for adequate precision measures was greater than 4, which is desirable. The ratio of 18.441 obtained in this study indicates an adequate signal.

Additionally, ANOVA fit statistics model for wear resistance as presented in Table 5 shows that the predicted R^2 0.8971 and adjusted R^2 0.9694 were in strong agreement as again change in value was less than 0.2. Signal to noise ratio for adeq precision measures was greater than 4, which is desirable. Observed ratio of 21.641 indicated an adequate signal.

ANOVA results for the FSP response for microhardness is presented in Table 6. It was found that the model F-value

of 43.93 implied that the model was significant. In addition, P-values of less than 0.0500 indicate that the model terms were significant. In this case, both controlled parameters such as tool rotation speed and number of passes were significant model terms for output response such as microhardness. Values greater than 0.1000 indicate the model

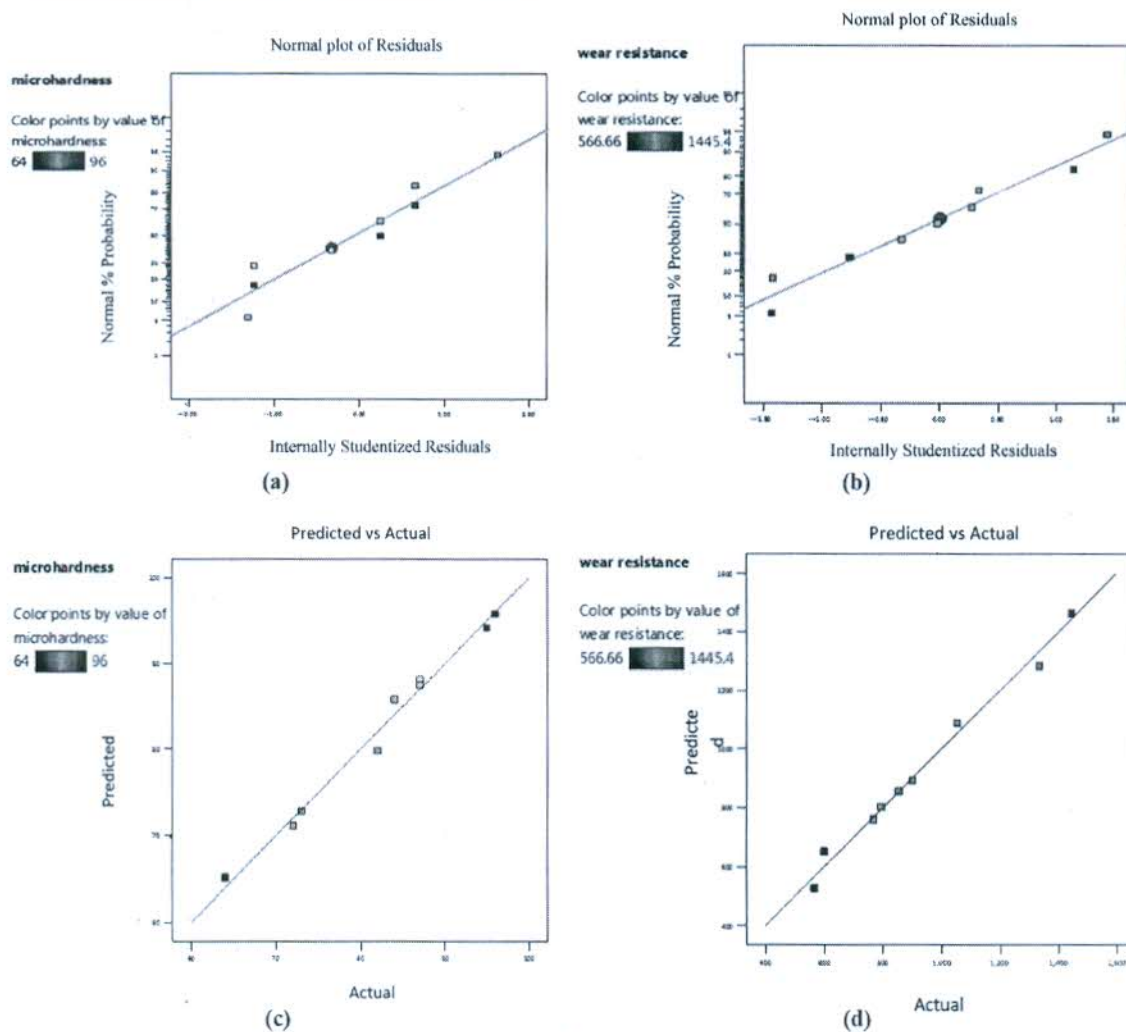
terms are not significant. As can be observed in Table 6, the combined effect of both parameters were not greatly influencing microhardness response.

ANOVA results for the FSP response such as wear resistance are presented in Table 7. It was found that the Model F-value of 51.64 implied the model significance.

Table 7 Response 2: Wear resistance

Source	Sum of Squares	df	Mean Square	F-value	p-value	
Model	7.261E + 05	5	1.452E + 05	51.64	0.0041	Significant
A-trs	2.736E + 05	1	2.736E + 05	97.31	0.0022	
B-no of pass	81683.00	1	81683.00	29.05	0.0125	
AB	20741.76	1	20741.76	7.38	0.0728	
A ²	3.499E + 05	1	3.499E + 05	124.42	0.0015	
B ²	121.73	1	121.73	0.0433	0.8485	
Residual	8436.06	3	2812.02			
Cor Total	7.345E + 05	8				

Figure 3 (a) Normal probability plot for studentized residuals for microhardness, (b) wear resistance, (c) plot of predicted vs actual response for microhardness, (d) plot of predicted vs actual response for wear resistance



Also, P-values of less than 0.0500 indicated that the model terms were significant. In this case tool rotation speed, number of pass and square values of tool rotation speed were significant model terms.

3. Results and discussion

The as processed FSPed specimens are shown in Figure 2(a) and 2(b). Using the existing empirical relationship, the influence of input variables namely, tool rotation speed and FSP pass number on the response properties of MMC such as micro hardness and wear were analyzed. The traditional residual plot graph and expected versus actual observed data for both responses is shown in Figure 3 (a-d). From Figure 3 (a) and 3(b) it can be observed that the residual was distributed randomly, and the developed model was found to be in tune with the experimental data.

3.1 Influence of tool rotation speed

Figure 4 demonstrates the influence of tool rotation speed and different number of passes on micro hardness and wear

resistance on response property. Tool rotational speed directly affected the generation of frictional heat within the FSP zone, in accordance with Rajakumar *et al.* (2011). The frictional heat determines the softening and amount of plasticized magnesium metal substrate. As it is evident from Figure 4 (a), with an increase in rotational speed from 800 to 1200 rpm, the microhardness of the developed composite decreased which was in agreement with earlier reported experiments (Azizieh *et al.*, 2011; Sathiskumar *et al.*, 2014, 2013). The micro hardness was found to be 92 Hv at 800 rpm and 64 Hv at 1200 rpm. This variation in micro hardness may be attributed to the presence of agglomerations. Additionally, this inverse relationship between tool rotational speed and hardness can be attributed to the fact that heat input increases the occurrence of grain growth that subsequently results in low hardness, as detailed by Thangarasu *et al.* (2014). Hence, the hardness of the composite surface at 1200 rpm was found to be lower.

Figure 5 (b) shows parabolic variation of wear resistance to the tool rotation speed. The observed nature of this

Figure 4 Plot showing the effect of TRS on (a) microhardness, (b) wear resistance, (c) contour plot showing interaction effect of TRS and No. of pass with microhardness, (d) 3D graph shows variation in microhardness with respect to change in TRS and No. of passes

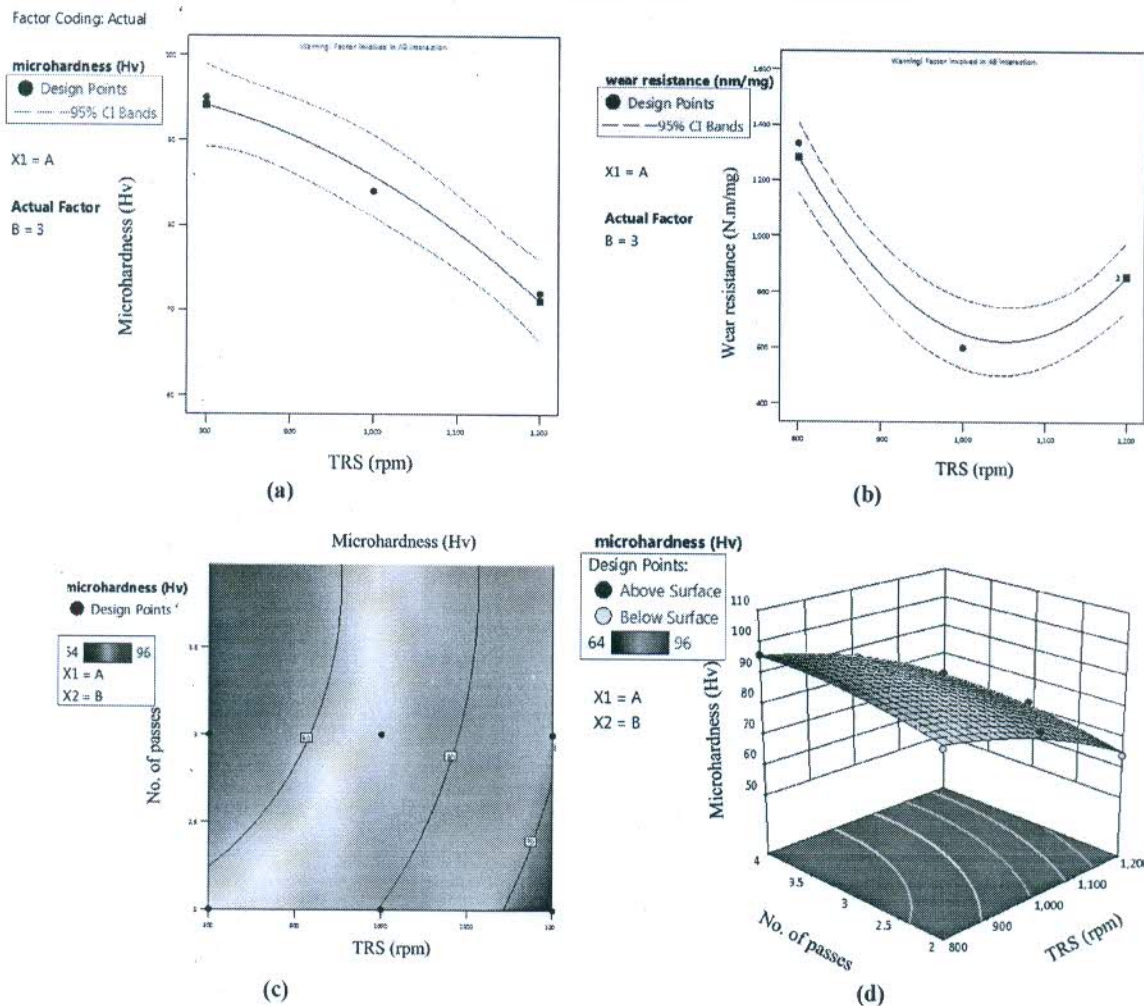
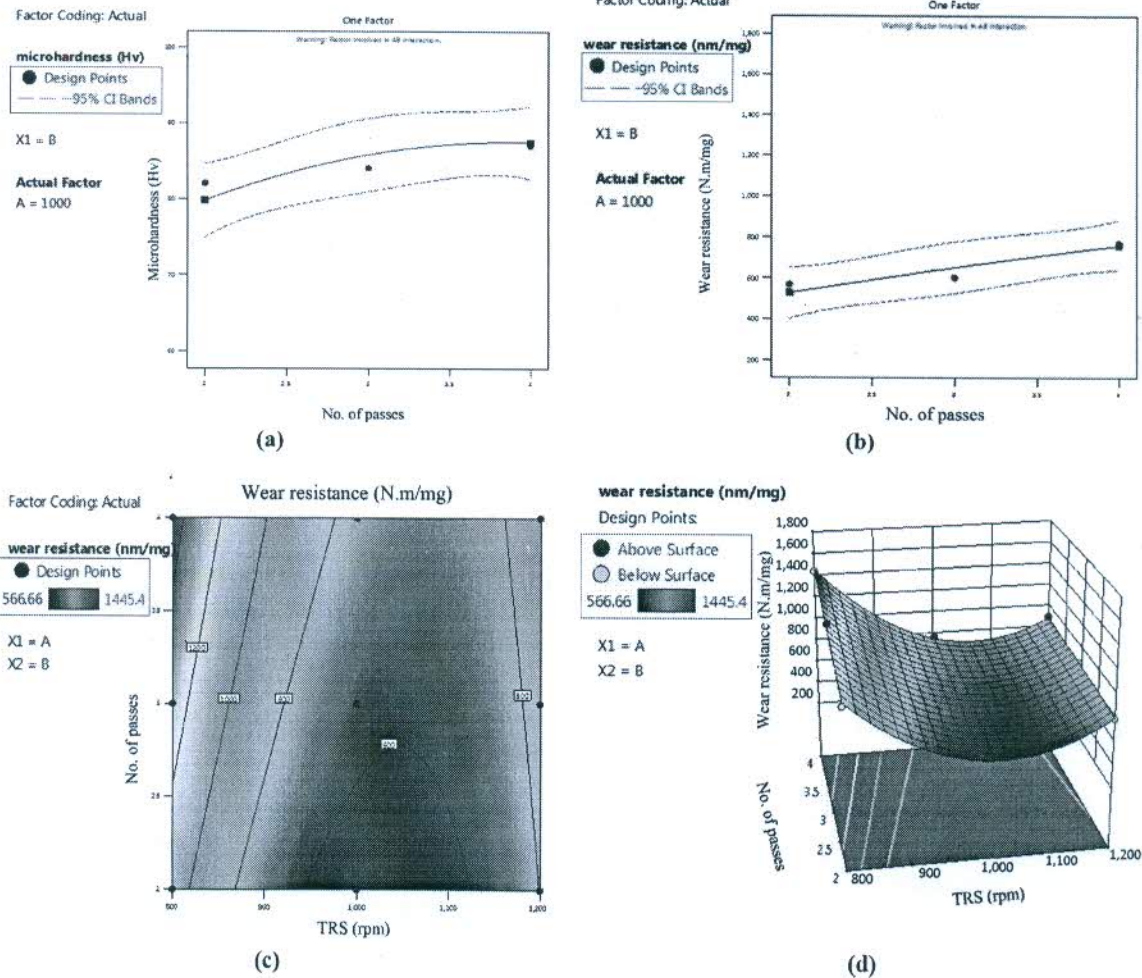


Figure 5 Effect of number of passes on (a) microhardness, (b) wear resistance, (c) contour plot showing interaction effect of no of passes



shape of curve was mainly because of the higher value of wear resistance at 1200 rpm. In spite of low value of hardness for FSPed sample processed at 1200 rpm, a higher value of wear resistance was observed and this may have been because of more homogenous distribution of nanoparticles, which is in consensus with Azizieh *et al.* (2011). It was notable that the wear rate was observed to be inversely related to microhardness in MMCs. The possible cause of wear resistance is minimum at an intermediately speed value is that FSPed samples developed at 1000 rpm causing a low integrity at the matrix–particle interface, and results in easy separation of nanoparticles from the matrix and during the wear test. These separations intensify the wear rate, because they act as abrasive particles between the counter side and pin. Lastly, a possible cause of high wear resistance for composites developed at 1200 rpm could attributed to the fact that the contact area between the sliding pin and the counter face is reduced by the protruding particles successfully because of homogenous dispersion. The applied load is well supported by the agglomeration of nanoparticles. Therefore, in the sample

FSPed at 1200 rpm, in spite of lower hardness values, the wear resistance was observed to be high compared to intermediate speed values because of more uniform distribution of the nanoparticles. This was again in strong agreement with what has been reported by Azizieh *et al.*, 2018.

As microhardness of the MMCs decreased, inferior values of wear resistance were noticed in form of higher metal removal during sliding wear. Consequently, the wear rate speeds up when rotational speed increases. Contour plots and 3D surface plots as presented in Figure 4 (c) and 4(d) shows the interaction between controlled FSP parameters to the response parameters.

3.2 Effect of number of pass

The influence of FSP pass number upon processed composites for microhardness and wear resistance are shown in Figure 5. As demonstrated in Figure 5, as the FSP pass number increased, the microhardness and wear resistance also increased which is in agreement with

Figure 6 SEM images for the composites processed at various combination of TRS and number of passes

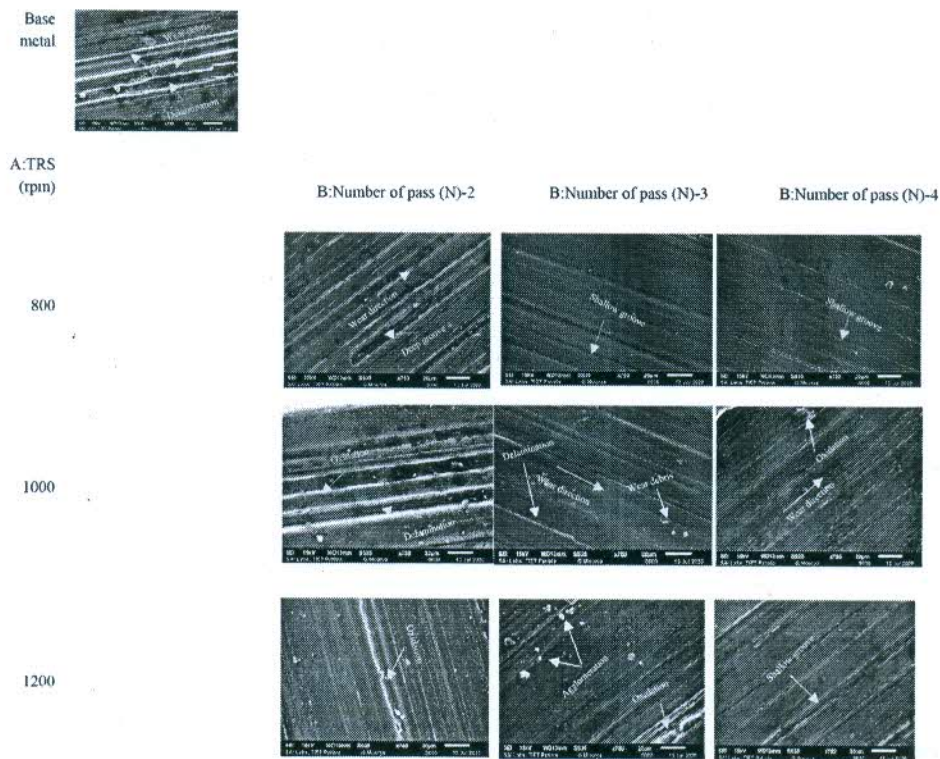


Table 8 Validation results

Sample no.	A:TRS (rpm)	No. of passes	Actual hardness	Predicted hardness	Deviation (%)	Actual wear resistance	Predicted wear resistance	Deviation (%)
1	900	2	83	84.87	2.2530	690.25	701.38	1.6130
2	1100	3	76	79.43	4.5131	630.10	648.32	2.8916
3	1100	4	78	81.10	3.9743	705.15	721.19	2.2746

Jabbari *et al.* (2015). This can be because of the fact that the number of passes:

- Increased the area filled with powder that produced smaller grains at the composite material.
- Every new pass forced dynamic recrystallization phenomena especially in all zones and gave rise to the production of reduced sized grains.

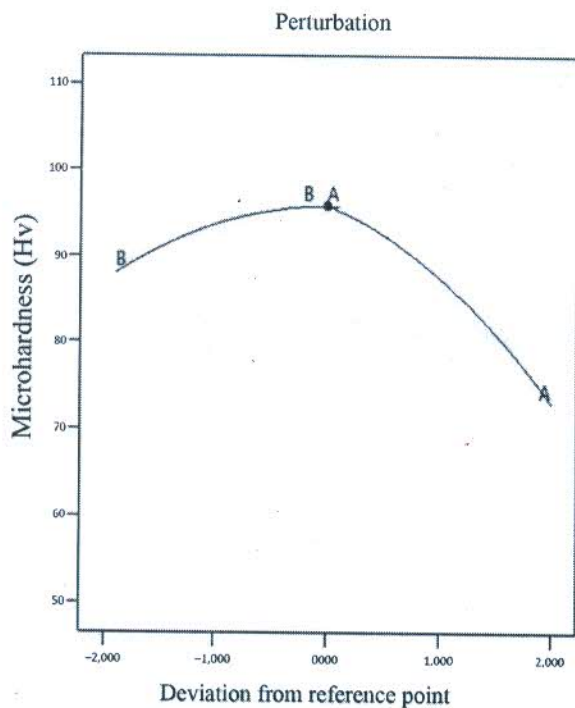
In addition, as reported by Faraji *et al.* (2011); the triangular tool finely dispersed the *n*-TiC particles and limited the growth of grains which consequently produced ultrafine grain size in the AZ61 matrix. Also, on the off chance that the entirety of the TiC particles isolated, and scattered, the theoretically evaluated grain size might be decreased extraordinarily in case of nano-size particles. Thus, in the event that one can totally scatter the *n*-TiC in the FSPed zone, it could deliver the nano-grain-sized composite. It appears that increasing FSP passes could be the ideal method for scattering the *n*-TiC particles consistently.

In fact, more homogenous particle distribution and reduced size grain sizes could be achieved via increasing number of passes. Also, it was observed that increasing the number of pass can give rise in hardness values up to 60%, which is way too high compared to a rise in hardness up to 45% achieved by Ram *et al.* (2019). Contour plots and 3D surface plots as shown in Figure 5 (c) and 5(d) shows the interactions between controlled FSP parameters to the response parameters.

3.3 Wear morphology

The investigation of wear tracks further affirmed the influence of the FSP parameters on the wear resistance conduct of the specimens. The SEM micrographs of the as received AZ61A and FSPed samples were taken to investigate morphology of the worn surfaces and included in Figure 6. As shown, the surface of base metal AZ61A displayed straight deep plows/grooves. This may be

Figure 7 Perturbation plot



attributed to high frictional heat that broke down the initial network of magnesium like $\beta\text{-Mg}_{17}\text{Al}_{12}$. This brittle and coarse phase demonstrated its inability to effectively act as an obstacle to wear, consequently it softened the material. Additionally, this heat caused plastic deformation, which lead to the formation of deep grooves. In addition, the presence of scratches on the base metal surface showed some evidence of abrasive wear. For the base metal, a range of adhesive and abrasive wear was observed which was in conjunction with earlier studies (Azizieh *et al.*, 2018; Madhusudhan Reddy *et al.*, 2013). However, deep grooves indicate severe adhesive wear and its domination, consequently the debris formed and massive surface damage on pin surface was found. This may also be related to the lower value of hardness for base material as contrasted to FSPed composites.

As shown in Figure 6, the wear component in the composite was unique as contrasted to base metal. Uniform-sized grains and homogenous distribution of TiC particles decidedly influenced the wear resistance. This was also the case with the addition of TiC particles in the base metal which:

- minimized the contact area of metal and counter part; and
- minimized direct load, which lead to a change from a severe wear to a mild wear.

For all manufactured composites, abrasive wear mechanism was observed to be the dominant wear mechanism up on considering the loose debris particles. These loose debris particles mainly showed up because of oxidizing MMCs and pulling of TiC during sliding.

However, FSPed composite surface processed at 1200 rpm showed micro cracks that could be attributed to good nanoparticle distribution which declined the immediate contact load and thus forestall the delamination. It merits referencing that for the specimen processed at 1000 rpm, delamination of the MMC layer was likewise found in some places. However, at 1200 rpm, metal matrix layer delamination was observed to be diminished.

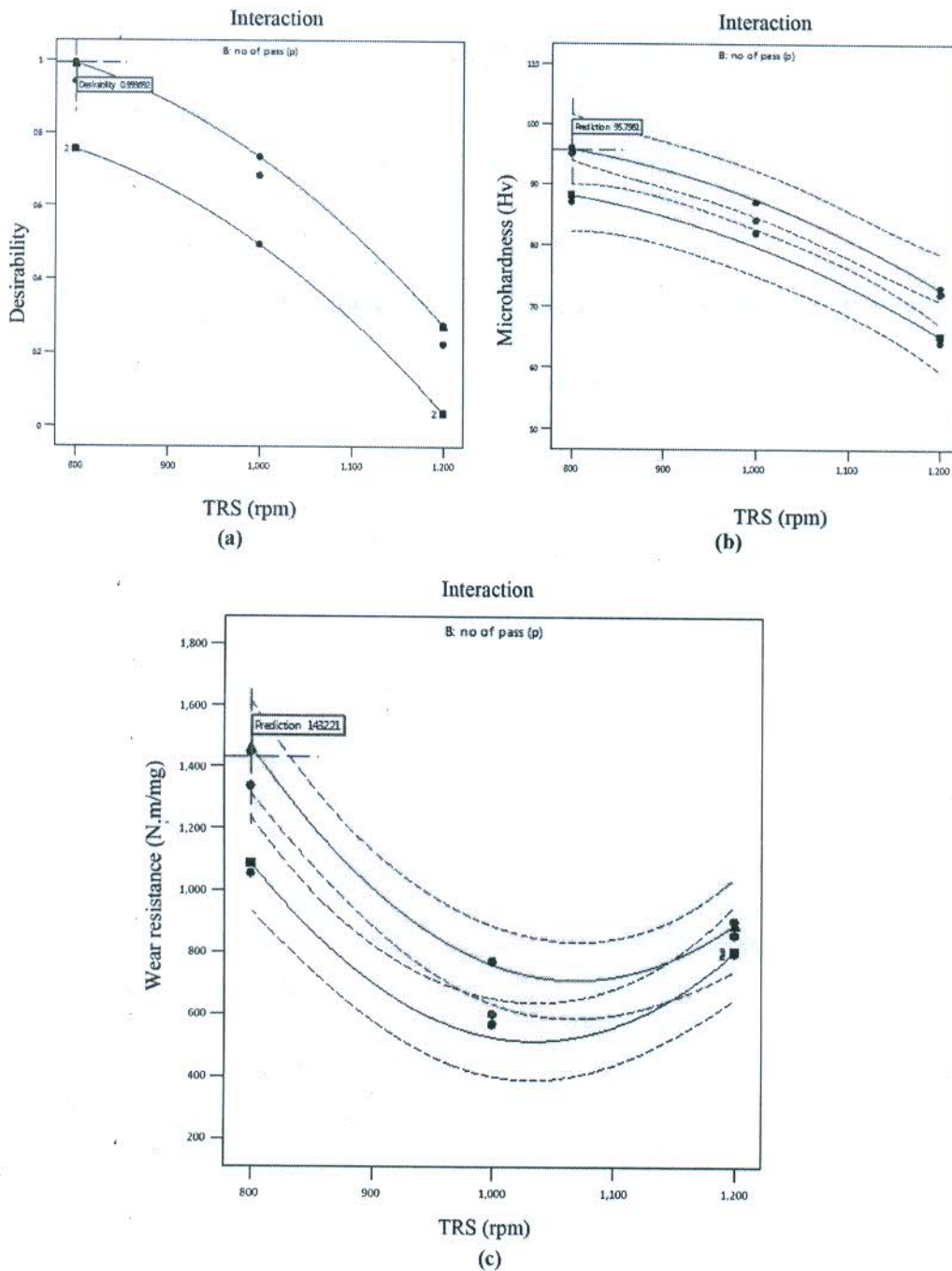
3.4 Model Validation

In this study, micro hardness and wear resistance were studied as a response parameter for examining the outcome of FSP process parameters. There are several statistical techniques available to solve multi response situations, within which a desirability approach is advocated because of its flexibility and simplicity. A series of tests were undertaken to validate models at different parameters, compared to the processing parameters used in model building. The outcomes are summarized in Table 8 and demonstrate good synergy between the developed model and the experimental data. A similar type of model validation was carried out by Akinlabi *et al.* (2014), however, closer values between predicted and actual responses was obtained in this work. These models can therefore be used to predict the performance of wear resistance, and the microhardness properties of the AZ61/TiC composite formed by FSP with a good degree of precision. As per perturbation plot seen in Figure 7, the steep curvature of the rotational speed and the number of passes suggest that the operating parameters significantly influenced the microhardness. Figure 8 shows the interaction effect of rotational speed and number of passes on microhardness and wear resistance properties. A significant interaction was observed between the number of passes and microhardness, as shown in Figure 8.

4. Conclusions

CCD-RSM was used in present work to develop a mathematical model for predicting microhardness and resistance to wear. Modelling was observed to be efficient and quadratic models were obtained for both the responses. The models were validated by additional experiments conducted at processing parameters beyond the processing parameters used in the model construction. Results from the design experiments were statistically analyzed, and models were developed to predict the wear resistance and microhardness properties of the AZ61A/n-TiC processed composites. The developed regression models were found to be significant for microhardness and wear resistance. It was observed that every single FSP variables are the most significant to influence responses according to equations 1 and 2. The maximum value of microhardness and wear resistance was obtained for tool rotational speed of 800 rpm, transverse speed of 40 m/min and four number of passes which was higher compared to the parent metal. It was found that the FSP could be utilized to improve the mechanical properties of MMC.

Figure 8 Interaction plot (a) desirability, (b) effect on microhardness, (c) effect on wear resistance



References

Akinlabi, E.T., Mahamood, R.M., Akinlabi, S.A. and Ogunmuyiwa, E. (2014), "Processing parameters influence on wear resistance behaviour of friction stir processed Al-TiC composites", *Advances in Materials Science and Engineering*, Vol. 2014.

Asadi, P., Faraji, G. and Besharati, M.K. (2010), "Producing of AZ91/SiC composite by friction stir processing (FSP)", *The International Journal of Advanced Manufacturing*

Technology, Vol. 51 Nos 1/4, pp. 247-260, doi: 10.1007/s00170-010-2600-z.

Azizieh, M., Kokabi, A.H. and Abachi, P. (2011), "Effect of rotational speed and probe profile on microstructure and hardness of AZ31/Al₂O₃ nanocomposites fabricated by friction stir processing", *Materials & Design*, Vol. 32 No. 4, pp. 2034-2041, doi: 10.1016/j.matdes.2010.11.055.

Azizieh, M., Larki, A.N., Tahmasebi, M., Bavi, M., Alizadeh, E. and Kim, H.S. (2018), "Wear behavior of AZ31/Al₂O₃ magnesium matrix surface nanocomposite fabricated via

- friction stir processing”, *Journal of Materials Engineering and Performance*, Vol. 27 No. 4, pp. 2010-2017, doi: 10.1007/s11665-018-3277-y.
- Chen, Z.W., Cui, S., Gao, W. and Zhu, T. (2010), “Microstructural evolution in various regions of stir zone during friction stir processing of Al-7Si-0.3Mg cast alloy”, Vol. 656, pp. 962-965. 10.4028/www.scientific.net/MSF.654-656.962.
- Dadashpour, M., Mostafapour, A., Yeşildal, R. and Rouhi, S. (2016), “Effect of process parameter on mechanical properties and fracture behavior of AZ91C/SiO₂ composite fabricated by FSP”, *Materials Science and Engineering: A*, Vol. 655, pp. 379-387, doi: 10.1016/j.msea.2015.12.103.
- Das, S., Mishra, R.S., Doherty, K.J., Cho, K.C., Davis, B. and DeLorme, R. (2016), “Magnesium based composite via friction stir processing”, *Friction Stir Welding and Processing VII, March*, pp. 245-252, doi: 10.1007/978-3-319-48108-1_25.
- Dinakaran, I., Zhang, S., Chen, G. and Shi, Q. (2019), “Development of titanium particulate reinforced AZ31 magnesium matrix composites via friction stir processing”, *Journal of Alloys and Compounds*, Vol. 820, p. 153071, doi: 10.1016/j.jallcom.2019.153071.
- Dinakaran, I., Zhang, S., Chen, G. and Shi, Q. (2020), “Materials science & engineering a titanium particulate reinforced AZ31 magnesium matrix composites with improved ductility prepared using friction stir processing”, *Materials Science and Engineering: A*, Vol. 772, p. 138793, doi: 10.1016/j.msea.2019.138793.
- Faraji, G., Dastani, O., Asghar, S.A. and Mousavi, A. (2011), “Effect of process parameters on microstructure and micro-hardness of AZ91/Al₂O₃ surface composite produced by FSP”, *Journal of Materials Engineering and Performance*, Vol. 20 No. 9, pp. 1583-1590, doi: 10.1007/s11665-010-9812-0.
- Gupta, M. and Wong, W.L.E. (2015), “Magnesium-based nanocomposites: lightweight materials of the future”, *Materials Characterization*, Vol. 105, pp. 30-46, doi: 10.1016/j.matchar.2015.04.015.
- Jabbari, A.H., Sedighi, M., Vallant, R., Huetter, A. and Sommitsch, C. (2015), “Effect of pass number”, *Rotational and Traverse Speed on Particle Distribution and Microstructure of AZ31/SiC Composite Produced by Friction Stir Processing*, pp. 765-770, doi: 10.4028/www.scientific.net/KEM.651-653.765.
- Khayyamin, D., Mostafapour, A. and Keshmiri, R. (2013), “The effect of process parameters on microstructural characteristics of AZ91/SiO₂ composite fabricated by FSP”, *Materials Science and Engineering: A*, Vol. 559, pp. 217-221, doi: 10.1016/j.msea.2012.08.084.
- Kumar, P.A., Madhu, H.C., Pariyar, A., Perugu, C.S., Kailas, S.V., Garg, U. and Rohatgi, P. (2020), *Materials Science & Engineering A Friction Stir Processing of Squeeze Cast A356 with Surface Compacted Graphene Nanoplatelets (GNPs) for the Synthesis of Metal Matrix Composites*. *Materials Science & Engineering A*, Vol. 769, p. 138517, doi: 10.1016/j.msea.2019.138517.
- Lin, C., Huang, W.S. and Liu, C. (2017), “Structural analysis and optimization of bicycle frame designs”, *Advances in Mechanical Engineering*, Vol. 9 No. 12, pp. 1-10, doi: 10.1177/1687814017739513.
- Madhusudhan Reddy, G., Sambasiva Rao, A. and Srinivasa Rao, K. (2013), “Friction stir processing for enhancement of wear resistance of ZM21 magnesium alloy”, *Transactions of the Indian Institute of Metals*, Vol. 66 No. 1, pp. 13-24, doi: 10.1007/s12666-012-0163-4.
- Markets, M.E. and Sheet, M.D. (2020), *Weblinks: Magnesium Applications Weblinks*, Magnesium Applications.
- Mishra, R.S. and Ma, Z.Y. (2005), “Friction stir welding and processing”, *Materials Science and Engineering: R: Reports*, Vol. 50 Nos 1/2, pp. 1-78, doi: 10.1016/j.mser.2005.07.001.
- Mishra, R.S., Ma, Z.Y. and Charit, I. (2003), “Friction stir processing: a novel technique for fabrication of surface composite”, *Materials Science and Engineering: A*, Vol. 341 Nos 1/2, pp. 307-310.
- Monteiro, W.A., Buso, S.J. and Silva, L.V. (1998), *Application of Magnesium Alloys in Transport*, pp. 1-14.
- Navazani, M. and Dehghani, K. (2015), “Investigation of microstructure and hardness of Mg/TiC surface composite fabricated by friction stir processing (FSP)”, *Procedia Materials Science*, Vol. 11, pp. 509-514, doi: 10.1016/j.mspro.2015.11.082.
- Neite, G., Kubota, K., Higashi, K. and Hehmann, F. (2006), *Magnesium-Based Alloys*, Mater. Sci. Technol, Wiley-VCH Verlag GmbH & Co. KGaA, doi: 10.1002/9783527603978.mst0082.
- Rajakumar, S., Muralidharan, C. and Balasubramanian, V. (2011), “Influence of friction stir welding process and tool parameters on strength properties of AA7075-T 6 aluminium alloy joints”, *Materials & Design*, Vol. 32 No. 2, pp. 535-549, doi: 10.1016/j.matdes.2010.08.025.
- Ram, B., Deepak, D. and Bala, N. (2019), “Role of friction stir processing in improving wear behavior of Mg/SiC composites produced by stir casting route”, *Materials Research Express*, Vol. 6 No. 2, doi: 10.1088/2053-1591/aaf1e4.
- Sardar, S., Karmakar, S.K. and Das, D. (2019), “Microstructure and tribological performance of alumina – aluminum matrix composites manufactured by enhanced stir casting method”, *Journal of Tribology*, Vol. 141, No. 4, doi: 10.1115/1.4042198.
- Sathiskumar, R., Dinakaran, I., Murugan, N. and Vijay, S.J. (2014), “Influence of tool rotational speed on microstructure and sliding wear behavior of Cu/B 4 C surface composite synthesized by friction stir processing”, *Transactions of Nonferrous Metals Society of China*, Vol. 25 No. 1, pp. 95-102, doi: 10.1016/S1003-6326(15)63583-X.
- Sathiskumar, R., Murugan, N., Dinakaran, I. and Vijay, S.J. (2013), “Prediction of mechanical and wear properties of copper surface composites fabricated using friction stir processing”, *Journal of Materials & Design*, Vol. 55, pp. 224-234, doi: 10.1016/j.matdes.2013.09.053.
- Sharma, V., Prakash, U. and Kumar, B.V.M. (2018), “Surface composites by friction stir processing: a review”, *Journal of Materials Processing Technology Surface Technology*, Vol. 224, pp. 117-134, doi: 10.1016/j.jmatprotec.2015.04.019.
- Sharma, S., Handa, A., Singh, S.S. and Verma, D. (2019), “Synthesis of a novel hybrid nanocomposite of AZ31Mg-Graphene-MWCNT by multi-pass friction stir processing

- and evaluation of mechanical properties”, *Materials Research Express*, Vol. 6 No. 12, doi: 10.1088/2053-1591/ab54da.
- Sunil, B.R., Reddy, G.P.K., Patle, H. and Dumpala, R. (2016), “Magnesium based surface metal matrix composites by friction stir processing”, *Journal of Magnesium and Alloys*, Vol. 4 No. 1, pp. 52-61, doi: 10.1016/j.jma.2016.02.001.
- Thangarasu, A., Murugan, N., Dinaharan, I. and Vijay, S.J. (2014), “Effect of tool rotational speed on microstructure and microhardness of AA6082/TiC surface composites using friction stir processing”, *Applied Mechanics and Materials*, Vol. 592-594, pp. 234-239, doi: 10.4028/www.scientific.net/AMM.592-594.234.
- Zohoor, M., Besharati Givi, M.K. and Salami, P. (2012), “Effect of processing parameters on fabrication of Al-Mg/Cu

composites via friction stir processing”, *Materials & Design*, Vol. 39, pp. 358-365, doi: 10.1016/j.matdes.2012.02.042.

Further reading

- Sardar, S. and Das, D. (2019), “Multi tribo – performance optimization of AA7075 – Al₂O₃ composites by grey based response surface methodology”, *Metals and Materials International*, 0123456789, doi: 10.1007/s12540-019-00573-z.

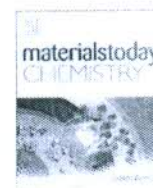
Corresponding author

Prem Sagar can be contacted at: jasujaprem@gmail.com

For instructions on how to order reprints of this article, please visit our website:

www.emeraldgrouppublishing.com/licensing/reprints.htm

Or contact us for further details: permissions@emeraldinsight.com



Controlled nano-particle dyeing of cotton can ensure low cytotoxicity risk with multi-functional property enhancement

A. Khandual^{a,*}, N. Rout^b, S.K. Verma^c, P. Patel^c, P. Pattanaik^b, Y. Luximon^d, A. Kumar^e, R.K. Nayak^f, M. Suar^g

^a College of Engineering & Technology, Bhubaneswar, Odisha, India

^b SOA, IITR, Deemed to Be University, Bhubaneswar, Odisha, India

^c School of Biotechnology, KBIT Deemed to Be University, Bhubaneswar, Odisha, India

^d School of Design, Hongkong Polytechnic University, Hong Kong

^e Department of Physics, TIT&S, Bhiwani, Haryana, India

^f School of Communication and Design, RMIT University, Viet Nam

ARTICLE INFO

Article history:

Received 2 May 2020

Received in revised form

12 July 2020

Accepted 16 July 2020

Available online 17 August 2020

Keywords:

Nano-textiles

Biocompatibility

Cell culture and toxicological assays

Moisture management test

Survivability analysis

ABSTRACT

The Nanoparticle (NP) and their oxides are being progressively used and expected to be more frequently used in textiles. Nanoparticle (NP) has higher toxicological risk than larger particles because of their physicochemical properties, chemical reactivity and biological activity. In fact, the stability of nano-oxide particles in the medium is always challenging as they lack functional groups to leverage upon textile materials directly. Thus, in many finishing processes, cross-linkers and/or adhesives are applied together with NP at the cost of inferior comfort, feel and fastness which tends to be toxic and prone to release NPs under common laundering, physical stress and sweat. This study shows that the diffusion of NPs into the fibre polymer matrix via dyeing technique could be much durable, safer in terms of cytotoxicity levels and easy to process for tailoring desired functional attributes. We studied the possibility of a simple application technique via dyeing of vinyl sulphone based reactive dye with four kinds of NPs followed by their cytotoxicity test using cell line A431. 1% silica dyed sample have shown highest (198.5%) increase in tensile strength followed by 2% silica and 2% CNT whereas a decrease in elongation is highest in the case of CNT 2% (5.31%) and significantly enhancing the moisture management properties in case of CNT and silica. The study showed promising results in dyeing with TiO₂, CNT (Carbon nanotubes), Silica and Alumina NPs in enhancing the mechanical, moisture management, and surface frictional properties to ensure comfortable and safe wear.

© 2020 Elsevier Ltd. All rights reserved.

Introduction

The pros and cons of environmental nanotechnology are frequently reported now a days. Recent study by Chris Toumey [1] has specifically reported, the use and claims on silver NPs for cloth washing by Samsung. Samsung introduced silver NP-based washers for textile clothing that claimed 99.9% protection from bacteria and keeps away from nasty smells for thirty days with just one wash cycle. However, the net environmental toxicity is concerned [2]. Toxicological survey undoubtedly suggests [2–4] that many NPs

have more risk of toxicity than larger particles because of their physicochemical properties, chemical reactivity (reactive oxygen species (ROS), including free radicals [5] resulting in oxidative stress, inflammation, prolong damage to proteins, membranes, and DNA [6] moreover, their biological activity are quite different [7,8]. Most of the other factors influencing toxicity are their shape, chemical composition, structure of the surface and charge, aggregation and solubility [9]. These can readily enter into the human body crossing membranes, cells, tissues, and organs compared to larger-sized particles [10]. They can be taken up by cell mitochondria [11–13], cell nucleus [14] and induce major structural damage to mitochondria [15,16], cause DNA mutation [17], and even result in cell death [18]. That's why many biogenic syntheses of nano-materials are being explored using different organisms which offer

* Corresponding author.

** Corresponding author.

E-mail addresses: khandual@coltech.ac.in (A. Khandual), m.suar@coltech.ac.in (M. Suar).

reliable, low-cost and environment-friendly alternative approach compared with classical chemical and/or physical methods [19,20].

Application of metal oxide NPs such as Alumina, silica, MgO [21], ZnO [22], TiO₂ [23], etc., CNT and silver [24] NPs have been reported improving physicochemical and other functional properties applied majorly through coating, sol-gel, plasma etc. [25] for broader range of application domains like wearable super capacitors [26]. Probably, Gang Sun and Dapeng Li should be credited to file the first patent related to NP dyeing of textiles on 22 Oct 2001, entitled "Dyeing textiles using NPs" which was granted on 23 May 2006 [27]. Later in 2007, they published related work [28]. Recently, some important applications to various textile fibers are being reported [29–31]. Goetz et al. [32] studied migration of Ag- and TiO₂ NPs from textiles into the artificial sweat under physical stress and developed an exposure Modeling. They found that dermal exposure to nano-objects and their aggregates and agglomerates (NOAA) from textiles can be considered comparably minor for TiO₂NOAA, but not for AgNOAA. Froggett et al. [33] reviewed well with the perspective of existing research on the release of nanomaterials from solid nanocomposites. In Fact, Textiles with silver NPs application share the most commercialized applications among another nanomaterial despite recent concerns about product safety [34–39]. However, a limited research has been reported in studying the dyeing ability and fastness properties [40] with enhanced functional properties, wearer comfort (moisture management test and surface frictional properties) along with cytotoxicity test and MMT test. All these are crucial factors for colorist, wearers' comfort

as well as the environmentalist. Here, we show the promising results of four types of NP such as TiO₂, Carbon NP, Alumina and Silica with enhanced mechanical, fastness and moisture management properties. In addition, we studied their surface friction and roughness properties to compare comfortable feel to the wearer.

Recent studies on toxicological risks of commercial nano-engineered functional textile have shown concern risk levels on sweating and common wear and tear in textile incorporated majorly through coating, spinning or sol-gel methods [32]. In fact, the stability of nano-oxide particles in the medium is always challenging; being an inorganic compound and lacking functional groups to leverage upon textile materials directly [41]. Thus, in many finishing processes of the fabrics, cross-linkers, resins, adhesives, binder, etc. are applied together with NP oxides to embed on the surface of the fabrics at the cost of inferior touch feel and fastness [42,43]. Undoubtedly, they are more toxic and prone to release NPs under physical stress and sweat. Many surface modifications of textiles and stabilizing nanoparticles require several steps of preparation, functionalization, final treatment, drying, curing and so on but are non-durable. Specifically, they can release nano-particle easily on washing or common laundering and also sweating. The entire process is very time consuming, high cost and limits high-scale manufacturing production [44,45].

In our previous study, we demonstrated a novel and simple way of incorporating TiO₂ NP with reactive vinyl sulphone class dyeing of cotton that economically can be practiced to enhance significant and lasting improvement in strength, wear resistance, stiffness and

Table 1
Tensile strength and elongation of control and NP dyed samples.

Sample	tensile strength (Kgf)	Elongation (mm)	TS percent increase	Elongation percent increase
Untreated	13.3	24.5	0.00	0.00
Alumina (3%)	35.4	24.5	166.17	0.00
Alumina (2%)	29.8	24.3	124.06	-0.82
Alumina (1%)	24.6	24	84.96	-2.04
Silica (3%)	35.9	24.3	169.92	0.82
Silica (2%)	37.4	23.9	181.20	2.45
Silica (1%)	39.7	23.8	198.50	-2.86
TiO ₂ (3%)	28.2	24.2	112.03	-1.22
TiO ₂ (2%)	24.6	23.7	84.96	-3.27
TiO ₂ (1%)	20	24	50.38	-2.04
CNT (3%)	31.9	23.4	139.85	-4.49
CNT (2%)	36.7	23.2	175.94	-5.31
CNT (1%)	31.6	23.5	137.59	-4.08

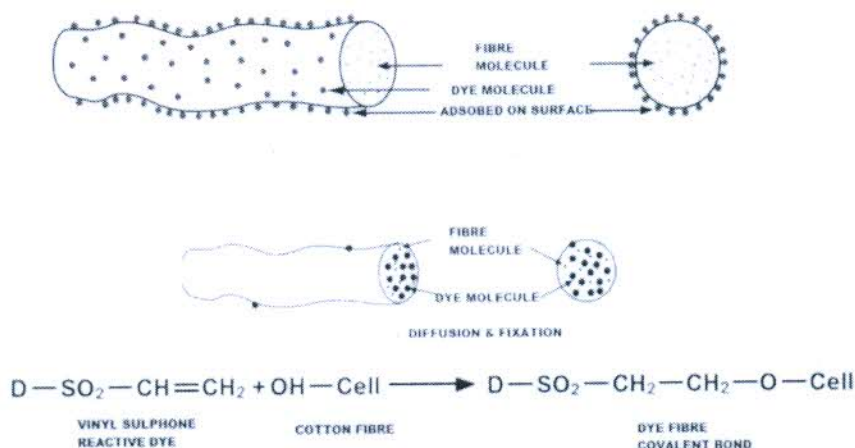


Fig. 1. Reactive dyeing system on Cotton.

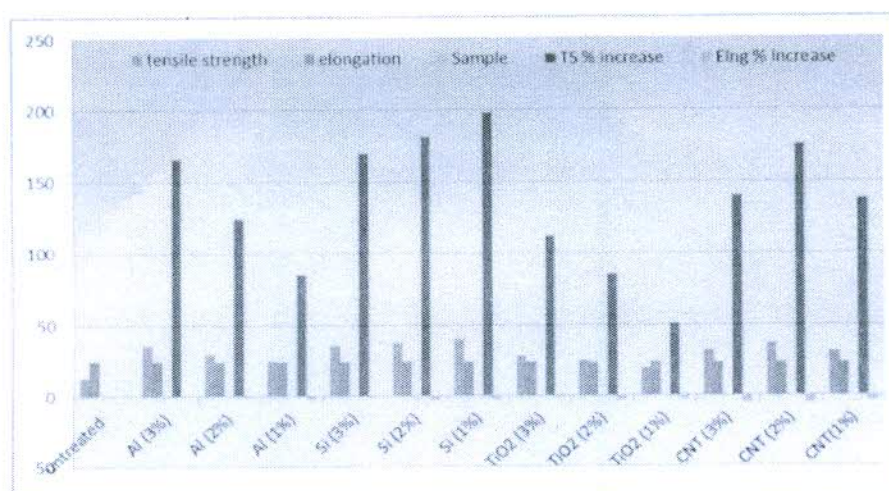


Fig. 2. Tensile strength and elongation of control and NP dyed samples.

UV protection [25]. The results from SEM, Raman, FTIR and UV-visible spectral analysis along with physical property tests confirmed the diffusion of nanoparticles in polymer matrices.

In this present investigation, we studied the diffusion of NPs into the fiber polymer matrix via dyeing technique that could be much safer in terms of cytotoxicity levels, durable and easy to process to tailor desired functional attributes. We studied here the possibility of a simple and eco-friendly application technique via dyeing of vinyl sulphone based reactive dye with four kinds of NPs followed by their cytotoxicity test using cell line A431 and MTT test. Promising results of four types of NP such as TiO₂, Carbon NP, Alumina and Silica by dyeing was achieved with enhanced mechanical property and moisture management properties. In addition, their surface roughness and frictional properties to compare comfortable feel to the wearer were analysed. A fiber matrix firm embedded system most likely to be achieved by Vander Waals forces of attraction Vis a Vis fiber, NP and reactive dye that also forms the covalent bond with cellulosic fibres [25,46]. The overview of reactive dyeing mechanism of dye migration from solution to the fibre surface, adsorption, diffusion and fixation on cotton by covalent bond formation was studied.

Materials & methods

Materials, NPs and dyeing

The cotton material used: dyeing technique followed has been described well by khandual et al. [25]. The NPs and dyes used are of following specifications.

1. The nano-alumina with trade name AEROXIDE® AluO₃: specific surface area (BET) of 100 m²/g primary particle size of 13 nm, obtained from Evonik, Degussa
2. Nano-silica with trade name AEROSIL® 300: specific surface area (BET) of 300 m²/g primary particle size of 7 nm, obtained from Evonik, Degussa
3. TiO₂ NP: Titanium (IV) Oxide -nanopowder, 21 nm particle size collected from Sigma-Aldrich, Mumbai
4. Carbon Nanotube (CNT), Prepared in the Lab by electric arc method, particle size 31 nm
5. Dye: Reactive Remazol Ultra RGB orange supplied by Dyestar, Hong Kong 1% (Dye + NP) means that the mixture contains 0.9 gm of the dye with 0.1 gm of NP in 100 mL of dye stock

solution and 50 gm/L Glauber's salt and 10 gm/L soda were taken for dyeing to be raised at 70 °C. The dyeing method was followed as per reference [22] followed by a hot wash, cold wash and soaping by non-ionic detergent. Ultrasonification was carried out at the initial stage for homogeneous mixer of dye and nano particle.

Scanning electron microscopy (SEM)

The control and NP dyed samples were analysed with Environmental scanning electron microscope (EP-SEM) of Zeiss, Model EVO 60 for SEM images along with EDEX results, these were provided in supplementary file.

Disk diffusion assay

Disk diffusion assay was conducted to check the antimicrobial capacity of the clothes embedded with NP and dye. *S. enteritidis* and

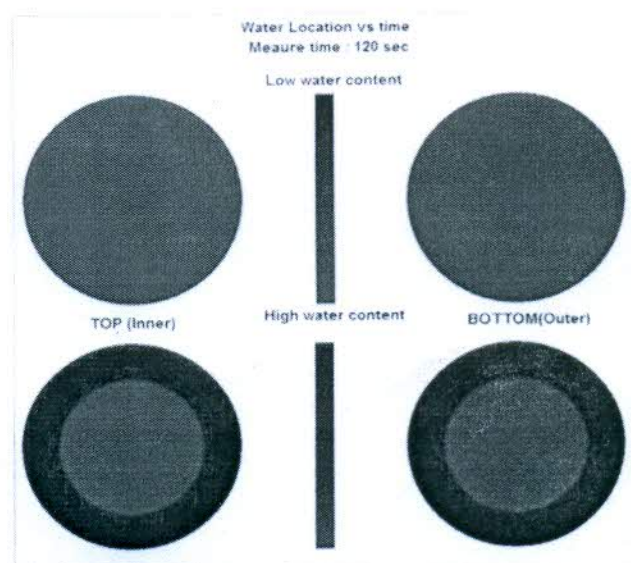


Fig. 3. MMT test. Water location vs. time: Lower: controlled sample, Upper: 2% CNT

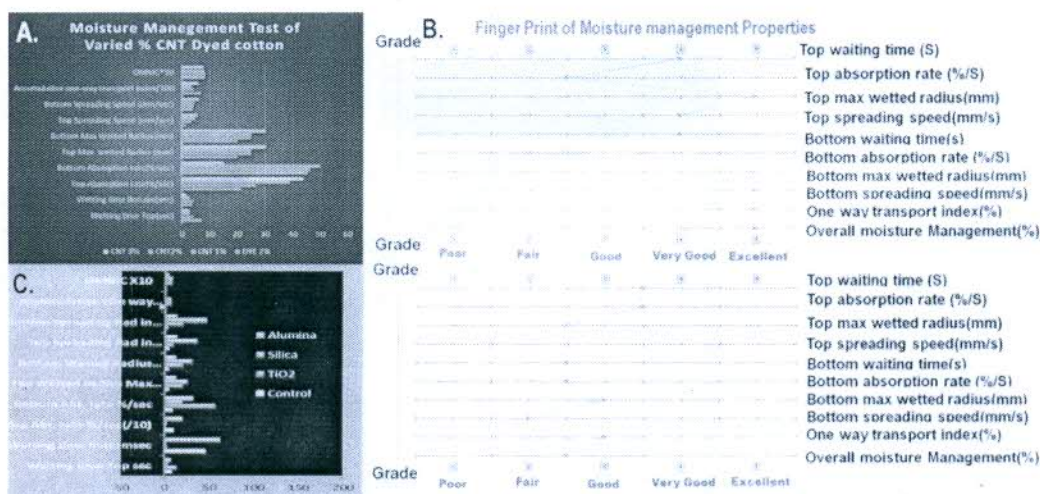


Fig. 4. (A) Influence on CNT % on MMT Properties (B) MMT test for overall rating: Lower: controlled sample, Upper: 2% CNT (C) MMT test for other Nano particles dyed with controlled sample at 2% shade.

E. coli strain were chosen for the assay. For assay, overnight culture of the bacterial strain cultured in Luria bertini medium at 370 °C in a shaking incubator was subcultured for 4 h till the attainment of 4.0 OD (600 nm). The bacterial strain were spread plate in a 60 mm petriplate contained with LB agar medium to obtain a lawn. 2 mm diameter of different clothes embedded with nanoparticles were placed on the lawn to observe the antibacterial effect.

Cell culture and toxicological assays

The human squamous epithelial cell line A431 was cultured in Dulbecco's Modified Eagle Medium (DMEM) medium supplemented with 10% Fetal bovine serum (FBS), 2 g/L sodium bicarbonate and 2 mM L-glutamine (complete medium), in 25 cm² tissue culture flasks in a humidified incubator at 37 °C supplied with 5% CO₂ in air atmosphere. For the MTT assay experiments, A431 cells were seeded in the wells of flat-bottom 96 well plates at 5 × 10⁴ cells per well in complete medium containing the fabrics impregnated with NPs. The non-impregnated cotton was taken as control. MTT was poured after 24 h and 48 h exposure. Followed by the completion of exposure time, the formazan crystals formed by MTT was dissolved by Dimethyl sulfoxide (DMSO). The Viability of cells was calculated in the relevance of control (no NPs), taken as 100%. For the morphological changes and microscopic analysis, the depleted culture medium was aspirated on the day of the experiment and replaced with 100 μL of DMEM medium. The treated cells were then incubated for 24 h. After incubation cells were taken for the microscopic examination.

MTT (3-(4, 5-dimethylthiazole-2-yl)-2, 5-biphenyltetrazolium bromide) assay is a color based assay which determines the viability of cells by measuring the color intensity of dissolved formazan crystals as an index of cellular mitochondrial dehydrogenase activity [47]. We tested the effect of TiO₂, SiO₂, Alumina and CNT NPs on A431 cell lines by exposing the cells for 24 h to the samples impregnated with 1%, 2% and 3% impregnation of these NPs. MTT Cell Viability Assay Cell Survivability was determined by MTT assay, which is a colorimetric assay depicted by measuring the intensity of purple color of buffer (11 gm SDS in 50 ml. of 0.02 M HCl and 50 ml. isopropanol) which dissolves the formazan crystals produced by the reduction of MTT. The absorbance was taken at 570 nm in enzyme-linked immunosorbent assay (ELISA) plate reader (Epoch,

Biotek, Germany). The amount of color product formed was proportional to the number of viable cells. Mean absorbance of Non-treated cells was taken as the reference value for calculating 100% cellular survivability [6].

Results and discussion

The cotton textiles were checked for their physical and biological properties after dyeing. Physical properties like mechanical strength, moisture management, light fastness, surface friction were analysed. Biological properties like antibacterial activity and cytotoxicity was determined (see Fig. 1).

Mechanical properties

Tensile strength test and elongation of the untreated and NP dyed fabric (warp way) was conducted by Digital Tensile Strength Tester, Globetex, Delhi and tabulated below (Table 1). The results have shown significant improvement in tensile strength with a nominal decrease in elongation. 1% silica dyed sample has shown highest (198.5%) increase in tensile strength followed by 2% silica and 2% CNT whereas a decrease in elongation is highest in the case of CNT 2% (5.31%). The graph was depicted in Fig. 2 and Fig. S1. The increased strength in case of silica can be attributed to the thermodynamic affinity of fibers form noncovalent interactions such as dipolar–dipolar and hydrogen bond, causing adhesion of silica nanoparticles and covalent bond between the cellulosic hydroxyl group and –Si–OH in silica particles [48–50]. Similar observations were found in case of other nanoparticles as shown in Fig. S2. The increased strength obviously attributed to the presence of nanoparticles in the core of the fiber matrix creating a strong physical bond: some may be due to the mechanical entrapment, aggregation, covalent and Vander Waals forces.

Moisture management test

The Moisture management tests were carried out in MMT, SDL Atlas. It has been found that significant variation in water penetration levels between controlled and treated sample. Fig. 3 depicts the water location vs. time (120 s) of controlled sample and 2% CNT dyed sample. As shown in Fig. 4a and b, the overall moisture

Table 2
Kawabata's evaluation system FB-4 reading of samples for surface friction and roughness.

samples	Weft			Warp		
	MIU	MMD	SMD	MIU	MMD	SMD
Dye 1%	0.205	0.0169	4.27	0.193	0.0228	4.835
Alumina 3%	0.168	0.0225	7.19	0.191	0.0159	4.69
Alumina 2%	0.176	0.0173	7.355	0.193	0.0222	4.16
Alumina 1%	0.173	0.011	5.81	0.192	0.0260	4.745
Silica 3%	0.153	0.0089	3.92	0.168	0.0225	7.19
Silica 2%	0.15	0.0077	4.715	0.156	0.0201	6.33
Silica 1%	0.153	0.0095	4.34	0.154	0.0211	6.735
TiO ₂ 1%	0.187	0.0142	3.125	0.189	0.0192	4.99
TiO ₂ 2%	0.192	0.0145	3.17	0.198	0.0175	4.41
TiO ₂ 3%	0.199	0.0215	3.22	1.88	1.57	4.88
CNT 3%	0.188	0.0134	3.57	1.94	0.88	3.355
CNT 2%	0.189	0.0215	3.22	1.88	2.16	7.235
CNT 1%	0.197	0.0187	2.955	1.87	2.55	4.38

management rating found out to be excellent (5) in the case of 2% CNT dyed sample as compared to controlled sample with a rating between 2 and 3. The parameters obtained clearly signified the results. Kim et al. reported the development of Bio-inspired, Moisture-Powered Hybrid Carbon Nanotube Yarn Muscles which can be actuated well by either changing relative humidity or water contact [51]. Wei Li et al. [52] recently developed "A yarn-like switch-type humidity sensing material, fabricated by infiltrating hydrophilic water-swelling polyvinyl alcohol (PVA) into a multi walled carbon nanotube (MWCNT) yarn. The humidity sensing material demonstrates excellent repeatability and stability, acceptable hysteresis and response time". CNTs are well known for tailoring moisture absorption properties of hybrid materials". In Fig. 4c. MMT test results for other Nano particles dyed with controlled sample at 2% shade are shown and the data was given in Table 3. The MMT Test results interpretation for control and nano dyed samples were shown in table no. 4 [53,54]. From the above figure and tables it is evident the MMT parameters are significantly

varying with the NP application. These tailored properties and controlled absorption could be explored for wide application in agriculture, food processing waste water treatments etc. which has been reported by different application technics [55,56]. The enhanced moisture management properties were seen in case of CNT and silicathen compared to TiO₂ followed by Alumina. Recently more interesting scopes on fluorescence and photocatalysis by various nanospheres has been reported, those have potentials for textile applications [57–60] (see Table 4).

Light fastness

Method- AATCC 16 test standard was used with Xenon arc lamp light fastness tester with the exposure time 20 AATCC fading units (AFU = 20 h). From the rating it is observed that the fastness to light is satisfactory and close to the parent reactive dye; exposure of light do not get influenced by presence of NP in the fabric and on the other way there is least chances of any reaction or degradation of fabric treated all four kinds of NP. Interestingly, the same phenomenon was obtaining while dyed with same class of ultra RGB blue reactive dye. This can ensure a strong fibre-nano-dye interlinking existing hereby. One test result image has been given below in Fig. 5. Literatures have reported that the durability of functional textiles along with lightfastness can be enhanced by application of nanoparticle or their combination for cotton and polyester [61–65]. The results were present on the scale of their fastness ranging from 0 to 10. Here we achieved good results i.e. a level of 5–6 as compared to the parent dye level of 4–5 (Fig. 5). The light fastness of the samples either similar or enhanced to higher level when nano particle is applied along with base dyes.

Surface friction and variation

Surface friction and variation were also studied in Kawabata's evaluation system FB-4, where MIU (Coefficient of friction), MMD (Mean deviation of MIU) and SMD (Geometrical roughness) (Table 2). The results have shown that the surface friction and

Table 3
MMT Test Results for control and nano dyed samples.

Moisture management test	Control Fabric	TiO ₂	Silica	Alumina	CNT
Wetting time Top (s)	9.125	13.406	4.203	7.2815	2.672
Wetting time Bottom (s)	45.9637	3.078	1.875	61.875	2.843
Top Absorption rate (percent/s)	103.7727	13.731	24.83	192.0076	38.8708
Bottom Absorption rate (percent/s)	9.4168	56.4955	20.1684	31.4327	49.9674
Top Max. wetted Radius (mm)	5	20	25	12.5	25
Bottom Max Wetted Radius (mm)	5	20	30	12.5	25
Top Spreading Speed (mm/s)	0.5421	0.97	3.5275	1.3535	4.7351
Bottom Spreading Speed (mm/s)	0.387	1.9801	4.6258	1.3122	4.4666
Accumulative one-way transport index	-543.6364	658.5499	605.1055	-83.9725	340.4473
OMMC	0.0091	0.7108	0.7782	0.3911	0.7949

Table 4
MMT Test Results interpretation for control and nano dyed samples.

Moisture management test	Control Fabric	TiO ₂	Silica	Alumina	CNT
Wetting time Top (s)	medium	medium	Fast	medium	very fast
Wetting time Bottom (s)	slow	fast	Very Fast	slow	very fast
Top Absorption rate (percent/s)	Very fast	slow	Slow	Very fast	medium
Bottom Absorption rate (percent/s)	very slow	fast	slow	Medium	medium-fast
Top Max. wetted Radius (mm)	No Wetting	Large	Very Large	Medium	very Large
Bottom Max Wetted Radius (mm)	No Wetting	Large	Very Large	medium	Very Large
Top Spreading Speed (mm/s)	very slow	Very Slow	Fast	Slow	very fast
Bottom Spreading Speed (mm/s)	very slow	Slow	Very Fast	slow	very fast
Accumulative one-way transport index	poor	excellent	excellent	Poor	very good
OMMC	poor	Very Good	Very Good	Fair	very good/Excellent

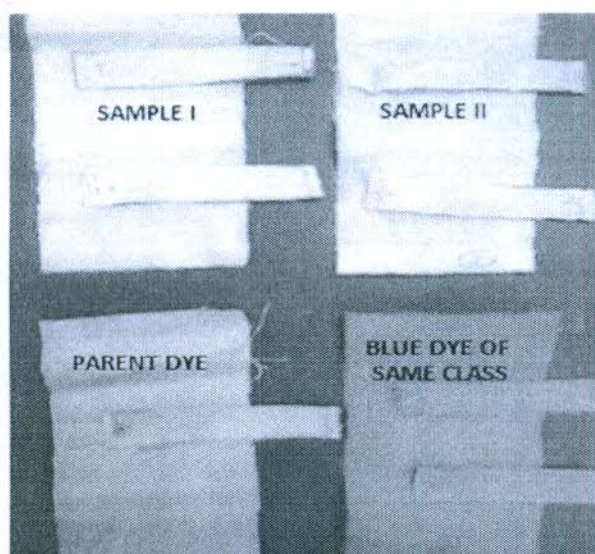


Fig. 5. Light Fastness Test of the textile dyed with different nanoparticles. Sample I and Sample II present different textiles compared with the parental dye.

roughness have been decreased in case of NP dyed samples. The observed result can be attributed to the diffusion of NPs in the textile matrix so observed in SEM and EDS results. However, TiO₂ 2% and CNT 3% NP dyed samples are much closer to controlled one. Silica NP dyed samples have shown a drastic reduction in surface friction and roughness characteristic of the samples followed by alumina [61].

Antimicrobial analysis

Nanoparticles have been shown to exhibit antimicrobial properties [66,67]. However, it is interesting to understand their antimicrobial behavior when embedded with textiles in order to understand their effect on their wearable properties. We have checked the antibacterial effect of clothes embedded with NPs with dye with two different bacterial strains (*S. typhi* and *E. coli*) to evaluate the effect of clothes on bacteria. As shown in Fig. 6 and Fig. 7, No inhibition zone was observed in control experiments and in the experimental set of clothes dyed with 1% and 3% NPs. The strange behavior can be attributed to the fact that the concentration of NP is too low to be diffused from the clothes. The NPs were attached to the fibers of the clothes firmly as interpreted from our physical analysis hence, were unable to get diffused showing no inhibition zone with bacteria. The exhibited properties can be considered beneficial with respect to the beneficial bacteria present at the skin.

Cytotoxicity test

Dermatological effects of NPs are questioned whether they are able to penetrate into or through the skin. Logically, if superficially bound NPs are present in the surface of the textile, it may cause more risk. *In vitro* studies reported that multi walled carbon nanotubes are capable of localizing within and initiating an irritation response in human epidermal keratinocytes, those are responsible for occupational exposure [32]. Similarly, it is well known that in order to avoid photo-oxidation of many metal oxides, commonly TiO₂ Silica is also used to act as protective adhesive [68]. However, the cytotoxic effect of the fabrics impregnated with these NPs is still not understood clearly. To address these facts, we

applied four kinds of NPs with dye at various concentration levels: 1%, 2% and 3% to the fabrics and studied their change in morphology and subsequently their effect on the viability of skin cell lines. It was found that the cell line A431 were almost alive or found to be infected with morphological changes in between 1 and 2% range after 48 h (Fig. 6). We can notice that silica at 2% level even harms Cell lines A431. As shown in Fig. 7, it was clearly observed that the viability of cells has depended on nature and percentage impregnation of NPs. It was observed that the viability was least in 3% in comparison to 1% and 2%. The A431 cells were showing their survivability in order TiO₂ > CNT > Alumina > Silica at all impregnation concentration. This observation was well supported by the bright field imaging of these cells when exposed to the corresponding samples (Fig. 7). Although alternative processes of nano application to textiles prevailing currently, they use much higher concentration levels of NPs that has to be paid much attention in terms of cytotoxicity: these processes involve lots of toxic material, organic solvents in several stages [25,69]. The MTT assay results (Fig. 8) supported the morphological analysis where the cell viability was found decreased to 43%, 86%, 55%, and 62% at 3% impregnation of Silica NP, TiO₂ NP, Alumina NP and CNT respectively. It has been found that the degree was in order TiO₂ > Alumina > Silica. Moreover, the viability of the cells was decrease by 10% at lower percentage of NP. The results depicted that cytotoxicity of the NP dyed textile varies with the nature and concentration of the NP. It is a matter of concern that silicone/polysiloxane are being extensively used for various functional finishes such as softeners, binder cross linkers etc [70], it has been observed from the MMT test that it is harmful even at very low concentration level.

It can be expected well to tailor various functional properties by applying NPs, but limited to be discussed here. Some of the SEM results has been provided as supplement material that confirms gradual diffusion and fixation of dyes into the textile polymer matrix of the textile substrate and in these cases, it reduces the chances of exposed NPs on the surface of the textile fibres.

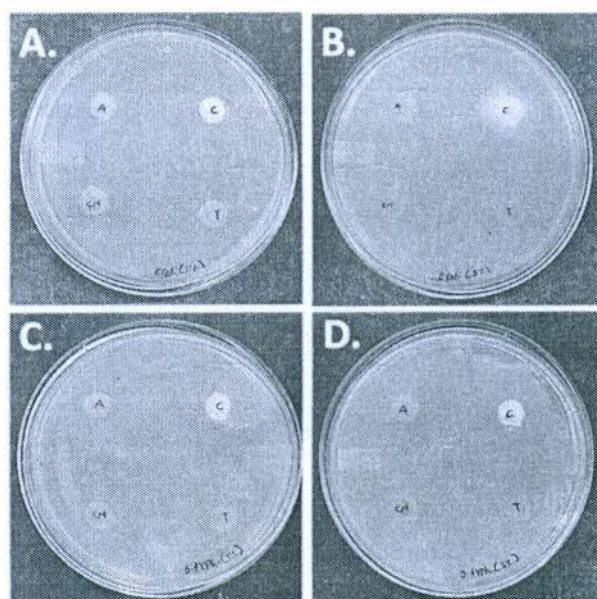


Fig. 6. Antibacterial activity of clothes embedded with NPs and dye. "A" presents Alumina, "C" presents Silica, "CN" presents CNT and "T" presents TiO₂ NP.

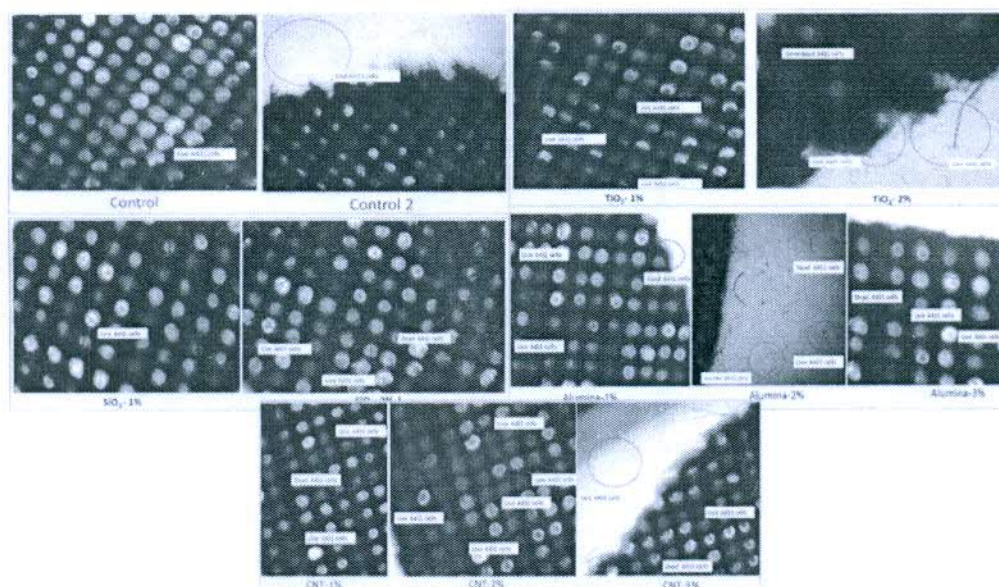


Fig. 7. Morphology of the cells accompanied with samples dyed with silica, TiO_2 , Alumina, and CNT NPs 1% & 2%.

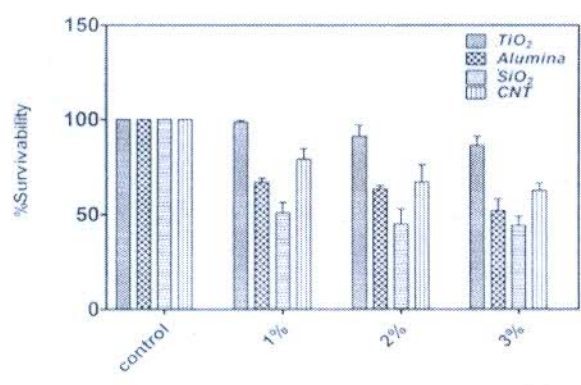


Fig. 8. Survivability analysis of A431 cells with samples dyed with different NPs.

Conclusion

In this novel study, we used four types of NP having average particle size ranging from 13 nm to 31 nm such as TiO_2 , Carbon NP, Alumina and Silica via simple dyeing of vinyl sulphone based reactive dye assisted by prior ultrasonic agitation at low concentrations i.e. 0.05 gm of nano particle with 0.95 gm dye for dyeing 100 gm fabric for 1% shade. The diffusion of NPs into the fiber polymer matrix via dyeing technique could be much safer in terms of cytotoxicity levels, durability and ease of application to tailor desired functional attributes. Promising results were achieved in terms of enhanced mechanical property and moisture management properties. In addition, their surface roughness and frictional properties were analysed to compare comfortable feel to the wearer. This will drastically lower the probability of NP release as they diffused predominantly to core, not in the surface, evidenced by significant improvement in mechanical properties. Safer application at lower level of concentrations were tested by cytotoxicity test using cell line A431 and MTT test. Interestingly, it has been found that it is possible to incorporate these NPs in an effective manner at 1–2% shade range rather than higher concentration of

3%, to reduce cytotoxicity risk level with enhanced strength, moisture management and improved surface feel.

As discussed earlier, the stability of nanoparticles in the medium is always challenging, being an inorganic compound and lacking functional groups to leverage upon textile materials directly. Thus, in many finishing processes of the fabrics, cross-linkers, resins, adhesives, binder, etc. are applied together with NP oxides to embed on the surface of the fabrics at the cost of inferior touch feel and fastness. Undoubtedly, they are more toxic and prone to release NPs under physical stress and sweat. The SEM with EDS results provided as the supplementary documents corroborate this fact that the optimum level of application ensures most of the NPs may be present on the core of the fiber. Most probably, therefore, previously NP treated fabrics are not recommended to be worn directly onto the skin or their toxicity tests have not been well reported. Keeping it in mind, we could be much safer in making the best use of low concentration NPs in dyeing textile for developing many functional properties of textiles to improve mechanical performances, UV protection, flame resistance and so on.

Declaration of competing interest

The authors declare that they have no known competing financial interests or personal relationships that could have appeared to influence the work reported in this paper.

Acknowledgements

We are thankful to TEQJP-III funding for CET, Bhubaneswar central laboratory for SEM with EDX analysis and ITC laboratory Hong Kong polytechnic university for Kawabata, FTT and MMT analysis of textile samples.

Appendix A. Supplementary data

Supplementary data to this article can be found online at <https://doi.org/10.1016/j.mtchem.2020.100345>.

References

- [1] C. Toumey, Quick lessons on environmental nanotech, *Nat. Nanotechnol.* 10 (2015) 566–567, <https://doi.org/10.1038/nnano.2015.144>.
- [2] M.A. Malik, M.Y. Wani, M.A. Hashim, F. Nabi, Nanotoxicity: dimensional and morphological concerns, *Adv. Phys. Chem.* 2011 (2011), <https://doi.org/10.1155/2011/450912>.
- [3] A.B. Seabra, N. Duran, Nanotoxicology of metal oxide nanoparticles, *Metals* 5 (2015) 934–975, <https://doi.org/10.3390/met5020934>.
- [4] Peter HM. Hoet, Irene Brüscke-Hohlfeld, Oleg V. Salata, Nanoparticles – known and unknown health risks, *J. Nanobiotechnol.* 2 (2004), <https://doi.org/10.1186/1477-3155-2-12>, 1ff.
- [5] J.S. Brown, K.L. Zeman, W.D. Bennett, Ultrafine particle deposition and clearance in the healthy and obstructed lung, *Am. J. Respir. Crit. Care Med.* 166 (2002) 1240–1247, <https://doi.org/10.1164/rccm.200205-399OC>.
- [6] S.K. Verma, E. Jha, P.K. Panda, A. Thirumurugan, S.K.S. Parashar, S. Patro, M. Suar, Mechanistic insight into size-dependent enhanced cytotoxicity of industrial antibacterial titanium oxide nanoparticles on colon cells because of reactive oxygen species quenching and neutral lipid alteration, *ACS Omega* 3 (2018) 1244–1262, <https://doi.org/10.1021/acsomega.7b01522>.
- [7] M. Ishihama, H. Y. I. P. M. DM, A. I. V. M. K. W. B. P. H. M. Formation and settlement of ultrafine atmospheric particles: a review of observations, *Environ. Int.* 2004, 3a.
- [8] K.J. Attwood, K.S. Levey, C.L. Tran, Nanoparticles: an occupational hygiene review, *Hum. and Exp. Toxicol.* 2004, 11.
- [9] H.J. Johnston, G. Hutchison, F.M. Christensen, S. Peters, S. Hankin, V. Stone, A review of the in vivo and in vitro toxicity of silver and gold particulates: particle attributes and biological mechanisms responsible for the observed toxicity, *Crit. Rev. Toxicol.* 40 (2010) 328–346, <https://doi.org/10.1080/10937540903394404>.
- [10] S.K. Verma, E. Jha, B. Sahoo, P.K. Panda, A. Thirumurugan, S.K.S. Parashar, M. Suar, Mechanistic insight into the rapid one-step facile biotransformation of antibacterial silver nanoparticles from bacterial release and their biogenicity and concentration-dependent in vitro cytotoxicity to colon cells, *RSC Adv.* 7 (2017) 40034–40045, <https://doi.org/10.1039/c7ra05943d>.
- [11] M. Holsappie, W.H. Farland, T.D. Landry, N.A. Monteiro Riviere, J.M. Carter, W. Farland, T. Landry, N. Monteiro Riviere, J. Carter, N. Walker, K. Thomas, Research strategies for safety evaluation of nanomaterials, part II: toxicological and safety evaluation of nanomaterials, current challenges and data needs, *Toxicol. Sci.* 88 (2005) 12–17.
- [12] N. Li, C. Sioutas, A. Cho, D. Schmitz, C. Misra, J. Sempf, M. Wang, T. Oberley, J. Froines, A. Nel, Ultrafine particulate pollutants induce oxidative stress and mitochondrial damage, *Environ. Health Perspect.* 111 (2003) 455–460, <https://doi.org/10.1289/ehp.6000>.
- [13] M. Geiser, B. Rothen-Rutishauser, N. Kapp, S. Schürch, W. Kreyling, H. Schulz, M. Semmler, V. Im Hof, J. Heyder, P. Gebr, Ultrafine particles cross cellular membranes by nonphagocytotic mechanisms in lungs and in cultured cells, *Environ. Health Perspect.* 113 (2005) 1555–1560, <https://doi.org/10.1289/ehp.6000>.
- [14] R. Savić, L. Luo, A. Eisenberg, D. Maysinger, Micellar nanocontainers distribute to defined cytoplasmic organelles, *Science* 300 (2003) 615–618, <https://doi.org/10.1126/science.1078192> (80-).
- [15] A. Hoshino, K. Fujioka, T. Oka, S. Nakamura, M. Suga, Y. Yamaguchi, K. Suzuki, M. Yasuhara, K. Yamamoto, Quantum dots targeted to the assigned organelle in living cells, *Microbiol. Immunol.* 48 (2004) 985–994, <https://doi.org/10.1148/MI480904985>.
- [16] V. Salnikov, Y.O. Lukyanenko, C.A. Frederick, W.J. Lederer, V. Lukyanenko, Probing the outer mitochondrial membrane in cardiac mitochondria with nanoparticles, *Biophys. J.* 92 (2007) 1058–1071, <https://doi.org/10.1524/biophysj.104.094335>.
- [17] K. Donaldson, V. Stone, Current hypotheses on the mechanisms of toxicity of ultrafine particles, *Ann. Ist. Super. Sanita* 39 (2003) 405–410.
- [18] R.F. Service, Nanotechnology grows up, *Science* 304 (2004) 1732–1734, <https://doi.org/10.1126/science.304.5678.1732> (80-).
- [19] S.K. Verma, E. Jha, P.K. Panda, A. Thirumurugan, M. Suar, Biological Effects of Green-Synthesized Metal Nanoparticles: A Mechanistic View of Antibacterial Activity and Cytotoxicity, 2019, pp. 145–171, https://doi.org/10.1007/978-3-319-01472-9_6.
- [20] S.K. Verma, E. Jha, K.J. Kiran, S. Bhat, M. Suar, P.S. Mohanty, Synthesis and characterization of novel polymer-hybrid silver nanoparticles and its biomedical study, *Mater. Today Proc.* 3 (2016) 1949–1957, <https://doi.org/10.1016/j.matpr.2016.04.058>.
- [21] S.K. Verma, K. Nisha, P.K. Panda, P. Patel, P. Kumari, M.A. Mallick, B. Sarkar, B. Das, Green synthesized MgO nanoparticles infer biocompatibility by reducing in vivo molecular nanotoxicity in embryonic zebrafish through arginine interaction elicited apoptosis, *Sci. Total Environ.* 713 (2020), <https://doi.org/10.1016/j.scitotenv.2020.136521>.
- [22] S.K. Verma, P.K. Panda, E. Jha, M. Suar, S.K.S. Parashar, Altered physiochemical properties in industrially synthesized ZnO nanoparticles regulate oxidative stress. Induce in vivo cytotoxicity in embryonic zebrafish by apoptosis, *Sci. Rep.* 7 (2017), <https://doi.org/10.1038/s41598-017-14039-y>.
- [23] S.K. Verma, E. Jha, P.K. Panda, M. Mukherjee, A. Thirumurugan, H. Makkar, B. Das, S.K.S. Parashar, M. Suar, Mechanistic insight into ROS and neutral lipid alteration induced toxicity in the human model with fins (Danio rerio) by industrially synthesized titanium dioxide nanoparticles, *Toxicol. Res.* 7 (2018) 244–257, <https://doi.org/10.1039/c7tx00300e>.
- [24] P. Paul, S.K. Verma, P. Kumar Panda, S. Jaiswal, B.R. Sahu, M. Suar, Molecular insight to influential role of Hha–TomB toxin–antitoxin system for antibacterial activity of biogenic silver nanoparticles, *Artif. Cells, Nanomed. Biotechnol.* 46 (2018) S572–S584, <https://doi.org/10.1080/21691401.2018.1503598>.
- [25] A. Khandual, A. Luximon, A. Sachdeva, N. Rout, P.K. Sahoo, Enhancement of functional properties of cotton by conventional dyeing with TiO₂ nanoparticles, *Mater. Today Proc.* 2 (2015) 3674–3683, <https://doi.org/10.1016/j.matpr.2015.07.128>.
- [26] L. Liu, Y. Yu, C. Yan, K. Li, Z. Zheng, Wearable energy-dense and power-dense supercapacitor yarns enabled by scalable graphene-metallic textile composite electrodes, *Nat. Commun.* 6 (2015), <https://doi.org/10.1038/ncomms8260>.
- [27] L.D. Gang, Sun, Dyeing Textiles Using Nanoparticles, 2003.
- [28] D. Li, G. Sun, Coloration of textiles with self-dispersible carbon black nanoparticles, *Dyes Pigments* 72 (2007) 144–149, <https://doi.org/10.1016/j.dyepig.2005.08.011>.
- [29] O.K. Alebeid, T. Zhao, Simultaneous dyeing and functional finishing of cotton fabric using reactive dyes doped with TiO₂ nano-sol, *J. Text. Inst.* 107 (2016) 625–635, <https://doi.org/10.1080/00405000.2015.1054209>.
- [30] D. Fakin, K.S. Kleinschek, A. Ojstrsek, The role of TiO₂ nanoparticles on the UV protection ability and hydrophilicity of polyamide fabrics, *Acta Phys. Pol., A* 127 (2015) 943–946, <https://doi.org/10.12693/APhysPolA.127.943>.
- [31] O. Kamal Alebeid, T. Zhao, Anti-ultraviolet treatment by functionalizing cationized cotton with TiO₂ nano-sol and reactive dye, *Textil. Res. J.* 85 (2015) 449–457, <https://doi.org/10.1177/0040517514549989>.
- [32] N. Von Goetz, C. Lorenz, L. Windler, B. Nowack, M. Heuberger, K. Hungerbühler, Migration of Ag- and TiO₂- (nano)-particles from textiles into artificial sweat under physical stress: experiments and exposure modeling, *Environ. Sci. Technol.* 47 (2013) 9979–9987, <https://doi.org/10.1021/es304329w>.
- [33] S.J. Froggett, S.F. Clancy, D.R. Boverhof, R.A. Canady, A review and perspective of existing research on the release of nanomaterials from solid nanocomposites, *Part. Fibre Toxicol.* 11 (2014), <https://doi.org/10.1186/s12937-014-11-17>.
- [34] P. Patel, P. Kumari, S.K. Verma, M.A. Mallick, Cellular and molecular insight of green synthesized silver nanoparticles, in: *Silver Nanoparticles – Heal. Saf.* 2019, <https://doi.org/10.5772/intechopen.90717> [Working Title].
- [35] S.K. Verma, E. Jha, P.K. Panda, A. Mishra, A. Thirumurugan, B. Das, S.K.S. Parashar, M. Suar, Rapid novel facile biosynthesized silver nanoparticles from bacterial release induce biogenicity and concentration dependent in vivo cytotoxicity with embryonic Zebrafish—A mechanistic insight, *Toxicol. Sci.* 161 (2018) 125–138, <https://doi.org/10.1093/toxsci/kfx204>.
- [36] J. Jura, R. Szmyd, A.G. Goralczyk, L. Skalniak, A. Cierniak, B. Lipert, F.L. Filon, M. Crosera, J. Borowczyk, E. Laczna, J. Drukala, A. Klein, Effect of silver nanoparticles on human primary keratinocytes, *Biol. Chem.* 394 (2013) 113–123, <https://doi.org/10.1515/bch-2012-0202>.
- [37] E. Vlachou, E. Chipp, E. Shale, Y.T. Wilson, R. Papini, N.S. Moiemien, The safety of nanocrystalline silver dressings on burns: a study of systemic silver absorption, *Burns* 33 (2007) 979–985, <https://doi.org/10.1054/burns.2007.07.014>.
- [38] S.W.P. Wijnhoven, C.A. Herberths, W.I. Hagens, A.G. Oomen, E.H.W. Heugens, B. Roszek, J. Bisschops, I. Gosens, D.I.K.V.A.N.D.E. Meent, S. Dekkers, W.I.M.H.D.E. Jong, R.E. Geertsma, M.V.A.N. Zijverden, Nano-silver – a review of available data and knowledge gaps in human and environmental risk assessment, *Nanotoxicology* 3 (2009) 109–138, <http://www.tandfonline.com/doi/abs/10.1080/17433590902725914>.
- [39] B. Sarkar, S.K. Verma, J. Akhtar, S.P. Netam, S.K. Gupta, P.K. Panda, K. Mukherjee, Molecular aspect of silver nanoparticles regulated embryonic development in Zebrafish (Danio rerio) by Oct-4 expression, *Chemosphere* 206 (2018) 560–567, <https://doi.org/10.1016/j.chemosphere.2018.05.018>.
- [40] D. Fakin, N. Veronovski, A. Ojstrsek, M. Bozic, Synthesis of TiO₂–SiO₂ colloid and its performance in reactive dyeing of cotton fabrics, *Carbohydr. Polym.* 88 (2012) 992–1001, <https://doi.org/10.1016/j.carbpol.2012.01.046>.
- [41] P. Kumari, P.K. Panda, E. Jha, N. Pramanik, K. Nisha, K. Kumari, N. Soni, M.A. Mallick, S.K. Verma, Molecular insight to in vitro biocompatibility of phytofabricated copper oxide nanoparticles with human embryonic kidney cells, *Nanomedicine* 13 (2018) 2415–2433, <https://doi.org/10.2217/nm-2018-0175>.
- [42] B. Baroli, M.G. Ennas, F. Loffredo, M. Isola, R. Pinna, M.A. Lopez-Quintela, Penetration of metallic nanoparticles in human full-thickness skin, *J. Invest. Dermatol.* 127 (2007) 1701–1712, <https://doi.org/10.1038/sj.jid.5700733>.
- [43] A.V. Zvyagin, X. Zhao, A. Guerden, W. Sanchez, J.A. Ross, M.S. Roberts, Imaging of zinc oxide nanoparticle penetration in human skin in vitro and in vivo, *J. Biomed. Opt.* 13 (2008), 064031, <https://doi.org/10.1117/1.3041492>.
- [44] R. Dastjerdi, M. Montazer, A review on the application of inorganic nanostructured materials in the modification of textiles: focus on anti-microbial properties, *Colloids Surf. B Biointerfaces* 79 (2010) 5–18, <https://doi.org/10.1016/j.colsurfb.2010.03.029>.
- [45] R. Dastjerdi, M. Montazer, S. Shahsavari, A new method to stabilize nanoparticles on textile surfaces, *Colloids Surf. A Physicochem. Eng. Asp.* 345 (2009) 202–210, <https://doi.org/10.1016/j.colsurfa.2009.05.007>.

- [46] M. Gorensk, Dye-fibre bond stabilities of some reactive dyes on cotton, *Dyes Pigments* 40 (1999) 225–233, [https://doi.org/10.1016/S0143-7208\(98\)00052-1](https://doi.org/10.1016/S0143-7208(98)00052-1).
- [47] S.K. Verma, E. Jha, P.K. Panda, A. Thirumurugan, S. Patro, S.K.S. Parashar, M. Suar, Molecular insights to alkaline based bio-fabrication of silver nanoparticles for inverse cytotoxicity and enhanced antibacterial activity, *Mater. Sci. Eng. C* 92 (2018) 807–818, <https://doi.org/10.1016/j.msec.2018.07.037>.
- [48] G. Nallathambi, T. Ramachandran, V. Rajendran, R. Palanivelu, Effect of silica nanoparticles and BTCA on physical properties of cotton fabrics, *Mater. Res.* 14 (2011) 552–559, <https://doi.org/10.1590/S1516-14392011005000086>.
- [49] F. Li, Y. Xing, X. Ding, Silica xerogel coating on the surface of natural and synthetic fabrics, *Surf. Coating Technol.* 202 (2008) 4721–4727, <https://doi.org/10.1016/j.surfcoat.2008.04.048>.
- [50] M. Jasurski, S. Bakardjeva, W. Doroszkoewicz, S. Brzezinski, G. Malinowska, D. Marcinkowska, M. Ornat, W. Strek, K. Maruszewski, Properties and applications of silica submicron powders with surface Ag nanostructures, *Mater. Sci. Pol.* 22 (2004) 137–144.
- [51] S.H. Kim, C.H. Kwon, K. Park, T.J. Mun, X. Lepro, R.H. Baughman, G.M. Spinks, S.J. Kim, Bio-inspired, moisture-powered hybrid carbon nanotube yarn muscles, *Sci. Rep.* 6 (2016), <https://doi.org/10.1038/srep23016>.
- [52] W. Li, F. Xu, L. Sun, W. Liu, Y. Qiu, A novel flexible humidity switch material based on multi walled carbon nanotube/polyvinyl alcohol composite yarn, *Sensor, Actuator, B Chem.* 230 (2016) 528–535, <https://doi.org/10.1016/j.smb.2016.02.108>.
- [53] B. guo Yao, Y. Li, J. yan Hu, Y. lin Kwok, K. wing Yeung, An improved test method for characterizing the dynamic liquid moisture transfer in porous polymeric materials, *Polym. Test.* 25 (2006) 677–689, <https://doi.org/10.1016/j.polymertesting.2006.03.014>.
- [54] A. RV, Moisture management properties of textiles and its evaluation, *Curr. Trends Fash. Technol. Text. Eng.* 3 (2018), <https://doi.org/10.19080/crtte.2018.03.565611>.
- [55] O. Sahu, N. Singh, Significance of bioadsorption process on textile industry wastewater, in: *Impact Prospect. Green Chem. Text. Technol.*, 2018, pp. 367–416, <https://doi.org/10.1016/B978-0-08-102491-1.00013-7>.
- [56] I. Rezić, T. Haramina, T. Rezić, Metal nanoparticles and carbon nanotubes—perfect antimicrobial nano-fillers in polymer-based food packaging materials, *Food Pack* (2017) 497–532, <https://doi.org/10.1016/B978-0-12-804302-8.00015-7>.
- [57] P. Khare, A. Bhati, S.R. Anand, Gunture, S.K. Sonkar, Brightly fluorescent zinc-doped red-emitting carbon dots for the sunlight-induced photoreduction of Cr(VI) to Cr(III), *ACS Omega* 3 (2018) 5187–5194, <https://doi.org/10.1021/acsomega.8b00047>.
- [58] S.J. Park, G.S. Das, F. Schütt, R. Adelung, Y.K. Mishra, K.M. Tripathi, T.Y. Kim, Visible-light photocatalysis by carbon-nano-onion-functionalized ZnO tetrapods: degradation of 2,4-dinitrophenol and a plant-model-based ecological assessment, *NPG Asia Mater.* 11 (2019), <https://doi.org/10.1038/s41427-019-0101-0>.
- [59] G.S. Das, S. Sarkar, R. Aggarwal, S.K. Sonkar, J.W. Park, K.M. Tripathi, T.Y. Kim, Fluorescent microspheres of zinc 1,2-dicarbomethoxy-1,2-dithiolate complex decorated with carbon nanotubes, *Carbon Lett.* 29 (2019) 595–603, <https://doi.org/10.1007/s42823-019-00058-4>.
- [60] K.M. Tripathi, A. Begum, S.K. Sonkar, S. Sarkar, Nanospheres of copper(III) 1,2-dicarbomethoxy-1,2-dithiolate and its composite with water soluble carbon nanotubes, *New J. Chem.* 37 (2013) 2708–2715, <https://doi.org/10.1039/c3nj00368j>.
- [61] W. Gao, The Fabrication of Structurally Coloured Textile Materials Using Uniform Spherical Silica Nanoparticles, 2016, <https://doi.org/10.13140/RG.2.2.25724.54403>.
- [62] P. Velmurugan, J. Shim, K.S. Bang, B.T. Oh, Gold nanoparticles mediated coloring of fabrics and leather for antibacterial activity, *J. Photochem. Photobiol. B Biol.* 160 (2016) 102–109, <https://doi.org/10.1016/j.jphotobiol.2016.03.051>.
- [63] M. Zhang, B. Tang, L. Sun, X. Wang, Protection of silica-coated ZnO nanoparticles on pre-dyed polyester fabrics against photofading, *J. Text. Inst.* 108 (2017) 95–101, <https://doi.org/10.1080/00405000.2016.1153912>.
- [64] F.A. Mohamed, H.M. Ibrahim, E.A. El-Kharadly, E.A. El-Alfy, Improving dye ability and antimicrobial properties of cotton fabric, *J. Appl. Pharmaceut. Sci.* 6 (2016) 119–123, <https://doi.org/10.7324/JAPS.2016.60218>.
- [65] M. Gorjanc, M. Sala, Durable antibacterial and UV protective properties of cellulose fabric functionalized with Ag/TiO₂ nanocomposite during dyeing with reactive dyes, *Cellulose* 23 (2016) 2199–2209, <https://doi.org/10.1007/s10570-016-0945-7>.
- [66] S.K. Verma, E. Jha, P.K. Panda, J.K. Das, A. Thirumurugan, M. Suar, S.K.S. Parashar, Molecular aspects of core-shell intrinsic defect induced enhanced antibacterial activity of ZnO nanocrystals, *Nanomedicine* 13 (2018) 43–68, <https://doi.org/10.2217/nmm-2017-0237>.
- [67] S. Das, N. Ranjana, A.J. Misra, M. Suar, A. Mishra, A.J. Tamhankar, C.S. Lundborg, S.K. Tripathy, Disinfection of the water borne pathogens *Escherichia coli* and *Staphylococcus aureus* by solar photocatalysis using sonochemically synthesized reusable Ag@ZnO core-shell nanoparticles, *Int. J. Environ. Res. Publ. Health* 14 (2017), <https://doi.org/10.3390/ijerph14070747>.
- [68] L. Dyshlyuk, O. Babich, S. Ivanova, N. Vasilchenko, V. Atuchin, I. Korolkov, D. Russakov, A. Prosekov, Antimicrobial potential of ZnO, TiO₂ and SiO₂ nanoparticles in protecting building materials from biodegradation, *Int. Biodeterior. Biodegrad.* 146 (2020), <https://doi.org/10.1016/j.ibiod.2019.104821>.
- [69] L. Hao, T. Gao, W. Xu, X. Wang, S. Yang, X. Liu, Preparation of crosslinked polysiloxane/SiO₂ nanocomposite via in-situ condensation and its surface modification on cotton fabrics, *Appl. Surf. Sci.* 371 (2016) 281–288, <https://doi.org/10.1016/j.apsusc.2016.02.204>.
- [70] X. Chen, Q. Zhou, Y. Zhang, J. Zhao, B. Yan, S. Tang, T. Xing, G. Chen, Fabrication of superhydrophobic cotton fabric based on reaction of thiol-ene click chemistry, *Colloids Surfaces A Physicochem. Eng. Asp.* 586 (2020) 124175, <https://doi.org/10.1016/j.colsurfa.2019.124175>.

VG4 Cipher: Digital Image Encryption Standard

Akhil Kaushik¹

Ph.D Scholar, CSE Department
Amity University, Gurugram
India

Dr. Vikas Thada²

Associate Professor, CSE Department
Amity University, Gurugram
India

Abstract—When it comes to providing security to information systems, encryption emerges as an indispensable tool, as it has been used extensively in the past few decades for securing stationary data as well as data in motion. With the rapid data transmission techniques and multimedia options available for data representation, the field of information security has become very significant. The state-of-art cryptographic technique is DNA encryption, which uses biological principles for safeguarding data. The use of Bio-inspired ciphers is becoming the de-facto safety standard, especially for digital images as they are a key source of extracting crucial information. Hence, image encoding becomes of ultimate importance when there is a need to send them via an insecure communication channel. The purpose of this research paper is to present a DNA- inspired cryptosystem that can be employed in the domain of image encryption that provides superior security with enhanced efficiency. The experimental outcomes prove that this novel cryptographic algorithm not only provides better security but also at a reasonable pace.

Keywords—DNA cryptography; cipher; information security; encryption; decryption

I. INTRODUCTION

With the epoch of information explosion, information has become the most crucial asset of any individual, corporate, or government. This vital data may contain the personal record of any person, trade secrets of any business organization, or official documents of any government and hence needs to be kept in a secure place. Besides the physical security needs, there is also a need for safety while this significant data during transmission over the vulnerable interaction channel. Cryptography is the remedial solution for such a situation which keeps the information correct and intact between sender and recipient by making the data in a mangled form. Cryptography depends on two things: encryption algorithm and encoding key. The key may be a shared secret key or may form a public-private key pair depending upon the nature of the encryption algorithm. Without the right encryption steps and correct key, the unveiling of secret data can be a herculean task for the adversaries. Thus, cryptography provides impenetrable data which will be meaningless for the eavesdropper [1]. The data is growing immensely as 'big data' and it can now be represented in various forms like text, image, sound, animation, video, etc. This extended volume and multimedia forms of data require modern crypto solutions that can provide information security from malevolent adversaries and uncover the actual information only to the intended recipient. There are a plethora of options available to provide robust security and not all options are suited for all sorts of media. Some ciphers work best on textual data but may perform poorly on video

data, although some security algorithms may perform brilliantly on all sorts of media. Every media form has its peculiar attributes that cause the deviation in the encryption process and outcomes [2].

The most prevalent form of media besides textual data is digital images as they are used widely for information storage and broadcast due to their enhanced data-carrying capacity. The images may contain classified data such as military maps, government documents, healthcare images. The security mechanisms for images can be done in two ways: steganography and cryptography. Image Steganography can be defined as the myriad ways of concealing confidential information in the images, while Image Cryptography alters the image's data to a garbled form making it irrelevant rather than hiding it. Earlier, both of these techniques were used individually, but nowadays they can be combined to provide an even stronger sanctuary solution. Image cryptography is primarily done in two ways: frequency-domain techniques and spatial-domain approaches. The frequency-domain techniques rely on the Fourier transformations, while the spatial-domain approaches simply involve the manipulation of pixels' data in such a way that the real information contained in the pixels of images get altered on the sender's side and gets reverted into the original shape and form on the receiver's side [3]. Apart from the pixel level, encoding can also be done at the bit level, adding more perplexity to the existing encryption systems. There can be innumerable methods of image encryption and the method under consideration in this study makes use of DNA computing.

DNA computing made its way into the modern world when Leonard Adleman experimented with biological data and discovered that biological methods can give productive outcomes while solving baffling computational problems in 1994. Later this phenomenon received greater appreciation and researchers invested their time and money to apply these newly fangled principles into the newer and unexplored domains. DNA cryptography is inspired by the natural process of translation and encoding genetic information in DNA sequences. DNA is the abbreviated form of Deoxyribonucleic Acid that encodes genomic information using enormous sequences of four nucleotide bases $\Sigma = \{A, C, G, T\}$. These chemical bases are Adenine (A), Cytosine (C), Guanine (G), and Thymine (T) can be connected into a variety of combinations to pass the genetic information from parents to their children. This information is present in the form of genes which are enormously long DNA distinguishable sequences using complementary pairs of bases and called genes [4], as shown in Fig. 1. There can be multiple ways in which DNA can be utilized in the cryptographic sphere like hiding classified information in long DNA sequences,

generating one-time pads, DNA intensification using Polymerase Chain Reaction (PCR) for using in data encryption, and many more.

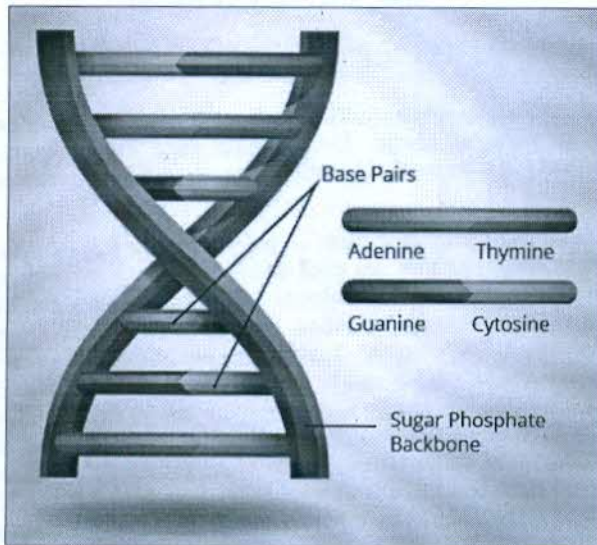


Fig. 1. DNA Structure [4].

The rest of the paper is organized as follows: Section II discusses the background and related work to the research. Section III highlights the system model and adversary model of the proposed research. Section IV details the stepwise proposed methodology for the presented work. Section V presents the simulation outcomes and examines the performance of the proposed cipher. Finally, Section VI entails the conclusion and the direction of future work.

II. RELATED WORK

As the name suggests, DNA cryptography is the amalgamation of biological methods and encryption. As discussed above, DNA computing was introduced in 1994 to solve intricate problems by Leonard Adleman and the concept grew stronger with time. In 1999, Cleland et. al. demonstrated the usage of DNA in steganography by hiding the renowned WWII phrase “June 6 attack; Normandy” in DNA strings [5]. Then, A. Gehani et al. demonstrated the myriad ways to encode data using DNA principles like OTP-based ciphers, Chip-based DNA microarray technology, and DNA steganography also. However, with the period of nearly 20 years, DNA cryptography has achieved new heights and plentiful novel DNA encoding algorithms have been developed, which have been listed below:

One exemplary work was proposed by Suri & Vijay (2017) which mixes a fast chaotic multi-image encryption algorithm with the AES encoding standard for a speedy encoding of multiple images. The concept is unique as it uses Cramer’s rule for decryption of digital images at the receiver’s end [6]. The use of biological methods in image encoding was also suggested by Enayatifar et al. (2017) that first brings the two-dimensional image into a single dimension and later applies permutation and diffusion parallelly for faster encryption. Both operations employ DNA sequences and results show quicker and securer output [7].

Niyat et. al. (2017) recommended the usage of non-uniform Cellular Automata (CA) for image cryptography. This non-uniform CA and hyperchaotic function create a stronger key image that generates a colossal number of random keys. Further usage of chaotic maps to add confusion and later using diffusion principles to create perplex cryptosystem [8]. The encoding of medical images is also a common practice and various studies have been conducted for the same. One such study is done by Akkasaligar & Biradar (2016) which blends DNA with chaotic theory to encode the odd and even pixels of medical images individually. This system is symmetric in nature that maintains integrity and efficiency along with security [9]. Ochani et al. (2017) also worked on the medical images using both steganography and cryptography. The chief technique here is to apply encryption on data and then hiding the patient’s vital encoded data in the cover medical image [10].

Another research done by Wang et. al. (2018) displayed that random numbers can also be used in the image encryption process. The authors have worked on both permutation and diffusion levels to increase the information security, besides including SHA-3 hashing with Chaotic systems to provide ultimate refuse against any unauthorized attacks [11]. Xiuli et. al. (2018) showed the embedding of DNA techniques in encryption. Initially, the image’s color is permuted and concerted into DNA codes. Consequently, DNA is used to produce random numbers that will be used to alter the pre-obtained DNA codes for further diffusion [12]. A similar approach was suggested by Rehman et. al. (2018) for encoding the colored images by combining SHA1 encoding, DNA complementary rules, and chaotic functions. The output obtained exhibited lesser noise and comparatively lower data loss [13].

Two-dimensional Logistic-Sine-Coupling map (2D-LSCM) can also be considered for encryption of colored images. It uses the typical confusion-diffusion structure i.e. transposing the pixels within the image first and then apply diffusion to further modify the pixels. This approach by Hua et. al. (2018) demonstrated better ergodicity than the traditional chaotic systems [14]. Another notable research was carried out by Li et al. (2018) for the encoding of multiple images simultaneously. First of all, Lifting Wavelet Transform (LWT) method is used to produce sparse images and then these scrambled images are XORed to further induce complexity. Finally, the images are compressed to form ghost images that can be traced only through bucket detector arrays [15].

Using DNA in image encryption is also verified by Sun (2018). Primarily, five-dimensional hyperchaotic systems are calculated to generate the chaotic sequences. Then, DNA is combined in several ways like DNA XOR operation, DNA complementary rules, DNA encoding, etc. to enhance the algorithm’s robustness. Besides these superior methods involved, the transposition is also done at two levels: pixel level and binary level [16]. A similar yet different approach was recommended by Zhang et al. (2018) that computed encoding key in two ways i.e. DNA sequencing and logistic chaos mapping. Later, these keys are applied to the plain image using DNA complementary rules to obtain the final ciphered image [17].

Liu et al. (2019) extended the image encryption using DNA to the next level by using 4-D memristive hyper-chaos to generate the chaotic matrices. Then, dynamic DNA is applied on the plain image to produce three matrices, and hence the combination of confusion, diffusion, and encryption creates vigorous cipher [18]. Zhang & Wang (2019) also demonstrated that using a three-dimensional DNA matrix to encode the digital images. First of all, numerous images are combined into a single image and then scramble using chaotic principles. Later on, multiple images are again taken away from the bigger image before applying diffusion using DNA codes and SHA-256 [19].

III. SYSTEM AND ADVERSARY MODEL

A. System Model

Fig. 2 shows the system model considered in this paper, in which there are three major components: Sender's end, Receiver's end, and Genetic Database. The sender's end consists of the user and the machine to generate and encode the message that needs to be sent over to the other end. The message has to be sent over the insecure public communication channel; hence the encoding must be done to keep it intact and away from prying eyes. The receiver's end is quite similar to the sender's end that encompasses the intended recipient and his/ her machine that not only accepts the transmitted message but also decodes it to obtain the original plaintext. However, the process of decryption is somewhat different from encryption depending upon whether it is symmetric or asymmetric cryptography. The third significant component of the model is the Genetic database, which is responsible to create, maintain and securely send the encryption key to the users. There are ample genetic databases that already contain the extremely long DNA sequences stored in the electronic form. The electronic form of DNA strings makes it easier enough for the administrators to store, maintain and give access to the authenticated users. It also eases the user to access, manipulate and regenerate the biological sequences by combining them in several ways. However, genetic databases also play a vivacious role in sharing the secret key that is used by sender and receiver. As the secret key used in the model is deduced from a specific DNA sequence, hence only its

sequence number in the genome database or its URL can be shared with the intended addressee via a safe and trusted channel rather than sending the entire genetic sequence over untrusted communication channels.

B. Adversary Model

In the system model, the real communicate takes place on the public insecure channel; hence there is a stout possibility of attacks to compromise the security. This is due to an imperious factor - an adversary who could try to catch the encoded message and try to either read or manipulate it. An adversary is defined as a computer wizard with malicious intent whose goal is to interrupt or halt the proper functioning of the cryptosystem. In this paper, the following threats are considered:

- **Shared Secret Key Security Threat:** As the communication under consideration is fairly dependent on the shared secret key that is generated using the DNA sequences stored in the genetic databases, hence if the key gets in the wrong hands, the whole system is compromised. Thus, the channel required to send this key must be trusted and secure enough to tackle this threat. Also, the property of backward secrecy should be followed while the generation of session key i.e. knowing one session key should not let the adversary extract other session keys.
- **Privacy Threat:** The message contents need to be kept private although the adversary may feel the message's presence but not its contents. If the adversary can read the message, he may replay the message multiple times or he may be able to modify the message contents or masquerade himself as an authenticated communicating party to gain undue advantage.
- **Physical Security Threat:** The physical security of all the crypto-system components must be of utmost priority as the attacker may try to physically damage or steal the devices or access the system's memory where session keys and messages are stored. Hence, the user credentials' information should be kept integrated and away from the hands of attackers.

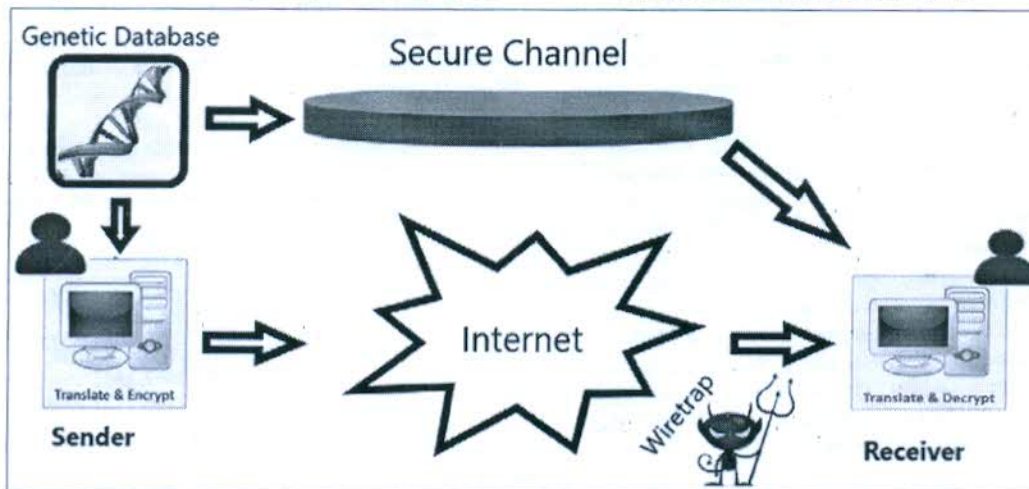


Fig. 2. System Model.

IV. PROPOSED SYSTEM

This section proposes the novel encoding system – VG4 cipher which is based on the existing VG1 cryptographic algorithm. VG1 cipher is a DNA Indexing cryptosystem that is a homophonic substitution cipher for textual data [20]. Several modifications have been done on the VG1 cipher for making it more efficient and secure to apply to digital images.

Image encryption is quite a tedious process with the inclusion of two steps: confusion and diffusion. Confusion refers to the permutation or transpositions of image components (blocks or pixels) so that the correlation among the pixels and the obvious redundancy gets altered. Another vital point is that the confusion step must be reversible to obtain the original image [21].

The second major operation is Diffusion which is stated as the process of altering the value of image components especially the value of pixels to make the encoding robust against differential and noise attacks. The diffusion procedure is done at two levels: block-level and pixel level. The encryption process in detail is described as follows:

- Step 1: The input is a color image of M & N dimensions, where M and N represent the width and height of the image.
- Step 2: The confusion step is done here at block level i.e. grouping of multiple pixels. The block size should be kept an even number and multiple of 8 for ease of operation. Here, the image is divided into 64 blocks and these 64 blocks are shuffled randomly.
- Step 3: There are two encoding keys used in the VG4 cipher. The first key is the 'Primary Key' which is deduced from the plethora of DNA sequences available from the genomic databases like GenBank, NCBI, DDBJ, EMBL-Bank, etc. Out of these ample DNA sequences, one peculiar DNA sequence is selected. In this particular DNA sequence, the position of every possible 4-DNA character combination is recorded in a separate dictionary. This dictionary contains position values of a specific DNA byte order (Ex: AATG) in the selected DNA sequence. This dictionary will form a homophonic substitution encryption cipher that works at the pixel level diffusion. An example of such a dictionary is demonstrated in Table I. The subsequent key is the 'Secondary Session Key' which is calculated prelude to applying diffusion at the block level. A set of session keys is produced (one for each block) by picking three random symbols from a set of pre-defined characters, $S = \{A-Z, a-z, 0-9, \#, @, !, \$, \%, \wedge, \&, *, \text{etc.}\}$ The secondary session key for each block thus consists of three characters, which are then changed to their binary equivalent.
- Step 4: Prelude to apply diffusion at the block level, a set of session keys is produced (one for each block) by picking three random symbols from a set of pre-defined characters, $S = \{A-Z, a-z, 0-9, \#, @, !, \$, \%, \wedge, \&, *, \text{etc.}\}$ The secondary session key for each block

thus consists of three characters, which are then changed to their binary equivalent. For every block, its combined RGB value is extracted and changed into the binary form so that the corresponding secondary session key can be applied to it. This process is repeated for every block in the image.

- Step 5: After applying diffusion at the block level, the next step is to apply the same at the pixel level. A pixel's RGB color code in decimal form is acquired using the NumPy library of Python. Using the VG1 encryption process, this decimal value is converted to the binary representation depending on the occurrence and frequency of the decimal values.
- Step 6: The binary data obtained from the previous step is then retransformed using shift-right or shift-left and then coded according to DNA rules (00-c, 01-a, 10-t, 11-g). This DNA encoding output converts all the binary data to DNA form.
- Step 7: The DNA homophonic substitution cipher is then applied on the output of step 6 and hence the 4-letter DNA codes are transformed into decimal numbers (index values in the given DNA sequence). Consequently, decimal values are changed into binary form and finally converted into a ciphered image. The whole encryption procedure is displayed in Fig. 3.

The proposed cryptographic algorithm is primarily based on symmetric encryption and henceforth the decryption procedure of the VG4 cipher is exactly opposite to the encoding process. The genomic sequences from which the primary key is crafted are shared through the reliable secure channel to the recipient. Similarly, the set of secondary session keys are also shared over to the other end. After the generation of encoding keys and receiving the ciphertext by the intended recipient, the next step is to convert the ciphertext into the DNA codes and then to binary form which is rotated into the reverse direction. Subsequently, the data is changed to decimal equivalent and then into pixel's RGB contents and the original image is conclusively recovered.

TABLE I. EXAMPLE OF KEY INDEXING

DNA Combination	Position Index in the DNA Sequence
GGTA	58, 80, 249, 619, 645, 671, 896, 1197, 1605, 2766, 2958, 2972
AGAG	130, 161, 242, 453, 1011, 1442, 1458, 1512, 1997, 2295, 2789
CAAG	27, 458, 611, 656, 924, 1059, 1332, 1518, 1521, 1539, 1584, 1647, 1695, 1698, 1734, 1767, 1779, 1885, 1933, 2166, 2225, 2365, 2401, 2625, 2700, 2754
AACT	271, 746, 1062, 1188, 1250, 1259, 1409, 1466, 1470, 1491, 1581, 1616, 1701, 1882, 1984, 2095, 2118, 2151, 2198, 2382, 2622, 2655, 2684
AAGG	10, 246, 366, 666, 1182, 1375, 1461, 1448, 1527, 1590, 1593, 1955, 2238, 2338, 2606, 2812, 2864
GGTG	521, 1754, 1877, 1992, 2442, 2531, 2618, 2675

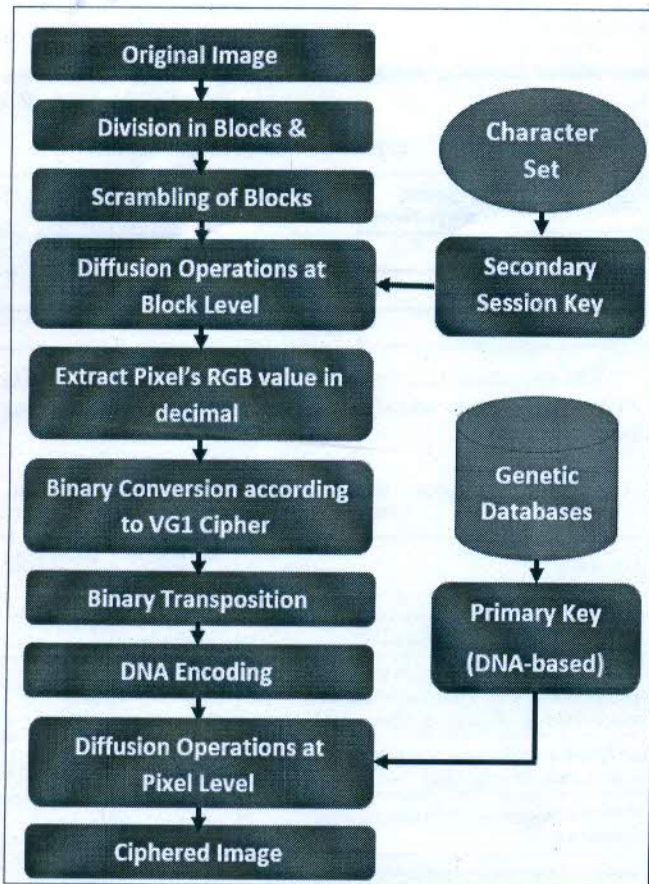


Fig. 3. Basic Block Diagram of VG4 Encryption Cipher.

V. SIMULATION RESULTS AND PERFORMANCE ANALYSIS

The proposed cryptographic algorithm can be implemented in any language that supports Unicode. It is implemented in Python Programming language using Google Colab IDE. It is also implemented on Jupyter Notebook on Intel Core i5 – 10th generation processor HP machine with 8GB RAM. Some crucial evaluation standards that focus on image encryption security are discussed and listed as follow:

A. Key Space Analysis

There is a total of nearly 420 billion DNA sequences available over genomic databases like EMBL-Bank, GenBank, NCBI, etc. Thus, first of all, the user needs to identify which genomic databases are exactly used for determining the primary key, otherwise, he will struggle for a lifetime to unearth it. Even if an attacker discovers DNA string is taken from NCBI, even then using the hit-&-trial method, he/she has to try 4163,000,000 combinations because there are 163 million nucleotide bases in NCBI and there are 4 bases -A, C, G, and T [22]. Thus, the probability of deciding accurate DNA sequence is $\frac{1}{163000000}$. Additional chaos will come into play if a longer biological series is chosen and out of this prolonged sequence only a fraction is extracted for spawning primary key. Hence, the huge keyspace for primary keys makes conventional attacks nearly impossible. Imperative consideration here is that the receiver only needs the correct

DNA number for reproducing the primary key, hence the whole DNA sequence need not be shared over the internet, rather only series numbers can be communicated through secure telephone or any other system.

B. Correlation

The adjacent pixels in any image are correlated to each other and measuring this correlation is of extreme importance when it comes to image cryptography. The input image usually has a high correlation between pixels, while the correlation in the ciphered image is desired to be as low as possible [23]. As depicted in Fig. 4(a), a positive correlation exists between pixels before encryption. However, the results obtained after encoding exhibit that the ciphered images have nearly 0 value of correlation, as shown below in Fig. 4(b). It means that the proposed cipher is successful in weakening the bond between adjacent pixels and makes it harder for the attacker during cryptanalysis.

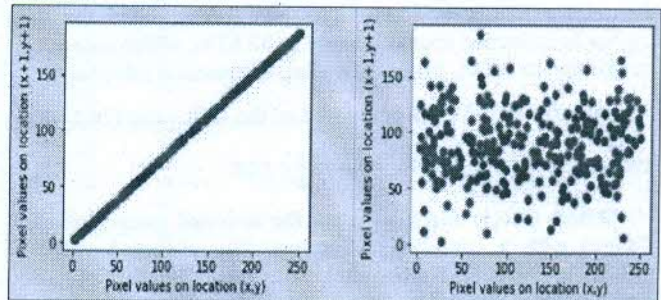


Fig. 4. Correlation between Adjacent Pixels in the Plain Image (a) and Ciphered Image (b) for a 512*512 Size Lena Image.

C. Histogram

The histogram analysis of the image cipher will demonstrate the pixel value distribution and it is desired to be uniform across the whole image. If the variance in histogram decreases in the enciphered image as compared to the plain image, then the cryptosystem is assumed to be fruitful [23]. As clearly observed from Fig. 5, the histogram of the plain image shows non-uniform dissemination, while the encoded image histogram has a uniform distribution pattern.

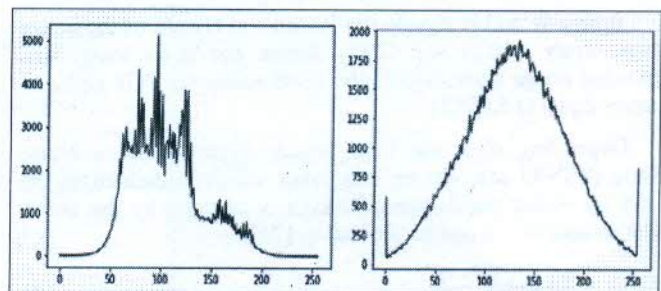


Fig. 5. Histogram of Plain Image (a) and Ciphered Image (b) for a 512*512 size Lena Image.

D. Analysis for Differential Attacks

Differential attacks are based on the idea of tracing the relationship between the original image and image obtained after encryption. Thus, the attacker tries to encode an image to obtain the ciphered image and then make some alterations in

the plain image to observe the subsequent changes in the newly attained encoded image. To measure these changes, there are two quantitative measures: The Number of Pixel Changing Rate(NPCR) and the Unified Average Changing Intensity(UACI). The NPCR for an image of dimension (W * H) is calculated by the following equation [24]:

$$NPCR = \frac{\sum_{i,j} D(i,j)}{W*H} * 100 \quad (1)$$

Where W is Width, H is Height, the value of i is between 1 and W, and the value of j lies within 1 and H. D(i, j) represents the difference between both images. The value of D(i, j) is 0 if the plain and encoded counterparts are the same, otherwise, the value equals 1. The lower bound of NPCR is 0% and the upper bound for NPCR is 100%. The NPCR calculated for VG4 cipher is estimated approximately at 97.65%, which means it is proximate to 100%, hence providing determined robustness.

Another factor UACI is computed as the following [24]:

$$UACI = \frac{1}{W*H} \left[\sum_{i,j} \frac{|C1(i,j) - C2(i,j)|}{255} \right] * 100 \quad (2)$$

Where C1(i,j) and C2(i,j) are the encoded images of plain images with a one-pixel difference. The observed value of UACI is 39.42% which simply means that the proposed cryptographic algorithm is quite sensitive to the minor changes in the plain image and provides substantial security against the differential attacks.

E. Analysis for Noise

The communication channels always contain some kind of noise, which will affect the enciphered image. There can be numerous kinds of noise and quantitative measures to check the effects of these noise on the image quality. The first one in this series is the Mean Square Error (MSE) which is computed as [25]:

$$MSE = \frac{1}{W*H} \sum_{i=1}^W \sum_{j=1}^H [I1(i,j) - I2(i,j)]^2 \quad (3)$$

Where W and H signify the Width and Height of the image respectively. I1(I,j) and I2(i,j) denote the plain image and encoded image correspondingly. MSE value for VG4 cipher is nearly equal to 0.00521.

Depending upon the MSE value, Peak Signal to Noise Ratio (PSNR) can also be computed which is defined as the ratio by which the decrypted image is affected by the noise. Mathematically, it can be defined as [25]:

$$PSNR = 10 \log \frac{(2^n - 1)^2}{MSE} \quad (4)$$

The PSNR value is measured for various noises like Salt & Pepper Noise (SPN), Speckle Noise (SN), and Gaussian Noise (GN) in the units – decibels. The PSNR value for 512*512 ‘lena.jpg’ for noise type SPN with parameters 0.001 is around 39.43. This result indicates detectable recovery from salt & pepper noise of up to 60%.

F. Timing Analysis

The performance analysis of any cryptographic algorithm depends upon security and speed. The encryption and decryption timings of the VG4 cipher are listed in the following Table II:

TABLE II. EXECUTION TIMINGS OF VG4 CIPHER

Image Size	Encryption Timings (Secs)	Decryption Timings (Secs)	Total Execution Timings (Secs)
512*512	40.3	37.6	77.9
700*400	53.2	44.7	97.9
1920*1080	210.6	199.5	410.1

The execution timings of VG4 cipher are compared with other state-of-art encoding algorithms in the following Table III:

TABLE III. COMPARISON OF EXECUTION TIMINGS OF VG4 CIPHER WITH EXISTING STANDARDS

Algorithm	Encryption (secs)	Decryption (secs)
Color image DNA encryption using NCA map-based CML and one-time keys [26]	1300.5	1300.7
Multiple-image encryption via lifting wavelet transform and XOR operation based on compressive ghost imaging scheme [15]	85.2	85.1
An AES-CHAOS-based hybrid approach to encrypt multiple images[6]	407.9	408.2
Multiple-image encryption using genetic algorithm [27]	149.7	144.5
Multiple-image encryption algorithm based on DNA encoding and chaotic system [19]	43	41.3
2D logistic-sine-coupling map for image encryption [14]	9.4	10.2
VG4 Cipher (Proposed)	40.3	37.6

VI. CONCLUSION

In the world of cybercrimes and online scams, a new defense is direly needed to guard the vital information, and for the same, the DNA cryptography approach reinforces the trust back into authenticated users. This paper presents a novel image encryption standard that uses biological principles in addition to traditional cryptography. First of all, the proposed algorithm uses two keys: primary key and secondary key. The primary key is deduced from a digital DNA sequence of long length and provides utmost security against brute-force attacks. The secondary key is also changed per session to enhance robustness. Both diffusion and confusion operations are applied to the image. Confusion or permutation of blocks are applied beforehand and then diffusion is applied at two levels. The secondary key works on a block of pixels and the primary key ensures encoding at the pixel level. The analysis for keyspace, histogram, correlation, etc. has been done and they determine the strength of enciphering algorithm. Also, the analysis for differential attacks and noise has been carried out and the desirable values of NPCR, UACI, PSNR, and MSE show better security and higher resistance against multiple attacks. The timing analysis done against the recent image encryption algorithms has been done and the results demonstrate the novel VG4 cipher is comparable to these modern standards both in encryption as well as decryption timings. Correspondingly, the execution (both encoding and decoding) timings are increasingly linearly with the increasing

size of images, which proves the computational complexity is linear.

In the future, the work can be manifold like chaotic functions like the Chen system or 3D logistic map can be introduced for confusion or diffusion. Another imperative future work could be improving the efficiency of the proposed cipher both in terms of security as well as execution timings.

REFERENCES

- [1] M. E. Saleh, A. A. Aly, & F. A. Omara, Data security using cryptography and steganography techniques (2016).
- [2] M. Jia, Y. Zhou, M. Shi, & B. Hariharan, A deep-learning-based fashion attributes detection model. arXiv preprint arXiv:1810.10148, (2018).
- [3] Z. Hua, Y. Zhou, & H. Huang, Cosine-transform-based chaotic system for image encryption. Information Sciences, 480, (2019) 403-419.
- [4] An online article "What is Chemical Structure of DNA" available at <https://empoweryourknowledgeandhappytrivia.wordpress.com/2017/03/29/what-is-the-chemical-composition-of-dna/> (2017).
- [5] A. Y. Niyat, & M. H. Moattar, Color image encryption based on hybrid chaotic system and DNA sequences. Multimedia Tools and Applications, 79(1), (2020) 1497-1518.
- [6] S. Suri & R. Vijay, An AES-CHAOS-based hybrid approach to encrypt multiple images, Recent Developments in Intelligent Computing, Communication and Devices, Springer, Singapore (2017) 37-43.
- [7] R. Enayatifara, A. H. Abdullah, I.F. Isnin, A. Altameem, & M. Leed, Image encryption using a synchronous permutation-diffusion technique. Opt Lasers Eng 90, (2017) 146-154.
- [8] A. Y. Niyat, M. H. Moattar, & M. N. Torshiz, Color image encryption based on hybrid hyper-chaotic system and cellular automata. Opt Lasers Eng 90, (2017) 225-237.
- [9] P. T. Akkasaligar, S. Biradar, Secure medical image encryption based on intensity level using chaos theory and DNA cryptography. International conference on computational intelligence and computing research, IEEE, Chennai, (2017).
- [10] A. Ochani, D. Jadhav, R. Gulwani, DNA Image encryption using modified symmetric key (MSK). International conference on inventive computation technologies, IEEE, Coimbatore, (2017) 1-4.
- [11] X. Wang, S. Wang, Y. Zhang, & C. Luo, A one-time pad color image cryptosystem based on SHA-3 and multiple chaotic systems. Optics and Lasers in Engineering 103, (2018) 1-8.
- [12] X. Chai, F. Xianglong, Z. Gan, Y. Lu & Y. Chen, A color image cryptosystem based on dynamic DNA encryption and chaos. Signal Processing, (2018).
- [13] A. U. Rehman, X. Liao, R. Ashraf, S. Ullah, & H. Wang, A color image encryption technique using exclusive-OR with DNA complementary rules based on chaos theory and SHA-2. Optik 159, (2018) 348-367.
- [14] Z. Hua, F. Jin, B. Xu & H. Huang, 2D logistic-sine-coupling map for image encryption, Signal Process., 149, (2018) 148-161.
- [15] X. Li, X. Meng, X. Yang, Y. Wang, Y. Yin, X. Peng, W. He, G. Dong, & H. Chen, Multiple-image encryption via lifting wavelet transform and XOR operation based on compressive ghost imaging scheme, Opt. Lasers Eng., 102, (2018) 106-111.
- [16] S. Sun, A novel hyperchaotic image encryption scheme based on DNA encoding, pixel-level scrambling and bit-level scrambling, IEEE Photon. J., 10(2), (2018) Art. no. 7201714.
- [17] T. T. Zhang, S. J. Yan, C. Y. Gu, L. Ren, & K. X. Liao, Research on image encryption based on dna sequence and chaos theory, Proc. 2nd Int. Conf. Mach. Vis. Inf. Technol. (CMVIT), 1004, (2018), 149-154.
- [18] Z. Liu, C. Wu, J. Wang, & Y. Hu, A color image encryption using dynamic DNA and 4-D memristive hyper-chaos, IEEE Access, 7, (2019) 78367-78378.
- [19] X. Zhang & X. Wang, Multiple-image encryption algorithm based on DNA encoding and chaotic system, Multimedia Tools Appl., 78(6), (2019), 7841-7869.
- [20] A. Kaushik & V. Thada, VG1 Cipher – A DNA Indexing Cipher, International Journal of Innovative Technology and Exploring Engineering, 9(3), 2020 221-226.
- [21] Z. Hua, B. Xu, F. Jin, & H. Huang, Image encryption using Josephus problem and filtering diffusion. IEEE Access, 7, (2019) 8660-8674.
- [22] E. W. Sayers, R. Agarwala, E. E. Bolton, J. R. Brister, K. Canese, K. Clark, R. Connor, N. Fiorini, K. Funk, T. Hefferon & J. B. Holmes, Database resources of the national center for biotechnology information. Nucleic acids research, 47(Database issue), D23, (2019).
- [23] C. Pak, & L. Huang, A new color image encryption using combination of the 1D chaotic map. Signal Processing, 138, (2017) 129-137.
- [24] R. Anushiadevi, V. Venkatesh, & R. Amirtharajan, An image mathcrypt-a flawless security via flawed image. International Conference on Applications and Techniques in Information Security, Springer, Singapore, (2019) 16-31.
- [25] S. Krivenko, M. Zriakhov, V. Lukin, & B. Vozel. MSE and PSNR prediction for ADCT coder applied to lossy image compression. 2018 IEEE 9th International Conference on Dependable Systems, Services and Technologies, (2018) 613-618.
- [26] X. Wu, K. Wang, X. Wang, H. Kan, and J. Kurths, Color image DNA encryption using NCA map-based CML and one-time keys, Signal Process., 148, (2018), 272-287.
- [27] S. Das, S. Mandal, & N. Ghoshal, Multiple-image encryption using genetic algorithm, Intelligent Computing and Applications, 343, (2015).

DESIGN AND SIMULATION OF A NOVEL STRUCTURE UWB PATCH ANTENNA

Ritu Yadav Research Scholar, Department of Electronics and Communication Engineering, Baba Mast Nath University Rohtak, Haryana

Dr. Anil Dudy, Assistant Professor, Department of Electronics and Communication Engineering, Baba Mast Nath University Rohtak, Haryana

Anil Kumar, Assistant Professor, CSE Department, TIT&S Engineering College, Bhiwani, Haryana
¹ritu12june@gmail.com*, ²anildudy@gmail.com and ³yadavanil82@gmail.com

Abstract

A new Ultra Wide Band (UWB) antenna is designed and simulated. Novel structure of patch antenna is able to provide broadband property of proposed design which is basic necessity for UWB application. The resonant frequency of antenna is observed at 10.6 GHz and 13.3 GHz with bandwidth 10.40 GHz to 10.75 GHz and 12.6 GHz to 13.9 GHz. Glass Epoxy substrate (FR4) with dielectric constant ($\epsilon_r = 4.4$), loss tangent ($\tan \delta$) equal to 0.02 has been used for the proposed patch antenna. The radiation pattern of purposed patch is broad side in direction of maximum radiation. Maximum gain observed by designed patch in operating range is 12.9 dB. With this, basic structure of patch antenna including working principle, basic feeding techniques, basic mathematical expression for calculating dimensions of patch are presented. Transmission line model for calculation the length and width of rectangular patch has been used which shows simplicity of fabrication and manufacturing. High Frequency Structure Simulator (HFSS) simulation platform is used for simulation. The simulation results in terms of return loss, Voltage Standing Wave Ratio (VSWR) and radiation pattern shows good agreement in performance.

Keywords: Bandwidth, Gain, Micro strip patch antenna, Radiation Pattern, Return Loss, VSWR.

Introduction

Concept of microstrip patch antenna was given by Bob Munson in 1950. But this concept of patch antenna did not come into picture till 1970. In 1970 with development of integrated circuits it was possible to fabricate patch antenna on a chip. In present time, from TV remote to fully automatic intelligent systems everything is wire free. To exchange a high volume of information with the help of electromagnetic waves a transducer is required which can convert information signal into electromagnetic waves and reverse. This transducer is known as 'antenna' which allows the devices to exchange information with the help of electromagnetic waves [1].

A variety of antenna are invented and used by researchers. But with time, it is observed that this antenna should be compact, ease to fabricate and cost should be less. These main objectives were fulfilled with the development of patch antenna.

A 'micro strip patch antenna' shown in Figure 1 consists of substrate, radiating patch and ground plane [2]. Patch antenna can be fabricated on printed circuit board. The lowest part is ground plane and the top most is patch. The substrate between ground plane and patch behaves as dielectric substrate. The distance between ground plane and patch behaves very important role in bandwidth of antenna [3]. A thicker substrate enhances gain but leads to surface wave excitation which disturbs the radiation pattern of antenna. The ground plane should extend beyond the edges of patch otherwise ratio of front to back wave can increases [3]. Increased dimensions of ground plane can increase the gain but diffraction at the edges increases and size of patch also increases which can reduce performance of patch antenna [4].

Main objective of this paper is to design a patch antenna for UWB application with wider bandwidth and acceptable performance in terms of acceptable return loss, VSWR, gain, directivity and bandwidth.

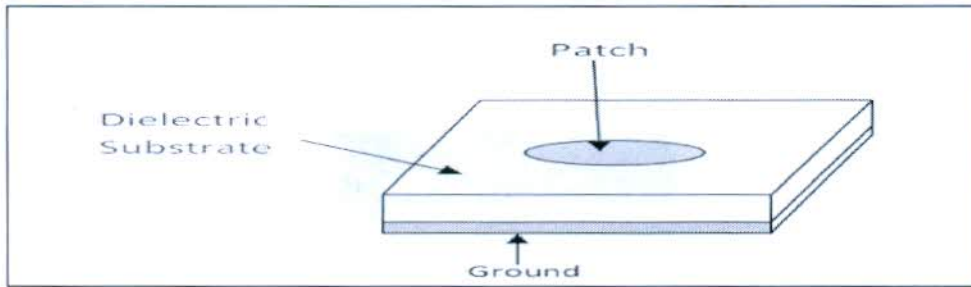


Figure 1. Structure of Micro Strip Patch Antenna

In this paper firstly basic working principle including various shapes of patch antennas, different feeding techniques, supporting literature review are discussed in brief. After basic concept of patch antenna adopted methodology is presented then designing of patch and simulation results are discussed. Followed by this conclusion and future scope is concluded in last.

Background

Basic working principle of antenna is fringing effect [4] as shown in Figure 2.

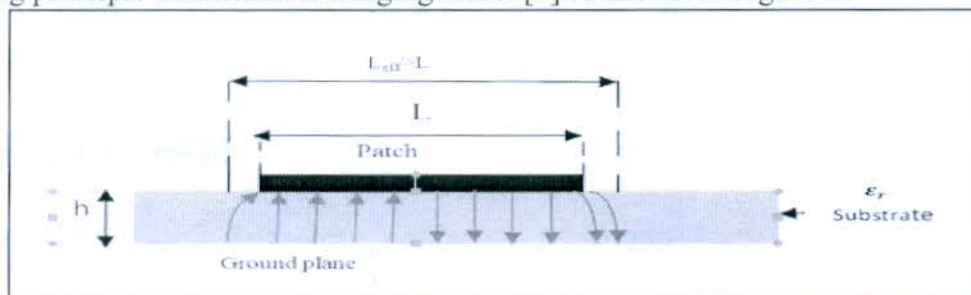


Figure 2. Fringing effect

Fringing occurs due to discontinuity observed by exciting current coming from feed line at the open end of feed line on patch. Due to this discontinuity value of current is minimum at the edges of patch while maximum current exists at the half of the length of the patch. This occurs because patch behaves as short circuited at the feeding point while it behaves as open circuited at the edges due to which maximum voltage +V exists at the edge while -V exists at the centre of patch due to fringing patch behaves as voltage radiator and starts radiating. Fringing effect allows patch to behave electrically wider compared to its dimensions [4]. EM waves pass through both air and substrate, due to which effective dielectric constant is to be introduced. This effective dielectric constant causes both fringing as well as wave transmission in the line.

Shapes of Microstrip Antenna

Various shapes of patch are designed and simulated by researchers. Different shapes of the microstrip patch attain the novel performance parameters.

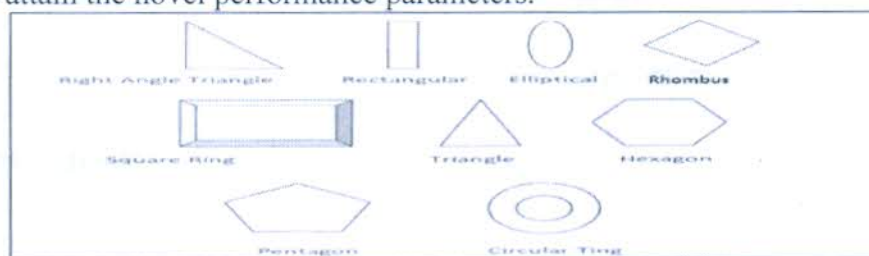


Figure 3. Basic shapes of Micro Strip Patch Antenna

So, to get the better and efficient one, the shape and dimensions of the microstrip patch must be defined properly. Basic shapes of the patch are shown in Figure 3 [5, 6].

Large number of physical parameters can characterize a patch antenna. Different shapes of patch with cuts and notches can affect the dimensions as well as performance of radiating patch. Thus a variety of patch antenna with different shapes can be designed and fabricated [6]. Length, width and thickness of radiating patch is calculated according to the operating frequency [7]. A variety of

substrate material with different values of permittivity and permeability can also affect the performance of patch antenna [8].

Feeding Patch Antennas

Feeding line through which radiating patch is excited also plays very important role in performance of patch antenna. Feeding line provides guided path from exciting origin up to radiating patch, so it is very important that input impedance of this feeding line should be matched with the impedance of radiating patch otherwise maximum of input will be reflected. Micro strip-line feed, Probe feed, Aperture coupled feed and proximity coupled feed are main kinds of feeding line [7].

Microstrip Line Feed

It is a feeding technique, microstrip feed line is directly connected with the microstrip patch. The size of the feed line is different than microstrip patch [8]. Microstrip line feed can be considered as extension of patch. The inset position can be adjusted to get the favorable results. It is simple to formulate and match. Spurious feed radiation limits the bandwidth of patch. The microstrip line feed is as shown in Figure 4.

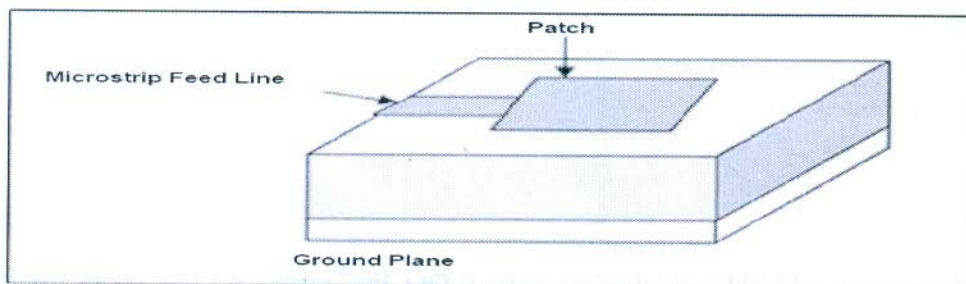


Figure 4. Microstrip Feed Line

Coaxial Probe Feed

In this feeding technique, central conductor of coaxial cable is linked to the microstrip patch of an antenna and external one is connected with ground plane [9]. Frequently the feed networks are cut off from the microstrip patch. Spurious radiation minimization, simple fabrication and competent feeding are the reward of coaxial feeding method. The coaxial probe feed is as shown in Figure 5.

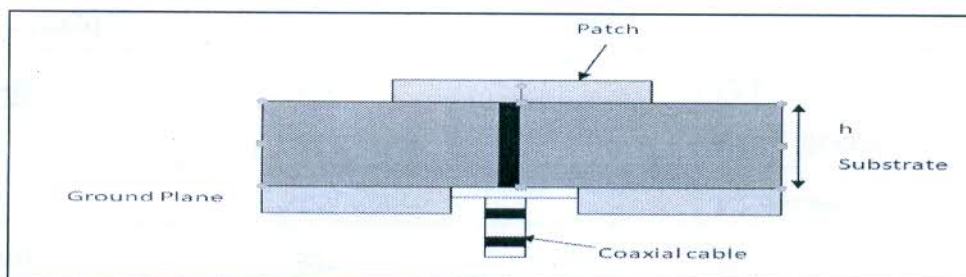


Figure 5. Coaxial Probe Feed

Aperture – Coupled Feed

This technology is having two substrates, which are dissimilar from each other and are alienated by a ground plane [10]. In this technique, the microstrip patch and feed line are united through a slot in the ground plane. Unadulterated polarization is the compensation of aperture coupled feeding method as shown in Figure 6.

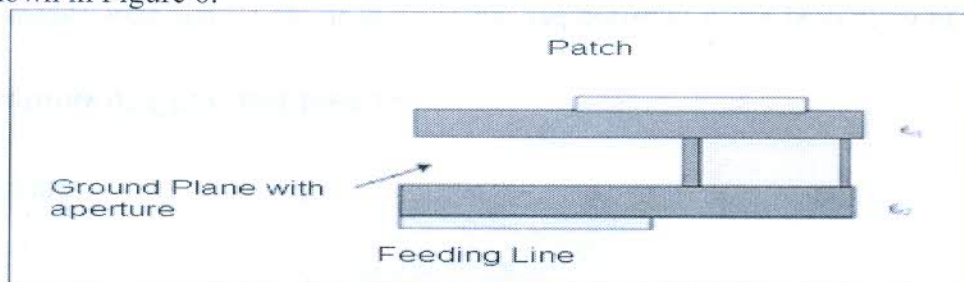


Figure 6. Aperture Feed Line

Researchers have simulated and proved how this feeding line can be optimized to get favorable results. According to requirement operating frequency or frequency on which antenna should resonant is selected. A huge area of wireless communication system is deploying microstrip patch antenna at the transmitting as well as at the receiving end.

Advantages of Microstrip patch Antennas [11, 12]

- Due to simple mathematical calculations microstrip patch antennas are low profile configurable.
- Uncomplicated and reasonably priced to fabricate using contemporary printed-circuit technology.
- Mechanically vigorous when mounted on firm surface.
- Patch shape is intended for flexible significant frequency, polarization, prototype, and impedance.
- Accumulation loads among the patch and the ground plane, (such as pins and varactor diodes), changeable resonant frequency, impedance, polarization, and prototype can be intended.

Disadvantages of Microstrip Antenna [11, 12]

- Squat efficiency.
- Reduced polarization transparency.
- Forged feed radiation.
- Contracted frequency bandwidth.

Due to mentioned shortcomings of patch antenna application of patch antenna is very limited. Researchers have introduced many solutions to these challenges like impedance matching devices, increasing the thickness of substrate, adding metamaterial with patch antenna [13] but again this enhances the complexity and cost of patch antenna [14].

Literature review

According to Ashish Kumar et.al thickness and dielectric constant of substrate governs the performance of a patch antenna. In this paper author has designed a rectangular patch antenna for resonating frequency 2.4 GHz and optimization is done by varying dielectric constant and substrate thickness. It is observed that decreased dielectric constant increases the bandwidth but size gets increased. So an optimization is done at three levels [15].

Satish Kumar et.al designed a rectangular patch for 5.6 GHz on simulation tool HFSS. Microstrip feeding line is used to excite the designed patch. FR4 epoxy substrate with dielectric constant 2.4 is chosen. Simulation results conclude that simple compact shape of patch can serve acceptable performance of patch antenna if dielectric constant is increased and height is decreased wisely [16].

A.A. Deshmukh et.al has designed a microstrip slotted antenna for wireless communication. A slotted E shape patch is designed with probe feeding technique on HFSS simulator. It is concluded that slots in patch is providing 30.3% bandwidth [17].

Norbahiah et.al purposed and designed a slotted patch antenna on simulator HFSS, operating between 1.56 GHz to 2.12 GHz. It is concluded that slots in patch gives novelty to the structure as well as high bandwidth is achieved [18].

F. Yang et.al designed E shaped patch antenna simulating on 1.9 GHz and 2.4 GHz. Bandwidth 21.2% and 32.3% bandwidth is covered by E-shaped patch antenna [19].

Author work by M. Abbaspour et.al has purposed a star-shaped patch antenna for frequency range from 4.0 to 8.8 GHz. 81% of bandwidth is reported [20]

A brilliant paper by F.Jolani et.al has designed a M-slot folded patch antenna. This folded patch provided 21.17% bandwidth [21].

M.T. Islam et.al designed a H shaped patch antenna. Results conclude purposed patch achieves bandwidth from 1.76 GHz to 2.38 GHz [22].

X. L. Bao et.al purposed a plus shaped antenna and 53% of bandwidth is offered by this shape of patch [23].

M. Albooyeh et.al purposed and designed a cross shaped patch antenna and 6.49% bandwidth is achieved [24].

Above reported paper motivates to design a novel structure of patch antenna for higher frequencies with better bandwidth and more than one resonating frequency.

In this paper a unique structure of patch simulating at higher frequency greater than 10 GHz with microstrip feeding line on Epoxy FR4 substrate is designed. Results are optimized to achieve wide bandwidth so that it can be applicable for ultra wide band applications. Purposed patch is designed and simulated on HFSS simulator. To analyze performance of this design basic performance plots obtained from simulator are presented and discussed.

Methodology

Operating frequency 10 GHz and FR4 Epoxy substrate with dielectric constant 4.4 and height 1.6 mm is chosen. A Transmission line model is used for calculation of dimensions of patch antenna [6, 7].

Step 1: Width of Patch Antenna

The width of patch antenna is calculated using the equation (1) [6]

$$W = \frac{C_0}{2f_r} \sqrt{\frac{2}{\epsilon_r + 1}} \dots\dots\dots (1)$$

Where, W= Width of the patch, Co= Speed of light, ϵ_r = value of the dielectric substrate and f_r is resonating frequency for which patch antenna is to be designed.

Step 2: Effective Refractive Index: ϵ_{reff}

Effective refractive index is a very important parameter for designing a patch antenna. It is responsible for the propagation of wave in the air as well as in the patch [6, 7].

$$\epsilon_{reff} = \frac{\epsilon_{reff} + 1}{2} + \frac{\epsilon_{reff} - 1}{2} \left[1 + 12 \frac{h}{w} \right]^{1/2} \dots\dots\dots (2)$$

Step 3: Length:

Due to fringing, electrically the size of the antenna is increased by an amount of (ΔL). Therefore, the actual increase in length (ΔL) of the patch is to be calculated using the following equation [3, 5, 6].

$$\frac{\Delta L}{h} = 0.412 \frac{(\epsilon_{reff} + 0.3) \left(\frac{w}{h} + 0.264 \right)}{(\epsilon_{reff} - 0.258) \left(\frac{w}{h} + 0.8 \right)} \dots\dots\dots (3)$$

Where ‘h’= height of the substrate The length (L) of the patch is now to be calculated using the below mentioned equation [3, 5, 6].

$$L = \frac{C_0}{2f_r \sqrt{\epsilon_{reff}}} - 2\Delta L \dots\dots\dots (4)$$

Step 4: Length (Lg) and Width (Wg) of Ground Plane:

Now the dimensions of a patch are known. The length and width of a substrate is equal to that of the ground plane. The length of a ground plane (Lg) and the width of a ground plane (Wg) are calculated using the following equations [7]:

$$L_g = 6h + L \dots\dots\dots (5)$$

$$W_g = 6h + W \dots\dots\dots (6)$$

Result and Discussion

Novel Structure of Patch Antenna:

Using above equations from 1 to 6 following novel structure of patch is designed at resonance frequency 10 GHz. Calculated Length and breadth of rectangular patch are 9.1 mm and 6.4 mm respectively. Figure 7 shows basic designing shapes used to design novel patch geometry.

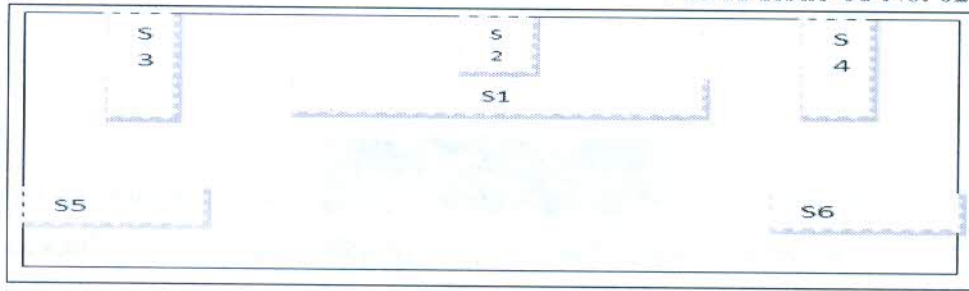


Figure 7. Layout of patch

In first simple rectangular patch is designed then small sub rectangle are designed and subtraction of these sub rectangle from main rectangle is done to achieve the desired shape of patch on HFSS as shown in Figure 8. Dimensions of sub rectangles are shown in table 1.

Table No.1: Dimensions of sub rectangle

Rectangle	X size in mm	Y size in mm
S1	3.5	0.5
S2	1	0.5
S3	0.5	1.5
S4	0.5	1.5
S5	1.5	0.5
S6	1.5	0.5

After subtraction following patch is developed on HFSS simulation tool as shown in Figure 8. Glass Epoxy substrate FR4 with height 1.6 mm is selected for simulation.

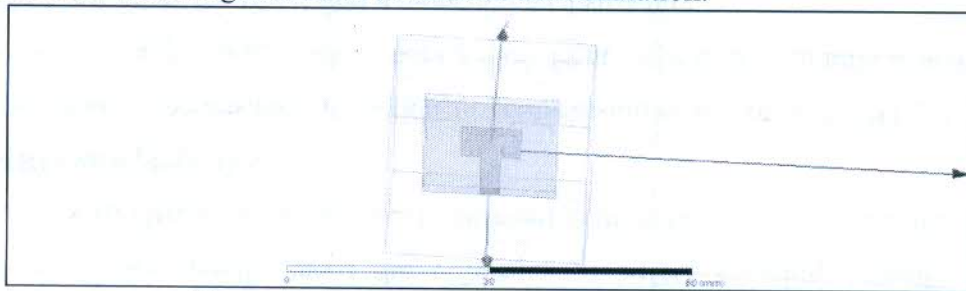


Figure 8. Novel Structure of Patch Antenna

Microstrip feed line with length 10 and width 3mm is adopted to feed the designed patch. After designing simulation is done on the same simulation tool i.e. HFSS. Following graphs are obtained to analyze the performance of designed novel patch.

Gain

Gain of an antenna is closely related to directivity of antenna. It counts efficiency as well as directional capabilities [15]. Gain of an antenna (in a given direction) is defined as “the ratio of the intensity, in a given direction, to the radiation intensity that would be obtained if the power accepted by the antenna were radiated isotropically” [6, 7].

$$\text{Gain, } G = 4\pi \frac{\text{Radiation intensity}}{\text{Total accepted input power}} \dots\dots\dots (7)$$

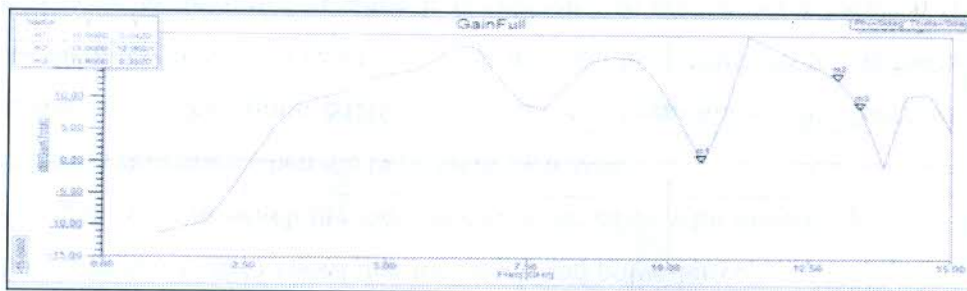


Figure 9. Simulation Graph between Gain vs. Frequency

Simulated graph for gain of designed patch in Figure 9 shows that at 10.6 GHz gain is 0.0420 dB while at 13.4 GHz it is 8.390 dB. Gain in positive range is considered acceptable range.

Return Loss

Return loss gives how well the device is matched [16]. It shows how much power is reflected when discontinuity between guided medium and air takes place. It is also known as constant of reflection constant [6].

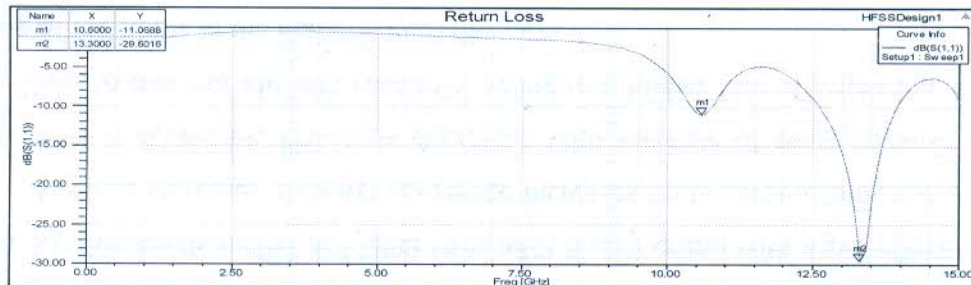


Figure 10. Simulation Graph between S(1,1) vs. Frequency

Simulation result shows graph between S (1, 1) vs. frequency range shown in Figure 10. The downfall of graph shows that patch antenna is resonating at two frequencies i.e. 10.6 GHz with return loss -11.0688 and at 13.3 GHz with return loss -29.6016, which shows that purposed patch is resonating at 10.6 GHz and at 13.3 GHz, so this patch antenna can be used for UWB application like satellite communication, inter space communication and downlink transmission.

Radiation Pattern

Radiation patterns also known as near field pattern or Fresnel pattern this refers to the positional reliance of the electromagnetic field in the near field [9, 10]. The near-field pattern is most commonly defined over a plane placed in front of the source, or over a cylindrical or spherical surface enclosing it [8].

Radiation pattern of designed patch is shown in Figure 11 and this shows maximum radiation along Z- axis.



Figure11. Radiation Pattern of Designed Patch Antenna at 10.6 GHz and 13.3 GHz.

Radiation pattern of designed patch shows that at resonating frequency 10.6 GHz patch antenna is radiating in broad side with 45 degree 3 dB beam width, while at 13.3 GHz radiation pattern shows maximum gain at 30 degree and beam width of 50 degree is observed.

Voltage Standing Wave Ratio (VSWR)

Voltage Standing Wave Ratio gives ratio of reflected wave to the transmitted wave between two different medium [7, 8]. VSWR is function of reflection coefficient. It is related to return loss by formula [7].

$$VSWR = \frac{1+\Gamma}{1-\Gamma} \dots\dots\dots (8)$$

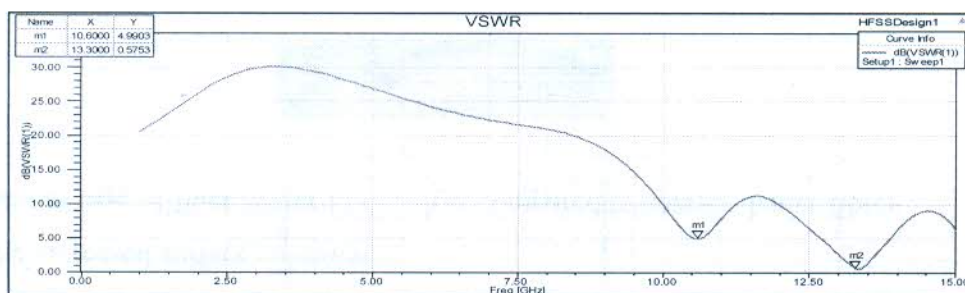


Figure 12. Simulation Graph between Frequency vs VSWR

Simulation graph shown in Figure 12 is drawn between VSWR vs. frequency. Graph shows at frequency 10.6 GHz VSWR is 4.9 dB and at frequency 13.3 GHz it is 0.575 dB. Value of VSWR at 10.6 GHz needs to be optimized while at 13.3 GHz a good value of VSWR is observed.

Bandwidth

Bandwidth shows the frequency range over which return loss is unacceptable range. In this range performance of antenna is in favorable condition and patch antenna can be used for the particular application. Generally frequency range having return loss less than -10db is considered as bandwidth of that particular microstrip patch antenna [11, 12].

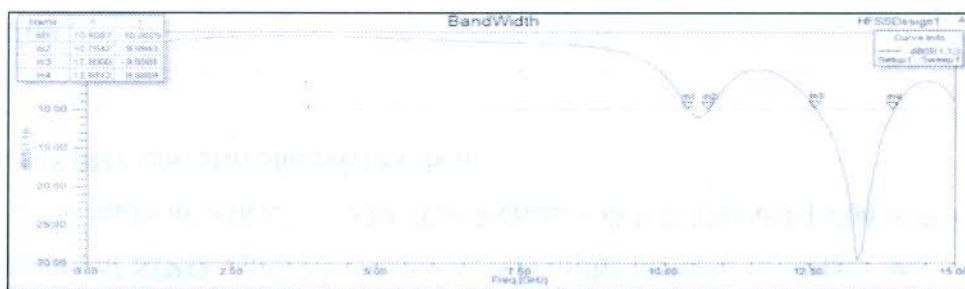


Figure 13. Simulation graph between Frequency vs S(1,1)

Simulation Results shown in Figure 13 shows bandwidth of .35 GHz with frequency range from 10.4 GHz to 10.75 GHz and bandwidth of 1.3 GHz is observed from 12.6 GHz to 13.9 GHz with return loss approximate -10db.

Conclusion and Future Scope

In this paper need of microstrip patch, its basic structure, basic feeding methods with advantages and disadvantages of microstrip patch antenna is discussed. A microstrip patch antenna for UWB frequency range has been successfully designed and simulated. All simulation results are summarized in table 2. Results show that it is a multi frequency operated antenna because it is resonating at two frequencies i.e. at 10.6 GHz and 13.3 GHz with return loss -11.06 dB and -29.6 dB respectively. A bandwidth of .35 GHz from 10.40 GHz to 10.75 GHz and 1.3 GHz from 12.60 GHz to 13.93 GHz has been confirmed at these two resonating frequencies. VSWR of purposed antenna at 10.6 GHz and 13.3 GHz is 4.9 db and 0.5 dB respectively.

Table No.2: Coefficients Simulated Results of purposed patch

Resonant frequency	10.6 GHz	13.3 GHz
Gain	0.04 dB	8.39 dB
Return loss	-11.06 dB	-29.06 dB
VSWR	4.9 dB	0.50 dB
Bandwidth	0.35GHz(10.4 GHz-10.75)	1.3 GHz(12.6 GHz-13.9 GHz)

A broad bandwidth is observed because of presence slots in the patch. Unique structure of patch allows this design to be multi frequency operated. In future performance of this patch can be enhanced with the aid of impedance matching devices or with the aid of metamaterial structures.

References

- [1] K. L. Wong, (1999), "Design of Nonplanar Microstrip Antennas and Transmission Lines", New York Wiley.
- [2] S. L. Latif, L. Shafai, (2005), and S. K. Shaema, "Bandwidth enhancement and size reduction of microstrip slot antenna," IEEE Trans. Antennas Propag., vol. 53, no. 3, pp. 994–1003.
- [3] I. J. Bahl and P. Bhartia, (1980), "Microstrip Antennas", Artech House
- [4] J. Q. Howel, (1972) ,"Microstrip antennas," in Proceedings of the Digest of the International Symposium of the Antennas and propagation Society, pp. 177–180.
- [5] R. H. Thaher and S. N. Alsaidy, (2016), "Design of Novel Wideband CPW Irregular Pentagonal Patch Antenna", International Journal of Computer Applications (0975 – 8887) Volume 139 – No.4, April pp.31-37.
- [6] C. A. Balanis, (2016) , "Antenna Theory: Analysis and Design", February 4th Edition.
- [7] W. L. Stutzman and, G. A. Thiele. (2012), "Antenna Theory and Design", 3rd Edition, Wiley Publications May.
- [8] J. R. James, P. S. Hall, and C. Wood, (1981), "Microstrip Antenna Theory and Design", Peter Peregrinus,.
- [9] G. Ramesh, (2001) "Microstrip Antenna Design Handbook", Artech House, Inc.
- [10] R. Garg, I. Bhartia, I. Bahl, and A. Ittipiboon, (2001), "Micro-Strip Antenna Design Handbook", Artech House, Boston, Mass, USA.
- [11] K. L. Wong, (2002) ,"Compact and Broadband Microstrip Antennas". New York: Wiley.
- [12] D. M. Pozar and B. Kaufman, (1987), "Increasing the bandwidth of a microstrip antenna by proximity coupling," Electronics Letters, vol. 23, no. 8, pp. 368–369.
- [13] R. Yadav and A. Dudy, (2020), "Performance analysis of microstrip patch antenna with aid of metamaterial", An International Conference on Cloud Computing (ICC-2020)",pp. 153-161.
- [14] H. F. Pues and A. R. Capelle, (1989), "Impedance-matching technique for increasing the bandwidth of microstrip antennas," IEEE Transactions on Antennas and Propagation, vol. 37, no. 11, pp. 1345–1354.
- [15] Ashish Kumar, Bimal Garg , (2011), "Rectangular Microstrip Patch Antenna Loaded With Double Orthogonal Crossed Slits In Ground Plane", International Journal of Advance Technology & Engineering Research, pp 675-702.
- [16] Sathish kumar , Arthika , Indhu , Elakkiya, (2020), "Design and Study of Rectangular Micro strip Patch Antenna for WLAN Applications", International Journal of Advanced Science and Technology Vol. 29, No. 7, pp. 3554-3558.
- [17] A. A. Deshmukh and K. P. Ray, (2009), "Compact broadband slotted rectangular microstrip antenna". IEEE Antennas and Wireless Propagation Letters, vol. 8, pp. 1410–1413.
- [18] Norbahiah Misran, Mohammed N. Shakib, Mohammad T. Islam, and Baharudin Yatim , (2009) ,"Design Analysis of a Slotted Microstrip Antenna for Wireless Communication", World Academy of Science, Engineering and Technology 49.
- [19] F. Yang, X. Zhang, Y. Rahmat-Samii, (2001) ,"Wide-band E-shaped patch antennas for wireless communications", IEEE Trans. Antennas Propag., vol. 49, pp. 1094-1100.
- [20] M. Abbaspour and H. R. Hassani, (2008) ,"Wideband star-shaped microstrip patch antenna", Progress in Electromagnetics Research Letters, vol. 1, pp. 61–68.
- [21] F. Jolani, A. M. Dadgarpour, and H. R. Hassani, (2008), "Compact M slot folded patch antenna for WLAN", Progress in Electromagnetics Research Letters, vol. 3, pp. 35–42.
- [22] M. T. Islam, M. N. Shakib, and N. Misran, (2009), "Broadband E-H shaped microstrip patch antenna for wireless systems", Progress in Electromagnetic Research, vol. 98, pp. 163–173.
- [23] X. L. Bao and M. J. Ammann, (2007), "Small patch/slot antenna with 53 input impedance bandwidth", Electronics Letters, vol. 43, no. 3, pp. 146–148.
- [24] M. Albooyeh, N. Komjani, and M. Shobeyri, (2008), "A novel cross slot geometry to improve impedance bandwidth of microstrip antennas", Progress in Electromagnetic Research Letters, vol. 4, pp. 63–72.

A Review on Trending Attacks: Phishing and Vishing attack

Archana Singh Parmar
T.I.T&S Bhiwani

Monika Sharma
T.I.T&S Bhiwani

Abstract - The Internet is a wide area network of computers connected around the world to facilitate data transmission and exchange. Due to the open nature of the Internet, all web-based services such as Online Banking are inherently subject to risks such as online theft of your Access Code/User ID/Username, PIN/Password, virus attacks, hacking, unauthorized access and fraudulent transactions. In today's world, 'sharing' has become the new norm, when it comes to financial details, we need to pay more attention and employ sound practices to keep our sensitive personal information safe and secure. A cyber-attack is an attempt to disable computers, steal data, or use a breached computer system to launch additional attacks. Cybercriminals can use a variety of methods to attack. This paper provides a basic explanation on most trending cyber-attacks, Phishing and vishing attack which is much similar with old phishing attack and discussed the scams in fashion nowadays to create awareness and several countermeasures to overcome them.

Keywords: Attacks, Cybersecurity, Phishing, Security, Vishing.

1. INTRODUCTION

Those days are gone when mobile phones were only used for calling, now even in India most of money transactions are carried through mobile phones. With the present dynamic technological developments, electronic information has grown in significance, businesses now conduct most of their day-to-day business undertakings electronically and this has drastically changed the level of information security threat. Now with this COVID-19 global forefront of mobile money services is an alternative to traditional banking. The Internet has a remarkable platform for common people communication. Persons with criminal mind have found a way of stealing personal information without meeting them and with the least risk of being caught. It is called Phishing. Over the years, since mobile money transaction services such as Google Pay and Paytm gained ground, criminals have

always devised ways of gaining access to individual's accounts". So in daily basis we are prone to cyberattacks.

A cyberattack is a malicious and deliberate attempt by an individual or organization to breach the information system of another individual or organization. Usually, the attacker seeks some type of benefit from disrupting the victim's network.

1.1 Cyber Attack Lifecycle model

1. Reconnaissance: Just like burglars and thieves, attackers carefully plan their attacks. They research, identify, and select targets, oftentimes using phishing tactics or extracting public information from an employee's LinkedIn profile or corporate websites. These criminals also scan for network vulnerabilities and services or applications they can exploit.

2. Weaponization & Delivery: Next, the attackers determine which methods to use. They may choose to embed intruder code within seemingly innocuous files like a PDF or Word document or email message. Or, for highly targeted attacks, attackers may craft deliverables to catch specific interests of an individual.

3. Exploitation: Once attackers gain access "inside" an organization, they can activate attack code on the victim's host and ultimately take control of the target machine.

4. Installation: Attackers will seek to establish privileged operations, root kit, escalate privileges, and establish persistence.

5. Command-and-Control: Attackers establish a command channel back through the Internet to a specific server so they can communicate and pass data back and forth between infected devices and their server.

6. Actions on the Objective: Attackers may have many different motivations for attack, and it is not always for profit. Their reasons could be data exfiltration, destruction of critical information.

2. PHISHING MECHANISM

The Cyber Security problems are increasing nowadays due to the growth of Internet worldwide. As Phishing links have different

features it becomes very difficult to mitigate different security issues. In Phishing attack attacker creates a replica of existing link or webpage to fool the user to get access to the personal information such as credit card or debit card passwords and try to convince the victim the message from the proper source.

The motive of phishing attack is to manipulate the attacker into providing confidential information about him/her. To perform such an attack, the attacker or phisher mimics a legitimate website. To mimic the web- site, he/she constructs a malicious site using a phishing website. This phishing Website would gather all the information on the target and provide it to the attacker. Usually, the targets are unable to distinguish between genuine and phishing websites causing them to fall into the traps set by the phisher.

The phishing attack lifecycle can be decomposed in :

- Planning,
- Setup,
- Attack,
- Collection,
- Fraud and
- Post attack action

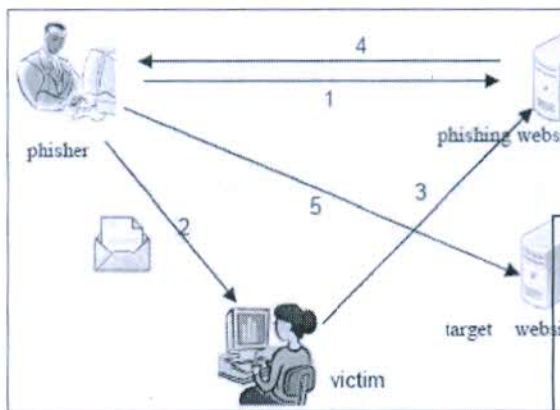


Fig 2.1: Phishing attack life cycle

Phishing attacks have several steps that attackers follow to obtain information. This can be explained in six steps. The steps are as follows:

- Plan
- Compose email
- Attack
- Gather data
- Fraud

The attacker starts the process by planning the attack. This step involves in deciding the legitimate website that has to be imitated and the victim whose information has to be gathered. Followed by planning, is composing an email that has to appear genuine for the victim to be lured into providing his/her data. The third part is sending the composed email to the target followed by gathering the information on the victim. The gathering of information phase occurs only if the victim has been tricked by the phisher. Using the victim’s information, the attacker commits cybercrimes such as credit card fraud, theft, etc.

Figure 2.2 shows the phishing mechanism and how the attackers manage to collect sensitive information about the target. It shows several steps involved in the attack.

Step 1 shows that the phisher composes an email with the help of a phishing website. This email is composed such that it appears to be genuine and legitimate.

Step 2, the attacker sends this composed email to the Target.

Step 3 indicates that the victim, unable to differentiate between genuine emails and phishing emails, tends to open the email.

The email then directs to the phishing website. The victim enters user login credentials in the webpage oblivious of the fact that it is a malicious site. The phishing website then provides the login credentials to the attacker. This is illustrated in step 4. In the last step, the phisher, using the data he has obtained from the phishing website, logs into the target website. Now, he would be able to access all the information of the victim. Thus, the process of phishing is completed.

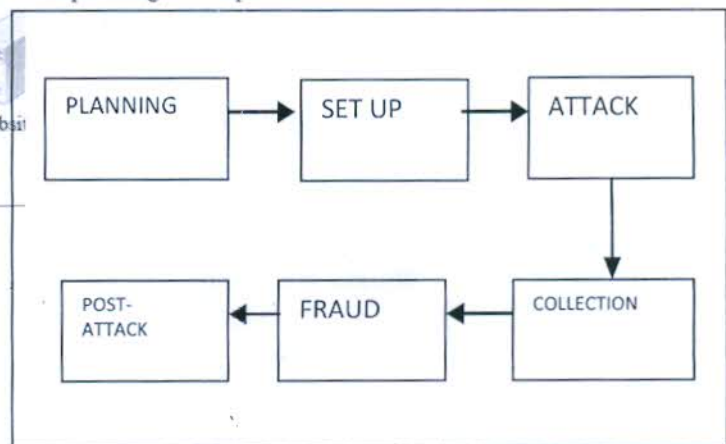


Fig 2.2 Phishing Attack mechanism

2.1 TYPES OF PHISHING ATTACKS

The attack can be performed in several ways. The motive for all the kinds are the same. The only variation amongst the types are the number of targets and the mechanism used to obtain the data.

The various types of phishing attacks are :

- E mail Phishing

- Spear Phishing
- Whaling
- Pharming
- *Deceptive Phishing*

2.1.1 Email phishing

Most phishing attacks are sent by email. The crook will register a fake domain that mimics a genuine organization and sends thousands of generic requests.

The fake domain often involves character substitution, like using 'r' and 'n' next to each other to create 'rn' instead of 'm'.

Alternatively, they might use the organization's name in the local part of the email address (such as paypal@domainregistrar.com) in the hopes that the sender's name will simply appear as 'PayPal' in the recipient's inbox.

There are many ways spot a phishing email, but as a general rule, you should always check the email address of a message that asks you to click a link or download an attachment.

2.1.2 Spear Phishing

Spear phishing describes malicious emails sent to a specific person. Criminals who do this will already have some or all of the following information about the victim:

- Their name
- Place of employment
- Job title
- Email address
- Specific information about their job role

2.1.3 Whaling

Whaling attacks occur when the phisher targets an individual at an executive position like CEO. The attacker would be profiling the victim for a considerable period before performing the attack. The attacker, similar to other types, would send an email to the target and manipulate him/her into providing information to the attacker. Whaling is considered a very dangerous attack since the people in executive bands have access to the organization's most confidential information.

2.1.4 Pharming

Pharming is another variation of phishing. Unlike the other techniques, it is not necessary to target individuals. The attack can victimize a large number of people without having to be targeted individually. Pharming is a form of online fraud involving malicious code and fraudulent websites. Cybercriminals install malicious code on your computer or server. The code automatically directs you to bogus websites without your knowledge or consent.

Pharming can be performed in two ways:

- The first method involves a code that is sent to the target via email that modifies all the local host files in the system. The URLs would be converted by the host files to number strings, used by the system to access web sites. This causes the target to be redirected to the malicious site in spite of entering the correct URL.
- The second method of performing pharming is through a technique called DNS Poisoning. In this method, the system's local host files are not corrupted but the domain name system table is modified. This results in the target being redirected to malicious websites without their knowledge. The target would be assuming they are accessing the legitimate websites, but because of DNS Poisoning, they would be accessing the malicious website.

Thus, the motive for all the variations of phishing are the same. Only the method and the technique used to obtain the information varies from one type to another.

3. VISHING MECHANISM:

Vishing, or voice phishing calls are a form of scam that aims to get prospective victims to share personal or financial information. Vishing is the practice of leveraging IP-based voice messaging technologies (primarily Voice over Internet Protocol, or VoIP) to socially engineer the intended victim into providing personal, financial or other confidential information for the purpose of financial reward. The term "vishing" is derived from a combination of "voice" and "phishing". Scam calls have risen significantly over the past couple of years. In 2017, scams represented only 3.7% of all incoming mobile calls. In 2021, that number reached nearly 40%.

Vishing is expected to have a much higher success rate than other phishing vectors because:

- Telephone systems have a much longer record of trust than newer, Internet-based messaging.
- A greater percentage of the population can be reached via a phone call than through e-mail.
- There is widespread adoption and general acceptance of automated phone validation systems.
- The telephone makes certain population groups, such as the elderly, more reachable.
- Timing of message delivery can be leveraged to increase odds of success.
- The telephone allows greater personalization of the social engineering message.
- Increased use of call centers means that the population is more accepting of strangers who may have accents asking for confidential information.

3.1 The most valuable information to the Visher is likely to be:

- Credit card details (including expiration data and card security codes) .
- Account numbers and their corresponding personal identification numbers (PINs)
- Birthdays
- Social Security numbers
- Customer loyalty card numbers
- Passport numbers.

3.2 Working OF Vishers

During a vishing phone call, a scammer uses social engineering to get you to share personal information and financial details, such as account numbers and passwords. The scammer might say your account has been compromised, claim to represent your bank or law enforcement, or offer to help you install software. Warning: It's probably malware.

Vishing is just one form of phishing, which is any type of message — such as an email, text, phone call or direct-chat message — that appears to be from a trusted source but isn't. The goal is to steal someone's identity or money.

It's getting easier to contact more people, too. Scammers can place hundreds of calls at a time using voice over internet protocol (VoIP) technology and can spoof the caller ID to make the call appear to come from a trusted source, such as your bank.

Vishing can be performed in several ways. These calls can have a real, live person on the other end of the phone line who is trying to scam you, or they can be fully automated where you are dealing with a robot only. Some types of voice phishing calls are even a hybrid of the two — where you will receive a call from an automated system that will then have a real person step in to take over the call.

3.2 Identity theft types of scams: -

- **The Internal Revenue Service (IRS)** — This vishing scam involves a malicious actor pretending to work with IRS. They will tell you that you owe taxes and, if you do not pay up immediately, that they're going to revoke your license, deport you, or throw you in jail. These scams involve trying to get the victim to provide their personal information and/or buy pre-paid gift cards. If you receive a phone call with this type of demand, hang up immediately. If you're still concerned, call the IRS directly.
- **Medicare** — This type of scam often involves someone calling and pretending to work for Medicare. They say that you are due to get a new Medicare card, but in order for you to receive the new card, they would need to first confirm your Medicare number. Obviously, this is not how Medicare operates, but people still frequently fall for this scam. If you provide your personal information, it can then be used to make bogus medical claims in your name and then the criminal pockets the money.
- **The Social Security Administration** — This particular scam involves someone calling and pretending to be from

Social Security Administration (SSA). They will feed you a line about how the SSA someone does not have all of your personal information, and that they need you to confirm it for you to receive the benefits you're entitled to. They will often threaten that if you don't provide the information, then you won't start to receive your Social Security benefits, or any benefits you already receive will be terminated. Like with the other examples we just mentioned, this is not how the SSA operates.

3.3 Consumers should do to protect themselves.

Here is some advice from security experts:

- Be aware. Consumers need to know that these scams exist.
- Be suspicious of all unknown callers. People should be just as suspicious of phone calls as they are of e-mails asking for personal information.
- Do not trust caller ID. Just because your caller ID displays a phone number or name of a legitimate company you might recognize, it doesn't guarantee the call is really coming from that number or company. Caller ID spoofing is easy.
- Ask questions. If someone is trying to sell you something or asking for your personal or financial information, ask them to identify who they work for, and then check them out to see if they are legitimate.
- Call them back. Again, if someone is selling you something or asking for information, tell them you will call them back and then either verify the company is legitimate, or if it's a bank or credit card company, call them back using a number from your bill or your card. Never provide credit card information or other private information to anyone who calls you.
- Report incidents. Report vishing calls. If you think you've been a victim of a vishing attack you can also contact, Internet crime complaint centre.

4. Conclusions:

Though not all people are victims to cybercrimes, they are still at risk. Crimes by computer vary, and they don't always occur behind the computer, but they executed by computer. Crimes done behind the computer are the 21st century problem. With the technology increasing, criminals don't have to rob banks, nor do they have to be outside in order to commit any crime. They have everything they need on their lap. Their weapons aren't guns anymore; they attack with mouse cursors and passwords.

Phishing and Vishing poses a huge threat to the e-commerce industry. Not only does it shatter the confidence of customers towards e-commerce and e-banking, but also causes electronic service providers tremendous economic loss. Vishing attack

prevention comes from both the user and the company side. Users should be ever mindful of such attacks and always foster a great deal of suspicion when being asked for critical information over the phone.

Hence it is essential to know about these attacks. So, awareness about phishing attacks and Vishing attack is very important as third person must not get access our hard-earned money.

REFERENCES

- [1] Ye Cao, Weili Han and Yueran Le - Anti-phishing based on automated individual white-list, Proceedings of the 4th ACM workshop on Digital Identity Management, pp. 51-60, October 2008.
- [2] Routhu Srinivasa Rao and Syed Taqi Ali - A Computer Vision Technique to Detect Phishing Attacks, 5th International Conference on Communication Systems and Network Technologies, IEEE, October 2015.
- [3] Madhusudhanan Chandrasekaran, Krishnan Narayanan and Shambhu Upadhyaya - Phishing Email Detection based on Structural Properties, IEEE, November 2015.
- [4] Rakesh Verma, Narasimha Karpoor, Nabil Hossain and Nirmala Rai - Automatic Phishing Email Detection based on Natural Language Processing Techniques, Research Gate, 2016.
- [5] Yi-Shin Chen, Huei-Sin Liu, Yi-Hsuan Yu and Pang-Chieh Wang, Detect Phishing by Checking Content Consistency, IEEE, 2017.
- [6]. K. Choia, J. Leeb and Y.ChunLijun, (2015) Voice phishing fraud and its modus operandi. Korea.
- [7]. Bezuidenhout, M., Mouton, F., & Venter, H. (August, 2010). "Social Engineering Attack Detection Model:SEADM," in Information Security for South Africa. IEEE, (pp. 1-8). Johannesburg, South Africa.
- [8]. Clarke, R.V. and Cornish, D.B. (1985) Modeling offenders' decisions: A framework for policy and research. In: M. Tonry and N. Morris (eds.) Crime and Justice: An Annual Review of Research. Chicago, IL: University of Chicago Press 6, pp. 147-185
- [9]. Mouton, F., Leenen, L., & Venter, H. S. (04 Feb. 2016). Social Engineering Attack Detection Model: SEADMv2. 2015 International Conference on Cyberworlds (p. 223). Pretoria, South Africa: CPS.
- [10]. L. Janczewski and L. Fu (2010) Social Engineering Based-Attack: Model and New Zealand Perspective. Proceeding of the International Multiconference on Computer Science and Information Technology pp. 847-853.

A Contemporary Ensemble Aspect-based Opinion Mining Approach for Twitter Data

Satvika¹

PhD Scholar, CSE Department
Amity University
Gurugram, India

Dr. Vikas Thada²

Associate Professor, CSE
Department, Amity University
Gurugram, India

Dr. Jaswinder Singh³

Associate Professor, CSE
Department, GJUS and T
Hisar, India

Abstract—Aspect-based opinion mining is one among the thought-provoking research field which focuses on the extraction of vivacious aspects from opinionated texts and polarity value associated with these. The principal aim here is to identify user sentiments about specific features of a product or service rather than overall polarity. This fine-grained polarity identification about myriad aspects of an entity is highly beneficial for individuals or business organizations. Extricating these implicit or explicit aspects can be very challenging and this paper elaborates copious aspect extraction techniques, which is decisive for aspect-based sentiment analysis. This paper presents a novel idea of combining several approaches like Part of Speech tagging, dependency parsing, word embedding, and deep learning to enrich the aspect-based sentiment analysis specially designed for Twitter data. The results show that combining deep learning with traditional techniques can produce excellent results than lexicon-based methods.

Keywords—Aspect-based sentiment analysis; dependency parsing; long short-term memory (LSTM); part of speech (POS) tagging; term frequency-inverse document frequency (TF-IDF)

I. INTRODUCTION

The past decade is undoubtedly dominated by data and its analytics. Now, anyone with an immense amount of data related to a domain and with the right tools to mine this colossal mountain of data is considered powerful. Surveys (either offline or online) are obsolete now as now more and more user is giving their opinions about myriad products and services on various social networking websites like Facebook, Instagram, LinkedIn, QQ, Telegram, Twitter, WhatsApp, WeChat, etc.[1]. All these social media platforms have been quite popular for exchanging opinions and sentiments and hence provide much-needed feedback about the specific products, services, vital events, organizations, or persons with the active participation of users. A lot of time, effort, and money has been put into analyzing user sentiments from a plethora of social sites especially Twitter due to the reason that tweets are limited to 140 characters[2]. This character limitation makes Twitter an easy and efficient tool for sentiment analysis, which can be pretty useful for organizations, who want to analyze related documents and make optimum changes to better suit their targeted customers. However, the sentiment analysis generally determines the overall opinion and hence may not be able to extract the precise essence needed to review that particular product or service.

This could be easily understood by the following example from a review about Cars: "Ford Mustang is awesome to drive, but the price is too high". This particular sentence basically talks about two different features of the subject (Ford Mustang) here i.e., "Driving Comfort" and "Price". Another notable point to comprehend is that a sentence may contain more than one aspect and the polarity of each aspect can be diverse. In the example shown above, "Driving comfort" is an undoubtedly positive polarity aspect while the "Price" aspect is declined more towards negative polarization. Hence to properly analyze the available data, a more detailed-level approach is needed, which is stated as the aspect-centered sentiment analysis. This methodology provides better insight for mining user opinions about the data under review. Overall, the sentiment analysis can be done at manifold stages that are document level, sentence phase, and aspect level[3]. Thus, in a nutshell, it can be stated that aspect-based sentiment analysis produces more fine-grained data analysis of user data.

In this research, an aspect-based sentiment mining problem is discussed on Twitter data and an efficient hybrid approach for the same has been proposed. The rest of this paper is organized as follows: Section II describes the numerous techniques used for aspect terms extraction. Section III gives an understanding of the projected framework. Section IV presents the outcomes of the proposed framework and evaluates them. Finally, Section V entails the conclusion and future work in the same direction.

II. ASPECT EXTRACTION TECHNIQUES

Sentiment analysis is usually defined as the computational study of a person's opinions or emotions or views about a particular entity. Nevertheless, an entity has certain features associated with it, which must be considered with utmost precaution as these characteristics define opinions at the atomic level. Aspects can be briefly stated as the attributes or traits of a product or service [4]. An Aspect extraction is a primary process of identifying these significant attributes and a considerate argument here is that aspect extraction aiming at no particular aspect or target is of circumscribed usage [5]. Hence aspect extraction is the most imperative step for pulverized opinion mining. There are two sorts of aspects, namely: implicit and explicit aspects. The explicit aspects are mentioned overtly in the opinionated sentence whereas the implicit aspects are expressed indirectly and that is why more challenging to discover. For example: "Mustang is a classic car from Ford, renowned as being the muscle car". In the

above sentence, “Ford” as the “brand” of the car is an explicit aspect, while “muscle car” refers to the implicit aspect “performance”. The subsequent step to aspect extraction is finding the sentiment polarity of recognized features; like in the above example “brand” aspect is neutral and the “performance” aspect is positive.

Some of the key techniques employed for finding aspects are shown in Fig. 1.

1) *Frequency-based approaches*: Considered as the most traditional approach, it chiefly employees tracing out the most commonly occurring words. One such technique is Part-of-Speech (POS) tagging which basically finds out the classification of words based on the grammar within a text like a noun, pronoun, verb, adjective or adverb, etc. POS tagging is not only the simplified syntactically tagging taught in school education, but it also tries to find the relationship between the word under consideration and the adjacent words. Thus, POS tagging is not generic but depends upon the sentence to sentence and finally, it can be said that it tries to extract speech tags based on the sentence context. Also, an imperative point is that POS tagging does not actually do the Natural Language Processing (NLP), but it is the precondition to handle a lot of NLP tasks. The main characteristic of POS tagging is that it finds the recurrent noun and noun phrases from the reviews as they are usually the aspects [7]. POS tagging on a review is demonstrated in Fig. 2.

However, it must be understood that some of the aspects identified by this approach may not be the key aspects and must be rendered. Another frequency-based tactic is Pointwise Mutual Information (PMI), which is figured as the variance of the common information between the feature and the related word [8]. Last but not the least is Term Frequency-Inverse Document Frequency (TF-IDF) methodology which evaluates how significant a word is to a document in a group of the corpus by calculating two terms. The first term (TF) is the frequency of a word appearing in a document, divided by the overall words’ tally in that document. The second term (IDF) is computed as the logarithm of the whole documents in the corpus divided by the number of documents where the particular word appears [9]. In simple words, TF-IDF is the statistical tool that keenly discovers the most vital words in the articles. An important feature of TF-IDF is that some words seem noteworthy due to their huge frequency in the text, but actually, they are insignificant like the, this, that, etc. [8]. Hence, TF-IDF can be described as the amalgamation of two algorithms that diminishes the weight of stopwords and recognizes the high opinionated words, which actually influence the sentiments contained in the documents.

2) *Relation-based approaches*: These techniques are based on discovering relations between features and the opinion words to identify aspects clearly. One such approach is Dependency Parsing – which is based on extracting the grammatical (or syntactic) structure of a sentence and finding the relation between vital words and the words which modify these vital words [10]. The second practice is called Double Propagation, which disseminates information among opinion

words and targets back and forth. This method comes under the semi-supervised category as it takes opinion word as the seed to start the process [11].

3) *Supervised machine learning*: The two most prominent aspect mining techniques Hidden Markov Model (HMM) and Conditional Random Fields (CRF) come under this category. HMM are a set of probabilistic visualization model that allows forecasting a sequence of hidden variables from a set of perceived variables. It is a great approach for tracing the aspects like it may predict the type of weather by observing the type of clothes worn by a person [12], as depicted in Fig. 3.

On the other hand, CRF is a discriminative model employed for predicting sequences where multiple variables are dependent on each other by imputing contextual information from previous labels [14]. Its main applications are in POS tagging and Named Entity Recognition (NER).

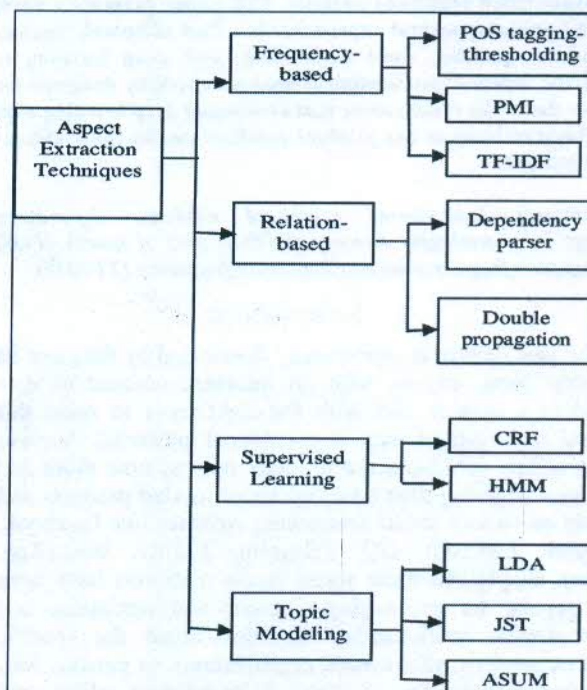


Fig. 1. Various Aspect-Extraction Approaches [6].

1315	NUM
RT	PROPN
TopGear	PROPN
It	PRON
delighted	VERB
us	PRON
in	ADP
dry	ADJ
autumnal	ADJ
Por	PROPN
....	PUNCT

Fig. 2. POS Tagging Output.

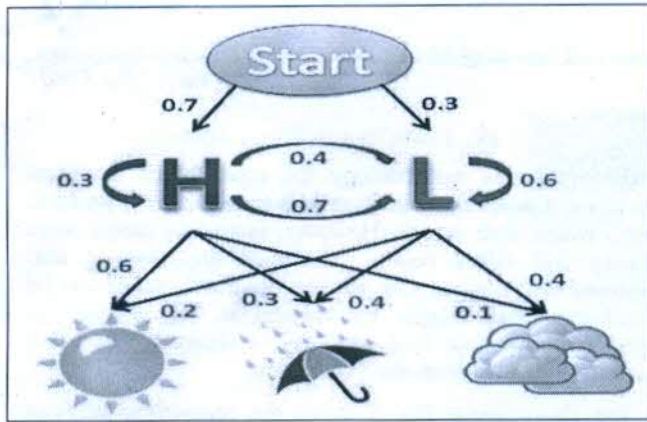


Fig. 3. Working of Hidden Markov Model [13].

4) Topic modeling: As the name suggests, it is a category of techniques used to automatically detect topics present in the text corpus. It comes under unsupervised learning for observing topics (a group of words) in a colossal amount of text clusters. Latent Dirichlet Allocation (LDA) is used to categorize text in a document to a certain topic by using Bag-of-Word (BOW) approach[15]. The prime objective of LDA is to match all the documents to the topics such that words in every document are customarily classified by those imagined topics. The next approach is Joint Sentiment Topic (JST) is the exquisite unsupervised technique that detects sentiments as well as the topics simultaneously from the text corpora by considering their mutual relations[16]. The next methodology categorized under topic modeling is the Aspect and Sentiment Unification (ASUM) model which automatically determines aspects and different sentiments towards these recognized aspects in one go. This model ascertains aspect-sentiment pair called 'senti-aspects' in an unsupervised way, explaining how much a particular word is related to aspect and sentiment [17].

III. PROPOSED FRAMEWORK

The focal emphasis is to conduct an exploration of aspect-based sentiment analysis conducted on Twitter data. The planned work consists of the following steps:

- 1) Data collection from Twitter.
- 2) Data pre-processing and preparation.
- 3) Aspect extraction from the data.
- 4) Aspect selection & polarity detection.
- 5) Tweet level Sentiment classification & Performance evaluation.

The first and foremost step is collecting data from Twitter, which is a social media networking site. There are numerous ways to extract data from Twitter; among which the most popular one is Twitter API Search, which allows us to retrieve the latest tweets about any topic. For doing so, a Twitter development account must be created first. Earlier, this method had a limitation on the number of tweets and also on the number of requests received per hour from a particular IP address [18].

After the data collection process from Twitter, the next work is to prepare the data for analysis and this process involves cleaning and pre-processing of data. The data from Twitter is not in a particular format and it must be cleansed beforehand like removing the links, emoticons without clear sentiment, new lines, hashtags and symbols like @, punctuation marks, etc. For effective aspect discovery, tweets, users who tweeted them, followers of users, count of retweets, date of the tweet, etc. are chosen from the whole data. After data collection and pruning, the next step is to pre-process it. The data pre-processing starts with the removal of stopwords i.e. removing the commonly occurring words like a, an, the, and, or, is, etc. as these words do not convey meaningful opinions. Then, all the words in the corpus are changed to lowercase for enhanced understanding and investigation. Afterward, the corpus is subjected to stemming and lemmatization i.e., words are reduced to their basic or root form. It is a highly recommended part because it reduces derivationally related forms of a word. For example: "programmable" is changed to "program" and "running" is converted to "run". One example of text before and after pre-processing is shown in Fig. 4.

Original Tweet: Tecney C900 Black Car DVD Sale, Price & Reviews Gearbest https://t.co/oM6s9jp8nn
Clean Tweet: Tecney C900 Black Car DVD Sale, Price amp Reviews Gearbest

Fig. 4. The Output obtained after Applying Pre-processing on Data.

Now, the data is ready for opinion mining and the foremost thing to do is finding aspects in these tweets. It can also be done in myriad ways as discussed in the above section. The aspect-extraction followed here is a hybrid one as multiple methodologies are combined for doing so including POS tagging, Dependency, etc. POS tagging is used to find the frequent nouns and noun phrases which tend to be the explicit aspects, while depending on parsing is brilliant for finding the implicit tags. For bigrams and trigrams, tokens are identified by checking words on the left side for 'proper Nouns' identified earlier. If the dependency is a compound or adjective modifier, then it is regarded as the aspect term. If the token is an 'adjective' or 'verb', the words on both sides (left and right) are examined for adverbial modifiers, open-clausal components, and 'auxiliary' dependencies and if it happens, they are regarded as aspect terms. For negation modification, words to the left of verbs and words on both left and right are diagnosed for adjectives and auxiliaries and in this case, the polarity of aspect is changed. Thus an ensemble of techniques is employed here to give the best output and providing every key aspect from the text corpora obtained after data preprocessing. The aspects can be ranked in decreasing order of frequency and selected on this basis. The next phase is detecting the polarity of each aspect and there are three types of polarities: positive, negative, and neutral. Positive polarity refers to the constructive and affirmative comments about the

aspect under consideration while negative polarity denotes the adverse and undesirable user views regarding that precise aspect and if the opinions do not fall under any of the above categories, it is considered as neutral polarity. Also, an imperative deliberation is that if an aspect has an equal number of positive and negative opinions, then it can be ignored. The algorithm for aspect-terms extraction can be described as the following:

- 1) Apply Tokenization first.
- 2) Prepare a list of stopwords, so that aspects, if identified on the stopword list, can be ignored.
- 3) Apply POS tagging for finding aspects.
- 4) The prime candidates for aspects are 'Nouns' or 'Proper Nouns' individually or in pair with Verbs/ Adverbs or Adjectives (explicit aspects).
- 5) For finding implicit aspects, dependency parsing is employed, along with bigrams and trigrams:
 - a) For a noun, check its dependency on its L.H.S. and if it is found to be 'compound', with an adjective or adjective modifier, then it should be an aspect-term.
 - b) For an adjective, check its dependency parsing on both L.H.S & R.H.S., if its dependency is auxiliary on L.H.S and 'negation modifier' on R.H.S, then is also identified as an aspect-term.
 - c) For a verb, if an adjective appears to its left or right and their dependency is 'adverbial modifier', then also it should be an aspect. Also, if an adjective appears on its L.H.S and dependency relation is negation modifier, the aspect is recognized.

Finally, the tweet level sentiments are analyzed using Vader Sentiment and Recurrent Neural Networks, and the results determined are verified in regard to state-of-art technologies. The overall process can be described by the Fig. 5 underneath.

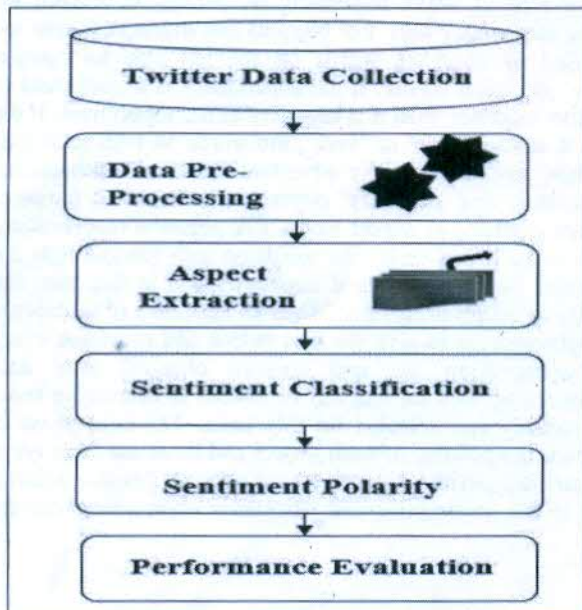


Fig. 5. Aspect-Based Sentiment Analysis Process.

IV. RESULTS AND EVALUATION

The ensemble methodology for aspect-based sentiment analysis is a novel approach that does excellent work for up to 49493 tweets data corpus. However, more data means more training and better results. The new algorithm is also employed on 'Scraped_Car_Review_ford.csv', which can be downloaded from Kaggle for verification. This dataset has 49493 reviews about ford cars. Fig. 6 shows the first five tweets downloaded from the Twitter site.

The above image Fig. 7 shows the comparison between tweet frequency and the number of followers for verified Twitter users. The data downloaded from Twitter is pre-processed as discussed in the above section and sample output is shown in Fig. 4 above. After pre-processing of data including tokenization and stemming, POS tagging is applied. After obtaining POS tags for each token, some special words with peculiar tags are selected and these are Nouns, Noun Phrases (like NNP, NNS & NNPS), Adjectives, and Adverbs because these tags are extremely helpful while identifying aspects.

The wordcloud is primarily an innovative tool that generates an aesthetic amalgamation of frequently occurring words. It puts together recurrent textual data into a beguiling visual representation and shows them in bigger and bolder fonts according to their frequency [19]. Fig. 8 shows the potential aspects identified by POS tagging and frequency distribution:

Fig. 9 demonstrates the top 20 frequent words occurring in the tweets according to their frequencies arranged in descending order.

While Noun and Noun phrases are the potential aspects, adjectives and adverbs support their claim when the dependency is checked between them. This is identified by applying dependency parsing between them, as illustrated below in Fig. 10.

After all the aspects are extracted, their polarity needs to be checked and for that Sentiwordnet can be used to check the opinion sentiment for all the mined aspects according to the tweets they are appearing in. Finally, the overall sentiment classification can be calculated using Vader Sentiment, which is a proficient tool for mining the sentiments. Fig. 11 shows the overall sentiment distribution of the downloaded tweets.

Tweets	User
RT @autocarindiamag: Happy #RepublicDay2020 to...	Serglus Barretto
Happy #RepublicDay2020 to all of you! \n\nOn...	Autocar India
RT @motoriseinc: With BMW updating the 7 Serie...	INClan
Update: Uber driver is watching video game rev...	Steven Ebert
RT @carsmagdotus: Collection of top car make a...	Fernando

Fig. 6. Sample of Tweets Downloaded from Twitter.

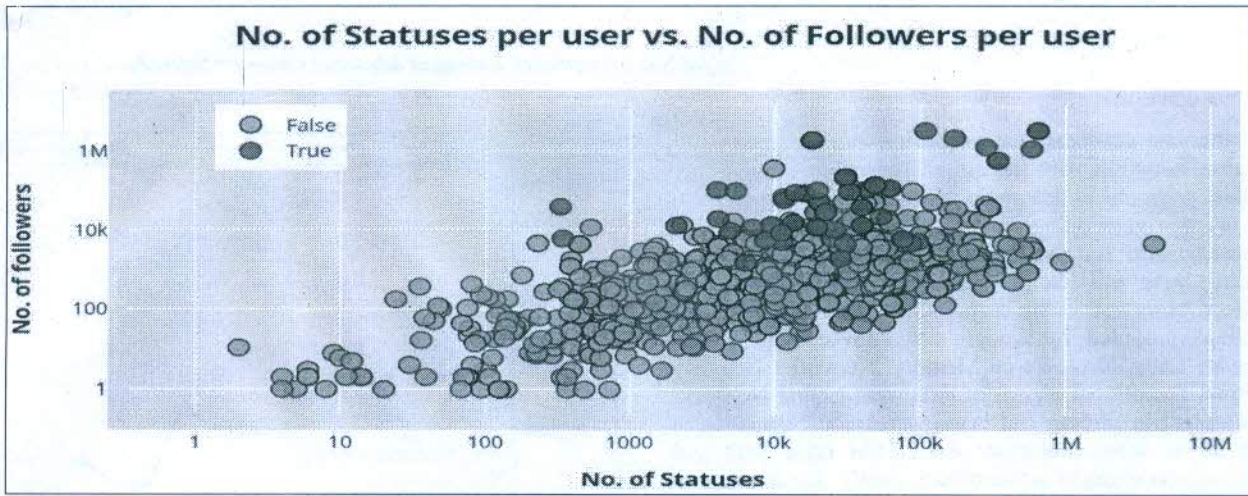


Fig. 7. No. of Statuses vs. No. of Followers.



Fig. 8. Wordcloud Showing Potential Aspects.

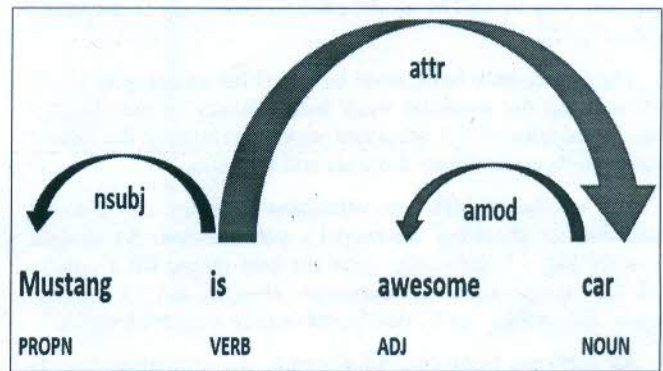


Fig. 10. Dependency Graph Example.

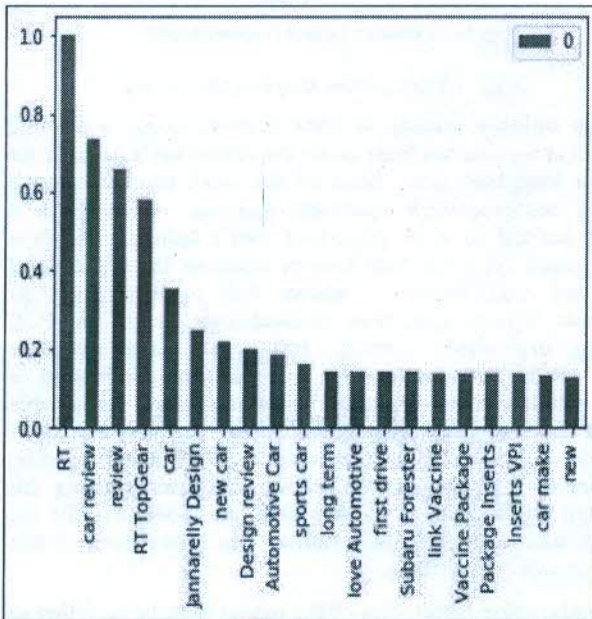


Fig. 9. Frequency Distribution of Potential Aspects.

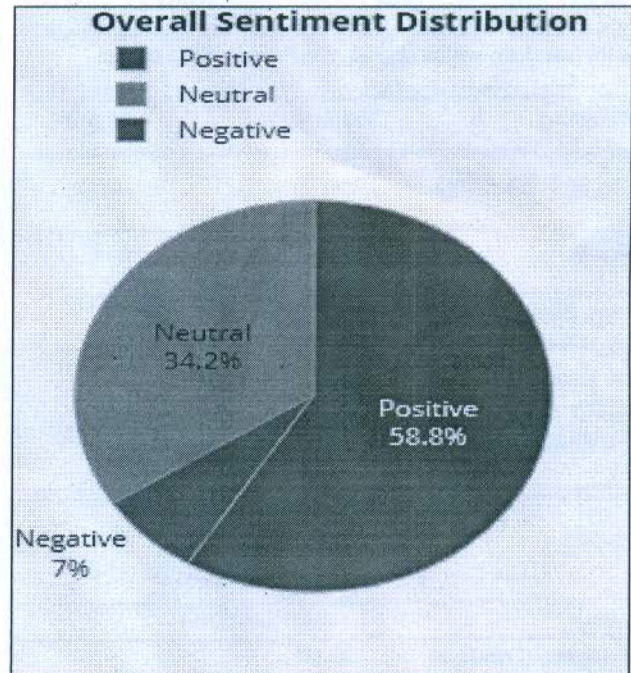


Fig. 11. Overall Sentiment Distribution.

An alternate sentiment categorization can be done using deep neural networks with the aid of TensorFlow and Keras. The model proposed in this paper is quite simple and contains three layers: embedding layer, a layer with LSTM functionality, and last but not least an output layer. The embedding layer will learn word embeddings for each, and every word contained in the corpus through pre-trained word embeddings provided by Google's word2vec. The second layer is of Long Short-Term Memory Networks (LSTM), which is an exceptional branch of Recurrent Neural Networks that are skilled in finding and learning relationships between features of an input sequence. An LSTM layer with 100 memory units is engaged in the model. Lastly, the dense layer provides uses a sigmoid activation function as it needs to classify the polarity of a tweet as either positive or negative. The summary of LSTM model used in this study is displayed in the Fig. 12.

The model once built, must be tested for accuracy to check if it is doing the intended work with efficacy or not. Table I lists the results of the proposed model, primarily the model score and its accuracy on the train and test data.

The validation loss and validation accuracy can also be identified for checking the model's performance. As evident from the Fig. 13, the model gave the best output till 5 epochs and then its performance decreases abruptly till 15 epochs. Hence, the epochs can be decreased to give a superior result.

As apparent from Fig. 14 beneath, the validation loss is quite high and hence the model overfits.

To conclude, the proposed model is evaluated for train and test data. The model shows 82% accuracy for training data but 99% for test data, which shows overfitting of the model.

Layer (type)	Output Shape	Param #
embedding_1 (Embedding)	(None, None, 100)	500000
lstm_1 (LSTM)	(None, 100)	80400
dense_1 (Dense)	(None, 1)	101
Total params: 580,501		
Trainable params: 580,501		
Non-trainable params: 0		

Fig. 12. Proposed Model's Summary.

TABLE I. RESULTS OF MODEL EVALUATION

Model Score	1.014088016230464
Model Accuracy (Train Data)	82.11%
Model Accuracy (Test Data)	99.95%

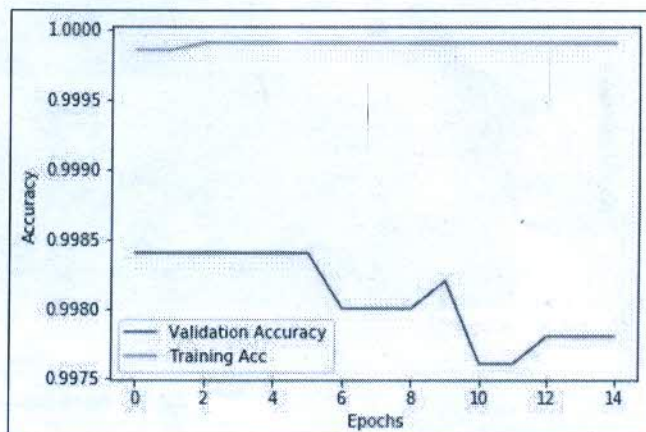


Fig. 13. Validation Accuracy of Proposed Model.

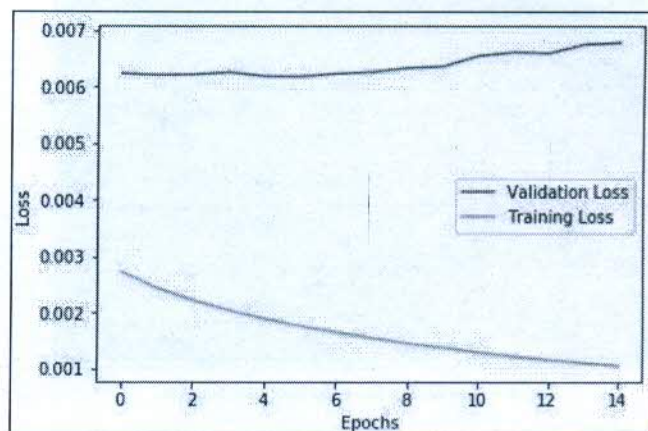


Fig. 14. Validation Loss of Proposed Model.

V. CONCLUSION AND FUTURE WORK

The opinion mining of user reviews about a specific product or service has been under the researcher's hammer for quite a long time now. Most of the work revolves around finding sentence-level sentiment analysis, which gives a bigger but not so clear picture of user's opinions. Hence a fine-grained approach that focuses more on the aspect-level sentiment classification is needed. This paper proposes an ensemble aspect extraction methodology based on POS tagging, dependency parsing, and dense neural networks which yields better outputs for sentiment analysis instead of using solo traditional methods. This research will be valuable for the individuals or commercial entities that may employ it for fine graining the existing users' opinion about specific features of their product or service and also targeting the potential customers. On the flip side, the model overfits the Twitter dataset under consideration. The future work of this research will be manifold.

Firstly, some parameters of the model must be modified to avoid overfitting. Secondly, several machine learning and deep learning classifiers can be employed for enhanced sentiment analysis. Finally, the most important prospect will be deploying it for more human languages like French, Spanish, Hindi or Tamil, etc.

REFERENCES

- [1] A. Gural, B. B. Cambazoglu, and P. Karagoz, Sentiment Focused Web Crawling, *CIKM'12, ACM Transactions on the web*, Maui, HI, USA, 2012.
- [2] O. Alqaryouti, N. Siyam, A. A. Monem, and K. Shaalan, Aspect-Based Sentiment Analysis Using Smart Government Review Data, *Applied Computing and Informatics*, 2019.
- [3] K. Bafna, and D. Toshniwal, Feature based summarization of customers' reviews of online products, In: *Proc. Comput Sci* 22, 2013, pp. 142–151.
- [4] Y. Zhang, and W. Zhu, Extracting implicit features in online customer reviews for opinion mining, In: *Proc. 22nd international conference on World Wide Web companion. International World Wide Web Conferences steering committee*, 2013, pp. 103–104.
- [5] R. Kumar, and R. Vadlamani, A Survey on Opinion Mining and Sentiment Analysis:Tasks, Approaches and Applications, *Knowledge Based Systems*, Vol. 89, No. 1, pp. 14-46, 2015.
- [6] P. More, and A. Ghotkar, A Study of Different Approaches to Aspect-based Opinion Mining, 2016.
- [7] B. Liu, and L. Zhang, A survey of opinion mining and sentiment analysis, In: *Proc. Mining Text Data. Springer US*, 2012, pp. 415–463.
- [8] A. M. Popescu, and O. Etzioni, Extracting product features and opinions from reviews, *Natural language processing and text mining. Springer*, pp. 9–28, 2007.
- [9] C. Quan, and F. Ren, Unsupervised product feature extraction for feature-oriented opinion determination, *Inf. Sci.* 272, pp. 16–28, 2014.
- [10] K. Liu, L. Xu, and J. Zhao, Co-extracting opinion targets and opinion words from online reviews based on the word alignment model, *IEEE Trans Knowl Data Eng.*, Vol. 27, No. 3, pp. 636–650, 2015.
- [11] G. Qiu, B. Liu, J. Bu, and C. Chen, Opinion word expansion and target extraction through double propagation, *Comput. Linguist*, Vol. 37, No. 1, pp. 9–27, 2011.
- [12] W. Jin, and H. H. Ho, A novel lexicalized hmm-based learning framework for web opinion mining, In: *Proc. 26th annual International Conference on Machine Learning*, 2009.
- [13] L. Rabiner, Predicting The Weather with Hidden Markov Models, [Blog], Retrieved from URL <http://guizzetti.ca/blogs/lenny/2012/04/predicting-the-weather-with-hidden-markov-models>, 2012.
- [14] L. Chen, L. Qi, and F. Wang, Comparison of feature-level learning methods for mining online consumer reviews. *Expert Syst Appl.*, Vol. 39, No. 10, pp. 9588–9601, 2012.
- [15] B. Ma, D. Zhang, Z. Yan, and T. Kim, An LDA and synonym lexicon based approach to product feature extraction from online consumer product reviews, *J Electron Commer Res.*, Vol. 14, No. 4, pp. 304–314, 2013.
- [16] F. Li, M. Huang, and X. Zhu, Sentiment analysis with global topics and local dependency, In: *Proc. Twenty-Fourth AAAI Conference on Artificial Intelligence*, 2010.
- [17] B. Liu, and L. Zhang, “A survey of opinion mining and sentiment analysis”, *Mining text data. Springer, Boston, MA*, pp. 415-463, 2012.
- [18] N. Zainuddin, A. Selamat, and R. Ibrahim, Hybrid sentiment classification on twitter aspect-based sentiment analysis, *Applied Intelligence*, Vol. 48, No. 5, pp. 1218-1232. 2018.
- [19] Y. Jin, Development of word cloud generator software based on python, *Procedia engineering*, Vol. 174, No. 1, pp. 788-792, 2017.

DESIGN AND SIMULATION OF A NOVEL STRUCTURE UWB PATCH ANTENNA

Ritu Yadav Research Scholar, Department of Electronics and Communication Engineering, Baba Mast Nath University Rohtak, Haryana

Dr. Anil Dudy, Assistant Professor, Department of Electronics and Communication Engineering, Baba Mast Nath University Rohtak, Haryana

Anil Kumar, Assistant Professor, CSE Department, TIT&S Engineering College, Bhiwani, Haryana
¹ritu12june@gmail.com*, ²anildudy@gmail.com and ³yadavanil82@gmail.com

Abstract

A new Ultra Wide Band (UWB) antenna is designed and simulated. Novel structure of patch antenna is able to provide broadband property of proposed design which is basic necessity for UWB application. The resonant frequency of antenna is observed at 10.6 GHz and 13.3 GHz with bandwidth 10.40 GHz to 10.75 GHz and 12.6 GHz to 13.9 GHz. Glass Epoxy substrate (FR4) with dielectric constant ($\epsilon_r = 4.4$), loss tangent ($\tan \delta$) equal to 0.02 has been used for the proposed patch antenna. The radiation pattern of purposed patch is broad side in direction of maximum radiation. Maximum gain observed by designed patch in operating range is 12.9 dB. With this, basic structure of patch antenna including working principle, basic feeding techniques, basic mathematical expression for calculating dimensions of patch are presented. Transmission line model for calculation the length and width of rectangular patch has been used which shows simplicity of fabrication and manufacturing. High Frequency Structure Simulator (HFSS) simulation platform is used for simulation. The simulation results in terms of return loss, Voltage Standing Wave Ratio (VSWR) and radiation pattern shows good agreement in performance.

Keywords: Bandwidth, Gain, Micro strip patch antenna, Radiation Pattern, Return Loss, VSWR.

Introduction

Concept of microstrip patch antenna was given by Bob Munson in 1950. But this concept of patch antenna did not come into picture till 1970. In 1970 with development of integrated circuits it was possible to fabricate patch antenna on a chip. In present time, from TV remote to fully automatic intelligent systems everything is wire free. To exchange a high volume of information with the help of electromagnetic waves a transducer is required which can convert information signal into electromagnetic waves and reverse. This transducer is known as 'antenna' which allows the devices to exchange information with the help of electromagnetic waves [1].

A variety of antenna are invented and used by researchers. But with time, it is observed that this antenna should be compact, ease to fabricate and cost should be less. These main objectives were fulfilled with the development of patch antenna.

A 'micro strip patch antenna' shown in Figure 1 consists of substrate, radiating patch and ground plane [2]. Patch antenna can be fabricated on printed circuit board. The lowest part is ground plane and the top most is patch. The substrate between ground plane and patch behaves as dielectric substrate. The distance between ground plane and patch behaves very important role in bandwidth of antenna [3]. A thicker substrate enhances gain but leads to surface wave excitation which disturbs the radiation pattern of antenna. The ground plane should extend beyond the edges of patch otherwise ratio of front to back wave can increases [3]. Increased dimensions of ground plane can increase the gain but diffraction at the edges increases and size of patch also increases which can reduce performance of patch antenna [4].

Main objective of this paper is to design a patch antenna for UWB application with wider bandwidth and acceptable performance in terms of acceptable return loss, VSWR, gain, directivity and bandwidth.

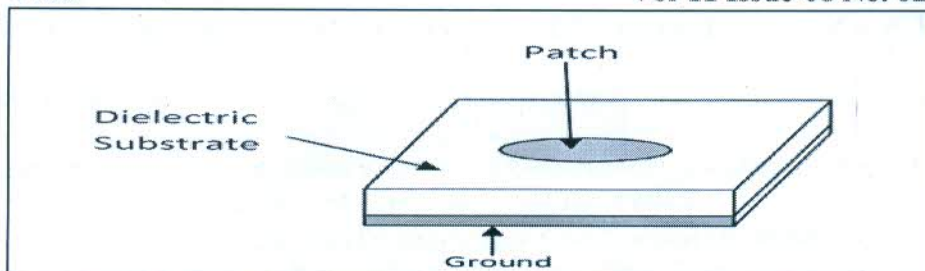


Figure 1. Structure of Micro Strip Patch Antenna

In this paper firstly basic working principle including various shapes of patch antennas, different feeding techniques, supporting literature review are discussed in brief. After basic concept of patch antenna adopted methodology is presented then designing of patch and simulation results are discussed. Followed by this conclusion and future scope is concluded in last.

Background

Basic working principle of antenna is fringing effect [4] as shown in Figure 2.

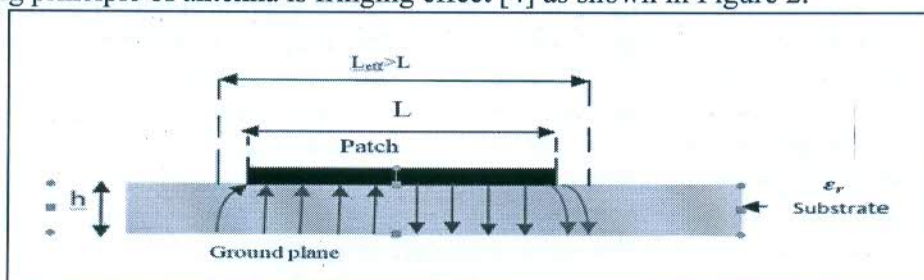


Figure 2. Fringing effect

Fringing occurs due to discontinuity observed by exciting current coming from feed line at the open end of feed line on patch. Due to this discontinuity value of current is minimum at the edges of patch while maximum current exists at the half of the length of the patch. This occurs because patch behaves as short circuited at the feeding point while it behaves as open circuited at the edges due to which maximum voltage +V exists at the edge while -V exists at the centre of patch due to fringing patch behaves as voltage radiator and starts radiating. Fringing effect allows patch to behave electrically wider compared to its dimensions [4]. EM waves pass through both air and substrate, due to which effective dielectric constant is to be introduced. This effective dielectric constant causes both fringing as well as wave transmission in the line.

Shapes of Microstrip Antenna

Various shapes of patch are designed and simulated by researchers. Different shapes of the microstrip patch attain the novel performance parameters.

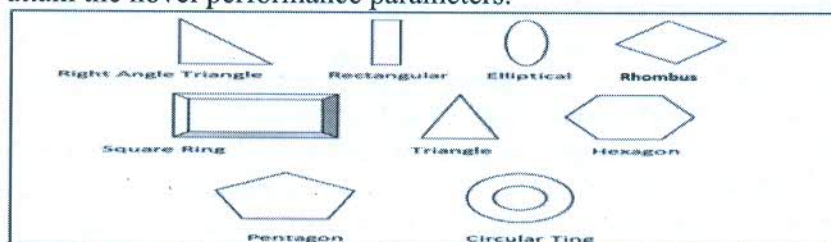


Figure 3. Basic shapes of Micro Strip Patch Antenna

So, to get the better and efficient one, the shape and dimensions of the microstrip patch must be defined properly. Basic shapes of the patch are shown in Figure 3 [5, 6].

Large number of physical parameters can characterize a patch antenna. Different shapes of patch with cuts and notches can affect the dimensions as well as performance of radiating patch. Thus a variety of patch antenna with different shapes can be designed and fabricated [6]. Length, width and thickness of radiating patch is calculated according to the operating frequency [7]. A variety of

substrate material with different values of permittivity and permeability can also affect the performance of patch antenna [8].

Feeding Patch Antennas

Feeding line through which radiating patch is excited also plays very important role in performance of patch antenna. Feeding line provides guided path from exciting origin up to radiating patch, so it is very important that input impedance of this feeding line should be matched with the impedance of radiating patch otherwise maximum of input will be reflected. Micro strip-line feed, Probe feed, Aperture coupled feed and proximity coupled feed are main kinds of feeding line [7].

Microstrip Line Feed

It is a feeding technique, microstrip feed line is directly connected with the microstrip patch. The size of the feed line is different than microstrip patch [8]. Microstrip line feed can be considered as extension of patch. The inset position can be adjusted to get the favorable results. It is simple to formulate and match. Spurious feed radiation limits the bandwidth of patch. The microstrip line feed is as shown in Figure 4.

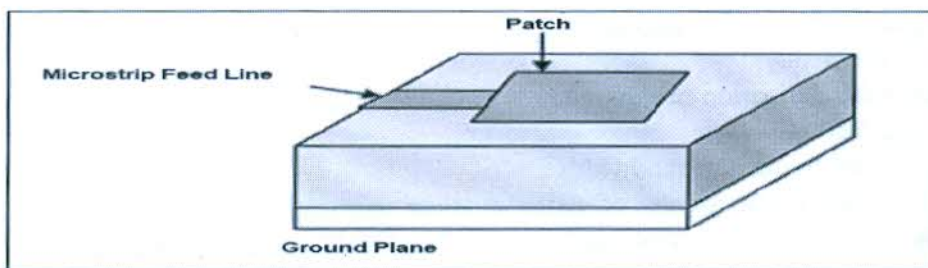


Figure 4. Microstrip Feed Line

Coaxial Probe Feed

In this feeding technique, central conductor of coaxial cable is linked to the microstrip patch of an antenna and external one is connected with ground plane [9]. Frequently the feed networks are cut off from the microstrip patch. Spurious radiation minimization, simple fabrication and competent feeding are the reward of coaxial feeding method. The coaxial probe feed is as shown in Figure 5.

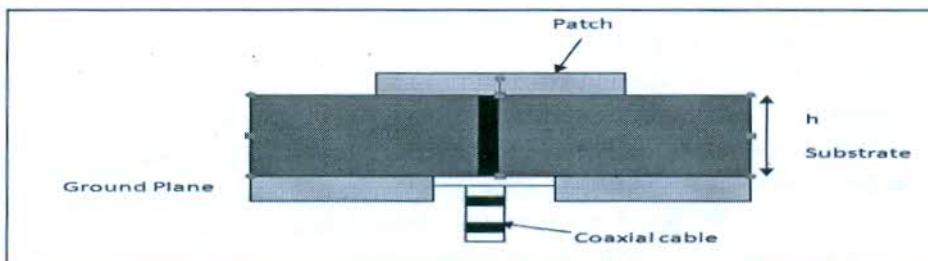


Figure 5. Coaxial Probe Feed

Aperture – Coupled Feed

This technology is having two substrates, which are dissimilar from each other and are alienated by a ground plane [10]. In this technique, the microstrip patch and feed line are united through a slot in the ground plane. Unadulterated polarization is the compensation of aperture coupled feeding method as shown in Figure 6.

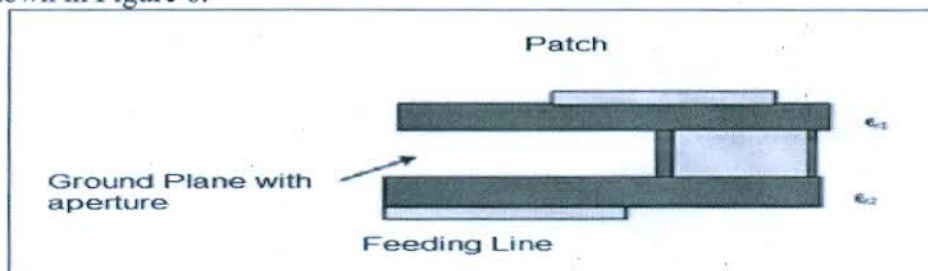


Figure 6. Aperture Feed Line

Researchers have simulated and proved how this feeding line can be optimized to get favorable results. According to requirement operating frequency or frequency on which antenna should resonant is selected. A huge area of wireless communication system is deploying microstrip patch antenna at the transmitting as well as at the receiving end.

Advantages of Microstrip patch Antennas [11, 12]

- Due to simple mathematical calculations microstrip patch antennas are low profile configurable.
- Uncomplicated and reasonably priced to fabricate using contemporary printed-circuit technology.
- Mechanically vigorous when mounted on firm surface.
- Patch shape is intended for flexible significant frequency, polarization, prototype, and impedance.
- Accumulation loads among the patch and the ground plane, (such as pins and varactor diodes), changeable resonant frequency, impedance, polarization, and prototype can be intended.

Disadvantages of Microstrip Antenna [11, 12]

- Squat efficiency.
- Reduced polarization transparency.
- Forged feed radiation.
- Contracted frequency bandwidth.

Due to mentioned shortcomings of patch antenna application of patch antenna is very limited. Researchers have introduced many solutions to these challenges like impedance matching devices, increasing the thickness of substrate, adding metamaterial with patch antenna [13] but again this enhances the complexity and cost of patch antenna [14].

Literature review

According to Ashish Kumar et.al thickness and dielectric constant of substrate governs the performance of a patch antenna. In this paper author has designed a rectangular patch antenna for resonating frequency 2.4 GHz and optimization is done by varying dielectric constant and substrate thickness. It is observed that decreased dielectric constant increases the bandwidth but size gets increased. So an optimization is done at three levels [15].

Satish Kumar et.al designed a rectangular patch for 5.6 GHz on simulation tool HFSS. Microstrip feeding line is used to excite the designed patch. FR4 epoxy substrate with dielectric constant 2.4 is chosen. Simulation results conclude that simple compact shape of patch can serve acceptable performance of patch antenna if dielectric constant is increased and height is decreased wisely [16].

A.A. Deshmukh et.al has designed a microstrip slotted antenna for wireless communication. A slotted E shape patch is designed with probe feeding technique on HFSS simulator. It is concluded that slots in patch is providing 30.3% bandwidth [17].

Norbahiah et.al purposed and designed a slotted patch antenna on simulator HFSS, operating between 1.56 GHz to 2.12 GHz. It is concluded that slots in patch gives novelty to the structure as well as high bandwidth is achieved [18].

F. Yang et.al designed E shaped patch antenna simulating on 1.9 GHz and 2.4 GHz. Bandwidth 21.2% and 32.3% bandwidth is covered by E-shaped patch antenna [19].

Author work by M. Abbaspour et.al has purposed a star-shaped patch antenna for frequency range from 4.0 to 8.8 GHz. 81% of bandwidth is reported [20]

A brilliant paper by F.Jolani et.al has designed a M-slot folded patch antenna. This folded patch provided 21.17% bandwidth [21].

M.T. Isalam et.al designed a H shaped patch antenna. Results conclude purposed patch achieves bandwidth from 1.76 GHz to 2.38 GHz [22].

X. L. Bao et.al purposed a plus shaped antenna and 53% of bandwidth is offered by this shape of patch [23].

M. Albooyeh et.al purposed and designed a cross shaped patch antenna and 6.49% bandwidth is achieved [24].

Above reported paper motivates to design a novel structure of patch antenna for higher frequencies with better bandwidth and more than one resonating frequency.

In this paper a unique structure of patch simulating at higher frequency greater than 10 GHz with microstrip feeding line on Epoxy FR4 substrate is designed. Results are optimized to achieve wide bandwidth so that it can be applicable for ultra wide band applications. Purposed patch is designed and simulated on HFSS simulator. To analyze performance of this design basic performance plots obtained from simulator are presented and discussed.

Methodology

Operating frequency 10 GHz and FR4 Epoxy substrate with dielectric constant 4.4 and height 1.6 mm is chosen. A Transmission line model is used for calculation of dimensions of patch antenna [6, 7].

Step 1: Width of Patch Antenna

The width of patch antenna is calculated using the equation (1) [6]

$$W = \frac{C_0}{2f_r} \sqrt{\frac{2}{\epsilon_r + 1}} \dots\dots\dots (1)$$

Where, W= Width of the patch, Co= Speed of light, εr = value of the dielectric substrate and fr is resonating frequency for which patch antenna is to be designed.

Step 2: Effective Refractive Index: εreff

Effective refractive index is a very important parameter for designing a patch antenna. It is responsible for the propagation of wave in the air as well as in the patch [6, 7].

$$\epsilon_{reff} = \frac{\epsilon_{reff} + 1}{2} + \frac{\epsilon_{reff} - 1}{2} \left[1 + 12 \frac{h}{w} \right]^{1/2} \dots\dots\dots (2)$$

Step 3: Length:

Due to fringing, electrically the size of the antenna is increased by an amount of (ΔL). Therefore, the actual increase in length (ΔL) of the patch is to be calculated using the following equation [3, 5, 6].

$$\frac{\Delta L}{h} = 0.412 \frac{(\epsilon_{reff} + 0.3) \left(\frac{w}{h} + 0.264 \right)}{(\epsilon_{reff} - 0.258) \left(\frac{w}{h} + 0.8 \right)} \dots\dots\dots (3)$$

Where ‘h’= height of the substrate The length (L) of the patch is now to be calculated using the below mentioned equation [3, 5, 6].

$$L = \frac{C_0}{2f_r \sqrt{\epsilon_{reff}}} - 2\Delta L \dots\dots\dots (4)$$

Step 4: Length (Lg) and Width (Wg) of Ground Plane:

Now the dimensions of a patch are known. The length and width of a substrate is equal to that of the ground plane. The length of a ground plane (Lg) and the width of a ground plane (Wg) are calculated using the following equations [7]:

$$L_g = 6h + L \dots\dots\dots (5)$$

$$W_g = 6h + W \dots\dots\dots (6)$$

Result and Discussion

Novel Structure of Patch Antenna:

Using above equations from 1 to 6 following novel structure of patch is designed at resonance frequency 10 GHz. Calculated Length and breadth of rectangular patch are 9.1 mm and 6.4 mm respectively. Figure 7 shows basic designing shapes used to design novel patch geometry.

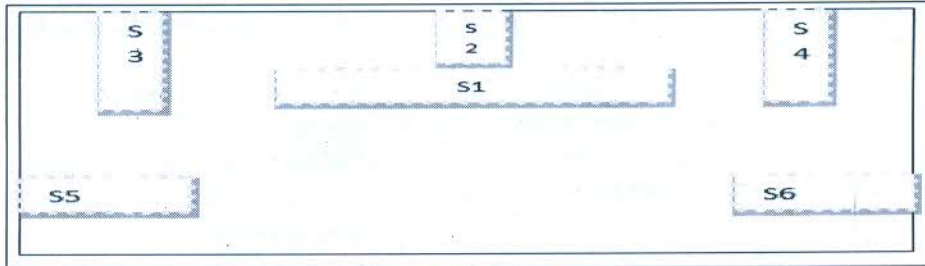


Figure 7. Layout of patch

In first simple rectangular patch is designed then small sub rectangle are designed and subtraction of these sub rectangle from main rectangle is done to achieve the desired shape of patch on HFSS as shown in Figure 8. Dimensions of sub rectangles are shown in table 1.

Table No.1: Dimensions of sub rectangle

Rectangle	X size in mm	Y size in mm
S1	3.5	0.5
S2	1	0.5
S3	0.5	1.5
S4	0.5	1.5
S5	1.5	0.5
S6	1.5	0.5

After subtraction following patch is developed on HFSS simulation tool as shown in Figure 8. Glass Epoxy substrate FR4 with height 1.6 mm is selected for simulation.

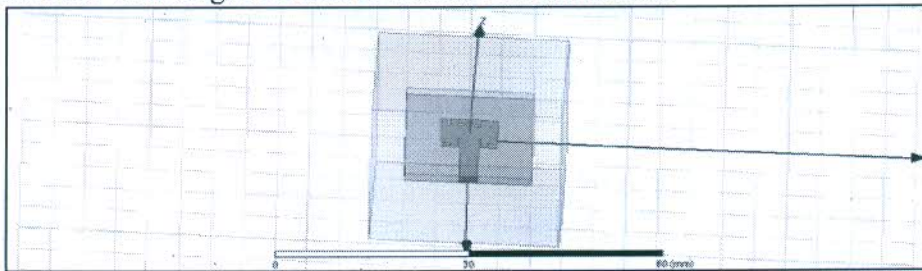


Figure 8. Novel Structure of Patch Antenna

Microstrip feed line with length 10 and width 3mm is adopted to feed the designed patch. After designing simulation is done on the same simulation tool i.e. HFSS. Following graphs are obtained to analyze the performance of designed novel patch.

Gain

Gain of an antenna is closely related to directivity of antenna. It counts efficiency as well as directional capabilities [15]. Gain of an antenna (in a given direction) is defined as “the ratio of the intensity, in a given direction, to the radiation intensity that would be obtained if the power accepted by the antenna were radiated isotropically” [6, 7].

$$\text{Gain, } G = 4\pi \frac{\text{Radiation intensity}}{\text{Total accepted input power}} \dots\dots\dots (7)$$

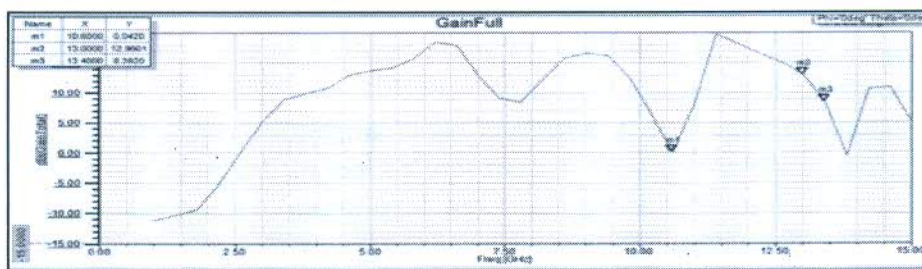


Figure 9. Simulation Graph between Gain vs. Frequency

Simulated graph for gain of designed patch in Figure 9 shows that at 10.6 GHz gain is 0.0420 dB while at 13.4 GHz it is 8.390 dB. Gain in positive range is considered acceptable range.

Return Loss

Return loss gives how well the device is matched [16]. It shows how much power is reflected when discontinuity between guided medium and air takes place. It is also known as constant of reflection constant [6].

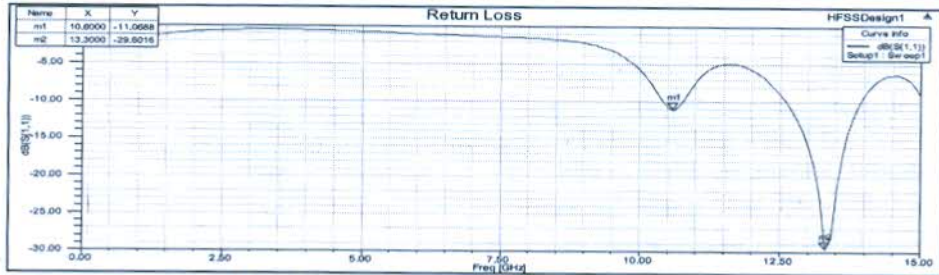


Figure 10. Simulation Graph between S(1,1) vs. Frequency

Simulation result shows graph between S (1, 1) vs. frequency range shown in Figure 10. The downfall of graph shows that patch antenna is resonating at two frequencies i.e. 10.6 GHz with return loss -11.0688 and at 13.3 GHz with return loss -29.6016, which shows that purposed patch is resonating at 10.6 GHz and at 13.3 GHz, so this patch antenna can be used for UWB application like satellite communication, inter space communication and downlink transmission.

Radiation Pattern

Radiation patterns also known as near field pattern or Fresnel pattern this refers to the positional reliance of the electromagnetic field in the near field [9, 10]. The near-field pattern is most commonly defined over a plane placed in front of the source, or over a cylindrical or spherical surface enclosing it [8].

Radiation pattern of designed patch is shown in Figure 11 and this shows maximum radiation along Z- axis.

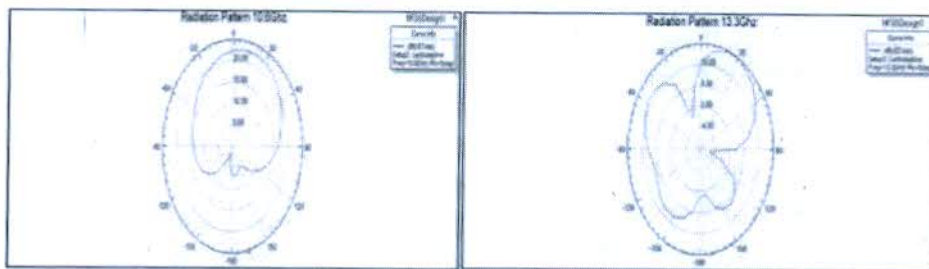


Figure11. Radiation Pattern of Designed Patch Antenna at 10.6 GHz and 13.3 GHz.

Radiation pattern of designed patch shows that at resonating frequency 10.6 GHz patch antenna is radiating in broad side with 45 degree 3 dB beam width, while at 13.3 GHz radiation pattern shows maximum gain at 30 degree and beam width of 50 degree is observed.

Voltage Standing Wave Ratio (VSWR)

Voltage Standing Wave Ratio gives ratio of reflected wave to the transmitted wave between two different medium [7, 8]. VSWR is function of reflection coefficient. It is related to return loss by formula [7].

$$VSWR = \frac{1+\Gamma}{1-\Gamma} \dots\dots\dots (8)$$

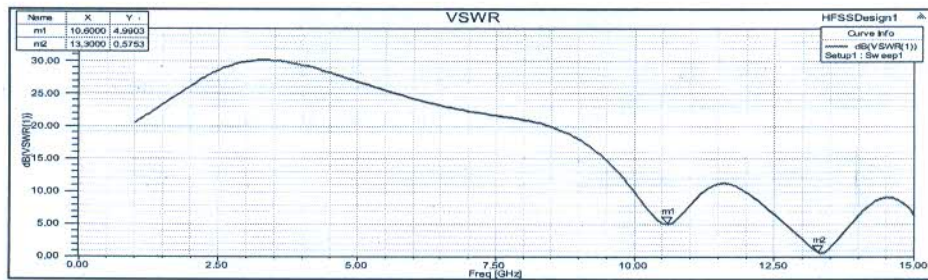


Figure 12. Simulation Graph between Frequency vs VSWR

Simulation graph shown in Figure 12 is drawn between VSWR vs. frequency. Graph shows at frequency 10.6 GHz VSWR is 4.9 dB and at frequency 13.3 GHz it is 0.575 dB. Value of VSWR at 10.6 GHz needs to be optimized while at 13.3 GHz a good value of VSWR is observed.

Bandwidth

Bandwidth shows the frequency range over which return loss is unacceptable range. In this range performance of antenna is in favorable condition and patch antenna can be used for the particular application. Generally frequency range having return loss less than -10db is considered as bandwidth of that particular microstrip patch antenna [11, 12].

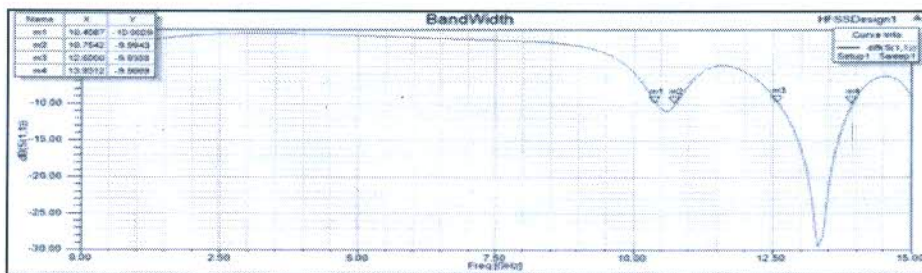


Figure 13. Simulation graph between Frequency vs S(1,1)

Simulation Results shown in Figure 13 shows bandwidth of .35 GHz with frequency range from 10.4 GHz to 10.75 GHz and bandwidth of 1.3 GHz is observed from 12.6 GHz to 13.9 GHz with return loss approximate -10db.

Conclusion and Future Scope

In this paper need of microstrip patch, its basic structure, basic feeding methods with advantages and disadvantages of microstrip patch antenna is discussed. A microstrip patch antenna for UWB frequency range has been successfully designed and simulated. All simulation results are summarized in table 2. Results show that it is a multi frequency operated antenna because it is resonating at two frequencies i.e. at 10.6 GHz and 13.3 GHz with return loss -11.06 dB and -29.6 dB respectively. A bandwidth of .35 GHz from 10.40 GHz to 10.75 GHz and 1.3 GHz from 12.60 GHz to 13.93 GHz has been confirmed at these two resonating frequencies. VSWR of purposed antenna at 10.6 GHz and 13.3 GHz is 4.9 db and 0.5 dB respectively.

Table No.2: Coefficients Simulated Results of purposed patch

Resonant frequency	10.6 GHz	13.3 GHz
Gain	0.04 dB	8.39 dB
Return loss	-11.06 dB	-29.06 dB
VSWR	4.9 dB	0.50 dB
Bandwidth	0.35GHz(10.4 GHz-10.75)	1.3 GHz(12.6 GHz-13.9 GHz)

A broad bandwidth is observed because of presence slots in the patch. Unique structure of patch allows this design to be multi frequency operated. In future performance of this patch can be enhanced with the aid of impedance matching devices or with the aid of metamaterial structures.

References

- [1] K. L. Wong, (1999), "Design of Nonplanar Microstrip Antennas and Transmission Lines", New York Wiley.
- [2] S. L. Latif, L. Shafai, (2005), and S. K. Shaema, "Bandwidth enhancement and size reduction of microstrip slot antenna," IEEE Trans. Antennas Propag., vol. 53, no. 3, pp. 994–1003.
- [3] I. J. Bahl and P. Bhartia, (1980), "Microstrip Antennas", Artech House
- [4] J. Q. Howel, (1972) ,"Microstrip antennas," in Proceedings of the Digest of the International Symposium of the Antennas and propagation Society, pp. 177–180.
- [5] R. H. Thaher and S. N. Alsaidy, (2016), "Design of Novel Wideband CPW Irregular Pentagonal Patch Antenna", International Journal of Computer Applications (0975 – 8887) Volume 139 – No.4, April pp.31-37.
- [6] C. A. Balanis, (2016) , "Antenna Theory: Analysis and Design", February 4th Edition.
- [7] W. L. Stutzman and, G. A. Thiele. (2012), "Antenna Theory and Design", 3rd Edition, Wiley Publications May.
- [8] J. R. James, P. S. Hall, and C. Wood, (1981), "Microstrip Antenna Theory and Design", Peter Peregrinus,.
- [9] G. Ramesh, (2001) "Microstrip Antenna Design Handbook", Artech House, Inc.
- [10] R. Garg, I. Bhartia, I. Bahl, and A. Ittipiboon, (2001), "Micro-Strip Antenna Design Handbook", Artech House, Boston, Mass, USA.
- [11] K. L. Wong, (2002) ,"Compact and Broadband Microstrip Antennas". New York: Wiley.
- [12] D. M. Pozar and B. Kaufman, (1987), "Increasing the bandwidth of a microstrip antenna by proximity coupling," Electronics Letters, vol. 23, no. 8, pp. 368–369.
- [13] R. Yadav and A. Dudy, (2020), "Performance analysis of microstrip patch antenna with aid of metamaterial", An International Conference on Cloud Computing (ICC-2020)",pp. 153-161.
- [14] H. F. Pues and A. R. Capelle, (1989), "Impedance-matching technique for increasing the bandwidth of microstrip antennas," IEEE Transactions on Antennas and Propagation, vol. 37, no. 11, pp. 1345–1354.
- [15] Ashish Kumar, Bimal Garg , (2011), "Rectangular Microstrip Patch Antenna Loaded With Double Orthogonal Crossed Slits In Ground Plane", International Journal of Advance Technology & Engineering Research, pp 675-702.
- [16] Sathish kumar , Arthika , Indhu , Elakkiya, (2020), "Design and Study of Rectangular Micro strip Patch Antenna for WLAN Applications", International Journal of Advanced Science and Technology Vol. 29, No. 7, pp. 3554-3558.
- [17] A. A. Deshmukh and K. P. Ray, (2009), "Compact broadband slotted rectangular microstrip antenna", IEEE Antennas and Wireless Propagation Letters, vol. 8, pp. 1410–1413.
- [18] Norbahiah Misran, Mohammed N. Shakib, Mohammad T. Islam, and Baharudin Yatim , (2009) ,"Design Analysis of a Slotted Microstrip Antenna for Wireless Communication", World Academy of Science, Engineering and Technology 49.
- [19] F. Yang, X. Zhang, Y. Rahmat-Samii, (2001) ,"Wide-band E-shaped patch antennas for wireless communications", IEEE Trans. Antennas Propag., vol. 49, pp. 1094-1100.
- [20] M. Abbaspour and H. R. Hassani, (2008) ,"Wideband star-shaped microstrip patch antenna", Progress in Electromagnetics Research Letters, vol. 1, pp. 61–68.
- [21] F. Jolani, A. M. Dadgarpour, and H. R. Hassani, (2008), "Compact M slot folded patch antenna for WLAN", Progress in Electromagnetics Research Letters, vol. 3, pp. 35–42.
- [22] M. T. Islam, M. N. Shakib, and N. Misran, (2009), "Broadband E-H shaped microstrip patch antenna for wireless systems", Progress in Electromagnetic Research, vol. 98, pp. 163–173.
- [23] X. L. Bao and M. J. Ammann, (2007), "Small patch/slot antenna with 53 input impedance bandwidth", Electronics Letters, vol. 43, no. 3, pp. 146–148.
- [24] M. Albooyeh, N. Komjani, and M. Shobeyri, (2008), "A novel cross slot geometry to improve impedance bandwidth of microstrip antennas", Progress in Electromagnetic Research Letters, vol. 4, pp. 63–72.

**DESIGN AND SIMULATION OF RECTANGULAR SPLIT RING RESONATOR
STRUCTURE OF METAMATERIAL**

Ritu Yadav Research Scholar, Department of Electronics and Communication Engineering, Baba Mast Nath University Rohtak, Haryana

Dr. Anil Dudy, Associate Professor, Department of Electronics and Communication Engineering, Baba Mast Nath University Rohtak, Haryana

¹ritu12june@gmail.com*, ²anildudy@gmail.com

Abstract

Based on a microstrip line loaded split ring resonator (SRR), a design of left handed metamaterial (LHM) unit cell has been presented. Using High Frequency System Simulator (HFSS), the unit cell is adjusted to have a negative return loss. In this paper Unit cell of rectangular Split Ring Resonator (RSRR) with microstrip structure is designed and simulated to construct metamaterial unit cells, which are novel artificial materials with a periodic layout much smaller than the guided wavelength and are appropriate for use in satellite communications. Over the frequency range of 15 GHz to 17 GHz, the proposed unit cell has a negative phase of return loss. Based on the S parameters recovered from a full wave simulator, a detailed step-by-step approach for getting the material parameters of a metamaterial structure is described in this work (HFSS).

Keywords: Floquet Plot, HFSS, Metamaterial, Return Loss, SRR

Introduction

To obtain an efficient antenna, the use of the unique features of Metamaterials [3] in small antennas is attempted. Veselago was the first to introduce Metamaterials in 1967. Metamaterials are materials that have been created by humans. Metamaterial is named after the Greek word Meta, which means "above/beyond/superior," since it has qualities that go beyond those of naturally occurring materials. The structural average cell size in Metamaterials is less than the guided wavelength. Its qualities are derived from its structure rather than from its composition. It's made up of a mix of metals and dielectric composite. The use of metamaterial structures in patch antennas has the advantage of improving antenna parameters such as gain and efficiency while also reducing antenna size for ease. Metamaterials are man-made materials with properties such as negative permittivity, negative permeability, and refractive index that aren't found in commonly used materials. Metamaterials have a -ve refractive index, which is the inverse of Snell's law, and are hence known as -ve index materials. The group and phase velocities of electromagnetic waves appear in the opposite direction due to the -ve refractive index, hence the propagation direction is reversed with regard to the energy flow direction. Negative μ_r and ϵ_r are found in nature, but not at the same time. When both μ_r and ϵ_r are negative, negative refraction can be achieved.

In the previous decade, a large number of publications have looked at the theoretical aspects and several key applications of Metamaterials in the microwave, terahertz, and optic domains [1-6]. Magnetic resonators of the split ring resonator (SRR) type are one of the most common metamaterial structures with negative permeability over restricted frequency bands. Although many types of SRR structures have been shown to be effective in narrowband applications, Metamaterials research has recently focused on the design of multiband and/or frequency adjustable Metamaterials. Park et al. [2] proposed the defective ground structure in 1999, based on the idea of photonic band-gap (PBG) structure and it has since been used in the construction of planar circuits and low pass filters [1-3]. The etching of a defective pattern in the ground plane causes the shield current distribution in the ground plane to be disrupted, resulting in a defective ground structure. This disruption has the potential to cause alter the equivalent capacitance and inductance of a transmission line to get the band-stop property and the slow-

wave effect. Split-ring resonators (SRRs) have been used to fabricate left-handed metamaterial (LHM) and build planar circuits with great success. Pendry et al. exhibited negative permeability around the resonance frequency of an array of SRRs [4]. The electromagnetic resonances in solo and coupled splitting resonators are investigated experimentally and numerically by Gay-Balmaz et al [5]. Markos et al. [6] studied the effect of ring thickness, inner diameter, radial and azimuthal gap, as well as the electrical permittivity of the board and the embedding medium on the resonance frequency of a periodic array of SRRs . In microstrip technology, Bonache et al. discovered the use of complementary circular split-ring resonators in the creation of compact narrow band-pass devices [7].

In this paper a two ring of Rectangular Split Ring Resonator (RSRR) is proposed with a microstrip structure on FR4 Epoxy substrate with height 0.25 mm. With this design of metamaterial unit cell, simulation and analysis of proposed rectangular SRR is discussed in following sections of this paper.

Design of Metamaterial Unit Cell

The description of the selected metamaterial structure, the design calculation of the unit cell structure, and the design and simulation results of the metamaterial unit cell with varied dimensions to see the influence of variations on the frequency region and the LHM property are all included here. Figure 1 depicts a schematic representation of the proposed multi-ring unit cell.

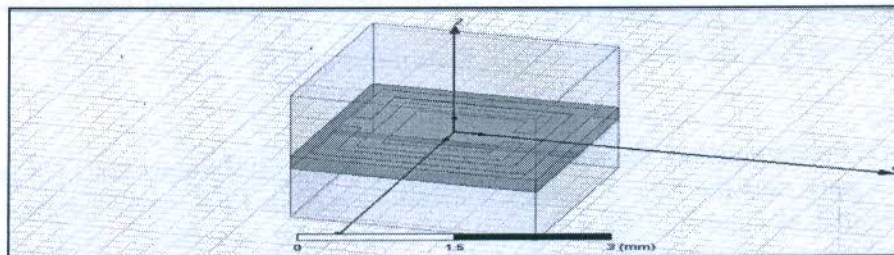


Figure 1. Simulation Setup of Purposed Unit Cell

For this research, the geometry and dimensions were chosen to be broadly compatible with earlier investigations. The unit cell is cubic, having a $d=2.5$ mm cell dimension. The loss tangent of 0.02 is considered for a 0.25 mm thick FR4 ($\epsilon=4.4$) substrate. On opposite sides of the substrate, a copper SRR and wire are installed. Copper has a thickness of 0.017 mm. The wire is 0.14 mm in width and runs the length of the unit cell. The SRR's outer ring measures 2.2 mm in length, with a line width of 0.2 mm on both rings. Each ring has a 0.3 mm gap, with a 0.15 mm gap between the inner and outer rings.

Simulation of Unit Cell and Analysis

The Simulation of Metamaterial unit cell is offered in this section.

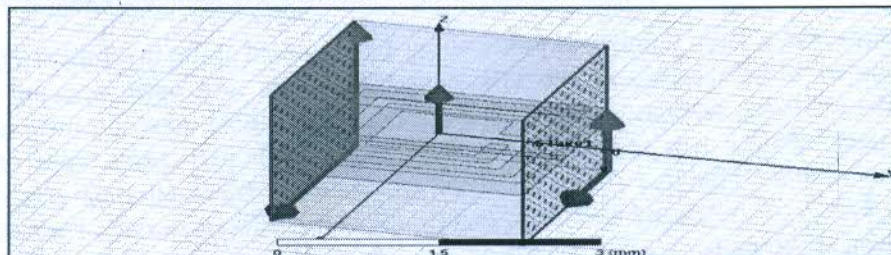


Figure 2. Simulated Model of First Master Slave Condition

Figure 2 shows the simulated assigned master 1 and slave 1 phase to excite the proposed unit cell without feeding line.

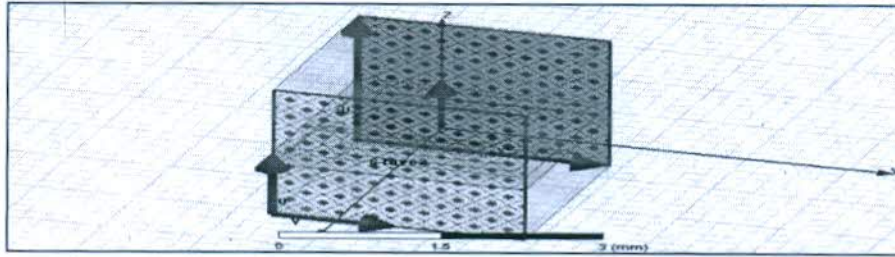


Figure 3. Simulated Model of Second Master Slave Condition

Figure 3 shows simulated second master and slave phase of proposed unit cell of rectangular SRR structure. To analyze the performance of designed unit cell without feeding line it is mandatory to assign master and slave boundary to the designed unit cell.

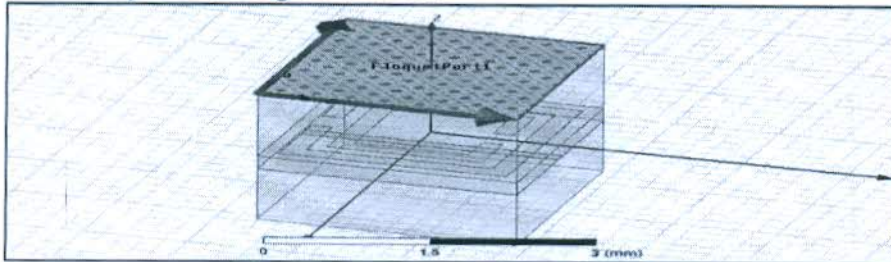


Figure 4. Assigned Floquet port 1

Figure 4 shows simulated assigned floquet port 1 on HFSS simulator with perfect E condition. After setting master slave condition second mandatory condition is to assign floquet port with either perfect electric or perfect magnetic condition.

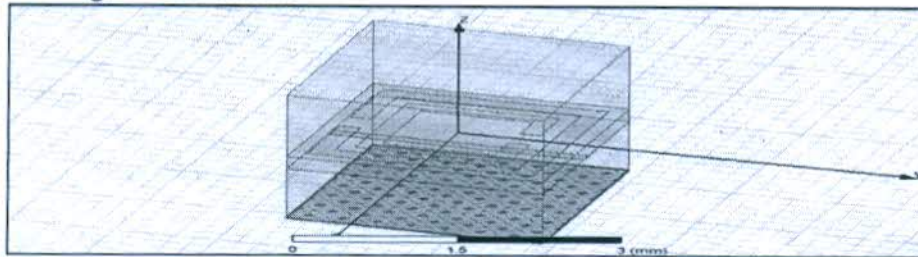


Figure 5. Assigned Floquet port 2

Figure 4 and 5 shows simulated assigned floquet port 1 and 2 of proposed unit cell of rectangular SRR structure.

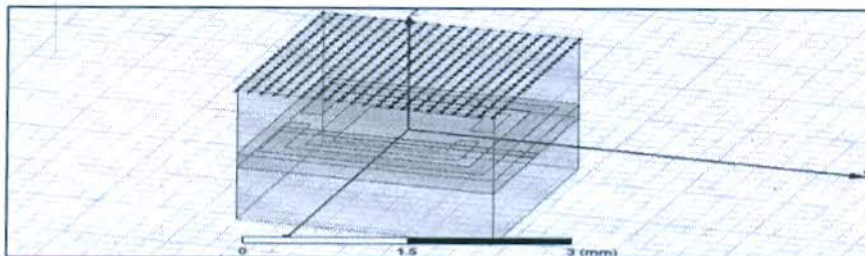


Figure 6. Distribution of current on first phase

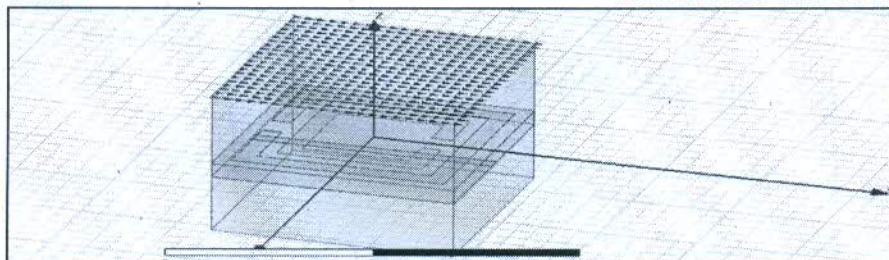


Figure 7. Distribution of current on first phase

Figure 6 and figure 7 shows simulation of distribution of phase current in two directions on first assigned port in HFSS simulator. Simulated images show that all boundary conditions are properly assigned.

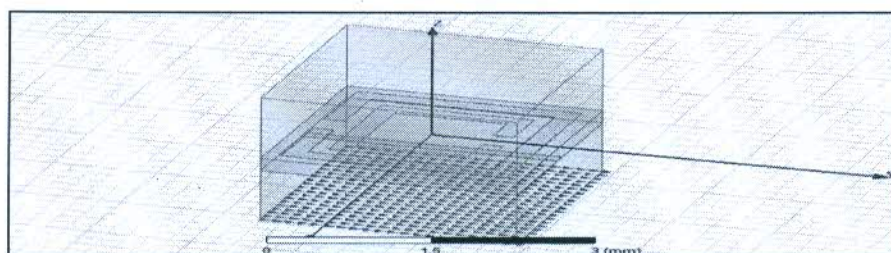


Figure 8. Distribution of Current on Second Phase

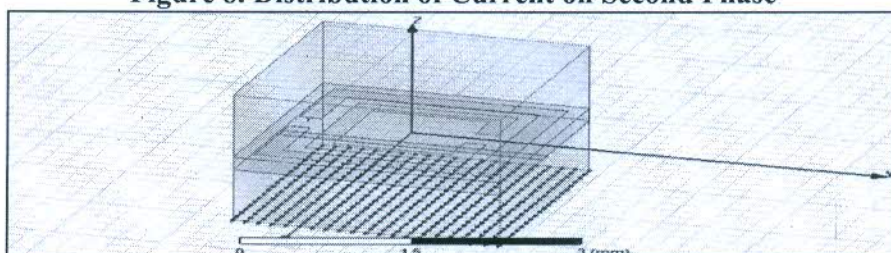


Figure 9. Distribution of Current on Second Phase

Figure 8 and 9 shows distribution of current on second phase. After setting the boundary condition the designed patch is excited and Floquet plot for port 1 and port 2 is drawn.

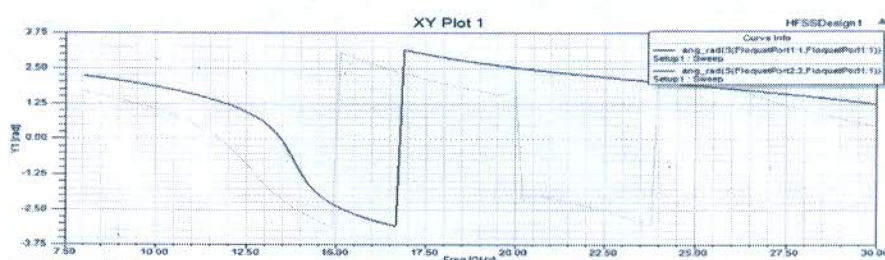


Figure 10. Angular Radian of S Parameter for port 1 and port 2

Simulated graph between S parameter vs. frequency is shown in figure 10. Simulated plot graph shows presence of negative S parameter in frequency range 15 GHz to 17 GHz. The "Floquet port" may imitate waves that are obliquely incident [8]. This obliquely incident wave is useful in instances where the incident wave's propagation direction coincides with the periodicity direction. The percentage of energy transported is provided by Floquet Port.

Conclusion and Future Scope

In this paper a rectangular split ring resonator with strip structure is designed. After assigning the boundary conditions floquet plot for port (1, 1) and for port (2, 2) is drawn to retrieve the S parameter properties. Negative phase of S parameter is observed between 15 GHz to 17 GHz. Presence of negative phase of S parameter indicates presence of negative refractive index. So proposed design is attaining the unusual electromagnetic properties and it can be adopted with microstrip patch antenna to provide enhanced performance of patch antenna for the application of satellite communication.

References

- [1] Yablonovitch, E., T. J. Gmitter, and K. M. Leung,(1991), "Photonic band structure: The face centered cubic case employing non-spherical atoms," *Physical Review Letters*, Vol. 67, No. 17, 2295–2298.
- [2] Park, J. I., C. S. Kim, J. Kim, et al.,(1999), "Modeling of a photonic band gap and its application for the low-pass filter design," Singapore: Asia Pacific Microwave Conference.
- [3] Kim, C. S., J. I. Park, A. Dal, et al.,(2000) ,"A novel 1-D periodic defected ground structure for planar circuits," *IEEE Microwave Guided Wave Lett.*, Vol. 10, No. 4, 131–133.
- [4] Pendry, J. B., A. J. Holden, D. J. Robbins, et al.,(1999) ,"Magnetism from conductors and enhanced nonlinear phenomena," *IEEE Trans. Microwave Theory Tech.*, Vol. 47, No. 11, 2075–2084.
- [5] Gay-Balmaz, P. and O. J. F. Martin,(2002), "Electromagnetic resonances in individual and coupled split-ring resonators," *Journal of Applied Physics*, Vol. 92, No. 5, 2929–2936.
- [6] Markos, P. and C. M. Soukoulis, (2002) "Numerical studies of left-handed materials and arrays of split ring resonators," *Physical Review E.*, Vol. 65, 036622-1–036622-8.
- [7] Bonache, J., F. Martin, F. Falcone, et al., (2005), "Application of complementary split-ring resonators to the design of compact narrow band-pass structures in microstrip technology," *Microwave and Optical Technology Letters*, Vol. 46, No. 5, 508–512.
- [8] HFSS TM, (2010), "Getting Started with HFSS: Floquet Ports," Technical Report.

“Corporate Social Responsibility – Buzzword for Business”

*Satish Khatak

Assistant Professor, ECE Department, TIT&S, Bhiwani.

**Monika Sharma

Assistant Professor, Management Department, TIT&S, Bhiwani.

Abstract

There is a growing investigation in all the aspects of ethics and CSR that manage the events of an organization and the corporate culture that encourage their business activities. It is very much desirable that we should take all the activities of business in association of ethics and performing corporate social responsibilities of business which prove advantage for the growth of the society. In our paper we have focused the concepts of Business Ethics as well as Corporate Social Responsibility with a perspective that notably CSR should be seen in the framework of an overall pattern of Business Ethics. Organizations now-a-days pays attention to their CSR activities through the framework of the stakeholder theory of the firm and put forward that CSR as practiced today is a breaking up of Business Ethics with other dimensions of an overall ethics framework still uncovered.

Keywords: CSR, Business Ethics, Corporate Culture.

Introduction

Business Ethics covers the zones of good standards and dynamic, administration issues and sets of accepted rules for a business. Beverungen and Case (2011) contend that "We may find that morals in business includes a fundamental disengagement identifying with amazing encounters emerging when things are strange" (Beverungen and Case, 2011) When distinguishing rehearses that reflect business morals, we end up in the region of profound quality and a definition of what establishes ethical quality. We comprehend that business moral as an idea is transforming, changing with regards to new advancements, better approaches for asset assembly and use, developing cultural practices and developing towards an interminably associated worldwide business organize. Developing widespread consciousness of the limit of regular assets, the developing riches isolate, and the unavoidable nearness of organizations in the individual resident's life through innovations, for example, large information and distributed computing, deliver business morals as a lot of standards rehearsed by a firm? Is it an indistinct idea hard to systematize or is it a translatable hypothesis with the capacity to be educated as a control in business colleges? (Beverungen and Case 2011). In the event that the standards are followed to guarantee legitimate consistence, will it as a general rule mirror the day to day rehearses followed by the firm? (Painter-Morland 2010).

In this paper, we plan to investigate Corporate Social Responsibility (CSR) with regards to business morals. The paper contemplates CSR as an idea and furthermore as a lot of activities installed in the ethicality of the business. Business associations are a necessary piece of the social, financial and ecological frameworks around them. Consequently, their exercise, structure and procedures need to assume liability for the effect they have on partners and on the general public which bolsters their reality. It isn't adequate to characterize CSR as constrained to business endeavors that connect with individuals or different parts of the earth as recipients characterized by the organization. The drop out impacts that an organization has on the more extensive network, today and tomorrow should be consolidated in CSR sharpening for morals and CSR to be dealt with reciprocally.

1.1. CSR with regards to Business Ethics

The regularizing partner hypothesis in CSR which draws its way of thinking from Ethics, avows that business organizations are "ethically" capable to care for the worries of a bigger gathering of partners which could incorporate proprietors, clients, merchants, representatives and network as opposed to its investors for example the proprietors of the business alone (Rodin 2005 pp561). The ideas of business morals and social obligation have unmistakable personalities. However, they are regularly used to allude to a similar contention or code. The term business morals should be "a mix of two extremely recognizable words, to be specific business and morals" (Dimitriades 2007 pp1).

CSR is then viewed as an expense charged on the profits got from the wrongs submitted by business to pay for a portion of the rights. Along these lines "the incomes gathered by charges related with transgression and misuse are

frequently reserved for reestablishing wellbeing and the earth, if not offering through and through impetuses for the assembling of progressively helpful items" (Fuller 2013 pp123).

One of the primary premise of the regularizing partner hypothesis is the idea that an association's inside procedures influences its recognized partners and should be founded on moral way of thinking and morals. All dynamic needs to consider the effect on the entirety of its partners and should have moral value of its own outside of the association's money related benefits (Donaldson and Preston 1995 as referred to in Parmar et al 2010).

1.2. Current Relevance of CSR

CSR has been a piece of moral and mindful strategic approaches for long. Nonetheless, the idea has picked up included footing in the wake of the globalized idea of the financial condition today (Jamail and Mirshak 2007). CSR works on the rule that corporates are obliged to meet their obligations to a bigger cluster of partners than its investors. Corporate Social Responsibility ought not be an extra approach by an organization, however be coordinated into its administration structure and technique.

CSR has additionally been characterized through the point of view of religion. Suthisak Kraisornsuthasinee states "Corporate social obligation (CSR), as an idea, addresses that benefit from business for some may come at the cost of others. Such a causal relationship could be grounded on the relativistic perspective on subordinate start what's more, the law of restriction" (Kraisornsthasinee 2012 Pp191).

Jamail and Mirshak (2007) state, "Increased enthusiasm for CSR lately has originated from the appearance of globalization and universal exchange, which have reflected in expanded business intricacy and new requests for upgraded straightforwardness and corporate citizenship. Besides, while governments have generally accepted sole duty regarding the improvement of the living states of the populace, society's needs have surpassed the capacities of governments to satisfy them. Right now, spotlight is progressively going to concentrate on the job of business in the public eye and dynamic organizations are looking to separate themselves through commitment in CSR. The discoveries propose the absence of a deliberate, centered, and standardized way to deal with

The felt requirement for Business Ethics as CSR has become so inescapable that even in the customary and what is seen as an enemy of natural segment, for example, the petroleum product industry, in a paper composed by staff at the International Petroleum Industry Environmental Conservation Association (IPIECA), the creators avow the requirement for a "decent human rights strategy and practice" (Owen and Sykes 2009 pp 131). The idea is presently picking up significance in the networks in which the business works, for encouraging the worldwide believability of the oil and gas organizations and furthermore to assist them with continuing to exist and participate in business. (Owens and Sykes 2009).

In India, perceiving the worries of the regularly expanding isolate between most by far of the majority and the progressively incredible and supplied organizations, the legislature has today enacted CSR as required with arrangements for the partnerships to report the reasons, in case of resistance. As far as possible have been characterized by a change to the Companies Bill 2011 that was passed in the Lok Sabha in December 2012. Open area organizations and privately owned businesses gaining over Rs.5 crores in net benefit must spend at least two levels of their benefits on CSR or report the explanations behind their inability to do as such (Goel, Sanghvi, Dahiya 2013).

1.3. Do great CSR rehearse compare with morals?

In any case, would consistence with all the standards and guidelines of CSR practice essentially imply that the business element is likewise following sound business morals rehearses? Are the exercises of the firm with regards to CSR and business morals fundamentally related? There are driving instances of organizations that conformed to CSR and administration standards on its substance, however would they say they were likewise moral?

Mallen Baker, a CSR authority states "CSR is never again characterized—on the off chance that it at any point truly was—by the procedure of how a lot of cash a business parts with, yet by how that business brings in its cash in any case."†

Management Conference in late 2001 that "Enron's Corporate Social Responsibility (CSR) team recorded its 'Achievements to Date', as:

- Secured board oversight of social/ecological execution
- Expressed help for Universal Declaration of Human Rights
- Completed corporate obligation team
- Developed and pilot-tried human rights review
- Developed security and human rights rules

- Established proper organizations with WBCSD [World Business Council on Sustainable Development], IBLF [International Business Leaders Forum], and CI [Conservation International]
- Identified language to reinforce code of morals
- Responding to partner worries on a continuous premise"

The incongruity of these cases in the light of what unfolded in the days to come is stunning most definitely.

Corporate monsters, for example, Enron and Satyam turn up as impolite stuns when the tricks are uncovered medium-term. No earlier indications of deceptive practices are unmistakable till the 'place of cards' breakdown. India's 'Enron', Satyam's CSR endeavors were praised all around. The organization that crumbled because of its the executives' swindling the organization and its investors financially received numerous honors including the Brilliant Peacock Global Award for Excellence in Corporate Governance, the Citizenship Partner of the Year Grant 2007 from Microsoft, Corporate Social Responsibility from Business World, Forbes' Top Asian Organization, was recorded among the best 13 Best-Managed Companies in India by Business Today, and was pronounced one among the 100 Leading Pioneering Technology Companies by the World Economic Forum. These grants gave a false representation of the truth behind the honor of the organization's lead including misrepresentation of records and demonstrating enormous money and fixed store adjusts in their monetary records when the organization as a general rule had no such balances. The money related misrepresentation included exaggerating the organization's money adjusts by more than 1 billion dollars, exaggerating of representative numbers by over 13,000 and withdrawal of the phantom worker pay rates by the association's originators, blowing up incomes by misrepresenting solicitations and producing of the organization's bank fixed store receipts.

References:

1. Beverungen, A., Dunne, S., Hoedemaekers, C. (2013). The financialisation of Business ethics. *Business Ethics: A European Review*. Volume 22 Number 1.
2. Beverungen, A., Case, P. (2011). Editorial introduction: where is business ethics? *Business Ethics: A European Review* Volume 20 Number.
3. Bjerregaard, T., Luring, J. (2013). Managing contradictions of corporate social responsibility: the sustainability of diversity in a frontrunner firm. *Business Ethics: A European Review* Volume 22 Number 2.
4. Bradley, R.L. (2009). Capitalism at Work: Business, Government, and Energy pp. 309–310. Carroll, A.B. (1991).
5. Freeman, R., E. (1999). Response: Divergent Stakeholder Theory. *The Academy of Management Review*, Vol. 24, No. 2 pp. 233-236.
6. Freeman, R.E., McVea, J. (n.d.) A Stakeholder Approach to Strategic Management. Darden Graduate School of Business Administration, University of Virginia. Working Paper No. 01-02.
7. Fuller, S. (2013). Never let a good crisis goes to waste': moral entrepreneurship, or the fine art of recycling evil into good. *Business Ethics: A European Review*. Volume 22 Number 1.
8. Goel, M., Sanghvi, T., Dahiya, K. (2013). Role of Corporate Social Responsibility in Entrepreneurship Development. Unpublished. Jamali, D., Mirshak, R. (2007).

*Book & Chapter
App
Journal*

JOURNAL

The

OF ENGLISH

English Language

LANGUAGE

Teachers' Association

TEACHING

of India

ISSN 0973-5208

(A Peer-Reviewed Journal)

ELT@I

A forum for
professional development

JOURNAL OF ENGLISH LANGUAGE TEACHING

(A Peer-Reviewed Journal)

VOLUME LXII, NUMBER 5, September-October 2020

Our Founder Editor & Publisher: (Late) Padmashree S. Natarajan

Editorial	2
Developing Socio-Cultural Competence in ESL Learners: Some Practical Techniques <i>K Venkat Reddy</i>	3
Writing Academic Essays <i>Dr Manoj Nanda</i>	13
How English Came to India: Language Education Policies in Colonial India <i>Chhayankdhar Singh Rathore</i>	19
Grammar Guru 10 <i>V Saraswathi</i>	24
The English Teacher's Role of Permanence <i>Kiran Shetty</i>	25
Mismatches in the Contents of Reading and Writing Tasks: Revisiting Schema Theory <i>P Bhaskaran Nair</i>	27
Teaching to Speak without Materials: Some Techniques <i>Arkapravo Banerjee</i>	32
Exploring Opportunities of Authentic Engagement in the English Classrooms <i>Nidhi Kunwar</i>	37
Promoting the Habit of Reading English Books in College Students <i>Pratima Talwar</i>	42
Reading Activity – Slow Reading <i>K Elango</i>	45
Manuscript submission guidelines for authors	47

Printed and published by

Dr. K. Elango on behalf of the Society for the Promotion of Education in India

Correspondence relating to the journal, *Journal of English Language Teaching*, should be addressed to the Chief Editor at: ramanipn@gmail.com and that relating to the association, English Language Teachers' Association of India (ELTAI), to: eltai_india@yahoo.co.in.

ELTAI Office: +91-44-26172789, 9344425159

The views expressed in the articles published in JELT are those of the authors only and do not necessarily reflect the stand of the editorial board.

Writing Academic Essays

Dr Manoj Nanda

ABSTRACT

The article discusses ideas and teaching tips on academic essay writing based on classroom practice. Often, students pay more attention to the content and less to the structure, including introduction, thesis statement, paragraphing, paraphrasing, mechanics of language, conclusion, and referencing. Students describe, rather than build, a sustained argument with critical analysis. An academic essay is sustained writing that answers a question, introduces a thesis, then expands it with reasoned arguments. The thesis is supported point-by-point with evidence from academic texts and credible sources. A salient pedagogic approach in developing these skills generates better academic essays.

Keywords: Academic essays; essay writing; teaching tips for writing.

Introduction

Writing academic essays is a challenge for students and teachers. Models such as PEAL (Point, Explanation, Analysis, and Link) and TEEES (Topic sentence, Explain, Elaborate, Evidence, and So what) provide frameworks for essay writing. Essay writing involves developing dual key skills: the ability to write analytical points within a paragraph, and the ability to structure a sustained argument in response to a specific statement. An essay must focus on and develop a central thesis and each paragraph must have a focus point to support the thesis or argument. An effective essay has a clear introduction, structure and format, mechanics of language, appropriate and adequate referencing, and a clear conclusion reflecting the thesis.

Writing the Introduction

The introduction is the key paragraph that clearly provides the focus and scope of the essay. It includes the topic, the focus points,

the thesis, and a concluding sentence.

What to write in the introduction

- Write a thesis statement (a single sentence), including the topic and the key focus areas, and the scope of the essay.
- Thesis statement – A thesis is a position statement either for or against a topic or problem. Adhere to the thesis statement throughout the essay; do not reverse your stand. The thesis is stated either as the first or the last sentence of the introduction.
- Do not include details on the topic (data) and any in-text citation in the introduction. Do not ask rhetorical question(s) in the introduction, for example, 'Should medical cannabis be legalised?' Instead, make a statement 'It is imperative that medical cannabis be legalised for health and well-being.' Rhetorical questions are not asked anywhere in an academic essay.

- Use the present tense, for example, ‘This essay examines, argues, analyses, etc.’ Do not write ‘This essay will examine, argue.’ However, the tense can change in the body of the essay depending on the arguments and context.
- Include a concluding sentence in the introduction, which will be expanded in the conclusion of the essay.

A Sample – Introduction

Research and clinical tests have been an essential part of developing safe and effective vaccines and administering vaccines is essential to safeguard health and wellbeing and thus vaccination should be mandatory as it has been proven to minimise the spread of disease. (Thesis) This essay examines vaccination (Topic) with an emphasis on societal fear of vaccines and risks (focus point 1), the research and advancement in vaccines, (focus point 2) and the essential role vaccines play in health of society (focus point 3). Various studies and research have argued that vaccination is an essential medical practice for better health and well-being. (Concluding sentence) (Kibin, 2018).

Structure and Format the Organised Paragraphs

A constructive structure and format provides a consistent flow of ideas, sustained argument, and comprehension. Structure and format include constructive paragraphs with an idea, use of appropriate linking devices (words), indented paragraphs, topic sentences, explaining and elaborating topic sentences with evidence, and providing a concluding statement to each idea in the

paragraph. For effective paragraphs, follow the TEEES model.

Sample paragraph (using the TEEES model)

First, vaccine safety and serious adverse effects are critical concerns for parents. (Topic sentence). Pockets of vaccine objectors, including those who delay vaccination or adopt a selective vaccination schedule, pose a risk to the community by threatening the circles of protection created by herd immunity. (Explain the topic sentence). Danchin and Nolan (2014) argued that for optimal and effective herd immunity, vaccine coverage above 90% is generally required and with the help of vaccination programs, this percentage can be achieved. (Elaborate and give evidence, use in-text citations). Lack of knowledge on developing immunity among the wider demography is a national concern in administering vaccination. Societal knowledge on vaccination needs to be enhanced. (Conclude by summing up the paragraph and introduce the next paragraph). Furthermore, there is still controversy whether parents should immunise their children for benefit to society or withhold vaccines for personal reasons. (mylearningadvisor, 2013)

The format or structure of the essay includes the introduction, body, and conclusion. A general rule is to write a FIVE-paragraph essay. The three focus points stated in the introduction of the essay (paragraph 1) are examined, argued, and analysed in the body of the essay (paragraphs 2-4). The focus points argue the thesis supported with research evidence using in-text citations. The conclusion is the fifth paragraph.

The five-paragraph essay:

Paragraph 1 – **Introduction**

Paragraph 2 (focus point 1)

Paragraph 3 (focus point 2)

Paragraph 4 (focus point 3)

Paragraph 5 – **Conclusion**

Body 1+3+1 = 5 paragraphs

(Taylor, 2012)

Conclusion

The concluding paragraph is a short summary that reflects and confirms the thesis and the key focus points. It has no new ideas or in-text citations, but rather has a few strong objective statements that support the thesis.

A sample concluding paragraph

In summary, research evidence argues for the safe development and the effective use of vaccines. Mandating laws on vaccination manifests progress, welfare, and safety of society. Such laws need to be instituted and implemented, stipulating that vaccines are necessary to help children and adults with medical issues or immunodeficiency disorders. Vaccines save lives. Societal fear of vaccines persists, but development and advancement in vaccines with further education and information protects individuals, families and community, and helps protect future generations by eradicating diseases.

Furthermore, the structure and format includes layout. The layout includes appropriate font and paragraph formatting: font size (12), font theme (Times New Roman), and paragraph (double space,

indented, justified), which gives the whole essay a clean, crisp, polished edge.

Structure and format:

- Indent all paragraphs with one space except the introductory paragraph.
- Use a topic sentence at the beginning of each paragraph (new idea or extension of the previous idea in a following paragraph). Explain or elaborate the key idea in the body of the paragraph including facts/figures and provide reference (in-text citation). Finish the paragraph with a concluding sentence on the idea expressed. (Write paragraphs using the TEEES model.)
- Begin a new paragraph with a linking word. The use of linking devices will depend on the context of the new paragraph. For example,

Open the introductory paragraph – *The current debate regarding..... / It is often argued...*

Introduce another viewpoint – *Although... / On the other hand...*

Show cause and effect – *As a consequence*

of... / Influence by...

To show significance of something –
Indicates... / Exemplifies...

Use comparative conjunctions – *However... / Nevertheless... / On the contrary...*

Use of additional conjunctions – *Moreover... / In addition...*

Conjunctions which exemplify and show results – *For example... / Therefore... / As a result...*

Use of temporal conjunctions – *Now... / Previously... / On another occasion...*

Causal conditional conjunctions –
Consequently... / Shaped by...

Ways to sum up or conclude – *It would seem that... / Thus, in summary... / There are many reasons...*

- Paraphrase all information to avoid plagiarism. Include in-text citation for all information, including paraphrased statements, concepts, technical terms, and historical information used verbatim with reference cited.
- Use statistics (data) within paragraphs to support arguments and evidence. Express statistical information in a short summary within the text and avoid details. Provide reference immediately after the statistical evidence.

Mechanics of Language

The mechanics of language ensures effective communication and makes the essay comprehensive and meaningful to the reader.

Correct mechanics of language includes:

- Correct use of spelling and grammar
- Sentence structure
- Paragraph and punctuation
- Using appropriate tone and register
- Linking ideas effectively through coherence and cohesion
- Using literary devices, for example, similes, metaphors, and so on
- Using a combination of simple, compound, and complex sentences
- Using appropriate tense
- Using full words and not contractions, like *cannot* instead of *can't*, *would not* instead of *wouldn't*.

Bibliography / Reference

Writing bibliography and reference is an important skill to develop. Academic essays use ideas from other sources as evidence to support arguments. Other sources help to make a point, add details, provide evidence, and demonstrate informed and scholarly writing. Acknowledge all sources used.

What do bibliography, reference, in-text citations, and annotated bibliography mean? Bibliography is a list of sources read or consulted during the research. It is a comprehensive alphabetical list of all sources browsed during the research of the topic. Reference or reference list includes only those sources closely read, referred to, and used in writing the essay. A referenced source is one used to delineate the information from the writing. In-text citation is a short reference to the author and year in the

paragraphs. An annotated bibliography is a short description for a reference, explaining the accuracy, validity, authenticity, and usefulness. Use a recommended referencing convention like Harvard or APA (American Psychological Association) (TAFE NSW, 2017).

Convention on Bibliography/Reference

- In-text citations need consistency. Use only author's surname and year, for example, (Smyth, 2018). Include the full stop after the citation and not at the end of the sentence. The citation is included as part of the sentence. Use corporate authors if the source has no individual author(s), for example, (The Guardian, 2020).
- Use full name of corporate author for the first time (in citation) and then use abbreviations, for example, British Broadcasting Corporation and then write BBC in subsequent citations of the same. Positioning in-text citations in the paragraph is a useful skill. Insert in-text citations at the beginning, middle or at the end of a paragraph, as appropriate. Varying the position of the in-text citations adds flow, sustains good academic convention, and gives a good scholarly rigour to the writing. Most essays include in-text citations at the end of every paragraph, making the essay monotonous. For example, in-text citations at the *beginning* of the paragraph: *Smith (2017) argued that higher education should be accessible to all.* In the *middle* of the paragraph, *Investment in public education is essential (Smith, 2017) as it enhances literacy.* At the *end* of a paragraph, after writing the

information... (*Smith, 2017*).

- For a direct quote, in-text citation follows immediately after the quote, including the page or paragraph number. For example, Smith (2017, p.6) stated "*investment in education is essential...*" Or Smith (2018, para 12) stated that "*investment in education is essential*". (NOTE: paragraph number is used if the publication has no page number, especially in an on-line publication).
- All references used need consistency following the required convention; references should be alphabetical.
- Use diverse sources to write the essay, rather than one or two sources from the bibliography. Use good academic, researched, and reputable published sources.
- For annotated references, comment on currency (when published, updated), relevance (usefulness), authenticity (who wrote it, correctness, truthfulness), and purpose (why is it written – to inform, argue, to show bias, to point out a fact, to share an opinion).

More Tips

- Do not use headings, subheadings, or bulleted list of points.
- Do not use personal pronouns (*I, we, they*, etc.) and slang/colloquialism.
- Do not use excessive punctuation, especially commas. Avoid it if not sure where to use.
- Do not ask a rhetorical question and

A Reliability Model for a Two Dissimilar Units Series System with Repair Time-Dependent Standby

Jai Bhagwan, Amit Manocha, Anil Taneja

Abstract: The present paper stochastically analyze a system comprising two dissimilar units (unit-1/unit-2) working in series configuration. System fails completely when either of the units gets failed. The repair time of unit-2 is considered to be much more as compared to the repair time of unit-1. So, to minimize the breakdown period of the system, a standby unit is provided against the second unit. Regenerative point technique (RPT) is used to develop a semi-markovian reliability model for the mentioned system. Optimum cut-off points concerning the profitability of the system have also been obtained. The model has applications in industries, particularly in aluminum industry.

Keywords: Dissimilar units, Optimum cut-off points, Repair time dependent standby, semi-Markov process, Series configuration

I. INTRODUCTION

The industries/organizations are now being modernized and focused on producing more reliable systems with increased availability and lesser break down time to achieve the set target. Redundancy is one of the most effective techniques, which may be used to enhance the performability of industrial systems and such systems have been analyzed by various researchers. Mokaddis et al. [1] analyzed standby system with three different operative stages. Parashar and Taneja [2] dealt with PLC hot standby system. A standby system with general life and repair time distribution was studied by Bieth et al. [3]. Mahmoud and Mosherf [4] discussed different types of failure and preventive maintenance in their study. Malhotra and Taneja [5] stochastically analysed a system wherein operability of more than one unit depends upon requirement. Manocha and Taneja [6] took arbitrary distribution for all random variables. El-Sherbeny [7] studied such systems with the concept of random change of units. Manocha et al. [8] investigated database system keeping hot standby unit under constant observation.

Dissimilar units system may also be observed in the industrial sector. Mokkaadis et al. [9] analysed a system by considering two types of repair and inspection of failed unit. Sadeghi and Roghanian [10] studied two unit warm standby system by considering two dissimilar units with imperfect

switching mechanism. Rahbi et al. [11] did the reliability analysis of rodding anode plant consisting of eight dissimilar units used in aluminum industry. Chopra and Ram [12] carried out reliability analysis of two dissimilar units parallel system using Gumbel-Hougaard family copula. In a two dissimilar unit series system, it may be observed that one of the two dissimilar units, whenever gets failed, may require more time to get repaired as compared to the other. These types of systems are used at a large scale in network communication, textile industry, aluminum industry etc. For such systems, if a unit gets failed, the whole system becomes non-functional and hence introduction of a standby unit may reduce the frequency of breakdowns. However, using standby units against both the units may be a costly affair. Therefore, to keep a balance between the cost of using standby units and breakdown time of the systems, one may use single standby unit against that unit whose recovery time after failure is more than the other.

The present study is an attempt to stochastically analyse a system comprising two dissimilar units connected in series (unit-1/unit-2), where a standby unit is kept against the second unit. In the system under consideration, let us assume that unit-2 takes more time to repair on failure as compared to the repair time of the first unit and hence breakdown period of system is much more in case of the failure of second unit. To reduce breakdown period of the system a standby unit is installed against unit-2. The product being manufactured by such a system is assumed to be first processed on unit-1 and then on unit-2. System fails completely if either unit-1 or unit-2 along with its standby after putting it into operation gets failed. The technique and the other assumptions taken in the present study are same as that taken in [2]. Optimum cut-off points for various costs which affect the profitability of the system have also been obtained.

II. NOTATIONS

O_1 / O_2	operative unit-1 / unit-2
S_2	standby unit for unit-2
ω_1 / ω_2	constant failure rate of unit-1 and 2
F_{r1} / F_{wr1}	unit-1 under repair/ waiting for repair
$F_{r2} / F_{R2} / F_{wr2}$	unit-2 under repair/repair from previous state/ waiting for repair
D_1 / D_2	down unit-1/unit-2
$g_1(t) / g_2(t)$	density function of repair time for unit-1 and 2

Note: For some other notations one may refer to [2] and [5].

Revised Manuscript Received on February 18, 2020.

* Correspondence Author

Jai Bhagwan, Department of Mathematics, Government P.G. Nehru College Jhajjar, Haryana, India. Email: jaichaudhary81@gmail.com

Amit Manocha*, Department of Mathematics, TIT&S, Bhiwani, Haryana, India. Email: amitmanocha80@yahoo.com

Anil Taneja, Department of Mathematics, Skyline University Nigeria, Kano, Nigeria, Email: dr.anilkraneja@gmail.com

III. TRANSITION DENSITIES & MEAN SOJOURN TIMES

Possible transitions for the model are shown in Fig.1. All the states except 3 and 4 are regenerative states.

States 0 and 2 are up, whereas 1, 3 and 4 are failed states.

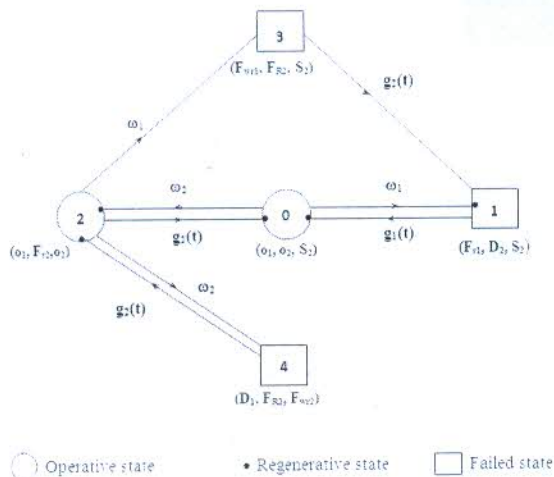


Fig.1. Transition diagram

Transition densities are:

$$\begin{aligned}
 q_{01}(t) &= \omega_1 e^{-(\omega_1 + \omega_2)t}, & q_{02}(t) &= \omega_2 e^{-(\omega_1 + \omega_2)t}, \\
 q_{10}(t) &= g_1(t), & q_{20}(t) &= e^{-(\omega_1 + \omega_2)t} g_2(t), \\
 q_{21}^{(3)}(t) &= (\omega_1 e^{-(\omega_1 + \omega_2)t} \odot 1) g_2(t), \\
 q_{22}^{(4)}(t) &= (\omega_2 e^{-(\omega_1 + \omega_2)t} \odot 1) g_2(t), \\
 q_{23}(t) &= \omega_1 e^{-(\omega_1 + \omega_2)t} \overline{G}_2(t)
 \end{aligned} \tag{1-7}$$

By the probabilistic argument, the non-zero elements p_{ij} are obtained as:

$$p_{ij} = \lim_{s \rightarrow 0} q_{ij}^*(s) \tag{8}$$

For the developed model, mean sojourn time and contribution to sojourn time are mathematically expressed as:

$$\mu_0 = \int_0^{\infty} e^{-(\omega_1 + \omega_2)t} dt, \quad \mu_2 = \int_0^{\infty} e^{-(\omega_1 + \omega_2)t} \overline{G}_2(t) dt \tag{9-10}$$

Thus, $m_{01} + m_{02} = \mu_0$, $m_{10} = -g_1^*(0) = K_1$ (say),

$$m_{20} + m_{23} + m_{24} = \mu_2, \quad m_{20} + m_{21}^{(3)} + m_{22}^{(4)} = -g_2^*(0) = K_2 \tag{11-14}$$

IV. RELIABILITY AND MTSF

If $rt_0(t)$ and $rt_2(t)$ denotes the CDF of first passage time from states 0 and 2 to a failed state respectively, then we have

$$\begin{aligned}
 rt_0(t) &= Q_{01}(t) + Q_{02}(t) \otimes rt_2(t) \\
 rt_2(t) &= Q_{23}(t) + Q_{24}(t) + Q_{20}(t) \otimes rt_0(t)
 \end{aligned} \tag{15-16}$$

Thus, the reliability of the system

$$R(t) = L^{-1} \{ [D(s) - N(s)] / sD(s) \} \tag{17}$$

and

$$MTSF = \int_0^{\infty} R(t) dt = N/D \tag{18}$$

where

$$\begin{aligned}
 N(s) &= \{ \omega_1 / (s + \omega_1 + \omega_2) \} \\
 &+ \{ \omega_2 (\omega_1 + \omega_2) / (s + \omega_1 + \omega_2)^2 \} \{ 1 - g_2^*(s + \omega_1 + \omega_2) \} \\
 D(s) &= 1 - \{ \omega_2 g_2^*(s + \omega_1 + \omega_2) / (s + \omega_1 + \omega_2) \} \\
 N &= \mu_0 + p_{02} \mu_2, \\
 D &= 1 - p_{02} p_{20}
 \end{aligned} \tag{19-22}$$

V. AVAILABILITY ANALYSIS

The recursive relations for point-wise availability $up_i(t)$, $i=0,1,2$ are:

$$\begin{aligned}
 up_0(t) &= a_0(t) + q_{01}(t) \odot up_1(t) + q_{02}(t) \odot up_2(t) \\
 up_1(t) &= q_{10}(t) \odot up_0(t) \\
 up_2(t) &= a_2(t) + q_{20}(t) \odot up_0(t) + q_{21}^{(3)} \odot up_1(t) \\
 &+ q_{22}^{(4)} \odot up_2(t)
 \end{aligned} \tag{23-27}$$

where $a_0(t) = e^{-(\omega_1 + \omega_2)t}$, $a_2(t) = e^{-(\omega_1 + \omega_2)t} \overline{G}_2(t)$

Thus, as time t approaches to infinity the availability is $up_0 = \lim_{s \rightarrow 0} \sup_{s \rightarrow 0} s N_1(s) / D_1(s) = N_1 / D_1$

where $N_1(s) = \{ 1 - q_{22}^{(4)*}(s) \} a_0^*(s) + q_{02}^*(s) a_2^*(s)$,

$$\begin{aligned}
 D_1(s) &= \{ 1 - q_{01}^*(s) q_{10}^*(s) \} \{ 1 - q_{22}^{(4)*}(s) \} \\
 &- q_{02}^*(s) \{ q_{10}^*(s) q_{21}^{(3)*}(s) + q_{20}^*(s) \},
 \end{aligned}$$

$$N_1 = (1 - p_{22}^{(4)}) \mu_0 + p_{02} \mu_2,$$

$$D_1 = (1 - p_{22}^{(4)}) (\mu_0 + p_{01} K_1) + p_{02} K_2 \tag{28-32}$$

VI. BUSY PERIOD ANALYSIS

The system of equations obtained for evaluating busy period of repairman $bt_i(t)$, $i=0,1,2$ are:

$$\begin{aligned}
 bt_0(t) &= q_{01}(t) \odot bt_1(t) + q_{02}(t) \odot bt_2(t) \\
 bt_1(t) &= l_1(t) + q_{10}(t) \odot bt_0(t) \\
 bt_2(t) &= l_2(t) + q_{20}(t) \odot bt_0(t) + q_{21}^{(3)} \odot bt_1(t) \\
 &+ q_{22}^{(4)} \odot bt_2(t)
 \end{aligned}$$

$$\text{where } l_1(t) = \overline{G}_1(t), \quad l_2(t) = \overline{G}_2(t) \tag{33-37}$$

Thus, in steady-state, we have

$$bt_0 = \lim_{s \rightarrow 0} \{ s N_2(s) / D_1(s) \} = N_2 / D_1$$

where

$$\begin{aligned}
 N_2(s) &= \{ q_{01}^*(s) - q_{01}^*(s) q_{22}^{(4)*}(s) + q_{02}^*(s) q_{21}^{(3)*}(s) \} l_1^*(s) \\
 &+ q_{02}^*(s) l_2^*(s),
 \end{aligned}$$

$$N_2 = \{ (1 - p_{22}^{(4)}) p_{01} + p_{02} p_{21}^{(3)} \} K_1 + p_{02} K_2 \tag{38-40}$$

EXPECTED NUMBER of VISITS BY REPAIRMAN

The equations for obtaining expected number of visits by repairman $ev_i(t)$, $i=0,1,2$ in specific unit of time, are:

$$\begin{aligned}
 ev_0(t) &= Q_{01}(t) \otimes \{ ev_1(t) + 1 \} + Q_{02}(t) \otimes \{ ev_2(t) + 1 \} \\
 ev_1(t) &= Q_{10}(t) \otimes ev_0(t) \\
 ev_2(t) &= Q_{20}(t) \otimes ev_0(t) + \\
 &Q_{21}^{(3)}(t) \otimes ev_1(t) + Q_{22}^{(4)}(t)
 \end{aligned}$$

In long run



$$ev_0 = \lim_{s \rightarrow 0} \{s N_3(s)/D_1(s)\} = N_3/D_1$$

$$\text{where } N_3(s) = \{1 - Q_{22}^{(4)**}(s)\} \{Q_{01}^{**}(s) + Q_{02}^{**}(s)\}$$

$$N_3 = (1 - p_{22}^{(4)}) \tag{41-46}$$

VII. PROFIT ANALYSIS

The profit equation, therefore, is

$$P_0 = C_R up_0 - C_B bt_0 - C_V ev_0 \tag{47}$$

where C_R = Revenue per unit up time

Table-I: Values of MTSF and Availability (up_0) w.r.t. ω_1 and α_2

ω_1 (per hr)	$\alpha_2=0.1$ (per hr)		$\alpha_2=0.15$ (per hr)		$\alpha_2=0.2$ (per hr)	
	MTSF (In hrs)	Availability (up_0)	MTSF (In hrs)	Availability (up_0)	MTSF (In hrs)	Availability (up_0)
0.001	828.77	0.9925	865.6	0.9939	894.07	0.9944
0.002	453.53	0.9874	464.18	0.9890	472.16	0.9895
0.003	312.18	0.9823	317.12	0.9840	320.78	0.9846
0.004	238	0.9773	240.82	0.9792	242.91	0.9798
0.005	192.31	0.9724	194.12	0.9744	195.45	0.9750
0.006	161.33	0.9675	162.59	0.9696	163.51	0.9703

Graphs of profit (P_0) with respect to the following have been plotted in Figs. 2 and 3.

- i) C_R for varied ω_1
- ii) C_B for varied C_V

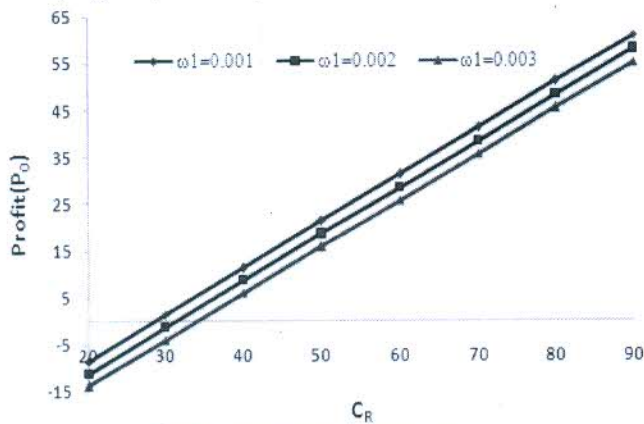


Fig.2. Profit (P_0) versus (C_R)

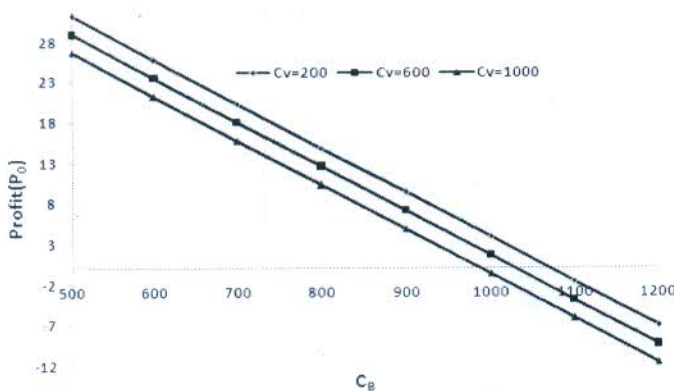


Fig.3. Profit (P_0) versus cost (C_B)

The above figures reveal what has been tabulated as follows:

C_B = Cost per unit time for engaging repair facility
 C_V = Repairman charges for each visit

VIII. RESULT AND DISCUSSION

Letting $g_1(t) = \alpha_1 e^{-\alpha_1 t}$, $g_2(t) = \alpha_2 e^{-\alpha_2 t}$; considering $\omega_2 = 0.005$ per hr, $\alpha_1 = 0.2$ per hr; and varying ω_1 , α_2 ; the values of MTSF and availability are tabulated as:

Table-II: Conditions for the profitability of the system

Assumed parametric values	Varied parameter	Condition for the system to be profitable(Optimum cut-off points)	Remark
$\omega_2 = 0.005$, $\alpha_1 = 0.2$, $\alpha_2 = 0.1$, $C_B = 500$, $C_V = 200$	$\omega_1 = 0.001$	$C_R > 28.64$	Otherwise, system will put to a loss
	$\omega_1 = 0.002$	$C_R > 31.33$	
	$\omega_1 = 0.003$	$C_R > 34.03$	
$\omega_1 = 0.001$, $\omega_2 = 0.005$, $\alpha_1 = 0.2$, $\alpha_2 = 0.1$, $C_R = 60$	$C_V = 200$	$C_B < 1070.12$	Otherwise, system will put to a loss
	$C_V = 600$	$C_B < 1028.54$	
	$C_V = 1000$	$C_B < 986.96$	

IX. CONCLUSION

The stochastic analysis is carried out for a system comprising two dissimilar units connected in series with a standby unit against that unit which has more recovery time after failure. Cost is always a crucial factor for any industry/organization and hence cut-off points for revenue/cost have been determined, finding numerical results for a particular case, which may be used to assess as to what value of the parameter under consideration should be taken in order to have a profitable system. Cost analysis may be done for other parameters of interest also in the similar way by the users of such systems.

REFERENCES

1. G.S.Mokaddis, S.W. Labib, and A.M. Ahmed, "Analysis of a two-unit warm standby system subject to degradation," *Microelectron. Reliab.*, vol.37 (4), 1997, pp.641-648.
2. B.Parashar, and G. Taneja, "Reliability and profit evaluation of a plc hot standby system based on a master- slave concept and two types of repair facilities," *IEEE T. Reliab.*, vol.56 (3), 2007, pp. 534-539.



3. B. Beith, L. Hong, and J. Sarkar, "A standby system with two repair persons under arbitrary life-and repair times," *Math. Comput. Modelling*, vol. 51, 2010, pp. 756-767.
4. M.A.W. Mahmoud, and M.E. Mosherrf, "On a two- unit cold standby system considering hardware, human error failures and preventive maintenance," *Math. Comput. Modelling*, vol. 51, 2010, pp. 736-745.
5. R. Malhotra, and G. Taneja, "Stochastic analysis of a two-unit cold standby system wherein both units may become operative depending upon the demand," *JQRE*, 2014, pp.1-13.
6. A. Manocha, and G.Taneja, "Stochastic analysis of a two-unit cold standby system with arbitrary distribution for life, repair and waiting times," *IJPE*, vol. 11(3), 2015, pp. 293-299.
7. M.S. El-Sherbeny, "Stochastic analysis of a system with cold standby, general distribution and random change in units," *AMIS*, vol.10 (2), 2016, pp. 565-570.
8. A. Manocha, S.Singh, and A. Taneja, "Analysis of hot standby database system with standby unit under constant observation," *AJMI*, vol.10 (1), 2018, pp. 25-32.
9. G.S. Mokaddis , G.S.Khalil, and H. Alhajri, Analysis of two dissimilar – unit cold standby redundant system subject to inspection and two types of repair," *IJMER*, vol.6(5), 2016, pp. 38-54.
10. M.Sadeghi, and E. Roghnia, "Reliability analysis of a warm standby repairable system with two cases of imperfect switching mechanism," *Scientia Iranica E*, vol. 24(2), 2017, pp.808-822.
11. Y. A. Rahbi, S. M. Rizwan, B. M. Alkali, A. Cowell and G. Taneja, "Reliability analysis of rodding anode plant in aluminum industry," *IJAER*, vol 12(16), 2017, pp. 5616–5623.
12. G. Chopra, and M. Ram, "Reliability measures of two dissimilar units parallel system using gumbel-hougaard family copula", *IJMMS*, vol. 4(1), 2019, pp. 116-130.

AUTHORS PROFILE



Jai Bhagwan is an Assistant Professor in Mathematics at Government P.G. Nehru College, Jhajjar, Haryana. He received his PhD in Mathematics from B.R.A. University, Agra. During 16 years of his teaching and research experience, he published around 9 research papers in journals of repute and contributed in 27 national/international conferences/seminar/workshop. He is in editorial committee of "Annals of Mathematical Physics": an International Journal by Serial Publications. He coauthored three books on Applied Mathematics and his area of interest is reliability modelling.



Amit Manocha is serving as an Assistant Professor(Mathematics) in Department of Applied Sciences at TIT&S, Bhiwani, Haryana, India. He has been teaching undergraduate/postgraduate engineering students since 17 years. He pursued his doctorate in Mathematics from NIT, Kurukshetra. Over 14 research papers in various reputed journals/proceedings owe to his credit. He has actively contributed and participated in various academic events like conferences, seminars etc His research areas are reliability modeling and applied mathematics.



Anil Taneja is a Professor and Head in the Department of Mathematics at Skyline University Nigeria, Kano (Nigeria). He qualified UGC-NET examination (mathematics) in year 2000. He did his PhD in the area of Reliability modelling from M.D. University, Rohtak, India. He published 12 research papers in national/international journals of repute and contributed in 20 national/international conferences/seminars. He has delivered expert lectures and chaired sessions in various conferences/seminars/workshops. With 25 years of teaching and administrative experience, he is actively involved in research areas like reliability modeling, queuing theory and information theory.



Functionalization of linen fabric using layer by layer treatment with chitosan and green tea extract

Sumit Saini, Ayush Gupta, Nagender Singh, Javed Sheikh*

Department of Textile and Fibre Engineering, Indian Institute of Technology (I.I.T.), Delhi, India



ARTICLE INFO

Article history:

Received 26 January 2019
Received in revised form 22 May 2019
Accepted 2 October 2019
Available online 15 October 2019

Keywords:

LBL assembly
Functionalization
Green tea extracts
Chitosan
Colour value

ABSTRACT

Development of multifunctional textile materials using green chemicals is a new quest of research. In the present work, the LBL treatment using chitosan (CH) and green tea extract (GTE) was utilized for the functionalization of linen fabric. The functionalized linen was characterized and functional properties of the modified linen viz. antioxidant property, antibacterial activity and UV protection were evaluated. The LBL finishing resulted in the coloured linen fabrics with antibacterial activity in the range 75–97%. Moreover, the treated fabrics also displayed an antioxidant property (58–96%) and the ultraviolet protection property (UPF > 22.5). The synergistic influence of CH and GTE was witnessed in imparting vital functional properties to linen using LBL technique.

© 2019 The Korean Society of Industrial and Engineering Chemistry. Published by Elsevier B.V. All rights reserved.

Introduction

Since last decade, the challenges faced by the textile finishing industry have consequentially intensified. The textile chemical processing is adversely impacting the ecological system, due to this strict legislation on industrial effluents has to be followed by the textile industry, which led to exploring the sustainable and advanced operations for textile finishing. Finishing of textile is a routine way of imparting functionalities to the textile surfaces without compromising the actual fabric properties. Textile finishing, especially functional finishing, process has grown in multiple dimensions with the use of various chemicals like natural extracts, synthetic chemicals and nanoparticles. The novel textile finishing techniques have opened the new horizon of value-addition opportunities in the textile and apparel sector. The recent trend in finishing is to impart the multifunctional properties such as wrinkle resistance, antioxidant activity, flame retardancy, UV protection and antibacterial activity.

Layer-by-layer self-assembly (LBL) is one of the most versatile methods available for modification of surface properties of polymers and it has advantages like its ability to control the thickness and applicability of variety of materials on large number of substrates. LBL technique involves the application of polyelectrolytes with opposite charges stepwise and there is no limitation of formation of by-products [1,2]. The LBL assemblies are based on

the alternate deposition of anionic and cationic electrolytes to fabricate layers on the textile substrate [3–5]. In 1990s Decher's group reported the polymeric multi-layer self-organization process [3]. Afterwards, the polymeric multi-layer films fabricated through LBL assembly were utilized to alter the surface properties of materials in machinery tools, electronic products, implants devices and medical devices [6,7].

The consumer awareness on the environmental issues and the need of eco-friendly finished textile materials are on a rise which necessitates the development of such products using green techniques [8]. Green tea (*Camellia sinensis*) leaves are the rich source various compounds such as catechin, amino acids, nucleotides, lipids, caffeine, minerals, carotenoid contents, chlorophyll, carbohydrates, organic acids, polyphenols, unsaponifiable, saponins and several low-volatility compounds [9,10]. Polyphenolic content of green tea has been reported to have many beneficial aspects and functional properties, such as anti-oxygenation antimicrobial activity, UV protection ability, and anti-carcinogenic activity [11–13].

In aqueous media the cellulose shows negative zeta potential while catechin shows anionic nature due to which catechin lacks affinity towards cellulose. Therefore, external agents are required to increase the affinity of catechin towards cellulose. Heavy metal salts are commonly used in mordanting of fabrics to improve the efficacy of natural dye and to enhance fastness [14,15]. However, the potential risk is always associated with the use of these metal ions because they can cause environmental problems and affect the aquatic life. Chitosan, an alkaline biomacromolecule, is an attractive alternative to metal salts. Therefore, in this study

* Corresponding author.

E-mail address: jnsheikh@iitd.ac.in (J. Sheikh).

chitosan was used as a mordant to enhance the affinity of GTE towards the linen fabric [16].

Chitosan is a natural linear polysaccharide comprised of *N*-acetyl- β -D-glucosamine and β -(1-4)-linked α -D-glucosamine and has many important features such as antimicrobial, biodegradability, cationic nature, non-allergic, and non-toxicity [17–19]. In acidic condition, chitosan present as a cation; where these cationic groups exert antibacterial activity. Therefore, the application of chitosan on the fabrics which will be coming in contact with the skin would be a possible option. Various applications of chitosan and its derivatives are explored in finishing of textile materials [20–26]. Chitosan can act a bridge between the cellulose and GTE because of ionic attraction [14]. Chitosan is a promising cationic electrolyte in the LBL technique. The innovative combinations of electrospinning and LBL techniques were reported. Chen et al. assembled chitosan and rectorite (REC) on the electrospun silk fibroin (SF) via electrostatic LBL. The resultant silk fibroin mats showed improvement in mechanical properties along with the excellent antibacterial activity against *Escherichia coli* and *Staphylococcus aureus* [27]. Tu et al. fabricated silk fibroin nanofibrous mats coated with carboxymethyl chitosan (CMC) by a combination of electrospinning and LBL self-assembly techniques to obtain better hydrophilicity, stronger mechanical properties and antibacterial properties [28]. In a similar fashion, Tian et al. coated bilayers of chitosan and epigallocatechin gallate (EGCG) or bilayers of chitosan–rectorite composite and EGCG on cellulose electrospun nanofibrous mats via LBL technique. The modified mats showed antibacterial activity and the mats coated with bilayers of chitosan–rectorite composite and EGCG showed delayed release of EGCG [29].

LBL method of application offers efficient functionalization of textile materials at low add-on levels. The application of CH and GTE as thin layers would be beneficial in terms of better functional properties without significant effect on the intrinsic properties of textile materials. Apart from this, the better attachment using cationic–anionic interactions would be beneficial. In the present work, LBL assembly was created by depositing thin alternate layers of cationic CH and anionic GTE onto linen fabric in order to impart multiple functionalities to the linen fabric. The colour imparted with subsequent treatments was evaluated. The efficacy of functional properties and their durabilities were explored.

Materials and methods

Materials

Jayshree Textiles, India has supplied the woven linen fabric (EPI-45, PPI-41, GSM-241.5). Green tea leaves (GTL) were purchased from a local supplier. Chitosan (Molecular weight- 150,000,

Degree of deacetylation- 90.1%, nitrogen content- 7.2%) was purchased from market and other chemicals (laboratory grade) were supplied by Merck Specialties Private Limited (India).

Methods

Extraction of colorant from green tea leaves

The 5% stock extract of green tea was prepared by boiling GTL (5gms) in water at 90°C for 60 min. Then the extract was filtered and used for the treatment.

LBL application of chitosan and GTL extract on the linen fabric

Chitosan (1%) was taken along with 2% acetic acid and stirred for 1 h at 60°C. The layer of chitosan on linen woven fabric was applied by keeping the linen fabric in chitosan solution for 2 min in shaking water bath. The fabric was squeezed (75% expression) and treated with the GTL extract for 2 min, as shown in Fig. 1. After the application of one layer, the fabric was dipped in DI water for 30 s to remove loosely held green tea extract. The procedure was repeated in order to put subsequent bilayers.

Characterization of the finished fabric

FTIR spectrometer (Thermo Scientific Nicolet iS50 FT-IR Spectrometer) was utilized to confirm the functional groups of GTL extract and chitosan on finished linen fabrics. The finished fabric was analyzed with 15-scans in the wavelength range of 400–4000 cm^{-1} with a resolution 4 cm^{-1} . A scanning electron microscope (Zeiss EVO 50) was used to scan a fabric surface at 5–6 K resolution. TGA was carried out using Perkin Elmer instrument in the atmosphere of nitrogen between 50°C to 800°C under a specific condition, i.e., temperature rate 20°C/min and gas flow rate 20 mL/min. XRD was carried out using instrument X' Pert Pro (Pan Analytical, Netherland) to identify the crystallinity of a material.

Analysis of color values of finished fabric

K/S value

Gretag Macbeth colour-eye 7000A spectrophotometer was used to measure the reflectance (%) of the finished linen fabric. The color values (K/S) was evaluated using the Kubelka Munk equation [30].

Evaluation of functional properties of finished linen fabric

UPF of the finished linen fabric samples were measured by laboratory instrument (UV–vis spectrometer) as per AS/NZS 4399:1996 standard [31]. The radical scavenging action of the

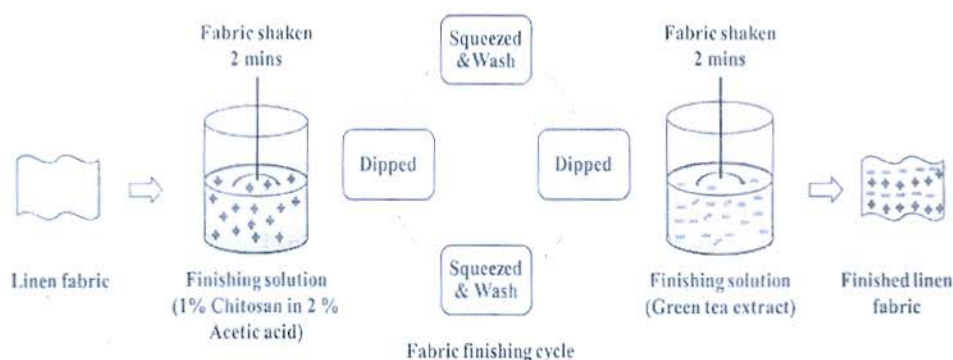


Fig. 1. Schematic of the LBL assembly with cationic chitosan and anionic GTL extract.

In order to confirm the changes in surface properties after the application of CT and GTE, the zeta potential of samples was measured (Malvern zetasizer, UK).

fabric was evaluated using DPPH radical with methanol as a solvent. The absorbance of the DPPH radical solution was measured at 517 nm, and the reduction in absorbance was used to calculate the antioxidant activity [32]. The antibacterial activity of the finished fabric samples against *S. aureus* was tested by using AATCC method-100 [33].

Results and discussion

Mechanism of finishing treatment and color values of finished fabrics

Chitosan (CH) is a cationic polymer which can hold anionic biomolecules of GTE. Generally, GTE contains various polyphenolic compounds which can result in a coloured complex in combination with chitosan. Thus the subsequent treatment of linen fabric with CH and GTE layers resulted in coloured linen fabric. The drying of the fabric after the application would result in a film of chitosan with attachment of GTE. The chitosan will be held by hydrogen bonding along with the interaction of film with the cellulose. The GTE and chitosan would interact through ionic linkages. A similar mechanism was reported in dyeing of cotton fabric by green tea extract using chitosan as a mordant [14].

The hypothesis was confirmed through zeta potential measurement of untreated, chitosan treated, and bilayer treated (CT + GTE) linen (Table 1).

As evident from Table 2, untreated linen showed negative zeta potential, which is generally shown by cellulosic fibres. This is attributed to presence of large number of hydroxyl groups. The chitosan-treated sample showed positive zeta potential, which may be attributed to the addition of protonated chitosan resulting in neutralization of negative zeta potential. The surface again showed shifting of zeta potential to negative side with the treatment of GTE. The anionic sites from the various polyphenolic compounds of GTE resulted in such shift. Even though zeta potential changes after subsequent addition of bilayers was not measured, it is obvious that the addition of positively charged chitosan would shift zeta potential toward positive side while anionic GTE would shift it to more negative side. The resultant zeta potential would be a combined effect of the extent of positive and negative sites imparted by the treatment of CT and GTE.

The subsequent bilayers were expected to form because of ionic interactions between CH and GTE. The colour values of the treated linen fabric increased with the increasing number of layers on the fabric (Table 2). This is obvious because the absorption of the light increases with the presence of higher quantity of chitosan-GTE extract. The subsequent layers add the higher amount of chitosan and green extract, thus resulting in higher color values. All the shades were found to have reddish–yellow tones (as represented by positive values of a^* and b^*). The tone became more redder–yellow as the layers of chitosan, and GTE extract increased. It was found that linen fibers showed low affinities to green tea colorants and a proper mordanting agent would be required to increase the affinity of linen fabric to GTE extract colorants. However, in presence of chitosan the cationic–anionic interactions resulted in pick-up of GTE biomolecules by the linen fabric. Chitosan layer thus act like a mordant to increase the uptake of GTE extract biomolecules on the linen fabric.

Table 1
Zeta potential and conductivity of linen samples.

Sample details	Zeta potential (mV)	Conductivity (mS/cm)
Unfinished	–1.63	0.0805
CH treated	0.880	1.30
1 bilayer treated (CH + GTE)	–1.32	0.0215

Table 2
 $L^*a^*b^*$ and K/S values of green tea extract and chitosan treated linen fabrics.

Sample no. (number of bilayers)	a^*	b^*	L^*	K/S
Unfinished	–1.26	6.18	91.81	0.29
1	3.11	15.92	83.54	1.57
2	3.44	16.51	82.55	1.84
5	3.04	16.38	82.12	2.13
8	4.58	17.93	79.74	2.31
10	3.35	16.76	76.68	2.38

Characterization of the finished fabric

The FTIR spectra of unfinished linen and finished linen (sample 10) are shown in Fig. 2. The characteristic peaks of finished linen corresponding to O–H stretch at 3339.1 cm^{-1} , C–H stretch at 2903.3 cm^{-1} , C=O of ester stretch at 1692 cm^{-1} , O–H bend at 1313.7 cm^{-1} , C–O–C symmetric stretch in a range of 1000 cm^{-1} – 1100 cm^{-1} were observed [34,35]. The FTIR spectrum of finished linen also displayed the amide bands at 3500 cm^{-1} – 3700 cm^{-1} and 1600 cm^{-1} – 1700 cm^{-1} , which suggest the N–H stretching/bending because of the presence of chitosan [36]. All these characteristic peaks correspond to the functional groups of chitosan and catechins. The FTIR spectra suggested the availability of green tea polyphenols. The new peak characteristic presence at 1023 cm^{-1} could be allocated to C–O–C bond of phenols, which suggested the attachment of tea polyphenols with linen fibers through chitosan [13].

SEM analysis

The surface morphology is one of the significant parameters for finished fabric which can provide further information and more details about the surface of finished fabric. SEM observations of finished linen fabric (with 10 layers) were carried out, and images are shown in Fig. 3.

The unfinished linen fabric showed a clean and smooth surface. The roughness can be observed on the surface of linen fabric finished with chitosan and GTE extract. The finished fabrics showed surface deposition, which may be attributed to the chitosan and GTE biomolecules.

Thermogravimetric analysis

TGA was utilized for the analysis of the degradation mechanism and thermal stability of finished linen by assessing the weight loss percentage of the sample as a function of temperature. The TGA curves of unfinished and finished linen fabrics are shown in Fig. 4 and weight loss values are summarized in Table 3.

The initial degradation temperatures (T_i) of unfinished and finished linen were 320°C and 325°C respectively. The finished linen fabric showed two-step degradation at 325°C and 500°C . The solid residue left at 700°C and mid-point degradation temperature (T_{50}) can be distinguished from the TGA curves. The finished linen fabric showed higher initial degradation temperature as compared to the unfinished linen fabric, which was because of the slow degradation of the top layer of GTE on the fabric [37]. However, finished linen fabric showed a slightly lower residue (9%) than the unfinished one (10%) at 700°C . Furthermore, no significant changes have been observed in the thermal properties of unfinished and finished fabric.

X-ray diffractometry

The XRD was utilized to measure the crystallinity of the fabric samples. The spectra are shown in Fig. 5 (a, b) regarding linen

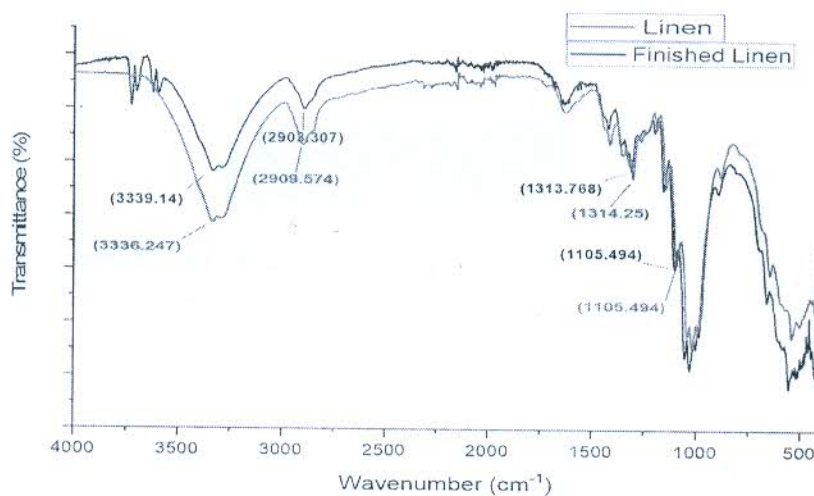


Fig. 2. FTIR spectra of unfinished and finished linen fabric (sample 10).

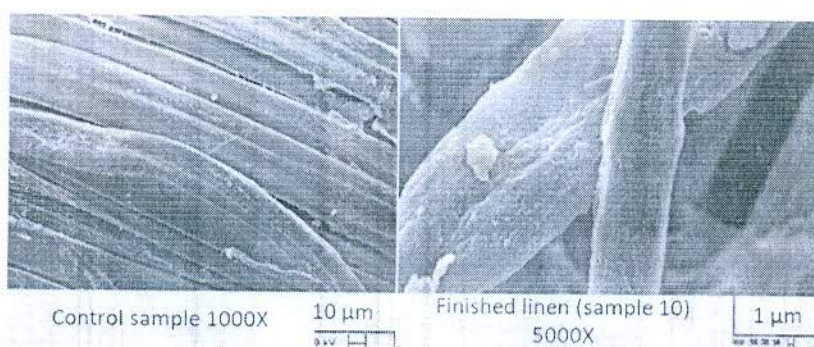


Fig. 3. SEM images of unfinished and finished linen fabric (sample 10).

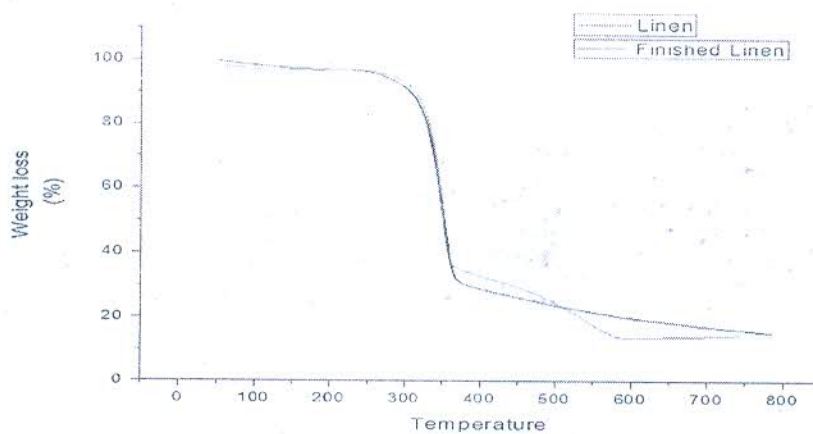


Fig. 4. TGA curve of unfinished and finished linen fabric.

Table 3
Description of the TGA curve obtained for unfinished and finished linen fabric.

Samples	T _i (°C)	T ₂₅ (°C)	T ₅₀ (°C)	T ₇₅ (°C)	Residue (%)
Linen	320	350	370	550	10
Finished linen (10 bilayers)	325	355	400	450	9

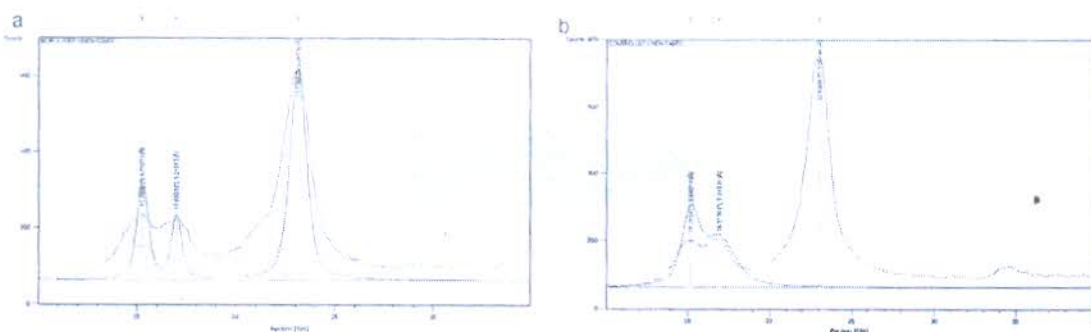


Fig. 5. (a) Unfinished linen fabric, (b) finished linen fabric.

obtained before and after treatment, showed the peaks corresponding to the typical profile of amorphous cellulose.

The strong peaks at $2\theta = 15.16^\circ$, 16.91° , and 23.03° are related to the crystallinity of cellulose [38]. From Fig. 5 (b), the finished linen fabric showed slight improvement in crystallinity. The peak intensities in case of finished linen is slightly higher than that of unfinished linen due to the occupancy of pores available in the amorphous region and hydrogen bonding between linen and chitosan. When layers of chitosan and GTL extract were applied on linen, the peaks were somewhat changed at the position ($2\theta = 15.29^\circ$, 17.00° , and 23.13°), indicating that no significant intercalation had occurred.

Functional properties of the finished fabric

The ultraviolet protection factor (UPF), antibacterial activity and antioxidant activity of unfinished and finished linen fabrics are shown in Table 4.

The finished linen displayed an excellent UV protection after deposition of 5 subsequent layers. UPF values increased with subsequent layers. The UV protection represents the blocking of transmittance of UV rays from the fabric. In this system, there were two contributors to the UV protection viz. the addition of barrier layer through deposition and the presence of active polyphenolic compounds in each layer which absorbs the UV light [39]. The antibacterial activity also showed enhancement with increasing number of layers. The finished linen with 10 layers showed a reduction of 97% of bacterial colonies. This is a significant value for the anti-bacterial finish on linen fabric. The finished fabric displayed efficient antibacterial activity which might be attributed to the presence of chitosan and green tea extracts. Chitosan is a cationic polysaccharide which can attach itself to the cell wall of bacteria causing the leakage of cell materials and also attacks the genetic material of bacteria, thus preventing the further growth [40]. Green tea extract contains various polyphenolic compounds like catechin, ferulic acid, etc. which are known for their antibacterial activity [41]. The finished fabric also displayed an excellent anti-oxidant property, the extent of which got increased with subsequent addition of layers. The potent radical scavenging activity was mainly attributed to the presence of green tea extract

[42]. The role of chitosan is also justified as it holds the green tea extract on the fabric firmly by ionic interactions. The green tea polyphenols are the responsible components for antioxidant activity; this is primarily due to the conjunction of hydroxyl groups and aromatic rings that unite their chemical structure which consequently neutralizes and binds the lipid-free radicals by hydroxyl groups of polyphenols [43].

Conclusion

In this study, the application of LBL assembly of chitosan and GTL extract in linen fabric finishing, and the effect of layers on color strength of the finished fabric and functional properties imparted on linen fabric was successfully studied. The role of green chemicals like chitosan and GTE biomolecules in developing coloured functional linen is established. The finished linen displayed an efficient multifunctional properties like antibacterial activity, UV protection and antioxidant activity. The attachment of various functional groups on the fabric, which were responsible for imparting functional properties, was confirmed through various characterizations. Hence, the natural resources like green tea and chitosan which are more environment-friendly can prove a good substitute of synthetic chemical for the textile finishing industry.

References

- [1] S. Richardson, M. Björnalm, F. Caruso, *Science* 348 (6233) (2015) 2491.
- [2] A. Elbakry, A. Zaky, R. Liebl, R. Rachel, A. Goeferich, M. Breunig, *Nano Lett.* 9 (5) (2009) 2059.
- [3] G. Decher, *Science* 277 (5330) (1997) 1232.
- [4] Y. Lvov, G. Decher, H. Moehwald, *Langmuir* 9 (2) (1993) 481.
- [5] V. Phivanartnuraks, T.J. McCarthy, *Macromolecules* 31 (6) (1998) 1906.
- [6] S.T. Dubas, J.B. Schlenoff, *Langmuir* 17 (25) (2001) 7725.
- [7] M. Joshi, R. Khanna, R. Shekhar, K. Jha, *J. Appl. Polym. Sci.* 119 (5) (2011) 2793.
- [8] R.C. Tang, H. Tang, C. Yang, *Ind. Eng. Chem. Res.* 49 (19) (2010) 8894.
- [9] B. Glover, J.H. Pierce, *J. Soc. Dyers Colour.* 109 (1) (1993) 5.
- [10] S. Noor, S. Ali, T. Hussain, *Asian J. Chem.* 27 (11) (2015) 4111.
- [11] J.B. Harborne, C.A. Williams, *Phytochemistry* 55 (6) (2000) 481.
- [12] G.F. Ferrazzano, I. Amato, A. Ingenito, A. De Natale, A. Pollio, *Fototerapia* 80 (5) (2009) 255.
- [13] Y. Ren, J. Gong, F. Wang, Z. Li, J. Zhang, R. Fu, J. Lou, *Dyes Pigm.* 134 (2016) 334.
- [14] S.H. Kim, *Fibers Polym.* 7 (3) (2006) 255.
- [15] J.E. Lee, H.J. Kim, M.C. Lee, *J. Korean Soc. Dyers Finish.* 13 (3) (2001) 11.
- [16] M.H. Han, *J. Korean Soc. Dyers Finish.* 12 (2) (2000) 51.
- [17] S. Lim, S.M. Hudson, *J. Macromol. Sci. Polym. Rev.* 43 (2003) 223.
- [18] M.M. Bashir, M.A. Khan, *J. Polym. Environ.* 21 (1) (2013) 181.
- [19] G. Duman, J.N. Chakraborty, *Fash. Text.* 2 (1) (2015) 13.
- [20] M.D. Ieu, J. Sheikh, C. Pradhan, *Melliand Int.* 20 (3) (2013) 171.
- [21] M.D. Ieu, J. Sheikh, L. Gomathi, *Melliand Int.* 19 (4) (2013) 229.
- [22] M. Sadeghi-Kiakhani, K. Gharanjig, M. Arami, *J. Ind. Eng. Chem.* 28 (2015) 78.
- [23] M. Sadeghi-Kiakhani, S. Safapour, *J. Ind. Eng. Chem.* 33 (2016) 170.
- [24] M.D. Ieu, J. Sheikh, P. Bhavsar, *Int. J. Biol. Macromol.* 54 (1) (2013) 125.
- [25] Y. S. Chung, K.-K. Lee, J.-W. Kim, *Text. Res. J.* 68 (10) (1998) 772.
- [26] S.K. Tiwari, M.M. Gharia, *AATCC Rev.* 3 (2003) 25.
- [27] J. Chen, G. Cheng, R. Liu, Y. Zheng, M. Huang, Y. Yi, H. Deng, *J. Colloid Interface Sci.* 523 (2018) 208.
- [28] H. Tu, G. Wu, Y. Yi, M. Huang, R. Liu, X. Shi, H. Deng, *Carbohydr. Polym.* 210 (2019) 9.

Table 4

UPF, antibacterial activity and antioxidant activity of unfinished and finished linen.

Sample No.	UPF value	Antibacterial activity (%)	Antioxidant activity (%)
Unfinished	9.85	Negligible	Negligible
1	22.55	75.30	58.06
2	23.47	79.50	70.85
5	52.81	88.40	85.50
8	83.32	95.25	89.19
10	88.16	97.00	95.89

- [29] J. Tian, H. Tu, X. Shi, X. Wang, H. Deng, B. Li, Y. Du, *Colloids Surf. B* 145 (2016) 643.
- [30] M.D. Teli, J. Sheikh, *Cellul. Chem. Technol.* 46 (1–2) (2012) 53.
- [31] AS/NZS 4399, Sun Protective Clothing Evaluation and Classification. (1996).
- [32] J. Sheikh, I. Bramhecha, *Int. J. Biol. Macromol.* 118 (2018) 896.
- [33] American Association of Textile Chemists and Colorists. AATCC Technical Manual, AATCC, 76, Research Triangle Park, NC, 2007.
- [34] S.Y. Oh, D.I. Yoo, Y. Shin, H.C. Kim, H.Y. Kim, Y.S. Chung, J.H. Youk, *Carbohydr. Res.* 340 (15) (2005) 2376.
- [35] J. Yao, Y. Liu, S. Yang, J. Liu, *J. Eng. Fibers Fabr.* 3 (2) (2008), doi:<http://dx.doi.org/10.1177/155892500800300205>.
- [36] M. Song, L. Li, Y. Zhang, K. Chen, H. Wang, R. Gong, *React. Funct. Polym.* 117 (2017) 10.
- [37] T. Zhang, H. Yan, L. Wang, Z. Fang, *Ind. Eng. Chem. Res.* 52 (18) (2013) 6138.
- [38] M.S. Khalil-Abad, M.E. Yazdanzhenas, M.R. Nateghi, *Cellulose* 16 (6) (2009) 1147.
- [39] M. Tian, X. Hu, L. Qu, M. Du, S. Zhu, Y. Sun, G. Han, *Appl. Surf. Sci.* 377 (2016) 141.
- [40] M. Kong, X.G. Chen, K. Xing, H.J. Park, *Int. J. Food Microbiol.* 144 (1) (2010) 51.
- [41] B.J. An, J.H. Kwak, J.H. Son, J.M. Park, J.Y. Lee, C. Jo, M.W. Byun, *Food Chem.* 88 (4) (2004) 549.
- [42] C.A. Rice-Evans, N.J. Miller, G. Paganga, *Free Radic. Biol. Med.* 20 (7) (1996) 933.
- [43] S.N. Senanayake, *J. Funct. Foods* 5 (4) (2013) 1529.



Download

International Journal of Biological Macromolecules

Volume 142, 1 January 2020, Pages 559-563

Functionalization of wool fabric using lignin biomolecules extracted from groundnut shells

Surya Bhushan, Ankit Kumar, Nagender Singh, Javed Sheikh

Show more

Outline | Share Cite

<https://doi.org/10.1016/j.ijbiomac.2019.09.130>

Get rights and content

Abstract

Food and agro-processing industries generate a huge quantity of solid waste which is rich in bio-macromolecules like lignin. The extraction of lignin biomolecules can help in the efficient management of such waste along with the generation of wealth from the waste. The groundnut shells are one of the lignin-rich wastes which could be utilized for the extraction of lignin biomolecules. The present work is an innovative approach involving the application of extracted lignin biomolecules for the value-addition to wool fabrics. Metallic mordants were utilized to get a wash-fast attachment of lignin with wool. The change in the appearance of wool fabrics was analyzed using reflectance spectroscopy. The finished fabrics were further evaluated for the functional properties like antioxidant activity, antibacterial activity and UV protection. The functionalized wool fabrics displayed a variety of shades with different combinations of groundnut shell lignin (GSL) and mordant. Thermal stability of treated wool fabrics was analyzed by thermogravimetric analysis. The functionalized wool fabrics showed significant antioxidant activity (69.5–84.5%), antibacterial activity (79.7–86.3%) and UV protection (UPF ratings of 50⁺).

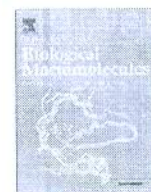
[View PDF](#)

Previous

Next

Keywords

Groundnut shell lignin; Antibacterial; Antioxidant; Wool



Functionalization of wool fabric using lignin biomolecules extracted from groundnut shells

Surya Bhushan, Ankit Kumar, Nagender Singh, Javed Sheikh*

Dept. of Textile Technology, Indian Institute of Technology, Delhi, India

ARTICLE INFO

Article history:

Received 10 June 2019
Received in revised form 24 September 2019
Accepted 29 September 2019
Available online 11 November 2019

Keywords:

Groundnut shell lignin
Antibacterial
Antioxidant
Wool

ABSTRACT

Food and agro-processing industries generate a huge quantity of solid waste which is rich in bio-macromolecules like lignin. The extraction of lignin biomolecules can help in the efficient management of such waste along with the generation of wealth from the waste. The groundnut shells are one of the lignin-rich wastes which could be utilized for the extraction of lignin biomolecules. The present work investigates an innovative approach involving the application of extracted lignin biomolecules for the value-addition to wool fabrics. Metallic mordants were utilized to get a wash-fast attachment of lignin with wool. The change in the appearance of wool fabrics was analyzed using reflectance spectroscopy. The finished fabrics were further evaluated for the functional properties like antioxidant activity, antibacterial activity and UV protection. The functionalized wool fabrics displayed a variety of shades with different combinations of groundnut shell lignin (GSL) and mordant. Thermal stability of treated wool fabrics was analyzed by thermogravimetric analysis. The functionalized wool fabrics showed significant antioxidant activity (69.584.5%), antibacterial activity (79.786.3%) and UV protection (UPF ratings of 50*).
© 2019 Elsevier B.V. All rights reserved.

1. Introduction

Recently, significant efforts have been made for the discovery of novel natural materials for functionalizing the textile substrates [1–3]. The natural materials with enhanced biodegradability and possible technological applications can diminish environment associated problems [4]. Apart from several types of synthetic materials used, several natural biomacromolecules perceive their position as efficient functional materials. Being biodegradable, economical, processable, renewable and non-toxic, along with their excellent chemical and physical properties, these materials are slowly replacing the conventional minerals [5,6]. Since the last decade, researchers are identifying the use of commercial, agricultural and industrial wastes as a more abundant, economical, and readily obtainable source of functional materials [7].

Groundnut (*Arachis hypogaea*), also known as peanut, is a global crop associated to the *Fabaceae* family. This crop's worldwide production is more than 10 million tonnes/year and the second-largest producer of groundnut in the world is India. The groundnuts processing industries produce the groundnut shells as a waste which is conventionally used as cattle feed and a source of biofuel [8]. The groundnut shells chemically comprise cellulose (35.7%), lignin (30.2%) hemicellulose (18.7%), and ash (5.9%) [6,9]. Even though

cellulose has gained more attention among researchers for its projected application as a raw material for the production of various materials, functional polymers and bio-based fuels [7], the exploration of lignin is limited and needs more investigations to open up its great potential [10,11]. There is an appreciable potential for lignin to serve as raw material for the extraction of various functional bio-molecules and it can be used for advanced engineering applications [12].

Lignin, which has the aromatic structure, is the dominant bio-renewable source on Earth [13]. Similar to other bio-renewable materials, lignin provides numerous properties such as antimicrobial activity, antioxidant activity, biodegradability [13]. Lignin is resistant to most of the microbial attacks unlike various polysaccharides, hemicellulose, and cellulose [14,15]. It is mainly comprised of sinapyl alcohols, p-coumaryl, and coniferyl, which are subdivided into phenylpropane units [15,17]. The presence of comparatively high contents of flavonoids and polyphenols such as luteolin, eriodictyol and 5, 7-dihydroxychromone in peanut shells was reported in the literature [18,19]. Wee et al. isolated four compounds with antioxidant activities from the methanolic extract of peanut shells which were identified as 5,7-dihydroxychromone, eriodictyol, 3,4,7-trihydroxyflavanone, and luteolin [20]. The chemical modification of lignin is possible because of the availability of ample functional groups which recommends the potential application of lignin in the formation of supramolecular aromatic chemicals [13,21]. In general, lignocellulosic biomass has been

Corresponding Author.

E-mail address: jnsheikh@iitd.ac.in (J. Sheikh).

<https://doi.org/10.1016/j.ijbiomac.2019.09.130>
0141-8130/© 2019 Elsevier B.V. All rights reserved.

considered as a waste material, and recently, some attempts have been made to exploit it as a source of useful functional biomolecules for textile applications [22,24]. It was proposed that the exploitation of lignin for development of value-added products will result in a substantial gain of the economy in the value-addition process [25]. In recent years, several important applications of lignin were reported. Culebras et al. utilized continuous melt spinning technique to prepare the precursor lignin blend fibres with thermoplastic polyurethane which were successfully converted into carbon fibres [26]. Culebras et al. studied the dielectric and thermal behaviour of modified kraft and organosolv lignin as a precursor of carbon fibre [27]. Vincent et al. investigated a cellulose-lignin based fibres as a precursor for the production of carbon fibres [28]. Dalton et al. manufactured bio-based carbon nanofibres from mixtures of lignin and poly-acrylonitrile to obtain thermoelectrical properties [29]. The lignin has been extensively used in many pharmaceutical applications. Pishnamazi et al. used natural polymers such as lignin, microcrystalline cellulose and lactose to improve the granulation of materials, which were further used for pharmaceutical applications [30]. In another study, Pishnamazi et al. investigated the influence of modified lignin on controlled release behavior of paracetamol at varying pH. The results suggested higher drug release and faster disintegration in case of modified lignin tablets [31]. Pishnamazi et al. also studied the effect of lignin in the manufacturing of aspirin tablets to control drug dissolution. The results suggested the higher release rate for the tablets containing lignin as compared to those without lignin [32].

The wool fibre is a superior textile material used for the luxury textiles items because of its warmness, smoothness, lightness, and softness. Wool fibre, being protein, is susceptible to microbial attack under specific condition [24,25]. It also lacks important functional properties like UV protection and antioxidant activity which are highly demanded in technical applications. In the present work, lignin bio-molecules were extracted from the groundnut shells using ultrasound sonication technique. The wool fabrics were functionalized using GSL by a pre-mordanting method. The functional properties of the modified wool fabrics were investigated. In short, the application of GSL in the preparation of economical multi-functional wool fabric was reported.

2. Experimental

2.1. Materials

The groundnut shells were procured from the local supplier. The wool fabric was purchased from the market (EPI-62, PPI-60, and GSM-175). All chemicals such as copper sulphate, ferrous sulphate, and potash alum were purchased from Merck Specialties Private Limited, India. The dried groundnut shells were crushed and powdered using a mixer-grinder and sieved to get a 2040 mesh fraction.

2.2. Methods

2.2.1. Extraction of GSL

The extraction of GSL was carried out using a method available in the literature [33,34] with slight modification in the solvent system and the process. The milled groundnut shells (5 gms) were put in 250 ml breaker, followed by addition of 100 ml of the ethanol-water mixture (10:90). The suspension was placed under probe sonicator and the sonication (100 W power with 35 kHz frequency) was continued for 30 min. The mixture was filtered, and the extract obtained (5%) was utilized for dyeing.

2.2.2. Mordanting of wool fabrics

For mordanting, different mordants were used such as potash alum (10% on weight of the fabric, owf), copper sulphate (1% owf), and ferrous sulphate (5% owf). The wool fabrics were separately immersed in different mordant solutions, keeping the M:L ratio of 1:10 and mordanting was carried out at 80 °C for 1 hr in a water bath (Julabo, USA).

2.2.3. Treatment of wool fabrics with GSL extract

Mordanted samples were squeezed and further subjected to treatment with GSL extract (100%, owf). The mordanted wool fabrics were immersed in a treatment bath (Julabo, USA) at 25 °C. The temperature of the bath was raised with a gradient of 3 °C/min and the treatment was continued at 90 °C for 1 hr. Subsequently, the treated fabrics were squeezed, followed by washing with cold water. The sample abbreviations are listed in Table 1.

2.2.4. Evaluation of functional properties of treated wool fabrics

Antioxidant activity of treated fabric was evaluated using the 2,2-diphenyl-1-picryl-hydrazil (DPPH) reagent [35]. The colony count method (AATCC 100-2004) was used for determining the antimicrobial activity of the treated samples [36]. The ultraviolet protection factor of finished wool samples was measured according to AS/NZS 4399:1996 standard using the UV-visible spectrometer [37].

2.2.5. Thermogravimetric analysis

To study the thermal stability of the sample, the finished wool samples were subjected to thermogravimetric analysis. The weight loss (%) of the fabrics was measured while the samples were being heated at a uniform rate of 20 °C/min in a nitrogen environment.

2.2.6. FTIR analysis

FTIR spectrometer (Thermo Scientific Nicolet iS50 FT-IR Spectrometer) was utilized to confirm the functional group of treated fabrics. The treated fabric was analyzed with 15-scans in the wavelength range of 4004000 cm⁻¹ with a resolution 4 cm⁻¹.

2.2.7. Colour value and fastness properties of the modified wool

The reflection method, utilizing a 10-degree observer, was employed to evaluate the depth of shade of treated fabrics. The

Table 1
Functional properties of wool fabrics.

Samples Code	Sample Details	Antioxidant activity ^a (%)	Bacterial reduction ^b (%)		UPF ^c
			<i>S. aureus</i>	<i>E. coli</i>	
Control	Control Sample	N	N	N	5.6
WGSL	Without mordant	75.5	45.5	55.25	
FGSL	Ferrous sulphate pre-mordanted	84.4	81.3	86.30	1653.7
CGSL	Copper sulphate pre-mordanted	69.5	80.5	84.50	753.6
AGSL	Alum pre-mordanted	79.9	79.7	81.70	705.1

N: negligible; S: average value of three determinations.

absorbance of the finished samples with GSL extract was measured on Spectra flash SF 300. The K/S values were calculated using the Kubelka-Munk equation. The scanned images of the dyed samples obtained through the spectrophotometer were also recorded.

To study the firm attachment of GSL with wool fabrics, the finished fabrics were subjected to washing fastness testing as per ISO 105C06-1M methods [38].

3. Results and discussion

3.1. Functional properties of treated wool fabrics

Antioxidant properties of the textile materials can be beneficial as it can scavenge the free radicals resulting in the prevention of the oxidative stress and thus lowering ageing related problems. The antioxidants are widely utilized in cosmetics and the antioxidant textiles can have added advantage as textile covers most parts of the human body and the effect is wash-durable. The antioxidant activity of wool samples was analyzed and the results are summarised in Tables 1. According to Table 1, wool fabrics treated with GSL extracts showed moderate to an excellent level of antioxidant activity with the radical scavenging in the range of 69.584.4%, depending on the type of mordant used for pre-mordanting. The FGSL exhibited the highest antioxidant value among all the samples. As evident from Table 1, the control sample showed negligible antioxidant activity indicating the insignificant role of functional groups like amino end-groups, carboxylic groups, and amide linkages in scavenging the DPPH radical. After the treatment with GSL without pre-mordanting, i.e. WGSL, the antioxidant activity was imparted. This indicates the role of bio-molecules from GSL in scavenging the free radical. Some phytochemical compounds containing hydroxyl, phenolic, and methoxy groups present in GSL extract play a significant role in increasing radical scavenger activity of lignin which results in excellent antioxidant activity. Also, because of the presence of phenolic hydroxyl groups in various polyphenolic compounds present in GSL extract, it shows a stabilizing effect and hence the radical scavenging.

It is interesting to note that WGSL also displayed a good level of antioxidant activity. This might be attributed to the free functionalities of the GSL in such cases. The antioxidant activity was further enhanced with pre-mordanting, except for CGSL.

It must be noted that the functional properties displayed by wool are dependent on the add-on of GSL, which is facilitated by the metal mordants, the efficiency of which generally varies in the individual cases of mordants. Antioxidant properties are mainly dependent on the add-on of GSL along with the free functionalities available for radical scavenging. Apart from this, it is evident that more GSL on fabric resulted in higher radical scavenging. The pre-mordanting resulted in the enhanced uptake of GSL along with the complexation of some of the functionalities of GSL. The combined effect resulted in better antioxidant activities in case of FGSL and AGSL, while the inferior effect in case of sample CGSL. WGSL displayed higher antioxidant activities as compared to CGSL which may be attributed to limited free functionalities in CGSL to stabilize the DPPH radical.

The antibacterial activity of treated wool fabrics was evaluated against *S. aureus* and *E. coli* bacteria, and the results are summarized in Table 1. The metallic mordants used for pre-mordanting of wool fabrics showed a toxic effect against the bacteria. As shown in the results, wool fabric treated with GSL extract after pre-mordanting using metallic mordants exhibited significant antimicrobial activity. The three different phenylpropane units such as sinapyl alcohols, p-coumaryl and coniferyl could be the responsible elements for antimicrobial activity of GSL extract [39]. The unmordanted sample (WGSL) however, displayed lower bacterial reduc-

tion, which does not qualify as antibacterial wool. In the presence of metallic mordants, the antibacterial activity showed enhancement which might be the combined effect of higher pick-up of biomolecules from the extract and the bactericidal effect of metal ions. So, it can be concluded that the GSL extract could be a promising source for antibacterial modification of wool in the presence of metallic mordants.

According to AS/NZS 4399:1996 standard, the UPF value of fabric higher than 50 indicates excellent UV protection offered by the fabric. The wool fabric treated with GSL extracts using different mordant showed UPF ratings of 50⁺ indicating the transmission of a negligible quantity of UV rays through the modified wool samples. Among the pre-mordanted samples, FGSL exhibited the highest UPF value (1653.7). Although UPF values achieved for CGSL and AGSL were lower than FGSL, all the ratings were in the excellent range (50⁺). The UPF values are dependent on the absorption of UV light by the substrate which lowers the transmission of UV light to human skin lying below it. The transmission of UV light was lowered significantly by the modified wool samples. The UV absorption by the biomolecules along with the complex between metal ions and the biomolecules are the main reasons behind such absorption and hence the enhanced UPF. Interestingly, different mordants showed varied UPF values; the ionic bridging achieved by metallic mordants between the lignin molecules and the fibres could be a possible reason for higher UPF values.

3.2. Thermogravimetric analysis

TGA provides characteristic curves over a specific heating rate and temperature range for a particular material based on its thermal stability.

As shown in Fig. 1, the control fabric started degrading at lower temperatures as compared to both FGSL and WGSL. This indicates the ability of lignin to enhance the thermal stability (in terms of Ti) of wool fabric. The characteristic and similar curves were obtained for FGSL and WGSL where the Ti was enhanced, while at higher temperatures, the samples showed greater weight loss as compared to control wool. Among the GSL-treated wool, FGSL showed slightly better thermal stability which might be attributed to the presence of metal ions (Fe) in the system. The weight loss values at 350 °C for WGSL, FGSL and FGSL were 50.05%, 25.22 and 15.2%, respectively. The ash formation at 700 °C was higher for control wool. The volatile degradation products obtained from lignin are aldehydes, alcohols, and phenolics with the formation of the gaseous product, e.g., CH₄, CO, CO₂ because of its branched characteristics and aromatic structure [40] which contributed to the enhancement in initial thermal stability of wool (till 350 °C). No

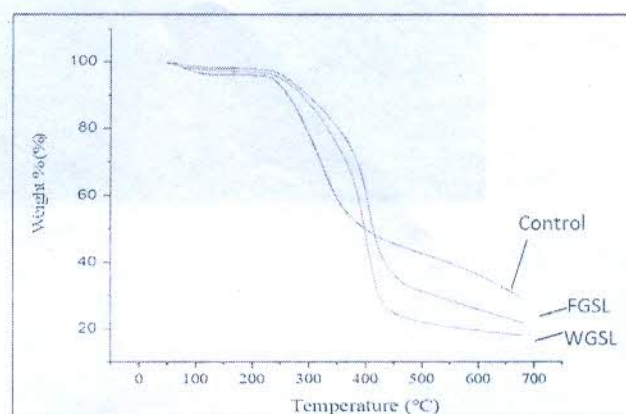


Fig. 1. Thermograms of wool fabrics.

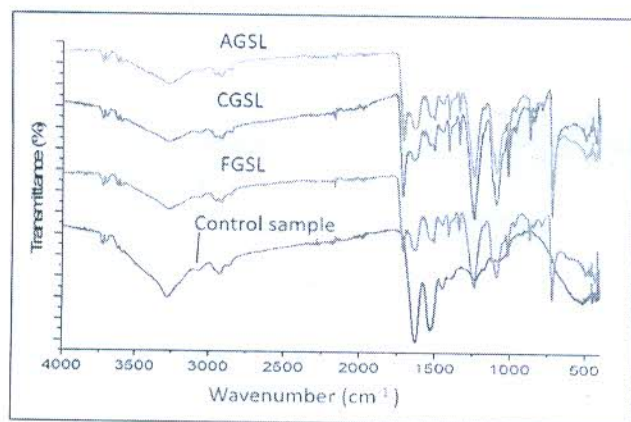


Fig. 2. FTIR analysis of wool fabric treated with GSL extract.

clear conclusions can be drawn from TGA analysis regarding the thermal stability of modified wool; however, the lower weight loss was evident at 350°C.

3.3. FTIR analysis

The FTIR spectra of control and modified wool fabrics were recorded and presented in Fig. 2.

A shift in peaks and formation of new peaks can be observed in the FTIR spectrum of finished fabrics. The significant change has been noticed in the peak intensity of —OH groups absorption band of treated fabrics. The peaks in the range 3250–3460 cm^{-1} was attributed to the hydroxyl groups (—OH) in phenolic and aliphatic structures. The CH stretching in aromatic methoxyl groups and aliphatic methyl and methylene groups of side chains was observed at 2900–3000 cm^{-1} . A new strong peak was observed at 1730 cm^{-1} which was attributed to C=O stretching in conjugated p-substituted aryl ketones of GSL extract. The treated fabric also displayed an aromatic C—O stretching vibrations (C—O stretching are those of the methoxyl and phenol groups) at 1200–1300 cm^{-1} . FTIR spectra of

treated fabric showed the characteristic peaks of GSL extract on wool fabric.

3.4. Colour values and fastness properties

The wool samples were analyzed for colour values and coordinates, and the results are summarized in Table 2. The finished fabrics displayed yellow-brown shades, the depth of which varied with mordant. The beautiful shades were obtained on wool are also presented in Table 2. The different mordants not only showed the effect on L^* , a^* , and b^* values but could also significantly affect the K/S values.


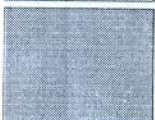


WGSL showed lower colour values indicating the tinting of wool using GSL. Among the pre-mordanted samples, FGSL showed highest colour value. CGSL also showed lighter shades. AGSL showed slightly higher colour values than WGSL. As shown in Table 2, L^* values showed similar trends like K/S where a sample with higher colour values showed a lower value of L^* . The significant tonal variations were observed among the treated wool (as indicated by a^* and b^* values).

The resistance of colour fading from the dyed wool samples was analysed using the washing fastness test. The fastness ratings for WGSL were inferior as compared to those of pre-mordanted samples. This confirms the wash-fast attachment of biomolecules from GSL extract on wool samples using metallic mordants. The ratings for change in the shade were in the range of very good to excellent. This verifies the insignificant fading of colour after the laundering treatment which can be taken as an indication of the durability of functional properties imparted to wool fabrics due to the presence of GSL biomolecules.

4. Conclusions

The lignin biomolecules were successfully extracted from the groundnut shells through the ultrasound-assisted extraction process and utilized for functionalization of wool fabrics in the presence of metallic mordants. The treated wool fabrics acquired beautiful shades along with functional properties. The treated wool fabrics displayed efficient bacterial reduction against *S. aureus* and

Table 2
Shade values for treated wool fabrics.

Sample code	L^*	a^*	b^*	K/S	Dyed fabrics	Washing Fastness	
						Change in shade	Staining
Control	90.87	1.45	9.65	0.235			
WGSL	77.60	0.52	10.96	0.722		2	34
FGSL	59.40	8.86	30.22	5.704		4	45
CGSL	60.70	0.31	16.19	2.911		4	45
AGSL	75.29	0.59	11.33	0.925		4	45

E. coli bacteria. The antioxidant activity and UV protection of the treated wool were also confirmed. The successful exploration of GSL in the novel application of functionalization of wool might open a new horizon in the field of functional finishing of textiles.

References

- [1] S. Basak, S.K. Chattopadhyay, S. Saxena, R. Narkar, Banana pseudostem sap and boric acid: a new green intumescent for making self-extinguishing cotton fabric, *Ind. J. Fibre Text. Res.* 43 (1) (2018) 36–43.
- [2] S. Basak, K.K. Samanta, S. Saxena, S.K. Chattopadhyay, M.S. Parmar, Self-extinguishable cellulosic textile from *Spinacia oleracea*, *Ind. J. Fibre Text. Res.* 42 (2) (2017) 215–222.
- [3] S. Basak, P.G. Patil, A.J. Shaikh, K.K. Samanta, Green coconut shell extract and boric acid: new formulation for making thermally stable cellulosic paper, *J. Chem. Technol. Biotechnol.* 91 (11) (2016) 2871–2881.
- [4] M. Shahid, F. Mohammad, Perspectives for natural product based agents derived from industrial plants in textile applications: a review, *J. Clean. Prod.* 57 (2013) 2–18.
- [5] N. Reddy, Y. Yang, Properties of natural cellulose fibers from hop stems, *Carbohydr. Polym.* 77 (4) (2009) 898–902.
- [6] S. Bano, Y.S. Negi, Studies on cellulose nanocrystals isolated from groundnut shells, *Carbohydr. Polym.* 157 (2017) 1041–1049.
- [7] R.J. Moon, A. Martini, J. Nairn, J. Simonsen, J. Youngblood, Cellulose nanomaterials review: structure, properties and nanocomposites, *Chem. Soc. Rev.* 40 (7) (2011) 3941–3994.
- [8] G.U. Raju, S. Kumarappa, Experimental study on mechanical properties of groundnut shell particle-reinforced epoxy composites, *J. Reinf. Plast. Compos.* 30 (12) (2011) 1029–1037.
- [9] K. Raveendran, A. Ganesh, K.C. Khilar, Influence of mineral matter on biomass pyrolysis characteristics, *Fuel* 74 (12) (1995) 1812–1822.
- [10] A.J. Ragauskas, G.T. Beckham, M.J. Biddy, R. Chandra, F. Chen, M.F. Davis, B.H. Davison, R.A. Dixon, P. Gilna, M. Keller, P. Langan, Lignin valorization: improving lignin processing in the biorefinery, *Science* 344 (6185) (2014) 1246843.
- [11] A. Duval, M. Lawoko, A review on lignin-based polymeric, micro- and nano-structured materials, *React. Funct. Polym.* 85 (2014) 78–96.
- [12] M.N. Collins, M. Nechifor, F. Tanas, M. Znoag, A. McLoughlin, M.A. Streyck, M. Culebras, C.A. Teac, Valorization of lignin in polymer and composite systems for advanced engineering applications: a review, *Int. J. Biol. Macromol.* 131 (2019) 828–849.
- [13] S. Laurichesse, L. AvOrous, Chemical modification of lignins: towards biobased polymers, *Prog. Polym. Sci.* 39 (7) (2014) 1266–1290.
- [14] W.O. Doherty, P. Mousavioun, C.M. Fellows, Value-adding to cellulosic ethanol: lignin polymers, *Ind. Crops Prod.* 33 (2) (2011) 259–276.
- [15] V.K. Thakur, M.K. Thakur, Recent advances in green hydrogels from lignin: a review, *Int. J. Biol. Macromol.* 72 (2015) 834–847.
- [16] J. Rencoret, J. Ralph, G. Marques, A. Gutiérrez, A.T. Martínez, J.C. del Río, Structural characterization of lignin isolated from coconut (*Cocos nucifera*) coir fibers, *J. Agric. Food Chem.* 61 (10) (2013) 2434–2445.
- [17] S.M. Roopan, An overview of natural renewable bio-polymer lignin towards nano and biotechnological applications, *Int. J. Biol. Macromol.* 103 (2017) 503–514.
- [18] V. Nepote, N.R. Grosso, C.A. Guzman, Extraction of antioxidant components from peanut skins, *Grasas Aceites* 53 (4) (2002) 391–395.
- [19] J. Qiu, L. Chen, Q. Zhu, D. Wang, W. Wang, X. Sun, X. Yin, F. Du, Screening natural antioxidants in peanut shell using DPPH/HPLC/DAD/TOF/MS methods, *Food Chem.* 135 (4) (2012) 2366–2371.
- [20] J.H. Wee, J.H. Moon, J.B. Eun, J.H. Chung, Y.G. Kim, K.H. Park, Isolation and identification of antioxidants from peanut shells and the relationship between structure and antioxidant activity, *Food Sci. Biotechnol.* 16 (1) (2007) 116–123.
- [21] M. Wawrzetkiewicz, P. Bartczak, T. Jesionowski, Enhanced removal of hazardous dye from aqueous solutions and real textile wastewater using bifunctional chitin/lignin biosorbent, *Int. J. Biol. Macromol.* 99 (2017) 754–764.
- [22] J. Sunthornvarabhas, S. Liengprayoan, T. Sawonsichon, Antimicrobial kinetic activities of lignin from sugarcane bagasse for textile product, *Ind. Crops Prod.* 109 (2017) 857–861.
- [23] S. Kadam, A. Sharma, S.U. Islam, I. Bramhecha, J. Sheikh, Utilization of Rice Straw as a Source of Biomolecules for Sustainable Multifunctional Finishing Vis a Vis Dyeing of Wool, *J. Nat. Fibers*. (2019). <https://doi.org/10.1080/15440478.2019.1581120>.
- [24] X. Hou, F. Fang, X. Guo, J. Wizi, B. Ma, Y. Tao, Y. Yang, Potential of sorghum husk extracts as a natural functional dye for wool fabrics, *ACS Sustain. Chem. Eng.* 5 (6) (2017) 4589–4597.
- [25] A.A. El-Kheir, S. Mowafi, M. Salama, A.A. El-Sayed, A. Kantouch, Imparting biocidal properties to wool fabrics using salicylanilide derivatives, *Egypt. J. Chem.* 56 (56) (2013) 435–447.
- [26] M. Culebras, A. Beaucamp, Y. Wang, M. Clauss, E. Frank, M.N. Collins, Bio-based structurally compatible polymer blends based on lignin and thermoplastic elastomer polyurethane as carbon fiber precursors, *ACS Sustain. Chem. Eng.* 6 (7) (2018) 8816–8825.
- [27] M. Culebras, M.J. Sanchez, A. Beaucamp, M. Carst, B.K. Kandola, A.R. Horrocks, G. Panzetti, C. Birkinshaw, M.N. Collins, Understanding the thermal and dielectric response of organosolv and modified kraft lignin as a carbon fibre precursor, *Green Chem.* 20 (19) (2018) 4461–4472.
- [28] S. Vincent, R. Prado, O. Kuzmina, K. Potter, J. Bhardwaj, N.D. Wanasekara, R.L. Hariman, A. Koutsomitropoulou, S.J. Eichhorn, T. Welton, S.S. Rabatekar, Regenerated cellulose and willow lignin blends as potential renewable precursors for carbon fibers, *ACS Sustain. Chem. Eng.* 6 (5) (2018) 5903–5910.
- [29] N. Dalton, R.F. Lynch, M.N. Collins, M. Culebras, Thermoelectric properties of electrospun carbon nanofibres derived from lignin, *Int. J. Biol. Macromol.* 121 (2019) 472–479.
- [30] M. Pishnamazi, S. Casilagan, C. Clancy, S. Shirazian, J. Iqbal, D. Egan, C. Edlin, D. M. Croker, G.M. Walker, M.N. Collins, Microcrystalline cellulose, lactose and lignin blends: process mapping of dry granulation via roll compaction, *Powder Technol.* 341 (2019) 38–50.
- [31] M. Pishnamazi, H. Hafizi, S. Shirazian, M. Culebras, G.M. Walker, M.N. Collins, Design of controlled release system for paracetamol based on modified lignin, *Polymers* 11 (6) (2019) 1059.
- [32] M. Pishnamazi, H.Y. Ismail, S. Shirazian, J. Iqbal, G.M. Walker, M.N. Collins, Application of lignin in controlled release: development of predictive model based on artificial neural network for API release, *Cellulose* 26 (10) (2019) 6165–6178.
- [33] M.F. Li, Y.M. Fan, F. Xu, K.C. Sun, Characterization of extracted lignin of bamboo (*Neosinocalamus affinis*) pretreated with sodium hydroxide/urea solution at low temperature, *BioResources* 5 (3) (2010) 1762–1778.
- [34] M.F. Li, S.N. Sun, F. Xu, R.C. Sun, Ultrasound-enhanced extraction of lignin from bamboo (*Neosinocalamus affinis*): characterization of the ethanol-soluble fractions, *Ultrason. Sonochem.* 19 (2) (2012) 243–249.
- [35] J. Sheikh, I. Bramhecha, Multifunctional modification of linen fabric using chitosan-based formulations, *Int. J. Biol. Macromol.* 118 (2018) 896–902.
- [36] American Association of Textile Chemists and Colorists, AATCC Technical Manual, AATCC, Research Triangle Park, NC, 2007, p. 76.
- [37] AS/NZS 4399, Sun protective clothing: evaluation and classification, 1996.
- [38] ISO Technical Manual, Geneva, Switzerland, 2006.
- [39] H.V. Lee, S.B.A. Hamid, S.K. Zain, Conversion of lignocellulosic biomass to nanocellulose: structure and chemical process, *Sci. World J.* 2014 (2014) 1–20.
- [40] Q. Liu, S. Wang, Y. Zheng, Z. Luo, K. Cen, Mechanism study of wood lignin pyrolysis by using TG/FTIR analysis, *J. Anal. Appl. Pyrol.* 82 (1) (2008) 170–177.



Download

Journal of Industrial and Engineering Chemistry

Volume 82, 25 February 2020, Pages 138-143

Functionalization of linen fabric using layer by layer treatment with chitosan and green tea extract

Sumit Saini, Ayush Gupta, Nagender Singh, Javed Sheikh

Show more

Outline | Share Cite

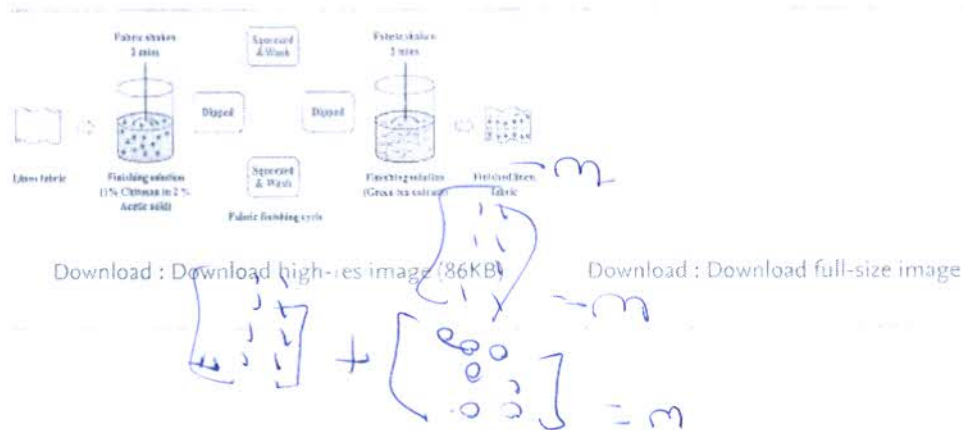
<https://doi.org/10.1016/j.jiec.2019.10.005>

Get rights and content

Abstract

Development of multifunctional textile materials using green chemicals is a new quest of research. In the present work, the LBL treatment using chitosan (CH) and green tea extract (GTE) was utilized for the functionalization of linen fabric. The functionalized linen was characterized and functional properties of the modified linen viz. antioxidant property, antibacterial activity and UV protection were evaluated. The finishing resulted in the coloured linen fabrics with antibacterial activity in the range 75–97%. Moreover, the treated fabrics also displayed an antioxidant property (58–96%) and the ultraviolet protection property (UPF > 22.5). The synergistic influence of CH and GTE was witnessed in imparting vital functional properties to linen using LBL technique.

Graphical abstract





Review

A comprehensive review of recent progress in fabrication of magnesium base composites by friction stir processing technique—A review

P. Sagar^{1,*} and A. Handa²

¹ Research Scholar, I.K. Gujral Punjab Technical University, Kapurthala, India

² Department of Mechanical Engineering, I.K. Gujral Punjab Technical University, Kapurthala, India

* **Correspondence:** Email: jasujaprem@gmail.com.

Abstract: Metal matrix composites (MMCs) are the next generation materials, globally popular for having numerous potential applications in aircraft, automobile and biomedical industry. Magnesium being continuously replacing other conventional materials however it is a hard to process material. Recently, friction stir processing (FSP) is drawing attention among researchers to fabricate MMCs. Using FSP, superior properties of magnesium based MMCs being successfully achieved. The primary aim of this paper is to review and provide a thorough summary of FSP synthesized magnesium based composites. Additionally the effect of secondary phase particles on the tribological behavior of produced composite materials is also summed up. Mechanical along with microstructural properties produced from stirred process and contribution of strengthening mechanism is addressed, as well.

Keywords: friction stir processing; metal matrix composites; magnesium; strengthening mechanism

1. Introduction

Metal matrix composite (MMC), widely known as the cluster of smartly developed engineered materials, synthesized by adding secondary phase reinforced micro, macro or nano particulates with parent materials of different chemical composition [1]. Continuous phase of metal is called matrix, and depending upon the chemical composition of matrix, composites are classified as metal matrix

composites (MMCs), ceramic matrix composite (CMC) and polymer matrix composite (PMC) [2]. MMC's recently are drawing interests of the researchers for not only they demonstrate firm bond with reinforced particles also develops no chemical alteration in terms of composition but also exhibits superior properties. MMC's clearly proven themselves as a promising candidate with their wide application in various fields [3,4]. Copper, magnesium, aluminum and titanium are commonly used matrix materials and TiC, MWCNTs, SiO₂, B₄C and Al₂O₃ few types of reinforced particles. Various manufacturing techniques like diffusion bonding [5], powder metallurgy [6–8], in situ fabrication [9], spray deposition [10], stir and squeeze casting [11–14] and vapor deposition been adopted by researchers to fabricate bulk MMCs [15,16]. All these manufacturing process of developing composites transform material from solid to liquid phase. On the flip side, techniques which do not have phase change process like solid state processing comparatively shows many merits over conventional phase change techniques. Friction stir processing (FSP) is a newly developed technique based on the principle of friction stir welding (FSW) [17]. And the principles along with recent progresses on friction stir welding and processing reported in [18]. Stirring action of FSP been successfully used to disperse secondary phase particles in the parent metal and producing next generation materials as MMCs [19]. Till now FSP is widely used to fabricate aluminum based composites [20–28]. Presently the world is more concerned about ecofriendly low-emission transportation vehicles with light-weight and maximum-performance. Magnesium been adopted by researchers and scientists over aluminum not for having density two-thirds that of aluminum also for its high strength-to-weight ratio [29]. Magnesium itself or its alloy doesn't meet the today need. For full filling this purpose few percentage of particulates need to be added in magnesium or its alloys. Addition of these particulates not only increases the microstructure of the composite but also enhanced it mechanical properties. Recently, Sunil et al. [30] summarized all work related to magnesium based composites. This paper present extended study of literature survey and review all recent development in the area of magnesium based composites fabrication by FSP. The demanding situations and future bearing of FSP are summed up.

2. Synthesis of composites with the aid of FSP

FSP in its least difficult structure comprises of a rotating tool that is non-consumable, which is dove into the work piece and afterward moved toward intrigue. The schematic outline of FSP is appeared in Figure 1.

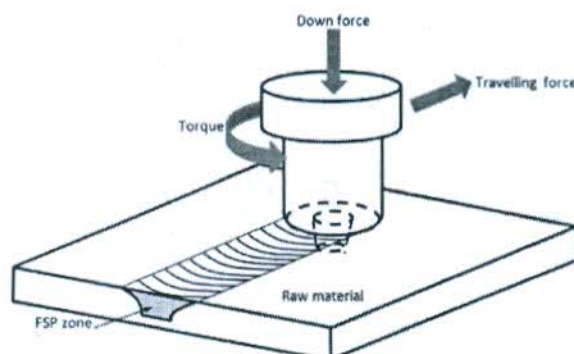


Figure 1. Schematic diagram of FSP technique.

FSP serves two essential capacities: (a) development of thermal energy thus deforming work piece material (b) mixing of secondary phase particles and form substrate. Intense rubbing of tool with material develop high frictional energy which results in producing enormous thermal energy. This thermal energy converts the metal into semi solid phase and makes it softer, while the turning of pin mixes and makes it flow around the pin. It then settle the soft metal depression at the back of the rotating tool. The material that flows around the tool is exposed to serious plastic deformation and heating, which prompts significant dynamic recrystallization thus refinement of microstructure in the stir zone (SZ) initiated [31].

2.1. FSP process variables

FSP machine process variables are classified into five categories. All these are the significant components that direct the successful achievement of the composite manufacture by FSP [32–40]. Variables are further divided into other various parameters. Figure 2 illustrates a schematic diagram of classification of the variables involved in the manufacture of the composite as well detailed by Rathee et al. [41].

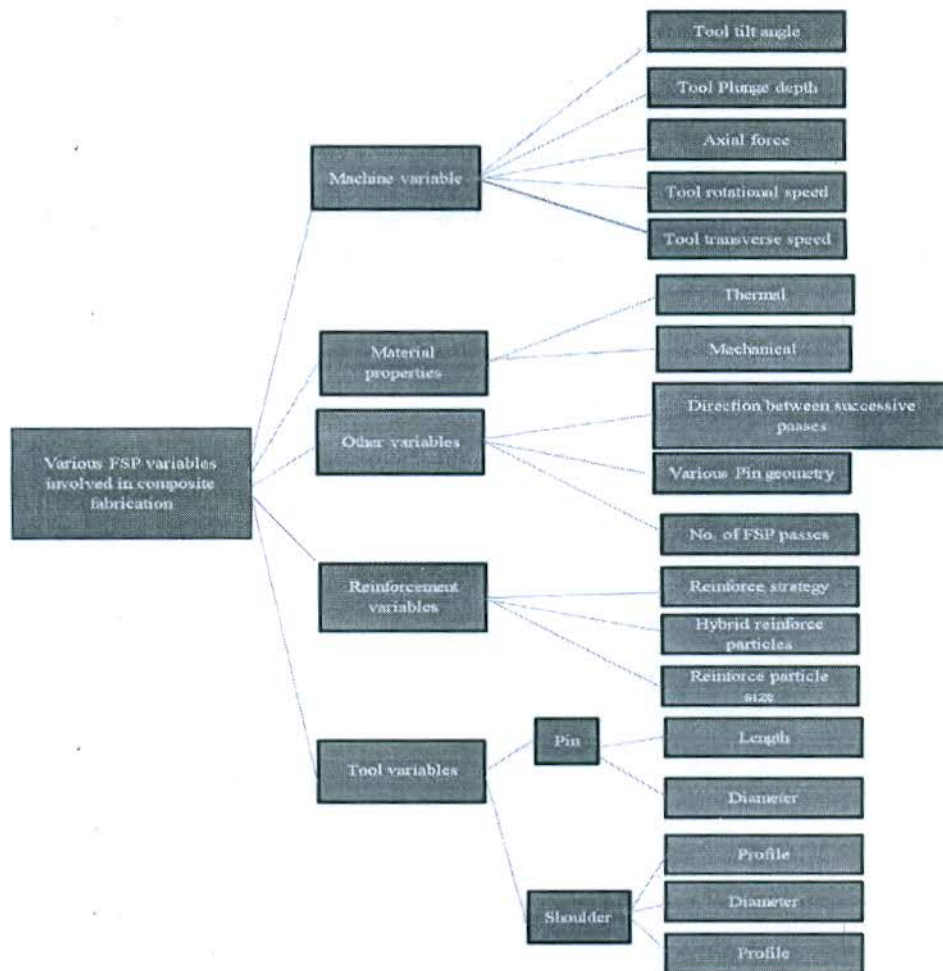


Figure 2. Various variables involved in FSP [41].

2.2. Doping method for reinforced particles

Prior investigations reveal that formation of composite materials was mainly via ceramic slurry layer for FSP process. Now a day's most common approaches for doping secondary phase particles into parent metal for composite manufacturing through FSP are shown schematically in Figure 3. Variety of secondary phase particles may be considered, as reported by literature, i.e., TiC, SiC, MWCNT, Al₂O₃, B₄C and SiO₂, etc.

- Hole drilling approach: Holes filling is a common strategy where required blind holes usually in straight/zig-zag pattern bored on top of the work piece and loaded up with reinforce particles. However, before final experimentation a pin less FSP tool is employed after loading of reinforced particles to avoid scattering of these particles.
- Groove filling approach: Groove filling is another common strategy in which a section is created on work piece and loaded up with reinforced particles. However, before final experimentation a pin less FSP tool is employed after loading of reinforced particles to avoid scattering of these particles.
- Sandwich approach: In this approach a layer of reinforced particles is prepared between parent material plates like a sandwich. High Thermal energy generated by tool breaks the particles and help in fabricating composite. However, uniform distribution may require increased number of passes.

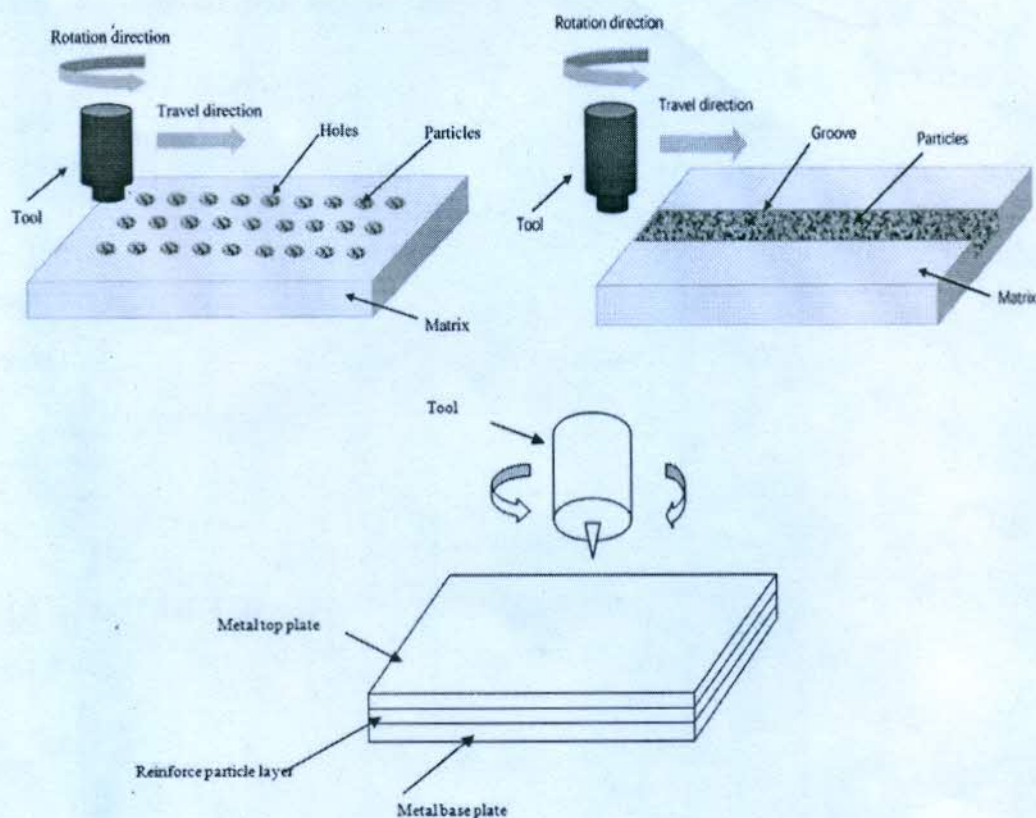


Figure 3. Schematic diagram of doping approaches [42].

2.3. Tool geometry

Tool geometry is a vital processing parameter which generates heat and guide material flow. The shoulder diameter affect heat generation at SZ and it is usually taken as, $D/d = 3$ (where D is shoulder diameter, d is pin diameter) [43]. Common types of tools used in FSP of magnesium based alloys are presented in Figure 4.

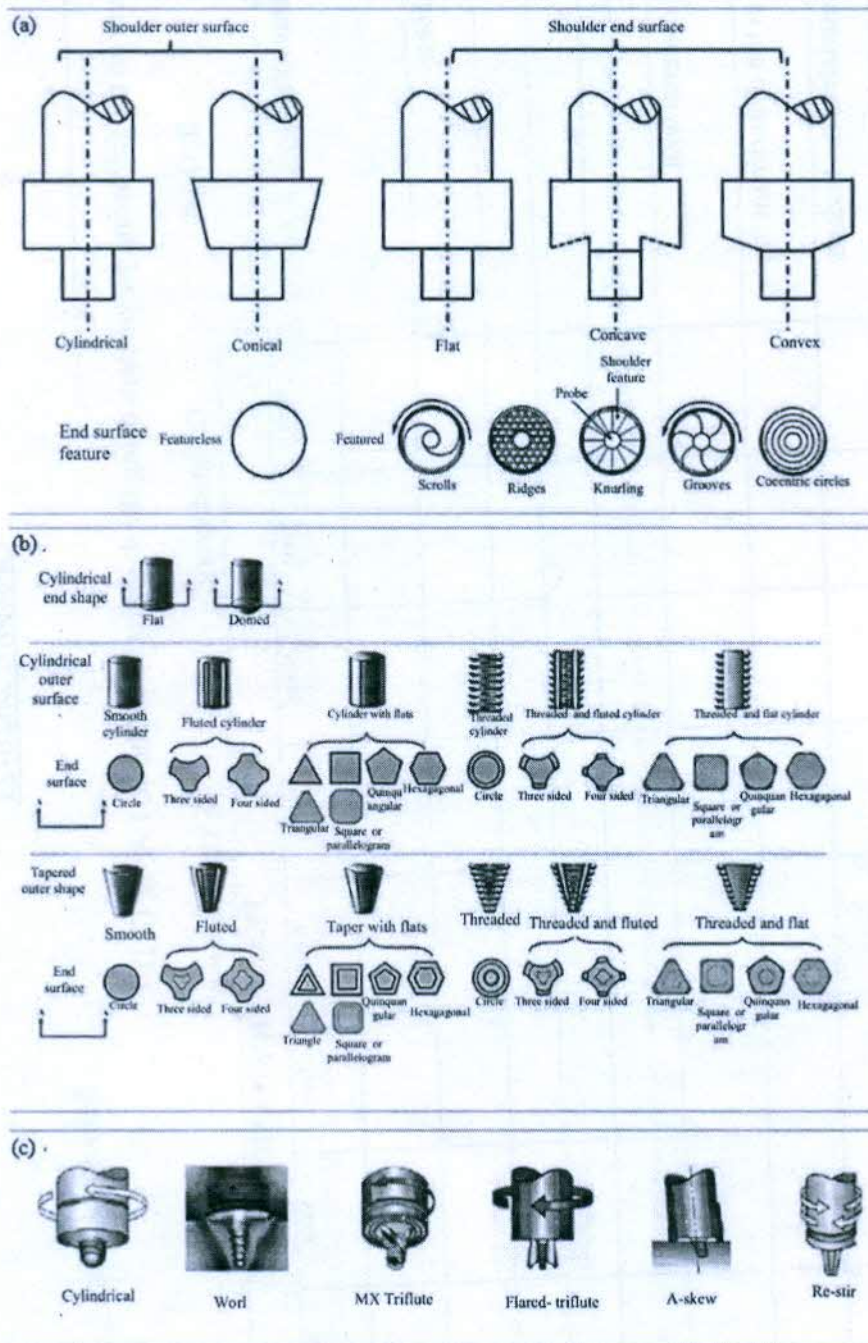


Figure 4. Common types of tools used for FSP processes [44].

3. Synthesis of Magnesium base composites with the aid of FSP

Most common magnesium alloys comprised of aluminum, zinc, thorium and uncommon earth. Using the ASTM alphanumeric designation system encourages grouping magnesium alloys by principal alloy composition like Mg–Al–Mn (AM), Mg–Al–Zn–Mn (AZ), Mg–Zr (K), Mg–Zn–Zr (ZK) with rare earth (ZE), Mg–Y–rare earth metal–Zr (WE). Initial two letters demonstrate the chief code for major alloying components followed by their concentration respectively. Last alphabet suggests alloy modification [45]. Studies considering major magnesium alloy for composite fabrication via FSP, as reported by the literature, are presented here.

3.1. AZ91Mg alloy

Asadi et al. [46] fabricate AZ91/SiC magnesium base composite considering square tool pin profile with three tool penetration depth (PD) 0.1, 0.2 and 0.3 mm and a tool tilt angle of 3°. They observed complete cracked processing zone for PD 0.1 mm, hole and tunneling cavity for PD 0.2 mm and sound surface quality for PD 0.3. They also studied the effect of tool rotational and tool transverse speed on grain size and micro hardness by considering groove filling approach for fabricating magnesium base AZ91 alloy with 5 μm SiC particles. They consider two 900 and 1400 rpm tool rotational speed and five 12.5, 25, 40, 50 and 63 mm/min tool transverse speeds. Finding of their research work suggests that best result for grain size and micro hardness were achieved at tool rotational speed of 900 rpm with transverse speed of 63 mm/min, i.e., 7.16 μm and 94 Hv. Asadi et al. [47] further extended their research for AZ91/SiC composite and suggests grain size increases with increase in rotational speed and lowers the micro hardness. Also it was noted that increasing transverse speed reduced the grain size, while the micro hardness increases. It was also added that changing the tool rotation speed resulting in fine grains and uniform distribution of particles. Faraji et al. [48] synthesized AZ91/Al₂O₃ composite by using friction stir processing. Their work included three different size nano particles ranging from nanometer to micrometer scale, i.e., 3000, 300 and 30 nm and two different tool geometries along with varying number of passes and also studies their effect on performance measures like grain size, cluster size, micro structure and mechanical properties. Findings of their work suggests that grain size in triangular tool is less than square tool but follows opposite trend in case of hardness. Finally the conclusion drawn from their work suggests that decrease in size of nanoparticle increases hardness of the composite. Khayyamin et al. [49] studied the effect of process parameters on micro structural characteristics of AZ91/SiO₂ composite fabricated by FSP. They fix tool rotation speed to 1250 rpm, tilt angle to 3° and number of passes to 4 passes with varying transverse speed to 20, 40 and 63 mm/min. They also examine metallurgical and mechanical properties by Optical Microscopy (OM), Scanning Electron Microscopy (SEM) and Vickers hardness tester. All optical microscopy and scanning electron microscopy tests were conducted on composites having all different passes and different transverse speed. Outline of the work concluded that grain size decreases and strength and hardness increase with increase in transverse speed. Increase number of pass increase hardness and reduce grain size. Faraji et al. [50] consider tool geometry of two types square and circular to examine the influence of process parameters on AZ91 with and without Al₂O₃ nano particles. It can be understood from the work that at tool rotation speed 900 rpm and transverse speed of 80 mm/min for square tool provides the best result with grain size 6 μm and microhardness 103 Hv as compared to 7.27 μm and 98.52 Hv

without particles. Ahmadkhaniha et al. [51] analyzed wear resistance on AZ91/Al₂O₃ as produced by FSP adopting groove filling approach with circular tool. They further consider different tool rotation speed, transverse speed and a fixed tool tilt angle of 3° to investigate mechanical and metallurgical properties. Finally outcome of the study suggests that tool rotation speed of 800 rpm and transverse speed 40 mm/min gives optimum results for grain refinement and wear behavior. Dadashpour et al. [52] introduced 10–15 nm SiO₂ particulates to study the fracture behavior AZ91C composite fabricated by FSP. H13 tool material was considered along with square pin geometry with a fixed tool rotational speed of 1250 rpm and feed rate 40 mm/min. Extreme refined grain from starting size of 140 to 4 μm was observed along with the hardness of 130 Hv and ultimate tensile stress of 239.6 MP for three FSP passes. Chen [53] mixes SiC particles and prepared a layer of surface composite on thixoformed AZ91 using FSP. Wear behavior of thixoformed AZ91/SiC was compared with thixoformed AZ91 alloy without composite surface. The authors concluded that found that increasing number of passes can minimize the agglomeration and maximize the SiC particles distribution. Further they reported reduced coefficient of friction and enhanced wear resistance of surface composite layer when compared with parent alloy. Very recently, Singh [54] developed AZ91/B₄C nano composite using drill hole approach with cylindrical tool rotating with 900 rpm and having feed of 45 mm/min. Three different sizes nano particles were considered for examine microhardness and wear behavior. Finally study concluded that average hardness, wear resistance increases and wear rate decreases as the reinforce particle size increases.

3.2. AZ31 Mg alloy

Morisada et al. [55] fabricate AZ31 magnesium alloy with SiC via using friction stir processing. They used SiC powder of mean diameter 1 μm into a groove of 1 × 2 mm of a 6 mm thick plate. A tool of columnar shape of material SKD61 with diameter 12 mm along with a probe of diameter 4 mm and length of 1.8 mm was used, also they fix the value of parameters like tool rotation 1500 rpm, tool tilt angle 3° and travel speed of range 25–200 mm/min for processing. OM, SEM and Transmission Electron Microscopy (TEM) tests were conducted to study the micro structural properties of the composite. Findings of the test reported a fine grain size, i.e., 6 μm in the developed AZ31/SiC as compared to the mean grain size, i.e., 79.1, 12.9 of as-received AZ31 and FSPed AZ31 respectively for the travel speed of 50 mm/min. Further they reported that as travel speed increase grain size of the composite decreases. Micro-vickers hardness tester with a load of 200 g was used to measure micro hardness and it shows a maximum value of 69.3 Hv for FSPed AZ31 with SiC particles and 48.1 Hv and 60.0 Hv for as-received AZ31 and FSPed AZ31 respectively. Morisada et al. [56] studied the influence of addition of multi walled carbon nano tubes on grain size and hardness of AZ31 magnesium composite prepared through friction stir processing. AZ31 rolled plate of 6 mm thickness with a groove of 1 × 2 mm, filled with multi walled carbon nanotubes of outer diameter 20–50 nm and of 250 nm length was used. A tool of columnar shape of material SKD61 with diameter 12 mm along with a probe of diameter 4 mm and length of 1.8 mm was used for fabrication. Good dispersion of nanoparticles was observed at 25 mm/min transverse speed and 1500 rpm tool rotation speed respectively. Hardness of 78 Hv was observed for AZ31/MWCNT as compared with hardness of 41 Hv of as received AZ31. Azizieh et al. [57] examine the effect of process parameters like tool profile, rotational speed and number of passes on micro structural and mechanical properties of FSPed fabricated AZ31/Al₂O₃. They used three kinds of Al₂O₃ particles

with mean diameters of 35, 350 and 1000 nm respectively. Rectangular shape of $60 \times 100 \times 10$ mm as cast AZ31 was used along with a groove of 1.2 mm width and 5 mm depth with a grain size of 70 μm . Varying geometry of tools, i.e., tool with a columnar probe without threads, a tool with a columnar probe with threads and a tool with columnar probe with threads and three flutes heat treated till 53HRC hardness along a fixed tool transverse speed of 45 mm/min, tool rotational speed of 800, 1000, 1200 rpm and tool tilt angle of 2° and FSP 2–4 times passes was adopted. OM, SEM and micro hardness tests was conducted to examine the etched sample. Finally cavity formation was noticed when non-threaded tool was used also they reported that use of threaded pin leads to good grain size along with uniform distribution of nano particles. In case of threaded pin with flute they observed low homogeneity along with tunneling effect. Azizieh et al. [58] synthesized AZ31/ Al_2O_3 composite by using friction stir processing. They considered parameters like rotational speed and number of passes to find out their effect on particle distribution, grain refinement, hardness and temperature changes in the magnesium metal composite. A constant travel speed of 45 mm/min, tool rotational speed of 800, 1000, 1200 rpm, tool tilt angle of 2° and FSP 2–4 times passes was adopted. Temperature in the stir zone was measured by the K-type thermocouple immersed in the stir region. Findings suggest that with increase in tool rotational speed average grain size, peak temperature and particle distribution increases. Also if number of passes increases nanoparticle agglomeration decreases and hardness increases which is good. Finally work concludes that at 800 rpm hardness is higher as compared to 1000 and 1200 rpm. Srinivasan et al. [59] developed AZ31B/ Al_2O_3 magnesium metal matrix nanocomposites through rotational friction welding. Authors, further examine the influence on mechanical and microstructure for the various controllable parameters like upsetting and friction time, upsetting and friction pressure. Cumulative effect of machine parameters and thermo mechanical stresses results in typical grain refinement in the SZ. Authors reported increase in friction time decrease joint efficiency. Microhardness variation is attributed due to distribution of heat produces by friction pressure and time. Chang et al. [60] synthesized metal matrix magnesium based composite AZ31/nano- ZrO_2 and nano- SiO_2 via FSP and examined both the microstructure and mechanical properties of. A tool with cylindrical probe with shoulder diameter 18 mm and pin length and diameter of 6 mm with 2° tilt angle along with pin rotation of 800 rpm and advancing speed of 45 mm/min was used. Two grooves each 6 mm in depth and 1.25 mm in width were cut, in which 10–20 vol% of nano-sized ZrO_2 and 5–10 vol% nano-sized SiO_2 particles was filled. Mechanical properties like vickers hardness was checked using a 200 gf load for 10 s along with optical microscopy, scanning and energy dispersive spectrometer was conducted to examine mechanical and metallurgical properties. Average grain size of composite produced 4P FSP resulted to be refined upto to 2–4 μm . Balakrishnan et al. [61] used magnesium alloy AZ31 with particulates like TiC to fabricate a magnesium matrix composite. They operate or execute or demonstrate the FSP by taking fixed tool rotational speed, transverse speed, and axial force on a 6 mm AZ31 plate by single pass. They engraved four different width (0, 0.4, 0.8, 1.2) and of equal depth 4.5 mm in the plate to introduced varying different fraction of the given (0, 6, 12, 18). Macrostructure and microstructure was studied by digital optical scanner and scanning electron microscope and it suggested TiC were properly distributed. Jiang et al. [62] dispersed nano SiO_2 reinforced by FSP into AZ31 Mg alloy. The main result reflects uniform grain refinement up to less than 1 μm and increase in hardness up to 1.83 times higher than that of the as-received AZ31 can be achieved. Sharma et al. [63] fabricated a novel hybrid nanocomposite AZ31/MWCNT–Graphene using multi-pass FSP with constant other parameters. Uniform, refined and more localized grains of average size

of 4.0 μm with lesser tensile twin fraction were reported for hybrid nano composites as shown in Figure 5.

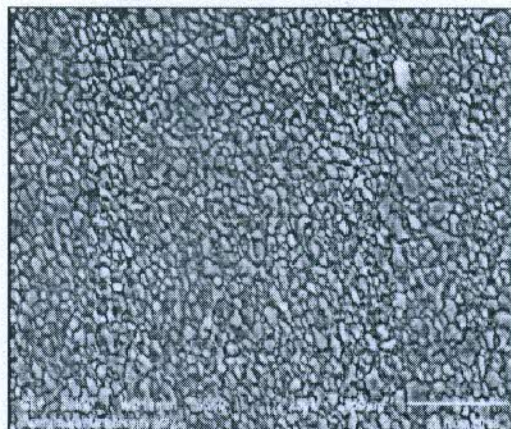


Figure 5. Microstructure of AZ31Mg–MWCNT–Graphene hybrid nanocomposite [63].

Also uniform dispersion of hybridized reinforce particles leads to significant enhancement of elastic modulus, tensile failure strains along with the improved mechanical properties like microhardness, i.e., 90.6 Hv and superior ultimate tensile strength as 49.23% as shown in Figure 6 with yield strength as 32.31%.

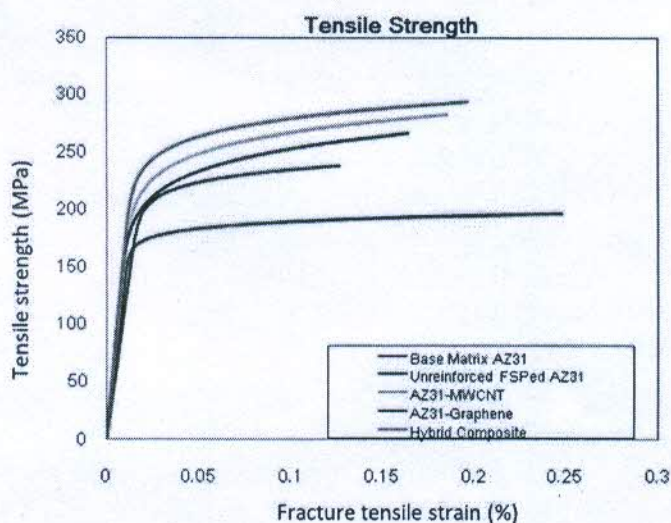


Figure 6. Tensile strengths of different specimens [63].

Huang et al. [64] executes the process of synthesized AZ31/SiC composite with a special FSP tool unlike other FSP tool. In this novel tool reinforce particles introduced via a hole prepared within this new direct friction stir process tool (DFSP). More than four times lesser grain was formed as compared to as cast magnesium alloy grain size of 16.57 μm . Authors further suggested groove or

hole filling step can completely be eliminated with new tool also better hardness can be achieved as compared to conventional FSP. Soltani et al. [65] synthesized AZ31B/CNT surface composite using FSP. For this research work author provides a suitable combination of transverse speed of 24 mm/min and rotational speed of 870 rpm for significant increase in hardness of 60 vickers and reduced grain size of less than 5 μm . Navazani and Dehghani [66] introduced 5 μm TiC particles for the fabrication of AZ31 magnesium base composite. Microstructural and hardness of the produced composite was examined. Authors suggested that three vital factors are responsible for dislocation of grain in composite i.e. dissimilar deformation behavior between particle and matrix, grain boundaries and thermal expansion. Finally, work suggests that defect free zone can be achieved at 1250 rpm and 50 mm/min with declined grain size. Sunil et al. [67] loaded nanohydroxyapatite reinforced particles into the groove of base AZ31 magnesium alloy in order to produce composite material. Authors mainly investigate the composite for biomedical applications and degradation of material. Wettability, cytotoxicity and vitro bioactivity in super saturated simulated field is been checked. Grain refinement upto 2 μm been the main reason of enhanced surface energy. Further authors concluded that dissolution of iron at FSP zone was within tolerance limit and hence its effect on corrosion is negligible. Newly, Sharma et al. [68] examined the influence of tool rotation speeds on mechanical and microstructure properties of fabricated a novel hybrid nanocomposite AZ31/MWCNT–Graphene using FSP. Optimum ratio of 1.6 and 0.3 vol% of MWCNT and grapheme was used. Author obtained various values of microhardness at different tool rotation speeds and presented them into a graph form as shown in Figure 7.

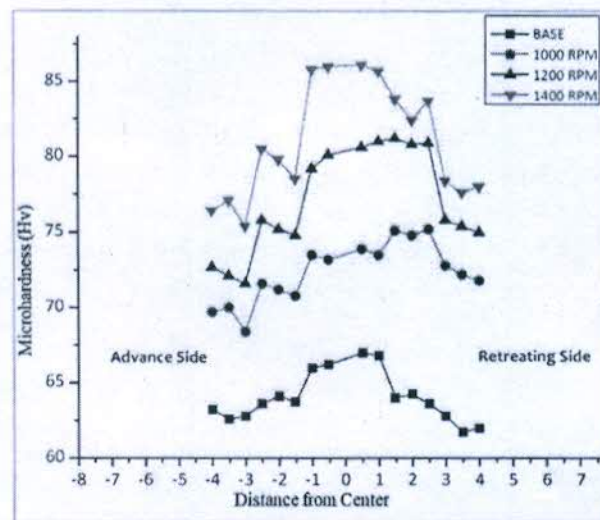


Figure 7. Range of microhardness at various tool rotation speeds [68].

3.3. WE43 and RZ5 Mg alloy

Das et al. [69] prepared a metal matrix composite WE43/B4C/6 vol% via friction stir processing. For the experimentation work they used $30 \times 5 \times 1.6 \text{ cm}^3$ of WE43 plate, B4C of 6 μm along with stepped tool. They drilled a set of holes into the plate for the friction processing and observe the microstructural and mechanical properties through scanning electron microscopy and tensile,

hardness tests. Finally they analyze reduction in grain size and increase in micro hardness for four passes as compare to single pass. Further they concluded that post treatment of composite at 210 °C for 48 h not only increase yield strength from 189–281 but also increase the ultimate tensile strength and elastic modulus with reduction in ductility and elongation to failure. Recently, Vedabouriswaran and Aravindan [70] introduced boron carbide (B₄C), MWCNT and a mixture of ZrO₂ + Al₂O₃ secondary phase particulates for production of magnesium rare earth alloy—RZ 5 based composite of by single pass FSP. Pinning effect cause by the reinforce particles produces refined grains of range 0.8 to 1.87 μm. Microhardness from 125 to 403 Hv was reached with increased ultimate tensile strength with range of 250–320 MPa.

3.4. AZ61 Mg alloy

Valle et al. [71] like Chang et al. [60] used backing plates as of cooper to speed up heat transfer rate between tool and work piece. They studied the effect of FSP on AZ61 via examining mechanical and micro structural properties. Grain refinement was achieved with maximum size 45 to 1.8 μm. Further authors reported that the surface created during FSP favors basal slip during the tensile test, leading to increase of ductility, a decrease in yield stress and a decrease in strain rate sensitivity in comparison with rolled AZ61 alloy. Lee et al. [72] created AZ61 based nanocomposite by mixing 5–10 vol% nanosized SiO₂ via FSP. Fix parameters with tool rotation 800 rpm and tool transverse 45 mm/min was employed. A back plate for cooling purpose for the whole procedure was deployed beneath. Succeeded FSP, authors declared that as number of passes increases nano-SiO₂ particles turns into a cluster of size going from 0.1 to 3 μm and the degree of grouping decreases. TEM contemplates that nano-SiO₂ particles stayed as shapeless and opposes change to crystalline stage during whole procedure. Du and Wu [73] processed magnesium base AZ61 alloy with rapid heat sink via FSP and achieved fine-microstructure at the processed zone with enhanced mechanical properties. Authors, observed average grain size less than 300 nm with mean micro hardness of 120–130 Hv, two times higher than that of AZ61 substrate. They further declares that one pass FSP under a high cooling rate may produces ultra-fine structure in AZ61 alloy with superior mechanical properties.

Literature survey concludes that various magnesium based composites were developed in past decade. All these composite materials shows improved microstrurtural and mechanical properties. Tribological performance, however, is by far the most commonly encountered industrial problem where the material is mainly influenced by speed, environmental conditions, and workload. Wear is a gradual and progressive material loss that is continuously subjected to rubbing action. Wear resistance of the composite metal matrix depends primarily on different microstructural features, such as particle size, volume fraction, reinforcement material distribution, and shape.

4. Tribological performance of some magnesium based composites

Tribological performance of magnesium based composites is an other parameter which have been succesfully studied and improved by the various researchers. Table 1 provides the brief summary of the work carried out so far pretaning to tribological performance of magnesuim based composites.

Table 1. Brief summary of the tribological performance of developed magnesium based composites as reported in literature.

Composite	Tool geometry	Grain size improvement	Machine parameters	Wear test specifications	Significant outcome	References
ZM21/SiC/B ₄ C	Straight cylindrical	40 μ m refined up to 20 μ m	1200 rpm, 50 mm/min	Pin on disc, load 0.5 kg, sliding speed 640 rpm for 6 km	Wear rate of composite decreases seventy six times to the base metal	Reddy et al. [74]
AZ91/Al ₂ O ₃ /SiC	Straight cylindrical	More refined grains as number of passes increases	730–1800 rpm, 14–80 mm/min with 1–4 passes	Tri pin on disc, load 50 N, sliding speed 1 mm/s for 500 m	Wear rate decreases as number of pass increases AZ91/Al ₂ O ₃ & AZ91/SiC gives almost same wear rate	Abbasi et al. [75]
AZ91/TiC	Straight cylindrical	More refined grains	900 rpm, 40 mm/min with PD = 0.3 mm	Pin on disc, load 5–10 N, sliding speed 1 m/s for 2000 m	Wear rate of composite decreases half to the base metal	Singh et al. [76]
AZ31/TiC	Straight cylindrical	More refined grains	800 rpm, 40 mm/min	Pin on disc, load 5–20 N, sliding speed 1 m/s for 1.5 km	At 20 N higher wear resistance was noticed	H. S. Arora et al. [77]
AE42 as cast and FSPed AE42	Straight cylindrical	40% reduction in grain size and reached upto 1.5 μ m	700 rpm, 60 mm/min	Pin on disc, load 5–20 N, sliding speed 0.3–3 m/s for 2500 m	Higher co-efficient of friction attended at low sliding velocities	Arora et al. [78]
As cast Mg/SiC	Threaded cylindrical	Grain size reduced from 170 to 3 μ m	1300 rpm, 50 mm/min	Pin on disc, load 1–5 Kg, sliding speed 1 m/s for 600 m	20% and 47% wear loss was noticed at 1 and 5 Kg	Ram et al. [79]
AZ31/Al ₂ O ₃	Threaded cylindrical	With development of refined grains hardness increases from 50 to 90 Hv	800, 1000, 1200 and 1400 rpm, 45 mm/min and 2° tilt angle	Pin on disc, load 10, 50 and 90 N, sliding velocity 0.12m/s for 600 m	Wear rate at 1000 and 1200 rpm is higher as compared to 800 rpm	Azizieh et al. [80]
AZ31/Fly ash	Straight cylindrical	Upto 4 μ m grain size achieved	1200 rpm and 40mm/min	Pin on disc, load 20 N, sliding velocity 1.0 m/s for 3000 m	FSP exhibits 33% lower wear rate as compared to stir cast	Dinakaran et al. [81]
AZ91/Al ₂ O ₃	Circular and square tool	Average grain size 5–10 μ m was obtained	900–1200 rpm, 40–80 mm/min with 3° tilt angle	Pin on disc, load 50 N, sliding velocity 1.0 mm/min for 500 m	Wear rate decreases more than three times to the base metal	Faraji and Asadi [82]
AZ31/MWCNT/Al ₂ O ₃	Cone shape	Much small size grains with microhardness 1.4 times higher than those of AZ31	1050 rpm, 33.4 mm/min	Pin on disc, disc rotation 200 rpm, load 0.65, 1.30, 1.95, 2.60 and 3.25 MPa	For load more to 1.95 MPa, the wear and friction coefficient of hybrid AZ31 composite is low and it only follows in case of 0.1% Al ₂ O ₃ and 0.2% CNTs composites	Lu et al. [83]

5. Strengthening mechanism and valuable equations

Considering the development of magnesium based metal matrix composites via FSP as reported in literature only selective strengthening mechanism hold good. Grain boundary and secondary phase

mechanism are the two strengthening mechanism and both of them are Hall–Petch relationship, and Orowan strengthening.

5.1. Hall–Petch strengthening

Hall–Petch strengthening mechanism have a vital role in the upgradation of major properties like strength of a composites, and it's contribution is directly depend on refined grains existing in metal matrix zone. And the pinning action exerted by the secondary phase particles give rise to the concept of grain boundary and grain size which is further expresses by Zener equation as shown in Eq 1 where the grain size of the matrix d_m that can be achieved [70].

$$d_m = 4\alpha d_p / 3v_p \quad (1)$$

Here d_p shows particle size, volume fraction of particles is v_p and α is a constant of proportionality. It may be concluded that newly developed grain size is highly influenced by the size of the reinforcement particles and its volume fraction. Hall–Petch relationship states that hardness is inversely proportional to grain size in other words any reduction in the grain size attributes to increase the yield strength. According to Hall–Petch Eqs 2 and 3 [84–87].

$$\Delta\sigma_{\text{Hall-Petch}} = K_y(d_{\text{composites}}^{-1/2} - d_{\text{matrix}}^{-1/2}) \quad (2)$$

where $d_{\text{composites}}$ and d_{matrix} are the average grain size of the composite and matrix and K_y is the strengthening coefficient.

$$\sigma_y = \sigma_o + K_y/\sqrt{d} \quad (3)$$

where σ_y is the yield stress, σ_o is a materials constant for the starting stress for dislocation movement (or yield strength before FSP), k_y is the strengthening coefficient (a constant specific to each material), and d is the average grain diameter. Based on similar theory [46–47] reported that increases the tool transverse speed, grain size reduces in SZ which further increases hardness at SZ. The influence of grain size on yield strength of magnesium alloys has also been reported in number of studies [59,60,64,69]. Azizieh et al. [81] and Huang et al. [64] based on average grain size uses further simplified Hall–Petch relationship and uses Eqs 4 and 5 for calculating microhardness of the samples.

$$H_v = 43 + 78d^{-1/2} \quad (4)$$

$$H_v = 40 + 72d^{-1/2} \quad (5)$$

where d is the average grain size. Rather Hung [88] established a generalized equation (Eq 6) for AZ series magnesium alloys. As reported in literature Figure 8 shows the ultra-refinement in grain size of magnesium composites as compared to base metal and Figure 9 shows the corresponding values of microhardness for magnesium composites when compared to base metal.

$$H_v = 56 + 348d^{-1/2} \quad (6)$$

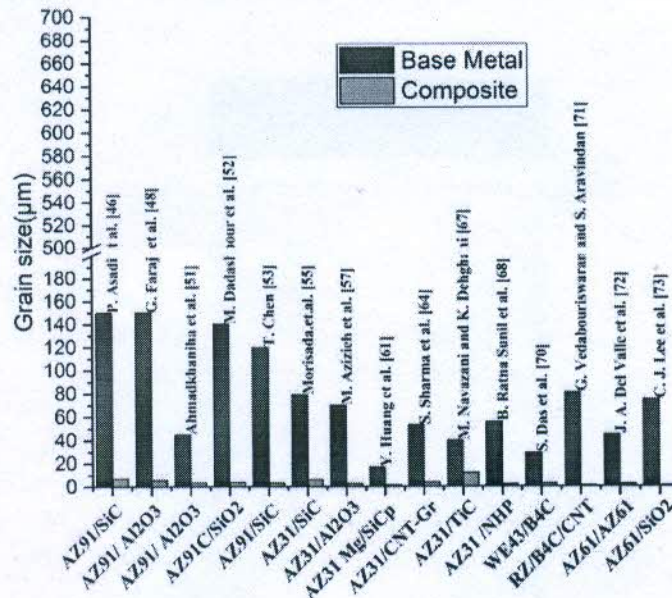


Figure 8. Comparisons of grain size values for fabricated magnesium base composites.

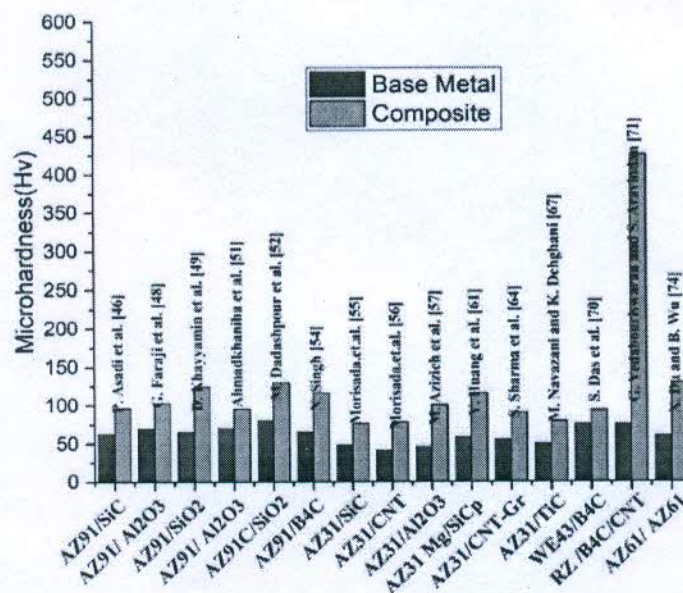


Figure 9. Enhancement in microhardness for various magnesium based composites as fabricated via FSP.

5.2. Orowan strengthening

Zhang and Chen [89] well explained the contribution of Orowan strengthening mechanism in reinforced metal matrix composites. Furthermore, Sanaty-Zadeh [90] studies different strengthening

mechanisms and it is worth maintaining that Hall–Petch strengthening mechanism is the most important factor, which should not be neglected even in micro-scale grain. Dadashpour et al. [52] concluded that in fabricating AZ/SiC magnesium based composite Orowan strengthening mechanism influence dislocation of grains, Vedabouriswaran and Aravindan [70] studies the effect of Orowan strengthening mechanism for fabricating magnesium based composite and concluded insignificant contribution of Orowan strengthening mechanism for their work. Sharma et al. [68] calculated as 58.65 MPa as the total contribution of Orowan strengthening by using Orowan equation as mention below in Eq 7.

$$\Delta\sigma_{\text{Orowan}} = (0.8 \times G_m \times M \times b)/L_p \quad (7)$$

where G_m is the shear modulus of alloy matrix, b is the magnitude of Burger's vector of the alloy matrix and M is Taylors factor. L_p is the inter-particle distance of the composites and can be calculated by equation mentioned below in Eq 8.

$$L_p = \sqrt{(\pi d_{\text{ref}}^2)/(2V_{\text{ref}})} \quad (8)$$

where, V_{ref} is the volume fraction of the hybrid reinforcements and d_{ref} is the average grain sizes of nano composites used.

6. Demanding situations and future bearings

Above studies of literature clearly concludes that new materials especially composite manufacturing could be effectively achieved via FSP. Various reinforcements have been successfully incorporated in metallic matrix by FSP. The grain refinement accomplished by FSP along with high hardness, expanded wear and erosion opposition is the one of a kind point of interest of this procedure. MMCs manufactured by FSP are typically a kind of defect free composites with homogeneous distribution of particles. FSP has indicated promising outcomes in different investigations. Copper, titanium, aluminum, and magnesium materials are the most commonly accepted materials used to supply FSP surface MMCs. Magnesium based components are among them a category of tough to process materials. It has been unmistakably reported in literature and in reality there is a lot of improvement for as long as decade that distinctive magnesium based surface composites can be effectively delivered by FSP. Very recently Huang [91] suggested that singly dispersed CNTs formed compact bonding with the matrix, which contributed to the grain refinement and the mechanical properties enhancement of the Mg–6Zn matrix. In addition, they explained about strengthening mechanism contributions to grain refinement, load transfer and Orowan looping mechanisms. Finally they achieved 144%, 156% and 87% higher values of yield strength, ultimate tensile strength and elongation of the FSPed CNTs/Mg–6Zn composites than those of the as-cast pristine Mg–6Zn alloy.

Apart from various applications of MMCs prepared by FSP yet production engineers are still wondering for the best outcome of the FSP process. Compound and articulate surfaces are hard to produce by FSP. More FSP passes could only have a homogeneous mixture of the reinforce particles into metal matrix, thereby increasing the cost of output. Tool wear is a significant issue in FSP particularly at high temperature. Basically this wear is due to prolonged contact between reinforce particles and tool pin. Literature also shows that various machine parameters affect the tool wear

such as tool rotation speed, transverse speed and axial force [92]. In addition, it was observed that considering tool wear, shear phenomenon is more dominating than drag, as demonstrated by Bist [92]. The development of wear-resistant tools is necessary for repeatable solid-state joining. Hence tungsten base and high carbon high chromium based tools are highly recommended for FSP processes.

Also high thermal energy generation and its controlled is an major issue [93]. These constraints confine the utilization of FSP to process hard surface composites. Flow of reinforce particles into the matrix is still wide area which need to be explore. Optimizing the FSP parameters and developing a model is still an area of future scope. Few recent developments such as fed friction stir technology reported in [94–95] may be considered for further improvement.

7. Conclusions

Literature study clearly summed up that even hard to processed material such as magnesium can be easily processed via FSP. Mainly two holes filling approach and groove filling approach been adapted for doping reinforce particles into the metal matrix. Every technique holds its advantages and limitations. Grain refinement, improved hardness, wear opposition, mechanical conduct, improved bioactivity and erosion obstruction are the normal perceptions in the entirety of the magnesium based composites produced by FSP. The relative contribution of Orowan strengthening effect increases with decreasing size of nanoparticles and Hall–Petch strengthening mechanisms increases with decreasing size of grains.

Also due to the stochastic nature of FSP machine parameters, an optimum combination of these parameters need to be established for producing defect free composite materials.

Dominant part of the work has been done utilizing AZ arrangement magnesium compounds. It is foreseen that composites of other magnesium combinations likewise will be created by FSP in future for a wide scope of uses.

Conflict of interests

All authors declare no conflicts of interest in this paper.

References

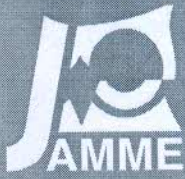
1. Smith W, Hashemi J, Prakash R (2008) *Materials Science and Engineering (SIE)*, 4 Eds., New York: McGraw Hill Education.
2. Clyne TW, Hull D (2019) *An Introduction to Composite Materials*, 3 Eds., Cambridge: Cambridge University Press.
3. Van Suchtelen J (1972) Product properties: a new application of composite materials. *Philips Res Rep* 27: 28–37.
4. Chung DDL (2010) *Composite Materials Science and Applications*, 2 Eds., New York: Springer.
5. Mukhin I, Perevezentsev E, Palashov O (2014) Fabrication of composite laser elements by a new thermal diffusion bonding method. *Opt Mater Express* 4: 266–271.

6. Bodukuri AK, Eswaraiyah K, Rajendar K, et al. (2016) Fabrication of Al–SiC–B₄C metal matrix composite by powder metallurgy technique and evaluating mechanical properties. *Perspect Sci* 8: 428–431.
7. Jiang QC, Wang HY, Ma BX, et al. (2005) Fabrication of B₄C particulate reinforced magnesium matrix composite by powder metallurgy. *J Alloy Compd* 386: 177–181.
8. Schubert T, Trindade B, Weißgärber T, et al. (2008) Interfacial design of Cu-based composites prepared by powder metallurgy for heat sink applications. *Mat Sci Eng A-Struct* 475: 39–44.
9. Wang X, Jha A, Brydson R (2004) In situ fabrication of Al₃Ti particle reinforced aluminium alloy metal–matrix composites. *Mat Sci Eng A-Struct* 364: 339–345.
10. Yang B, Wang F, Zhang JS (2003) Microstructural characterization of in situ TiC/Al and TiC/Al–20Si–5Fe–3Cu–1Mg composites prepared by spray deposition. *Acta Mater* 51: 4977–4989.
11. Hashim J, Looney L, Hashmi MSJ (1999) Metal matrix composites: production by the stir casting method. *J Mater Process Tech* 92: 1–7.
12. Uozumi H, Kobayashi K, Nakanishi K, et al. (2008) Fabrication process of carbon nanotube/light metal matrix composites by squeeze casting. *Mat Sci Eng A-Struct* 495: 282–287.
13. Hu H (1998) Squeeze casting of magnesium alloys and their composites. *J Mater Sci* 33: 1579–1586.
14. Dhanashekar M, Kumar VSS (2014) Squeeze casting of aluminium metal matrix composites—An overview. *Procedia Eng* 97: 412–420.
15. He CN, Zhao NQ, Shi CS, et al. (2009) Mechanical properties and microstructures of carbon nanotube-reinforced Al matrix composite fabricated by in situ chemical vapor deposition. *J Alloys Compd* 487: 258–262.
16. Delhaes P (2002) Chemical vapor deposition and infiltration processes of carbon materials. *Carbon* 40: 641–657.
17. Mishra RS, Ma ZY (2005) Friction stir welding and processing. *Mat Sci Eng R* 50: 1–78.
18. Meng X, Huang Y, Cao J, et al. (2020) Recent progress on control strategies for inherent issues in friction stir welding. *Prog Mater Sci* 115: 100706.
19. Sharma V, Prakash U, Kumar BVM (2018) Surface composites by friction stir processing: A review. *J Mater Process Tech* 224: 117–134.
20. Ni DR, Wang JJ, Zhou ZN, et al. (2014) Fabrication and mechanical properties of bulk NiTiP/Al composites prepared by friction stir processing. *J Alloys Compd* 586: 368–374.
21. Thangarasu A, Murugan N, Dinaharan I, et al. (2015) Synthesis and characterization of titanium carbide particulate reinforced AA6082 aluminium alloy composites via friction stir processing. *Arch Civ Mech Eng* 15: 324–334.
22. Salehi M, Farnoush H, Mohandesi JA (2014) Fabrication and characterization of functionally graded Al–SiC nanocomposite by using a novel multistep friction stir processing. *Mater Design* 63: 419–426.
23. Byung-Wook AHN, Don-Hyun C, Yong-Hwan KIM, et al. (2012) Fabrication of SiCp/AA5083 composite via friction stir welding. *T Nonferr Metal Soc* 22: s634–s638.
24. Sagar P, Handa A (2020) Selection of tool transverse speed considering trial run experimentations for AZ61/TiC composite developed via friction stir processing using triangular tool. *Mater Today Proc* In press.

25. Guo J, Amira S, Gougeon P, et al. (2011) Effect of the surface preparation techniques on the EBSD analysis of a friction stir welded AA1100–B₄C metal matrix composite. *Mater Charact* 62: 865–877.
26. Yang M, Xu C, Wu C, et al. (2010) Fabrication of AA6061/Al₂O₃ nano ceramic particle reinforced composite coating by using friction stir processing. *J Mater Sci* 45: 4431–4438.
27. Feng AH, Ma ZY (2007) Formation of Cu₂FeAl₇ phase in friction-stir-welded SiCp/Al–Cu–Mg composite. *Scripta Mater* 57: 1113–1116.
28. Lim DK, Shibayanagi T, Gerlich AP (2009) Synthesis of multi-walled CNT reinforced aluminium alloy composite via friction stir processing. *Mat Sci Eng A-Struct* 507: 194–199.
29. Gupta M, Ling MN (2011) *Magnesium, Magnesium Alloys and Magnesium Composites*, 1 Ed., Hoboken: John Wiley and Sons.
30. Sunil BR, Reddy GPK, Patle H, et al. (2016) Magnesium based surface metal matrix composites by friction stir processing. *J Magnes Alloy* 4: 52–61.
31. Mishra RS, Mahoney MW, McFadden SX, et al. (1999) High strain rate superplasticity in a friction stir processed 7075Al alloy. *Scripta Mater* 42: 163–168.
32. Dinaharan I, Murugan N, Parameswaran S (2012) Developing an empirical relationship to predict the influence of process parameters on tensile strength of friction stir welded AA6061/0–10 wt% ZrB₂ in situ composite. *Trans Indian Inst Met* 65: 159–170.
33. Dolatkhan A, Golbabaee P, Givi MKB, et al. (2012) Investigating effects of process parameters on microstructural and mechanical properties of Al5052/SiC metal matrix composite fabricated via friction stir processing. *Mater Design* 37: 458–464.
34. Zohoor M, Givi MKB, Salami P (2012) Effect of processing parameters on fabrication of Al–Mg/Cu composites via friction stir processing. *Mater Design* 39: 358–365.
35. Thangarasu A, Murugan N, Dinaharan I, et al. (2014) Influence of traverse speed on microstructure and mechanical properties of AA6082–TiC surface composite fabricated by friction stir processing. *Procedia Mater Sci* 5: 2115–2121.
36. Bauri R, Janaki Ram GD, Yadav D, et al. (2015) Effect of process parameters and tool geometry on fabrication of Ni particles reinforced 5083 Al composite by friction stir processing. *Mater Today Proc* 2: 3203–3211.
37. Patel VV, Badheka V, Kumar A (2016) Influence of friction stir processed parameters on superplasticity of Al–Zn–Mg–Cu alloy. *Mater Manuf Process* 31: 1573–1582.
38. Salehi M, Farnoush H, Mohandesi JA (2014) Fabrication and characterization of functionally graded Al–SiC nanocomposite by using a novel multistep friction stir processing. *Mater Design* 63: 419–426.
39. Hoda MDN, Singari RM, Arulmoni VJ (2016) Friction stir processing (FSP) of copper and enhancement of its mechanical properties using graphite powder. *IJRSI* 3: 58–65.
40. Sathiskumar R, Murugan N, Dinaharan I, et al. (2013) Prediction of mechanical and wear properties of copper surface composites fabricated using friction stir processing. *Mater Design* 55: 224–234.
41. Rathee S, Maheshwari S, Siddiquee AN, et al. (2018) A review of recent progress in solid state fabrication of composites and functionally graded systems via friction stir processing. *Crit Rev Solid State* 43: 334–366.
42. Li K, Liu X, Zhao Y (2019) Research status and prospect of friction stir processing technology. *Coatings* 9: 129.

43. Vijay SJ, Murugan N (2010) Influence of tool pin profile on the metallurgical and mechanical properties of friction stir welded Al-10 wt% TiB₂ metal matrix composite. *Mater Design* 31: 3585–3589.
44. Zhang YN, Cao X, Larose S, et al. (2012) Review of tools for friction stir welding and processing. *Can Metall Quart* 51: 250–261.
45. Kirkland NT, Birbilis N (2014) Introduction to magnesium biomaterials, *Magnesium Biomaterials*, 1 Ed., Cham: Springer, 1–12.
46. Asadi P, Faraji G, Besharati MK (2010) Producing of AZ91/SiC composite by friction stir processing (FSP). *Int J Adv Manuf Tech* 51: 247–260.
47. Asadi P, Givi MKB, Faraji G (2010) Producing ultrafine-grained AZ91 from as-cast AZ91 by FSP. *Mater Manuf Process* 25: 1219–1226.
48. Faraji G, Dastani O, Asghar SA, et al. (2011) Effect of process parameters on microstructure and micro-hardness of AZ91/Al₂O₃ surface composite produced by FSP. *J Mater Eng Perform* 20: 1583–1590.
49. Khayyamin D, Mostafapour A, Keshmiri R (2013) The effect of process parameters on microstructural characteristics of AZ91/SiO₂ composite fabricated by FSP. *Mat Sci Eng A-Struct* 559: 217–221.
50. Faraji G, Dastani O, Mousavi SAAA (2011) Microstructures and mechanical properties of Al₂O₃/AZ91 surface nanocomposite layer produced by friction stir processing. *P I Mech Eng B-J Eng* 225: 1331–1345.
51. Ahmadkhaniha D, Heydarzadeh Sohi M, Salehi A, et al. (2016) Formations of AZ91/Al₂O₃ nano-composite layer by friction stir processing. *J Magnes Alloy* 4: 314–318.
52. Dadashpour M, Mostafapour A, Yeşildal R, et al. (2016) Effect of process parameter on mechanical properties and fracture behavior of AZ91C/SiO₂ composite fabricated by FSP. *Mat Sci Eng A-Struct* 655: 379–387.
53. Chen T, Zhu Z, Ma Y, et al. (2010) Friction stir processing of thixoformed AZ91D magnesium alloy and fabrication of surface composite reinforced by SiCps. *J Wuhan Univ Technol* 25: 223–227.
54. Singh N, Singh J, Singh B, et al. (2018) Wear behavior of B₄C reinforced AZ91 matrix composite fabricated by FSP. *Mater Today Proc* 5: 19976–19984.
55. Morisada Y, Fujii H, Nagaoka T, et al. (2006) Effect of friction stir processing with SiC particles on microstructure and hardness of AZ31. *Mat Sci Eng A-Struct* 433: 50–54.
56. Morisada Y, Fujii H, Nagaoka T, et al. (2006) MWCNTs/AZ31 surface composites fabricated by friction stir processing. *Mat Sci Eng A-Struct* 419: 344–348.
57. Azizieh M, Kokabi AH, Abachi P (2011) Effect of rotational speed and probe profile on microstructure and hardness of AZ31/Al₂O₃ nanocomposites fabricated by friction stir processing. *Mater Design* 32: 2034–2041.
58. Azizieh M, Kim HS, Kokabi AH, et al. (2011) Fabrication of AZ31/Al₂O₃ nanocomposites by friction STIR processing. *Rev Adv Mater Sci* 28: 85–89.
59. Srinivasan M, Loganathan C, Balasubramanian V, et al. (2011) Feasibility of joining AZ31B magnesium metal matrix composite by friction welding. *Mater Design* 32: 1672–1676.
60. Chang CI, Wang YN, Pei HR, et al. (2007) Microstructure and mechanical properties of nano-ZrO₂ and nano-SiO₂ particulate reinforced AZ31–Mg based composites fabricated by friction stir processing. *Key Eng Mater* 351: 114–119.

61. Balakrishnan M, Dinaharan I, Palanivel R, et al. (2015) Synthesize of AZ31/TiC magnesium matrix composites using friction stir processing. *J Magnes Alloy* 3: 76–78.
62. Jiang Y, Yang X, Miura H, et al. (2013) Particles reinforced magnesium alloy produced by friction stir processing. *Rev Adv Mater Sci* 33: 29–32.
63. Sharma S, Handa A, Singh SS, et al. (2019) Synthesis of a novel hybrid nanocomposite of AZ31Mg–Graphene–MWCNT by multi-pass friction stir processing and evaluation of mechanical properties. *Mater Res Express* 6: 126531.
64. Huang Y, Wang T, Guo W, et al. (2014) Microstructure and surface mechanical property of AZ31 Mg/SiCp surface composite fabricated by direct friction stir processing. *Mater Design* 59: 274–278.
65. Soltani M, Shamanian M, Niroumand B (2015) Surface characteristics improvement of AZ31B magnesium by surface compositing with carbon nano-tubes through friction stir processing. *Int J Adv Des Manuf Technol* 8: 85–95.
66. Navazani M, Dehghani K (2015) Investigation of microstructure and hardness of Mg/TiC surface composite fabricated by friction stir processing (FSP). *Procedia Mater Sci* 11: 509–514.
67. Sunil BR, Kumar TSS, Chakkingal U, et al. (2014) Nano-hydroxyapatite reinforced AZ31 magnesium alloy by friction stir processing: A solid state processing for biodegradable metal matrix composites. *J Mater Sci Mater Med* 25: 975–988.
68. Sharma S, Handa A, Singh SS, et al. (2019) Influence of tool rotation speeds on mechanical and morphological properties of friction stir processed nano hybrid composite of MWCNT–Graphene–AZ31 magnesium. *J Magnes Alloy* 7: 487–500.
69. Das S, Mishra RS, Doherty KJ, et al. (2016) Magnesium based composite via friction stir processing. In: Mishra R, Mahoney MW, Sato Y, et al., *Frict Stir Weld Process VII*, Cham: Springer, 245–252.
70. Vedabouriswaran G, Aravindan S (2018) Development and characterization studies on magnesium alloy (RZ 5) surface metal matrix composites through friction stir processing. *J Magnes Alloy* 6: 145–163.
71. Del Valle JA, Rey P, Gesto D, et al. (2012) Friction stir processing of the magnesium alloy AZ61: Grain size refinement and mechanical properties. *Mater Sci Forum* 706: 1823–1828.
72. Lee CJ, Huang JC, Hsieh PJ (2006) Mg based nano-composites fabricated by friction stir processing. *Scripta Mater* 54: 1415–1420.
73. Du X, Wu B (2009) Using two-pass friction stir processing to produce nanocrystalline microstructure in AZ61 magnesium alloy. *Sci China Technol Sci* 52: 1751–1755.
74. Madhusudhan Reddy G, Sambasiva Rao A, Srinivasa Rao K (2013) Friction stir processing for enhancement of wear resistance of ZM21 magnesium alloy. *Trans Indian Inst Met* 66: 13–24.
75. Abbasi M, Bagheri B, Dadaei M, et al. (2015) The effect of FSP on mechanical, tribological, and corrosion behavior of composite layer developed on magnesium AZ91 alloy surface. *Int J Adv Manuf Tech* 77: 2051–2058.
76. Singh J, Lal H, Bala N (2013) Investigations on the wear behavior of friction stir processed magnesium based AZ91 alloy. *Int J Mech Eng Robot Res* 2: 271–274.
77. Arora HS, Singh H, Dhindaw BK, et al. (2012) Improving the tribological properties of mg based AZ31 alloy using friction stir processing. *Adv Mater Res* 585: 579–583.
78. Arora HS, Singh H, Dhindaw BK (2013) Wear behaviour of a Mg alloy subjected to friction stir processing. *Wear* 303: 65–77.



Role of tool rotational speed on the tribological characteristics of magnesium based AZ61A/TiC composite developed via friction stir processing route

P. Sagar ^{a,*}, A. Handa ^b

^a Ph.D Research Scholar, I.K. Gujral Punjab Technical University, Kapurthala, India

^b Department of Mechanical Engineering, I.K. Gujral Punjab Technical University, Kapurthala, India

* Corresponding e-mail address: jasujaprem@gmail.com

ORCID identifier: <https://orcid.org/0000-0003-2804-9458> (P.S.)

ABSTRACT

Purpose: A new composite material was prepared and Different properties such as hardness and tribological behaviour of the fabricated metal matrix composite (MMC) was investigated and compared with the base AZ61A magnesium alloy.

Design/methodology/approach: For the current research work, state-of-the-art technology, Friction stir processing (FSP) was performed to develop magnesium based AZ61A/TiC composite at optimized set of machine parameters.

Findings: Increasing tool rotational speed ultimately leads in enhanced hardness, which further gives superior tribological properties as compared to base AZ61A alloy. Wear observations suggests a combination of abrasive and adhesive wear mechanism.

Research limitations/implications: More microstructural and mechanical properties can be examined.

Practical implications: The idea behind selecting AZ61A is mainly due to its increasing use in bicycle pedals and military equipment's where at certain places it needs to encounter friction. In this current work, microhardness study and wear behaviour of AZ61A/TiC composite processed via FSP were examined.

Originality/value: Paper is completely new and no work has been done till date considering this material and preparing composite with nanoparticles TiC.

Keywords: Friction stir processing, AZ61A magnesium alloy, Microhardness, Wear

Reference to this paper should be given in the following way:

P. Sagar, A. Handa, Role of tool rotational speed on the tribological characteristics of magnesium based AZ61A/TiC composite developed via friction stir processing route, Journal of Achievements in Materials and Manufacturing Engineering 101/2 (2020) 60-75. DOI: <https://doi.org/10.5604/01.3001.0014.4921>

PROPERTIES

1. Introduction

There is an increasing interest in lightweight, maximum performance, eco-friendly and low-emission vehicles. In this respect, magnesium is being increasingly preferred over aluminium not just for its 66% lower density but also for its higher strength to weight ratio [1]. In addition, magnesium constitutes almost 2.7% of the earth's crust, is the sixth most abundant element in the earth's crust and third most abundant dissolved mineral in seawater [1]. In spite of these advantages, insufficient hardness and relatively poor protection from wear constraints the extensive use of magnesium alloys. To enhance its mechanical properties, a specific percentage of secondary phase reinforcement particles is required to be incorporated with the base magnesium or its alloys to produce magnesium matrix composites (MMC). Various manufacturing techniques have been studied such as Mukhin et al. [2] used diffusion bonding to fabricate composites of YAG, Yb:YAG, Yb:GGG, and TGG crystals, Bodukuri et al. [3], Jiang et al. [4], and Schubert et al. [5] fabricated Al-SiC-B₄C MMC, reinforced MMC and copper based composites by powder metallurgy. Also *in situ* fabrication [6], spray deposition [7], stir and squeeze casting [8-11] and vapor deposition methods have been adopted by researchers to fabricate bulk MMCs [12-13]. All these manufacturing processes of developing composites transform the material from solid to liquid phase.

On the flip side, the techniques which do not have a phase change process such as solid state processing entails many merits over conventional phase change techniques. Novel, Friction stir processing (FSP) operates on the friction stir welding principle (FSW) [14]. Stirring action of FSP has been successfully used to disperse secondary phase particles in the parent metal and producing the next generation materials such as MMCs [15,16]. In the most recent times, various researchers have utilized the FSP procedure to improve wear and hardness of these MMCs. Reddy et al. [17] incorporated SiC and B₄C particles through hole filling approach into the upper surface of magnesium base ZM21 alloy to develop a surface composite. It was found that there was no formation of intermetallic compounds and a strong bond was formed between carbide particles and the metal matrix. Furthermore, they investigated properties such as microhardness and dry sliding wear on the developed composite. They found similar values of hardness of base metal and FSPed alloy without reinforced particles. ZM21/B₄C composite demonstrated higher values of hardness compared to ZM21/SiC. As far as the wear properties are concerned, adhesive wear mechanism was observed and it was presumed that almost 70% wear opposition for ZM21/B₄C was obtained in contrast with the base metal.

Aabbsi et al. [18] developed two surface composites namely, AZ91/SiC and AZ91/Al₂O₃ via groove filling approach. Wear, mechanical properties, and corrosion resistance were examined and compared with as cast AZ91. The AZ91/SiC developed higher values of hardness, ultimate tensile strength, and percent elongation compared to AZ91/Al₂O₃ and base metal, which was attributed to the increase in number of passes. The wear test was conducted as per ASTM G99 standard on TRI-PIN-ON-DISK equipment using a stainless steel disk as a counter face along with a sliding speed of 1 mm s⁻¹, contact force of 50 N, and total distance of 500 m. Cylindrical pins with 5 mm diameter and 40mm height were prepared from the samples using wire cut machine. They concluded that the wear rate for AZ91/SiC and AZ91/Al₂O₃ was almost same but superior to the base metal. Singh et al. [19] introduced TiC reinforced particles into the blind holes drilled on AZ91 magnesium alloy surface to develop MMC via FSP. Wear performance was examined using pin-on-disc wear testing with two loads of 5 N and 10 N and resulting wear rate for these loads were examined. Rectangular pin specimens with cross sectional dimensions of 5 mm x 5 mm and 10 mm in length were machined from the as cast as well as FSPed AZ91 alloy for the wear tests. The counter face material used was a stainless steel disc with hardness value of nearly 220 Hv. Wear test were conducted and it was found that FSPed samples exhibited lower wear rate and higher wear resistance in contrast with as cast AZ91. Similarly, Arora et al. [20] investigated the tribological characteristics of AZ31/TiC composite as fabricated via FSP. Experimentation with single pass FSP process along with undersurface cooling was executed. Microhardness and wear test results concluded that the composite with single pass and undersurface cooling demonstrated enhanced microhardness and lesser wear rate. Arora et al. [21] compared wear behaviour of as cast AE42 magnesium alloy with FSPed AE42 samples. The authors concluded that FSPed AE42 alloy demonstrated decreased wear rate and enhanced hardness which was attributed to grain refinement. Furthermore, this study concluded that at low velocity and higher loads, surface delamination, plastic deformation and abrasive wear existed. Ram et al. [22] used pure magnesium and reinforced SiC particles to develop a novel composite via FSP. Enhanced microhardness of up to 45% and lower wear rate up to 47% was achieved. Finally, for the as cast, composite abrasive wear mechanism was found to be the dominant factor. Azizieh et al. [23] synthesized AZ31/Al₂O₃ nanocomposite and examined the response of various parameters on hardness and wear behaviour. Authors considered varying tool rotation speeds of 800, 1000, 1200 and 1400 rpm with fixed tool transverse speed of 45 mm/min

and 2° tool tilt angle. It was found that due to refined grain formation, hardness increased from 50 Hv to 90 Hv and wear rate at 1000 and 1200 rpm was higher compared to that 800 rpm. Faraji and Asadi [24] in another study fabricated AZ91/Al₂O₃ and obtained three times lower wear rate in contrast to the base metal. Recently, Dinaharan et al. [25] used fly ash to develop AZ31 magnesium base composite via processing route of stir cast and FSP. They obtained grain size of up to 4 μm and 33% lower wear rate for FSP compared to stir cast. In addition, they claimed superior wear resistance and microhardness of the composite developed via FSP. Very recently, Patle [26] examined sliding wear behaviour of as fabricated AZ91/B₄C via FSP route. They found that the addition of B₄C particles could enhance hardness of base metal, and leads to lower wear rate. They observed abrasive, severe adhesive, oxidative and delamination as major wear mechanisms at two different sliding velocities.

Literature survey shows that very little work has been carried out studying tribological behaviour of magnesium based AZ61A/TiC composite and compared with AZ61A magnesium alloy. The idea behind selecting AZ61A was mainly due to its increased use in bicycle pedals and military equipment where it needs to encounter friction

[27-29]. In this work, microhardness study and wear behaviour of AZ61A/TiC composite processed via FSP was conducted.

2. Experimental details

2.1. As received material

In this work, plates of magnesium, alloy AZ61A with dimensions of 200 mm×100 mm×6 mm were used. Table 1 presents the complete configuration of parent AZ61A magnesium alloy.

2.2. Reinforce particles

Nano titanium carbide (n-TiC) with 80 nm average particle sizes and 99.99% purity were used for the current study. Whereas Figure 1 represents Scanning electron microscopy (SEM), Energy-dispersive X-ray spectroscopy (EDSX) and X-ray diffraction (XRD) results obtained for nano reinforcement used in experiment. Table 2 presents the atomic and weight percentage of nano TiC reinforcement particles.

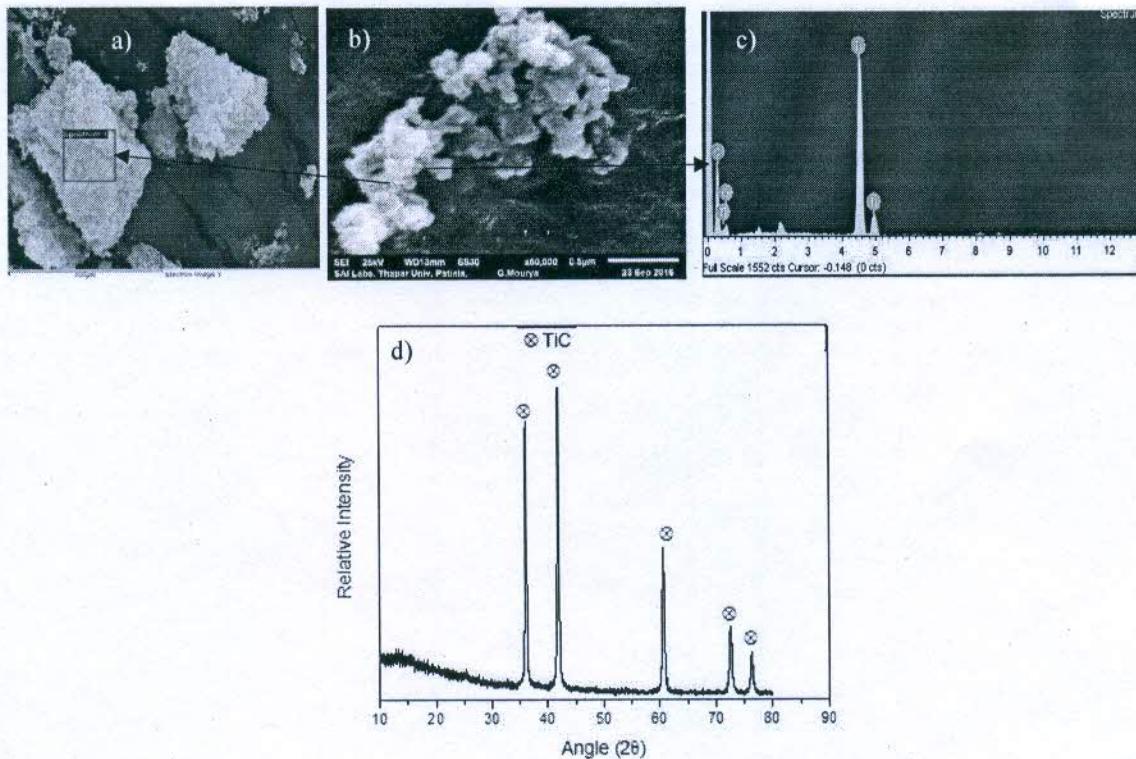


Fig. 1. a) SEM image of TiC powder, b) SEM image showing the average grain size, c) EDS spectra showing abundance of TiC particles, d) XRD image of TiC powder

Table 1.

Chemical composition of as supplied magnesium AZ61A alloy

Element	Aluminium	Zinc	Manganese	Silicon	Iron	Copper	Nickel	Magnesium
Actual content, %	6.26	0.78	0.27	0.032	0.0021	0.011	0.0026	-----
Allowable range of content, %	5.8-7.2	0.4-1.5	0.15-0.50	0.05	0.005	0.05	0.005	Balance

Table 2.

Chemical composition of secondary phase TiC particles

Element	C K	O K	Ti K	Final %
Weight, %	35.86	17.15	46.99	100 %
Atomic, %	59.25	21.28	19.47	100 %

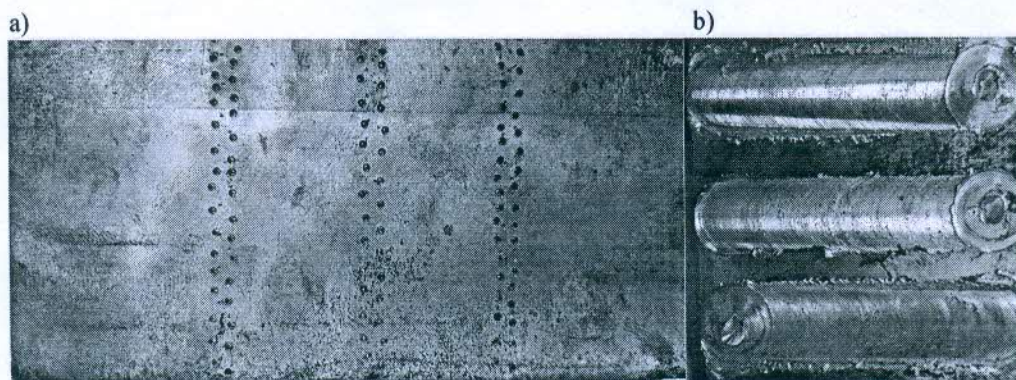


Fig. 2. a) Design sequence of blind holes made into AZ61A plate; b) pictorial view of FSPed surface

2.3. Fabrication of composite

Firstly, to consolidate the secondary phase particles, a grid of blind holes in zig-zag pattern with size $\text{Ø}2 \text{ mm} \times 4 \text{ mm}$ were injected into the plate as shown in Figure 2. FSP was implemented using two high carbon high chromium (HCHCr) tools. The first tool had a shoulder but no pin was employed to cover the top of the holes after implanting TiC powder into the holes to prevent the scattering of particles during FSP. The second tool had a triangular pin profile with a shoulder diameter of 16 mm, making root diameter 6 mm and pin length 4 mm. Figure 2 (b) shows the pictorial view of the crown surface appearance of FSPed surfaces. Nearly 21 % of volume fraction of TiC was added as theoretically calculated by using formula [30].

Theoretical volume fraction = $\frac{\text{Total volume of reinforcement particles}}{\text{Total volume of the processing zone}} \times 100$

Total volume of reinforcement particles = Numbers of holes \times Volume of each blind hole

Volume of cylindrical hole = $\pi r^2 \times \text{Depth of hole}$

Total volume of the processing zone = Working length \times Pin Length Tool \times Shoulder diameter

Six samples were prepared through FSP under various conditions as shown in Table 3. FSP experiments were conducted utilizing a modified dedicated vertical milling machine.

Table 3.

Processing parameters for FSP of AZ61A/TiC

Parameter	Value 1	Value 2	Value 3
Tool rotation speed, rpm	800	1000	1200
Transverse speed, mm/min	40	40	40
No. of passes	3	3	3

2.4. Microstructure and microhardness test

The standard metallurgical practice were carried out to prepare the processed specimens. The specimens for optical microscopy were prepared by particular polishing with varying grit size SiC. Double disc polishing machine was used for mechanical polishing with emery papers of size 80,

100, 150, 220, 320, 500, 800, 1000, 1500 and 2000, respectively and with water as a lubricant. Further polishing was carried out with diamond paste. Polished specimens were then etched by 100 ml ethanol, 5 gm picric acid, 4 ml acetic acid, and 10 ml water for 15-20 sec. Prepared specimens than examined under image analysing software attached with the microscope which construct the grain boundaries completely and measured the grain size. For better results, all the optical images were taken within 25 minutes of sample preparation.

Microstructure investigations were done using optical microscopy (OM- Leica, Germany make) and measurement of microhardness was done by Vickers indentation method by applying a total load of 500gm for a dwell time of 15 sec. as per ASTM specifications. Hardness values were examined along a horizontal line underneath 1.5 mm from top surface at equal intervals of 0.5 mm between adjacent points. A total of thirty-three values were taken for a distance of 8 mm to the either side of the central line passing through stir zone. At every indentation point, three values were taken and mean value was considered.

2.5. Wear test

Machine and experiment detail

For examining wear and friction characteristics, pins of size Ø3 mm × 30 mm were prepared from base metal and from composites via wire cut electric discharge machining. All the experiments were done as per ASTM G99 standard and were examined using pin-on-disc tribotester (DUCOM

TR-20 LE), as shown schematically in Figure 3. Basic geometry of pin and disc is presented in Figure 4.

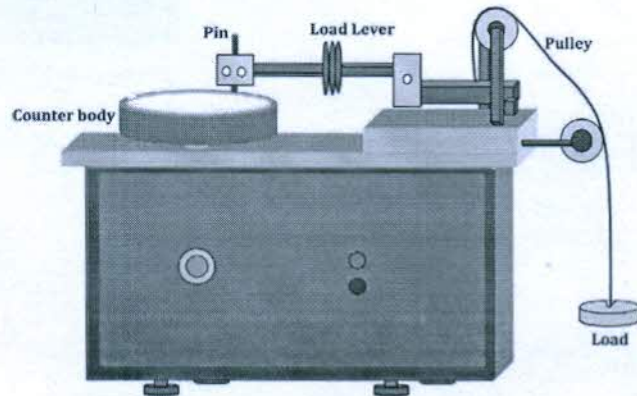


Fig. 3. Pictorial view of pin-on-disc tribotester [31]

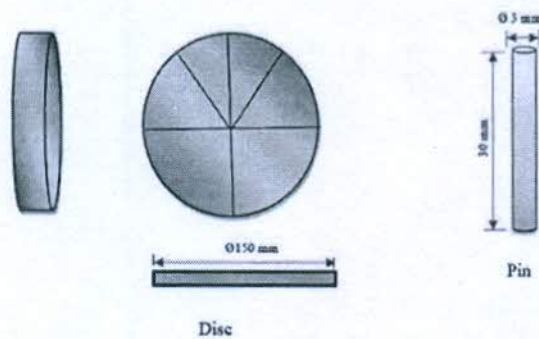


Fig. 4. Basic geometry of pin and disc

Table 4. Final wear rate of composite as well base metal at various FSP conditions

	RPM	TS (mm/min)	LOAD (N)	Initial height (IH)	Final Height (FH)	Change in height ($\Delta h = IH - FH$)	Volumetric loss (VL) = $\pi r^2 \Delta h$ (mm ³)	Wear rate = VL/S.D (mm ³ /m)
Composite	800	40	10	30	29.56916	0.43084	3.04539254	0.006090785
	800	40	20	30	29.41379	0.58621	4.14362538	0.008287251
	1000	40	10	30	29.38102	0.61898	4.37526013	0.00875052
	1000	40	20	30	29.28752	0.71248	5.03616488	0.01007233
	1200	40	10	30	29.43218	0.56782	4.01363567	0.008027271
	1200	40	20	30	29.34579	0.65421	4.62428338	0.009248567
Base metal			10	30	29.28452	0.71548	5.05737038	0.010114741
Base metal			20	30	29.057265	0.94273	6.66372234	0.013327445

Steel disc (EN31) of hardness of 60 HRC was used as a counter surface and prepared by silicon carbide papers of grit size 800 and 1000 preceded by acetone cleaning. All wear analysis was conducted for sliding distance of 500 m, time 600s, disc rpm 400, and varying load of 10 and 20 N. Volumetric loss was determined as a function of loss of height multiplying it with the cross-sectional area of pin. Further wear rate was calculated considering volumetric loss as a function of the sliding distance. Worn surfaces and the underlying wear mechanism were analyzed by scanning electron microscopy (JEOL, JSM-F100). Final values of calculated wear rate are presented in Table 4.

3. Results and discussion

3.1. Microstructure and microhardness

The obtained microstructures of monolithic AZ61A and FSPed processed specimens are shown in Figure 5 and Figure 6. Figure 5 shows the optical micrographs of the as received AZ61A magnesium base alloy. The typical microstructure of AZ61A alloy is characterized by coarse β -Mg₁₇-Al₁₂ and α -Mg compound with discontinuous network at grain boundary. It was observed that unrefined coarse grains were distributed in the metal matrix. Additionally, clusters of small crystals were observed alongside segregated large crystals. The average grain size of the base was about 75 μ m.

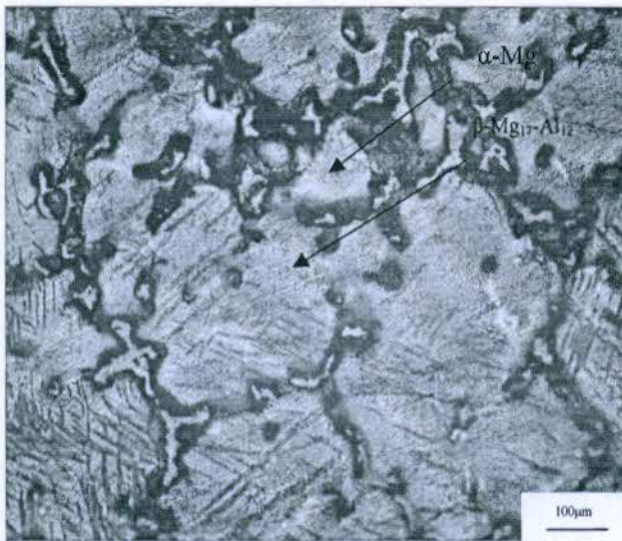


Figure 5. Optical micrograph of monolithic AZ61A base metal

AZ61A magnesium alloy incorporated with secondary phase TiC particles and further processed at various tool rotation speed. The specimen shows that coarse magnesium grains were not able to handle rigorous action of tool and broke up into tiny grains. Figure 6, presents microstructure images of different zones at 200 X. In almost all the specimens, stir zone (SZ) exhibited finer grains, which may be attributed to dynamic recrystallization, and heat generation, which is in agreement with several other studies [32-36]. In Figure 6, FSPed specimen processed at 800 rpm showed refined microstructure up to 3 μ m that may be due to nucleation of TiC and pinning of grain boundaries with nano reinforce particles. In addition fixed volume fraction of nano reinforce particles achieves better distribution and results in developing obstacles to growing grain boundary, which is in tune with Azizieh et. al [37]. In case of tool speed of 1000 rpm the OM reveals refined grains (up to 4.3 μ m) at stir zone as shown in Figure 6. However, at some places agglomeration was noticed which can be attributed to improper distribution of secondary phase particles in metal flow. As tool rotation speed increased to 1200 rpm, the microstructure images reveal that as heat input increased the grain growth (up to 5 μ m) occurred consequently larger grains were noticed at this parameter, which is in agreement with [37,38]. However, simultaneously shattering effect of rotation cause uniform distribution of secondary phase particle.

Microhardness

Microhardness values of the FSPed specimens was examined along the horizontal line passing through stir zone of cross section and presented in Figure 7. As received base metal AZ61A bore hardness of 60 HV. The hardness of the stir zone for all FSPed samples was considerably higher in contrast to the base magnesium alloy. This may be attributed to refined and small sized grains at the stir zone due to dynamic crystallization of FSP. As per the Hall-Petch equation, the grain size holds an inverse relationship with hardness. As grain size decreases, the hardness increases. Additionally, Orowan strengthening mechanism contribution that influence dislocation of grains in reinforced metal matrix composites. At higher rotational speed 1200 rpm, heat input increases and grain growth occur that consequently results in low hardness, as detailed by Azizieh et. al [23]. Hence as tool rotational speed increases, the microhardness of the composite decreases, these findings are in confirmation with the findings of Sathiskumar et. al [38]. Hardness value for 1200 rpm processed sample was observed to be 72 HV, which was the lowest compared to 84 HV at 1000 rpm and 95 HV at 800 rpm.

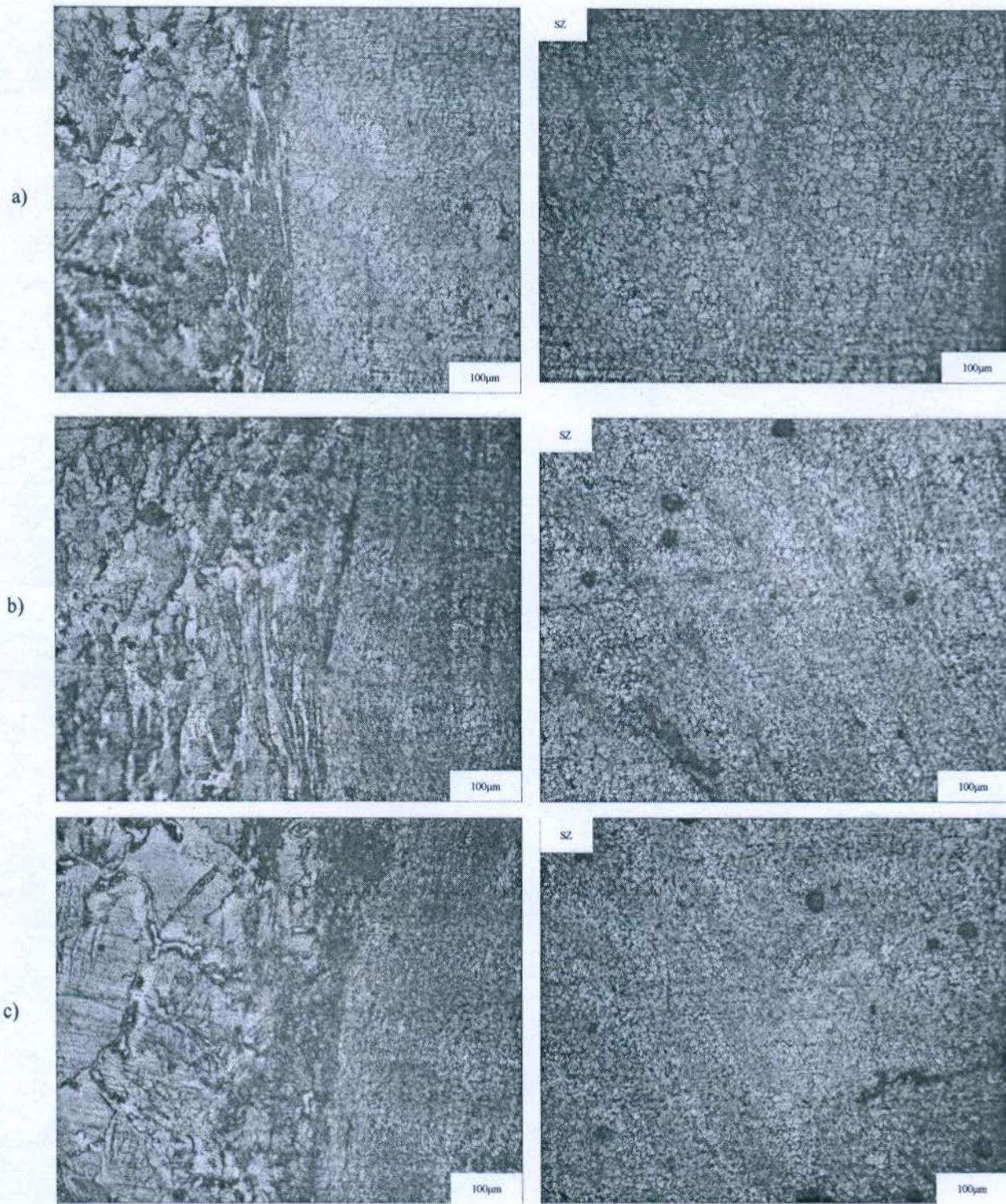


Fig. 6. Microstructure at 200 X for interface and stir zone of FSPed specimen processed: a) at 800 rpm, b) at 1000 rpm, c) at 1200 rpm

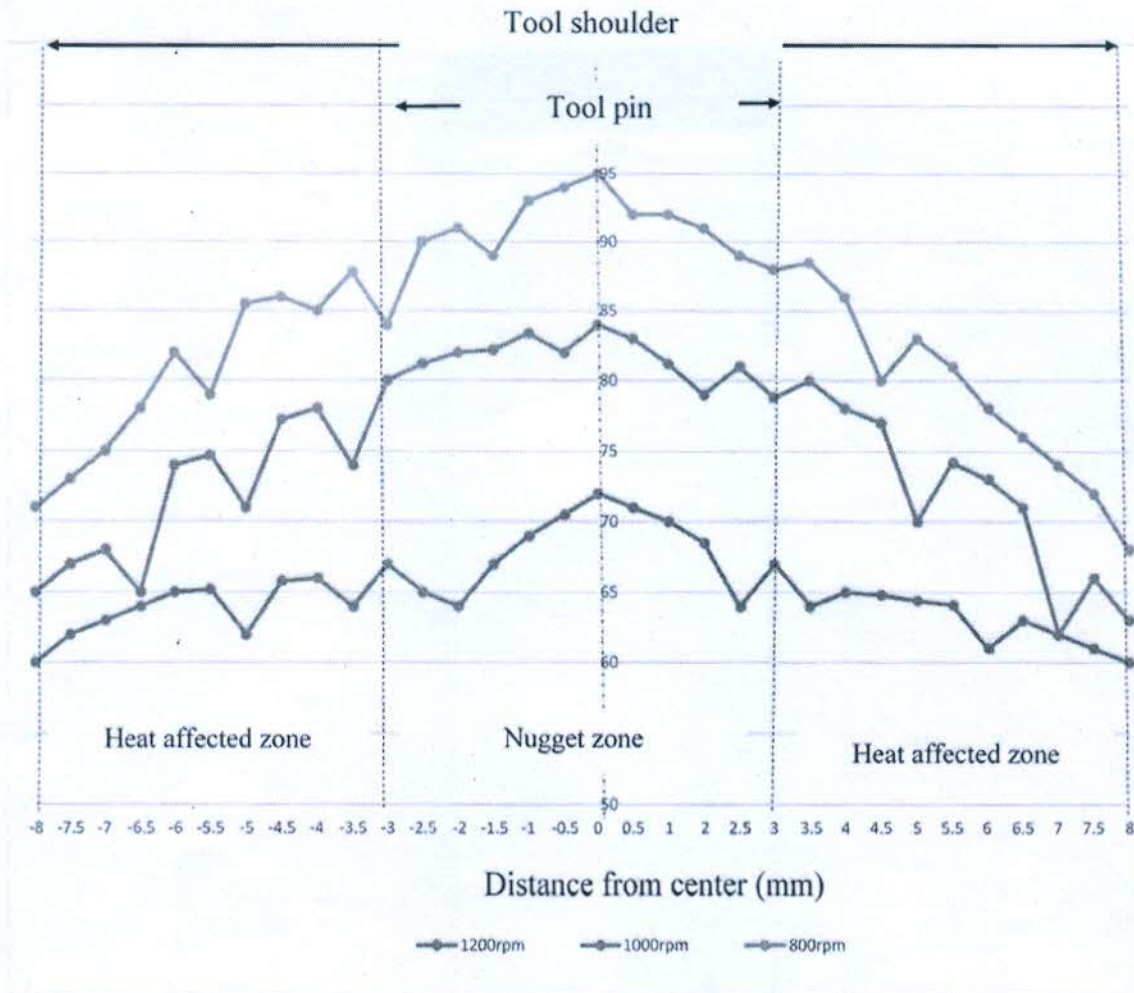


Fig. 7. Hardness values for FSPed composites processed at different tool rotation speed

3.2. Wear performance

Final values of wear rate were calculated with respect to the sliding distance. In addition, entire values for the composite along with the base material considering varying load are presented in tabular form in Table 4.

Figures 8 and 9, shows that the specimen processed at 800 rpm shows lower value of height loss with respect to time as contrasted with composite developed at 1000 rpm, 1200 rpm and the base metal. This may be attributed to low tool rotational speed producing smaller grains, higher hardness resulting in lesser wear [30,39]. In spite of low value of hardness for FSPed, the sample processed at 1200 rpm had, lower value of wear rate and low height loss was observed due to more homogenous distribution of nanoparticles in consensus with Azizieh et. al [23].

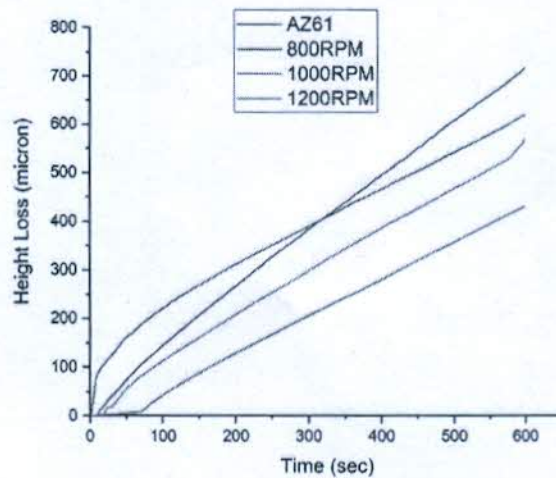


Fig. 8. Height loss of all specimens with respect to time at 10 N

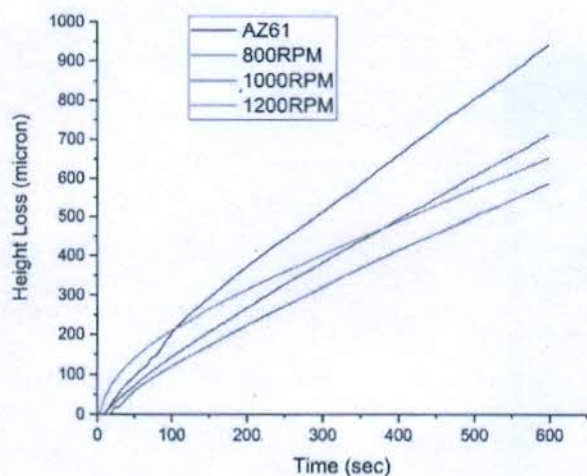


Fig. 9. Height loss of all specimens with respect to time at 20 N

Plots shown in Figure 10, represents findings of wear rate comparison between AZ61A base metal and FSPed processed composites examined at various FSP parameters and tribological loads. As was observed in Figure 8, the magnesium base AZ61A metal wear rate was high compared to the processed composites.

As observed in Figure 10, with increase in applied load, the wear rate increases for both base metal and developed composites, which is in agreement with the Archard's wear equation [40]. However, at an elevated value of load, wear rate for the base metal increases sharply as shown in Figure 10, which reflects mild to severe delamination of the surface, also reported by Ram et. al [22]. Apparent changes take place in wear rate of metal matrix composites (MMCs) at

increased load and it shows lower values of wear rate compared to the base metal. In other words, wear resistance is comparatively high for developed composites at high load. In FSP samples, refined grains and uniformly distributed secondary phase particles results in hardened surface which has also been reported by various researchers [34, 41-46]. This low wear rate and resistance to wear be due to the (a) addition of secondary phase particles develops enhanced values of hardness for FSP composite, (b) additive TiC particulate content not only minimizes the contact area of composite and counter surface, additionally it opposes the cutting activity of the counterface adequately (c) grain boundary and secondary phase mechanism i.e. Hall-pitch and Orowan mechanism contributes in development of hardness and strength of composite, resulting in greater load bearing capacity.

3.3. Coefficient of friction

Amplitude of friction coefficient to the function of time for base metal and for composites samples are shown in Figure 11. The friction coefficient fluctuations for initial time frame is extremely high, which might be due to the new disc surface introduction to the pin. To obtain precise values and to remove the material stored on plate, steel disc was cleaned before each run. As observed in Figure 11, at 10 N higher variations are obtained for all specimens. However, extensive variation in friction coefficient with high amplitudes for base metal at 10 N is noticed while these progressions for FSPed composites were not all that broad. Mainly this fluctuation is an outcome of adhesion of the pin to counterside. Moreover SEM images also suggests that abrasive wear also occurs. Therefore, at 10 N adhesive wear

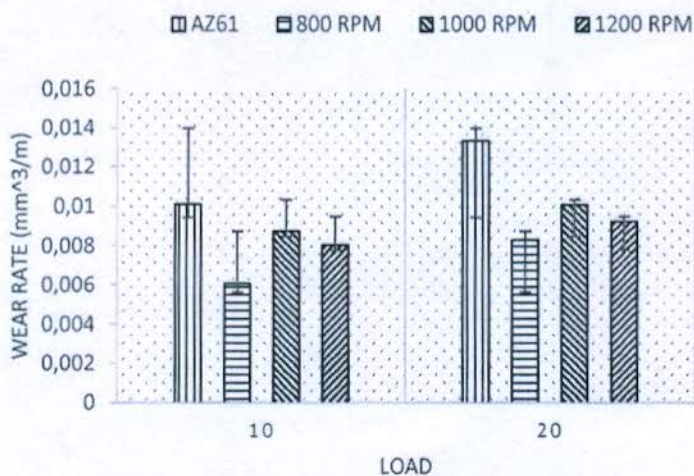


Fig. 10. Wear rate plots of base metal AZ61A and FSPed composites

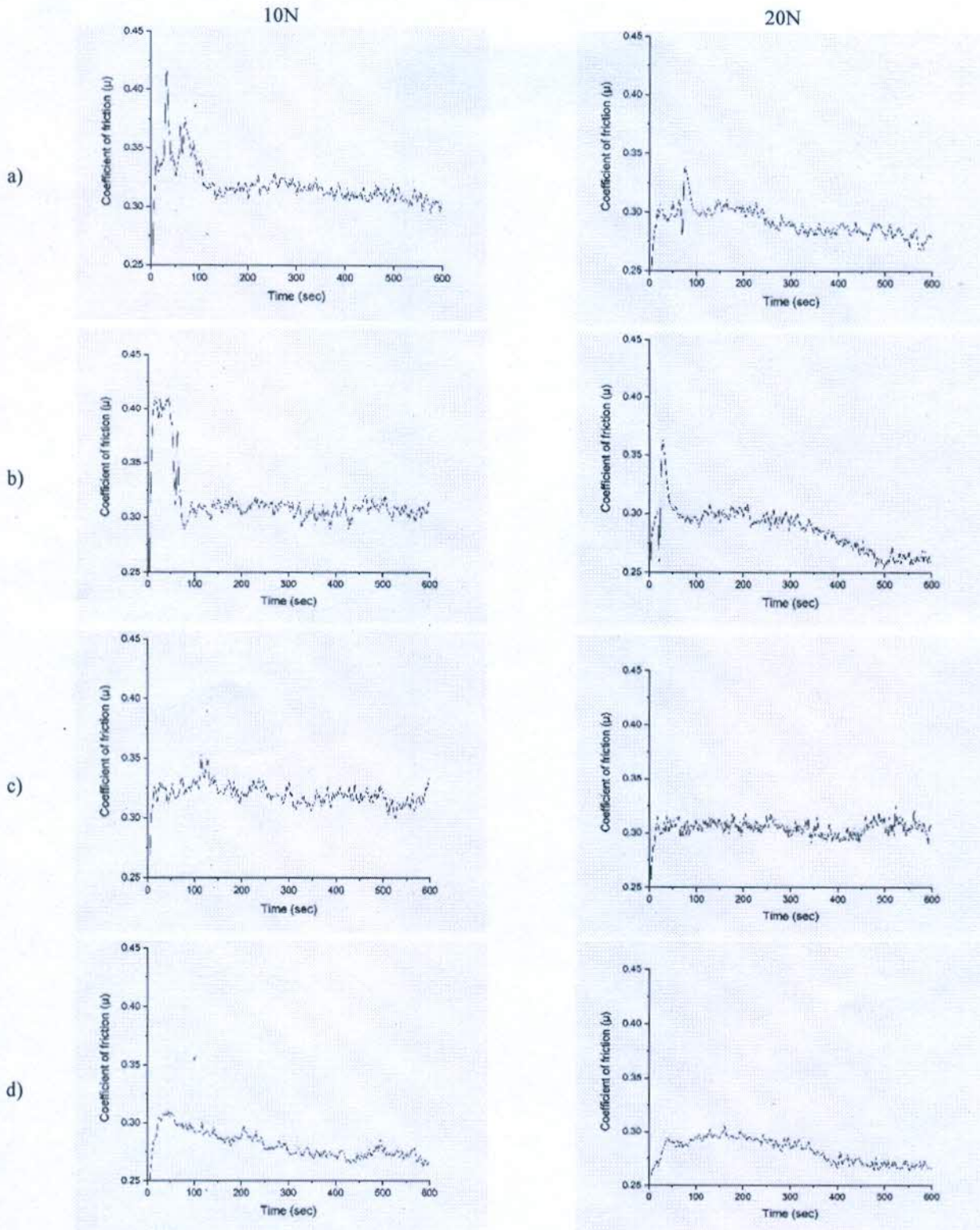


Fig. 11. Coefficient of friction values with respect to time a) for base metal AZ61A b) for FSPed specimen processed at 800 rpm c) for FSPed specimen processed at 1000 rpm. d) for FSPed specimen processed at 1200 rpm

mechanism is dominant consequently develops higher values of friction coefficient for base metal when compared to developed composites. In subsequent samples distribution of TiC particles acted as thin film and gives rise to selective material removal, hence decrease the mean friction coefficient as can be seen in Figure 12. As friction coefficient reduced, the actuating shear stress on the sliding surface decreases and results in resistance to wear. In case of FSPed composites processed at 1200 rpm in spite of low hardness values, it is uniform distribution of particles that leads it to homogeneity, which prevents large variation in friction coefficient.

When load increases, the variations in fluctuation decreases in all specimens as shown in Figure 11. Also, the base metal mean friction coefficient of all FSPed composites decreased as the applied load increased. This may be attributed to high thermal energy developed, which softened the materials. Additionally for FSPed specimens, mixing of secondary phase particles minimize the direct contact area and direct contact load, hence decrease in the friction coefficient was noticed. This behaviour can also be ascribed to hardness. Therefore, at low applied load hardness is acting as a prevailing variable. In any case, at enhanced load values, friction coefficient was mainly influenced by wear mechanism i.e. delamination. Therefore, the composite with low friction coefficient worn less which is in agreement with Lu et al. [47].

3.4. Wear mechanism

SEM micrographs of the as received AZ61A and FSPed samples were taken to investigate the morphology of the worn surfaces and included in Figures 13 and 14. As can be observed in Figures 13 and 14, the surface of base metal

AZ61A shows straight deep plows/grooves. This may be attributed to frictional heat that breaks into the initial network of magnesium like $\beta\text{-Mg}_{17}\text{Al}_{12}$. This brittle and coarse phase shows its inability to effectively act as an obstacle to wear, consequently it softening of the material. Additionally this heat generates good amount of plastic deformation, which leads to the formation of deep grooves. The presence of these deep grooves could also be brought about by microploughing, a sub mechanics of abrasion. Also, the appearance of scratches on the base metal surface shows some evidence of abrasive wear. For base metal, a range of adhesive and abrasive wear was observed which is in conjunction with [17,23]. However, deep grooves indicate severe adhesive wear and its domination, consequently debris formed and massive surface damage on pin surface was found. This may be also be related to lower value hardness for base material as contrasted to FSPed composites. When applied load increase to 20N it is evident from Figure 12 that base metal forms more cracks and has widened grooves.

As is shown in Figures 13 and 14, the wear component in the composite is unique and different compared with the base metal. Uniform grains and homogenous distribution of TiC particles decidedly influenced the wear resistance. EDS images also validates the presence of TiC particles in almost all the MMCs. Also the addition of TiC particles in the base metal, a) minimized contact area of metal and counter part b) minimized direct load, which lead to change in the severe wear to mild wear. For all manufactured composites, thus, the abrasive wear mechanism was found to be the dominant wear mechanism by the loose debris particles. These loose debris particles mainly shows up due to oxidizing MMCs and pulling of TiC during sliding.

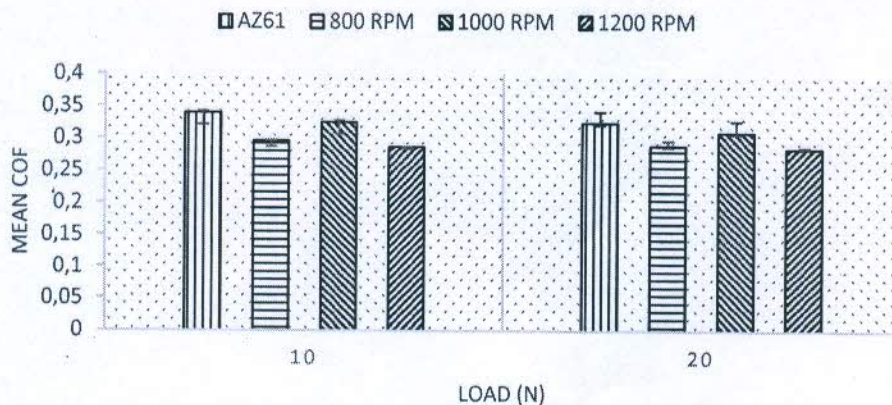


Fig. 12. Values of mean coefficient of friction as a function of load

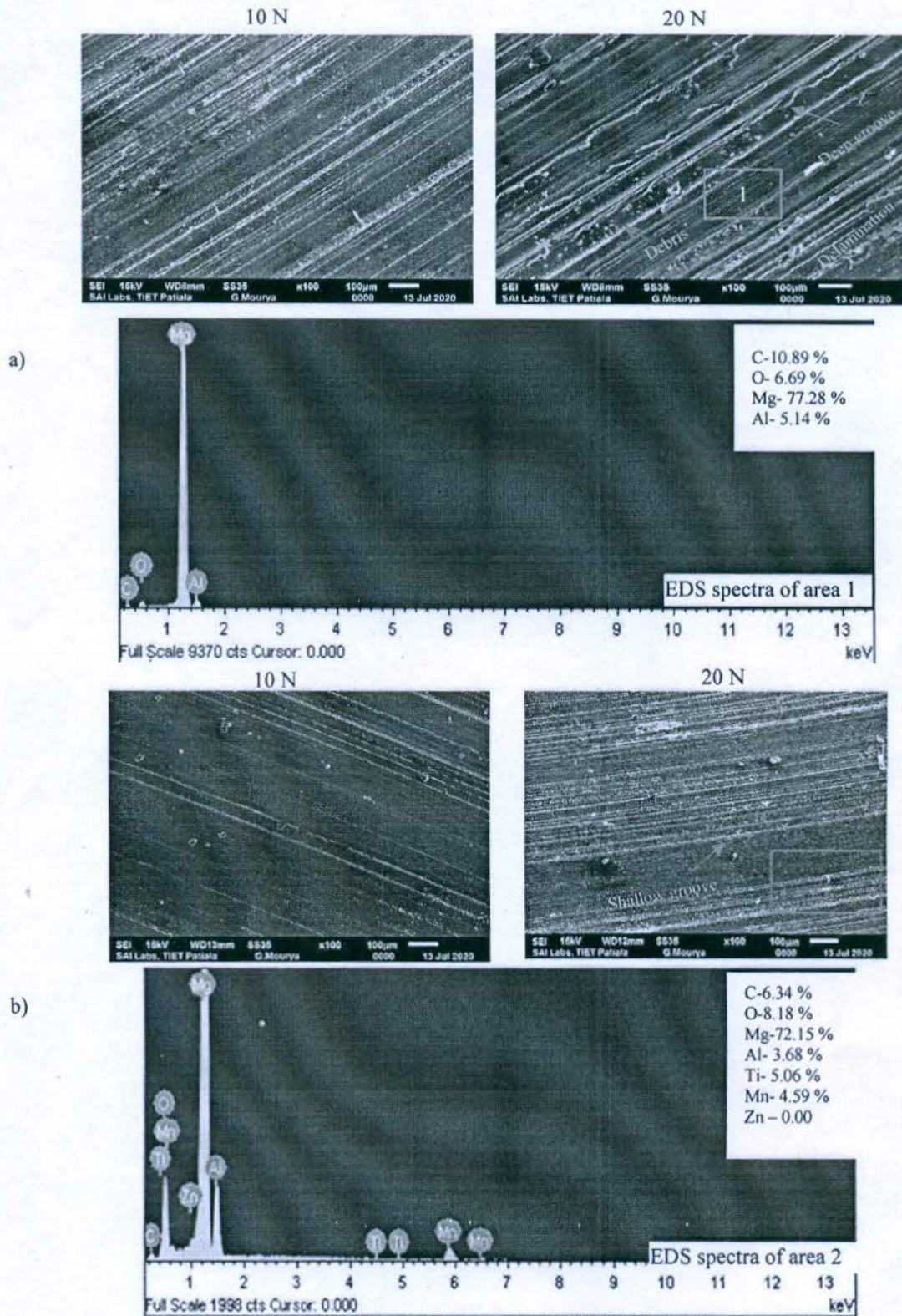


Fig. 13. SEM micrographs and corresponding EDS of worn surfaces; a) for base metal AZ61A, b) for FSPed specimen processed at 800 rpm

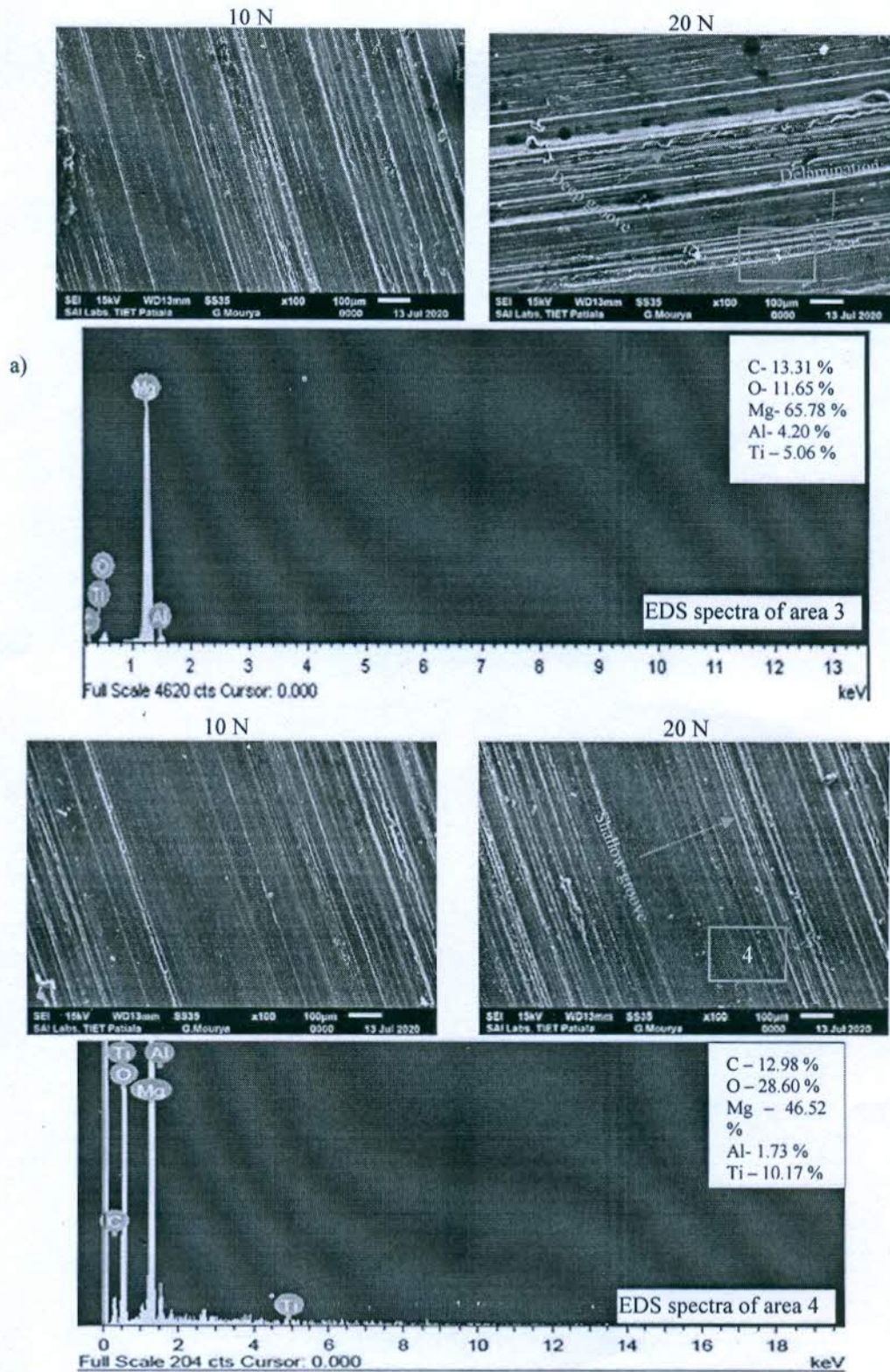


Fig. 14. SEM micrographs and corresponding EDS of worn surfaces; a) for FSPed specimen processed at 1000 rpm, b) for FSPed specimen processed at 1200 rpm

Generally, enhanced load creates frictional heating that causes changes in morphology of worn surfaces from fine scratches to grooves. However, FSPed composite surface processed at 1200 rpm showed microcracks that may be due to good nanoparticle distribution, which reduced the immediate contact load and thus forestalled the delamination. It merits referencing that for the specimen processed at 1000 rpm and 10 N or 20 N delamination of the MMCs layers was likewise found in some places. However, at 1200 rpm and 10 N metal matrix layer delamination was observed to be diminished.

4. Conclusions

In this work magnesium, based AZ61A/TiC composites were effectively manufactured utilizing FSP. The tribological characteristics of the as-got AZ61A and fabricated composites were examined. The main findings of the examination can be summed up as follows:

1. Presence of secondary phase TiC particles and grain refinement directly influenced hardness and wear rate of the composites.
2. Enhanced hardness was achieved for composite fabricated at 800 rpm i.e. 95 HV which is way too high as contrasted to the hardness of AZ61A base metal i.e. 60 HV.
3. For composites, a lower wear rate was observed compared to base metal that may be attributed to increased hardness values.
4. For lower value of loads, composites showed lower friction coefficients due to reinforced particles load bearing abilities.
5. Worn surface morphology was greatly influenced by tool rotational speeds. Due to high hardness and uniform particle distribution of specimen prepared at 800 rpm and 1200 rpm, worn surface appeared to be smooth with few shallow grooves.

Acknowledgements

The authors would like to thank I.K. Gujral Punjab Technical University, Kapurthala, India for giving us the opportunity to carry on this research work. Also authors are highly thankful to Dr Pavel Somavat, A.P, University of Texas, USA for his valuable suggestions.

References

- [1] M. Gupta, N. Sharon, Magnesium, Magnesium alloys and magnesium composites, J. Wiley and Sons, 2010.
- [2] I. Mukhin, E. Perevezentsev, O. Palashov, Fabrication of Composite Laser Elements by a New Thermal Diffusion Bonding Method, *Optical Materials Express* 4/2 (2014) 266-271. DOI: <https://doi.org/10.1364/OME.4.000266>
- [3] A.K. Bodukuri, K. Eswaraiah, K. Rajendar, V. Sampath, Fabrication of Al-SiC-B₄C Metal Matrix Composite by Powder Metallurgy Technique and Evaluating Mechanical Properties, *Perspectives in Science* 8 (2016) 428-431. DOI: <https://doi.org/10.1016/j.pisc.2016.04.096>
- [4] Q.C. Jiang, H.Y. Wang, B.X. Ma, Y. Wang, F. Zhao, Fabrication of B₄C Particulate Reinforced Magnesium Matrix Composite by Powder Metallurgy, *Journal of Alloys and Compounds* 386/1-2 (2005) 177-181. DOI: <https://doi.org/10.1016/j.jallcom.2004.06.015>
- [5] Th. Schubert, B. Trindade, T. Weißgärber, B. Kieback. Interfacial Design of Cu-Based Composites Prepared by Powder Metallurgy for Heat Sink Applications, *Materials Science and Engineering: A* 475/1-2 (2008) 39-44. DOI: <https://doi.org/10.1016/j.msea.2006.12.146>
- [6] X. Wang, A. Jha, R. Brydson, In Situ Fabrication of Al₃Ti Particle Reinforced Aluminium Alloy Metal-Matrix Composites, *Materials Science and Engineering: A* 364/1-2 (2004) 339-345. DOI: <https://doi.org/10.1016/j.msea.2003.08.049>
- [7] B. Yang, F. Wang, J.S. Zhang, Microstructural Characterization of in Situ TiC/Al and TiC/Al-20Si-5Fe-3Cu-1Mg Composites Prepared by Spray Deposition, *Acta Materialia* 51/17 (2003) 4977-4989. DOI: [https://doi.org/10.1016/S1359-6454\(03\)00292-1](https://doi.org/10.1016/S1359-6454(03)00292-1)
- [8] J. Hashim, L. Looney, M.S.J. Hashmi, Metal matrix composites: production by the stir casting method, *Journal of Materials Processing Technology* 92-93 (1999) 1-7. DOI: [https://doi.org/10.1016/S0924-0136\(99\)00118-1](https://doi.org/10.1016/S0924-0136(99)00118-1)
- [9] H. Uozumi, K. Kobayashi, K. Nakanishi, T. Matsunaga, K. Shinozaki, H. Sakamoto, T. Tsukada, C. Masuda, M. Yoshida, Fabrication Process of Carbon Nanotube/Light Metal Matrix Composites by Squeeze Casting, *Materials Science and Engineering: A* 495/1-2 (2008) 282-287. DOI: <https://doi.org/10.1016/j.msea.2007.11.088>
- [10] H. Hu, Squeeze Casting of Mg Alloy and Their Composites, *Journal of Materials Science* 33 (1998) 1579-1589. DOI: <https://doi.org/10.1023/A:1017567821209>
- [11] M. Dhanashekar, V.S. Senthil Kumar, Squeeze casting of aluminium metal matrix composites – an overview, *Procedia Engineering* 97 (2014) 412-420. DOI: <https://doi.org/10.1016/j.proeng.2014.12.265>

- [12] C.N. He, N.Q. Zhao, C.S. Shi, S.Z. Song, Mechanical Properties and Microstructures of Carbon Nanotube-Reinforced Al Matrix Composite Fabricated by in Situ Chemical Vapor Deposition, *Journal of Alloys and Compounds* 487/1-2 (2009) 258-262. DOI: <https://doi.org/10.1016/j.jallcom.2009.07.099>
- [13] P. Delhaes, Chemical Vapor Deposition and Infiltration Processes of Carbon Materials, *Carbon* 40/5 (2002) 641-657. DOI: [https://doi.org/10.1016/S0008-6223\(01\)00195-6](https://doi.org/10.1016/S0008-6223(01)00195-6)
- [14] R.S. Mishra, Z.Y. Ma, Friction Stir Welding and Processing, *Materials Science and Engineering R: Reports* 50/1-2 (2005) 1-78. DOI: <https://doi.org/10.1016/j.mser.2005.07.001>
- [15] H.S. Arora, H. Singh, B.K. Dhindaw, Composite Fabrication Using Friction Stir Processing – a Review, *International Journal of Advanced Manufacturing Technology* 61/9-12 (2012) 1043-1055. DOI: <https://doi.org/10.1007/s00170-011-3758-8>
- [16] V. Sharma, U. Prakash, B.V. Manoj Kumar, Surface Composites by Friction Stir Processing: A Review *Journal of Materials Processing Technology* 224 (2015) 117-134. DOI: <https://doi.org/10.1016/j.jmatprotec.2015.04.019>
- [17] G. Madhusudhan Reddy, A. Sambasiva Rao, K. Srinivasa Rao, Friction Stir Processing for Enhancement of Wear Resistance of ZM21 Magnesium Alloy, *Transactions of the Indian Institute of Metals* 66/1 (2013) 13-24. DOI: <https://doi.org/10.1007/s12666-012-0163-4>
- [18] M. Abbasi, B. Bagheri, M. Dadaei, H.R. Omidvar, M. Rezaei, The Effect of FSP on Mechanical, Tribological, and Corrosion Behavior of Composite Layer Developed on Magnesium AZ91 Alloy Surface, *International Journal of Advanced Manufacturing Technology* 77/9-12 (2015) 2051-2058. DOI: <https://doi.org/10.1007/s00170-014-6577-x>
- [19] J. Singh, H. Lal, N. Bala, Investigations on the wear behaviour of friction stir processed magnesium based AZ91 alloy, *International Journal of Mechanical Engineering and Robotics Research* 2/3 (2013) 271-274.
- [20] H.S. Arora, H. Singh, B.K. Dhindaw, H.S. Grewal, Improving the Tribological Properties of Mg Based AZ31 Alloy Using Friction Stir Processing, *Advanced Materials Research* 585 (2012) 579-583. DOI: <https://doi.org/10.4028/www.scientific.net/AMR.585.579>
- [21] H.S. Arora, H. Singh, B.K. Dhindaw, Wear Behaviour of a Mg Alloy Subjected to Friction Stir Processing, *Wear* 303/1-2 (2013) 65-77. DOI: <https://doi.org/10.1016/j.wear.2013.02.023>
- [22] B. Ram, D. Deepak, N. Bala, Role of Friction Stir Processing in Improving Wear Behavior of Mg/SiC Composites Produced by Stir Casting Route, *Materials Research Express* 6/2 (2019) 026577. DOI: <https://doi.org/10.1088/2053-1591/aaf1e4>
- [23] M. Azizieh, A.N. Larki, M. Tahmasebi, M. Bavi, E. Alizadeh, H.S. Kim. Wear Behavior of AZ31/Al₂O₃ Magnesium Matrix Surface Nanocomposite Fabricated via Friction Stir Processing, *Journal of Materials Engineering and Performance* 27/4 (2018) 2010-2017. DOI: <https://doi.org/10.1007/s11665-018-3277-y>
- [24] G. Faraji, P. Asadi, Characterization of AZ91/Alumina Nanocomposite Produced by FSP, *Materials Science and Engineering: A* 528/6 (2011) 2431-2440. DOI: <https://doi.org/10.1016/j.msea.2010.11.065>
- [25] I. Dinaharan, S.C. Vettivel, M. Balakrishnan, E.T. Akinlabi, Influence of Processing Route on Microstructure and Wear Resistance of Fly Ash Reinforced AZ31 Magnesium Matrix Composites, *Journal of Magnesium and Alloys* 7/1 (2019) 155-165. DOI: <https://doi.org/10.1016/j.jma.2019.01.003>
- [26] H. Patle, B. Ratna Sunil, R. Dumpala, Sliding Wear Behavior of AZ91/B₄C Surface Composites Produced by Friction Stir Processing, *Materials Research Express* 7/1 (2020) 016586. DOI: <https://doi.org/10.1088/2053-1591/ab6a55>
- [27] W.A. Monteiro, S.J. Buso, L.V. Silva, Application of Magnesium Alloys in Transport, in: W.A. Monteiro (ed.), *New Features on Magnesium Alloys*, IntechOpen, 1998, 1-14. DOI: <https://doi.org/10.5772/48273>
- [28] C.-C. Lin, S.-J. Huang, C.-C. Liu, Structural analysis and optimization of bicycle frame designs, *Advances in Mechanical Engineering* 9/12 (2017) 1-10. DOI: <https://doi.org/10.1177/1687814017739513>
- [29] Weblinks: Magnesium Applications. Available from: https://www.tms.org/Communities/FTAttachments/Mg%20Applications_Corporate.pdf
- [30] S. Sharma, A. Handa, S.S. Singh, D. Verma, Synthesis of a Novel Hybrid Nanocomposite of AZ31Mg-Graphene-MWCNT by Multi-Pass Friction Stir Processing and Evaluation of Mechanical Properties, *Materials Research Express* 6/12 (2019) 126531. DOI: <https://doi.org/10.1088/2053-1591/ab54da>
- [31] A.P. Sekhar, D. Das, Influence of Artificial Aging on Mechanical Properties and High Stress Abrasive Wear Behaviour of Al-Mg-Si Alloy, *Metals and Materials International* (2019). DOI: <https://doi.org/10.1007/s12540-019-00399-9>
- [32] J.A. Valle, Friction Stir Processing of the Magnesium Alloy AZ61: Grain Size Refinement and Mechanical

- Properties, *Materials Science Forum* 706-709 (2012) 823-1828. DOI: <https://doi.org/10.4028/www.scientific.net/MSF.706-709.1823>
- [33] D. Khayyamin, A. Mostafapour, R. Keshmiri, The Effect of Process Parameters on Microstructural Characteristics of AZ91/SiO₂ Composite Fabricated by FSP, *Materials Science and Engineering: A* 559 (2013) 217-221. DOI: <https://doi.org/10.1016/j.msea.2012.08.084>
- [34] S. Das, R.S. Mishra, K.J. Doherty, K.C. Cho, B. Davis, R. DeLorme, Magnesium Based Composite Via Friction Stir Processing., in: R. Mishra, M.W. Mahoney, Y. Sato, Y. Hovanski, R. Verma (eds), *Friction Stir Welding and Processing VII*, Springer, Cham, 245-252. DOI: https://doi.org/10.1007/978-3-319-48108-1_25
- [35] G. Vedabouriswaran, S. Aravindan, Development and characterization studies on magnesium alloy (RZ 5) surface metal matrix composites through friction stir processing, *Journal of Magnesium and Alloys* 6/2 (2018) 145-163. DOI: <https://doi.org/10.1016/j.jma.2018.03.001>
- [36] D. Ahmadkhaniha, M. Heydarzadeh Sohi, A. Salehi, R. Tahavvori, Formations of AZ91/Al₂O₃ nanocomposite layer by friction stir processing, *Journal of Magnesium and Alloys* 4/4 (2016) 314-318. DOI: <https://doi.org/10.1016/j.jma.2016.11.002>
- [37] M. Azizieh, H.S. Kim, A.H. Kokabi, P. Abachi, B.K. Shahraki, Fabrication of AZ31/Al₂O₃ nanocomposites by friction stir processing, *Reviews on Advanced Materials Science* 28/1 (2011) 85-89.
- [38] R. Sathiskumar, I. Dinaharan, N. Murugan, S.J. Vijay, Influence of Tool Rotational Speed on Microstructure and Sliding Wear Behavior of Cu/B₄C Surface Composite Synthesized by Friction Stir Processing, *Transactions of Nonferrous Metals Society of China* 25/1 (2014) 95-102. [https://doi.org/10.1016/S1003-6326\(15\)63583-X](https://doi.org/10.1016/S1003-6326(15)63583-X)
- [39] P. Asadi, M.K. Besharati Givi, G. Faraji, Producing Ultrafine-Grained AZ91 from as-Cast AZ91 by FSP, *Materials and Manufacturing Processes* 25/11 (2010) 1219-1226. DOI: <https://doi.org/10.1080/10426911003636936>
- [40] J.F. Archard, Contact and rubbing of flat surfaces, *Journal of Applied Physics* 24/8 (1953) 981-988. DOI: <https://doi.org/10.1063/1.1721448>
- [41] G. Faraji, O. Dastani, S. Ali Asghar, A. Mousavi. Effect of Process Parameters on Microstructure and Micro-Hardness of AZ91/Al₂O₃ Surface Composite Produced by FSP, *Journal of Materials Engineering and Performance* 20 (2011) 1583-1590. DOI: <https://doi.org/10.1007/s11665-010-9812-0>
- [42] M. Dadashpour, A. Mostafapour, R. Yeşildal, S. Rouhi. Effect of Process Parameter on Mechanical Properties and Fracture Behavior of AZ91C/SiO₂ Composite Fabricated by FSP, *Materials Science and Engineering: A* 655 (2016) 379-387. DOI: <https://doi.org/10.1016/j.msea.2015.12.103>
- [43] M. Azizieh, A.H. Kokabi, P. Abachi, Effect of Rotational Speed and Probe Profile on Microstructure and Hardness of AZ31/Al₂O₃ Nanocomposites Fabricated by Friction Stir Processing, *Materials and Design* 32/4 (2011) 2034-2041. DOI: <https://doi.org/10.1016/j.matdes.2010.11.055>
- [44] M. Navazani, K. Dehghani, Investigation of Microstructure and Hardness of Mg/TiC Surface Composite Fabricated by Friction Stir Processing (FSP), *Procedia Materials Science* 11 (2015) 509-514. DOI: <https://doi.org/10.1016/j.mspro.2015.11.082>
- [45] R. Bauri, G.D. Janaki Ram, D. Yadav, C.N. Shyam Kumar, Effect of Process Parameters and Tool Geometry on Fabrication of Ni Particles Reinforced 5083 Al Composite by Friction Stir Processing, *Materials Today: Proceedings* 2/4-5 (2015) 3203-3211. DOI: <https://doi.org/10.1016/j.matpr.2015.07.115>
- [46] M. Zohoor, M.K. Besharati Givi, P. Salami, Effect of Processing Parameters on Fabrication of Al-Mg/Cu Composites via Friction Stir Processing, *Materials and Design* 39 (2012) 358-365. DOI: <https://doi.org/10.1016/j.matdes.2012.02.042>
- [47] D. Lu, Y. Jiang, R. Zhou, Wear Performance of Nano-Al₂O₃ Particles and CNTs Reinforced Magnesium Matrix Composites by Friction Stir Processing, *Wear* 305/1-2 (2013) 286-290. DOI: <https://doi.org/10.1016/j.wear.2012.11.079>



© 2020 by the authors. Licensee International OCSCO World Press, Gliwice, Poland. This paper is an open access paper distributed under the terms and conditions of the Creative Commons Attribution-NonCommercial-NoDerivatives 4.0 International (CC BY-NC-ND 4.0) license (<https://creativecommons.org/licenses/by-nc-nd/4.0/deed.en>).

2019-20

Intelligent Textiles and its applications: An overview

Satish Khatak

Department of ECE, The Technological Institute of Textile & Sciences, Bhiwani- 127021(Haryana)

To Cite this Article

Satish Khatak, "Intelligent Textiles and its applications: An overview", *International Journal for Modern Trends in Science and Technology*, 6(9S): 68-71, 2020.

Article Info

Received on 25-August-2020, Revised on 08-September-2020, Accepted on 12-September-2020, Published on 18-September-2020.

ABSTRACT

Intelligent wearable clothing can be seen as textiles that possess the capability of sensing and responding to environmental changes. The clothing sense the physical activity of the person and his environment, monitor and analyze it, and accordingly attempts to respond in most appropriate manner. Intelligent textiles are laced with embedded electronics sensors and other circuitry into fabric thereby resulting in smart outfits capable of an array of diverse applications. Intelligent textiles find applications in defense sectors, railways, firefighters, police, skydivers, sports-persons and other professional activities. The aim of this study is to highlight the protective applications of wearable intelligent textiles and their significance in the present context.

KEYWORDS: Intelligent, Textiles, Defense, Sensors, Smart, Technology.

I. INTRODUCTION

"Intelligent textiles" are fabrics that have been designed and developed with innovative technologies that offer added advantage to the wearer. They have the capability to sense, monitor, process information, analyze, and react accordingly. They may be wearable and also they have monitoring and computation, as well as wireless information transfer capabilities. Some sensors and other computational elements are embedded in intelligent textiles, as well as built into yarns, with the aim of collecting useful information, monitoring vital statistics, and transferring them remotely for further processing. Intelligent textiles can be broadly divided into two main categories as aesthetic textile and performance enhancing textiles. The examples of aesthetic textile include fabrics that glow and fabrics that can alter colour. These fabrics may collect energy from the environment by harnessing sensations, sound or heat, reacting to these inputs.

Also the colour changing and lighting scheme can also work by embedding the fabric with electronic battery or cell that can power it. On the other hand Performance enhancing intelligent textiles are proposed for use in athletic, extreme sports, military and other such applications. They are designed to regulate body temperature and blood pressure of the wearer, decrease wind resistance, and control muscle vibration and these results in improved athletic performance. Other intelligent fabrics have also been developed for protective clothing, to guard against extreme hazardous environmental conditions, such as radiation and the effects of space travel, to safeguard firefighters against fire and heat etc. The other sectors such as health and beauty industry are getting benefits of these innovations, which range from drug-releasing medical textiles, to fabric with moisturizer, perfume, and anti-aging properties. In case of electronic textiles the emphasis is given on the flawless integration of textiles with

electronic elements like microcontrollers, sensors, and actuators or any other active or passive components. Also they may be wearable or non-wearable as there are electronics textiles which found application in interior design. The challenging side for embedding electronic function in the clothing are flexibility, life, lightweight, comfort-level, conductivity, good process ability, good wear ability and cost effective. The research in this field is growing so rapidly that with new technologies we can integrate several electronic devices directly into textile & apparel products using common resources enhancing the mobility, comfort & convenience of such device to a great extent.

II. WORKING PRINCIPLE

When we talk about intelligent Textile it is having some advance features as compared to the smart textile. As smart textile senses the environment the intelligent textiles also have the capability to sense parameters from the environment but along with that they analyze and process it, and respond accordingly. So we can say that intelligent textiles have to perform some basic functions to complete its task. These are

1. Sensors:-With the help of sensors it is going to gather some parameters heat, temperature, pressure velocity etc from the environment. These sensors should have very high sensitivity and accuracy. They should also have small size and light in weight.

2. Processing, Monitoring and Analyzing Unit:-With the help of this section the intelligent textile is going to make an appropriate decision as per the stimulation and some predetermined data. It may contain microcontroller units and other electronic circuitry

3. Actuators.- This is the unit which gives response as per the stimulation captured by the sensors

Apart from these, if we want to transfer the vital information or data to a remote location for further monitoring, controlling and recording purpose we may require some more electronic circuitry.

III. DEVELOPMENTAL STAGES OF INTELLIGENT TEXTILES

Functionally the development can be understood as follows-

1. Passive smart Textiles:-These are composed of devices or materials which are going to sense the environment. They are basically having sensor only, which respond the stimulus by showing

change in electric or thermal resistance, colour, shape etc. The best example is dresses which have inbuilt thermistors to log body temperature over the time.

2. Active Smart Textiles: - These not only senses the external environment condition but also respond to it. In these actuator is there which respond to a particular stimulus from the environment. We are having temperature sensing shirts which rolls up the sleeves if the body temperature rises beyond some predetermined values.

3. Intelligent Textile:-These are having capability to sense, react and adapt accordingly.

4. Textile integrated with Artificial Intelligence:-If these extra smart textiles are embedded with artificial intelligence, than they reach at next higher level of intelligence. They can than analyze more smartly and make decisions of their own like human beings, by means of virtual mind.

IV. APPLICATION AREAS

1. Sports Activities:-The intelligent Textiles with the aim to improve performance of sports person and personal comfort, plays a very crucial role. A smart sock with a foot pressure measurement technology and walking distance measurement that can be used to measure sports performance. The various electronic parts of this product can be separated in order to clean and wash the textile part of the socks. The collected data is sent wirelessly to a mobile application running into a Smartphone. With this intelligent device, the athletes can see and monitor the pressure profile of the foot sole and then practice their gait cycle to achieve a better performance. A sports person can wear intelligent bands, jackets, caps to continuously monitor the pulse rate, blood pressure, body temperature, fatigue. The necessary data can be sent to remote location where it can be analyzed and may be used to improve the performance of the sports person. Similar types of devices can be used by sky divers, swimmers or other sports persons to monitor, analyze and improve their performance.[1,3]

2. Health sector:-Smart and Intelligent textiles which are being utilized by health care industry are proving to be a boon to this sector. Intelligent wearable textile which are basically composed of various embedded sensors, actuators, microcontrollers which not only senses, register, monitor and analyze the physical and mental health of the person but it also transmit the

necessary data from the patient to the medical expert.

There are diverse applications in medical sectors where these electronic or intelligent textiles are extensively used. To ease the symptoms of Seasonal Affective Disorder (SAD), electro-luminescent wire being explored by creating bedding that emits light. Intelligent bras are there which have the capability to detect symptoms of breast cancer at an early stage so that it can be treated and cured. For the monitoring of respiration system, Heart pumping system, and other physical activity, various wireless enabled intelligent garments have been developed and still some are in pipeline. These are going to be very helpful for the persons who are prone to heart attack as these wearable intelligent textiles will detect the early signs and warn the wearer and simultaneously sent the data to the person who is monitoring such a person. Intelligent shirts are also developed in which the conductive fibers and various sensors are embedded which measures and monitor respiration system. The "tricoder for babies" are there which tracks vital as well as changes in body temperature. The increasing demand of these wearable intelligent textiles from health care sector is going to help in developing more advance types of such intelligent textiles embedded with artificial intelligence.[6]

3. Military and Defense sector

Due to technological advancement in electronic sector it is now possible to develop very small sized electronics devices which can be embedded in textiles and can be used in defense sector. This will give new dimensions to military and defense security. In adverse environmental conditions and hazardous situations faced by soldiers, there is a need of real time information system to give protection and survivability to them. This will help in improving performance and other capabilities of the defense forces and emergency response services. The requirements for such situations are to monitor vital signs and ease injuries while also monitoring environment hazards such as toxic gases. The intelligent textile in military can be utilized in two ways. Firstly, Personal protective garments and individual equipments which includes battle uniforms, ballistic protection vests and helmets, chemical protection suits, belts, ropes, suspenders and field-packs. Secondly, defense systems and weapons like parachutes, shelters tent houses etc. The enhanced security to both these can be provided with intelligent textiles. If a soldier get injured during war or any other

situation and he is wearing an Intelligent jackets than this information is automatically transferred to the nearby controlling and monitoring unit and necessary medical or any other help can be provided to the injured soldier. The soldier can himself monitor his pulse rate, blood pressure and other parameters through the embedded intelligent systems in the jacket. Intelligent materials are being developed to equip the army of future with uniforms which help in heal, shield, and protect them against chemical and biological warfare[2]. The work is also going on to develop such a uniform that is almost invisible and soft clothing that can become a rigid cast when a soldier break his or her leg. Also with the help of sensors in jacket he can monitor his surroundings. So this combination of electronics and textile will largely benefit the defense personals. No doubt much more is need to done to develop best possible intelligent protective wearable textiles in this sector.[5,7]

4. Safety purpose

Intelligent jackets and shirts especially for the protection of public safety personnel, namely firefighters, rescue teams, police officers are being developed with all necessary advanced safety features. They will be used in conjunction with a wireless- enabled radio system. The intelligent jacket or shirt can monitor the health and safety of public safety personnel, victims trapped in a building or underneath rubble with the ability to detect the exact location of the victims through positioning capability. In addition to monitoring vital signs, the system can detect the extent of falls, and the presence of harmful gases. It can also facilitate two- way voice and video communication. An integration of sensors and flexible light emitting displays with textile can help in designing a wearable warning signal generating jacket. This can receive and respond to stimuli from body, enabling a warning signal to be displayed and sent. The sensors in the jacket keeps on monitoring the vital body parameters and if something unusual happens, same is indicated through flash of light and a wireless communication system could send a distress signal to a remote location. Textiles integrated with electronic sensory devices driven by global positioning system can detect one's exact location anytime and in any weather. Fabric area networks (FANs) make it possible with the help of electronic devices to exchange required information, power and control signals within the user's personal space and remote locations[8].

5. Fashion and Lifestyle

The development of high tech intelligent textiles for initial high-value applications such as extreme sports will eventually find its way into street fashion. There are fabrics with moisture management systems being used for fast evaporation of sweat. Fabrics with UV protection, anti allergic and anti bacterial capabilities are available. There are intelligent dresses and sleep suit which emits scents depending on your mood and requirement. Intelligent fibers are being developed that can change colour and its shape as per your command. The conductive fibers could change colour on command from an electric signal that alters the reflective quality of this special fiber. Thereby increasing function as well as fashion. Intelligent Textile with thermoregulation properties are also being developed. These textiles contain phase change materials which react immediately with change in surrounding temperatures, and the temperature in different parts of the body. When there is a rise in temperature, the phase changing material microcapsules react by absorbing heat and storing this energy in the liquefied phase change materials. When temperature falls again, the microcapsules release this stored heat energy and the phase change material solidify again. There are also interactive fibers which incorporates electronics that are activated by a power source[4]. There are wearable electronics which can be used in intelligent wearable textiles to dial mobile numbers, control music from mp3 player etc. The examples includes business suit with a mobile phone incorporated, sportswear to monitor heart rate, aerobic outfits with music players incorporated and club wear which changes colour. This is only being possible because of integration of electronics and textiles.[9,10]

V. FUTURE PROSPECTS

In the coming years the fibertronics will become advanced and in such situation all the electronic functions such as computing, fast and reliable communication, power sources, etc are embedded in fiber itself. The nano-technology will give new horizons to the intelligent textiles. Embedded optical fiber and micro-porous breathable fabrics will be more effectively and efficiently utilized in development of intelligent textiles. Weather proof and water proof systems needs to be developed. Lots of improvements are still needed in current technologies to make it more reliable, authentic, durable and economical so that it will reach to every corners of life of a common man.

VI. CONCLUSION

This paper summarizes the main concept of Intelligent Textiles and its some of the current and future possible applications. Due to advancement in electronics, the devices are becoming smaller and smaller and it is becoming easier to integrate them with the fibers. The current technological shortcoming will be removed very soon in the coming years and more reliable, high performance and efficient intelligent textile devices will be available in future.

REFERENCES

- [1]. "Wearable sensors for Human Activity Monitoring: A Review". S.C.Mukhopadhyay, Massey University on March 2015.
- [2]. "A Review of smart Clothing in Military", Sofiascataglini, Johan Gallant and Giuseppe Andreoni, Conference paper on May 2015.
- [3]. "Wearable Electronics and Smart Textiles: A Critical Review", MatteoStoppa Alessandro Chiolerio, Center for Space Human Robotics, Istituto Italiano di Tecnologia, Corso Trento 21, 10129 Torino, Italy. Received: 14 May 2014; in revised form: 2
- [4]. "Applications of Smart and Interactive Textiles". Textile Learner. Saddamhusen Jamadar. Archived from the original on 2013-06-12. Retrieved 2013-04-21.
- [5]. "Smart Shirt." Wikipedia. Wikimedia Foundation, 22 Aug.2012. Web. 07 Oct. 2012. <http://en.wikipedia.org/wiki/Smart_shirt>.
- [6]. "Smart textiles for healthcare: applications and technologies",Viktorija Mečnikal Ms.sc.; Melanie Hoerr2 Dipl.-Ing.; Ivars Krieviņš1 Assoc.prof. Dr.sc.ing.; Anne Schwarz2 Dr.sc.ing. Institute of Textile Technology and Design of Riga Technical University, Latvia1; Institut fuer Textiltechnik of RWTH Aachen University, Germany2 viktorija.mecnika@rtu.lv, ivars.krievins@rtu.lv1; melanie.hoerr@ita.rwth-aachen.de, anne.schwarz@ita.rwth-aachen.de2
- [7].http://www.army.mil/article/133577/Body_sensors_to_help_Soldiers_in_future_conflicts
- [8]. "Electronic Textiles: Fiber- Embedded Electrolyte -Gated Field-Effect Transistors for e-Textiles", Hamedi, M.; Herlogsson, L.; Crispin, X.; Marcilla, R.; Berggren, M.; Inganäs, O. (22 January 2009). *Advanced Materials*. John Wiley & Sons, Inc. doi:10.1002/adma.200990013.PMID 21162140 - via Wiley Online Library.
- [9]. "Smart Fabrics and Interactive Textile Enabling Wearable Personal Applications: R&D States of the Art and Future Challenges", A.Lymberis, R.Paradiso, 30th Annual International IEEE EMBS conference, Vancouver, British Columbia, Canada, August 20-24, 2008.
- [10]. "Interactive electronic textile development" Dina Meoli and Traci May-plumle; *Journal of Textile and Apparel, Technology and Management*; Volume 2(2), Spring 2002.



Contents lists available at ScienceDirect

Materials Today: Proceedings

journal homepage: www.elsevier.com/locate/matpr

Selection of tool transverse speed considering trial run experimentations for AZ61/TiC composite developed via friction stir processing using triangular tool

P. Sagar^{a,*}, A. Handa^b^a PhD, Research scholar, I.K. Gujral Punjab Technical University, Kapurthala, India^b Department of Mechanical Engineering, I.K. Gujral Punjab Technical University, Kapurthala, India

ARTICLE INFO

Article history:

Received 12 June 2020

Received in revised form 26 June 2020

Accepted 28 June 2020

Available online xxxx

Keywords:

Friction stir processing

Magnesium base Alloy

TiC

Optical Microscopy

Grain refinement

ABSTRACT

In this present work, an effort has been applied to fabricated AZ61/TiC magnesium based metal matrix composite. The effect of tool transverse speed and specimen holding time after etchant application has been studied before final design and run of experiments. A set of zig-zag holes were prepared into the 200 mm × 100 mm × 6 mm thick AZ61A plate and compacted with TiC particles. A fixed three pass Friction stir processing (FSP) was performed out employing a fixed tool rotation speed of 850 rpm and varying tool transverse speed of 25 mm/min, 100 mm/min and 170 mm/min. Optical microscopy (OM) was used to study the grain refinement. The results indicate that for tool rotational speed of 850 rpm and transverse speed of 25 mm/min better grains were formed at stir zone (SZ) and poor grains were observed once the specimen analyzed after 25 min of etching.

© 2020 Elsevier Ltd. All rights reserved.

Selection and Peer-review under responsibility of the scientific committee of the 2nd International Conference on Future Learning Aspects of Mechanical Engineering.

1. Introduction

Until today, Friction stir welding (FSW) is used to join material same or different. In last few decades FSP is been developed for developing metal matrix composites based on the principle of FSW [1]. FSP is widely used to fabricate aluminum composites used in submarine, space engineering, railways, electronics and automobile industry [2,3]. In past few recent years, FSW/FSP is also used to fabricate magnesium based metal matrix composites which has been globally investigated [4–15]. Magnesium been adopted by researchers and scientists over aluminum not for having density two-thirds that of aluminum also for its high strength-to-weight ratio [16]. Presently the world is more concerned about ecofriendly low-emission transportation vehicles with light-weight and maximum-performance. Magnesium possesses increased strength to weight ratio hence reduces the weight of the construction and minimize power requirement of a vehicle. Magnesium in its base form lacking in various applications thus improvement of its properties is required to extend its application. Hence for achieving this few per-

centage of particulates need to be added in magnesium or its alloys. Addition of these particulates not only increases the microstructure of the composite but also enhanced its mechanical properties. Reinforced particles plays vital role in increasing the properties of the base metal. Therefore, there is a worldwide interest to further develop and investigate magnesium based composites. FSP tool generates high amount of heat which softens the base metal and allow proper mixing of particulates into it. One method of fabricating magnesium based composite is creating a matrix of hole in zig-zag pattern with required depth and diameter in the parent metal, compact the holes with reinforce particles, plunge the tool and traverse along the holes [17,18]. A metal matrix composite (MMC) provides improved metallurgical and mechanical properties. Few studies of developing MMC are reported in literature. M. Balakrishnan et al. [19], used magnesium alloy AZ31 with particulates like TiC to fabricate an MMC. They operate or execute or demonstrate the FSP by taking fixed tool rotational speed, tool transverse speed and tool axial force on a 6 mm AZ31 plate by single pass. They engraved four different width [0, 0.4, 0.8, 1.2] and of equal depth 4.5 mm in the plate to introduced varying different fraction of the given [0, 6, 12, 18]. Macrostructure and microstructure was studied by digital optical scanner and scanning electron microscope and it was suggested TiC were properly distributed. D. Khayyamin et al. [20], studied the

* Corresponding author.

E-mail addresses: jasuaprem@gmail.com (P. Sagar), handaaamic2002@gmail.com (A. Handa).<https://doi.org/10.1016/j.matpr.2020.06.537>

2214-7853/© 2020 Elsevier Ltd. All rights reserved.

Selection and Peer-review under responsibility of the scientific committee of the 2nd International Conference on Future Learning Aspects of Mechanical Engineering.

effect of process parameters on micro structural characteristics of AZ91/SiO₂ composite fabricated by FSP. They fix tool rotation speed to 1250 rpm, tilt angle to 3° and number of passes to 4 passes with varying transverse speed to 20, 40 and 63 mm/min. They also examine metallurgical and mechanical properties by optical microscopy, scanning electron microscopy (SEM) and vickers hardness tester. Outline of the work concluded that grain size decreases and strength and hardness increase with increase in transverse speed. Increase number of pass increase hardness and reduce grain size. Morisada et al. [21], fabricate AZ31 magnesium alloy with SiC via using FSP. They used SiC powder of mean diameter 1 μm into a groove of 1 mm × 2 mm of a 6 mm thick plate. A tool of columnar shape of material SKD61 with diameter 12 mm along with a pin of diameter 4 mm and length of 1.8 mm was used, also they fix the value of parameters like tool rotation 1500 rpm, tilt angle 3° and travel speed of range 25–200 mm/min for processing. OM, SEM tests was conducted to investigate the micro behavior of the composite. Findings of the test reported a fine grain size i.e. 6.0 μm in the FSPed AZ31 with SiC particles as compared to the mean grain size i.e. 79.1, 12.9 of as-received AZ31 and FSPed AZ31 respectively at the travel speed of 50 mm/min. Further they reported that with increased travel speed grain size of the composite decreases. Micro-vickers hardness testing apparatus with a load of 200 g was used to measure micro hardness and it shows a maximum value of 69.3 Hv for FSPed AZ31 with SiC particles and 48.1Hv and 60.0Hv for as-received AZ31 and FSPed AZ31 respectively.

The aim of the present work is to apply FSP technique for producing magnesium based composite with TiC as reinforcement and to analyze the grain refinement of MMC.

2. Experimental procedure

In this current work, AZ61A magnesium alloy is used. Plates of AZ61A with size 200 mm × 100 mm × 6 mm were brought from Shandong Hongtai science and technology co.ltd. China. The result of chemical analysis of the magnesium anode in percent weight is presented in Table 1. TiC is used as reinforcement particles with average size of 80 nm. SEM image showing the average size of the powder particles is shown in Fig. 1. Energy-dispersive X-ray spectroscopy (EDSX) images of powder showing abundance of Titanium and Carbide particle is shown in Fig. 2 and weight and atomic percentage of the particulates is presented in Table 2. A matrix of zig-zag pattern holes with precise depth of 4 mm and diameter 2 mm were drilled into the plate with a pattern as shown in Fig. 3. FSP was carried out with HCHCr tool. Initially setting up of the powder into the holes was carried out by pin less tool and for subsequent passes triangular tool was used with tool shoulder diameter 21 mm and pin length 4 mm as shown in Fig. 4. The volume fraction of the reinforce particles was calculated by using formula [17]:

$$V_t = Tsd \times Pl \times Twl$$

$$V = \pi r^2 \times Dh$$

$$V_r = V \times N$$

Table 1
Complete chemical composition of as cast AZ61A.

Element	Content %	Content by weight
Aluminum	6.26	5.8–7.2
Zinc	0.78	0.4–1.5
Manganese	0.27	0.15–0.5
Silicon	0.032	0.05 max
Iron	0.0021	0.005 max
Copper	0.011	0.05 max
Nickel	0.0026	0.005max
Magnesium	-----	Bal

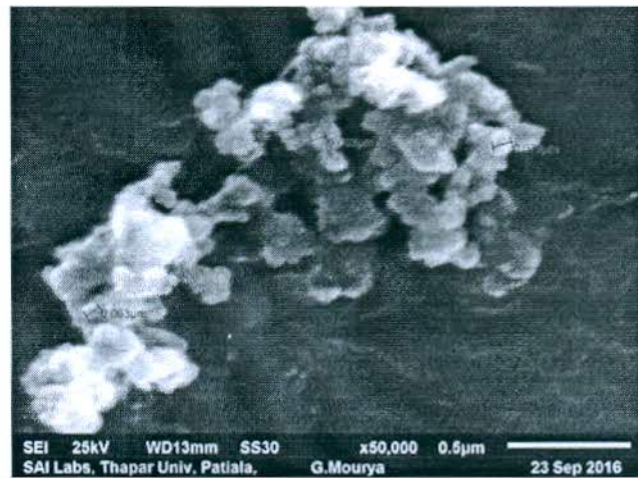


Fig. 1. SEM image of reinforced TiC particles showing average size.

$$V_f = (V_r \div V_t) \times 100$$

Where, V_t = Total volume of the processing zone; Tsd = Tool shoulder diameter; Pl = Pin Length, Twl = Total working length; Dh = Depth of hole; V = volume of cylindrical hole; V_r = Volume of reinforcement particles; N = Total number of cylindrical holes; V_f = Volume fraction

In view for avoiding bending and lateral movement of the plate a fixture has been designed as shown in Fig. 5.

FSP was performed on CNC vertical milling machine and all the process parameters adopted is presented in Table 3.

A fixed three pass FSP was carried out and all three experiments were successfully completed. Fig. 6 shows the surface appearance of the synthesized composite. All these friction stir processed specimens were taken out and polished as per standard metallographic procedure.

Double disc polishing machine was used for mechanical polishing with emery papers of size 80, 100, 150, 220, 320, 500, 800, 1000, 1500 and 2000 and water as lubricant. Further polishing was carried out with diamond paste. Polished specimen then etched by 100 ml ethanol, 5 gm picric acid, 4 ml acetic acid, and 10 ml water for 15–20 sec. All the optical images were taken within 25 min of sample preparation. Fig. 7 shows the OM images for the specimen kept on hold for more than 25 min after etching.

3. Result and discussion

FSP technique was successfully executed for developing AZ61A/TiC with fixed volume fraction of 21.53% reinforcement particles inserted in thirty six holes for 100 mm length. Macrograph image for the successfully developed composite is shown in Fig. 8. It clearly shows that penetrating and rigorous stirring causes properly bonded groove. Also the pin length is sufficient for not producing defect at the bottom. Vigorous rubbing of the tool produces heat due to friction between tool and material. This frictional heat plasticize the magnesium metal alloy and converting it into semi solid phase. Packed TiC particles also brake down due to friction heat and transverse action of tool moves the plasticize composite from advancing side to retarding side and forge this behind the tool. Quality tool stirring with specific rings are almost visible on surface. OM images reveal that specimen kept on hold for more than 25 min develops a thin layer of etchant and dust over composite material. Fig. 9 Shows the OM images of different zones of the composite at tool rotation speed 850 rpm and tool transverse speed of 25 mm/min.

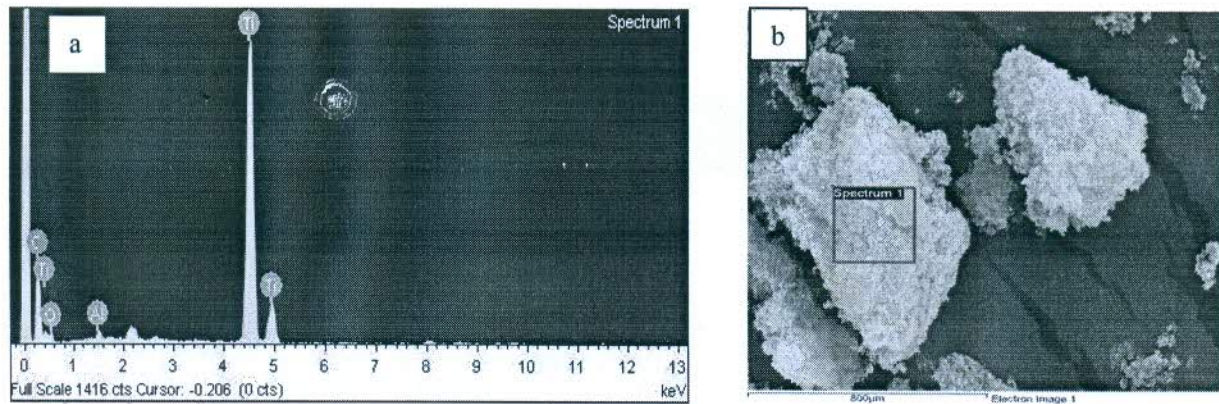


Fig. 2. EDS images of TiC powder (a) energy diagram for spectrum1, (b) electron image captured for spectrum1.

Table 2

Reinforcement particle TiC complete chemical composition.

Element	C K	O K	Al K	Ti K	Total
Weight %	29.21	13.50	0.90	56.39	100%
Atomic %	54.21	18.81	0.74	26.24	100%

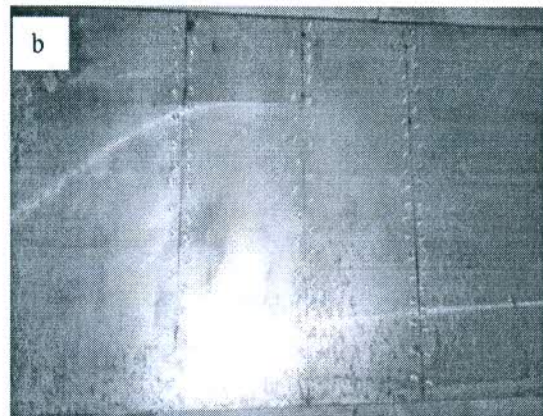
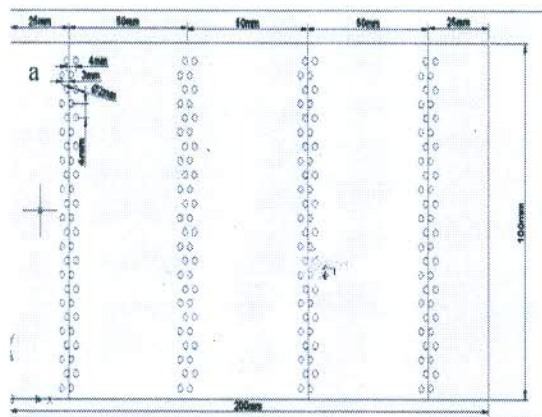


Fig. 3. Pattern of holes drilled into the AZ61A plate (a) schematic diagram, (b) photographic view of zig-zag pattern of holes.

Triangular probe with pin length 4mm.

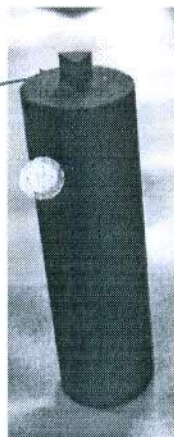


Fig. 4. Triangular tool used for FSP.

Dispersion of the TiC of TiC particle into the AZ61 matrix are presented. Only the travel speed determines the heat due to friction as tool rotational speed is fixed.

According to figure, for this trial experimentation comparatively increased heat flow and good flow viscosity of the metal around stir zone was observed. As reported by the author [22] grain refinement is due dynamic recrystallization, and that developed due to heat by tool rotation. So new grains almost at the entire processed zone are formed. More refined grains can be seen at SZ and are properly glued to the boundaries. OM images for tool rotation speed 850 rpm and 100 mm/min are shown in Fig. 10.

Localized refined grains at some places and bimodal population of some highly deformed grains are seen at heat affected zone and interface of heat affected and the thermal heat affected zone. This inadequate mixing is due to too fast tool transverse speed that leads to improper breaking of TiC particles. Less time generation of along with inadequate heat generation. Major defects like tunnel, crack, piping, pin hole and voids are not present on the top surface for 850 rpm tool rotation speed and for tool transverse speed of 25 and 100 mm/min. As the transverse speed of the tool increased to very high value, the stirring effect of tool becomes weaker and produces a weld flaw because no material particle at the retreating side enters into the advancing side. So a clear crack

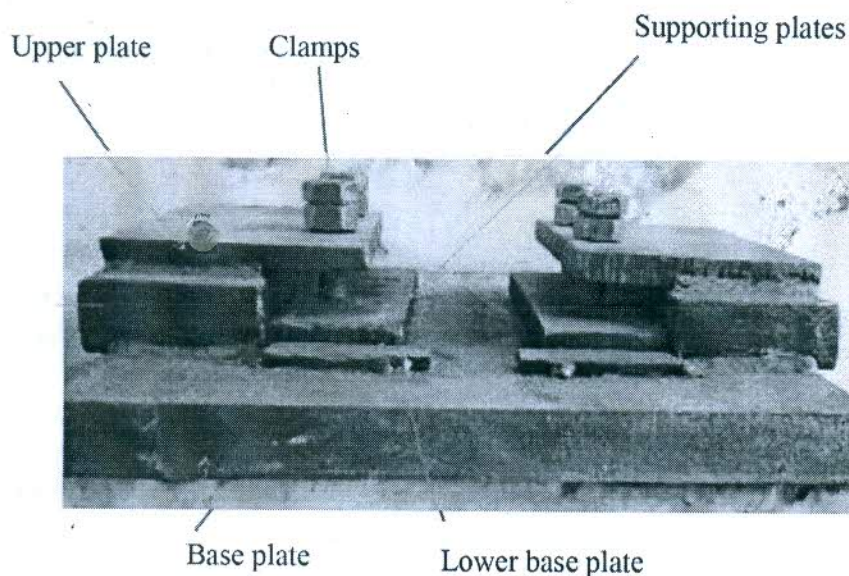


Fig. 5. Specially designed fixture for refraining movement.

Table 3
A combination of typical FSP parameters.

Experiment no.	Tool rotation speed	Transverse speed
1	850 rpm	25 mm/min
2	850 rpm	100 mm/min
3	850 rpm	170 mm/min

is visible on the upper half of the plate for transverse speed of 170 mm/min. as shown in Fig. 6 (c).

4. Conclusions

AZ61/TiC MMCs were successfully synthesized by using the novel method FSP. OM is used to study refinement of grain. The following conclusions were derived from the present work.

1. Friction stir processing is a sound technique for producing magnesium based Metal Matrix composites.

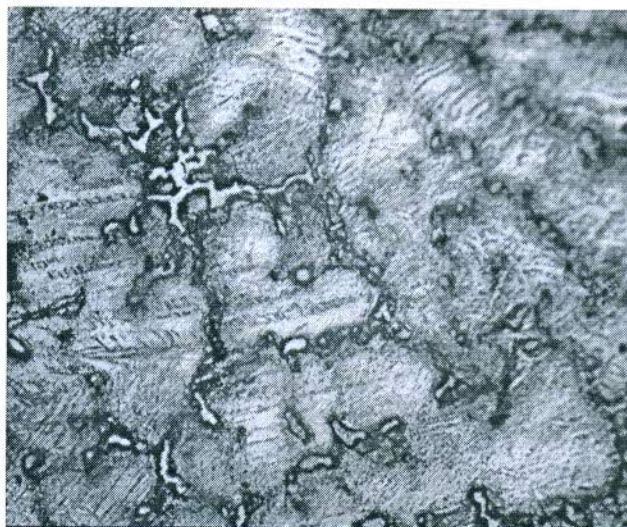


Fig. 7. Optical micrograph image of stir zone for specimen kept more than 25 min after etching.

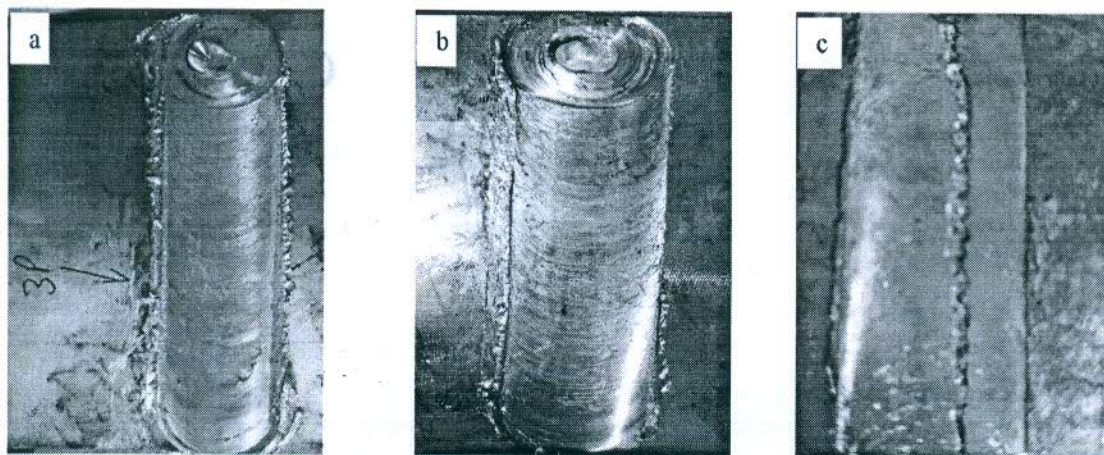


Fig. 6. Surface appearance of AZ61A MMC (a) at 850 rpm and 25 mm/min. (b) at 850 rpm and 100 mm/min. (c) at 850 rpm and 170 mm/min.

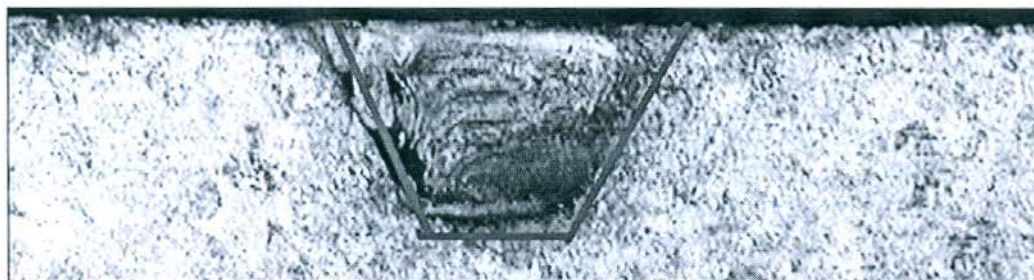


Fig. 8. Optical macrograph image of FSPed specimen.

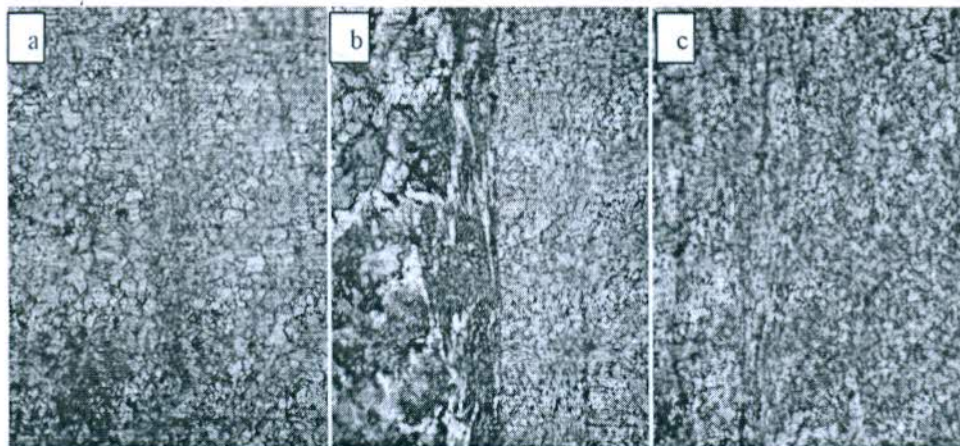


Fig. 9. Microstructure images of synthesized AZ61/TiC at tool rotation speed of 850 rpm and transverse speed of 25 mm/min. (a) SZ (b) Interface between Base metal and Heat affected zone (c) Interface between Heat affected zone and Thermal heat affected zone.

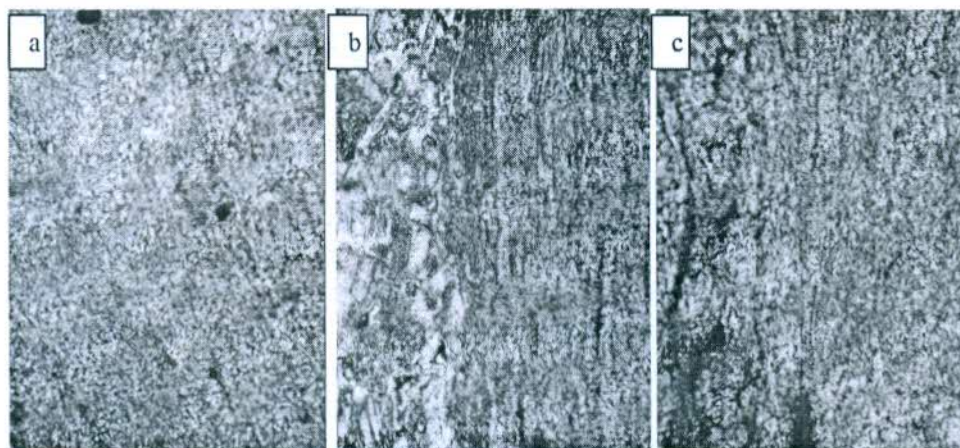


Fig. 10. Microstructure images of synthesized AZ61/TiC at tool rotation speed of 850 rpm and transverse speed of 100 mm/min. (a) SZ (b) Interface between Base metal and Heat affected zone (c) Interface between Heat affected zone and Thermal heat affected zone.

2. Fine dispersion of TiC into the alloy material is related to the tool travel speeds. A good dispersion of the TiC is obtained at 850 rpm and 25 mm/min transverse speed. New refined grains obtained at stir zone.
3. Low quality grains appeared for specimen kept on hold for more than 25 min after etching.
4. Metal matrix composite is fabricated successfully and without any crack formation.
5. There were no chemical reaction seen between TiC particles and parent metal.

Declaration of Competing Interest

The authors declare that they have no known competing financial interests or personal relationships that could have appeared to influence the work reported in this paper.

Acknowledgements

The authors would like to thank I.K. Gujral Punjab Technical University, Kapurthala, India for giving us the opportunity to carry

on our research work. All persons who have made substantial contributions to the work reported in the manuscript (e.g., technical help, writing and editing assistance, general support), but who do not meet the criteria for authorship, are named in the Acknowledgements and have given us their written permission to be named. If we have not included an Acknowledgements, then that indicates that we have not received substantial contributions from non-authors.

References:

- [1] R.S. Mishra, Z.Y. Ma, I. Charit, Friction stir processing: A novel technique for fabrication of surface composite, *Mater. Sci. Eng. A* 341 (1–2) (2003) 307–310, [https://doi.org/10.1016/S0921-5093\(02\)00199-5](https://doi.org/10.1016/S0921-5093(02)00199-5).
- [2] K. Kumar, P. Gulati, A. Gupta, D.K. Shukla, A review of friction stir processing of aluminium alloys using different types of reinforcements, *Int. J. Mech. Eng. Technol.* 8 (7) (2017) 1638–1651.
- [3] Y.X. Gan, D. Solomon, M. Reinbolt, Friction stir processing of particle reinforced composite materials, *Materials (Basel)* 3 (1) (2010) 329–350, <https://doi.org/10.3390/ma3010329>.
- [4] B.R. Sunil, G.P.K. Reddy, H. Patle, R. Dumpala, Magnesium based surface metal matrix composites by friction stir processing, *J. Magnes. Alloy* 4 (1) (2016) 52–61, <https://doi.org/10.1016/j.jma.2016.02.001>.
- [5] C.I. Chang, Y.N. Wang, H.R. Pei, C.J. Lee, X.H. Du, J.C. Huang, Microstructure and mechanical properties of nano-ZrO₂ and nano-SiO₂ particulate reinforced AZ31-Mg based composites fabricated by friction stir processing, *Key Eng. Mater.* 351 (2007) 114–119, <https://doi.org/10.4028/0-87849-451-0.114>.
- [6] P. Asadi, G. Faraji, M.K. Besharati, Producing of AZ91/SiC composite by friction stir processing (FSP), *Int. J. Adv. Manuf. Technol.* 51 (1–4) (2010) 247–260, <https://doi.org/10.1007/s00170-010-2600-z>.
- [7] P. Asadi, M.K. Besharati Givi, G. Faraji, Producing ultrafine-grained AZ91 from as-cast AZ91 by FSP, *Mater. Manuf. Process.* 25 (11) (2010) 1219–1226, <https://doi.org/10.1080/10426911003636936>.
- [8] M. Azizieh, A.H. Kokabi, P. Abachi, Effect of rotational speed and probe profile on microstructure and hardness of AZ31/Al₂O₃ nanocomposites fabricated by friction stir processing, *Mater. Des.* 32 (4) (2011) 2034–2041, <https://doi.org/10.1016/j.matdes.2010.11.055>.
- [9] M. Azizieh, H.S. Kim, A.H. Kokabi, P. Abachi, B.K. Shaharaki, Fabrication of AZ31/Al₂O₃ nanocomposites by friction stir processing, *Rev. Adv. Mater. Sci.* 28 (1) (2011) 85–89.
- [10] G. Madhusudhan Reddy, A. Sambasiva Rao, K. Srinivasa Rao, Friction stir processing for enhancement of wear resistance of ZM21 magnesium alloy, *Trans. Indian Inst. Met.* 66 (1) (2013) 13–24, <https://doi.org/10.1007/s12666-012-0163-4>.
- [11] C.J. Lee, J.C. Huang, P.J. Hsieh, Mg based nano-composites fabricated by friction stir processing, *Scr. Mater.* 54 (7) (2006) 1415–1420, <https://doi.org/10.1016/j.scriptamat.2005.11.056>.
- [12] M. Soltani, M. Shamanian, B. Niroumand, Surface characteristics improvement of AZ31B magnesium by surface compositing with carbon nano-tubes through friction stir processing, *ADMT J.* 8 (1) (2015) 85–95.
- [13] X. Du, B. Wu, Using two-pass friction stir processing to produce nanocrystalline microstructure in AZ61 magnesium alloy, *Sci. China Ser. E Technol. Sci.* 52 (6) (2009) 1751–1755, <https://doi.org/10.1007/s11431-008-0210-x>.
- [14] D. Ahmadvani, M. Heydarzadeh Sohi, A. Salehi, R. Tahavvori, Formations of AZ91/Al₂O₃ nano-composite layer by friction stir processing, *J. Magnes. Alloy* 4 (4) (2016) 314–318, <https://doi.org/10.1016/j.jma.2016.11.002>.
- [15] D. Sameer Kumar, K.N.S. Suman, C. Tara Sasanka, K. Ravindra, P. Poddar, S.B. Venkata Siva, Microstructure, mechanical response and fractography of AZ91E/Al₂O₃ (p) nano composite fabricated by semi solid stir casting method, *J. Magnes. Alloy* 5 (1) (2017) 48–55, <https://doi.org/10.1016/j.jma.2016.11.006>.
- [16] M. Gupta, N. Sharon, "Magnesium, Magnesium alloys and magnesium composites" J.Wiley and Sons Magnesium. 2010. Print ISBN: 9780470494172 | Online ISBN: 9780470905098 DOI: 10.1002/9780470905098.
- [17] S. Sharma, A. Handa, S.S. Singh, D. Verma, Synthesis of a novel hybrid nanocomposite of AZ31Mg-Graphene-MWCNT by multi-pass friction stir processing and evaluation of mechanical properties, *Mater. Res. Express* 6 (12) (2019), <https://doi.org/10.1088/2053-1591/ab54da>.
- [18] S. Das, R.S. Mishra, K.J. Doherty, K.C. Cho, B. Davis, R. DeLorme, Magnesium based composite via friction stir processing, *Frict. Stir Weld. Process. VII (March)* (2016) 245–252, https://doi.org/10.1007/978-3-319-48108-1_25.
- [19] M. Balakrishnan, I. Dinaharan, R. Palanivel, R. Sivaprakasam, Synthesize of AZ31/TiC magnesium matrix composites using friction stir processing, *J. Magnes. Alloy* 3 (1) (2015) 76–78, <https://doi.org/10.1016/j.jma.2014.12.007>.
- [20] D. Khayyamin, A. Mostafapour, R. Keshmiri, The effect of process parameters on microstructural characteristics of AZ91/SiO₂ composite fabricated by FSP, *Mater. Sci. Eng. A* 559 (2013) 217–221, <https://doi.org/10.1016/j.msea.2012.08.084>.
- [21] Y. Morisada, H. Fujii, T. Nagaoka, M. Fukusumi, Effect of friction stir processing with SiC particles on microstructure and hardness of AZ31, *Mater. Sci. Eng. A* 433 (1–2) (2006) 50–54, <https://doi.org/10.1016/j.msea.2006.06.089>.
- [22] S. Sharma, A. Handa, S.S. Singh, D. Verma, Influence of tool rotation speeds on mechanical morphological properties of friction stir processed nano hybrid composite of MWCNT-Graphene-AZ31 magnesium, *J. Magnes. Alloy* 7 (3) (2019) 487–500, <https://doi.org/10.1016/j.jma.2019.07.001>.



Cloud Data double Security Using DES and ECC

Archana Singh Parmar ¹,
Monika Sharma ²,

¹Assistant Professor, Department of Information Technology, India

²Assistant Professor, Department of Information Technology, India

Abstract - Data security is, protecting data from ill- conceived get to, utilize, intrusion, change, examination, recording or destruction. Cloud computing is a network-based service that provide sharing of resources such as virtual machine, storage, network, software and applications etc. It helps to reduce capital costs since that cloud users only need to rent resources according to their requirements and pay the services they use. It is very flexible since users can access its service in any place through internet. However, a variety of security concerns such as integrity, availability and privacy act as barriers for cloud users to adopt the cloud service. The key issue in effective execution of Cloud Computing is to adequately deal with the security in the cloud applications. To secure the Cloud means secure the treatments (calculations) and storage (databases hosted by the Cloud provider). In this research paper, the proposed work plan is to eliminate the concerns regarding data privacy using two cryptographic algorithms back to back to enhance the security in cloud and provide the digital signature as per different perspective of cloud customers.

Key Words: Cloud Computing, Elliptical Curve Cryptography, Cryptography 1.

INTRODUCTION

Cloud computing provides a new way of services by organizing various resources and providing them to users based on their demands. It also plays a crucial role in the next generation mobile networks and services (5G) and Cyber-Physical and Social Computing (CPSC). Cloud computing and capacity arrangements give clients and ventures different qualities to store and process their information in third-party data centers that might be arranged a long way from the user running in remove from over a city to over the world. Cloud computing counts on sharing of resources to attain endurance and economy of scale, similar to a utility (like the electricity grid) over an electricity network. Storing data in the cloud greatly decreases storage load of users and brings them access comfort, thus it has become one of the most important cloud services. Possibilities guarantee that, cloud computing enables organizations to keep away from forthright infrastructure costs (e.g. purchasing servers). Likewise, it engages associations to focus on their core businesses instead of investing energy and supports on computer infrastructure. Cloud computing enables undertakings to get their applications up and running speedier, with enhanced sensibility and less maintenance. Be that as it may, concerns are starting to create about how safe Cloud is? as more data on people and organizations are being put in the cloud. Disregards to all the hype surrounding the cloud, enterprise customers are still unwilling to place their business in the cloud. One of the real concerns which lessens the development of Cloud computing is security and impediment with data security and information protection keep on infecting the market. Cloud information storage augments the danger of data spillage and ill-conceived get to. The architecture of cloud poses certain dangers to the security of the existing technologies when deployed in a cloud environment. Cloud service users need to be alert in interpreting the risks of data intrusion in this new environment.[1] The security concerns with respect to cloud computing are end-user data security, network traffic, file systems and host machine security which can be addressed with

the help of cryptography to a considerable level. "Security and privacy are indeed interrelated because the security is provided without having privacy but the privacy is not maintained without security.

2. LITERATURE SURVEY

1. Wang, L., Tao, J., & Kunze, M. in their research paper "Scientific cloud computing: Early definition and experience" says that, Computing clouds equips users with services to access hardware, software, and data resource. Some clouds service models are:

i) HaaS: Hardware as a Service

Hardware as a Service was proposed possibly at 2006. As an outgrowth of rapid advances in hardware virtualization, IT automation and usage metering and pricing, users could buy IT hardware - or even an entire data center/computer center- as a pay-as-you-go subscription service. The HaaS could be flexible, scalable and manageable to meet your needs.

ii) SaaS: Software as a Service

Software or application is hosted as a service and provided to customers across the Internet, which excludes the requirement to install and run the application on the customer's local computer. SaaS therefore amends the customer's headache of software maintenance, and decreases the expense of software purchases by on demand pricing.

iii) DaaS: Data as a Service

Data in various formats, from various sources, could be accessed via services to users on the network. Clients could, for instance, control remote information simply like work on local disk or access data semantically on the Internet.

3. Cryptographic Algorithms :

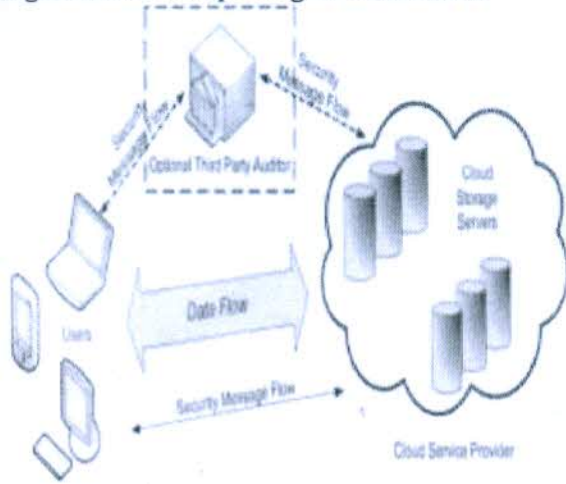
- 1) Data Encryption Standards (DES)
- 2) Advanced Encryption Standards (AES)
- 3) Triple - DES
- 4) RSA
- 5) Blowfish
- 6) ECC

These algorithms can be applied successfully in cloud environment.

Three entities involved in the cloud computing are users, cloud service providers and the third-party auditors. Securing the data in cloud service required cryptographic encryptions which isolates the users from accessing others information or workload. The data stored in the cloud server was encrypted and the user access the data from the cloud server will decrypt the data with the key provided for access. The encryption is the process of converting the plain information into a chipper text. The chipper text is an order less or meaningless information which is generated by the encryption algorithm in the certain pattern. Decryption is the process of converting the chipper text into the original plain text. The decryption algorithm reverses the process of encryption to generate the plain text. The main aim of the encryption algorithm is to generate a tough chipper text which should be ordered to decrypt without using the proper decrypt key. The size of the key proportionally toughens the decryption of chipper text without a proper key.

Selecting the encryption algorithm is very important. The quality of the encryption algorithm should be maintained strictly. The algorithm looks promising may be very easy to break. A tougher encryption algorithm to be selected to secure the data from attack.

Fig.1: Cloud computing Architecture



4. Data Security Issues

As many are moving to cloud storages, there are many potential attacks attempted few of them are:

a) **Denial of Service(DoS) attacks:**

b) **Side Channel attacks:**

By placing a malicious virtual machine to a target cloud server an attacker can launch a side channels attack.

c) **Authentication attacks:**

There are many different ways to authenticate users, and methods used are a frequent target of attackers.

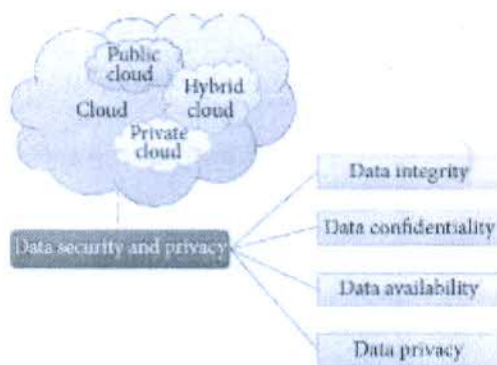
d) **Man-in-the-middle cryptographic attacks:**

e) **Inside-job:**

Here person, employee or staffs who have the knowledge of system can attack the cloud system.

Security aspects can be classified as data integrity, confidentiality, availability and privacy as show in figure below.

Fig 2: Various security concepts



5. Cloud Computing Entities

Figure 3 shows the cloud computing entities:

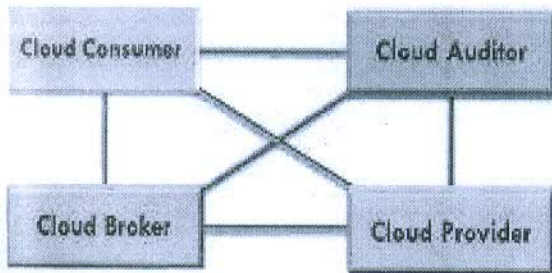


Fig3 : Cloud Computing Entities

- i) **Cloud Consumer:** One who uses a cloud provider's resources, from a company to an individual.
- ii) **Cloud Auditor:** The goal of Cloud Audit is to provide cloud service providers with a way to make their performance and security data readily available for potential customers.
- iii) **Cloud Broker:** the Service brokers concentrate on the negotiation of the relationships between consumers and providers. There are two major roles for brokers: SLA Negotiation and VM Monitor. The SLA Manager takes care that no Service Level Agreement (SLA) is violated and VM Monitor the current stated of virtual machines periodically at specific amount of time[2].
- iv) **Cloud Provider:** The Company who makes the cloud available to others. They are in charge of maintenance/ upkeep of the cloud and, of course, making sure it is always available to the cloud user.

6 Proposed system

- 1) For Encryption of text files:
Upload Text file.
Implementing the DES algorithm of Encryption to generate Cipher text 1.
Implementing the ECC algorithm of Encryption to generate Digital Signature as cipher text2
Store cipher text1 and Cipher Text2 into Database.
- 2) For Decryption of text files:
Read Cipher Text2 from Database.
Implementing the ECC algorithm of Decryption to decode digital signature cipher text2
Implementing the DES algorithm on cipher1 of Decryption to generate Plain text.
Display Plain Text to User

7. Algorithm of DES and ECC

7.1 Digital Encryption Std :

The Data Encryption Standard (DES) [2] is a symmetric- key block cipher published as FIPS-46 in the Federal Register in January 1977 by the National Institute of Standards and Technology (NIST). At the encryption site, DES takes a 64- bit plaintext and creates a 64-bit cipher text, at the decryption site, it takes a 64- bit cipher text and creates a 64-bit plaintext, and same 56 bit cipher key is used for both encryption and decryption. The encryption process is made of two permutations (P-boxes), which we call initial and final permutation, and sixteen Feistel rounds [10]. Each round uses a different 48-bit round key generated from the cipher key according to a predefined algorithm as shown in figure

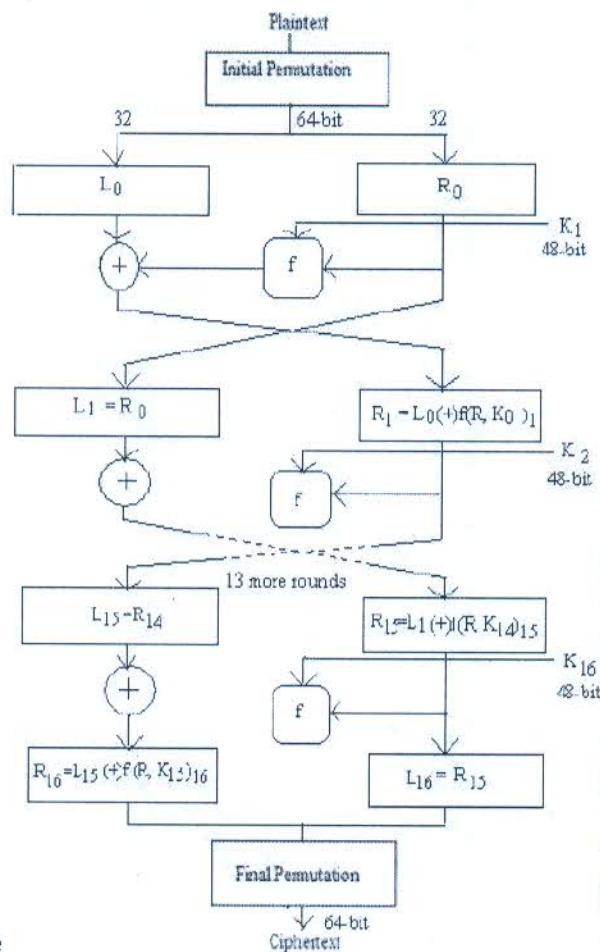


Fig 4: DES cycle

7.2 Elliptical Curve Theory

1. Algorithms for data security using ECC

Assume we have two organizations A and B. A and B act as public clouds with data, software and applications. A want to send data to B's cloud securely and data should be authenticated. Here we can use digital signature and encryption to data with ECC in order to send secure data from A to B. Suppose B wants a document from A's cloud, B's user will initialize a request to A's user, A's user select the corresponding document from A's cloud data storage and then apply hash function, it will give message digest. Sign the message digest with his private key by A's software. It is called digital signature. Encrypt digitally signed signature with B's public key using ECC algorithm. Encrypted cipher message will be send to B. B's software decrypt the cipher message to this document with his private key and verify the signature with A's public key.

We assume both A and B agree to some public-known data item:

The elliptic curve equation: $y^2 = x^3 + ax + b$, where $4a^3 + 27b^2 \neq 0$ The elliptic

group computed from elliptic curve equation A, B taken from the elliptic group

Then we have some algorithms for data security using ECC

Key generation

I.

II.

A selects random integer d_A , which is A's private key A generates a public key $P_A = d_A * B$

III. B selects a private key d_B and generates a public key $P_B = d_B * B$

IV. A generates the security key $Key = d_A * P_B$

V. B generates the security key $Key = d_B * P_A$ Signature

Generation

I. For signing a message m by sender of cloud A, using A's private key d_A

II. Calculate $e = \text{HASH}(m)$, where HASH is a cryptographic hash function, such as SHA-1

III. Select a random integer k from $[1, n-1]$

IV. Calculate $r = x_1 \pmod n$, where $(x_1, y_1) = k * B$. If $r = 0$, go to step III

V. Calculate $s = k^{-1}(e + d_A * r) \pmod n$. If $s = 0$, go to step III

VI. The signature is the pair (r, s)

VII. Finally, send signature (r, s) to B

Encryption algorithm Assume A send an encrypted message to B

I. A takes plaintext message m , and encodes it onto a point, p_m , from the elliptic group

II.

III.

IV

A chooses another random integer, k from interval $[1, p-1]$

The cipher text is a pair of points $pc = [(kB), (pm + k * PB)]$

Send cipher text pc to B

Decryption algorithm

B will decrypt cipher text pc

I. B computes the product of the first point from pc and its private key dB , which is $kB * dB$

III. B takes this product and subtracts it from the second point from pc , $(pm + k * PB) - kB * dB$, since $PB = dB * B$, so the difference is pm

III. Finally, B decodes pm to get the message m Signature Verification

If B wants to authenticate A's signature, B must have A's public key PA

Verify that r and s are integers in $[1, n-1]$

Calculate $e = \text{HASH}(m)$, where HASH is the same function used in the signature generation

III. Calculate $w = (s - 1) \% n$

IV. Calculate $u1 = e * w \% n$ and $u2 = r * w \% n$

V. Calculate $(x1, y1) = u1 * B + u2 * PA$

VI. The signature is valid if $x1 = r \% n$, otherwise invalid

9. Advantages of ECC Algorithm

Many cryptographic algorithms are introduced to perform asymmetric key generation for encryption and decryption process. In that RSS algorithm is a widely used method for cryptographic function. But the RSS algorithm needs more powerful processors and the memory unit. To overcome these limitations ECC based algorithm is developed to provide the tighter encryption technique which challenges the hackers technologies. In 2010 the researchers in cryptosystem concluded that the keys with longer size would provide maximum security over the attack, but the theory is no longer succeed. Lengthening of key size results to the undesirable effects on encryption. In the case of RSA algorithm doubling the size of the key decreased the performance of the algorithm. The advantage of the ECC algorithm based on the key size is analysed to better than the RSS algorithm. Table 1 shows the performance of the RSS and the ECC algorithm based on the key size.

Key Size of ECC	The key size of RSS	The ratio of the key size
160	1024	1:6
224	2048	1:9
256	3072	1:12
384	7680	1:20
512	15360	1:30

Table 1 : Comparison od ECC and RSA

Table 1 clearly shows that the performance of the ECC algorithm is higher than the RSS algorithm even in smaller key size. Increasing the key size of ECC increases the performance of it, but the RSS needs to increase more than double the value of it to match the performance of the ECC algorithm. Moreover, the speed of generating the key is 1000 time faster than the RSA algorithm.

10. Application of ECC algorithm in Cloud

ECC algorithm undergoes the four-step procedure to provide security in cloud architecture. The four steps include Connection generation, account creation, authentication and data exchange. Two initial steps were undergone for the first time connection. Connection generation and account creation were performed by the user to generate a cloud application interface. HTTPS and SSL protocols are used to generate communication with the cloud systems. The third process is authentication. The authentication is performed by applying the connection ID which is generated during the account creation process. And the ECC algorithm plays at the data exchange process. The Data was encrypted and shared with the cloud storage, and the user who downloads the data from the cloud should decrypt the downloaded data with the appropriate private key. The sender encrypts the data with the public key, and the user decrypts it using the private key. The data in the middle (in cloud storage) is in the form of chipper data. This provides the security in handling cloud storage or virtualisation.

11. Conclusion:

Cloud Computing can become more secure using cryptographic algorithms. Cryptography is the art or science of keeping messages secure by converting the data into non readable forms.

But the existing cryptographic algorithms are single level encryption algorithms. Cyber criminals can easily cracked single level encryption. Hence we propose a system which uses multilevel encryption and decryption to provide more security for Cloud Storage.

As our proposed algorithm is a Multilevel Encryption and Decryption algorithm. Thus, in our proposed work, only the authorized user can access the data by confirming the Digital Signature . Even if some intruder (unauthorized user) gets the data accidentally or intentionally, he must have to decrypt the data at each level which is a very difficult task without a valid key. It is expected that using multilevel encryption will provide more security for Cloud Storage than using single level encryption.

12. REFERENCES

- [1]S. Subashini, V. Kavitha -Anna University Tirunelveli, India," A survey on security issues in service delivery models of cloud computing"ELSEVIER- Journal of Network and Computer Applications Volume 34, Issue 1, January 2011,
- Jashanpreet Pal Kaur, Rajbhupinder kaur, Yadavindra College of Engineering, Talwandi Sabo, Bathinda Punjab, "Security Issues and Use of Cryptography in Cloud Computing" International Journal of Advanced Research in Computer Science and Software Engineering, Volume 4, Issue 7, July 2014, ISSN: 2277 128X.
- Wang, L., Tao, J., & Kunze, M. (2008). "Scientific cloud computing: Early definition and experience". Proceedings of the 10th IEEE International Conference on High Performance Computing and Communications, Austin, TX, 825-830.
- Reservoir Project [URL]. <http://www-03.ibm.com/press/us/en/pressrelease/23448.wss/>, access on June 2008.
- Amazon Elastic Compute Cloud [URL]. <http://aws.amazon.com/ec2>, access on Nov. 2007.
- IBM Blue Cloud project [URL]. <http://www-3.ibm.com/press/us/en/pressrelease/22613.wss/>, access on June 2008.
- Nimbus Project [URL].<http://workspace.globus.org/clouds/nimbus.html/>,access on June 2008.
- Status Project [URL]. <http://www.acis.ufl.edu/vws/>, access on June 2008.
- OpenNEbula Project [URL].<http://www.opennebula.org/>, access on Apr.2008.
- G. Devi , M. Pramod Kumar, "Cloud Computing: A CRM Service Based on a Separate Encryption and Decryption using Blowfish algorithm" International Journal Of Computer Trends And Technology Volume 3 Issue 4, ISSN: 2231-2803, pp. 592-596,2012.
- Rashmi Nigoti, Manoj Jhuria and Dr.Shailendra Singh, "A Survey of Cryptographic Algorithms for Cloud Computing" International Journal of Emerging Technologies in Computational and Applied Sciences,Vol. 4, pp.141-146, March-May 2013.
- Wayne Jansen ,Timothy Grance, "Guidelines on Security and Privacy in Public Cloud Computing", NIST Special Publication,NIST SP - 800- 144 ,80 pp., 2011.
- G. Lin, D. Fu, J. Zhu, and G. Dasmalchi, "Cloud Computing: IT asa Service," IT Professional, vol. 11, pp. 10-13, Mar./Apr.2009.

15. Rachna Arora, Anshu Parashar, "Secure User Data in Cloud Computing Using Encryption Algorithms", International Journal of Engineering Research and Applications (IJERA), Vol. 3, pp.1922-1926, Jul-Aug 2013.
16. Zhidong Shen, Li Li , Fei Yan, Xiaoping Wu , "Cloud Computing System Based on Trusted Computing Platform", International Conference on Intelligent Computation Technology and Automation, Volume 1, pp.942-945, 2010.
17. Pearson, S., Benameur, A., Privacy, "Security and Trust Issues Arises from Cloud Computing", Cloud Computing Technology and Science (CloudCom), IEEE Second International Conference, pp.693-702, 2010.
18. Lizhe Wang, Gregor von Laszewski, Marcel Kunze, Jie Tao, Cheng Fu, Xi He, Andrew Younge, "Cloud Computing: A Perspective Study", New Generation Computing- Advances of Distributed Information Processing, Volume 28, pp.137-146, 2010.
19. Puneet Jai Kaur, Sakshi Kaushal, "Security Concerns in Cloud Computing", Communication in Computer and Information Science Volume 169, pp.103-112, 2011.
20. Priyanka Arora, Arun Singh, Himanshu Tyagi, "Evaluation and Comparison of Security Issues on Cloud Computing Environment", World of Computer Science and Information Technology Journal, pp.179-183, 2012.

|





Artificial Intelligence Design Suggestions for Apparel Retail Counters

Dr. Nidhi Sharma¹ | Dr. Alok Sharma²

¹Department of Computer Engineering, TIT&S, Bhiwani, Haryana, India

²Om Sterling Global University, Hisar, Haryana, India

To Cite this Article

Dr. Nidhi Sharma and Dr. Alok Sharma, "Artificial Intelligence Design Suggestions for Apparel Retail Counters", *International Journal for Modern Trends in Science and Technology*, 6(9S): 242-244, 2020.

Article Info

Received on 25-August-2020, Revised on 08-September-2020, Accepted on 12-September-2020, Published on 18-September-2020.

ABSTRACT

Artificial Intelligence is the requirement felt widely in retail industry support system, especially in Apparel Retail counters. On different occasions, functions, parties and celebrations, the shopping is done using these Apparel retail counters. Artificial Intelligence is an area of computer science which simulates the human intelligence and human sensory abilities. So, Artificial Intelligence is becoming an imperative tool for the retail counters to enhance the quality, improve customer's experience, automation, and to lower the operating costs. This paper will discuss how Artificial Intelligence is influencing the retail counters by automation of cash management, improving customer's experience and providing other supports for adjustment of prices and prediction of prices considering seasonal as well as occasional effects.

KEYWORDS: Artificial Intelligence, Supervised learning, Unsupervised learning, Retail Counters, AI Chatboot.

INTRODUCTION

With the emergence of 24/7 Internet, the customers can save their time and can shop online at their own convenience. AI machines which facilitate retail counters are working with the following major components (support system) in them. First, sensing devices and second, calculation support system along with output devices like vocal communication, printouts and displays in different forms. As per sensing devices are concerned, most of them are camera, barcode readers, sound recorder, electronic sensors etc. Thus for logical programming feature, calibration, decision support system mainly supervised and unsupervised learning concepts are used.

Supervised learning:

In case of supervised learning previous (old) data is available in database to guide the decision taken by AI machine. In case of supervised learning complete guidance and help is available to calibrate the system such that all future decisions are correct.

Unsupervised learning:

In case of Unsupervised learning previous (old) data is not available in database to guide the decision taken by AI machine. In case of unsupervised learning no guidance and help is available to calibrate the system and chances of right decision are probable only not guaranteed.

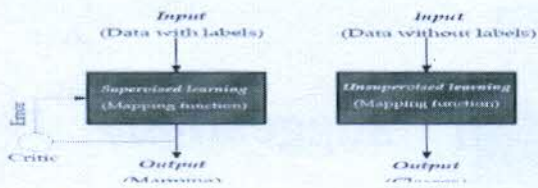


Fig1: Types of Learning Techniques in Retail Counters

AI DESIGN SUGGESTIONS FOR RETAIL COUNTERS

Artificial Intelligence is influencing the retail counters by automation of cash management, improving customer's experience and providing other supports for adjustment of prices and prediction of prices considering seasonal as well as occasional effects. Some of the applications of Artificial Intelligence in retail counter are:

- 1) Cash management without human help,
- 2) Customer guide to assist in shopping and to provide assistance in store,
- 3) Adjustment of Prices and Prediction of Prices.

1) CASH MANAGEMENT WITHOUT HUMAN HELP

Now a days, the warehouses in developed countries are taking help of robots for cash management. For this work, Robots considers two main conditions:

- 1) If customer pick any item
- 2) If customer put back any item

The item picked by customer is consider as purchased item and item kept back is considered as unpurchased. So this way, Number of item purchased cost towards customer bill and on exit from warehouse customer has to pay only for purchased items. By doing so, with the help of simple robots with sensors and billing facility like a robotised POS (Point of sale) facility this feature of cash management is handled. For this facility the concept of limited supervised learning technique is used as an example of all situations of POS(Point of sale) are available from many years in the database of warehouses to make the robotised management of cash counters. This process of cash management without human needs more electronic sensors and printing devices rather than complicated Artificial Intelligence programming. That's why, the limited supervised learning is mention in the above lines.

2) CUSTOMER GUIDE TO ASSIST IN SHOPPING AND TO PROVIDE ASSISTANCE IN STORE

This feature is to help the customer in shopping and to improve customer shopping experience. Customers used to chat with a counter clerk known as Chatboot who knew the products and assembled orders. It matches with artificial passenger application of AI in Vehicle in which to accompany the driver, to monitor drivers activity and to improve his comfort, to entertain him, to make him aware of risky situation(warnings), to refresh his mood if driver feels bore many sensors are fitted inside the vehicle. Similarly, in retail counter AI Chatboot should help customer in improving his shopping skills by making customer aware of various schemes available, discounts, observing his shopping interest, making customer aware of all possible options of purchase of item of customer's interest responding customer's query, providing best answers to Customer's Query, helping customer in locating items, upcoming schemes and sales, other facilities available like sanitization, rules and regulations in CORONA like situations do's and Donot's. For providing this type of facility in warehouses using AI the requirement of system are:

- a) Updating of various schemes, tokens, discounts and other data required to handle query of customer in AI Chatboot machine database
- b) A database with all possible values of features of all available items for best purchase options of every item in the warehouse.
- c) A track record of likes and dislikes pattern of previous customer behaviour
- d) Sensors to judge the behaviour of customer and react accordingly with AI logical support to answer in best way.

For providing this type of facility to warehouses requires supervised learning of AI system from the data available in database of warehouse about shopping patterns and queries came across in the past.

Next requirement is the calibration of system to judge the personality of customer with the help of various type of sensors and logical support available in the AI Chatboot.

Normally, supervised learning with available database mentioned above is sufficient to handle the query of customers but for more advance systems personality judgement may be included to enhance the Quality of work which requires calibration of system in starting to judge human behaviours for better results.

3) ADJUSTMENT OF PRICES AND PREDICTION OF PRICES

The price adjustment systems are used to fix prices of items by monitoring the outcomes of different price strategies. To adjust the prices, calculations are made by analysing costs, quality and other parameters of available products in market, various promotions activities, sale data and its trends along with other available data. During price adjustment all type of customers are considered, target of sale are to be met by presenting the best offers and getting new customers to boost sales.

For price forecasting (prediction) the market demand of the product, seasonal effects, characteristics and date of release of new products etc are considered.

This feature for support of retail counter requires maximum efforts in comparison of other supports where data is quantitatively verifiable from the available database to give best results. This feature to handle adjustment of prices and prediction of prices requires critical reasoning support, inclusion of all affecting parameters, and calibration of system to give good results.

CONCLUSION

In this paper the use of AI with design suggestions in Apparel retail counters is discussed. It has been observed from above discussion that AI machines take decisions mostly in two ways:

- 1) The decision is quantitatively verifiable from the available database of Retail counters. In such cases, the possibility of taking wrong decisions by AI machines is nil. So, such types of machines for handling such scenarios are suggested for medium and large retail counters. As are the first two cases of application in the paper i.e cash management without human and Chatbot to improve customer experience. Similar types of automation machines with nearly similar features are visible now a days for tickets generation on metro platforms.
- 2) In some cases AI machines are used for critical analysis and predictions where decision of AI machine is not verifiable from available database. So there are chances of mistake in decision making as machine has to be calibrated based on many factors which requires the supervision of core technical team to take right decisions and inclusion of upcoming factors which come with

time in picture. Such AI machines are suggested to be used in large scale industry counters where a team of intellectuals to monitor is affordable.

REFERENCES

- [1] <http://www.aindralabs.com>
- [2] <http://www.insider-trends.com>
- [3] <http://www.v-count.com>
- [4] <http://www.altexsoft.com>

VG1 Cipher – A DNA Indexing Cipher

Akhil Kaushik, Vikas Thada

Abstract: When it comes to providing security to information systems, encryption emerges as an indispensable tool, as it has been used intensively in past few decades for securing stationary data as well as data in motion. Earlier, the security of an encryption algorithm lied in the manipulation of characters among a word or group of words, which is called the classical age of cryptography. This age ended when indigenous mathematical equations came into play and modern ciphers like DES and RSA were designed to mark the modern cryptographic era. This period witnessed two world wars and rise of machines instead of manual calculation for data secrecy. But, the time kept moving on and new advances in the information security field surfaced like Elliptical Curve Cryptography and Quantum Cryptography which added new dimensions to the secret world of confidential communication over unsecure channels. The latest addition in this count is the DNA cryptography which has combined the laws of biology with computing to form unbreakable ciphers at least theoretically. This paper introduces a new DNA cipher which is bound to provide more robust ways to safeguard vital data.

Keywords: DNA Cryptography, cipher, information security, encryption, decryption.

I. INTRODUCTION

Even before the advent of technology, the human race has been profoundly in love with information. This information whether religious, personal or social has always been of great interest to rivals, gossip lovers or revolutionists. Hence, since beginning of civilization there was requirement of safeguarding this confidential information and myriad ways were adopted for it like Scytale, Heliography, Caesar cipher, Pigeon cipher, etc.[12] This growth increased quadruple folds with the time, especially during the world wars. Information security refers to the technique of protecting information from unauthorized access, use, disclosure, disruption and modification. Governments, military, corporations, financial institutions, hospitals, and private businesses amass a great deal of confidential information about their employees, customers, products, research, and financial status. Most of this information is now collected, processed and stored on electronic media and transmitted across networks to other computers. Encryption clearly addresses the need for confidentiality of information, in process of storage and transmission. Popular application of multimedia technology and increasingly transmission ability of network gradually leads us to acquire information directly and clearly through multimedia and hence the security of multimedia data has become inevitable. The following sections talk about the growth of cryptography with the human evolution.

II. CLASSIC CRYPTOGRAPHY

This is considered as the golden era of cryptology where the tools and tricks for encryption were in the infancy stage.

Revised Manuscript Received on January 05, 2020

* Correspondence Author

Akhil Kaushik*, PhD Scholar, CSE Department, Amity University, Gurugram, Haryana, India.

Dr. Vikas Thada, CSE Department, Amity University, Gurugram, Haryana, India.

It all started when a genius king designed Caesar cipher which was basically a substitution cipher i.e. replacing each character by its third character[13]. This was designed to be used for military operations and it instigated a large number of ciphers based on the idea of transposition and substitution. Transposition means changing the order of characters in a word while substitution means replacing a character with another one. Further development included polyalphabetic substitution instead of just mono-alphabetic i.e. if a character is repeated a number of times, it is replaced by different characters to make it more robust[14]. Additionally, new and fresh ideas were given for encoding like the Playfair cipher, where a matrix of English characters is formed in a 5 by 5 square (combining I and J together). Here, a particular word is used as a key which is written first and then the remaining letters were put in that matrix to form a dissimilar cipher text each time[15]. To put it in simple words, this was a substitution cipher which worked in a pair of words. This brilliant idea paved the way for other revolutionized ciphers like the Rail-fence cipher, Hill Cipher and Vigenere Cipher.

samplemessage
+ keykeykeykeyk
= cekzpcwiqceo

Fig 1: Example of Vigenere Cipher[11]

The Vigenere cipher was considered unbreakable at that time, but it also failed due to short length of the key and its repetition in accordance of the plaintext. This predicament gave birth to the idea of One-Time Pads (OTPs) which used random letters each time as the encryption key. The point here was to use a key one time only and destroy it after encryption. This sounds perfect in theory, but practically, it is hard to generate truly random characters or even numbers by humans and computers[13].

samplemessage
+ hqnyjiefsehpb
= zqznumqjkw hvf

Fig 2: Example of One-Time Pad (OTP)[5]

The remainder of the paper is organized as follows. Section III gives some insight on the conventional cryptography and Section IV talks about the popular cryptographic domains i.e. Elliptic Curve Cryptography and Quantum Cryptography. The primary ideas DNA encryption are discussed in Section V and the next paragraph i.e. Section

VG1 Cipher – A DNA Indexing Cipher

VI compares the contemporary cryptology with DNA cryptology. Section VII proposes the novel encryption algorithm and Section VIII simplifies the idea with an example. The performance analysis of the proposed cipher is done in Section IX, while conclusion and future work are proposed in Section X.

III. CONVENTIONAL CRYPTOGRAPHY

As discussed in the above section, classic cryptology was based on the characters in a human language and their manipulation. Due to the limited numbers of characters in any human language, this approach become brittle with the timeline and a new set of techniques was needed. The old era of classic cryptology was gone and new age of conventional cryptology started.

<p>Key: FAUZANCE</p> <p>01000110010000010101010101011010</p> <p>00100000101001110010000110100010</p> <p>Plaintext: DISASTER</p> <p>010001000100100101010011010000010</p> <p>1010011010101000100011010101010010</p> <p>Ciphertext: DISASTER</p> <p>01010111101001010000010011011110</p> <p>110001010111011001110000101011</p> <p>Ciphertext: DISCSTER</p> <p>11111011010101000100100100101111</p> <p>11101110100001101001110101110111</p>
--

Fig 3: Avalanche effect on DES[1]

This era marked the classic ciphers which used complex mathematical equations and mechanical devices like Enigma, BOMBE, etc. to produce highly efficient and perplex cipher texts, which were immune to the crypto attacks used earlier. The modern encryption ciphers use publicly known yet bamboozling mathematical algorithms and their secrecy is maintained through the secret key, which must be securely shared among the communicating parties[16]. Some of the popular ciphers of this age are DES, 3DES, etc. which mostly come under the symmetric category of ciphers i.e. they used one key only for encoding and decoding of data. Furthermore, the conventional ciphers are good exhibitors of the avalanche effect i.e. a small change in either the secret key or the plaintext causes a considerable change in the ciphertext. For example: changing the fourth character of the word "DISASTER" from 'A' to 'C' causes change in 35 bits which is quite significant, as shown in the figure above[1]. Later on in 1976, mathematical innovation by Whitfield Diffie and Martin Hellman gave birth to the idea of public key cryptography which revolutionized the security sector. The asymmetric algorithms based on the modular arithmetic uses has two different keys (per user): one for encryption and other for decryption. This approach has two benefits: first

the eavesdropper cannot decode the messages even if he/ she knows the mechanism and second the user just needs two keys for communication rather than having a lot of secret keys (one shared secret key between each pair of users).

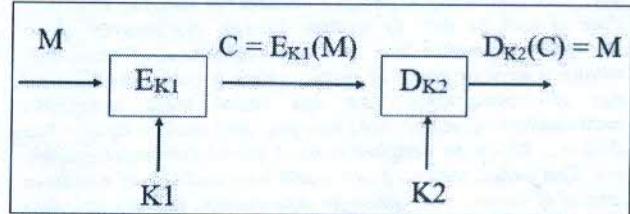


Fig 4: Block scheme of Public Key Cryptography[4]

Nevertheless the public key cryptography concept channeled the growth of other ideas like sharing secret key (Diffie-Hellman algorithms and its myriad versions), digital signatures to provide non-repudiation, digital watermarking for protecting intellectual property rights and one-way hash functions for providing authentication, which added further dimensions to the world of information security[1]. Additionally, the conventional cryptology can also be bifurcated on the basis of amount of data encoded each time the algorithms runs. If the encoding of data is done character by character, it is known as stream cipher and if the data is encrypted in chunks, it is called as block cipher. Obviously, the block ciphers have the upper hand over stream ciphers when it comes to speed and efficiency. Some popular block ciphers are DES, 3DES, IDEA, etc. and some well-known stream ciphers are A5, RC4, SEAL, Hughes XPD/ KPD, etc.

IV. ECC AND QUANTUM CRYPTOGRAPHY

As stated above, the public-key cryptography paved the way for future developments in the safe communication and one of the elite thought is Elliptical Curve Cryptography (shortened as ECC). ECC depends on the notion of using elliptical curves to generate the pair of private key and public key instead of using product of two extreme large prime numbers for the same. Elliptical curves are basically the binary curves which are equally proportioned over the x-axis and their maximum value is kept limited by finite field theory. The two primary concepts used for producing keys in ECC are Point Addition and Point Doubling. Another chief predicaments to remember is that elliptical curves prove to be slower and inaccurate when it comes to real number's calculation[2].

ECC is highly beneficial over the traditional ciphers as it produces keys of smaller length yet robust and this key feature makes it more useful for mobile applications where low battery consumption and lesser computing power is desired. Another pluses of using ECC over well-known Public key algorithms like RSA are faster key generation, quicker hardware implementation and rapid encryption and decryption processes' computation[3].

Another crypto variant used now-a-days is the Quantum Cryptography, which is using laws of nature to encode the messages at the physical layer and hence the need of security at upper layers is eliminated. Instead of using bits as the atomic information unit, the quantum computers use "qubits" which is photon (by default). The '0' and '1' state of a photon depends upon its polarity either vertical or

horizontal and its primary usage is key distribution rather than data encryption.

The most vital feature of quantum key distribution is its strength against the man-in-the-middle attack i.e. if the message is intercepted and then retransmitted by someone, then the qubits settle on a solo state and hence the recipient know not to trust the message as according to the Heisenberg's uncertainty principle the eavesdropper activity must cause an irrevocable modification in the quantum states[4]. Although this technique is a bit expensive at the moment, but it works excellent to encode the fiber optics network. Further, this technique is yet to prove its worth over larger distances and diminishing the higher error rates. Some highlighted applications of the quantum cryptology are encoded video calls, online voting in Switzerland and smart cards.

V. DNA CRYPTOGRAPHY

As the name suggests, DNA cryptography is the combination of DNA and encryption. This is a newly emerged specific set security system based on the idea of biology. It all started when Leonard Adleman used a biological approach to unravel the illustrious traveling salesman (or Hamilton) problem in 1994 and paved the way to handle complex mathematical problems[17]. This renowned research took the world like a twister and several other academicians contributed their part to prove that DNA computing can prove advantageous and myriad operations can be applied like DNA slicing, DNA polymerization, PCR amplification, etc. to give answers to the unknown problematical questions.

DNA encryption was first proposed by Ashish Gehani et al in 2004, when their research article in Springer enlightened the use of DNA principles in symmetric encryption, DNA chip and One-Time Pad generation[5]. Then the exploration in the arena of DNA cryptology expanded like a bubble like the YAEA algorithm implementation by Sherif T. Amin in 2006[6], Asymmetric Key algorithm, DNA digital coding, PCR amplification concepts by Guangzhao Cui in 2008[7], DNA chip based encryption by LaixueJia in 2010[8], etc to mention the few among illustrious research work done so far. All of the above research paper suggest one common thing i.e. the parallel processing provided by DNA computing offers exponentially fast solutions to the enigmatic and big mathematical problems.

VI. MODERN CRYPTOGRAPHY VS DNA CRYPTOGRAPHY

DNA cryptography is still in its infancy stage when we compare to modern cryptography and it will take some time and deep research to grow fully as a standalone application. Some basic difference between modern cryptology and DNA encryption can be understood by the following table:

TABLE I. MODERN CRYPTOGRAPHY VS DNA CRYPTOGRAPHY[9]

	Operations	Time Complexity	Storage Medium	Storage Capacity	Security
Modern Cryptography	Binary numbers	In seconds	Silicon chips	In GBs	Complex Maths

DNA Cryptography	DNA strands	In Hours	DNA chips	In TBs	Biology & Maths
------------------	-------------	----------	-----------	--------	-----------------

As clearly elucidated from the table, a scholar can figure why DNA cryptography has not yet replaced the modern cryptography. Although DNA cryptology offers several advantages like huge storage capacity and parallel processing, but two important lacunas that need to be comprehend are the time complexity and its inability to work as a standalone alternative to modern encryption. DNA encoding rather serves as a support to the modern cryptography[10].

VII. THE PROPOSED CIPHER

The proposed encryption algorithm is based on the idea of amalgamation of mathematical perplexity and DNA Indexing. Usually, the indexing mechanisms are being used for data searching and processing, however here the DNA indexing is used to make the cipher stouter and harder to guess for the eavesdropper. For this, a chromosomal sequence is downloaded from any publicly available genomic databases like GenBank, NCBI, DDBJ, etc. This chromosomal sequence is made up of copious DNA nucleotide bases (A,C,G or T) as shown in the figure below:

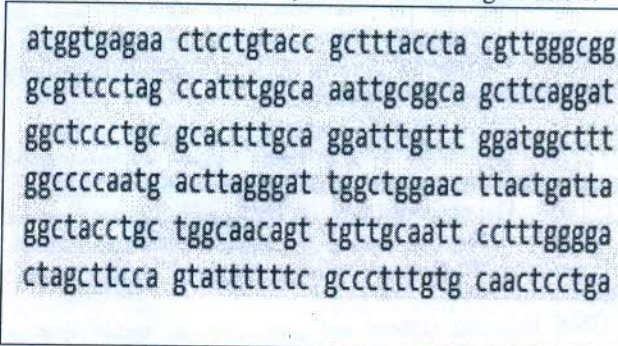


Fig 6: A fragment of DNA sequence downloaded from NCBI

According to DNA coding principle, one byte is transformed into a sequence of four DNA letters. Hence, a search is performed on every possible byte sequence and its various positions in the chromosomal sequence are stored in a table (as shown in Table II below):

TABLE II. KEY INDEXING OF GENETIC DATABASE

GGTA	58, 80, 249, 619, 645, 671, 896, 1197, 1605, 2766, 2958, 2972
AGAG	130, 161, 242, 453, 1011, 1442, 1458, 1512, 1997, 2295, 2789
AATA	27, 458, 611, 656, 924, 1059, 1332, 1518, 1521, 1539, 1584, 1647, 1695, 1698, 1734, 1767, 1770, 1885, 1933, 2166, 2225, 2365, 2401, 2625, 2700, 2754
AACT	271, 746, 1062, 1188, 1250, 1259, 1409, 1466, 1470, 1491, 1581, 1616, 1701, 1882, 1984, 2095, 2118, 2151, 2198, 2382, 2622, 2655, 2684
CTGC	10, 246, 366, 666, 1182, 1375, 1461, 1527, 1590, 1593, 1955, 2238, 2338, 2606, 2812, 2864



VG1 Cipher – A DNA Indexing Cipher

GGTG	521, 1754, 1877, 1992, 2422, 2531, 2618, 2675
------	---

Hence, for each byte of data, there are multiple position values which can be substituted one at a time and that too randomly. An important consideration here is to have a sufficiently long DNA sequence in order to obtain an extensive number of replacements for a byte. The encoding algorithm is primarily a stream cipher that works as follows:

- 1) The plaintext is read from input file.
- 2) The message is converted into ASCII code (or UTF-8).
- 3) Individual characters are arranged according to their number of occurrences and the total count of dissimilar characters is calculated.
- 4) Each character is then transformed to binary '1' according to its occurrence in message and the previously recognized characters are stored as binary '0'.
- 5) The output of step 4 is divided bitwise and transposed to add complexity.
- 6) DNA coding is then applied to the data.
- 7) The output from previous phase is then encoded using DNA homophonic substitution cipher.
- 8) The encoded data (in the form of integers) is then retransformed according to ASCII values (or UTF-8), which is the final ciphertext and is stored back in the file.

DNA Indexing ciphers are symmetric in nature that is encryption and decryption is done using same key and the process is reverse and identical. However, the receiver need to know identification number of the chromosomal sequence used as encoding key to complete the decryption process.

VIII. EXAMPLE OF THE PROPOSED ALGORITHM

As displayed in the figure 6 below, the decimal coding represent here ASCII or UTF-8 coding which transform the English characters to decimal values. Then the count of dissimilar characters and the frequency of each character is displayed. The next step illustrates the binary conversion of all characters. After binary conversion, the transposition of characters is done in the following way:

Input (000 01 100)

0	0	0
0	X	1
1	0	0

Output (001 00 010)

As displayed, the input data is stored in a 3*3 matrix (keeping the center cell empty to accommodate 8 bits in 9 cells). The data is stored row-wise, but read column-wise to add another step in complexity. After operations at digital level, DNA coding is implemented. It can be done in multiple ways; one simple way is to encode using following table:

TABLE III. DNA CODING

Binary Code	DNA Chromosome
00	a
01	c
11	t
10	g

The intermediate output received after DNA encoding is then subjected to homophonic substitution, which is done according to the chosen index positions of the 4-chromosomal DNA as shown in the table II. The key sequence indicate the length of position number of the substitution done in the previous step. Finally, the cipher text is achieved after reconversion according to the decimal coding.

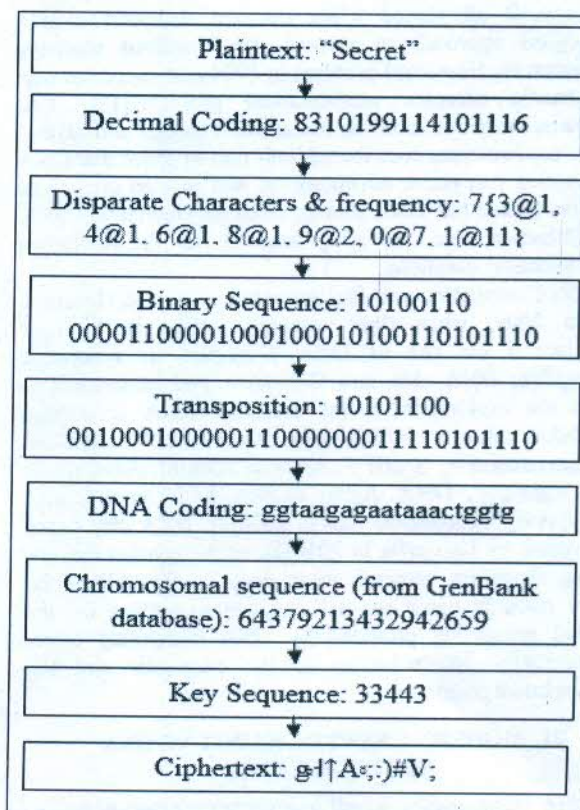


Fig. 6: Working of proposed cipher

IX. PERFORMANCE ANALYSIS

The performance of cryptosystems can be evaluated on two vital criterias: security and computational complexity. The proposed encryption algorithm is based on the theory of homophonic substitution provided by the DNA Indexing. The security provided in the proposed algorithm is three – fold. Firstly, the concept of modern cryptography (i.e. perplex mathematical function) is applied here which transmutes decimal numbers to the binary sequence depending upon its frequency. Secondly, the binary transformations are done to alter the binary sequences generated earlier. This binary operations add extra layer of refuge to the encryption system. Last but not the least, the DNA coding and chromosomal sequence from a genetic database to further mystify the encoded data. These three

layers of encryption should be robust enough for safeguarding small amount of data. The homophonic substitution in VG1 cipher offers more uniform distribution of the Ciphertext and will be not show analogy to the

plaintext distribution. Another security aspect of proposed cipher is its robustness against the Ciphertext-only attacks as well as known-plaintext attacks due to the fact that each plaintext value corresponds to not just one, but numerous Ciphertext values. The brute-force attack against VG1 cipher can be possible, but a number of factors need to be considered. Firstly, the genetic sequence must be identified, which is kind of herculean task given plenty of publicly available genetic databases and plethora of DNA sequences within each (at least a million). For example: Suppose NCBI has genetic sequence which has at least 45000 nucleotide bases and each sequence is composed of A,C,G & T, then possible number of keys become 4^{45000} , which can prove to be a colossal job for hacker. Moreover, the binary operations also need to be taken care of. A vital point for deliberation here is that instead of sharing a long DNA sequence (already available on the internet), only it's ID from the genetic database needs to be shared and for the same, we can use any public-key cryptosystem. The computational complexity of an algorithm depends upon two major things: time complexity and memory requirements. The time complexity of the algorithm depends primarily on two factors: encryption and decryption time taken by the algorithm. However, importing the chromosomal sequence from file and then DNA indexing is a much bigger task and consumes the maximum amount of time. This time is nearly 10 times the time to encrypt the whole file. The total time taken to import the DNA Indexing file and to encode the input file of different file sizes is given below:

TABLE IV. TIME COMPLEXITY FOR VG1 ENCRYPTION PROCESS

Plaintext Size (in KiloBytes)	Execution Time (seconds)
256	13.27
512	28.59
768	40.23
1000	64.65

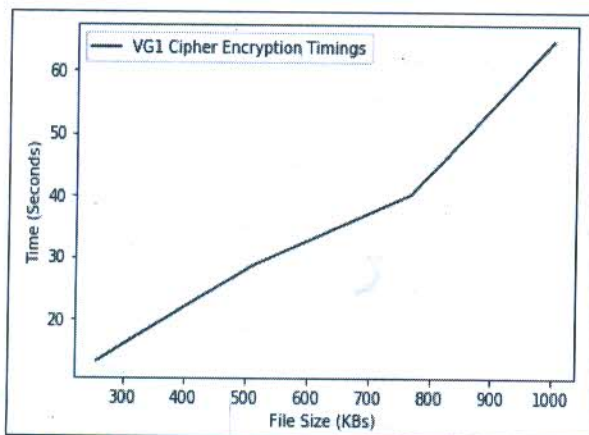


Fig. 7: Encoding Time Calculation of VG1 cipher

The total time taken to import the DNA Indexing file and to decode the received file of different file sizes is given below:

TABLE V. TIME COMPLEXITY FOR VG1 DECRYPTION PROCESS

Plaintext Size (in KiloBytes)	Execution Time (seconds)
256	15.74
512	30.11
768	41.68
1000	66.63

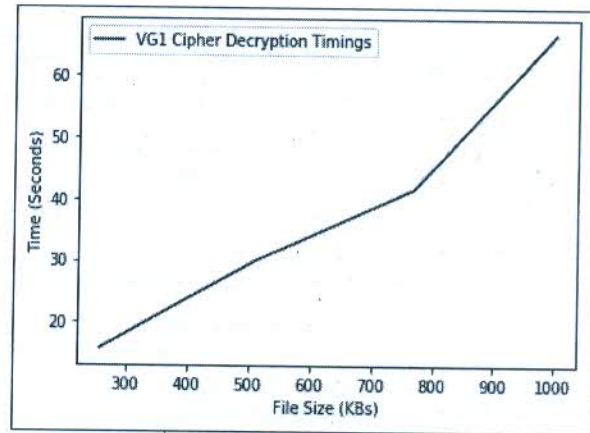


Fig. 8: Decoding Time Calculation of VG1 cipher

As evident from the above graphs, there is a positive correlation between file sizes and for encoding and decoding timings of VG1 cipher, which means the execution time upsurges with growing file sizes. Encryption and Decryption timings has been tested on a machine using Intel i5 2.2GHz processor, 4 GB RAM and Windows 10 Pro Operating System. The programming language used to implement VG1 cipher is Python version 3.7.3 64-bit using Spyder IDE.

X. SUMMARY & FUTURE SCOPE

In the world of cybercrimes and online scams, a new defense is needed to guard the vital information and once again a new form of cryptography emerges for the rescue. This new tool is called DNA Cryptology and it is derived from the roots of computing and biology. This paper give some insights on DNA encoding and designate how it can be used as a side-kick to the modern cryptography to safeguard the significant information. This paper also proposes a new encryption algorithm "VG1 Cipher" which provides a novel approach to DNA Indexing methodology which is not only fast but also produces highly secure ciphertext. The proposed algorithm is based on DNA Indexing and Modern Cryptography, which makes it more efficient and faster than its counterparts.

The next step chromosomal sequence signify the homophonic substitution taken from the genetic database downloaded from either GenBank or NCBI i.e. there are several positions. The key sequence indicate the length of position number of the substitution done in previous step. Finally, the cipher text achieved at the end is shown as the final step.

REFERENCES

1. M. Kumar et. al., "Comparing Classical Encryption with Modern Techniques", S-JPSET, Vol. 1, Iss. 1, Dec. 2010, pp. 49-54.
2. J. Zargar, M. Manzoor & T. Mukhtar, "Encryption/ Decryption using Elliptical Curve Cryptography", International Journal of Advanced Research in Computer Science, Vol. 8, Iss. 7, July 2017, pp. 48-51.
- a. Ibrahim, W. Cheruiyot & M. W. Kimwele, "Data Security in Cloud Computing with Elliptic Curve Cryptography", International Journal of Computer, Vol. 26, Iss. 1, 2017, pp. 1-14
3. R. J. Hughes et. al., "Quantum Cryptography", Contemp. Phys. 36, 1995, pp. 149-190.
4. Gehani, T. LaBean, and J. Reif, "DNA-Based Cryptography", Lecture Notes in Computer Science 2950, Springer, pp. 167-188, 2004
5. S.T. Amin, M. Saeb, S. El-Gindi, "A DNA-Based Implementation of YAEA Encryption Algorithm", Computational Intelligence, pp. 120-125, 2006.
6. G. Cui et. al., "An Encryption Scheme Based on DNA Microdots Technology", Journal of Computational and Theoretical Nanoscience, Vol. 12, Iss. 7, pp. 1434-1439, 2015.
7. L. XueJia et. al., "Asymmetric encryption and signature method with DNA technology", Science China Information Sciences, Vol. 53, No. 3, pp. 506-514, 2010.
8. S. Karthiga & E. Murugavalli, "DNA Cryptography", International Research Journal of Engineering and Technology, Vol. 5, Iss. 3, Mar 2018, pp. 3987-3991.
9. S. Kalso, H. Kaur & V. Chang, "DNA Cryptography and Deep Learning using Genetic Algorithm with NW algorithm for Key Generation", Springer Journal of Medical System, Vol. 42, Iss. 17, Oct. 17.
10. E. P. Dummit, "A Tour of Classical and Modern Cryptography", University of Rochester, 2015, an online article available at https://math.la.asu.edu/~dummit/docs/talk_sums_cryptography_talk.pdf.
11. A. Kahate, "Cryptography and Network Security", Tata McGraw Hill, New Delhi, India, 2012.
12. P.P Charles & P.L Shari, "Security in Computing: 4th edition", Prentice-Hall, Inc., 2008.
13. W. Stallings, "Cryptography and Network Security Principles and Practice," Fourth edition, Prentice hall, 2007.
14. J. Katz and Y. Lindell, Introduction to Modern Cryptography: Principles and Protocols, 1st ed. USA: Chapman & Hall/ CRC, 2007.
15. A.S. Tanenbaum, "Computer Networks", Fourth Edition, Prentice hall, 2004.
16. J. Hoffstein, J. Pipher & J.H. Silverman, An Introduction to Mathematical Cryptography, 1st ed. USA: Springer, 2010.

AUTHORS PROFILE



Akhil Kaushik has received the Master degree in Information Technology from Central Queensland University, Melbourne, Australia. Currently he is pursuing his doctorate degree in CSE Department of Amity University, Gurugram, Haryana, India. He has more than 10 years of teaching experience and nearly 6 years of research experience with contribution at International level in various proceedings like IEEE, IJCEE, ICFN, ICNIT, etc. His research interest includes network security, cryptography and machine learning.



Dr. Vikas Thada has received the doctorate degree from Dr. KNM University, Jaipur, India. Currently he is employed as Associate Professor in CSE Department, Amity School of Engineering & Technology, Amity University, Gurugram, Haryana, India. He has more than 16 years of teaching experience and over 7 years of research experience. He has numerous publications in international journals and is author of number of books on programming, data structures, algorithms etc. His chief research interests are genetic algorithm, cryptography and network security, design and analysis of algorithm and web technologies.

Coating of multi-walled carbon nanotubes on cotton fabric via conventional dyeing for enhanced electrical and mechanical properties

Cite as: AIP Conference Proceedings 2142, 140019 (2019); <https://doi.org/10.1063/1.5122532>
Published Online: 29 August 2019

Anil Kumar, Jasvir Dalal, Sajjan Dahiya, Amal Chowdhury, A. Khandual, Anil Ohlan, Rajesh Punia, and A. S. Maan



View Online



Export Citation

ARTICLES YOU MAY BE INTERESTED IN

Profit analysis of a uni-directional and non revertible 1+1 protection switching scheme in optical communication process

AIP Conference Proceedings 2142, 170011 (2019); <https://doi.org/10.1063/1.5122608>

Influence of defects on the diffusion of helium in uranium dioxide: Molecular dynamics study

AIP Conference Proceedings 2142, 020002 (2019); <https://doi.org/10.1063/1.5122325>

Excellent photoelectrical properties of ZnO thin film based on ZnO/epoxy-resin ink for UV-light detectors

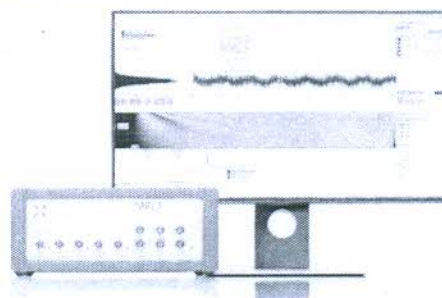
AIP Conference Proceedings 2142, 120004 (2019); <https://doi.org/10.1063/1.5122500>

Challenge us.

What are your needs for periodic signal detection?



Zurich Instruments



Coating of Multi-walled Carbon Nanotubes on Cotton Fabric via Conventional Dyeing for Enhanced Electrical and Mechanical Properties

Anil Kumar^{1,2, a)}, Jasvir Dalal^{1, b)}, Sajjan Dahiya^{1, c)}, Amal Chowdhury¹,
A. Khandual^{3, d)}, Anil Ohlan^{1, e)}, Rajesh Punia^{1, f)} and A. S. Maan^{1, g)}

¹Department of Physics, Maharshi Dayanand University, Rohtak-124001, India.

²Department of Applied Sciences and Humanities, The Technological Institute of Textile and Sciences, Bhiwani-127021, India.

³Department of Textile Engineering, The College of Engineering & Technology (CET), Bhubaneswar-751003, Odisha, India

^{a)}Corresponding author; anilkstits@gmail.com.

^{b)}jasvirdalal2012@gmail.com.

^{c)}sajjandahiya1@gmail.com.

^{d)}khandual123@gmail.com.

^{e)}anilohlan@gmail.com.

^{f)}rajeshpoonial3@gmail.com.

^{g)}asmaan66@rediffmail.com.

Abstract. In this paper, uniform and durable deposition of multi-walled carbon nanotubes (MWCNTs) on cotton fabric by conventional dyeing method with is reported. MWCNTs were synthesized by arc discharge method in deionized water and purified. Synthesized MWCNTs were analyzed by XRDs and TEM analysis. Purified MWCNTs were incorporated on cotton fabric with reactive vinyl sulphone class dyeing and confirmed by Raman spectroscopy and FE-SEM. It has been observed that there is effective improvement in strength, bending length and flexural rigidity of fabric. Sheet resistance of cotton fabric was also enhanced by 10⁵ fold. Results remain same even after 10 laundries washing which confirm the durability of deposition.

Keywords: MWCNTs, cotton fabric, dyeing, mechanical properties, sheet resistance.

INTRODUCTION

Nanotechnology has been proven vital enough in improving the performance of textile materials and thereby increasing its utility in the market. Numerous nanomaterials e.g. Ag nanoparticles, ZnO, MgO, TiO₂, graphene oxides etc. were used to produce special or multifunctional textile fabrics e.g. antibacterial, electrical conductivity, super hydrophobic, EMI shielding, self-cleaning and fire retardant [1-6]. Since after discovery of carbon nanotubes by Sumi Iijima in 1991, it also became fascinating nanomaterial due to its chemical, electrical and mechanical properties [7-8]. It is widely used in supercapacitor, sensors, optoelectronics, biomaterial science, EMI shielding materials [9-12]. It is also used to design smart textile as electrical conducting, self-cleaning, hydrophobic, antibacterial active, fire resistant or antistatic etc [13-14].

Uniform and stable deposition of nanomaterials on textile material is critical issue due to its agglomeration and chemical inertness. Various techniques were carried out for coating of nanoparticles on fabric including dip-dry-

curing, plasma, layer by layer, sol-gel, spray-coating, nip and dip, electro-less deposition, and chemical vapor deposition [15-17]. But most of coating techniques are time consuming, complex and costly. Maintaining biocompatibility, comforts and strength of coated is also big issue because large amount of dispersing and crosslinking agents were used in these methods. A simple, cheap and mass scale coating technique is needed for uniform deposition on nanoparticles on cotton fabric. In this work, high quality MWCNTs were synthesized by arc discharge method and purified by acidic treatment. Synthesized MWCNTs were uniformly deposited on cotton fabric by conventional dyeing method and its electrical conductivity and mechanical property was measured. Durability of coating was also analyzed.

EXPERIMENTAL

In this method, MWCNTs were synthesized by arc discharge method in deionized method. During the process, two graphite rods of diameter 6mm each were dipped nearly 3cm inside the deionized water. When 20- 25 V potential difference was provided to electrodes by DC power supply and electrodes were brought in contact to ignite arc and followed by immediate separation about 1mm to sustain arc in water. Direct electric current in range of 75-100 A was passed through electrodes. During the process, the electrode as anode get shorten and carbon shoot in the form of MWCNTs and impurities were deposited on cathode. The carbon soot accumulated over cathode was removed by knife and followed by purification to remove amorphous carbon and impurity. After purification, 100, 200, 300, 400 and 500 mg MWCNTs were mixed in each 100ml aqueous solution containing 1% dye at 50 °C and mixed by magnetic stirrer for 30 minutes at 500 rpm and followed by sonication for 2 hour in bath sonicator. Just after the mixing, dyeing process was carried out in dyeing machine and followed the process depicted in fig. 1(a). According to recommendations of dye supplier, soda and NaOH (alkali) were added in fixation stage. After dyeing, samples were taken out of beaker dyeing machine for cold wash, soaping with non-ionic detergent and hot wash. Cotton fabric dyed with solution of MWCNTs/dye composite having 0, 100, 200, 300, 400 and 500mg MWCNTs are termed as sample-0, sample-1, sample-2, sample-3, sample-4 and sample-5 respectively. Synthesized MWCNTs and its deposition on cotton fabric were analyzed by various characterization techniques.

Resistance of material depends upon nature and dimensions of material and it is the ratio of voltage (V) to electric current (I) flow. In case of coating thin film of conducting or semiconductor material on non-conducting surface or textile fabric where thickness of film is very tough to measure with accuracy, sheet resistance (R_s) is more important. This is because sheet resistance only depend upon nature and uniformity of coating material and independent on length and gap between electrodes and measuring technique. It can be defined as ratio of electric resistivity (ρ) to film thickness (t) i.e. $R_s = \rho/t$. $R = \frac{\rho L}{td}$. Where R is bulk resistance. But $\frac{\rho}{t} = R_s$ or $R_s = \frac{Rd}{L}$ is called sheet resistance and its unit is Ohm per sq. cm. Sheet resistance of cotton fabric coated with MWCNTs by conventional dyeing method was measured by laboratory equipment (two electrodes system) as shown in fig. 1(c). Strength and elongation of cotton

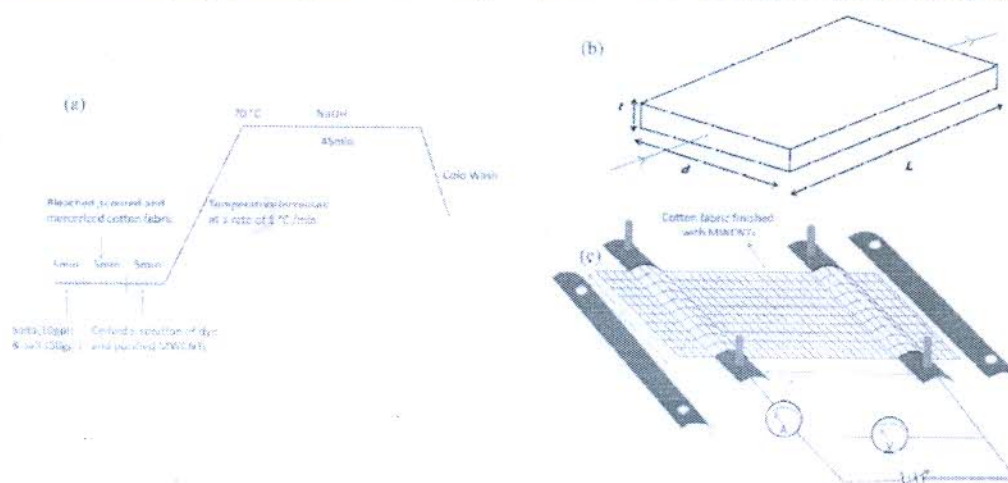


Figure 1-a) shows schematic diagram show different steps used to dye cotton fabric, (b) Diagram of film through which electric current is passed and (c) Schematic diagram of laboratory equipment for measurement sheet resistance of dyed cotton fabric

fabric untreated and treated with MWCNTs at varying concentration were measured on an Instron tensile tester according to ASTM D5034. Bending length and flexural rigidity were measured on Shirley tester by using formula $G = w \cdot c^3 / \text{gm-cm}$, where G is the rigidity, w is mass per unit area of fabric (gm/cm^2) and c is bending length (cm) [18]. During testing, standard atmospheric conditions were maintained.

RESULTS and DISCUSSION

Fig.2 (a) shows the XRD patterns of graphite and MWCNTs synthesized by arc discharge method. The characteristic peak at 25.9° in MWCNTs and at 26.5° in graphite powder are corresponding to C (002) plane. Sharp

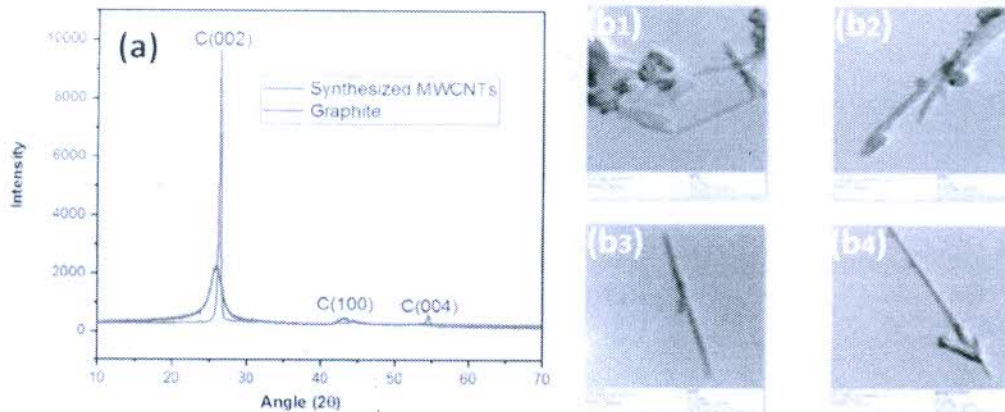


Figure 2. (a) XRD pattern of graphite powder and MWCNTs synthesized by arc discharge method. (b₁ and b₂) TEM images of as synthesized MWCNTs before and (b₃ and b₄) after purification.

decrease in peak intensity and its shift is attributed to an increase in the sp^2 , C-C layers spacing [19]. Other peaks observed at 42.7° and 53° are related to the reflection from the (100) and (004) planes. TEM images of synthesized MWCNTs before purification were shown by fig.2 (b₁ and b₂) and purification shown by fig.2 (b₃ and b₄). XRD pattern and TEM Images confirm the synthesis MWCNTs by arc discharge method.

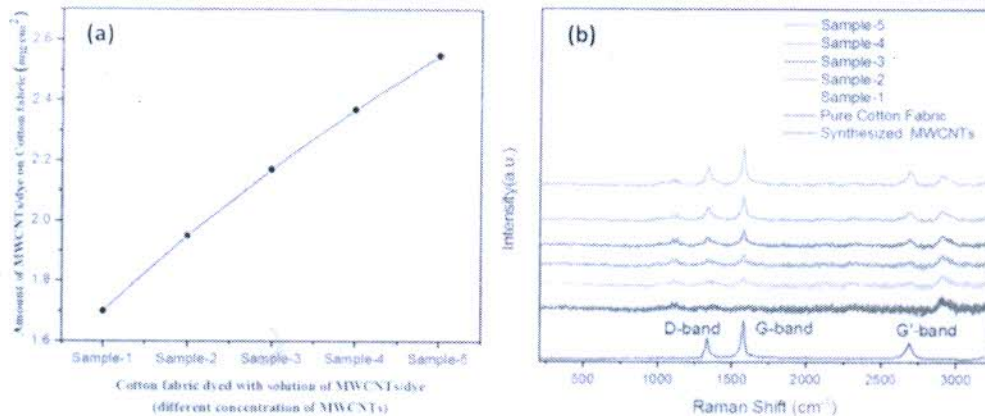


Figure 3. (a) Loading of MWCNTs/dye (mg/cm^2) on cotton fabric after dyeing and (b) Raman spectra of dyed cotton fabric

After dyeing of cotton fabric with solution of MWCNTs/dye composite at different concentration of MWCNTs, weight of samples (before and after dyeing) was measured. Mass of MWCNTs/dye composite per cm^2 deposited on

different cotton samples is shown in fig. 3(a). It is revealed from the graph that with increase of concentration of MWCNTs in solution, areal density of MWCNTs /dye composite on fabric also increases. To further confirm the

deposition of MWCNTs on cotton fabric, the Raman spectrum of synthesized MWCNTs, control cotton fabric and fabric dyed with MWCNTs/dye composite were presented in fig. 3(b). No one effective peak is observed in Raman graph related to control cotton fabric. The graph of MWCNTs has effective peaks at 1337, 1574 and 2690 cm^{-1} which are corresponding to D-band, G-band and G'-Band respectively [20]. Dyed cotton fabric also has all these effective peaks which confirm that fabric is successfully coated with synthesized MWCNTs. It is also observed from Raman spectra that intensities of MWCNTs peaks increases as fabric is dyed with higher concentration of MWCNTs in solution. It may be owing to higher amount of MWCNTs loading on cotton fabric. The FE-SEM micrographs of cotton fibres (sample-5) before and after the deposition of MWCNTs are shown in fig. 4(a) and (b). Image of cotton fibre is smooth before dyeing but rough after dyeing. Roughness of surface is due to deposition of MWCNTs on surface of cotton fabric, as being observed in figure fig. 4(b).

The coated fabric shows significant electrical conductivity. Sheet resistance of fabrics dyed with various MWCNTs concentrations are shown in fig 5(a). The sheet resistance of sample-1, sample-2, sample-3, sample-4 and sample-5 obtained are 5486, 2435, 385.6, 18.19 and 0.433 $\text{M}\Omega/\text{sq}$ respectively. This is due to higher amount MWCNTs loading and formation of conducting path on the surface of cotton fibers. The resistivity of samples decreased by 10^5 fold. After 10 times washing of dyed cotton fabric, its surface resistance increased from 0.433 to 0.489 $\text{M}\Omega/\text{sq}$. This variation is very small and confirms its durability.

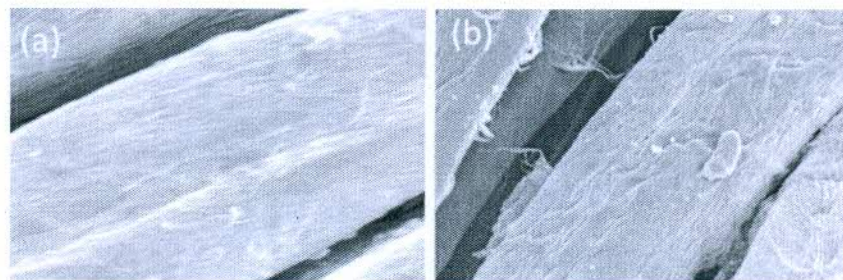


Figure 4. (a) and (b) FE-SEM images of cotton fabric before and after dyeing

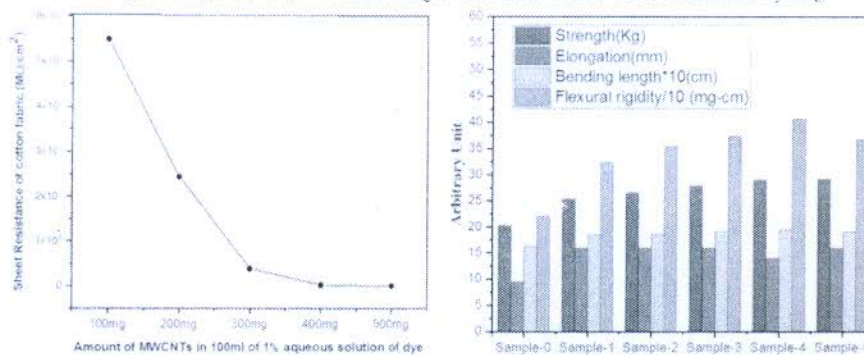


Figure 5. (a) and (b) show graph of sheet resistance and mechanical properties of cotton fabric dyed with solution of different MWCNTs concentrations.

The mechanical properties (strength, elongation, bending length and flexural rigidity) of cotton fabrics dyed with different solution of MWCNTs/dye mixtures having different concentration of MWCNTs were shown in fig. 5 (b). It has been observed that strength of dyed fabric increases as fabric is treated with higher concentration of MWCNTs solution. This may be due to strong van der Waals forces between MWCNTs and cotton yarn surface because MWCNTs have very high surface area [21]. Other mechanical properties of fabrics also register higher values as sample is loaded with MWCNTs as clearly shown in fig. 5(b).

CONCLUSION

TEM and XRD analysis confirmed the synthesis of high quality of MWCNTs by arc discharge method. Synthesized MWCNTs were successfully deposited on cotton fabric by conventional dyed method which was

clearly substantiated by Raman spectroscopy and FE-SEM images. Cotton fabric finished with MWCNTs has enhanced electrical conductivity and mechanical property. Further, the finishing is observed to be highly durable. So, deposition of MWCNTs on cotton fabric by conventional dyeing method is very effective and may help for uniform deposition of other nanoparticles on cotton fabric.

ACKNOWLEDMENT

The authors are thankful to DST, New Delhi and UGC, New Delhi for providing financial support under DST-FIST (SR/FST/PSI-162/2011) and UGC-SAP {F530/5/DRS/2012(SAP-1)} schemes, respectively.

REFERENCES

1. N. Jones, B. Ray, K. T. Ranjit and A. C. Manna, *FEMS microbiology letters* **279** (1), 71-76 (2008).
2. N. Onar, A. C. Akşit, M. F. Ebeoglugil, I. Birlık, E. Celik and I. Ozdemir, *Journal of applied polymer science* **114** (4), 2003-2010 (2009).
3. I. Perelshtein, G. Applerot, N. Perkas, G. Guibert, S. Mikhailov and A. Gedanken, *Nanotechnology* **19** (24), 245705 (2008).
4. S. Chen, X. Li, Y. Li and J. Sun, *ACS nano* **9** (4), 4070-4076 (2015).
5. R. Perumalraj, B. Dasaradan, R. Anbarasu, P. Arokiaraj and S. L. Harish, *The Journal of The Textile Institute* **100** (6), 512-524 (2009).
6. D. Wu, M. Long, J. Zhou, W. Cai, X. Zhu, C. Chen and Y. Wu, *Surface and Coatings Technology* **203** (24), 3728-3733 (2009).
7. R. Saito, G. Dresselhaus and M. S. Dresselhaus, *Physical properties of carbon nanotubes*. (World Scientific, 1998)
8. S. Iijima and T. Ichihashi, *nature* **363** (6430), 603 (1993).
9. E. T. Thostenson, Z. Ren and T.-W. Chou, *Composites science and technology* **61** (13), 1899-1912 (2001).
10. C. Li, E. T. Thostenson and T.-W. Chou, *Composites Science and Technology* **68** (6), 1227-1249 (2008).
11. C. Lin, L. Hu, C. Cheng, K. Sun, X. Guo, Q. Shao, J. Li, N. Wang and Z. Guo, *Electrochimica Acta* **260**, 65-72 (2018).
12. W. Zhou, T. Yamaguchi, K. Kikuchi, N. Nomura and A. Kawasaki, *Acta Materialia* **125**, 369-376 (2017).
13. Y. Liu, J. Tang, R. Wang, H. Lu, L. Li, Y. Kong, K. Qi and J. Xin, *Journal of Materials chemistry* **17** (11), 1071-1078 (2007).
14. O. Breuer and U. Sundararaj, *Polymer composites* **25** (6), 630-645 (2004).
15. M. Stoppa and A. Chiolerio, *Sensors* **14** (7), 11957-11992 (2014).
16. J. McCann and D. Bryson, *Smart clothes and wearable technology*. (Elsevier, 2009).
17. K. Cherenack, C. Zysset, T. Kinkeldei, N. Münzenrieder and G. Tröster, *Advanced materials* **22** (45), 5178-5182 (2010).
18. N. Abbott, *Textile Research Journal* **21** (6), 435-441 (1951).
19. D. Bera, G. Johnston, H. Heinrich and S. Seal, *Nanotechnology* **17** (6), 1722 (2006).
20. L. Bokobza and J. Zhang, *Express Polymer Letters* **6** (7) (2012).
21. K. Jost, G. Dion and Y. Gogotsi, *Journal of Materials Chemistry A* **2** (28), 10776-10787 (2014).



In situ decoration of silver nanoparticles on single-walled carbon nanotubes by microwave irradiation for enhanced and durable anti-bacterial finishing on cotton fabric

Anil Kumar^{a,1}, Jasvir Dalal^a, Sajjan Dahiya^a, Rajesh Punia^a, K.D. Sharma^c, Anil Ohlan^{a,*}, A.S. Maan^b

^a Department of Physics, Maharshi Dayanand University, Rohtak 124001, India

^b Department of Applied Sciences and Humanities, The Technological Institute of Textile and Sciences, Bhawan 127021, India

^c Department of Microbiology, PGIMS, Rohtak 124001, India



ARTICLE INFO

Keywords

Ag-SWCNTs nanocomposites
In situ synthesis
Microwave irradiations
Cotton fabric
Anti-bacterial activity

ABSTRACT

Present communication reports microwave-assisted process to decorate single-walled carbon nanotubes (SWCNTs) with silver nanoparticles (Ag-NPs) to induce excellent and durable anti-bacterial activity in cotton fabric. Pristine SWCNTs were functionalized (f-SWCNTs) through acidic treatment for nucleation, followed by reduction of silver ion by microwave heating to produce Ag-NPs decorated SWCNTs (Ag-SWCNTs). Functionalization and decoration of Ag-NPs on SWCNTs were characterized by FTIR, XRD, RAMAN spectroscopy and FE-SEM. Microwave irradiation time was optimized and it was observed that complete reduction of Ag ions on SWCNTs from its precursor (AgNO_3) took place within 40 s of microwave irradiation time. For antibacterial activity measurement and comparison, pristine SWCNTs, Ag-NPs and Ag-SWCNTs composite were individually coated on different cotton fabrics via dip-dry-curing process. Deposition of these particles on cotton fabrics were confirmed by FE-SEM and Raman spectroscopy. Antibacterial property of all coated fabrics was evaluated qualitatively against *Staphylococcus aureus* (*S. aureus*) as gram positive and *Escherichia coli* (*E. coli*) as gram negative pathogenic bacteria. It was observed that the fabric coated with Ag-SWCNTs show excellent anti-bacterial activity against both types of bacteria. Sufficient antibacterial activity of Ag-SWCNTs coated fabrics was observed even after 20 washing.

1. Introduction

Cotton is the most important natural cellulose used as raw material for textiles and clothing production for domestic and medical purposes due to comfortability, skin affinity, biodegradability, cheap, and easy availability [1]. However, compared to synthetic polymer fibers, cotton fibers have a drawback of providing favorable conditions for bacteria breeding due to moisture retaining property, biocompatibility and large surface area. It has been reported that cotton fabrics used in hospital application such as bandages, bed sheets, lab coats etc. have a huge numbers of microorganisms and odor generating bacteria [2,3]. Therefore, for value addition to cotton fabric, antibacterial activity is required. Certain nanomaterials having antibacterial activity such as copper, copper oxide, titanium dioxide, Magnesium oxide, zinc oxide [4–6] etc. have been reported so far. Recently, Zhang et al. synthesized TiO_2/ZnO nanocomposites as effective antibacterial material [9].

Silver (Ag), is well known as effective antibacterial material for variety of bacterial species [10,11]. Huag et al. reported the anti-bacterial properties of ZnO decorated silver nano-rods [12]. Physical and chemical properties of silver particles are significantly changed as their size is reduced to nanoscale resulting in improve the anti-bacterial property. Small particle size might be beneficial because it results in high aspect ratio, which allows greater interaction with bacteria. Improved antibacterial property may be due to increased density of edges and corner sites on the surfaces of silver nanoparticles. Atoms at edges and corners have dangling bonds which easily interact with thiol groups of bacterial cells resulting damage their reproduction and respiratory system. Chemical properties, particle size and shape appear to be the most significant parameters to determine the antibacterial activity of silver [13].

However, the Ag-NPs exhibit two major shortcomings at nanoscale level: (i) instability in size of silver nanoparticles leads to agglomeration

Corresponding authors.

E-mail addresses: anilohlan@mvscs.com (A. Ohlan), asm@mvscs.com (A.S. Maan).

Received 10 February 2018; accepted 29 September 2018

Received 4 September 2018; Received in revised form 27 September 2018; Accepted 27 September 2018

Available online 01 October 2018

0272-8842/ © 2018 Elsevier Ltd and Techna Group S.r.l. All rights reserved.

of particles and reduces antibacterial activity and (ii) at high concentrations, the Ag-NPs could exhibit a highly toxic potential to human cells. The main reason of Ag-NPs-mediated cytotoxicity is ascribed to the induction of reactive oxygen species (ROS) due to release of silver ions [14,15]. Thus the application of novel nanostructures as alternatives for decorating Ag-NPs on supporting materials is important with a view to improve the antibacterial performance of materials and minimize adverse effects of silver.

Since after discovery of carbon nanotubes (CNTs), it became a new fascinating material among other nanoscale materials and has been widely used due to its exceptional structural stability, excellent electrical conductivity and thermal and mechanical properties [16–18]. CNTs have been reported to have excellent properties such as high surface area and chemical stability. Castle et al. reported that the strong adhesion of nanoparticles on functionalized CNTs makes the Ag-NPs less toxic because they are not released easily to human cells [19]. Additionally, antibacterial activity of CNTs was discovered which triggered environmental and health applications of CNTs [20,21]. CNTs are categorized as single wall carbon nanotubes (SWCNTs) and multi-wall carbon nanotubes (MWCNTs). It is reported that SWCNTs show more antibacterial activity as compared to MWCNTs due to large surface area and more interaction with bacteria [22]. Interaction of bacteria with CNTs damages the cell membrane resulting in their death [23]. In addition, individually dispersed SWCNTs are reported to be more toxic to bacteria than aggregated SWCNTs as individual CNTs have greater interaction with bacteria as compared to aggregated tubes due to large surface area [24]. Yang et al. observed that longer SWCNTs exhibit stronger antibacterial activity as shorter SWCNTs aggregate themselves without involving many bacterial cells [25]. Therefore, SWCNTs can be used to deposit the Ag-NPs due to larger surface area (for strong adhesive force between Ag and SWCNTs and SWCNTs and cotton fabric), compatibility with cellulosic fabric, high stability and outstanding antimicrobial activity. To date, a number of authors have reported various methods for the preparation of CNT/Ag composites, such as reduction in N-N DMF, silver mirror reaction, electron assisted reduction, ultra-sonication, vapor phase deposition, photochemical reaction, ethanol as reducing agent, γ -irradiation, high temperature reduction etc [26–34]. However, all of these methods are disadvantageous due to one or more reason such as the chemical reduction method induces impurities like reducing agent and stabilizing agent (capping) in CNTs/Ag composites which harm human cells. Reduction of silver ions via γ -irradiation requires costly equipment and high energy consumption while reduction through vapor phase deposition is time consuming and a complicated process. The most critical issue is to control aggregation of Ag NPs and impurities and for this purpose, an efficient and simple approach without using toxic chemicals, reducing and capping agents is required. The synthesis of nanostructured materials via microwave irradiation is one such technique which offers advantages such as simple and fast synthesis procedures, improved reaction kinetics, uniform heat distribution and minimal structural damage [35–37]. Wadhawan et al. reported that SWCNTs are very good microwaves absorbent and one can raise its temperature to 500–650 °C with in few seconds [38]. In addition, as prepared SWCNTs can be further purified by microwave technique without damaging its structure [39].

In present work, microwave-assisted synthesis process is reported to decorate carboxylates SWCNTs with Ag-NPs for enhanced antibacterial activity. The microwave-assisted process completely reduces silver precursor within 40 s, leading to synthesis of Ag-NPs of size about 60 nm on SWCNTs. Anti-bacterial activity measurements were carried out and indicate that Ag-SWCNTs nanocomposite coated cotton fabric shows excellent and durable anti-bacterial activity against *E. coli* as gram-negative and *S. aureus* as gram-positive pathogenic bacteria than cotton fabric coated with pristine SWCNTs and Ag-NPs individually.

2. Experimental

2.1. Materials

Pristine SWCNTs (diameter ~ 1.5 nm, length ~ 5 μ m, purity > 85% and specific surface area 422 m²/gm) procured from United Nanotech Innovations, Bangalore (India) and were used after purification. Silver Nitrate and other required chemical of analytical grade make Merck (India) and Nutrient agar, MacConkey agar and peptone broth make HiMedia Laboratories (India) were used. 100% Cotton fabric (plain weave, EPI 96, PPI 64, and surface density 92 g/m²) was used after scouring and bleaching. All chemicals were used without purification. Distilled water was used throughout the experiment.

2.2. Purification and functionalization of SWCNT

SWCNTs were purified to remove amorphous carbon and the metal catalyst particles used to grow SWCNTs. During this process, 100 mg of SWCNTs were sonicated for one hour in 100 ml solution 3 M of hydrochloric acid to decrease size of agglomerated CNTs. Thereafter, the mixture was heated at 70 °C under stirring rate of 300 rpm for 24 h by magnetic stirrer and was filtered using 0.22 μ m pore PTFE membrane. Several washing were carried out with distilled water until the pH reached neutral value. Purified SWCNTs (p-SWCNT) were dried at 70 °C for 24 h [40]. Functionalized SWCNTs (f-SWCNTs) were prepared by oxidation of p-SWCNTs in mixture of sulfuric acid and nitric acid [41]. For this purpose, 60 mg of p-SWCNTs were added in mixture of 100 ml acid solutions of 98% H₂SO₄ and 70% HNO₃ at volume proportion 3:1 and refluxed at 80 °C for 6 h. To remove acidic content, the mixture was filtered and washed several times with distilled water until pH value reached to neutral and at last dried at 70 °C overnight.

2.3. Microwave-assisted process to decorate Ag-NPs on f-SWCNTs

In this process, 40 mg of f-SWCNT was mixed in 90 ml distilled water and followed by sonication for 2 h at 20 °C to obtain homogeneous dispersion. Thereafter, 10 ml of 0.001 M AgNO₃ was added and it was further sonicated for 30 min. The resulting solution was filtered using 0.22 μ m pore PTFE filter and was dried at 70 °C for 48 h to recover AgNO₃ treated f-SWCNTs. Finally, dried material was crushed to fine powder and heated using household microwave oven at average power 500 W for time intervals of 10, 20, 30, 40, and 50 s (Figs. 1–3).

2.4. Preparation of aqueous dispersion of Ag-SWCNTs, pristine SWCNTs and Ag NPs and deposition on cotton fabric surface

In present case, 10 mg of Ag-SWCNTs (Ag-SWCNTs composite prepared after irradiating microwave for 40 s) were mixed in 20 ml distilled water and solution was ultra-sonicated for 2 h in bath sonicator. The resulting suspensions were centrifuged at 6000 rpm speed for 1 h and finally, 90% of supernatant was collected from all solutions. Now, collected supernatant was stable and uniform. For uniform deposition of Ag-SWCNTs on cotton fabric dip-dry-curing process was opted. In this method, scoured and bleached cotton fabrics of size 3 × 3 cm² were immersed in beakers containing 20 ml prepared uniform aqueous dispersions of Ag-SWCNTs and dry at 70 °C for 10 min and finally cured at 130 °C for 3 min in hot air oven. Above steps are repeated five times. Same process was used to prepare aqueous dispersion of pristine SWCNTs and deposition on cotton fabric. Pristine Ag-NPs were prepared and coated on cotton fabric according to reference to compare antibacterial activity [42].

2.5. Characterization

To confirm the attachment of carboxyl groups on purified SWCNTs after acidic treatment, FT-IR spectroscopy was used. The spectra were

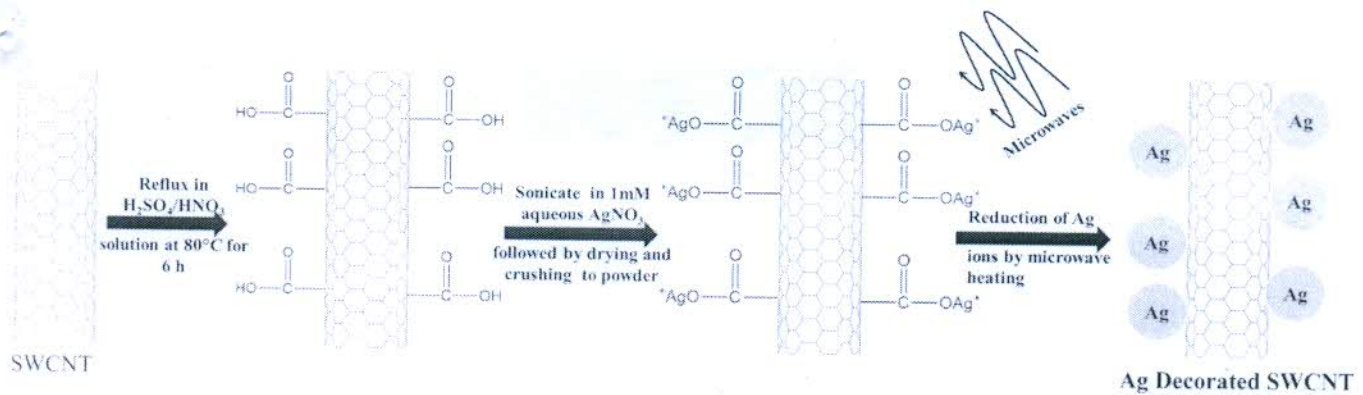


Fig. 1. Schematic diagram of functionalization of SWCNTs and decoration of Ag-NPs on SWCNTs by microwave irradiation.

recorded in KBr on Thermo iS50 FT-IR at wave number range 400–4000 cm⁻¹. To study the effect of acidic treatment for functionalization, deposition of Ag-NPs by microwave irradiation on the surface of SWCNTs and to confirm coating of different nanoparticles on cotton fabric, Raman spectra was recorded using Raman spectrometer (Renishaw) using 532nm laser at room temperature. Surface morphology of control and coated cotton fabrics were examined by field emission scanning electron microscopy (FESEM; Hitachi Japan, 4300S, SE/N). All samples for the measurements were prepared by fixing 5 mm × 5 mm sections to the support directly. To examine Ag-NPs on SWCNTs, X-rays diffraction pattern was recorded at scan rate 2°/min. at angle (2θ) from 10 to 90° using Rigaku MiniFlex-600 with monochromatic Cu Kα radiation of wavelength 1.540598 Å.

2.6. Antibacterial activity

Cotton fabrics provides excellent environment for microorganism growth. Therefore, its surface was modified with prepared Ag-SWCNTs nanocomposites to impart antibacterial property. The antibacterial activity of cotton fabric coated with Ag-SWCNTs was evaluated qualitatively against *Escherichia coli* (*E. coli*-ATCC 25922) as a Gram-negative organism and *Staphylococcus aureus* (*S. aureus*-ATCC 25923) as a Gram-positive organism according to AATCC (American Association of Textile Chemists and Colourists) Method 147. For comparison, antibacterial activity of pristine cotton fabric, cotton fabric coated pure SWCNTs and pristine Ag-NPs were also analysed by same method. In this analysis, inhibition zone test was used. In typical procedure, 100 μl bacterial suspensions containing *S. aureus* strain with concentration of 10⁵ colonies forming units per millilitre (CFUs/ml) was spread on

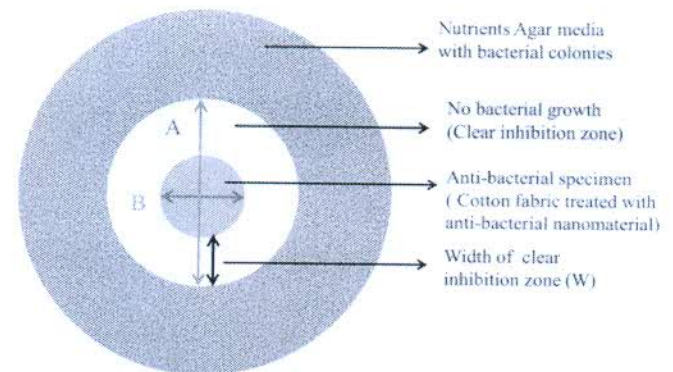


Fig. 3. Schematic diagram for determination of inhibition zone width.

nutrient agar plate by sterilized cotton swab and same CFU concentration was used to spread *E. coli* stains on MacConkey agar plate and left to dry for few minutes in sterilized atmosphere. Finally, autoclaved pristine and treated cotton swatches in circular shape (diameter-5 mm) were placed on corresponding agar plates and incubated at 37 °C for 24 h. The width of clear inhibition zone was measured according to formula given below

$$W = (A - B) / 2 \quad (1)$$

where W is width of clear zone of inhibition; A is total diameter of test fabric + clear zone and B is diameter of the test fabric (in mm). Diameter of test fabric and clear inhibition zone were measured by travelling microscope attached with scale of least count 0.001 mm.

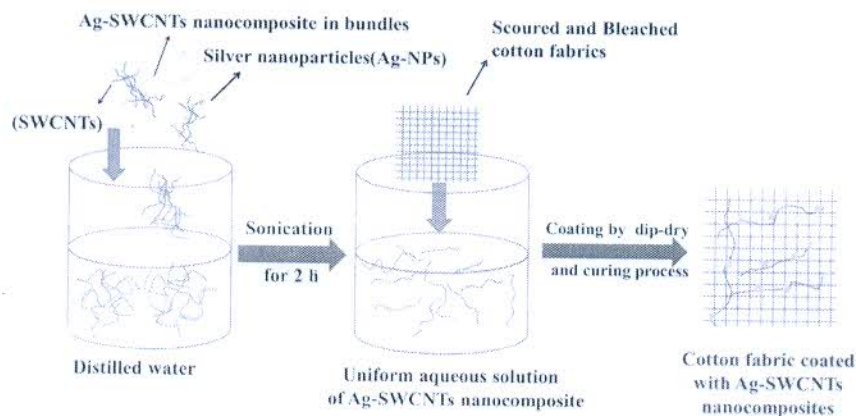


Fig. 2. Schematic diagram of preparation aqueous dispersion of Ag-SWCNTs nanocomposites and deposition on cotton fabric.

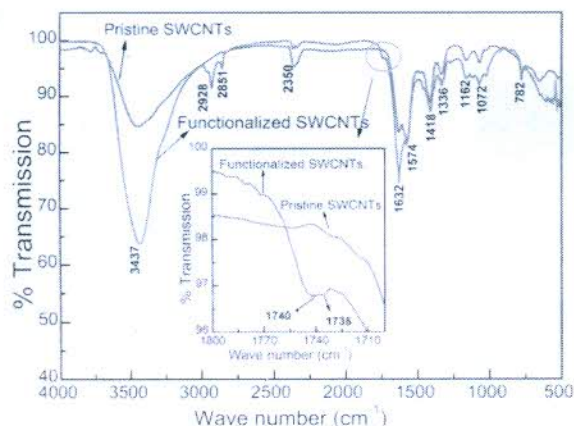


Fig. 4. FT-IR spectra of purified and functionalized SWCNTs.

3. Results and discussion

3.1. Functionalization of SWCNTs

FT-IR spectra analysis was carried out to confirm the functionalization of SWCNTs after treatment with acid mixture ($\text{H}_2\text{SO}_4/\text{HNO}_3$). Fig. 4 shows the FT-IR spectra of pristine and acid-treated SWCNTs. After treatment, a strong peak was appeared at about 3437 cm^{-1} as compare to pristine SWCNTs and corresponding to stretching mode of hydroxyl groups (O–H) [43,44]. Increase in peak intensity at position 1632 cm^{-1} can be attributed to asymmetrical COO- stretching after strong oxidation [45]. New peaks at 1740 , 1735 , 2851 and 2928 cm^{-1} also appeared after acidic treatment. The peak at 1740 cm^{-1} was assign to C=O stretching vibration mode and indicates the presence of COOH groups in free state and peak at 1735 cm^{-1} was also related to C=O stretching vibration mode which indicate COOH groups are attached to surface of SWCNTs [46]. Peaks at 2851 and 2928 cm^{-1} were assigned to CH_2/CH_3 bending and stretching modes, indicate the presence of hydrocarbons [44–47]. Simultaneous increase in intensities of peaks at C=O and O–H reveal that the COOH groups are successfully attached on the surface of SWCNTs.

To further confirm the presence of SWCNTs and attachment of carboxyl groups, Raman spectroscopy of samples was performed. It can differentiate SWCNTs from other carbon based nanomaterials e.g. graphite, fullerenes, MWCNT and Graphene. It also reveals the structural and electronic properties of SWCNTs [48]. Fig. 5 shows the Raman spectra of pristine and acid-treated SWCNTs. In Fig. 5b, the pristine SWCNTs has strong peak at 1598 cm^{-1} (G-band) that represent

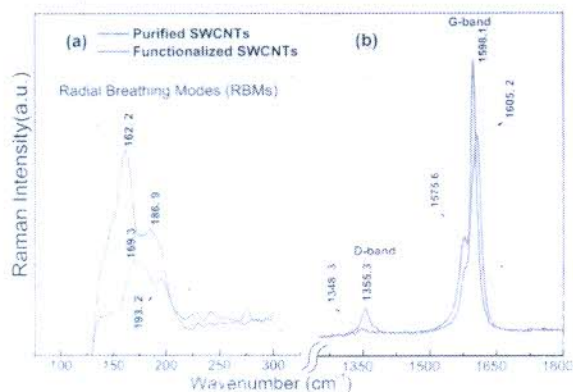


Fig. 5. Raman spectra of purified and functionalized SWCNTs: (a) radial breathing modes (RBMs) at small scale and (b) D-band and G-band at large scale.

crystalline arrangement of carbon according to sp^2 hybridization and weak peak at 1348 cm^{-1} (D-band) represent the defects or disorder of carbons in sp^2 network. Low value of intensities ratio of D-band to G-band (I_D/I_G) i.e. 0.018 shows highly pure SWCNTs and existence of less defects in sp^2 network of carbons [49]. The Raman spectra of acid treated SWCNTs has intense peak at D-band and slightly diminished peak at G-band as compare to spectra of pristine SWCNTs. Increase in intensities ratio (I_D/I_G) from 0.018 to 0.085 indicate that large amount of defects were induced or carboxyl groups were attached to SWCNTs structure after acid treatment [50]. Raman peaks from 100 to 300 cm^{-1} known as Radial breathing modes (RBMs) of SWCNTs provide information about structure and aggregation of SWCNTs. In Fig. 5a, RBMs of pristine and treated SWCNTs were effectively changed. There are two main peaks in RBMs of pristine SWCNTs spectra, at 162.2 and 186.9 cm^{-1} which corresponds to SWCNTs of a diameter 1.54 and 1.32 nm respectively. Diameter of tubes were calculated by using equation $\omega_{RBM} = A/d+B$ where ω_{RBM} is RBM shift, d is diameter of SWCNTs, $A = 234\text{ cm}^{-1}\text{ nm}$ and $B = 10\text{ cm}^{-1}$ [51]. D band, G band and RBMs peaks in Raman spectra were upshifted by 7 cm^{-1} after acidic treatment which is attributed to intercalation of COOH groups in SWCNTs bundles [52]. Accordingly, it is clear that COOH groups were successfully attached to SWCNTs.

3.2. Decoration of silver nanoparticles of SWCNTs

XRD measurements were carried out to confirm the decoration of SWCNTs with silver nanoparticles. Fig. 6 shows the typical X-ray diffraction pattern for SWCNTs decorated with Ag nanoparticles by irradiating microwave for different time intervals. In all samples, positions of major peaks are same, five effective peaks at 2θ value of 38.2 , 44.2 , 64.4 , 77.3 and 81.5° are observed which are assigned to (111), (200), (220), (311) and (222) lattice planes of silver respectively. These peaks suggest that SWCNTs are decorated with Ag-NPs and have face centred cubic structure (FCC) [53]. It is depicted from the graph that with increase of microwave irradiation time from 10 to 40 s , intensity of peaks corresponding to Ag-NPs increases and after 40 s heights of peaks became almost saturate and sharp (FWHM decreases significantly). This may suggest that deposition of number of silver nanoparticles on SWCNTs increases initially (reduction of AgNO_3 into Ag-NPs) then become constant and further size of deposited Ag-NPs increases due to collapsing via overheating [38].

The size of nanoparticles was calculated by using Scherrer's equation and average size of decorated Ag-NPs were found to be 41 , 43 , 47 , 54 , and 88 nm when samples were irradiated by microwave for 10 , 20 , 30 , 40 and 50 s respectively. XRD peak at 25.8° is assigned to graphite

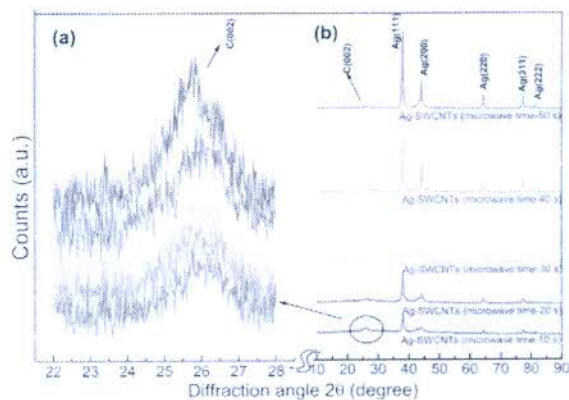


Fig. 6. XRD patterns of SWCNTs decorated with Ag-NPs by irradiating microwave for time intervals 10 , 20 , 30 , 40 and 50 s : (a) XRD peak of carbon lattice plane (002) at small scale and (b) XRD peaks of silver lattice planes at large scale of all samples.

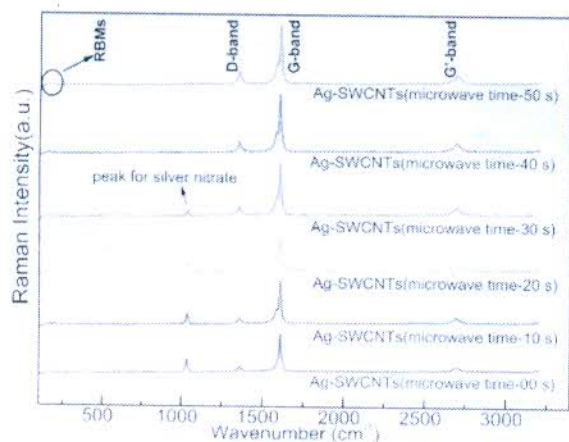


Fig. 7. Raman spectra of SWCNTs decorated with Ag-NPs by irradiating microwaves for time intervals 0, 10, 20, 30, 40 and 50 s.

structure of carbon particles. Broad and weak band about this position ensures that SWCNTs bundles were small in size and highly purified [54]. We can conclude that microwave irradiation time of 40 s is sufficient to reduce AgNO_3 to Ag-NPs and if we further increase microwave irradiation time then size of Ag-NPs gets increased. Fig. 6a shows XRD pattern at peak 25.8° of samples irradiated by microwave at different time intervals. Intensity of peaks decreases as microwave irradiation time increases which indicates the removal of graphitic particle. In addition, the method helps to purify the SWCNTs sample.

Decoration of SWCNTs with Ag-NPs (Ag-SWCNTs) was also analysed by using Raman scattering and the data is presented in Fig. 7. Here, Raman spectra of Ag-SWCNTs nanocomposite synthesized by microwave heating at different time intervals were compared. The result shows that intensities of RBMs, D-band, G-band and G'-band of SWCNTs increases as microwave irradiation time on samples was increases from 0 to 40 s but after that there was no significant increase in their intensity. Rise in these peaks is attributed to SERS (surface enhancement of Raman spectra) effect of decorated Ag-NPs on SWCNTs [55–57]. Raman peak at 1031 cm^{-1} is assigned to AgNO_3 and its intensity decreases as time of microwave irradiation is increased and finally, the peak almost disappeared when sample was heated by microwave for 40 s [58]. It is also clear from Raman analysis that 40 s microwave irradiation time is enough to reduce Ag ion from its precursor. Raman spectra also show that peaks related to SWCNTs were redshift by $7\text{--}9\text{ cm}^{-1}$ which can be attributed to removal of free carboxyl groups, oxygen, nitrogen gases due to oxidation and de-

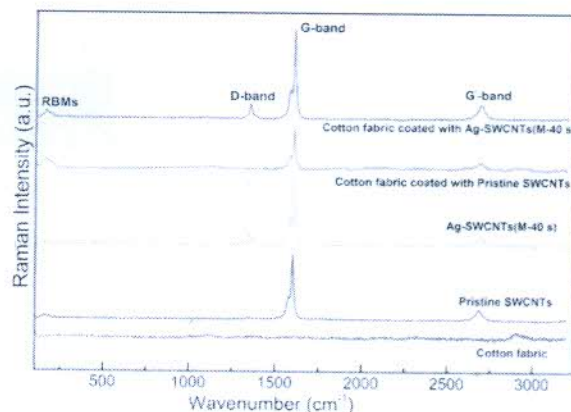


Fig. 9. Raman spectra of control cotton fabric, pristine SWCNTs, Ag-SWCNTs (m-40) nanocomposites and cotton fabric coated with pristine SWCNTs and Ag-SWCNTs (m-40) nanocomposites.

intercalation under microwave annealing [52]. The ratio of intensities of D-band to G-band (I_D/I_G) is found to be 0.122, 0.136, 0.149, 0.162, 0.173, and 0.223 when samples were irradiated by microwave for 0, 10, 20, 30, 40, and 50 s respectively. It indicates that when samples were heated by microwave for 0–40 s then disorder in SWCNTs surface remains same because I_D/I_G ratios were not effectively increased. When microwaves were incident on samples for 50 s then I_D/I_G ratio increases significantly which means large number of disorder in SWCNTs surface appears. The reason may be accounted as when samples were heated by microwave for 40 s then deposition of Ag-NPs at nucleation (at disorder sites) on SWCNTs surface took place. Whereas when sample was heated by microwave for 50 s then local temperature on SWCNTs surface attains a very high value [38]. We may conclude from Raman and XRD pattern that 40 s microwave irradiation time is enough and most appropriate for complete reduction of Ag from its precursor (AgNO_3) and microwave heating also helps to purify the SWCNTs.

To induce the antibacterial properties into cotton fabric, Ag-SWCNTs synthesized by irradiating microwave for 40 s (Ag-SWCNTs (m-40)) were coated on cotton fabric by dip-dry-curing process and its FE-SEM image was taken. Fig. 8 shows the FE-SEM image and histogram related to silver nanoparticles size distribution on SWCNTs surface. It is clearly seen from image that Ag-NPs were uniformly decorated on SWCNTs and most of Ag-NPs size varies from 30 to 80 nm. Nearly same result was calculated by using Scherrer's formula.

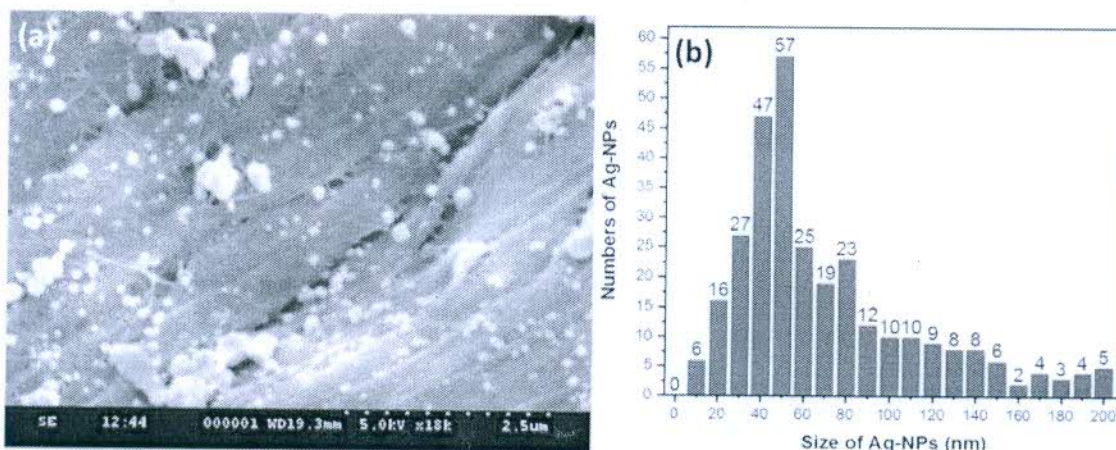


Fig. 8. (a) FE-SEM image of Ag-SWCNTs nanocomposite coated on cotton fabric and (b) Size distribution of silver nanoparticles decorated on SWCNTs (extracted from FE-SEM image).

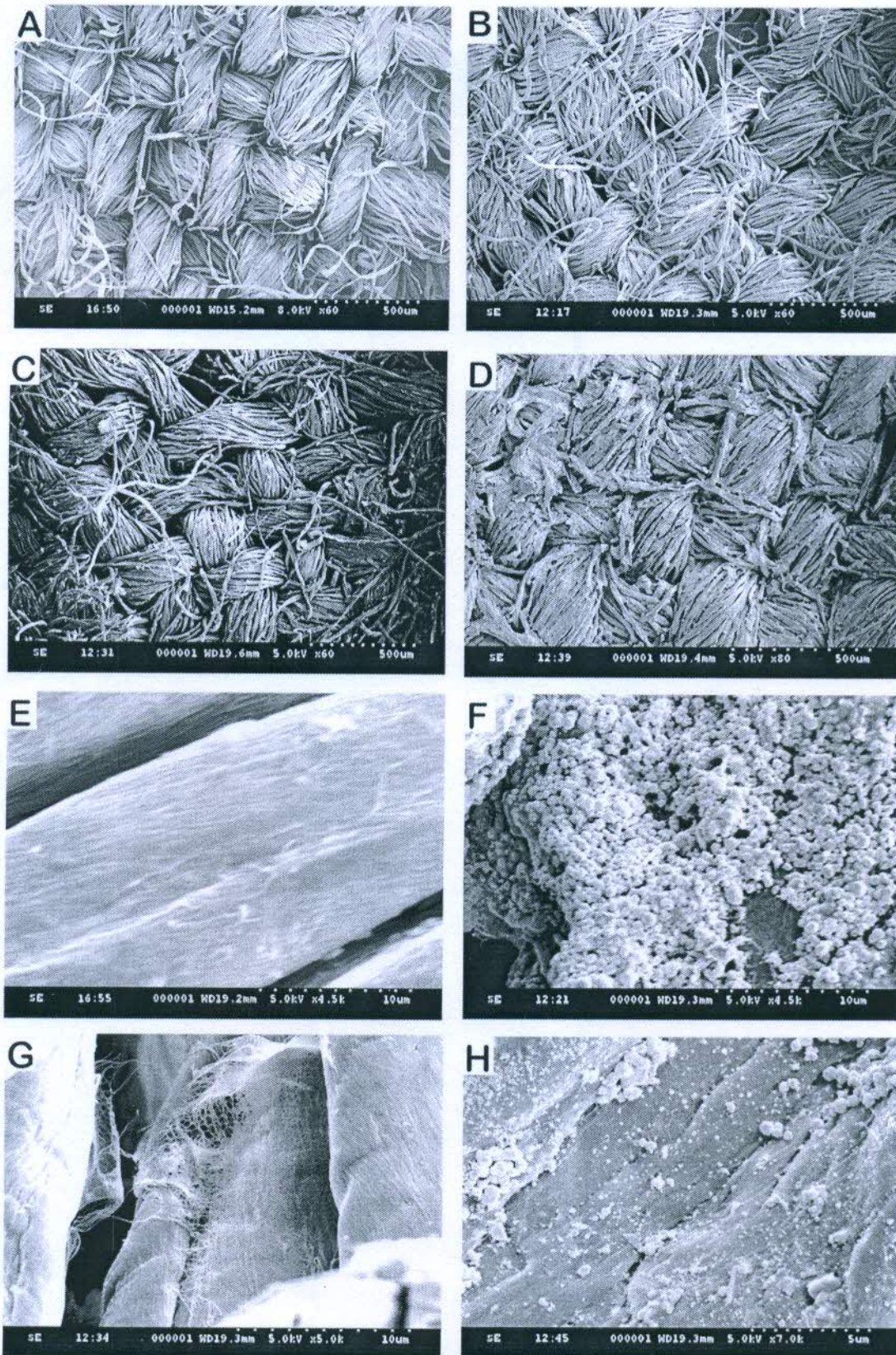


Fig. 10. FE-SEM images: A&E (control cotton fabric), B&F (cotton fabric coated with pristine Ag-NPs), C&G (fabric coated with purified SWCNTs) and D&H (cotton fabric treated Ag-SWCNTs composite) at different magnification.

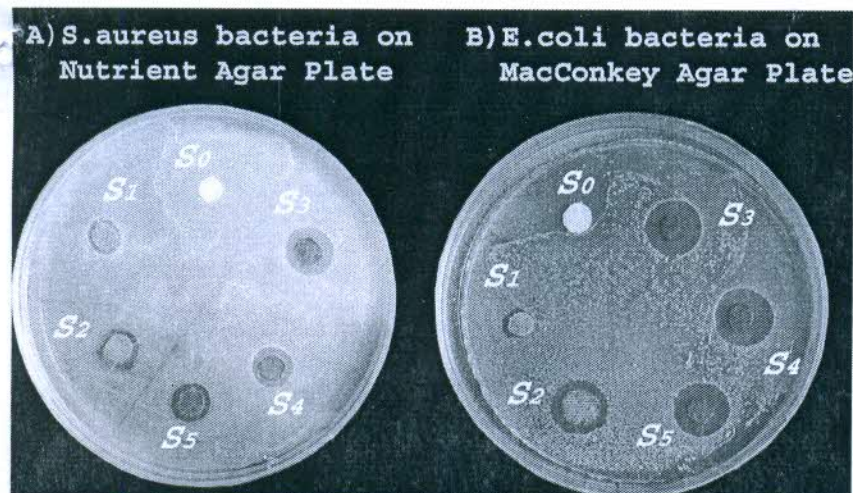


Fig. 11. Photo view of inhibition zone (Antibacterial activity) about uncoated and coated cotton fabric: (A) Nutrient agar plate containing *S. aureus* bacteria and (B) MacConkey agar plate containing *E. coli* bacteria. Inhibition zone about circular cotton swatches S_0 (uncoated cotton fabric), S_1 (cotton fabric coated with purified SWCNTs), S_2 (cotton fabric coated with pristine Ag-NPs), S_3 (cotton fabric coated with Ag-SWCNTs (m-40) nanocomposites before washing), S_4 (cotton fabric coated with Ag-SWCNTs (m-40) nanocomposites after 10 washings) and S_5 (cotton fabric coated with Ag-SWCNTs (m-40) nanocomposites after 20 washings).

Table 1

Antibacterial activity assessment against *S. aureus* and *E. coli* bacteria of cotton fabric finished with pristine SWCNTs, Ag-NPs, Ag-SWCNTs nanocomposite (after 0, 10 and 20 times washings).

Name of sample	Description of sample	Number of washings	Inhibition zone width of <i>S. aureus</i> bacteria (mm)	Inhibition zone width of <i>E. coli</i> bacteria (mm)
S_0	Control cotton fabric	0	0	0
S_1	SWCNTs coated cotton fabric	0	1.149 ± 0.053	0.576 ± 0.169
S_2	Ag-NPs coated cotton fabric	0	1.787 ± 0.246	2.103 ± 0.202
S_3	Ag-SWCNTs(m-40) coated cotton fabric	0	2.402 ± 0.213	3.498 ± 0.132
S_4	Ag-SWCNTs(m-40) coated cotton fabric	10	1.863 ± 0.219	3.361 ± 0.381
S_5	Ag-SWCNTs(m-40) coated cotton fabric	20	1.526 ± 0.197	2.931 ± 0.163

Table 2

Antibacterial activity of different types of nanomaterials against *S. aureus* and *E. coli* bacteria (Inhibition zone width).

Nano-particles as anti-bacterial material	Method to synthesizes Nanomaterial	Method to deposition of nanoparticles on cotton fabric	Width of inhibition zone against <i>S. aureus</i> (mm)	Width of inhibition zone against <i>E. coli</i> (mm)	Ref.
Silver nanoparticles	Wet chemical route	–	–	1.5	[15]
5,5-dimethylhydantoin (DMH)	–	Pad-dry-plasma-cure method	1.611	–	[65]
AgCl embedded in a silica matrix	–	Pad-dry-cure and exhaustion methods	–	~ 1	[66]
Silver nanoclusters/silica composite	–	Radio frequency (RF) co-sputtering	2–3	< 1	[67]
Zinc oxide	Wet chemical route	In situ synthesis	< 3	–	[68]
Ag/ZnO nanocomposites	Chemical reduction method	Pad-dry-cure method	< 1	–	[69]
Monochlorotriazine triethylphosphite guanidine (MCTPG)	Wet Chemical route	–	–	–	–
Silver chloride compounds (Silpure)	Dip-dry method	2.8	2.9	[70]	–
Ag-NPs-alginate composite	–	Pad-dry-cure	1.66	–	[71]
Ag-SWCNTs	Chemical reduction by microwave irradiation	Pad-dry-cure method	3	2	[22]
		Dip-dry-cure method	2.4	3.5	Present work

3.3. Attachment of pristine SWCNTs, Ag-NPs and Ag-SWCNTs to cotton fabric individually

To confirm the deposition of pristine SWCNTs and Ag-SWCNTs on cotton fabric Raman spectroscopy were recorded. Fig. 9 shows the Raman graphs of control cotton fabric, pristine SWCNTs, Ag-SWCNTs (m-40), cotton fabric coated with pristine SWCNTs and cotton fabric coated with Ag-SWCNTs (m-40). No one effective peaks are observed in Raman graph related to control cotton fabric. The graph corresponding to pristine SWCNTs coated cotton fabric has all effective peaks related

to SWCNTs which confirm the coating of SWCNTs on fabric. Raman graph of the fabric coated with Ag-SWCNTs (m-40) has enhanced peaks about RBMs, D-band, G-band and G' -band of SWCNTs which confirmed the coating of Ag-SWCNTs because enhancement can be attributed to SERS effect of Ag-NPs decorated on SWCNTs [59,60].

To further confirm the deposition of different nanoparticles on cotton fabric FE-SEM images were taken. Fig. 10 displays the FE-SEM images of control cotton fabric (A & E), cotton fabric treated with pristine Ag-NPs (B & F), cotton fabric treated with pristine SWCNTs (C & G), and cotton fabric treated Ag-SWCNTs (D & G) at different

magnification. It is clearly seen from Fig. 10(E) that the surface of control cotton fibre is clean and smooth. From Fig. 10(F), it is seen that the surface of cotton fibre is completely encapsulated by large number of spherical coagulated Ag-NPs which confirm the presence of pristine silver nanoparticles. Fig. 10(G) shows that cotton fibre is covered with network of nanotubes which confirm that fabric is coated with pristine SWCNTs. It is clearly observed from Fig. 10(H) that the surface of cotton fabric treated with Ag-SWCNT nanocomposite also covered with SWCNTs where individual silver nanoparticles are decorated uniformly.

3.4. Antibacterial performance of modified cotton fabric

The antibacterial activities of control and modified cotton fabrics were evaluated against *S. aureus* as gram positive and *E. coli* as gram negative pathogenic bacteria by inhibition zone test. Durability of antibacterial activity of cotton fabric modified by Ag-SWCNTs (m-40) nanocomposite was evaluated after 10 and 20 washings. Fig. 11 represents the visual aspect of antibacterial performance of uncoated and coated cotton fabric and Table 1 demonstrates the data of inhibition zone width. The data in Table 1 and images of agar plates containing bacteria in Fig. 10 show that all cotton swatches coated with different particles show anti-bacterial activity against both type of bacteria. It is also revealed from images and data that fabric coated with Ag-SWCNTs (m-40) has best antibacterial performance against both types of bacteria in comparison to unmodified cotton fabric and fabrics modified with other nanoparticles. While cotton fabric coated with pristine Ag-NPs portrayed moderate and fabric coated with pristine SWCNTs show least anti-bacterial activity. Cotton fabric coated with pristine SWCNTs has slightly more anti-bacterial activity against *S. aureus* as compare to *E. coli*. It is also observed that fabric coated with pristine Ag-NPs and Ag-SWCNTs (m-40) show more antibacterial performance against *E. coli* in comparison to *S. aureus*. The antibacterial performance of Ag-SWCNTs (m-40) coated fabric against both bacteria was slightly decreased after 10 and 20 washings but still comparable with fabric coated with Ag-NPs. Wash durability of antibacterial properties of cotton fabric coated with SWCNTs/Ag may attribute to strong adhesion of SWCNTs with underlying cotton fabric via large Vander wall forces and hydrogen bonding [61].

Excellent antibacterial performance of decoration of silver nanoparticles on SWCNTs surface may have number of reasons. When Ag-NPs interact with cell membrane of bacteria then nanoparticles react with proteins by getting attached to the thiol group and the proteins get inactivated. In this way, reproduction process of bacteria reduces and membrane also gets damaged. Some Ag-NPs may release silver ions which penetrate the bacteria cell and damage the DNA, or attack the respiratory chain, finally leading to cell death [62–64]. Smaller size of silver nanoparticles might have enhanced antibacterial activity which is attributed to increased density of edges and corner sites on the surfaces (more interaction of Ag-NPs with bacteria can take place). Additionally, the edges and corners have more co-ordinately unsaturated atoms (dangling bonds) so silver ions can easily release. These released silver ions disturb the respiratory system of bacteria which results in its death [13]. Therefore, excellent antibacterial performance of cotton fabric coated with Ag-SWCNTs nanocomposite may attribute to control size of silver nanoparticles and their well distribution on SWCNTs surface.

The antibacterial properties of cotton fabric finished with different materials were tabulated in Table 2. Data in Table 2 show that cotton fabric coated with Ag-SWCNTs nanocomposite had better antibacterial performance against *S. aureus* bacteria than AgCl embedded in a silica matrix, Ag/ZnO nanocomposites, Silver chloride compounds and slightly less than AgNPs-alginate composite, Monochlorotriazine triethyl phosphite guanidine (MCTPG) and ZnO but Ag-SWCNTs coated cotton fabric had more inhibition zone width against *E. coli* bacteria than fabric coated with all other materials.

4. Conclusions

We have demonstrated microwave assisted process to decorate Ag-NPs on SWCNTs for antibacterial active material without using strong reducing and capping agents. FT-IR and Raman spectroscopy analysis confirmed the attachment of carboxyl groups to surface of SWCNTs after refluxing in concentrated acidic solution for nucleation. Raman spectroscopy, XRD pattern and FESEM Images confirmed that Ag-NPs were uniformly decorated on SWCNTs within 40 s by irradiating microwave energy of average power 500 W at frequency 2450 MHz. To evaluate and compare the antibacterial activity, Ag-NPs decorated SWCNTs, Pristine SWCNTs and Pristine Ag-NPs were individually coated on different cotton fabrics by dip-dry-curing process. Raman spectroscopy and FE-SEM images confirmed the uniform coating of these particles on cotton fabric. Among these three nanoparticles coated cotton fabrics, the fabric modified by Ag-SWCNTs nanocomposite exhibit strongest antibacterial activity against both type of pathogenic bacteria *E. coli* as gram-negative and *S. aureus* as gram-positive. It is also reported that cotton fabric coated with Ag-SWCNTs nanocomposite have excellent antibacterial activity even after 20 washings. These results suggest that deposition of silver nanoparticles on SWCNTs by microwave heating can be good choice as an anti-bacterial material and have great potential to develop antibacterial fabric for textile industries.

Acknowledgements

The authors are thankful to DST, New Delhi and UGC, New Delhi for providing financial support under Department of Science and Technology, New Delhi (India) (DST-FIST) (SR/FST/PSI-162/2011) and University Grants Commission, New Delhi (India) (UGC-SAP) (F530/5/DRS/2012(SAP-1)) schemes, respectively.

References

- [1] S. Gordon, Y.-J. Hsieh, *Cotton: Science and Technology*, Woodhead Publishing, 2006.
- [2] J.W. Smith, R.L. Nichols, Barrier efficiency of surgical gown: are we really protected from our patients' pathogens? *Arch. Surg.* 126 (1991) 756–763.
- [3] S.A. Lavar, R.L. Nichols, J.W. Smith, A.C. Muzik, P.F. Pearce, Isolation gown: a false sense of security? *Am. J. Infect. Control* 20 (1992) 185–191.
- [4] A. Berendtsch, R. Khajou, M.E. Yazdanzhan, Fabrication of superhydrophobic and antibacterial surface on cotton fabric by doped silica-based sols with nanoparticles of copper. *Nanosc. Res. Lett.* 6 (2011) 394.
- [5] X. He, G. Zhang, X. Wang, R. Han, X. Huang, L. Qiu, B. Tang, X. Zhang, Biocompatibility, corrosion resistance and antibacterial activity of TiO₂/CaO coating on titanium. *Ceram. Int.* 43 (2017) 16185–16195.
- [6] H. Meriani, M. Alizadeh, N. Hadji, Synthesis of zirconium doped copper oxide (CuO) nanoparticles by the Pechini route and investigation of their structural and antibacterial properties. *Ceram. Int.* 44 (2018) 20289–20308.
- [7] R. Zhang, X. Liu, Z. Xiong, Q. Huang, X. Yang, H. Yan, J. Ma, Q. Jiang, Z. Shen, Silver-ionic nanostructured TiO₂/ZnO coating with antibacterial capacity and cytocompatibility. *Ceram. Int.* 44 (2018) 9711–9719.
- [8] M. Saha, D. Pedkova, J. Boyo, I. Perelshtein, A. Goshanker, T. Tzanov, Durable antimicrobial cotton textiles coated photochemically with ZnO nanoparticles embedded in an in-situ enzymatically generated bioadhesive. *Carbohydr. Polym.* 189 (2018) 198–203.
- [9] A.-K. Im, J.Y. Kim, H.-S. Kim, S. Cho, Y. Park, Y.S. Kim, Wound healing and antibacterial activities of chondroitin sulfate and acharan sulfate-reduced silver nanoparticles. *Nanotechnology* 24 (2013) 395102.
- [10] H. Klaseen, A historical review of the use of silver in the treatment of burns. II. Renewed interest for silver. *Burns* 26 (2000) 131–138.
- [11] M.A. Raza, Z. Kamal, A. Raut, A.N. Sabir, S. Biaz, S. Naseem, Alzein and shape dependent antibacterial studies of silver nanoparticles synthesized by wet chemical routes. *Nanomaterials* 6 (2016) 73.
- [12] Y. He, A.M. Jones, S. Garg, A.N. Pflam, I.D. White, Silver nanoparticles—reactive oxygen species interactions: application of a charging—discharging model. *J. Phys. Chem. C* 115 (2011) 5461–5468.
- [13] P.P. Fu, Q. Xia, H.-M. Hwang, P.C. Ray, H. Yu, Mechanisms of nanotoxicity: generation of reactive oxygen species. *J. Food Drug Anal.* 22 (2014) 64–75.
- [14] S. Iijima, Helical microtubules of graphitic carbon. *Nature* 354 (1991) 56.
- [15] R. Saito, G. Dresselhaus, M.S. Dresselhaus, *Physical Properties of Carbon Nanotubes*, World Scientific, 1998.
- [16] P. Lu, L. Gu, M.J. Meziani, X. Wang, P.C. Ray, J.M. Vega, L. Cao, Y.B. Sim, Advances in bioapplications of carbon nanotubes. *Adv. Mater.* 21 (2009) 130–152.

- [171] S. H. Cho, E. G. Cho, H. J. Park, S. H. Cho, H. J. Park, S. H. Cho, M. Terrones, S. H. Cho, Hydroxyl-functionalized and N-doped multiwalled carbon nanotubes decorated with silver nanoparticles preserve cellular function, *ACS Nano* 5 (2011) 2458–2468.
- [118] J. H. Schaffman, M. Elmehrich, Antibacterial activity of electrospun polymer mats with incorporated narrow diameter single-walled carbon nanotubes, *ACS Appl. Mater. Interfaces* 3 (2011) 462–468.
- [119] Y. Bai, L.S. Park, S.J. Lee, T.S. Bae, E. Watari, M. Do, M.H. Lee, Aqueous dispersion of surfactant-modified multiwalled carbon nanotubes and their application as an antibacterial agent, *Carbon* 49 (2011) 3663–3671.
- [120] S. Kang, M. Pinaud, L.D. Pfefferle, M. Elmehrich, Single-walled carbon nanotubes exhibit strong antimicrobial activity, *Langmuir* 23 (2007) 8670–8673.
- [121] S. Kang, M. Hertzberg, D.E. Rodrigues, M. Elmehrich, Antibacterial effects of carbon nanotubes: size does matter!, *Langmuir* 24 (2008) 6409–6413.
- [122] S. Liu, J. Wei, L. Huo, N. Tang, M.W. Chang, R. Yu, Y. Yang, Y. Chen, Sharper and faster “nano darts” kill more bacteria: a study of antibacterial activity of individually dispersed pristine single-walled carbon nanotube, *ACS Nano* 3 (2009) 3891–3892.
- [123] C. Yang, J. Manouq, Y. Tang, L. Yang, Antimicrobial activity of single-walled carbon nanotubes: length effect, *Langmuir* 26 (2010) 16013–16019.
- [124] B.C. Ma, E.Z. Tang, J.-K. Kim, Effect of CNT decoration with silver nanoparticles on electrical conductivity of CNT/polymer composites, *Carbon* 46 (2008) 1497–1505.
- [125] D.F. Andrade, M.F. Costa, Synthesis and characterization of silver nanoparticles decorated carbon nanotube composites, *J. Nanomater.* 2014 (2014) 90.
- [126] X. Tang, S.-H. Cho, S. Cho, N. Zhang, B. Fan, R. Li, X. Liu, Y. X. Pan, Immobilization of human hepatitis Ag nanoparticles on carbon nanotubes using electro-assisted reduction: antibacterial performance, *ACS Appl. Mater. Interfaces* 5 (2013) 17069–17073.
- [127] J. Y. Jung, Y. Hayashi, H. Takizawa, Synthesis of carbon nanotube/silver nanocomposites by ultrasonication, *Mater. Trans.* 51 (2010) 1769–1772.
- [128] I. Menéndez Zúñiga, C. Torres Torres, M. Trejo-Valdez, R. Torres Martínez, J. Coronado-Sodi, J.R. Vargas-García, Influence of silver decoration on the nonlinear optical absorption exhibited by multiwall carbon nanotubes, *J. Nanopart.* 164 (2014) 2334.
- [129] N.N. Dind, N.V. Ouy, T.Q. Hai, A. T. Le, Decoration of silver nanoparticles on multiwalled carbon nanotubes: antibacterial mechanism and ultrastructural analysis, *J. Nanomater.* 16 (2015) 63.
- [130] Y. Seo, J. Hwang, J. Kim, Y. Jeong, M.P. Hwang, J. Choi, Antibacterial activity and cytotoxicity of multi-walled carbon nanotubes decorated with silver nanoparticles, *Bull. J. Nanomed.* 9 (2014) 4621.
- [131] J. Ovescanin, A. Kikles, Z. Kacarevic-Popovic, M. Mitric, Z. Rakocovic, D. Trpkov, G. Noskovic, Functionalization of carbon nanotubes with silver clusters, *Appl. Surf. Sci.* 256 (2010) 7048–7055.
- [132] A.J. Haide, M. Mohammed, R.A.J. Al-Mulla, D.S. Ahmed, Synthesis of silver nanoparticles decorated carbon nanotubes and its antimicrobial activity against growth of bacteria, *Res. Limos.* 25 (2014) 803–807.
- [133] Y. He, Y. Liu, H. Qian, Z. Li, J. Chen, Coating colloidal carbon spheres with CdS nanoparticles: microwave-assisted synthesis and enhanced photocatalytic activity, *Langmuir* 26 (2010) 18770–18775.
- [134] G. Calvino, R.A. Davoglio, J.W. Harris, J.F. Marco, E.C. Pereira, S.R. Baggio, H. Varela, A. Queiro, Microwave-assisted synthesis of Pd/Au nanoparticles with enhanced electrocatalytic activity for the oxidation of formic acid, *Electrochim. Acta* 53 (2008) 58–64.
- [135] P.H. Santiago, C. Kaciroti, M.F. Thillipremu, High-speed but not magic: microwave-assisted synthesis of ultra-small silver nanoparticles, *Langmuir* 34 (2017) 142–153.
- [136] A. Wadhawan, D. Garroti, J.M. Perez, Nanoparticle-assisted microwave absorption by single-wall carbon nanotubes, *Appl. Phys. Lett.* 83 (2003) 2683–2685.
- [137] Y. Chen, Z. Qian, S. Mitra, Microwave-induced controlled purification of single-walled carbon nanotubes without sidewall functionalization, *Adv. Funct. Mater.* 17 (2007) 3985–3991.
- [138] C. Ferrate, C. Kim, H. Gutierrez, L. Pan, E. Drake, P.C. Brédas, Tebunliny and oxidation of single-walled carbon nanotubes in amide solvents, *J. Am. Chem. Soc.* 126 (2004) 6095–6105.
- [139] S. Hussain, P. Jha, A. Chouksey, R. Raman, S. Islam, F. Islam, P. Choudhary, Spectroscopic investigation of modified single wall carbon nanotube (SWCNT), *J. Mod. Phys.* 2 (2011) 538–543.
- [140] B.Y. Lee, H.K. Park, Y.M. Lee, S. Kim, S.B. Park, A practical procedure for producing silver nanocoated fabric and its antibacterial evaluation for biomedical applications, *Chem. Commun.* (2007) 2959–2961.
- [141] L. Wang, L. Ge, T.E. Rufford, J. Chen, W. Zhou, Z. Zhu, Y. Radolph, A comparison study of catalytic oxidation and acid oxidation to prepare carbon nanotubes for filling with Bi nanoparticles, *Carbon* 49 (2011) 2022–2032.
- [142] D.E. Fanning, M.A. Vanucci, A DRIFTS study of the formation of surface groups on carbon by oxidation, *Carbon* 33 (1993) 721–730.
- [143] J. Zhang, H. Zou, Q. Qing, Y. Yang, Q. Li, Z. Liu, Y. Guo, Z. Liu, Effect of chemical oxidation on the structure of single-walled carbon nanotubes, *J. Phys. Chem. B* 107 (2003) 3712–3718.
- [144] V. Gomez-Serrano, I. Barja-Alameda, C. E. Durán-Villal, J. Pastor-Villégas, Formation of oxygen structures by air activation: A study by Raman spectroscopy, *Carbon* 37 (1999) 1517–1525.
- [145] A.R.K. Kumar, S.-J. Jung, W.-J. Yang, Effective adsorption of chromium (VI)/Cr(III) from aqueous solution using ionic liquid functionalized multiwalled carbon nanotubes as a super sorbent, *J. Mater. Chem. A* 3 (2015) 7044–7057.
- [146] A.C. Dillon, J. Gennett, K.M. Jones, J.L. Alleman, P.A. Parilla, M.J. Heben, A simple and complete purification of single-walled carbon nanotube materials, *Adv. Mater.* 11 (1999) 1354–1358.
- [147] M. Itkis, D. Perea, S. Niyogi, J. Lovy, J. Tang, A. Yu, C. Kang, R. Jung, R. H. Hsu, Optimization of the Ni–Y catalyst composition in bulk electric arc synthesis of single-walled carbon nanotubes by use of near-infrared spectroscopy, *J. Phys. Chem. B* 108 (2004) 12770–12775.
- [148] M. Milosević, J. Kirtić, M. Halman, H. Kuzumcu, Periodic resonance excitation of intertube interaction from quasicontinuous distributed helicities in single wall carbon nanotubes, *Phys. Rev. Lett.* 84 (2000) 1324.
- [149] M. Martínez, M. Callejos, A. Benito, M. Cochet, T. Seeger, A. Anson, J. Schreiber, C. Gordon, C. Marčić, O. Chauvet, Sensitivity of single wall carbon nanotubes to oxidative processing: structural modification, intercalation and functionalization, *Carbon* 41 (2003) 2247–2256.
- [150] W. Wu, M. Wu, Z. Sun, G. Li, Y. Ma, X. Liu, X. Wang, X. Chen, Morphology controllable synthesis of silver nanoparticles: optical properties study and SERS application, *J. Alloy. Compd.* 579 (2013) 117–123.
- [151] S.-W. Han, S.-J. Oh, L.-S. Tan, J.-B. Baek, One-pot purification and functionalization of single-walled carbon nanotubes in less-corrosive poly (phosphoric acid), *Carbon* 46 (2008) 1841–1849.
- [152] F. Liu, Z. Cao, C. Tang, L. Chen, Z. Wang, Ultrahigh diamond-like carbon film coated silver nanoparticles-based substrates for surface-enhanced Raman spectroscopy, *ACS Nano* 4 (2010) 2643–2648.
- [153] S. Suzuki, M. Yoshimura, Chemical stability of graphene coated silver substrates for surface-enhanced Raman scattering, *Sci. Rep.* 7 (2017) 14851.
- [154] Perelshtein, G., Appierot, N., Perkas, G., Guibert, S., Mikhailov, A., Gedanken, Sonochemical coating of silver nanoparticles on textile fabrics (nylon, polyester and cotton) and their antibacterial activity, *Nanotechnology* 19 (2008) 245705.
- [155] Martina, R. Wiesinger, D. Jembrih-Simbürger, M. Schreiner, Micro-Raman characterization of silver corrosion products: instrumental set up and reference database, *P-Preserv. Sci.* (2012) 1–8.
- [156] J. Zhang, X. Zhang, C. Lai, H. Zhou, Y. Zhu, Silver-decorated aligned CNT arrays as SERS substrates by high temperature annealing, *Opt. Express* 21 (2013) 21157–21166.
- [157] Y.-C. Chen, R.J. Young, J.V. Macpherson, N.H. Wilson, Single-walled carbon nanotube networks decorated with silver nanoparticles: a novel graded SERS substrate, *J. Phys. Chem. C* 111 (2007) 16167–16173.
- [158] H. Song, K. Ko, I. Oh, B. Lee, Fabrication of silver nanoparticles and their antimicrobial mechanism, *Eur. Cells Mater.* 11 (2006) 58.
- [159] J.S. Kim, E. Kuk, K.N. Yu, J.-H. Kim, S.J. Park, H.J. Lee, S.H. Kim, Y.K. Park, Y.H. Park, C.-Y. Hwang, Antimicrobial effects of silver nanoparticles, *Nanomed. Nanotechnol. Biol. Med.* 3 (2007) 95–101.
- [160] S. Prabhu, E.K. Poulouse, Silver nanoparticles: mechanism of antimicrobial action, synthesis, medical applications, and toxicity effects, *Int. Nano Lett.* 2 (2012) 32.
- [161] C.-E. Zhou, C.-W. Kan, J.P. Macfutura, J.K.-H. Tsai, Regenerable Antibacterial cotton fabric by plasma treatment with dimethylhydantoin: antibacterial activity against *S. aureus*, *Coatings* 7 (2017) 11.
- [162] B. Tomić, B. Simonović, B. Oreš, M. Žerjav, H. Schreiers, A. Simonović, Z. Samardžija, Antimicrobial activity of AgCl embedded in a silica matrix on cotton fabric, *Carbohydr. Polym.* 75 (2009) 618–626.
- [163] M. Jbran, S. Perero, M. Mhola, G. Miano, A. Ferri, M. Ferraris, C. Balagna, Antimicrobial functionalization of cotton fabric with silver nanoclusters/silica composite coating via RF co-sputtering technique, *Cellulose* 24 (2017) 2311–2345.
- [164] M. Shater-Khalilabadi, M.F. Yazdanzhas, Bifunctionalization of cotton textiles by ZnO nanostructures: antimicrobial activity and ultraviolet protection, *Text. Res. J.* 83 (2013) 993–1004.
- [165] M. Bănescu, V. Musat, T. Teodor, V. Badilita, B. Mălbîg, Photocatalytic and antimicrobial Ag–ZnO nanocomposites for functionalization of textile fabrics, *J. Alloy. Compd.* 610 (2014) 244–249.
- [166] C. Dong, P. He, Z. Lu, S. Wang, S. Su, J. Liu, J. Zhang, P. Zhu, Preparation and properties of cotton fabrics treated with a novel antimicrobial and flame retardant containing triazine and phosphorus components, *J. Therm. Anal. Calorim.* 131 (2018) 1079–1087.
- [167] S. Ghosh, S. Yadav, N. Reynolds, Antibacterial properties of cotton fabric treated with silver nanoparticles, *J. Text. Inst.* 101 (2010) 917–924.
- [168] M. Zahra, H.B. Ahmed, M. El-Rafie, Surface modification of cotton fabric for antibacterial application by coating with AgNPs–alginate composite, *Carbohydr. Polym.* 108 (2014) 145–152.
- [169] R. Zhang, X. Liu, Z. Xiong, Q. Huang, X. Yang, H. Yan, J. Ma, Q. Peng, Z. Shen, Novel micro/nanostructured TiO₂/ZnO coating with antibacterial capacity and cytocompatibility, *Ceram. Int.* (2018).
- [170] S.-C. Huang, K.M. Jhsieh, T.W. Chang, Y.C. Chen, C.-T.R. Yen, T.-C. Lo, C.F. Liu, E.-Y. Yu, T.-I. Wang, H. Chen, ZnO nanoflakes on silver wires with antibacterial effects, *Ceram. Int.* 42 (2016) 7848–7851.
- [171] A.S.K. Kumar, S.-J. Jung, W.-J. Yang, Effective adsorption of chromium (VI)/Cr(III) from aqueous solution using ionic liquid functionalized multiwalled carbon nanotubes as a super sorbent, *J. Mater. Chem. A* 3 (2015) 7044–7057.
- [172] K. Joshi, G. Dion, Y. Gogotsi, Textile energy storage in perspective, *J. Mater. Chem. A* 2 (2014) 10776–10787.

Modelling and analysis of two-unit hot standby database system with random inspection of standby unit

Amit Manocha*

Department of Mathematics,
T.I.T.S.,
Bhiwani, Haryana 127021, India
Email: amitmanocha80@yahoo.com
*Corresponding author

Gulshan Taneja

Department of Mathematics,
M.D. University,
Rohtak, Haryana 124001, India
Email: drgtaneja@gmail.com

Sukhvir Singh

Department of Information Technology,
iNurture Education Solutions Pvt. Ltd.,
Bangalore, Karnataka 560052, India
Email: boora_s@yahoo.com

Rahul Rishi

Department of Computer Science,
U.I.E.T.,
M.D. University,
Rohtak, Haryana 124001, India
Email: rahulrishi@rediffmail.com

Abstract: Stochastic model for a two-unit hot standby database system comprising of one operative (primary unit) and one hot standby unit has been developed. The primary unit acts as production unit which is synchronised with hot standby unit through online transfer of archive redo logs. The data being saved in the primary unit gets simultaneously stored in the hot standby unit. The different modes of failure of primary database have been considered. To avoid loss of data, random inspection of the standby unit is carried out by a database administrator (DBA) to see as to whether redo log files are created/updated in standby unit or not. The repair of the failed unit and creation/update of redo log files are also done by the DBA. The system is analysed using semi-Markov process and regenerative point technique. Mathematical expressions for various performance measures of the system

have been obtained along with cost-benefit analysis of the system. Numerical analysis has been done to validate the derived results. Bounds for various parameters have also been obtained with regard to profitability of the system.

Keywords: database system; hot standby; random inspection; semi-Markov process; regenerative point technique; stochastic modelling; system effectiveness; cost-benefit analysis; profitability; bounds.

Reference to this paper should be made as follows: Manocha, A., Taneja, G., Singh, S. and Rishi, R. (2019) 'Modelling and analysis of two-unit hot standby database system with random inspection of standby unit', *Int. J. Mathematics in Operational Research*, Vol. 15, No. 2, pp.156–180.

Biographical notes: Amit Manocha is working as an Assistant Professor in Department of Mathematics at Technological Institute of Textile and Sciences, Bhiwani, Haryana, India. He has been teaching mathematics to BTech/MTech students for last the 16 years. He did his PhD in Mathematics from National Institute of Technology, Kurukshetra. He has been involved in research activities from the last 14 years and published 13 research papers in various journals of national/international repute and proceedings of the conferences. He has participated in around 12 national/international conferences/seminars. He is an active member of various academic societies/associations. His area of interest is reliability modelling.

Gulshan Taneja is a Professor in the Department of Mathematics, MD University, Rohtak, Haryana, India with 29 years of teaching and research experience. He is an Associate Editor/Editor/Reviewer of some journals. He supervised 24 PhD/MPhil dissertations and completed two research projects successfully. He has published over 100 research papers in journals of repute and over 35 in the proceedings of conferences. He contributed in over 50 conferences, organising seven out of them. He authored six books and edited six books/proceedings of conferences. He is an office bearer/member of various academic societies/associations. His areas of interest are reliability modeling, queuing theory and information theory.

Sukhvir Singh is working as an Academic Head-North in Department of Information Technology, iNurture Education Solutions Pvt. Ltd., Bangalore, Karnataka, India. He has more than 20 years of teaching and research experience. He received his Master degree in Technical Sciences from State University of Armenia. He did his PhD in Engineering and Technology from Maharshi Dayanand University, Rohtak. He has published over 50 research papers in national/international journals and proceedings of various conferences. He has delivered expert lectures in various conferences/seminars/workshops. His areas of interest are reliability, software engineering, computer networks and network and information security.

Rahul Rishi is a Professor of Computer Science and Engineering at the University Institute of Engineering and Technology, Maharshi Dayanand University, Rohtak, Haryana, India. He did his BTech, MTech and PhD in the area of computer science. He has over 100 research publications in national and international journals and conferences of repute. He has supervised 11 students for PhD and 50 students for MTech dissertations. With a teaching experience of 20 years, he is actively involved in research in the areas of reliability, databases, soft computing and antennas.

1 Introduction

Data management in terms of handling, security, reliability and availability is imperative factor in today's technological era and globalised work situations. With the comprehensive progress in computation speed of automated systems, online business and financial transactions have become easier and faster with the use of database systems. The continuous data archiving is important for supplementary reporting as well as prevention in case of catastrophic failure of the primary database unit and that can be achieved by using a standby unit. Reliability models for various systems considering the concept of catastrophic failure was developed by some researchers such as Kumar and Kapoor (2013) and Ram and Manglik (2016). Kumar and Kapoor (2013) did the economic and performance evaluation of base transceiver system wherein, different modes of operation of the system and catastrophic failure were taken into account. Ram and Manglik (2016) proposed a mathematical model for multi-state complex repairable manufacturing system with four types of failure, i.e., common cause, partial, human and catastrophic failure. Supplementary variable technique and Laplace transform were used to evaluate various reliability characteristics. Cost-benefit and sensitivity analysis were also carried out.

However, the catastrophic failures in case of hot standby database system, which are worth considering, are not addressed in earlier studies. The study of reliability and availability of a system comprising primary as well as standby database is very important as in such automated systems, even a small error may further lead to failure and put a substantial adverse impact on its operation. Such systems are commonly designed by Oracle corporation (RDBMS Oracle and open source DBMS MySQL), Microsoft Corporation (Microsoft Access and Microsoft SQL Server) and IBM (DB2). These systems play pivotal role in handling and securing data for various industries like telecommunication, automobile, gas and oil, transportation, education, medical, finance, marketing, banking, textile, garments sectors, etc. Singh et al. (2013) examined the reliability and availability of database system with number of standby units provided by system provider. Cost factor for having multiple standby units was not taken into consideration by the authors. Gaikwad and Raut (2014) reviewed various issues of threats that may damage the integrity and reliability of database system along with taking into account the level, requirement, guidelines and techniques for database security. Khattab et al. (2015) introduced a layer-by-layer tuning framework (MAG) to predict, analyse and control the performance of database systems which was mainly based on the neural networks.

Manocha et al. (2017) investigated the stochastic behaviour of database system comprising two units – one primary and the hot standby. The hot standby database unit is kept in synchronisation with primary database unit and redo log files are created/updated online in it, if everything is going fine. However, the possibility of non-creation/non-updation of redo log files in it cannot be ruled out and this is observed only at the time of failure of primary unit. This may cause the serious loss of data and hence there is need to introduce the concept of random inspection of the standby unit to ensure the proper creation/updation of redo log files in it and this will lead to the enhancement of reliability and availability of the system.

Thus, keeping the above in view, our aim is to develop a more reliable and less costlier model and hence the present study deals with a database system comprising one primary production database unit synchronised with a hot standby unit through online

transfer and simultaneous archiving of redo log together with the random inspection by the database administrator (DBA). The rest of the paper is structured as follows. In Section 2, review of literature relevant to the study is discussed. Section 3 gives brief description of the system along with the assumptions made to carry out the analysis. The methodology and nomenclature used are mentioned in Sections 4 and 5, respectively. By making use of semi-Markov processes and regenerative point technique, modelling of the system is done in Section 6. Transition probabilities and mean sojourn times are also obtained in this section. Mathematical expressions for various measures of system effectiveness are obtained in Section 7. Section 8 is devoted to the cost-benefit analysis of the system. Numerical results are given in Section 9. Concluding remarks are offered in Section 10.

2 Review of literature

An extensive work on modelling of various systems has been done in the field of reliability by various researchers including the following:

Tuteja and Taneja (1992) studied the cost-benefit analysis of a two-unit warm standby system. They considered failure of main unit directly from normal state or via a partial failure along with two types of repair facilities- regular repairman and an expert repairman.

Singh and Mishra (1994) carried out profit analysis for two-unit cold standby system. They considered different modes of failure of unit i.e. entering the system into the total failure mode from the normal failure mode only after passing through the partial failure mode. A single repair facility was considered in their study.

Mokaddis et al. (1997) analysed a single server two-unit (priority and ordinary) warm standby system subjected to degradation of priority unit from excellent to good level as well as good to satisfactory level before it gets failed. The priority unit has priority for both operation as well as repair.

Parashar and Taneja (2007) collected data on various rates/costs for PLC hot standby system. They developed stochastic model to evaluate the reliability and profit for such a system configured in master-slave concept. The real practical situations were incorporated in their study.

El-Damcese (2009) did the reliability and availability analysis of a K-out-of-(M + S): G warm standby system. The time varying failure and repair rates in presence of common-cause failure were taken into consideration.

Beith et al. (2010) studied a two-unit cold standby system with regular repairman as well as visiting expert. The concept of random and deterministic patience time for regular repairperson was discussed assuming that the expert leaves only after repairing all the units which fail during his stay at the system.

Mahmoud and Mosherf (2010) did the stochastic analysis of a two-unit cold standby system considering hardware, human error failure and preventive maintenance. All the time distributions were taken arbitrary in their study. Various measures of system effectiveness were obtained and cost analysis was carried out.

Mathews et al. (2011) carried out reliability analysis of an identical two-unit parallel continuous casting plant using the maintenance data collected from a steel production plant.

Shakuntla et al. (2011) carried out reliability analysis of a polytube manufacturing plant having four subunits. Supplementary variable technique was used to derive Chapman-Kolmogorov differential equations. Effect of various failure/repair rates of subunits were discussed on the overall availability of the system.

Jain and Gupta (2013) obtained the reliability indices for a repairable system consisting of single repairman, who can take multiple vacations. The imperfect coverage of faults during major failures was also taken into account. The authors proposed an optimal replacement policy to maximise the expected profit in the long-run for the system.

Jain and Gupta (2014) used an irreducible Markov process to analyse the availability of repairable redundant system consisting of N -non-identical components and S -warm standby components. Concept of three types of failure subjected to common cause failure of the system with single repair facility was dealt with. Sensitivity analysis of the system with respect to different parameters was also done.

Yusuf et al. (2014) analysed a 2-out-of-4 cold standby system stochastically. The concept of four types of failure dealt by four different repairmen was taken into consideration. System reliability indices and profit functions were obtained using Kolmogorov's forward equation method.

Yusuf (2015) evaluated availability of the system subjected to minor deterioration after imperfect repair. The optimal availability level of system was also obtained numerically.

Jia et al. (2016) introduced active switching policy in addition to common switching policy for two-unit standby system without repair. Expressions for survival function and mean time to system failure (MTSF) were determined. They proposed system with active switching policy to be more reliable than common switching policy system.

Kumar and Batra (2016) developed a stochastic model for printed circuit board manufacturing process. Various performance indicating measures of the system were obtained. Numerical results were obtained using the values of various parameters estimated on the basis of the data collected.

Goyal et al. (2017) developed probabilistic model for solar thermal power plant. Three types of failure, which generally occurs in the plant, were taken into account while developing the model. System was analysed using Markov process and supplementary variable technique.

3 System description and assumptions

Figure 1 shows the functioning of two-unit hot standby database wherein redo log files are created at primary site and are archived at the standby site which acts as a hot standby. The standby database unit is kept in synchronisation with primary database unit through online redo log files. On failure of the primary unit, the standby unit becomes the production unit and the failed unit goes under repair of the DBA instantaneously. The following mutually exclusive and exhaustive situations may be observed on failure of the primary unit:

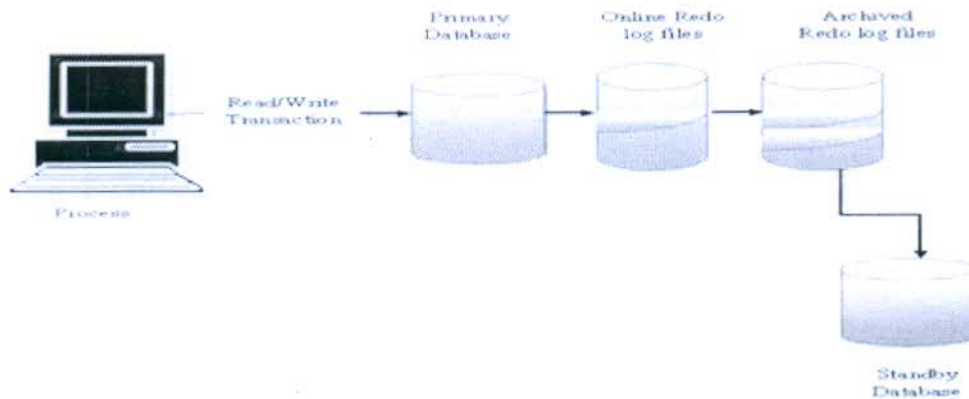
- 1 standby unit working in synchronous with primary unit
- 2 redo log files are not updated in standby unit

3 redo log files are not created in standby unit.

In either of the above mentioned situations, redo log files are created/updated in the standby unit by the DBA before making it to act as production database, i.e., like primary unit. Cost for using the standby unit during the time it act as the primary unit is paid by the user itself. Random inspection of the standby unit is performed by the DBA to check whether the standby unit is synchronous with primary unit so as to avoid any of the above mentioned three situations on failure of the primary unit. The proposed system has a single repair facility, i.e., DBA who performs random inspection of the standby unit, undertakes the repair of the failed unit and creates/updates redo log files in standby database unit, if required.

The cost incurred for engagement of the DBA is meted out by the user. It is assumed that after each repair, the system works as good as new. All failure times are assumed to have exponential distribution whereas repair times, time for creating/updating of redo log files and time to inspection have general distributions.

Figure 1 Two-unit hot standby database system



4 Material and methods

Branson and Shah (1971) used semi-Markov process to analyse the reliability of two-unit standby system with exponential failure time and general repair time distributions. Srinivasan and Gopalan (1973) concentrated on regenerative point technique while analysing a probabilistic model for a two-unit warm standby system with single repair facility. In the proposed study, semi-Markov process and regenerative point technique have been used to develop a discrete state space and continuous time stochastic model for a two-unit hot standby database system, wherein standby unit is kept under random inspection. Various measures of system effectiveness such as MTSF, mean time to failure of primary database unit (MTFP), availability of primary database unit, busy period of DBA, expected number of visits by the DBA and finally, the expression for the profit function is obtained by formulating recursive relations using convolutions, Laplace-Stieljes, Laplace transforms. etc. MATLAB/MS Excel is used to accomplish the numerical analysis done on the basis of data collected on database system from various users of the system. Bounds for profitability of the system have also been obtained.

5 Nomenclatures

λ	Constant failure rate of primary database unit
α	constant failure rate of standby database unit
p_1	probability that hot standby unit is synchronous with primary unit on the failure of primary unit
p_2	probability that redo log files are not updated in hot standby database unit on the failure of primary database unit
p_3	probability that redo log files are not created in hot standby database unit on the failure of primary database unit
$q_1/q_2/q_3$	probability that after random inspection standby database unit is working fine/redo log files are not updated in standby database unit/redo log files are not created in standby database unit
$M_i(t)$	probability that primary database unit up initially in regenerative state i is up at time t without passing through any other regenerative state or returning to itself through one or more non-regenerative states
$g(t)/G(t)$	pdf/cdf of the time for repairing the primary database unit
$g_1(t)/G_1(t)$	pdf/cdf of the time for repairing the standby database unit
$h_1(t)/H_1(t)$	pdf/cdf of the time for updating the redo log files in the standby database unit
$h_2(t)/H_2(t)$	pdf/cdf of the time for creating the redo log files in the standby database unit
$i(t)/I(t)$	pdf/cdf of the time for undertaking the standby database unit for inspection
$q_{ij}(t)/Q_{ij}(t)$	pdf/cdf of time for the system transits from regenerative state i to j
$q_{ij}^{(k)}(t)/Q_{ij}^{(k)}(t)$	pdf/cdf of time for the system transits from regenerative state i to j via non-regenerative state k
\otimes/\odot	symbol for Stieltjes/Laplace convolution
**/*	symbol for Laplace-Stieltjes/Laplace transformation.

6 Modelling of the system

Symbols for the states of the system are:

P_0	primary database unit is operative
$H_s/H_r/H_R$	hot standby (database)/under repair/repair from previous state
S_0	hot standby database unit is used as primary database unit

$S_r/S_w/S_R$	hot standby unit (used as primary database unit) is under repair/waiting for repair/repair from previous state
$F_r/F_w/F_R$	failed unit under repair/waiting for repair/repair from previous state
$P_f H_S A \bar{D}$	primary database unit fails and redo log files are not updated in hot standby database unit
$P_f H_S \bar{A}$	primary database unit fails and redo log files are not created in hot standby database unit
$H_S A \bar{D}$	redo log files are not updated in hot standby database unit
$H_S \bar{A}$	redo log files are not created in hot standby database unit.

Considering these symbols, the system can be in any one of the following states:

State 0	(P_0, H_S)
State 1	$(P_0, H_S A \bar{D})$
State 2	$(P_0, H_S \bar{A})$
State 3	$(P_f H_S A \bar{D})$
State 4	$(P_f H_S \bar{A})$
State 5	(F_r, S_0)
State 6	(P_0, H_r)
State 7	(F_w, H_R)
State 8	$(F_w, H_S A \bar{D})$
State 9	$(F_w, H_S \bar{A})$
State 10	(F_R, S_w)
State 11	(P_0, S_r)
State 12	(F_w, S_R)

Possible transitions of the system are shown in Figure 2

Here, $E = \{0, 1, 2, 3, 4, 5, 6, 11\}$ is a set of regenerative states and $\bar{E} = \{7, 8, 9, 10, 12\}$ is a set of non-regenerative states. States 7, 8, 9, 10 and 12 are failed states, whereas 3 and 4 are down states. Let $T_0 (\equiv 0), T_1, T_2, \dots$ be the epochs at which system enters to any state $i \in E$ and let X_n be the state visited at epoch in T_{n+1} , i.e., just after transition at T_n . Then, $\{X_n, T_n\}$ is a Markov-renewal process with state space E . Let $q_{ij} = P\{X_{n+1} = j, T_{n+1} - T_n \leq t \mid X_n = i\}$ semi-Markov kernel over E . The transition probability matrix (t.p.m.) of the embedded Markov chain is, therefore, given by

$$P = (p_{ij}) = [q_{ij}(\infty) = q(\infty)]$$

where

$$p_{00} = \int_0^{\infty} e^{-(\lambda+\alpha)t} q_1 i(t) dt$$

$$p_{01} = \int_0^{\infty} e^{-(\lambda+\alpha)t} q_2 i(t) dt$$

$$p_{02} = \int_0^{\infty} e^{-(\lambda+\alpha)t} q_3 i(t) dt$$

$$p_{03} = \int_0^{\infty} p_2 \lambda e^{-(\lambda+\alpha)t} \bar{I}(t) dt$$

$$p_{04} = \int_0^{\infty} p_3 \lambda e^{-(\lambda+\alpha)t} \bar{I}(t) dt$$

$$p_{05} = \int_0^{\infty} p_1 \lambda e^{-(\lambda+\alpha)t} \bar{I}(t) dt$$

$$p_{06} = \int_0^{\infty} \alpha e^{-(\lambda+\alpha)t} \bar{I}(t) dt$$

$$p_{10} = \int_0^{\infty} e^{-\lambda t} h_1(t) dt$$

$$p_{15}^{(8)} = \int_0^{\infty} (\lambda e^{-\lambda t} \odot 1) h_1(t) dt$$

$$p_{20} = \int_0^{\infty} e^{-\lambda t} h_2(t) dt$$

$$p_{25}^{(9)} = \int_0^{\infty} (\lambda e^{-\lambda t} \odot 1) h_2(t) dt$$

$$p_{35} = \int_0^{\infty} h_1(t) dt$$

$$p_{45} = \int_0^{\infty} h_2(t) dt$$

$$p_{50} = p_{11,0} = \int_0^{\infty} e^{-\lambda t} g(t) dt$$

$$p_{5,11}^{(10)} = p_{11,5}^{(12)} = \int_0^{\infty} (\lambda e^{-\lambda t} \odot 1) g(t) dt$$

$$p_{60} = \int_0^{\infty} e^{-\lambda t} g_1(t) dt$$

$$p_{65}^{(7)} = \int_0^{\infty} (\lambda e^{-\lambda t} \odot 1) g_1(t) dt$$

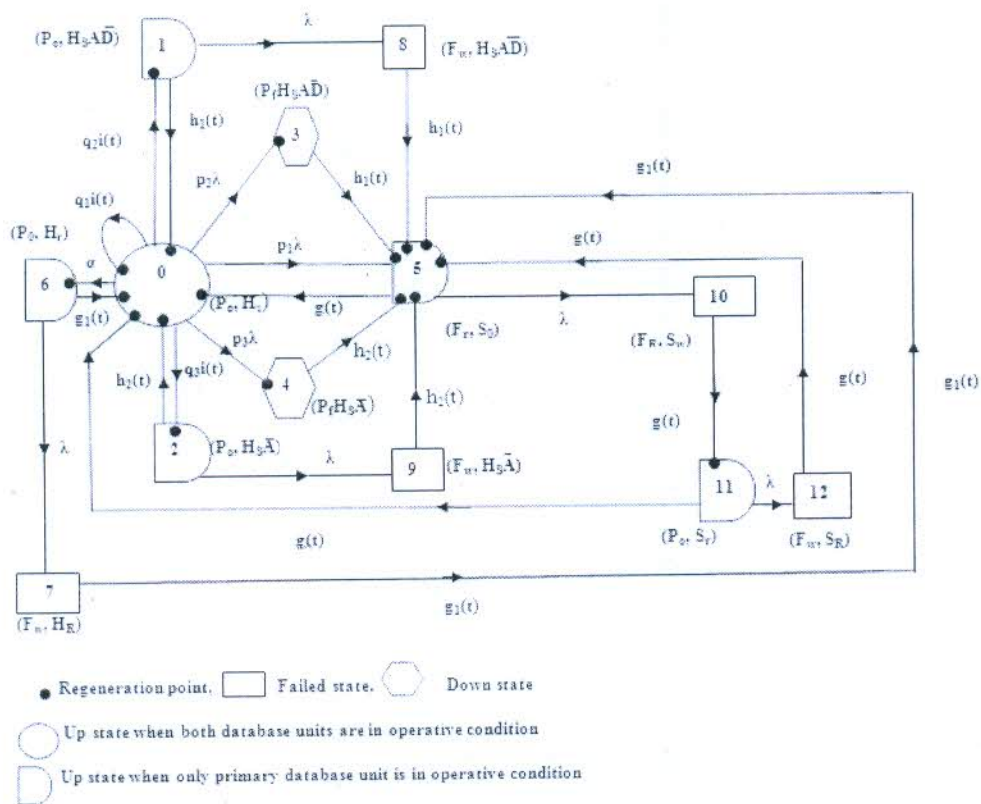
$$p_{5,10} = p_{11,12} = \int_0^{\infty} \lambda e^{-\lambda t} \bar{G}(t) dt$$

$$p_{18} = \int_0^{\infty} \lambda e^{-\lambda t} \bar{H}_1(t) dt$$

$$p_{29} = \int_0^{\infty} \lambda e^{-\lambda t} \bar{H}_2(t) dt$$

$$p_{67} = \int_0^{\infty} \lambda e^{-\lambda t} \bar{G}_1(t) dt$$

Figure 2 State transitions



It can be verified that:

$$p_{00} + p_{01} + p_{02} + p_{03} + p_{04} + p_{05} + p_{06} = 1$$

$$p_{10} + p_{18} = 1$$

$$p_{10} + p_{15}^{(8)} = 1$$

$$p_{20} + p_{29} = 1$$

$$p_{20} + p_{25}^{(9)} = 1$$

$$p_{35} = p_{45} = 1$$

$$p_{50} + p_{5,10} = 1$$

$$p_{50} + p_{5,11}^{(10)} = 1$$

$$p_{60} + p_{67} = 1$$

$$p_{60} + p_{65}^{(7)} = 1$$

$$p_{11,0} + p_{11,12} = 1$$

$$p_{11,0} + p_{11,5}^{(12)} = 1$$

Mean sojourn time in regenerative state i is defined as the time of stay in state i before transition to any other state. If T denotes the sojourn time in state i , then the mean sojourn time is

$$\mu_i = \int_0^{\infty} P(T > t) dt$$

Considering the above result, we can obtain the following expressions:

$$\mu_0 = \int_0^{\infty} e^{-(\lambda+\alpha)t} \bar{I}(t) dt$$

$$\mu_1 = \int_0^{\infty} e^{-\lambda t} \bar{H}_1(t) dt$$

$$\mu_2 = \int_0^{\infty} e^{-\lambda t} \bar{H}_2(t) dt$$

$$\mu_3 = \int_0^{\infty} \bar{H}_1(t) dt$$

$$\mu_4 = \int_0^{\infty} \bar{H}_2(t) dt$$

$$\mu_5 = \mu_{11} = \int_0^{\infty} e^{-\lambda t} \bar{G}(t) dt$$

$$\mu_6 = \int_0^{\infty} e^{-\lambda t} \bar{G}_1(t) dt$$

The unconditional time taken by system to transit for any regenerative state j when it (time) is counted from the epoch of entrance into state i is mathematically stated as

$$m_{ij} = \int_0^{\infty} t dQ_{ij}(t) = q_{ij}^*(0)$$

Thus:

$$m_{00} + m_{01} + m_{02} + m_{03} + m_{04} + m_{05} + m_{06} = \mu_0$$

$$m_{10} + m_{18} = \mu_1$$

$$m_{10} + m_{15}^{(8)} = m_{35} = \mu_3$$

$$m_{20} + m_{29} = \mu_5$$

$$m_{20} + m_{25}^{(9)} = m_{45} = \mu_4$$

$$m_{50} + m_{5,10} = \mu_5$$

$$m_{50} + m_{5,11}^{(10)} = m_{11,0} + m_{11,5}^{(12)} = -g^*(0) = K_5(\text{say})$$

$$m_{60} + m_{67} = \mu_6$$

$$m_{60} + m_{6,5}^{(7)} = -g_1^*(0) = K_6(\text{say})$$

$$m_{11,0} + m_{11,12} = \mu_{11}$$

7 Measures of system effectiveness

7.1 Mean time to system failure

Let $\phi_i(t)$, where $i \in E$ be c.d.f. of the first passage time from regenerative state i to a failed state. Regarding the failed state as absorbing state and employing the arguments used for regenerative processes, we have the following recursive relations for ' $\phi_i(t)$ '.

$$\begin{aligned} \phi_0(t) = & Q_{00}(t) \otimes \phi_0(t) + Q_{01}(t) \otimes \phi_1(t) + Q_{02}(t) \otimes \phi_2(t) + Q_{03}(t) \otimes \phi_3(t) \\ & + Q_{04}(t) \otimes \phi_4(t) + Q_{05}(t) \otimes \phi_5(t) + Q_{06}(t) \otimes \phi_6(t) \end{aligned}$$

$$\phi_1(t) = Q_{18}(t) + Q_{10}(t) \otimes \phi_0(t)$$

$$\phi_2(t) = Q_{29}(t) + Q_{20}(t) \otimes \phi_0(t)$$

$$\phi_3(t) = Q_{35}(t) \otimes \phi_5(t)$$

$$\phi_4(t) = Q_{45}(t) \otimes \phi_5(t)$$

$$\phi_5(t) = Q_{5,10}(t) + Q_{50}(t) \otimes \phi_0(t)$$

$$\phi_6(t) = Q_{67}(t) + Q_{60}(t) \otimes \phi_0(t)$$

Taking Laplace-Stieljes transformation of the above equations and solving them for $\phi_0^{**}(s)$, we have

$$\phi_0^{**}(s) = N(s) / D(s)$$

where

$$N(s) = Q_{06}^{**}(s)Q_{67}^{**}(s) + Q_{02}^{**}(s)Q_{29}^{**}(s) + Q_{04}^{**}(s)Q_{45}^{**}(s)Q_{5,10}^{**}(s) + Q_{01}^{**}(s)Q_{18}^{**}(s) \\ + Q_{05}^{**}(s)Q_{5,10}^{**}(s) + Q_{03}^{**}(s)Q_{35}^{**}(s) + Q_{03}^{**}(s)Q_{35}^{**}(s)Q_{5,10}^{**}(s)$$

and

$$D(s) = 1 - Q_{00}^{**}(s) - Q_{01}^{**}(s)Q_{10}^{**}(s) - Q_{02}^{**}(s)Q_{20}^{**}(s) - Q_{03}^{**}(s)Q_{35}^{**}(s)Q_{50}^{**}(s) \\ - Q_{04}^{**}(s)Q_{45}^{**}(s)Q_{50}^{**}(s) - Q_{05}^{**}(s)Q_{50}^{**}(s) - Q_{06}^{**}(s)Q_{60}^{**}(s)$$

The reliability of the system at time t is given by,

$$R(t) = L^{-1} \left[\frac{1 - \Phi_0^{**}(s)}{s} \right]$$

Now, the MTSF when the system starts from state '0' is

$$MTSF = \int_0^{\infty} R(t) dt = \lim_{s \rightarrow 0} R_0^*(s) = N / D$$

where

$$N = \{ \mu_0 + p_{01}\mu_1 + p_{02}\mu_2 + p_{03}(\mu_3 + \mu_5) + p_{04}(\mu_4 + \mu_5) + p_{05}\mu_5 + p_{06}\mu_6 \}$$

and

$$D = (1 - p_{00} - p_{01}p_{10} - p_{02}p_{20} - p_{03}p_{50} - p_{04}p_{50} - p_{05}p_{50} - p_{06}p_{60}).$$

7.2 Mean time to failure of primary database unit

Let $TP_i(t)$, where $i \in E$ be the c.d.f. of the first passage time of primary database unit from regenerative state i to the state where it is failed. By using arguments of theory of regenerative processes, we have the following recursive relations for ' $TP_i(t)$ '.

$$TP_0(t) = Q_{03}(t) + Q_{04}(t) + Q_{05}(t) + Q_{00}(t) \otimes TP_0(t) + Q_{01}(t) \otimes TP_1(t) \\ + Q_{02}(t) \otimes TP_2(t) + Q_{06}(t) \otimes TP_6(t)$$

$$TP_1(t) = Q_{18}(t) + Q_{10}(t) \otimes TP_0(t)$$

$$TP_2(t) = Q_{29}(t) + Q_{20}(t) \otimes TP_0(t)$$

$$TP_6(t) = Q_{67}(t) + Q_{60}(t) \otimes TP_0(t)$$

Taking Laplace-Stieljes transformation of above equations and solving them for $TP_0^{**}(s)$, we have

$$TP_0^{**}(s) = N_1(s) / D_1(s)$$

where

$$N_1(s) = Q_{03}^{**}(s) + Q_{04}^{**}(s) + Q_{05}^{**}(s) + Q_{01}^{**}(s)Q_{18}^{**}(s) + Q_{02}^{**}(s)Q_{29}^{**}(s) + Q_{06}^{**}(s)Q_{67}^{**}(s)$$

and

$$D_1(s) = 1 - Q_{00}^{**}(s) - Q_{01}^{**}(s)Q_{10}^{**}(s) - Q_{02}^{**}(s)Q_{20}^{**}(s) - Q_{06}^{**}(s)Q_{60}^{**}(s)$$

Now, the MTFP when the system start from state '0' is

$$\text{MTFP} = \lim_{s \rightarrow 0} \{1 - TP_0^{**}(s)\} / s = N_1 / D_1$$

where

$$N_1 = \{\mu_0 + p_{01}\mu_1 + p_{02}\mu_2 + p_{06}\mu_6\}$$

and

$$D_1 = (1 - p_{00} - p_{01}p_{10} - p_{02}p_{20} - p_{06}p_{60}).$$

7.3 Availability of primary database unit (AP_0)

Let $AP_i(t)$, where $i \in E$ be the probability that the primary database unit is in upstate at instant t given that the system entered regenerative state i at $t = 0$. By using arguments of theory of regenerative processes, we have the following recursive relations for ' $AP_i(t)$ '.

$$AP_0(t) = M_0(t) + q_{00}(t) \odot AP_0(t) + q_{01}(t) \odot AP_1(t) + q_{02}(t) \odot AP_2(t) + q_{03}(t) \odot AP_3(t) \\ + q_{04}(t) \odot AP_4(t) + q_{05}(t) \odot AP_5(t) + q_{06}(t) \odot AP_6(t)$$

$$AP_1(t) = M_1(t) + q_{10}(t) \odot AP_0(t) + q_{15}^{(8)}(t) \odot AP_5(t)$$

$$AP_2(t) = M_2(t) + q_{20}(t) \odot AP_0(t) + q_{25}^{(9)}(t) \odot AP_5(t)$$

$$AP_3(t) = q_{35}(t) \odot AP_5(t)$$

$$AP_4(t) = q_{45}(t) \odot AP_5(t)$$

$$AP_5(t) = q_{50}(t) \odot AP_0(t) + q_{5,11}^{(10)}(t) \odot AP_{11}(t)$$

$$AP_6(t) = M_6(t) + q_{60}(t) \odot AP_0(t) + q_{6,5}^{(7)}(t) \odot AP_5(t)$$

$$AP_{11}(t) = M_{11}(t) + q_{11,0}(t) \odot AP_0(t) + q_{11,5}^{(12)}(t) \odot AP_5(t)$$

where

$$M_0(t) = e^{-(\lambda+\alpha)t} \bar{I}(t)$$

$$M_1(t) = e^{-\lambda t} \bar{H}_1(t)$$

$$M_2(t) = e^{-\lambda t} \bar{H}_2(t)$$

$$M_6(t) = e^{-\lambda t} \bar{G}_1(t)$$

$$M_{11}(t) = e^{-\lambda t} \bar{G}(t)$$

Taking Laplace transform of the above equations and solving them for $AP_0^*(s)$, we have

$$AP_0^*(s) = N_2(s)/D_2(s)$$

where

$$\begin{aligned} N_2(s) = & \{1 - q_{11,5}^{(12)*}(s)q_{5,11}^{(10)*}(s)\} \{M_0^*(s) + q_{02}^*(s)M_2^*(s) + q_{01}^*(s)M_1^*(s) + q_{06}^*(s)M_6^*(s)\} \\ & + q_{5,11}^{(10)*}(s) \{q_{03}^*(s)q_{35}^*(s) + q_{06}^*(s)q_{65}^{(7)*}(s) + q_{05}^*(s) + q_{04}^*(s)q_{45}^*(s) \\ & + q_{01}^*(s)q_{15}^{(8)*}(s) + q_{02}^*(s)q_{25}^{(9)*}(s)\} M_{11}^*(s) \end{aligned}$$

and

$$\begin{aligned} D_2(s) = & \{1 - q_{00}^*(s) - q_{06}^*(s)q_{60}^*(s) - q_{01}^*(s)q_{10}^*(s) - q_{02}^*(s)q_{20}^*(s)\} \{1 - q_{11,5}^{(12)*}(s)q_{5,11}^{(10)*}(s)\} \\ & - \{q_{03}^*(s)q_{35}^*(s) + q_{04}^*(s)q_{45}^*(s) + q_{06}^*(s)q_{65}^{(7)*}(s) + q_{05}^*(s) + q_{01}^*(s)q_{15}^{(8)*}(s) + q_{02}^*(s)q_{25}^{(9)*}(s)\} \\ & \{q_{50}^*(s) + q_{5,11}^{(10)*}(s)q_{11,0}^*(s)\} \end{aligned}$$

In steady-state, the availability of primary database unit, is given by

$$AP_0 = \lim_{t \rightarrow \infty} AP_0(t) = \lim_{s \rightarrow 0} sAP_0^*(s) = N_2/D_2$$

where

$$\begin{aligned} N_2 = & (1 - p_{11,5}^{(12)}p_{5,11}^{(10)}) \{ \mu_0 + p_{01}\mu_1 + p_{02}\mu_2 + p_{06}\mu_6 \} \\ & + (1 - p_{00} - p_{01}p_{10} - p_{02}p_{20} - p_{06}p_{60}) p_{5,11}^{(10)}\mu_{11} \end{aligned}$$

and

$$\begin{aligned} D_2 = & (1 - p_{11,5}^{(12)}p_{5,11}^{(10)}) \{ \mu_0 + (p_{01} + p_{03})\mu_3 + (p_{02} + p_{04})\mu_4 + p_{06}\mu_6 \} \\ & + (1 - p_{00} - p_{01}p_{10} - p_{02}p_{20} - p_{06}p_{60}) (K_5 + p_{5,11}^{(10)}K_5) \end{aligned}$$

Similarly, employing the arguments used for regenerative process, as discussed above, other measures of system effectiveness are obtained and are given as follows.

7.4 Expected time for which standby database unit worked as primary database unit (S_0)

Let $S_i(t)$, $i \in E$, be the probability that the standby database unit is working as primary database unit at instant t , given that the system entered regenerative state i at $t = 0$. In steady-state, expected time for which standby database unit worked as primary database unit, is given by

$$S_0 = \lim_{t \rightarrow \infty} S_0(t) = \lim_{s \rightarrow 0} sS_0^*(s) = N_3/D_2$$

where $N_3 = (1 - p_{00} - p_{01}p_{10} - p_{02}p_{20} - p_{06}p_{60})\mu_5$.

7.5 Busy period analysis of DBA

7.5.1 Expected time for updating the redo log files in standby database unit (AU_0)

Let $AU_i(t)$, $i \in E$, be the probability that DBA is busy in updating redo log files in standby database unit at instant t , given that the system entered regenerative state i at $t = 0$. In steady-state, expected time for updating the redo log files in standby database unit, is given by

$$AU_0 = \lim_{t \rightarrow \infty} AU_0(t) = \lim_{s \rightarrow 0} sAU_0^*(s) = N_4/D_2$$

where $N_4 = (1 - p_{11,5}^{(12)} p_{5,11}^{(10)}) (p_{01} + p_{03}) \mu_3$.

7.5.2 Expected time for creating redo log files in standby database unit (AC_0)

Let $AC_i(t)$, $i \in E$, be the probability that DBA is busy in creating redo log files in standby database unit at instant t , given that the system entered regenerative state i at $t = 0$. In steady-state, expected time for creating the redo log files in standby database unit, is given by

$$AC_0 = \lim_{t \rightarrow \infty} AC_0(t) = \lim_{s \rightarrow 0} sAC_0^*(s) = N_5/D_2$$

where $N_5 = (1 - p_{11,5}^{(12)} p_{5,11}^{(10)}) (p_{02} + p_{04}) \mu_4$.

7.5.3 Expected time for repairing primary database unit (BP_0)

Let $BP_i(t)$, $i \in E$, be probability that DBA is busy in repairing the primary database unit at instant t , given that the system entered regenerative state i at $t = 0$. In steady-state, total fraction of time for which primary database unit is under repair, is given by

$$BP_0 = \lim_{t \rightarrow \infty} BP_0(t) = \lim_{s \rightarrow 0} sBP_0^*(s) = N_6/D_2$$

where $N_6 = (1 - p_{00} - p_{01}p_{10} - p_{02}p_{20} - p_{06}p_{60}) (K_5 + p_{5,11}^{(10)} K_5)$.

7.5.4 Expected time for repairing standby database unit (BH_0)

Let $BH_i(t)$, $i \in E$, be probability that DBA is busy in repairing the standby database unit at instant t , given that the system entered regenerative state i at $t = 0$. In steady-state, total fraction of time for which standby database unit is under repair, is given by

$$BH_0 = \lim_{t \rightarrow \infty} BH_0(t) = \lim_{s \rightarrow 0} sBH_0^*(s) = N_7/D_2$$

where $N_7 = (1 - p_{5,11}^{(10)} p_{11,5}^{(12)}) p_{06} K_6$.

7.6 Expected number of visits by DBA (V_0)

Let $V_i(t)$, $i \in E$, be the expected number of visits by the DBA, given that the system entered regenerative state i at $t = 0$. In steady-state, expected number of visits by the DBA per unit time, is given by

$$V_0 = \lim_{t \rightarrow \infty} V_0(t) = \lim_{s \rightarrow 0} sV_0^{**}(s) = N_8/D_2$$

where $N_8 = (1 - p_{00})(1 - p_{5,11}^{(10)} p_{11,5}^{(12)})$.

On the basis of the above measures, the cost-benefit analysis is carried out as in the following section.

8 Cost-benefit analysis

The revenue and cost functions lead to the profit function of a firm. As the profit is excess of revenue over the cost of production, the profit function takes the form

$$P(t) = \text{Expected revenue in } (0, t] - \text{Expected total cost in } (0, t]$$

Thus, for the model discussed in the present paper, the expected profit per unit time incurred to the system, in steady-state, is given by

Profit (P) = (Revenue generated by the system) – (cost incurred when the standby database is used as primary database + cost for updating the redo log files in standby database unit + cost for creating the redo log files in standby database unit + cost for which the DBA is busy for repairing primary database unit + cost for which the DBA is busy for repairing standby database unit + cost per visit of the DBA + cost of initial installation + cost for which the DBA is busy for random inspection of standby database unit), i.e.,

$$P = (C_0 A P_0) - (C_1 S_0 + C_2 A U_0 + C_3 A C_0 + C_4 B P_0 + C_5 B H_0 + C_6 V_0 + 2CI + K)$$

where

- C_0 revenue per unit uptime
- C_1 cost per unit time for which standby database unit worked as primary database unit
- C_2 cost per unit time for updating the redo log files in standby database unit
- C_3 cost per unit time for creating the redo log files in standby database unit
- C_4 cost per unit time for which DBA is busy for repairing primary database unit
- C_5 cost per unit time for which DBA is busy for repairing standby database unit
- C_6 cost per visit of DBA
- CI cost per unit time of initial installation
- K cost per unit time for random inspection of standby database unit.

9 Numerical results and discussions

9.1 Input variables

For numerical calculations we consider repair times, time for creating/updating redo log files and the time for undertaking the standby unit for inspection follow exponential distribution, i.e.,

$$g(t) = \eta e^{-\eta t}, g_1(t) = \alpha_1 e^{-\alpha_1 t}, h_1(t) = \gamma_1 e^{-\gamma_1 t}, h_2(t) = \gamma_2 e^{-\gamma_2 t} \text{ and } i(t) = \gamma e^{-\gamma t}$$

The estimates of various probabilities, rates and costs for primary database unit as well as for the standby database unit obtained on the basis of the data collected are given as follows:

- Probability that standby unit is synchronous with primary unit on the failure of primary database unit (p_1) = 0.1628.
- Probability that redo log files are not updated in standby database unit on the failure of primary database unit (p_2) = 0.0465.
- Probability that redo log files are not created in standby database unit on the failure of primary database unit (p_3) = 0.7907.
- Constant failure rate of primary database unit (λ) = 0.00205 per hr.
- Constant repair rate of primary database unit (η) = 0.6529 per hr.
- Constant failure rate of standby database unit (α) = 0.00087 per hr.
- Constant repair rate of standby database unit (α_1) = 0.8533 per hr.
- Cost per unit time for which DBA is busy for repairing primary database unit (C_4) = INR 7326.
- Cost per unit time for which DBA is busy for repairing standby database unit (C_5) = INR 8750.

The values of above mentioned input variables have been taken as fixed as obtained from the collected data. However, for some parameters/variable, the data were not available and hence, their values have been assumed as mentioned in the Sections 9.3 to 9.9.

9.2 Output variables

The output variables, here, are various measures of system effectiveness including MTSF, availability of primary database unit and profit function. Results of the effects of various input variables on the output variables have been obtained and have been shown in the following sub-sections.

9.3 Effect of rate (γ) on MTSF for different values of rate (γ_2)

MTSF of the system is calculated by varying the rate (γ) for different values of rate (γ_2) and keeping the other parameters constant as $q_1 = 0.75$, $q_2 = 0.1$, $q_3 = 0.15$ and $\gamma_1 = 12$.

The results are tabulated as in Table 1. It is observed that MTSF decreases with the increase in the values of rate (γ) and it has higher values for higher values of rate (γ_2).

Table 1 Values of MTSF w.r.t. rate (γ) for different values of rate (γ_2)

γ	MTSF (in hrs)		
	$\gamma_2 = 2$	$\gamma_2 = 2.5$	$\gamma_2 = 3$
0.01	154,293.4	161,865.7	167,345.5
0.011	150,386.2	158,330.9	164,112.1
0.012	146,651.2	154,916.1	160,978.8
0.013	143,091.4	151,647	157,950.5
0.014	139,687.6	148,493.2	155,011.7
0.015	136,480.2	145,508.3	152,233.8
0.016	133,412.4	142,641.5	149,551
0.017	130,479.6	139,884.2	146,960.9

9.4 Effect of rate (γ_1) on availability of primary database (AP_0) for different values of rate (γ_2)

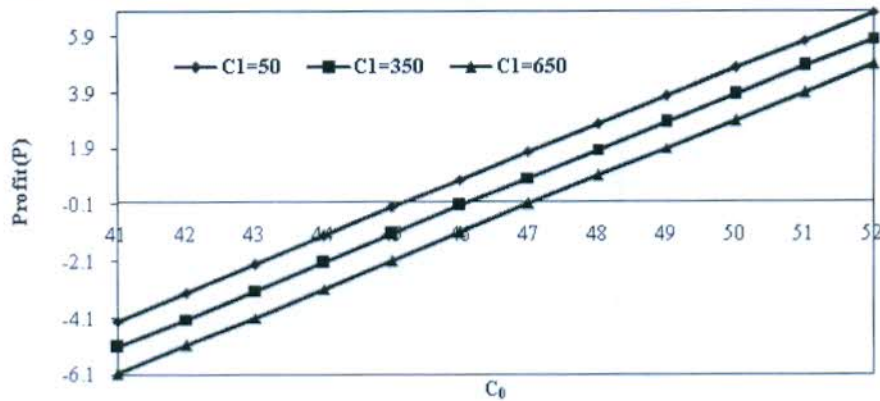
For $q_1 = 0.75$, $q_2 = 0.1$, $q_3 = 0.15$ and $\gamma = 0.02$, Table 2 shows the behaviour of availability of primary database unit (AP_0) w.r.t. rate (γ_1) for different values of rate (γ_2). It is interpreted that availability increases with the increase in the rate (γ_1) and has higher values for higher values of rate (γ_2).

Table 2 Values of (AP_0) w.r.t. rate (γ_1) for different values of rate (γ_2)

γ_1	Availability(AP_0)		
	$\gamma_2 = 2$	$\gamma_2 = 2.5$	$\gamma_2 = 3$
5	0.996047	0.996208	0.996315
6	0.99605	0.996211	0.996318
7	0.996052	0.996213	0.99632
8	0.996054	0.996215	0.996322
9	0.996055	0.996216	0.996323
10	0.996056	0.996217	0.996324
11	0.996057	0.996218	0.996325
12	0.996058	0.996219	0.996326

9.5 Effect of revenue (C_0) on profit (P) for different values of cost (C_1)

The profit (P) of the system has been calculated with respect to revenue (C_0) for different values of cost (C_1) by fixing another parameters such as $q_1 = 0.75$, $q_2 = 0.1$, $q_3 = 0.15$, $\gamma_1 = 12$, $\gamma_2 = 3$, $\gamma = 0.02$, $CI = 5$, $K = 2$, $C_2 = 50$, $C_3 = 150$ and $C_6 = 100$. Figure 3 reveals the behaviour of profit (P) with respect to revenue (C_0) for different values of cost (C_1).

Figure 3 Profit (P) versus revenue (C_0) for different values of cost (C_1)

It is observed that:

- 1 Profit (P) increases with increase in values of (C_0) and it has higher values for lower values of cost (C_1).
- 2 For $C_1 = 50$, the profit is positive, zero or negative according to $C_0 > \text{or} = \text{or} < 45.20$. Hence, for $C_1 = 50$, the revenue should be more than 45.20 to get some profit.
- 3 For $C_1 = 350$, the profit is positive, zero or negative according to $C_0 > \text{or} = \text{or} < 46.14$. Hence, for $C_1 = 350$, the revenue should be more than 46.14 to get some profit.
- 4 For $C_1 = 650$, the profit is positive, zero or negative according to $C_0 > \text{or} = \text{or} < 47.08$. Hence, for $C_1 = 650$, the revenue should be more than 47.08 to get some profit.

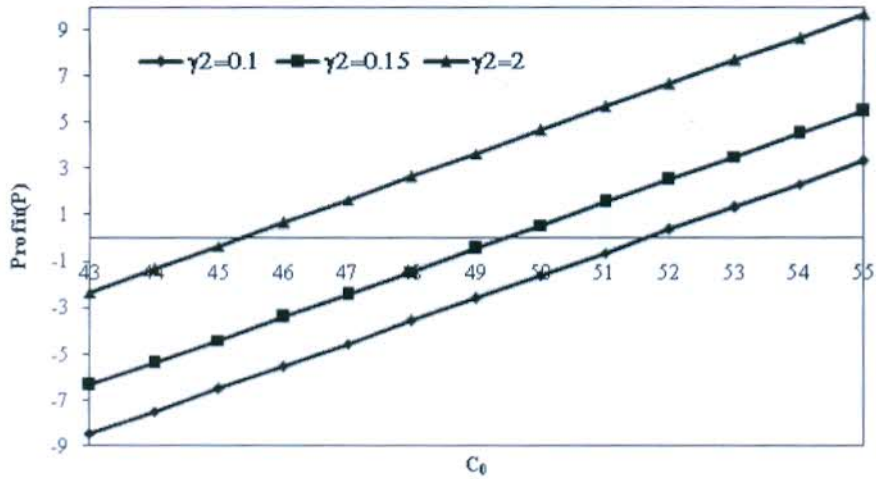
9.6 Effect of revenue (C_0) on profit (P) for different values of rate (γ_2)

Figure 4 depicts the behaviour of profit (P) with respect to revenue (C_0) for different values of rate (γ_2). By considering other parameters as $q_1 = 0.75$, $q_2 = 0.1$, $q_3 = 0.15$, $\gamma_1 = 12$, $\gamma = 0.02$, $C_1 = 5$, $K = 2$, $C_1 = 50$, $C_2 = 50$, $C_3 = 150$ and $C_6 = 100$. It is interpreted that profit (P) increases with increase in the revenue (C_0) and has higher values for higher values of rate (γ_2).

Further:

- 1 For $\gamma_2 = 0.1$, the profit is positive, zero or negative according to $C_0 > \text{or} = \text{or} < 51.62$. Hence, for $\gamma_2 = 0.1$, the revenue should be more than 51.62 to avoid loss.
- 2 For $\gamma_2 = 0.15$, the profit is positive, zero or negative according to $C_0 > \text{or} = \text{or} < 49.44$. Hence, for $\gamma_2 = 0.15$, the revenue should be more than 49.44 to avoid loss.
- 3 For $\gamma_2 = 2$, the profit is positive, zero or negative according to $C_0 > \text{or} = \text{or} < 45.31$. Hence, for $\gamma_2 = 2$, the revenue should be more than 45.31 to avoid loss.

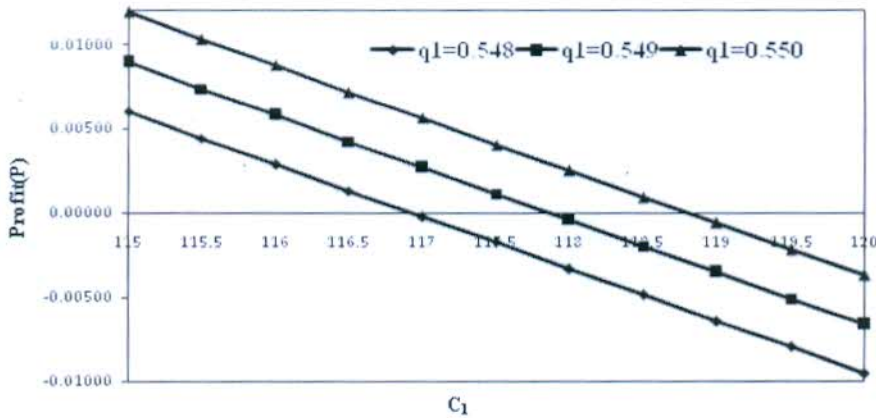
Figure 4 Profit (P) versus revenue (C_0) for different values of rate (γ_2)



9.7 Effect of cost (C_1) on profit (P) for different values of probabilities (q_1)

Behaviour of profit (P) of the system is analysed w.r.t. cost (C_1) per unit time for which the standby database unit worked as primary unit for different values of probability that after the random inspection standby database unit is working fine (q_1). By taking $q_2 = 0.1$, $q_3 = 1 - (q_1 + q_2)$, $\gamma_1 = 12$, $\gamma_2 = 3$, $\gamma = 0.02$, $CI = 5$, $K = 2$, $C_0 = 46$, $C_2 = 50$, $C_3 = 150$ and $C_6 = 100$, it is interpreted from Figure 5 that the profit (P) decreases with increase in cost (C_1) and has higher values for higher values of probability (q_1).

Figure 5 Profit (P) versus cost (C_1) for different values of probabilities (q_1)



Moreover, it is observed that:

- For $q_1 = 0.548$, the profit is positive, zero or negative according to $C_1 \leq$ or ≥ 116.93 . Hence, for $q_1 = 0.548$, the cost per unit time for which standby database unit is used as primary unit should not be more than 116.93 so that the system should not be put to any loss.

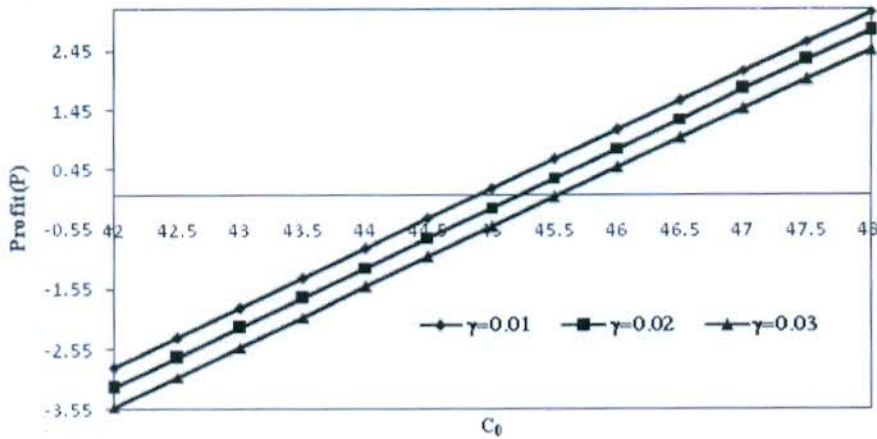
- 2 For $q_1 = 0.549$, the profit is positive, zero or negative according to $C_1 \leq$ or $\Rightarrow 117.8$. Hence, for $q_1 = 0.549$, the cost per unit time for which standby database unit is used as primary unit should not be more than 117.8 so that the system should not be put to any loss.
- 3 For $q_1 = 0.550$, the profit is positive, zero or negative according to $C_1 \leq$ or $\Rightarrow 118.8$. Hence, for $q_1 = 0.550$, the cost per unit time for which standby database unit is used as primary unit should not be more than 118.8 so that the system should not be put to any loss.

9.8 Effect of cost (C_0) on profit (P) for different values of rate (γ)

Figure 6 reveals the behaviour of profit with respect to revenue (C_0) for different values of rate (γ) of undertaking the standby database for inspection. The values of other parameters are assumed as $q_1 = 0.75$, $q_2 = 0.1$, $q_3 = 0.15$, $\gamma_1 = 12$, $\gamma_2 = 3$, $C_1 = 50$, $C_2 = 50$, $CI = 5$, $K = 2$, $C_3 = 150$ and $C_6 = 100$. It is observed that the profit increases with increase in the revenue and has higher values for lower values of rate (γ).

- 1 For $\gamma = 0.01$, the profit is positive, zero or negative according to $C_0 > \text{or} =$ or < 44.87 . Hence, for $\gamma = 0.01$, the revenue should be more than 44.87 for the system to be profitable.
- 2 For $\gamma = 0.02$, the profit is positive, zero or negative according to $C_0 > \text{or} =$ or < 45.20 . Hence, for $\gamma = 0.02$, the revenue should be more than 45.20 for the system to be profitable.
- 3 For $\gamma = 0.03$, the profit is positive, zero or negative according to $C_0 > \text{or} =$ or < 45.52 . Hence, for $\gamma = 0.03$, the revenue should be more than 45.52 for the system to be profitable.

Figure 6 Profit (P) versus revenue (C_0) for different values of rate (γ)

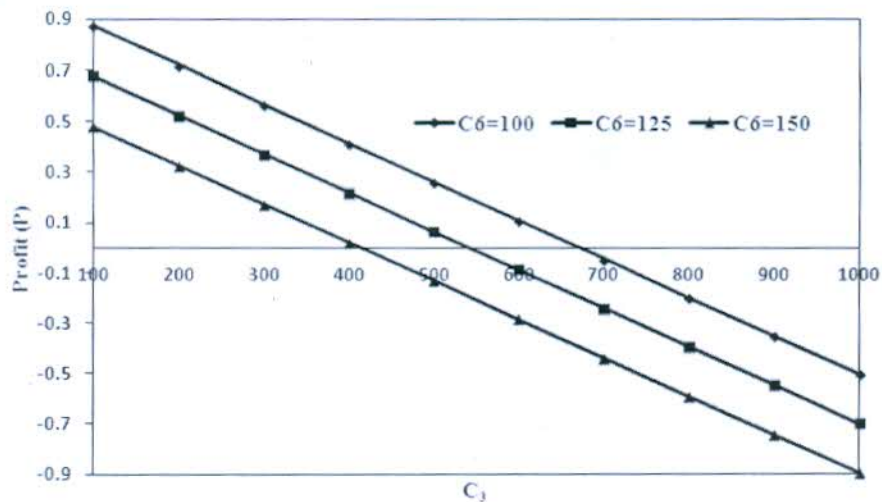


9.9 Effect of cost (C_3) on profit (P) for different values of cost (C_6)

For $q_1 = 0.75$, $q_2 = 0.1$, $q_3 = 0.15$, $\gamma_1 = 12$, $\gamma_2 = 3$, $\gamma = 0.02$, $C_0 = 46$, $C_1 = 50$, $C_2 = 50$, $CI = 5$ and $K = 2$, Figure 7 depicts the behaviour of profit (P) with respect to cost (C_3) per unit time for creating the redo log files in standby database unit for different values of cost (C_6) per visit of the DBA. It is observed that profit decreases with increase in the cost (C_3) and has higher values for lower values of cost (C_6).

- 1 For $C_6 = 100$, the profit is positive, zero or negative according to $C_3 < \text{or} = \text{or} > 670.56$. Hence, for $C_6 = 100$, the cost for creating the redo log files in standby database unit should not be more than 670.56 to have some positive profit.
- 2 For $C_6 = 125$, the profit is positive, zero or negative according to $C_3 < \text{or} = \text{or} > 542$. Hence, for $C_6 = 125$, the cost for creating the redo log files in standby database unit should not be more than 542 to have some positive profit.
- 3 For $C_6 = 150$, the profit is positive, zero or negative according to $C_3 < \text{or} = \text{or} > 413.47$. Hence, for $C_6 = 150$, the cost for creating the redo log files in standby database unit should not be more than 413.47 to have some positive profit.

Figure 7 Profit (P) versus cost (C_3) for different values of cost (C_6)



10 Conclusions

In this paper, we have developed and analysed a stochastic model on a standby database system wherein standby unit is kept under random inspection of DBA. Various measures of system effectiveness have been obtained. Cost/revenue always remains a significant and decisive factor while developing a model for a particular system and hence, bounds for revenue, cost per unit time for which the standby database unit works as a primary database unit and the cost per unit time for creating the redo log files in standby unit have been obtained. Lower bounds obtained for revenue per unit uptime are quite useful with regard to profitability of the system. The upper bounds obtained for the cost per unit time

for which the standby database unit works as a primary database unit and cost per unit time for creating the redo log files in standby unit helps in finding maximum amount to be paid by the user so that system is not put to any loss. Any company/organisation using such systems may apply the model developed in the present study for obtaining the bounds for the parameters of interest in the similar fashion which will help them take various productive and operational decisions.

The limitation of the study has been that the authors were not provided with the data on revenue and various rates/costs including the rate of creating/updating redo log files, cost during which standby works as primary unit, cost of creating/updating redo log files, cost of random inspection, etc. and the values for such parameters have been assumed for numerical analysis. Had the data for all the parameters been available with the authors, the study would have been more effective.

10.1 Future scope

In the present study, a two-unit hot standby database system is considered wherein redo log files may be created/updated in the hot standby unit at the time of inspection, or failure of primary unit. Future scope of the study is that a model may be developed for such a system wherein primary and hot standby unit may be interchanged randomly having some negotiation with the provider of the system regarding the cost of using a unit as primary unit. Redo log files may be created/updated, if required, when units are interchanged. This may decrease the constant load on a primary unit and also the chances of loss of data. However, this aspect needs to be studied and compared with the present study taking various parameters into consideration to see under what conditions which of the two models is better.

Acknowledgements

The authors are grateful to the reviewers/editor for their valuable comments and suggestions.

References

- Beith, B., Hong, L. and Sarkar, J. (2010) 'A standby system with two types of repair persons', *Applied Stochastic Models in Business and Industry*, Vol. 26, No. 5, pp.577–594.
- Branson, M.H. and Shah, B. (1971) 'Reliability analysis of systems comprised of units with arbitrary repair time distributions', *IEEE Transactions on Reliability*, Vol. R-20, No. 4, pp.217–223.
- El-Damcese, M.A. (2009) 'Analysis of warm standby systems subject to common-cause failures with time varying failure and repair rates', *Applied Mathematical Sciences*, Vol. 3, No. 18, pp.853–860.
- Gaikwad, T.R. and Raut, A.B. (2014) 'A review on database security', *International Journal of Science and Research*, Vol. 3, No. 4, pp.372–374.
- Goyal, N., Ram, M. and Kaushik, A. (2017) 'Performability of solar thermal power plant under reliability characteristics', *International Journal of System Assurance Engineering and Management*, Vol. 8, No. 2, pp.479–487.

- Jain, M. and Gupta, R. (2013) 'Optimal replacement policy for a repairable system with multiple vacations and imperfect fault coverage', *Computers & Industrial Engineering*, Vol. 66, No. 4, pp.710–719.
- Jain, M. and Gupta, R. (2014) 'Availability analysis of repairable redundant system with three types of failures subject to common cause failure', *Int. J. Mathematics in Operational Research*, Vol. 6, No. 3, pp.271–296.
- Jia, X., Chen, H., Cheng, Z. and Guo, B. (2016) 'A comparison between two switching policies for two-unit standby system', *Reliability Engineering and System Safety*, Vol. 148, pp.109–118.
- Khattab, A., Algergawy, A. and Sarhan, A. (2015) 'MAG: a performance evaluation framework for database systems', *Knowledge-Based Systems*, Vol. 85, pp.245–255.
- Kumar, R. and Batra, S. (2016) 'Cost-benefit and performance analysis of a stochastic model on printed boards manufacturing process', *Int. J. Mathematics in Operational Research*, Vol. 8, No. 4, pp.490–508.
- Kumar, R. and Kapoor, S. (2013) 'Economic and performance evaluation of stochastic model on a base transceiver system considering various operational modes and catastrophic failures', *Journal of Mathematics and Statistics*, Vol. 9, No. 3, pp.198–207.
- Mahmoud, M.A.W. and Mosherf, M.E. (2010) 'On a two-unit cold standby system considering hardware, human error failures and preventive maintenance', *Mathematical and Computer Modeling*, Vol. 51, Nos. 5–6, pp.736–745.
- Manocha, A., Taneja, G. and Singh, S. (2017) 'Stochastic and cost-benefit analysis of two-unit hot standby database system', *International Journal of Performability Engineering*, Vol. 13, No. 1, pp.63–72.
- Mathews, A.G., Rizwan, S.M., Majumdar, M.C., Ramchandarann, K.P. and Taneja, G. (2011) 'Reliability analysis of identical two unit parallel CC plant system operative with full installed capacity', *International Journal of Performability Engineering*, Vol. 7, No. 2, pp.179–187.
- Mokaddis, G.S., Labib, S.W. and Ahmed, A.M. (1997) 'Analysis of a two-unit warm standby system subject to degradation', *Microelectronics Reliability*, Vol. 37, No. 4, pp.641–648.
- Parashar, B. and Taneja, G. (2007) 'Reliability and profit evaluation of a PLC hot standby system based on a master-slave concept and two types of repair facilities', *IEEE Transactions on Reliability*, Vol. 56, No. 3, pp.534–539.
- Ram, M. and Manglik, M. (2016) 'An analysis to multi-state manufacturing system with common cause failure and waiting repair strategy', *Cogent Engineering*, Vol. 3, No. 1, pp.1–20.
- Shakuntla, S., Lal, A.K., Bhatia, S.S. and Singh, J. (2011) 'Reliability analysis of polytube industry using supplementary variable technique', *Applied Mathematics and Computation*, Vol. 218, No. 8, pp.3981–3992.
- Singh, S., Rishi, R., Taneja, G. and Manocha, A. (2013) 'Reliability and availability analysis of database system with standby unit provided by the system provider', *International Journal of Soft Computing and Engineering*, Vol. 3, No. 2, pp.235–237.
- Singh, S.K. and Mishra, A.K. (1994) 'Profit evaluation of a two-unit standby redundant system with two operating modes', *Microelectronics Reliability*, Vol. 34, No. 4, pp.747–750.
- Srinivasan, S.K. and Gopalan, M.N. (1973) 'Probabilistic analysis of a two-unit system with a warm standby and a single repair facility', *Operations Research*, Vol. 21, No. 3, pp.748–754.
- Tuteja, R.K. and Taneja, G. (1992) 'Cost-benefit analysis of a two-server, two-unit, warm standby system with different types of failure', *Microelectronics Reliability*, Vol. 32, No. 10, pp.1353–1359.
- Yusuf, I. (2015) 'Availability modeling and evaluation of a repairable system subject to minor deterioration under imperfect repair', *Int. J. Mathematics in Operational Research*, Vol. 7, No. 1, pp.42–51.
- Yusuf, I., Suleiman, K., Bashir, Y. and Ali, U.A. (2014) 'Stochastic modelling and analysis of a repairable 2-out-of-4 system', *Int. J. Mathematics in Operational Research*, Vol. 6, No. 1, pp.23–34.



International Journal of Advance Engineering and Research Development

Volume 6, Issue 02, February -2019

STUDIES ON EFFECT OF RING FRAME DRAFTING PARAMETERS ON YARN FAULTS USING FACTORIAL DESIGN TECHNIQUE

Dr. Suman Bhattacharyya¹, Chandra Prakash Sharma²

¹Textile Department, TIT&S College, Bhiwani-127021, Haryana,

²Textile Department, TIT&S College, Bhiwani-127021, Haryana.

Abstract: Drafting process being the most important operation in ring frame which influences the major quality parameters of yarn, spinners were becoming increasingly concerned to optimize the parameters of drafting process in ring frame. Faults in yarn which are considered to be major causes of rejection and down grading of fabric and reduced productivity in all the downstream processes are largely influenced by ring frame drafting variables e.g. back zone roller setting, break draft and spacer size. In the present work, the effect of afore said ring frame drafting parameters on different categories of yarn faults are studied in detail using factorial design technique (Box –Behnken design of experiment.)

Keywords: Back zone setting, Break draft, spacer size, drafting faults, thick faults, slub, thin fault design of experiment

I. INTRODUCTION

The seldom occurring faults in yarn are the major factor responsible for rejection and down grading of yarn and fabrics and low productivity in the downstream processes due to higher end breakage. Furthermore, new generation high speed looms and knitting machines place more stringent demands on the fault level in the yarn. Thus, spinners are becoming increasingly concerned to reduce the fault level in the yarn. Accordingly, many experimental and theoretical researches on drafting in ring frame have been carried out with an aim to control the drafting process to improve quality of yarn. Most of the research works carried out hitherto considered the effect of ring frame drafting variables on generation of yarn fault in isolation [1, 2, 3, and 4]. There is notable absence of literatures on the combined effect of ring frame drafting parameters on generation of different types of seldom occurring faults. Hence, the present study is undertaken to analyze in detail the effect of important drafting variables e.g. back zone setting, break draft and spacer size on different categories of faults employing Box- Behnken design of experiment.

II. MATERIAL AND METHOD

2.1 Material

The specifications of polyester and viscose fibres used in the study are given in the Table 1

Table 1
Specification of polyester, and viscose

Fibre characteristic	Polyester	Viscose
Length (mm)	44	44
Fineness (denier)	1.4	1.5

2.1 Preparation of sample:

Standard process and machine parameters as adopted by the industry is followed for preparation of polyester- viscose (70:30) blended roving of hank 1.0 Ne. Twenty roving bobbins are collected from the same doff of a roving frame and creeled on the same set of spindles of ring frame to rule out any variation in the experimental results due to machine conditions. It is ensured that all the parameters (other than the variable ones) are identical in all the spindles. In total 15 numbers of samples of 30^s Ne having twist multiplier of value 3 were prepared on LR-6 medium cradle ring frame for all the combinations by using three-variable factorial design as suggested by Box and Behnken (Table 2). The actual levels of variables were taken within the range commonly adopted by industries and mentioned in Table 3. For each combination total 40 bobbins (2 complete doff) were prepared.

Table 2
Experimental Plan (Box and Behnken) for Preparation Ring Yarn
(Coded Values)

Combination No	Break draft	Back zone setting	Spacer size
1	-1	-1	0

2	-1	+1	0
3	+1	-1	0
4	+1	+1	0
5	-1	0	-1
6	-1	0	+1
7	+1	0	-1
8	+1	0	+1
9	0	-1	-1
10	0	-1	+1
11	0	+1	-1
12	0	+1	+1
13	0	0	0
14	0	0	0
15	0	0	0

Table 3
Actual Values of The Process Parameters of Yarn Spinning Corresponding to Coded Levels

Coded levels	Actual Values		
	Break draft	Back zone setting(mm)	Spacer size(mm)
-1	1.17	70	3.0
0	1.24	75	3.5
+1	1.30	80	4.0

2.1 Measurement of yarn faults: Measurement of seldom occurring yarn faults, which occur at infrequent intervals, was done in which classify the yarn faults in following categories:

Slub - 25 classes by 5 level limits of 0 to 4 and 5 length limits of A to E.

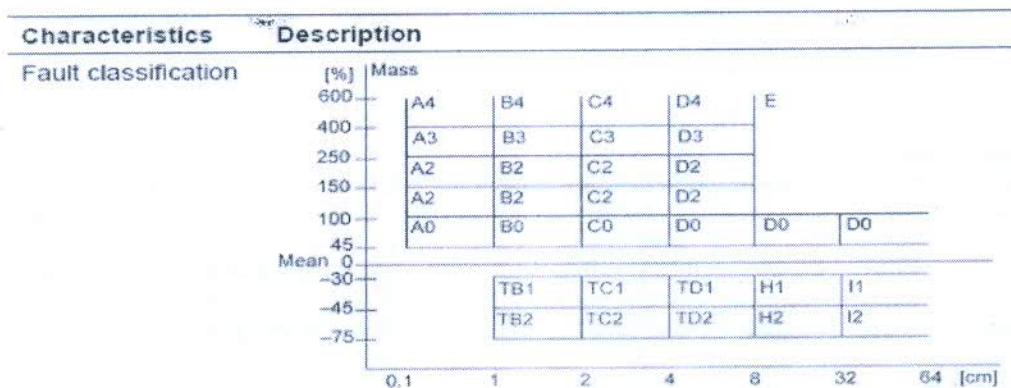
Thick Place: 15 classes by 3 level limits of TK1, TK2, and TK3 and 5 length limits of L1 to L5.

Thin Place:-15 classes by 3 level limits of TN1, TN2, and TN3 and 5 length limits of L1 to L5.

Drafting faults: C₃, D₃ and C₄, D₄

The CFT -II classifies the yarn faults in 40 classes as shown below in Table-4 [5] :

Table 4



Testing condition:

Winding Speed – 500 m/min

Total Length of tested material approximately 150 km for each sample

III. RESULT AND DISCUSSION

The experimental results for different characteristics of the yarn samples prepared for different combinations of break draft, back zone setting and spacer size is given in the yarn the Table5. Mathematical models (in form of regression equations) were developed to predict various physical properties of yarn using SYSTAT 12 statistical package are given

in Table 6. The corresponding significant tests of model equations were carried out on the basis of adjusted coefficient of determination (R^2_{adjusted}), and standard error. Higher the value of R^2_{adjusted} , stronger is the correlation between dependent and independent variables and the regression equation derived is considered to be more significant.

Table 5 Test Results for Seldom Faults Yarn Samples

Combination No.	Objectionable Drafting Faults/ 100 km	Total slub / 100 km	Total	
			Thin faults/ 100 km	Total Thick faults / 100 km
Y ₁	21	1213	1855	1118
Y ₂	30	1291	1907	1153
Y ₃	27	1178	1870	1152
Y ₄	32	1224	1928	1171
Y ₅	25	1313	1983	1124
Y ₆	41	1198	1917	1217
Y ₇	29	1255	1859	1295
Y ₈	53	1326	1925	1181
Y ₉	32	1187	1876	1153
Y ₁₀	46	1151	1973	1219
Y ₁₁	29	1275	1881	1281
Y ₁₂	50	1318	1920	1335
Y ₁₃	22	1279	1977	1304
Y ₁₄	16	1187	1886	1287
Y ₁₅	13	1213	1928	1181

Table 6. Response Surface Equation for Various Yarn Faults

Properties	Response surface equation	R^2_{adj}	S.E.
drafting fault	$3782.82-2466.19*x_1-36.54*x_2-552.35*x_3-3.45*x_1*x_2+59.88*x_1*x_3+.70*x_2*x_3+1037.09*x_1*x_1+0.26*x_2*x_2+63.50*x_3*x_3$	0.89	3.85
slub total	$11036.68-15259.70*x_1+127.66*x_2-3126.55*x_3-0.68*x_1*x_2+1441.59*x_1*x_3+7.9*x_2*x_3+4738.25*x_1*x_1-0.8*x_2*x_2+105.83*x_3^2$	0.34	46.0
total thick	$-40655.81+49785.95*x_1+218.15*x_2+1392.11*x_3-.67*x_1*x_2-1546.01*x_1*x_3-1.2*x_2*x_3-17617.52*x_1*x_1-1.32*x_2*x_2+90.83*x_3*x_3$	0.26	68.01
total thin	$-6313.98+5979.69*x_1+168.42*x_2-1017.81*x_3-0.05*x_1*x_2+1052.51*x_1*x_3-5.8*x_2*x_3-3972.83*x_1*x_1-0.98*x_2*x_2+26.33*x_3*x_3$	0.32	49.27

3.1 Objectionable drafting Faults

Results of Drafting Faults (/100km) for the experimental samples are given in Table 5. High value of R^2_{adjusted} (0.894) (Table 6) shows that the regression model derived for the drafting fault is significant and correlates well with the independent variables. This is also evident from Fig1. It can be seen from the fig 2 and fig 3 response surface plot that drafting faults is significantly affected by spacer size. Besides the size of the spacer, break draft also affects incidence of drafting fault. The effect of back zone setting is marginal and significant only at higher level.

Effect of Break Draft

It can be inferred from Fig 1 that the effect of beak drafts is more prominent at higher level (beyond 1.24). At higher break draft level, stick-slip effect is more prominent. This is because the fibres are subjected to static and dynamic friction in quick succession and the movement of the fibres becomes more erratic [6] . This leads to substantial increase in drafting fault after drafting in front zone (specially belonging to D₃ and D₄ categories).

Design-Expert® Software
 Trial Version
 Factor Coding: Actual

Drafting faults (/100km)
 13  53

X1 = A: Break Draft
 X2 = B: Back Zone Setting

Actual Factor
 C: Spacer Size = 3.03

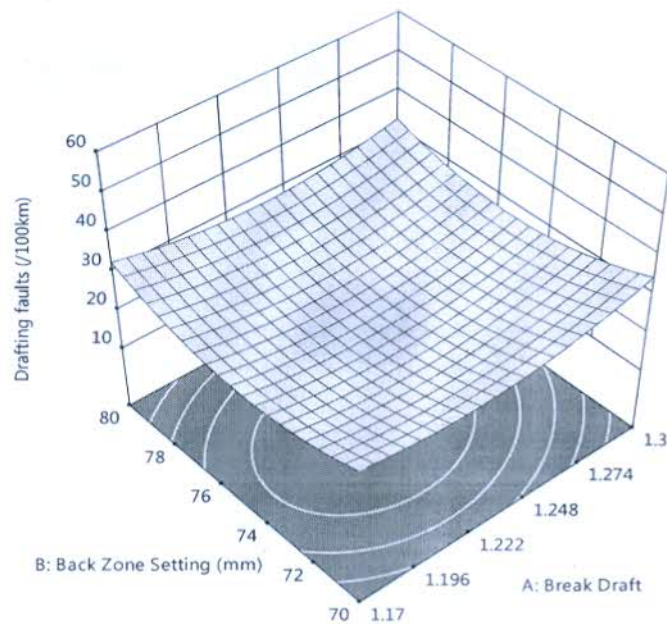


Fig 1 –Effect of Break Draft and Back Zone Setting on Drafting Faults(/100km)

Effect of Back Zone Setting:

Response surface plot fig 2 shows that the effect of back zone setting and spacer size on drafting faults. The incidence of higher drafting fault with wider back zone setting may be ascribed to the relatively higher level of floating fibres. With the widening of the gap between the friction field created by the back roller and middle roller, movement of the floating fibre will be uncontrolled in this zone creating mass variation [6]. These are extended in length by the amount of draft in the main drafting zone and counted as infrequent drafting fault.

Design-Expert® Software
 Trial Version
 Factor Coding: Actual

Drafting faults (/100km)
 ● Design points above predicted value
 ○ Design points below predicted value
 13  53

X1 = B: Back Zone Setting
 X2 = C: Spacer Size

Actual Factor
 A: Break Draft = 1.17

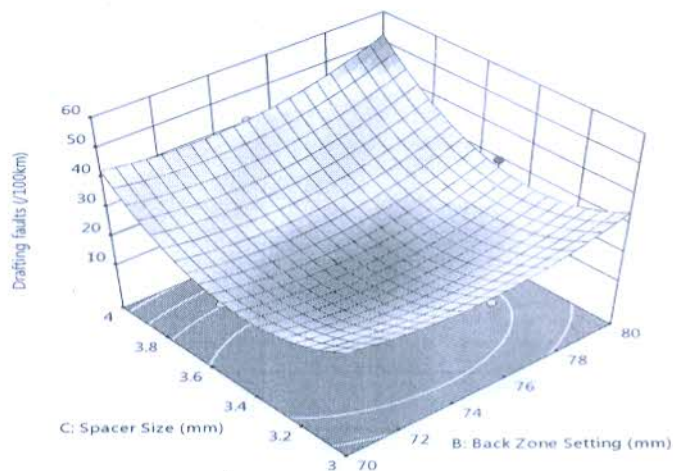


Fig 2 – Effect of Back Zone Setting and Spacer Size on Drafting Faults(/100km)

Effect of Spacer Size:

Response surface plot Fig 3 shows that number of drafting faults decrease initially up to an optimum spacer size and then increases sharply with increase in size. This may be attributed to the fact that for narrower the apron nip opening, same number of fibres will pass through narrower gap causing increased cohesion among the fibres. Thus, fibres are subjected to greater strain and are more resistant to drafting. Thus, drafting fault reduces initially up to a certain optimum size [7]. Beyond this, control over the fibres by the aprons is reduced and the movement of the fibres will become more irregular leading to higher drafting faults.

Design-Expert® Software

Trial Version

Factor Coding: Actual

Drafting faults (/100km)

● Design points above predicted value

○ Design points below predicted value

13  53

X1 = A: Break Draft

X2 = C: Spacer Size

Actual Factor

B: Back Zone Setting = 70

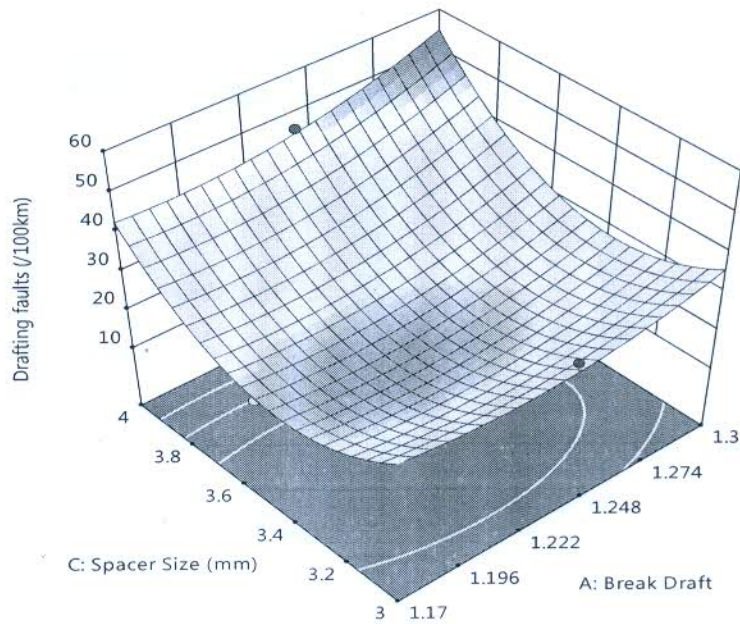


Fig 3 – Effect of Break Draft and Spacer Size on Drafting Faults(/100km)

3.2 Total Slub

The low value of R^2_{adjusted} (0.345) and Fig 4 confirms that the regression model for total slub is fairly weak. This is because of the fact that total slub measured by the Keisokki classifault tester [5] include all categories of short thick faults originating both from poor opening at preparatory stage and faulty drafting at ring frame, the former being much higher in number, overshadowed the effect of drafting.

Design-Expert® Software

Trial Version

Slub total

Color points by value of

Slub total:

1151  1326

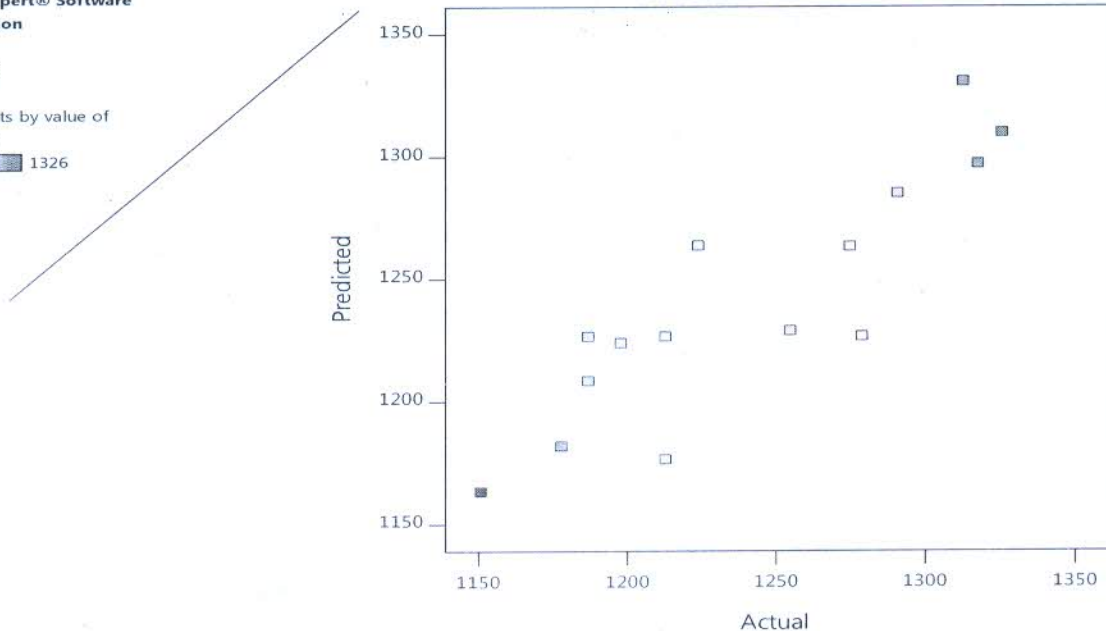


Fig 4 - Correlation Between Predicted Vs Actual Value of Total Slub Faults

3.3 Total Thick Fault:

Results of the Total Thick Faults (/100km) for the experimental samples are given in Table 5. The low value of R^2_{adjusted} (0.063) confirms that the regression model for total thick faults is fairly weak. It is also evident from the Fig 5 that the experimental data fit poorly to the straight line from the analysis of the ANOVA. It is clear that there is no significant effect of any of the spinning process variables on the number of long thick in the yarn.

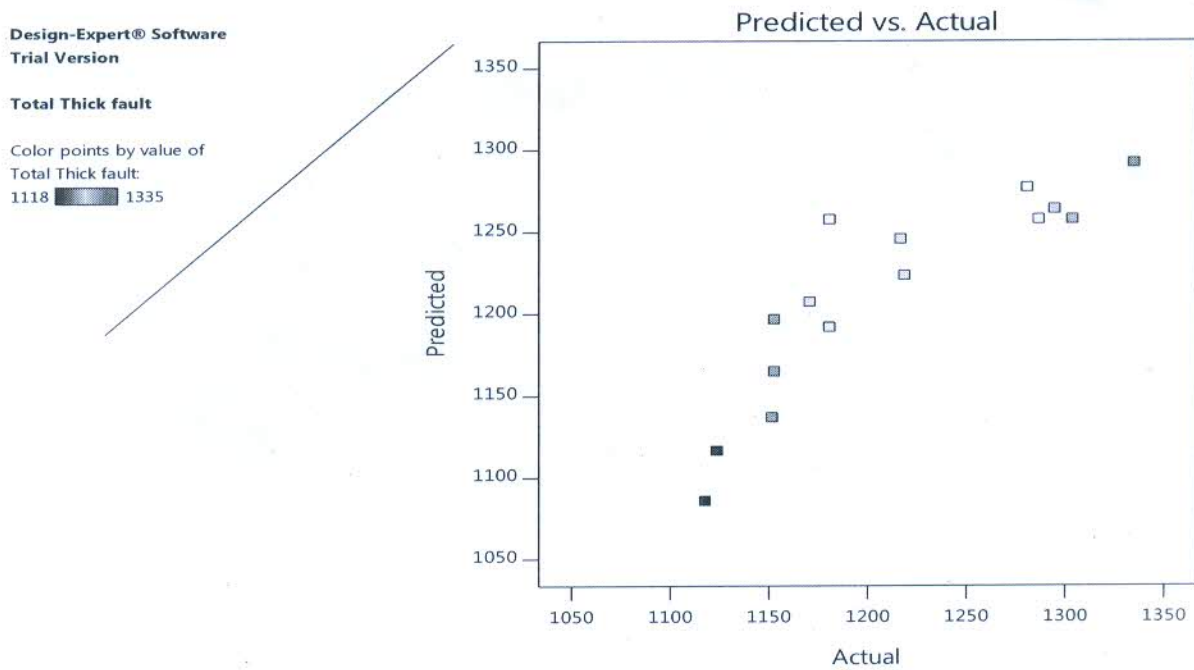


Fig 5 - Correlation Between Predicted Vs Actual Value of Total Thick Faults

3.4 Total Thin Fault:

Results of the Total Thin Faults(/100km) for the experimental samples are given in Table 5. The low value of $R^2_{adjusted}$ (0.100) and Fig 6 confirms that the regression model for total thin fault is fairly weak. This is because of the fact that total thin faults originate due to stretching and none of the drafting parameters considered for this study can influence the generation thin faults.

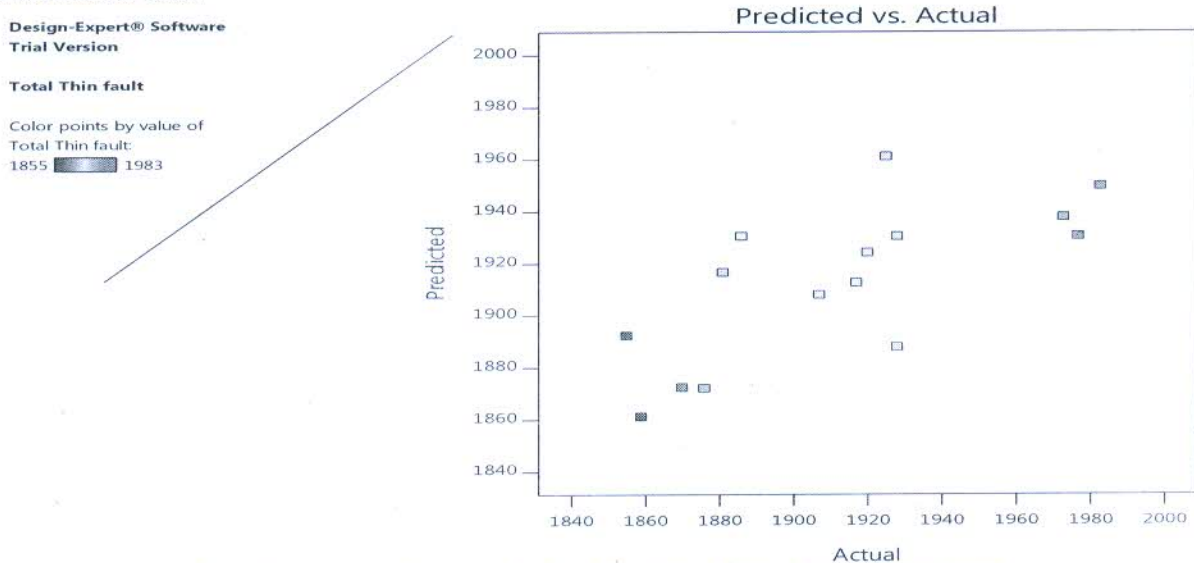


Fig 6 - Correlation Between Predicted Vs Actual Value of Total Thin Faults.

III. CONCLUSION

1. It can be concluded that number of objectionable drafting faults (C3, C4, D3 and D4) is significantly affected by spacer size. Besides the size of the spacer, break draft also affects incidence of drafting fault. The effect of back zone setting is marginal and significant only at higher level.
2. Total number of slub in the yarn is not significantly any of the parameters considered in the study. This may be due the fact that total slub measured by the Keisokki classifault tester include all categories of short thick faults originating both from poor opening at preparatory stage and faulty drafting at ring frame, the former being much higher in number, overshadowed the effect of drafting
3. Total thick and total thin faults are not affected by any of the spinning process variables

VI. REFERENCES

1. V. Ramachandran, Journals of the Textile Association (Bombay), sept-oct, 1996, No. 3, Page No. 153
2. R. N. Yadav, Man-Made Textile India, 36, No. 5, May 1993, Page No. 185-188.
3. K Kumaraswamy and I Sheriff, Journals of Textile Association, Vol.40, November 1979, No.6, page 213.
4. Vishwanath C.S, Jumdar C. R, Indian Textile Journal, 102, No.1, October 1991, 90-93.
5. Classifault
6. W. Klein, The Rieter Manual of Spinning, Vol. 1 – The Technology of short-staple Spinning
7. Dr. N. Balasubramanian, Curbing yarn faults, The Indian Textile Journal, May (1997), page. 12-23.

Characterization of Warp Knitted Spacer Fabric for Application in Sports Bra

Mrinal. K. Datta^{1*}, B.K. Behera², and Ashvani Goyal³

¹Northern India Textile Research Association, Ghaziabad 201002, India

²Indian Institute of Technology, Delhi 110 016, India

³The Technological Institute of Textile and Sciences, Bhiwani, Haryana 127021, India

(Received January 15, 2019; Revised March 29, 2019; Accepted May 26, 2019)

Abstract: Women's breasts contain limited anatomic support. Sporting activities create an excessive movement of breasts. It causes generation of continuous stress on the cooper ligaments. Excessive stress on cooper ligaments creates discomfort, pain, embarrassment and also causes the breasts to sag. The effectiveness in reducing breast movement depends on various factors. The factors are related to breast sizes, breast stiffness, running and jumping speed of sport woman and fabric structural parameters by which sports bra are made. However, no work has investigated and characterized spacer fabric based on the curvature of inner body parts under the bra. Characterization of spacer fabric is required on the basis of the real life simulation. The reaction force acting on the breasts during spherical compression of spacer fabric needs to be analyzed. Air and moisture transmission through the fabric, thermal resistance and moisture management properties also need to be characterized along with compression properties. Samples were developed to characterize spacer fabric for the above requirement. This paper analyzes to understand the behavior of warp knitted spacer fabric for spherical compression with different diameter of the spheres and its thermal, air and moisture related comfort characteristics. Finite Element Analysis (FEA) is also done for compression property of spacer fabric. It is concluded that spacer fabric may be considered as a very effective component of sports bra for controlling breast movement without compromising with comfort of sports women.

Keywords: Warp knitting, Spacer fabric, Technical textile, Sports bra, Specialty fabric

Introduction

Women's breasts contain limited anatomic support. It has lack of muscles and bones. It is made of several specialized glandular tissues as well as fatty tissues. Tissues in the breast help to maintain structural integrity, shape and size while cooper's ligaments provide support to keep the breast in position [1]. Sporting activities create an excessive movement of the breasts. It causes generation of continuous stress on the cooper ligaments. Excessive stress on cooper ligaments creates discomfort, pain, embarrassment and also causes the breasts to sag. Hence, sports bras are designated sturdier than everyday bras. It effectively limits breast motion and reducing breast discomfort, compared with everyday bras. It reduces the chances of damaging the cooper ligaments in the breast during high-impact sporting activity [2-4].

Traditionally, sports bras are either compression type or encapsulation type [5]. Compression bra restricts breast movement by compressing and flattening breasts against the body. Compressing forces acting on breasts may cause breast discomfort and distortion of shape. An encapsulation bra contains two individual cups that separately support and hold the breasts in place. It causes limited breast discomfort and distortion of shape. There is a difference in opinions regarding effectiveness of two types of bra regarding reducing breast movement. Starr *et al.* [6] claim that the vertical displacement of breast in compression bras was larger than encapsulation bras though it was challenged by Mc Ghee and Steele [7]. For both cases, effectiveness in reducing

breast movement depends on various factors. The factors are related to breast sizes, breast stiffness, running and jumping speed of sport woman and fabric structural parameters by which sports bra are made.

Many researchers [8-12] have analyzed on the kinetics of the female body and breasts during the sports activities. Video motion-capture technology is used by some researchers [6,7,13-19] for better understanding of breast motion. It is reported that during sporting activities repeated loading and repeated vertical displacement of breasts take place, which significantly increase with time, responsible for tissue strain [15,20]. Many researchers have published their work on breast comfort in relation with breast movement like displacement, velocity and acceleration [13,18,21].

However, only a few researches have investigated the effect of fabric structural parameter on performance of sports bra [22,23]. Knitted fabric is mostly preferred as a sports bra fabric since it extends greatly in all directions. Lin *et al.* [19] have investigated on the sports bra made of dynamic moisture transfer fabrics. Lower skin temperature was reported with bra made of single jersey fabric. Many researchers [24-27] have shown the application of warp knitted spacer fabric as a component of sports bra, like molded bra cups [24,28], sports bras[25], bra wings [26], wire casings [27], shoulder straps, and the backing of hook-and-eye closures [3].

Curvature of inner body parts under the bra varies widely. It varies with the shape and size of breast and body. Many literatures [29-32] have emphasized the need for assessment of the properties of spacer fabrics in accordance with the curve surface of the human body in order to simulate the

*Corresponding author: mkd2222000@gmail.com

realistic requirement. Liu *et al.* [29,30] analyzed the spacer fabric's performance with a hemispherical drop-weight impact tester. The compression behavior of spacer fabrics was simulated with finite element method (FEM) with a different curve surface by researchers [31,32] for better understanding of their characteristics. However, no such work has investigated and characterized spacer fabric based on the curvature of inner body parts under the bra. Characterization of spacer fabric is required to be based on real life simulation. The reaction forces acting on breast during spherical compression of spacer fabric need to be analyzed. Air and moisture transmission through the fabric, thermal resistance and moisture management properties need to be characterized along with compression properties. Hence, the objective of this paper is to understand the behavior of warp knitted spacer fabric for spherical compression with different diameter of the spheres and its thermal, air and moisture related comfort characteristics.

Experimental

Materials

100 % polyester multifilament (20 tex/96 f) yarn is used to produce front and back surface structures and 100 % monofilament polyester is used as a spacer yarn for sample preparation.

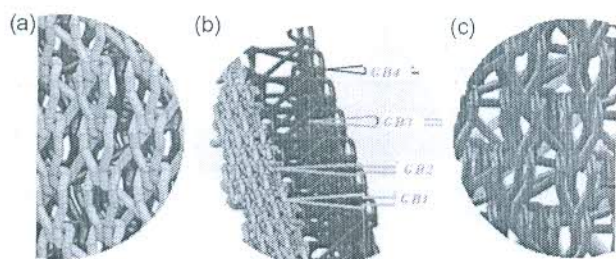


Figure 1. Spacer fabric with four guide bars structure; (a) Face structure made by GB1 & GB2, (b) spacer yarn made by GB3, and (c) back fabric made by GB4.

Preparation of Fabric Samples

Four guides bar warp knit structures (see Figure 1) were produced by double-needle-bed Raschel knitting machine. Guide Bar 1 (GB1) & Guide Bar 2 (GB2) were utilized for face structures. Hexagonal mesh (H), Rhombic mesh (R), Tricot structure (T), Pillar with inlay (P) were produced as a face structures. Stitch notation of structures is shown in Table 1. Guide Bar 4 (GB4) was utilized for back structure

Table 1. Structure of spacer samples

Structure	Representation of stitch notation and threading pattern
Rhombic mesh (R)	Guide Bar 1: 1-0-0-0/1-2-2-2/2-3-3-3/2-1-1-1// (1 Threaded and 1 Empty) Guide Bar 2: 2-3-3-3/2-1-1-1/1-0-0-0/1-2-2-2// (1 Threaded and 1 Empty) (see Figure 2a)
	Guide Bar 3: 1-0-1-0/2-1-2-1// (1 Threaded and 1 Empty)
	Guide Bar 4: 1-1-1-0/1-1-1-2// (fully threaded.) (see Figure 2e)
Hexagonal mesh (H)	Guide Bar 1: (1-0-3-3/3-2-1-1)x2/1-0-3-3/3-2-4-4/(5-4-3-3/3-2-4-4)x2/5-4-3-3/3-2-2-2// (2 Threaded and 2 Empty) Guide Bar 2: (5-4-3-3/3-2-4-4)x2/5-4-3-3/3-2-1-1/(1-0-3-3/3-2-1-1)x2/1-0-3-3/3-2-4-4// (2 Threaded and 2 Empty) (see Figure 2b)
	Guide Bar 3: 1-0-1-0/3-2-3-2// (2 Threaded and 2 Empty)
	Guide Bar 4: 1-1-1-0/1-1-1-2// (fully threaded.) (see Figure 2e)
Tricot structure (T)	Guide Bar 1: 1-0-1-1/1-2-1-1// (1 Threaded and 1 Empty) Guide Bar 2: 1-2-1-1/1-0-1-1// (1 Threaded and 1 Empty) (see Figure 2c)
	Guide Bar 3: 1-0-1-0// (1 Threaded and 1 Empty)
	Guide Bar 4: 1-1-1-0/1-1-1-2// (fully threaded.) (see Figure 2e)
Pillar with inlay structure (P)	Guide Bar 1: 1-0-1-1// (2 Threaded and 2 Empty) Guide Bar 2: 0-0-0-0/5-5-5-5/4-4-4-4/5-5-5-5/0-0-0-0/1-1-1-1// (2 Threaded and 2 Empty) (see Figure 2d)
	Guide Bar 3: 1-0-1-0// (2 Threaded and 2 Empty)
	Guide Bar 4: 1-1-1-0/1-1-1-2// (fully threaded.) (see Figure 2e)

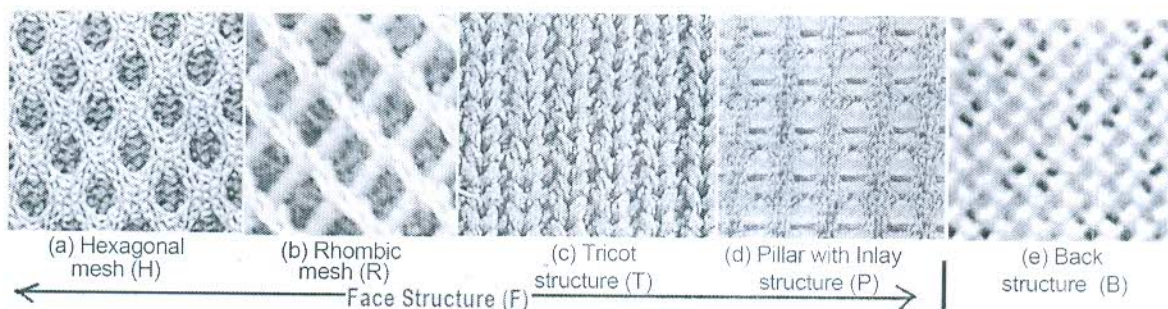


Figure 2. Surface structure of samples; (a) rhombic structure (R), (b) hexagonal structure (H), (c) tricot (T), (d) pillar with inlay (P), and (e) back fabric structure.

Table 2. Summary of variables

Serial no.	Face fabric surface structure	Distance between needle bars (mm)	Spacer yarn linear density (tex)	Sample code
1	Hexagonal mesh	6.5	28	H
2	Rhombic mesh	6.5	28	R
3	Tricot	6.5	28	T
4	Pillar with inlay	6.5	28	P
5	Hexagonal mesh	6.5	22	HD2
6	Hexagonal mesh	6.5	18	HD3
7	Hexagonal mesh	6.5	14	HD4
8	Hexagonal mesh	4.5	28	HS1
9	Hexagonal mesh	5.5	28	HS2
10	Hexagonal mesh	7.5	28	HS4

(B). There was no difference for back guide bar structures for the samples. It was a close lap structure with one needle space under lap. Visual appearance of face and back structures are shown in Figure 2. Guide Bar 3 (GB3) knits both needle beds in succession with monofilament spacer yarn with linear density 28 tex (dia 0.2 mm). Three other monofilament spacer yarns with linear density 22 tex (dia 0.18 mm), 18 tex (dia 0.16 mm) and 14 tex (dia 0.14 mm) were also taken for samples preparation with only Hexagonal mesh (H) structure. Above structures are coded as HD2, HD3 and HD4 respectively.

Thickness of spacer fabric is an important characteristic. Thickness can be controlled by adjusting the space between two needle bars. Four samples with varying thicknesses were developed by keeping distance between needle bar 4.5 mm, 5.5 mm, 6.5 mm and 7.5 mm. Identifications of above samples were denoted as HS1, HS2, H and HS4 respectively. Summary of variables is shown in Table 2.

FEM Analysis of Fabric Compression

The experimental setup of fabric compression performance was simulated in Abaqus/CAE 6.12-1 platform. The parts of models (see Figure 3) were developed in Solidworks platform and imported into Abaqus for Finite Element Analysis (FEA). The variables were kept same as per sample plan. Young's modulus, density of polyester yarn and Poisson's ratio were taken as 6773.3 MPa, $1.38 \times 10^3 \text{ kg/m}^3$ and 0.3 respectively and same for upper plate, lower plate and spheres were considered as 200 GPa $7.872 \times 10^3 \text{ kg/m}^3$, and 0.29 respectively [32]. Fabric material was considered as polyester with isotropic behavior as there is no anisotropy in structure of fabric. The section was taken as solid homogeneous as per actual circumstances. Element type was taken as Standard 3D Stress with an eight-node linear brick, reduced integration and hourglass control. It typically manifests as a patchwork of zig-zag or hourglass like

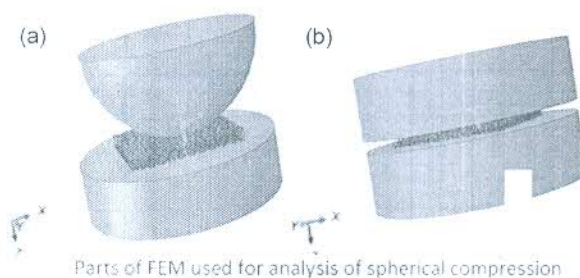


Figure 3. Parts of FEMs were developed in Abaqus/CAE 6.12-1 platform; (a) spherical compression with 10 cm diameter and (b) spherical compression with infinite diameter.

element shapes, where individual elements are severely deformed, while the overall mesh section is undeformed. This happens on hexahedral 3D solid reduced integration elements and on the respective tetrahedral 3D shell elements. Analysis was done in General-Dynamic-Explicit procedure as it perfectly matches with actual circumstances with step time of one second with the default iterative nonlinear solver. Yarn to yarn and yarn to steel coefficient of friction was considered isotropic in all directions with a value of 0.3 and frictional formulation was used as Penalty in Abaqus/CAE 6.12-1.

Boundary conditions, were taken for the above analysis, are shown below.

- Bottom of lower disc was pinned.
- Upper disc and sphere have no displacement and rotation with respect to X and Y axes but have movement only in Z axis direction.
- Velocity of upper disc and spheres were chosen in such a way that these can compress and allow recovering strictly 70 % at step time.

Compression Test of Fabric

Compression was measured by INSTRON 3382 device with reference to the standard ASTM D575. 10 cm×10 cm samples were tested with an upper plate speed 1 mm/min. Upper flat plate of Instron is a 15 cm diameter circular plate. Spherical compression was measured by four different non-

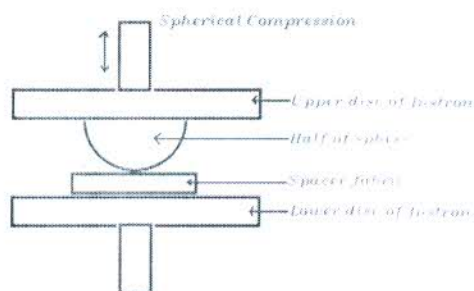


Figure 4. Spherical compressibility measurement by INSTRON device.

compressible semi spheres. Diameters of spheres were taken as 4 cm, 6 cm, 8 cm and 10 cm. Material was also tested without sphere that may be considered as a sphere with infinite diameter. Each semi sphere was placed separately in between spacer fabric and upper plate (see Figure 4). Maximum 0.7 compression strain was applied on the above test.

Characterization of Comfort Properties of Sports Bra Fabric

Air Permeability

Air permeability is defined as the rate of flow of air through a perpendicular measured area at a prescribed air pressure. Tests were performed by Air Permeability Tester-Textest FX-3300 according to standard ISO 9237. The air pressure differential between the two surfaces was taken 100 Pa.

Thermal Resistance

Dry thermal resistance was tested using sweating guarded hot plate under steady state condition by using test method ISO 11092. Sweating guarded hot plate can be used for assessing the performance of dry thermal insulation of a fabric wearing next to the skin. Thermal resistance was measured by maintaining bottom plate temperature $35 \pm 0.5^\circ\text{C}$ which was considered normal skin temperature of a human being and air temperature $20 \pm 0.5^\circ\text{C}$. Relative humidity was maintained at 65%. Air velocity was maintained at 1 m/s. Measurement was done by placing fabric on the test plate with the side normally facing the human body [33]. The total thermal resistance of dry heat transfer (R_{ct}) is measured by following formulation [33]

$$R_{ct} = (T_s - T_a)A/H_c$$

where, R_{ct} : resistance to dry heat transfer provided by the fabric system and air layer (Km^2/W)

A : area of the plate test section (m^2)

T_s : surface temperature of the place ($^\circ\text{C}$)

T_a : air temperature ($^\circ\text{C}$)

H_c : power input (W)

Water Vapor Resistance

Water vapor resistance or evaporating resistance was tested using sweating guarded hot plate under Isothermal condition by using test method ISO 11092. Sweating guarded hot plate can also be used for assessing the breathability of a fabric wearing next to the skin.

Water vapor resistance was measured by maintaining bottom plate temperature and air temperature $35 \pm 0.5^\circ\text{C}$. Relative humidity was mentioned at $40 \pm 4\%$. Air velocity was maintained at 1 m/s. Measurement was done by placing fabric on the test plate with the side normally facing the human body. Distilled water was used to the test plate and guard section to mimic the sweating mechanism of human skin and allowed sweat to evaporate through the fabric [33].

The total evaporating resistance (R_{et}) is measured by

following formulation [33]

$$R_{et} = (P_s - P_a)A/H_E$$

where, R_{et} : resistance to evaporation heat transfer provided by the fabric system and air layer ($\text{kPa m}^2/\text{W}$)

A : area of the plate test section (m^2)

P_s : water vapor at the plate surface (kPa)

P_a : the water vapor pressure in the air (kPa)

H_E : power input (W)

Moisture Management Tests

The test method produces objective measurements of liquid moisture management properties of textile fabric. It is based on water resistance, water repellency and water absorption characteristic of the fabric structure, including the fabric's geometric and internal structure and wicking characteristics of its fibers and yarns [34]. In this test method, perspiration generated from the body was mimicked. Several moisture management related properties of the fabrics were reported, including top and bottom wetting time (second), top and bottom absorption rate (% second), top and bottom wetting radius (millimeter), top and bottom spreading speed (millimeter/sec), cumulative one way transport capacity and overall moisture management capacity [34]. It is contributing to overall rating of comfort. The test can provide an idea of about person's microclimate, which is a critical factor in achieving body comfort. The Moisture management behavior of samples was tested using MMT according to AATCC TM 195 test method.

Results and Discussion

Effect of Radius of Curvature of Sphere on Fabric Compression

Five spheres with different diameters 4 cm, 6 cm, 8 cm, 10 cm and infinite (∞) [flat surface] were taken to analyze the effect of the radius of curvature of the sphere on fabric compression so that it becomes practically possible to do experiments with $10\text{ cm} \times 10\text{ cm}$ sample dimension with said standard. The effect is shown in Figure 5. The sphere denoted as S4, S6, S8, S10 and flat having diameter of 4 cm,

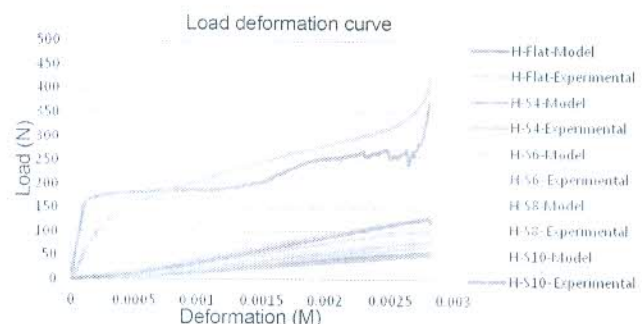


Figure 5. Effect of diameter of sphere on reaction force acted on sphere.

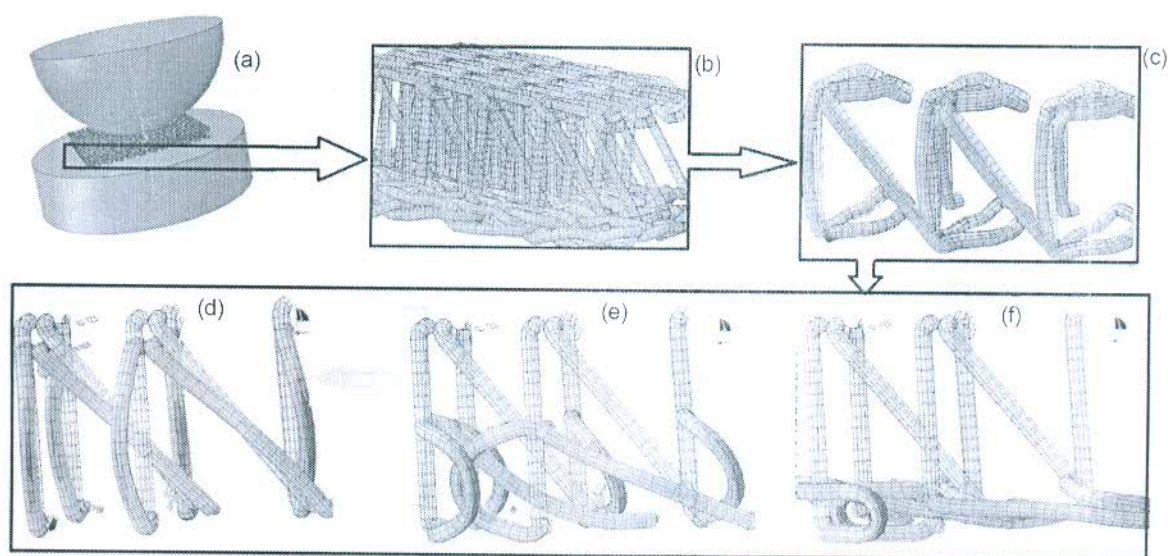


Figure 6. Stress distribution (Von mises) on elements of spacer yarn at different level of compression.

6 cm, 8 cm, 10 cm and ∞ respectively. The fabric structure was taken as Hexagonal mesh fabric. Hence, it is denoted as sample code H. It was observed that reaction force generated due to compression was linearly proportional with deformation with finite diameter sphere. It was further observed that experimental and FEM based reaction force, acted on center of the sphere with infinite diameter sphere, increased up to 428.61 N and 371.35 N respectively at 70 % deformation. Whereas, it was only 131.2 N and 130.85 N with 10 cm diameter sphere (S10) respectively. It was also observed that with decrease in diameter of sphere from 10 cm to 4 cm reaction force acted on center of sphere further decreased.

The observed fact is due to bending of monofilament yarns. The bending of monofilament takes place with contact with sphere which causes stress at the center of monofilament yarn (see Figure 6). Generated stress at monofilament causes reaction force on the sphere. With the increase in the diameter of sphere more number of monofilament bend at a time. More reaction force acts on a sphere with larger diameter. From the above fact, it can be concluded that spacer fabric provides more pressure to larger breast size than a smaller one. Large breast being associated with heavier mass requires more reaction force to control its movement during sporting activity. So spacer fabric may be a very effective component of the sports bra to control breast movement for different breast size, if structural parameters are controlled properly.

Effect of Linear Density of Spacer Yarn on Force Deformation Behavior

To minimize breast movement, it is necessary to control structural parameters of spacer fabric. Spacer yarn linear

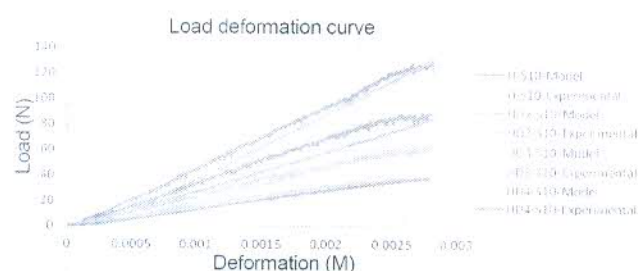


Figure 7. Effect of linear density (diameter) of monofilament yarn on force acting on sphere.

density is one of the important structural parameters that can be control the forces acting on the breasts. Four samples with different monofilament diameters denoted as H, HD2, HD3 and HD4 were compressed with spherical (S10) intender.

It was observed (see Figure 7) that reaction force acted on sphere was linearly proportional with deformation for all cases. It was further observed that experimental and FEM based maximum force generated for H-sample with sphere (S10) increased up to 131.2 N and 130.85 N respectively at 70 % deformation. Whereas, it was only 37.16 N and 39.1 N respectively with HD4 sample. Diameter of monofilament has relation like $H > HD2 > HD3 > HD4$. Hence, reaction force acting on sphere decreases with decrease in diameter monofilament yarn.

It is already explained in the previous section that bending of monofilament yarns played a predominant role on reaction force acting on the sphere. Higher the diameter of monofilament higher is the bending rigidity. It causes higher

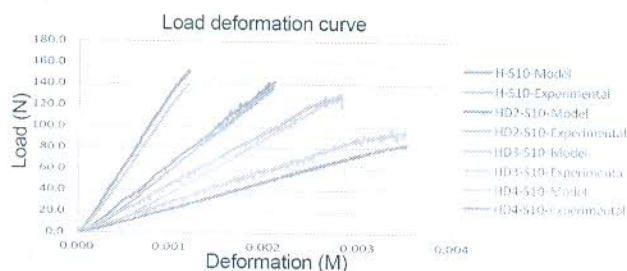


Figure 8. Effect of spacer fabric thickness on load deformation curves spherical compression.

stress generation on monofilament and subsequently higher reaction force. From the above fact, it can be concluded that the diameter of the spacer yarn needs to be optimized to control the reaction force acted on the breast. The force required for controlling breast movement can be increased or decreased by increasing or decreasing diameter of monofilament yarn.

Effect of Fabric Thickness on Force Deformation Behavior of Fabric

Spacer fabric thickness is one of the important structural parameters need to be controlled for controlling the reaction force acting on the breasts. Four different types of samples denoted as HS4, H, HS2 and HS1 were compressed with spherical (S10) intender. Thickness of samples has the order like HS4 > H > HS2 > HS1.

It was observed (see Figure 8) that slope of load deformation curve increased with lower thickness fabric. This is indicated that for same deformation, thinner fabric gives higher load than thicker fabric. The observation is for both experimental and FEM based data.

Reason behind the fact is that it is due to higher stress distribution at the center of spacer yarn with thinner sample. Thinner sample has a shorter length of spacer yarn than thicker sample. Shorter spacer yarns generate more reaction force than a longer one at the same percentage of deformation. From the above fact, it can be concluded that the thickness of spacer fabric needs to be optimized to control the reaction force acted on the breasts. The force required for controlling breast movement can be increased by decreasing thickness of fabric.

Energy Absorption during Compression

Sporting activity creates excessive movement of breasts. Energy produced during the movement of breast needs to be absorbed to control that movement. The energy can be absorbed during compression of spacer fabric and stored energy can be released during reversed directional movement of the breast. Compression energy, the energy required to compress fabric, is one of the important parameters needs to be analyzed. Energy can be calculated by calculating area

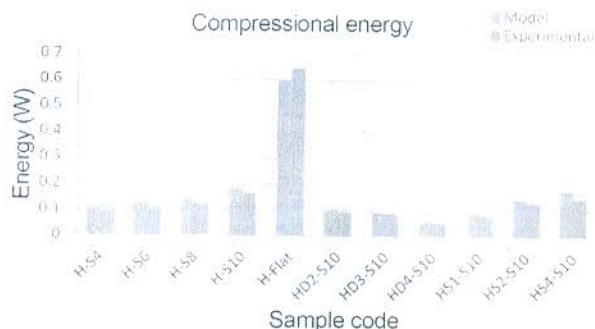


Figure 9. Absorbed energy (in watts) during interaction with sphere.

under the load-deformation curve. The energy calculated from FEM and experimental data are shown Figure 9.

It was observed from experimental and model based data that energy absorption was highest for infinite diameter sphere and lowest for 4 cm diameter sphere (S4). It was also observed that with decrease in diameter of sphere from 10 cm to 4 cm energy absorption decreases. Higher diameter of monofilament absorbed more energy than the lower diameter of monofilament and in the same fashion thicker fabric absorbed more energy than thinner fabric.

Reason behind these facts can be understood from the bending behavior of monofilament yarn. Bending of monofilament yarns takes place in contact with the sphere, which causes absorption of energy. As the diameter of the sphere is increasing, more is the number of monofilament bend at a time. Hence, more energy is absorbed during bending. Higher diameter of monofilament has higher bending rigidity. High bending rigidity causes higher absorption of energy. Thinner fabric has shorter spacer yarn than thicker fabric. It is known that Energy=Distance× Force. Reaction force obtained, after compressing lower thickness fabric, is more at a similar percentage of deformation. Whereas, distance required for compressing at 70 % deformation is less than that of high thickness fabric. Shorter spacer yarns deformed lesser amount than longer one. Hence, longer monofilament or thicker fabric absorbs more energy.

From the above fact, it can be concluded that spacer fabric absorbed more energy from larger breast size than a smaller one. Large breast being associated with heavier mass require more energy absorption to restrict movement during sporting activity. So spacer fabric acted as self adjusting structure to control breast movement irrespective of breast size. Higher diameter monofilament absorbed more energy. Hence, it will control breasts movement more effectively than that of lower diameter.

Comparison of Model Result with Experimental Values

Error of the prediction of load deformation curve obtained

Table 3. Percentage of error of prediction between model and experimental result

	H-Flat	H-S4	H-S6	H-S8	H-S10	HD2-S10	HD3-S10	HD4-S10	HS1-S10	HS2-S10	HS4-S10	Avg
E_L	27.2	23.7	21.1	30	27.6	22.2	32.2	30.9	16	30.6	26.8	26.2
E_e	6.7	17.5	17.1	22.2	8.9	15.3	6.8	12.7	13.3	18.7	21.3	14.6

is calculated by error percentage by following a formula

$$EL (\%) = \frac{1}{n} \sum_{i=0}^n \left| \frac{L_i^0 - L_i'}{L_i'} \times 100 \right|$$

where, L_i^0 is load value for i th deformation obtained from Models and L_i' is load value for i th deformation obtained from experiment. n (where, $n > 450$) is number of point considered on load deformation curves with equal spacing.

The deviation of prediction of compression energy is calculated by error percentage (Ee)

$$Ee (\%) = \frac{E_m - E_x}{E_x} \times 100$$

where, E_m is compression energy based on model. E_x is compression energy based on experiment. Error (Ee)% is shown in Table 3. It is observed that model based results have very good agreement with experimental results.

Comfort Characteristic of Sports Bra Fabric

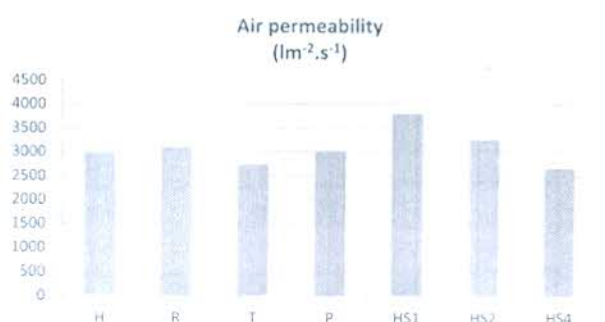
During a sporting activity lot of heat and moisture are generated in microclimate within the bra. It should be transmitted through the bra fabric at a much faster rate than the rate of generation. Spacer fabric to be used as a component of the bra should be characterized with good air permeability and moisture vapor permeability. Thermal resistance should be in accordance with external climatic condition. Bra fabric should have very good moisture management properties so that moisture generated due to excess sweating should be removed out of microclimate.

Air Permeability of Spacer Fabric

It was observed from the Figure 10 that different surface structures have different air permeability values. The value of air permeability has the order in sequence $R > P > H > T$.

The observed results are due to the openness of surface structure. Tricot structure is a compact structure at its face side. Compact structure provides more resistance to passage of air. R, P and H structures are porous surface structure. A porous structure provides easy passage of air, hence more permeability to air is observed.

Four samples with varying thickness were taken for study. It was observed that the air permeability of the samples were inversely proportional to their thickness (see Figure 10). This is because thicker fabric provides more resistance to passage of air. Hence, higher air permeability is obtained in thinner fabric.

**Figure 10.** Air permeability of spacer sample.

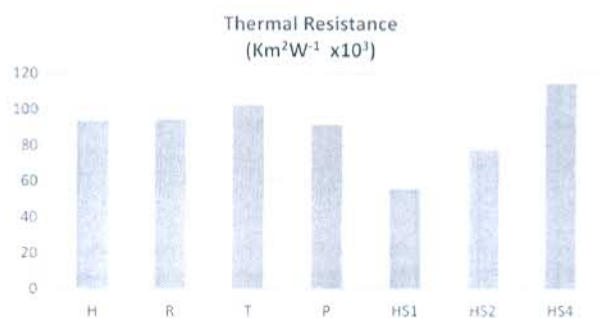
Thermal Resistance of Spacer Fabric

It was observed (see Figure 11) that different structures have different thermal resistances. Tricot structure has maximum thermal resistance. Whereas, Pillar and inlay structure has lowest thermal resistance value. Compact structure provides more resistance to passage of air. Hence, it is having higher thermal resistance, whereas other structures are having porous surface. A porous structure provides easy passage of air, hence more permeability to air, but at the same time it provides less thermal resistance.

Four samples with varying thickness were taken for study. It was observed (see Figure 11) that thermal resistance is directly proportional to fabric thickness. Thicker fabric provides more resistance to passage of air and hence keeps static air in its body. Static air results in more thermal resistance, hence thicker fabric provides more thermal resistance.

Water Vapor Resistance of Spacer Fabric

It was observed (see Figure 12) that different structures

**Figure 11.** Thermal resistance of spacer samples.

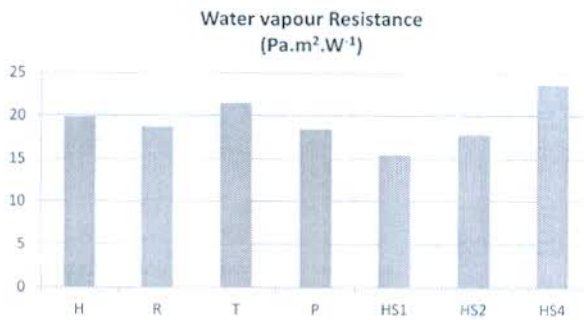


Figure 12. Water vapour resistance of spacer samples.

have different water vapor resistance characterization. It is observed that Tricot structure has maximum water vapor resistance and Pillar and inlay structure has lowest water

vapor resistance value. Compact structure provides more resistance to passage of air. Hence it has higher water vapor resistance. H, R and P structures are porous at its face side. A porous structure provides easy passage of air, hence more permeability to air, but less resistance to water vapor.

Four samples with varying thickness were taken for study. It is observed that water vapor resistance directly proportional to the thickness of the samples. Thicker fabric provides more resistance to passage of air and hence keeps static air in its body which causes more water vapor resistance.

Moisture Management Properties of Spacer Fabric

Moisture management property is another important characteristic for a sports bra fabric. Sporting activity generates a lot of moisture within the microclimate of bra due to excessive sweating. Bra fabric should have the

Table 4. Moisture management test result of spacer samples

Code	TOP	Bottom	TOP	Bottom	TOP max	Bottom max	TOP	Bottom	Accumulative one way transport index (%)	OMMC
	Wetting time (sec)	Wetting time (sec)	Absorption rate (%/sec)	Absorption rate (%/sec)	Wetted radius (mm)	Wetted radius (mm)	Spreading speed (mm/sec)	Spreading speed (mm/sec)		
H	11.6	8.6	22.3	47.4	15	30	1.4	4.4	425.71	0.85
HD2	12.6	9.5	24.6	51.9	14	31	1.3	4.8	523.76	0.84
HD3	10.6	7.4	20.6	42.7	16	29	1.4	4.2	478.98	0.83
HD4	11.6	6.4	23.6	46.9	15	30	1.3	5.9	567.76	0.84
R	10.2	3.7	10.3	52.7	10	30	0.9	8.3	612.11	0.86
T	8.6	6.9	21.9	50.5	17	32	1.8	3.8	345.57	0.77
P	9.6	3.8	12.8	48.9	11	28	1.1	6.9	576.87	0.86
HS1	5.6	4.8	37.4	82.8	16	29	1.5	4.1	697.65	0.89
HS2	7.5	5.8	29.6	76.7	13	30	1.4	4.0	612.67	0.87
HS4	28.6	6.6	12.8	36.6	10	32	1.3	5.7	412.98	0.79

Table 5. Grading of spacer samples

Code	TOP	Bottom	TOP	Bottom	TOP max	Bottom max	TOP	Bottom	Accumulative one way transport index (%)	OMMC
	Wetting time (sec)	Wetting time (sec)	Absorption rate (%/sec)	Absorption rate (%/sec)	Wetted radius (mm)	Wetted radius (mm)	Spreading speed (mm/sec)	Spreading speed (mm/sec)		
H	3	3	2	3	3	5	2	5	5	5
HD2	3	3	2	4	3	5	2	5	5	5
HD3	3	3	2	3	3	5	2	5	5	5
HD4	3	3	2	3	3	5	2	5	5	5
R	3	4	2	4	2	5	1	5	5	5
T	3	3	2	4	3	5	2	4	4	4
P	3	4	2	3	2	5	2	5	5	5
HS1	3	4	3	4	3	5	2	5	5	5
HS2	3	3	2	4	3	5	2	5	5	5
HS4	2	3	2	4	2	5	2	5	5	4

capability to transport that perspiration out of the microclimate. Results obtained from moisture management tests are shown in Table 4. Grade of fabric as per the test is shown in Table 5. It is observed that all spacer structures have very good moisture management properties. It is due to open and porous structure. Hence, any of the spacer structure can be used in sports bra. All samples used for study can easily transmit moisture out of microclimate.

Conclusion

It can be concluded that spacer fabric may be a very effective component of the sports bra to control breast movement for different breast sizes, if structural parameters controlled properly.

Structural parameters like spacer yarn diameter, thickness may be controlled to adjust the required force for controlling breast movement. The force required for controlling breast movement can be increased or decreased by increasing or decreasing diameter of monofilament yarn. Higher diameter of monofilament and thicker fabric absorb more energy. At same percentage of deformation, thinner fabric gives higher load than thicker fabric. Tricot structure is a compact structure provides more resistance to passage of air and moisture. R, P and H structures provide easy passage of air and moisture. A higher air permeability and moisture vapor permeability are obtained with thinner fabric. Thermal resistance is directly proportional to fabric thickness. Tricot structure has a maximum thermal resistance. Where, as Pillar and inlay structure has lowest thermal resistance value. All spacer fabrics have very good moisture management properties. Hence, Spacer fabric may be considered as a very effective component of sports bra for controlling breast movement without compromising with comfort of sports women.

References

1. C. W. Patrick, *Annu. Rev. Biomed. Eng.*, **6**, 9 (2004).
2. K. Okabe, T. Kurokawa, *J. Home Economics of Japan*, **56**, 379 (2005).
3. Y. W. Man, "Advances in Women's Intimate Apparel Technology", Woodhead Publishing Series in Textiles, 2016.
4. N. L. Shivitz, "Adaptation of Vertical Ground Reaction Force Due to Changes in Breast Support in Running", Master of Science Thesis, Oregon State University, 2001.
5. W. Yu, J. Fan, S. C. Harlock, and S. P. Ng, "Innovation and Technology of Women's Intimate Apparel", Woodhead Publishing Series in Textiles, 2006.
6. C. Starr, D. Branson, R. Shehab, C. Farr, S. Ownbey, and J. Swinney, *J. Text. Apparel Technol. Manage.*, **4**, 1 (2005).
7. D. E. McGhee and J. R. Steele, *Med. Sci. Sport. Exer.*, **42**, 1333 (2010).
8. A. A. Zadpoor, A. A. Nikooyan, and A. R. Arshi, *Journal of Biomechanics*, **40**, 2012 (2007).
9. B. M. Nigg and W. Liu, *Journal of Biomechanics*, **32**, 849 (1999).
10. J. Vance and A. Hreljac, *J. Hamill, Eur. J. Appl. Physiol.*, **87**, 403 (2002).
11. M. F. Bobbert, M. R. Yeadon, and B. M. Nigg, *Journal of Biomechanics*, **25**, 223 (1992).
12. K. A. Christina, S. C. White, and L. A. Gilchrist, *Human Movement Science*, **20**, 257 (2001).
13. J. C. Scurr, J. L. White, and W. Hedger, *J. Sports Sci.*, **29**, 55 (2011).
14. H. Pontzer, J. H. Holloway, D. A. Raichlen, and D. E. Lieberman, *J. Exp. Biol.*, **212**, 523 (2009).
15. K. Bowles and J. R. Steele, *J. Sci. Med. Sport*, **6**, S67 (2003).
16. A. Milligan, C. Mills, J. Corbett, and J. Scurr, *J. Sports Sci.*, **33**, 2025 (2015).
17. B. R. Mason, K. A. Page, and K. Fallon, *J. Sci. Med. Sport*, **2**, 134 (1999).
18. J. Scurr, N. Brown, J. Smith, A. Brasher, D. Risius, and A. Marczyk, *J. Adolesc. Health*, **58**, 167 (2016).
19. X. Lin, Y. Li, J. Zhou, X. Cao, J. Hu, Y. Guo, S. Sun, R. Lv, Y. Lin, Q. Ye, and H. Leung, *Text. Res. J.*, **85**, 2030 (2015).
20. A. Milligan, C. Mills, J. Corbett, and J. Scurr, *J. Sports Sci.*, **33**, 2025 (2015).
21. B. R. Mason, K. A. Page, and K. Fallon, *J. Sci. Med. Sport*, **2**, 134 (1999).
22. L. J. Lawson and D. Lorentzen, *Cloth. Text. Res. J.*, **8**, 55 (1990).
23. M. Lu, J. Qiu, G. Wang, and X. Dai, *Materials Today Communications*, **6**, 28 (2016).
24. J. Kaye and M. D. Abbott, *U. S. Patent*, 7214120B2 (2007).
25. H. Heath and S. Krueger, *U. S. Patent*, 8690634 B2 (2014).
26. M. Scheininger, S. Castellano, and D. Gilliland, *U. S. Patent*, 7867057 B2 (2011).
27. M. He, *U. S. Patent*, 8317568 B2 (2012).
28. J. Yip and S. P. Ng, *J. Mater. Process Technol.*, **209**, 58 (2009).
29. Y. P. Liu, W. M. Au, and H. Hu, *Text. Res. J.*, **84**, 422 (2014).
30. Y. P. Liu, H. Hu, and W. M. Au, *Text. Res. J.*, **84**, 312 (2014).
31. M. K. Datta, B. K. Behera, and A. Goyal, *J. Ind. Text.*, **48**, 1489 (2019).
32. D. Zhaoqun, M. Li, Y. Wu, and L. He, *J. Ind. Text.*, **46**, 1362 (2015).
33. ASTM F1868 - 17 <https://www.astm.org/Standards/F1868.htm>
34. AATCC 195-2017 https://www.techstreet.com/standards/aatcc-195-2017?product_id=2018816#jumps

Prediction and analysis of compression behaviour of warp-knitted spacer fabric with cylindrical surface

Mrinal K Datta¹, B K Behera² and Ashvani Goyal³

Abstract

Nowadays, applications of spacer fabric cover wider areas of technical textile. It is used in the automotive textile, personal protective clothing, sports textile, foundation garments, pads for swimwear, buffer clothing, medical textile etc. It does possess good recovery to compression, high bulk with relatively lightweight and very good moisture permeability. Almost in all applications, spacer fabrics are compressed by different parts of human body. Body parts have different shapes and curvatures. In all standard methods, spacer fabric compressibility is measured by a pair of flat circular plate which cannot represent a human body. The contour of body can be assumed as cylindrical with varying radius of curvature. So, it is necessary to understand the mechanism of compression of spacer fabric with cylindrical surface in order to understand the performance of the fabric under real-world dynamics. In this research, an effort is being made to predict the compression behaviour of warp-knitted spacer fabric by flat as well as cylindrical surface. Finite Element Models were designed on Abaqus/CAE platform to meet above requirement with variable circumstances. Experimental setup was also made to analyse cylindrical and flat compression at different circumstances. Results show that flat compression and cylindrical compression are largely deferred in terms of shape of load-deformation curve and compressional energy. Effect of variables on compression behaviour was also analysed. Model results were validated with experimental values. It is found that the proposed model has got a good agreement with the experimental results.

¹Textile Technology, Northern India Textile Research Association, Ghaziabad, India

²Textile Engineering, Indian Institute of Technology, Delhi, India

³Textile Technology, The Technological Institute of Textile and Sciences, Bhiwani, India

Corresponding author:

Mrinal K Datta, Northern India Textile Research Association, HIG H5A Sector 23, Raj Nagar, Sanjay Nagar, Ghaziabad, Uttar Pradesh 201002, India.

Email: mkd22222000@gmail.com

Keywords

Warp knitting, spacer fabric, finite element analysis, cylindrical compression, compressional energy

Introduction

Warp-knitted spacer fabrics comprise two outer layers that are connected together but kept apart by an inner layer of spacer monofilaments [1]. Spacer fabrics possess good resilience to compression, high bulk with relatively lightweight and very good moisture permeability with thermoregulation [2, 3]. In addition, spacer fabrics are good at pressure relief [3–5]. The unique combination of these characteristics made this fabric suitable for a wide range of applications.

Nowadays, applications of spacer fabric cover wider areas, from a simple replacement of foam in bags to diversified areas of technical textiles. It is used in the areas of automobile textile (as a cushions [6] or car seats [7]), personal protective clothing (as a cushioning material [8–10]), sports textile [11], and foundation garments (functional bra support [12]), pads for swimwear [13], buffer clothing [14], medical textile (knee braces [15]), geo-textile, civil engineering, etc. However, engineering design of spacer architecture is still at its infancy.

Almost in all above applications, spacer fabrics are compressed by different parts of human body. Radius of curvature of various parts of human body changes with age and varies with gender. It also varies from one person to another person. Not only this, different parts of a human body have different shapes and curvatures. Hence, the contour of body can be assumed as cylindrical with varying radius of curvature. Many authors have described assessment of protective properties of warp-knitted spacer fabrics in hemispherical form, in order to simulate the realistic requirement of human body protection [16–18]. In all standard methods, spacer fabric compressibility is measured by a pair of circular plate which is basically a flat surface and cannot represent truly a human body in its shape. So, it is necessary to understand the mechanism of compression of spacer fabric with cylindrical surface. On the above circumstances, this paper aims to understand behaviour of warp-knitted spacer fabric under the compressive load by flat as well as cylindrical surface. An effort is also being made to predict the compression behaviour in order to understand the performance of the fabric under real-world dynamics.

Experimental details

Preparation of fabric samples

It was found that four-guide bar structures are the most popular commercial structures due to economical advantage over six-guide bar structures but hardly any research work had been done with four-guide-bar structures. Hence, all the samples in the study were produced double-needle bad Raschel knitting machine with four-guide bars. Two front guide bars (GB1 & GB2) knit a base fabric on the front

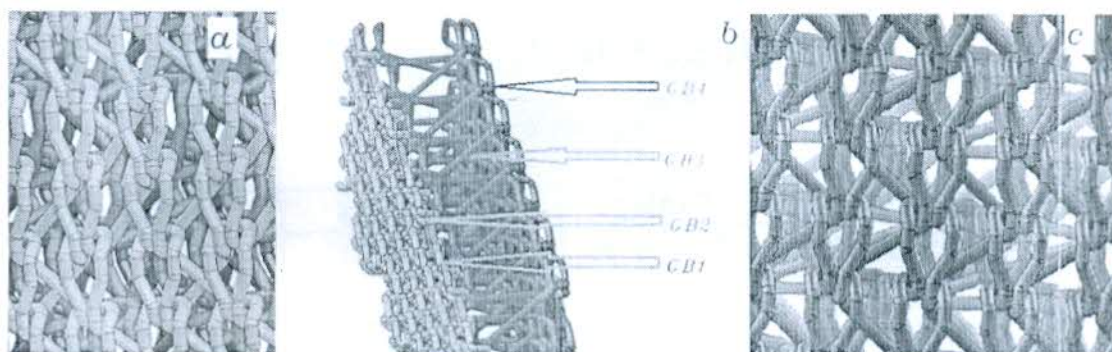


Figure 1. Four-guide bars construction of spacer fabric. (a) Face fabric made of two guide bars yarn (GB1 & GB2). (b) Spacer yarn in between face and back fabric (GB3). (c) Back fabric made of back guide bar yarn (GB4).

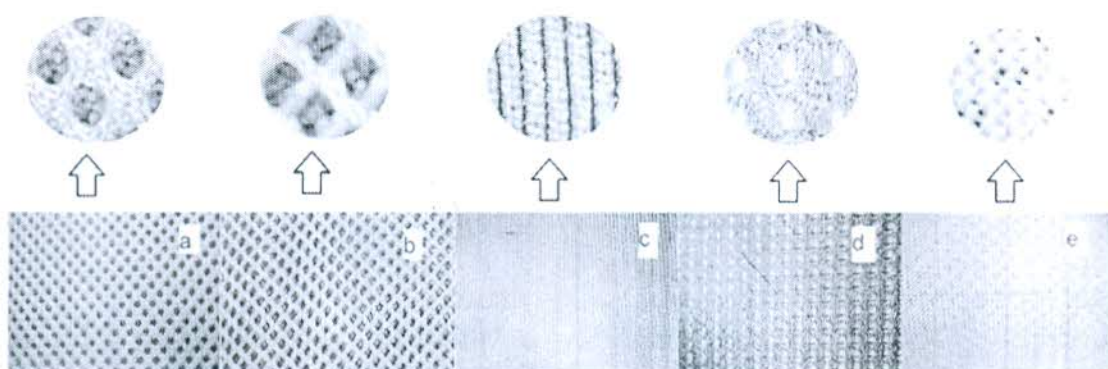


Figure 2. Face and back fabric surface structure. (a) Rhombic Mesh (R). (b) Hexagonal Mesh (H). (c) Full Tricot (T). (d) Pillar with inlay structure (P). (e) Close lap structure with one needle space under lap.

needle bar and one back guide bar (GB4) knit base fabric on the back needle bar. One spacer guide bar (GB3) knits on both needle beds in succession (see Figure 1). Back needle bar structure was kept same for all of the samples. It was close lap structure with one needle space under lap.

All the samples were produced by polyester filament yarn. Multifilament yarn of 20 tex/96 f was used in both front guide bars and back guide bar. Monofilament yarns were used in the spacer guide bar. Four different surface structures namely Hexagonal mesh (H), Rhombic mesh (R), Full Tricot structure (T), Pillar with inlay structure (P) were developed at front needle bar for investigation with spacer yarn linear density 28 tex (dia 0.2 mm) (See Figure 2). Three others spacer yarn linear density 22 tex (dia 0.18 mm), 18 tex (dia 0.16 mm) and 14 tex (dia 0.14 mm) were also taken for samples preparation. Three other Hexagonal mesh (H) structures were produced by using those monofilament spacer yarns. They are identified in this paper as HD2, HD3 and HD4, respectively. Table 1 gives a summary of all structures.

Table 1. Chain notations for front and back guide bar surface structures.

Chain notation (with type of threading)	Appearance
Rhombic mesh (R) GB1: 1-0-0-0/1-2-2-2/2-3-3-3/2-1-1-1/(1 Threaded and 1 Empty) GB2: 2-3-3-3/2-1-1-1/1-0-0-0/1-2-2-2/(1 Threaded and 1 Empty) GB3: 1-0-1-0/2-1-2-1/(1 Threaded and 1 Empty) GB4: 1-1-1-0/1-1-1-2/(fully threaded.)	Front fabric: See Figure 2(a) Back fabric: See Figure 2(e)
Hexagonal mesh (H) GB1: (1-0-3-3/3-2-1-1) × 2/1-0-3-3/3-2-4-4/(5-4-3-3/3-2-4-4) × 2/5-4-3-3/3-2-2-2/(2 Threaded and 2 Empty) GB2: (5-4-3-3/3-2-4-4) × 2/5-4-3-3/3-2-1-1/(1-0-3-3/3-2-1-1) × 2/1-0-3-3/3-2-4-4/(2 Threaded and 2 Empty) GB3: 1-0-1-0/3-2-3-2/(2 Threaded and 2 Empty) GB4: 1-1-1-0/1-1-1-2/(fully threaded.)	Front fabric: See Figure 2(b) Back fabric: See Figure 2(e)
Full Tricot structure (T) GB1: 1-0-1-1/1-2-1-1/(1 Threaded and 1 Empty) GB2: 1-2-1-1/1-0-1-1/(1 Threaded and 1 Empty) GB3: 1-0-1-0/(1 Threaded and 1 Empty) GB4: 1-1-1-0/1-1-1-2/ (fully threaded.)	Front fabric: See Figure 2(c) Back fabric: See Figure 2(e)
Pillar with inlay structure (P) GB1: 1-0-1-1/(2 Threaded and 2 Empty) GB2: 0-0-0-0/5-5-5-5/4-4-4-4/5-5-5-5/0-0-0-0/1-1-1-1/(2 Threaded and 2 Empty) GB3: 1-0-1-0/(2 Threaded and 2 Empty) GB4: 1-1-1-0/1-1-1-2/(fully threaded.)	Front fabric: See Figure 2(d) Back fabric: See Figure 2(e)

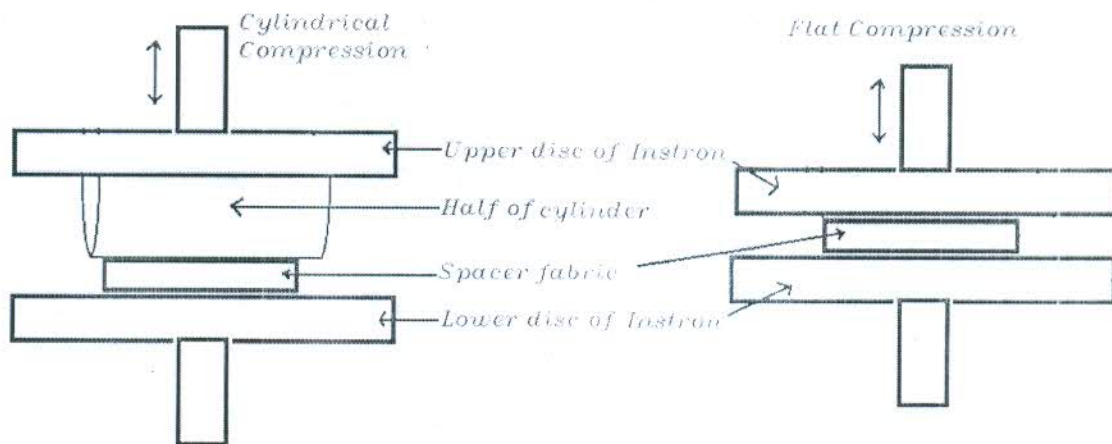
The space between two surface layers is also an important structural feature of a warp-knitted spacer fabric. That space can be control by adjusting distance between two needle bars. Sample H was developed by keeping distance 6.5 mm. Other three samples were produced with a distance between two needle bars of 4.5, 5.5 and 7.5 mm, respectively. Those samples were denoted as HS1, HS2 and HS4, respectively. Table 2 gives summary of all variables used for samples preparation.

Compression tests

An INSTRON 3382 device was used to measure flat plate compression with reference to the standard ASTM D575. A pair of circular plates with a diameter of 15 cm were used. The compression speed was set to 1 mm/min. The samples' size was 10 cm × 10 cm. To measure cylindrical compression, four cylinders (with diameter of 4, 6, 8 and 10 cm) made of non-compressible material were taken. Cylinders were cut vertically to get two equally divided half cylinders and one half cylinder was placed separately in between spacer fabric and upper plate. Double-sided adhesive tape was used to stick flat surface of half-cylinder with upper plate to

Table 2. Summary of variables used for samples preparation.

Serial No	Sample code	Monofilament yarn linear density (tex)	Distance between needle bars (mm)	Face surface structure
1	H	28	6.5	Hexagonal mesh
2	R	28	6.5	Rhombic mesh
3	T	28	6.5	Full Tricot
4	P	28	6.5	Pillar with inlay
5	HD2	22	6.5	Hexagonal mesh
6	HD3	18	6.5	Hexagonal mesh
7	HD4	14	6.5	Hexagonal mesh
8	HS1	28	4.5	Hexagonal mesh
9	HS2	28	5.5	Hexagonal mesh
10	HS4	28	7.5	Hexagonal mesh

**Figure 3.** Measurement of compressibility by cylindrical upper plate and flat upper plate, respectively.

avoid slippage during compression (see Figure 3). All compression tests were conducted to compress the material with maximum compression strain of 0.70, thereafter allowed to recover at same speed mentioned above.

Models

Finite element models were developed in Abaqus/CAE 6.12-1 platform to measure compression performance under different variable situations as per sample plan. The parts of models (see Figure 4) were designed in Solidworks platform and imported to Abaqus. In Finite Element Models [FEMs], Young's modulus, Poisson's ratio and density of polyester yarn were taken 6773.3 MPa, 0.3 and

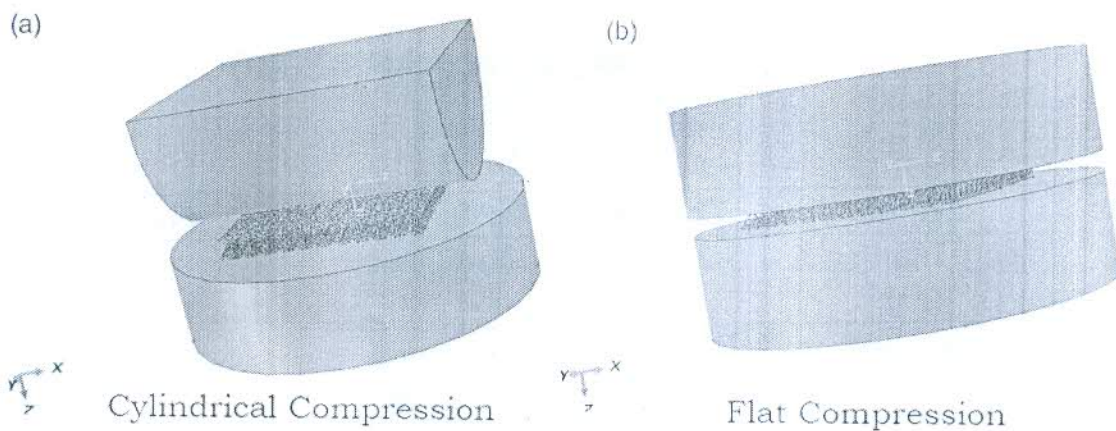


Figure 4. Parts of FEMs were developed in Abaqus/CAE 6.12-1 platform. (a) Cylindrical compression. (b) Flat compression.

$1.38 \times 10^3 \text{ kg/m}^3$, respectively. It was assumed that upper plate, lower plate and cylinder were made of solid hard material. Young's modulus, Poisson's ratio and density of solid hard material were considered as 200 GPa, 0.29 and $7.872 \times 10^3 \text{ kg/m}^3$, respectively [18]. Solid homogeneous sections were taken. Isotropic polyester material was considered for analysis. 'Standard 3D Stress' type of elements was used with an eight-node linear brick, reduced integration and hourglass control. Analysis was done in 'General-Dynamic-Explicit' procedure with step time of 1 s with default iterative nonlinear solver. Yarn to yarn and yarn to steel frictional coefficient was considered 0.3. Directionality of frictional properties was considered 'isotropic' and frictional formulation was used as 'Penalty' in Abaqus/CAE 6.12-1. Lower disc bottom face was pinned. Upper disc and cylinder having no displacement and rotation with respect to X- and Y-axes. Velocity of upper plate and cylinder was taken in such a way to compressed and allowed to recover 70%.

Results and discussion

Compression and recovery characteristics

Spacer fabric samples were compressed and allowed to recover by two different methods. First method was flat compression, where it was compressed and allowed to recover by upper flat disc of Instron device. Second method was cylindrical compression, where it was compressed and allowed to recover by a cylinder by keeping cylinder at bottom of upper disc of Instron device. Finite element models were also designed to meet above situation of experimental environment. Contours of von Mises stress developed in FEM are computed at an element levels. Those images help us to understand magnitude of stress develop on different regions of spacer fabric during dynamic compression and recovery activity. For clear understanding, only a small portion of spacer yarn is shown (see Figure 5). It is observed that higher stress is concentrated at centre of vertical parts of spacer yarn, which causes recovery at removal of deforming forces.

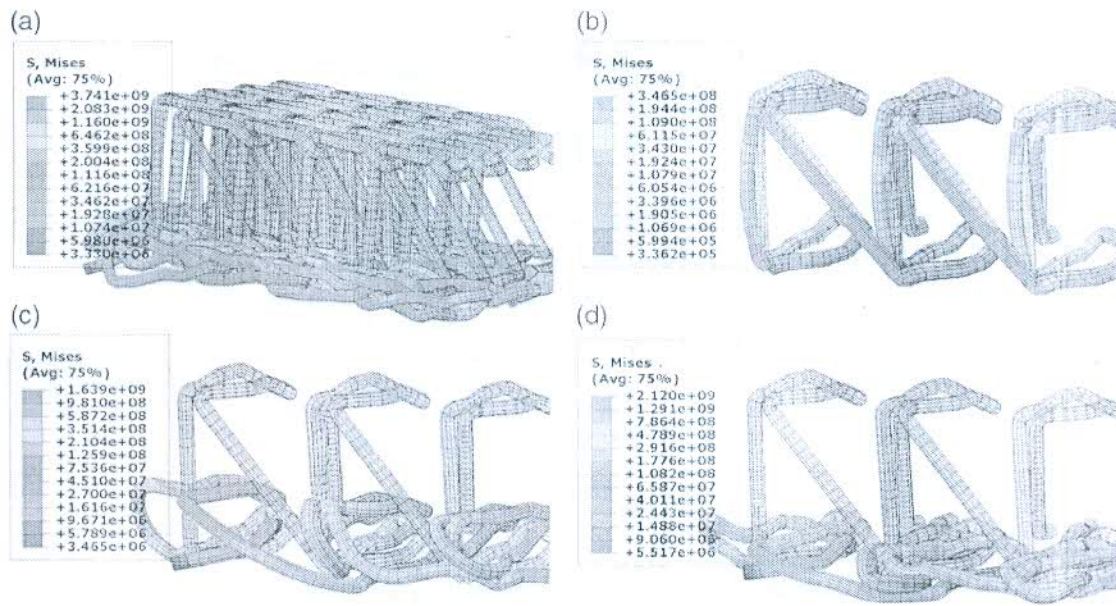


Figure 5. Von Mises stress distribution on elements of spacer yarn during compression. (a) At 70% compression of spacer yarn structure. (b) At 10% compression of spacer loops. (c) At 50% compression of spacer loops. (d) At 70% compression of spacer loops.

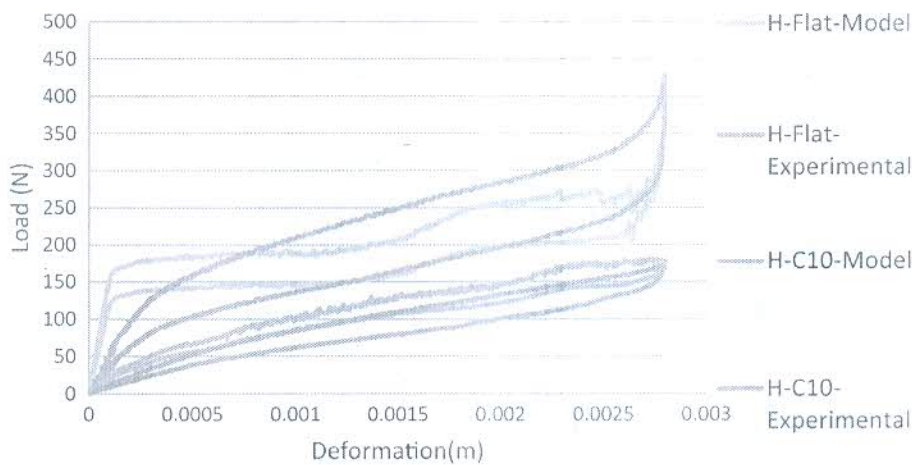


Figure 6. Compression and recovery curves.

Flat and cylindrical compression and recovery curves obtained from the model and experiment of Hexagonal mesh fabric (Sample code H) are shown in Figure 6. (Other samples having similar trend are not shown in this figure.) It is observed from figures that load-deformation behaviour of spacer fabric under compression by flat surface and cylindrical surface largely differ. The difference is clearly depicted from all the figures (see Figures 6–10) of load-deformation curves. In flat compression, spacer fabric is compressed uniformly by its whole flat surface. Shape of curves obtained during compression by flat surface can be divided in three sections (see Figure 6).

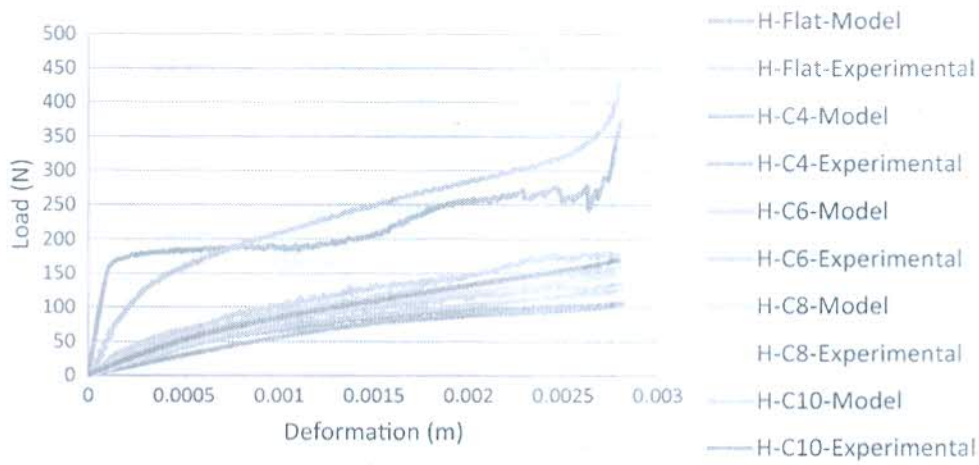


Figure 7. Effect of radius of curvature of cylinder on load-deformation curve.

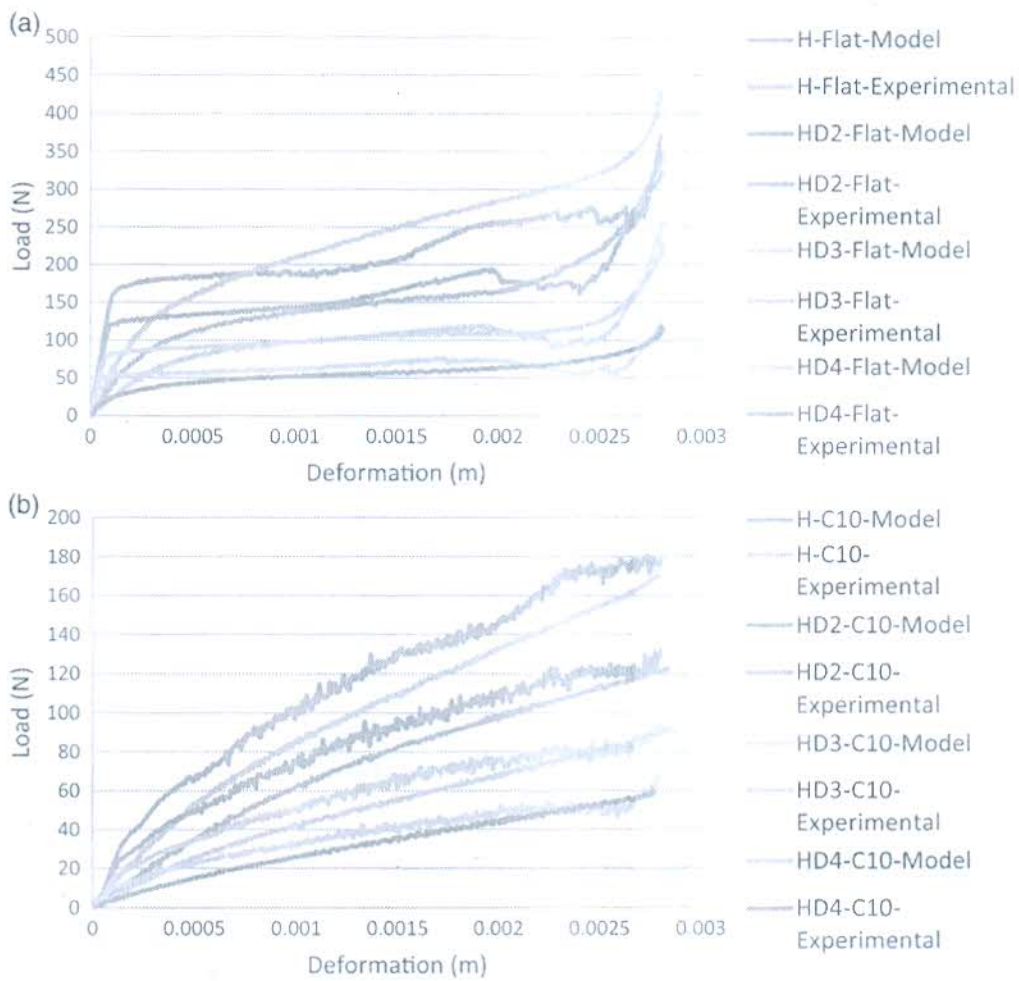


Figure 8. Effect of linear density (diameter) of monofilament on load-deformation curve for flat and cylindrical compression. (a) Flat compression. (b) Cylindrical compression.

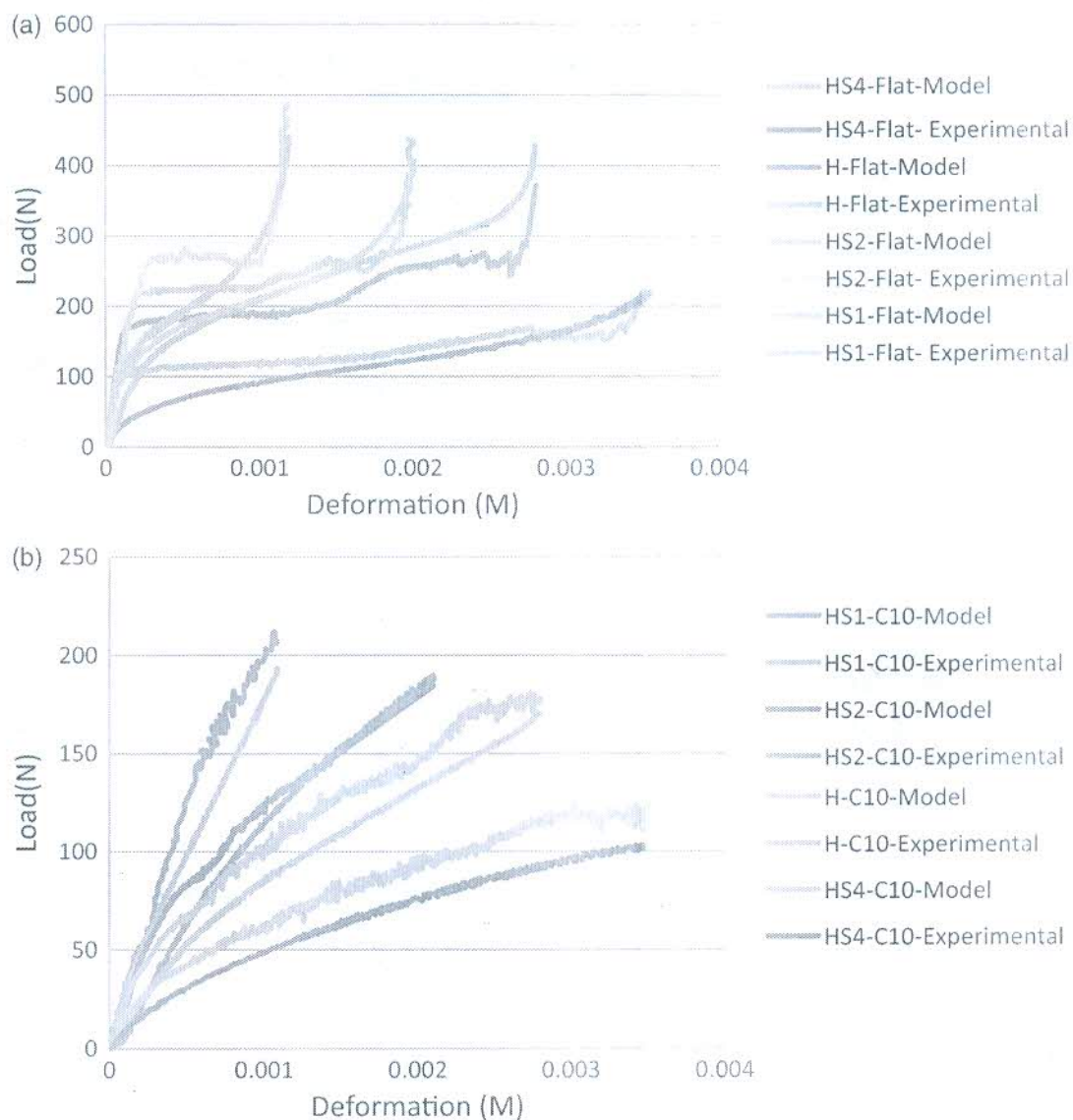


Figure 9. Effect of spacer fabric thickness on load-deformation curves for flat and cylindrical compression. (a) Flat compression. (b) Cylindrical compression.

In first section, load increases suddenly on contact. At contact, monofilament yarns resist downward movement of upper surface. Hence, load increases sharply till bending of monofilaments starts. In second section, load increases very slowly as bended monofilaments cannot resist downward movement. In this section, fabric is compressed and free space present in the structure of fabric reduces gradually. In third section, again load increases sharply as free space almost removed in earlier stage. The shape of the recovery curves is almost similar to the compression curves but in reverse direction and lagged behind the compression curves. At start of recovery, load decreases suddenly, thereafter decreases gradually and finally recovers fully.

However, in case of cylindrical compression, no such clearly distinguishing section is observed. Load gradually increases with deformation. Rate of increment of

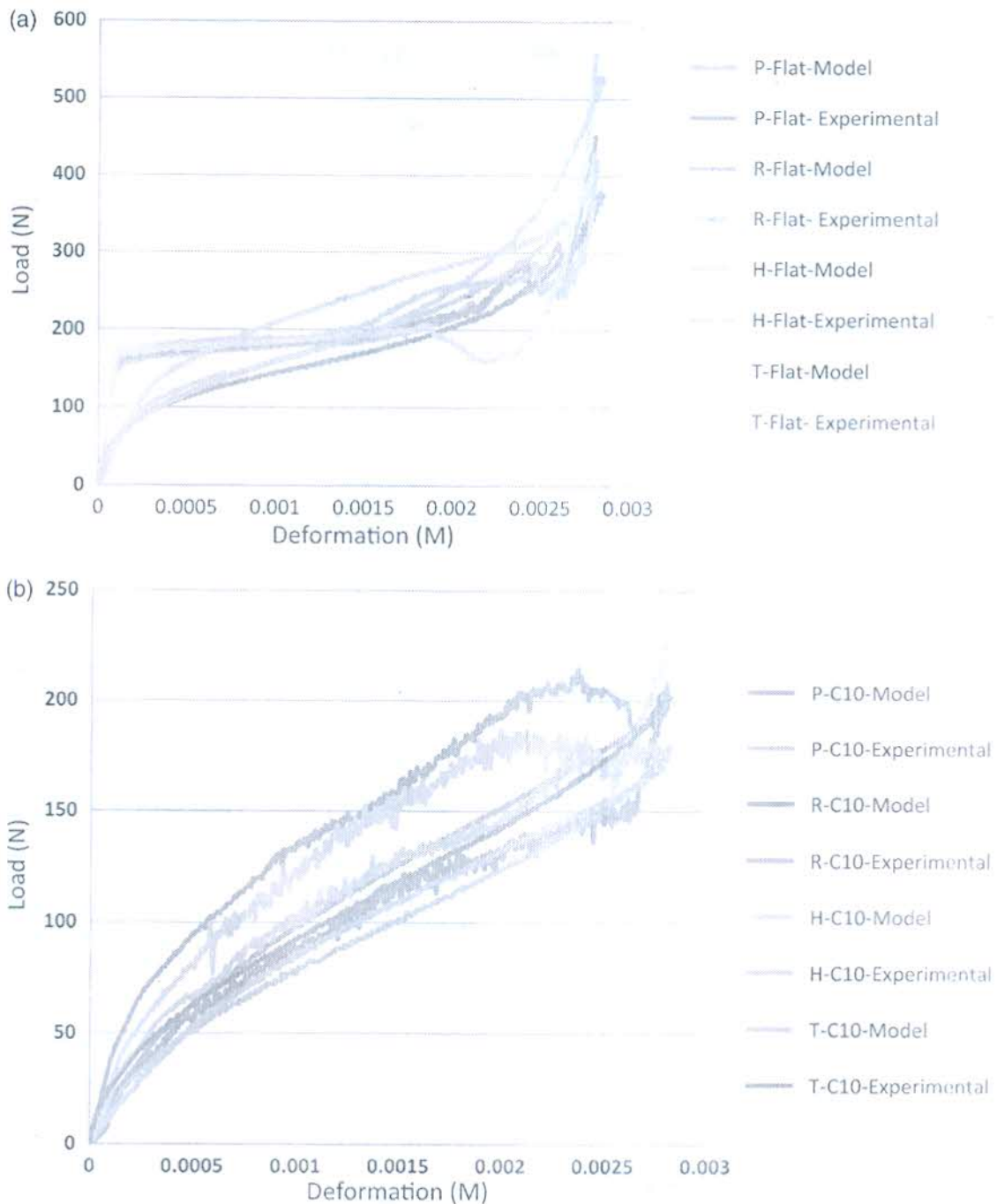


Figure 10. Effect of spacer fabric surface structure on load-deformation curves for flat and cylindrical compression. (a) Flat compression. (b) Cylindrical compression.

load with deformation is lower than that of flat compression. In flat compression, whole upper surface of fabric is compressed at a time, whereas cylindrical compression starts from a line. Gradually it spreads towards front and back side of that line. Initially, bending of monofilament starts from that contact line; thereafter, it spreads to its back and front side. Shape of recovery curve is almost similar

to compression curve from reverse direction and recovery curve lagged behind the compression curve.

Effect of radius of curvature of cylinder

Four cylinders with different diameters 4, 6, 8 and 10 cm were taken for experiment. Similarly, FE models were also designed to replicate experimental conditions. In Figure 7, the cylinder denoted as C4, C6, C8 and C10, having diameter of 4, 6, 8 and 10 cm, respectively. Flat surface may be considered as cylinder of infinite diameter that is also considered for comparison.

It is observed from experiment and from FEM that load increases up to 428.61 and 371.35 N, respectively, at 70% deformation for flat compression of Hexagonal Mesh (see Figure 7). Similar values for cylindrical compression with 10 cm diameter cylinder (C10) were only 169.41 and 177.86 N, respectively. The values reduce with reducing diameter of cylinder. As cylinder moves downward, bending of monofilaments takes place. Rate at which monofilament yarns bend depends on diameter of cylinder. That finally determines the rate of increase of load in load-deformation curve.

Effect of linear density of spacer yarn

Linear density of monofilament spacer yarn is one of the important factors of compressibility of spacer fabric. Four different linear densities of monofilament were taken for sample preparation. Flat and cylindrical (by C10) compressibility were measured and similar finite element models were also designed to replicate experimental condition. Effect of linear density (diameter) of monofilament on load-deformation curve is shown in Figure 8. It is observed that coarser diameter of monofilaments leads to higher load at same deformation. With increase in diameter of monofilament, it is observed that bending rigidity of filament increases that leads to increase slope of load-deformation curve (see Figure 8). Above effect is observed for flat as well as cylindrical compression for both experimental- and model-based load-deformation curves.

Effect of fabric thickness

The effect of fabric thickness on load-deformation curve is shown in Figure 9. It is observed that load required to deform thicker fabric (HS4) is lesser than that of thinner fabric (HS1) at same percentage of deformation. The trend is similar for both flat and cylindrical compression though in cylindrical compression fabric deform at lower deforming force. Spacer fabrics having higher thickness have longer length of monofilaments. Long monofilaments can easily bend than shorter ones. Hence, low-thickness fabric has more load bearing capability than thicker spacer fabric. It is also observed that load for cylindrical compression is always lower than flat compression.

Effect of fabric structure

Load-deformation curve also depends on surface structure of spacer fabric. That is depicted from Figure 10. Four different structures were taken under study. It is found that Tricot structure, which is most compact surface structure (visual appearance), shows higher load (Model 557.52 N, Exp 528.37 N) at 70% deformation, whereas other structures, comparatively open structures (visual appearance), show lower load than Tricot structure at 70% deformation value. Though flat and cylindrical compression have shown similar trend but effect is less prominent in case of cylindrical compression (see Figure 10). Load bearing capability of any material depends on its compactness of structure. Tricot structure is more compact structure, hence it is deformed at higher load, whereas other structures require lower deformative force.

Error of prediction of load-deformation curve

Error of prediction of load-deformation curve is calculated by error percentage

$$E_{LDC} (\%) = \frac{1}{n} \sum_{i=0}^n \left| \frac{y_i^0 - y_i'}{y_i'} \cdot 100 \right| \quad (1)$$

where y_i^0 is load value for i -th deformation obtain from Models and y_i' is load value for i -th deformation obtain from experiment. n (where $n > 450$) is number of point consider on load-deformation curves in equal spacing (See Table 3). It is found that predicted load-deformation curves are validated with experimental curves with an average error percentage of 26.8. Hence, the predicted results have got a good agreement with the experimental results.

Compressional energy

Compressional energy is the energy required to compress fabric. It is the area under load-deformation curve. Compressional energies are calculated from FEM and

Table 3. Percentage of error of prediction of load-deformation curve in between model and experimental results.

H-flat	H-C4	H-C6	H-C8	H-C10	HD2-flat	HD2-C10	HD3-flat
27.2	26.6	21.1	22.0	22.4	28.6	26.5	28.8
HD3-C10	HD4-flat	HD4-C10	HS1-flat	HS1-C10	HS2-flat	HS2-C10	HS4-flat
26.4	31.6	30.3	26.4	20.9	21.5	28.84	35.6
HS4-C10	P-flat	P-C10	R-flat	R-C10	T-flat	T-C10	Avg
27.8	28.5	11.1	27.5	36.7	34.4	24.4	26.8

experiment with all variable circumstances is shown in Figure 11. It depends on radius of curvature of cylinder (see Figure 11(a)). Higher the radius of curvature more the energy required to compress the material, because more area is compressed with it. Flat surface is a cylinder of infinite radius, hence flat compressional energy is higher than that of cylindrical compression. The effect of linear density of spacer yarn on compressional energy is shown in Figure 11(b). It is observed that spacer fabric with finer spacer yarn requires lower energy to compression. Finer linear density of monofilament yarn having lower bending rigidity than that of coarser one, easily bends at low load. Hence, lower energy is required to compress material. Compressional energy also depends on thickness of spacer fabric (see Figure 11(c)). It is found that compressional energy increases with increase in thickness up to 4 mm after that it decreases. It is known that $\text{Energy} = \text{Force} \times \text{Distance}$. It is already discussed in previous sections that force required to compress lower thickness fabric is more at similar percentage of deformation, whereas distance required to compressing at 70% deformation is less than that of high-thickness fabric. Hence, above effect is the result of combined effect of force and distance. Effect of structure is shown in Figure 11(d). It is observed that four different

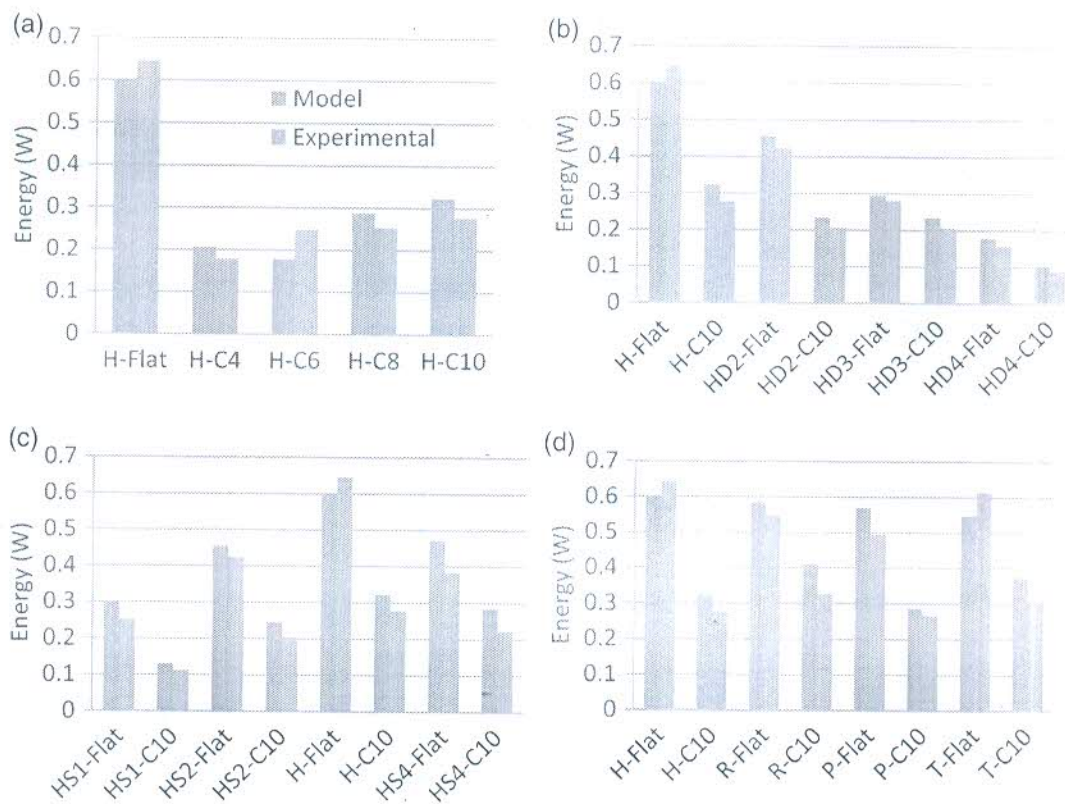


Figure 11. (a) Effect of radius of curvature on compressional energy, (b) effect of linear density (diameter) of monofilament on compressional energy for flat and cylindrical compression, (c) effect of spacer fabric thickness on compressional energy for flat and cylindrical compression, (d) effect of spacer fabric surface structure on compressional energy for flat and cylindrical compression.

Table 4. Percentage of error of prediction compressional energy in between model and experimental results.

H-flat	H-C4	H-C6	H-C8	H-C10	HD2-flat	HD2-C10	HD3-flat
6.74	15.85	14.29	13.68	16.60	7.73	13.66	4.96
HD3-C10	HD4-flat	HD4-C10	HS1-flat	HS1-C10	HS2-flat	HS2-C10	HS4-flat
9.66	13.23	16.48	18.74	17.91	6.89	6.59	14.23
HS4-C10	P-flat	P-C10	R-flat	R-C10	T-flat	T-C10	Avg
26.66	14.96	7.07	6.41	25.65	10.87	21.17	13.48

structures under study have almost same compressional energy with minute deviation. Hence, no conclusion can be drawn regarding effect of structure.

Error of prediction compressional energy

Error of prediction of compressional energy is calculated by error percentage (E_{CM})

$$E_{CM}(\%) = \frac{E_M - E_E}{E_E} \times 100 \quad (2)$$

where E_M is compressional energy based on model. E_E is compressional energy based on experiment. Error (E_{CM}) % is shown in Table 4. It is found that predicted compressional energies are validated with experimental values with an average error percentage of 13.48, the predicted results have got a good agreement with the experimental results.

Conclusion

It may be concluded from above discussion that results obtained from FEM are comparable with experimental results with certain percentage of acceptable error. Load-deformation curves and results of compressional energy, obtained from FEM-based and experimental-based, have shown similar trend with an average error percentage of 26.79 and 13.48, respectively. Flat compressibility and cylindrical compressibility behaviour of spacer fabrics differ to a certain extent. Behaviour of spacer fabrics compressibility depends on radius of curvature of cylinder. In case of higher radius of curvature, more reaction force is obtained from similar level of deformation percentage. Hence, compressional energy also becomes higher for higher radius of curvature. Compressibility properties also depend on linear density of spacer yarn. Finer denier yarn gives low reaction force than coarser denier. Thickness plays an important role on compressibility behaviour of spacer fabric. It is observed, under above study, that 4 mm fabric gives maximum reaction force at 70% deformation. Initially, reaction force increases with increase in thickness, thereafter, decreases at a certain level of

deformation percentage. Structure has certain influence on compressibility behaviour of fabric. Different structures may have different compressibility behaviours.

Declaration of conflicting interests

The author(s) declared no potential conflicts of interest with respect to the research, authorship, and/or publication of this article.

Funding

The author(s) received no financial support for the research, authorship and/or publication of this article.

References

- [1] Shikhzadeh M, Ghane M, Eslamian Z, et al. A modeling study on the lateral compressive behavior of spacer fabrics. *J Tex Ins* 2010; 101: 795–800.
- [2] Rothe D. Warp knitted spacer fabric – design and application fields. *Knit Tech* 2001; 4: 14–16.
- [3] Schwabe D, Mohring U and Bartels VT. Development of textiles for or coverings and pads. *Melliand-Textilberichte* 2005; 6: E95–E96.
- [4] Heide M. Development of functional warp knitted spacer fabrics as operating table covers. *Melliand-Textilberichte* 2002; 6: 411–442.
- [5] Ye X, Hu H and Feng X. An experimental investigation on the properties of the spacer knitted fabrics for pressure reduction. *Res J Tex Apparel* 2005; 9: 52–57.
- [6] Xiaohua Y, Hong H and Xunwei F. Development of the warp knitted spacer fabrics for cushion applications. *J Ind Tex* 2008; 37: 213.
- [7] Ye X, Fingueiro R, Hu H, et al. Application of warp-knitted spacer fabric in car seats. *J Tex Ins* 2007; 98: 337–344.
- [8] Rock M and Lohmueller K. Three-dimensional knit spacer fabric for footwear and backpacks. Patent 5896758, USA, 1999.
- [9] Goodwin EL. Protective device using a spacer fabric. Patent 2006/0287622 A1, USA, 2006.
- [10] Sorensen BB. A device for protection of the hips. Patent EP1684604, Europe, 2007.
- [11] Bruer SM and Smith G. Three-dimensionally knit spacer fabric: a review of production techniques and application. *J Tex Apparel Tech Manag* 2005; 4: 23–25.
- [12] Yip J and Ng SP. Study of three-dimensional spacer fabrics: molding properties for intimate apparel application. *J Mater Process Tech* 2009; 209: 58–62.
- [13] Bagherzadeh R, Montazer M, Latifi M, et al. Evaluation of comfort properties of polyester knitted spacer fabrics finished with water repellent and antimicrobial agents. *Fiber Polym* 2007; 8: 386–392.
- [14] Liu YP, Hu H, Long HR, et al. Impact compressive behavior of warp-knitted spacer fabrics for protective applications. *Tex Res J* 2012; 82: 773–788.
- [15] Pereira S, Anand SC, Rajendran S, et al. A study of the structure and properties of novel fabrics for knee braces. *J Ind Tex* 2007; 36: 279.
- [16] Liu YP, Au WM and Hu H. Protective properties of warp-knitted spacer fabrics under impact in hemispherical form. Part I: impact behavior analysis of a typical spacer fabric. *Text Res J* 2014; 84: 422–434.

- [17] Liu YP, Hu H and Au WM. Protective properties of warp-knitted spacer fabrics under impact in hemispherical form. Part II: effects of structural parameters and lamination. *Tex Res J* 2014; 84: 312–322.
- [18] Zhaoqun D, Ming L, Yuanxin W, et al. Analysis of spherical compression performance of warp-knitted spacer fabrics. *J Ind Tex* 2015; 46: 1362–1378.

QUALITY ASPECTS OF VISCOSE YARNS PRODUCED ON DIFFERENT SPINNING SYSTEM

¹Ashvani Goyal, ²Sangeeta Goyal

¹Assistant Professor, ²Assistant Professor

¹Department of Textile Technology, ²Department of Mathematics

¹The Technological Institute of Textile & Sciences, Bhiwani 127 021, Haryana, India

²Govt. College for Women, Bahadurgarh, Haryana, India

Abstract: This paper investigated the properties of 100% viscose yarn produced on Ring, Rotor, Compact, Siro and Siro compact spinning system. The yarn produced on Siro compact spinning system is found to be superior in terms of tensile strength, extensibility, abrasion resistance and hairiness. Further, the diameter of compact yarn is found to be least whereas the Siro yarn has highest yarn diameter. The unevenness of Siro yarn is least among all the yarns compared.

Index Terms- Siro, siro compact, viscose yarn, ring yarn

I. INTRODUCTION

Properties of spun yarns are mainly affected by fibers properties and yarn structure. Yarn structure is principally influenced by the spinning system. In fact, each spinning system tends to produce a distinctive yarn structure. Recent refinements in spinning technologies have yielded significant improvement in yarn structure. The Siro, rotor, Siro compact, compact and ring spun yarns are the new spinning systems to have made a breakthrough until recently [1-4]. Of the various structural parameters for staple yarns, fibers migration has a crucial influence on the yarn mechanical properties. Thus, the need for precise and concise information about fibre migration becomes important for better understanding of yarn structure and hence yarn mechanical behaviour. The work presented here aims to analyse change in properties in Siro, rotor, Siro compact, compact and ring spun yarns.

In the past decades, all the new spinning processes have been developed to achieve a better yarn quality and mechanical properties as well as higher production per spinning unit. Manufacturing methods impose certain constraints on the disposition and arrangement of fibers in the yarn body. The Siro, rotor, Siro compact, compact and ring spun yarns spinning systems propose fundamental modifications to the conventional ring spinning process with the aim of altering the geometry of the spinning triangle.

During the two last decades, there have been several investigations on the properties of Siro-spun yarns and their advantages over conventional yarns [4,5]. The researchers have demonstrated that Siro-spun yarns enjoy better properties in many ways investigated the effect of fiber fineness and strand spacing & other qualities on Siro-spun yarn properties. They reported that, the optimal changes for 100% viscose yarns produced by different spinning systems. There have been few investigations in terms of structural parameters about the yarns. The researchers have put their emphasis on comparing the hairiness of different spinning system of yarns. Breaking strength of these yarns about 15% higher than that of conventional ring spun yarns. This study investigates the differences between Siro, rotor, Siro compact, compact and ring spun yarns with reference to their migratory and inner structural parameters.

In this paper, we studied the properties of yarn which are produced on different spinning systems. 100% Viscose yarns of 30^s are produced on Ring, Rotor, Compact, Siro and Siro compact spinning system. The yarns produced by different spinning system have various specific properties and hence it affects the structural and physical properties of the yarn. In our project, we study and compare the properties of yarn made-up on above mentioned spinning systems.

II. MATERIAL AND METHODS

2.1 Preparation of Yarn Samples

The yarns used for study were made of 100% viscose fiber. A predetermined quantity of the fibres is taken, and yarns of 100% viscose are made up by five different spinning systems having same count of 30Ne. The list of the yarn samples produced and the corresponding variables are given in Table 1.

2.2 Testing method

2.2.1 Measurement of Yarn Strength and Elongation

Measurement of yarn strength and elongation was tested on Tensorapid 3 with the following parameters:

- Clamp speed: 400m/min
- Testing length: 500mm
- Pre-tension: 92cN

Table 1- Sample Plan

S. No	Count	Fibre Blend	Blend Ratio	Yarn Spinning System
1	30Ne	Viscose	100%	Ring Spinning
2	30Ne	Viscose	100%	Rotor Spinning
3	30Ne	Viscose	100%	Compact Spinning
4	30Ne	Viscose	100%	Siro Spinning
5	30Ne	Viscose	100%	Siro Compact Spinning

2.2.2 Measurement of Yarn Diameter

Yarn diameter was measured by projection microscope. Yarn was first passing through a disc type tensioner attached to the instrument, so that yarn remains tight under testing under tension head. After adjusting the focus than magnified diameter was read from projection screen. Fifty observations were taken for each sample at random. Yarn diameter was calculated by dividing the observed diameter reading by the magnification power.

2.2.3 Measurement of Yarn Unevenness, Imperfections & Hairiness

The yarn unevenness, imperfection and hairiness were measured by Uster Evenness Tester- 5. The parameters set on the instrument were as follows:

- Material speed: 400 m/min
- Evaluating time: 1 min
- Sensitivity level: Thick (+50%)
- Thin (-50%)
- Neps (+200%)

Hairiness H represents the total length of protruding fibres with reference to the sensing length of 1cm of yarn.

2.2.4 Measurement of Yarn Abrasion Resistance

Abrasion resistance of all the yarn samples was determined by CSI Universal abrasion tester. By winding a yarn sheet on wrap reel, specimen was prepared for flexing and abrasion. The number of ends in the specimen has been calculated according to ASTM standards D 1379-55T

Following Parameters were used

No. of threads/specimen	92
Flex weight, lbs	2.0
Spigot weight, lbs	0.5
No. of sample for each variable	6

III. RESULTS AND DISCUSSION

3.1 Yarn Tenacity

Figure 1 shows the effect of spinning systems on single yarn strength of 100% viscose yarn. It can be seen from the Figure 1 that Siro compact yarn shows highest single yarn strength followed by Siro spun yarn and compact spun yarn whereas rotor spun yarn being weakest. Compact spun yarn is weaker than Siro compact spun yarn because the straight and parallel bundle of core fibers held together by higher twist. Rotor is weakest owing to the bipartite structure in which the yarn strength is derived mainly from the helically twisted core fibers. The same trend is also observed by Tyagi *et. al.* [6] where Siro compact spun yarn shows highest single yarn strength due to the enhanced inter-fiber cohesion through fiber consolidation brought out by superior alignment and extent of continuous fibers.

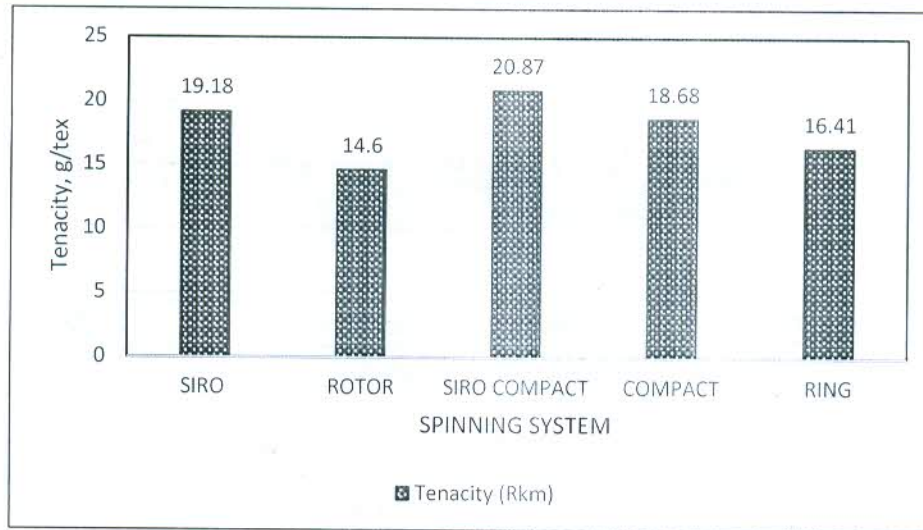


Figure 1- Effect of Spinning System on Yarn Tenacity

3.2 Yarn Elongation

Figure 2 shows the effect of spinning systems on elongation of 100% viscose yarns. It can be seen from the figure that Siro compact yarn shows highest elongation value followed by Siro yarn whereas ring yarn shows least elongation values. The highest elongation of Siro compact yarns is due to its structure and fiber migration phenomena. The high breaking extension of Siro spun yarns than the ring yarns, can be ascribed to the presence of lower value of hooked, looped and disoriented fibers [7].

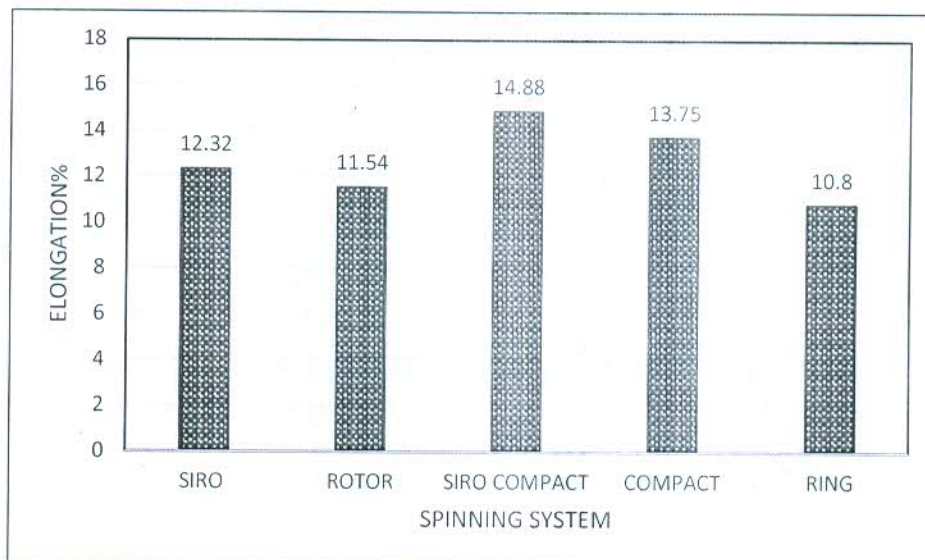


Figure 2-Effect of Spinning System on Elongation

3.3 Yarn Diameter

Figure 3 shows that for yarns with same material, yarn diameter is greater for Siro spun process than ring spun yarn. Different spinning processes produce different degrees of yarn density because of the different patterns of fibre compactness imposed by yarn twisting and spinning process. For instance, a Siro-spun yarn will typically exhibit higher degree of compactness than a comparable ring spun yarn due to the true twist with the high tension used in Siro spinning [8]. The higher value of Siro spun yarn diameter indicates that it is bulkier than the ring-spun yarn. The packing density calculated from the yarn diameter is higher for ring spun yarns as compared to the Siro spun yarns which have least packing density.

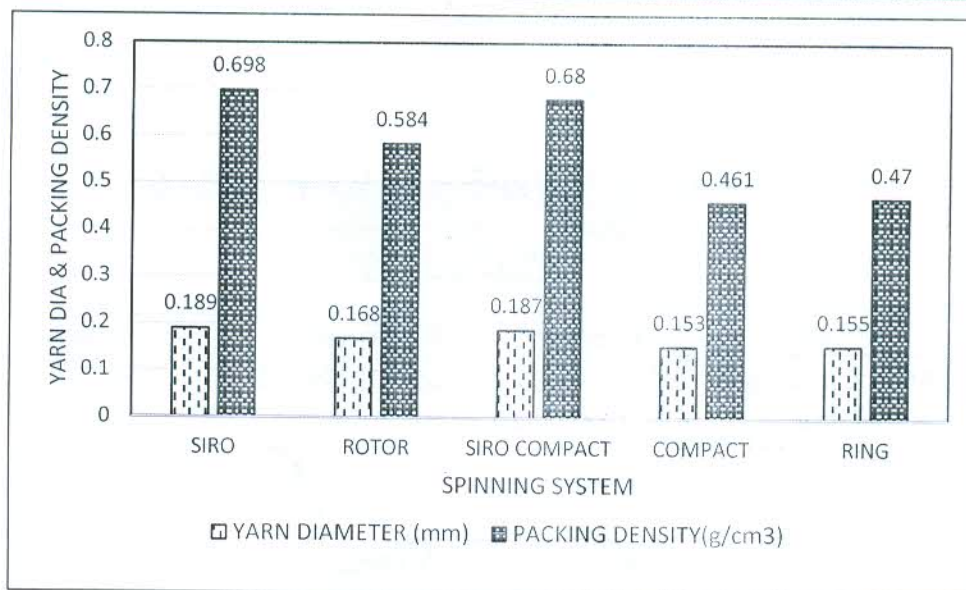


Figure 3- Effect of Spinning System on Yarn Diameter and Packing Density

3.4 Hairiness

Hairiness and hairiness variation are shown in Figure 4. Upon the general observation of spinning system, it is found that ring yarn has highest value of hairiness while Siro compact has least hairiness. The low hairiness of rotor spun yarn are because the wrapper fibers cover the main body of fibers to some extent preventing the ends of core fibers protruding out of yarn. In the ring spinning, many factors contribute to hairiness like spindle speed, twist factor, spinning geometry and the fibers which emerge from the front roller nip have no control which is the main factor in contribution for higher hairiness values [9]. The hairiness variation for yarns spun are directly proportional to the hairiness values of the yarn i.e., highest for ring spun yarns and lowest for Siro compact yarns.

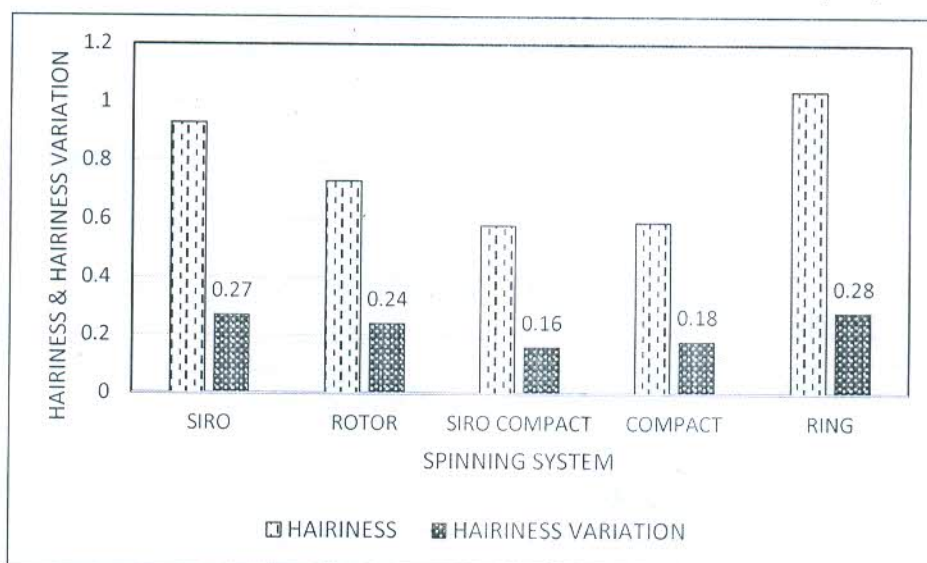


Fig. 4-Effect of Spinning Systems on Hairiness and Hairiness Variation

3.5 Unevenness

Figure 5 shows the effect of spinning systems on unevenness of 100% viscose yarns. It can be clearly observed that Siro spun yarn is most regular followed by yarns from other spinning systems. Rotor spun yarns have higher values of $U\%$ [7]. The Siro Spun yarns is more even than an equivalent rotor spun yarns. This can be attributed to the fact that the Siro spun yarns is spun on a high draft system, where at very high drafting speed, the tensile force acting on fibers readily overcome the fibre inertial effects and frictional effects, leading to smoother fibre movement and thus presence of uniform number of fibers in yarn cross section along its length.

Figure 5 also shows the effect of spinning systems on $CVm\%$ of 100% viscose yarns. $CVm\%$ values are like that of the unevenness values with having higher for rotor spun yarns and least for the Siro compact yarns.

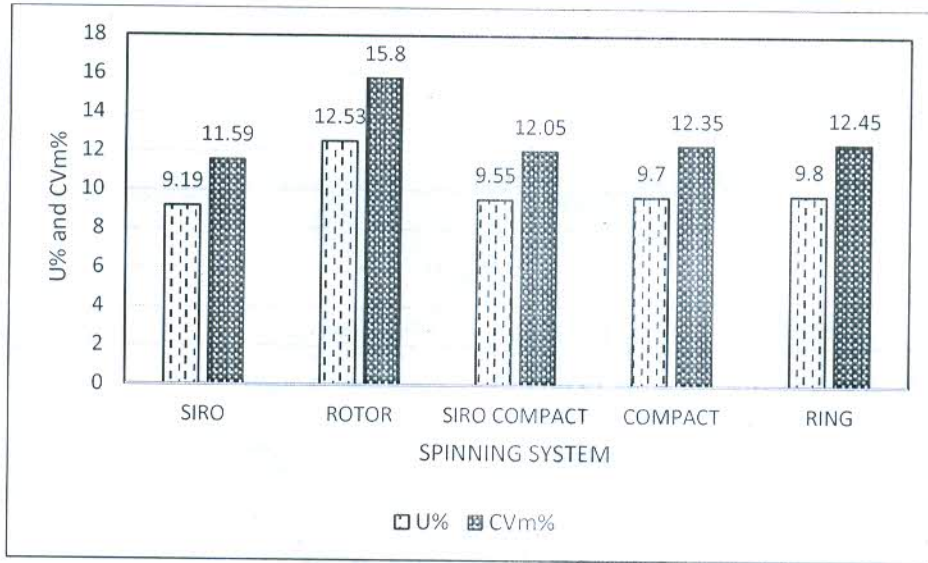


Figure 5- Effect of spinning systems on U% and CVm %

3.6 Imperfections

Figure 6 shows the effect of spinning systems on imperfection of 100% viscose yarns. It is clear from the graph that Siro compact yarn shows least yarn imperfection followed by ring yarn. In a study by Ramachandran and Nagarajan [9], the yarn quality is superior in the Siro compact spinning in terms of imperfection values. It is because in the Siro compact spinning process, the processes like speed frame is eliminated and moreover the drafting irregularities are less as compared to the rotor spinning system. The same trend is also confirmed by Ahmed and Syduzzaman [10]. Further, Ring spun yarn is more even and has fewer imperfections than an equivalent rotor spun yarn. This can be attributed to the fact that the ring spun yarn is spun on a high draft system, where at very high drafting speed, the tensile force acting fibers readily overcome the fiber inertial effects and frictional effects, leading to smoother fiber movement and thus presence of uniform number of fibers in yarn cross section along its length.

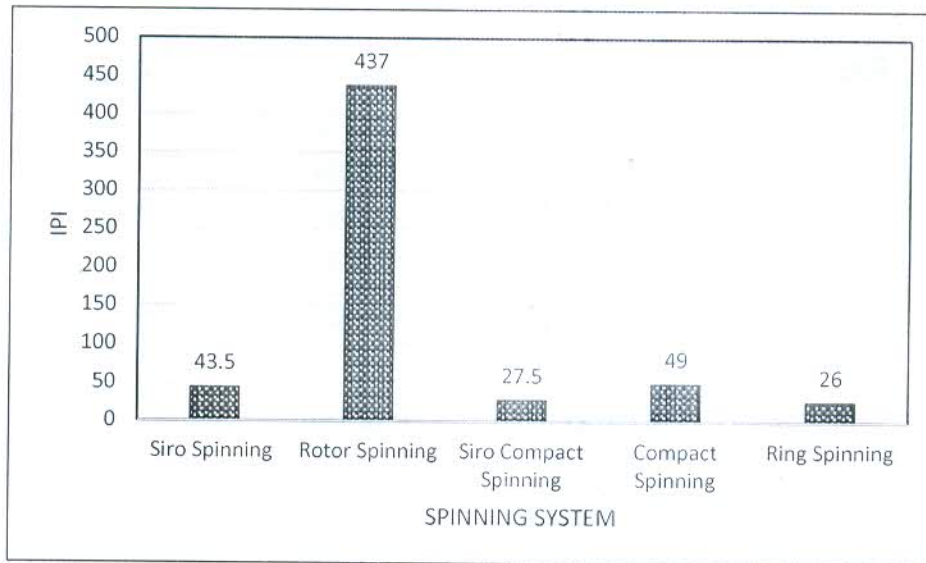


Figure 6 - Effect of spinning system on Total IPI

3.7 Abrasion Resistance

Figure 7 shows the effect of spinning systems on abrasion resistance of 100% viscose yarns. It is clear from the graph that a Siro compact spun yarn displays higher abrasion resistance which shows better property regarding the abrasion, while its counterpart ring spun yarn shows least abrasion resistance. Higher abrasion resistance of Siro compact spun yarns may be due to the higher compactness, which increases the fiber cohesion and offer better resistance to plucking action of abradant [11].

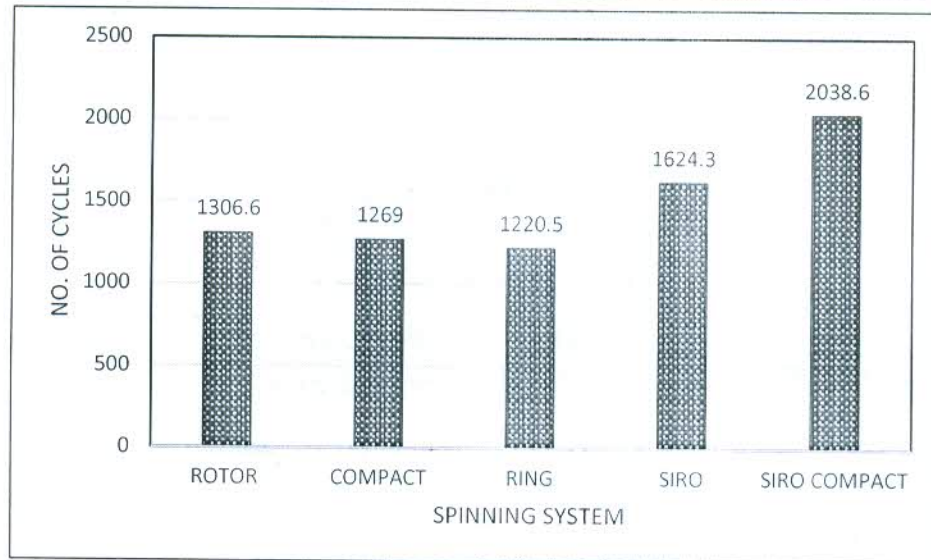


Figure 7- Effect of Spinning System on Abrasion Resistance

IV. CONCLUSIONS

- 4.1. Siro Compact spun yarns have high single yarn strength and tenacity whereas the rotor spun yarns shows the weakest yarn strength and tenacity. Beneath the Siro compact yarns, the compact yarns have the higher yarn strength and tenacity values among all other spinning systems.
- 4.2. The Ring Yarns have low elongation value than a Siro compact spun yarn which have the highest elongation% values among all other spinning systems.
- 4.3. Compact spun yarns have the least yarn diameter as compared to yarns from other spinning systems whereas Siro spun yarns having highest yarn diameter. The packing density of the yarns are directly related to the yarn diameter values.
- 4.4. The Siro compact spun yarns have the least hairiness factor among all the yarns while that of the ring yarns have highest hairiness. The hairiness variation is directly to the hairiness factor and hence respective yarns have better results.
- 4.5. Regarding the unevenness property of a yarn, the Rotor spun yarn is more uneven than yarns produced form all other spinning system. Siro yarns are the best yarns regarding the unevenness property as they have the less value of it.
- 4.6. The Siro Compact yarn is best in terms of abrasion resistance.

REFERENCES

- [1] W. Klein, "Technology of Short Staple Spinning", The Textile Institute, Manual of Textile Technology, All volumes.
- [2] NCUTE publications on Yarn Manufacturing, Indian Institute of Technology, Delhi.
- [3] <https://www.swicofil.com/consult/textile-applications/wool-type-spinning/Siro-spinning>
- [4] <http://www.swicofil.com/products/001cotton.html> (accessed on 22 October 2013)
- [5] Ashvani Goyal, D.P Gon, Amit Sareen & Virender Verma. *A Comparative study of ELITWIST Yarn with Siro & other yarns.*
- [6] Tyagi, Ashvani Goyal Chattopadhyay. (2013). Low stress & recovery characteristics of blended ring and rotor yarns, Vol.38, pp 331-339.
- [7] Lawrence C A, Foster W, Wilding M, Howard A & Kudo R. *A study of the structure and properties of Spun Yarns.* Paper presented at VI International IZMIR Textile symposium.
- [8] <http://www.indiantextilejournal.com/articles/FAdetails.asp?id=552>
- [9] Ramachandran T, Nagarajan. (2016) Comparison of Yarn Quality of Ring & Rotor Spun Yarns for Denim Fabric Manufacture. International Conference on Systems, Science, Control, Communication, Engineering and technology: 772-775.
- [10] Sharif Ahmed, Md. Syduzzaman and Md. Sultan Mahmud. (2015). Comparative studies on Ring, rotor and compact spun yarn. *European Scientific Journal*, Vol.11, pp. 100-105.
- [11] Dhamija S & Manshahia M, *Indian Journal Fibre Textile Research*, 32(2007)295.

Bio-Bleaching of Cotton with H₂O₂ Generated from Native and Immobilized Glucose Oxidase

By Amit Madhu and J. N. Chakraborty, Dr. B. R. Ambedkar National Institute of Technology, Jalandhar

Abstract

Enzymatically-generated hydrogen peroxide (H₂O₂) using glucose oxidase (GOX) is a sustainable alternative for cotton textile bleaching. GOX catalyzes the oxidation of glucose to gluconic acid with generation of H₂O₂ as a side product for bleaching. This work involves the study of cotton fabric bleaching with enzymatically-generated H₂O₂. Enzyme and glucose concentrations significantly affect peroxide generation as well as bleaching and were optimized using statistical experimental design in reference to maximum whiteness. Furthermore, the sustainability of this bleaching system was premeditated by GOX immobilization. GOX was covalently immobilized onto a natural and inexpensive support (chitosan) based on statistical experimental design results. The immobilization improved whitening results as well as allowing repeated application of enzyme for H₂O₂ generation, which was successively implemented for cotton textile bleaching.

Key Terms

Bleaching, Chitosan, Cotton, Enzyme Immobilization, Glucose Oxidase, Hydrogen Peroxide

Introduction

Textile bleaching removes natural pigments present in fibers that discolor the substrate. Traditionally, whitening was achieved with chlorine- and oxygen-containing oxidizing agents. In the last few decades, hydrogen peroxide (H₂O₂) has been accepted as a universal bleaching agent because it is a more environmentally-friendly (e.g., it can decompose into oxygen and water) and is a versatile application processes.¹ Enzymatically, the discoloration of natural impurities can be achieved using laccase/mediator systems, peroxidases, and in situ generated peroxide or peracids by glucose oxidases (GOX) for cotton-based textiles.² The use of GOX for producing H₂O₂ can be a sustainable method for bio-bleaching. GOX enzymes are electron-transfer oxidases, which catalyze the oxidation of glucose to gluconolactone in the presence of oxygen, and in turn spontaneously yield gluconic acid as well as H₂O₂ as a byproduct for bleaching purposes.³⁻⁵

Generation of peroxide with GOX requires slightly acidic to neutral conditions at low temperatures; the bleaching effect of H₂O₂ under these conditions is insignificant. High temperature (80-90 °C) and alkaline (pH 11) conditions for bleaching provide efficient results,⁶⁻¹⁰ and the assistance of ultrasound energy also improves fabric whiteness due to increased enzyme reaction.¹¹ Several researchers investigated the activation of generated H₂O₂ with different activators such as Prestogen SP,³ peroxidases,¹² and peracid precursors^{9,13-16} to enable bleaching at low temperature in neutral media. Integration of pre-treatment with GOX enzyme and dyeing was also studied by researchers to minimize energy consumption.^{17,18}

The important parameters for H₂O₂ generation with GOX are pH, temperature, and sufficient aeration.¹⁹⁻²¹ A considerable increase in H₂O₂ generation was observed by aeration rather than by mechanical agitation.^{7,10} In preliminary trials, we also observed that the concentration of GOX, amount of glucose, and the incubation time were the prime factors for peroxide generation,^{7,8,21} while maximum H₂O₂ generation did not ensure maximum whiteness from the bleaching bath. In 2017, Reis and coworkers optimized the peroxide generation and bleaching processes separately for one-step pre-treatment of knitted cotton textiles using GOX enzyme.²² The focus on parameter optimization, however, should be directed towards the bleaching process. Therefore, in the present study, we adopted experimental design to optimize parameters for whiteness instead of H₂O₂ generation.

The industrial application of this system was quite limited due to the enzyme expense. In addition, a higher quantity of enzymatically-produced peroxide was needed to accomplish a bleaching equivalent to that of conventional bleaching. Immobilization of the GOX enzyme, however, can overcome the problems associated with use of the native enzyme and can ensure long-term application due to easy recovery and recycling. The first textile application using immobilized GOX was reported in 1999 by Opwis, with cyanuric chloride-mediated attachment to cotton—with subsequent release of H₂O₂ at levels high enough to support adequate bleaching.²³ In other research, GOX was covalently immobilized on two inexpensive and commercially-available supports, viz. alumina and glass. High protein immobilization yields, as well as sufficient bleaching levels were

attained. Glass permitted a higher generation rate of H_2O_2 (0.35 g/L) due to its porous morphology and thus bound more protein; however, alumina produced a higher operational stability and permitted reuse.²⁴

The support material plays a very significant role in the performance of immobilized enzymes. Stability under working conditions, availability at low cost, and adequately large surface area, together with the least diffusion limitations, are the important criteria for selecting support materials for industrial applications.²⁵ In previous studies,^{23,24,26} the supports used were hydrophobic and poorly diffuse, whereas, in the present work, GOX was immobilized on a natural, inexpensive, biocompatible, and hydrophilic support material: chitosan. Experimental design was used to optimize the process of immobilization for maximum conjugate activity, with Fourier transform infrared (FTIR) spectroscopy and enzyme assays confirming bond formation. The H_2O_2 generated with native, as well as immobilized, GOX were successively used for cotton fabric bleaching. The reusability of immobilized enzyme was studied for five consecutive cycles. The purpose of this study was to establish GOX- H_2O_2 cotton fabric bleaching for industrial application.

Experimental

Materials

Cotton fabric (plain weave, 172 g/m², epi×ppi: 65 × 56, warp and weft count: 30 Ne), Gluzyme Mono 10000 BG (10,000 glucose oxidase units (GODU)/g, Novozymes), D(+)-Glucose (Merck), water soluble chitosan (chitosan chloride, India Sea Food Ltd.), and glutaraldehyde (25%, Thomas Baker) were used. All other chemicals used were of analytical grade and were procured from SD Fine Chemicals Ltd., India. Gluzyme Mono 10000 BG (*Aspergillus oryzae*) is a commercially-available product of glucose oxidase (GOX) and a cost-effective alternative to GOX from *Aspergillus niger*.

H_2O_2 Generation Using GOX

H_2O_2 was generated by means of the GOX enzyme using glucose as the substrate. The enzyme was added in small doses to counteract the time dependent deactivation of the enzyme and a buffer was used for pH control to avoid enzyme deactivation caused by decreased pH.^{5,23} The medium (50 mL) was prepared in Erlenmeyer flasks using a buffer. The experiments were carried out with constant aeration at 5 L/min from a pressurized oxygen cylinder through a glass tube introduced into the solution and mechanical agitation of 100 rpm.

Preliminary experiments were performed at optimal temperature and pH for maximum generation of H_2O_2 from enzyme. The final optimization to achieve maximum whiteness on cotton fabric was determined using statistical experimental design. The design variables were chosen that

potentially affected H_2O_2 generation as well as whiteness, and the range of each variable was selected based on primary optimization. The experimental combination and the levels of these variables in coded and actual values are illustrated in Table I.

Table I.
Design Matrix for H_2O_2 Generation from GOX Enzyme

Independent Variables	Coded Levels			Responses
	-1	0	+1	
X_1 : Enzyme (g/L)	1	1.5	2	H_2O_2 (g/L)
Y_1 : Glucose (g/L)	10	20	30	Whiteness (CIE)
Z_1 : Incubation Time (min)	90	120	150	—

Determination of H_2O_2 Concentration

The concentration of H_2O_2 was determined by potassium permanganate titration in acidic medium using AATCC TM102-2002.²⁷

Bleaching Process

For conventional bleaching, the desized and scoured samples were bleached at a material to liquor ratio (LR) of 1:20 with varying H_2O_2 concentrations (2, 4, 6, 8, and 10% owf), 5 g/L of sodium hydroxide, and 2 g/L of sodium silicate at pH 11, various temperatures (75, 85, 95, and 105 °C), and various times (30, 60, 90, and 120 min).

For enzymatic bleaching, samples were placed in the GOX- H_2O_2 bath and the bath was activated by raising the temperature to 85 °C and pH 11 using NaOH. The gluconic acid produced with the oxidation of glucose acted as a chelating agent for metal ions, thus, the use of additional stabilizers was not required in the bleaching bath.^{7,24,28} The bleaching experiments were carried out in an Innolab water bath shaker. Continuous stirring was performed with a glass rod to ensure uniform bleaching. After the requisite time, the samples were washed with hot and cold water, and finally dried.

Fabric Whiteness

The whiteness of the bleached samples was measured using a Premier Colorscan SS 5100A according to AATCC TM110-2005 and represented in CIE.²⁷ All determinations were performed in triplicate and the result represented as the mean value.

Immobilization of GOX Enzyme on Chitosan Beads

Chitosan beads were prepared from water soluble chitosan.²⁹⁻³¹ These beads (5 g) were activated with aqueous glutaraldehyde solution (% v/v) at room temperature (RT) under mild stirring. GOX immobilization was performed in two steps using glutaraldehyde as a cross-linking agent (Scheme 1).³² Following the activation for given time, the

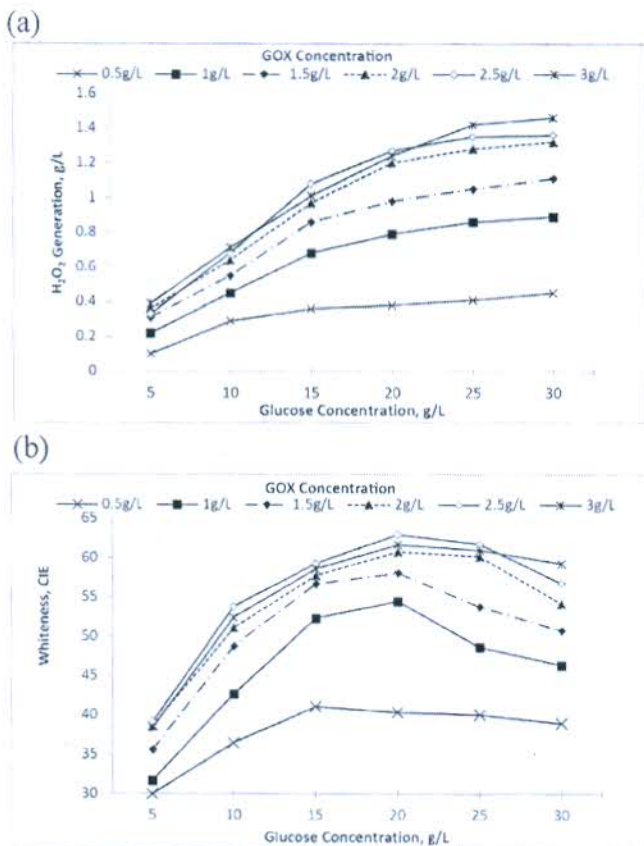


Fig. 2. (a) H_2O_2 generation at various GOX concentrations using varying amounts of glucose and (b) whiteness obtained at various GOX concentrations using varying amounts of glucose.

GOX generates H_2O_2 efficiently at all temperatures. A temperature of $40\text{ }^\circ\text{C}$ was chosen for further investigation because it gave the greatest H_2O_2 generation. Reduction of H_2O_2 production at higher temperature may be due to enzyme denaturation.^{25,26} Irrespective of temperature, maximum generation of H_2O_2 was observed at pH 5.5 in the above experiments. For all further experiments, the temperature and pH were kept constant at these values.

Primary Optimization

For preliminary studies, H_2O_2 was generated by varying concentrations of GOX enzyme using different glucose amounts and bleaching experiments were performed using the peroxide. Peroxide generation increased with enzyme concentration (0.5 to 2 g/L) as shown in Fig. 2a, which consecutively resulted in increased whiteness (Fig. 2b). The difference in peroxide generation and whiteness was very insignificant for 2 g/L and 2.5 g/L GOX concentrations. For the GOX concentration of 3 g/L, decreased whiteness was observed even with greater peroxide generation. The whiteness obtained with 0.5 g/L of GOX was insufficient, therefore, GOX was used at concentrations ranging from 1 to 2.5 g/L during further experiments.

Invariably, H_2O_2 generation increases with glucose content at all enzyme concentrations. For each enzyme concentration, after a particular concentration of glucose was reached, an insignificant change in H_2O_2 generation was observed (Fig. 2a). Whiteness also showed a similar trend with the glucose concentration. Hence, an optimal amount of enzyme and glucose was required for bleaching, beyond which no additional improvement was observed.

Final Optimization

Finally, to optimize enzymatic bleaching using GOX enzyme, experimental design was used (Table III). Statistical analysis of design was performed using a trial version of Design Expert-10.0.3. Results show that the enzyme and glucose concentrations, and time, favored H_2O_2 generation, with enzyme concentration having the most significant effect, followed by time of incubation and glucose concentration (Table IV).

The response surface obtained for significant interaction factors is shown in Fig. 3. H_2O_2 generation increased with increased GOX and glucose concentrations. The higher concentration of reactants favored the reaction, resulting in more peroxide generation, while the higher concentration of GOX in the bleaching bath necessitated high concentrations of glucose. The increase in incubation time also favored H_2O_2 generation and the higher GOX and glucose concentrations required prolonged incubation times for reaction completion.

Table III. Results of Cotton Fabric Bleaching using H_2O_2 Generated from GOX Enzyme

Run No.	X_1 Enzyme (g/L)	Y_1 Glucose (g/L)	Z_1 Incubation Time (min)	R_1 H_2O_2 Generation (g/L)			R_2 Whiteness (CIE)		
				I	II	Avg.	I	II	Avg.
1	2	20	150	1.2	1.09	1.15	63.9	61.5	62.7
2	1.5	20	120	0.83	0.85	0.84	59.3	60.1	59.7
3	1.5	20	120	0.84	0.83	0.83	59.8	59.2	59.4
4	1.5	30	90	0.8	0.77	0.78	54.2	54.8	54.6
5	1	20	150	0.74	0.75	0.74	48.9	50.2	49.6
6	2	30	120	1.1	0.99	0.99	59.8	59.6	59.7
7	1.5	20	120	0.87	0.86	0.86	59.6	60.5	60.1
8	1	30	120	0.79	0.8	0.79	49.9	49.7	49.8
9	1	20	90	0.65	0.62	0.63	45.1	44.7	44.9
10	1.5	30	150	0.91	0.91	0.89	58.2	55.4	56.8
11	1.5	10	150	0.91	0.9	0.9	57.9	57.3	57.6
12	1	10	120	0.58	0.6	0.59	44.4	44.8	44.6
13	1.5	10	90	0.66	0.68	0.67	52.5	54.1	53.3
14	2	20	90	0.95	0.93	0.94	61.9	61.7	61.8
15	2	10	120	1.1	0.97	0.98	60.4	61	60.7

Table II. Design Matrix for GOX Immobilization on Chitosan Beads using Glutaraldehyde

Independent Variables	Coded Levels			Responses
	-1	0	+1	
X ₁ : Enzyme (mg/mL)	0.4	0.8	1.2	Enzyme Loading (%)
Y ₁ : Glutaraldehyde (% v/v)	1	2.5	4	H ₂ O ₂ (g/L)
Z ₁ : Activation Time (h)	2	4	6	—

beads were washed with sodium acetate buffer to remove unbound glutaraldehyde. The activated chitosan beads were then immobilized with different concentrations of GOX enzyme at RT for 12 h under mild stirring. The effect of immobilization parameters were studied using experimental design (Table II).

The immobilized beads were filtered and washed to eliminate unbound protein and the enzyme loading percentage was measured for each run. The conjugate activity of immobilized GOX was evaluated in terms of H₂O₂ generation with reaction of glucose as described earlier.

The Fourier transform infrared-attenuated total reflection (FTIR-ATR) spectra of chitosan beads, glutaraldehyde activated beads, and immobilized beads were recorded between 4000 and 400 cm⁻¹ using a Bruker Eco Alpha FTIR spectrophotometer.

Enzyme Loading (Protein Assay)

The amount of protein in the solution was determined according to the Bradford method, using bovine serum albumin (BSA) as the protein standard. The amount of immobilized enzyme was calculated from the protein content in the solution before and after immobilization.

Results and Discussion

Conventional H₂O₂ Bleaching

In initial trials, it was observed that the high concentration of oxidant and elevated temperatures resulted in a significant fabric strength loss. Keeping the strength loss to 10–15% as a reference,^{33–35} the conventional bleaching parameters were set to 4% (owf) or 0.5 g/L H₂O₂ at 85 °C for 60 min to obtain a sufficient CIE Whiteness Index value of 60.

H₂O₂ Generation using GOX

Initial Parameter Selection

GOX enzymes from different strains are active under different conditions. The recommended range for the provided GOX was 30 to 50 °C within a pH of 4 to 6. Initial experiments were carried out using 2 g/L of enzyme and 20 g/L glucose at 25, 40, and 55 °C at pH 4.5, 5, 5.5, and 6 to obtain maximum generation of H₂O₂ (Fig. 1).

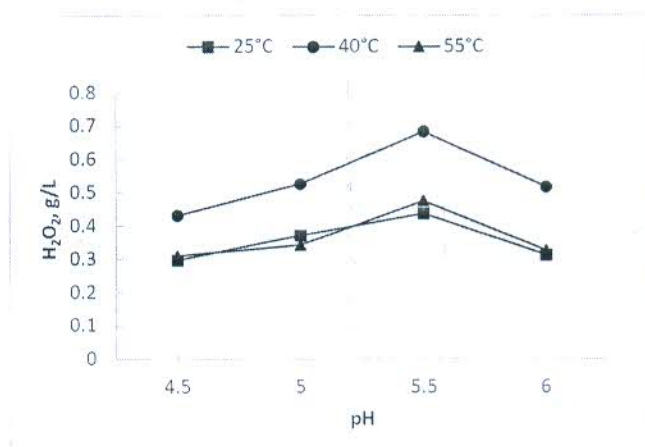
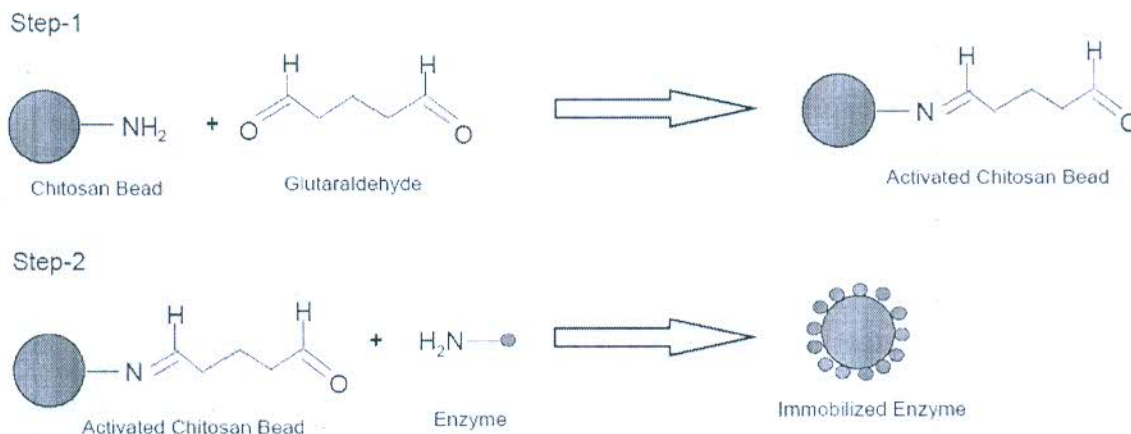


Fig. 1. Optimum pH and temperature for H₂O₂ generation with GOX enzyme.



Scheme 1. Immobilization of GOX on chitosan beads using glutaraldehyde.

	R_1 : H_2O_2 (g/L)	R_2 : Whiteness (CIE)
Equation	$0.84 + 0.164X_1 + 0.04Y_1 + 0.08Z_1 - 0.05 X_1 Y_1$	$59.73 + 7X_1 + 0.59Y_1 + 1.51Z_1 - 1.55 X_1 Y_1 - 3.43X_1^2 - 2.6Y_1^2 - 1.55Z_1^2$
R^2	0.947	0.983
Adjusted R^2	0.925	0.965
Predicted R^2	0.868	0.886
Lack to Fit (p-value)	0.1092 Not Significant	0.069 Not Significant

Similarly, statistical analysis for whiteness shows that the coefficients for quadratic terms of enzyme, glucose, and time were very significant (i.e., these factors had very large effects on the bleaching). The linear effect of enzyme and time was also significant, whereas for glucose it was very small (Table IV). For interaction effects, only the interaction between enzyme and glucose was significant.

The response surface for whiteness (Fig. 3) indicates that bleaching increased with GOX enzyme and glucose concentrations. Whiteness values reached 60 (CIE) when increasing the enzyme concentration from 1 to 2 g/L with 10–15 g/L of glucose. Similar levels of whiteness were obtained easily with lower enzyme concentrations by increasing the glucose amount. But, at high concentrations of glucose (30 g/L) and enzyme (2.5 g/L), whiteness decreased even with increased H_2O_2 generation. This may be due to increased gluconic acid formation or residual glucose in the bath, which may significantly affect bleaching.

For enzymatic bleaching, a higher quantity of enzymatically-produced H_2O_2 was required to achieve the bleaching effect equivalent to that of conventional methods. In conventional

bleaching, a minimum concentration of 0.5 g/L of H_2O_2 was required to achieve a whiteness (CIE) value of 60 while ~0.8–0.85 g/L of enzymatically-produced hydrogen peroxide provided equivalent bleaching results. This might be due to the presence of glucose and enzyme in the bleaching bath, resulting in lower whiteness values. To study the impact of their presence in the bleaching bath, two separate series of experiments were performed.

In one series, 2–10 g/L of glucose was added in the bleaching bath containing 2 g/L of GOX enzyme and 0.6 g/L of H_2O_2 . Each bath was used for bleaching cotton samples and the consumption of H_2O_2 was measured (Fig. 4). In absence of glucose, the maximum consumption of H_2O_2 was observed with lower bleaching results due to rapid decomposition of H_2O_2 (as no gluconic acid was produced). The graph indicates that the presence of glucose had a stabilizing effect on H_2O_2 and resulted in improved whiteness up to a certain concentration of glucose. Higher concentrations of glucose over-stabilized the bleaching bath and resulted in decreased H_2O_2 consumption. Therefore, the reduction of the bleaching power of peroxide was reflected in decreased whiteness.

In the second series, the interaction of protein in the bleach bath was studied with addition of 0.5–2.5 g/L GOX in the bath containing 0.6 g/L H_2O_2 . The enzyme also had a stabilizing effect on the generated peroxide, resulting in reduced whiteness values. As the protein concentration increased in the bleaching bath, the H_2O_2 consumption decreased and resulted in lower whiteness values (Fig. 5). Both of these experiments confirm that the presence of excess glucose and enzyme in the bleaching bath resulted in reduced whiteness values due to over-stabilization of H_2O_2 (Fig. 6). The higher concentrations of both glucose and GOX favored H_2O_2 generation, but were unfavorable for whiteness.

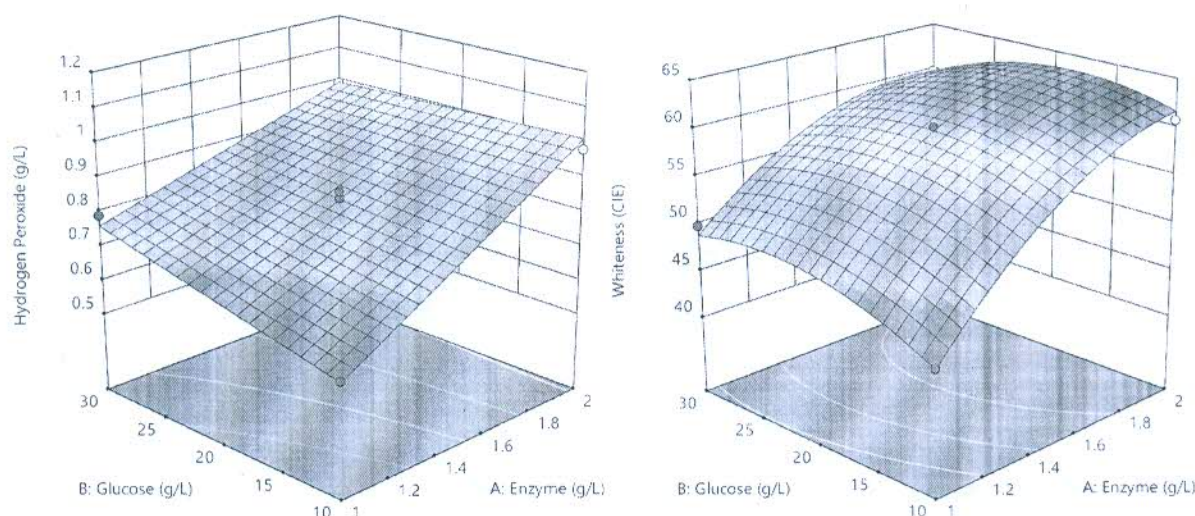


Fig. 3. Effect of GOX enzyme and glucose concentration on (a) peroxide generation and (b) cotton fabric whiteness.



Fig. 4. Impact of glucose in cotton fabric bleaching bath.

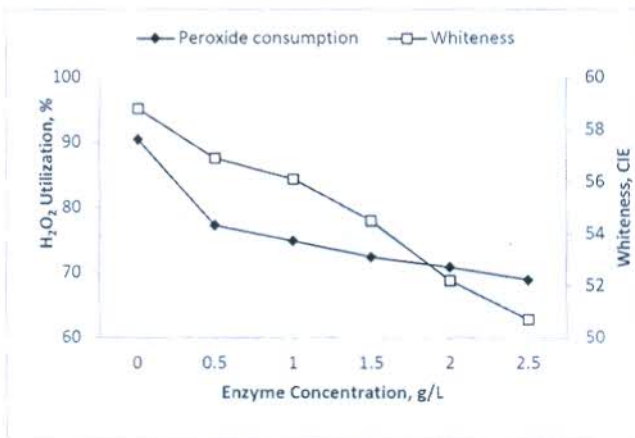


Fig. 5. Impact of enzyme in cotton fabric bleaching bath.

Optimal Bleaching Conditions using GOX Enzyme

To obtain the optimal values of parameters with respect to achieving the maximum whiteness value R_2 , numerical analysis was performed with respect to the desirability function ($DF1$) in Eq. 1.

$$\text{Desirability Function } DF1 = f(X_1, Y_1, Z_1) \quad \text{Eq. 1.}$$

X_1 is the enzyme concentration (g/L) set in range, Y_1 is the glucose concentration (g/L) set to the minimal value, Z_1 is the incubation time (min) set in the 90–150 min range, and R_1 is the H_2O_2 concentration set in the 0.8–0.9 g/L range.

The H_2O_2 generation range was set based on the preliminary trials that indicated the concentrations of enzymatically-generated H_2O_2 required to achieve sufficient whiteness values (60) when compared to conventional bleaching. Since controlling the cost of chemicals is paramount for industrial applications, these were kept to a minimum. Numerical optimization of the design gave the following results: 1.8 g/L of GOX with 12 g/L of glucose with 110 min of incubation time satisfied the function $DF1$ at a desirability of 1. The results obtained experimentally for H_2O_2 generation and whiteness values also validated the model at a significance level of 95%. Finally, these optimized reaction conditions were used for bleaching using H_2O_2 generated with free and immobilized GOX.

GOX Immobilization

GOX was covalently immobilized on chitosan beads using glutaraldehyde as a crosslinking agent. In initial trials, it was observed that the enzyme amount, concentration of glutaraldehyde, and time of incubation were influencing factors for immobilization. Higher enzyme loading did not give higher conjugate activity. Hence to optimize these parameters, statistical design was employed as per experiments in Table V and the loading percentage was evaluated for each run along with the GOX conjugate activity.

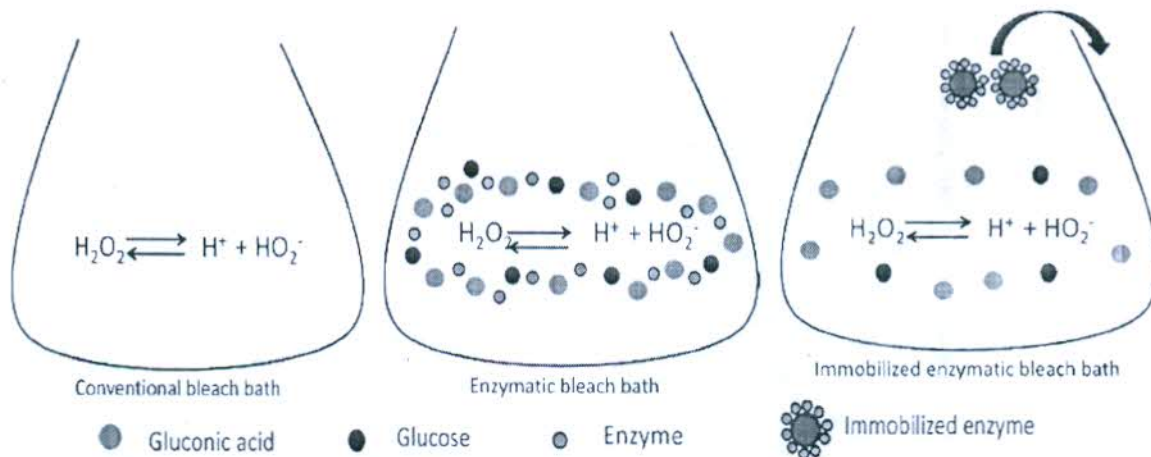


Fig. 6. Comparative bleaching bath composition depicting over-stabilization of peroxide.

Table V. Results of GOX Immobilization at Varying Parameters

Run No.	X ₁ Enzyme (mg/mL)	Y ₁ Glutaraldehyde (% v/v)	Z ₁ Activation Time (h)	R ₁ Enzyme Loading (%)			R ₂ Conjugate Activity (H ₂ O ₂ Generation, g/L)		
				I	II	Avg.	I	II	Avg.
1	0.8	2.5	4	85.8	85.4	85.6	0.60	0.56	0.58
2	1.2	2.5	2	82.0	83.2	82.6	0.51	0.49	0.5
3	1.2	4	4	85.1	84.5	84.8	0.34	0.37	0.35
4	1.2	2.5	6	83.8	83.9	83.8	0.48	0.44	0.46
5	0.8	1	6	79.6	80.5	80.1	0.31	0.35	0.33
6	0.8	4	2	85.7	86.7	86.2	0.48	0.47	0.47
7	0.4	2.5	6	80.5	82.5	81.5	0.26	0.25	0.26
8	0.8	4	6	86.8	86.0	86.4	0.42	0.41	0.41
9	0.8	2.5	4	86.1	85.5	85.8	0.53	0.57	0.55
10	0.4	4	4	82.3	81.9	82.1	0.22	0.25	0.23
11	0.4	2.5	2	79.6	79.7	79.6	0.31	0.29	0.3
12	0.8	2.5	4	85.8	85.4	85.6	0.57	0.57	0.57
13	0.8	1	2	78.7	78.6	78.6	0.36	0.39	0.37
14	0.4	1	4	75.7	76.6	76.1	0.29	0.23	0.07
15	1.2	1	4	78.4	79.1	78.8	0.41	0.39	0.4

Table VI. Statistical Analysis Results of GOX Immobilization

	R ₁ : Enzyme Loading (%)	R ₂ : Conjugate Activity (g/L)
Equation	$85.67 + 1.34X_1 + 3.24Y_1 + 0.6Z_1 - 3.08X_1^2 - 2.13Y_1^2 - 0.71Z_1^2$	$0.57 + 0.11X_1 + 0.036Y_1 - 0.023Z_1 - 0.053X_1Y_1 - 0.16X_1^2 - 0.145Y_1^2 - 0.027Z_1^2$
R ²	0.9916	0.9944
Adjusted R ²	0.9853	0.9889
Predicted R ²	0.9667	0.9606
Lack to Fit (p-value)	0.0617 Not Significant	0.594 Not Significant

Furthermore, the design was analyzed to obtain a statistical model for maximal GOX conjugate activity. The analysis shows that the concentration of enzyme, glutaraldehyde, and time significantly affect GOX immobilization for a statistical model at a 95% confidence limit. According to estimated coefficients, the proposed model is shown in Table VI. It is apparent from the coefficients that the GOX enzyme and glutaraldehyde concentrations were acting in favor of conjugate activity, while their quadratic terms negatively influenced the activity. The interaction factors were also significant, but they negatively influenced the activity. The linear enzyme concentration was the major influencing factor for conjugate activity. The value of correlation coefficient R² and the non-significant lack to fit the p-value validated the predicted model. Moreover, a small difference between the predicted R² and the adjusted R² further supported the regression model (Table VI).

The response surfaces (Figs. 7a and b) indicate that conjugate activity increased with GOX enzyme concentration from 0.4 to 0.9 mg/mL while, for concentrations higher than 0.9 mg/mL, it became constant. Initially, the activity increased in accordance with the amount of protein bound, while higher enzyme loadings on the support did not give higher activity. This could be explained by the increase in enzyme concentrations favoring bond formation and by the increase of enzyme loading over the support. The higher concentrations of enzyme can cause aggregation/clustering over the support, which result in steric hindrance and reduced conjugate activity even after high enzyme loadings.²⁹ Maximal conjugate activity

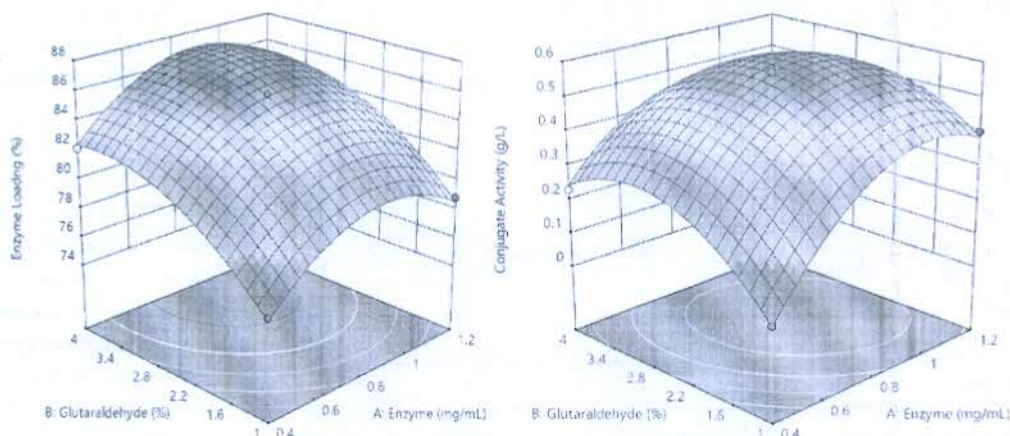


Fig. 7. Effect of GOX enzyme and glucose concentration on (a) loading percent and (b) conjugate activity.

was observed for glutaraldehyde concentrations ranging from 2.2 to 3.4%. Increased glutaraldehyde concentrations undoubtedly increased protein loading, but resulted in multipoint attachment, reducing the activity.³² Similarly, longer cross-linking times increased the conjugate activity, with 4 h being sufficient for maximum activity.

Optimal GOX Immobilization Conditions

To obtain the optimal parameter values for immobilization with respect to the maximum conjugate activity R_4 , numerical analysis was performed with respect to the desirability function (DF_2) in Eq. 2.

$$\text{Desirability Function } DF_2 = f(X_2, Y_2, Z_2) \quad \text{Eq. 2.}$$

X_2 is the GOX concentration (mg/mL) set in the 0.4 to 1.2 mg/mL range, Y_2 is the glutaraldehyde (% v/v) concentration set in the 1 to 4% range, Z_2 is the crosslinking time (h) set in the 2 to 6 h range, and R_3 is the enzyme loading (%).

Numerical analysis was used for parameter optimization and the values of 0.95 mg/mL GOX enzyme with 3% glutaraldehyde and 4 h of crosslinking satisfied the function DF_2 with a desirability of 1. The values obtained experimentally for enzyme loading and conjugate activity with these optimized parameters validated the model at a 95% significance level.

Table VII.
Characteristics of Free and Immobilized GOX Enzyme

Enzyme Sample	Protein (mg)	Activity (g/L)	η_{protein} (%)	η_{activity} (%)	Optimum pH	Optimum Temperature
Free Enzyme	7.4	0.781	100	100	5.5	40-45 °C
Immobilized Enzyme	6.27	0.58	85.73	74.35	5.5	40-45 °C

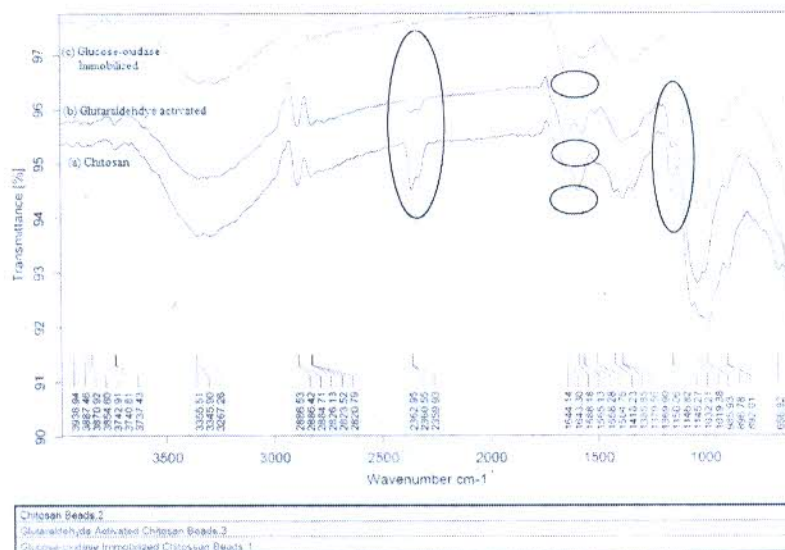


Fig. 8. FTIR spectra of (a) chitosan beads, (b) glutaraldehyde activated chitosan beads, and (c) immobilized GOX on chitosan beads.

Immobilized GOX Characterization

The defined optimal conditions characteristics of free and immobilized GOX were evaluated and are presented in Table VII. GOX activity was reduced after immobilization, while no change in optimum pH and temperature was observed for the immobilized GOX enzyme. This was expected because immobilization normally results in structural rearrangements in enzyme conformation and microenvironment due to the attachment on the polymeric support. Many studies with GOX also showed that the conjugate activity decreased after immobilization while the enzyme stability increased.^{4,26,36}

The FTIR spectra of chitosan beads (Fig. 8) show the characteristic absorption peaks at 1588 ($-\text{NH}_2$) and 1380 cm^{-1} ($-\text{CH}_2$) bending. The absorption bands at 1150 (anti-symmetric stretching of the C-O-C bridge), 1040, and 985 cm^{-1} (skeletal vibrations involving C-O stretching) were characteristic of its saccharide structure. The activated and immobilized chitosan beads show a peak at 1644 cm^{-1} attributed to imine bond ($-\text{C}=\text{N}-$) formation from the interaction of glutaraldehyde and amine groups present in chitosan and enzyme crosslinked with glutaraldehyde. This region of the spectrum contained overlapped peaks corresponding to $-\text{NH}$ and $-\text{C}=\text{N}-$ stretching of the newly-formed Schiff's base. The peak corresponding to 1150 cm^{-1} ($-\text{C}-\text{O}-\text{C}$ bridge) was reduced in intensity due to formation of new bonds. (Fig. 8). The peaks corresponding to 1588 (amine) and 2362 cm^{-1} (amine stretching) were also reduced after bond formation in this spectrum. Thus, the FTIR results confirmed the covalent immobilization of GOX enzyme on chitosan beads using glutaraldehyde as a crosslinking agent.³⁷⁻⁴⁰

H_2O_2 Generation using Immobilized GOX

H_2O_2 generation for bleaching was evaluated and compared for both immobilized and free GOX using the same equivalent amount of each. Aliquots of reaction mixtures were separated at various time intervals and H_2O_2 generation was measured (Fig. 9). The amount of H_2O_2 generation using immobilized GOX was less than that of free GOX with the equivalent enzyme amount. It was also observed that H_2O_2 generation also increased with increased incubation time and became constant beyond 180 min with immobilized GOX. For free GOX, an incubation time of 120 min was sufficient for maximal peroxide generation. Immobilization restricted enzyme mobility and reduced its interaction with the reaction media. An additional concentration (20–25%) of immobilized GOX enzyme was required to generate H_2O_2 equivalent to that of the free GOX enzyme.

Cotton Fabric Bleaching Results

The performance of free and immobilized GOX enzymes for bleaching cotton fabric was compared at equivalent H₂O₂ concentrations. Results from conventional H₂O₂ bleaching of cotton fabric were also obtained for benchmarking purposes.

The immobilized GOX was successfully used for in situ H₂O₂ generation to bleach cotton textiles. Comparable whiteness values were obtained with enzymatically-generated and conventional peroxide (Table VIII). Application of the immobilized GOX enzyme slightly increased whiteness values compared to the free GOX enzyme. This observation

was also reported by Tzanov in 2002 with GOX immobilized on alumina.²⁴ This may be due to the reduced interaction of protein with the bleaching liquor as the enzyme is eliminated after H₂O₂ generation. The comparative bleaching bath compositions of these bleaching methods suggest the over-stabilization of H₂O₂ in the presence of glucose and GOX enzyme as explained earlier. It was concluded that only an additional 10% of the enzymatically-produced H₂O₂ was required with use of the immobilized GOX, while for the free GOX enzyme, 30% additional H₂O₂ provided whiteness values equivalent to that of the conventional H₂O₂ bleaching.

Immobilized GOX Enzyme Reuse

As enzyme immobilization allows recovery, the immobilized GOX (7-g beads) was used for H₂O₂ generation for five consecutive cycles and conjugate activity was measured after each cycle. The activity of immobilized GOX was reduced after each cycle and reached less than 50% for 4th and 5th cycles (Fig. 10a). The peroxide generated from each cycle was used for cotton bleaching and a good whiteness value (>50 CIE) was obtained for up to three consecutive cycles (Fig. 10b). Insufficient peroxide generation due to reduced activity restricted its further application.

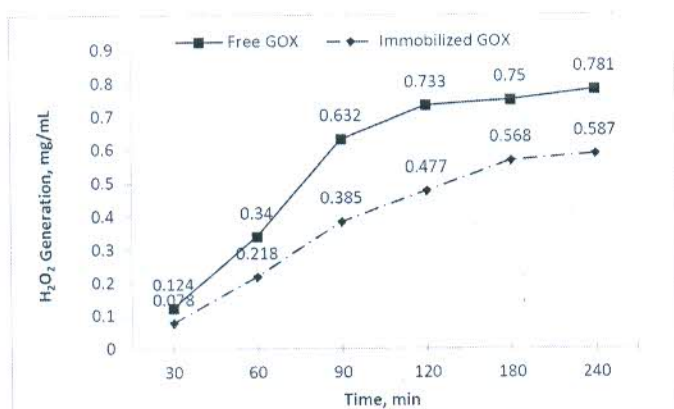


Fig. 9. Comparative peroxide generation using free and immobilized GOX enzyme.

Table VIII. Comparison of Cotton Fabric Bleaching Results with Free and Immobilized GOX Enzyme

Process	H ₂ O ₂ Concentration (g/L)				Whiteness (CIE)			
	I	II	III	Avg.	I	II	III	Avg.
Conventional H ₂ O ₂	0.76	0.77	0.81	0.78	62.2	62.4	62.9	62.5
Free GOX	0.78	0.81	0.81	0.8	57.2	57.8	58.4	57.8
Immobilized GOX	0.84	0.81	0.83	0.82	60.4	59.8	60.2	60.1

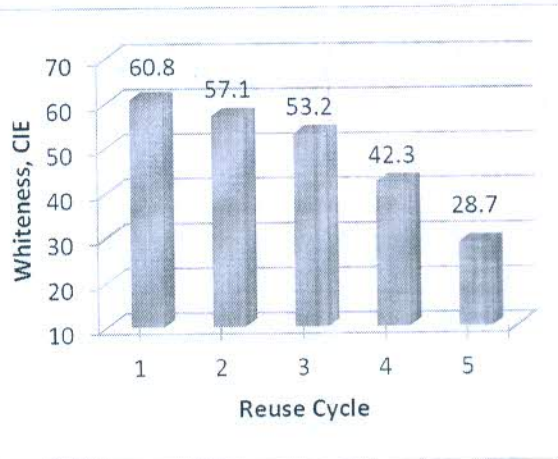
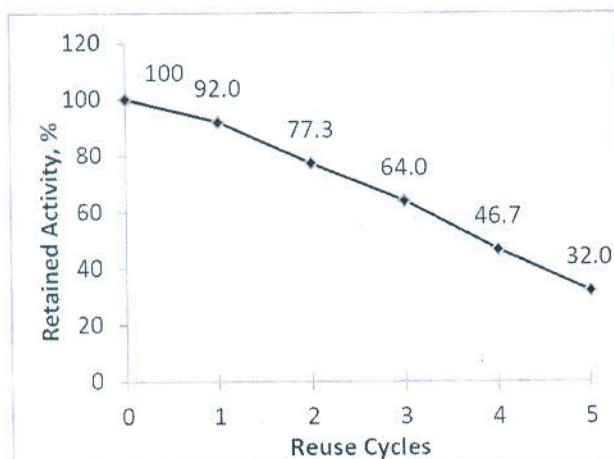


Fig. 10. (a) Activity retained and (b) cotton fabric whiteness obtained with immobilized GOX after each use cycle.

Conclusions

Hydrogen peroxide generation using glucose oxidase (GOX) depended significantly on enzyme and glucose concentrations, and time of incubation. Higher concentrations of enzyme and glucose favored hydrogen peroxide (H_2O_2) generation, but were unsuitable for cotton fabric bleaching due to over-stabilization of the bleaching bath. Statistical experimental design showed that the 1.8 g/L of GOX with 12 g/L of glucose were optimal for H_2O_2 generation to obtain sufficient whiteness. In conventional bleaching, 0.5 g/L of H_2O_2 provided a whiteness value of CIE 60 to cotton fabric, while in the enzymatically-generated bleaching bath, due to interactions of glucose and GOX, a higher concentration (0.8–0.85 g/L) of H_2O_2 was required to achieve the equivalent bleaching results.

The use of immobilized GOX enzyme for H_2O_2 generation improved the whiteness value and 0.55–0.6 g/L H_2O_2 provided cotton fabric bleaching results equivalent to that of conventional H_2O_2 bleaching. Concentrations of enzyme and glutaraldehyde and time of activation were the significant factors for immobilization of GOX on chitosan. Statistical experimental design was used and these results showed that the loading percent increased with the enzyme and glutaraldehyde concentrations, but the conjugate activity decreased. Use of 0.9 mg/mL of GOX enzyme with 3% glutaraldehyde solution followed by 4 h of activation gave the maximal conjugate activity.

In addition, the immobilized GOX enzyme can be reused for H_2O_2 generation, whereas the free GOX enzyme was lost after a single use. In this study, appropriate bleaching results were obtained for up to three consecutive uses with immobilized enzyme, although the reduced activity (40% residual activity) restricted their further application. Thus, the industrial feasibility of this process is worth further study, with recycling of immobilized enzyme providing a potential economic benefit, as well as improved cotton fabric bleaching results due to the absence of protein in the bleaching bath.

References

- Karmakar, S. R. *Chemical Technology in the Pre-Treatment Processes of Textiles*; Elsevier Science B.V.: Amsterdam, Netherlands, 1999.
- Basto, C.; Tzanov, T.; Cavaco-Paulo, A. *Ultrasonics Sonochemistry* **2007**, *14*, 350–354.
- Buschle-Diller, G.; Yang, X. D.; Yamamoto, R. *Textile Research Journal* **2001**, *71* (5), 388–394. <http://doi.org/10.1177/004051750107100504>.
- Dubey, M. K.; Zehra, A.; Aamir, M.; Meena, M.; Ahirwal, L.; Singh, S.; Shukla, S.; Upadhyay, R. S.; Bueno-Mari, R.; Bajpai, V. K. *Frontiers in Microbiology*, June 8, 2017, 1–22. <http://doi.org/10.3389/fmicb.2017.01032>.
- López, C.; Cavaco-Paulo, A. *Engineering in Life Sciences* **2008**, *8* (3), 315–323. <http://doi.org/10.1002/elsc.200700060>.
- Aniş, P.; Davulcu, A.; Eren, H. A. *Fibres and Textiles in Eastern Europe* **2009**, *73* (2), 87–90.
- Farooq, A.; Ali, S.; Abbas, N.; Fatima, G. A.; Ashraf, M. A. *Journal of Cleaner Production* **2013**, *42* (October), 167–171. <http://doi.org/10.1016/j.jclepro.2012.10.021>.
- Ramadan, A. R. *Journal of Textile and Apparel Technology and Management* **2008**, *6* (1), 1–12.
- Tavčer, P. F. *Biocatalysis and Biotransformation* **2012**, *30* (1), 20–26. <http://doi.org/10.3109/10242422.2012.644437>.
- Tzanov, T.; Calafell, M.; Guebitz, G. M.; Cavaco-Paulo, A. *Enzyme and Microbial Technology* **2001**, *29* (6–7), 357–362. [http://doi.org/10.1016/S0141-0229\(01\)00388-X](http://doi.org/10.1016/S0141-0229(01)00388-X).
- Davulcu, A.; Eren, H. A.; Avinc, O.; Erismis, B. *Cellulose* **2014**, *21*, 2973–2981. <http://doi.org/10.1007/s10570-014-0273-8>.
- Opwis, K.; Knittel, D.; Schollmeyer, E.; Hoferichter, P.; Cordes, A. *Engineering in Life Sciences* **2008**, *8* (2), 175–178. <http://doi.org/10.1002/elsc.200720237>.
- Hebeish, A.; Ramadan, M. A.; Hashem, M.; Sadek, B.; Abdel-Hady, M. *Research Journal of Textile and Apparel* **2013**, *17* (1), 94–103.
- Li, M.; Hinks, D. *AATCC Review* **2012**, *12* (5), 46–51.
- Spicka, N.; Tavcer, P. F. *Textile Research Journal* **2012**, *83* (6), 566–573. <http://doi.org/10.1177/0040517512458346>.
- Špička, N.; Tavčer, P. F. *Materiali in Tehnologije* **2013**, *47* (4), 409–412.
- Ali, S.; Khatri, Z.; Khatri, A.; Tanwari, A. *Journal of Cleaner Production* **2014**, *66* (March), 562–567. <http://doi.org/10.1016/j.jclepro.2013.11.035>.
- Eren, H. A.; Anis, P.; Davulcu, A. *Textile Research Journal* **2009**, *79* (12), 1091–1098. <http://doi.org/10.1177/0040517508099388>.
- Ali, S.; Khatri, Z.; Tanwari, A. *Int. J. Chem. Environ. Eng.* **2011**, *2*, 295–301.
- Desai, U. R.; Desai, P. V. *International Journal of Life Sciences Research* **2015**, *3* (2), 25–28.
- Saravanan, D.; Vasanthi, N. S.; Senthil-Raja, K.; Das, A.; Ramachandran, T. *Indian Journal of Fibre & Textile Research* **2010**, *35* (September), 281–283.
- Reis, C. Z.; Fogolari, O.; Oliveira, D.; de Arruda Guelli Ulson de Souza, S. M.; de Souza, A. A. U. *Canadian Journal of Chemical Engineering* **2017**, *95* (11), 2048–2055. <http://doi.org/10.1002/cjce.22891>.
- Opwis, K.; Knittel, D.; Kele, A.; Schollmeyer, E. *Starch/Stärke* **1999**, *51* (10), 348–353. [http://doi.org/10.1002/\(SICI\)1521-379X\(199910\)51.1.1.1](http://doi.org/10.1002/(SICI)1521-379X(199910)51.1.1.1).
- Tzanov, T.; Costa, S. A.; Guebitz, G. M.; Cavaco-Paulo, A. *Journal of Biotechnology* **2002**, *93* (1), 87–94. [http://doi.org/10.1016/S0168-1656\(01\)00386-8](http://doi.org/10.1016/S0168-1656(01)00386-8).
- Sheldon, R. A. *Adv. Synth. Catal.* **2007**, *349*, 1289–1307.
- Soares, J. C.; Moreira, P. R.; Queiroga, A. C.; Morgado, J.; Malcata, F. X.; Pintado, M. E. *Biocatalysis and Biotransformation* **2011**, *29* (January), 1–15. <http://doi.org/10.3109/10242422.2011.635301>.
- AATCC Technical Manual; AATCC: Research Triangle Park, NC, USA, 2007, Vol. 82, 151–152.
- Ramachandran, S.; Fontanille, P.; Pandey, A.; Larroche, C. *Food Technology and Biotechnology* **2006**, *44* (2), 185–195.
- Chen, H.; Zhang, Q.; Dang, Y.; Shu, G. *Advance Journal of Food Science and Technology* **2013**, *5* (7), 932–935.
- Tripathi, P.; Kumari, A.; Rath, P.; Kayastha, A. M. *Journal of Molecular Catalysis B: Enzymatic* **2007**, *49* (1–4), 69–74. <http://doi.org/10.1016/j.molcatb.2007.08.011>.
- Pospiskova, K.; Safarik, I. *Carbohydrate Polymers* **2013**, *96*, 545–548.
- Betancor, L.; Fernando, L.; Hidalgo, A.; Alonso-Morales, N.; Mateo, G. D. C.; Fernandez-Lafuente, R.; Guis, J. M. *Enzyme and Microbial Technology* **2006**, *39*, 877–882. <http://doi.org/10.1016/j.enzmictec.2006.01.014>.
- Fijul-Kabir, S. M.; Iqbal, M. I.; Sikdar, P. P.; Akhter, A. *European Scientific Journal* **2014**, *10* (36), 200–210.

34. Imran, M. A.; Hussain, T.; Memon, M. H.; Abdul Rehman, M. M. *Journal of Cleaner Production* **2015**, *108* (February), 494–502. <http://doi.org/10.1016/j.jclepro.2015.08.073>.
35. Naser, A.; Haque, A.; Islam, A. *International Journal of Scientific & Technology Research* **2015**, *4* (4), 40–43.
36. Madhu, A.; Chakraborty, J. N. *Journal of Cleaner Production* **2017**, *145*, 114–133. <http://dx.doi.org/10.1016/j.jclepro.2017.01.013>.
37. Aybastier, Ö.; Şahin, S.; Işık, E.; Demir, C. *Analytical Methods* **2011**, *3* (10), 2289. <http://doi.org/10.1039/c1ay05218g>.
38. Çetinus, Ş. A.; Öztop, H. N.; Saraydin, D. *Enzyme and Microbial Technology* **2007**, *41* (4), 447–454. <http://doi.org/10.1016/j.enzmictec.2007.03.014>.
39. Li, B.; Shan, C. L.; Zhou, Q.; Fang, Y.; Wang, Y. L.; Xu, F.; Han, L. R.; Ibrahim, M.; Guo, L. B.; Xie, G. L.; Sun, G. C. *Marine Drugs* **2013**, *11* (5), 1534–1552. <http://doi.org/10.3390/md11051534>.
40. Tavano, O. L.; Fernandez-Lafuente, R.; Goulart, A. J.; Monti, R. *Process Biochemistry* **2013**, *48* (3), 1054–1058. <http://dx.doi.org/10.1016/j.procbio.2013.05.009>.

Author

J. N. Chakraborty, Dr. B. R. Ambedkar National Institute of Technology, Jalandhar 144011, India; phone +91.941.713.9036; fax +91.181.269.0932; chakrabortyjn@gmail.com.

©opy

What you're reading is more than just copy. It's also copyrighted. So before you head over to the photocopier, make sure you have permission. Contact the publisher or visit www.copyright.com.

 **COPYRIGHT CLEARANCE CENTER**

Functional Dyeing of Cellulose-based (Linen) Fabric Using *Bombax Ceiba* (Kapok) Flower Extract

Javed Sheikh*, Nagender Singh, and Mayuri Srivastava

Department of Textile Technology, Indian Institute of Technology (I.I.T.), Delhi 110016, India
(Received April 17, 2018; Revised September 11, 2018; Accepted November 18, 2018)

Abstract: Linen fiber, which is claimed to be more comfortable than cotton, is an important textile fiber obtained from *Linum usitatissimum* (Flax) plant. However, the lack of functional properties of linen limits its application in functional textile products. Nowadays, use of natural colorant for textile dyeing has become an attractive option for sustainable textile coloration. Kapok flower is an unexplored source of natural dyestuff which can also be utilized for functionalization of cellulose-based textiles. In the current work, kapok flower extract (KFC) was utilized as a functional dye for dyeing of linen fabric in the presence of metallic mordants. The dyed fabrics were evaluated for coloration properties (color values, color coordinates, and fastness properties) as well as functional properties viz. antibacterial activity, UV protection, and antioxidant activity. The satisfactory level of dyeing with acceptable fastness ratings was achieved on linen fabrics. The dyed fabrics displayed an excellent antibacterial activity against gram-positive and gram-negative bacteria. The efficient level of UV protection and radical scavenging (antioxidant activity) was also obtained. The mechanism of functional modification of linen using KFC was discussed.

Keywords: Linen, Kapok, Dyeing, Antibacterial, UPF, Antioxidant

Introduction

Linen fiber is an important natural fiber obtained from flax (*Linum usitatissimum*) plant. It is an upcoming fiber for textile applications with most suitable properties for the products like apparels, bedsheets, and many technical textiles. However, being cellulosic, it lacks very important functional properties like antibacterial activity, UV protection, and flame retardancy. With the development of textile-based wellness products, the antioxidant activity of the substrates is highly demanded. Hence functional modification of such cellulose-based fiber is the new quest for research.

A huge amount of plant sources has been identified for extraction of different vibrant colors and their multifunctional requirements in textile processing and other disciplines. In order to obtain attractive natural dyes, various parts of plants like their flowers, stem, pellets, and also animals have been utilized. Natural dyes, as compared to synthetic dyes, have better biodegradability and compatibility with the environment. These benefits have led to an increasing customer demand for natural coloration of textile products. However, most of the natural dyes suffer from limitations like availability of limited shades, low reproducibility, inferior fastness, requirement of mordant, and higher cost, which restricts the commercial exploration of natural dyes. In most of the natural dyes, the dye-mordant combination governs the properties of dyed materials and the said limitations thus can be overcome using suitable combination of dye and mordant. There are continuous investigations in the various species of plants for identifying new sources of natural dyes

and natural mordants [1-13].

The continuous research in the field of natural dyes had led to an exploration of many functional properties of the natural-dyed substrates. The plant extracts based functional finishing of various textile fibers has been reported [14-25].

Kapok plant contains about 26 genera and nearly 150 pantropical species. It is commonly known as *purani*, *pagun*, *roktosimul*, *ceiba*, and *Indian bombax*. Bombax or red silk cotton is an important medicinal plant and widely found in Australia, tropical Asia, and northeast Africa [26,27]. In India, it is found at low altitudes to high altitudes specifically in autumn/winter/spring seasons [28]. Kapok plant has several medicinal properties such as hepatoprotective, anti-inflammatory, antiangiogenic, anti-HIV, antioxidant activities, etc. and is extensively used for curing diseases [29-31]. Kapok flower retains red without fading over a week after falling on the ground [32], which indicates the resistance of kapok colorant towards fading in the presence of sunlight. In short, KFC can be utilized as functional natural dye. However, the literature regarding the use of KFC as a natural dye for textiles is rather scarce. Chung *et al.* studied the dyeing performance of kapok flower colorant on wool fabrics and achieved remarkable results [33].

In the present work, we are reporting the first application of kapok flower colorant (KFC) in simultaneous dyeing and multifunctional modification of linen fabric. The coloration of linen fabric using KFC and metallic mordants was reported. The efficacy of imparted functional properties viz. antioxidant property, UV protection factor, and antibacterial activity was also studied.

*Corresponding author: jnsheikh@iitd.ac.in

Experimental

Materials

Linen fabrics (EPI-45, PPI-41, and GSM-241.5) were supplied by Jayshree Textiles. The received fabrics were washed, dried, and further used for dyeing. The kapok flowers (red colored) were collected from Institute campus. All the chemicals used in the study were of laboratory grade, which were purchased from Sigma Aldrich and Merck Specialties Private Limited, India.

Method

Extraction of KFC

Kapok flowers were dried in an oven at 45 °C for 24 h and powdered in a mixer-grinder. Extraction of KFC was carried out using an aqueous extraction method. The kapok flower powder (5 g) was suspended in water (100 ml) and the extraction was carried out at 90 °C for 60 min using a water bath (Khera, India). After the completion of extraction time, the liquor was filtered to collect the extract. The volume of the final extract was made to 100 ml using water and the prepared stock solution of KFC (5 %) was used for dyeing. In order to study the absorption pattern of extract in UV-Visible region, the KFC extract was analyzed using a UV-Vis spectroscopy (Shmadzu, Japan).

Mordanting and Dyeing of Linen Fabric

The pre-mordanting process was used for this experiment. The mordants used for this study were different metallic salts such as copper sulfate, ferrous sulfate, and potash alum which were used in the concentration of 1 %, 5 %, and 10 % (on weight of fiber, owf), respectively. The metal salts were dissolved in distilled water to make an M:L ratio of 1:10. The fabric samples were immersed in the mordant solution and treated at 90 °C for 60 min. After mordanting, the fabric samples were removed, squeezed, and subjected to further dyeing process.

The mordanted samples were dyed with the KFC (20 % shade owf) by using the M:L ratio of 1:10. The mordanted fabric samples were dipped in dye extract and dyeing was carried out in a water bath at 90 °C for 60 min. After the completion of dyeing, the samples were removed from the dye solution and washed with cold water for 10 min. The sample names were abbreviated as AKFC (alum mordanted and dyed), CKFC (copper sulfate mordanted and dyed), and FKFC (ferrous sulfate mordanted and dyed).

FTIR Analysis

FTIR spectra of the dyed fabrics were recorded using a Thermo Scientific Nicolet iS50 FTIR Spectrometer. The samples were recorded and analyzed with 15 scans in the wavenumber range 400-4000 cm^{-1} with a 4 cm^{-1} resolution.

Color Strength Measurement

The reflectance (R %), CIE $L^*a^*b^*$ values and color strength (K/S value) of the dyed fabric samples were analyzed

using a spectrophotometer (Color-EYE 7000A). The method involves Kubelka-Munk K/S equation. K/S value denotes the fabric color strength. Based on the reflectance (R %), color strength value can be calculated by the following formula:

$$K/S = \frac{(1-R)^2}{2R}$$

where K is absorption coefficient) and S is scattering coefficient.

Fastness Test

The dyed fabrics were analyzed for washing fastness according to standard test method ISO II [34]. The rubbing fastness was evaluated as per the standard test method ISO105-X12.

Antimicrobial Activity

The antibacterial activity was assessed by using the agar plate method (AATCC 100-2004) [35]. The ability of the fabric samples to prevent microbial growth and retention was evaluated using *S. aureus* (a gram-positive bacterium) and *E. coli* (a gram-negative bacterium) cultures. The following equation was used to calculate the bacterial reduction:

$$\text{Bacterial reduction (\%)} = \frac{(B-A)}{A} \times 100$$

where A =the number of bacterial colonies recovered from the inoculated treated test specimen swatches in the jar incubated for 24 h contact period and B =the number of bacterial colonies recovered from the inoculated untreated control test specimen swatches in the jar immediately after inoculation (at 0 contact time).

Antioxidant Activity

The antioxidant activity of the dyed fabric samples was tested using the 2,2-diphenyl-1-picryl-hydrazil (DPPH) reagent, as per method available in the literature [36]. One-inch square samples of linen were added to a test tube which is containing 4 ml of freshly prepared DPPH radical (1.0×10^{-4} mol/l) in a methanol solution and the reaction was allowed for 30 min at 25 °C in the dark using a shaking incubator. The decolorizing result of the samples was analyzed by measuring the absorbance at 517 nm by a UV-VIS spectrophotometer (Shimadzu, Japan). The following formula was used to determine the antioxidant activity (%):

$$\text{Antioxidant activity (\%)} = \frac{(A_c - A_s)}{A_c} \times 100$$

where A_c is absorbance of the control and A_s is absorbance of the sample.

Ultraviolet Protection Factor (UPF)

The ultraviolet protection factor (UPF) of the dyed samples was evaluated as per AS/NZS 4399:1996 standard [37] using a UV-visible spectrometer (Cary, USA). The UPF was determined by using following formula;

$$UPF = \frac{\sum_{290}^{400} E_{\lambda} S_{\lambda} \Delta\lambda}{\sum_{290}^{400} E_{\lambda} S_{\lambda} T_{\lambda} \Delta\lambda}$$

where S_{λ} (Erythema action spectrum), E_{λ} (solar irradiance), $\Delta\lambda$ (wavelength increment), and T_{λ} (specimen spectral transmittance).

The UPF range and the corresponding category of protection is available in the literature [37].

Results and Discussion

Characterization of KFC Extract and Dyed Sample

The FTIR spectra of extracted and purified KFC were recorded using a Thermo Scientific Nicolet iS50 FT-IR Spectrometer with a wavenumber range of 4000-400 cm^{-1} and the most characteristic functional chemical groups are present in the colorant are shown in Figure 1. The characteristics peaks were observed at 3270 cm^{-1} (O-H stretching band), 2920 cm^{-1} (CH-vibration), 2110 cm^{-1} (CH_2 symmetric stretching), 1730 cm^{-1} (C=O stretching vibration), 1610 cm^{-1} (C=C stretching and -N-H stretching), 1440 cm^{-1} (CH_2 deformation, C-H deformation), 1290 cm^{-1} (C-O stretching vibration), 1050 cm^{-1} (C-O and C-O-C vibration), 778 cm^{-1} (-C-H vibration).

The FTIR spectrum of KFC showed various peaks indicating the presence of natural pigments like anthocyanin and carotenoid. The presence of these pigments was reported in earlier studies from various researchers [38,39]. Apart from this, kapok flowers contains various active compounds like flavones (apigenin, cosmetin, isovitexin, linarin, saponarin, vicianin 2, xanthomicrol [40], flavonols (3,5-dihydroxy-4'-methoxy-flavon 7-yl-O- α -l-rhamnopyranosyl-(1 \rightarrow 6)- β -d-glucopyranoside [41], kaempferol, quercetin [42]), anthocyanidins and anthocyanins (cyanidin-3,5-diglucoside [43], pelargonidin-5- β -d-glucoside, cyanidin-7-methyl-ether-3- β -d-glucoside [44], triterpenes (α -amyryn [40]), etc.

The FTIR spectra of undyed and dyed fabric samples are shown in Figure 2.

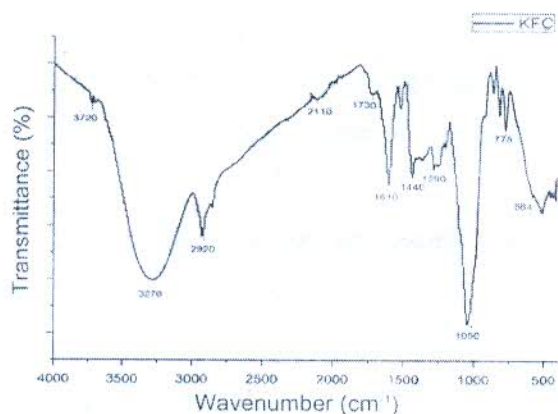


Figure 1. FTIR of KFC extract.

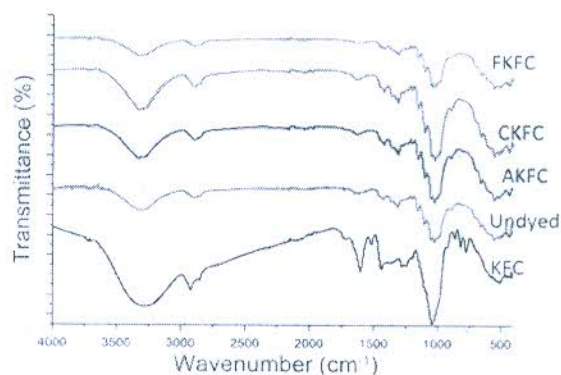


Figure 2. FTIR of undyed sample, KFC extract, AKFC, CKFC, and KFCC.

No significant difference was observed between the FTIR spectra of undyed and dyed linen samples. The dyed fabrics showed some changes in the peaks between 1500-1750 cm^{-1} . A change in the peak intensity of absorption band of -OH groups was observed between dyed and undyed fabrics. The change can be observed in peak intensity at 2920 cm^{-1} when linen dyed with KFC. The peak intensity change between 2800-2950 cm^{-1} may be attributed to the C-H groups of from KFC. A significant change of peak intensity was observed in various peaks viz. 1440-1750 cm^{-1} assigned to the C=O vibration at 1730 cm^{-1} , C=C stretching and -N-H stretching at 1610 cm^{-1} and CH_2 deformation, C-H deformation at 1440 cm^{-1} . This might be attributed to complex formed between metal ions and KFC with the cellulose backbone. As the metal ions are held on cellulose because of -OH groups which later form a complex with the active compound of KFC extract, a big shift in FTIR spectrum was not expected. Apart from this, linen itself contains various functional groups which are identical to those present in KFC extracts which makes it difficult for FTIR spectrum to give very clear distinction between undyed and dyed linen.

Color Values of the Dyed Sample

Most of the natural dyes have no or moderate affinity for textile substrates and mordants must be used to improve the color strength and fastness. To improve dye affinity, there is a need of mordanting agent which can produce a molecular bond between the fiber and dye molecules. The metal salts like potash alum, copper sulfate, ferrous sulfate, etc. form complex with dye molecules and show efficient mordanting action for the natural dyes. After mordanting, the metal salts attached to the fibers attract the dye molecules towards the fibers and finally develops the link between the dye molecules and the fiber by forming stable complexes. Most of the metallic mordants attached to any textile fiber, chemically combine with particular chemical functional groups present in the natural dyes and bond with the help of hydrogen bonds, ionic bonds, and other important bonding

Table 1. Color values and color coordinates of dyed samples

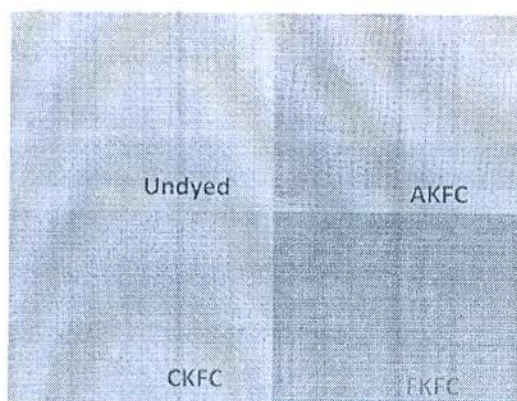
Sr. no.	Sample	Mordant concentration	L^*	a^*	b^*	K/S
1	Undyed		91.39	-0.89	5.10	0.23
2	AKFC	10	78.11	-0.95	14.15	1.04
3	CKFC	1	73.14	2.77	16.75	1.14
4	FKFC	5	56.12	-0.39	10.28	4.13

forces [45]. The validation of the requirement of mordant for dyeing of linen fabric using KFC has been confirmed as the fabric dyed without mordant showed negligible color strength which was further reduced after washing.

The color strength of dyed samples was evaluated with the help of Kubelka-Munk equation and the results are presented in Table 1.

The satisfactory color strength was observed on dyed linen fabrics, which indicates the suitability of KFC as a natural dye. The beautiful shades were built on linen fabric (Figure 3), the depths and tones of which varied with mordant type. The AKFC, CKFC, and FKFC showed yellow-brown, brown, and grey shades, respectively. The use of different mordants not only caused the variations in hue and significant changes in color strength (K/S values), but also affected the brightness index values and L^* values. The importance of mordants in providing the higher color strength values to dyed fabric may be attributed to their ability to form complexes between the fiber and the dye molecules thus resulting in fixation of higher amount of dye on fiber. Combination of kapok colorant and linen was affected by the presence of metal ions, resulting in a change in shade. The highest K/S value was found in case of FKFC sample which represents ability of Fe ion to interact with higher number of dye molecules.

Table 1 shows CIE $L^*a^*b^*$ values in which positive value a^* and b^* represent red and yellow shades while a negative value of a^* and b^* represent green and blue shades, respectively. The AKFC, CKFC, and FKFC displayed green-

**Figure 3.** Dyed linen fabrics using kapok flower extract.**Table 2.** Fastness properties of dyed samples

Sr. no.	Sample	Wash fastness		Rubbing fastness	
		Change in shade	Staining	Dry	Wet
1	AKFC	3-4	4	4-5	4
2	CKFC	4	4-5	4-5	4
3	FKFC	4	4-5	4-5	4

yellow, red-yellow, and green-yellow tones, respectively. This gives an immense potential where a shade and tone of the dyed fabrics can be varied using different mordants when a single natural dye is available for dyeing.

Fastness Properties of Dyed Sample

Fastness properties, which indicate the resistance of dye on dyed fabric to come out in presence of various agencies, were evaluated and the results are summarized in Table 2.

The washing fastness varied with the use of different mordants; however, all samples viz. AKFC, CKFC, and FKFC displayed an acceptable level of fastness. This further confirms the wash-fast interaction between dye and fiber using metallic mordants. The efficient mordanting action was achieved because of a complex formation between the dye and mordant which holds the dye firmly on cellulose and prevents bleeding in the wash liquor. The wash fastness achieved may also be attributed to the formation of an additional bond between the fiber, metal ions, and KFC molecules, which could overcome the force applied during washing. Staining was negligible on the adjacent fabric used for testing of wash fastness which also indicates limited affinity of KFC towards cellulose in the absence of mordant. All dyed samples displayed excellent rubbing fastness indicating stability of dye-mordant complex during an abrasive action. Among all mordants studied, FKFC was found to give the best fastness; however, it is also the question of optimization of mordant and dye concentration.

Antimicrobial Activity of Dyed Fabrics

The microbial contamination on textile materials is considered as a severe limitation for its use in health and hygiene applications. The efficacy of dyed fabrics as

Table 3. Antibacterial and antioxidant properties of kapok colorant dyed linen fabrics

Sr. no.	Sample	Bacterial colony reduction (%)		Radical scavenging activity (%)
		<i>E. coli</i>	<i>S. aureus</i>	
1	Undyed	N	N	7.52
2	AKFC	84	78	89.39
3	CKFC	95	88	90.27
4	FKFC	97	92	91.87

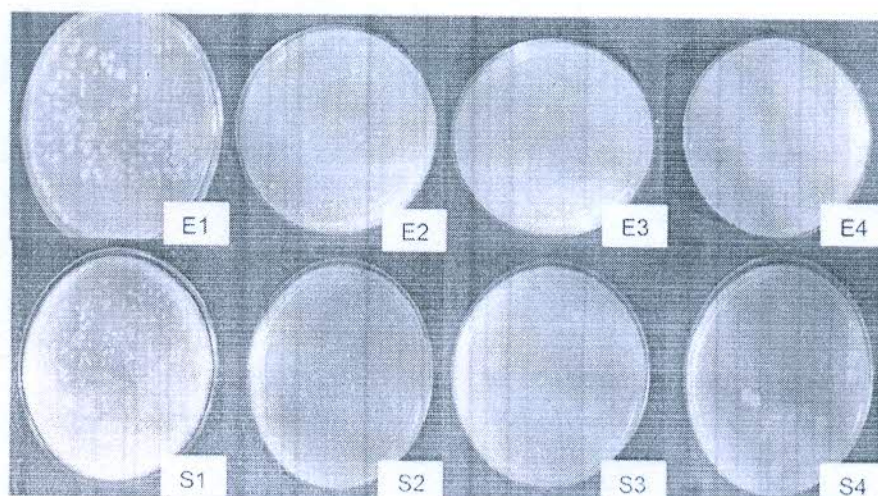


Figure 4. Pictorial representation of Antibacterial activity of dyed fabrics; (E1) Blank *E. coli*, (E2) AKFC against *E. coli*, (E3) CKFC against *E. coli*, (E4) FKFC against *E. coli*, (S1) Blank *S. aureus*, (S2) AKFC against *S. aureus*, (S3) CKFC against *S. aureus*, and (S4) FKFC against *S. aureus*.

antibacterial material was evaluated against gram positive and gram negative bacteria and the results are presented in Table 3. The pictorial presentation of bacterial colony reduction is presented in Figure 4.

The dyed fabrics displayed varying level of antibacterial activity which is ultimately dependent on the mordant-dye combination; however, all dyed samples can be regarded as antibacterial materials. In general, the dyed samples displayed better antibacterial properties against *E. coli* as compared to that against *S. aureus*. The antibacterial activity of KFC dyed fabrics was ranked in the order FKFC > CKFC > AKFC and the trend was valid against both *S. aureus* and *E. coli*. This is due to the fact that metal ions of mordants exhibit toxic effects against the pathogens and prevent bacteria attack [46] along with the inherent antibacterial properties of KFC. The presence of various active compounds like flavones, flavonols, kaempferol, quercetin, anthocyanidins and anthocyanins, pelargonidin-5- β -d-glucoside, cyanidin-7-methyl-ether-3- β -d-glucoside triterpenes (α -amyrin), etc. are known for antimicrobial properties and thus also impart antibacterial properties to the dyed samples. In case of natural dyeing, the antibacterial activity of dyed fabric is a combined effect of the mordant-dye complex. The non-leaching type of mechanism of antibacterial activity is expected in such cases where the active compound does not leach out and kill the bacteria. It remains bound to fiber and kills the bacterium coming in contact with it.

Antioxidant Properties of Dyed Samples

Results in Table 3 clearly showed the absence of antioxidant activity in case of undyed linen; however, all dyed samples show efficient radical scavenging activity. The tannins and flavonoids contain a huge number of free,

glycosylated, and esterified hydroxyl groups attached to the aromatic and heterocyclic rings which are responsible for radical scavenging activity. The number and position of these free hydroxyl groups on the ring affect the radical scavenging activity significantly. DPPH is a stable radical and can easily undergo scavenging in the presence of antioxidant compounds containing hydroxyl groups which can scavenge radicals and help protect human cells against oxidative damage [47,48]. The antioxidant activity of dyed fabrics was mainly due to the presence of polyphenolic compounds and flavonoids which have the tendency to transfer hydrogen or electron thus stabilizing free radical. In case of dyed linen samples, the antioxidant activity depends on the amount of KFC extract, containing polyphenolic compounds, exhausted on the fiber as well as the free functionalities of the biomolecules present on the dyed sample. All dyed samples displayed an excellent antioxidant activity indicating the availability of sufficient phenolic groups for the scavenging of DPPH radical.

UV Protection of Dyed Samples

The UV radiation emitted by the sun has a broad spectrum from the high to low-energy with varying wavelengths, which is classified as UVC (below 280 nm), UVB (280-315 nm), and UVA (315-400 nm). It is highly desirable to develop UV protective clothing that can protect user from harmful effects of such radiations. In general, lower value of UV transmittance indicates better UV protection property of the sample [49-53]. The UV protection offered by dyed samples are presented in Figure 5 and Table 4. As evident from Figure 5, the UV transmittance spectra showed a significant difference between the dyed fabric samples and undyed sample.

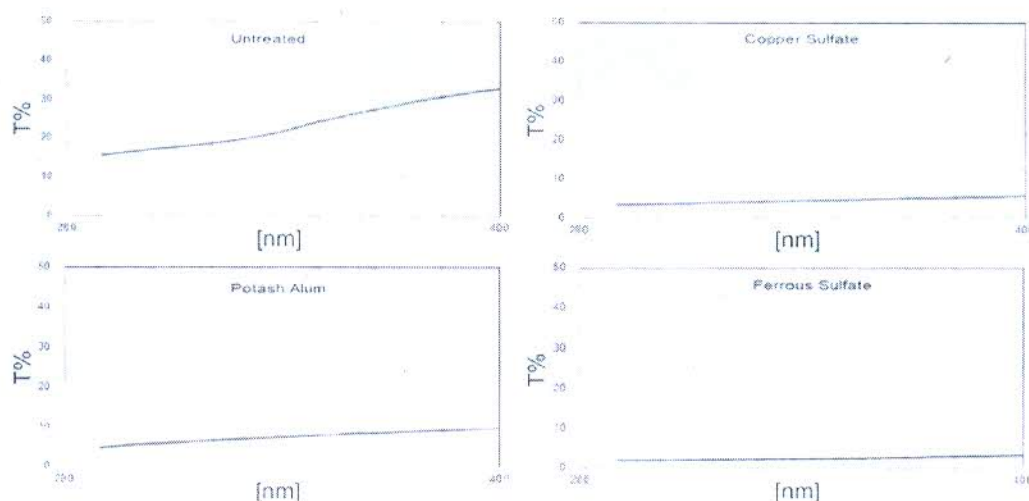


Figure 5. UV transmittance spectra of the undyed and dyed fabric samples.

Table 4. Comparison of UV transmittance spectra of the untreated and dyed fabric samples

Mordant	UVA	UVB	UPF
	315-400 nm	290-315 nm	290-400 nm
Undyed	25.46	16.80	5.62
AKFC	8.08	5.66	16.29
CKFC	4.72	3.56	26.73
FKFC	2.55	1.90	50.38

The UV transmittance of the undyed linen was higher than the dyed samples. This is well reflected in UPF value of untreated linen which was found to be 5.62. Hence the poor UV protection offered by the undyed sample.

Evidently, less UV transmittance was detected when fabric samples were dyed with KFC that ultimately displayed good UV protection properties. As shown in Table 4, it is clearly noticed that different mordants had different effects on the spectral transmittance of fabrics dyed with KFC. However, the UPF values displayed by all dyed samples were satisfactory to provide efficient UV protection. This may be due to the metal salts bridging the fibers and the dyes molecules resulting in the formation of differently coordinated complexes of π -bonds [52]. Therefore, fabrics dyed with KFC can block ultraviolet radiation. The UPF of FKFC was 50.38 which shows better ultraviolet protection as compared to that of AKFC and CKFC. The KFC dyed wool fabric was reported to offer efficient UV protection [33]. The UV-Visible spectra of KFC showed (Figure 6) strong absorption in UV region which clearly indicates the reason behind the enhanced UPF of dyed fabrics.

In short, the functional properties of the dyed samples were found dependent on the color values of the dyed samples. This is obvious because the higher color values

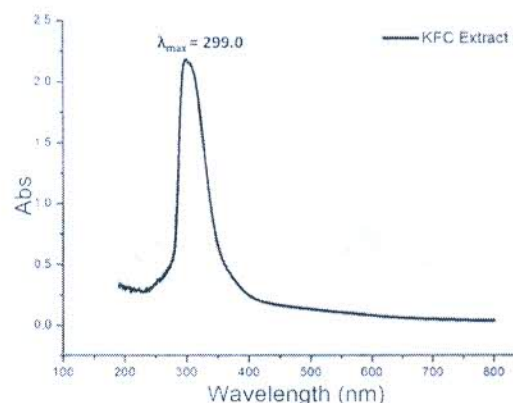


Figure 6. UV-Visible spectra of KFC extract.

indicate the presence of higher amount of biomolecules on fabric which are responsible for imparting functional properties to the linen fabric. Hence, among the dyed samples, FKFC displayed the best antimicrobial properties, UV protection, and radical scavenging activity.

Conclusion

The successful development of multifunctional linen was carried out using kapok flower colorant as a natural dye. Beautiful shades were obtained on linen using KFC. All the dyed samples showed excellent color strength along with satisfactory fastness ratings. The change in shade from reddish to brownish yellow and grey was observed depending on the presence of metal ions in the mordants. The KFC dyed linen demonstrated interesting radical scavenging activity and antimicrobial properties against both gram-positive and gram-negative bacteria. All dyed samples also displayed higher UPF values indicating efficient UV

protection offered by such substrates. It can be concluded that the kapok flower extract is a functional dye when utilized in the presence of metallic mordants which can serve as a promising candidate of natural dyestuff and can be used in simultaneous dyeing and textile finishing to impart antibacterial, antioxidant, and ultraviolet protection properties to cellulose-based biological macromolecules.

Acknowledgement

Authors gratefully acknowledge Science and Engineering Research Board (SERB, India) for ECRA funding (project File no. ECR/2017/001041).

References

1. P. Guinot, A. Rogé, A. Gargadennec, M. Garcia, D. Dupont, E. Lecoeur, L. Candelier, and C. Andary, *Color Technol.*, **122**, 93 (2006).
2. E. Yi and J. Choi, *Fiber Polym.*, **9**, 646 (2008).
3. A. K. Samanta and P. Agarwal, *Indian J. Fibre Text. Res.*, **34**, 384 (2009).
4. R. Siva, *Curr. Sci.*, **92**, 916 (2007).
5. A. Pal, Y. C. Tripathi, R. Kumar, and L. Upadhyay, *J. Pharm. Res.*, **10**, 154 (2016).
6. W. Khwanchit, V. Meeyoo, and S. Chavadej, *Sol. Energy Mater. Sol. Cells*, **91**, 566 (2007).
7. S. Hao, J. Wu, Y. Huang, and J. Lin, *Sol. Energy*, **80**, 209 (2006).
8. J. Sheikh, P. S. Jagtap, and M. D. Teli, *Fiber Polym.*, **17**, 738 (2016).
9. S. Islam, L. J. Rather, M. Shahid, M. A. Khan, and F. Mohammad, *Ind. Crops Prod.*, **59**, 337 (2014).
10. M. Yusuf, S. Islam, M. A. Khan, and F. Mohammad, *Optik*, **127**, 6087 (2016).
11. R. J. Rather, S. Islam, M. Shabbir, M. N. Bukhari, M. Shahid, and M. A. Khan, *J. Environ. Chem. Eng.*, **4**, 3041 (2016).
12. P. S. Vankar, R. Shanker, and S. Wijayapala, *Pigm. Resin Technol.*, **38**, 242 (2009).
13. M. Shabbir, S. Islam, M. N. Bukhari, L. J. Rather, M. A. Khan, and M. A. Mohammad, *Text. Cloth Sustain.*, **2**, 7 (2016).
14. J. Banupriya and V. Maheswari, *J. Text. Sci. Eng.*, **3**, 1 (2013).
15. S. N. Chattopadhyay, N. C. Pan, A. K. Roy, S. Saxena, and A. Khan, *J. Text. Inst.*, **104**, 808 (2013).
16. M. Joshi, S. W. Ali, and S. Rajendran, *J. Appl. Polym. Sci.*, **106**, 793 (2007).
17. M. Rattanaphol, K. Jiri, W. Jakob, and V. Martina, *Fibres Text. East. Eur.*, **19**, 94 (2011).
18. S. Han and Y. Yang, *Dyes Pigm.*, **64**, 157 (2005).
19. E. Koh and K. H. Hong, *Dyes Pigm.*, **103**, 222 (2014).
20. S. Islam, S. A. Wani, and F. Mohammad, *Int. J. Biol. Macromol.*, **109**, 907 (2018).
21. S. Islam and G. Sun, *ACS Sustain. Chem. Eng.*, **5**, 7451 (2017).
22. P. Pisitsak, N. Tungsombatvisit, and K. Singhanu, *J. Cleaner Prod.*, **174**, 1215 (2018).
23. L. J. Rather, S. Islam, M. Azam, M. Shabbir, M. N. Bukhari, M. Shahid, M. A. Khan, Q. M. R. Haque, and F. Mohammad, *RSC Adv.*, **6**, 39080 (2016).
24. L. J. Rather, S. Akhter, R. A. Padder, Q. P. Hassan, M. Hussain, M. A. Khan, and F. Mohammad, *Dyes Pigm.*, **139**, 812 (2017).
25. M. Shabbir, L. J. Rather, and F. Mohammad, *Ind. Crops Prod.*, **119**, 277 (2018).
26. D. D. Chakraborty, V. Ravi, and P. Chakraborty, *Int. J. Pharm. Sci. Res.*, **1**, 66 (2010).
27. C. Bhavsar and G. S. Talele, *Bangladesh J. Pharmacol.*, **8**, 102 (2013).
28. John A. Parrotta, "Healing Plants of Peninsular India", CABI Publishing, 2001.
29. T. O. Vieira, A. Said, E. Aboutabl, M. Azzam, and T. B. Creczynski-Pasa, *Redox Rep.*, **14**, 41 (2009).
30. V. Lakshminarasimhan, M. Lenin, and P. Varalakshmi, *Phytother. Res.*, **16**, 514 (2002).
31. Y.-J. You, N.-H. Nam, Y. Kim, K.-H. Bae, and B.-Z. Ahn, *Phytother. Res.*, **17**, 341 (2003).
32. M. A. Abdullah, A. U. Rahmah, and Z. Man, *J. Hazard. Mater.*, **177**, 683 (2010).
33. T. W. Chung, P. F. Ng, Q. Chen, and B. Fei, *World J. Text. Eng. Technol.*, **1**, 23 (2015).
34. E. R. Trotmann, "Dyeing and Chemical Technology of Textile Fibers", England: Charles Griffin and Company Ltd., 1984.
35. American Association of Textile Chemists and Colorists. AATCC Technical Manual, 76, Research Triangle Park, NC: AATCC (2007).
36. J. Sheikh and I. Bramhecha, *Int. J. Biol. Macromol.*, **118**, 896 (2018).
37. AS/NZS 4399:1996, Sun Protective Clothing-Evaluation and Classification, 1996.
38. N. Li, N. Pan, D. Li, and S. Lin, *Int. J. Photoenergy*, **2013**, Article ID 598753 (2013).
39. H. Hug, M. Bader, P. Mair, and T. Glatzel, *Appl. Energy*, **115**, 216 (2014).
40. A. M. EL-Hagrassi, M. M. Ali, A. F. Osman, and M. Shaaban, *Nat. Prod. Res.*, **25**, 141 (2011).
41. S. A. Rizvi and O. C. Saxena, *Arzneimittelforschung*, **24**, 285 (1974).
42. H. Gopal and R. K. Gupta, *J. Pharm. Sci.*, **61**, 807 (1972).
43. R. Scogin, *Aliso*, **11**, 377 (1986).
44. G. S. Niranjan and P. C. Gupta, *Planta Med.*, **24**, 196 (1973).
45. M. Shahid, S. Islam, and F. Mohammad, *J. Cleaner Prod.*, **53**, 310 (2013).
46. A. K. Prusty, T. Das, A. Nayak, and N. B. Das, *J. Cleaner*

- Prod.* **18**, 1750 (2010).
47. S. Kandhasamy and S. C. Kang, *Saudi J. Biol. Sci.*, **20**, 319 (2013).
48. S. N. Das, P. V. Jagannath, and S. C. Dinda. *Asian Pac. J. Trop. Biomed.*, **2**, S1382 (2012).
49. D. Grifoni, L. Bacci, S. D. Lonardo, P. Pinelli, A. Scardigli, F. Camilli, F. Sabatini, G. Zipoli, and A. Romanic. *Dyes Pigm.*, **105**, 89 (2014).
50. D. Grifoni, L. Bacci, G. Zipoli, L. Albanese, and F. Sabatini, *Dyes Pigm.*, **91**, 279 (2011).
51. A. Springsteen, R. Yurek, M. Frazier, and K. Carr, *Anal. Chim. Acta.* **380**, 155 (1999).
52. X. X. Feng, L. L. Zhang, J. Y. Chen, and J. C. Zhang, *J. Cleaner Prod.*, **15**, 366 (2007).
53. K. Hoffmann, P. Kesners, A. Bader, A. Avermaete, P. Altmeyer, and T. Gambichler, *Skin Res. Technol.*, **7**, 223 (2001).



Sustainable Functional Coloration of Linen Fabric Using *Kigelia Africana* Flower Colorant

Javed Sheikh, Nagender Singh & Dipak Pinjari

To cite this article: Javed Sheikh, Nagender Singh & Dipak Pinjari (2021) Sustainable Functional Coloration of Linen Fabric Using *Kigelia Africana* Flower Colorant, Journal of Natural Fibers, 18:6, 888-897, DOI: [10.1080/15440478.2019.1658260](https://doi.org/10.1080/15440478.2019.1658260)

To link to this article: <https://doi.org/10.1080/15440478.2019.1658260>



Published online: 31 Aug 2019.



Submit your article to this journal [↗](#)



Article views: 198



View related articles [↗](#)



View Crossmark data [↗](#)



Citing articles: 2 View citing articles [↗](#)



Sustainable Functional Coloration of Linen Fabric Using *Kigelia Africana* Flower Colorant

Javed Sheikh^a, Nagender Singh^a, and Dipak Pinjari^b

^aDepartment of Textile Technology, Indian Institute of Technology (I.I.T.), Delhi, India; ^bNational Center for Nanoscience and Nanotechnology, University of Mumbai, Mumbai, India

ABSTRACT

Natural dyes are gaining momentum in the textile industry due to their non-toxic and eco-friendly nature. The enhanced demand of natural-dyed functional textile materials resulted in increased interest among the research community to explore new sources of natural dyes which could be utilized for functional coloration of textile materials. *Kigelia Africana* flower is known for various medicinal properties and thus can be utilized for functional coloration of textile materials. In the current study, the pre-mordanting process has been exploited to evaluate the dyeing condition of the linen fabrics by using different mordants such as; alum, ferrous sulfate, and copper sulfate. The effect of mordants on the color strength of the dyed fabrics was analyzed and correlated with wash fastness tests results. The dyed fabrics analysis has been carried out in terms of their color strength and color coordinates ($L^*a^*b^*$). The functional properties like radical scavenging activity, antibacterial activity, and UV protection properties were thoroughly investigated to determine the functionality of dyed fabrics. The dyed samples displayed satisfactory fastness and color strength along with efficient antibacterial, antioxidants and UV protection properties.

KEYWORDS

Kigelia Africana; dyeing; antibacterial; UPF; antioxidant

关键词



非洲基格里亚; 染色; 抗菌; 抗氧化剂

摘要

天然染料以其无毒、环保的特性在纺织工业中得到了发展。对天然染色功能性纺织材料的需求增加，使得研究界对探索可用于纺织材料功能性染色的天然染料的新来源越来越感兴趣。非洲基格里亚花以其多种药用特性而闻名，因此可用于纺织材料的功能性着色。在目前的研究中，我们利用预媒染剂工艺，通过使用明矾、硫酸亚铁和硫酸铜等不同的媒染剂来评估亚麻织物的染色条件。分析了媒染剂对染色织物色强度的影响，并与耐洗性试验结果进行了关联。根据染色织物的颜色强度和颜色坐标 ($L^*A^*B^*$) 进行了染色织物分析。对染色织物的清除自由基活性、抗菌活性、防紫外线性能等功能性进行了深入的研究，以确定其功能性。染色后的样品显示出令人满意的牢度和色强度，以及有效的抗菌、抗氧化剂和紫外线防护性能。

Introduction

In today's scenario, the textile industry is one of the major polluting industry around the globe (Saleh, YA, and El-Badry 2013). There is a huge requirement of freshwater to process the textile materials. Almost 250 times more water is required for processing of one-ton of textile materials (Mongkhorrattanasit et al., 2011). During the textile processing, a massive amount of industrial effluent is getting generated which contains chemicals, dyes, and salts which pollute the environment (Saleh, YA, and El-Badry 2013). The effective effluent treatment plants and use of environment friendly dyes and chemicals are the pathways to reduce the overall impact of textile processing on the environment (Anttha and Prasad 2007). Several studies suggested that some of the synthetic dyes are

CONTACT Javed Sheikh  jnsheikh@iitd.ac.in  Department of Textile Technology, Indian Institute of Technology (I.I.T.), Delhi, India

© 2019 Taylor & Francis

allergic to human skin, non-biodegradable and few others are having the potential to cause cancer (Sachan and Kapoor 2004). The use of synthetic dyes and hazardous products is banned or restricted to import/export by many developed and developing countries (Baliarsingh et al. 2012; Bechtold et al. 2003; Bhatti et al. 2010; Sachan and Kapoor 2004). Currently, the textile industry is moving towards the developing green dyes (natural products) for sustaining textile industries because of its impressive characteristics such as environmental compatibility (Angelini et al. 1997; Goodarzian and Ekrami 2010), biodegradability (Khan et al. 2014), health benefits, simple extraction methods under mild reaction conditions (Grifoni et al. 2014). Natural dyes are obtained from plants mainly contain pigments such as a flavonoid, anthocyanin, chlorophyll, and carotenoids (Baliarsingh et al. 2012; Hussein et al. 1997). Many researchers have studied the impact and effect of natural dyes in functionalization of textile fibers and found remarkable results. Koh and Hong investigated the ability of spent coffee extract to impart antimicrobial and antioxidant properties to the cotton fabric. The finished cotton fabrics inhibited the growth of gram-positive *S. aureus*. Also, the finished fabric displayed increased antioxidant activity in proportion to the increased concentration of the spent coffee extract (Koh and Hong 2017). Rehman et al. extracted the natural dye from pomegranate peel via ultrasonic method and applied the extracted dye on the pre-mordanted lyocell fabrics. The dyed fabric showed excellent color strength, colorfastness and also showed suitable antibacterial properties against *S. aureus* microorganisms (Rehman et al. 2018). Halysh et al. prepared low-cost sorbents based on walnut shell for sorption of dyes and metal ions (Halysh et al. 2018). Rossi et al. extracted natural colorant from eucalyptus wood using steam extraction method. The obtained colorant was used to dye cotton, nylon, and wool fabric. The dyed fabrics showed very good washing fastness (Rossi et al. 2017). Pisitsak et al. replaced traditional mordanting agents with by-product of protein recovered from the oil extraction process of Antarctic krill (*Euphausia superba*). The cotton fabric was pre-mordanted using Antarctic krill protein and then dyed with natural dye extracted from the bark of *Xylocarpus granatum*. The dyed fabrics exhibited excellent colorfastness and showed durable UV protection properties (Pisitsak, Tungsombatvisit, and Singhanu 2018).

Kigelia Africana flowers have dark red or maroon trumpet-shaped flower having a velvety appearance on the inside of petals and contain sugary-rich fluid and are fragrant (Agyare et al. 2013; Shalini et al. 2018). *Kigelia* belongs to 'Bignoniaceae' family, and the *Kigelia Africana* is the only species in the *Kigelia* genes. *Kigelia Africana* contains flavonoids, terpenoids, coumarins and saponins compounds (Asekun, Olusegun, and Adebola 2007). Flavonoids are accountable for the coloration of flower and are obtainable in substantial amounts in the *Kigelia Africana* flower (Harborne and Williams 2000). These plants parts have high medicinal values and are used for the treatment of many skin-ailments including boils, eczema, syphilis, fungal infections, psoriasis, leprosy, and cancer (Houghton and Jäger 2002).

Various methods for the extraction of dyes from natural resources such as aqueous extraction, alkali/acid extraction, solvent extraction, enzymatic extraction, microwave, and ultrasonic-assisted extraction, and super critical fluid extraction are reported in literature. The nature of dyes needs to be understood for the selection of ideal extraction process. The natural dyes are slight expensive because of the limited natural resources. On the other hand, synthetic dyes are easily available with affordable price and offer wide variety of shades however because of toxicity these are harmful to human body (Mansour., 2018). Most of the natural dyes do not show affinity for textile fibers and suffer from a limitation of narrow shade/color range with low wash fastness of the dyed textiles. The use of mordant not only improves the affinity between fiber and dye but also alters the hue of dyes. Hence, different mordants may change the shade of a specific dye from dark, bright or sometimes vigorously change the final color of the dyed fabric. Furthermore, mordanting can enhance the dye performance and provides wide-range of colors spectrum on natural as well as synthetic fibers with superior wash fastness (Manhita et al. 2011; Samanta and Agarwal 2009; Shahid and Mohammad 2013; Yi and Cho 2008).

Linen is cellulosic textile fiber obtained from the flax plant. It is an important textile material with different characteristics. The fabric which is produced by the linen fiber possess certain solar

protection properties which are dependant on the extent of removal of impurities from the fibre during processing. However, because of cellulosic nature, it can be attacked by microorganism and lacks antioxidant ability. Hence, it is important to develop a functional linen fabric by imparting antibacterial and antioxidant properties using natural material.

The current research work reports the first application of *Kigelia Africana* flower extracts in sustainable functional coloration of linen fabric. The metallic mordants, in the safer limits, were used to study the possibility of various shades and the corresponding dye-fiber interactions. The functional properties imparted to the dyed linen viz. antibacterial action, UV protection, and antioxidant activity were also explored. In short, the novel source of natural dye was reported for the dyeing vis-à-vis functionalization of linen fabric.

Experimental

Materials

The linen fabric (epi = 45, ppi = 41, GSM = 241.5) was procured from Jayshree Textiles, India. The *Kigelia Africana* flowers, in the family 'Bignoniaceae' selected for the present study, were collected from the local campus (Coordinates: latitude 28°32'42"N and longitude 77°11'32"E). All chemicals such as copper sulfate, ferrous sulfate, and potash alum were purchased from Merck Specialties Private Limited, India.

Methods

Extraction of colorants

The collected flowers were thoroughly washed with deionized water to detach sand/dust particles followed by drying in sunlight. Then, the flowers were ground into a powder form using a mixer grinder. The colorant was extracted typically in deionized water to keep the solvents free process. The flowers powder was added to deionized water, keeping liquor ration (M:L) 1:10. The mixture was kept at a temperature 80°C for 60 min under continuous stirring. Then, filtration of the solution was carried out to separate out the residue and the extract was further used as the dyeing colorant.

Mordanting and dyeing

The pre-mordanting method was adopted for mordanting the linen fabrics using different mordants such as potash alum (10% on weight of fabric, owf), copper sulfate (1% owf), and ferrous sulfate (5% owf). The linen fabrics were separately immersed in different mordant solutions, keeping the M:L ratio of 1:10 at 80°C for 60 min with constant stirring in a water bath. After mordanting, linen fabrics were squeezed and further subjected for dyeing. Dyeing was carried out by keeping 1:10 liquor ratio (M: L) in separate baths. The mordanted linen fabrics were dyed using KAFC colorant (20% owf). The dyeing process was started at room temperature and the temperature was raised to 80°C at the gradient of 3°C/min. The dyeing was continued at 80°C for 60 min. The dyed fabrics were then washed with cold water followed by drying. The sample names were abbreviated as AKAFC (alum mordanted and dyed), CKAFC (copper sulfate mordanted and dyed) and FKAFC (ferrous sulfate mordanted and dyed).

Determination of color and fastness properties of dyed linen

The colorimetric properties (color values and color coordinates) of the dyed fabrics were examined using Gretag Macbeth Color-Eye 7000A spectrophotometer. The color values (K/S) were evaluated using Kubelka Munk equation. The dyed linen fabrics were examined for washing fastness and rubbing fastness using ISO 105C06A1M and ISO 105-X12 methods, respectively (ISO Technical Manual, 2006).

Evaluation of functional properties of dyed linen

The antibacterial activity of dyed linen against *E. coli* and *S. aureus* cultures was determined by the agar plate method (AATCC 100–2004) (AATCC Technical Manual, 2007). The antioxidant activity of the dyed fabrics was evaluated using the procedure available in the literature (Natarajan and Gupta 2017; Sheikh and Bramhecha 2018) using 1, 1-diphenyl-2-picrylhydrazyl (DPPH). Ultraviolet protection factor (UPF) of the dyed linen was determined with AS/NZS 4399:1996 standard using the UV-Visible spectrometer (AS/NZS 4399, 1996).

FTIR analysis

In order to identify the functional groups of undyed and dyed samples, FT-IR spectra of undyed and dyed fabric were generated on Thermo Scientific Nicolet iS50 FT-IR Spectrometer. The fabrics were analyzed with 15-scans in the wavelength range of 400–4000 cm^{-1} with a resolution 4 cm^{-1} .




Results and discussion

Color analysis of the dyed samples

Color co-ordinates and color strength (K/S) values of dyed fabric samples are tabulated in Table 1. In general, the variety of shades with varying tones were obtained for all the mordants used. Color values obtained were satisfactory in all the combinations of dye and mordant. The different mordants caused not only the enormous changes in their K/S values, but also changes in brightness index and L^* values. The ferrous sulfate and copper sulfate manifest the higher K/S values due to their potential to form stable complexes with the dye components. The unique combination of *Kigelia Africana* flower colorant and linen was affected by pre-mordanting with metal ions, shows a change in shade. As can be seen from Table 1, the beautiful shades were obtained by using the metallic mordants and KAFC. The ionic interaction between KAFC and different metal ions not only changes the dye shades but it can also resulted in different tones. It must be emphasized that the mordants used in this study are the representatives of various mordants available for natural dyeing and the combinations of KAFC with others can also explore new shades on linen. Several research studies repeatedly used the ferrous sulfate and copper sulfate as a mordant for natural dyeing because of their ability to strongly hold the dyes on the textiles which results in excellent wash and rubbing fastness. The beauty of natural dye is that the variety of shades can be produced using a single natural dye with number of different mordants, either alone or in combinations.

The K/S (color strength) value were calculated and are presented in Table 1. The satisfactory coloristic efficiency obtained for all dyed samples indicate the suitability of KAFC as natural dye. In

Table 1. Color measurement values for dyed linen fabric.

Sample Name	L^*	a^*	b^*	K/S	Shade Obtained
AKAFC	71.57	0.28	6.92	1.94	
CKAFC	70.90	0.75	11.59	2.00	
FKAFC	59.86	-1.41	7.77	2.38	

general, cellulosic fibers present difficulty in dyeing using natural dyes and building darker shades on them is difficult as compared to the case of protein fibers. The dye content of the natural dye extract is limited, unlike synthetic dye, which results in lighter shades of dyed fabrics especially on cellulosic ones. In general, all dyed samples showed yellower tones (positive value of b^*) due to the presence of phenolic content in KAFC such as flavonoids, terpenoids, coumarins, and saponins compounds; however, there were variations in red-green tones. AKAFC and CKAFC displayed red-yellow tones, while FKAFC displayed green-yellow tones.

Fastness properties of the dyed linen

The fastness properties of the dyed fabrics are the indication of dye-fiber chemical interaction and it affects the suitability of the dyed fabrics for a particular application. The fastness properties of the dyed linen are evaluated and presented in Table 2. The dyed fabrics displayed excellent washing fastness which showed no variation with respect to the mordant used for dyeing. The ratings were identical for all the dyed samples. As a result of negligible removal of dye from dyed samples, the staining was negligible which was reflected in washing fastness ratings on staining scale. The rubbing fastness ratings were satisfactory. The dry rubbing fastness ratings were in the range of "very good" to "excellent". Wet rubbing fastness ratings were inferior than the dry rubbing ones; however, these were in the range of "good" to "very good" which can be considered as satisfactory levels of fastness. The fastness ratings indicate a strong interaction between mordant and KAFC inside the fiber thus preventing the bleeding of shade during the washing cycles and abrasive action.

Functionalities of the dyed linen

Kigelia Africana flower contains large quantities of flavonoids, mainly anthocyanins, which are the glycosides where the sugar molecule is attached to a functional group via a glycosidic bond which makes the dye color more stable. Apart from this, it contains luteolin and flavonol quercetins two more structures belonging to the group flavonoids which are known for their antioxidant properties. *Kigelia Africana* flower also contains various functional compounds like terpenoids (iridoids and naphthoquinones), coumarin, etc. The major iridoids found in the KAF are minescoside and specioside while the main naphthoquinone pigment present is Kigelinone. All of these terpenoids are known to possess good antibacterial properties (Atawodi and Olowoniyi 2015; Gabriel and Olubunmi 2009; Harborne and Williams 2000; Yang et al. 2014).

The antibacterial properties of dyed linen are summarized in Table 3. The results in Table 3 clearly indicate the efficient antibacterial activity of dyed fabric against both bacteria, the extent of which varied with the mordant-dye combination. Even though the level of antibacterial activity was moderate, it can be improved using higher shade (%) of the dye. The antibacterial activity in case of natural dyed fabrics is a combined effect of mordant and dye. The metallic mordants are known for antibacterial activity; however, the durability of the properties would not be achieved as these would be washed out on subsequent washing cycles. The natural dyeing using KAFC resulted in the formation of mordant-dye complex inside the fiber which can't be washed out easily and it can withstand subsequent washing treatments (as confirmed by fastness ratings). KAFC also contains various functional compounds, as discussed in previous paragraph, which are known for their

Table 2. Fastness ratings for dyed linen fabrics.

Sample Name	Wash Fastness		Rubbing Fastness	
	Change in shade	Staining	Dry	Wet
AKAFC	4-5	4-5	4-5	3-4
CKAFC	4-5	4-5	4-5	3-4
FKAFC	4-5	4-5	4-5	4

Table 3. Antibacterial and antioxidant activities of dyed fabrics.

Sample Name	Bacterial Colony reduction ^S (%)		Radical scavenging activity ^S (%)
	<i>E. coli</i>	<i>S. aureus</i>	
Undyed	N	N	7.52
AKAFC	76	65	71.39
CKAFC	84	81	86.76
FKAFC	86	85	94.46

S-Average value of three determinations; N- negligible

antimicrobial activities. The KAFC-dyed fabrics show high antibacterial activity (%) against *E. coli*, but the moderate level of activity against *S. aureus*, the actual extent of which was varied among individual samples. Among the dyed samples, FKAFC showed an excellent antibacterial property while potash alum showed the least value.

According to Table 3, dyed linen fabric displayed high antioxidant activity in the range 71.39–94.46% depending on the mordant-dye combination. The undyed fabric displayed negligible antioxidant activity.

The large cellulosic units of linen with a huge number of free glycosylated and hydroxyl groups which will attach to the heterocyclic and aromatic rings of tannins and flavonoids found in *Kigelia Africana* flower are responsible for providing antioxidant activity. The number and position of free hydroxyl on the rings significantly affect the antioxidant activity of these polyphenols. With maximum absorption at 517 nm, DPPH is a stable radical and can easily subject to scavenging by an antioxidant thus go scavenging with hydroxyl groups (Das, Patro, and Dinda 2012; Sowndhararajan and Sun 2013). Therefore, dyed linen can help to resist oxidative damage of the human body cells. Interestingly, the dyed linen fabric showed varied antioxidant activities when mordanted with alum, copper, ferrous mordants. This phenomenon could be explained because of the fact that copper and ferrous ions interact with more dye molecules as compared to alum which results in high dye affinity and high antioxidant activities.

The UV protection offered by the dyed fabrics was evaluated and the results are presented in Table 4. The UV radiation emitted by the sun has a wide-spectrum ranging from the high energy to low energy. The wavelength below (280 nm) belongs to UVC band and wavelength (280–315 nm) to (315–400 nm) belongs to UVB band & UVA band, respectively. In this experiment, the UV transmittance was evaluated including UVA and UVB through the fabric samples. If the UV transmittance of fabric is less, then there is a better ultraviolet protection property of the fabric (Springsteen et al. 1999). To analyze the efficacy of UV protection offered by the dyed linen, the UV transmittance values of the dyed and undyed fabrics were compared.

The UV transmittance spectra show a noticeable difference between the dyed and undyed fabrics as shown in Figure 1, Table 4. The undyed fabric showed significantly higher transmittance values than those of dyed damples. The undyed fabric's UVB value and UVA value (16.80% and 25.46%) shows the poor resistance to UV radiations. However, UVB value should be <6.7% for active UV resistance. Undyed fabric's UPF value 5.62 also confirms the poor ultraviolet protection offered by undyed linen fabric. However, dyed fabrics exhibit less UV transmittance thus good to excellent UV resistance. It is observed that different mordants had varied effects on the UV transmittance spectra

Table 4. Comparison of UV transmittance values of the undyed and dyed fabric.

UV transmittance Sample Name	UVA	UVB	UPF
	315–400nm	290–315nm	290–400nm
Undyed	25.46	16.80	5.62
AKAFC	7.43	6.06	16.33
CKAFC	3.25	2.87	34.59
FKAFC	3.28	2.19	44.95

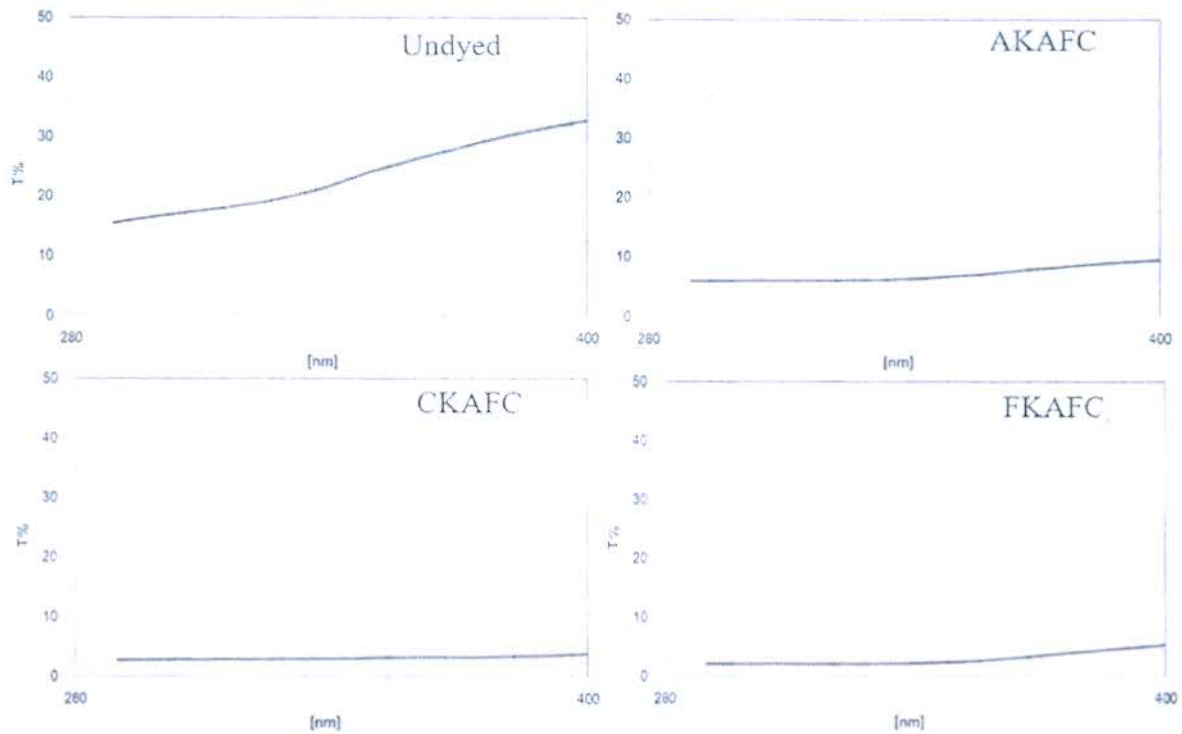


Figure 1. UV transmittance spectra of the undyed and dyed fabric samples.

of dyed fabric with *Kigelia Africana* flower colorant as shown in Table 4. The increased UPF value with different metallic mordants can be due to the metallic salts bridging the dyes molecules and the fibers leading to the formation of differently coordinated complexes of π -bonds (Feng et al. 2007). The FKAFC showed higher UPF (44.95) as compared to other dyed samples. Other dyed samples (AKAFC and CKAFC) showed UPF in satisfactory range. Hence, it can be concluded that the fabrics dyed with KAFC can block ultraviolet radiation. Moreover, the resultant garment stitched from such fabrics can adequately protect the wearer skin from UV radiation (Hoffmann et al. 2001).

FT-IR investigation

The FT-IR spectra of KAFC extract were recorded and presented in Figure 2. Moreover, Figure 3, shows the FTIR spectra of dyed linen fabrics. FTIR spectrum of KAFC shows the presence of major and broad peak at 3304 cm^{-1} assigned to OH groups indicating the presence of various compounds rich in hydroxyl groups. The other peaks evident are at 2925 cm^{-1} (C-H stretching vibration) and 1700 cm^{-1} (C-O stretching of carboxylic acid). The presence of flavonoids and polyphenolic compounds in the KAFC is thus confirmed. A slight shift in peaks can be observed between undyed and dyed fabrics FT-IR spectra. The peak intensity at $3800\text{--}3000\text{ cm}^{-1}$ attributed to the hydroxyl groups ($-\text{OH}$) of undyed linen. The significant change has been noticed in the peak intensity $-\text{OH}$ groups absorption band of dyed fabrics using different mordants as shown in Figure 3. This might be because of introduction of polyphenolic compounds and flavonoids after dyeing. The change in peak intensity at $2800\text{--}2950\text{ cm}^{-1}$ attributed to the C-H groups of KAFC. Furthermore, at $1100\text{--}1350\text{ cm}^{-1}$ change in peaks can be noticed in FT-IR spectra of dyed linen fabric, which indicates the C-O-C and C-O vibration.

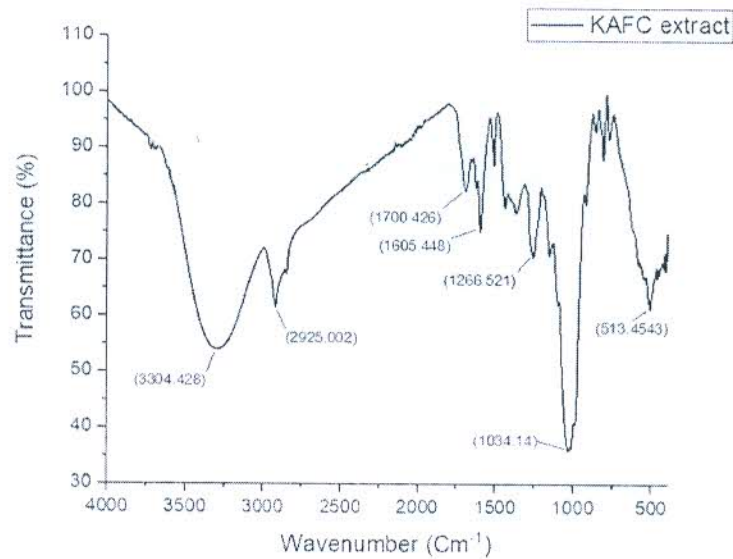


Figure 2. FTIR spectra of KAFC extract.

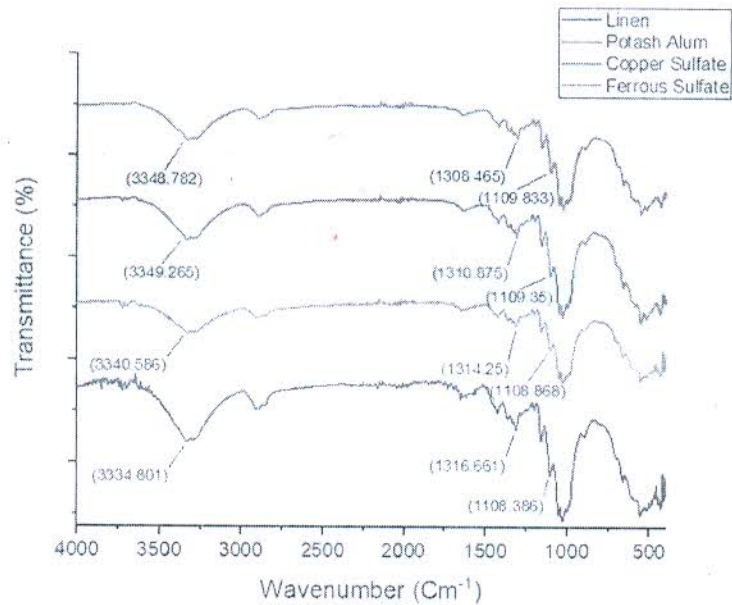


Figure 3. FTIR of undyed linen and dyed linen fabrics.

Conclusions

The current study successfully confirms the possible use of natural dyes extracted from *Kigelia Africana* flowers to impart the antioxidant, antibacterial, and UV-protection to the linen fabric. The KAFC resulted in beautiful shades on linen fabric in presence of various metallic mordants. Dyed fabrics displayed moderate to efficient antibacterial activities against *E. coli* and *S. aureus*. The efficient UV protection was also confirmed. The radical scavenging action of such dyed linen was superior and can explore the scope of naturally dyed linen in cosmetic textiles. This work explored a green option for functional coloration of linen fabrics using a novel natural dye.

Acknowledgments

Authors gratefully acknowledge Science and Engineering Research Board (SERB, India) for ECRA funding (project File no. ECR/2017/001041).

Funding

This work was supported by the Science and Engineering Research Board [ECR/2017/001041].

References

- Agyare, C., A. S. Dwobeng, N. Agyepong, Y. D. Boakye, K. B. Mensah, P. G. Ayande, and M. Adarkwa-Yiadom. 2013. Antimicrobial, antioxidant, and wound healing properties of *Kigelia africana* (Lam.) Beneth and *Strophanthus hispidus* DC. *Advances in Pharmacological Sciences*. doi:10.1155/2013/692613.
- American Association of Textile Chemists and Colorists. 2007. *AATCC Technical Manual*, Vol. 76. Research Triangle Park, NC: AATCC.
- Angelini, L. G., L. Pistelli, P. Belloni, A. Bertoli, and S. Panconesi. 1997. Rubia tinctorum a source of natural dyes: agronomic evaluation, quantitative analysis of alizarin and industrial assays. *Industrial Crops and Products* 6 (3-4):303-11. doi:10.1016/S0926-6690(97)00021-6.
- Anththa, K., and S. N. Prasad. 2007. Developing multiple natural dyes from flower parts of Gilmour. *Current Science* 92:12. AS/NZS 4399. Sun protective clothing evaluation and classification; 1996.
- Asekun, O. T., E. Olusegun, and O. Adebola. 2007. The volatile constituents of the leaves and flowers of *Kigelia africana* Benth. *Flavour Fragrance Journal* 22 (1):21-23. doi:10.1002/ffj.1723.
- Atawodi, S. E., and O. D. Olowoniyi. 2015. Pharmacological and therapeutic activities of *kigelia africana* (Lam.) benth. *Annual Research & Review in Biology* 5 (1):1-17. doi:10.9734/ARRB/2015/8632.
- Baliarsingh, S., A. K. Panda, J. Jena, T. Das, and N. B. Das. 2012. Exploring sustainable technique on natural dye extraction from native plants for textile: identification of colourants, colourimetric analysis of dyed yarns and their antimicrobial evaluation. *Journal of Cleaner Production* 37:257-64. doi:10.1016/j.jclepro.2012.07.022.
- Bechtold, T., A. Turcanu, E. Ganglberger, and S. Geissler. 2003. Natural dyes in modern textile dyehouses—how to combine experiences of two centuries to meet the demands of the future? *Journal of Cleaner Production* 11 (5):499-509. doi:10.1016/S0959-6526(02)00077-X.
- Bhatti, I. A., S. Adeel, M. A. Jamal, M. Safdar, and M. Abbas. 2010. Influence of gamma radiation on the colour strength and fastness properties of fabric using turmeric (*Curcuma longa* L.) as natural dye. *Radiation Physics and Chemistry* 79 (5):622-25. doi:10.1016/j.radphyschem.2009.12.006.
- Das, S. N., V. J. Patro, and S. C. Dinda. 2012. Evaluation of anti-inflammatory, anti-diabetic activity of Indian *Bauhinia vahlii* (stem bark). *Asian Pacific Journal of Tropical Biomedicine* 2 (3):S1382-S1387. doi:10.1016/S2221-1691(12)60421-3.
- Feng, X. X., L. L. Zhang, J. Y. Chen, and J. C. Zhang. 2007. New insights into solar UV-protective properties of natural dye. *Journal of Cleaner Production* 15:366-72. doi:10.1016/j.jclepro.2005.11.003.
- Gabriel, O. A., and A. Olubunmi. 2009. Comprehensive scientific demystification of *Kigelia africana*: a review. *African Journal of Pure and Applied Chemistry* 3 (9):158-64.
- Goodarziyan, H., and E. Ekrami. 2010. Wool dyeing with extracted dye from pomegranate (*Punica granatum* L.) peel. *World Applied Sciences Journal* 8 (11):1387-89.
- Grifoni, D., L. Bacci, S. Di Lonardo, P. Pinelli, A. Scardigli, F. Camilli, F. Sabatini, G. Zipoli, and A. Romani. 2014. UV protective properties of cotton and flax fabrics dyed with multifunctional plant extracts. *Dyes and Pigments* 105:89-96. doi:10.1016/j.dyepig.2014.01.027.
- Halysh, V., O. Sevastyanova, A. V. Riazanova, B. Pasalskiy, T. Budnyak, M. E. Lindström, and M. Kartel. 2018. Walnut shells as a potential low-cost lignocellulosic sorbent for dyes and metal ions. *Cellulose* 25 (8):4729-42. doi:10.1007/s10570-018-1896-y.
- Harborne, J. B., and C. A. Williams. 2000. Advances in flavonoid research since 1992. *Phytochemistry* 55 (6):481-504.
- Hoffmann, K., P. Kesners, A. Bader, A. Avermaete, P. Altmeyer, and T. Gambichler. 2001. Repeatability of in vitro measurements of the ultraviolet protection factor (UPF) by spectrophotometry with automatic sampling. *Skin Research and Technology* 7:223-26.
- Houghton, P. J., and A. K. Jäger. 2002. The sausage tree (*Kigelia pinnata*): ethnobotany and recent scientific work. *South African Journal of Botany* 68 (1):14-20. doi:10.1016/S0254-6299(15)30434-8.
- Hussein, S. A., H. H. Barakat, I. Merfort, and M. A. Nawwar. 1997. Tannins from the leaves of *Punica granatum*. *Phytochemistry* 45 (4):819-23. doi:10.1016/S0031-9422(96)00888-6.
- ISO Technical Manual, Geneva, Switzerland, 2006.

- Khan, A. A., N. Iqbal, S. Adeel, M. Azeem, F. Batool, and I. A. Bhatti. 2014. Extraction of natural dye from red calico leaves: Gamma ray assisted improvements in colour strength and fastness properties. *Dyes and Pigments* 103:50–54. doi:10.1016/j.dyepig.2013.11.024.
- Koh, E., and K. H. Hong. 2017. Preparation and properties of cotton fabrics finished with spent coffee extract. *Cellulose* 24 (11):5225–32. doi:10.1007/s10570-017-1466-8.
- Manhita, A., V. Ferreira, H. Vargas, I. Ribeiro, A. Candeias, D. Teixeira, T. Ferreira, and C. B. Dias. 2011. Enlightening the influence of mordant, dyeing technique and photodegradation on the colour hue of textiles dyed with madder—A chromatographic and spectrometric approach. *Microchemical Journal* 98 (1):82–90. doi:10.1016/j.microc.2010.12.002.
- Mansour, R. 2018. Natural Dyes and Pigments: Extraction and Applications. *Handbook of Renewable Materials for Coloration and Finishing*, M. Yusuf, ed., 75–102. USA: Wiley Scrivener.
- Mongkhlorattanasit, R., J. Kryštůfek, J. Wiener, and J. Studničkova. 2011. Natural dye from eucalyptus leaves and application for wool fabric dyeing by using padding techniques. *Natural dyes*, E. A. Kumbasar, ed. InTech., 57–78. Rijeka, Croatia. Available from <http://www.intechopen.com/books/natural-dyes/natural-dye-from-eucalyptus-leaves-and-application-for-woolfabric-dyeing-by-using-padding-technique>
- Natarajan, S., and D. Gupta. 2017. In situ colouration of wool. *The Journal of the Textile Institute* 108 (10):1822–27. doi:10.1080/00405000.2017.1292648.
- Pisitsak, P., N. Tungsombatvisit, and K. Singhanu. 2018. Utilization of waste protein from Antarctic krill oil production and natural dye to impart durable UV-properties to cotton textiles. *Journal of Cleaner Production* 174:1215–23. doi:10.1016/j.jclepro.2017.11.010.
- Rehman, F., N. Sanbhal, T. Naveed, A. Farooq, Y. Wang, and W. Wei. 2018. Antibacterial performance of Tencel fabric dyed with pomegranate peel extracted via ultrasonic method. *Cellulose* 25 (7):4251–60. doi:10.1007/s10570-018-1864-6.
- Rossi, T., P. M. S. Silva, L. F. De Moura, M. C. Araújo, J. O. Brito, and H. S. Freeman. 2017. Waste from eucalyptus wood steaming as a natural dye source for textile fibers. *Journal of Cleaner Production* 143:303–10. doi:10.1016/j.jclepro.2016.12.109.
- Sachan, K., and V. P. Kapoor. 2004. Eucalyptus bark dye: Standardization of extraction and eco-friendly dyeing profiles. *Colourage* 51 (9):41–44.
- Saleh, M. S., A. E. B. YA, and K. El-Badry. 2013. Dyeing of cationized cotton fabrics with natural dye extracted from acacia. *International Journal of Textile Science* 2 (2):30–35.
- Samanta, A. K., and P. Agarwal. 2009. Application of natural dyes on textiles. *Indian Journal of Fibre & Textile Research* 34:384–99.
- Shahid, M., and F. Mohammad. 2013. Recent advancements in natural dye applications: a review. *Journal of Cleaner Production* 53:310–31. doi:10.1016/j.jclepro.2013.03.031.
- Shalini, S., N. Prabavathy, R. Balasundaraprabhu, T. S. Kumar, D. Velauthapillai, P. Balraju, and S. Prasanna. 2018. Studies on DSSC encompassing flower shaped assembly of Na-doped TiO₂ nanorods sensitized with extract from petals of *Kigelia Africana*. *Optik* 155:334–43. doi:10.1016/j.ijleo.2017.10.173.
- Sheikh, J., and I. Bramhecha. 2018. Multifunctional modification of linen fabric using chitosan-based formulations. *International Journal of Biological Macromolecules* 118:896–902. doi:10.1016/j.ijbiomac.2018.06.150.
- Sowndhararajan, K., and C. K. Sun. 2013. Free radical scavenging activity from different extracts of leaves of *Bauhinia vahlii* Wight & Arn. *Saudi Journal of Biological Sciences* 20 (4):319–25. doi:10.1016/j.sjbs.2012.12.005.
- Springsteen, A., R. Yurek, M. Frazier, and K. F. Carr. 1999. In vitro measurement of sun protection factor of sunscreens by diffuse transmittance. *Analytica Chimica Acta* 380:155–64. doi:10.1016/S0003-2670(98)00577-7.
- Yang, A. H., X. Y. Shi, X. Li, F. F. Li, Q. Q. Zhang, S. X. Jiang, J. Z. Cui, and H. L. Gao. 2014. Spectroscopic and electrochemical studies on the evaluation of the radical scavenging activities of luteolin by chelating iron. *RSC Advances* 4:25227–33. doi:10.1039/c4ra01396d.
- Yi, E., and J. Y. Cho. 2008. Color analysis of natural colorant-dyed fabrics. *Color Research & Application* 33 (2):148–57. doi:10.1002/col.20390.



Research Journal of Textile and Apparel

Recovery and reuse of immobilized α -amylase during desizing of cotton fabric

Amit Madhu, J.N. Chakraborty,

Article information:

To cite this document:

Amit Madhu, J.N. Chakraborty, (2018) "Recovery and reuse of immobilized α -amylase during desizing of cotton fabric", Research Journal of Textile and Apparel, <https://doi.org/10.1108/RJTA-12-2017-0052>

Permanent link to this document:

<https://doi.org/10.1108/RJTA-12-2017-0052>

Downloaded on: 19 September 2018, At: 20:29 (PT)

References: this document contains references to 43 other documents.

To copy this document: permissions@emeraldinsight.com

Access to this document was granted through an Emerald subscription provided by

Token:Eprints:YDTKKW7ETFHMPQNW16TW:

For Authors

If you would like to write for this, or any other Emerald publication, then please use our Emerald for Authors service information about how to choose which publication to write for and submission guidelines are available for all. Please visit www.emeraldinsight.com/authors for more information.

About Emerald www.emeraldinsight.com

Emerald is a global publisher linking research and practice to the benefit of society. The company manages a portfolio of more than 290 journals and over 2,350 books and book series volumes, as well as providing an extensive range of online products and additional customer resources and services.

Emerald is both COUNTER 4 and TRANSFER compliant. The organization is a partner of the Committee on Publication Ethics (COPE) and also works with Portico and the LOCKSS initiative for digital archive preservation.

*Related content and download information correct at time of download.

2018-19

Recovery and reuse of immobilized α -amylase during desizing of cotton fabric

Desizing of cotton fabric

Amit Madhu and J.N. Chakraborty

Department of Textile Technology, National Institute of Technology, Jalandhar, India

Abstract

Purpose – Enzymatic desizing using α -amylase is the conventional and eco-friendly method of removing starch based size. Conventionally, enzymes are drained after completion of process; being catalysts, they retain their activity after reaction and need to be reused. Immobilization allows the recovery of enzymes to use them as realistic biocatalyst. This study aims to recover and reuse of α -amylase for desizing of cotton via immobilization.

Design/methodology/approach – This paper investigates the application of α -amylase immobilized on Chitosan and Eudragit S-100 for cotton fabric desizing. A commercial α -amylase was immobilized on reversibly soluble-insoluble polymers to work out with inherent problems of heterogeneous reaction media. The immobilization process was optimized for maximum conjugate activity, and immobilized amylases were applied for grey cotton fabric desizing.

Findings – The desizing performance of immobilized amylases was evaluated in terms of starch removal and was compared to free enzyme. The immobilized amylases showed adequate desizing efficiency up to four cycles of use and were recovered easily at the end of each cycle. The amylase immobilized on Eudragit is more efficient for a particular concentration than chitosan.

Practical implications – Immobilization associates with insolubility and increased size of enzymes which lead to poor interactions and limited diffusion especially in textiles where enzymes have to act on macromolecular substrates (heterogeneous media). The selection of support materials plays a significant role in this constraint.

Originality/value – The commercial α -amylase was covalently immobilized on smart polymers for cotton fabric desizing. The target was to achieve immobilized amylase with maximum conjugate activity and limited constraints. The reversibly soluble-insoluble polymers support provide easy recovery with efficient desizing results in heterogeneous reaction media.

Keywords Cotton, Chitosan, Immobilization, Amylase, Desizing, Enzyme

Paper type Research paper

Introduction

Enzymatic desizing using α -amylase is the most commercial method for the desizing of grey cotton after acid desizing process. α -amylase catalyses the hydrolysis of 1, 4 linked glucose units of starch-based size to water soluble maltose and larger oligosaccharides. The use of α -amylase for desizing not only is eco-friendly but also avoids the fibre damage in comparison to hydrolytic and oxidative desizings (Karmakar, 1999).

Conventionally, the amylases are used in soluble form to hydrolyse starch and drained along with the desizing products. As the enzymes are biocatalysts, they retain their activity after reaction and need to be reused. The solubility of native enzyme and desizing products restricts their separation and may involve additional cost of separation. Thus, the immobilization can be the alternative way to use enzymes as realistic biocatalyst which not



Characterization of immobilized amylases

The immobilization may lead to the change in thermal and pH stability of enzymes. Therefore, it is necessary to characterize the immobilized enzymes for their optimum working temperature and pH before application. The effect of pH on amylase activities of native and immobilized enzymes was monitored using different acetate, phosphate and carbonate buffer solutions of different pH at temperature 50°C. Similarly to study the effect of temperature, these amylases were incubated at pH 5.5 with varying temperature from 20° to 100°C. The activities of immobilized amylases at different pH and temperature were measured using DNSA method as described earlier.

Enzymatic desizing of cotton fabric

Grey cotton fabric treated with desired concentration of amylase (per cent, w/v) in buffer with a liquor ratio of 1:30 at different temperatures and time using incubator shaker (Innolab). Continuous stirring was done at 80 rpm for efficient desizing, and after completion of process directly, hot washing was done for native amylase samples while the immobilized enzyme was filtered, separated and then fabric sample was hot washed at 90°C for 10 min succeeded by a thorough wash at 50°C.

Analysis of treated cotton fabric

Fabric sample analysis. The fabric samples were conditioned and weighted until constant weight to calculate weight loss per cent for assess size removal. The assessments were carried out in duplicates. Further, the water absorbency of samples was evaluated as per the AATCC Test Method 79-2000 and physical properties: bending length and tensile strength (warp-wise) were measured according to ASTM-D 1388-16 and ASTM D5034-95, respectively.

Estimation of starch content using anthrone reagent. Grey cotton was treated in perchloric acid to extract starch. In hot acidic medium starch got hydrolysed to glucose and dehydrated to hydroxymethyl furfural which forms a green coloured product with anthrone. Fabric sample (0.4 g) was treated with perchloric acid (54 per cent, 6.5 ml) and water (5 ml) at 0°C for 20 min. Extracted solution (0.5 ml) was pipette out in a test tube and made up the volume to 1 ml with distilled water. Anthrone reagent (4 ml) was added to it and heated for 10 min in a boiling water bath. Test tube was rapidly cooled and the intensity of green colour was observed at λ_{\max} (630 nm) using UV-visible spectrophotometer (Perkin Elmer, Lambda-25). The amount of starch was then estimated by comparing this absorbance value with the known absorbance from the standard starch-anthrone curve (Hodge and Hofreiter, 1962). Further, the desizing efficiency can be calculated using equation (2):

$$\text{Desizing efficiency (\%)} = 1 - \frac{\text{Starch in sized specimen}}{\text{Starch in grey specimen}} \quad (2)$$

TEGEWA scale rating. Residual starch size was also assessed with TEGEWA scale (violet scale calibrated from 1 to 9) by spotting samples with a solution of iodine in potassium iodide.

FTIR spectroscopy. To ascertain the removal of starch after desizing process, the functional group analysis was carried out based on FTIR spectrum. FTIR spectra of samples were taken using BRUKER ECO ATR Alpha spectrometer. The transmittance spectrum was obtained after 16 scans for 400-4000 cm^{-1} wave-number range for each sample.

only allows their recovery but also improves the stability, extends their useful life and improves action in some cases too (Pan *et al.*, 2009; Sahinbaskan and Kahraman, 2011; Shukla and Jajpura, 2005).

In textile chemical processing, immobilized enzymes need to act on insoluble macromolecular substrates; therefore, the poor interaction, limited diffusion and incomplete separation of immobilized enzymes are the common constraints. Immobilization using smart (reversibly soluble-insoluble) polymers has been suggested as a means to solve the inherent problems of the heterogeneous reaction media. Enzyme immobilized on such supports could catalyse reaction in its soluble state and can be easily separated in insoluble form by simply adjusting the pH (Cong *et al.*, 1995; Soares *et al.*, 2011).

Many methods of immobilization, coupled to a wide spectrum of supports, have been revealed. However, the selection of method or support simply depends on their end use. Immobilized amylases show improved stability and offer economic benefits by their enhanced use in repeated-batch, or continuous mode (Pandey *et al.*, 2000). A comparative study on different matrices for immobilization of α -amylase was done in many works (Singh, 2014; Shukla and Jajpura, 2005). A lot of work has been reported on immobilization of amylases on various conventional supports: glass beads (Kahraman *et al.*, 2007), silica (Leng *et al.*, 2003), alumina (Reshmi *et al.*, 2006), adsorption on zirconia (Reshmi *et al.*, 2007), dialdehyde cellulose (Varavinit *et al.*, 2002) and reversibly soluble-insoluble polymers (Aksoy *et al.*, 1998; Cong *et al.*, 1995; Hoshino *et al.*, 1989; Madhu and Chakraborty, 2017) for their repeated use in starch hydrolysis, but their practical application for textile desizing (heterogeneous system) is rarely reported. Some work was reported in starch stain removal of textiles using amylase: amylase entrapped in agarose and agar matrices was reused efficiently for five cycles (Prakash and Jaiswal, 2011) and immobilized on glass beads to mix with detergent for stain removal in several cycles (Dhingra *et al.*, 2006). Sahinbaskan and Kahraman (2011) only reported the desizing of grey cotton fabric using amylase immobilized on acrylatedepoxydized soya bean oil resin, where the immobilized amylase can give significant starch-removal up to three reusability cycles in assistance to ultrasound.

In the present work, a commercially available α -amylase was covalently immobilized on two different soluble-insoluble supports: chitosan and Eudragit S-100 using cross-linking agents. Chitosan, a natural polyaminosaccharide (copolymer of N-acetyl-D-glucosamine and D-glucosamine), is an ideal smart support for enzyme immobilization because of economy, its hydrophilicity, biocompatibility, biodegradability and antibacterial properties (Chang and Juang, 2007; Krajewska, 2004; Tripathi *et al.*, 2007). Eudragit S-100 is a synthetic soluble-insoluble copolymer of methacrylic acid and methyl methacrylate and extensively used to immobilize a variety of enzymes (Smith *et al.*, 2008; Silva *et al.*, 2006a; Yu *et al.*, 2013). The main reason for their selection as support material is that these are inexpensive reversibly soluble-insoluble polymers: chitosan (natural) and Eudragit (synthetic). These polymers are suitable for bio-catalytic applications in soluble phase at favourable pH range which can be recovered in insoluble phase at specific pH.

Immobilization processes were optimized for conjugate activity, and the immobilized amylases were characterized for optimum pH and temperature. Then these competent immobilized amylases were used for grey cotton fabric desizing, and the starch-removal was evaluated using anthrone reagent and percentage weight loss. The removal of size was also qualitatively assessed with TEGEWA scale rating and Fourier transform infra-red (FTIR) analysis. Sustainability of the process was discovered with reusability of immobilized amylases for repeated desizing cycles. The easy availability of the commercial amylases and the ease of its immobilization on inexpensive matrices make them suitable for industrial applications.

Material and methods

Cotton fabric (Plain weave, 172 g/m², epi×ppi: 65 × 56, warp and weft count 30 Ne), commercial α-amylase (Palkozyme Plus, Maps Enzyme Limited), water soluble chitosan (chitosan chloride, India sea food Ltd. Coimbatore), Eudragit® S-100 (Evonik India Pvt. Ltd, Mumbai; anionic copolymer of methacrylic acid and methyl methacrylate in approx. 1:2), glutaraldehyde (25 per cent, Thomas baker), DNSA (3,5-Dinitrosalicylic acid, SD Fine) and Carbodiimide hydrochloride/carbodiimide (1-Ethyl-3-(3-diethylaminopropyl), Sigma-aldrich) were used. All other chemicals used were of analytical grade and were procured from SD Fine Chemicals Ltd., India.

Immobilization of amylase on chitosan beads

Chitosan beads were prepared from the soluble chitosan powder according to method described in Tripathi *et al.* (2007), Chen *et al.* (2013) and Pospiskova and Safarik (2013). To form a covalent network with enzyme, these beads were activated with glutaraldehyde solution. Chitosan beads (1 gm) were suspended in different glutaraldehyde solutions under mild magnetic stirring at neutral pH and room temperature (25°C) for varying activation time. Following the activation, beads were thoroughly washed with sodium acetate buffer to make it free from glutaraldehyde. The activated chitosan beads were then immobilized with different amylase solutions at three different temperatures (4°, 25° and 40°C) for varying time under mild stirring. Further, these immobilized beads were filtered, washed with 0.1 M phosphate buffer (pH 7) and stored in refrigerator at 4°C.

Immobilization of amylase on Eudragit S-100

Eudragit S-100 solutions of different concentrations were prepared in phosphate buffer at pH 7 and varying amount of carbodiimide coupling agent was added in these solutions with continuous stirring for 10 min. Subsequently, different α-amylase solutions were also added at room temperature (25°C) and kept under stirring for varying immobilization time. The pH of the mixture was reduced to 4.5 with acetic acid to precipitate the Eudragit-amylase conjugate. The precipitate was separated by centrifugation (11,000×g) at room temperature for 10 min and washed in 0.01 M acetate buffer at pH 4.5 for 10 min. The precipitate was further dissolved in phosphate buffer at pH 7 and re-precipitated with acetic acid solution at pH 4.5. Finally, the Eudragit-amylase precipitate was re-dissolved in 100 ml buffer of pH 7.6 for use (Cong *et al.*, 1995; Silva *et al.*, 2006b; Yu *et al.*, 2013).

Amylase activity assessment

The activity of α-amylase was estimated using DNSA method. The amount of reducing sugar (glucose) formed due to enzyme reaction was quantified in terms of absorbance value using standard glucose curve and activity was evaluated using equation (1) (Miller, 1959).

$$\text{Activity of amylase (U/ml)} = \frac{\text{Glucose produced (}\mu\text{g)}}{\text{Volume of enzyme (ml)} \times \text{Incubation time (min)}} \quad (1)$$

Enzyme loading of the immobilized amylase

The enzyme loading was calculated by detecting the changes in absorbance before and after enzyme immobilization using 2,4,6-trinitrobenzenesulfonic acid according to Yu *et al.* (2012).

Immobilization of amylase on Eudragit S-100

Similarly, here the amylase was covalently immobilized on Eudragit S-100 polymer using carbodiimide as cross-linking agent. In this process, the polymer concentration, carbodiimide concentration, enzyme per cent and immobilization time has significant impact and needs to be optimized for maximum conjugate activity.

Effect of Eudragit concentration. Amylase was immobilized onto Eudragit S-100 and the effect of polymer concentration was studied by varying its amount from 0.5 to 3 per cent (w/v). Then, after the activation with 0.4 per cent carbodiimide for 10 mins, 1 per cent α -amylase was immobilized on Eudragit polymer. The Eudragit concentration has a positive effect on conjugate activity. It increases with polymer concentration and reached maximum for 2 per cent with enzyme loading of 65 per cent. The reduction in activity was observed (Figure 6) for higher polymer concentrations, even though most of the enzyme added was coupled (80.4 per cent enzyme loading). This reduction in activity observed due to either enzyme denaturation by the coupling conditions or steric hindrance caused by intermolecular binding at higher Eudragit concentrations.

Effect of carbodiimide concentration. 2 per cent Eudragit polymer solution was prepared and 1 per cent α -amylase was immobilized without and with varying concentration (w/v) of carbodiimide as coupling agent. In absence of carbodiimide, the non-covalent type of immobilization takes place which results insufficient enzyme

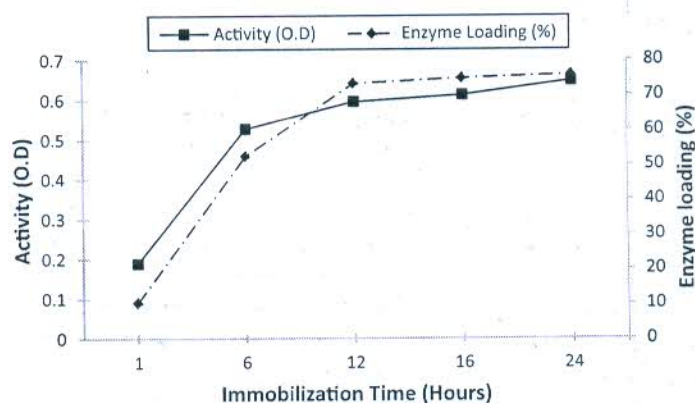


Figure 5.
Effect of immobilization time on conjugate activity and enzyme loading

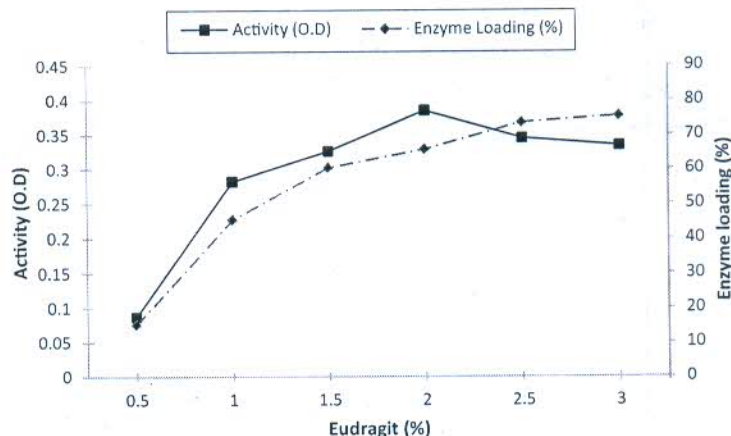


Figure 6.
Effect of Eudragit polymer concentration on conjugate activity and enzyme loading

as described earlier. The activity of these immobilized amylases was evaluated, and the effect of cross-linking time on conjugate activity is demonstrated in Figure 2. With increase in cross-linking time, the enzyme loading and conjugate activity increases and the conjugate activity reached maximum for 3 h cross-linking. Further, over the conjugate activity reduces while no significant change in enzyme loading was observed. Initially, the increase in cross-linking time leads to more glutaraldehyde attachment which increase enzyme loading and for 3 h the enzyme loading as well activity reached maximum as the support gets saturated. While prolong cross-linking time exhibit instability in (-OH-NH₂-) linkage of glutaraldehyde-chitosan due to overcrowding and enzyme loading become stagnant. However, the decrease in activity on prolong cross-linking might be related to the increase in glutaraldehyde dimer formation and denaturation of enzyme caused by excessive interaction of glutaraldehyde.

Effect of enzyme concentration. Chitosan beads activated with 2.5 per cent glutaraldehyde for 3 h were now immobilized with different concentrations of amylase solution (1, 3, 5, 7 and 9 per cent), and the reaction was carried out at three different temperatures (4°C, 25°C and 40°C) for 24 h. Finally, the activity of different immobilized amylases was measured and shown in (Figures 3 and 4). The effect of immobilization temperature, shown in Figure 3, clearly indicates that there was no significant difference in the conjugate activities on immobilization at 4°C and 25°C, while reduced activities were observed at higher temperature (40°C). Therefore, the immobilization can be efficiently done at 4°C or 25°C, and as the room temperature is easy to maintain, the further immobilization was carried out at 25°C.

The enzyme concentration was found to be one of the significant factors in influencing the immobilization. As the different concentrations of enzyme were used for immobilization here, i.e. the retained activity is considered (instead conjugate activity), which is the per cent of conjugate activity to the initial enzyme activity taken for immobilization (Zhou, 2010). The retained activity initially increases with increase in enzyme concentration while at concentrations higher than 5 per cent the retained activity decreases rapidly in spite of increase in enzyme loading to 62.7 per cent, shown in Figure 4. The increase in enzyme amount will increase the chance of attachment with glutaraldehyde and favour immobilization to obtain higher enzyme loadings. While after an optimum concentration the aggregation or oversaturation of enzyme over the support results in steric hindrance and reduce retained activity.

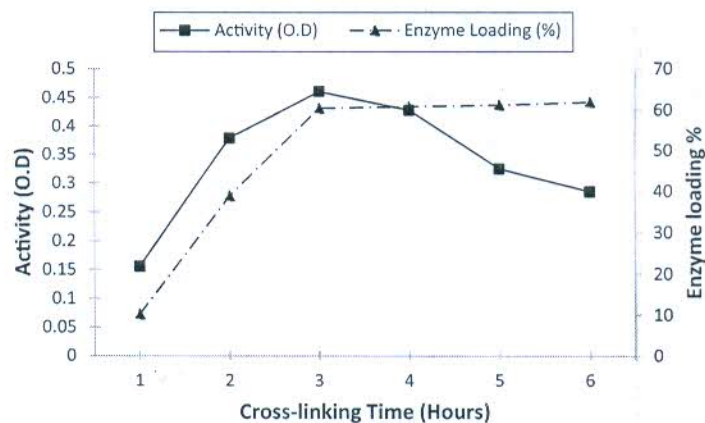


Figure 2.
Effect of bead activation time on covalent chitosan amylase activity and enzyme loading

Reusability analysis

To study the reusability of immobilized amylases, the immobilized amylases were separated from desizing liquor, and their residual activity was estimated after each cycle by taking initial activity as 100 per cent.

Results and discussion

Immobilization of amylase on chitosan

The amylase was covalently immobilized on chitosan beads using glutaraldehyde as cross-linking agent. The factors like glutaraldehyde per cent, cross-linking time, enzyme amount and incubation time has significant impact on the immobilization, i.e. it was necessary to optimize them for maximum conjugate activity.

Effect of glutaraldehyde concentration. Initially, 1 g of chitosan beads were added in 10 ml of different per cent glutaraldehyde solutions, after cross-linked for 6 h at 25°C the beads were washed with distilled water. Then these activated beads were added to 5 per cent (v/v) amylase solution at neutral pH, and the reaction was carried out at room temperature for 24 h. Finally, the conjugate activity of chitosan-amylase was evaluated and plotted against the glutaraldehyde concentration, shown in Figure 1.

The conjugate activity increases with increase in glutaraldehyde concentration and reached maximum for 2.5 per cent glutaraldehyde with enzyme loading of 58.4 per cent. Increasing concentration of glutaraldehyde makes the support more reactive which increase enzyme loading and results in increased conjugate activity. However, further increase in glutaraldehyde concentration from 2.5 to 5 per cent, the conjugate activity decreased gradually even after the enzyme loading increased to 67.8 per cent. This could be attributed to the fact that the higher concentrations of glutaraldehyde cause the excessive bound aldehydes on chitosan which increase enzyme loading. While this extensive interaction bring conformational changes in enzyme structure due to multipoint attachment and ultimately reduce the conjugate activity. Similar results have also been reported by many researchers in immobilization of amylases (El-Ghaffar and Hashem, 2009; Zufahair *et al.*, 2017) and β -galactosidase (Chang and Juang, 2007; Chen *et al.*, 2013; Zubriene *et al.*, 2003) on chitosan as support.

Effect of cross-linking time. Now, 1 gm of chitosan beads were added into 10 ml of 2.5 per cent glutaraldehyde solution in five different beakers and kept for varying cross-linking time from 1 to 6 h at 25°C and then immobilized with 5 per cent amylase solution

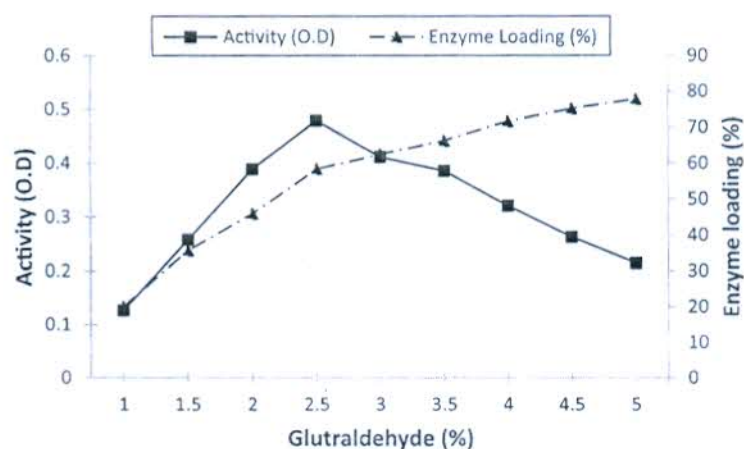


Figure 1.
Effect of
glutaraldehyde
concentration on
conjugate activity
and enzyme loading

as described earlier. The activity of these immobilized amylases was evaluated, and the effect of cross-linking time on conjugate activity is demonstrated in Figure 2. With increase in cross-linking time, the enzyme loading and conjugate activity increases and the conjugate activity reached maximum for 3 h cross-linking. Further, over the conjugate activity reduces while no significant change in enzyme loading was observed. Initially, the increase in cross-linking time leads to more glutaraldehyde attachment which increase enzyme loading and for 3 h the enzyme loading as well activity reached maximum as the support gets saturated. While prolong cross-linking time exhibit instability in (-OH-NH₂) linkage of glutaraldehyde-chitosan due to overcrowding and enzyme loading become stagnant. However, the decrease in activity on prolong cross-linking might be related to the increase in glutaraldehyde dimer formation and denaturation of enzyme caused by excessive interaction of glutaraldehyde.

Effect of enzyme concentration. Chitosan beads activated with 2.5 per cent glutaraldehyde for 3 h were now immobilized with different concentrations of amylase solution (1, 3, 5, 7 and 9 per cent), and the reaction was carried out at three different temperatures (4°C, 25°C and 40°C) for 24 h. Finally, the activity of different immobilized amylases was measured and shown in (Figures 3 and 4). The effect of immobilization temperature, shown in Figure 3, clearly indicates that there was no significant difference in the conjugate activities on immobilization at 4°C and 25°C, while reduced activities were observed at higher temperature (40°C). Therefore, the immobilization can be efficiently done at 4°C or 25°C, and as the room temperature is easy to maintain, the further immobilization was carried out at 25°C.

The enzyme concentration was found to be one of the significant factors in influencing the immobilization. As the different concentrations of enzyme were used for immobilization here, i.e. the retained activity is considered (instead conjugate activity), which is the per cent of conjugate activity to the initial enzyme activity taken for immobilization (Zhou, 2010). The retained activity initially increases with increase in enzyme concentration while at concentrations higher than 5 per cent the retained activity decreases rapidly in spite of increase in enzyme loading to 62.7 per cent, shown in Figure 4. The increase in enzyme amount will increase the chance of attachment with glutaraldehyde and favour immobilization to obtain higher enzyme loadings. While after an optimum concentration the aggregation or oversaturation of enzyme over the support results in steric hindrance and reduce retained activity.

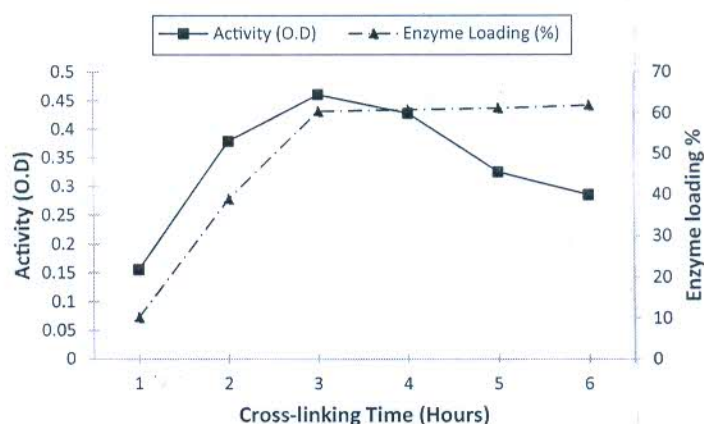


Figure 2.
Effect of bead activation time on covalent chitosan amylase activity and enzyme loading

increases with increase in immobilization time from 2 to 6 h and reached maximum for 6 h. Further with increase in immobilization time over 6 h, the activity decreases rapidly (Figure 9). An immobilization time of 2 h was insufficient for immobilization and results in very low conjugate activity. Further, increase in time of immobilization increase conjugate activity due to more enzyme loading. But the enzyme loading become stagnant after 6 h of immobilization while the conjugate activity reduced for prolong immobilization. This may be due to the fact that a long immobilization time can cause enzyme denaturation by multipoint attachment and results in reduced activity. Thus, the immobilization time of 6 h was accepted as optimum for further immobilization.

Thus, overall, the maximum conjugate activity was obtained on 2 per cent Eudragit activated with 0.2 per cent EDC for 1.5 per cent amylase concentration in 6 h of immobilization time and can be considered as optimum for further application.

Characteristics of the immobilized amylases

After optimizing the immobilization parameters, the amylase was immobilized on chitosan and Eudragit with these parameters, and their characteristics were evaluated, shown in Table I. The activity of amylase reduced after immobilization while on Eudragit the conjugate activity was more as compared to the chitosan. The reason for the decreased activity on immobilization is that the immobilization associates with increase enzyme size and insolubility which results in poor interaction with substrate and limited diffusion which solely depend on the properties of the support material.

Further, the effects of temperature and pH on native and immobilized amylases activity are shown in Figures 10 and 11. The optimum temperature of native and Eudragit immobilized amylase was at around 60°C while for chitosan immobilized amylase it shifts to 70°C also with some increase inactivity at lower temperatures. This increase in optimum

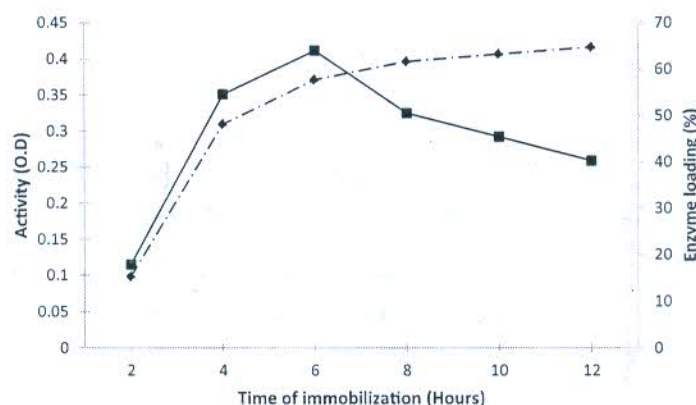


Figure 9.
Effect of time of immobilization on conjugate activity and enzyme loading

Enzyme	Activity (U/mL)	Enzyme loading (%)	Optimum pH	Optimum temperature
Native amylase	1352	—	5.5	55°-60°C
Chitosan-amylase conjugate	560	52.4	5.5	70°C
Eudragit-amylase conjugate	849	63.1	7	55°-60°C

Table I.
Characteristics of both immobilized amylases

Notes: Each experiment was done in duplicate. The difference in individual readings was less than 5%

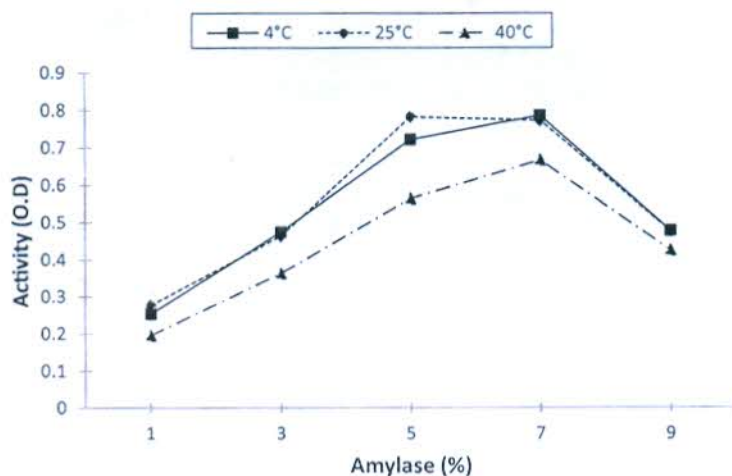


Figure 3. Effect of enzyme concentration and immobilization temperature on conjugate activity

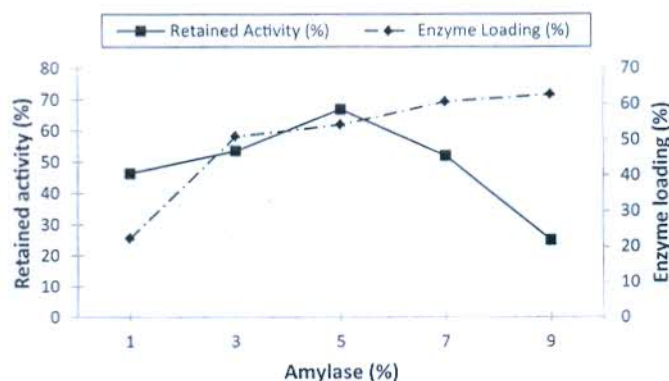


Figure 4. Effect of enzyme concentration on retained activity and enzyme loading

Effect of immobilization time. The chitosan beads activated with glutaraldehyde were added to 5 per cent amylase solution for varying time (1, 6, 12, 16 and 24 h) of immobilization at 25°C. After immobilization, the activity of each immobilized amylase was measured and plotted (Figure 5) against the immobilization time. With increase in immobilization time, the enzyme loading increase and reached maximum to 73.3 per cent within 12 h and then remained nearly constant on prolonged incubation. The conjugate activity also show a similar trend of reaching maximum within 12 h and remains unchanged afterwards. The reported results attribute to the fact that initially the incubation time of 1 to 6 h was too short to get sufficient enzyme binding and results in lower loading per cent with reduced conjugate activity. While, with the extension of the immobilization time, the reaction gradually proceeds and favours the enzyme loading which in turn increases the conjugate activity. The immobilization time of 12 h is optimum to get sufficient enzyme loading to achieve utmost conjugate activity.

Thus, overall, the 2.5 per cent glutaraldehyde concentration with 3 h of activation results in sufficient cross-linking and the immobilization with 5 per cent amylase for 12 h of incubation provide maximum conjugate activity.

was also observed when α -amylase immobilized on chitosan and Amberlite (Tripathi *et al.*, 2007) and chitosan (Zusfahair *et al.*, 2017) due to enzyme and support interactions.

Application of native and immobilized amylases for cotton fabric desizing

Native amylase. Initially, the desizing was carried out with different process parameters using native amylase to obtain most favourable conditions. The desizing efficiency was evaluated in terms of absorbance value of anthrone reagent test, represented in Table II. The results clearly indicate that the desizing efficiency increases with increase in enzyme concentration and a concentration greater than 4 per cent is required to obtain sufficient desizing at 60°C with 90 min of treatment. Increase in treatment time from 30 to 90 min also show significant increase in desizing efficiency, while no change in efficiency was observed from 90 to 120 min of treatment for a specific concentration. The temperature greater than 70°C reduces enzyme activity (observed in Figure 10) and results in somewhat reduced desizing efficiency at that temperature, shown in Table II.

Immobilized amylases. The desizing using Eudragit immobilized amylase was performed at neutral pH, while for native and chitosan, immobilized amylases pH 5.5 was maintained using acetate buffer. Eudragit immobilized amylase efficiently remove starch at neutral pH, but an inadequate desizing efficiency (TEGEWA rating 4) was observed with chitosan immobilized amylase. This may be due to the limited diffusion of immobilized amylase because of insolubility of chitosan. So, for the further desizing using chitosan immobilized amylase pH 3-4 was maintained at which chitosan amylase conjugate become soluble.

The results of enzymatic treatment using native and immobilized amylases are shown in Table III. The desizing with immobilized amylases was performed using the same amylase units as used for the native. The results revealed that the weight loss (percentage) was significant which obviously confirms the removal of starch-based impurities and almost similar trend was observed for native and chitosan immobilized amylase. Weight loss increases with increased amylase concentration and reaches maximum (12 per cent) with 4 per cent native amylase, while around 8 per cent of chitosan immobilized amylase reproduce similar results. It may be due to the limited diffusion of immobilized amylase or the reduced activity at acidic pH.

The performance of different enzymatic desizing processes was also analysed in terms starch content (anthrone reagent test) and TEGEWA rating. Results in Table III clearly indicate that the chitosan immobilized amylase showed 73.6per cent of starch removal with a TEGEWA scale rating of 7-8 at the maximum concentration (8 per cent) of usage. Higher the TEGEWA rating means lower the residual starch content and TEGEWA scale rating 6 or higher is requisite for the effective desizing (Au and Holme, 1999; Dalvi *et al.*, 2007; Wang *et al.*, 2012).

Parameters Enzyme %	30 min		60 min		90 min		120 min	
	60°C	70°C	60°C	70°C	60°C	70°C	60°C	70°C
0	0.948	0.937	0.932	0.921	0.946	0.941	0.932	0.943
2	0.624	0.673	0.563	0.684	0.562	0.672	0.512	0.521
4	0.464	0.514	0.371	0.456	0.258	0.375	0.255	0.369
6	0.412	0.487	0.289	0.361	0.173	0.328	0.169	0.335
8	0.325	0.452	0.211	0.278	0.128	0.287	0.135	0.276

Note: Each experiment was done in duplicate

Table II.
Application of native
amylase for cotton
fabric desizing

loading (20 per cent) and leads to the lower conjugate activity. While the addition of carbodiimide in 0.2 per cent improves the enzyme loading to 67 per cent due to activated carboxyl groups and provide higher activity (Figure 7). However, the excessive amount of carbodiimide causes the partial cross-linking of enzyme molecules restricted their conformation mobility and thus led to the loss in enzyme activity in spite of increased enzyme loading to 80 per cent.

Effect of enzyme concentration. Similarly, the 2 per cent Eudragit polymer solution was activated with 0.2 per cent carbodiimide for 10 mins and varying concentration of amylase from 0.5 to 3 per cent (v/v) was immobilized on it. The enzyme concentration had significant impact on the activity. Figure 8 depicts that with the increase of concentration from 0.5 to 1.5 per cent, the retained activity increases and reached to maximum at 1.5 per cent, while for higher concentrations, it reduces significantly. However, the enzyme loading peak maximum at 2 per cent concentration and become stagnant afterwards. The decrease in activity at higher enzyme concentrations could be attributed to the fact that the support was oversaturated with higher enzyme amount which leads to steric hindrance. This clustering effect had already been observed by other researchers Dourado *et al.* (2002), Silva *et al.* (2006b), Smith *et al.* (2008) and Zhou (2010). Thus, the 1.5 per cent amylase was accepted as optimum for further immobilization over the Eudragit.

Effect of immobilization time. The activated Eudragit polymer was immobilized with 1.5 per cent amylase solution at 25°C for 2 to 12 h of incubation. Initially, the conjugate activity

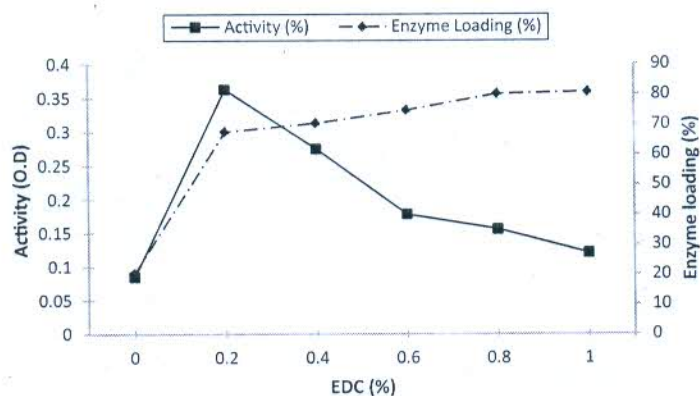


Figure 7.
Effect of carbodiimide concentration on conjugate activity and enzyme loading

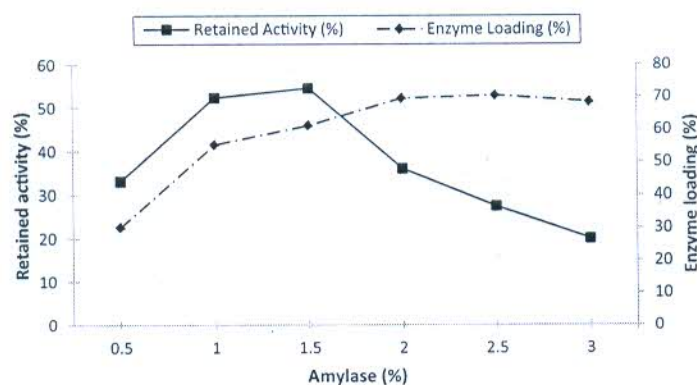


Figure 8.
Effect of enzyme concentration on retained activity and enzyme loading

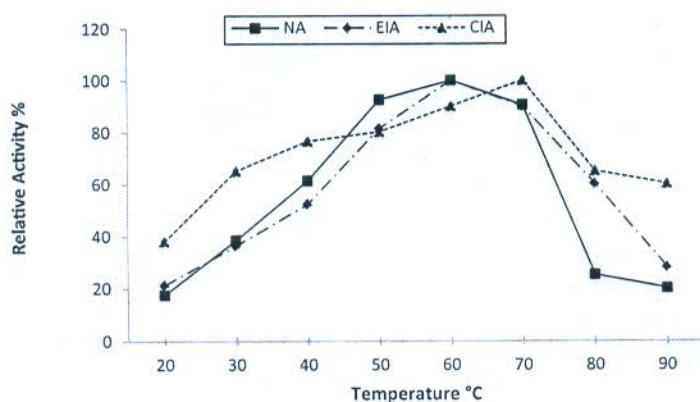


Figure 10. Effect of temperature on relative activities of the native and immobilized amylases

Notes: NA – native amylase, EIA – Eudragit S-100 immobilized amylase, CIA – Chitosan immobilized amylase

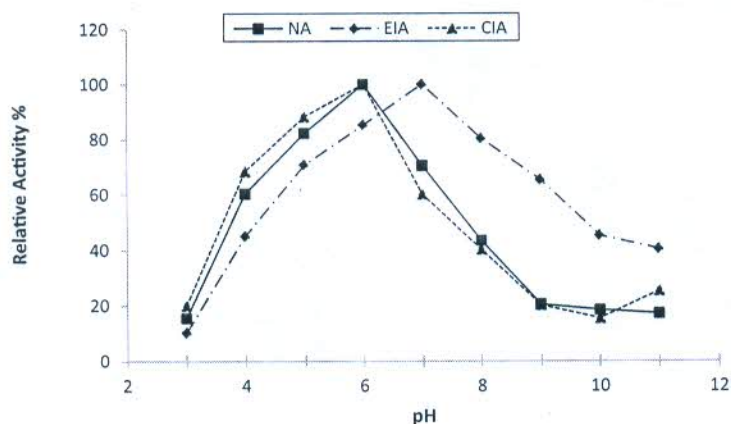


Figure 11. Effect of pH on relative activities of the native and immobilized amylases

Notes: NA – native amylase, EIA – Eudragit S-100 immobilized amylase, CIA – Chitosan immobilized amylase

temperature of α -amylases after immobilization on supports has been reported in several studies (Chang and Juang, 2005; Fang *et al.*, 2016; Shukla and Jajpura, 2005; Tavano *et al.*, 2013). The conformational change in enzyme structure by covalent bond formation via amino groups with support brings about the changes in thermal stability of immobilized amylases. Similar increase in thermal stability of amylase was also observed in Tripathi *et al.* (2007) on immobilization with Amberlite and chitosan.

The optimum pH of native amylase was 5.5-6, and it remains same on immobilization with chitosan, while it shifts to 7 for Eudragit immobilized amylase. Figure 11 clearly indicates that the Eudragit-amylase conjugate shows higher activity in pH above 7, while chitosan-amylase conjugate shows some increased activity in acidic pH range. It is clear from the fact that the anionic nature of Eudragit S-100 matrix results solubility above pH 5.5 which shifts the optimum pH of conjugate to alkaline side (Dourado *et al.*, 2002; Silva *et al.*, 2006b; Yu *et al.*, 2012). While for the chitosan the pH less than 6.5 favour the solubility (Krajewska, 2004) which shifts the optimum pH to acidic side. A similar shift in optimum pH

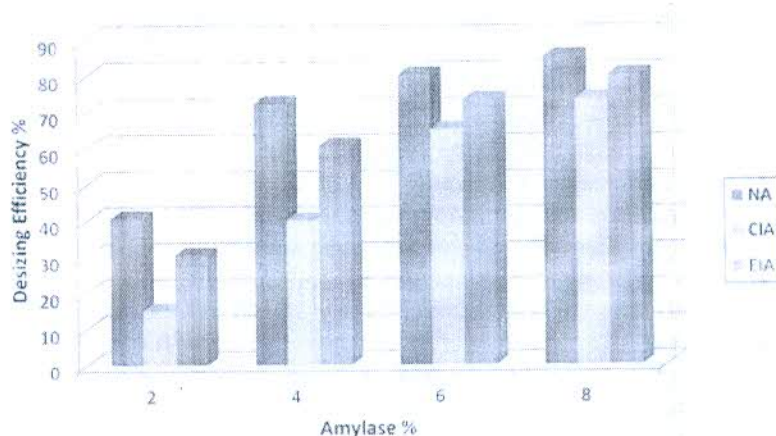
The Eudragit immobilized amylase also shows significant weight loss and a concentration of 6 per cent gives 73.4 per cent desizing efficiency comparable to native amylase. Results of anthrone test and TEGEWA rating also confirms that the covalent Eudragit amylase can give equivalent desizing efficiency to native amylase when applied in a concentration higher than 4 per cent. While the Eudragit immobilized amylase is more efficient in terms of starch removal than chitosan immobilized amylase for a particular concentration (Figure 12). TEGEWA rating of 7-8 is acquired with 6 per cent Eudragit immobilized amylase which is corresponding to 8 per cent chitosan immobilized amylase application, and the results of anthrone reagent test also support this inference with desizing efficiency of 73 per cent.

Treatment with native and immobilized amylases showed similar levels of bending length and tensile strength for the fabric samples (Table III). Removal of starch associates with decrease in stiffness, i.e. reduces the bending length (Saravanan *et al.*, 2011). So the lower bending length in native and immobilized amylases desized samples confirms the efficient removal of size. The tensile strength does not show any significant changes in enzymatically desized samples. No significant improvement in water absorbency was observed in desized samples compared to sized sample, i.e. not mentioned in the results.

Figure 13 represents the FTIR of sized and desized cotton fabrics with, chitosan immobilized amylase, Eudragit immobilized amylase. FTIR spectrum of cotton fabric shows characteristic peaks and the comparative study of the spectrums of sized and desized cotton fabrics show some significant differences in intensity of peaks. The strong peaks in range $3850-3550\text{ cm}^{-1}$ become more predominant in the desized samples attributed to the increase in O-H stretching in primary and secondary hydroxyl groups of cellulose, while a strong absorption band in range $3450-3250\text{ cm}^{-1}$ and $700-470\text{ cm}^{-1}$ reduced significantly indicating the removal of polymeric hydroxyl groups related to starch.

Peaks in region 3560 cm^{-1} (O-H stretch in monomeric compounds like fatty alcohols), 2900 cm^{-1} (corresponding to asymmetric and symmetric stretching of $-\text{CH}_3$ group in long chain alkyls like waxy matters) and around 2360 cm^{-1} and $1650-1750\text{ cm}^{-1}$ (corresponding to pectic substances) shows a considerable increase in intensity in desized cotton due to exposure of impurities by removal of starch coating from cotton yarn surface. Also, the peak intensities in the region $1315-1365\text{ cm}^{-1}$ and $1100-1155\text{ cm}^{-1}$ (corresponding to stretching and bending of aliphatic esters and fatty acid chains) reduces in desized samples, possibly due to removal of some fatty matters by hot wash given after enzyme treatment (Chung *et al.*, 2004).

Figure 12. Desizing efficiency w. r.t amylase concentration of native and immobilized amylases (NA – native amylase, EIA – Eudragit S-100 immobilized amylase, CIA – Chitosan immobilized amylase)



Sample	Treatment	Amylase (%)			Weight loss (%)	Anthrone reagent test		TEGEWA test (Rating)	Bending length (cm)	Tensile strength (kgf)
		0	2	4		Starch content (630nm)	Desizing efficiency %			
Grey cotton Control Native amylase	-	-	-	-	-	0.967	-	1	4.2	38.5
	0	0.21	7.83	11.42	12.49	0.935	3.31	2	4.1	38.6
	2	7.83	11.42	12.49	12.68	0.573	40.71	4	3.9	38.5
	4	11.42	12.49	12.68	3.53	0.266	72.5	8-9	3.2	37.2
Chitosan-amylose conjugate	6	12.49	12.68	7.85	10.21	0.189	80.48	8-9	2.9	36.3
	8	12.68	3.53	10.21	7.85	0.141	85.4	9	2.9	35.8
	2	3.53	10.21	7.85	10.21	0.820	10.21	3	4.1	38.2
	4	7.85	10.21	11.59	6.23	0.579	40.12	4-5	3.8	38.1
Eudragit-amylose conjugate	6	10.21	11.59	10.16	10.92	0.336	65.26	6	3.5	37.4
	8	11.59	6.23	10.16	10.92	0.255	73.6	7-8	3.2	36.9
	2	6.23	10.16	10.92	12.18	0.672	30.5	4	4.2	37.9
	4	10.16	10.92	12.18	-	0.379	60.78	5-6	3.7	37.1
						0.257	73.4	7-8	3.2	36.4
						0.189	80.42	8	3.1	36.2

Note: Reading shown here is the average of three readings

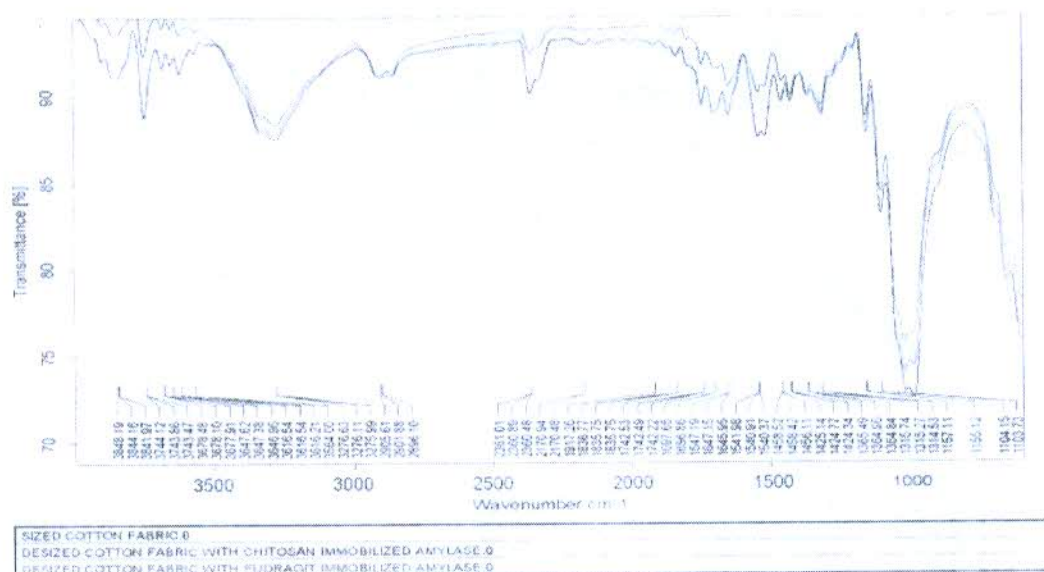
Desizing of cotton fabric

Table III.
Application of immobilized amylases for cotton fabric desizing

Table IV.
Reusability analysis
of immobilized
amylases for cotton
fabric desizing

Reuse cycles	Chitosan α -amylase (8% amylase) Anthrone reagent test			Eudragit α -amylase (8% amylase) Anthrone reagent test		
	Starch content absorbance (630 nm)	Desizing efficiency (%)	TEGEWA scale rating	Starch content absorbance (630nm)	Desizing efficiency (%)	TEGEWA Scale Rating
Grey fabric	0.967	—	1	0.967	—	1
1	0.192	80.1	7-8	0.131	86.5	8-9
2	0.245	74.7	7	0.169	82.5	7-8
3	0.287	70.3	6-7	0.204	78.9	7-8
4	0.379	60.8	6	0.331	65.8	6-7
5	0.419	56.7	4-5	0.366	62.2	6

Note: Each experiment was done in duplicate



Desizing of cotton fabric

Figure 13. FTIR spectra of sized and desized cotton fabrics with chitosan and Eudragit immobilized amylases

Reusability of immobilized amylases

Reusability of biocatalysts is a key factor for their cost-effective industrial application and immobilization allows the possibility to recover and reuse of the enzymes. The Eudragit immobilized amylase insoluble below pH 4, while the chitosan immobilized amylase insoluble in alkaline pH. Thus, immobilized amylases can be easily separated after completion of desizing process due to their pH-dependent soluble-insoluble nature and reused. The reusability was studied up to five cycles, and the retained activity of immobilized amylases was calculated after each cycle, shown in Figure 14. The Eudragit immobilized amylase retained 52 per cent, while chitosan immobilized retained 45 per cent of their original activity, i.e. showing a high reusability.

The results for the application of these immobilized amylases for five desizing cycles are shown in Table IV. The results clearly confirm that the Eudragit immobilized

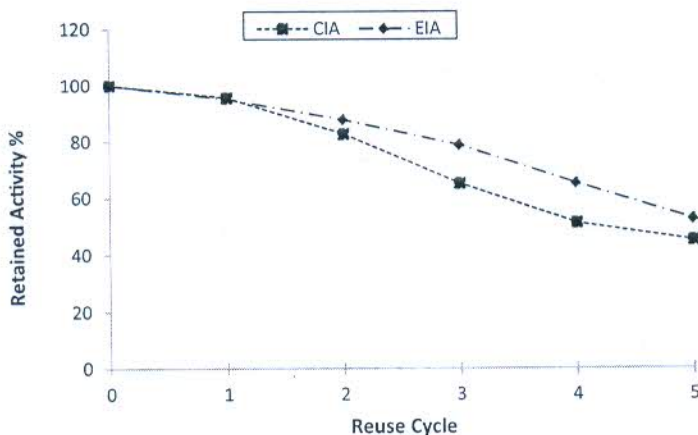


Figure 14. Retained activity of immobilized amylases (CIA – Chitosan immobilized amylase, EIA – Eudragit S-100 immobilized amylase) after several cycles of repeated use (initial activity was taken as 100%)

- Dalvi, P., Anthapan, P., Darade, N. and Kanoongo Adivarekar, R. (2007), "Amylase and pectinase from single source for simultaneous desizing and scouring", *Indian Journal of Fiber & Textile Research*, Vol. 32 No. 4, pp. 459-465.
- Dhingra, S., Khanna, M. and Pundir, C.S. (2006), "Immobilization of α -amylase onto alkylamine glass beads affixed inside a plastic beaker: kinetic properties and application", *Indian Journal of Chemical Technology*, Vol. 13, pp. 119-121.
- Dourado, F., Bastos, M., Mota, M. and Gama, F.M. (2002), "Studies on the properties of celluclast/eudragit L-100 conjugate", *Journal of Biotechnology*, Vol. 99 No. 2, pp. 121-131, available at: [http://doi.org/10.1016/S0168-1656\(02\)00178-5](http://doi.org/10.1016/S0168-1656(02)00178-5)
- El-Ghaffar, M.A. and Hashem, M.S. (2009), "Immobilization of α -amylase onto chitosan and its amino acid condensation adducts", *Journal of Applied Polymer Science*, Vol. 112 No. 2, pp. 805-814, doi: 10.1002/app.29292.
- Fang, S., Chang, J., Lee, Y., Hwang, E., Heo, J.B. and Choe, Y. (2016), "Immobilization of α -amylase from *exiguobacterium* sp. DAU5 on chitosan and chitosan-carbon bead: Its properties", *Journal of Applied Biological Chemistry*, Vol. 59 No. 1, pp. 75-81, available at: <http://dx.doi.org/10.3839/jabc.2016.014>
- Hodge, J.E. and Hofreiter, B.T. (1962), in *Methods in Carbohydrate Chemistry*, Whistler, R.L. and Be Miller, J.N. (Eds), Academic Press, New York.
- Hoshino, K., Taniguchi, M., Netsu, Y. and Fuji, M. (1989), "Repeated hydrolysis of raw starch using amylase immobilized on a reversibly soluble-insoluble carrier", *Journal of Chemical Engineering of Japan*, Vol. 22 No. 1, pp. 54-59.
- Kahraman, M.V., Bayramoglu, G., Kayaman-Apohan, N. and Gungor, A. (2007), " α -amylase immobilization on functionalized glass beads by covalent attachment", *Food Chemistry*, Vol. 104 No. 4, pp. 1385-1392, doi: 10.1016/j.foodchem.2007.01.054.
- Karmakar, S.R. (1999), *Chemical Technology in the Pre-Treatment Processes of Textiles*, Elsevier Science B.V., Amsterdam.
- Krajewska, B. (2004), "Application of chitin and chitosan-based materials for enzyme immobilizations: a review", *Enzyme and Microbial Technology*, Vol. 35 No. 2-3, pp. 126-139, doi: 10.1016/j.enzmictec.2003.12.013.
- Leng, H.L., Douglas, G.M. and Gordon, A.H. (2003), "Hydrolysis of starch particles using immobilized barley α -amylase", *Biochemistry Engineering Journal*, Vol. 13 No. 1, pp. 53-62.
- Madhu, A. and Chakraborty, J.N. (2017), "Developments in application of enzymes for textile processing", *Journal of Cleaner Production*, Vol. 145, pp. 114-133, available at: <http://dx.doi.org/10.1016/j.jclepro.2017.01.013>
- Miller, G.L. (1959), "Use of dinitrosalicylic acid reagent for determination of reducing sugars", *Analytical Chemistry*, Vol. 31 No. 3, pp. 426-428.
- Pan, C., Hu, B., Li, W., Sun, Y., Ye, H. and Zeng, S. (2009), "Novel and efficient method for immobilization and stabilization of β -D-galactosidase by covalent attachment onto magnetic Fe₃O₄ chitosan nanoparticles", *Journal of Molecular Catalyst B: Enzymatic*, Vol. 61 No. 3-4, pp. 208-215, available at: <http://dx.doi.org/10.3839/jabc.2016.014>
- Pandey, A., Soccol, C.R., Thomaz, and Soccol, V. (2000), "Biopotential of immobilized amylases", *Indian Journal of Microbiology*, Vol. 40 No. 1, pp. 1-14.
- Pospiskova, K. and Safarik, I. (2013), "Low-cost easy-to-prepare magnetic chitosan micro-particles for enzyme immobilization", *Carbohydrate Polymers*, Vol. 96 No. 2, pp. 545-548.
- Prakash, O. and Jaiswal, N. (2011), "Immobilization of a thermostable amylase on agarose and agar matrices and its application in starch stain removal", *World Applied Sciences Journal*, Vol. 13 No. 3, pp. 572-577.

RJTA

- Zhou, J. (2010), "Immobilization of cellulase on a reversibly soluble-insoluble support: properties and application", *Journal of Agricultural and Food Chemistry*, Vol. 58 No. 11, pp. 6741-6746, available at: <http://doi.org/10.1021/jf100759c>
- Zubriene, A., Budriene, S., Gorochovceva, N., Romaskevicius, T., Matulionis, E. and Dienys, G. (2003), "Immobilization of hydrolases onto chitosan microparticles", *Chemija (Vilnius)*, Vol. 14 No. 4, pp. 226-230.
- Zusfahair, N.D.R., Kartika, D., Fantoni, A. and Zuliana, A.L. (2017), "Bacillus thuringiensis HCB6 amylase immobilization by chitosan beads", *IOP Conf. Series: Materials Science and Engineering*, Vol. 172, p. 012068, doi: 10.1088/1757-899X/172/1/012068
-

Corresponding author

J.N. Chakraborty can be contacted at: chakrabortyjn@gmail.com

amylase was more efficient compared chitosan immobilized amylase in terms of desizing efficiency. TEGEWA rating more than 6 was obtained with Eudragit immobilized amylases for five reuse cycles, while chitosan immobilizes amylase give up-to 60 per cent desizing efficiency in four reuse cycles (Table IV). The TEGEWA rating more than 6 also confirms the adequate starch removal from samples, i.e. both the chitosan and Eudragit immobilized amylases can be reused for three to four repeated cycles for efficient desizing.

Conclusions

A commercial amylase was immobilized on reversibly soluble-insoluble polymers chitosan and Eudragit S-100 by covalent bonding. The immobilization parameters were optimized for both the immobilization processes to obtain maximum conjugate activity. The Eudragit immobilized amylase retains 62.7 per cent of activity, while on immobilization with chitosan, the retained activity reduced to 41.5 per cent. The solubility of support material plays significant role in the conjugate activity. Thus, optimum pH for chitosan immobilized amylase remains 5.5-6, while for Eudragit immobilized shifts to neutral. Immobilized amylases efficiently desize the starch-sized cotton fabrics. Application of 8 per cent chitosan immobilized amylase, and 6 per cent Eudragit immobilized amylase can provide desizing efficiency equivalent (70 per cent) to 4 per cent of native amylase. The amylase immobilized on Eudragit is more efficient for a particular concentration than chitosan. The immobilized amylases can be easily separated due to reversible soluble-insoluble polymer supports and can be reused up to four repeated cycles with TEGEWA rating higher than 6. The retained activity of 45 per cent for chitosan immobilized and 52 per cent for Eudragit immobilized amylase was observed even after five desizing cycles. Thus, Eudragit S-100 can be the suitable support material for the desizing application of α -amylase. Further, the fundamental knowledge of enzyme-support compatibility and enzyme characteristics may explore ideas to get maximum conjugate activity for more repeated cycles.

References

- Aksoy, S., Tumturk, H. and Hasirci, N. (1998), "Stability of alpha amylase immobilized on poly (methyl methacrylateacrylic acid) microspheres", *Journal of Biotechnology*, Vol. 60 Nos 1/2, pp. 37-46.
- Au, C.K. and Holme, I. (1999), "The alkali desizing of woven cotton fabrics", *Research Journal of Textile and Apparel*, Vol. 3 No. 1, pp. 16-30.
- Chang, M. and Juang, R. (2005), "Activities, stabilities, and reaction kinetics of three free and chitosan-clay composite immobilized enzymes", *Enzyme and Microbial Technology*, Vol. 36 No. 1, pp. 75-82, doi: 10.1016/j.enzmictec.2004.06.013.
- Chang, M. and Juang, R. (2007), "Use of chitosan-clay composite as immobilization support for improved activity and stability of β -glucosidase", *Biochemical Engineering Journal*, Vol. 35 No. 1, pp. 93-98, doi: 10.1016/j.bej.2007.01.003.
- Chen, H., Zhang, Q., Dang, Y. and Shu, G. (2013), "The effect of glutaraldehyde cross-linking on the enzyme activity of immobilized β -galactosidase on chitosan bead", *Advance Journal of Food Science and Technology*, Vol. 5 No. 7, pp. 932-935.
- Chung, C., Lee, M. and Choe, E.K. (2004), "Characterization of cotton fabric scouring by FTIR ATR spectroscopy", *Carbohydrate Polymers*, Vol. 58 No. 4, pp. 417-420.
- Cong, L., Kaul, R., Dissing, U. and Mattiasson, B. (1995), "A model study on Eudragit and polyethyleneimine as soluble carriers of α -amylase for repeated hydrolysis of starch",

A CONTEMPORARY REVIEW ON ASPECT-BASED SENTIMENTAL ANALYSIS

¹Satvika, ²Dr. Vikas Thada

¹PhD Scholar, ²Associate Professor

¹Computer Science and Engineering Department

¹Amity University, Gurgaon, India

Abstract : Social media sites are gaining popularity across the world and they are being used in every sphere of life. Even, in India social media platforms are being used for all purposes ranging from movie reviews to political campaigns to digital marketing of products. One key application of social media which is under tremendous research is the sentimental analysis of users. As most of the people are active on the social networking sites and are using these platforms to launch their emotions about any specific product or service or even idea; hence sentimental analysis is the vital and focal point of research. Prior to purchase a product or service, consumers frequently surf the Web for expert reviews, but progressively also for suggestions of other consumers, expressed in blogs, social networks etc. Many useful suggestions are exhibited in text-only form (like in tweets). It is then prudent to extract aspects (like screen, battery) from the texts that discuss a particular entity (like a smartphone), i.e., sort out what is being discussed, and also estimate aspect sentiment scores, polarity i.e., how negative or positive the sentiment for each aspect is. These two goals are jointly termed as Aspect Based Sentiment Analysis. This review is based on this Aspect-based sentimental analysis concept.

IndexTerms - Aspect, Sentiment Analysis, NLP, Social Media, Machine Learning.

I. INTRODUCTION

Social media platforms and, in particular, microblogging services such as Twitter, Tumblr, and Weibo are increasingly being adopted by users to access and publish information about a great variety of topics. These new mediums of expression enable people to connect to each other, and voice their opinion in a simple manner[1]. Sentiment analysis or opinion mining refers to the application of techniques from fields such as natural language processing (NLP), information retrieval and machine learning, to identify and extract subjective information from textual datasets [2].

One of the most popular sentiment analysis tasks is the automatic classification of documents or sentences into sentiment categories such as positive, negative, and neutral. These sentiment classes represent the writer's sentiment toward the topic addressed in the message. Sentiment analysis applied to social media platforms has received increasing interest from the research community due to its importance in a wide range of fields such as business, sports, and politics. Several works claim that social phenomena such as stock prices, movie box-office revenues, and political elections, are reflected by social media data [3][4] and that opinions expressed in those platforms can be used to assess the public opinion indirectly[5].

II. MACHINE LEARNING

If computer science is the systematic characterization of the computations that we can perform efficiently, what, then, is machine learning? To solve a problem with a computer, one first designs an appropriately efficient algorithm that solves the problem and then implements that algorithm in hardware or software. If we cannot specify the algorithm, then we cannot solve the problem with direct programming. Machine learning extends what we can do with computers by letting us solve problems even when we are unable to manually design an algorithm to solve them. Using examples of correct behaviour, we can specify an algorithm non-constructively. Thus a machine learning algorithm is a meta-algorithm for creating algorithms from data that defines what they should produce.

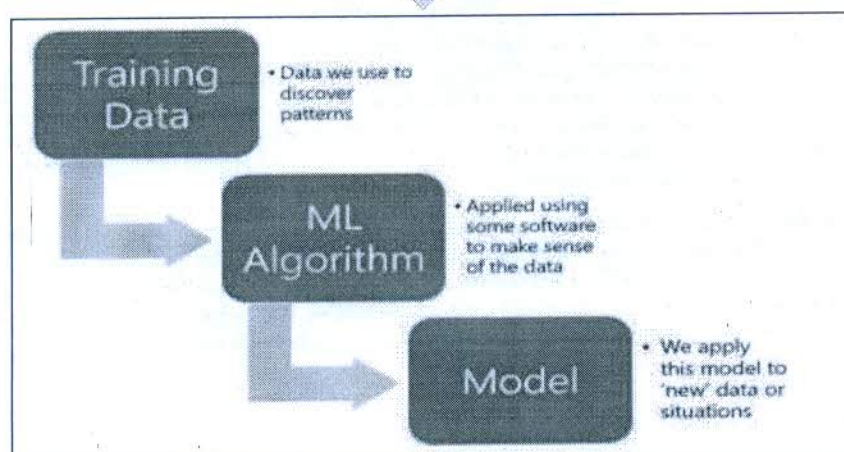


Fig. 1: Working of Machine Learning[6]

Meta-algorithms give us a powerful new way of interacting with computers by telling them what they should compute instead of how they should compute it. Extending our ability to solve problems with computers is reason enough to study machine learning, but it is far from the

only reason. Just as studying learning helps us understand what we can practically compute, we must also study computation in order to inform our understanding of learning.

Machine learning as a scientific discipline examines the computational basis of learning; thus it is essential even if we are only interested in how humans and animals learn. These two central motivations support each other. Trying to solve problems using computational models of learning sheds light on our understanding of the brain, and, by the same token, what we learn about the brain can serve as inspiration for designing learning machines. Basically, Machine Learning allows to tackle problems (tasks) that don't have an exact solution like recommendations, predictions or clustering.

Studying machine learning has scientific value both as a way to understand computation and as a way to understand learning, but for science to matter it must have a positive impact on the world. By always maintaining a connection to important practical problems, one increases the chance that their research on machine learning will have such a positive impact. One great property of the field of machine learning is that its methods can help us solve many specific problems of practical and commercial interest. However, if as researchers our only concern is making scientific progress, should we still labour over specific applications of our more general methods? Obviously we need to try new methods on actual problems to make sure that they work, but perhaps we can start with a new method and then look for problems it can attack.

Alternatively, we can start with a problem and then do whatever it takes to solve it; sometimes solving a problem will require new methods and sometimes not, but in either case good research will help us learn the limitations and advantages of existing methods as well as what aspects of the problem are important.

III. NATURAL LANGUAGE PROCESSING

With the growth of computers and internet, computer linguistics has become an imperative field. Basically computational linguistics began soon after the development of the first computers. This area of Artificial Intelligence which explores how computers can be made to understand and manipulate natural language text or speech to do incredible improvement in communication is known as Natural Language Processing. NLP will not only perk up communication between humans and computers, but also communiqué between computers and computers. The aim of NLP is to enhance ability of computers to extract valuable information and to improvise it like a human expert will do.

Natural language processing (NLP) has fascinated researchers since the advent of AI as a discipline in the 1950s, appearing both in philosophical arguments about the nature of intelligence and in applications. In fact, Turing proposed his famous imitation game that required a computer to communicate in human language only a few years before the first machine translation demo. Human language seems to be an important distinction between humans and other animals making language processing tasks natural members of the AI-set. Beyond any potential implications for AI research, software able to extract useful information from text automatically is of immense practical value simply because of the ubiquity of natural language text on the internet.

Text data have very different qualitative properties than data from other modalities and these properties provide important challenges for machine learning. Tokens, characters, and words are inherently discrete whereas pixel values are discrete merely because of digital quantization. Zipf distributions abound in NLP and the large fraction of words that are rare words demands machine learning models with powerful generalization abilities. Unlabelled data are often plentiful, but even in the largest unlabelled text corpora many particular constructions or phrases of interest will still only occur rarely. Human users also have very high standards for correctness and precision for text processing systems since an error in a single word can have non-local effects on the meaning of an utterance. Because massive collections of text data provide exciting opportunities for machine learning research, there is an extensive literature on natural language processing[7].

IV. LITERATURE REVIEW

M. Bouazizi & T. Ohtsuki[8] state that although opinion mining and sentimental analysis of social networking sites are undergoing immense research. However, most of the researchers ignore the bigger picture and are binary or ternary classification based i.e. considering user view as either positive, negative or neutral. The authors focus on multi-class classification i.e. seven different classes for matching user's exact sentiment. For this, a graphical-user interface (SENTA) has also been developed by authors which provides ease of use and better understanding. The experimental results show that 81.3% accuracy has been achieved in the case of binary or ternary classification and a solid 60.2% accuracy even in the case of multi-class classification of user views.

Y. Wu et. al[9] discuss that the emerging size of social media data is a boon not only for the solution providers (or data owners), but also for the end users. This colossal availability of social media data can help the end users achieve a great understanding of society, however it working contrarily. This is where "visual analytics" to aid the common man to fully exploit this variable and immensely-sized multimedia social data. The authors have divided the available state-of-art techniques into two wide categories: information gathering and understanding user conduct. A comprehensive survey is also proposed by the authors here to fully undermine the structured and unstructured social media analysis techniques.

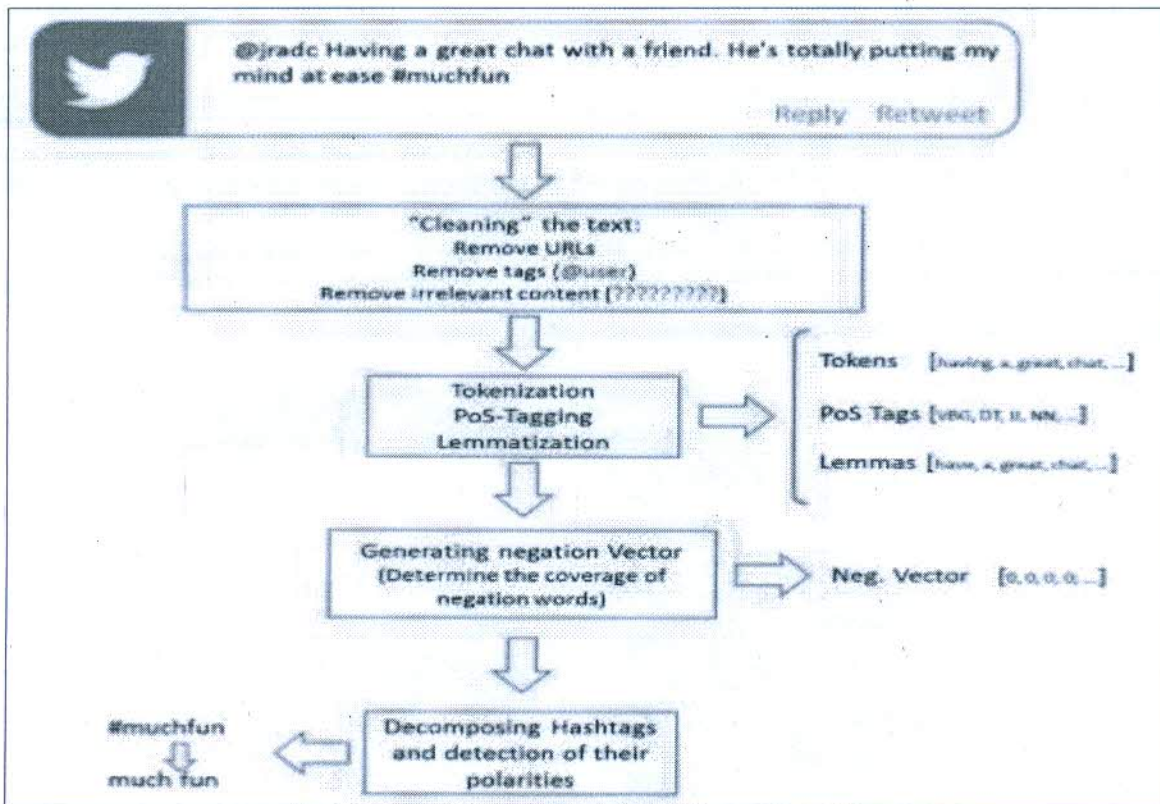


Fig 2: Working of SENTA (GUI tool) for Multi-class Classification[8]

X. Zhou et. al[10] address a grave problem of recognizing anonymous users which seem identical but are present widely on the social media platforms. Due to availability of user profiles publicly, duplication and personification of users for varied purposes is present extensively, hence using a cross-platform approach to identify such users will prove to be a prodigious benefit both in theory and practice of social computing.

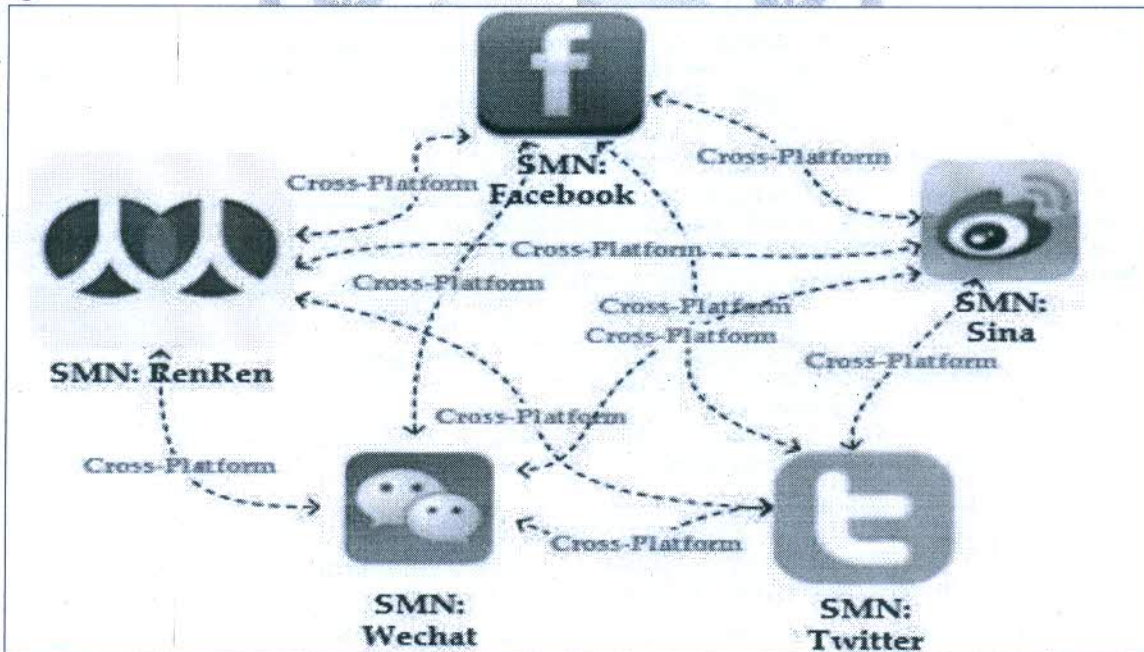


Fig 3: Cross-platform research to merge a variety of SMNs[10]

However, the present methodologies implementing user's location, writing pattern and network structure for distinguishing anonymous users are not yielding the expected results. Hence, the authors propose a novel method for the same i.e. Friend Relationship-Based User Identification (FRUI) algorithm which is based on the concept that no two users on the social networking sites share the same friendship cycle unless they are the same person.

N. D. Doulamis et. al[11] focus on a specific social micro-blogging site Twitter and gave a particular approach to detect the vital events on Twitter. The twitter events could be short-timed (trending currently) or long-timed (submitted recently) and their identification could yield

superior structuring of user content. As the conventional techniques available seem inadequate, a fuzzy-based model is developed by the eminent authors to entirely capture real-life data and twitter dynamics. In addition to it, a word-clustering graph has also been implemented to properly identify an event.

N. Cao et. al[12] have worked on an ingenious concept that is detecting anomalous users present on the social media networks and for this herculean task they have deployed unsupervised learning techniques. The paper also discusses how the visualization techniques can be used for better understanding of user social behavior depending upon user's social relations and communication. Keeping all the above points in mind, TargetVue – a system is developed for anomaly detection, which is depicted as follow:

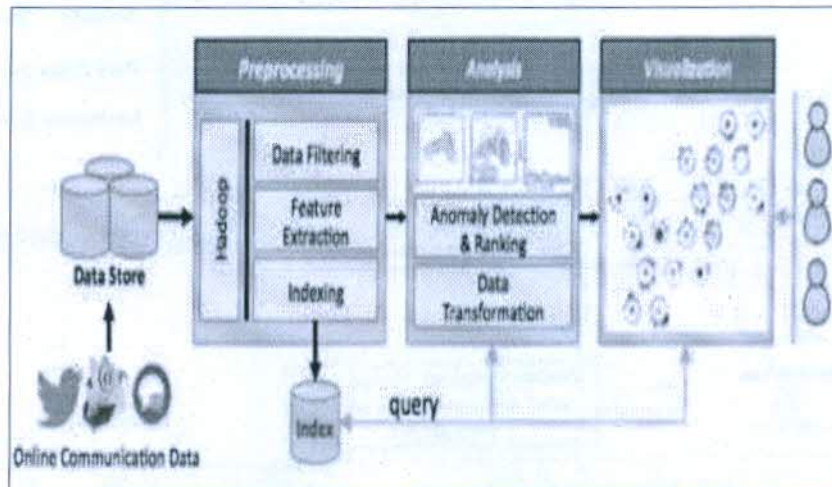


Fig 4: Working of TargetVue – the anomaly detection system[26]

Y. Zhang et. al[13] concentrated on a vital area of social media which is the security aspect. The authors have taken Twitter as a case example of social networking sites and have analysed how the trending topics in Twitter is affecting people's behaviour and mood. Twitter trends are very popular these days and if in hands of wrong people, they may use social sites for spreading hate and hate crimes, which will be a curse for the society. It was also found out that there are numerous fake accounts on Twitter and spammers use them for their own advantage i.e. manipulating the trending topics, hence highlighting the news they want for money or for fun or with bad intentions.

Z. Liu & B.J. Jansen[14] have focused on the information seeking part of the social media networks and have traced that it's a natural drift in a mundane man's life to go to social network sites for searching information. All the vital sites such as Facebook, Twitter, etc. help their users to join specific groups in which they are interested in and such groups notify their members of all the vivacious information on a given subject. The question classification has been done on two basis: subjective and objective. Based on this classification, a predictive model has been proposed to instigate the subjectivity orientation of user questions.

G. I. Parisi et. al[15] have established the idea of lifelong learning through novel deep learning methods. The traditional deep learning approaches focus on the supervised pattern where a group of training data is already given to the machine based upon which it classifies things and learn, however a new method is required for action recognition from videos. This could be achieved with the help of self-organizing deep neural architectures; which in turn uses unsupervised learning methodologies through recurrent neural networks which are arranged hierarchically.

M. Bouazizi & T. Ohtsuki[16] present a brilliant and challenging idea of using machine learning for detecting sarcasm in tweets. Sarcasm represents soft irony in the language, which is hard to detect even by humans, hence it could be a daunting task for the computer. The authors have proposed a pattern-based tactic for sarcasm analysis through which they can categorize each tweet as sarcastic or non-sarcastic. To achieve their target, the Weka tool is used in conjunction with the Libsvm. The experimental results have shown greater efficiency upto 83.1%, which is way better than the state-of-art technologies.

J. Lin and A. Kolcz[17] have tried to bundle Twitter with Hadoop-based, Pig-centric analytics platform. As data is increasing globally at a tremendous rate, so does the data warehousing and data mining techniques. One such platform is Pig, which not only provides the predictive capability but also the analytic capabilities for huge data available. It is stated that the common tasks involved in social sites analysis can be easily implemented with the help of Pig platform, which is also open-source. This paper uses a supervised model for training of the machine.

V. Carchiolo et. al[18] brought a new application of social media sentimental analysis. They suggest that the Twitter can be used as a tool to predict the health related issues and diseases' dynamics. As the health data from hospitals and health centres is not easily available because of various legal and ethical constraints, Twitter can be used as a tool for collection of such data. After the data collection, this data undergoes the numerous machine learning and Natural language processing tools to predict the concern and spread of a disease in a specific geographical area. The whole process mentioned above is shown below:

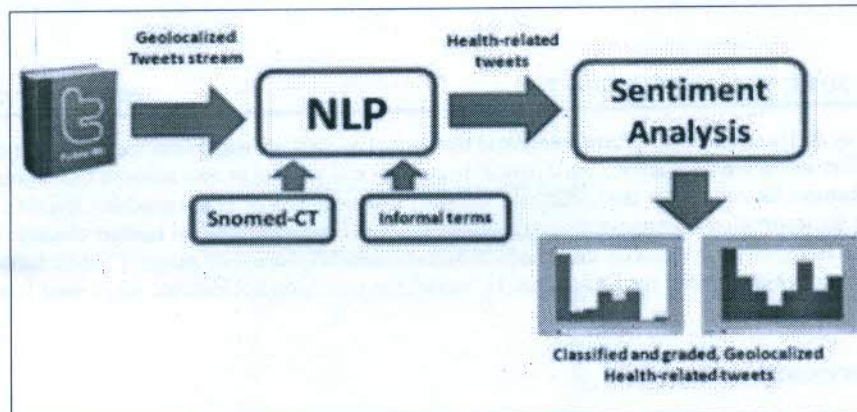


Fig 5: Application Architecture to study Dynamics of Diseases through Twitter[18]

H. Anber et. al[19] have got new insights on the sentimental analysis done with the help of Twitter. Myriad social media networks like Facebook, Twitter, Instagram, LinkedIn behave in dissimilar ways and to distinguish each, authors have considered two major factors: Homophily and Reciprocity. Homophily refers to the tendency of contacting similar users at a higher rates than other and Reciprocity refers to the relation of following a user and getting followed back. Like in Facebook, if a user is friend with someone, they relation is reciprocal i.e. both are each other's friend, but in Twitter relationship is mostly following updates from a celebrity and thus mostly unidirectional. Depending upon this, Tweets can be used to analyse the social behaviour towards any social event.

M. Ben-Ari & F. Mondada[20] have published a detailed article on how the machine learning basically works. They have used statistical techniques primarily Linear Discriminant Analysis (LDA) based on the supervised learning approach. LDA is a kind of a classification algorithm of machine learning which is helpful in detecting patterns and also to forecast outcomes without explicit programming. This is a how an artificially intelligent robotic arm can be used to distinguish between balls of different colours.

L. Jiang et. al[21] too have taken the case study of micro-blogging site – Twitter for sentimental analysis. Usually a binary classification of tweets is done i.e. marking them as positive or negative, however this is target-independent strategy which is not full-proof. Hence, a target-dependent strategy is needed to fill in the gaps, which decides by taking not just 1 tweet, but all the related tweets into account. The experimental results show that the target-dependent approach is much better than the target-independent one.

M. Pennacchiotti & A.M. Popescu[22] have proved the worth of Natural Language Processing in the Twitter Sentimental Analysis. Their approach is taking three key points into consideration which are political orientation, soft corner for a particular business and ethnicity for user classification. All the above mentioned features can be predicted considerably well by careful consideration of linguistic aspects of user tweets, tweet content and their respective behaviour on Twitter. Here, the Latent Dirichlet Allocation (LDA) model is used primarily for the linguistic characteristics.

H. Becker et. al[23] have tried to characterize the social media platforms especially Twitter (because of its short messaging feature) for identification of real-events. For this, they have taken into account millions of tweets (nearly 2,600,000 tweets) and have used machine learning approach to classify them as event-based or non-event based tweets. An online-clustering technique that groups together similar tweets about a real event are grouped together. Based upon this several key factors can be improved like prioritization, filtering of content and ranking of events.

P. Juneja and U. Ojha[24] suggest that if Twitter Sentimental Analysis can be used to predict the market trends or fashion trends, then they can also be used for prediction of elections. The research in this paper is twofold: one aspect is based on whether Twitter can be used to predict the outcomes of Delhi Corporation Elections and other feature compares all the available social media classifiers to identify the best tool for it. The investigational outcomes show that Multinomial Naïve Bayes classifier is the most accurate sentiment predictors with 78%. Also, depending upon various political events like rallies or speeches, the sentiments of public get inclined towards a political party.

G. Gautam & D. Yadav[25] advocate that Twitter Sentimental Analysis is also a major tool for classification of user reviews. So, they have used machine learning approach with semantic analysis for classifying the tweets and user reviews about a particular product. The procedure described here is first pre-processing the available dataset, then extract the feature vector (adjective), finally apply copious classification algorithms and compare their results.

P. Kumar et. al[26] state that Twitter as a data analysis tool is under-utilized. Only, two chief territories are pulling in more enthusiasm for the examination group, the feeling mining and assessment investigation. An assessment examination of general's conclusions mined from the well known smaller scale blogging site Twitter is performed. The real accentuation of this paper is set on assessing precision of various machine learning calculations for the errand of twitter notion investigation.

K. Kang et. al[27] contributed immensely by detecting user's psychological states through the user tweets. In this context, the authors have taken into account not only text, but also other multimedia like images, emoticons, etc. to identify the depressive users. Apart from this the tweets of depressive and non-depressive users are analysed to clearly distinguish their characteristics. Identification of depressive users can predict the mood swings of users and ultimately prevent possible suicides.

E. Chaniotakis & C. Antoniou[28] state that social networking sites are used in every sphere of life including transportation. With the help of its myriad characteristics like combining temporal, textual and spatial information from social media, continuous information flow, message content, etc. a colossal amount of information can be generated which can be analysed to delineate hidden patterns regarding rider's satisfaction and examination of the relationship between mobility and social media networks.

G. T. Giancrifofaro & A. Panangadan[29] have integrated the textual as well as image data for the sentimental analysis for the purpose of transportation studies. The social media platform used here is Instagram and also takes into account California Department of Transportation (Caltrans). Numerous features like comment data, captions and images are submitted to the machine learning network, so that the prediction of sentiments regarding transportation. The classification accuracy reaches close to reported human classification agreement (approximately 80%). This indicates that transportation agencies can completely automate the process of gauging public sentiment toward their services and performance from multimedia based social media sources. However, the results do not indicate that visual features are more informative than text features.

V. SUMMARY AND DISCUSSION

Table I: Summary of Research Work

Author	Year	Source	Major Contribution
M. B. Ari and F. Mondada[20]	2018	Springer	Using LDA in supervised learning
M. Bouazizi and T. Ohtsuki[8]	2017	IEEE Translations	Multi-class Sentimental Analysis
P. Juneja and U. Ojha[24]	2017	8 th ICCCNT Conference	Analysing Twitter to predict 2014 elections
E. Chaniotakis & C. Antoniou[28]	2016	IEEE Intelligent Systems	Relationship between social media and transportation
G. T. Giancrifofaro and A. Panangadan[29]	2016	19 th ITSC Conference	Analysing Instagram data for California Department of Transportation
H. Anber, A. Salah and A. A. Abd El-Aziz[19]	2016	IJCEE	Analysing sentiments based on Homophily and Reciprocity
K. Kang, C. Yoon and E. Y Kim[27]	2016	IEEE Conference	Identifying depressive users through social media
M. Bouazizi and T. Ohtsuki[16]	2016	IEEE Tranlations	Sarcasm detection
P. Kumar, T. Choudhury, S. Rawat and S. Jayaraman[26]	2016	IEEE Conference	Assessing precision of various machine learning calculations
Y. Zhang, X. Ruan, H. Wang, H. Wang and S. He[13]	2016	IEEE Transactions	How mischievous people spread hate crimes through Twitter
Z. Liu and B. J. Jansen[14]	2016	IEEE Transactions	Difference between subjective and objective questions
N. Cao, C. Shi, S. Lin, J. Lu, Y.R Lin and C. Y Lin[12]	2015	IEEE Transactions	Classifying user's behaviour
N. D Doulamis, D. Anastasios, D. Doulamis, P. Kokkinos and E. M Varvarigos[11]	2015	IEEE Transactions	Detecting various vital events (both short-timed and long-timed)
V. Carchiolo, A. Longheu, and M. Malgeri[18]	2015	Springer	Extraction of health related information
X. Zhou, X. Liang, H. Zhang and Y. Ma[10]	2015	IEEE Transactions	Identifying anonymous identical users on different social platforms
G. Gautam and D. Yadav[25]	2014	IEEE	Classifications of user sentiments in Twitter
J. Lin and A. Kolcz[17]	2012	ACM	Use of open-source platform for data mining
H. Becker, M. Naaman and L. Gravano[23]	2011	5 th AAAI Conference	Identifying real events through Twitter
L. Jiang, M. Yu, M. Zhou, X. Liu and T. Zhao[21]	2011	ACL	Target dependent sentimental analysis
M. Pennacchiotti and A.M	2011	5 th AAAI	Using NLP in sentiment analysis

Popescu[22]		Conference	
Y. Wu, N. Cao, D. Gotz, Y. P Tan and D. A. Keim[9]	1997	IEEE Transactions	Using visual analytics to help to exploit vastly available data

VI. CONCLUSIONS

This research paper reviews the recent work done on the current hot topic "Sentimental Analysis" and the crux of study are the following. The actual sentiment conveyed by a word depends on subjective judgment of a person, which is hard to diagnose by a machine. Social networking sites use a lot of informal words or slangs. This rich diversity makes the opinion mining and sentimental analysis task a herculean one both in terms of time as well as cost. Use of sarcasm both in terms of words or even emoticons is hard to infer. Most of the research on sentimental analysis is based on binary opinions (positive or negative) or ternary opinions (positive, negative or neutral) only, however most of the scholarly work ignores the aspect-based part of opinions.

REFERENCES

- [1] B. J. Jansen, M. Zhang, K. Sobel and A. Chowdury, "Twitter power: Tweets as electronic word of mouth", *Journal of the American Society for Information Science and Technology*, vol. 60, no. 11, 2009, pp. 2169–2188.
- [2] B. Pang and L. Lee, "Opinion mining and sentiment analysis. Foundations and Trends in Information Retrieval", *Foundations and trends in information retrieval*, vol. 2, no. 1, 2008, pp. 1–135.
- [3] J. Bollen, H. Mao and X.J Zeng, "Twitter mood predicts the stock market", *Journal of computational science*, vol. 2, no. 1, 2011, pp. 1–8.
- [4] S. Asur and B.A. Huberman, "Predicting the future with social media", *Proceedings of the 2010 IEEE/WIC/ACM International Conference on Web Intelligence and Intelligent Agent Technology*, vol. 1, Washington, DC, USA: IEEE Computer Society, 2010, pp. 492–499.
- [5] B. O'Connor, R. Balasubramanyan, B.R Routledge and N.A Smith, "From Tweets to Polls: Linking Text Sentiment to Public Opinion Time Series", *Proc. Fourth International AAAI Conference on Weblogs and Social Media*, AAAI Press, 2010, pp. 122–129.
- [6] "AI and Machine Learning in finance - are we doomed?". [Online]. Available: <http://www.linkedin.com/pulse/ai-machine-learning-finance-we-doomed-sanjay-bhandari>. [Accessed: Jan. 19, 2003]
- [7] A. Kaushik and A. Kumar, "A Novel Solution based Approach to NLP", *International Conference on Reliability, Infocom Technology and Optimization(ICRITO)*, Lingaya's University, Faridabad, Nov 2010.
- [8] M. Bouazizi and T. Ohtsuki, "Pattern-Based Approach for Multi-Class Sentiment Analysis in Twitter", vol. 5, no. 7, *IEEE Transactions and Content Mining*, August 18, 2017, pp. 20617 – 20639.
- [9] Y. Wu, N. Cao, D. Gotz, Y. P Tan and D. A. Keim, "A Survey on Visual Analytics of Social Media Data", *IEEE Transactions on Multimedia*, DOI 10.1109/TMM.2016.2614220, 2016. *Wireless LAN Medium Access Control (MAC) and Physical Layer (PHY) Specification*, IEEE Std. 802.11, 1997.
- [10] X. Zhou, X. Liang, H. Zhang and Y. Ma, "Cross-Platform Identification of Anonymous Identical Users in Multiple Social Media Networks", *IEEE Transactions on Knowledge And Data Engineering*, DOI 10.1109/TKDE.2015.2485222, 2015.
- [11] N. D. Doulamis, D. Anastasios, D. Doulamis, P. Kokkinos and E. M Varvarigos, "Event Detection in Twitter Microblogging", *IEEE Transactions on Cybernetics*, 2015.
- [12] N. Cao, C. Shi, S. Lin, J. Lu, Y.R Lin and C. Y Lin, "TargetVue: Visual Analysis of Anomalous User Behaviors in Online Communication Systems", *IEEE Transactions on Visualization And Computer Graphics*, vol. 22, no. 1, Jan. 2016, pp. 280–289.
- [13] Y. Zhang, X. Ruan, H. Wang, H. Wang and S. He, "Twitter Trends Manipulation: A First Look Inside the Security of Twitter Trending", *IEEE Transactions on Information Forensics And Security*, 2016.
- [14] Z. Liu and B. J. Jansen, "Understanding and Predicting Question Subjectivity in Social Question and Answering", *IEEE Transactions on Computational Social Systems*, vol. 3, no. 1, Mar. 2016.
- [15] G. I. Parisi, J. Tani, C. Weber and S. Wermter, "Lifelong learning of Human actions with deep neural network self-organization", *Elsevier Neural Networks*, vol. 96, 2017, pp. 137–149.
- [16] M. Bouazizi and T. Ohtsuki, "A Pattern-Based Approach for Sarcasm Detection on Twitter", *IEEE Transactions and Content Mining*, 2016.
- [17] J. Lin and A. Kolcz, "Large-Scale Machine Learning at Twitter", *SIGMOD '12*, Copyright ACM 978-1-4503-1247-9/12/0, May 20–24, 2012, Scottsdale, Arizona, USA, pp. 793–804.
- [18] V. Carchiolo, A. Longheu, and M. Malgeri, "Using Twitter Data and Sentiment Analysis to Study Diseases Dynamics", *Springer International Publishing, ITBAM2015*, Switzerland, 2015, pp. 16–24.
- [19] H. Anber, A. Salah and A. A. Abd El-Aziz, "A Literature Review on Twitter Data Analysis", *International Journal of Computer and Electrical Engineering*, vol. 8, no. 3, June 2016, pp. 241–249.
- [20] M. B. Ari and F. Mondada, "Machine Learning - Elements of Robotics", 2018.[Online] Available: https://doi.org/10.1007/978-3-319-62533-1_14. [Accessed: Dec. 24, 2017].
- [21] L. Jiang, M. Yu, M. Zhou, X. Liu and T. Zhao, "Target-dependent Twitter Sentiment Classification", *Proc. of the 49th Annual Meeting of the Association for Computational Linguistics*, Portland, Oregon, June 19–24, 2011, pp. 151–160.
- [22] M. Pennacchiotti and A.M Popescu, "A Machine Learning Approach to Twitter User Classification", *Fifth International AAAI Conference on Weblogs and Social Media*, 2011, pp. 281–288.
- [23] H. Becker, M. Naaman and L. Gravano, "Beyond Trending Topics: Real-World Event Identification on Twitter", *Fifth International AAAI Conference on Weblogs and Social Media*, 2011, pp. 438–441.
- [24] P. Juneja and U. Ojha, "Casting Online Votes: To Predict Offline Results (Using Sentiment Analysis by machine learning Classifiers)", *8th ICCNT 2017*, July 3–5, 2017, IIT Delhi, Delhi, India, 2017.
- [25] G. Gautam and D. Yadav, "Sentiment Analysis of Twitter Data Using Machine Learning Approaches and Semantic Analysis", 978-1-4799-5173-4/14/\$31.00 © IEEE, 2014.

- [26] P. Kumar, T. Choudhury, S. Rawat and S. Jayaraman, "Analysis of Various Machine Learning Algorithms for Enhanced Opinion Mining using Twitter Data Streams", 2016 IEEE International Conference on Micro-Electronics and Telecommunication Engineering, 2016, pp. 265-270.
- [27] K. Kang, C. Yoon and E. Y Kim, "Identifying Depressive Users in Twitter Using Multimodal Analysis", IEEE BigComp 2016, 2016, pp. 231-238.
- [28] E. Chaniotakis and C. Antoniou, "Mapping Social Media for Transportation Studies", IEEE Intelligent Systems, 2016.
- [29] G. T. Giancrifofaro and A. Panangadan, "Predicting Sentiment toward Transportation in Social Media using Visual and Textual Features", 2016 IEEE 19th International Conference on Intelligent Transportation Systems (ITSC), Windsor Oceanico Hotel, Rio de Janeiro, Brazil, November 1-4, 2016, pp. 2113-2118.



RESEARCH

Open Access



Enzyme washing of indigo and sulphur dyed denim

A. K. Patra^{1*}, Amit Madhu¹ and Neeraj Bala²

*Correspondence:

arunkpatra@rediffmail.com

¹The Technological Institute

of Textile & Sciences,

Bhiwani 127 021, India

Full list of author information

is available at the end of the

article

Abstract

A wide ranging finish effects have been given to denim fabrics in industrial scale to make it more fashionable and functional. Among the numerous wet and dry treatments given, worn out looks of various kinds have received the maximum attention. In this context, herein, two denim fabrics, one dyed with vat indigo and the other with sulphur black were enzyme washed. The enzymes used were acid cellulase and neutral cellulase and the treatments were done at varying concentrations, time and mechanical agitation. The trials so taken were based on design of experiments, and the effect was analysed in terms of decrease in colour depth and weight loss. Back staining of fabric during the wash was also checked and acid enzyme despite higher colour removal, caused significant staining in sulphur dyed quality. Attempt was made to contain this back staining by suitable treatment. The application conditions of cellulases on the denim qualities were also optimized for fading effect.

Keywords: Acid cellulase, Back staining, Colour strength, Denim, Fading, Neutral cellulase

Introduction

Denim as a fabric, has received the widest acceptance among all textile products. It has had an incredible influence on consumers both socially and culturally (Paul 2015). This twill cotton fabric usually has warp threads indigo dyed while weft remains plain white. The warp faced fabric therefore looks blue on one side and white on reverse. The warp being ring dyed, creates denim's fading characteristics, which is unique compared to every other textile material. With changing times, many new variants of denim came into existence. Denim washing is one of the key areas in getting the faded look. Earlier stone washing used to be done to achieve soft feel and the desired appearance. During washing, the pumice stone, scraps off the dye particles from the yarn surface in the denim fabric. Due to the ring dyeing of denim fabric and heavy abrasion during stone washing process, the faded effect is achieved. Oxidative bleaching agent with or without the addition of stones have also been used to get fading effect. Difficulty in removing residual pumice from fabric, damage to equipment and clogging of machine drainage passage due to particulate material proved to be major drawbacks with the technique (Heikinheimo et al. 2000). Later on use of enzymes became a sustainable option to get the worn out look in denim. The enzymes used are cellulase enzymes, specifically acting on the cellulose part, mainly on the surface of the fabric. This gives the desired look

and at the same time, removes hairiness from surface thus giving a smooth and soft feel. Enzymes are substrate specific in their action, unaffected by the others. They are primarily used in textiles to promote hydrolysis of the required substrate (Patra 2003).

A fair amount of experimental research on enzyme wash, has also been carried out in last two decades or so. Denim fabric has been treated with *Trichoderma Reesei* cellulases and compared for stone washing denim fabrics (Heikinheimo et al. 2000). The redeposition of indigo after treating with cellulase has been examined to certain extent (Andreus et al. 2000). Campos et al. (2000) investigated the indigo-cellulase interactions for cellulases from different fungal origins. However differing from all these, in the present work, two denim fabrics of similar weave and dyed with different classes of dyes are treated with acid cellulase and neutral cellulase. The laboratory scale treatments were done varying their concentration and time. Standard steel balls were also used in the bath to enhance the rigours of treatment. The levels of the process parameters were changed based on design of experiment. Since washing of denim is sometimes accompanied by back staining, treatment with a commercial anti back staining agent was also done. Out of the various dyes used for denim, indigo vat and sulphur colours are the more common ones and hence they were taken for the study.

Methods

Materials

Grey denim fabrics of two different colours were taken for the study. The fabrics of 2/1 twill with 7 s warp count and 10 s weft count had following specifications.

Dark blue indigo dyed: epi 49; ppi 49; gsm 210.

Sulphur black dyed: epi 50; ppi 51; gsm 220.

The enzymes used for the denim washing are from Novozymes with specifications as given below (Table 1).

For desizing of the sized warp yarn Invazyme ADC of Huntsman was used while acetic acid used was of L R grade. A bleached plain woven cotton fabric with 40 s yarn was used for back staining.

Enzymatic fading

To start with, the standard test for dye on fibre was done to conform vat dye and sulphur colour on the two fabrics. Then, in both the denim qualities, fabric was first desized with 5 g/l of the amylase enzyme at 60–65 °C for 60 min. The pH was maintained at 5–6 using

Table 1 Enzyme specifications

Name	Type	Strength (ECU ^a /g)	Recommended conditions	
			pH	Temperature (°C)
Cellusoft Conc. L	Acid cellulase	1500	4.5–5.5	40–50
Neutrancell CLD	Neutral cellulase	2400	6.5–7.5	25–35
Denimax core 1380S	Anti backstaining	–	6.5–7.5	40–55

^a ECU—amount of enzyme producing one n mole of reducing sugar as glucose in 1 s

acetic acid and MLR was kept 1:30. After desizing, the enzyme was deactivated by raising the temperature of water bath to 80 °C for 10 min. Then fabric was rinsed with warm water followed by cold water. It was then dried in an oven and checked for size removal with Iodine drop test. After passing the test, fabric was taken for further treatments.

The two denim qualities were treated with the cellulase enzymes under recommended conditions. These enzymes in ready to use form, were applied in different concentrations with varying parameters like time and mechanical agitation. The two denim fabrics as mentioned were of different colours and enzymatic fading action was supposed to differ from fabric to fabric. The enzymes were applied at concentrations of 0.5, 1.25 and 2% and treatment time was 30, 45 and 60 min for acid enzyme while it was 60, 75 and 90 min for the neutral cellulase. Desized samples were given the treatment in Infra red dyeing machine with required number of steel balls. An MLR of 1:30 was maintained while pH of the bath was adjusted with acetic acid. After the specified time of treatment, hot and cold wash were given followed by soaping with Lissapol D 1 g/l at 80 °C for 15 min. Then hot and cold wash were given and finally samples were dried.

Experimental design

To study the individual and interactive effects of the concentration of enzymes, treatment time and mechanical agitation and optimize the results, Box Behnken design was used. These three variables were chosen as they were expected to potentially affect the fading process. The limits of each variable were chosen based on the preliminary investigations. Colour strength, weight loss percentage and back staining values were taken as response factors. The three levels of the variables and the set of experimental combinations for all the three types of enzymes are shown in following tables (Tables 2, 3).

The other parameters namely temperature and pH maintained for the acid cellulase was 40–50 °C and 4.5–5.5, while it was 25–35 °C and pH of 6.5–7.5 for neutral enzyme. All the treatments were carried out at 45 rpm in Infra Red dyeing machine with digital programming system. The pH was maintained with acetic acid while temperature was monitored every 10 min. The contour plots obtained from the values in the observation tables were used for interpretation. Further, ridge analysis was used for optimization of values in the experimental design region.

Test methods

The extent of fading was determined by measuring the colour strength of the treated samples in Premier Colorscan SS 5100A spectrophotometer. The measurement was done using the formula

Table 2 Experimental conditions for the enzyme fading

Variables	Coded levels for different enzymes					
	Acid enzyme			Neutral enzyme		
	- 1	0	+ 1	- 1	0	+ 1
Concentration (%)	0.5	1.25	2	0.5	1.25	2
Time (min)	30	45	60	60	75	90
Mechanical agitation (number of steel balls)	0	5	10	0	5	10

Table 3 Experimental design based on coded levels

Sample no.	Time	Enzyme conc.	Mechanical agitation
E1	-1	-1	0
E2	1	-1	0
E3	-1	1	0
E4	1	1	0
E5	-1	0	-1
E6	1	0	-1
E7	-1	0	1
E8	1	0	1
E9	0	-1	-1
E10	0	1	-1
E11	0	-1	1
E12	0	1	1
E13	0	0	0
E14	0	0	0
E15	0	0	0

$$\text{Colour strength, } K/S = (1 - R)^2/2R$$

where R reflectance.

The effect of enzyme on cellulose was tested by finding the % age weight loss as per ASTM D 3776. Since enzyme action on denim often causes undesirable back staining, the intensity of the staining was also measured in terms of K/S . To check the impact of treatments on stiffness of the denim qualities, bending length was measured in Shirley Stiffness tester as per BS 3356 standard test method.

Results and discussion

Effect of acid cellulase on dark blue indigo dyed denim fabric

The impact of process parameters namely, enzyme concentration, time and mechanical agitation using Cellusoft Conc. L was studied on the K/S value of dark blue indigo and sulphur black dyed denim fabric using Box-Behnken design. The values so obtained for the vat dyed fabric were,

Multiple R	0.965
Squared multiple R	0.931
Adjusted squared multiple R	0.805
Standard error of estimate	0.459

The response model evaluated in this study is significant, with coefficient of determination R^2 of 0.931 at a confidence level of 95%. The response surface equation obtained for the K/S value is as follows:

$$\begin{aligned} \frac{K}{S} \text{ value} = & 18.725 - 0.470X - 0.332Y - 1.164Z \\ & + 0.185X^2 - 0.054Y^2 + 0.294Z^2 \\ & - 0.205XY - 0.11YZ + -0.072XZ \end{aligned}$$

where, X concentration, Y treatment time and Z mechanical agitation.

The model is very significant, as is evident from its F value ($F_{\text{model}} = 7.442$) and very low probability value ($p = 0.020$) obtained from analysis of variance (Table 4).

The trend in colour fading under actual experimental conditions are shown by the K/S value in Table 5, while the contour plots for the interactive effects are in Fig. 1a–c.

It was observed that colour strength of denim fabric decreased significantly after they were exposed to enzyme treatment particularly at higher concentrations of the enzyme. A portion of the primary wall of cotton is always in contact with enzyme during washing and hence at the contact point, surface of fibers are decomposed by the aqueous solution of the enzyme. Consequently, enzyme washed denim become duller and color is faded. As a result, the indigo colored warp yarn in denim fabric tends to restore its original white color, because warp yarns are surface dyed. The results show that increasing the enzyme concentration from 0.5 to 2% (owf) has effect on change in color strength.

Figure 1a, c also indicate that K/S value decreased with increasing treatment time. This is likely due to the fact that longer enzyme treatment time will prolong degradation of cellulose and the time for further abrasion. With regards to the effect of mechanical agitation, it is clear from Fig. 1b, c that the K/S value decreases with increase in mechanical agitation caused by number of steel balls. In fact, increasing steel balls leads to higher

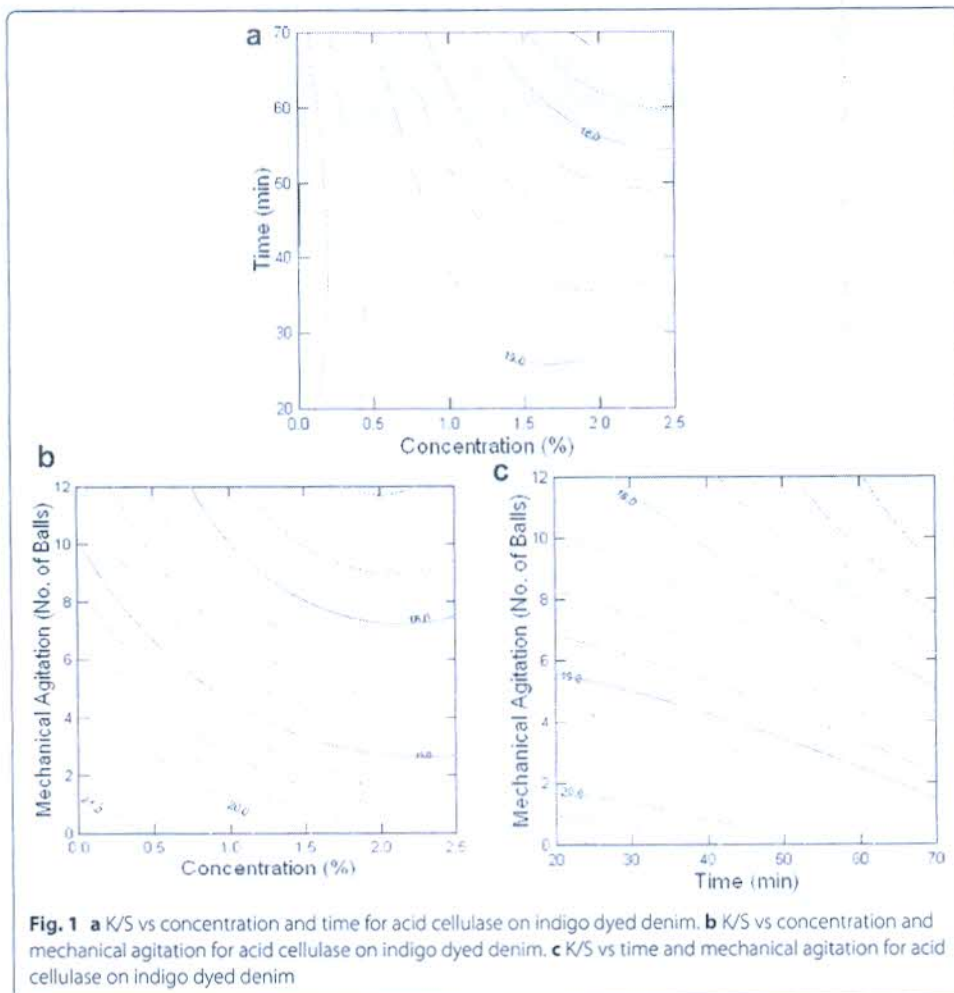
Table 4 Analysis of variance table

Source	df	Sum of squares	Mean squares	F-ratio	p value
Regression	9	14.128	1.570	7.442	0.020
Residual error	5	1.055	0.211		
Total error	14	15.182			

Table 5 Experimental conditions and results for the effect of acid cellulase on dark blue INDIGO DYED denim

Concentration (%)	Time (minutes)	Mechanical agitation (No. of steel balls)	K/S value	Weight loss (%)
0	0	0	22.32 ^a	–
0.5	30	5	19.38	2.94
2	30	5	19.17	3.01
0.5	60	5	18.94	3.72
2	60	5	17.91	4.55
0.5	45	0	20.79	3.03
2	45	0	19.39	4.52
0.5	45	10	18.87	5.16
2	45	10	17.75	5.35
1.25	30	0	20.63	3.04
1.25	60	0	20.17	4.75
1.25	30	10	17.78	3.59
1.25	60	10	17.27	5.09
1.25	45	5	18.99	4.44
1.25	45	5	18.38	4.32
1.25	45	5	18.79	4.52

^a K/S value of desized denim fabric is 22.32



removal of dye particles along with protruding surface fibers. Hence more prominent fading effects are observed i.e. K/S value decreases.

Optimum conditions for the K/S value

With the help of ridge analysis method of optimization of process variables, optimum fading with Cellusoft Conc. L enzyme is found to be at concentration 1.25–1.55%, time about 45–52 min and with 5–8 steel balls at 95% confidence level.

Effect of acid cellulase on sulphur black dyed denim fabric

Similarly the effect of Cellusoft Conc. L treatment parameters when studied on the K/S value of sulphur black dyed denim fabric, the values obtained are

Multiple R	0.954
Squared multiple R	0.910
Adjusted squared multiple R	0.747
Standard error of estimate	1.202

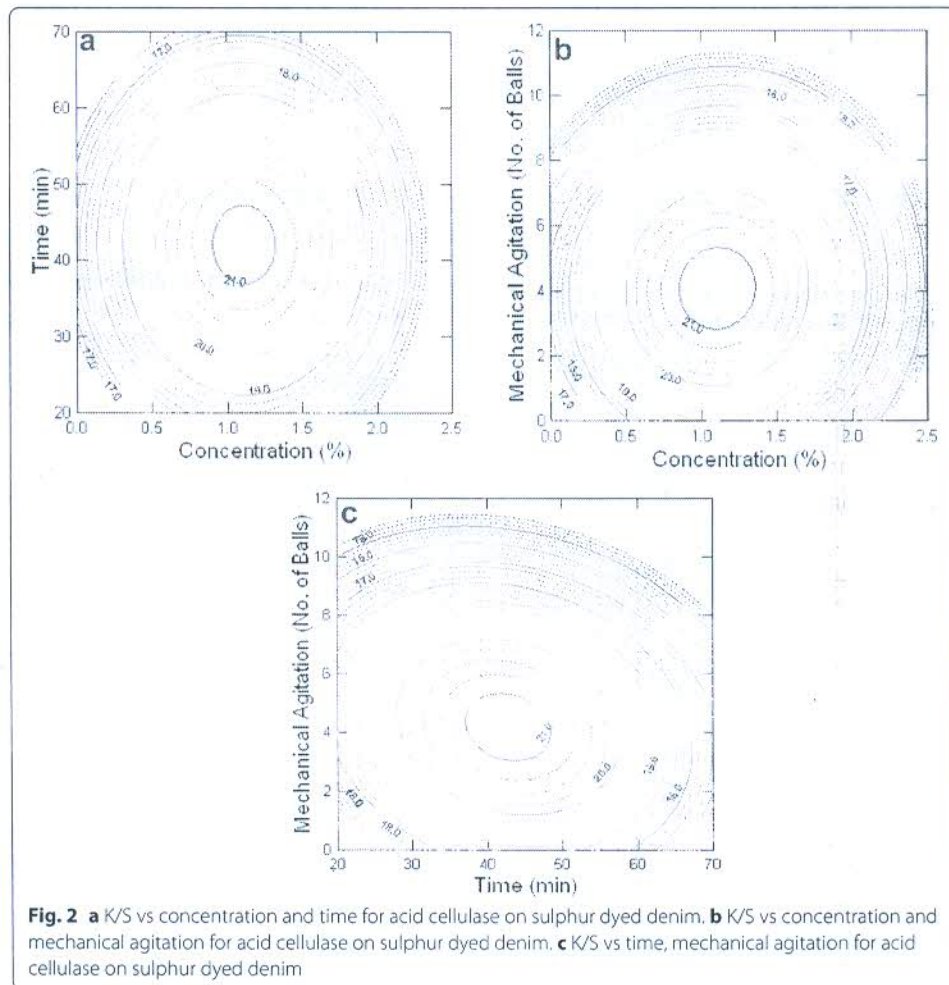
The response model evaluated in this study is significant, with a coefficient of determination R^2 of 0.910 at a confidence level of 95%. The response surface equation obtained for the K/S value is as follows:

$$\begin{aligned} \frac{K}{S} \text{ value} = & 21.046 - 0.683X - 0.486Y - 1.205Z \\ & - 1.856X^2 - 1.234Y^2 - 3.349Z^2 \\ & - 0.022XY - 0.665YZ + 0.18XZ \end{aligned}$$

where X concentration, Y treatment time and Z mechanical agitation.

This model is quite significant, as per its F value ($F_{\text{model}} = 5.597$) and very low probability value ($p = 0.036$).

It can be seen from Fig. 2a, b that the color strength of denim fabric decreased significantly after they were exposed to cellulase treatment particularly at concentrations of 1–2%. During washing, fiber surfaces are hydrolyzed by the catalysis of the cellulase and the treated fabric becomes duller and color is faded. The hair-like cotton fibrils are likely to be degraded first and partly detached from the main fiber chain and sulphur dye bonds are broken from the yarn surface. Rotating fabric inside the machine with



steel balls, hydrolyzes more bonds due to mechanical friction and restores original white color. The longer treatment time also accelerates this reaction (Fig. 2c). The fading in each of the trials is as indicated in Table 6.

Optimum conditions for the K/S value

Using ridge analysis method of optimization, optimum fading with Cellusoft Conc. L enzyme is obtained at concentration of 1.25–1.33%, time about 45–48 min and with 5–9 steel balls.

Effect of neutral cellulase enzyme on dark blue indigo dyed denim fabric

The correlation aspects for treatment of above fabric with Neutrancell CLD are as follows.

Multiple R	0.960
Squared multiple R	0.921
Adjusted squared multiple R	0.779
Standard error of estimate	0.474

The response model evaluated in this study is significant, with a coefficient of determination R^2 of 0.921 at a confidence level of 95%. The response surface equation obtained for the K/S value is as follows

$$\begin{aligned} \frac{K}{S} \text{ value} = & 19.514 - 0.337X - 0.624Y - 0.729Z \\ & - 0.052X^2 + 0.343Y^2 - 0.935Z^2 \\ & - 0.288XY + 0.385YZ + 0.093ZX \end{aligned}$$

where X concentration, Y treatment time and Z mechanical agitation.

Table 6 Experimental conditions and results for the effect of acid cellulase on sulphur black dyed denim fabric

Concentration (%)	Time (minutes)	Mechanical agitation (No. of steel balls)	K/S value	Weight loss (%)
0	0	0	26.88 ^a	–
0.5	30	5	19.38	2
2	30	5	17.06	2.49
0.5	60	5	18.89	2.94
2	60	5	16.48	3.19
0.5	45	0	16.67	2.56
2	45	0	15.95	2.73
0.5	45	10	15.37	3.5
2	45	10	15.36	4.5
1.25	30	0	18.43	2.07
1.25	60	0	18.36	2.4
1.25	30	10	15.89	3.37
1.25	60	10	13.15	4.5
1.25	45	5	21.60	2.44
1.25	45	5	20.97	3.06
1.25	45	5	20.55	2.1

^a K/S value of desized fabric is 26.88

The computed F ratio (6.487) and p value 0.027 (less than 0.05) shows that the model is significant.

In Fig. 3b, c plots, the interactive effect of variables indicates reduction in the color strength value with the increase in the level of mechanical agitation. This may be due to the fact that by increasing the number of steel balls applied, the abrasion of the fabric surface will increase which creates more accessible sites for enzyme attack. The combined effect of enzyme and mechanical action facilitates removal of indigo dye trapped in cellulose fibre (Cavaco-Paulo et al. 1999). Also, the fading increased with increasing treatment time as understood from Fig. 3c, for reasons similar to that in acid enzymes. With regards to the effect of concentration of enzyme, as expected the K/S value decreases with increasing enzyme concentration. However the fading is less compared to that with acid enzyme as observed from the values in Table 7.

Optimum conditions for the K/S value

Using ridge analysis method, optimum fading with Neutrancell CLD enzyme can be achieved at concentration of 1.25–1.33%, time 75–76 min and with 5–10 steel balls at 95% confidence level.

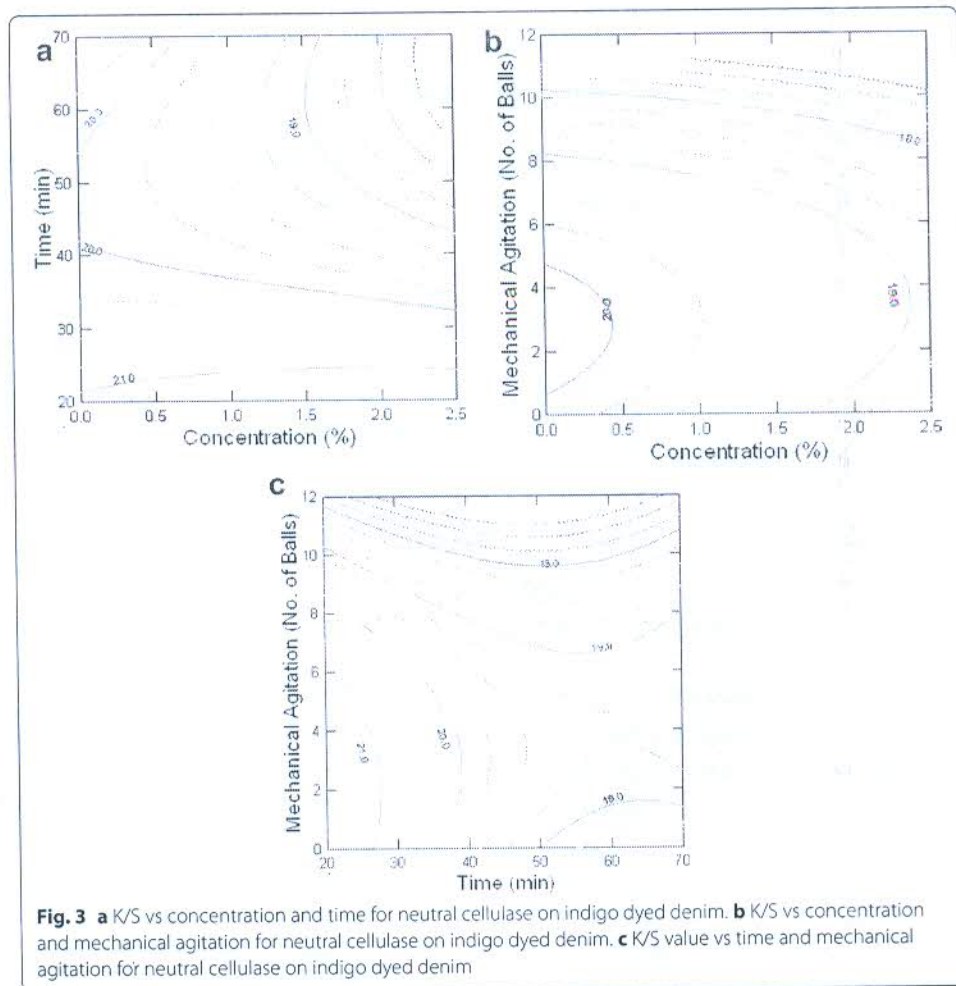


Table 7 Experimental conditions and measured values for neutral cellulase for dark blue indigo dyed denim fabric

Concentration (%)	Time (minutes)	Mechanical agitation (No. of steel balls)	K/S value	Weight loss (%)
0	0	0	22.32 ^a	–
0.5	60	5	20.68	0.47
2	60	5	20.48	1.41
0.5	90	5	19.70	0.57
2	90	5	18.35	2.23
0.5	75	0	19.35	0.45
2	75	0	18.59	1.32
0.5	75	10	18.27	1.49
2	75	10	17.88	2.94
1.25	60	0	20.70	0.53
1.25	90	0	19.07	1.00
1.25	60	10	18.00	0.94
1.25	90	10	17.82	1.97
1.25	75	5	19.88	0.80
1.25	75	5	19.12	0.81
1.25	75	5	19.52	0.74

^a K/S value of desized fabric is 22.32

Effect of neutral cellulase on sulphur black dyed denim fabric

The effect of enzyme Neutrancell CLD in terms of concentration, process time and mechanical agitation on the K/S value of sulphur black dyed denim fabric was studied as per experimental design and values obtained are shown.

Multiple R	0.988
Squared multiple R	0.977
Adjusted squared multiple R	0.936
Standard error of estimate	0.533

The response model evaluated in this study is significant, with a coefficient of determination R² of 0.977 at a confidence level of 95%. The response surface equation obtained for K/S value is as follows

$$\begin{aligned} \frac{K}{S} \text{ value} = & 19.143 - 0.310X - 1.378Y - 1.785Z \\ & - 0.661X^2 - 1.1001Y^2 - 1.739Z^2 \\ & + 0.355XY - 0.947YZ - 0.094ZX \end{aligned}$$

where X concentration, Y treatment time and Z mechanical agitation.

From the analysis of variance, the computed F-ratio and p value are 23.563 and 0.001 (less than 0.05) respectively which shows that the model is significant.

Considerable fading is observed for all the experimental samples as shown in Table 8. From contour plots (Fig. 4a–c), it can be seen that significant fading effect is obtained particularly at medium to higher concentrations on treatment with Neutrancell CLD enzyme. This is likely to be due to the fact that sulphur black dye being a dark shade have higher dye content on the fabric surface and during washing, along with the hydrolysis of

Table 8 Experimental conditions and measured value for neutral cellulase for sulphur black dyed denim fabric

Concentration (%)	Time (minute)	Mechanical agitation (No. of steel balls)	K/S value	Weight loss (%)
0	0	0	26.88 ^a	–
0.5	60	5	19.67	1.66
2	60	5	18.09	2.01
0.5	90	5	16.16	1.44
2	90	5	15.99	2.12
0.5	75	0	18.51	1.44
2	75	0	18.33	1.51
0.5	75	10	15.33	1.61
2	75	10	14.78	1.91
1.25	60	0	18.69	0.63
1.25	90	0	17.88	1.07
1.25	60	10	16.82	0.87
1.25	90	10	12.21	1.15
1.25	75	5	18.25	0.97
1.25	75	5	19.46	0.96
1.25	75	5	19.70	0.95

^a K/S value of desized fabric is 26.88

the surface fibre, sulphur dye-fibre bonds are also broken and higher amount of sulphur dye is removed from the fabric surface and faded look is obtained on the fabric surface. Higher mechanical agitation and longer treatment time assists this chemical reaction.

Optimum conditions for the K/S value

By applying ridge analysis method, optimum fading with Neutrancell CLD enzyme can be achieved at concentration in the range 1.25–1.28%, time about 75–82 min and with 5–9 steel balls at 95% confidence level.

Comparative analysis of action of enzymes on denim fabrics

To compare the effects of the two enzymes on the K/S value of the differently dyed varieties of denim fabrics, the K/S value of optimized samples are considered as shown in Fig. 5a. The fading effect of dark blue indigo and sulphur black dyed denims after enzymatic washing with Cellusoft Conc. L and Neutrancell CLD enzymes are shown in terms of K/S values. The enzymatic bio-washed denim samples showed an obvious decrease in K/S value as compared to the desized sample (control) due to the removal of surface dye particles along with the removal of short surface fibrils during treatment. The denim fabric treated with Cellusoft Conc. L enzyme showed higher fading effect compared to Neutrancell CLD enzyme, as the former is acidic in nature. Acid enzyme is more aggressive on the cotton cellulose (denim fabric) and causes more dye particles removal compared to neutral cellulase (Klahorst et al. 1994). The two cellulase enzymes differ in their amino acid compositions. The higher number of adsorption sites on acid enzyme is the likely cause for its stronger action (Campos et al. 2000). The result of weight loss (shown in Fig. 5b) also confirms the severity of Cellusoft Conc. L enzyme with greater weight loss %. Neutrancell CLD being neutral enzyme has milder action hence lower hydrolysis

level causing less weight loss % with lower reduction in the K/S value observed in indigo dyed denim samples.

Interestingly, the trend shown by sulphur dyed denim fabric is different from indigo dyed denim. This may be due to the reason that the dye removed from denim material after the treatment with cellulase cause back staining or re-deposition and re-coloration of black threads and black coloration of white threads, resulting in less contrast between black and white threads. Moreover, higher amount of dye is present on the surface of the fabric and hence more dye is released in the bath, thus resulting in heavy back staining. Cellusoft Conc. L being an acid enzyme shows higher level of back-staining as compared to neutral enzyme and results in less contrast or higher K/S value. Also sulphur dye particles have less affinity towards neutral cellulase as compared to acid cellulase. Thus, chances of back-staining are less and better contrast and higher reduction in K/S value is achieved with Neutrancell CLD.

Further study on back-staining

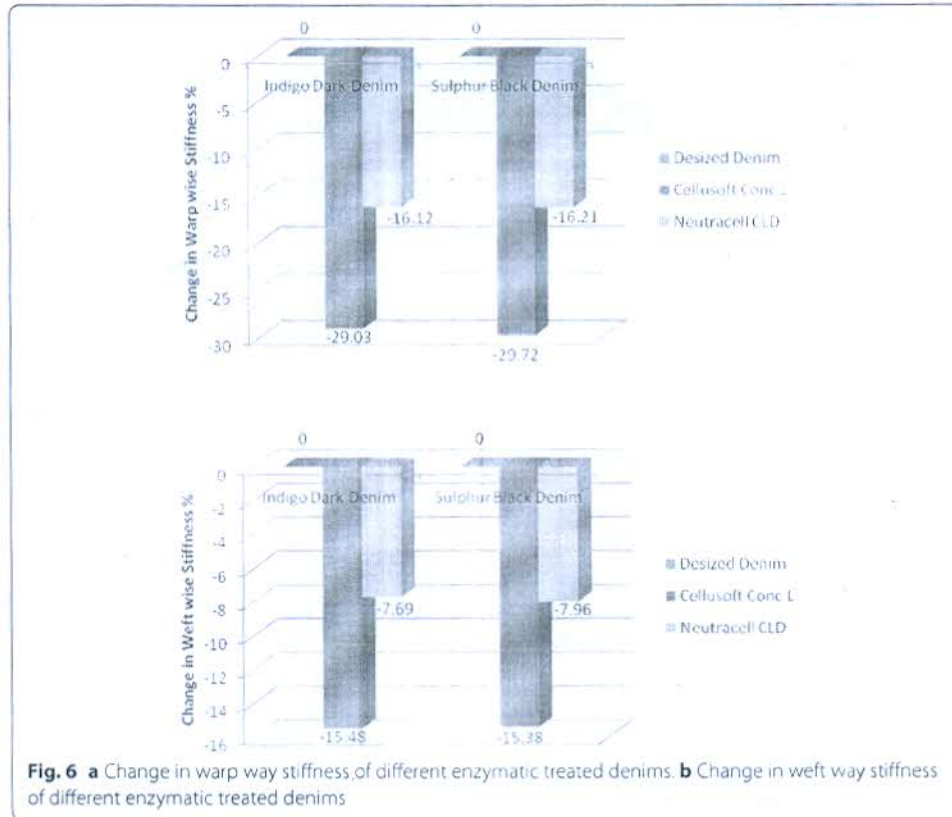
To study the effect of Denimax core-1380 on back-staining the K/S values of white cotton pocket material attached to both the denim fabrics was assessed with or without treatment of 1% of the stain regulating agent. In case of indigo dyed denim samples, no substantial difference was observed in the K/S values of white cotton pocket material, with or without the treatment. The fading effect of sulphur dyed denim samples with two different enzymes before and after Denimax core 1380 S treatment are shown in Fig. 5c and also for white cotton pocket lining fabric in Fig. 5d. The possible explanation for back staining in sulphur colour is as follows.

During enzyme washing, cellulose is degraded and sulphur dye is released. The cellulase enzymes are temporarily bound to the cellulose by means of an anchor. The surface fibre possibly gets split in terms of 1,4- β glycoside composition (Kumar et al. 1997). After this process it is made available for further hydrolysis reaction. The cellulose is degraded hydrolytically by cellulases partially until it becomes glucose. The glucose to some extent is likely to reduce the sulphur dye, both on the fibre and in the treatment liquor (Akram 2010). This reduced form has limited affinity to cellulose fibre and thus soils the weft thread and the pocket lining. The acid cellulase enzymes have a strong effect on cellulose hydrolysis and create more glucose formation, resulting in increased back staining of the denim garment. Neutral cellulase as compared to acid cellulase, are less aggressive and hence there is less back staining.

It is clear from Fig. 5c, d that the enzymatic washing along with Denimax core 1380 S imparts significant reduction in K/S value (back-staining) of the white cotton fabric (pocket material) as well as denim fabric surface. The K/S value (back-staining) for white cotton lining fabric is found reduced up to 48.22% by adding Denimax enzyme along with Cellusoft Conc. L enzymes. This may be due to the fact that Denimax core 1380 S is formulated with special anti redeposition agents to ensure minimal back-staining of the fabric.

Changes of fabric stiffness (bending length) after different enzymatic washing

The change in the stiffness of the fabrics after enzymatic treatment for both warp and weft way are shown in Fig. 6a, b. The stiffness of both denim materials reduced compared



to respective desized control samples. This may be due to the fact that the cotton fibres are loosened by degradation and partly detachment of fibrils causing increased softness. Moreover the rubbing action due to steel balls has a great influence on the increased softness of the denim fabrics. Consequently, bending length was less and stiffness got reduced. It is clear from the figures that the Cellusoft Conc. L has great influence on the stiffness in both warp and weft directions. Stiffness value was reduced up to 29.72 and 15.48% in warp direction and weft direction respectively. Neutrancell CLD being milder in action, showed lower reduction in stiffness.

Moreover, the figures show that in the warp wise direction reduction in stiffness is higher as compared to weft direction. This could be attributed to the construction of fabrics which were 2 ends up warp face twill weave. As a result warp yarns face higher amount of friction than weft yarns. The figures also shows that trend of reduction in stiffness in both warp and weft way direction treated with both the enzymes are similar for indigo and sulphur dyed denims. This may be because the effect of enzymes on stiffness is independent of the dye applied to the fabric.

Conclusions

The treatment of denim fabrics with cellulase enzymes gave effective results in terms of colour fading. The fading effect achieved was shown by the change in colour strength while the removal of surface fibres was clear from the loss in weight of the denim qualities. The effect was more in case of acid cellulase due to their stronger action than

neutral cellulose. However, in sulphur dyed fabric, the back staining was significant in case of acid enzyme, because of high colour removal and subsequently its redeposition. The application of anti-back staining agent was found to be quite useful in this case. Good softness was achieved in both the fabric qualities, shown in terms of decrease in bending length.

Authors' contributions

AKP, AM and NB carried out the enzyme studies on denim, participated in the sequence alignment and drafted the manuscript. All authors read and approved the final manuscript.

Author details

¹The Technological Institute of Textile & Sciences, Bhiwani 127 021, India. ²Panipat Institute of Engineering and Technology, Panipat 132 102, India.

Competing interests

The authors declare that they have no competing interests.

Ethics approval and consent to participate

Not applicable.

Publisher's Note

Springer Nature remains neutral with regard to jurisdictional claims in published maps and institutional affiliations.

Received: 27 July 2017 Accepted: 19 October 2017

Published online: 28 January 2018

References

- Akram, R. (2010) Anti back staining method for denim. Retrieved February 23, 2015, from <http://www.denimprocessing.blogspot.in/2010/01/anti-backstaining-method-for-denim.html>.
- Andreas, J., Campose, R., Gubitz, G., & Cavaco-Paulo, A. (2000). Influence of cellulases on indigo back staining. *Textile Research Journal*, 70(7), 628–632.
- Campos, R., Cavaco-Paulo, A., Andreas, J., & Gubitz, G. (2000). Indigo-cellulase interactions. *Textile Research Journal*, 70(6), 532–536.
- Cavaco-Paulo, A., Morgado, J., Andreas, J., & Kilburn, D. (1999). Interactions of cotton with CBD peptides. *Enzyme Microbial Technology*, 25, 639–643.
- Heikinheimo, L., Buchert, J., Miettinen-Oinonen, A., & Suminen, P. (2000). Treating of denim fabrics with *Trichoderma Reesei* cellulases. *Textile Research Journal*, 70(11), 969–973.
- Klahorst, S., Kumar, A., & Mullins, M. (1994). Optimizing the use of cellulose enzymes. *Textile Chemist & Colorist*, 26(2), 13–18.
- Kumar, A., Yoon, M., & Purtell, C. (1997). Optimizing the use of cellulose enzymes in finishing cellulosic fabrics. *Textile Chemist & Colorist*, 29(4), 37–42.
- Patra, A. K. (2003). Enzymes for wet-processing pretreatments. *Textile Asia*, 34(9), 46–51.
- Paul, R. (2015). Denim and jeans: an overview. In *Denim: manufacture, finishing and application*, (pp. 1–11). Woodhead Publishing, Cambridge.

Submit your manuscript to a SpringerOpen[®] journal and benefit from:

- Convenient online submission
- Rigorous peer review
- Open access: articles freely available online
- High visibility within the field
- Retaining the copyright to your article

Submit your next manuscript at ► springeropen.com



Journal of Emerging Technologies and Innovative Research

An International Open Access Journal

www.jetir.org | editor@jetir.org

Certificate of Publication

The Board of

Journal of Emerging Technologies and Innovative Research (ISSN : 2349-5162)

Is hereby awarding this certificate to

Satvika

In recognition of the publication of the paper entitled

**A CONTEMPORARY REVIEW ON ASPECT-BASED SENTIMENTAL
ANALYSIS**

Published In JETIR (www.JETIR.org) ISSN UGC Approved & 5.87 Impact Factor

Published in Volume 5 Issue 7 , July-2018

EDITOR IN CHIEF



JETIR1807685

Research Paper Weblink <http://www.jetir.org/view?paper=JETIR1807685>

Registration ID : 185338



Comparative Analysis of Vertical Fragmentation Techniques in Distributed Environment

Mukta Goel¹, Shalini Bhaskar Bajaj²

¹Assistant Professor, IT, TIT&S, Bhiwani, Haryana, India, ²Professor, CSE, AUH, Gurugram, India
¹rishu.muk@gmail.com, ²shalinivimal@gmail.com

Abstract: Distributed database management system is a software system that manages the distributed database system and makes distribution transparent to the user. Efficient distributed databases can be designed using database fragmentation, allocation and replication. Fragmentation can be applied horizontally or vertically. In this paper, various algorithms used in vertical fragmentation techniques are reviewed and compared. Algorithms reviewed are Apriori algorithm, Enhanced Minimum Spanning Tree algorithm, Modified Bond energy algorithm and Knowledge Oriented clustering technique. These algorithms result in fragmented database and further allocation and replication can be applied to these fragments.

Keywords: EMST, KO, MBEA, ECRUD Matrix, AUM.

I. INTRODUCTION

In distributed database system, database may be stored at multiple sites. Logically it belongs to the same system but is distributed geographically at multiple locations. These locations or sites are interconnected with each other through a network. Accessing the remote site provides some delay that is not desired, so this delay can be overcome by using database fragmentation technique. Database is divided into small fragments. Fragmentation can be done horizontally or vertically [1]. Horizontal fragmentation provides all the attributes to the users. Dividing database horizontally can reduce communication cost as fragments are allocated to those sites where they are most frequently accessed. But sometimes the user is not interested in all the attributes. In that case the horizontal fragmentation does not provide useful results as attributes are duplicated in different fragments. When only some attributes of a database are required by the user, then instead of horizontal fragmentation, vertical fragmentation is done. Vertical fragmentation divides the database according to columns i.e. now fragments are formed in terms of attributes instead of complete row. The attributes that are used frequently can now be placed in same fragment. For vertical fragmentation various algorithms can be applied: Apriori, Enhanced Minimum Spanning Tree, Modified bond energy and Knowledge based clustering.

After fragmentation, allocation techniques are required to distribute the fragments to their respective sites in the network. These techniques are most important in distributed databases and treated separately [2]. In

allocation, the fragment F is assigned to site S if it is most frequently accessed by site S. If a fragment is not accessed frequently at the site, then a copy of fragment can be allocated to that site. Assigning a copy of a fragment to a site is called replication. Allocation of fragments can be done at all sites, i.e. full replication or at selective sites, i.e. partial replication. The rest of the paper is organized as follows. Section (II) describes the formation of attribute usage matrix which will be used as the first step in all the algorithms. Section (III) describes the steps followed by all the vertical fragmentation techniques mentioned above. In Section (IV), allocation and replication of fragments is discussed. Section (V) concludes the various techniques described in section (III).

II. ATTRIBUTE USAGE MATRIX (AUM)

For fragmenting database vertically, usage of attribute at particular site is considered. Vertical fragmentation techniques use the Attribute Usage Matrix (AUM) [3]. AUM is 2-D matrix showing whether the attribute is accessed by query or not. If an attribute A is accessed by a query Q executing at site S then usage (A) at site S is represented by 1, otherwise 0. Usage of all attributes is represented as Attribute Usage Matrix. The following example shows the formation of Attribute Usage Matrix.

Example of Attribute Usage Matrix:

Consider a relation Emp with attributes Eid, Ename, Salary and City. Queries Q1, Q2, Q3 and Q4 are applied on the relation as shown below.

Q1: Find the Salary of Employee, if Eid is given

Select Salary

from Emp

where Eid = value;

Q2: Find the Eid, Ename and Salary of all Employees

Select Eid, Ename, Salary From Emp;

Q3: Find the name of Employee living in particular City

Select Ename

From Emp

Where City = value;

Q4: Find total Salary of Employees living in same City

Select sum (Salary)

From Emp

Group by City

Consider A1—Eid, A2—Ename, A3—Salary, A4—City. In AUM, rows represent queries and columns represent attributes as shown in Table 1. Value of each cell in the matrix will be either 0 or 1. Condition for inserting value in AUM is:

If A_i is used by Q_i then 1
 Otherwise 0

Table I. Attribute Usage Matrix (AUM)

	A1	A2	A3	A4
Q1	1	0	1	0
Q2	1	1	1	0
Q3	0	1	0	1
Q4	0	0	1	1

After AUM is formed a similarity matrix is generated, called Attribute Similarity Matrix (ASM) as shown in Table 2. This table is formed between the attributes of a relation. Number of queries accessing both attributes A_i and A_j together is shown in this matrix and this is called similarity between attributes. For example, A1 and A3 are accessed together 2 times by queries Q1 and Q2. This value is stored in ASM under column A3 and row A1 of attributes. Every cell in ASM shows access frequency of two attributes A_i and A_j together.

Table II. Attribute Similarity Matrix (ASM)

	A1	A2	A3	A4
A1	0	1	2	0
A2	1	0	1	1
A3	2	1	0	1
A4	0	1	1	0

Highly accessed attributes are placed together in same fragment. Now these AUM and ASM matrices will be used by different vertical fragmentation approaches discussed in section III to achieve fragmentation.

III. DISTRIBUTED DATABASE VERTICAL FRAGMENTATION TECHNIQUES

1. Apriori Approach:

In this approach [4] frequent item sets of attributes are determined. Frequent item sets are sets of those attributes which are called together very often by different sites. Frequent item sets are formed for a prescribed sites (support), i.e. for $\min(\text{support}) = 3$, an attribute must appear at least in 3 queries. The value 3 is support measure called $\min(\text{support})$. For generating frequent item sets, Attribute Usage Matrix of Table 1 is used. First of all support for each attribute is calculated separately. The attributes having value equal to or greater than $\min(\text{support})$ are called frequent items. Then list of all pairs of frequent items is generated so that they all meet or exceed the $\min(\text{support})$ value. If any pair is not frequent then its larger set cannot be frequent. So these item sets are pruned at this step. Then frequent sets of triples will be found excluding the pruned pairs of item sets. Frequent item sets of length k can be generated and all must follow the $\min(\text{support})$ value. For generating different combinations of attributes $\min(\text{support})$ can be varied. In this way using Apriori algorithm on Attribute Usage Matrix, frequent item sets of attributes are obtained. These frequent item sets are considered as fragments of the database. Each Fragment consists of different combination of attributes. Now fragments can be allocated and replicated to various sites.

Algorithm 1:

C_k : candidate item set of size k

L_k : frequent item set of size k

1. $L_1 = \text{find frequent 1-item set}$

2. For ($k=1; L_k \neq \text{null}; k++$)

{
 $C_{k+1} = \text{candidates generated from } L_k$
 }

3. For each transaction t in database

{
 Increment the count of all candidates in C_{k+1} that are contained in t
 }

4. $L_{k+1} = \text{Candidate in } C_{k+1} \text{ with } \min(\text{support})$

In Algorithm 1, fragmentation is done at initial stage. Different combination of attributes can be retrieved on the basis of $\min(\text{support})$. If $\min(\text{support})$ is higher, some important combinations may be lost. If $\min(\text{support})$ is lower, irrelevant combinations may be there. Main advantage of this approach is that it doesn't involve much calculation. The disadvantage is that it may not cover all attributes.

2. Enhanced Minimum Spanning Tree (EMST) Approach:

In this approach [5] an enhanced minimum spanning tree is formed using Attribute Usage Matrix (AUM) and Attribute Similarity Matrix (ASM), shown in Table 1 and 2 respectively. ASM matrix is used to represent the similarity measure between attributes, i.e. how many times the attributes of the relation are accessed together. From ASM, Enhanced Minimum Spanning Tree is generated. In the tree each node is represented as an attribute and the weight of edge between nodes specify the similarity measure. Minimum spanning tree is used to find out the shortest path between two nodes, but here it is used to find out the similarity between two attributes. So, rather than picking minimum weight edge, it will pick up the edge with highest weight because weights on the tree represent the frequency that how many times these two attributes are called together and it should be high. Following algorithm is used to generate enhanced minimum spanning tree:

Algorithm 2:

Input: ASM matrix, fragment K

Output: List of fragments

1. Transform the ASM into a graph G.
2. Generate minimum spanning tree.
3. Create the graph G by selecting any one vertex V.
4. Initialize Empty graph EG with the selected vertex V.
5. Select a list of edges E from G such that at most one vertex of edge E is in EG.
6. From E select the edge M with Maximum weight.
7. Add M to EG.
8. Repeat from step 5 until all vertices are added to EG.
9. Partition the relation removing K-1 edges from EG.

If the value of K = 2, then the edge with minimum weight is removed and tree is divided into two fragments. Now these fragments can be allocated to the sites. If more fragments are required then value of K can be increased. For example, If K = 3 then, K-1 = 2, edges will be removed and total fragments formed will be 3. Every time the edge removed will be of minimum weight so that the fragments will consist of attributes with highest similarity measure. This approach results in fragments that cover all attributes.

3. Modified Bond Energy (MBEA) Algorithm:

In bond energy algorithm, similarity between two attributes is calculated using affinity measure [6]. It is based on simultaneous access of attributes A_i and A_j by query Q_k as shown in Table 1. Along with AUM, frequency of query at particular site and access per execution is also considered. Affinity is calculated by

$$Aff(A_i, A_j) =$$

$$\sum_{use(Q_k, A_i)=1 \wedge use(Q_k, A_j)=1} \sum_{\forall S_l} freq_l(Q_k) * acc_l(Q_k)$$

$$use(Q_k, A_i) = 1, \text{ if } A_i \text{ is used by } Q_k$$

$$freq_l(Q_k) = \text{access frequency of query } k \text{ on site } l$$

$$acc_l(Q_k) = \text{access per execution of query } k \text{ on site } l$$

After calculating Affinity, clusters of attributes are generated using the split function. Split permutes the rows and columns of Affinity matrix and cluster matrix is generated. Permutation maximizes the global affinity measure.

In modified approach, when the two attributes have concurrent occurrence in a query then its similarity is considered and for the same query concurrent absence of the attributes could be considered as a weighted measure of similarity. Attribute Affinity Measure is modified and is denoted as S_{ij} .

$$S_{ij} = n_{11} + n_{00}/n_{11} + n_{00} + w_1(n_{01} + n_{10})$$

This formula gives the match between two attributes directly. Here n_{11} and n_{00} show number of simultaneous presence and absence of attributes. In denominator, n_{10} and n_{01} represent that only one attribute is accessed by the query at a time. Weights are assigned to dissimilar pairs on the basis of their contribution to the similarity. In this approach less similar attributes are separated correctly.

4. Vertical Fragmentation Based on Knowledge Oriented (KO) Clustering Technique:

In this approach, similarity between two attributes is calculated and is denoted as affinity [7]. Attributes which are accessed maximum number of times together by various queries have highest affinity. Attribute Usage Matrix and Attribute Similarity Matrix are used to calculate similarity. After constructing these matrices, reference measure for each attribute is calculated. Reference measure determines that how many times an attribute is accessed by a particular query and is denoted as $M(q_i, A_j)$. The following algorithm is used to construct fragments:

Algorithm 4:

1. Construct Attribute Usage Matrix
2. Calculate the reference measure of transaction q_i on attribute A_j
3. Calculate reference feature vector of each pair of attributes, such as VA_p and VA_r
4. Obtain similar matrix using $S(A_p, A_r)$

5. Place the attributes with highest similarity in same fragment.

In Algorithm 4, Reference measure of transaction q_i on attribute A_j is denoted by $M(q_i, A_j)$.

$$M_{ij} = M(q_i, A_j) = \text{Use}(q_i, A_j) * f_i$$

M_{ij} is the frequency with which transaction q_i reference attribute A_j .

f_i is frequency of execution of q_i on the sites. $\text{Use}(q_i, A_j)$ is obtained from AUM as shown in Table 1. So, M_{ij} obtain the frequency with which transaction q_i refers to attribute A_j .

VA_j is reference feature vector of attribute A_j with reference to the transactions (q_1, q_2, \dots, q_m). So VA_j will be:

$$VA_j = M_{1j}, M_{2j}, \dots, M_{mj} \text{ with respect to } q_1, q_2, \dots, q_m$$

The similarity measure of two attributes A_p and A_r now has two feature vectors with respect to transactions (q_1, q_2, \dots, q_m):

$$VA_p = (M_{1p}, M_{2p}, \dots, M_{mp})$$

$$VA_r = (M_{1r}, M_{2r}, \dots, M_{mr})$$

$$S(A_p, A_r) = \frac{\sum_{i=1}^m M_{ip} * M_{ir}}{\sqrt{\sum_{i=1}^m M_{ip}^2} * \sqrt{\sum_{i=1}^m M_{ir}^2}}$$

The result of this equation generates similarity matrix and give the similarity value for each pair of attributes. Attributes having the highest similarity are placed in same fragment. Least similar attributes are placed in different fragment. This provide multiple fragments and each fragment consist of similar attributes. In this approach there is no need to generate tree as in algorithm 2, but many calculations has to be done.

IV. ALLOCATION AND REPLICATION

Using one of the above techniques fragments are generated. But fragmentation does not work alone. Fragments are of no use unless these are provided to some site. For this, allocation procedures are used. Various allocation procedures can be used. One is allocation on the basis of site usage. For this, Site usage matrix can be formed. This matrix represents the usage of fragments on a particular site, i.e. how frequently a fragment is accessed by a particular site. Suppose fragment F_k has maximum frequency at site S_j then it will be allocated to S_j . The fragments with frequency less than $\max(\text{freq})$ are replicated at their respective sites. Only allocation is not sufficient so replication is also applied along with allocation [8, 9]. Another approach is use of CRUD matrix for allocation and replication. This matrix is used

to define create, read, update and delete operations performed by queries at site S_j . Mainly two operations are considered for allocation and replication: update and read. The site at which more update operations are performed on fragment F_k , will be allocated F_k and the site at which more read operations for F_k are performed, F_k is replicated there. Each fragment is allocated to at least one site and replicated at more than one site.

V. COMPARISON

The techniques described in section III are compared and Table 3 shows the various parameters considered.

First parameter is usage of CRUD (Create, Read, Update and Delete) operations. If any one of these operations is performed then its entry is recorded in AUM. Use of CRUD matrix reduces the complicated calculations. There is no requirement of empirical data about the frequency of user queries.

Second parameter, similarity measure, shows how many times the attributes are accessed together by same queries. Two ways are there to show the similarity between two attributes: formation of ASM, as shown in Table 2, and forming frequent item sets as used in Apriori algorithm. Both methods require AUM as an input.

Third parameter is Query Accessed Frequency measure. This shows how many times a query is accessed by different sites.

Fourth parameter is Storage Cost. It determines the cost of storing the attributes at particular site. This cost is considered so that it will be easy to find out whether a particular fragment should be allocated to that site or not. If cost is very high then fragment is not allocated to that site.

Fifth parameter is Communication Cost between sites. If a user is on local site S_i and accessing a particular fragment from remote site S_j then communication cost between S_i and S_j is considered. If it is high then it is better to replicate the fragment at local site instead of accessing the remote site.

Sixth parameter is Allocation. After fragmentation, allocation of fragments to the sites is done. Fragment is placed on the site where the access frequency of that fragment is highest.

Seventh parameter is Replication. Fragments can be placed at one site or more than one sites. Replicas of fragments are created and copied on the sites where the access frequency is high. Some algorithms cover only fragmentation and some cover all techniques like fragmentation, allocation and replication.

Table III. Comparison of Techniques

	EMST	KO	Apriori	MBEA
CRUD	Yes	No	No	No
Similarity Measure	ASM	ASM	Frequent Item Set	ASM
QueryAccessed Frequency measure	No	Yes	Yes	Yes
Storage Cost	No	No	No	Yes
Communication Cost between Sites	No	No	No	Yes
Allocation	Yes	No	No	Yes
Replication	Yes	No	No	No

VI. CONCLUSION

As shown in Table 3, only EMST technique uses enhanced CRUD matrix. This technique does not involve empirical data about query executions and does not take into consideration location of sites. It covers allocation and replication of fragments with multiple transactions at each site. EMST is graph based technique while KO and MBEA use similarity measure for making fragments. Number of fragments formed in KO and MBEA are decided on the basis of similarity, but in EMST and Apriori, user decide the number of fragments to be formed. Only fragmentation is of no use until it is provided to some site. So allocation is also discussed in EMST and MBEA. Allocation at one site does not provide good results every time so replication of the fragment is required at other sites. Sites are chosen for allocating replicas of fragments on the basis of the number of accesses for that particular fragment. This comparison provides a comprehensive study of various vertical fragmentation techniques proposed in literature and will provide a future direction to the researchers.

VII. REFERENCES

[1] S.I. Khan and A.S.M. Latiful Hoque, (2012) "Scalability and Performance Analysis of CRUD Matrix Based Fragmentation Technique for Distributed Database", 15th IEEE International Conference on Computer and Information Technology (ICCIT), 22-24 Dec, Chittagong, Bangladesh.

[2] Hassan I. Abdalla and Ali A. Amer, (2012) "Dynamic Horizontal Fragmentation, Replication and Allocation Model in DDBSs", IEEE International Conference on

Information Technology and e-Services, 24-26 March, pp. 1-6.

[3] Shahidul Islam Khan, Dr. A. S. M. Latiful Hoque, (2010) "A New Technique for Database Fragmentation", International Journal of Computer Applications, Volume 5- No.9, pp. 20-24.

[4] Ramesh Dharavath, Vikas Kumar, Chiranjeev Kumar, Amit Kumar, (2013) "An Apriori-Based Vertical Fragmentation Technique for Heterogeneous Distributed Database Transactions", Intelligent Computing, Networking, and Informatics, Advances in Intelligent Systems and Computing, Springer, New Delhi, vol 243, pp. 687-695.

[5] Ahmed E. Abdel Raouf, Nagwa L. Badr, M. F. Tolba, (2015) "An Optimized Scheme for Vertical Fragmentation, Allocation and Replication of a Distributed Database", IEEE Seventh International Conference on Intelligent Computing and Information Systems (ICICIS' 15), 12-14 December, pp. 506-513.

[6] Hossein Rahimi, Fereshteh-Azadi Parand, Davoud Riahi, (2016) "Hierarchical Simultaneous Vertical Fragmentation and Allocation using Modified Bond Energy Algorithm in Distributed Databases", Applied Computing and Informatics, Saudi Computer Society, King Saud University, pp. 1-7.

[7] Van Nghia Luong, Ha Huy CuongNguyen and Van Son Le, (2015) "An improvement on fragmentation in distribution Database Design Based on Knowledge-Oriented Clustering Techniques", IJCSIS, Vol. 13, No. 5.

[8] Ahmed E. Abdel Raouf, Nagwa L. Badr, M. F. Tolba, (2017) "Distributed Database System (DSS) Design over a Cloud Environment", Multimedia and Forensic Security, Springer International Publishing, Chapter 10, pp. 97-115.

[9] Jon Olav Hauglid, Norvald H. Ryeng, Kjetil Norvag, (2010) "DYFRAM: Dynamic Fragmentation and Replica Management in Distributed Database System", Distributed Parallel Databases, Springer Open Access, Vol. 28, pp. 157-185.



Functionalization of wool fabric using kapok flower and bio-mordant

Gurpartap Singh^a, Prasun Mathur^b, Nagender Singh^b, Javed Sheikh^{b,*}^a Dept. of Textile Chemistry, Technological Institute of Textile and Sciences, Bhiwani, India^b Dept. of Textile and Fibre Engineering, Indian Institute of Technology, Delhi, India

ARTICLE INFO

Keywords:

Wool
Tamarind seed coat
Kapok flower
Functional wool

ABSTRACT

The use of sustainable techniques for simultaneous colouration and functionalization of textiles is gaining momentum. The colouration of wool by kapok flower extract (KFE) utilizing pre-mordanting technique using tannin-based natural mordant could impart important functional properties to the dyed fabrics. In this study, the wool fabrics were mordanted using tamarind seed coats extract (TSCE) and further dyed with KFE. The effect of TSCE and KFE concentration on the colour values of dyed fabrics was analysed using various concentrations of TSCE and KFE. The dyed fabrics were evaluated for colouration properties (colour values, fastness properties) as well as functional properties like antibacterial and antioxidant activity. The dyed fabrics without pre-mordanting displayed satisfactory colour values ($K/S > 1.89$) along with satisfactory colour fastness (ratings > 3); however, the pre-mordanted wool displayed enhanced colour values and improved fastness ratings. The dyed wool also showed an excellent antibacterial activity (bacterial colony reduction $> 95\%$) against *E. coli* and *S. aureus*. The antioxidant activity of dyed fabrics was found in the range of 79–95%. A novel and sustainable way of functional dyeing of the wool was confirmed.

1. Introduction

In order to achieve sustainable dyeing, considerable emphasis has been given to the use of natural dyes for the colouration of textiles. Generally, synthetic dyes are widely used across the globe for a large number of industrial and domestic applications. Although, synthetic dyes has a better substantivity, affinity, fastness, and durability as compared to those of natural dyes and their natural counterparts, the shift from synthetic to natural dyes has been seen in the recent time mainly due to the toxicity and environmental issues associated with some of the synthetic dyes. Therefore, the use of eco-friendly dyes and pigments for dyeing of textiles is in high demand. Moreover, naturally occurring colourant offers several benefits like sustainability, biocompatibility, biodegradability and less effluent load. Apart from this, various functional properties can be imparted to textile materials using natural dyes (Shahid et al., 2019; Sharma et al., 2019; Ganesan and Karthik, 2017; Yadav et al., 2019; Shabbir et al., 2018; Baaka et al., 2018; Nazari, 2017). Hence natural dyes could be utilized for functional colouration of textile materials.

With the revival in the interest of scientific community towards the exploration of natural dyes, variety of research work dealing with dyeing of fibers such as cotton, linen, jute, wool, and silk using different

types of natural dyes was reported. There is a wide interest in the research community to explore new sources of natural dyes. Kapok plant is a natural resource which consists of around 150 pantropical species and about 26 genera (Chakraborty et al., 2010). Literature reports the various properties of kapok such as anti-HIV, anti-angiogenic, anti-inflammatory, antibacterial, antioxidant, UV protective, and hepato-protective (Vieira et al., 2009; Vidya et al., 2002). The kapok flower contains natural pigments like anthocyanin and carotenoid along with various biomolecules like flavones, flavonols, kaempferol, quercetin and anthocyanidins (El-Hagrassi et al., 2011; Rizvi and Saxena, 1974; Gopal and Gupta, 1972; Scogin, 1986; Niranjana and Gupta, 1973). Therefore, it will be interesting to explore the application of kapok flower extract as a textile dyestuff to impart functional properties to textiles. Some reports regarding dyeing of textile fibers using kapok flower colourant are available in literature (Chung et al., 2015; Sheikh et al., 2019).

Natural dyes show poor affinity for textile substrates. Therefore mordants have been extensively used for fixation of dyes on the textiles (Unzel and Akgerman, 2000; Mathur and Gupta, 2003). The mordants can be metallic or natural. Metal mordants such as chromium salts, ferrous salts and aluminium salts can be harmful to ecology and sometimes lead to permanent staining on the fabrics (Kamel et al., 2011).

* Corresponding author.

E-mail address: jnsheikh@iitd.ac.in (J. Sheikh).<https://doi.org/10.1016/j.scp.2019.100184>

Received 6 April 2019; Received in revised form 18 August 2019; Accepted 6 October 2019

Available online 22 October 2019

2352-5541/© 2019 Elsevier B.V. All rights reserved.

Thus, it is important to use the mordant which does not cause any environmental issue (Tepparin et al., 2012).

Rather et al. reported the ecological dyeing of woollen yarn with natural dye in the presence of natural tannin extracts (gallnut, pomegranate peel and babool bark) as biomordants and concluded a full potential of these bio-mordants to replace metallic mordants in wool dyeing (Rather et al., 2016). Haji, reported the dyeing of wool using *Runex Hymenosepolus* root as a natural mordant and *Berberis vulgaris* wood extract as natural dye (Haji, 2010). Baaka et al. reported the ultrasonic assisted dyeing of wool with grape pomace colourant using metallic mordant alum and various biomordants like chlorophyll-a, tannic acid and nimosa extract (Baaka et al., 2017). İsmal reported the dyeing of wool using natural dye of prina, a by-product of olive oil, using various biomordants such as pomegranate, rind, rosemary, valex, thuja and iris germanica. The fabrics pre-mordanted using biomordants showed equivalent fastness properties to those of fabrics pre-mordanted using metal salts (İsmal, 2017).

Tamarind seed coat (TSC) is a good source of tannins which could be utilized as a bio-mordant in natural dyeing of textiles. Tannins can crosslink fibers molecules; thus, the tannin-containing extracts could be used to retain the colour on the fabric (Tsuda et al., 1994a). Prabhu et al. determined the tannin class and total phenolic contents of tamarind seed coat extract and confirmed the presence of condensed tannins with total phenolic content of 365.12 mg/g gallic acid equivalent. They suggested the presence of phenolic OH groups which could be effectively utilized as mordant for natural dyeing of cotton, wool and silk (Prabhu and Teli, 2014). Several researches utilized of tamarind seed extract as a mordant in natural dyeing of textiles (Prabhu and Teli, 2014; Teli et al., 2012a, 2012b, 2013a, 2013b, 2013c, 2014; Sheikh et al., 2016). Efficient extraction of natural mordant from TSC using microwave (Teli et al., 2013a) and ultrasound assisted (Sheikh et al., 2016) techniques was reported. Efficient mordanting action of TSCE was also confirmed in natural dyeing of new fibers like bamboo rayon (Teli et al., 2013b, 2014), soyabean protein fiber (Teli et al., 2012a) and milk fiber (Teli et al., 2013c). The tamarind seed coat has been reported for its excellent antioxidant, antimicrobial and lipid peroxidation reducing properties (Lourith et al., 2009; Tsuda et al., 1995; Siddharaju, 2007). There are various components which are responsible for the antioxidant activity of tamarind seed coats like 2-hydroxy 3,4-dihydroxyacetophenone, methyl 3,4-dihydroxybenzoate, 3,4-dihydroxy phenylacetate and (-)-epicatechin (Tsuda et al., 1994b, 1995).

Even though a vast literature is available in the area of natural dyeing of wool, the reports regarding simultaneous dyeing and functionalization of wool using a combination of kapok flowers extract (KFE) and tamarind seed coats extract (TSCE) are not available. Hence, the dyeing of wool with KFE using a pre-mordanting using TSCE was attempted for the first time. The dyeability along with dye-fiber interactions were explored. The functionalities imparted to dyed wool fabrics were also studied towards their efficacies.

2. Materials and methods

2.1. Materials

The 100% wool fabric (EPI- 60/2, PPI-52/2, GSM-140), was supplied by WRA (Wool Research association) Thane, Mumbai, India. The fabric was scoured using 2gm/L nonionic soap at 80 °C for 20 min and further used for dyeing. The kapok (*Bombax ceiba*) flowers were collected from the local campus. Tamarind seeds were purchased from the local market.

2.2. Methods

2.2.1. Extraction of mordant and dye

Kapok flowers and tamarind seeds were dried in an oven. The flowers were crushed using mixer grinder to obtain a powder. Tamarind seeds were crushed using mortar and pestle to separate the seed coats which were

powdered using mixer grinder. The extraction of mordant and dye was done using the aqueous method. Stock solution (5%) of TSCE was prepared by heating the mixture of TS powder (5 gms) in 100 ml DI water at 90 °C for 60 min under continuous stirring. The extract was then filtered using nylon filter cloth (200 mesh), made to 100 ml using DI water and used for mordanting. The KFE was prepared in a similar manner.

2.2.2. Pre-mordanting and dyeing of wool fabrics

The exhaust method was used for pre-mordanting and dyeing of wool fabrics. During the pre-mordanting process, the wool fabrics were treated with different concentrations (5% owf, 10% owf, and 15% owf) of TSCE at 90 °C for 60 min. After that, the treated fabrics were squeezed and subjected to dyeing. The mordanted wool fabrics were dyed using KFE with different shade percentages (10% owf, 20% owf, 30% owf) at 90 °C for 60 min. The fabrics were further washed with cold water and dried. The pre-mordanting and dyeing were carried out in separate baths by keeping material to liquor ratio of 1:20 in rota dyer (Texlab, India).

2.2.3. Measurement of colour values and evaluation of fastness properties of dyed wool

The colour measurement (CIE L*, a*, b* and K/S) was done using Gretag Macbeth Colour-Eye 7000A spectrophotometer. The K/S values were calculated using the Kubelka Munk equation as given below:

$$K/S = \frac{(1-R)^2}{2R}$$

where, K/S represents the ratio of absorption coefficient to scattering coefficient, and R is the reflectance.

The washing fastness with respect to a change in colour and stain was measured using ISO 105-C06:1994 method. The wet and dry rubbing fastness was determined using crockmeter as per ISO 105-X12:2001 (ISO Technical Manual, 2006) standard. Light fastness was evaluated using ISO 105-B02 test method (ISO Technical Manual, 2006).

2.2.4. Evaluation of functional properties of dyed wool













The antibacterial properties of dyed fabrics were measured using AATCC 100 method against *E. coli* and *S. aureus* (AATCC 100, 2007). During the antimicrobial test, all fabric samples were inoculated with bacteria cultures, and then incubated under ambient conditions for 24 h. In a further process, the inoculated fabric samples were submerged in 20 ml of quenching solution and the containers were stirred for the transportation of bacteria from the fabric to the quenching solution. Then the fabric samples were removed, and 1 ml of the quenching solution containing the transferred bacteria was serially diluted with distilled water. A fixed volume of each dilution (100 µl) was inoculated onto agar plates and the plates were incubated at 37 °C for 24 h. The following equation was used to calculate the bacterial reduction:

$$\text{Bacterial Reduction (\%)} = \frac{(B - A)}{A} \times 100$$

where A = the number of bacterial colonies recovered from the inoculated treated test specimen swatches in the jar incubated for 24 h contact period and B = the number of bacterial colonies recovered from the inoculated untreated control test specimen swatches in the jar immediately after inoculation (at 0 contact time).

The antioxidant properties of dyed wool fabrics were measured in terms of radical scavenging activity using the 2,2-diphenyl-1-picrylhydrazyl (DPPH) assay method available in the literature (Sheikh and Esmailchacha, 2018). The fabric samples (1*1 inch) were kept in contact with 4 ml solution of DPPH radical (10⁻⁴ mol/l) prepared in methanol. The fabrics were kept in contact with solution for 30 mins and the reduction in absorbance of DPPH radical was measured at 517 nm.

Table 1
Colour values of dyed wool fabrics (at wavelength- 420 nm).

Sample No.	TSCE (%) owf	KFE (%) owf	K/S ^a	Increase in K/S (% with respect to unmordanted)	L*	a*	b*	Wool fabric image
1	Nil	10	1.89	0	74.25	1.69	9.30	
2		20	2.06	0	73.52	1.28	9.54	
3		30	2.15	0	72.51	1.54	10.36	
4	5	10	2.66	40.74	64.75	5.50	11.18	
5		20	2.66	29.12	66.42	5.38	11.95	
6		30	2.85	32.55	66.26	5.25	12.46	
7	10	10	2.90	53.43	63.13	6.78	12.10	
8		20	3.01	46.11	63.36	6.88	12.79	
9		30	3.44	60	57.02	4.41	8.46	
10	15	10	2.92	54.49	62.55	7.18	11.94	
11		20	3.19	54.85	62.26	7.23	12.32	
12		30	3.33	54.88	61.43	7.44	13.15	

^a Average value of three determinations, std. deviation $\pm 2\%$.

3. Results and discussion

3.1. Colour measurement

The colour values of dyed wool fabrics, pre-mordanted with TSCE and dyed with KFE extract, are tabulated in Table 1. Samples 1–3 were dyed without pre-mordanting process where the increase in colour strength with increase in dye concentration was observed. This indicates affinity of KFE towards the wool fabrics. Wool is a protein-based fiber and some free-amino end groups are available for dyeing. KFE extract consists of biomolecules which are anionic in nature. Thus, the

mechanism of dyeing could be the ionic interaction between fiber and KFE biomolecules. Similar observations were made by Chung et al. (2015). Higher colour values were achieved in case of dyed wool which were pre-mordanted using TSCE. The pre-mordanted and dyed wool fabrics have significantly enhanced colour values which were found increasing with the increase in mordant concentrations; however, the extent of increase at a fixed mordant concentration was lower with respect to increase in dye concentration. This validates the role of TSCE as a mordant. The role of mordant is to hold the dye, thus ensuring higher exhaustion and fixation along with better dye-fiber interactions which might be ensured through fastness ratings. The role of TSCE as a

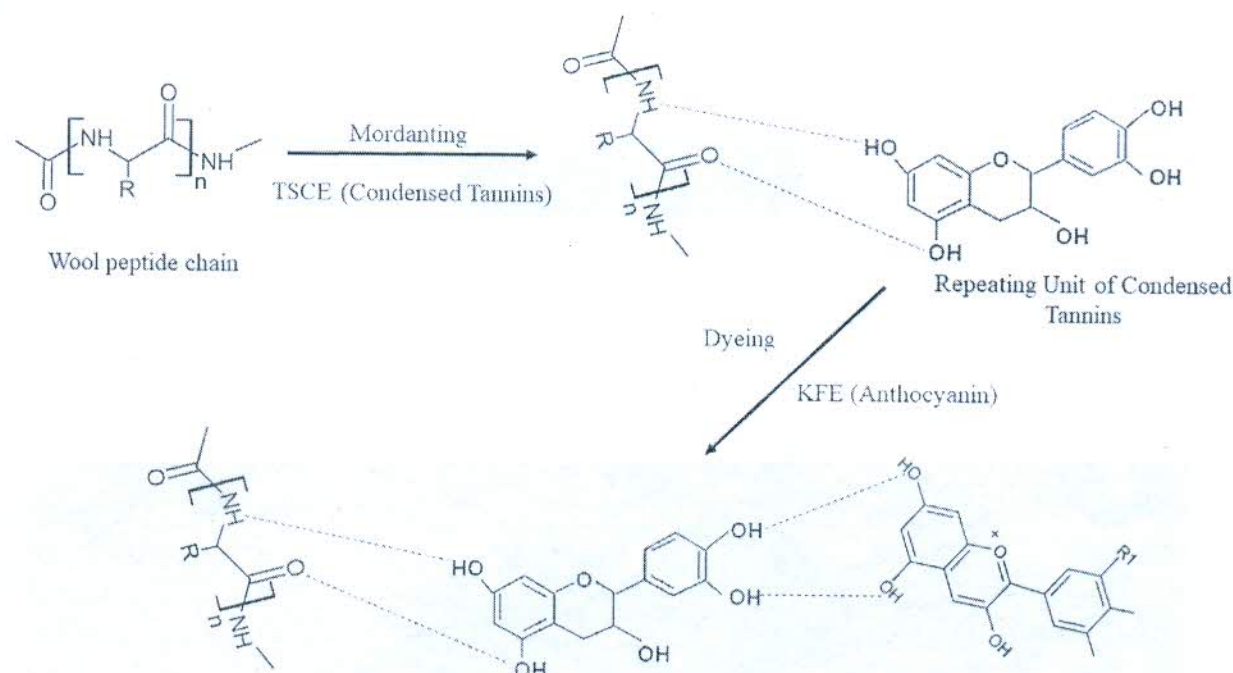


Fig. 1. Schematic diagram of the interaction of anthocyanin from KFE, condensed tannin from TSCE with wool peptide chain.

Table 2
Fastness ratings of dyed wool.

Sample No.	TSCE (%) owf	KFE (%) owf	Rubbing fastness		Washing fastness		Light fastness
			Dry	Wet	C	S	
1	Nil	10	4	3	3-4	4-5	3
2		20	4	3	3-4	4-5	3
3		30	4	3	3-4	4-5	3
4	5	10	4-5	3-4	4	4-5	4
5		20	4-5	3-4	4	4-5	4
6		30	4	3-4	4	4-5	4
7	10	10	4-5	3-4	4-5	4-5	4
8		20	4-5	3-4	4-5	4-5	5
9		30	4-5	3-4	4-5	4-5	5
10	15	10	4-5	4	4-5	4-5	5
11		20	4-5	3-4	4-5	4-5	5
12		30	4-5	3-4	4-5	4-5	5

mordant was already confirmed through various studies available in the literature (Prabhu and Teli, 2014; Teli et al., 2012a, 2012b, 2013a, 2013b, 2013c, 2014; Sheikh et al., 2016). TSCE contains condensed tannins which show affinity for wool fiber. There is ample opportunity of formation of H-bonding thereafter between the mordanted wool and KFE which results in better colour values. The interaction between wool fibre, TSCE and KFE biomolecule is represented in Fig. 1.

The dyed samples 1-3 (without pre-mordanting) showed redder-yellow tones (indicated by positive values of a^* and b^*). After dyeing of pre-mordanted samples, the samples showed higher values of a^* and b^* .

3.2. Fastness properties

The fastness properties of wool fabrics were evaluated and summarized in Table 2. The dry rubbing fastness of wool fabrics dyed with and without mordant was found in the acceptable range; however, the pre-mordanted samples displayed better fastness properties. The wet rubbing fastness rating was comparatively inferior which might be because of lower resistance of dye on fabric, especially on the surface to wet crocking. It must be noted that the dye present on the surface of the

fabrics is generally responsible for poor resistance which comes out during abrasive rubbing and stains the white fabric thus resulting in poor ratings. This is also an indication of poor dye-fiber interaction. In case of pre-mordanted samples (4-12), the rubbing fastness ratings were higher indicating the better resistance of the dye on dyed fabric. Even though the dyed wool sample pre-mordanted with 15% TSCE were darker, the fastness ratings were identical to those of other pre-mordanted samples. The acid-dyed wool samples with such fastness ratings are generally acceptable.

The washing fastness for samples 1-3 were found in the range of "Good" to "Very good". This also indicates a good interaction between wool fiber and KFE biomolecules. The rating showed negligible variation in case of pre-mordanted samples and the general ratings for washing fastness were in the acceptable range. The slight improvement (1/2 scale) in washing fastness was observed with increase in mordant concentration. The results assured that there is an enough interaction between dye molecules and wool through TSCE mordant. The tannin-based natural mordants make a bridge between dye molecules and fibers by chemical interaction which firmly holds the dye on fibers and results in an improved washing and rubbing fastness. Light fastness showed the similar trend where samples 1-3 showed slightly inferior but

Table 3
Antibacterial activity of dyed wool.

Sample No.	TSCE (%) owf	KFE (%) owf	Bacterial Colony Reduction (%) ^a	
			<i>E. coli</i>	<i>S. aureus</i>
3	Nil	30	95.00	96.35
6	5		96.55	96.27
9	10		97.22	97.14
12	15		99.44	99.87

^a Average value of three determinations.

Table 4
Antioxidant activity of dyed wool.

S. no.	Mordant concentration (%) owf	Dye concentration (%) owf	Absorbance at 517 nm	Antioxidant activity ^b (%)
1.	Nil	Nil	1.130 ^a	28.48 ^a
2.	Nil	30	0.851	46.13
3.	5		0.323	79.55
4.	10		0.275	82.59
5.	15		0.086	94.55

^a For undyed wool fabric.

^b Average value of three determinations.

acceptable ratings while the pre-mordanted samples showed better light fastness (ratings ≥ 4)

3.3. Antibacterial properties

The representative samples (with different TSCE concentrations at 30% (owf) KFE) were subjected to antibacterial testing and the results of antibacterial activity of dyed wool against *E. coli* and *S. aureus* are tabulated in Table 3. An excellent bacterial colonial reduction (BCR %) by all the dyed samples was observed. It is interesting to note that the samples 1–3 also displayed antibacterial activity. This might be attributed to the presence of polyphenolic compounds in the KFE. As expected, bacterial colony reduction by the dyed wool increased with an increase in the concentration of mordant. This happened due to the presence of polyphenolics, tannins, and flavonoids in the KFE and TSCE. These may hinder the bacterial growth in the agar plates. Herein, TSCE used as a mordant which itself is a natural ingredient and have condensed tannins which are astringent in nature. The phenolic composition of TSCE offers significant antibacterial properties. The phenolic constituents interact with the bacterial cell membrane which degrade the membrane and affect the permeability of membrane (Chandra et al., 2017). In natural dyeing, the achieved antibacterial properties are expected to be a combined result of dye and mordant. In this case, the non-leaching bacterial inhibition mechanism is expected where active components remain bound to fibers and inhibit the growth of bacteria coming in contact with them.

3.4. Antioxidant properties of dyed wool

The antioxidant activity was evaluated using the DPPH method by measuring the reduction in absorbance of DPPH radical in contact with wool fabrics at 517 nm. Table 4 shows the significant values of radical scavenging by dyed wool. The antioxidant activity of undyed wool fabric was 28.48% which was improved after dyeing. The polyphenolics and flavonoids in kapok flower along with the condensed tannins from tamarind seed coat extracts are responsible for the antioxidant property. There are many active components present in tamarind seed coats which are antioxidant (Prabhu and Tel, 2014; Lourith et al., 2009; Tsuda et al., 1994b, 1995; Siddhraj, 2007). These components interact with free radicals and stabilize the free radical. Thus, the dyed wool fabrics showed excellent antioxidant activity. Reports regarding antioxidant activity of linen dyed using KFE and metallic mordants are available in

literature (Shrikh et al., 2019). The various biomolecules in KFE are also capable of scavenging free radicals and the combined effect of TSCE and KFE resulted in enhanced antioxidant activity of dyed wool.

4. Conclusions

The kapok flower colourant was successfully extracted and utilized in dyeing of wool fabrics using tamarind seed coat extract as a natural mordant. The dyed wool fabrics showed very beautiful shades of colours. The wool fabrics dyed using pre-mordanting showed improvement in colour values and colour fastness to washing and rubbing. The functional properties, i.e. antibacterial (>95%) and antioxidant (79–95%) were found quite effective which can provide efficient protection against bacteria and free radicals. This complete sustainable approach of functionalization cum dyeing was confirmed using natural resources. Even though costing of such dyeing will be higher than that of conventional dyeing using synthetic dyes, the reported combination can be scaled up for specialized fabrics where sustainable dyeing and functional finishing is desired.

Acknowledgement

Authors gratefully acknowledge Science and Engineering Research Board (SERB, India) for ECRA funding (project File no. ECR/2017/001041).

References

- AATCC 190. 2007. Antimicrobial Activity Assessment of Textile Materials: Agar Plate Method. AATCC Technical Manual.
- Baoka, N., Haddad, W., Ben Ticha, M., Amorim, M.T.P., M'Henri, M.F., 2017. Sustainability issues of ultrasonic wool dyeing with grape pomace colourant. *Nat. Prod. Res.* 31 (14), 1655–1662.
- Baoka, N., Ben Ticha, M., Haddad, W., Amorim, M.T.P., M'Henri, M.F., 2018. Upgrading of UV protection properties of several textile fabrics by their dyeing with grape pomace colorants. *Fibers Polym.* 19 (2), 307–312.
- Chakraborty, D.D., Ravi, V., Chakraborty, P., 2010. Phytochemical evaluation and TLC protocol of various extracts of *Bombax ceiba* Linn. *Int. J. Pharm. Sci. Res.* 1 (8), 66–73.
- Chandra, H., Bishnoi, P., Yadav, A., Patil, B., Mishra, A., Nautiyal, A., 2017. Antimicrobial resistance and the alternative resources with special emphasis on plant based antimicrobials: a review. *Biomol. Res.* 16.
- Chung, T.W., Ny, P.F., Chan, Q., Fu, B., 2015. Dyeing performance of Kapok flower colourant on wool fabrics. *World J. Text. Eng. Technol.* 1, 23–27.
- El-Deghany, A.M., Ali, M.M., Osman, A.I., Shaban, M., 2011. Phytochemical, antibacterial and biological studies of *Bombax malabaricum* Poivre's. *Nat. Prod. Res.* 25, 141–151.
- Gunson, P., Luo, H., 2017. Analysis of colour strength, colour fastness and antimicrobial properties of silk fabric dyed with natural dye from red prickly pear. *Fruit. J. Text. Inst.* 108 (7), 1173–1179.
- Gujral, H., Gupta, R.K., 1972. Chemical constituents of salmali (*malabarica* schott and endl. Flowers). *J. Pharm. Sci.* 61, 807–808.
- Guzel, B., Akgerman, A., 2000. Mordant dyeing of wool by supercritical processing. *J. Supercrit. Fluids* 18 (3), 247–252.
- Haj, A., 2010. Functional dyeing of wool with natural dye extracted from *Berberis orientalis* L. and *Rumex* heterosepium (L.) as biomordant. *Iran. J. Chem. Eng. (Int. Eng. Ed.)* 29 (3), 55–60.
- ISO Technical Manual. Geneva, Switzerland, 2006.
- Ismail, O.E., 2017. Greener natural dyeing pathway using a by-product of olive oil, prima and biomordants. *Fibers Polym.* 18 (4), 773–785.
- Kamel, M.M., Abdelghaffar, P., El-Zawahry, M.M., 2011. Eco-friendly dyeing of wool with a mixture of natural dyes. *J. Nat. Fibers* 8 (4), 289–307.
- Lourith, N., Kanlayavattanakul, M., Chanpirom, S., 2009. Free radical scavenging efficacy of Tamarind seed coat and its cosmetics application. *J. Health Res.* 23 (4), 159–162.
- Mathur, J.P., Gupta, N.P., 2003. Use of natural mordant in dyeing of wool. *Indian J. Fiber Text. Res.* 28 (1), 90–93.
- Nazari, A., 2017. Efficient mothproofing of wool through natural dyeing with walnut hull and lemon against *Dermeestes maculatus*. *J. Text. Inst.* 108, 255–265.
- Nirmala, G.S., Gupta, P.C., 1971. Antibiotics from the flowers of *Bombax malabaricum*. *Phyto Med.* 24, 196–199.
- Prabhu, J. G., Tel, M.D., 2014. Eco-dyeing using Tamarindus indica L. seed coat tannin as a natural mordant for fabrics with antibacterial activity. *J. Saudi Chem. Soc.* 18 (6), 861–872.
- Rath, J.S., Shaban, M., Fokhri, B.N., Shrikh, M., Khan, M.A., Mohammad, F., 2019. Eco-friendly dyeing of woolen yarn with *Adiantum species* natural dye in the presence

- of biomordants as an alternative copartner to metal mordants. *J. Environ. Chem. Eng.* 4 (3), 3041–3049.
- Rizvi, S.A., Saxena, O.C., 1974. New glycosides, terpenoids, colouring matter, saponin and fatty compounds from the flowers of *Sida alba malabarica*. *Arzneimittelforschung* 24, 285–287.
- Scragin, R., 1986. Reproductive phytochemistry of *Bombax ceiba*: floral ambucyane and nectar constituents. *Aliso* 11, 377–385.
- Shabbir, M., Bathel, L.J., Mohammad, F., 2018. Economically viable UV protection and antioxidant finishing of wool fabric dyed with *Tagetes erecta* flower extract: valorization of marigold. *Ind. Crops Prod.* 119, 277–282.
- Shahid, M., Islam, Shahid ul, Rather, L.J., Manzoor, N., Mohenmad, F., 2019. Simultaneous shade development, antibacterial, and antifungal functionalization of wool using *Punica granatum* L. Peel extract as a source of textile dye. *J. Nat. Fibers* 16 (4), 555–566.
- Sharma, A., Kadam, S., Mathur, P., Shahid-ul-Islam, Sheikh, J., 2019. Re-using henna natural dyeing wastewater for coloration and multifunctional finishing of linen fabric. *Sustain. Chem. Pharm.* 11, 17–22.
- Sheikh, J., Bramhecha, J., 2018. Multifunctional modification of linen fabric using chitosan based formulations. *Int. J. Biol. Macromol.* 118, 896–902.
- Sheikh, J., Jagtap, P.S., Teli, M.D., 2016. Ultrasound assisted extraction of natural dyes and natural mordants vis-a-vis dyeing. *Fibers Polym.* 17 (5), 738–743.
- Sheikh, J., Singh, N., Srivastava, M., 2019. Functional dyeing of cellulose based (linen) fabric using *Bombax ceiba* (Kapok) flower extract. *Fibers Polym.* 20 (2), 312–319.
- Siddhuraju, P., 2007. Antioxidant activity of polyphenolic compounds extracted from defatted raw and dry heated *Tamarindus indica* seed coat. *LWT-Food Sci. Technol.* 40 (6), 982–990.
- Teli, M.D., Sheikh, J., Kamble, M., 2012. Simultaneous dyeing and antibacterial finishing of soyabean protein fabric using catechu and natural mordants. *J. Text. Assoc.* 73 (4), 227–233.
- Teli, M.D., Sheikh, J., Mahalle, K., Labade, V., Trivedi, R., 2012. Application of Tamarind seed coat in dyeing of cotton and silk using catechu and henna. *J. Text. Assoc.* 73 (2), 90–95.
- Teli, M.D., Sheikh, J., Jagtap, P.S., 2013. Microwave assisted extraction of natural dyes and natural mordants vis-a-vis dyeings. *Asian Dye* 10 (4), 32–38.
- Teli, M.D., Sheikh, J., Kamble, M., Trivedi, R., 2017. Simultaneous natural dyeing and antibacterial finishing of bamboo rayon using catechu and natural mordants. *J. Text. Assoc.* 78 (2), 68–74.
- Teli, M.D., Sheikh, J., Vallias, R., Yasin, P., 2013. Dyeing of milk fibre with marigold and natural dyes. *J. Text. Assoc.* 74 (1), 12–17.
- Teli, M.D., Sheikh, J., Kamble, M., Trivedi, R., 2014. Temple wares marigold dyeing and antibacterial finishing of bamboo rayon using natural mordants. *Int. Dyer* 199 (1), 28–32.
- Teppan, S., Sae-be, P., Suesat, J., Chumnum, S., Hongmang, W., 2012. Dyeing of cotton, bombyx mori and eri silk fabrics with the natural dye extracted from tamarind seed. *Int. J. Biosci. Biochem. Bioinform.* 2 (3), 159.
- Tsuda, T., Watanabe, M., Ohshima, K., Yamamoto, A., Kawakishi, S., Osawa, T., 1994. Antioxidative components isolated from the seed of tamarind (*Tamarindus indica* L.). *J. Agric. Food Chem.* 42 (12), 2671–2674.
- Tsuda, T., Watanabe, M., Ohshima, K., Yamamoto, A., Kawakishi, S., Osawa, T., 1994. Antioxidative components isolated from the seed of Tamarind (*Tamarindus indica* L.). *J. Agric. Food Chem.* 42, 2671–2674.
- Tsuda, T., Mizuno, K., Ohshima, K., Kawakishi, S., Osawa, T., 1995. Supercritical carbon dioxide extraction of antioxidative components from tamarind (*Tamarindus indica* L.) seed coat. *J. Agric. Food Chem.* 43 (11), 2803–2806.
- Vidya, L., Lenin, M., Varalakshmi, P., 2002. Evaluation of the effect of triterpenes on urinary risk factors of stone formation in pyridoxine deficient hyperoxaluric rats. *Photother. Rev.* 16 (6), 514–518.
- Vieira, F.O., Said, A., Abouabdi, E., Azzam, M., Greczynski-Pasa, T.B., 2009. Antioxidant activity of methanolic extract of *Bombax ceiba*. *Redox Rep.* 14 (1), 41–46.
- Yadav, R., Anubhav, Mathur, P., Sheikh, J., 2019. Antibacterial, UV protective and antioxidant linen obtained by natural dyeing with Henna. *Cellul. Chem. Technol.* 53 (3–4), 357–362.

AROMA CUM ANTIBACTERIAL FINISHING OF COTTON WITH INCLUSION COMPLEX OF β -CYCLODEXTRIN-CO-CHITOSAN AND OIL OF LAVENDER

*Shelly Khanna¹, Amandeep Kaur¹

¹ Fashion & Apparel Engineering department, The Technological Institute of Textiles and Sciences, Bhiwani, Haryana, India

Email: sh_khanna2002@yahoo.com

Abstract: Host-guest complex of β -cyclodextrin-co-chitosan and lavender was employed for the combined aroma cum anti-bacterial finishing of cotton textiles. The modified host viz. β -cyclodextrin-co-chitosan was synthesized with the use of β -cyclodextrin citrate as the intermediate for the achievement of the satisfactory yield of the host. FTIR analysis was carried out for the characterization of β -cyclodextrin-co-chitosan and also the surface modification of the functionalized cotton with the modified host. ¹HNMR spectra of the inclusion complex of β -cyclodextrin-co-chitosan and Lavender had confirmed the formation of a strong complexation between the two compounds. The functional as well as physical properties as aroma retention, anti-bacterial assessment, tensile strength, crease recovery, bending length and air permeability were investigated both for the host-guest complexed cotton and lavender alone treated cotton. The aroma retention and a strong inhibition zone was found more pronounced in the functionalized cotton instead of the oil alone treated cotton, which can be a promising and potential cadre of application of multi faceted textiles.

Keywords: Host-guest, β -cyclodextrin-co-chitosan, anti-bacterial, β -cyclodextrin citrate, FTIR, ¹HNMR

1. INTRODUCTION

Aromas have been used widely in different fields such as textile, medicine, food, tobacco, leather, papermaking, cosmetics and many more because of their antibacterial effect, sedative effect and tranquillization[1-3]. Nowadays, finishing a textile with aroma is an important commercial target and an engineering challenge. Pure aroma compounds and essential oils have been used traditionally in folk medicine for a long time. Aroma finishing has been increase in demand since last one decade, as well as tremendous competition in the market, opens up opportunities for value addition to all forms of textile materials[4]. Over the last 50 years, plants are utilized as a potential source of natural aromas in the form of essential oils. It is reported that the essential oils with high aromatic index offers advantage of insect

repellency and prohibit the growth of microorganisms[5]. Aroma finished textiles are an important entry into the field of textiles for trend conscious people[6]. A fragrant finished fabric is the one, where, the aroma is attached and incorporated into the fabric surface in a way that the aroma is slowly released, refreshing the mood and emotions of human being. Finishing a textile with long term aroma and with not much change in physical properties of textile is a desirable commercial goal as well as a textile chemistry and engineering challenge with two aspects; the amount of aroma applied to the textile must have good durability and the aroma is released in a slow and controlled manner. The aromatic matter was added in traditional dyeing, printing or finishing processes producing a perfumed fabric. However, the durability of aroma imparted was analyzed to be poor. Addition of aromatic matter into synthetic fiber polymer during fiber formation can create a fragrant fiber that exhibit good aroma durability. But, the limitations of this method was the time from fiber formation to final product, loss of fiber properties due to the presence of aroma, loss of aroma during textile processing, difficulty in changing the aroma, and inability to use this technique on natural fibers[7]. Many other techniques are also available to impart aroma into textiles, however, the need and development of the techniques which not only enhance the slow release property but also not affect the properties of textile is yet to be clearly defined.

The aroma compounds are volatile substances that can easily vaporize to give sense of smell. The most difficult task in preparing the aroma therapeutic textile is to prolong the lifetime of aroma. Micro-encapsulation technique is an effective solution of this difficulty[8,9] but it suffers from a number of limitations as external stimuli is needed to activate the microcapsules, loading of microcapsules can be carried out once in their life time and fabric hand gets stiffer as binders are a necessity for adhering and

fixing microcapsules to the textile surfaces. Instead, the macromolecular containers as cyclodextrins can be preferentially loaded with the newer guests every time after the depletion of the guest molecules and fabric handle is also maintained softer without any adverse effect on other functional properties. Also, β -CDs considered as the environmental friendly microcapsules because they are biodegradable and non-toxic[10].

The cyclodextrins are produced by certain microorganisms of cultivated starch and are non-reducing cyclically linked oligosaccharides, which are capable of forming inclusion compounds with molecules that fit into their cone-shaped hydrophobic cavity[11]. These cavities of cyclodextrins can hold liquid, gases and solid particulates properly and can act as a slow releasing host with the prospects of refilling the cavities again with a variety of guests. As a result of the inclusion compounds between the host-guest associations, the physico-chemical properties of the compounds are changed, i.e. the vapour pressure of volatile substance is reduced, stability against light or air is enhanced, harmful and/or unpleasant odour in the surrounding may be eliminated[12]. No hydrogen and covalent bonds are formed or broken during the formation of such host-guest complexes[13]. β -Cyclodextrin (β -CD) is the most commonly used derivative of cyclodextrins as these are the cheapest, nontoxic for oral use, causes no skin irritation, no skin sensitisation, no mutagenic effect, does not cause any problems in water and are also biodegradable[14]. β -CD can be incorporated onto textile by means of spraying, printing, padding, grafting, surface coating, impregnation and ink jet printing[15] but it suffers from a major limitation that it has no inherent affinity for any fibre. Different mechanisms are used to fix β -CD on textile substrates viz. grafting with the use of crosslinking agents such as polycarboxylic acids onto cotton, [15,16,17] wool,[15,18] polyester [19,20] polyamide [21] and polyacrylonitrile fibres [22]. Resins such as epichlorohydrin can also be used to fix β -CD to cellulose [23,24]. The derivatives as Monochlorotriazine β -CD and hydroxylpropyl β -CDs are also gaining importance among durable host-guest complexes. Chitosan is utilized in the textile industry as an antimicrobial agent due to its inherent ability to provide protection against allergies and infections, diseases, coupled with moisture retention and wound healing capabilities [25].

Thus, an attempt was carried out to synthesize β -CD-co-chitosan, characterization with FTIR and HNMR for the development of inherently durable fragrant cum anti-microbial textiles for hi-end niche market with the infusion of lavender essential oil.

2. EXPERIMENTAL

2.1 Materials

Thoroughly pre-treated 2/1 twill woven cotton fabric possessing epi (64), ppi (78), warp (2/40 Ne^s), weft (2/20 Ne^s) and gsm (236) was used as control for finishing with Lavender essential oil for aroma as well as anti-microbial finishing. All the analytical grade chemicals, viz. β -cyclodextrin (β -CD; M.W~1134.98 g/mol), citric acid anhydrous (M.W 192.129 g/mol), formic acid, sodium hypophosphite, silicon softener, sodium hydroxide, ethanol, oil, Isopropanol and lavender were supplied by SDFL, Mumbai. Chitosan (M.W 50000 g/mole) was sourced from India sea food (regd.) from Kochi, Kerala. Water bath (Laboratory glassware co. Ambala), Electronic pH meter (PH-009(I)), Electronic weighing balance (CAS Model MW -11 series), UV/Visible spectrophotometer (Lab India analytical UV 3000⁺), Orbital shaker (Bio-Technology Lab, M.D.U Rohtak), Padding mangle (Electronic and Engg. Company), Drying oven (Kaypee udyog, Ambala), Laundrometer (RBE, Mumbai), Digital Tensile strength tester (Globe Tex Industries), Shirley Stiffness tester, Crease recovery tester (Shirley), Air permeability tester (Prolific) and FTIR (Perkin Elimer) were used for the assessment of aroma stability; anti microbial activity (AATCC: 147-2004) and effect on physical properties as Tensile strength (IS: 1969-1968), Stiffness (IS: 6490-1971), Crease recovery (IS: 4681-1968) and Air permeability (IS: 11056-1984).

2.2 Methods

2.2.1 Calibration and Optimization of lavender for aroma analysis

Calibration of lavender was done by measuring the aroma of different concentrations of lavender as (1, 2, 3, 4, 5, 6, 7, 8, 9 and 10 %) in 100% ethanol. Maximum wavelength (λ_{max} ~344nm) of lavender was measured by taking any concentration of oil in ethanol as a blank sample through UV/Visible spectrophotometer. Concentration versus absorbance curve was plotted on UV/Visible spectrophotometer according to Beer Lambert's law. A calibration curve was thus obtained and it was used for the detection of unknown concentration of aroma in the sample.

Ten oil concentrations (1, 2, 3, 4, 5, 6, 7, 8, 9 and 10 %) in 100% ethanol were prepared. Ten cotton samples were independently immersed in each concentration of oil for 1 min, followed by padding (2dip, 2nip) and Drying (at room temperature). The release of oil was investigated for the optimization of oil concentration with the extraction of oil as- Extraction of oil was done by taking 0.1g of each

treated sample, immersing in 100 % ethanol with 1:50 ML followed by heating of test tube at 50°C in water bath for 5 minutes, cooling and finally removing the samples from the solutions. Absorbance of each concentration of lavender was measured with the help of UV/Visible spectrophotometer at $\lambda_{\text{max}} \sim 344\text{nm}$. The same procedure was repeated after a time span of 2 hours each up to 72 hours by exposing samples in dirt and dusty environment. Effect of time on aroma retention was also measured by calculating unknown concentration of aroma.

2.2.2 Synthesis and characterization of β -CD-co-chitosan

The synthesis of β -CD-co-chitosan was carried out according to the previous procedure without any major modification i.e. by a two step process-synthesis of β -CD citrate followed by its modification for the production of β -CD-co-chitosan. β -CD citrate concentration (0.54g) was introduced into a solution containing chitosan (0.6g) dissolved in formic acid concentration (0.4ml/1g chitosan) using M:L (1:15). The reaction mixture was then magnetically stirred and heated at 100°C for 3 hour at the end the reaction, the product was precipitated by adding 100 ml of NaOH solution (0.2 N). The sample was thoroughly washed with distilled water till natural (pH- 7) to ensure the removal of un-reacted β -CD-C. Finally, treated cotton was washed with acetone and oven dried at 60°C for 24 hours²⁶. FTIR was used to characterize the synthesized component.

2.2.3 Application and characterization of β -CD-co-chitosan on cotton

Cotton was treated with 80 gpl of synthesized β -CD-co-chitosan in the aqueous medium of formic acid to aid its solubility via pad, dry, cure and rinsing technique on cotton. FTIR was used to characterize the presence of β -CD-co-chitosan on cotton as a modification of control.

2.2.4 Treatment of control and β -CD-co-chitosan functionalized cotton with lavender

Control and β -CD-co-chitosan functionalized cotton were treated with lavender by taking its optimized concentration as discussed in section 2.2.1. Cotton was immersed in the optimized concentration with 100 % ethanol (v/v) for 1 minute, padded at 1 Kpa (2dip and 2 nips) and finally air dried at room temperature. ¹H-NMR spectra was investigated for the inclusion complex formation between β -CD-co-chitosan and lavender.

2.2.5 Performance evaluation of oil treated cotton

The treated cotton was evaluated for the aroma release; Qualitative and Quantitative assessment, laundering durability, tensile strength, bending length, crease recovery, air permeability and antimicrobial activity. Comparative analysis of physical and functional properties was performed for oil treated non-functionalized and β -CD-co-chitosan functionalized cotton. **Qualitative Aroma release** was carried out as – Intensity of scent was performed by a group of 5 persons in which, standard sample of each recipe was first given to the panel to rank the test specimen. Evaluation was done for the treated samples which were packed in an airtight polythene bag so that there was no release of aroma in between evaluation due to air or light. Panel was allowed to take 3-4 whiffs for each sample in an open corridor and rank them in prepared rating scale from 1 to 5. Coding of preference was done and analyzed to obtain relative results of scent intensity. The rating was between '5' which meant the strongest scent and '0' which meant no scent. The higher the rating, the stronger the aroma intensity on the finished sample would be. The aroma retention was observed for 72 hours after the treatment. **Quantitative Aroma release-** UV/Visible spectroscopy was used for the quantitative evaluation of % retained aroma as- The aroma was extracted from 0.1g of cotton samples (oil alone and host- oil complex) immersed in 100 % ethanol with 1:50 ML ratio then test tube heated at 50°C in water bath for 5 minutes, cooled it, followed by removing the cotton samples from the ethanol solutions. Absorbance of the extracted aroma was measured with UV/Visible spectrophotometer at λ_{max} . The observations were taken at 0, 2, 4, 6, 12, 24, 48 and 72 hours to find the % retained aroma intensity after predetermined time span and to evaluate the aroma release rate. Release rate was calculated using Equation 1.

Equation 1:

$$\text{Release rate of fragrance} = \frac{\text{Immediate concentration} - \text{concentration after: hours}}{\text{Immediate concentration}} \times 100 \quad \text{-- 1}$$

Laundering durability was assessed as- 4 cm x 10 cm strips of oil treated cotton were washed according to ISO 105-C01:1989 with 5 gpl of soap solution with M:L of 1:50 at 40°C \pm 2°C for 30 minutes. Washed cotton were rinsed with running tap water for 10 minutes and dried at room temperature. % retained aroma was observed according to the procedure earlier mentioned. **Tensile strength** of cotton was carried with a gauge length of 8" inches (IS: 1969-1968). **Bending length** was measured with IS:6490-1971, **Crease recovery** was measured with a test

method (IS:4681-1968), Air permeability was determined by testing using (IS:11056-1984) and AATCC Test Method 147-2004 standard was followed for anti-bacterial testing. Parallel streak method is a qualitative method to determine antibacterial activity of diffusible antimicrobial agents on treated textile materials. The average width of a zone of inhibition along a streak on either side of the test specimen was calculated using the following equation: $W = (T - D)/2$; where: W = width of clear zone of inhibition in mm, T = total diameter of test specimen and clear zone in mm, D = diameter of the test specimen in mm.

3. Results and Discussion

3.1 Calibration and Optimization of lavender

The lavender was required to be calibrated against blank at λ_{max} for the evaluation of % retained aroma on cotton. The graph was plotted between absorbance values (Abs) and concentrations of lavender (Conc.) in mol/l. The slope of the linear line was calculated. The equation is: $y = mx + b$ or $Abs = (Slope \times Conc.) + 0 = 0.088 \times concentration$ as shown in Figure 1. The optimization of lavender was obtained at λ_{max} using UV/Visible spectrophotometer after time spans of 2 hours each up to 72 hours as shown in Table 1 and retained fragrant oil with time in Figure 2.

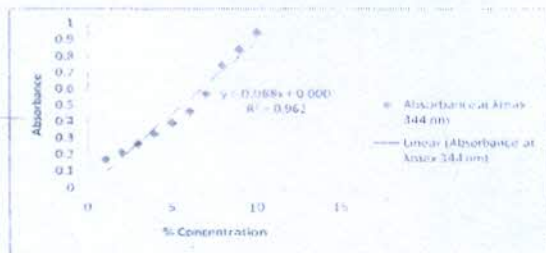


Figure 1. Calibration curve of Lavender oil

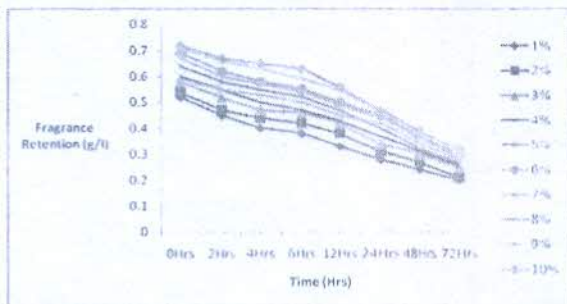
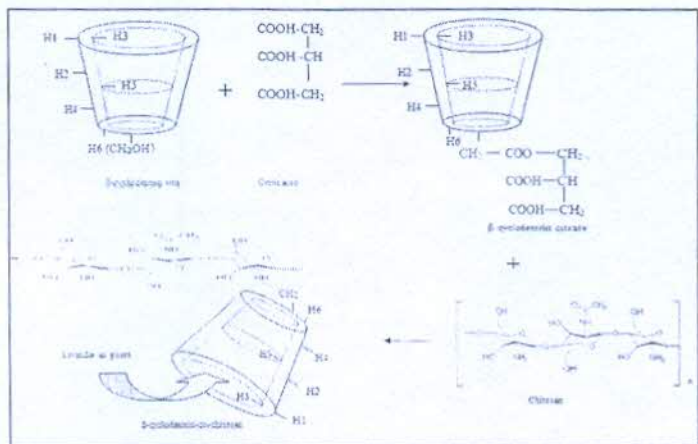


Figure 2. Effect of time on fragrance retention at various concentrations

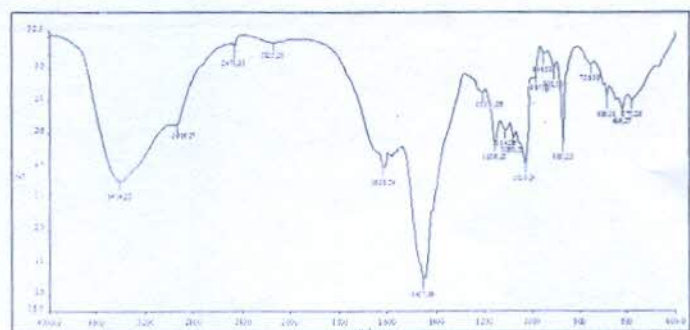
It was observed that at 6% lavender, maximum absorbance was obtained which indicated that at this concentration, maximum lavender was deposited on cotton. Higher absorbance indicated more quantity of lavender extracted into the solution and hence confirmed the presence of more lavender on the cotton too.

3.2 Synthesis and Characterization of synthesized β -CD-co-chitosan

The reaction mechanism of β -CD-co-chitosan synthesis is shown below in Reaction 1. It can be inferred that the β -CD citrate was used as the intermediate for the attachment of chitosan to the β -CD ring, which was later removed as citric acid in the form of by-product and further neutralized in the presence of an alkali. The degree of substitution of chitosan with β -CD rings varied as per the citric acid concentration.



Reaction 1. Synthesis mechanism of β -CD-co-chitosan



a)

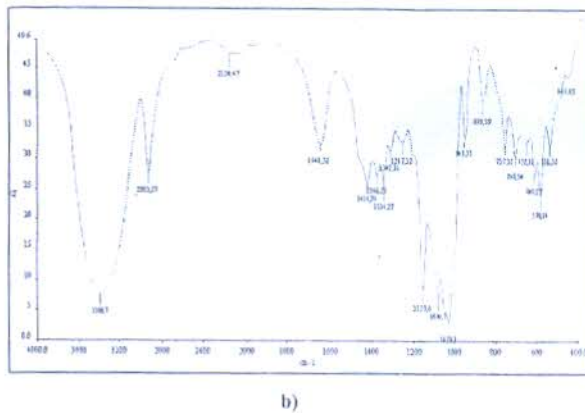
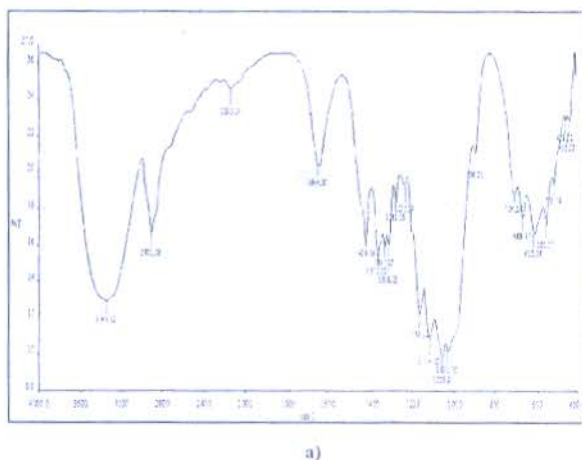


Figure 3. FTIR of a) native β -CD b) β -CD-co-chitosan

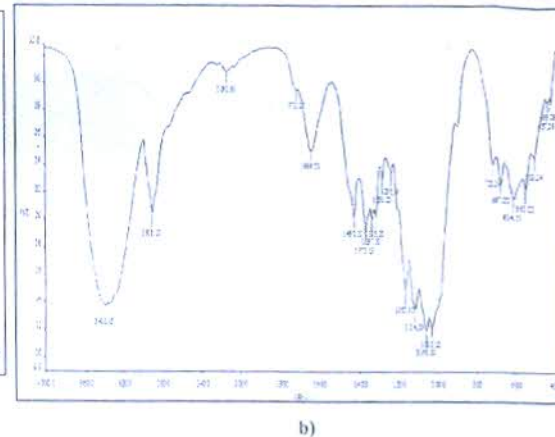
The comparative FTIR spectra of β -CD and β -CD-co-chitosan had shown that native β -CD presented the strong absorption band at 3388 cm^{-1} assigned to O-H stretching. The characteristic peaks of β -CD at 1029 and 2925 cm^{-1} that are related to C-O and C-H stretching were also detected. By comparing the transmittance spectra of β -CD and β -CD-co-chitosan, an additional absorption peak of 3404 cm^{-1} , attributed to O-H stretching and N-H stretching was observed. The absorption bands at 1114 cm^{-1} (C-O stretching) and 1628 and 1457 cm^{-1} (C=O of amide I and II) were the characteristic peaks of β -CD-co-chitosan. The FTIR had confirmed the modification of the native β -CD with the chitosan group (Figure 3).

3.3 Characterization of β -CD-co-chitosan on cotton

The application of β -CD-co-chitosan on cotton was assured by the modification of the treated cotton as compared to control by the use of FTIR spectra.



a)



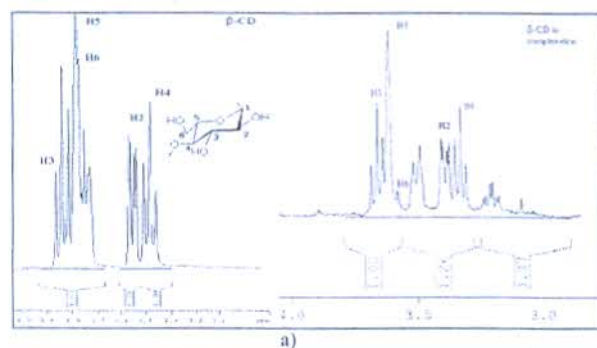
b)

Figure 4. FTIR spectra of a) control b) cotton functionalized with β -CD-co-chitosan (%T Vs cm^{-1})

FTIR-spectra of cotton treated with β -CD-co-chitosan indicated strong additional ester peak at 1730 cm^{-1} . This peak indicates the formation of carboxylic ester of β -CD-co-chitosan with cellulosic hydroxyl groups of cotton to be functionalized, which was not apparent in the control as shown in Figure 4 a and b. Also, the treated cotton had shown O-H and N-H stretching (-NH₂ in primary amides) at 3348 cm^{-1} in comparison to 3411 cm^{-1} in control.

3.4 ¹HNMR analysis of inclusion complex of β -CD-co-chitosan and lavender

The control and cotton functionalized with β -CD-co-chitosan both were treated with 6% lavender in ethanol medium for aroma finishing as described in section 2.2.4. HNMR spectra were investigated to assess the formation of inclusion complex between β -CD-co-chitosan and lavender as a host-guest system as a comparison of both the compounds in their pure states as shown in Figure 5.



a)

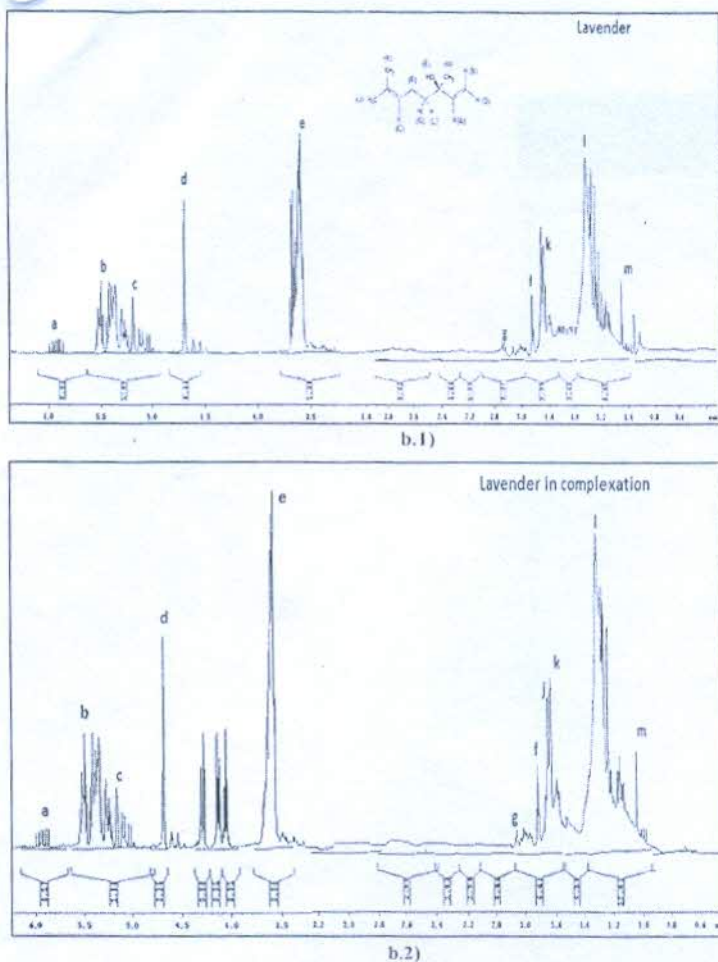


Figure 5. HNMR of a) β -CD in pure and complexed form with lavender b.1) lavender in pure state b.2) lavender in complexed state with β -CD (concentration of pure compounds~ 10mM; concentration of β -CD: lavender ~ 5mM; 5mM)

The respective chemical shifts ' δ ' and induced chemical shifts ' $\Delta\delta$ ' (The induced shift, is defined as the difference in chemical shifts in the absence and in the presence of the other reactant) as detailed in Table II. The chemical and induced chemical shifts of β -CD and lavender in free as well as in compounded state had revealed evident shifts in the β -CD and oil in free and complexed state. This signified the formation of dynamic complexes between the anchor and the guest. The chemical shifts had shown significant entrapment of oil molecules into the cavities as the induced shifts of proton H5> H3 was found for lavender.

The above table shows that induced chemical shifts were pronounced in both the host (β -CD-co-chitosan) and the guest (Lavender) during complexation process. H3 and H5 protons in β -CD-co-chitosan and Hj and Hk protons in lavender had shown the maximum shift when complexed together. This had

also shown that no newer peaks were formed in the complexed spectra of host-guest system; that could be assigned to the fact that complexation was a dynamic process, the included oil being in a faster exchange between the free and bound states.

3.5 Performance evaluation of lavender treated control and functionalized cotton

3.5.1 Qualitative analysis-

Aroma evaluation was done qualitatively by panel judgment for scent intensity as shown in Table III. Cotton finished with both the techniques gave noticeable scent intensity after 24 hours but cotton treated with lavender alone did not retain any aroma after 24 hours, on the other, oil treated functionalized cotton was scented even after 72 hours. The reason might be the cavities of β -CD that were capable of holding aroma of lavender. Along with this, ester linkages between cotton and β -CD-co-chitosan also stabilize as well as suppress the release of lavender. This was attributed to the slow release of lavender from the surface of cotton.

3.5.2 Quantitative analysis-

For the Quantitative assessment of the aroma retention, it was observed that there was an increase in release rate of fragrance from both categories of finished cotton with span of time i.e. about 91.72% oil was released from lavender alone cotton but only 36.33% was sublimated from the Host guest-complexed cotton. The initial release of oil was primarily dependent upon the presence of oil either alone on the fabric or in the complex form. Minimum aroma oil's release rate was observed from cotton with host-guest complex (β -CD-co-chitosan and lavender) as per the quantitative evaluation of extracted lavender from the lavender treated cotton as it retained maximum fragrance even after 72 hours. The reason might be the linkage of β -CD chitosan and cotton to retain the fragrance even after long span of time as seen in Figure 6.

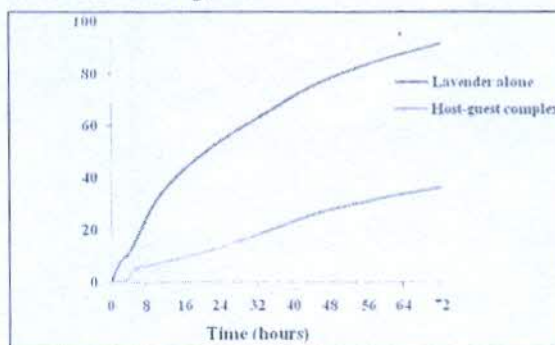


Figure 6. % Release of lavender from treated cotton with time

3.5.3 Laundering durability

The durability to laundering of the lavender treated cotton was investigated as shown in Figure 7. Lavender when applied alone on cotton gave significant release in fragrance after three washing cycles. Aroma was released by almost 25.8 % after 3rd subsequent wash due the weak interactive forces between cotton and lavender resulting in its quicker release. On the other, host-complexed cotton had shown a significant improvement in aroma durability as aroma release rate was significantly low (10.53% after 3rd wash). This was attributed to the cavities of β -CD which were capable of forming inclusion complex with the lavender as guest. The lavender dimensionally fitted into the cavities of host molecules, thereby, releasing the aroma in a suppressed manner. Thus, to improve the retention of fragrance for longer duration, lavender was enclosed with β -cyclodextrin as host.

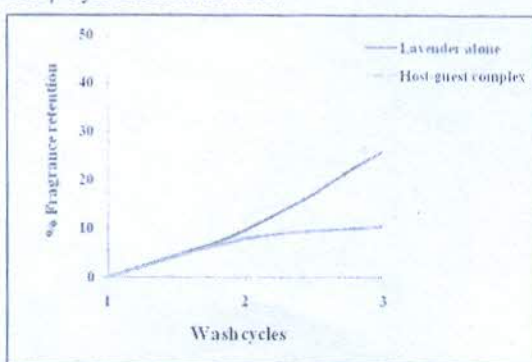


Figure 7. Effect of wash treatments on % fragrance retention of treated cotton

3.5.4 Effect of aroma treatment on physical properties of cotton

The effect of aroma treatment on physical properties of cotton alone and host-complexed cotton is detailed in Table IV.

Tensile strength (TS) had shown an increase when cotton was finished with lavender alone and also with the complex of β -CD-co-chitosan and lavender. The tensile strength of cotton finished with β -CD-co-chitosan and lavender shows higher tensile strength of the two treatments due to the ester linkage between modified host and hydroxyl groups of cotton which lessened the restriction of segmental movement of cellulosic chains in the fiber and prevented the fiber from being tendered severely. The above results had shown that host-complex treatment had added bit **stiffness**

(**BL**) to the treated cotton due to mechanical deposition of finishing chemicals in the open interstices of the fabric or due to cross linking reaction between cellulosic molecules of fiber and β -CD-co-chitosan; due to this, extra cross linking chains were developed between fiber segments that increased the abrasion resistance of fiber segments, thereby restricting the bending of fibers which made the fabric more rigid. The change in the **crease recovery (CR)** angle of treated cotton is elucidated in the above Table. Crease recovery angle of cotton treated with β -CD-co-chitosan shows minimum recovery angle as compared to the other treatment due to the deposition of finishing chemicals in the pores of cotton and physical bonding between adjacent molecular chains of cotton and chitosan. There was a noticeable change in the **air permeability (AP)** of treated cotton due to the closing of open interstices due to mechanical deposition of β -CD-co-chitosan as a film on cotton. In addition, swelling of hydrophilic cotton would had changed the fabric porosity and thickness that resulted in decrease of air permeability of both the treated cotton as compared to control.

3.5.5 Assessment of anti-bacterial activity of control and treated cotton

The three specimens of control, lavender treated cotton and lavender treated functionalized cotton were investigated for ant-bacterial activity. Nil activity was seen for the control (A), little was observed for the lavender alone treated cotton (B) and maximum inhibition zone was observed for cotton finished with host-guest complex of β -CD-co-chitosan-Lavender (C). The reason might be the presence of chitosan, as it is a cationic antimicrobial agent particularly for external disinfection and the target site of the cationic biocides is the cell envelope of bacteria. Chemical modification of chitosan via it's coupling with β -CD improves its antimicrobial activity due to the enhancement of dissolution of chitosan and the creation of carboxyl groups along with chitosan molecules serve in the dissolution of phospholipids area and causing leakage of intercellular components and finally the death of the microorganisms as shown in Figure 8.

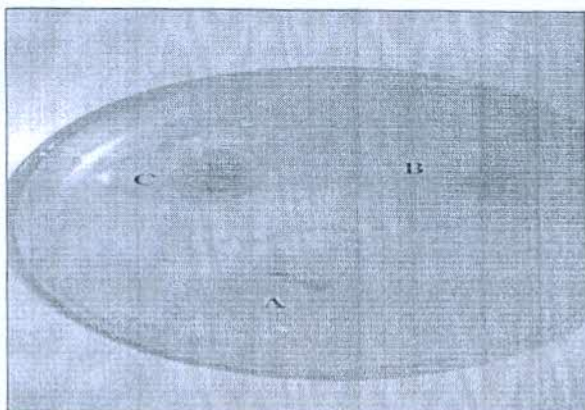


Figure 8. Inhibition of control and treated cotton A. control B. Lavender alone treated cotton C. Lavender treated on host-guest complexed cotton

4. CONCLUSIONS

β -CD-co-chitosan was synthesized and characterized for the development of modified host-guest system to impart aroma and anti-bacterial finishing. Aroma release (Qualitative and Quantitative) and laundering durability was excellent for the β -CD-co-chitosan and Lavender inclusion complex rather than when lavender treated alone on cotton. The physical properties viz. tensile strength had shown an improvement due to the use of the modified host, on the other, bending, crease recovery and air permeability were only marginally affected. The combination of chitosan and lavender had shown appreciable antibacterial activity and inhibition zone for the development of antibacterial cum aroma finished textiles.

References

- M. Toda, and K. Morimoto, "Effect of lavender aroma on salivary endocrinological stress markers", *Arch. Oral B.* vol. 53, pp. 964-968, 2006.
- G. Kyle, "Evaluating the effectiveness of aromatherapy in reducing levels of anxiety in palliative care patients: Results of a pilot study", *Complementary Ther. Clinical Practice*, vol. 12, 2, pp. 148-155, 2006.
- N. Gordon, "Microencapsulation in textile finishing", *Rev. Prog. Coloration*, vol. 321, pp. 57-64, 2001.
- G. Buchbauer, "Methods in Aromatherapy Research", *Perfume and Flavorist*, vol. 21, pp. 31-36, 2006.
- Matsushi-Shikiso Chemical Co. Ltd. "Fixing Odors to Textiles. High-Performance-Textiles", vol. 8, 2000.
- S.Y. Cheng, C.W.M. Yuen, C.W. Kan, and Cheuk, K.K.L., "Imparting cosmetic effects on textile" *Colourage*, vol. 8, pp. 68-78, 2008.
- S. Li, J. E. Lewis, N. M. Stewart, L. Qian, and H. Boyter, "Effect of finishing methods on washing durability of microencapsulated aroma finishing" *J of Tex Inst.*, vol. 99, 2, pp. 177-183, 2008.
- Shirley Institute, "New Finishes Using Microencapsulation", *Textile Month*, vol. 5, pp. 49, 1988.
- W-P. Mei, "Application of Microencapsulation Technology in Textile Coloration and Finishing" *Journal-China-Textile-Institute*, vol. 5, 3, pp. 188-191, 1995.
- T. Boonsod, *Finishing cotton and silk fabric with Glyoxal- β -cyclodextrin complexes*. Graduate School, Kasetsart University, 2007.
- H. J. Buschmann, D. Knittel, and E. Schollmeyer, "Resin finishing of cotton in the presence of cyclodextrins for depositing fragrances", *Melliand Textilbericht*, vol. 72, 3, pp. 198-199, 1991.
- H. J. Buschmann, "The Use of Cyclodextrins in Textile Processes" *J of Tex Inst.*, vol. 89, pp. 554-561, 1998.
- M. Singh, R. Sharma, and U.C. Banerjee, "Biotechnological applications of cyclodextrins", *Biotech. Adv.*, vol. 20, 5-6, pp. 341-359, 2002.
- A. Grigoriu, and O. Popescu, *Applications of cyclodextrines in textiles - A review*. Technical University of Iasi, 2011.
- B. Martel, "Polycarboxylic acids as crosslinking agents for grafting cyclodextrins onto cotton and wool fabrics: Study of the process parameters", *J. Appl. Poly Sc.*, vol. 83, 7, pp. 1449-1456, 2002.
- J. Andreaus, "Application of cyclodextrin in textile processes". *Quimica Nova*, vol. 33, pp. 929-937, 2010.
- B. Voncina, and L. A. Marechal, "Grafting of cotton with β -cyclodextrin via poly (carboxylic acid)", *J. Appl. Poly Sc.*, vol. 96, 4, pp. 1323-1328, 2005.
- B. Martel, M. Morcellet, D. Ruffin, F. Vinet, and M. Weltrowski, "Capture and controlled release of fragrances by CD finished textiles" *J Incl Phenom Macrocycl Chem.*, vol. 44, pp. 439-442, 2002.
- B. Martel, M. Morcellet, D. Ruffin, L. Ducoroy, and M. Weltrowski, "Finishing of polyester fabrics with cyclodextrins and polycarboxylic acids as crosslinking agents", *J Incl Phenom Macrocycl Chem.*, vol. 44, 1, pp. 443-446, 2002.
- B. Voncina, V. Vivod, and W. Chen, "Surface modification of PET fibers with the use of β -cyclodextrin", *J. Appl. Poly Sc.*, vol. 113, 6, pp. 3891-3895, 2009.
- Y. E. Ghoul, "Mechanical and physico-chemical characterization of cyclodextrin finished polyamide fibers". *J Incl Phenom Macrocycl Chem.*, vol. 57, 1, pp. 47-52, 2007.
- M. Weltrowski, M. Morcellet, and B. Martel, "Fiber with improved complexation qualities and cation exchange properties" *US Patent 7048769*, 2006.
- J. Szejtli, "Cyclodextrins in the textile industry". *Starch-Stärke*, vol. 55, 5, pp. 191-196, 2003.
- J. Szejtli, B. Zsádon, E. Fenyvesi, O. Horváth, and F. Tudos, "Sorbers of cellulose basis capable of forming inclusion complexes and a process for the preparation thereof", *US Patent. 6/288764*, 1982.
- P. K. Dutta, S. Tripathi, and J. Dutta, "Chitin and Chitosan: chemistry, properties and applications", *J of Scientific and Industrial Res.*, vol. 63, pp. 20-31, 2004.
- EI-T. Khaled, A. G. Mohamed, and EI-Rafie. Safaa, "Novel method for preparation of β -cyclodextrin/grafted chitosan and its application", *Carbohydr. Polym.*, vol. 63, pp. 385-392, 2006.

Table I. Absorbance index of lavender at various concentrations

Oil%	Absorbance Index							
	Time span (hours)							
	0	2	4	6	12	24	48	72
1	0.029	0.023	0.018	0.016	0.012	0.007	0.003	0
2	0.031	0.025	0.022	0.02	0.016	0.01	0.006	0.001
3	0.035	0.029	0.025	0.024	0.02	0.013	0.009	0.004
4	0.037	0.032	0.027	0.025	0.021	0.015	0.01	0.005
5	0.04	0.035	0.032	0.029	0.025	0.018	0.011	0.006
6	0.045	0.038	0.035	0.032	0.027	0.023	0.015	0.009
7	0.036	0.032	0.03	0.027	0.023	0.02	0.013	0.007
8	0.043	0.037	0.034	0.031	0.026	0.022	0.014	0.008
9	0.047	0.042	0.039	0.036	0.032	0.024	0.016	0.01
10	0.048	0.043	0.041	0.039	0.033	0.025	0.017	0.011

Table II. Chemical shifts of Protons of β -CD and Lavender

Protons	β -CD-co-chitosan			Lavender oil			
	CS	CS	IS $\Delta \delta$	Protons	CS	CS	IS $\Delta \delta$
	$\delta_{\beta\text{-CD free}}$	δ^*_{C}	($\delta_{\beta\text{-CD free}} - \delta^*_{\text{C}}$)	$\delta_{\text{L free}}$	δ^*_{C}	($\delta_{\text{L free}} - \delta^*_{\text{C}}$)	
H3	3.8322	3.666	-0.1659	H _B	5.4424	5.5032	-0.0608
H5	3.7438	3.612	-0.1314	H _C	5.1804	5.1196	-0.0708
H6	3.7158			H _D	4.9653	4.6949	-0.0004
H2	3.5336			H _E	3.6036	3.5969	-0.0067
H4	3.4469			H _F	1.7231	1.7226	-0.0005
		H5 > H3		H _G	1.8531	1.8591	0.006
				H _J	1.6580	1.6686	0.0106
				H _K	1.6486	1.6569	0.0083
				H _L	1.3742	1.3739	0.0003
				H _M	1.050	1.0498	-0.0002

CS= Chemical shift; IS= Induced Shift; $\delta_{\beta\text{-CD free}}$ = β -CD in free state; δ^*_{C} = β -CD/ Lavender in complex; $\delta_{\text{L free}}$ = Lavender in free state

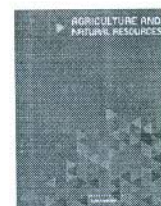
Table III. Qualitative evaluation of fragrance through scent intensity rating

Techniques	Scent intensity rating							
	0 hrs	2 hrs	4hrs	6hrs	12hrs	24hrs	48hrs	72hrs
Lavender alone	+++++	++++	+++	++	+	+	-	-
Host-guest complex	+++++	+++++	++++	++++	++++	++++	+++	+++

Table IV. Effect of aroma treatment on physical properties of cotton

Type of cotton treatment	TS Warp (kgf)	BL Warp (cm)	CR Ø	AP (lph)
Control	50.1	2.275	99.1	39.1
Lavender alone treated	51.7(3.19%)*	2.4(5.49%)	100.5(1.41%)	35.00 (10.66%)
Host-guest complex treated	63.5(26.74%)	3.21(41.1%)	100.2(1.1%)	31.67 (19.16%)

*Data in Parenthesis() shows the % change in the physical property subject to treatment



Research article

Antibacterial activity assessment of woolen fabric treated with natural dyes and chitosan

Manisha Yadav^a, Nagender Singh^a, Amandeep Kaur^b, Omprakash Sahu^{c,*}

^a Apparel Production, Ethiopian Institute of Textile and Fashion Technology, Bahir Dar University, Ethiopia

^b Fashion and Apparel Engineering, The Technological Institute of Textile and Sciences, Bhiwani Haryana, India

^c Department of Chemical EngineeringUIE, Chandigarh University, Mohali Punjab

Article Info

Article history:

Received 3 August 2017

Revised 26 October 2018

Accepted 5 November 2018

Available online 30 April 2019

Keywords:

Antimicrobial activity,

Chitosan,

Mordant,

Natural dye,

Wool fabric.

Abstract

In the textile industry, the finishing process has an important role in the antibacterial characterization of fabrics. Antibacterial growth was investigated in woolen fabric with natural biopolymeric material (chitosan) and natural dyeing (turmeric and madder). The effect of mordant concentration was studied in terms of dyeing concentration, dyeing temperature and dyeing time on the color strength. The results indicated that colorant absorption coefficient/colored substrate scattering coefficient (K/S) values increased with an increase in the chitosan and dyeing concentrations. The highest K/S value for turmeric was 2% chitosan, 55°C dyeing temperature and 105 min and for madder was 2% chitosan, 73°C temperature and 75 min at 9% shade. Good fastness properties were also achieved using both dyes. The results confirmed that the combination of chitosan and natural dye enhanced the antibacterial activity of woolen fiber against *Escherichia coli* and *Staphylococcus aureus*. The impregnation of chitosan in the fabric structure was also examined using scanning electron micrographs.

Introduction

Natural dyes are easily available and provide a sustainable alternative option as a coloring material and they have been used, since the nineteenth century to dye cotton, wool and silk (Shahid and Mohammad, 2013). The demand for natural dyes has reduced due to synthetic dyes becoming more popular in small and large-scale industry, though in developing countries still, some synthetic dyes like azo are used for textiles, leather, toys and plastics product (Ahlström et al., 2005) and may have harmful effects (Sen et al., 2016). Synthetic dyes have their own drawbacks in terms of health, safety and being environment-friendly and are banned in many countries (Singh et al.,

2002; Crini et al., 2008). As an alternative, natural dyes have numerous advantages such as resistance to moth invasion, anti-allergic, safer for body contact, non hazardous, economical and recyclable and therefore should be considered as a sustainable colorant for the textile industry (Siva, 2007; Erdawati et al., 2013; Swamy et al., 2014). Natural dyes can be classified according to the nature of raw material such as plants, insects and minerals, and among these, dyes derived from plants have substantial antibacterial quality (Mirjalili et al., 2013). *Turmeric (Curcuma longa)* is one such dye; it has been extracted from medicinal plants and used for coloring purposes (Mirjalili et al., 2014). The pigment extract from *C. longa* is known to be a curcuminoid, with small amounts of demethoxy curcumin and bisdemethoxy curcumin,

* Corresponding author.

E-mail address: ops0121@gmail.com (O. Sahu)

online 2452-316X print 2468-1458/Copyright © 2019. This is an open access article, production and hosting by Kasetsart University of Research and Development institute on behalf of Kasetsart University.

<https://doi.org/10.34044/j.anres.2019.53.2.14>

as shown in Fig. 1 (Bechtold et al., 2009). Turmeric has unique biochemical properties, so that it has been used in wound-healing and for its anti-inflammatory, anticancer, anti-proliferative, antifungal, and antibacterial activity (da Silva et al., 2018). Mirjalili et al. (2013) reported that turmeric shows good antibacterial, wash fastness and dye uptake properties with cotton and silk fabric. In addition, wool fabrics also showed excellent fastness, durability and antibacterial activity properties, when treated with other natural dyes (green tea, turmeric, saffron petals) and aluminum sulfate as a mordant using five washing cycles and 5 hr light exposure (Ghaheh et al., 2014). Madder is another natural dye derived from the roots of *Rubia tinctoria*. The main coloring constituents in madder are mixture of purpurin and munjistin, as shown in Fig. 2 (Saxena et al., 2014). In the middle ages, madder red was expensive in Europe and was typically used for special occasions (Chenciner, 2003). Madder can produce a range of reddish colors from pink to deep scarlet and is applied in the form of chips or powder (Schmidt-Przewoźna, and Brandys, 2016). In an acidic medium, it produces vivid oranges and rich browns on wool fabrics, medium shades of salmon and rose on silk fabrics and paler shades of oranges and salmons on cotton fabrics (Bechtold et al., 2009).

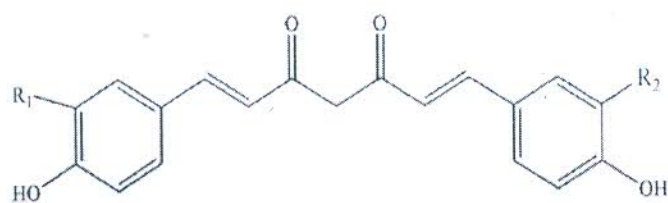


Fig. 1 Structures of curcumin (R1 = OCH₃ and R2 = OCH₃ is curcumin; R1 = R2 = H is bisdemethoxycurcumin; R1 = OCH₃ and R2 = H is demethoxycurcumin)

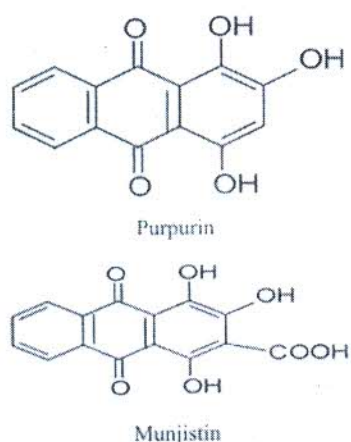


Fig. 2 Structures of purpurin and munjistin

Most of the natural dyes have antibacterial properties but they need some substitute along with mordants (Teli et al., 2013). Application of metallic mordants in the textile dyeing process could cause environmental hazards and be harmful. Hence another choice is a natural mordant like chitosan (Teli et al., 2014). Chitosan is

biopolymeric material containing antibacterial properties (Bano et al., 2017). It is a good supplementary agent in textile printing that can be extracted from the shrimp shell waste (Suryawanshi et al., 2019). Treatment with chitosan enhanced the color strength of dyed fabric as well acting as a good shrink-resistance agent for wool (Davidson et al., 1994; Dev et al., 2009). Nowadays, the textile industry is looking for sustainable production and consumption to address global environmental and economic issues; therefore, natural products are an alternative option in various applications in the textile industry.

The aims of this research work were: 1) to investigate the quality of natural dye madder and turmeric dyes with natural mordant chitosan for woolen fabrics; 2) to examine the effects of chitosan concentration, dye shade percentage, dyeing temperature and dyeing time on the color strength of dyed fabrics; and 3) to assess the antibacterial activity of woolen fabrics treated with mordant and both dyes.

Materials and Methods

Materials

Fabric: The mill-scoured pure (100%) wool fabric was supplied by Madan Textiles Industry Punjab, India. The specifications of the wool fabric are given in Table 1.

Chitosan: The chitosan derivative chitosan chloride was supplied by India Sea Food (regd.) Kochi, Kerala, India. The specifications of the chitosan are given in Table 2.

Chemicals: The acetic acid, hydrogen peroxide, sodium pyrophosphate and sodium hydroxide used in the experiments were all laboratory grade.

Natural Dyes: Raw turmeric root and madder dye powder were purchased from a local market in Bhiwani Haryana, India. Turmeric powder was extracted from the root, with the latter boiled for 1 hr followed by filtration and the residual impurities discarded. The madder dye powder was used in the original form as received (Ali et al., 2011).

Table 1 Fabric specifications

Variable	Specification
Fabric	100% wool
EPI/PPI	34/46
Weave	Twill(2/1)weave
GSM	136

EPI/PPI = End Per Inch/Pick Per Inch; GSM = Gram Per Squar.

Table 2 Specifications of chitosan chloride

Variable	Detail
Chemical name	Chitosan chloride
Source	Chemically modified from chitin flakes
Appearance and color	Powder & off white
Solubility	Water soluble
Density	>0.6gm/ml

Pre-treatment

Oxidation of wool with hydrogen peroxide

Oxidation of wool with hydrogen peroxide was carried out using the exhaustion method at pH 9. The fabric sample (1 g) and solvent (30 mL) were used at a liquor ratio 1:30. The treatment of fabric was completed with 18 mL/L hydrogen peroxide and 2 g/L of sodium pyrophosphate at 70°C for 1 hr. After that, the sample was washed carefully and dried under ambient conditions (Julia et al., 1998).

Pre-mordanting using chitosan

After oxidation, the wool samples were immersed in the chitosan solution at a liquor ratio of 1:20. The chitosan solution was prepared by dissolving different concentrations of chitosan (1–2%) in deionized water. The exhaustion procedure was carried out for 1 hr at 60°C. The samples were then rinsed properly and dried properly (Chen et al., 2007).

Dyeing procedure

The treated wool samples were dyed in a dye bath, containing a measured amount of dye and acetic acid (4g/L) with a liquid ratio of 1:30. After that, the sample was heated at different temperatures for different periods, as shown in Fig. 3. The samples were rinsed with cold water and subsequently with a nonionic detergent (3g/L) using a liquor ratio of 1:30 at 45°C for 40 min. Finally, the samples were rinsed with distilled water and dried at ambient temperature.

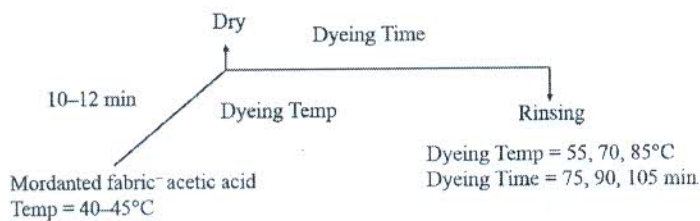


Fig. 3 Dyeing process of mordanted wool fabric at dyeing temperature 55, 70, 85°C and time 75, 90, 105 min

Optimization of dyeing conditions

To optimize the suitable conditions, dyeing was carried out at different concentrations of chitosan, different temperatures and different times, as detailed in Table 3. The experiments were optimizing using the Design Expert software version 7.1 (Stat-Ease, Inc.; Minneapolis, MN, USA) and different runs were formulated as shown in Table 4. Three different percentages (3%, 6% and 9%) of both dyes were used to obtain light, medium and dark shades, respectively (Prabu et al., 2002).

Table 3 Levels of variables chosen for design of experiment

Chitosan concentration (% w/w)	Dyeing temperature (°C)	Dyeing time (min)
1 (-1)	55 (-1)	75 (-1)
1.5 (0)	70 (0)	90 (0)
2 (+1)	90 (+1)	105 (+1)

Table 4 Box-Behnken design for three independent variables

Experimental Run	Chitosan (% weight per weight)	Dyeing time (min)	Dyeing temperature (°C)
1	1.5	75	85
2	1.5	90	70
3	2.0	105	70
4	1.0	105	70
5	1.5	90	70
6	1.0	90	85
7	1.0	90	55
8	2.0	90	85
9	1.5	75	55
10	1.5	90	70
11	1.5	105	85
12	1.5	105	55
13	1.0	75	70
14	1.5	90	70
15	2.0	75	70
16	1.5	90	70
17	2.0	90	55

Testing and analysis methods

Testing method

Color strength

The color yield, expressed as a K/S value using Equation 1, with a wavelength range of 400 nm to 700 nm with 10 nm intervals measured using a spectrophotometer (Gretag Macbeth color eye 7000A; X-Rite; Grand Rapids, MI, USA) and calculated in accordance with the Kubelka-Munk equation (Teli et al., 2014), as shown in Equation 1:

$$K/S = (1-R)^2/2R \quad (1)$$

where K is the absorption coefficient, depending on the concentration of colorant; S is the scattering coefficient, caused by the colored substrate; and R is the reflectance of the colored substrate.

Analysis method

Fastness testing

Fastness testing of dyed fabric samples was determined according to IS:764–1984 methods using a Sasmira Launder-O-Meter (Mumbai, India) followed with the IS-3 wash fastness method. The wash fastness rating was examined using a grey scale as per ISO-05-A02 (loss of shade depth) and ISO-105-A03 (extent of staining). Color

fastness to rubbing (dry and wet) was assessed according to the IS: 766-1984 method using a manual-operated crock meter and grey scale as per ISO-105-AO3 (Kumaresan et al., 2013).

Antimicrobial activity

The treated samples were investigated for antimicrobial properties using the AATTC Test Method (AATCC 100–2004). The *E. coli* method was used to test bacterial activity with a Gram-negative bacterium *S. aureus* and a pathogenic Gram-positive bacterium (Khan et al., 2011). A circular (4 cm diameter) fabric swatch was cut and the untreated wool fabric was used as a control sample. The dilution medium was nutrient broth and the neutralizer was sodium hydroxide. Antimicrobial activity on the wool fabric was examined using a comparative study for the reduction in colony number between treated and untreated fabrics after incubation. The results were expressed as the percentage reduction of bacteria (*R*) using Equation 2:

$$R (\%) = (A-B) / A * 100\% \quad (2)$$

where *A* and *B* are the numbers of bacteria recovered from the untreated and dyed treated wool fabric swatches, respectively.

Result and Discussion

K/S (Color strength)

The K/S values obtained for turmeric and madder dye with respect to all shades are shown in Tables 5 and 6, respectively. The results were analyzed statistically to determine the optimum parameters and desirability function of the experimental design. The analysis of variance model had coefficient of determination (R^2) values in the range 0.8–0.9 for all shades. Increased chitosan concentration after oxidation increased the K/S value. This might have been due to the simple formation of the amino groups of chitosan and the hydroxyl groups of the wool fabrics after oxidation (Ali et al., 2011). Similarly, the K/S value increased with increased dyeing time and concentration. The color strength was higher at 105 min treatment compared to 75 min; there was different percentage shade increases with both dyes at the different 3%, 6% and 9% dye concentrations. These were attributed to an increase in the driving force for dye transport toward the fiber surface, due to the increased higher concentration gradient of dye occurring in two phases (Zhang et al., 2017). The dyeing temperature did not have a prominent effect on the K/S values. The interaction results of different parameters for turmeric and madder are presented in Figs. 4A–4D and Figs. 5A–5D, respectively.

Table 5 Colorant absorption coefficient/colored substrate scattering coefficient (K/S) values for turmeric-dyed wool samples

Experiment number	K/S _{T3}	K/S _{T6}	K/S _{T9}
1	2.091	3.603	3.566
2	2.809	4.311	4.282
3	4.760	6.370	6.442
4	3.450	5.041	5.002
5	2.311	3.912	3.884
6	2.259	3.761	3.726
7	2.682	4.191	4.146
8	4.000	5.512	5.472
9	2.548	4.101	4.061
10	2.331	3.836	3.827
11	3.087	4.589	4.545
12	3.670	5.220	5.240
13	2.819	4.402	4.367
14	2.387	3.889	3.841
15	4.010	5.570	5.462
16	2.205	3.711	3.767
17	4.110	5.710	5.770

K/S_{T3}, K/S_{T6} and K/S_{T9} representing K/S values for 3%, 6% and 9% shade of turmeric dyed wool, respectively. Values shown as mean of three values.

Table 6 Colorant absorption coefficient/colored substrate scattering coefficient (K/S) values for madder dyed wool samples

Experiment number	K/S _{M3}	K/S _{M6}	K/S _{M9}
1	1.252	4.235	4.797
2	1.245	4.136	4.876
3	4.01	6.824	7.198
4	3.12	6.12	6.465
5	1.897	4.778	5.107
6	1.123	3.947	4.298
7	1.356	4.236	4.798
8	3.021	5.836	6.187
9	1.639	4.502	5.007
10	1.125	3.947	4.298
11	1.352	4.514	4.905
12	1.542	4.601	5.007
13	1.602	4.592	4.954
14	1.528	4.403	4.787
15	4.21	7.11	7.55
16	1.132	4.013	4.573
17	3.221	6.223	6.651

K/S_{M3}, K/S_{M6} and K/S_{M9} representing K/S values for 3%, 6% and 9% shade of madder dyed wool, respectively. Values shown as mean of three values.

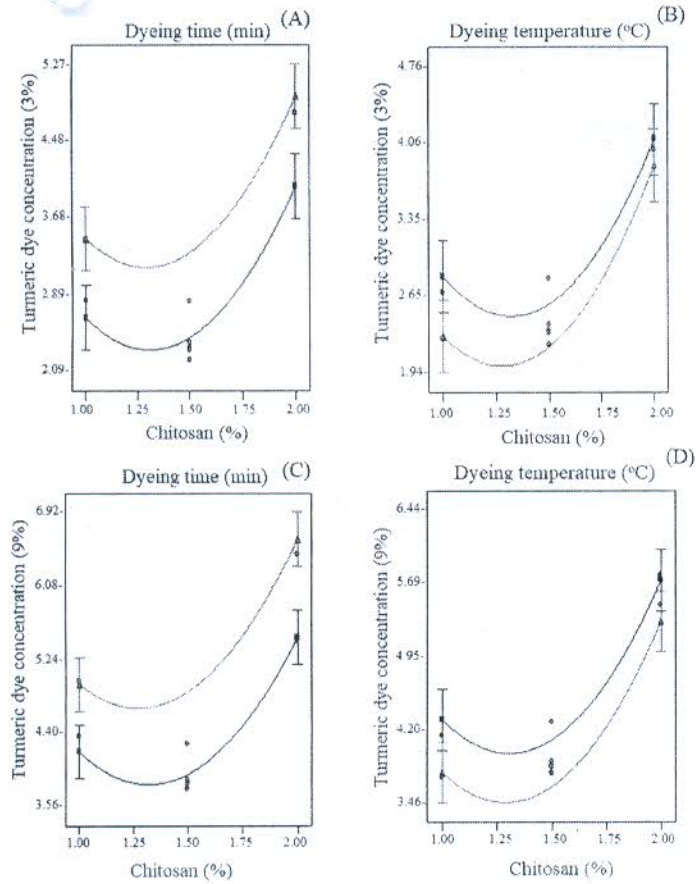


Fig. 4 Interaction graphs of various parameters for turmeric: (A) chitosan percentage and time (T3%); (B) chitosan percentage and temperature (T3%); (C) chitosan percentage and time (T9%); (D) chitosan percentage and temperature (T9%).

The sorption of chitosan on raw wool fabric was due to ionic interaction between the negative charges of carboxylic groups ($-COO^-$) in the polypeptide macromolecule and the protonated amino groups (NH_3^+) of chitosan. The deacetylated derivative of chitin (protonated form (NH_3^+) in aqueous solution at pH <6) is shown in Fig. 6. In the case of bleached wool, an additional vacancy at cysteic groups (SO_3^-) possibly resulted in higher cross-linking of chitosan, and the proposed mechanism is shown in Fig. 7. The turmeric dye has ionizable $-OH$ groups as auxochromes, which attached to the sites available in bleached chitosan-treated wool fiber as shown in Fig. 8. In aqueous medium at optimum pH, these ionizable groups of turmeric were dissolved due to conversion in anionic forms (Rafols et al., 2017). In addition, chitosan formed a strong bond with the sulphonic acid group on the surface of bleached wool which may result in further attraction and react with the turmeric dyes, leading to an increased dyeing rate and a reduction in dyeing time. However, the optimum time obtained was less for madder as it has a greater number of ionizable OH groups compared to turmeric.

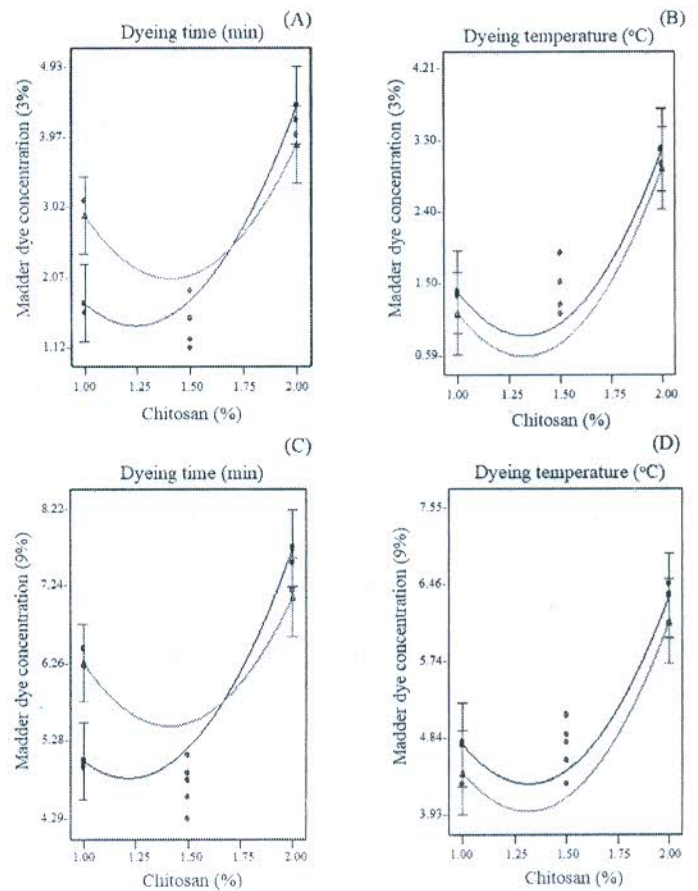


Fig. 5 Interaction graphs of various parameters for madder: (A) chitosan percentage and time (M3%); (B) chitosan percentage and temperature (M3%); (C) chitosan percentage and time (M9%); (D) chitosan percentage and temperature (M9%).

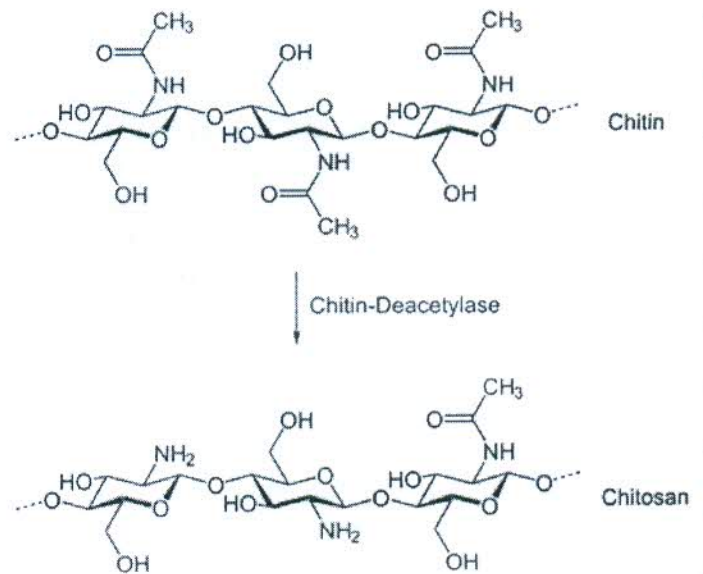


Fig. 6 Deacetylation of chitin to form chitosan

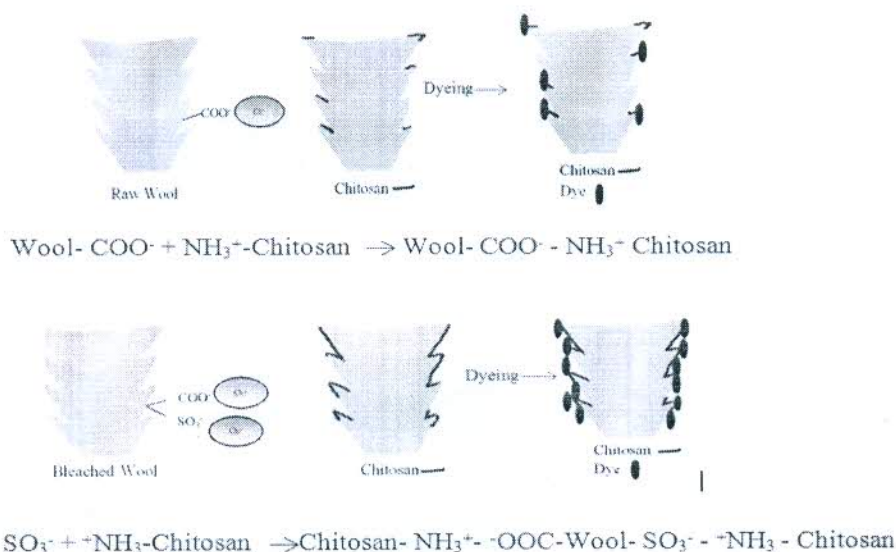


Fig. 7 Proposed mechanism of wool and chitosan attachment

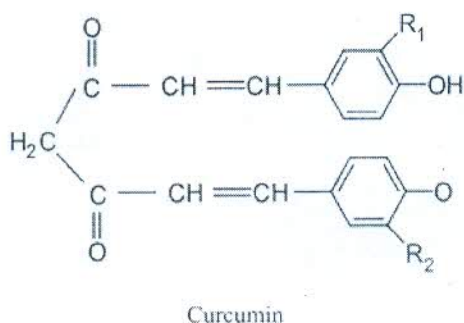


Fig. 8 Ionizable -OH groups of turmeric

The micrograph structures of wool at different chitosan percentages are presented in Fig. 9A and 9B. It was observed that the chitosan percentage on the raw wool increased with the increased concentration of chitosan from 1% to 2%. The values of optimized parameters satisfying the desirability criteria for 'maximizing the K/S value' for turmeric and madder as obtained using the software are given in Tables 7 and 8. Table 7 shows no significant differences (almost similar values of K/S) between the optimized values for 6% and 9% shades for turmeric dyes. Similarly, for madder (Table 8), there were similar values for chitosan (approximately 2%), dyeing time (approximately 105min) and different temperature (approximately 67°C and 55°C) and no significant differences in the K/S values. The effect of an increase in temperature was only for limited time, as for further increase in temperature, there were no changes in the K/S values.

The structural properties of treated and untreated wool fabric with chitosan and dyes were examined using Fourier-transform infrared spectroscopy. The biochemical interaction between chitosan and wool fiber polymer was investigated using the changes in the peaks from the characteristic spectra (Fig. 10). In general, no major changes were observed in bands or their intensities for all test fabrics. The broad absorption band which appeared in the range

of 3700–2900 cm^{-1} indicates the presence of -OH groups in the cellulose polymer (Martínez-Sanz et al., 2011). The presence of -NH₂ group in the treated fabric was responsible for introducing a cationic site in the wool polymer resulting in improved dye exhaustion and also interaction with microorganisms for antibacterial properties. Again, the spectrum near 2500 cm^{-1} corresponding to the symmetric stretching of methylene (-CH₂-) groups (Babu et al., 2015) and 1500 cm^{-1} related to the C=O stretch of esters were found to be similar in all the tested samples. The absorption peak that appeared at 1300 cm^{-1} for chitosan-treated wool fabric suggested the formation of a Schiff base (C=N double bond) between the aldehydic carbonyl group of cellulose and the amino group of chitosan (Tian et al., 2017). All three samples showed peaks near 1320 and 1100 cm^{-1} being related to -O- bending of C-O-H alcohol groups (Rusu et al., 2016) and 960 cm^{-1} corresponding to C-O mainly to C₃-O₃H secondary alcohol (Bakshi et al., 2018). Moreover, the peak at 700 cm^{-1} corresponding to asymmetric out-of-phase ring stretching of C₁-O-C₄ β-glucosidic bonds increased after the dyeing process (Araujo et al., 2018). The increase in the percentage absorption of dye in mordanted samples may have been due to the formation of a chemical bridge between the dye and fabric through natural mordant which was fixed on the fiber and enhanced the fixation of dye (Islam et al., 2016).

Color fastness

Color fastness indicates the resistance of a material to any change in any of its color characteristics (Ramalingam et al., 2016). The results of color fastness are shown in Tables 9 and 10 for turmeric and madder, respectively. It can be clearly seen from both tables that the fastness properties were excellent for both of dyes. This might have been due to electron-donating groups (OH groups) in the dye structure being capable of forming a complex, that doesn't participate during washing or rubbing (Das, 2011).

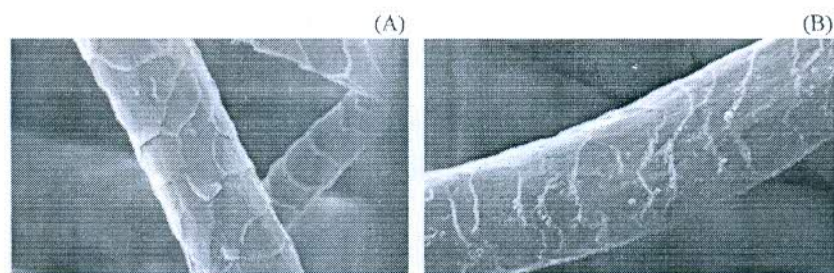


Fig. 9 Macrograph images showing chitosan percentage increase on raw wool with rising concentration: (A) 1% chitosan; (B) 2% chitosan

Table 7 Optimized parameters for turmeric dyed samples to achieve maximum colorant absorption coefficient/colored substrate scattering coefficient (K/S) value

Shade (%)	Chitosan (%w/w)	Dyeing time (min)	Dyeing temperature (°C)	K/S	Desirability
3%	1.97	105	55	4.9	1
6%	1.98	105	67	6.4	1
9%	1.96	104	56	6.5	1

w/w = weight per weight.

Table 8 Optimized parameters for madder dyed samples to achieve maximum colorant absorption coefficient/colored substrate scattering coefficient (K/S) value

Shade (%)	Chitosan (%w/w)	Dyeing time (min)	Dyeing temperature (°C)	K/S	Desirability
3%	1.99	75	75	4.2	1
6%	2	76	59	7.2	1
9%	2	75	73	7.6	1

w/w = weight per weight.

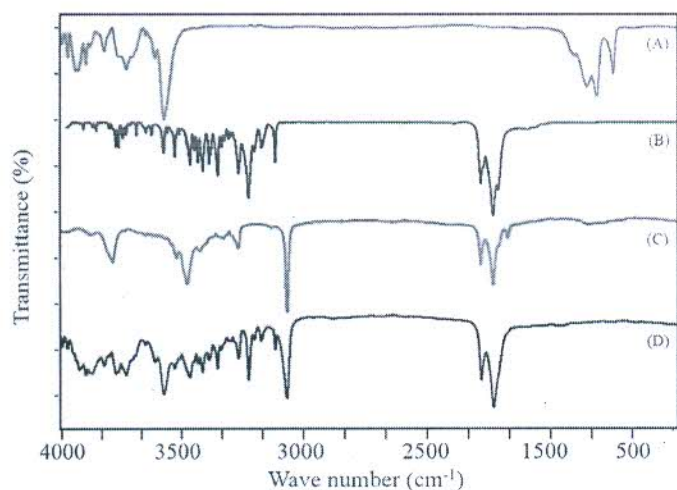


Fig. 10 Fourier-transform infrared spectroscopy images: (A) pure wool fabric; (B) treated with chitosan; (C) treated with chitosan and turmeric; (D) treated with chitosan and madder

Table 9 Color fastness for turmeric dye

Turmeric dye (%)	Wash fastness		Rubbing fastness	
	Color change	Color staining	Dry	Wet
3	4–5	4–5	4–5	3–4
6	4	4–5	4	3–4
9	4–5	4–5	5	4

Table 10 Color fastness for madder dye

Madder dye (%)	Wash fastness		Rubbing fastness	
	Color change	Color staining	Dry	Wet
3	4–5	5	5	4–5
6	5	5	5	4–5
9	4–5	4–5	5	4

Antibacterial assessment

The antibacterial activity of un-mordant-dyed and mordant-dyed fabrics was examined against *S. aureus*, *E. coli*, and *P. aeruginosa* and the results are shown in Table 11. With 2% chitosan as mordant, maximum color strength was achieved, as this was identified as the optimum mordant concentration. All experimental samples of turmeric and madder had high antibacterial activity against the tested microorganisms (bacteria). This could be attributed to the linkage of chromophores to the glycoside in natural dyes. It was also noted that the antibacterial activity of dyed samples showed significant increases after mordanting and dye concentration increases.

This research concluded that natural dyes and mordant are effective substitutes for synthetic dyes to reduce adverse environmental and economic conditions. The dyeing of wool fabric with natural dyes was successfully carried out using chitosan as an eco-friendly mordant. The K/S values varied with the dye and mordant percentage combination; hence the parameters were optimized to produce a maximum K/S

value for both dyes. The results showed a maximum K/S value at turmeric was 2% chitosan, 55°C dyeing temperature and 105 min and for madder was 2% chitosan, 73°C temperature and 75 min at 9% shade. Moreover, the fixation of chitosan as a mordant on wool fabric was confirmed using scanning electron micrographs. The color fastness property for both wool fabrics was excellent. The turmeric and madder were suitable as an antibacterial agent for *E. coli* and *S. aureus* microorganisms and this increased with increased dye and mordant concentrations. Further investigation should investigate different organisms with different mordants and different types of fabric.

Table II Antibacterial activity of dyed woolen fabrics

Fabric sample	Bacterial reduction (%)	
	<i>S. aureus</i>	<i>E. coli</i>
Turmeric		
Unmordanted + 3% turmeric	94.2	93.0
Mordanted + 3% turmeric	99.4	99.2
Mordanted + 6% turmeric	99.6	99.5
Mordanted + 9% turmeric	99.8	99.7
Madder		
Unmordanted + 3% madder	95.3	96.2
Mordanted + 3% madder	99.2	99.1
Mordanted + 6% madder	99.5	99.4
Mordanted + 9% madder	99.6	99.7

Conflict of Interest

The authors have no conflicts of interest to declare.

Acknowledgments

The authors acknowledge Fashion and Apparel Engineering, The Technological Institute of Textile and Sciences, Bhiwani Haryana, India for funding and facilities.

Reference

- Ahlström, L.H., Eskilsson, C.S., Bjorklund, E. 2005. Determination of banned azo dyes in consumer goods. *Trends Analyt. Chem.* 24: 49–56.
- Ali, N.F., Mohamedy, R.S.R.E.L., El-Khatib, E.M. 2011. Antimicrobial activity of wool fabric dyed with natural dyes. *Research Journal of Textile and Apparel.* 15: 1–10.
- Araujo, C., Freire, C.S.R., Nolasco, M.M., Ribeiro-Claro, P.J., Rudic, S., Silvestre, A.J., Vaz, P.D. 2018. Hydrogen bond dynamics of cellulose through inelastic neutron scattering spectroscopy. *Biomacromolecules* 19: 1305–1313.
- Babu, K., Pal, N., Bera, A., Saxena, V.K., Mandal, A. 2015. Studies on interfacial tension and contact angle of synthesized surfactant and polymeric from castor oil for enhanced oil recovery. *Appl. Surf. Sci.* 353: 1126–1136.
- Bakshi, P.S., Selvakumar, D., Kadirvelu, K., Kumar, N.S. 2018. Comparative study on antimicrobial activity and biocompatibility of N-selective chitosan derivatives. *Reac. Funct. Polym.* 124: 149–155.
- Bano, I., Arshad, M., Yasin, T., Ghauri, M.A., Younus, M. 2017. Chitosan: A potential biopolymer for wound management. *Int. J. Biol. Macromol.* 102: 380–383.
- Bechtold, T., Mussak, R. 2009. *Handbook of natural colorants*. John Wiley & Sons, West Sussex, UK.
- Chen, P-H, Hwang, Y-H, Kuo, T-Y, Liu, F-H, Lai, J-Y, Hsieh, H-J. 200. Improvement in the properties of chitosan membranes using natural organic acid solutions as solvents for chitosan dissolution. *J. Med. Biol. Eng.* 2: 23–28.
- Chenciner, R. 2003. *Madder red: A history of luxury and trade*. Routledge United Kingdom.
- Crini, G., Badot, P.M. 2008. Application of chitosan, a natural amino polysaccharide, for dye removal from aqueous solutions by adsorption processes using batch studies: A review of recent literature. *Pro. Polym. Sci.* 33: 399–447.
- da Silva, A.C., de Freitas Santos, P.D., do Prado Silva, J.T., Leimann, F., Bracht, L., Gonçalves, O.H. 2018. Impact of curcumin nano formulation on its antimicrobial activity. *Trends Food Sci. Technol.* 72: 74–82.
- Das, P. 2011. Application of vegetable dyes in carpet industry. In: *National Workshop and Seminar on "Vegetable dye and its application on textile"*. Bhadohi (U.P.), India, pp. 84–90.
- Davidson, R.S., Xue, Y. 1994. Improving the dyeability of wool by treatment with chitosan. *Color. Technol.* 110: 24–29.
- Dev, V.G., Venugopal, J., Sudha, S., Deepika, G., Ramakrishna, S. 200. Dyeing and antimicrobial characteristics of chitosan treated wool fabrics with henna dye. *Carbohydr. Polym.* 75: 646–650.
- Erdawati, G.M., Fithriyah, N.H. 2013. The application of chitosan for environmentally benign process of curcumin dyeing of silk fabrics. *Jo. B App. Sci. Res.* 3: 5–14.
- Ghaheh, F.S., Mortazavi, S.M., Alihosseini, F., Fassihi, A., Nateri, A.S., Abed, D. 2014. Assessment of antibacterial activity of wool fabrics dyed with natural dyes. *J. Clean Prod.* 72: 139–145.
- Islam, M., Hasan, K.F., Deb, H., Faisal, A.M.M., Xu, W. 2016. Improving the fastness properties of cotton fabric through the implementation of different mordanting agents dyed with natural dye extracted from marigold. *American Journal of Polymer Science and Engineering* 4: 171–176.
- Julia, M.R., Cot, M., Erra, P., Jovic, D., Canal, J.M. 1998. The use of chitosan on hydrogen peroxide pretreated wool. *Tex. Chem. Col.* 30: 78–83.
- Khan, M.I., Ahmad, A., Khan, S.A., Yusuf, M., Shahid, M., Manzoor, N., Mohammad, F. 2011. Assessment of antimicrobial activity of catechu on its dyed substrate. *J. Clean. Prod.* 19: 1385–1394.
- Kumaresan, M., Palanisamy, P.N., Kumar, P.E. 2013. Comparison of fastness properties and colour strength of dyed cotton fabrics with eco-friendly natural dyes. *The Exp.* 8: 483–489.
- Martínez-Sanz, M., Lopez-Rubio, A., Lagaron, J.M. 2011. Optimization of the nanofabrication by acid hydrolysis of bacterial cellulose nanowhiskers. *Carbohydr. Pol.* 85: 228–236.
- Mirjalili, M., Abbasipour, M. 2013. Comparison between antibacterial activity of some natural dyes and silver nano particles. *J. Nanost. Chem.* 3: 1–3.
- Mirjalili, M., Karimi, L. 2013. Extraction and characterization of natural dye from green walnut shells and its use in dyeing polyamide: Focus on antibacterial properties. *J. Chem.* 14: 115–119.
- Mirjalili, M., Karimi, L. 2014. Antibacterial dyeing of polyamide using turmeric as a natural dye. *Aut. Res. J.* 13: 51–56.
- Prabu, H.G., Sundarajan, M. 2002. Effect of the bio-salt trisodium citrate in the dyeing of cotton. *Color. Technol.* 118: 131–134.

- Rafols, C., Subirats, X., Rubio, J., Rosés, M., Bosch, E. 2017. Lipophilicity of amphoteric and zwitterionic compounds: A comparative study of determination methods. *Talanta*. 162: 293–299.
- Ramalingam, S., Sreeram, K.J., Raghava Rao, J., Unni Nair, B. 2016. Organic nanocolorants: Self-fixed, optothermal resistive, silica-supported dyes for sustainable dyeing of leather. *ACS Sust. Chem. Eng.* 4: 2706–2714.
- Rusu, R.D., Simionescu, B., Oancea, A.V., et al. 2016. Analysis and structural characterization of pigments and materials used in Nicolae Grigorescu heritage paintings. *Spectrochim Acta A Mol. Biomol. Spectrosc.* 168: 218–229.
- Saxena, S., Raja, A.S.M. 2014. Natural dyes: Sources, chemistry, application and sustainability issues. In: *Roadmap to Sustainable Textiles and Clothing*. Springer, Singapore, pp. 37–80.
- Schmidt-Przewoźna, K., Brandys, A. 2016. Utilization of contaminated lands for cultivation of dye producing plants. *Bioremediation and Bioeconomy* 2: 329–359, doi.org/10.1016/B978-0-12-802830-8.00014-9
- Sen, S.K., Raut, S., Bandyopadhyay, P., Raut, S. 2016. Fungal decolouration and degradation of azo dyes: a review. *Fung. Bio. Rev.* 30: 112–133.
- Shahid, M., Mohammad, F. 2013. Recent advancements in natural dye applications: A review. *J. of Clean. Pro.* 53: 310–331.
- Singh, K., Singh, S., Butola, B.S. 2002. The German ban-A realistic appraisal. *Colourage*. 49: 43–47.
- Siva, R. 2007. Status of natural dyes and dye-yielding plants in India. *Curr. Sci.* 92: 916–925.
- Suryawanshi, N., Jujjavarapu, S.E., Ayothiraman, S. 2019. Marine shell industrial wastes—an abundant source of chitin and its derivatives: constituents, pretreatment, fermentation, and pleiotropic applications—a revisit. *Int. J. Environ. Sci. Technol.* 4: 1–22.
- Swamy, V.N., Gowda, K.N., Sudhakar, R. 2014. Dyeing properties of natural dye *Syzygium cumini* on silk. *Journal of The Institution of Engineers (India): Series E* 95: 11–17.
- Teli, M.D., Sheikh, J., Shastrakar, P. 2013. Exploratory investigation of chitosan as mordant for eco-friendly antibacterial printing of cotton with natural dyes. *Journal of Textiles* 5: 95–112.
- Teli, M.D., Sheikh, J., Shastrakar, P. 2014. Eco-friendly antibacterial printing of wool using natural dyes. *J. Tex. Sci. Eng.* 6: 25–37.
- Tian, X., Yan, D., Lu, Q., Jiang, X. 2017. Cationic surface modification of nanocrystalline cellulose as reinforcements for preparation of the chitosan-based nanocomposite films. *Cellulose* 24: 163–174.
- Zhang, Y., Huang, G., An, C., et al. 2017. Transport of anionic azo dyes from aqueous solution to gemini surfactant-modified wheat bran: Synchrotron infrared, molecular interaction and adsorption studies. *Sci. Total Environ.* 595: 723–732.

FAE



Thermal and mass transport properties of polyester-cotton plated fabrics in relation to back layer fibre profiles and face layer yarn types

Yamini Jhanji, Deepti Gupta & Vijay Kumar Kothari

To cite this article: Yamini Jhanji, Deepti Gupta & Vijay Kumar Kothari (2018) Thermal and mass transport properties of polyester-cotton plated fabrics in relation to back layer fibre profiles and face layer yarn types, The Journal of The Textile Institute, 109:5, 669-676, DOI: [10.1080/00405000.2017.1363948](https://doi.org/10.1080/00405000.2017.1363948)

To link to this article: <https://doi.org/10.1080/00405000.2017.1363948>



Published online: 10 Aug 2017.



[Submit your article to this journal](#)



Article views: 202



[View related articles](#)



[View Crossmark data](#)



Citing articles: 1 [View citing articles](#)

Thermal and mass transport properties of polyester–cotton plated fabrics in relation to back layer fibre profiles and face layer yarn types

Yamini Jhanji^a, Deepti Gupta^b and Vijay Kumar Kothari^b

^aDepartment of Fashion & Apparel Engineering, Technological Institute of Textiles & Sciences, Bhiwani, India; ^bDepartment of Textile Technology, Indian Institute of Technology, New Delhi, India

ABSTRACT

Clothing plays an important role in maintaining thermal equilibrium between a human body and the ambient environment by serving as a medium for heat, moisture vapour and liquid moisture transfer. The ability of fabric to maintain this equilibrium is related to thermo-physiological comfort. Plating is an innovative knitted fabric production technique to obtain bi-layered fabrics. An attempt has been made to engineer plated knit structures with such a combination of fibre cross section in the back (inner/next to skin) and the yarn type in the face (outer) layer, so that a rapid liquid transfer from back layer by wicking and quick liquid absorption and evaporation by the face layer can be achieved. Plated fabrics using the combination of triangular polyester fibre in the back and carded cotton yarn in the face layer showed the higher thermal resistance, higher absorbent capacity and would be warmer to the initial touch. However, the combination of combed cotton yarn with triangular polyester fibre resulted in fabrics with the higher air permeability, moisture vapour transmission rate and transplanar wicking.

ARTICLE HISTORY

Received 17 July 2016
Accepted 25 July 2017

KEYWORDS

Comfort; knits; plated; microclimate; moisture management

Introduction

Clothing plays an important role in maintaining the thermal equilibrium between human body and the ambient environment by serving as a medium for the heat, moisture vapour and liquid moisture transfer (Stankovic, Popovic, & Poparic, 2008). The ability of fabric to maintain this equilibrium is related to thermo-physiological comfort.

The acceptability of textile fabrics for varied applications like the sportswear, active wear and inner wears depend on thermo-physiological comfort aspects, which involve thermal properties, the air permeability, moisture vapour and liquid moisture transfer properties. The transient thermal behaviour of textiles, which give an indication of warm–cool feeling on first brief skin contact with fabric is also believed to contribute to the overall comfort of textile fabrics (Majumdar, Mukhopadhyay, & Yadav, 2010; Ozdil, Marmarali, & Kretzschmar, 2007; Pac, Bueno, Renner, & Kasmi, 2001). The most challenging job for the researchers is the designing of clothing which meets the requirements of the wearer in different environmental conditions and at different activity levels. At the low level of activity, the person perspires in the vapour form (insensible perspiration). However, an increase in activity level and ambient temperature is followed by the onset of liquid sweat (sensible perspiration). Clothing should thus be able to provide the wearer comfort in changing ambient conditions and at different activity levels. Heat exchange between the clothing and the environment is achieved through dry flux (conduction, convection and radiation) during an insensible perspiration and latent flux during the sensible perspiration. The

dry flux is dependent on the insulation property of the textiles, while the latent flux depends on the moisture vapour and liquid moisture transfer properties (Kothari & Sanyal, 2003). Dry skin micro climate and wearer comfort is thus ensured by the rapid moisture transportation or sweat diffusion from the body to the environment (Su, Fang, Chen, & Wu, 2007). Diffusion of water vapour through fibre layers, absorption-desorption of vapour by the fibres and transmission of water vapour by forced convection are the means, by which the moisture transfer through textiles occur. However, liquid moisture flow through textile materials takes place by the mechanism of wetting and wicking. Wetting is the initial process of fluid spreading, where the fibre–liquid interface displaces the fibre–air interface. Soon after the process of wetting, wicking comes into action as water wets the fibres and enters the inter-fibre capillary channels (Patnaik, Rengasamy, Kothari, & Ghosh, 2006).

Plating is an innovative knitted fabric production technique to obtain bi-layered fabrics. Plated knit structures are characterized by distinct yet integrated face (outer) and back (inner/next to skin) layers. The flexibility in selection of contrastingly different fibre and yarn constituents in the two layers of plated fabrics make them suitable and versatile for applications like inner wears, sportswear, active wear, etc. The main elements of two-layered plated knitted structures are: (a) Back (Inner) layer: this is the separation layer which is in direct skin contact. The conductive and diffusive hydrophobic components of this layer help in removal and transportation of sweat to the outer layer. (b) Face (Outer) layer: this is the absorption layer which is in contact

with the environment. The absorptive hydrophilic components of this layer provide large area for sweat absorption and evaporation to the outside environment (Bivainyte & Mikucioniene, 2011; Geraldes, Lubos, Araujo, Belino, & Nunes, 2008).

A gamut of fibre, yarn and fabric variables is reported to affect the comfort aspects of fabrics. Fibre properties like the fibre length, fibre type, fibre fineness, cross-sectional shape, composition of fibre mix, friction, crimp, molecular orientation, yarn structure, yarn count, yarn twist and yarn spinning technologies are suggested as the major contributors to the moisture vapour and liquid moisture transmission and wearing comfort in textiles (Behera & Singh, 2013; Karaca, Kahraman, Omeroglu, & Becerir, 2012; Tyagi, Krishna, Bhattacharya, & Kumar, 2009).

Published literature reveals that the sizeable amount of research is focused on studying the effect of fibre and yarn variables on mechanical and comfort properties of textiles.

Karaca et al. (2012) compared thermal comfort properties of fabrics woven from different cross-sectional shaped polyester fibres and concluded that fabrics produced from hollow fibres had the low thermal insulation, air permeability and water vapour permeability; however, fabrics using trilobal polyester fibres had the high air and water vapour permeability and lower thermal conductivity compared to round fibre fabrics. Varshney, Kothari, and Dhamija (2010) studied the effect of polyester profile on physiological properties of polyester fabrics and suggested that fabrics using non-circular fibres offered more resistance to the heat flow. Das, Das, Kothari, Fanguiero, and Araujo (2008) studied the effect of fibre cross-sectional shape on moisture transmission properties of the fabrics and suggested that the wicking rate through fabrics increased, while the water vapour permeability reduced as the fibre shape factor increased. Matsudaira and Kondo (1996) suggested that more water could be absorbed by polyester fibres by making grooved or non-grooved hollow in the fibre due to the increase in space ratio and surface area of fibre in their studies on moisture transport properties of fabrics having the different ratio of space to polymer in the fibre cross section. Behera and Singh (2013) suggested that low stress mechanical properties and hand behaviour of fabric was altered by the change in the cross-sectional shape of filaments in their studies on polyester multifilament yarn fabrics. Singh and Nigam (2013) compared carded, combed and compact spun yarn woven fabrics for their comfort performance and reported that compact weft yarn fabrics showed the high water vapour permeability and were found suitable for the summer wear shirting. The yarn type used can significantly influence thermal properties of knitted fabrics as suggested by Singh and Nigam (2013) who observed that combed yarn fabrics would exhibit higher thermal conductivity and thermal absorptivity however reduced thermal resistance as compared to carded yarn fabrics. Likewise, moisture vapour and liquid moisture transfer properties of combed yarn fabrics are expected to be higher compared to fabric composed of carded yarn owing to absence of hairs and hence uninterrupted passage through inter-yarn spaces.

Ozdil et al. (2007) studied the thermal comfort properties of carded and combed yarn rib knitted fabrics and observed an increase in thermal conductivity, thermal absorptivity and water vapour permeability of fabrics knitted with combed yarns. Oglakcioglu and Marmarali (2010) studied the effect of yarn type on thermal comfort properties of cotton knitted fabrics and

observed that fabrics knitted with the double plied yarn had the higher thermal conductivity, thermal absorptivity and thermal resistance compared to single plied yarn fabrics.

An interesting avenue to explore further is the suitable combination of different fibres and yarns in the face and back layers of plated knit structures in order to control overall thermal and mass transfer properties of structures. The change in fibre type may not make substantial difference to thermal properties, as thermal properties of textiles are related to enclosed air and fabric thickness more as compared to fibre type. However, owing to difference in moisture absorption and diffusivity properties of two different fibres used in two layers of plated knits, a considerable difference in moisture transfer properties is anticipated as the structure is made entirely of polyester or cotton and also if fibre positions are altered in face and back layers. Thermal properties may not be affected much as the fabric is reversed or position of fibres is altered with cotton in inner and polyester in the outer layer. The same hold true if fabrics are made entirely of one fibre i.e. either 100% polyester or 100% cotton. The above statement has been validated by research on comfort properties of polyester/cotton, polypropylene/cotton and nylon/cotton-plated knitted fabrics (Jhanji, Gupta, & Kothari, 2015a). Researchers found that samples varied marginally in thermal resistance values, supporting the fact that thickness and enclosed layer of still air are the greatest determinants of insulation of textile structures. Fabrics constructed with same cover factor and all other variables constant just varying in fibre type would have nearly same thickness and would offer similar thermal properties. It was concluded by researchers that type of fibre used has no effect on thermal insulation properties or moisture vapour transmission rate of plated knit fabrics if all other construction parameters remain the same.

Moisture transmission properties are expected to be affected if fabric is reversed, i.e. cotton in back (next to skin) layer and polyester in the face (outer) layer owing to difference in hydrophilicity of the two fibres. A study has been conducted and reported to study the moisture management properties of plated knit structures by altering the position of polyester and cotton fibre in face and back layer (Jhanji, Gupta, & Kothari, 2015b). It has been reported that liquid moisture transmission properties of fabric with cotton in inner layer are inferior compared to fabrics where cotton is used in the outer layer. Fabric with polyester in inner layer was classified as moisture management fabric with excellent grade for overall moisture management capacity while fabric with cotton in inner and polyester in outer layer was classified as fast absorbing and slow drying fabric. Fabric made entirely of cotton would exhibit inferior wicking properties. Cotton inhibits the liquid movement through capillaries due to blockage of inter-fibre capillaries caused by water absorption by fibres. Polyester on the other hand, provides sufficient drag for liquid movement along the capillaries owing to its hydrophobicity and accordingly, fabrics with 100% polyester and fabrics using polyester in inner and cotton in outer layer would exhibit higher wicking.

Researchers have reported that fibre variables like fibre fineness, fibre cross-sectional shape and yarn variables like the yarn twist, yarn count and yarn structure affects the different mechanical and comfort properties of textiles. Most of the studies are focused on thermal comfort properties of woven fabrics

and comparison of different knit structures. However, there are few studies devoted to systematic studies on the effect of fibre profile and yarn types on thermal as well moisture vapour and liquid moisture transfer properties of single jersey plated fabrics, although the use of such structures is increasing rapidly owing to the flexibility in the selection of different fibre and yarn combinations in two layers of the same fabric. The present study, therefore attempts to investigate the effect of back layer fibre profile and face layer yarn type on thermal and mass transport properties of polyester-cotton plated fabrics. Back layer in the direct skin contact should be able to conduct and diffuse sweat to the face layer, while the face layer should rapidly absorb the sweat for the quick evaporation. An attempt has been made to select such a combination of fibre profile in the back and yarn type in the face layer, so that the rapid liquid transfer from the back layer by wicking and quick liquid absorption and evaporation by the face layer can be achieved.

Material

Cotton (J-34) of upper half mean length of 29.2 mm, mean length of 24.3 mm and 4.32 micronaire and polyester fibres of 2.2 dtex and staple length of 44 mm were used in the production of yarn samples. Cotton carded and combed roving of 0.9 hank were used to spin 246 dtex single ring spun carded and combed yarns in blow room. Polyester fibres of circular and triangular profile were used to spin 246 dtex single ring spun yarns on 6/S LMW pilot plant ring frame. The yarns used were Z twisted with 677.6 turns/metre. The four yarn samples in total were used for the preparation of four single jersey plated fabrics. All the samples were prepared in the plating relationship with the carded and combed ring spun cotton yarn in the face and polyester fibres of two different profiles in the back layer. Figure 1 shows schematics of face and back layer of developed fabric samples. The fabric samples were prepared on the hand operated flatbed knitting machine (Elex, China) with the machine gauge of 14, needle bed of 42 inches and 588 needles in each bed. All the machine parameters were kept constant to obtain the fabrics of same cover factor.

Methods

The prepared yarn samples were tested for their diameter and hairiness values. Comfort-related properties of the resultant fabrics were also tested. Yarn diameter was determined by SMZ1500 digital microscope. Hairiness values for yarn samples were measured on the Zweigle Hairiness meter (Model G566). Thickness of fabric samples was determined at 10 different positions by the thickness gauge (ASTM D 1777-96, 2007) and average values were recorded. Aerial density of samples was determined according to ASTM D-1059 on the electronic balance. Five tests were conducted for each sample and the average value of aerial density in g/m^2 was recorded. Fabric porosity was calculated as the ratio of fabric density and fibre density expressed as a percentage. Thermal properties of prepared samples were measured on the Alambeta instrument. Air permeability of plated fabrics was measured on the TEXTEST FX 3300 air permeability tester (ASTM D 737-04). The measurements were taken at 10 different positions for each test sample. Moisture vapour transmission rate of test samples was determined at five different positions of test sample by the MVTR cell method. Absorbent capacity and transplanar wicking of plated fabrics were determined on the Gravimetric Absorbency Tester (GATS) in accordance with ASTM D-5802 and five values were recorded for each sample.

Results and discussion

Thermal absorptivity

Thermal absorptivity is the transient thermal property of textiles and indicates the feeling of warmth-coolness of fabric on the first brief skin contact with fabric. Fabrics using triangular polyester fibre and carded cotton yarn exhibit the lower value of thermal absorptivity; thereby, they are providing feeling of warmth at the brief initial skin contact. High thickness and porosity of fabrics incorporating triangular fibres might have led to low values of thermal absorptivity. Edges of triangular fibre inhibit the close packing of fibres in the structure (Figure 2) as opposed to more uniform, regular surface of circular fibres ultimately resulting in more open fabric structure (Varshney et

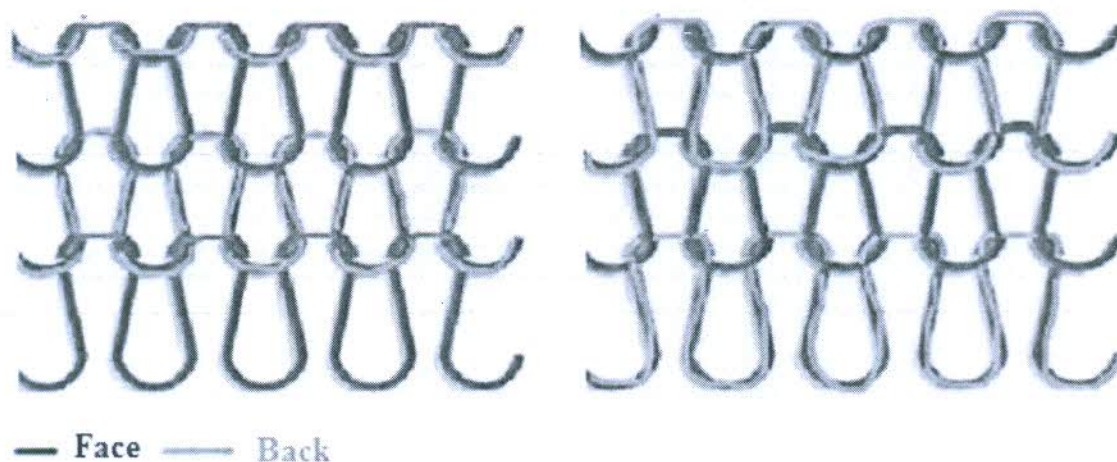


Figure 1. Schematics showing face & back layer of plated fabric.

al., 2010). Yarn hairiness and surface roughness are believed to affect the thermal absorptivity by the way they change the contact area between the fabric and skin. Carded yarns owing to the high hairiness tend to form the thick, insulating air layer reducing the contact between the fabric and skin; and therefore, exhibit

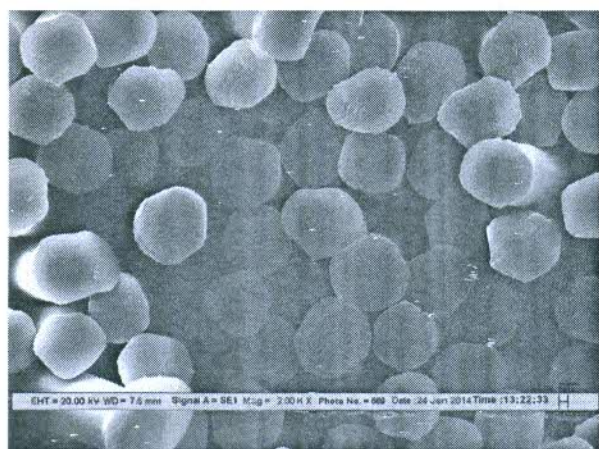
the lower thermal absorptivity compared to their combed yarn counterparts as shown in Figure 3.

Thermal resistance

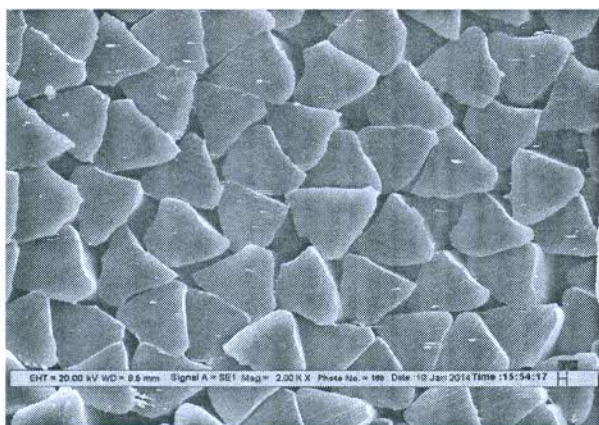
Figure 4 illustrate the effect of back layer fibre profile and face layer yarn type on thermal resistance of plated fabrics. Thermal resistance of fabrics using the combination of triangular polyester fibre and carded cotton yarn was higher compared to fabrics of circular fibres and combed cotton yarns. Incorporation of triangular fibres resulted in bulkier yarn as suggested by the high yarn diameter for the polyester yarn using the triangular fibre and high air volume fraction in the fabric structure due to the high fabric porosity value (Table 1). Moreover, triangular fibre fabrics were observed to be thicker and less dense compared to their circular counterparts. Fabric thickness, along with the air volume fraction dictates the thermal insulation properties of porous textile structures. In the light of above argument, the high thermal resistance of triangular polyester fibre fabrics is well justified. Yarn type, yarn spinning system, yarn count are known to affect thermal properties by affecting the fabric's bulk properties. High thermal resistance of carded yarn fabrics may be attributed to the hairy structure of carded yarn, which enables the formation of thick, insulating air layer. Air being the better thermal insulator than fibrous materials preventing the heat loss, and hence the high thermal resistance was observed for carded yarn fabrics.

Air permeability

The flow of air through inter-yarn spaces is an important means of providing comfort in hot, humid conditions. Yarn and fabric structural parameters affect air permeability properties of textiles by influencing the shape and area of channels, through which the air flow occurs (Raj & Sreenivasan, 2009). Plated fabrics knitted with the triangular polyester fibre and combed cotton yarn were observed to be more permeable to passage of air as shown in Figure 5. Triangular fibres are distinct from circular fibres in having edges, which may restrict the tight packing of fibres in the yarn structure with the consequence that the fabric structure becomes more open and fabric porosity increases.



(a)



(b)

Figure 2. SEM of polyester fibre cross section (a) Circular (b) Triangular.

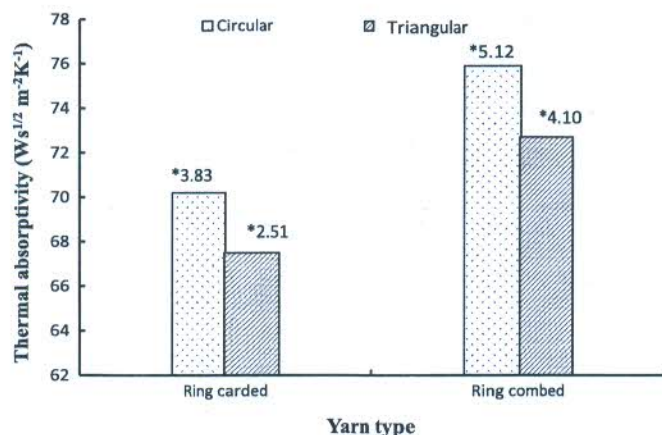


Figure 3. Thermal absorptivity of carded and combed yarn fabrics with varying polyester fibre profile.

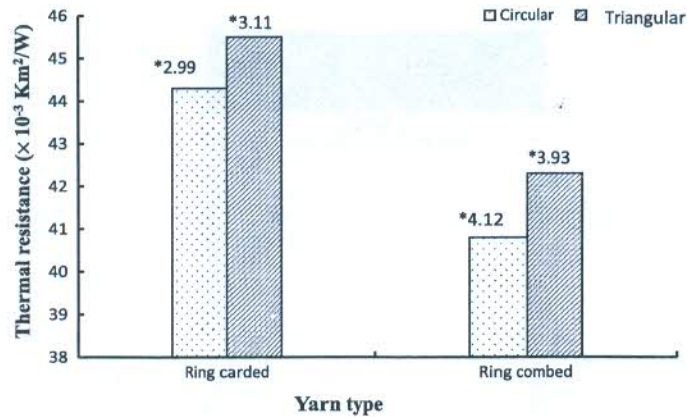


Figure 4. Thermal resistance of carded and combed yarn fabrics with varying polyester fibre profile.

Table 1. Plated fabric details.

Sample code	PET Fibre cross section	Yarn type	Yarn spinning system	Yarn diameter (mm)	Uster yarn hairiness (H)	Thickness (mm)	Aerial density (g/m ²)	Bulk density (kg/m ³)	Porosity (%)
RC2.2	Circular	Carded	Ring	0.215	22.21	0.960	239	248.95	82.94
RM2.2	Circular	Combed	Ring	0.181	18.14	0.95	248	261.05	82.11
RCT2.2	Triangular	Carded	Ring	0.195	12.13	0.99	245	247.47	83.05
RMT2.2	Triangular	Combed	Ring	0.216	10.55	0.98	247	258.16	82.73

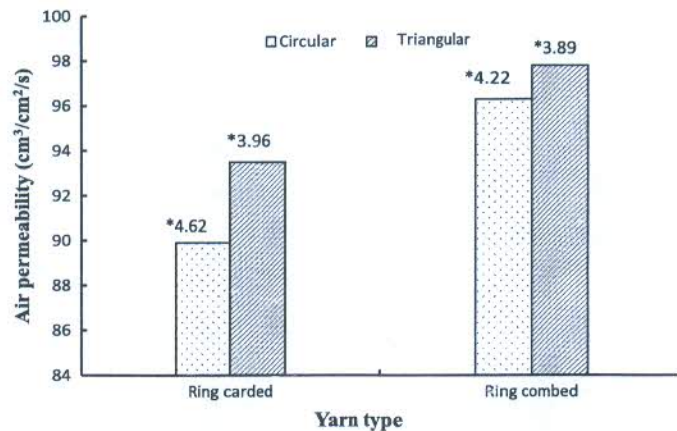


Figure 5. Air permeability of carded and combed yarn fabrics with varying polyester fibre profile.

Increase in the fabric porosity and inter-yarn spaces due to loose packing of fibres might have led to corresponding increase in air permeability of triangular polyester fibre fabrics. Less tortuous and continuous path is required for air flow through fabrics. The presence of protruding hair fibres in carded yarn fabrics might have blocked the inter-yarn pores; thereby, lowering the air permeability, however the absence of hairs in the combed yarn enable the unrestricted air passage through inter-yarn pores and correspondingly the high air permeability of combed yarn fabrics.

Moisture vapour transmission rate

Moisture transmission properties of textiles are crucial to maintain the dry skin microclimate as sweat accumulation near the

skin may add to feeling of wetness and discomfort for the wearer. Figure 6 suggests that changing the back layer fibre profile to triangular and use of combed cotton yarn in the face layer resulted in augmented values of moisture vapour transmission rate of tested fabrics. Moisture diffusion through fabrics depends on the fibre's moisture diffusivity and fabric porosity. Free open spaces enable an easy passage of moisture vapour through fabrics. In the present study, the fabrics were knitted with same fibre (polyester) in the back layer, hence the difference in moisture vapour transmission rate due to difference in moisture diffusivity of fibres had to be ruled out. However, the difference in fibre cross-sectional shape brings about the difference in inter-yarn spaces available for the moisture diffusion. High porosity of triangular fibre fabrics seems to be the probable reason for the high moisture passage through these fabrics. Carded yarns had

high hairiness values (Table 1) compared to their combed yarn counterparts. The inter-yarn spaces might have been blocked by the hairy structure of ring yarn; thereby, restricting free passage of moisture vapour, which is unlikely to happen in combed yarn fabrics having low hairiness resulting in high moisture vapour transmission in the combed yarn fabrics.

Transplanar wicking

Wicking properties of textiles are crucial for effective liquid moisture transfer. Fibre cross-sectional shape determines the size and geometry of capillary spaces between fibres and consequently determines the wicking rates (Cimilli, Nergis, Candan, & Ozdemir, 2010; Das et al., 2008; Tyagi et al., 2009). Plated fabrics with the triangular polyester fibre and combed cotton yarn in distinct back and face layers, respectively, showed the higher values of transplanar wicking compared to their circular fibre and carded yarn counterparts as shown in Figure 7. Non-circular fibre profile, i.e. triangular shape is characterized by the high shape factor and high specific surface area as compared to the circular fibre. High capillary pressure as a result of high specific surface area of triangular fibre fabrics account for their higher wicking values compared to circular fibre fabrics. Results are in accordance with the findings of Varshney et al., 2010 and

Das et al., 2008. Low yarn diameter of combed yarn compared to the carded yarn promote the formation of numerous capillaries of small diameter. The lower the capillary diameter, the greater will be the pressure created inside the capillary providing means for liquid flow. Moreover, the hairy structure of carded yarn may disrupt the continuity of capillaries and can even block some inter-yarn capillaries; combed yarn on the other hand seems to be forming more continuous capillaries owing to more uniform and less hairy structure. High transplanar wicking of combed yarn fabrics can therefore be explained well in the light of above arguments.

Absorbent capacity

Figures 8 and 9 show absorbent capacity of test fabrics with the different polyester profile and yarn type, respectively. Plated fabrics with triangular polyester fibre in the back and carded cotton yarn in the face layer showed higher absorbent capacity.* Water absorbency through the inter-fibre and inter-yarn channel is dependent on the number of capillaries formed, diameter of capillary and tortuosity of channels. Besides, the capillary geometry, bulk properties particularly fabric thickness, aerial density and porosity also governs the weight of water initially absorbed and held by fabrics. Fibres of varying cross-sectional shapes have

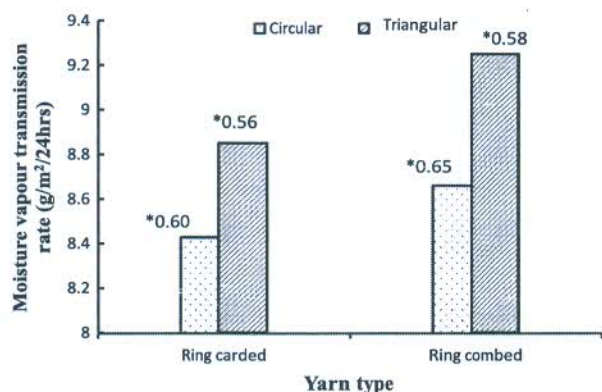


Figure 6. Moisture vapour transmission rate of carded and combed yarn fabrics with varying polyester fibre profile.

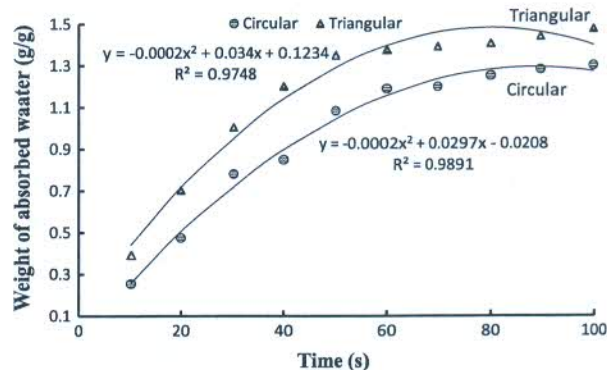


Figure 8. Absorbent capacity of fabrics with different polyester fibre profiles.

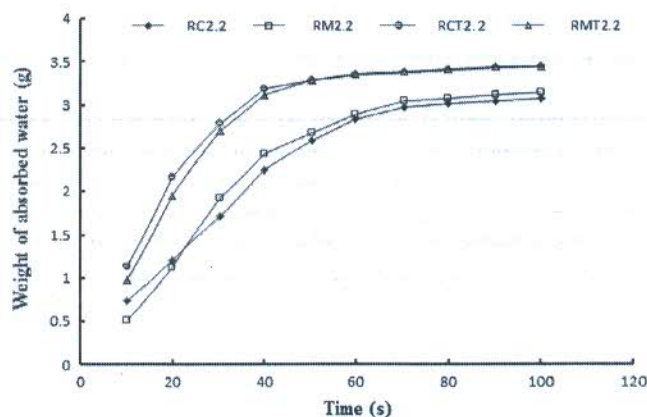


Figure 7. Transplanar wicking of test samples.

Note: RC2.2: ring carded circular; RM2.2: ring combed circular; RCT2.2: ring carded triangular; RMT2.2: ring combed triangular; PET dtex 2.2.

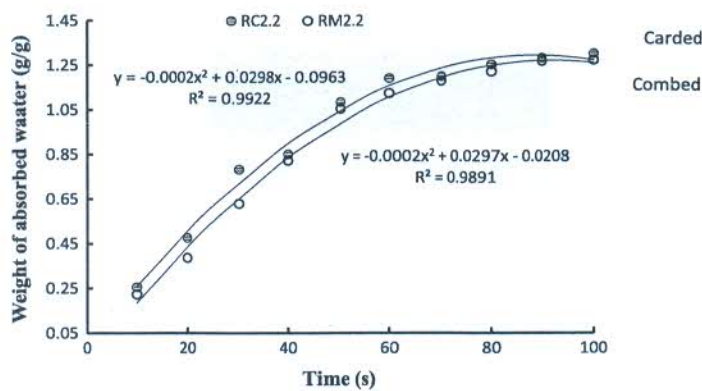


Figure 9. Absorbent capacity of fabrics with different yarn types.
Note: RC2.2: ring carded circular; RM2.2: ring combed circular.

the ability to reflect the increased or decreased capillarity, which in turn may affect the water uptake on wetting and water retention on drying (Cimilli et al., 2010). Triangular fibres resulted in fabrics of open structure and high porosity. Water entrapment increases with the increase in pore size and pore volume and hence the higher absorbent capacity for triangular fibre fabrics. High fabric thickness along with the high fabric porosity leading to the increased air volume fraction may have resulted in more water entrapment by pores; and hence the high water absorbing capacity of carded yarn fabrics (Figure 9).

Conclusions

The present study was aimed to investigate the influence of back layer fibre profile and face layer yarn type on thermal and mass transport properties of polyester–cotton plated fabrics. Both fibre profile and yarn type are found to affect the thermal, moisture vapour and liquid moisture transfer properties of developed plated fabrics. The understanding obtained from the study can serve as a useful insight for the development of plated fabrics with correct selection of fibre profile and yarn type in the distinct back and face layers, respectively. Plated fabrics using combination of triangular polyester fibre in the back and carded cotton yarn in the face layer showed the high thermal resistance, higher absorbent capacity and would be warmer to initial touch as indicated by the low value of thermal absorptivity.

However, the combination of combed cotton yarn in the face layer with the triangular polyester fibre in the back (next to the skin) layer resulted in fabrics with the high air permeability, moisture vapour transmission rate and transplanar wicking.

The findings of the study help to conclude that the use of triangular fibre in the back layer generally perform better than their circular counterparts in thermal properties, air and moisture vapour permeability as well as liquid moisture transfer properties. As far as face layer yarn types are concerned, the carded yarn seems to perform better in cold conditions and low activity levels as characterized by the high thermal resistance, low thermal absorptivity, low air and moisture vapour permeability and transplanar wicking. The combed yarns seem suitable for use in fabrics intended for warm climates and at high activity level as they exhibit the higher thermal absorptivity, air and moisture vapour permeability and high transplanar wicking.

Eventually, it can be concluded that plated fabrics for cold conditions to be worn at low activity levels can be designed with the combination of triangular fibre in the back and carded yarn in the face layers. However, triangular fibres in the back along with combed yarns in the face layers may be selected for plated fabrics meant for warm and high activity conditions.

Disclosure statement

No potential conflict of interest was reported by the authors.

References

- Behera, B. K., & Singh, M. K. (2013). Role of filament cross-section in properties of PET multifilament yarn and fabric. Part II: Effect of fibre cross-sectional shapes on fabric hand. *The Journal of The Textile Institute*, 1–12. doi:10.1080/00405000.2013.774132
- Bivainyte, A., & Mikucioniene, D. (2011). Air and water vapour permeability of double-layered weft knitted fabrics. *Fibres and Textiles in Eastern Europe*, 19, 69–73.
- Cimilli, S., Nergis, B. U., Candan, C., & Ozdemir, M. (2010). A comparative study of some comfort properties of different fibre types. *Textile Research Journal*, 80, 948–957.
- Das, B., Das, A., Kothari, V. K., Fanguiero, R., & Araujo, M. (2008). Effect of fibre diameter and cross-sectional shape on moisture transmission through fabrics. *Fibres & Polymers*, 9, 225–231.
- Geraldes, M. J., Lubos, H., Araujo, M., Belino, N. J. R., & Nunes, M. F. (2008). Engineering design of the thermal properties in smart and adaptive knitting structures. *Autex Research Journal*, 8, 30–34.
- Jhanji, Y., Gupta, D., & Kothari, V. K. (2015a). Comfort properties of plated knitted fabrics with varying fibre type. *Indian Journal of Fibre & Textile Research*, 40, 11–18.
- Jhanji, Y., Gupta, D., & Kothari, V. K. (2015b). Moisture management properties of plated knits with varying fibre types. *The Journal of The Textile Institute*, 106, 663–673.
- Karaca, E., Kahraman, N., Omeroglu, S., & Becerir, B. (2012). Effects of fiber cross sectional shape and weave pattern on thermal comfort properties of polyester woven fabrics. *Fibres & Textiles in Eastern Europe*, 3, 67–72.
- Kothari, V. K., & Sanyal, P. (2003). Fibers and fabrics for active sportswear. *Asian Textile Journal*, 55–56.
- Majumdar, A., Mukhopadhyay, S., & Yadav, R. (2010). Thermal properties of knitted fabrics made from cotton and regenerated bamboo cellulosic fibres. *International Journal of Thermal Science*, 30, 1–7.
- Matsudaira, M., & Kondo, Y. (1996). *The Journal of The Textile Institute*, 87, 409–416.
- Oglakcioglu, N., & Marmarali, A. (2010). Thermal comfort properties of cotton knitted fabrics in dry and wet states. *Tekstil Ve Konfeksiyon*, 3, 213–217.

- Ozdil, N., Marmarali, A., & Kretzschmar, S. D. (2007). Effect of yarn properties on thermal comfort of knitted fabrics. *International Journal of Thermal Science*, 46, 1318–1322.
- Pac, M., Bueno, M., Renner, M., & Kasmi, S. (2001). Warm cool feeling relative to tri biological properties of fabrics. *Textile Research Journal*, 71, 806–812.
- Patnaik, A., Rengasamy, R. S., Kothari, V. K., & Ghosh, A. (2006). Wetting and wicking in fibrous material. *Textile Progress*, 38, 1–105.
- Raj, S., & Sreenivasan, S. (2009). Total wear comfort index as an objective parameter for characterization of overall wear ability of cotton fabrics. *Journal of Engineered Fibers & Fabrics*, 4, 29–41.
- Singh, M. K., & Nigam, A. (2013). Effect of various ring yarns on fabric comfort. *Journal of Industrial Engineering*, 1–7. doi:10.1155/2013/206240
- Stankovic, S. B., Popovic, D., & Poparic, G. B. (2008). Thermal properties of textile fabrics made of natural and regenerated cellulose fibres. *Polymer Testing*, 27, 41–48.
- Su, C. L., Fang, J. X., Chen, X. H., & Wu, W. Y. (2007). Moisture absorption and release of profiled polyester and cotton composite knitted fabrics. *Textile Research Journal*, 77, 764–769.
- Tyagi, G. K., Krishna, G., Bhattacharya, S., & Kumar, P. (2009). Comfort aspects of finished polyester-cotton and polyester-viscose ring and MJS yarn fabrics. *Indian Journal of Fibre & Textile Research*, 34, 137–143.
- Varshney, R. K., Kothari, V. K., & Dhamija, S. (2010). A study on thermo-physiological comfort properties of fabrics in relation to constituent fibre fineness and cross-sectional shapes. *The Journal of the Textile Institute*, 101, 495–505.

Prediction of thermo-physiological properties of plated knits by different neural network architectures

Y Jhanji^{1,a}, D Gupta² & V K Kothari²

¹Department of Fashion & Apparel Engineering, The Technological Institute of Textiles & Sciences, Bhiwani 127 021, India

²Department of Textile Technology, Indian Institute of Technology Delhi, New Delhi 110 016, India

Received 4 August 2015; revised received and accepted 6 July 2016

Thermo-physiological properties of polyester-cotton plated knits have been predicted using two different network architectures (NA1 & NA2). NA1 consists of four individual networks working in tandem with common set of inputs and NA2 consists of one network giving four outputs. It is found that network architecture NA1 is able to predict the thermo-physiological properties of plated fabrics better as compared to NA2 network architecture. Sensitivity analysis is performed to judge the sensitivity or the importance of each input parameter in determining thermo-physiological properties of plated fabrics. The most sensitive parameter in prediction of thermal resistance is total yarn linear density, filament fineness for thermal absorptivity, loop length for air permeability and moisture vapour transmission rate.

Keywords: Neural network, Polyester-cotton plated knit, Thermo-physiological properties

1 Introduction

Thermo-physiological properties of textiles are crucial to provide comfortable microclimate to the wearer by managing controlled movement of heat, moisture vapour and liquid moisture from skin through clothing to environment. Along with the objective evaluation, prediction of thermo-physiological properties of textiles is equally challenging and crucial for characterization and designing of fabrics for any desired application before the actual commencement of fabric production. The thermo-physiological properties of textile materials can be predicted by mechanistic, statistical models and soft computing techniques.

Mechanistic models are useful tools in understanding the fundamentals and physics involved in heat and moisture transfer through textiles.

However, the assumptions considered in the simplification of mechanistic models may not be valid in all conditions and can lead to high prediction errors in real conditions owing to inherent variability in the textile structures. Statistical models can give good prediction performance, provided a large data set is presented to make the model and a relationship exists between input parameters and response variables. Statistical models fail to present satisfactory analysis of relationship in such cases. Artificial neural network is a stochastic (based on probabilistic method) and heuristic

model (action based on prior experience)¹⁻³. It simulates the functioning of a biological neuron and every component of the network is analogous to the actual constituents or operations of a biological neuron^{1, 4}. ANN has the ability to learn any kind of linear/non-linear relationship between input and output parameters during training and to make prediction based on the training experience. ANN also shows the ability of generalization by predicting values of responses for new unseen data set not used during the network training. Correct network training can drastically reduce the error between actual and predicted values. Selection of appropriate number of hidden layers, number of neurons in each hidden layer and division of data set into training and test set is a tricky process, as it dictates the training process and ultimately the network's performance. Training of ANN is followed by evaluation of the network performance separately for training and the testing data. Coefficient of determination (R^2) between experimental (target) and predicted values, mean absolute percentage error (MAPE) and mean square error (mse) are some of the statistical parameters with which performance of ANN is appraised.

Several researchers²⁻⁹ have attempted the prediction and optimization of various performance properties of textiles by using artificial neural network, statistical and theoretical models. Bhattacharjee and Kothari⁶ developed multi-layered feed forward neural networks to predict steady state and transient thermal properties

^aCorresponding author.
E-mail: yjhanji@gmail.com

of woven fabrics and concluded that better prediction of thermal behavior of fabrics can be achieved in case of different neural networks for different outputs. Shabridharan and Das¹⁰ compared ANN and statistical model for prediction of thermal properties of multilayered fabrics and obtained low mean absolute percentage error for ANN as compared to statistical model. Fayala *et al.*⁸ developed a three layered neural network with four input nodes corresponding to four inputs, viz fibre conductivity, fabric weight, porosity and air permeability to predict thermal conductivity of knitted fabrics and finally suggested that the developed model could predict thermal conductivity with correlation coefficient of 0.91. Pattanayak and Mittal¹¹ developed feed forward artificial neural network using two hidden layers and 20 neurons in each layer for prediction of air and water vapour permeability of knitted apparel fabrics and obtained error % between measured and predicted values of network lying within tolerance limit. Alibi *et al.*⁵ studied the relationship between elastic properties of knitted fabrics and structural parameters like knitted structure, yarn count, gauge, weight per unit area and thickness by ANN model and observed the robustness of the model in the prediction of elastic properties of fabrics. Majumdar *et al.*¹² predicted the single yarn tenacity of ring- and rotor- spun yarns using ANN and found good prediction performance of the developed model with mean error less than 5% for ring and rotor yarns. Baldua *et al.*¹³ developed artificial neural network and response surface model for prediction of air- jet textured yarn properties and obtained low level of prediction error for ANN. Ozkan *et al.*¹⁴ used feed forward and general regression neural networks for prediction of nips stability and number of nips, and concluded that former model shows better

performance (at most 6%) than the latter in terms of prediction accuracy on train and test data sets.

Although some studies have discussed^{6,10-11} prediction of thermal properties i.e. thermal resistance, thermal conductivity of woven and knitted fabrics, none of the studies give a detailed review of the modelling of comfort properties particularly thermal absorptivity and moisture vapour transmission rate of plated knitted fabrics. Moreover, very few studies are devoted to the prediction of thermo-physiological properties such as thermal properties, air permeability and moisture vapour transmission rate collectively. In the present work therefore, attempts have been made to model the thermo-physiological properties of plated knitted fabrics from constructional parameters like yarn linear density, filament fineness and loop length using two different network architectures and to compare developed models in terms of their prediction performance and robustness. Sensitivity analysis has also been undertaken to evaluate the relative importance of each input parameter on the thermo-physiological properties.

2 Materials and Methods

2.1 Materials

A total of 50 C/PET (cotton polyester) plated knitted fabrics were used for the study. Out of the 50 samples, 40 samples (80%) were presented as training set to neural network and remaining 10 samples (20%) were used as the testing set. All the samples were prepared on flat knitting machine (Elex, China) with machine gauge of 14, needle bed of 42 inches and 588 needles on each bed. The machine had two needle beds called front and rear bed. The front bed was utilized for the preparation of single jersey plated fabrics. Fabric specifications of test set are shown in Table 1.

Table 1 — Specifications of test set

Sample code	Back LD, tex	Filament fineness, dtex	Total LD tex	Loop length mm	Thermal resistance $\times 10^{-3}$ km^2/W	Thermal absorptivity $\text{Ws}^{1/2}/\text{m}^2\text{K}$	Air permeability $\text{cm}^3/\text{cm}^2/\text{s}$	MVTR $\text{g}/\text{m}^2/24\text{h}$
CPET3	11.1	2.31	40.63	6.4	20.5	84.0	156.1	5.99
CPET6	11.1	1.54	40.63	5.0	20.5	94.1	113.1	5.10
CPET10	11.1	1.54	40.63	7.1	24.5	70.1	168.2	6.13
CPET15	11.1	1.1	40.63	7.1	31.2	68.5	155.0	5.99
CPET27	16.7	2.31	46.2	6.0	22.8	92.5	96.5	5.15
CPET30	16.7	2.31	46.2	7.1	25.5	74.2	133.0	5.98
CPET32	26.1	3.62	55.63	6.0	23.8	111.9	95.0	3.66
CPET35	26.1	3.62	55.63	7.1	29.2	81.3	131.0	5.82
CPET41	33.3	4.62	72.70	5.0	31.1	149.5	59.8	3.05
CPET45	33.3	4.62	72.70	7.1	35.1	131.0	127.3	5.01

LD – Yarn linear density, MVTR – Moisture vapor transmission rate.

2.2 Methods

2.2.1 Objective Evaluation

Thermal properties such as thermal resistance and thermal absorptivity were measured using Alambeta (Sensora, Czech Republic). In this instrument fabric is kept between hot and cold plate. The heat transfer from hot plate to cold plate through fabric is determined by the instrument. Air permeability of fabrics was determined by FX 3300 air permeability tester (Textest AG, Switzerland) at a pressure of 98 Pa according to ASTM D 737. Moisture vapour transmission rate of the fabrics was tested on moisture vapour transmission cell (MVTR cell) (Grace, Cryovac division). Amount of water vapour that transmits through 100 inch² fabric area during period of 24 h can be determined by this instrument rapidly.

Difference in humidity maintained on two sides of test fabric positioned in MVTR cell enables moisture vapour transmission rate to be determined according to the following equation:

$$MVTR = (269 \times 10^{-7}) \left(\Delta RH\% \times \frac{1440}{t} \right) H \quad \dots (1)$$

where $\Delta RH\%$ is the average difference in successive % RH values; t , the time interval (min); and H , the amount of water in g/m³ of air at cell temperature.

2.2.2 Development of Artificial Neural Network

Multilayered back propagation feed forward neural network was used to predict the thermo-physiological properties of plated fabrics. All the programming was done using MATLAB software neural network toolbox.

Sigmoid transfer function 'tansig' was used for input and hidden layers and a linear function 'purelin' was used for the output layer. Normalization was

applied to both input and target vectors. 'mapminmax' function was used to normalize inputs and targets to fall in the range of -1 to 1. Network was trained using 'trainlm' function which is Levenberg-Marquardt algorithm. Structural elements of different network architectures are presented in Table 2.

Two different network architectures (NA1 & NA2) were developed and compared for their prediction performance. Network architecture (NA1) – consisted of four sequential networks (NN1, NN2, NN3 and NN4) working in tandem with input layer of 4 nodes in turn corresponding to four input parameters, namely back layer yarn linear density, filament fineness, total yarn linear density and loop length, and an output layer of 1 node corresponding to the property to be predicted. Back layer in the study is referred to inner/next to skin layer. Polyester yarns of 11.1, 16.7, 26.1 and 33.3 tex were used in the back/inner layer. Four levels of loop length i.e. 5, 6, 6.4 and 7.2 mm were selected for the present study. The levels of loop lengths were selected to engineer fabrics of slack, medium and tight construction. However, GSM was not included in the list of input parameters as yarn linear density directly influences the GSM of fabrics. Hence, only yarn linear density was selected as one of the input parameters owing to its influence on GSM.

The four different networks fed with common set of inputs gave individual single outputs i.e. output of NN1 was thermal resistance, output of NN2 was thermal absorptivity, air permeability and moisture vapour transmission rates were the outputs of NN3 and NN4 respectively. Three layered network with one input layer, one hidden layer and one output layer was used for the four networks. The number of

Table 2— Structural elements of different network architectures

Elements	Individual networks				Combined network TR, TA, AP, MVTR
	NN1	NN2	NN3	NN4	
Output parameters	TR	TA	AP	MVTR	
Input parameters	Back LD, filament fineness, total LD, LL				Back LD, filament fineness, total LD, LL
Number of nodes in input layer	4	4	4	4	4
Number of hidden layers	1	1	1	1	2
Number of nodes in hidden layers	7	4	7	7	5,10
Transfer function between input & hidden layer	Tansig	tansig	tansig	tansig	tansig
Transfer function between hidden & output layer	Purelin	purelin	purelin	purelin	purelin
Training rule	LM algorithm	LM algorithm	LM algorithm	LM algorithm	LM algorithm

TR— Thermal resistance, TA— Thermal absorptivity, AP— Air permeability, MVTR— Moisture vapour transmission rate, LD— Yarn linear density, LL— Loop length, tansig— Tan sigmoid, purelin— linear transfer functions and, LM—Levenberg- Marquardt algorithm.

neurons was fixed after many trials at 7, 4, 7 and 7 for NN1, NN2, NN3 and NN4 respectively (Table 2). Trial and error method was employed i.e. working with different number of hidden layers and neurons and the combination that gave maximum coefficient of determination and minimum error was selected for networks. Figure 1 shows the network architecture of NA1.

Network architecture (NA2) – consisted of single network with same set of input parameters as in NA1 but with four nodes in the output layer corresponding to four predicted properties, namely thermal resistance, thermal absorptivity, air permeability and moisture vapour transmission rate. Four layered network with one input layer, two hidden layers with 5 and 10 neurons and one output layer was used for the network as shown in Table 2. Figure 2 shows the network architecture of NA2.

Figure 3 shows the weights and bias connections between input, hidden and output layers for individual network with thermal resistance as output. Weights and bias connections between input, two hidden and

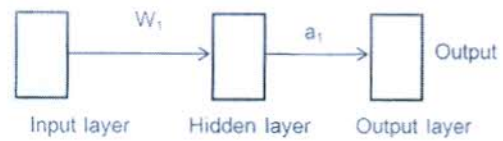


Fig. 1 — Network architecture of NA1 for individual thermo-physiological properties (thermal resistance, thermal absorptivity, air permeability and moisture vapour transmission rate)

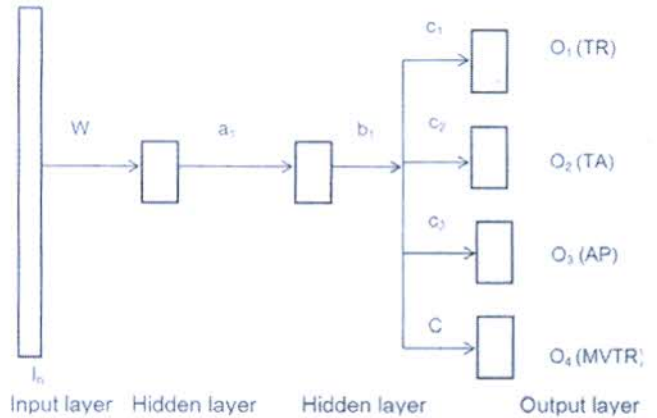


Fig. 2 — Network architecture for combined network with four outputs (TR — thermal resistance, TA — thermal absorptivity, AP — air permeability and MVTR — moisture vapour transmission rate)

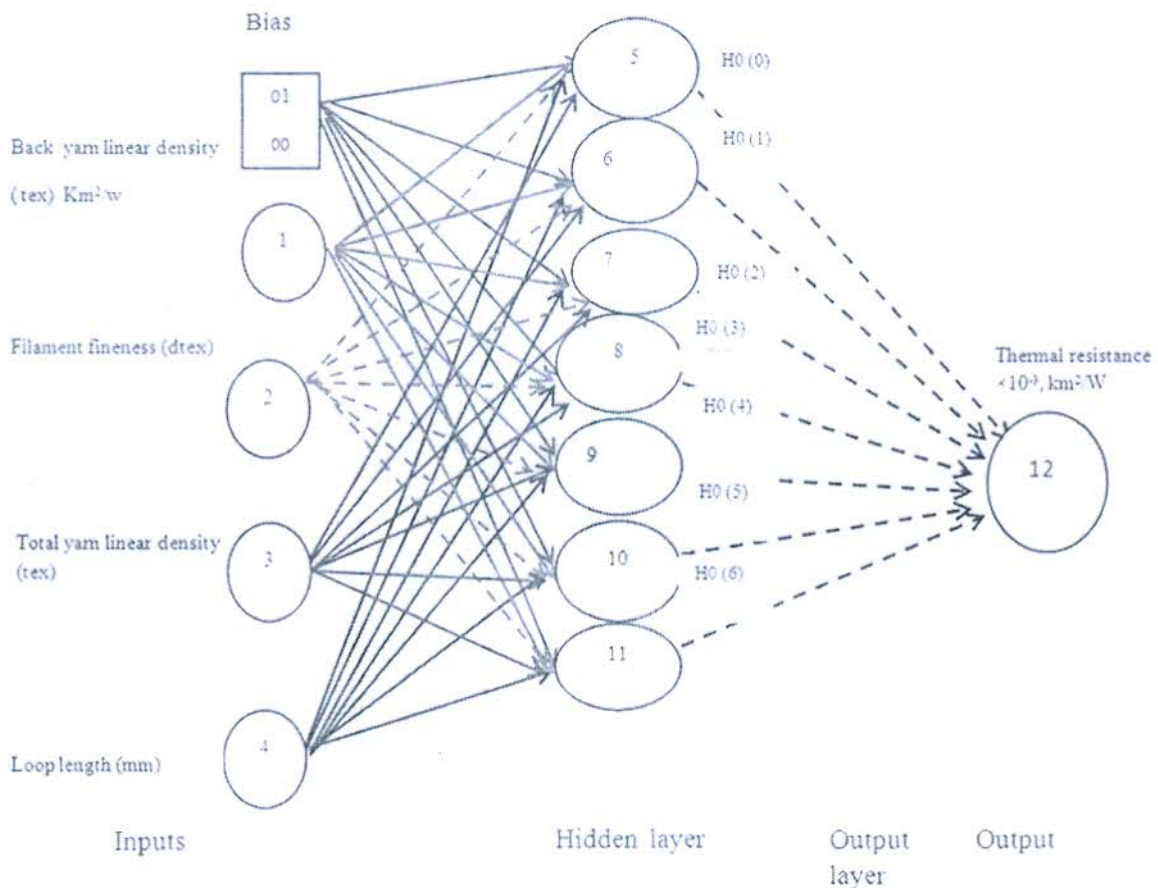


Fig. 3 — Weight and bias connections and different layers of individual network

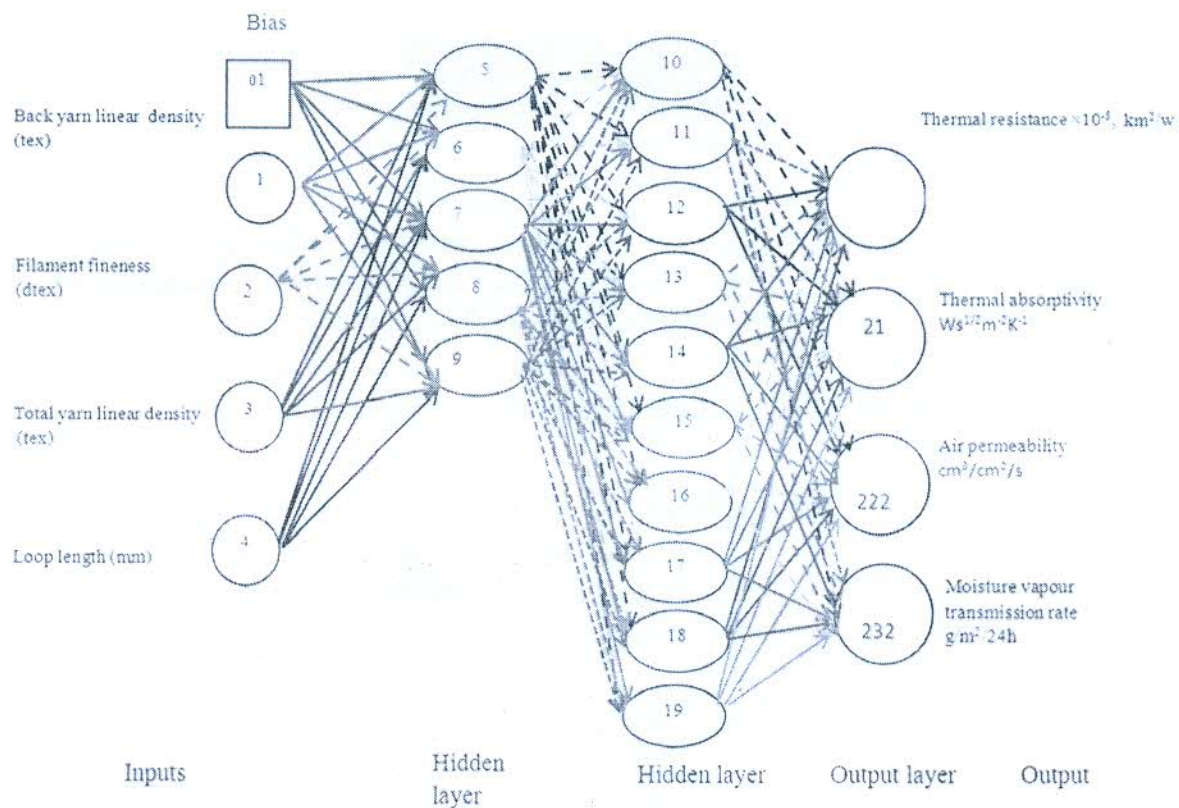


Fig. 4— Weight and bias connections and different layers of combined network

one output layer for combined network with four outputs is shown in Fig. 4.

2.2.3 Sensitivity Analysis

Sensitivity analysis was performed to judge the sensitivity or the importance of each input parameter in determining thermo-physiological properties of plated fabrics. Each input was eliminated once from the optimized neural network and then trained again up to the optimum level.

3 Results and Discussion

3.1 Prediction Performance

Prediction performance of the two different network architectures i.e. individual networks (NN1, NN2, NN3 & NN4) & combined network has been compared in terms of mean absolute percentage error (MAPE) and coefficient of determination (R^2). Individual errors between experimental and ANN predicted values and mean absolute percentage error of thermal resistance, thermal absorptivity, air permeability and moisture vapour transmission rate are calculated and summarized in Table 3.

Mean absolute percentage errors for thermal resistance, thermal absorptivity, air permeability and

moisture vapour transmission rate were found to be 2.03, 3.1, 3.15 and 2.58% for training data set and 4.84, 5.13, 7.40 and 7.25% respectively for test data set for individual networks to predict four properties individually.

Mean absolute percentage errors are found to be 5.03, 8.61, 10.45 and 18.23% for thermal resistance, thermal absorptivity, air permeability and moisture vapour transmission rate respectively for combined network used to obtain four outputs.

Individual error % and mean absolute percentage errors for all four properties under consideration are found to be lower for individual networks compared to combined network, suggesting that individual networks (each giving one output) can predict the thermo-physiological properties in close agreement with experimental values as compared to combined network giving four outputs. Individual networks (NN1, NN2, NN3 & NN4) include less number of hidden layers and less number of epochs (10, 32, 18 & 16) to reduce performance function (Table 4)

Combined network consume higher processor memory for 101 iterations, and training time is also higher for combined network (1.46 s) as compared to

Table 3 — Individual errors between experimental and predicted values of tested properties

Sample code	Thermal resistance $\times 10^{-3}$, km^2/W		Thermal absorptivity $\text{Ws}^{1/2}/\text{m}^2\text{K}$		Air permeability $\text{cm}^3/\text{cm}^2/\text{s}$		Moisture vapour transmission rate $\text{g}/\text{m}^2/24\text{h}$	
	Experimental	Predicted	Experimental	Predicted	Experimental	Predicted	Experimental	Predicted
CPET3	20.50	21.135 (3.10)	84.0	83.74 (0.31)	156.13	152.48 (2.34)	5.99	6.26 (4.55)
CPET6	20.50	21.200 (3.42)	94.1	85.18 (9.48)	113.13	126.38 (11.71)	5.10	4.81 (5.77)
CPET10	24.50	26.593 (8.54)	70.1	72.22 (2.99)	168.20	154.89 (7.91)	6.13	6.69 (9.12)
CPET15	31.20	32.455 (4.02)	68.5	72.10 (5.25)	155.00	148.97 (3.89)	5.99	6.44 (7.45)
CPET27	22.80	22.417 (1.68)	92.5	87.48 (5.43)	96.50	90.46 (6.26)	5.15	5.56 (8.00)
CPET30	25.50	26.395 (3.51)	74.2	73.36 (1.14)	133.00	130.94 (1.55)	5.98	6.27 (4.78)
CPET32	23.87	23.345 (2.20)	111.9	97.25 (13.11)	95.00	81.44 (14.28)	3.66	4.64 (26.92)
CPET35	29.22	26.356 (9.80)	81.32	87.37 (7.44)	131.00	128.52 (1.89)	5.82	5.86 (0.60)
CPET41	31.10	33.847 (8.83)	149.5	141.90 (5.12)	59.80	55.70 (6.85)	3.05	3.07 (0.78)
CPET45	35.06	36.219 (3.30)	131.0	132.40 (1.07)	127.30	105.66 (17.00)	5.01	5.24 (4.53)
MAPE		4.84		5.13		7.37		7.25

Values in parenthesis are Error%, MAPE— Mean absolute percentage error.

Table 4— Performance parameters of different network architectures

Parameter	Thermal resistance $\times 10^{-3}$, km^2/W		Thermal absorptivity $\text{Ws}^{1/2}/\text{m}^2\text{K}$		Air permeability $\text{cm}^3/\text{cm}^2/\text{s}$		Moisture vapour transmission rate, $\text{g}/\text{m}^2/24\text{h}$	
	NN1	Combined network	NN2	Combined network	NN3	Combined network	NN4	Combined network
Network architecture	4-7-1	4-5-10-4	4-4-1	4-5-10-4	4-7-1	4-5-10-4	4-7-1	4-5-10-4
Epochs	10	101	32	101	18	101	16	101
Performance ratio	0.9	0.9	0.9	0.9	0.9	0.9	0.9	0.9
Average elapsed time, s	1.5	1.46	0.5	1.46	1.25	1.46	0.45	1.46
MAPE	4.59	5.03	5.13	8.61	7.40	10.45	7.25	18.23
Max. error %	9.80	10.13	13.10	22.71	17.0	26.47	26.9	51.66
Min. error%	1.68	0.25	0.31	0.99	1.55	0.18	0.60	0.85
r^2	0.92	0.89	0.95	0.84	0.93	0.89	0.90	0.90

individual networks which takes 0.93s to converge (Table 4). Figures 5 (a) – (d) show the relationship between experimental and network predicted values of the thermo-physiological properties i.e. thermal resistance, thermal absorptivity, air permeability and moisture vapour transmission rate respectively. R^2 values are over 0.9 for all the thermo-physiological properties, suggesting robustness and generalization power of the network architectures giving four different outputs, as four individual models are able to explain 90% variability in the test data set.

Individual networks giving four single outputs predict the thermo-physiological properties with good

coefficient of determination (0.92, 0.95, 0.93 and 0.9) for thermal resistance, thermal absorptivity, air permeability and moisture vapour transmission rate respectively. The mean absolute percentage errors are also found less as compared to the errors obtained from the combined network (Table 4). R^2 values obtained from the combined network such as 0.89, 0.84, 0.89 and 0.90 (Table 4) for the four outputs are found lower than NA1, suggesting that NA1 architecture shows better prediction ability.

Mean absolute percentage error which indicates the difference in target and predicted values is higher for prediction of air permeability and moisture vapour

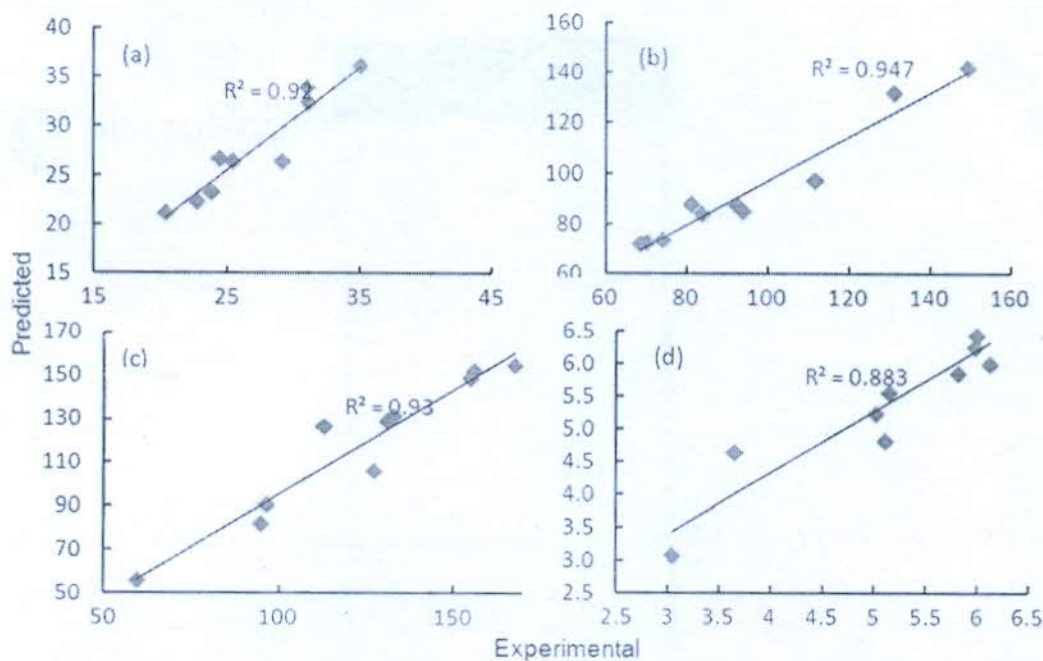


Fig. 5 — Correlation between experimental and ANN predicted [(a) thermal resistance ($\times 10^{-3} \text{ km}^2/\text{W}$), (b) thermal absorptivity ($\text{Ws}^{1/2}/\text{m}^2\text{K}$), (c) air permeability ($\text{cm}^3/\text{cm}^2/\text{s}$) and (d) moisture vapour transmission rate ($\text{g}/\text{m}^2/24\text{h}$)]

transmission rate as compared to thermal properties for both network architectures. However, mean absolute percentage error for the two properties is higher in combined network as compared to that in individual networks. The input parameters selected for the network construction such as back yarn linear density, filament fineness, loop length and total yarn linear density influence the fabrics bulk properties like thickness, fabric weight and are the determinants of thermal properties. Selection of the input parameters can influence the prediction performance of the developed networks. The selected input parameters are found sufficient for prediction of thermal properties. However, air permeability depends on the openness of the fabric structure and fabric porosity. The exclusion of porosity as one of the input parameters might be the reason for high mean absolute percentage error in prediction of air permeability. Moisture vapour transmission rate through fabrics depends on free air spaces in the fabric for moisture diffusion and moisture diffusivity of the fibres. Hydrophilic and hydrophobic nature of the fibre can affect the moisture diffusion through textiles significantly. The inclusion of constituent fibres as one of the input parameters to neural network may result in lowering the error percentage in prediction of moisture vapour transmission rate. The predicted thermo-physiological properties of

plated fabrics by NAI are in close agreement with target outputs (experimental values) which proves the robustness and generalization ability of the network.

3.2 Sensitivity Analysis

MSE (mean square error) ratio ranks the sensitivity or the importance of input parameters of neural network. MSE ratio of test data set before and after exclusion of input parameters is used for the sensitivity analysis (Table 5). Change in MSE is noted after exclusion of each input parameter from network architecture, as shown in following equation:

$$\text{MSE}_{\text{ratio}} = \frac{\text{MSE}_e}{\text{MSE}_{ei}} \quad \dots (2)$$

where MSE_e is the mse after excluding respective input parameters; and MSE_{ei} , the mse before excluding input parameters.

Higher $\text{MSE}_{\text{ratio}}$ indicates that the corresponding excluded parameter is more sensitive in determining the thermo-physiological properties. Based on $\text{MSE}_{\text{ratio}}$, input parameters are ranked according to sensitivity with rank 1 given to the most sensitive parameter and 4 to the least sensitive input parameter in determining thermo-physiological properties of plated fabrics. Decreasing order of sensitivity of input parameters in determining thermal resistance is total yarn linear density, filament fineness, back layer yarn linear density and loop length. Hence; based on sensitivity

Effect of Sewing Process on Tensile Properties of Sewing Threads in Denim Garment

Vishal Trivedi^{1*}, Girendra Pal Singh² & Shelly Khanna³

¹(Department of Textile Technology, Panipat Institute of Engineering and Technology,

²(Department of Fibres & Textiles Processing Technology, Institute of chemical Technology,

³(Department of Fashion & Apparel Engg. The Technological Institute of Textile & Sciences,

Abstract

The objectives of study were to analyse the effect of different sewing process on tensile behaviour of sewing thread in denim garments. In this study six types of sewing threads were used to stitch denim fabric using lockstitches and chainstitches in lapped seam. Tensile behaviour of all sewing threads were compared in terms of tenacity, initial modulus and breaking energy for lockstitch and chainstitch process. The reduction in all the tensile properties were observed for all type of sewing thread for both the sewing process. Tensile properties of sewing thread were identified at fixed sewing machine speed (RPM), Stitch density (SPI) and needle size. A direct current shunt motor is used for single needle lockstitch and chainstitch (feed of the arm) machine. For chainstitch process tensile properties of all sewing threads were found poor as compared to lockstitch process. From this study it can be concluded that lockstitch is more stronger than chainstitch for superior mechanical properties.

Keywords

Direct current shunt motor, Lock and chain stitch, Sewing Thread, Stitch density, Tensile Properties.

1. Introduction

Clothing manufacturing is the process of making garment/apparel from flat fabric to match the shape of the Human body. This flat/ two-dimensional fabric is converted into three-dimensional garment after stitching [1]. Sewing a textile fabric is a very pin pointed operation which is governed by a broad spectrum of parameters like the type of sewing machine, the stitching velocity, the structure of sewing operation, the method and the ability of worker, the selection of stitching parameters, seam appearance (straightness, proper stitches). The seam tensile performance (strength, elasticity) is the result of a combination of all these factors [2]. Many typical sewing problems occur such as skip stitches, thread breakage, fabric damage, faulty seam appearance, needle damage, which reduces productivity and seam quality [3].

Seam strength is dependent on the thread strength; a reduction in thread strength during sewing will lead to lower seam strength than expected [4]. Therefore, in order to minimize the thread strength reduction, it is important to understand the contribution of different

machine elements or processes during sewing. During high-speed sewing, the dynamic and thermal loadings are found to be the major causes of strength reduction of needle thread, which can go up to 30-40 per cent [5]. The type of sewing thread and the selection of seams play a major role in seam quality. These parameters have great significance role garment durability, especially for the fashionable denim garments [6]. When a needle penetrates in the fabric, the upper and the lower threads loop insert within the fabric. The fabric yarns are bent, stressed, and attempting to return to their original positions, but are prevented by the sewing threads [7]. The fabric structural jamming is the most influenced by the sewing thread diameter alongside with other factors such as fabric properties, seam type, stitch density [8].

In Lock stitch interlacing occurs, stitch formation is done by using 2 threads (needle thread+ bobbin thread). A rotary hook catches the needle thread loop as it passes around the bobbin and interlocks the 2 threads. Lock stitches have a neat appearance and most secure stitch.

In chain stitch interlacing and interloping occurs, it requires one or more needle threads that form loops as they pass through the fabric and inter-loop with the looper thread on the underside. It is more durable and used extensively on apparel [9].

*All the correspondences should be addressed to,
Mr. Girendra Pal Singh,
Department of Fibres & Textiles Processing Technology,
Institute of chemical Technology, Mumbai, India
Email : singhgirendra2000@gmail.com

This research focuses on the effect of different sewing thread and sewing process on mechanical properties of sewing thread in denim garments and to find suitable combination of sewing thread and sewing process for denim garments. The mechanical properties (breaking load, breaking extension and breaking energy) of the different sewing thread unraveled from the seams in the lock stitched and chain stitched denim fabrics were compared with those of the parent sewing thread.

2. Material and Methods

2.1. Selection of sewing threads

The sewing threads used in this work procured from Vardman yarns & threads Ltd. Hoshiarpur, Punjab (INDIA). Two different types core spun ((Poly-Poly & Poly-cotton) sewing threads having three different counts were selected as per compatibility with the fabric GSM. Physical characteristics of different selected sewing threads were analysed and reported in Table 2.1.

Note: T (gm/tex) - Tenacity, M (gm/tex) - Modulus, B (J) - Breaking Energy, Friction co-eff. - Friction coefficient against metal surface, Y to Y abrasion - Yarn to yarn abrasion (cycle at break)

The twist per inch was measured by Twist tester as

Table 2.1: Physical characteristics of sewing threads

Code	Tex Size	Ply	TPI	T(gm/tex)	M(gm/tex)	B (J)	Friction Co-eff.	Y to Y Abrasion	Shrinkage (%)
PC90	90	2	14.37	34.34	211.8	1.13	0.08	1890	0.6
PC105	105	3	11.78	43.39	217.4	3.48	0.12	2340	0.8
PC120	120	3	11.52	47.14	251.0	4.56	0.17	1962	0.46
PP90	90	2	13.9	48.86	258.3	2.19	0.07	1666	0.21
PP105	105	3	11.12	51.90	259.6	3.55	0.12	2013	0.12
PP120	120	3	10.65	54.05	250.5	4.55	0.16	1816	0.18

per ASTM standard D-1422 and friction coefficient and abrasion resistance were measured using the Lawson Hemphill friction meter as per ASTM standard D-3108 & yarn abrasion tester as per ASTM standard D-6611 respectively. Sewing thread shrinkage is calculated according to boiling water shrinkage method (ASTM D-204). The tensile characteristics of all the parent threads were tested on Instron tensile tester - 4411 as per standard ASTM D-2256.

2.2 Denim fabric specification

The selected denim fabric construction and structure were analyzed and reports in Table 2.2.

Table 2.2: Construction Parameter of denim fabric

Fabric	Classical Denim
Fabric composition	100% Cotton
GSM	326 (10.50oz/yd2)
EPI	72
PPI	40
Warp Count	7.50 Ne
Weft Count	9 Ne
Weave	2/1 Twill
Fabric Thickness	0.77mm (Single Layer)

Fabric GSM was measured with an electronic weighing balance. End and Pick density were measured using the pick glass. Fabric thickness was measured with the help of R & B Thickness Tester.

2.3 Sewing of denim fabric

Single needle Lockstitch machine (JUKI-DDL-8300N) and Chain stitch machine (Feed off the arm MS-191) were used for sewing of denim fabric at the speed of 1500 stitches per minute with needle size 21 (130

Nm) having stitch density 8 SPI. The Lapped seam L5a type was used to stitch two layers of fabrics. The fabric samples were cut to convenient sizes of 24x2.5 inches (for making lapped seam and easily unraveling of threads from the sample) and weft way lapped seam are stitched. Identical settings of foot pressure and needle thread tension were maintained at the same level for all the seams produced. Sixty samples were prepared on both machines for each type of sewing thread.

The needle threads were extracted from the stitched denim fabric after cutting thread from supply package and carefully removed at constant pressure avoid extension and loss of twist. Tensile testing of needle thread before and after sewing was tested at a gauge length of 500mm (20 inches) on Instron tensile testing machine as per ASTM standard D-2256.

Percentage reduction in tenacity, Initial modulus and Breaking energy for all types of sewing threads were calculated using following formula [9].

$$\text{Change (\%)} = \frac{T \text{ After sewing} - T \text{ Parent thread}}{T \text{ Parent thread}} \times 100$$

T = Tenacity in gm/tex

3. Results and Discussions

3.1 Effect of sewing process on the tensile properties of unraveled Polyester-Cotton (PC) sewing threads

The tensile properties of PC core spun sewing thread before and after sewing were shown in Table 2.1 and Table 3.1 respectively.

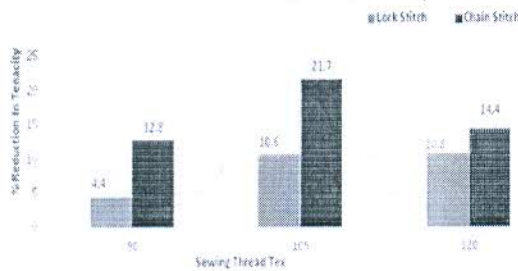


Figure 3.2 : Percentage reduction in tenacity of unraveled PC sewing threads

The decrease in tenacity was observed in all PC unraveled sewing threads as shown in Fig 3.2 As yarn count (Tex) increases, % loss in tenacity increases in sewing threads unraveled from lock stitched denim fabric which can be attributed to the abrasion of sewing thread between needle and fabric. This abrasion was more for 120 Tex yarn because of the higher surface area which causes pulling out of more fibres on the surface of yarn which was confirmed by microscopic analysis of thread (Fig.3.5).

The percentage loss in tenacity was more in all threads unraveled from chain stitched denim fabric as compared to threads unraveled from lock stitched denim fabric because lock stitch unraveled needle threads have to reach up to the fabric bed. But the tension fluctuations in the interlacing processes for lock stitches might have compensated for energy losses due to the combined effect of interloping and interlacing stitch formation processes in chain stitches.

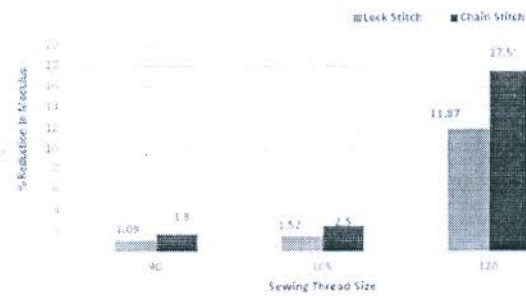


Figure 3.3 : Percentage reduction in modulus of unraveled PC sewing threads

An increasing % loss in modulus for PC core spun sewing thread has been observed for the increasing

Table 3.1: Percentage reduction in tensile properties of unraveled PC sewing threads

Sewing Threads	90 Tex		105 Tex		120 Tex	
	Lock stitch	Chain stitch	Lock stitch	Chain stitch	Lock stitch	Chain stitch
Property						
Tenacity(gm/tex)	32.8	29.9	38.8	34.0	42.0	40.3
% Reduction in Tenacity	4.4	12.8	10.6	21.7	10.8	14.4
Initial modulus (gm/tex)	209.5	208.1	214.1	212.0	221.2	207.0
% Reduction in Initial modulus	1.09	1.8	1.52	2.5	11.87	17.5
Breaking Energy(J)	1.08	1.02	2.82	2.64	3.79	3.56
% Reduction in Breaking Energy	4.4	9.73	18.96	24.13	16.88	21.92

Tex from 90 Tex to 120 Tex as shown in Fig-3.3. This can be attributed to the increased abrasive damage which causes displacement of plies and loosening of structure and also the non contribution of the higher no. of surface fibers in thread tension leading to a higher loss in initial modulus for coarser needle threads.

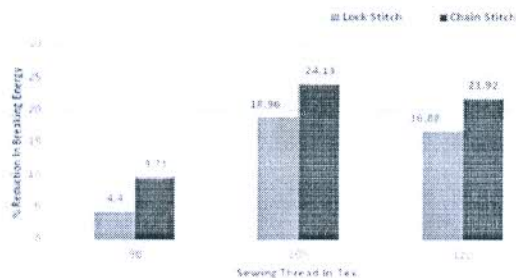


Figure 3.4 : Percentage reduction in breaking energy of unraveled PC sewing threads

The breaking energy of a thread is directly related to the tenacity. As thread count (Tex) increases, the energy required to break the thread also increases for the parent threads (Table 2.1). The needle threads unraveled from the chain stitches show the similar trends as for tenacity for the same threads (Table 3.1). The % loss in breaking energy was highest for 105 Tex for thread unraveled from lock stitched and chain stitched denim fabrics. The % loss for thread unraveled from lock stitched denim fabric was lesser as compared to thread unraveled from chain stitched denim fabric for all sewing thread (Fig 3.4). The greater loss in energy to break for needle threads of chain stitch owe to the fact that greater fabric thickness along with four fabric

layers that the needle threads have to pierce to make its way into the seam configuration.

The effect of abrasion between needle and fabric on the surface of sewing threads can be seen in Fig 3.5. From figures, it can be observed that in parent thread fibres on the surface were very less. The amount of fibres pull out due to abrasion was found more on the surface of thread unraveled from chain stitched denim fabric as compared to the surface of thread unraveled from lock stitched denim fabric. These more surface fibres cause more deterioration in mechanical properties of sewing thread during chain stitch process.

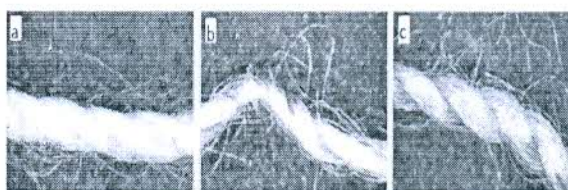


Figure 3.5 : The effect of abrasion between needle and fabric on the surface of PC sewing threads
(a: Parent thread, b: Lock stitch unraveled thread, c: Chain stitch unraveled thread)

3.2 Effect of sewing process on the tensile properties of unraveled PP needle sewing threads

The tensile properties of Poly-Poly core spun sewing thread before and after sewing were shown in Table 2.1 & Table 3.6 respectively.

Table 3.6 : Percentage reduction in tensile properties of unraveled PP sewing threads

Sewing Threads	90 Tex		105 Tex		120 Tex	
	Lock stitch	Chain stitch	Lock stitch	Chain stitch	Lock stitch	Chain stitch
Tenacity(gm/tex)	46.80	44.51	46.86	45.44	50.60	48.50
% Reduction in tenacity	4.21	8.92	9.71	12.44	6.38	10.26
Initial modulus (gm/tex)	254.4	255.3	252.4	249.3	225.8	214.6
% Reduction in initial modulus	1.5	1.16	2.77	3.96	9.86	14.33
Breaking Energy(J)	2.10	1.99	3.10	2.86	4.08	3.78
% Reduction in breaking energy	4.10	9.13	12.67	19.43	10.32	16.92

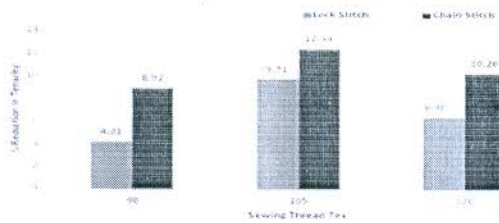


Figure 3.7 : Percentage reduction in tenacity of unraveled PP sewing threads

The decrease in tenacity was observed in all PP unraveled sewing threads. As yarn count (Tex) increases, % loss in tenacity increases in sewing threads unraveled from lock stitched denim fabric which can be attributed to the abrasion of sewing thread between needle and fabric. This abrasion was more for 120 Tex yarn because of higher surface area which causes pulling out of more fibres on surface from yarn which was confirmed in microscopic analysis of Thread (Fig 3.10). The PP unraveled needle threads show higher loss of reduction in tenacity with the increasing coarseness of threads for chain stitches as compared to lockstitch unraveled needle threads.

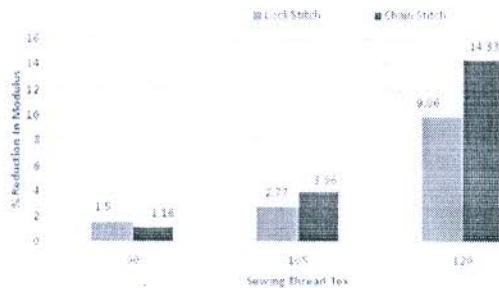


Figure 3.8 : Percentage reduction in modulus of unraveled PP sewing threads

An increasing % loss in modulus for PP core spun sewing thread has been observed for the increasing Tex number from 90 Tex to 120 Tex. The contribution to loss in the modulus is more for coarser threads than for the finer needle threads might be due to the more dynamic loading of coarser than finer Tex needle threads.

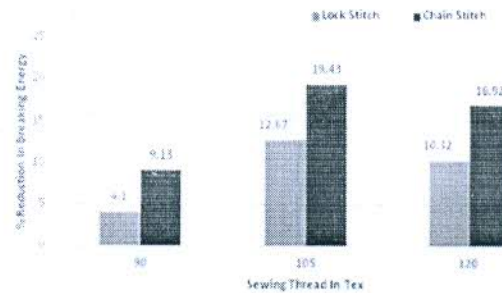


Figure 3.9 : Percentage reduction in breaking energy of unraveled PP sewing threads

The breaking energy of PP unraveled threads is observed in exact accordance with the trend of the PP threads for tenacity. The coarser the threads, more the abrasion & frictional contacts with the machine elements, thus reduced residual strength and more loss in thread tenacity and breaking energy for chain stitches. The % loss for thread unraveled from lock stitched denim fabric was lesser as compare to thread unraveled from chain stitched denim fabric for all sewing thread. The % loss in breaking energy was highest for 105 Tex yarn for thread unraveled from lock stitched and chain stitched denim fabrics.

The effect of abrasion and damages surfaces of unraveled needle sewing thread for lock stitch and chain stitch are shown by the microscopic images of all the sewing thread. Microscopic images of parent, lock stitch & chain stitch PP needle sewing thread shown in the fig 3.10.

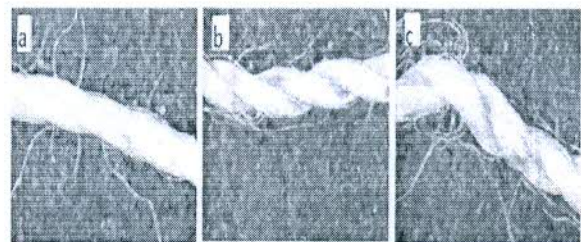


Figure 3.10 : The effect of abrasion between needle and fabric on the surface of PC sewing threads(a: Parent thread, b: Lock stitch unraveled thread c: Chain stitch unraveled Thread)

4. Conclusions

The tensile characteristics of sewing thread are highly influenced by the stitching process. The tenacity of PC lock stitch unraveled needle thread is slightly

higher than the residual tenacity of the chain stitch unraveled needle threads. The coarser PC sewing thread shows higher tenacity loss as compared to finer sewing threads. As tex size increases initial modulus increases for PC core spun sewing threads. The initial modulus of PC chain stitch unraveled needle thread is slightly lesser than the lock stitch unraveled needle thread except for 120 tex size. The breaking energy of the unraveled needle threads from the lock stitches shows the similar trends as for tenacity for the same threads. The PP core spun unraveled needle threads shows an increasing trend of reduction in tenacity with the increasing coarseness in tex size of threads for chain stitches just as PC core-spun sewing threads. The change % in the initial modulus loss for PP lock stitch unraveled needle thread increases as tex size increases and shows a similar trend as PC lock stitch needle thread. The breaking energy of the PP needle thread shows the same trend as for tenacity of PP needle thread. According to the results lock stitch is stronger than chain stitch needle thread. So it can be concluded that lock stitching process is more suitable sewing process for denim garment construction as compared to chain stitching process because during this process reduction in tensile properties is lesser.

References

1. Vinay Kumar Midha, V. K. Kothari, R. Chattopadhyay and A. Mukhopadhyay, Effect of Workwear Fabric Characteristics on the Changes in Tensile Properties of Sewing Threads after Sewing, *Journal of Engineered Fibers and Fabrics*, 5(1), (2010).
2. A. K. Choudhary and Amit Goel, Effect of Some Fabric and Sewing Conditions on Apparel Seam Characteristics, *Journal of Textiles*, 2, 1-7, (2013).
3. D. Samuel Wesley* and R. S. Rengasamy, Changes in Tensile Properties of Needle Thread in Lock Stitch Sewing, *Fibers and Polymers*, 18(2), 390-399, (2017)
4. Harold Carr and Barbara Lathom, *The technology of clothing manufacture*, Blackwell publishing, second edition, (2004).
5. GribaaSabria, Sami Ben Amar and Dogui A, 'Influence of sewing parameters upon the tensile behavior of textile assembly', *International Journal of Clothing Science & Technology*, 18(4), 235-246, (2006).
6. Ramachandran T and Ramesh Babu V, Analysis of performance of seams and sewing threads in woven fabric', *The Textile Magazine*, 49(2), 34-42, (2007).
7. Nagwa Ali Abou Nassif, Investigation of the Effects of Sewing Machine Parameters on the seam quality, *Life Science Journal*, 10(2), (2013).
8. Andreja Rudolf, Jelka Geršak, Anna Ujhelyioval, and Majda Sfiligoj Smole, Study of PES Sewing Thread Properties, *Fibers and Polymers*, 8(2), 212-217, (2007).
9. Mazari A and Havelka Antonin , Influence of needle heat during sewing process on tensile properties of sewing thread, *Tekstilec*, 56(4), 345-352, (2013).

□ □ □

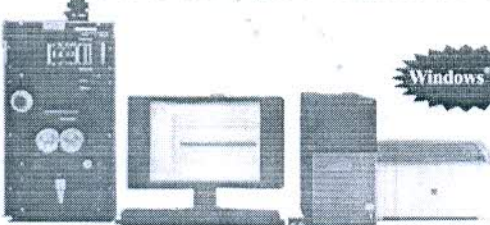
ADVERTISEMENT INDEX			
Advertise in	A-14	Meera Industries Limited	Gatefold
CEO Conclave	A-8	PNB Housing Finance Limited	Cover3
Grasim Industries limited	Gatefold	Precision Rubber Ind. Pvt. Ltd.	A-12
GTTES	A-6	Reliance Industries Ltd.	Cover 1
Hometex	A-13	Rieter India Ltd.	A-3
International Conference - Textile 4.0	A-4	Rieter India Ltd. (Components)	Cover 2
ISTE	A-2	Trutzschler India	A-9
ITMA 2019	A-10	Unitech Techmech	Cover 4
ITMACH	A-12	W.T.C.	A-7
ITTA	A-11	Web Advertise	A-15
Lakshmi Machine Works	A-1	Meera Industries Limited	Gatefold

- Yarn Structure", *Fibres & Textiles in Eastern Europe*, Vol. 3, 2015, P.54-57.
6. Iqbal SMF, "Influence of yarn structure produced in different spinning systems on the properties of yarn", *IJAR*, Vol.4, No.4, 2018, P.172-176.
 7. Cheng K.P.S, Yuen C.H., "Siro And Two-Fold Yarns", *Research Journal of Textile and Apparel*, Vol. 1, No.1, 1997, P.64-70, <https://doi.org/10.1108/RJTA-01-01-1997-B008>.
 8. Sharma I. C., Pandey A., Janveja A., Sharma N., "Comparison of Properties of Siro spun and conventional two fold yarns and of their fabrics", *Indian Journal of Textile Research*, Vol. 11, 1986, P.15 18.
 9. Advantages of bamboo yarn and bamboo fabric, www.bambrotex.com, (Accessed on 01/01/2017).
 10. Stalder H. and Rusch A., "Successful compact spinning process", *Intl. Textile Bulletin.*, Vol. 48, No.1,2002, P 42-43.
 11. Stalder H., "A new spinning process - ComforSpin", *MelliandTextilber.*, Vol.80, No.3, 2000, P.133-135.
 12. EliTeCompactSet V5, Suessen brochure leaflets, <https://www.suessen.com>.
 13. Artzt P., "The effect of different spinning processes on yarns", *ITB*, Vol.49, 2003, P. 40-43.
 14. Sundaresan S., Balu R., & Mohanraj R., "Effect of Strand spacing of SIRO Compact yarn on fabric properties", Vol. 2, No. 4, 2016, P. 172-179.
 15. Long Li & Hongqin Yan, "Tensile Properties of Regenerated Bamboo Yarn" *Fibres & Textiles in Eastern Europe*, Vol. 20, No. 1, 2012, P.18-23.

□ □ □

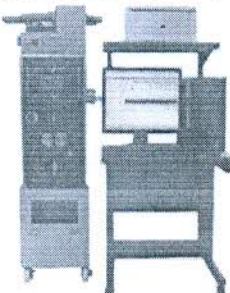
Quality Control Solutions from *Kaisokki* JAPAN

LABORATORY TESTING INSTRUMENTS & YARN CLEARERS



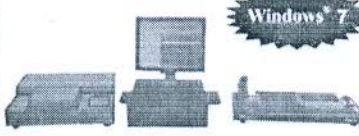
Windows 8.1

OPTICAL HAIRINESS & DIAMETER TESTER LASERSPOT LST - V++



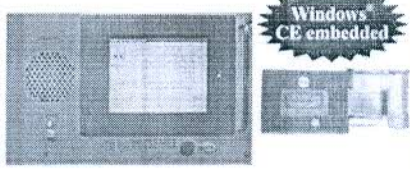
Windows 8.1

EVENNESS TESTER KET V++/C
(for filament yarn)
NEW MODEL



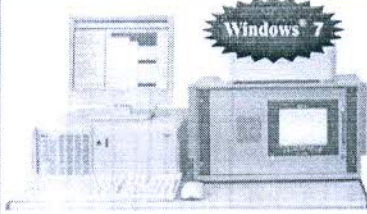
Windows 7

FIBER LENGTH DISTRIBUTION TESTER CLASSIFIBER KCF V/LS
Individual Fiber length 6mm - 30 mm available.



Windows CE embedded


YARN CLEARER TRICHORD FLEX WITH FOREIGN FIBER DETECTION



Windows 7

YARN FAULT CLASSIFYING SYSTEM CFT TRICHORD FLEX

Exclusive Sales-Service Agent for India
Thymas Electronics Pvt. Ltd.
 "YOGIDHARA", 2 Nandanvan Society, Indubhai Patel Road, Aikapun, Vadodera 390 007, Gujarat, India
 Phone : 0265 2312730 / 2351634. Webpage : www.thymas.com Email : thymasltd@gmail.com, tepi26@yahoo.com



Journal of the TEXTILE Association

RESEARCH

Open Access



Mosquito repellent activity of cotton functionalized with inclusion complexes of β -cyclodextrin citrate and essential oils

Shelly Khanna and J. N. Chakraborty*

*Correspondence:
chakrabortyjn@hotmail.com
National Institute
of Technology,
Jalandhar 144011, India

Abstract

With the progress of time, demand for healthy and hygienic clothing has gone up tremendously. Fabrics and apparels finished with mosquito repellent finishes belong to one of such highly looked out clothing's. The present study aims at synthesis, characterization and optimization of β -Cyclodextrin citrate (β -CD CA) followed by its complexion with essential oils of cedarwood, clove, eucalyptus, peppermint, lavender and jasmine for the assessment of repellent efficacy against *Anopheles Stephensi* by means of arm in cage assays on cotton. Protection time, repellency (%), biting (%) and mortality (%) of inclusion complexes encapsulated with oils were evaluated. Two way ANOVA and post hoc analysis had affirmed the significant effect of essential oil type on bio-assay. Lavender and cedarwood had provided the longest protection times (210 and 160 min respectively); jasmine and peppermint were least effective showing protection times of 20 and 60 min whereas oils of eucalyptus and clove behaved as feeding deterrents. Peppermint and lavender were effective as potential repellents and cedarwood had shown supreme mortality against arthropods. Jasmine was the weakest repellent due to its flower-nectar stimulating upshot for *Anopheles stephensi*.

Keywords: β -cyclodextrin citrate, Repellent efficacy, *Anopheles stephensi*, Protection time, % mortality, Inclusion complexes, Bio-assay, Feeding deterrents

Introduction

Due to the increased awareness about health and hygiene, people increasingly demand their clothing to be hygienically afresh and functional as market has been expanded for specialty clothing (Karolia and Mendapara 2005). Mosquito repellence with the use of textiles is a promising area of functionality. Many species of mosquitoes are the vectors of numerous fatal diseases, with no effective vaccines against the ailments caused by them. Personal protection is one of the approaches to prevent mosquito bites. The only way to avoid the disorders is to keep away from the mosquito bites. Mosquito repellent textiles are one of the revolutionary ways to advance the textile field by providing immensely needed features of driving away the mosquitoes. It protects the human beings from the bite of mosquitoes, and thereby promising safety from the mosquito borne diseases such as malaria, dengue fever, chicken guinea and filarial (Prabha and Vasugi 2012). Both natural as well as synthetic repellents are exploited against mosquitoes. But

natural repellents as essential oils are the upcoming genre of scientific interest due to their non-toxic, non-sticky, non-irritating and eco-friendly nature; however, essential oil repellents tend to being short-lived in their effectiveness due to their high volatility and requirement of frequent re-application. This problem has been tried to be overcome with the controlled release of oils from the textiles using monomolecular inclusion complexes with β -cyclodextrin (β -CD) in native form (Songkro et al. 2012), β -CD with crosslinking agents as polycarboxylic acids namely citric acid, BTCA, acrylic acid (Martel et al. 2002a, b; Voncina and Marechal 2005; El-Tahlawy et al. 2007; Specos et al. 2013), MCT β -CD (Hebeish et al. 2008; Romi et al. 2005; Abdel-Mohdy et al. 2008, 2009; Shahba et al. 2011; Hebeish et al. 2009, 2010) on varied substrates. The use of citric acid as crosslinking agent for β -CD had been extensively reported for cotton for diversified functionalities (Aly et al. 2004; Fahmy 2004; Martel et al. 2002b; Ramchandran 2009; Dehbadi et al. 2014; Kasprzyk et al. 2010; Fouda and Fahmy 2011) but the use of β -CD CA as a host for mosquito repellent finishing has been worked and cited scarcely (Samanta et al. 2016). Also, the process parameters for attachment of β -CD CA on textile substrates as individual parameters during reaction has been reported, that too rarely without any emphasis on their interactions (Martel et al. 2002b; El-Tahlawy et al. 2006; Ramchandran 2009). As the reactivity of citric acid towards cellulose is higher than that towards β -CD, results in different desired reaction conditions of citric acid towards cellulose and β -CD, necessitated the requirement of a two-step procedure. (Martel et al. 2002b).

Thus, the aim of present work was the synthesis, characterization, optimization of a novel modified cyclodextrin host (β -CD CA) for inclusion complexation with essential oils and its application on cotton for adjudgement of potential of inclusion complexes against malaria causing arthropods scientifically.

Methods

Materials

Thoroughly pre-treated plain woven cotton fabric possessing epi (76), ppi (70), warp (42.8 Ne⁵), weft (38 Ne⁵) and gsm (136), six categories of essential oils (Eos)- clove (CO), cedarwood (CdO), eucalyptus (EO), peppermint (PO), lavender (LO) and Jasmine (JO) were used. All the analytical grade chemicals, viz. β -cyclodextrin (β -CD), citric acid (CA), sodium hypophosphite (SHP), ethanol and Isopropanol were supplied by SDFL, Mumbai. FTIR-spectroscope (*Perkin Elmer, US*), Bruker Avance II NMR Spectrometer (*Saif, PU, Chandigarh, India*), Thermogravimetric Analyser (*SDT Q600 V20.9 Build 20; NITRA, Gaziabad, India*), Water bath (*Laboratory glassware Co.*), Padding mangle (*Electronic & Engg. Company*), Electronic weighing balance (*CAS Model MW -11 series*), Drying oven (*Kaypee Udyog, India*), Soxhlet, freeze drier, Laundrometer (*RBE*), Tensile tester (*Globe Tex Industries*) and Computer colour matching (*Macbeth colour-eye*) were the equipment used to evaluate the physical properties of the functionalized cotton. Arm in cage/cloth cage was used for the assessment of bio-assay of mosquito repellence.

Synthesis and characterization of β -cyclodextrin citrate (β -CD CA)

The synthesis of β -CD CA was carried out according to the procedure described previously by (El-Tahlawy et al. 2006) without any major process modifications using β -CD,

CA and SHP in molar ratios 1:2:2. FTIR, TGA and $^1\text{H-NMR}$ (for resonances of protons for structural confirmation) were used for the characterization of synthesized $\beta\text{-CD CA}$.

Solubility analysis of $\beta\text{-CD CA}$ in water and ethanol

The solubility of $\beta\text{-CD CA}$ was analyzed in water and ethanol for the assessment of modification of modified $\beta\text{-CD}$ according to Eq. 1.

Solubility%

$$= \frac{\text{Initial weight of } \beta\text{-CD CA in solution} - \text{Final weight of } \beta\text{-CD CA as residue on filter paper}}{\text{Initial weight of } \beta\text{-CD CA in solution}} \quad (1)$$

Optimization of process parameters of $\beta\text{-CD CA}$ attachment on cotton

The optimization of process variables for $\beta\text{-CD CA}$ attachment on cotton was accomplished with response surface methodology using 3^3 Box and Behnken factorial design. $\beta\text{-CD CA}$ concentration (60, 70, 80 gpl), Time of curing (4, 6, 8 min) and Temperature of curing (100, 130, 160 °C) were taken as three independent variables for the assessment of independent responses viz. % Graft yield, % change in Tensile strength, % change in yellowness index and Wash durability (up to 5 washes) of functionalized cotton. The attachment of modified host on cotton was affirmed by FTIR and TGA. Design Expert software version 7.1.2 (State-ease Inc., Minneapolis, USA) was used for statistical analysis and model-fitting of responses. % Graft yield (GY%) was determined from the gain in weight of cotton due to the attachment of $\beta\text{-CD CA}$ after the removal of unattached host according to Eq. 2. *Tensile strength* was determined according to the ASTM D5034-1995 using digital tensile strength tester. *Wash durability* was evaluated as % retained weight gain after washing as- $\beta\text{-CD CA}$ treated cotton samples were washed according to ISO 105-C03:1989 with 5 gpl of soap and 3 gpl of Na_2CO_3 , with a M:L 1:50 followed by laundering 60 ± 2 °C for 30 min. Rinsing with tap water for 10 min and drying at room temperature after each wash cycle was done. *Yellowness Index* was used to determine the degree to which a cotton sample's colour shifts away from an ideal white using Macbeth color eye matching system with D65 illuminant (AATCC test method 110-2000). FTIR was further used to adjudge the presence of $\beta\text{-CD CA}$ on cotton after 5 washings.

$$\text{Weight gain (\%)} = (W_f - W_i)/W_i \times 100 \quad (2)$$

where W_f and W_i represent final and initial fabric weight respectively.

Synthesis, characterization and application of inclusion complexes of $\beta\text{-CD CA-Eos}$ on cotton

$^1\text{H-NMR}$ was used for the determination of stoichiometry and binding constants between $\beta\text{-CD CA-Eos}$ in solution state with Job's plot (or continuous variation method) and Scott's method (y-reciprocal plot). For this, two stock solutions of $\beta\text{-CD CA}$ and oil both having 10 mM concentration were prepared. Based on these two equimolar solutions, a series of 5 sample solution using magnetic stirrer at 4000 rpm for 25 mins were prepared containing both the oil and host at constant volume with varying proportions, so that a wide range ($0 < r < 1$) of the ratio $r = [X]/([H] + [G])$ was sampled, where $X = G$ or H and $[H]$ and $[G]$ are the total concentrations of the $\beta\text{-CD CA}$ and oil to achieve

the total concentration $[H] + [G] = [M] = 10$ mM i.e. {(2.8 mM), (4.6 mM), (5.5 mM), (6.4 mM), (8.2 mM)} with dry mixing technique using magnetic stirrer at 4000 rpm for 25 min to achieve a uniform and stable complex. The chemical shift $\Delta\delta$ was measured and plotted as a function of 'r' for Job's plot. The Scott's method (or γ -reciprocal plot) was used to investigate the extent of the intermolecular binding as a constant between oils and β -CD CA according to the Eq. 3. The synthesis of inclusion complexes (ICs) of β -CD CA-Eos with the optimized β -CD CA concentration (from the previous section) and oils at 14, 16 and 18 $\mu\text{L}/\text{cm}^2$ (v/v of 100% ethanol) was carried out by dry mixing followed by freeze drying the complex using freeze drier (at -22 °C for 12 h; $+20$ °C for next 8 h and at 30 °C for 6 h). The freeze dried fine powder was applied on cotton at optimized conditions of curing time and temperature. TGA were carried out for the anchorage of ICs on cotton.

$$\frac{[OIL]}{\Delta\delta_{obs}} = \frac{[OIL]}{\Delta\delta_c} + \frac{1}{K_a \times \Delta\delta_c} \quad (3)$$

where, [OIL] molar concentration of oils (mM), $\Delta\delta_{obs}$ chemical shift difference observed for MCT β -CD proton resonances for a given oil concentration, $\Delta\delta_c$ difference in chemical shift between the complexed and free MCT β -CD at saturation, K_a binding constant.

Repellence assessment-arm-in cage bioassay

Mosquito repellence activity was assessed with the test cage described as "Laboratory testing of non-commercial mosquito repellent formulations on skin employing laboratory reared mosquitoes" (ASTM-E951-83; Jantan and Zaki 1999; Masetti and Maini 2006) in cage ($30 \times 30 \times 30$ cm³) with an aspirator tube. Laboratory bred and reared 5–10 days old female *Anopheles stephensi* mosquitoes were used. Adults were fed with 10% sucrose solution prior to testing and were starved by providing them only water for 15 h. Around 150 adult female mosquitoes were taken to conduct a single bioassay test, 100 of which were exposed to the ICs treated cotton (in 4 replicates of around 25 mosquitoes). The remaining 50 were used for control in 2 replicates (WHO 2013). Bio-assay was determined with-

$$\begin{aligned} \text{Protection time (PT)} &= \text{Time elapsed between application of oil and second successive bite} \\ \% \text{Repellency (\%R)} &= (C - T)/C \times 100 \end{aligned}$$

where, C is the number of biting or landing on the control, T is number of biting or landing on the treated area calculated at the end of each test.

$$\% \text{Mortality (\%M)} = \text{No. of mosquitoes dead/Total number of mosquitoes in the cage} \times 100$$

$$\% \text{Biting/landing (\%B)} = B \text{ or } L/\text{Total number of mosquitoes in the cage} \times 100,$$

where, B/L is the total number of biting or landings at the end of each test.

Cotton samples (650 cm² area) were treated with ICs and draped over the top of the left forearm. A rubber glove was worn to cover the hand and wrist. Right arm with ethanol treated cotton was taken as a reference. An initial 3 min exposure period was observed for mosquito behaviour followed by observations after every 10, 20, 30, 40,

50 min, 1 h and after that a small 3 min interval for every 30 min up to 6 h. Mortality was noted after 24 h, % B and % R were noted after 6 h observation period.

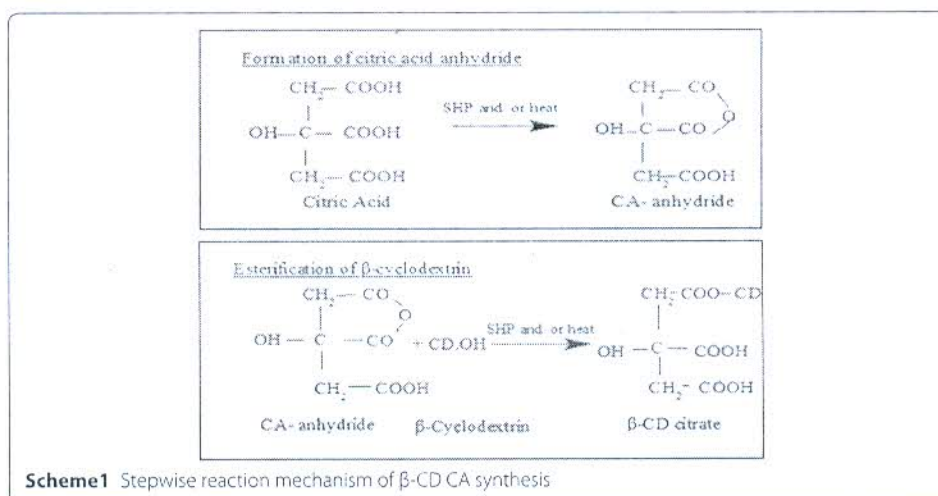
Statistical analysis

Two-way ANOVA was used to assess the effect of all Eos type and concentrations (14, 16 and 18 $\mu\text{L}/\text{cm}^2$) on the bio-assay. One way analysis of variance followed by Tukey–Kramer post hoc analysis was used to compare the bio-assay for six oils at 18 $\mu\text{L}/\text{cm}^2$ concentration. A value of $p \leq 0.05$ was considered statistically significant.

Result and discussions

Synthesis and characterization of β -CD CA

The % yield of synthesis was satisfactory at 63.96 with DS of β -CD CA of 0.28–0.42 and MW at 1310. The reaction proceeds by the formation of a reactive cyclic anhydride intermediate by the dehydration of two adjacent carboxyl groups under curing conditions for the substitution of the primary hydroxyl groups of β -CDs with the elimination of water. The reaction mechanism for β -CD CA synthesis is depicted in Scheme 1. FTIR had shown the presence of the strong absorption band at 3308 cm^{-1} as compared to 3388 and 3296 cm^{-1} in β -CD and 3445 cm^{-1} in citric acid assigned to O–H stretching. The characteristic peaks of 2931 cm^{-1} in β -CD, 3284 cm^{-1} in CA and 2928 cm^{-1} in β -CD CA are related to C–O and C–H stretching were detected. An additional extended absorption peak at 1715 cm^{-1} was observed in β -CD CA and in CA at 1695 cm^{-1} (absent in β -CD) attributed to C=O stretching of citrate moieties in CA and β -CD CA. Further, both β -CD and β -CD CA had shown the evidence of carbon in cyclic rings at 1029 and 1020 cm^{-1} as shown in Fig. 1a. β -CD CA had shown thermal decomposition as a measure of % weight change by TGA with $T_g = 235\text{ }^\circ\text{C}$ and $T_p = 315\text{ }^\circ\text{C}$ (Fig. 1b). $^1\text{H-NMR}$ allows the observation of specific resonances of the various protons located within the cyclodextrin cavity. H3 and H5 atoms are located in the interior cavity; H1, H2, H4 and H6 are located on the exterior of the cavity (Levy et al. 2001). H2–H6 are attributed to the cyclodextrin ring whereas, Ha and Ha' are the chemical shifts of citric acid backbone. The chemical shifts for β -CD CA are H2 (3.3680), H3 (3.6083), H4 (3.3114), H5 (3.6560), H6 (3.5), Ha (2.5167) and Ha' (2.5688 ppm).



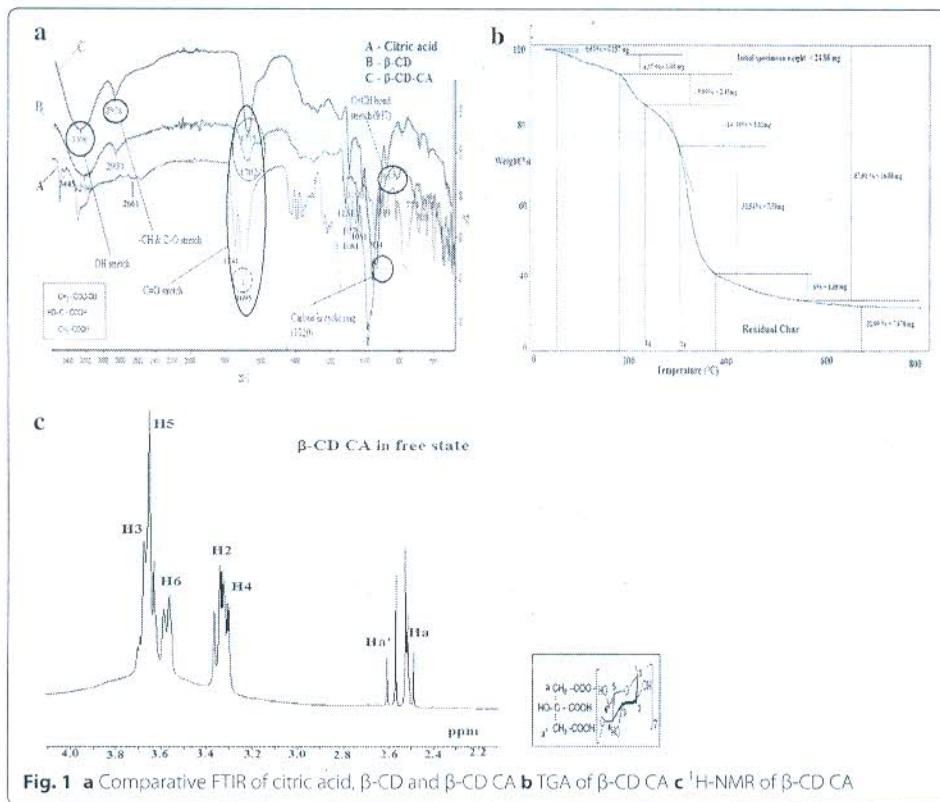


Fig. 1 a Comparative FTIR of citric acid, β -CD and β -CD CA b TGA of β -CD CA c ¹H-NMR of β -CD CA

Solubility of β -CD CA

The substitution of native β -CD had increased its solubility in both water and ethanol due to extreme high solubility of CA itself in both media even at very low temperatures. With increase in β -CD CA concentration in aqueous media, the restriction to the solubility increased due to the increased number of strained cyclodextrin rings. Water was chosen to be used as the working medium. An increase of 51% (at 60 gpl) up to 91% (at 100 gpl) was found for β -CD CA as compared to native β -CD.

Optimization of process parameters of β -CD CA attachment on cotton

The reaction mechanism of β -CD CA with cellulose can be described as—the two carboxyl groups present in citric acid dehydrate to form a reactive cyclic anhydride that further, reacted with the secondary -OH groups of β -CD to form β -CD CA. After this, the remaining carboxyl groups at the end of β -CD CA chain might have reacted with the -OH groups of cellulose. (Dong et al. 2014) as shown in Fig. 2a). FTIR analysis had affirmed the presence of modified host on functionalized cotton with the C=O strong ester group at 1742 cm⁻¹, which was not revealed by control as shown in Fig. 2b). TGA had shown that the presence of β -CD CA on cotton due to the reduction of Tg of control had reduced from 290 °C up to 248 °C and Tp had reflected a change from 383 to 365 °C solely due to the adherence of reactive host (β -CD CA) on cotton that had its own Tg and Tp at lower temperatures of 235 and 315 °C.

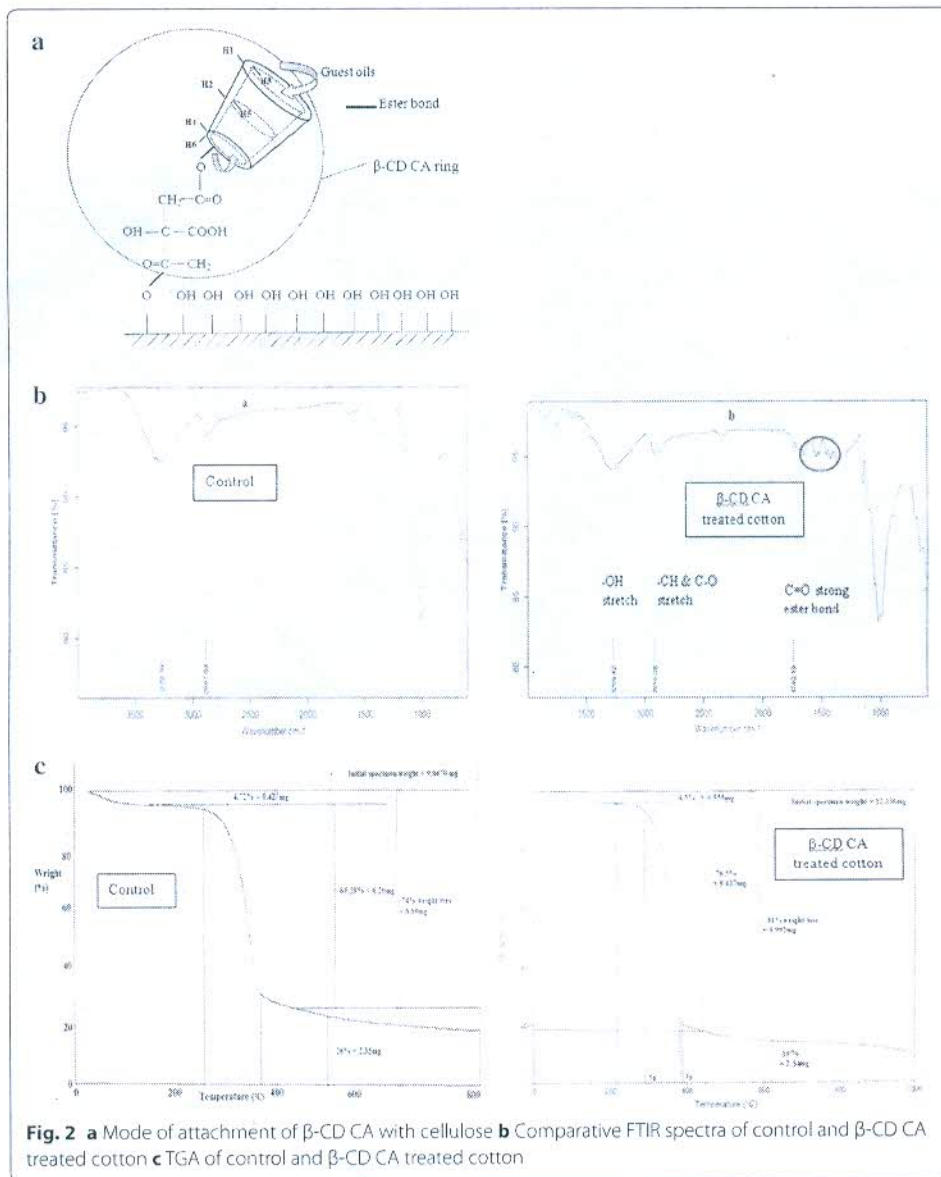


Fig. 2 a Mode of attachment of β -CD CA with cellulose b Comparative FTIR spectra of control and β -CD CA treated cotton c TGA of control and β -CD CA treated cotton

A desirability function (DF) = $f\{GY, TS, YI, WD\}$ was designed for the optimization of process parameters as—GY% is % graft yield targeted to 'maximum', TS is % loss in tensile strength targeted to 'minimum', YI is % change in yellowness index targeted to 'minimum' and WD is wash durability of host treated cotton in terms of % retained weight gain targeted to 'maximum'. The statistical analysis of dependent responses is shown in Tables 1 and 2.

Graft yield (%)

It had shown dependence on β -CD CA concentration and curing temperature (Fig. 3a). With the increase in concentration and temperature from (60 gpl and 100 °C) to (80 gpl and 160 °C) for 6 min, GY had increased from 5.69% up to 7.62% due to the increase in the availability of the β -CD CA molecules for attachment on cotton as the higher

Table 1 Experimental responses of β -CD CA treatment on cotton

Run no.	Independent variables			Responses							
	Concentration (gpl)	Temperature of curing ($^{\circ}$ C)	Time of curing (min)	GY* (%)	TS* (%)	YI* (%)	WD*				
							1st	2nd	3rd	4 th	5 th ^a
1.	60	130	8	5.26	9.52	8.74	5.20	4.66	3.98	3.16	2.45
2.	80	100	6	7.08	17.54	14.21	6.91	6.17	5.88	5.73	5.45
3.	80	130	8	7.75	18.78	18.33	7.61	7.14	6.62	6.42	5.72
4.	60	160	6	5.76	9.36	8.83	5.34	4.78	4.12	3.65	2.98
5.	70	130	6	6.01	12.03	11.72	5.94	5.22	4.87	4.67	4.22
6.	70	100	4	5.69	10.22	11.14	5.44	5.11	4.78	3.66	2.67
7.	60	130	4	5.18	9.32	8.11	4.87	4.22	3.69	2.87	2.18
8.	70	130	6	6.19	12.13	11.06	5.93	5.27	4.87	4.13	3.45
9.	70	160	4	6.04	10.97	11.46	5.83	5.11	4.88	4.52	4.03
10.	70	160	8	6.67	11.32	13.62	6.29	6.06	5.62	4.98	4.49
11.	70	100	8	5.47	10.73	10.79	5.22	5.02	4.81	4.20	3.74
12.	60	100	6	5.46	9.26	8.29	5.27	5.11	4.53	3.76	2.94
13.	70	130	6	6.23	12.07	11.03	6.09	5.83	5.29	4.88	4.29
14.	80	160	6	7.62	19.17	17.86	7.44	6.61	6.18	5.91	5.77
15.	80	130	4	7.02	17.97	13.64	6.88	6.11	5.77	5.62	5.24
16.	70	130	6	6.01	12.11	11.02	5.81	5.34	5.10	4.87	4.23
17.	70	130	6	6.19	12.08	11.14	5.92	5.73	5.34	4.96	4.27

* GY graft yield, TS loss in tensile strength, YI change in yellowness index, WD Wash durability up to 1, 2, 3, 4, 5th wash (% retained weight gain)

^a WD after 5th wash considered for the analysis

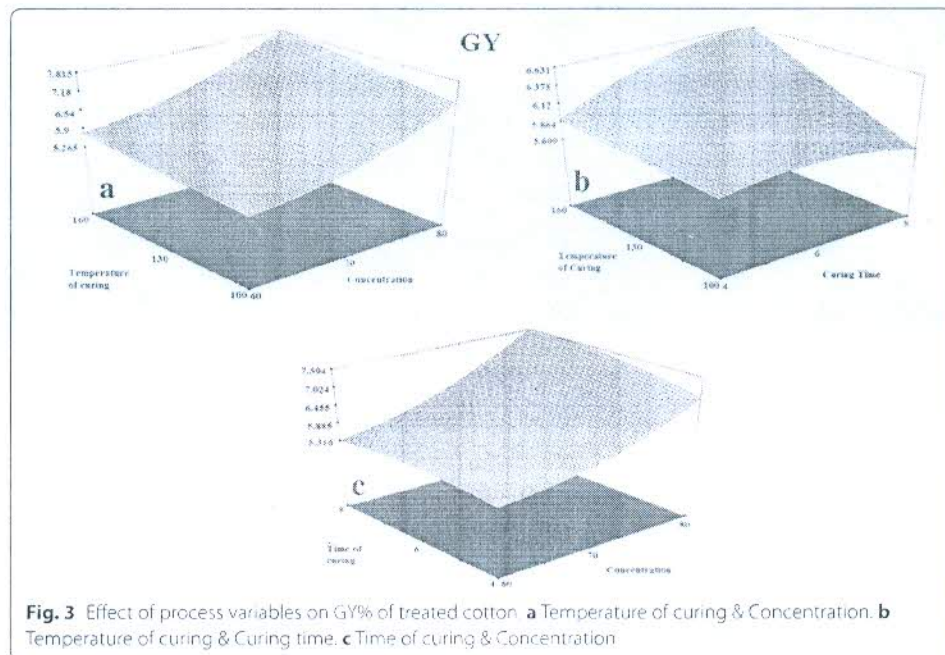
Table 2 Statistical analysis for desirability (Model equations)

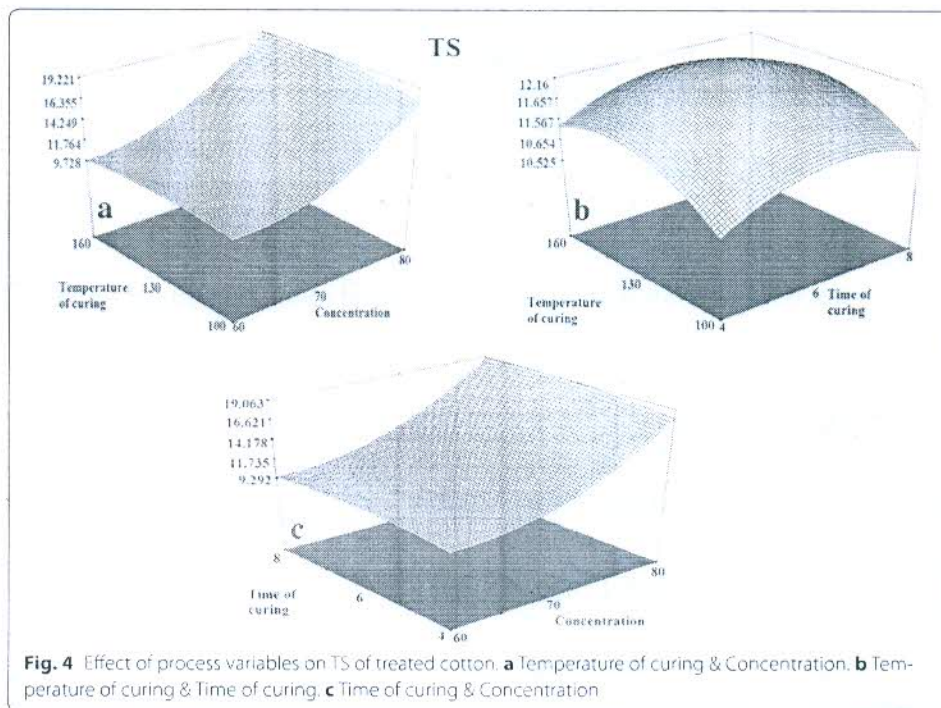
Response	Model equations	R ²	Adjusted R ²	Predicted R ²	Lack of fit (Prob > F)
Y1, GY%	$6.13 + 0.98X_1 + 0.3X_2 + 0.15X_3 + 0.34X_1^2 - 0.17X_3^2 + 0.16X_1X_3$	0.9773	0.9480	0.705	0.0763; Not significant
Y2, TS	$12.08 + 4.50X_1 + 0.38X_2 + 0.23X_3 + 2.42X_1^2 - 0.67X_2^2 + 1.54X_3^2 + 0.15X_1X_2 + 0.38X_1X_3$	0.9998	0.9996	0.998	0.068; Not significant
Y3, YI	$11.19 + 3.76X_1 + 0.92X_2 + 0.89X_3 + 0.78X_1^2 + 0.33X_2^2 + 0.23X_3^2 + 1.01X_1X_2 + 0.63X_2X_3 + 0.68X_1X_3$	0.9854	0.9667	0.8038	0.0536; Not significant
Y4, WD	$4.01 + 1.45X_1 + 0.31X_2 + 0.31X_3$	0.9048	0.8828	0.8271	0.4601; Not significant

concentration increases the diffusion of β -CD CA into the vicinity of cellulose fibres. But the use of high temperature might be harmful for the fibre as a result of citrate degradation as shown in Fig. 3b). The interaction of β -CD CA concentration with curing time had also influenced the grafting ratio as change in the process parameters from (60 gpl and 4 min) up to (80 gpl and 8 min) at 130 °C reflected the increase in GY from 5.18% up to 7.75% due to the favourable conditions of temperature and time of curing to graft high proportion of host molecules on the cotton (Fig. 3c).

Loss in tensile strength (%)

The combined effect of β -CD CA concentration and curing temperature on TS of functionalized cotton is shown in (Fig. 4a). With the increase in concentration at all the temperatures, there is an increase in TS% due to the acid-catalysed cellulose depolymerisation and cross linking of cellulosic chains that limited the mobility of the chains to equalize the distribution of stress on individual chains, within the substantial range of 9.26% at (60 gpl and 100 °C) up to 19.17% at (80 gpl and 160 °C) for 6 min. TS was

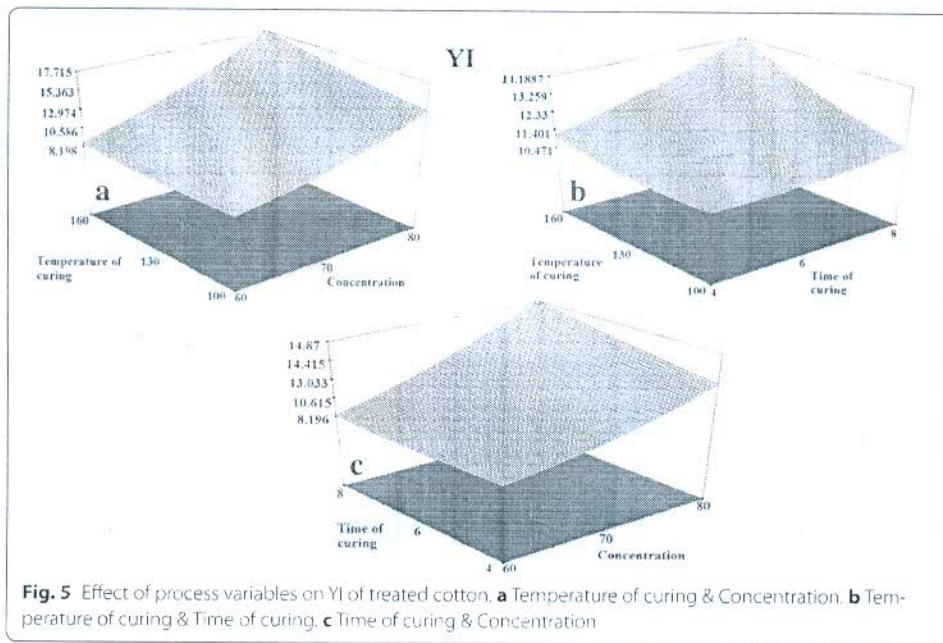




lesser up to 70 gpl but as concentration increased from 70 to 80 gpl, TS had increased due to the increased formation of cross links and presence of β -CD CA on cotton that augmented degradation of treated cotton at the higher temperatures. The effect of curing temperature and time is shown in Fig. 4b). The increase in the levels from (4 min and 100 °C) up to (8 min and 160 °C) at 70 gpl, TS increased at lower level but decreased at their highest levels i.e. TS increased from 10.22 to 12.03% as the levels increased from the interactions (4 min and 100 °C) to (6 min and 130 °C) but it fell to 11.32% at 8 min and 160 °C, TS lowered down followed by its shooting up at the middle level due to the rapid cross linking of the citrate chains to cotton but as temperature and time both increased, citrate degradation affected TS as no more crosslinking was achieved but with the tenderness of cotton (Fig. 4c).

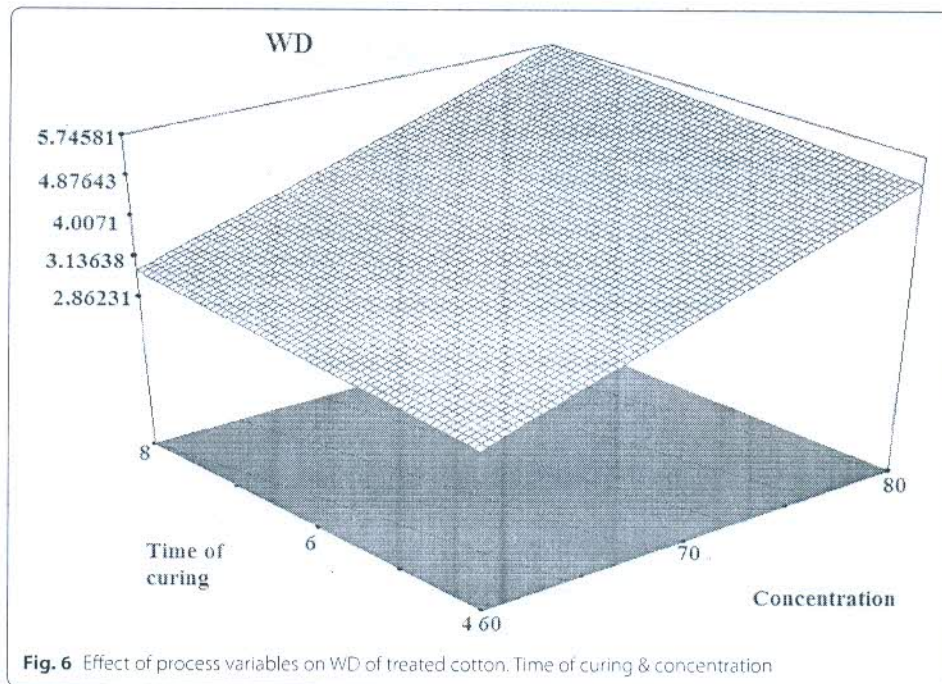
Change in yellowness index (%)

It is evident from Fig. 5a that more the amount of the host on cotton leads to the increase of the yellowness at all levels of curing temperature, i.e. with the increase in the citrate concentration, the yellowness index increased because citrate component of β -CD CA is known to cause fabric yellowing. The major reason of cotton yellowing in presence of β -CD CA is the formation of unsaturated *cis*- and *trans*-aconitic acids (primarily at higher curing temperatures) prior to the formation of anhydrides through dehydration. The effect of curing temperature at low β -CD CA concentrations was lesser significant on the yellowness of cotton, whereas, at higher levels of concentration and temperature, the YI changed from 17.86% from 8.29%. The combined effect of curing time and temperature did not bring a substantial change in YI (Fig. 5b). The interaction of concentration and curing time followed the same trend as with the concentration and temperature on YI (Fig. 5c).



Wash durability

WD was affected mainly by the concentration of β -CD CA present on cotton as can be seen in Fig. 6. With the increase in the host concentration from 60 to 80 gpl, WD increased after 5 subsequent washes that depended on the amount of citrate host present on cotton, higher the amount of the β -CD CA molecules in the vicinity of the cellulose, greater is the grafting ratio.

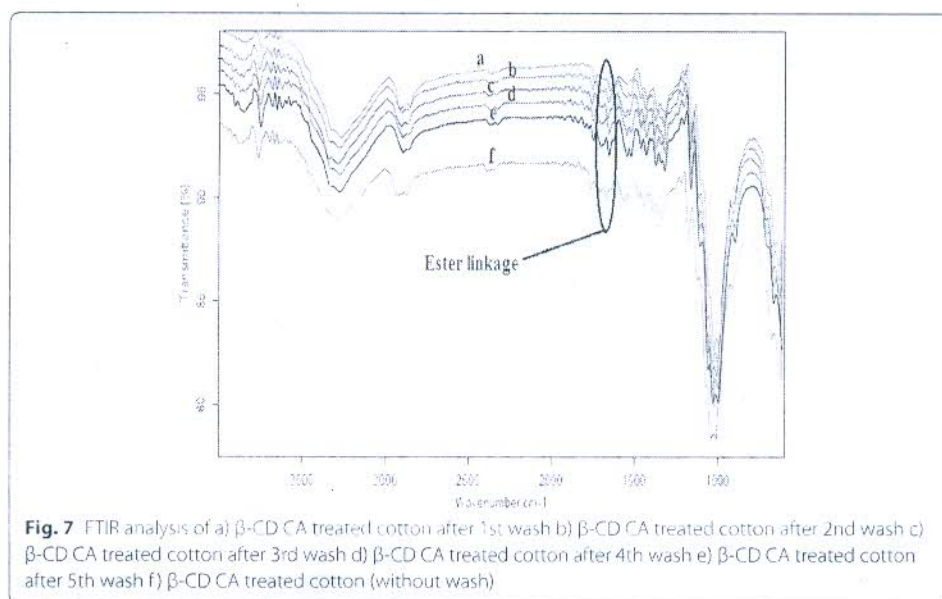


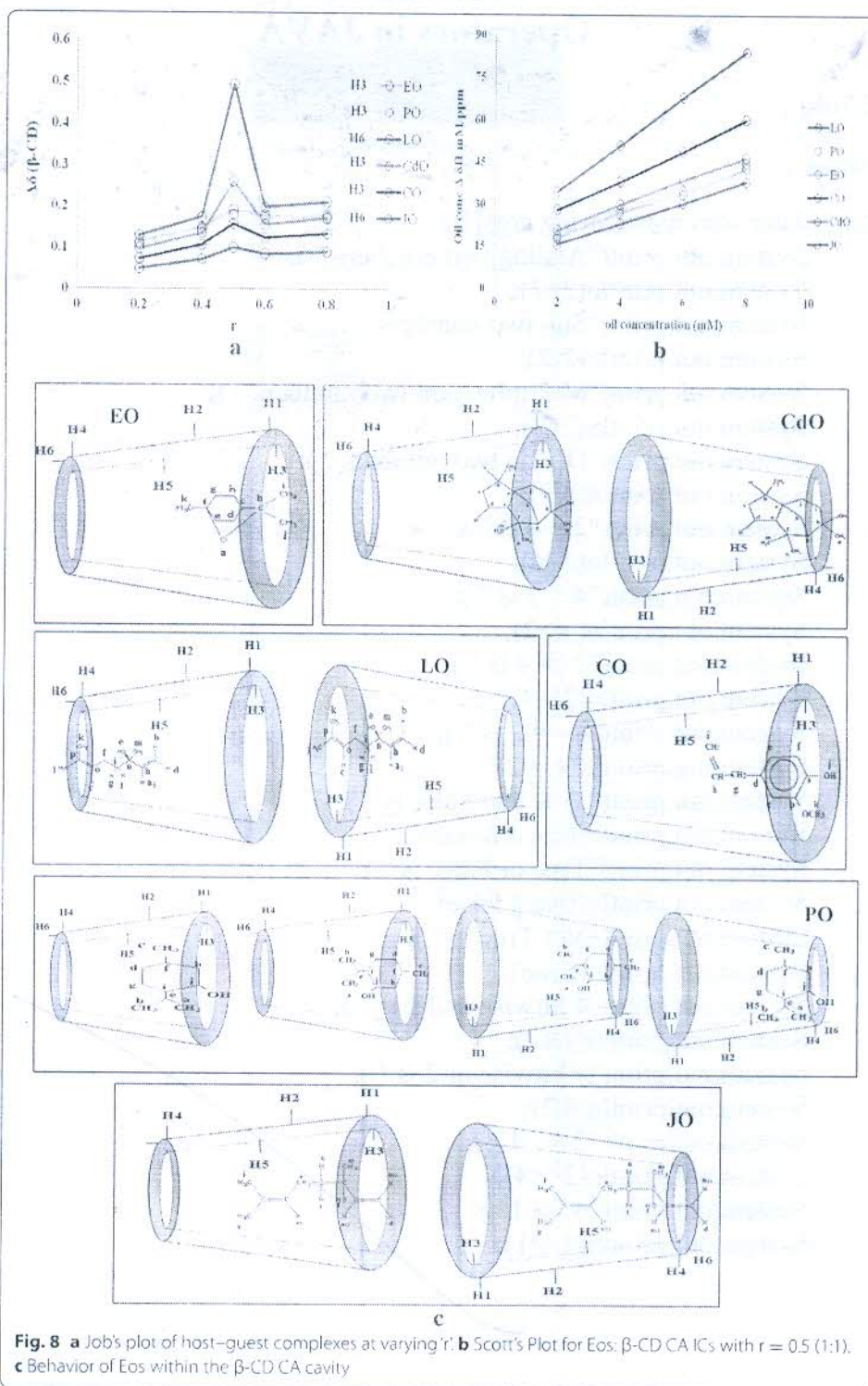
The optimized variables for attachment of β -CD CA on cotton were 63.46 gpl (concentration), 160 °C (curing temperature) and 7.15 min (curing time) having experimental validation of $R^2 = 0.987$. FTIR spectra had revealed the presence of ester linkage intact even after 5 subsequent wash treatments as in unwashed functionalized cotton (Fig. 7).

Synthesis, characterization and application of ICs of β -CD CA-Eos on cotton

The Job's plot had demonstrated that $\Delta\delta$ β -CD CA ('H' resonance) was maximum at 'r' = 0.5 and highly symmetrical shape depicting the complexes of all Eos-host had 1:1 stoichiometry (Fig. 8a) and binding constants between oils- β -CD CA were given by Scott's plot as shown in Table 3 and Fig. 8b). Also, the direction and extent of penetration of Eos into the cavity was also determined with $^1\text{H-NMR}$ spectra (Fig. 8c). The trend of binding constant of Eos with host was $\text{CO-}\beta\text{-CD CA} < \text{LO-}\beta\text{-CD CA} < \text{CdO-}\beta\text{-CD CA} < \text{EO-}\beta\text{-CD CA} < \text{PO-}\beta\text{-CD CA} < \text{JO-}\beta\text{-CD CA}$. For EO, partial penetration of the oil molecules from the tail side into the wider rim was observed. PO had been observed with the possibility of inclusion of the oil from either side of the chain and from both sides of cavity. LO was enclosed into the cavity from either of the rims through tail side. Entry of CO could be from either of the two sides of the chain via wider opening of the cavity but the possibility of complexation from the tail side is more due to the non-polar nature of the functional groups present in this part of the chain. CdO was entrapped partially into the cavity from either of the two sides but penetration of oil from the head side of chain is more probable due to its lesser polar nature than the other side. JO had shown full inclusion into the cavity from both rims from the tail side. Also, it was observed that all Eos were partially entrapped into the cavity except JO that was fully trapped into the cavity.

A comparative TGA of β -CD CA, control, β -CD CA treated cotton and IC functionalized cotton is shown in Fig. 9. It can be inferred that T_p of control at 383 °C was shifted to 365 °C after treatment with β -CD CA, that further reduced to 355 °C when treated

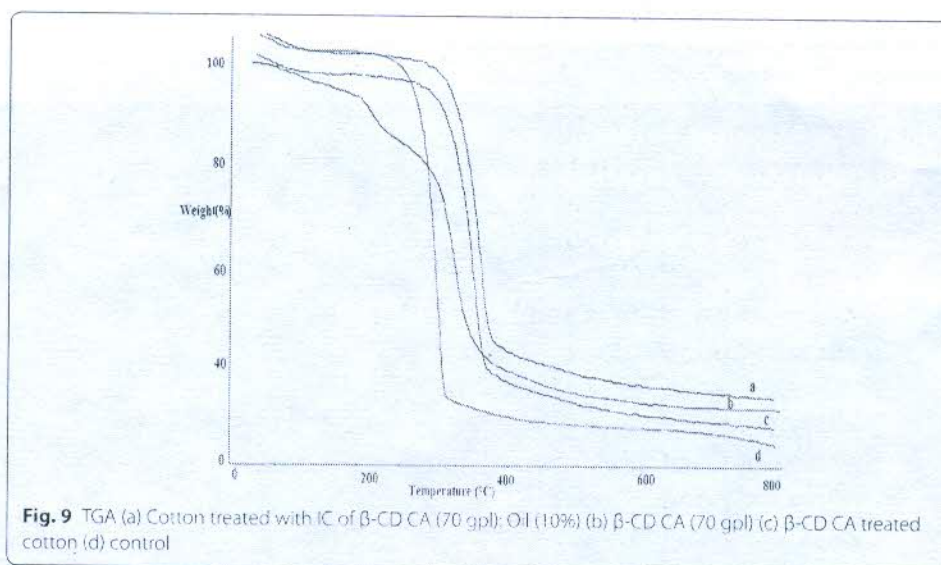




with host-oil complexes. The char residue also had shown a substantial change from 19% (control), 26% (β-CD CA treated cotton) and further, 29% (for complex treated cotton). This change was observed because of the presence of IC, from which evaporation of oil

Table 3 ¹H-NMR data of oil conc/ $\Delta\delta H$ for binding constants between ICs of Eos & β -CD CA

Oil conc. (mM)	Oil conc./ $\Delta\delta H$					
	EO (H3)	PO (H3)	LO (H6)	CdO (H3)	CO (H3)	JO (H6)
2	17.99	18.74	34.39	20.72	27.98	15.67
4	26.99	27.92	50.91	29.9	37.96	23.07
6	33.61	34.98	67.98	38.62	48.79	30.39
8	42.87	44.96	84.17	46.64	60.12	38.13
Y-reciprocal equation	$4.063x + 10.05$	$4.286x + 10.22$	$7.920x + 24.76$	$4.324x + 12.35$	$5.362x + 16.9$	$3.735x + 8.14$
R ²	0.996	0.996	0.997	0.999	0.996	0.999
Binding constant (M ⁻¹)	404	419	319	350	317	460



had taken place, followed by the decomposition of β -CD CA and cellulose. Further, ICs of β -CD CA-Eos were synthesized for application on cotton at 63.46 gpl host and 14, 16 and 18 $\mu\text{L}/\text{cm}^2$ Eos. The freeze dried ICs were applied on cotton via pad, dry and cure at 160 °C and for 7.15 min.

Repellence assessment-arm-in cage bioassay

Statistical analysis

Eo type had a significant effect on the bio-assay. PT with $\{F(5,17) = 3.3, p < 0.05\}$, % R with $\{F(5,17) = 3.3, p < 0.05\}$, % B with $\{F(5,17) = 3.3, p < 0.05\}$ and % M with $\{F(5,17) = 3.3, p < 0.05\}$ had confirmed that the bio-assay of all Eos was significantly different from each other. The effect of oil concentrations on the repellent activity was significantly different for % M $\{F(2,17) = 4.1, p = 0.02\}$ and % R $\{F(2,17) = 4.1, p = 0.005\}$, but not for % B $\{F(2,17) = 4.1, p = 0.14\}$ and PT $\{F(2,17) = 4.1, p = 0.98\}$.

The one-way ANOVA showed a significant effect of the factor Eo ($F(5,23) = 144.4$; $p < 0.05$). Mean comparisons had shown that % M of all Eos except CO (44%) and EO (40%) was statistically significant. % R for CdO (48.5%) and CO (51.5%), CO (51.5%) and LO (55%), EO (60%) and PO (64%) and EO (60%) and LO (55%) were not significantly different than the other Eos groups. % B for CdO (39%) and CO (37%), LO (35%) and CdO (39%), CO (37%) and LO (35%) and EO (30%) and PO (27%) was insignificant than other Eos (Table 4).

The repellent activity of Eos against *Anopheles Stephensi* mosquitoes is shown in Table 5 and Fig. 10. During the initial 3 min exposure, only JO and control had shown mosquito landing. In the 1st h of exposure of treated cotton, other than JO and control; PO and EO also had shown few mosquito bites (2 B and 1 B) due to the reason that PO was the one with the lowest % release from the IC functionalized cotton that wasn't able to ward the mosquitoes away from the cotton's surface. But, EO was released to a considerably greater extent; even then it had allowed the bites. The bio-assay for the IC treated cotton followed the following pattern-Mean PT (minutes): JO < PO < EO < CO < CdO < LO Mean % R: JO < CdO < CO < LO < EO < PO Mean % M: JO < LO < PO < EO < CO < CdO Mean % B: JO > CdO > CO > LO > EO > PO

PT-LO had shown the longest PT and JO was with the least PT due to the fastest % release of LO and slowest for JO from IC. EO and CO gave shorter PTs due to their deterrent behavior against mosquito biting and landing. PO had low PT due to its slower % release initially, which wasn't able to retard mosquitoes from landing and biting. % B and % R-JO and CdO had shown poor % B and %R, due to lowest % release of JO in the initial hours and high tendency of CdO to lure mosquitoes for landing. EO and CO did not allow the mosquitoes to land and thus, deterred bites, despite the initial bites. Due to the quickest sublimation of CO from the cavities of β -CD CA, % B was higher and thus, lower % R. LO had allowed lesser %B and thus, higher % R and optimum repellent activity. PO was the one giving the highest % R and lowest %B due to the highest % retention level after 6 h that might had helped to repel mosquitoes away from the cotton surface. CdO and JO had shown the highest and lowest %M among all the Eos. Rest Eos had shown the intermediate levels of %M in between CdO and JO. The preferential behavior of Eos towards arthropods was due to their respective compositions as monoterpenes and sesquiterpenes are the most active constituents of oils that reflect mosquito repellent activity. Monoterpenes are more volatile than the sesquiterpenes due to their molecular weight, thus 1,8 cineole (EO), linalool (LO), menthol (PO) and Eugenol (CO) are the most common monoterpenes that evaporated the fastest to give

Table 4 Post hoc analysis for mosquito repellence of ICs of Eos- β -CD CA

Oil type	CdO	CO	EO	PO	LO	JO
% M	50 \pm 3.2 ^{a*}	44 \pm 2.0 ^{ab*}	40 \pm 3.2 ^{bc*}	33 \pm 2.0 ^{abcd*}	21 \pm 0.0 ^{abcde*}	12 \pm 2.3 ^{bcde}
% R	48.5 \pm 3.0 ^a	51.5 \pm 3.0 ^b	60 \pm 3.46 ^{abc}	64.25 \pm 2.5 ^{abd}	55 \pm 2.3 ^{de}	39.5 \pm 2.89 ^{abcde}
% B	39 \pm 2.0 ^a	37 \pm 2.0 ^b	30 \pm 2.3 ^{bc}	27 \pm 2.0 ^{abd}	35 \pm 2.0 ^{cde}	46 \pm 2.31 ^{abcde}

*Various super-indices, i.e. a, b, c, d and e indicate statistical differences in repellence between the Eos ($p < 0.05$ ANOVA) and Tukey Kramer post hoc analysis. ^a Statistical difference of CdO with other Eos, ^b Statistical difference of CO with other Eos, ^c Statistical difference of EO with other Eos, ^d Statistical difference of PO with other Eos, and ^e Statistical difference of LO with other Eos.

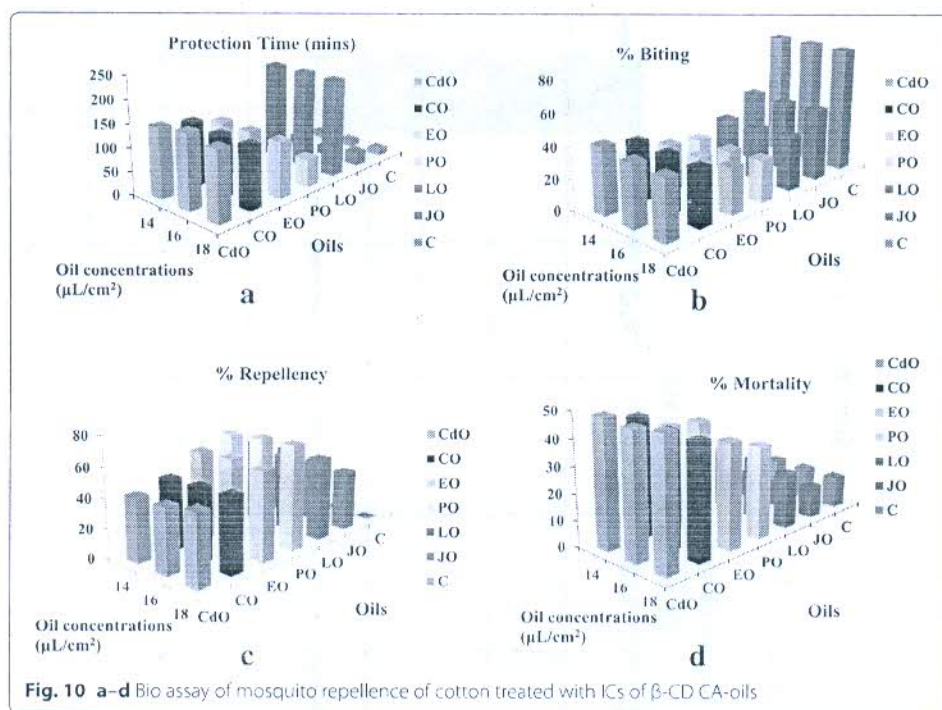
Table 5 Bio-assay of mosquito repellence-oils on β -CD CA functionalized cotton

Oil type Oil conc(μ L/cm ²)	CdO ^a			CO ^a			EO ^a			PO ^a			LO ^a			JO ^a			C
	14	16	18	14	16 ^b	18	14	16	18	14	16	18	14	16	18	14	16	18	Alcohol
Total mosq (for 4 tests)	100	100	100	100	100	100	100	100	100	100	100	100	100	100	100	100	100	100	50 (for 2 tests)
Initial 3 min. exposure (mean)	0L	0L	0L	0L	0L	0L	0L	0L	0L	0L	0L	0L	0L	0L	0L	0L	0L	0L	10L
Bites after 1st hr	0B	0B	0B	0B	0B	0B	1B	1B	1B	1B	1B	2B	0B	0B	0B	2B	2B	1B	12L, 4B
Mean M ^a after 24 h	12.25	12	12.5	11.5	11	11	9.75	10	10	8.5	8.25	8.75	5.75	5.75	5.25	2.25	2.75	2.75	3
Mean PT (mins) ^b	150 ^b	160 ^b	150 ^b	140 ^b	135 ^b	135 ^b	120 ^b	120 ^b	120 ^b	60 ^b	60 ^b	60 ^b	210 ^b	210 ^b	210 ^b	23 ^b	20 ^b	30 ^b	15
Mean bites/landings	10.75	10.5	9.75	9.75	9.5	9.25	7.25	6.75	6.5	6.75	6.5	6.75	8.5	8.25	8.75	11.5	11.25	11.5	20
Mean R% ^a	43.25 ^a	44.5 ^a	48.5 ^a	48.5 ^a	50 ^a	51.5 ^a	60 ^a	61.5 ^a	60 ^a	64.25 ^a	65.5 ^a	64.25 ^a	55 ^a	56 ^a	55 ^a	39.5 ^a	40.75 ^a	39.5 ^a	0
S.D.	2.5	2.89	3	3	3.46	3	3.46	3	3.46	2.5	2.89	2.5	2.3	2	2.3	2.89	2.5	2.89	0
Mean M% ^a	49 ^a	48 ^a	50	46	44	44	39	44	40	34	33	35	23	23	21	10	10	12	12
S.D.	2.3	3.2	3.2	2.31	2.31	2	2	3.2	3.2	2.3	2	2	2	2.3	0	2.3	2.3	2.3	0
Mean M% ^b	43 ^b	40 ^b	39 ^b	39 ^b	38 ^b	37 ^b	30 ^b	29 ^b	30 ^b	27 ^b	26 ^b	27 ^b	34 ^b	34 ^b	35 ^b	46 ^b	45 ^b	46 ^b	80 ^b

C control; L landing; M mortality; PT protection time; R repellency; B biting

^a Means of the parameters followed by their S.Ds. are significantly different ($p < 0.05$, by two-way ANOVA) for all oils

^b Indicate the columns are not significantly different ($p > 0.05$, by two-way ANOVA) for all the oil concentrations



the quickest effect on the mosquitoes. On the other hand, oxygenated sesquiterpenes (as β -caryophyllene in CdO) was the slowest to release thereby giving the sustained release.

Conclusions

The solubility of β -CD CA in water had shown a tremendous increase as compared to native β -CD. Interaction of β -CD CA concentration and curing temperature was most influential on graft yield, tensile strength, yellowness index and durability. $^1\text{H-NMR}$ spectral analysis revealed only partial inclusion of Eos into cyclodextrin cavity except JO. The phenomenon of inclusion complexation exerted a thermo-chemical influence on treated cotton and altered its thermal behaviour. Oils of Jasmine is the weakest against mosquitoes as it worked as an attractant simulating flower nectar Eucalyptus and Clove are the feeding deterrents, Lavender and Peppermint are potential mosquito repellents and Cedarwood is an effective mosquito killer.

Authors' contributions

SK and JNC planned the work. SK carried out the work and drafted the manuscript. Both the authors read and approved the final manuscript.

Competing interests

The authors declare that they have no competing interests.

Ethics approval and consent to participate

Not applicable.

Publisher's Note

Springer Nature remains neutral with regard to jurisdictional claims in published maps and institutional affiliations.

Received: 21 June 2017 Accepted: 19 October 2017

References

- Abdel-Mohdy, F., Fouda, M. M. G., Rehan, M. F., & Aly, A. S. (2008). Repellency of controlled-release treated cotton fabrics based on cypermethrin and prallethrin. *Carbohydrate Polymers*, 73(1), 92–97.
- Abdel-Mohdy, F., Fouda, M. M. G., Rehan, M. F., & Aly, A. S. (2009). Repellency of controlled-release treated-cotton fabrics based on permethrin and bioallethrin against mosquitoes. *The Journal of The Textile Institute*, 100(8), 695–701.
- Aly, S. A., Hashem, A., & Hussein, S. S. (2004). Utilization of chitosan citrate as crease-resistant and antimicrobial finishing agent for cotton fabric. *Indian Journal of Fibre & Textile Research*, 29, 218–222.
- Dehbadi, V. A., Buschmann, H. J., & Gutmann, J. S. (2014). A novel approach for fixation of β -cyclodextrins on cotton fabrics. *Journal of Inclusion Phenomena and Macrocyclic Chemistry*, 79(3–4), 459–464. <https://doi.org/10.1007/s10847-013-0368-0>
- Dong, C., Ye, Y., Qian, L., Zhao, G., He, B., & Xiao, H. (2014). Antibacterial modification of cellulose fibres by grafting β -cyclodextrin and inclusion with ciprofloxacin. *Cellulose*, 21, 1921–1932.
- El-Tahlawy, K., El-Nagar, K., & Elhendawy, A. G. (2007). Cyclodextrin-4 Hydroxy benzophenone inclusion complex for UV protective cotton fabric. *Journal of the Textile Institute*, 98(5), 453–462.
- El-Tahlawy, K., Gaffar, M. A., & El-Rafei, S. (2006). Novel method for preparation of β -cyclodextrin-grafted chitosan and its application. *Carbohydrate Polymers*, 63, 385–392.
- Fahmy, H. M. (2004). Enhancing some performance properties of ester crosslinked cotton fabric by pre-quaternization. *Egyptian Journal of Chemistry*, 47(6), 627–639.
- Fouda, M. M. G., & Fahmy, H. M. (2011). Multifunctional finish and cotton cellulose fabric. *Carbohydrate Polymers*, 86, 625–629.
- Hebeish, A., El Shafel, A., & Shaarawy, S. (2009). Synthesis and characterization of multi-functional cotton containing cyclodextrin and butylacrylate moieties. *Polymer Plastics Technology and Engineering*, 48(8), 839–850.
- Hebeish, A., Hamdy, I. A., El-Sawy, S., & Abdel-Mohdy, F. A. (2010). Preparation of durable insect repellent cotton fabric through treatment with a finishing formulations containing cypermethrin. *The Journal of The Textile Institute*, 101(7), 627–634.
- Hebeish, A., Hamdy, I. A., El-Sawy, S. M., & Fouda, M. M. G. (2008). Preparation of durable insect repellent cotton fabric: Limonene as insecticide. *Carbohydrate Polymers*, 74(2), 268–273.
- Jantan I and Zaki Z M (1999). Development of environment-friendly insect repellents from the leaf oils of selected Malaysian plants. *ASEAN Review of biodiversity and environmental conservation (ARBEC)*, 1–7.
- Karolia, A., & Mendapara, P. (2005). Application of antimicrobial and fragrance finish in combination by microencapsulation on cotton. *Journal of the Textile Association*, 66(4), 155–159.
- Kasprzyk W, Bednarsz S and Bogdal D (2010). Sorption properties of β -Cyclodextrin- citric acid derivatives, *14th International electronic conference on synthetic Organic chemistry (ECSOC-14)*, 1–7.
- Levy, E., Moctezuma, E., Strouse, J., & Agaribay, M. A. G. (2001). Spectrometric and 2D NMR studies on the complexation of chlorophenols with cyclodextrins. *Journal of Inclusion Phenomena and Macrocyclic Chemistry*, 39, 41–46.
- Martel, B., Morcellet, M., Ruffin, D., Vinet, F., & Weltrowski, M. (2002a). Capture and controlled release of fragrances by CD finished textiles. *Journal of Inclusion Phenomena and Macrocyclic Chemistry*, 44, 439–442.
- Martel, B., Weltrowski, M., Ruffin, D., & Morcellet, M. (2002b). Polycarboxylic acids as crosslinking agents for grafting cyclodextrins onto cotton and wool fabrics: Study of the process parameters. *Journal of Applied Polymer Science*, 83(7), 1449–1456.
- Masetti, A., & Maini, S. (2006). Arm in cage to compare skin repellents against bites of *Aedes albopictus*. *Bulletin of Insectology*, 59(2), 157–160.
- Prabha, R., & Vasugi, R. N. (2012). Filarial repellent finish using medicinal plants. *Indian Journal Science*, 1(1), 74–76.
- Ramchandran, T. (2009). Optimization of process parameters for crease resistant finishing of cotton fabric using citric acid. *Indian Journal of Fibre and Textile Research*, 34, 359–367.
- Romi, R., Nostro, P. L. O., Bocci, E., Ridi, F., & Baglioni, P. (2005). Bioengineering of a cellulosic fabric for insecticide delivery via grafted cyclodextrin. *Biotechnol Progress*, 21, 1724–1730.
- Samanta, A. K., Hossain, A., Bagchi, A., & Bhattacharya, K. (2016). Simultaneous dyeing and fragrance finishing of cotton fabric. *Journal Material Science & Application*, 2(4), 25–34.
- Shahba, A. F., Osama, H., Mohamed, P., & Mohamed H. (2011). Development of Longer-Lasting insect repellence cellulosic based curtain fabrics. *Material Science and Applications*, 2(3), 200–208. <https://doi.org/10.4236/msa.2011.23025>.
- Songkro, S. H. N., Jaisawang, J., Maneenuan, D., Chui home, T., & Kaewnopparat, N. (2012). Investigation of inclusion complexes of citronella oil, citronellal and citronellol with β -cyclodextrin for mosquito repellent. *Journal of Inclusion Phenomena and Macrocyclic Chemistry*, 72, 339–355.
- Specos, M. M. M., Zannoni, V., Topollan, D., Arata, J., Vivod, V., Garcia, J., et al. (2013). *Controlled release of mosquito repellents by cyclodextrins treated textiles*. Istanbul: The International Istanbul Textile Congress.
- Voncina, B., & Marechal, A. M. L. (2005). Grafting of cotton with β -Cyclodextrin via poly (carboxylic Acid). *Journal of Applied Polymer Science*, 96, 1323–1328.
- World Health Organization (2013). *Guidelines for laboratory and field testing of long-lasting insecticidal nets*, WHO/HTM/NTD/WHOPES/2013.1, ISBN 978 92 4 150527 7.

A New Color based Symmetric Encryption Algorithm

Ajit Singh¹, Kamal Sardana²
 Assistant Professor¹, Assistant Professor²
 Department of Computer Engineering¹
 Department of Electronics and Communication Engineering²
 The Technological Institute of Textile & Sciences, Bhiwani^{1,2}, India^{1,2}

Abstract:- In today's environment, an electronic security being an important aspect for high performance communication networks. Therefore a secure policy need to assure the security and privacy of information that is sent over the electronic communication media is in great need. So in this paper, we have introduced a newer a color based symmetric cryptographic approach which is being implemented in secure and reliable path selection based policy system to achieve security in ISP's networks.

Keywords:- Policy Based Routing, BGP (Border Gateway Protocol), ISP (Internet Service Provider), Encryption, Decryption.

INTRODUCTION

Cryptography is the way to achieve security by secret writing message to make them non-readable. Secret writing enables you to store sensitive data or transfer it across insecure networks so that it cannot be masqueraded by an attacker. In today's world, most of the means of secure data, code storage and transmission depend on cryptographic techniques.

There are two basic types of cryptography: Symmetric key cryptography (Secret key cryptography) and Asymmetric key cryptography (Public key cryptography). In secret key cryptography, a single key is used by both sender and receiver. For this type of cryptography, it is obvious that the secret key must be known to both the sender and the receiver. The cumbersome problem with this approach is key distribution through a highly unsecured channel. There are few well known examples are DES, RC2, IDEA etc. Asymmetric key cryptography is mainly used to solve the problem of key distribution. In this, two keys are used; private and public keys. Public key is used for encryption and private for decryption purpose. Because users tend to use two keys: public key which is known to public and private key which is known only to the user. There is no need for key distribution through insecure channel, but due to it's relying on mathematical function and large scale computationally it is not efficient for small devices. RSA and Digital signature are well known asymmetric key cryptography.

According to TACIT[8], a cryptographic algorithm consider to be secured if the cost required to break an algorithm is greater than the value of encrypted data then we consider safe. Several cryptanalyst has carried out the study of the requirements for secure use of encryption algorithm.

- It requires a strong encryption algorithm. Moreover, the attacker who knows the algorithm and has access to one or more cipher text would not be able to interpret the plain text from the cipher text.
- Sender and receiver must interchange the private key via a secure fashion.

Realizing the importance of securing the information in communication media, at most care is taken to propose a cryptographic algorithm which produces color cipher rather than text cipher on the basis of hexadecimal color value and some suitable mathematical logic concept, which is being applied on BGP routers to achieve secure and reliable path selection based policy system. In this policy, administrator can implement a policy which defines certain administrative rules and service level agreements corresponding to different characteristic path selection mechanism. When BGP routers receive a packet, it can check the nature of packet against the policy. If it matches, then secure and reliable path selection based policy determine which path to follow rather than pre-defined path. So, this new introduced policy will be helpful to enhance the security, network performance and to meet the customized routing services.

II. ENCRYPTION ALGORITHM

- Step 1. Read the character from the text file and get their ASCII value.
- Step 2. Convert the ASCII value into 8-bit binary string as $b_0b_1b_2b_3b_4b_5b_6b_7$.
- Step 3. A 16-bit binary string is formed by applying binary string expansion method as $b_4b_5b_6b_7b_0b_1b_2b_3b_4b_5b_6b_7b_0b_1b_2b_3$.
- Step 4. Perform XOR operation on binary string with 16-bit specific key k.
- Step 5. Now perform reverse operation on binary string.
- Step 6. On the nature of key, an 8-bit specific number and specified operation is chosen from a key specific look-up table and perform that specified operation on the binary string with that number.
- Step 7. Convert the resultant binary string into decimal equivalent number.
- Step 8. Now convert the decimal value into hexadecimal equivalent number.
- Step 9. Then corresponding to hexadecimal value, color cipher is to be generated.
- Step 10. Continue step (1) to (10) for the next character of file until EOF is not encountered.

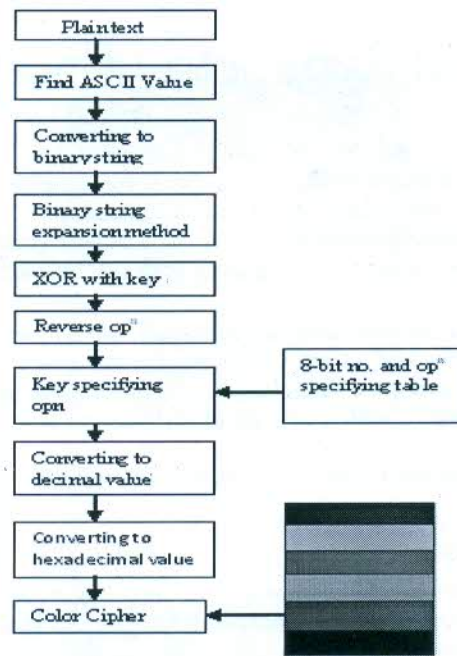


Fig1: Flow Chart of color based Encryption technique

III. DECRYPTION ALGORITHM

- Step 1. Scan the first color from the color cipher and get the corresponding hexadecimal value.
- Step 2. Convert the hexadecimal value into decimal equivalent number.
- Step 3. Corresponding binary value is evaluated.
- Step 4. On the nature of key, an 8-bit specific number and specified reverse operation is chosen from a key specific look-up table and perform that specified reverse operation on the binary string with that number.
- Step 5. Now perform reverse operation on binary string.
- Step 6. Perform XOR operation on binary string with 16-bit specific key k.
- Step 7. Apply binary string reduction method by truncating 4-bit from front and rear end of string.
- Step 8. Corresponding decimal value is calculated.
- Step 9. The ASCII character corresponding to it is determined i.e. plain text.
- Step 10. Repeat the step (1) to (9) till the EOF.

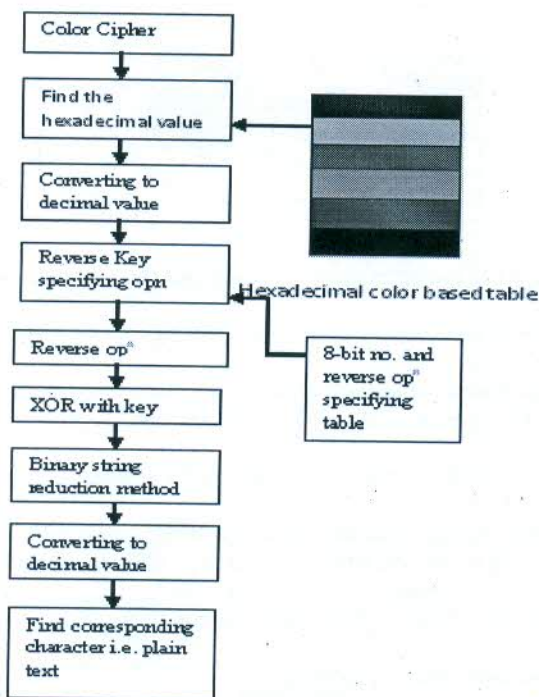


Fig 2: Flow Chart of color based Decryption technique

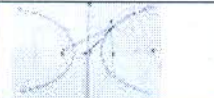

IV. KEY DISTRIBUTION TECHNIQUE

In secret key cryptography, a single key is used by both parties. So, it is obvious that the secret key must be known to both the sender and the receiver. But the cumbersome problem with this approach is key distribution through a highly unsecured channel. Here we have introduced a new key distribution system which is based on geometrical co-ordinate system in which sender and receiver will generate a key k by using the following procedure as:

- Sender will generate a coordinate point (X_1, Y_1) and similarly receiver (X_2, Y_2) , then both exchange between them.
- Now both sender and receiver familiar with (X_1, Y_1) and (X_2, Y_2) . From this we calculate m , where $m = \lceil (|Y_2 - Y_1| / |X_2 - X_1|) \rceil$.
- Then we can calculate g , where $g = \lceil (m^{X_1 * Y_2} + m^{X_2 * Y_1}) \rceil$.
- On the nature of m , we can randomly choose a geometric image from a pre-defined geometric image table, i.e. Table 1.
- Generate functional equation corresponding to image and calculate p , where $p = \lfloor f(X_2, Y_2) \rfloor$.
- Finally, generate 16-bit key as $k = (p(\text{specified operation})g) \text{ mod } 65536$.

Table 1: Geometrical Image Table

Nature of "m"	Geometric Images
$m \in$ prime no. & $m \in (1, 1000)$	
$m \in$ non-prime no. & $m \in$ (above 65536)	
$m \in$ prime no. & $m \in (1000, 9999)$	
$m \in$ non-prime no. & $m \in (1, 1000)$	

m ∈ non-prime no. & m ∈ (1000, 65536)	
m ∈ prime no. & m ∈ (above 9999)	

V. CASE STUDIES

Let we encrypt the character ‘S’ from the text file having content “SATYAGRAHA”. So first, we generate the 16-bit secret key by following procedure as:

Sender and receiver generates (19, 37) and (27, 51) coordinates points, and exchange between them.

Then sender calculates $m = 1.75$, and $g = 59871413$.

On the nature of m , sender choose a line image from a pre-defined table and get their corresponding equation i.e. $f(X, Y) = Y - X + 1$.

Finally, sender will generate $k = 31387$ by performing $k = (15 * 59871413) \text{ mod } 65536$.

For Encryption

Step 3. Apply the algorithm on first character of the file having the content “SATYAGRAHA” i.e. “S”, ASCII value of “Y” is 83.

Step 4. Corresponding 8-bit binary string is 01010011.

Step 5. Generate 16-bit binary string by applying expansion method as 0011010100110101.

Step 6. Perform XOR operation on resultant string of step (5) with the key ($k = 31387$) i.e. 0100111110101110.

Step 7. Reversing the binary string i.e. 011101011110010.






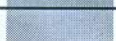




Step 8. Perform a specified operation (multiplication here) with a specific number (91 here) i.e. 1010011110110100000110.

Step 9. Corresponding decimal value is 2747654.

Step 10. Now convert the 2747654 into hexadecimal value i.e. 29ED06.

Step 11. Finally the color corresponding to the character “S” is “██████████”. That is our secure color cipher.

Similarly other character will be treated and the resultant color cipher of “SATYAGRAHA” will be

Character	Hexadecimal Value	Color Cipher
S	3CB8A6	
A	4E9EFF	
T	4B0D71	
Y	4E9EFF	
A	1FDF13	
G	4E9EFF	
R	4B68CC	
A	4D8CEE	
H	4E9EFF	
A	4DE849	

Color Cipher of “SATYAGRAHA”

Fig 3: Encrypted Plain Text

VI. SECURE AND RELIABLE PATH SELECTION BASED POLICY ROUTING

In today’s networking environment, ISPs play a crucial role in keeping the Internet well-connected and stable, as well as providing network services that meet the needs of other networks. All the services offered by ISPs fundamentally rely on routing, the process of discovering paths in a network along which to send traffic to reach other destinations. Managing routing through some policies is essential in ISPs’ to achieve high performance. By configuring many routers in its network, an ISP implements policy that reflect its business relationships with neighboring networks, and adjusts routing protocols to select paths with desirable properties. In spite of its obvious importance, today’s ISP routing management practices follows policy based routing which are surprisingly primitive. For example, even though different networks today may have very different preferences for the kinds of paths they would like to use (e.g., a financial institution may prefer the most secure and reliable paths that do not traverse any untrusted networks, whereas a provider of video conferencing, live information broadcasting or voiceover-IP service may prefer paths with the lowest latency and fast data transmission while an advertising agency prefer path having low cost or normal

data transmission), today's ISPs simply are not capable of providing such customized routing services a router is only allowed to select a single best path and only that path may be offered to its neighbors. By using secure and reliable path selection based policy, customer can implement a policy on a BGP decision router which defines certain rules and parameters corresponding to different characteristic path selection mechanism. When BGP routers receive a packet, it can check the nature of packet against the policy. If it matches, then secure and reliable path selection based policy determine which path to follow rather than pre-defined path.

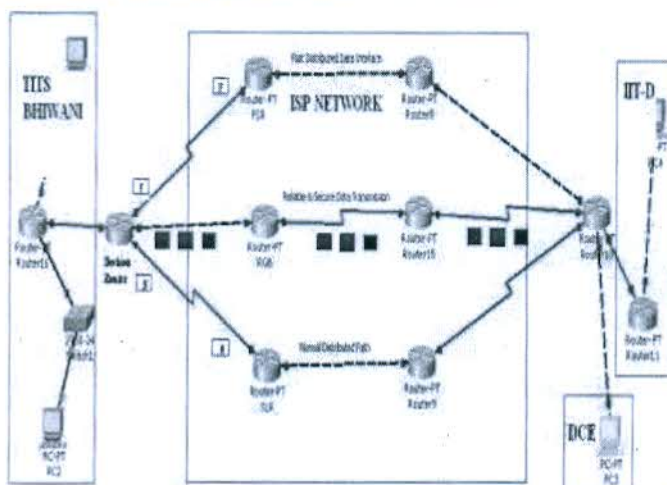


Fig 4: Secure and reliable path selection based policy System

In above ISP network, we have implemented a secure color based encryption and decryption algorithm on BGP decision router and router-10 to meet the importance of electronic security to the information that is sent over highly vulnerable and untrusted electronic communication media. Beside this, we have also imposed a secure and reliable path selection based policy on BGP decision router with the help of network simulator packet tracer which will provide the path on the nature or priority of incoming packet that violates the traditional path vector routing. Now if we need to have a secure and reliable data transmission or packet comes from IP address class 2, then BGP will provide a secure and reliable path to that packet. Also if nature of traffic demands fast transmission or comes from IP address class 1, then it will follow the fast distributed data interface path. Finally, normal distributed path will be available for slow transmission; low priority and IP address class 3 packets. So, this new introduced policy will be helpful to enhance the network performance and to meet the customized routing services. In this, we have discussed about three traffic classes which are categorized as:

Class 1: Traffic that demands services like video-conferencing, client meetings, live support etc.

Class 2: Traffic that demands services like secure transaction with the client will be categorized in this class except video-conferencing.

Class 3: This class mainly supports extranet services for the unauthorized clients.

VII. ROUTER CONFIGURATION

```
Router>enable
Router#config t
Enter configuration commands, one per line. End with CNTL/Z
Router(config)#interface fa 0/0
Router(config-if)#ip address 192.168.122.2 255.255.255.0
Router(config-if)#description line Fast Distributed Data Interface Line
Router(config-if)#no shut
LINK-5-CHANGED: Interface FastEthernet0/0, changed state to up
Router(config-if)#exit
Router(config)#interface s 0/1
Router(config-if)#ip address 192.168.124.5 255.255.255.0
Router(config-if)#clockrate 500000
Router(config-if)#description line Reliable and secure data transmission Line
Router(config-if)#no shut
LINK-6-CHANGED: Interface serial 0/1, changed state to up
Router(config-if)#exit
Router(config)#interface s 0/0
Router(config-if)#ip address 192.168.128.3 255.255.255.0
Router(config-if)#description line Normal Distributed Path
Router(config-if)#no shut
LINK-7-CHANGED: Interface serial 0/0, changed state to up
Router(config-if)#exit
Router(config)#access-list 1 permit 192.168.0.0 0.0.0.255 ?
log Log matches against this entry
```

```

<cr>
Router(config)#route-map PBR permit 10
Router(config-route-map)#match ip address 1
Router(config-route-map)#match fastEthernet
Router(config-route-map)#set interface fa 0/0
Router(config-route-map)#end
Router# show route-map
route-map PBR, permit, sequence 10
Match clauses:
  ip address (access-lists): 1
  fastEthernet
Set clauses:
  interface fa 0/0
Router(config)#route-map PBR permit 10
Router(config-route-map)#match ip address 2
Router(config-route-map)#match RelialeSecure
Router(config-route-map)#set interface S 0/1
Router(config-route-map)#end
Router# show route-map
route-map PBR, permit, sequence 10
Match clauses:
  ip address (access-lists): 2
  RelialeSecure
Set clauses:
  interface S 0/1
Router(config)#route-map PBR permit 10
Router(config-route-map)#match ip address 3
Router(config-route-map)#match NormalPath
Router(config-route-map)#set interface S 0/0
Router(config-route-map)#end
Router# show route-map
route-map PBR, permit, sequence 10
Match clauses:
  ip address (access-lists): 2
  NormalPath
Set clauses:
  interface S 0/0

```



VIII. CONCLUSION

The paper has demonstrated a color based symmetric encryption algorithm which is more secure as compared to existing ones and to the best of our concern it would be difficult to intruders for cryptanalysis. Moreover, we have also implemented this newer approach on secure and reliable policy based routing which will provide different characteristics path on the basis of nature, priority, type of service (ToS) or defined class of incoming packet. The main emphasis of this policy is to provide a secure and reliable path, and that will be provided by applying the encryption and decryption techniques on BGP routers and also by configuring them. So, this new introduced policy will be helpful to enhance the security, network performance by partitioning the single link load into three link, and also helpful to meet the customized routing services by providing the required services to the customers. And the proposed direction for the future work would be to analyze the following factors:

1. Hardware implementation of this algorithm using VLSI techniques on BGP router.
2. Compression technique could be implemented along with encryption procedure to achieve high performance in terms of security and bandwidth utilization.
3. Introduce time and location dependent encoded look-up tables.
4. Performance analysis of this one with existing ones in terms of throughput, memory requirement, power consumption and security towards intruders.
5. Introduce the enhanced one or more complex policy in network traffic like ISP.
6. Introduce modified form of this one which can be efficiently used in small devices.

REFERENCES

- [1] P.Gope, "Multi Operator Delimiter based Data Encryption Standard (MODDES)", ICCNT 2009.
- [2] P.Gope, "A comparative study of performance based crypto analysis features for standard Data Encryption Algorithms with (MODDES)", ICCNT 2009.
- [3] Twenty Second National Radio Science Conference (NRSC 2005), RDEA Algorithm.
- [4] Daemen, Jjmen, V.: "AES Proposal: Rijndael", Banksys/Katholieke, R Universiteit Leuven, Belgium, AES submission, June 1998.
- [5] W.Stallings "Cryptography and network security principles and practice," Fourth edition, Prentice hall, 2007.

- [6] Computer Networks by Andrew S. Tanenbaum, Fourth Edition, Prentice hall, 2004.
- [7] P.Gope," Extended Multi Operator Delimiter Based Data Encryption Standard(X-MODDES)," ICFN, 2010, China.
- [8] P. Gope, A. Singh, "An Efficient Cryptographic Approach for Secure Policy Based Routing", ICNCS, 2011, Kanyakumari, India.
- [9] A. Singh "An Improved Two-factor Authenticated Key exchange Protocol in Public Wireless LANs", IEEE Xplore Digital Library, ACCT2012, India.
- [10] A. Singh "A Novel Approach towards Mutual Authentication and Key Exchange Protocol based on Elliptic Curve", IEEE Xplore Digital Library, ACCT2012, India.
- [11] <http://www.cisco.com>.
- [12] <http://thepackettracer.blogspot.com>.
- [13] http://watchguard.com/.../policy_based_routing_configuration_f.html.
- [14] D. R. Stinson, "Cryptography Theory and Practice", CRC Press, Inc., 2002.
- [15] E. Crawley et. al. "A framework for QoS based Routing in the Internet", RFC 2386, Aug 1998.



GOVERNANCE SYSTEM FOR FAILURE ANTICIPATION IN HYBRID/OPTICAL NETWORKS

Satish Khatak

Assistant Professor, Department Of Electronics and Communication,
The Technological Institute Of Textile & Sciences, Bhiwani (Haryana)

Rajeev Sharma

Assistant Professor, Department Of Electronics and Communication,
The Technological Institute Of Textile & Sciences, Bhiwani (Haryana)

ABSTRACT:

To fulfill the enormous growth in voice, data & multimedia applications, Optical networks (SDH and DWDM) have been introduced for exploring higher bandwidth & better QOS. Problems arise when integrating the whole new optical infrastructure with current IP backbone, including controlling data path and network management. Network Management System (NMS) is a service that employs a variety of tools, applications, and devices to assist network administrators on monitoring and maintaining network and keeping the network working with high quality of services. The aim of this paper is to review the design of a multi-agent based network management support system with well-organized representation of the formal semantics of networks alarm management in hybrid networks containing DWDM, SDH and IP technologies & experiential knowledge related to NMS fault diagnosis functional area.

Cite this Article: Satish Khatak and Rajeev Sharma, Governance System for Failure Anticipation in Hybrid/Optical Networks. *International Journal of Advanced Research in Engineering and Technology*, 9(1), 2018, pp. 68–77.
<http://iaeme.com/Home/issue/IJARET?Volume=9&Issue=1>

1. INTRODUCTION

As networks face increasing bandwidth demand and diminishing fiber availability, network providers are moving towards a crucial milestone in network evolution. The Optical networks, based on the emergence of the optical layer in transport networks, provide higher capacity and reduced costs where fiber systems are employed, technologies and components that provide routing, grooming, and restoration at the wavelength level as well as wavelength-based services. In optical networks, two main technologies are covered. **DWDM (Dense Wavelength-Division Multiplexing)** DWDM technologies can be used for all-optical data transmission. With the latest equipments up to 192 client data signals can be converted to wavelengths and then transmitted simultaneously over a single fiber [5]

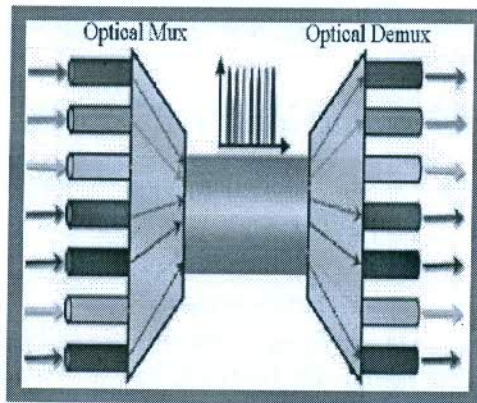


Figure 1 DWDM

A multi-channel fiber optic transmission system in which one fiber transmits No of client signals provided by different Wavelength optical carriers it is used to overcome overcome fiber exhaust / lack of fiber availability problems (Better utilization of available fiber) Easier capacity expansion Wave length leasing instead of Bandwidth leasing **SONET/SDH** Synchronous digital transmission was first introduced in the early 1980's and has matured since then with the standardization of SONET and the Synchronous Digital Hierarchy (SDH). SONET/SDH uses Time-division multiplexing technique which specific number of time slots from SONET/SDH links can be allocated to individual circuits./light paths SDH networks have many advantages such as flexible bandwidth allocation, ease of multiplexing and demultiplexing, ease of transition to higher bit rates in the future to keep up with the evolution of transmission technology, and enhanced operations OAM capabilities with the capability to implement a distributed network management system as part of an overall Telecommunications Management Network (TMN) solution [4] .There is a need in parts of a telecommunications network to transport a partially filled payload comprising low and medium capacity signals. These data signals could be or therefore, if all above technologies are deployed, hybrid network is constructed of three layers: DWDM, SONET/SDH and IP as shown in Fig.2. In the bottom layer, dark fiber footprints form the topology of DWDM network. Wavelengths in these fibers are then converted into SONET/SDH signals that construct the second layer. Finally, IP devices are connected with each other through SONET/SDH circuits/light paths.

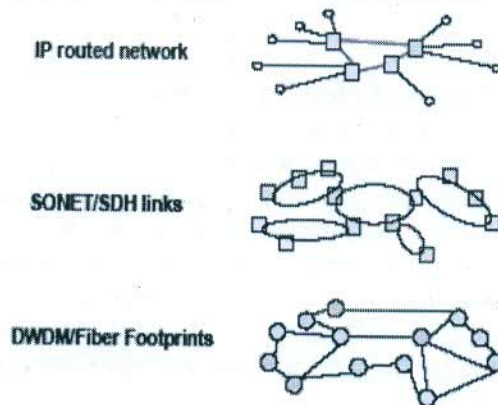


Figure 2 Hybrid network

A. DIGITAL NETWORK ARCHITECTURE

Figure 3 illustrates the basic architecture of a typical digital telecommunications network with both network management and restoration capabilities. This kind of network is typically based on three types of elements: (a) customer premises equipment, (b) nodal equipment and (c) facilities that connect nodes to nodes or nodes to customer premises. The NMS and the RS (Restoration system) are external to the network and are connected to the dedicated network via a separate communications network. The communications network does not carry customer traffic but only network alarm and status information plus maintenance and control commands

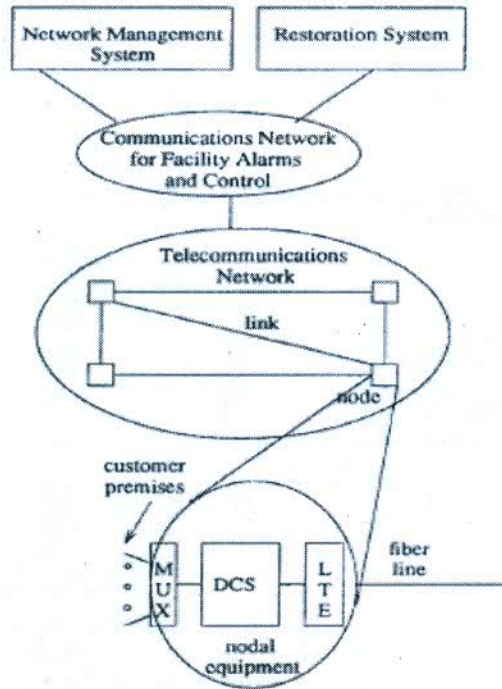


Figure 3 Network Architecture Networks.

Currently and with increasing rapidity, major network providers are deploying fiber optic technology as the technology of choice for their transport networks, both domestic and international. In general, primary rate bearers at data rates of 1.544 or 2.048 Mb/s are viewed as the fundamental building blocks of a transmission network. These bearers carry multiplexed service circuits (also called applications) across physical facilities and through nodal equipments (e.g., cross-connects and multiplexers) constituting a digital telecommunications network. End-end service circuit connections (which typically would operate at rates of 2.4 kb/s or above) are shown in Figure 3. At the access node, a customer circuit is multiplexed with other customers' service circuits up to the primary rate level for packing efficiency via a multiplexer (MUX) and then cross connected at bearer channel level (64 kb/s) for proper routing via a Digital Cross-connect System (DCS). Then within the access node the bearer is cross-connected to a Line Terminating Equipment (LTE) for long-haul transport. At the egress node, the facility is terminated at an LTE, the bearer is cross-connected in the DCS at a channel level appropriate for local routing, and then the bearer is demultiplexed to recover the original service circuit from it.

B. ALARM CORRELATION CROSSES IP AND OPTICAL LAYERS

The typical network layer hierarchy in hybrid networks in Fig. 4. Assuming that there are f fibers run in the same conduit. For each fiber, there are w wavelengths which are converted into oc-192 (for SONET) or STM-64 (for SDH) signals. Average x SONET/SDH circuits traverse each oc-192 or STM-64 link. End users connect their IP clients (router, switch or PC) to the termination point of light paths to utilize the end-to-end bandwidth assigned from underlying optical infrastructure. If network breakdown occurs in single layer, network alarms from all affected layers would appear concurrently. Therefore, correlation could be done from bottom layer up. In order to compute the complexity of alarm correlation, five cases are discussed as follows:

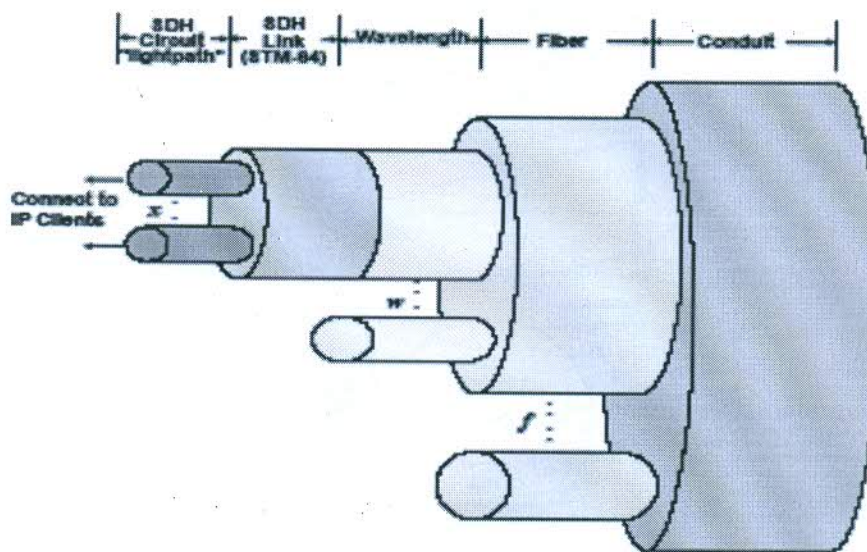


Figure 4 Network Layer Hierarchy in Hybrid Networks.

Case1. Client signal loss

The complexity of this case is Opt (1) since there would be a single alarm from light path termination point.

Case2. SONET/SDH link loss of signal

For the broken SONET/SDH link, we have to omit alarms from n light paths that traverse over it. Hence the complexity of this case is Opt (n).

Case3. Wavelength fail

If transponder malfunctions, the wavelength cannot convert to SONET/SDH signal and will cause SONET/SDH link loss of signal. The complexity is the same as Case 2 Which is Opt (n)

Case4. Single fiber cut

In case of fiber cut, all w wavelengths are malfunctioned, including n light paths for each wavelength. In order to correlate these alarms, the computation complexity is Opt (wn).

A. DIGITAL NETWORK ARCHITECTURE

Figure 3 illustrates the basic architecture of a typical digital telecommunications network with both network management and restoration capabilities. This kind of network is typically based on three types of elements: (a) customer premises equipment, (b) nodal equipment and (c) facilities that connect nodes to nodes or nodes to customer premises. The NMS and the RS (Restoration system) are external to the network and are connected to the dedicated network via a separate communications network. The communications network does not carry customer traffic but only network alarm and status information plus maintenance and control commands

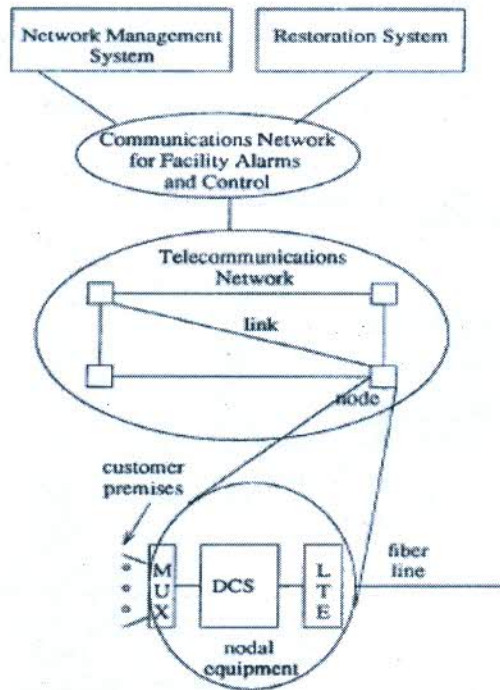


Figure 3 Network Architecture Networks.

Currently and with increasing rapidity, major network providers are deploying fiber optic technology as the technology of choice for their transport networks, both domestic and international. In general, primary rate bearers at data rates of 1.544 or 2.048 Mb/s are viewed as the fundamental building blocks of a transmission network. These bearers carry multiplexed service circuits (also called applications) across physical facilities and through nodal equipments (e.g., cross-connects and multiplexers) constituting a digital telecommunications network. End-end service circuit connections (which typically would operate at rates of 2.4 kb/s or above) are shown in Figure 3. At the access node, a customer circuit is multiplexed with other customers' service circuits up to the primary rate level for packing efficiency via a multiplexer (MUX) and then cross connected at bearer channel level (64 kb/s) for proper routing via a Digital Cross-connect System (DCS). Then within the access node the bearer is cross-connected to a Line Terminating Equipment (LE) for long-haul transport. At the egress node, the facility is terminated at an LTE, the bearer is cross-connected in the DCS at a channel level appropriate for local routing, and then the bearer is demultiplexed to recover the original service circuit from it.

Case5. Conduit collapsed

If the conduit collapsed due to road construction or destruction, all f fibers in the conduit are cut concurrently. The complexity for each fiber is $Opt(wn)$ according to Case 4. As a result, total time complexity is $Opt(fwn)$.

From the above discussion, it is concluded that the worst case complexity for cross-layer correlation is $Opt(fwn)$. Furthermore, there are several modules in DWDM layer such as pre-amplifier, multiplex/de-multiplex, and booster, each represents single sub-layer.

In general, we suppose that there are total l layers/sub-layers and the dimension of each layer is D_i , where $i=1\sim l$. The time complexity for the total correlation process is $O(D_1 D_2 \dots D_l)$

C. CORRELATION DIAGRAM AND PROPOSED ALARM CORRELATION ALGORITHM

In this section, a novel alarm correlation algorithm that simplifies root-cause analysis. A predetermined correlation diagram is required. The proposed algorithm finds the root cause from top layer down according to the diagram. In order to construct the alarm correlation diagram, we have to analyze all possible alarms in the hybrid system. As shown in Fig. 5, the alarms are classified into L layers.

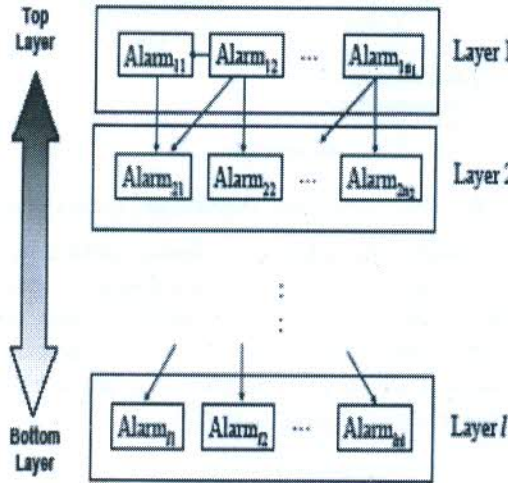


Figure 5 Alarm Correlation Diagram

Assume that there are k alarms in any layer let this layer is i , where $i=1\sim L$. Therefore, there are alarms $Alarm_{i1}, Alarm_{i2}, \dots, Alarm_{ik}$ in Layer i . If Alarm xy is caused by Alarm mn , we draw a Directed link from Alarm xy to Alarm mn . Noted that $m \geq x$ for most cases because top layer alarms are triggered by same or lower layer alarms while disruptions from top layers do not affect lower layers. Any single alarm maybe caused by multiple alarms. For example, Alarm $_{11}$ is caused by Alarm $_{21}$ while Alarm $_{12}$ may be caused by Alarm $_{21}$ or Alarm $_{22}$ in Fig. 5. The flow of the proposed alarm correlation algorithm is illustrated in Fig. 6, the algorithm processes from top layer down. Alarms are firstly categorized by layers and are then examined alarms from the top-most layer. If there is any possible alarms exist in this layer, we follow the entire correlation path to bottom

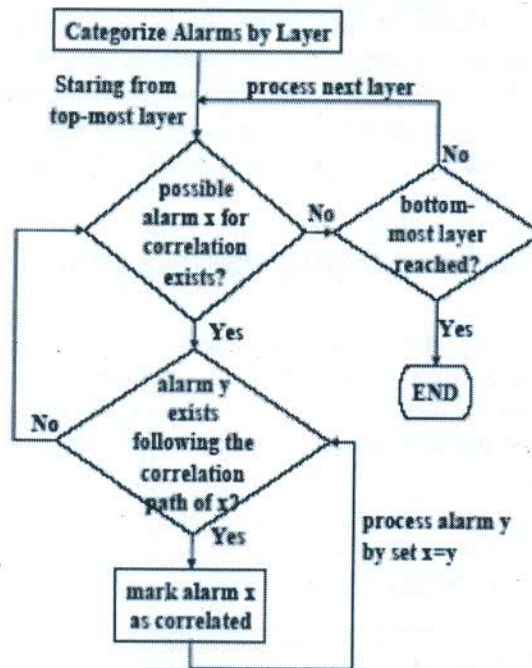


Figure 6 Alarm Correlation Algorithm Process Flow

Layers and mark these alarms as correlated. Same iterations are processed toward bottommost layer. After the process finished, the residual alarms that are not marked are the root-causes of network impairments. From previous section, time complexity of traditional alarm correlation process is in proportion to the product of dimensions at each layer. We assume that the maximum number of correlation path is p from alarm correlation diagram. The complexity of proposed correlation algorithm is $Opt(pL)$.

D. Experiment scenario and correlation diagram

In this section, real case scenarios are experimented according to previous section. These tests are performed at testbed in TWAREN optical lab. From the test results, the alarm correlation diagram is illustrated

1) TWAREN Optical Lab

It is a hybrid network that employs both IP and SDH technologies. In order to support pilot projects for cutting edge experiments, TWAREN deployed an optical network laboratory supported both next-generation SDH and DWDM. The laboratory is equipped with CISCO ONS 15454 optical switches, which support SDH modules and DWDM network modules in single chassis. Therefore, hybrid network architecture that supports IP, SDH and DWDM can be Designed and deployed using single product. The network topology is depicted in Fig. 7. Simulation of three sites called A, B and C. In site A, there are two ONS shelves that operate in DWDM and SDH layer separately. In site B and C, both DWDM and SDH modules can be installed in a single shelf. The DWDM equipment in site .Functions as ROADM to provide direct wavelengths between B and C. For each site, there is a CISCO 7609 router connected to SDH terminations of ONS Site B and C are simply DWDM leaf nodes

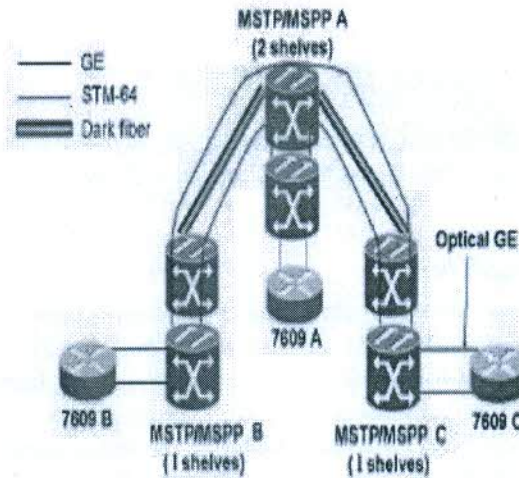


Figure 7 Network Topology of TWAREN Optical lab

For each site, there is a CISCO 7609 router connected to SDH terminations of ONS. By connecting CISCO 7609 routers to the SDH terminations, this topology acts as hybrid architecture to serve both IP network and optical network.

2. TEST SCENARIOS AND RESULTS

In order to simulate the link breakdown in several layers, the examination of the device cards in ONS 15454, which is illustrated in Fig. 8(a) is done. Dark fiber is connected to OSC-SCM (Optical Service Channel Combiner/Splitter Module) module, where the proprietary optical service channel is dropped for management operations while other data channels are delivered to de-multiplexer (32-DMX) and wavelength select and switch (32-WSS) modules for wavelength separation and switching (including local add drop). In this lab environment, 32 wavelengths could be de multiplexed from each dark fiber. For local add-drop, each wavelength is connected with transponder (TXP-MR-10G) for conversion to client signal, which is STM-64 in this configuration. Through the switching backplane of ONS, SDH circuits/light paths are provisioned over STM-64 links and terminated at Gigabit Ethernet cards (CE (Customer equipment or ML cards)). During the test, a light path is provisioned between Site A and C. Light path terminations at A and C are connected to routers at each site. The design follows four test scenarios to simulate link breakdown at each layer, which is referred to Fig. 8 (b). Table 1 lists the generated alarms in each test scenario. Each white row indicates a major alarm while each gray row indicates a critical alarm.

Test1. Client signal loss

Client signal loss can be simulated simply by shutdown of the router interface that connects to light path termination. As a result, we can easily observe that CE/ML card at near end delivers a "**Carrier Loss on LAN**" alarm to address the problem. The CE/ML card at the far end of the light path termination simultaneously issues a "**Transport Layer Failure**" alarm to notify that the client IP signal cannot be detected from this light path.

Test2. SONET/SDH link loss of signal

The link between STM-64 and transponder is unplugged such that cards to enforce loss of signal for a SDH link. From Table both near and far end of light paths that traverse this SDH link will send "**Transport Layer Failure**" alarms which reveal that there are signal detection

problems on these Light paths. In SDH and wavelength layer, only signal receives is "Loss of Signal" alarms from near end STM-64 and transponder cards. No alarm is generated at the far end site in optical layer.

Test3. Transponder/wavelength fail

Critical indicates a severe, service-affecting alarm that needs immediate correction. Major is still a serious alarm, but the failure has less of an impact on the network. To simulate transponder/wavelength fail a Link is removed between transponder and 32-WSS cards. Again, "Transport Layer Failure" alarms are issued by terminations of all affected light paths. In wavelength layer, both transponders at near end and far end generate "Incoming Payload Signal Absent" alarm to indicate the missing wavelength. But only near end 32-WSS card issue the same "Incoming Payload Signal Absent" alarm. Surprisingly, there is no "Loss of Signal" alarm in SDH layer.

Test4. Single fiber cut

In the last scenario, dark fiber is unplugged from OSCCSM module to represent single fiber cut. We obtain "Transport Layer Failure" alarms at light path termination as predicted. OSC-CSM at two ends of the dark fiber issue "Loss of Signal" alarm to warn fiber cut problem. At wavelength layer, only the transponders at ROADM site (site A in the configuration) will send "Incoming Payload Signal Absent" alarm to indicate wavelength fail. There is no reception of any "Loss of Signal" alarm in SDH layer, same as in test 3.

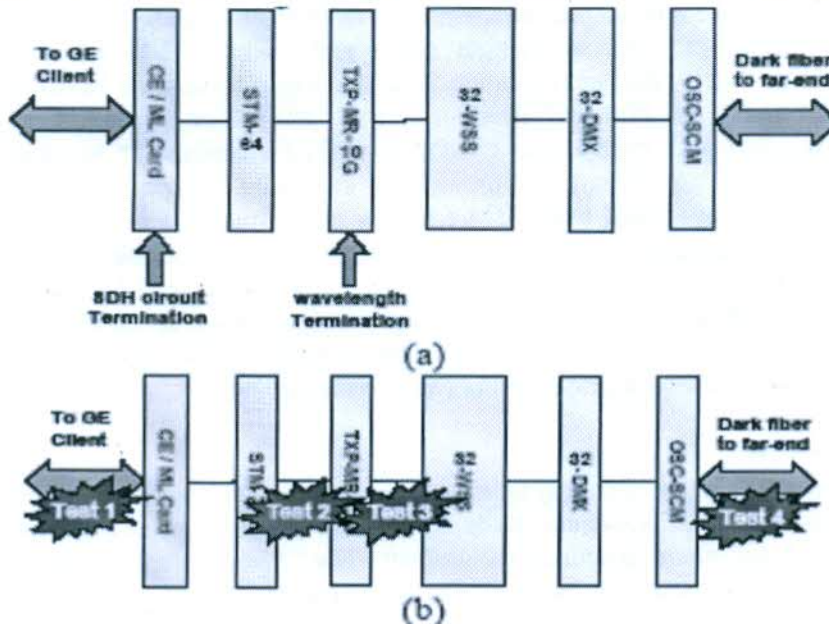


Figure 8 (a) Device cards of ONS 1544 (b) Link Breakdown Test Scenarios

In observation, the experimental results are quite different from analysis in previous section. For instance, in a fiber cut situation, 2wx alarms are issued in IP/light path termination layer, 2w alarms in both SDH and wavelength layer and 2 alarms at fiber layer. The experiment has equivalent results with IP/light

TABLE I GENERATED ALARMS IN EACH TEST SCENARIO

Scenario	Alarm Description	Alarm source (near-end or far-end)	Affected card/module
Test 1	Carrier loss on LAN	near	CE/ML
	Transport Layer Failure	far	CE/ML
Test 2	Transport Layer Failure	near and far	CE/ML
	Loss of Signal	near	STM-64
	Loss of Signal	near	TXP-MR-10G
Test 3	Transport Layer Failure	near and far	CE/ML
	Incoming Payload Signal Absent	near and far	TXP-MR-10C
	Incoming Payload Signal Absent	near	32-WSS
Test 4	Transport Layer Failure	near and far	CE/ML
	Incoming Payload Signal Absent	ROADM site	TXP-MR-10C
	Loss of Signal	near and far	OSC-CSM

Correlation Diagram

path termination layer (*Transport Layer Failure*) and fiber layer (*Loss of Signal*), but only the transponder at ROADM site will send alarm (*Incoming Payload Signal Absent*) in wavelength layer and no alarms generated in SDH layer. Apparently, device vendor has processed part of Correlation. It is very interesting that because ONS15454 integrates DWDM, SDH and IP access layers within single device, cross-layer information could be obtained easily. For example, if a transponder detects signal absent in wavelength layer, the STM-64 card connected to it should also have the same problem and therefore the alarm for STM-64 card could be ignored. It is the reason why there are no alarms in SDH layer in our test scenarios 3 and 4. In test 2, the link is unplugged between transponder and STM-64 cards at the near end. Because the underlying DWDM/wavelength layer remains intact, far end transponder and STM-64 cards will not issue loss of signal.

Although part of alarms between wavelength layer and SDH layer could be correlated, further analysis of alarms between IP/light path layer and optical-related layers is still required.

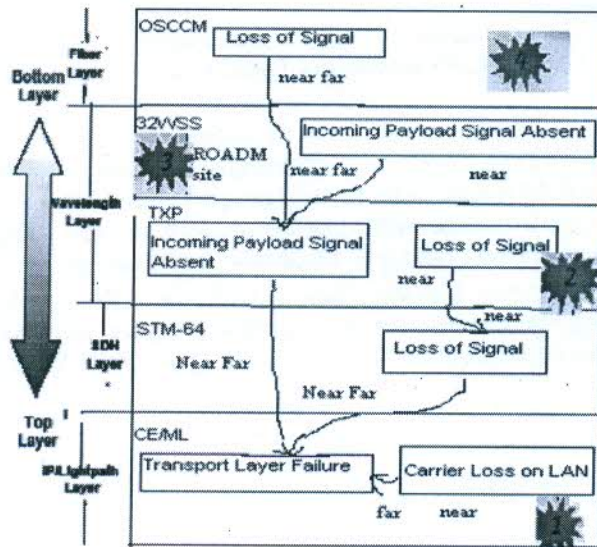


Figure 9 Alarm Correlation Diagram from Experiment

Therefore, the alarm correlation diagram is designed as shown in Fig.9 according to the experiment results. This diagram compensates for vendor's partial correlation and will help network operators/engineers to discover the actual location of network obstruction by executing the proposed alarm correlation algorithm described in previous section.

3. CONCLUSION

The intent behind this paper is to highlight the need for a fully integrated transmission network with flavors of SDH, DWDM & IP technologies to cater future demands of high bandwidth & flexible IP architecture. Secondly some basic framework is suggested to have common TMN platform for SDH, DWDM, and IP layers of network so that the operators can have single source of debugging. Alarm analysis of network in case of failure at any of the layer. This will simplify the network operations spread across different Network elements (NE) of different technologies. IP & SDH standards being already very mature only thing required is a streamlined correlation between alarms and PM parameters. With the use of OTN standards in DWDM the correlation with DWDM layers can also be strengthened. The proposed correlation diagrams & process flow compensate for such partial correlation function & will help operators and network engineers to locate the RCA (route cause analysis) of typical issues.

REFERENCES

- [1] Cheng Lai Cheah, Mohd Khazani Abdullah, Siti Barirah, Mohd Adzir Mahdi and Borhanuddin Mohd Ali. An Adaptive Error Correction Scheme for SDH Based Wavelength Division Multiplexed Optical Networks 1-4244-0000-7/05/\$20.00 02005
- [2] Cisco ONS 15454 SDH Troubleshooting and Maintenance Guide, Release 3.3, Cisco Press.] Dr. M. O. Mansour AT&T Bell Laboratories Automatic Restoration of Telecommunication Network 1995 IEEE
- [3] Miyazawa, M., Ogaki, K., Kashihara, S., Ogino, N., Furuya, H., Nakamura, H., Otani, T.: Multi-layer Network Management System integrated with a Network Planning Tool for IP/Optical integrated network, Proceedings of Optical Fiber Communication Conference, pp. 1-9. (2007)
- [4] Morkel, P.R., Farbert, A., Schwandner, A., Schubert, G., Rozensweig, G., Maki, J.J., Hotchkiss, A., Ming Ding, Sun, G., ElAhmadi, S.: Integrated IP-Optical Network Demonstration of DWDM Router-to-Router IP Transport Over 574km SMF Fiber Link Using 11.1Gbit/s OTN Pluggable Interface with Integrated G.709 and FEC, Proceedings of Optical Fiber communication/National Fiber Optic Engineers Conference, pp.1-6. (2008)
- [5] Te-Lung Liu, Hui-Min Tseng, Hui-Min Chen, Jen-Wei Hu, Chu-Sing Yang and C. Eugene Yeh Design of Alarm Management System in Hybrid IP/Optical Networks 2009 International Conference on Advanced Information Networking and Applications Workshops

Emerging Prospects of Photonic Crystal Fibers

Satish Khatak¹, G.P. Singh²

¹Research Scholar, Mewar University, Rajasthan, India

²Govt. Dungar College, Bikaner, Rajasthan, India

Abstract- Photonic crystal fibers are the periodic structures of air holes running along the fiber around a solid or hollow core. These present a diversity of new and improved features beyond what conventional optical fibers can offer. Due to their unique geometric structure, and superior control of guiding properties, PCFs present special properties and capabilities that lead to an spectacular potential for various applications. in optical communications and various other areas. This paper will review recent developments and discuss the emerging prospects in this field.

1. Introduction

A remarkable development has taken place in the last few decades within the field of optical components having a full or partly periodic structure incorporated. Such artificial optical materials are often called photonic crystals, because they form an optical equivalent to the electronic crystals in semiconductors, and they appear both as key elements in novel optical fibres and in integrated optical devices[9]. The most mature class of components are the optical fibres (often named photonic crystal fibres, microstructured fibres, or holey fibres). The appearance of photonic crystal fibers (PCFs) in 1996 was a breakthrough in fiber optic technology given that these fibers not only had new properties as they could overcome many limitations intrinsic to conventional optical fibers. PCF geometry is defined by a periodic arrangement of air holes running along the entire length of the fiber, centered on a solid or hollow core. The major difference between both kinds of fibers relies on the fact that the waveguide properties of photonic crystal fibers are not from spatially varying glass composition, as in conventional fiber, but from an arrangement of very tiny and closely spaced air holes which go along the whole length of fiber. In comparison with standard optical fibers, photonic crystal fibers can be made of a single material and have several geometric parameters which can be controlled offering large flexibility of design. These fibers also offers the possibility of light guiding in a hollow core, giving new perspectives in fields such as nonlinear fiber optics, fiber lasers, supercontinuum generation, particle guidance, and fiber sensors [3,4]. Therefore, there is a high curiosity of the research and

scientific community in employing photonic crystal fibers in all kind of fields.

2. PCF Modes

2.1 Index Guided Mode (Holey Fiber)

This comprise a arranged micro structural array of air holes called the solid core surrounded by pure silica cladding of refractive index 1.462. Owing to the large refractive index contrast between air (1.000) and silica (1.462) here the light is guided by modified total internal reflection which is totally a function of wavelength [3]. The Fig. 1 refers to the effective refractive index profile for Photonic Crystal Fiber. Effective Refractive Index is a number that measures the phase delay per unit length in PCF relative to phase delay in vacuum.

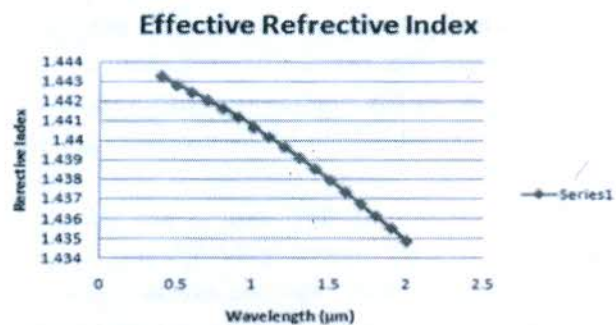


Fig. 1. Graph for Effective Refractive index distribution profile for PCF structure (Circular air holes)[4]

This differs PCF from the conventional fibers wherein light is propagated by the mechanism of total internal reflection at the core cladding interface

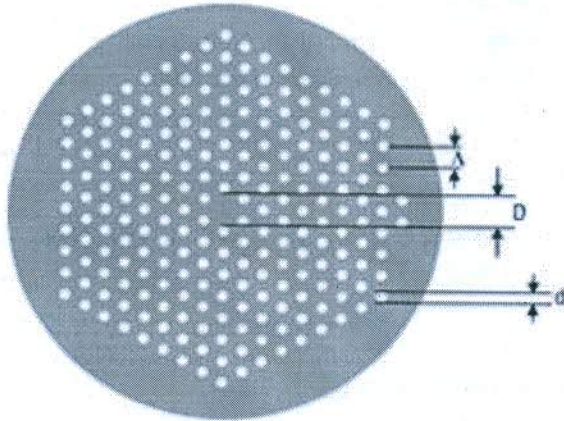


Fig. 2. Holey fibers [5]

In Fig. 2, the PCF consists of a missing air hole in the center of diameter 'D' and the pitch is labeled as 'Λ' which measures the distance between the centers of the neighboring air holes. The hole size is labeled as 'd'.

2.2 Photonic Band gap Mode

In this the central part of the array of air holes is replaced by a bigger hole of much bigger diameter as compared to the encompassing holes, then the fiber so obtained is called the Photonic band-gap fiber. As here the periodicity of the structure is broken, the flaw so introduced causes a change in its optical properties [3], [6]. The method that guides light in the fiber is photonic band-gap according to which if the frequency of the external light matches the band-gap frequency, the light gets trapped in the hole and thus is guided throughout the length. Therefore there is no need of having a greater refractive index of the core. The figure given below is a PBG fiber with a hollow cavity in the center. Fig. 3 illustrates the PBG Fiber showing a large air hole in the center surrounded by an array of air hole

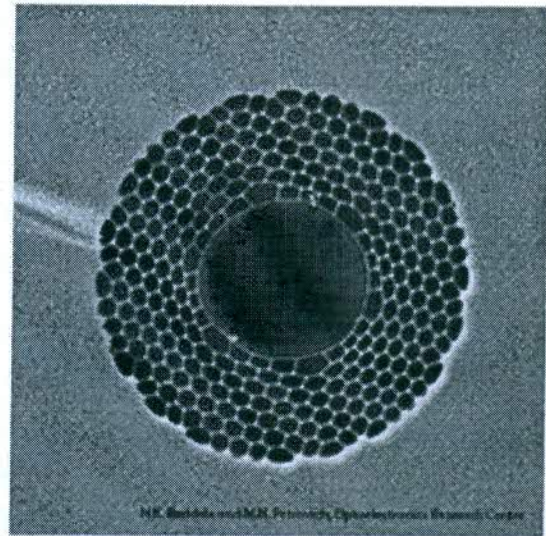


Fig. 3. Band Gap Fibers [7]

3. Features gained through PCF structure

A very important property observed in PCF's is that it acts as Single Mode Fiber for a wide range of wavelengths from about 300 nm to beyond 2000 nm and that too with a large mode-field diameter.

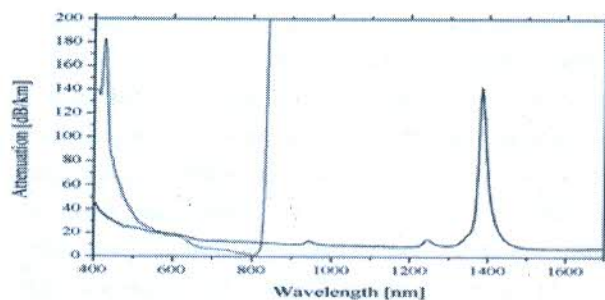


Fig. 4. Difference in Attenuation spectral of conventional optical fiber (red) and PBG fiber (black)

The above Fig. 4 shows the difference in Attenuation spectral of conventional optical fiber (red) and PBG fiber (black). The attenuation is lesser in case of Photonic Band-gap fibers as the light is guided through the hollow core. PCF's with larger core carry more optical power. Size of the air holes can be controlled and adjusted so as to minimize dispersion by shifting the point of zero dispersion in the visible light region. PCFs can easily attenuate higher wavelengths and so

they can control Raman Scattering. They have no. of air holes which provide large surface area to gather more amount of light and thus an increased Numerical Aperture (NA) is obtained i.e. 0.6 or 0.7 of MMF. Larger holes may be filled with different liquids and gases. Gas filled PCFs are greatly used in Fiber Optics Sensor, non linear spectral broadening and variable power attenuation.

4. Application areas

The use of microstructures in optical fibres have opened new developments in various areas of fiber applications, and it is interesting that each of these areas actually takes advantage of different aspects of the increased physical performance enabled by the location of microstructures in the fibers. One of the highly interesting possibilities of the photonic crystal fibers lies in the ability to confine light in a very small cross section area through the use of high index contrast between holes and glass. This is used in the so-called highly nonlinear photonic crystal fibers HNL-PCFs [2]. The opposite possibility is explored in the case of so-called large-mode-area photonic crystal fibers, LMA-PCFs, which moves the nonlinear limitations to higher power levels by spreading of light to larger areas than possible in conventional fibers.

The possibility of microstructuring does, however, hold further interesting possibilities, and one is to obtain very high numerical apertures. When these possibilities are combined in an optimal manner, one of the most promising applications of photonic crystal fibers appears in the rapidly developing area of compact high-power doped PCF fiber lasers and amplifiers [3]. These may have primary applications in areas such a high-power laser-based material processing and biomedical applications, but will also find unique applications within optical communications, including, for example, broadband video distribution in the cable TV's hybrid-fiber-coax (HFC) networks or free-space optical communications.

In future optical networks one of the enabling technologies is tunable component elements or subsystem modules including reconfigurable routers, switches etc. Thus, the development of a technology platform that allows construction of tuning components is critical. Lately, photonic bandgap fibers, filled with liquid crystals, have proven to be candidates for such a

platform. Photonic bandgap fibers provide specific wave-propagating properties that are powerfully related to the design of the air holes in the cladding of the fiber. These wave-guiding properties may be altered by filling the air holes with a material, for example a liquid crystal that changes optical properties when subjected to, for example, an optical or an electrical field [4]. The usage of these two basic properties allows design of tuneable optical devices for reconfigurable optical networks.

Among the very fascinating topics in the area of research on photonic crystal fibers are the possibilities for crafting the waveguide dispersion in these devices. This is already used in the design of dispersion controlled highly nonlinear PCFs [2]. Several applications of these dispersion-flattened high-nonlinearity PCF for optical communications have been demonstrated in nonlinear optical signal processing, including wideband tunable wavelength conversion, nonlinear signal conditioning and reshaping, optical signal regeneration, ultrashort optical pulse compression, etc. [5-8,10-11].

With the flexibility in design and the ability to tailor the dispersion properties of these fibers it may also be visualized that better and more efficient dispersion compensating elements can be developed by the use of very high dispersion values obtainable in PCFs. Such dispersion compensating fiber or DCM (dispersion-compensating module) may substitute the current DCFs in future high-capacity DWDM systems for long-haul and metro networks.

Photonic crystal fiber-based sensing technology is still at its emerging stage when compared to fields such as supercontinuum generation. Nevertheless, the perspectives to achieve commercial availability of sensing solutions based in these fibers are optimistic.

The area of sensing is the one with more patents using PCFs: for the detection of adsorbates on the interior surfaces of the PCF air holes; by the functionalization of the air holes in the cladding of the PCF for detection of chemical and biological agents through SERS ; an analyte can be inserted in the half-core of the PCF in order to be identified by a spectroscopy interaction; or even by producing a resonator using a solid core PCF coil to measure an analyte

Temperature sensing with PCFs also has some patents. Temperature measurement was developed by filling the fiber

with a temperature-sensitive fluid or accordingly with its fluorescent characteristic and, even more, by using Hi-Bi PCF Sagnac loop mirrors with a partial perfusion or with a PCF long-period grating differential demodulation. Humidity sensors patents based on tapered and perfuse PCFs and on injection-type PCFs were also formulated. Patents were completed for a PCF refractive index sensor based on polarization interference, as well as for a real-time measurement of fluid flow concentration based in a PCF. An all-fiber liquid level sensor and a current sensor through a PCF Bragg grating were developed. A hollow-core PCF was used for a Fabry-Perot interferometer in order to obtain a displacement sensor patent; and a multiparameter sensor patent was completed based in a PCF. The number and content of patents based on PCFs is growing through the years, showing an open possibility for future commercial exploitation.

5. Conclusions

The variety of unaccustomed features of PCF, beyond what conventional fibers can offer, leads to an increase of possibilities for new and improved applications in various fields. The amount and quality of photonic crystal fiber sensors developed nowadays, shows that photonic crystal fiber is a technology with an outstanding potential for sensing applications which unlock the path for a commercial scenario. They can be used as the basic long-distance optical signal transmission medium. The potential for using PCF for telecom-level transmission seems to be there. Recent research results indicated that using hole-assisted structured, "holey fibers" with much more bending tolerance (low loss even at a very small bending radius) have been developed and deployed.

References:

- [1] A. Bjarklev, "Photonic crystal fibers: fundamentals to emerging applications," (Tutorial) CMM1, CLEO '05, May 2005, Baltimore, Maryland, USA.
- [2] K. P. Hansen, J. R. Folkenberg, C. Peucheret and A. Bjarklev, "Fully dispersion controlled triangular-core nonlinear photonic crystal fiber," OFC 2003 Postdeadline Paper PD2-1, Atlanta, Georgia, March 2003.
- [3] Richard E. Kennedy and J. R. Taylor, "All fiber, integrated, kilowatt level subpicosecond chirped pulse Yb amplification system using an air-core photonic Bandgap fiber," CMM1, CLEO '05, May 2005, Baltimore, Md., USA.
- [4] M. W. Haakestad, T. T. Larsen, M. D. Nielsen, H. E. Engan and A. Bjarklev, "Electrically tunable fiber device based on a nematic liquid crystal filled photonic Bandgap fiber," ECOC'04 Postdeadline Paper Th.4.3.2, Sept. 2004, Stockholm, Sweden.
- [5] K. K. Chow, C. Shu, Chinlon Lin and A. Bjarklev, "Polarization-insensitive widely tunable wavelength converter based on four-wave mixing in a dispersion-flattened nonlinear photonic crystal Fiber," *IEEE Photonics Technology Letters*, vol. 17, p. 624, March 2005.
- [6] K. K. Chow, C. Shu, Chinlon Lin, and A. Bjarklev, "All-optical signal restoration by spectral filtering of self-phase modulation in nonlinear photonic crystal fiber," in Proc. ECOC '04, Paper We4.P.104, Sept. 2004, Stockholm, Sweden.
- [7] K. K. Chow, C. Shu, Chinlon Lin, and A. Bjarklev, "All-optical pulse compression and reshaping by spectral filtering from self-phase modulation in a nonlinear photonic crystal fiber," CLEO '05, May 2005, Baltimore, Maryland, USA.
- [8] Zhaoxin Wang, Chinlon Lin, K. K. Chow, Yuen-Ching Ku, and Anders Bjarklev, "Nonlinear suppression of interferometric crosstalk with dispersion imbalanced loop mirror using dispersion flattened high-nonlinear photonic crystal fiber," CLEO '05, May 2005, Baltimore, Maryland, USA.
- [9] Satish Khatak, G.P. Singh "Photonic Crystal Fiber –A novel medium for light propagation" *IJARSE*, Vol.No.3, Issue No. 8, August, 2014.
- [10] Rajeev Sharma, Harish Nagar, G.P. Singh "Accurate Numerical Simulation Of Higher Order Soliton Decomposition in presence of TOD and Self-Steeptening" *IJARET*, Vol-7, Issue-1, Jan-Feb 2016, pp. 54-59
- [11] Rajeev Sharma, Harish Nagar, G.P. Singh. "Investigation of self frequency variation of higher order soliton in optical fiber" *IJSER*, Vol-7, Issue-3, March 2016, pp. 997-1000

SOLITONS IN PCF

Satish Khatak¹, G.P. Singh²

Abstract-Solitons are steady and firm nonlinear travelling waves that sustain their shape and speed in interactions. Optical solitons have shown tremendous potential globally in the various domains and because of this lots of research activities are going on and these have attracted much curiosity and interest in the research and industrial cosmos. In this paper, we give a brief overview of the basic idea of temporal solitons, simulate it and see its possible applications and the challenges in the field of Photonic Crystal fiber communications.

Keywords: PCF, Solitons

1. INTRODUCTION

The word soliton refers to steady and firm nonlinear travelling waves that sustain their shape and speed in interactions. Solitons have been discovered in many branches of Physics. In the context of Photonic Crystal Fibers, solitons are not only of fundamental interest but also have practical applications in the field of optical communications. James Scott Russel was the first scientist who discovered a soliton wave in 1834 when he unexpectedly detected in the narrow water canal a smoothly shaped water pile that to his surprise was able to propagate in the canal without an evident change in its shape a few kilometers along. The actual reason of propagation of this solitary wave was not interpreted for a many years until suitable mathematical model was formed in the 1960's together with a method of solving nonlinear equation with the help of inverse scattering method [5]-[8].

The activity of modulation disequilibrium tells that propagation of a continuous-wave (CW) beam inside optical fibers is intrinsic unstable because of the nonlinear phenomenon of SPM and leads to formation of a pulse train in the anomalous dispersion regime of optical fibers.

2. PULSE PROPAGATION IN OPTICAL FIBER

The propagation of light can be precisely described mathematically with Maxwell equations. When equations for magnetic and electric fields are combined together one get

$$\nabla^2 \vec{E} - \frac{1}{c^2} \frac{\partial^2 \vec{E}}{\partial t^2} = \frac{1}{\epsilon_0 c^2} \frac{\partial^2 \vec{P}}{\partial t^2} \quad (1)$$

Where c is the speed of light in the vacuum and ϵ_0 is the vacuum permittivity. The induced polarization P consists of two parts:

$$\vec{P}(\vec{r}, t) = \vec{P}_L(\vec{r}, t) + \vec{P}_{NL}(\vec{r}, t) \quad (2)$$

Where $P_L(r,t)$ and $P_{NL}(r, t)$ are related to electric field by relations:

¹ Research Scholar, Mewar University, Rajasthan, India

² Govt. Dungar College, Bikaner, Rajasthan, India

$$\vec{P}_L(\vec{r}, t) = \epsilon_0 \int_{-\infty}^{+\infty} \chi^{(1)}(t-t') \cdot \vec{E}(\vec{r}, t') dt' \quad (3)$$

$$\vec{P}_{NL}(\vec{r}, t) = \epsilon_0 \iiint_{-\infty}^{+\infty} \chi^{(3)}(t-t_1, t-t_2, t-t_3) * \vec{E}(\vec{r}, t_1) \vec{E}(\vec{r}, t_2) \vec{E}(\vec{r}, t_3) dt_1 dt_2 dt_3 \quad (4)$$

Where $\chi^{(1)}$ and $\chi^{(3)}$ are the first and third order susceptibility tensors.

For healthier interpreting a soliton pulse propagation in fibers it is essential to set up our modeling on the mathematical expression (1). We will suppose that a solution for electric field E have a form:

$$E(r,t) = A(Z,t) F(X,Y) \exp(i\beta_0 Z) \quad (5)$$

where $F(X, Y)$ is transverse field distribution which corresponds to the fundamental mode of single mode fiber.

The time dependence of $A(Z,t)$ implies that all spectral components of the pulse may not propagate at the same speed inside the optical fiber because of chromatic dispersion. This effect is included by modifying the refractive index as

$$\tilde{n} = n(\omega) + n_2 |E|^2 \quad (6)$$

The frequency dependence of $n(\omega)$ plays an important role in the formation of temporal solitons. It leads to broadening of optical pulse in the absence of nonlinear effects. To obtain an equation satisfied by the pulse amplitude $A(Z, t)$, it is useful to work in the Fourier domain for including the effects of chromatic dispersion and to treat the nonlinear term as a small perturbation. The Fourier transform of $\tilde{A}(Z, \omega)$ is found to satisfy

$$\frac{\partial \tilde{A}}{\partial z} - i[\beta(\omega) + \Delta\beta - \beta_0] \tilde{A} \quad (7)$$

Where $\beta(\omega) = k_0 n(\omega)$ and $\Delta\beta$ is the nonlinear part defined as

$$\Delta\beta = k_0 n_2 |A|^2 \frac{\iint_{-\infty}^{\infty} |F(X,Y)|^4 dx dy}{\iint_{-\infty}^{\infty} |F(X,Y)|^2 dx dy} \quad (8)$$

Above equation implies that each spectral component within the pulse envelope acquires a phase shift whose magnitude is both frequency and intensity dependent as it propagates down the fiber. Taking the inverse transform of Eq.(7) and obtain the propagation for $A(Z,t)$. Expanding β in Taylor series around the carrier frequency ω_0 .

$$\beta(\omega) = \beta_0 + \beta_1(\omega - \omega_0) + \frac{1}{2} \beta_2 (\omega - \omega_0)^2 + \dots \quad (9)$$

Where $\beta_m = (d^m \beta / d\omega^m)$, $m=1, 2, 3, \dots$. Substituting Eq.(9) in Eq.(7) and taking inverse transform we obtain the equation for $A(Z, t)$ as

$$\frac{\partial A}{\partial z} + \beta_1 \frac{\partial A}{\partial z} + \frac{i\beta_2}{2} \frac{\partial^2 A}{\partial t^2} = i\gamma |A|^2 A \quad (10)$$

The parameters β_1 and β_2 include the effect of dispersion to first and second orders, respectively. Physically, $\beta_1 = 1/v_g$, where v_g is group velocity accompanying with the pulse and takes into account the dispersion of group velocity. For this reason, β_2 is called the group velocity dispersion (GVD) parameter. Parameter γ is nonlinear parameter that takes into account the nonlinear properties of a fiber medium. Parameter β_1 is in true case always positive but on the other hand parameters $\lambda Z D$ and γ can be in some specific case either positive or negative. The parameter β_1 is closely associated in practice with better known parameter called dispersion parameter - D (ps/nm/km). The relation between them is in the form:

$$D = \frac{d}{d\lambda} \left(\frac{1}{v_g} \right) = - \frac{2\pi c}{\lambda^2} \beta_2 \tag{11}$$

As, the dispersion parameter D is a monotonically increasing function of wavelength, crossing a zero point at wavelength λ_{ZD} , which is called a zero chromatic dispersion wavelength. If a system operates with wavelengths above λ_{ZD} , where D is positive, β_2 must be negative and a fiber is said to work in anomalous dispersion mode. If the fiber is run below λ_{ZD} , the D is negative and β_2 must be positive. In this case a fiber is said to operate in normal dispersion mode. As far as the nonlinear parameter γ is concerned, it can be generally either positive or negative, depending on the material of the wave guide. For silica fiber is parameter γ positive but for some other materials it can be negative. More specifically, equation (10) has only two solutions, in the form of either dark or bright soliton. Corresponding to the light pulse there is the bright soliton but a pulse shaped dip in CW light “background” is the dark soliton. In other words, the dark soliton is in a fact negation of the bright soliton. Where there is maximum of light in the bright soliton, there is minimum of the light in the dark soliton and vice versa.. A waveguide in which there is either the positive nonlinearity parameter or fiber is in anomalous dispersion regime or the negative nonlinear parameter but is in normal dispersion regime, only then the bright soliton can propagate in it.

3. SIMULATION AND RESULT

Equation (10) can be normalized in the form

$$i \frac{\partial u}{\partial z} - \frac{\partial^2 u}{\partial \tau^2} \pm |u|^2 u = 0 \tag{12}$$

By using simple conversion

$$\tau = (t - \beta_1 Z) / T_0, z = Z / L_D, u = \frac{\sqrt{|\gamma| L_D}}{A} \tag{13}$$

Where T_0 is pulse width and $L_D = T_0^2 / |\beta_2|$ is the dispersion length. Using inverse scattering method reveals the solution of above mentioned equation has a form:

$$u(z, \tau) = N \cdot 2 / (e^\tau + e^{-\tau}) \cdot e^{iz/2} = N \operatorname{sech}(\tau) e^{iz/2} \tag{14}$$

If N is integer, it represents the order of the soliton pulse. Very interesting situation comes when $N=1$.

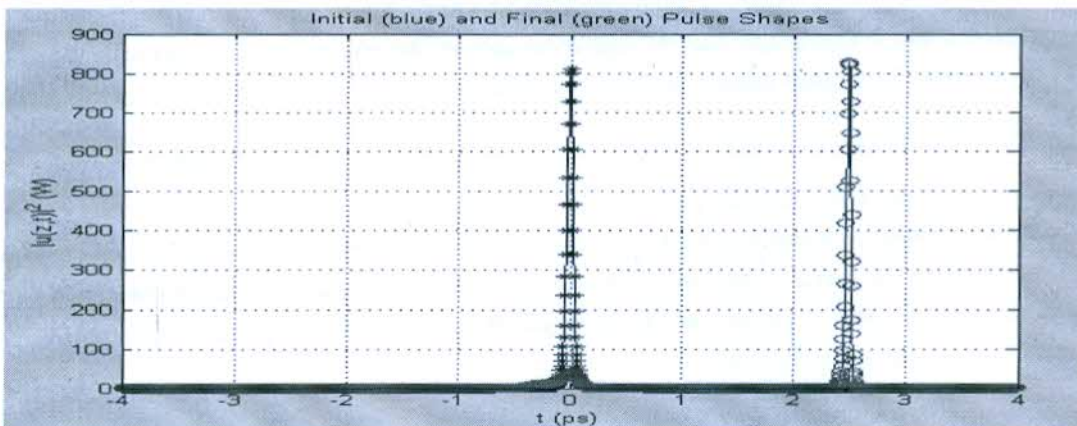


Figure: 1 Pulse intensity versus propagation time

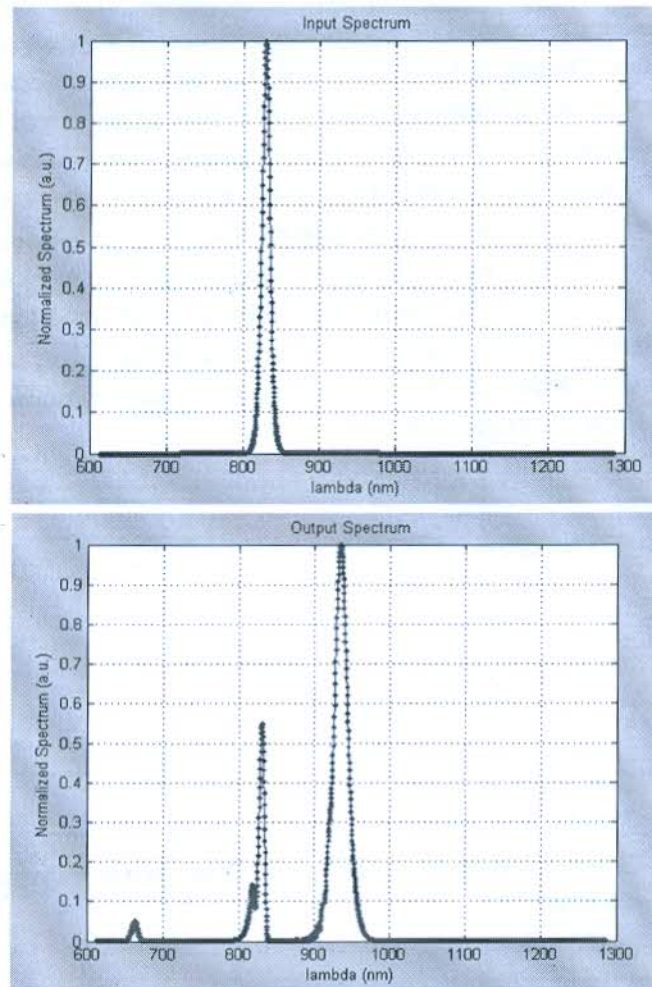


Figure: 2 Input Spectrum Vs. Output Spectrum

As seen from figure 1 and 2 that in this case of first order soliton, the pulse does not change its shape at all as it propagates in optical fiber. In contrast when N is higher than one, pulse shape is not stable and change periodically with

soliton period. $Z_0 = (\pi/2) LD$ At the end of every period Z_0 the soliton resembles its initial simple pulse shape. This shows that inclusion of higher terms alter the pulse in time and quicken its broadening.

By seeing the solitonic behavior there is a fascinating expectation of using the PCFs as dispersion compensating or dispersion managed fibers for optical communication systems. It is evident that for telecommunication purposes the soliton of first order is most suitable, because in this application is necessary to keep a pulse shape stable.

N defines the order of soliton and is defined by:

$$N = T_0 \sqrt{\frac{\gamma P_0}{\beta_2}} \quad (15)$$

Where T_0 corresponds to input pulse width, P_0 is pulse peak power. β_2 takes into account group velocity dispersion and γ is nonlinear parameter of the fiber material.

4. CONCLUSIONS:

In this paper a numerical analysis based on simulations have been exploited to know the behavior of the propagation of solitonic pulses in nonlinear PCF. The investigation has been done in time and frequency domain to fully study the nonlinear effect. Several discussion based on numerical result have been conducted.

REFERENCES

- [1] AGRAWAL, Govind P. "Applications on Nonlinear Fiber Optics". San Diego: Academic Press, 2001. 458 s. ISBN 0-12-045144-1.
- [2] KIVSHAR, Yuri S., AGRAWAL, Govind P. "Optical Solitons: From Fibers to Photonic Crystals". San Diego: Academic Press, 2003. 540 s. ISBN 0-12-410590-4.
- [3] PORSEZIAN, K., KURIAKOSE, V.C. "Optical Solitons: Theoretical and Experimental Challenges." 1st edition. Berlin: Springer, 2003. 406 s. ISBN 3-540-00155-7.
- [4] Satish Khatak, G.P. Singh "Photonic Crystal Fiber – A novel medium for light propagation" IJARSE, Vol. No 3, Issue No. 8, August, 2014.
- [5] Satish Khatak, G.P. Singh "Affects of Varying the parameters on Supercontinuum in PCF" IJAREEIE, Vol. 3, Issue 9, September 2014, pp. 12058-12067.
- [6] Rajeev Sharma and G P Singh, "Optical Soliton & Application Thereof" IJECIERD Vol. 4, Issue IV Aug 2014, pp. 71-76
- [7] Rajeev Sharma and G P Singh "Analysis of Fundamental & Higher Order Solitonic Propagation in Optical Fiber" IJRET, Vol. 2, Issue IV, July 2014, pp. 77-80
- [8] Rajeev Sharma, Harish Nagar, G.P. Singh "Accurate Numerical Simulation Of Higher Order Soliton Decomposition in presence of TOD and Self-Steepening" IJARET, Vol-7, Issue-1, Jan-Feb 2016, pp. 54-59
- [9] Rajeev Sharma, Harish Nagar, G.P. Singh. "Investigation of self frequency variation of higher order soliton in optical fiber" IJSER, Vol-7, Issue-3, March 2016, pp. 997-1000
- [10] Rajeev Sharma and G P Singh, "Numerical Simulations of Collision Behaviors of Optical Soliton in a Kerr Law Media" IJECIERD Vol. 4, Issue IV Aug 2014, pp 51-54

Dispersion Management in Photonic Crystal Fibers

Satish Khatak¹, G.P. Singh²

¹Research Scholar, Mewar University, Rajasthan, India

²Govt. Dungar College, Bikaner, Rajasthan, India

Abstract: Optical fibers have low losses, enormous bandwidth, and capability to realize high speed transmission networks. As the photonic crystal fibers offer high flexibility in its design they have attracted great interest in many research areas. Recent studies and analysis showed that dispersion properties of PCF are expected to exhibit some unusual features and these will decide whether the PCF is potentially capable to be used in telecommunication and other related applications. In this paper we look upon these properties and its management.

1. Introduction

The optical fiber has been an ideal medium for transmitting large amount of data over very long distances for the last several decades because of their low losses, enormous bandwidth and capability to realize high speed transmission networks. After the evolution of PCF, it has shown its prospective as a high data rate, large information carrying capacity and suitable for long distance transmission medium [1]. Photonic crystal fibers are the periodic structures of air holes running along the fiber around a solid or hollow core and because of the design flexibility they have shown an enormous potential over conventional fibers in many application areas. From the practical point of view, several feasibility studies need to be undertaken which include investigating its transmission characteristics and reliability over wide wavelength regions and comparing it with the existing technology of conventional fibers regarding applications and specifications matters required to replace the existing fibers revolutionary impact to the progress of the optical communications in the future. [4,5]

Polarization effects can have a huge impact on the operation of fiber-based devices and communication systems. In particular, polarization-mode dispersion can limit long distance high bit-rate data transmission. [4]

Hollow-core PCFs are well geometrically organized fibers with glass cladding incorporating arrays of air holes throughout its length. The core is formed by removing several unit cells of material from the cladding. In this structure cladding with holes is having a two dimensional photonic bandgap that can restrict and guide light to the core for wavelengths having a minimum-loss λ_c , even when the core is hollow and filled with air. In contrast, a conventional fiber light is propagated by TIR so its core must have a higher refractive index as compared with the cladding. Particularly soft glasses and polymers (plastics) can also be used in the fabrication of preforms for photonic crystal fibers by extrusion. There is a great flexibility in designing and arranging the holes leading to PCFs with very unique and important properties. All these tailored fibers can be considered as specialty fibers. [1,2]

2. Dispersion and Attenuation in PCF

The attenuation as low as about 0.15 dB/km in conventional fibers is observed by basic scattering and absorption processes in the high-purity glass which means that there are very less possibilities to further reduce it. But in case of HC-PCF over 99 % of the light is propagated in air and avoid these loss mechanisms, making Hollow-core photonic crystal fibers bright and suitable nominee as future ultra-low loss telecommunication fibers. Although, the lowest loss determined in Hollow-core photonic crystal fibers is 1.7 dB/km, though we have since reduced this to 1.2 dB/km [1,4]. So it is of utmost important to understand and analyze the primary limitations of this loss. As already mentioned that only a little fraction of the light propagates in silica, so the effect of material non-linearities is insignificant and the PCF do not suffer from the same limitations on loss as conventional fibers does.

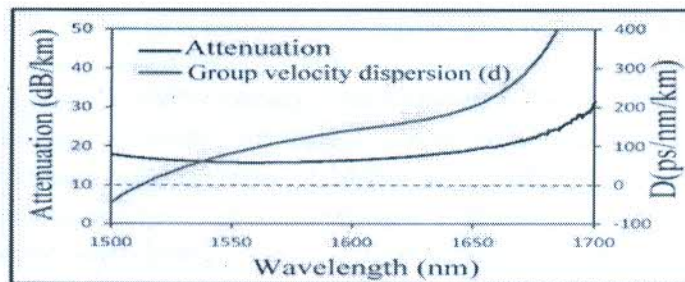


Figure 1 Attenuation and Dispersion curve as a function of wavelength

In the above figure 1 we have shown typical variation in attenuation and the dispersion as a function of wavelength. On the left vertical axis attenuation in dB/km and on right vertical axis dispersion in ps/nm/km are shown. From this we can see that at a wavelength 1500 nm dispersion effect is minimum and it keep on increasing as we move towards right hand side and shows abrupt increase in dispersion at about 1665 nm, as can be seen by red curve. On the other hand attenuation factor is almost constant from 1500 nm to 1650 nm but after that it shows slight increase, as can be seen by black curve. At around 1540 nm wavelength, the attenuation and dispersion curve are intersecting. [4,5]

3. Dispersion Management

In a fiber-optic communication system, information is transmitted over a fiber by using a coded sequence of optical pulses whose width is determined by the bit rate B of the system. Dispersion-induced broadening of pulses is undesirable as it interferes with the detection process and leads to errors if the pulse spreads outside its allocated bit slot ($T_B = 1/B$). Clearly, GVD limits the bit rate B for a fixed transmission distance L . The dispersion problem becomes quite critical when optical amplifiers are used to compensate for fiber losses because L can exceed thousands of kilometers for long-haul systems. [2,4]

A helpful measure of the information-transmission capacity is the bit rate–distance product BL. This section discusses how the BL product is controlled by fiber dispersion and how it can be improved by using the technique of dispersion management.

3.1 Dispersion-Induced Pulse Broadening

The effect of GVD on optical pulses transmitting in a linear dispersive medium are studied by setting $\gamma = 0$ in Eq.1

$$i \frac{\partial A}{\partial z} = - \frac{i\alpha A}{2} + \frac{\beta_2}{2} \frac{\partial^2 A}{\partial T^2} - \gamma |A|^2 A = 0 \quad (1)$$

If we define the normalized amplitude $U(z, T)$ and $U(z, T)$ satisfies the following linear partial differential equation:

$$i \frac{\partial U}{\partial z} - \frac{\beta_2}{2} \frac{\partial^2 U}{\partial T^2} = 0 \quad (2)$$

This equation is identical to the paraxial wave equation that administer diffraction of CW light and becomes one and the same when diffraction appears in only one transverse direction and β_2 is replaced by $-\lambda/(2\pi)$, where λ is the wavelength of light. For this cause, the dispersion-induced temporal effects have a close equivalence with the diffraction-induced spatial effects.

Equation (2) is readily solved by using the Fourier-transform method.

If $\hat{U}(z, \omega)$ is the Fourier transform of $U(z, T)$ such that

$$U(z, T) = \frac{1}{2\pi} \int_{-\infty}^{+\infty} \hat{U}(z, \omega) \exp(-i\omega T) d\omega \quad (3)$$

then it satisfies an ordinary differential equation

$$i \frac{\partial \hat{U}}{\partial z} - \frac{1}{2} \beta_2 \omega^2 \hat{U} = 0 \quad (4)$$

Whose solution is given by

$$\hat{U}(z, \omega) = \hat{U}(0, \omega) \exp\left(\frac{i}{2} \beta_2 \omega^2 z\right) \quad (5)$$

Equation (5) shows that GVD modifies the phase of every spectral component of the pulse by an amount that bank on both the frequency and the propagated distance. Although such phase changes do not change the pulse spectrum, they can modify the pulse shape. By putting Eq. (5) in Eq.(3), the solution of Eq. (2) is given by

$$U(z, T) = \frac{1}{2\pi} \int_{-\infty}^{+\infty} \hat{U}(0, \omega) \exp\left(\frac{i}{2} \beta_2 \omega^2 z - i\omega T\right) d\omega \quad (6)$$



$$\text{Where } \hat{U}(0, \omega) = \int_{-\infty}^{+\infty} \hat{U}(0, T) \exp(i\omega T) dT \quad (7)$$

Equations (6) and (7) can be used for input pulses of arbitrary shapes

3.2 GVD Induced Limitations

Consider first the case in which pulse broadening is dominated by the large spectral width σ_ω of the source. For a Gaussian pulse, the broadening factor can be obtained. Assuming that the contribution of the β_3 term is negligible together with $C=0$ and $V_\omega \gg 1$, the RMS pulse width σ is given by

$$\sigma = [\sigma_0^2 + (\beta_2 L \sigma_\omega)^2]^{1/2} = [\sigma_0^2 + (DL\sigma_\lambda)^2]^{1/2} \quad (8)$$

where L is the fiber-link length and σ_λ is the RMS spectral width of the source in wavelength units.

One can relate σ to the bit rate B by using the criterion that the broadened pulse should remain confined to its own bit slot ($T_B=1/B$) commonly used criterion is $4B\sigma < T_B$; for a Gaussian pulse, notably about 95% of the pulse energy remains within the bit slot when this condition is satisfied. The limiting bit rate is obtained using $4B\sigma < 1$. Assuming, $\sigma_0 \ll \sigma$ this condition becomes

$$BL|D|\sigma_\lambda < 1/4 \quad (9)$$

As an illustration, consider the case of multimode semiconductor lasers for which $\sigma_\lambda \approx 2$ nm. If the system is operating near $\lambda = 1.55 \mu\text{m}$ using standard fibers, $D \approx 16$ ps/(km-nm). For a 100-km-long fiber, GVD reduce the bit rate to relatively low values of only 80 Mb/s. on the other hand, if the system is designed to operate near the zero-dispersion wavelength (occurring near 1.3 μm) such that $|D| < 1$ ps/(km-nm), the BL product increases to beyond 100 (Gb/s)-km[4].

3.3 Dispersion Compensation

Although operation at the zero-dispersion wavelength is most desirable from the standpoint of pulse widening, other examination may preclude such a design. For example, at most one channel can be located at the zero dispersion wavelength in a wavelength-division-multiplexed (WDM) system. Moreover, strong four-wave mixing occurring when GVD is relatively low forces WDM systems to operate away from the zero-dispersion wavelength so that each channel has a finite value of β_2 . Of course, GVD induced pulse broadening then becomes of serious concern. The technique of dispersion management provides a solution to this context. It comprise of combining fibers with different traits such that the average GVD of the entire fiber link is quite low while the GVD of each fiber section is chosen to be large enough to make the four-wave-mixing effects negligible[6,7]. As a general rule, a periodic dispersion map is used with a period equal to the amplifier spacing (typically 50–100 km). Amplifiers compensate for accumulated fiber losses in each section. Between each pair of amplifiers, just two kinds of fibers, with opposite signs of β_2 , are combined to reduce the average dispersion to a small value. When the average GVD is set to zero, dispersion is totally compensated. Such a dispersion-compensation technique takes benefit of the linear nature of eq.2

The basic idea can be understood from Eq. (6) representing the general solution of Eq. (2). For a dispersion map consisting of two fiber segments, eq.(6) becomes the condition for dispersion compensation can be written as

$$D_1 L_1 + D_2 L_2 = 0 \quad (10)$$

Equation (10) can be satisfied in numerous different ways. If two segments are of equal lengths ($L_1=L_2$), the two fibers ought to have $D_1 = -D_2$. Fibers with equal and opposite values of GVD can be made by shifting the zero dispersion wavelength appropriately at some stage in the manufacturing process. [8,9] However, a large quantity of standard fiber is already installed in existing lightwave systems. Because this fiber has anomalous GVD with $D=16$ ps/(km-nm), its dispersion can be compensated by the help of a relatively short segment of dispersion-compensating fiber (DCF), designed to have 'normal' GVD with values of $D > -100$ ps/(km-nm).

3.4 Compensation of Third-Order Dispersion

When the bit rate of a single channel exceeds 100 Gb/s, one must use ultra short pulses (width ~ 1 ps) in each bit slot. For such short optical pulses, the pulse spectrum becomes broad enough that it is not easy to compensate GVD over the entire bandwidth of the pulse (because of the frequency dependence of β_2).

The simplest solution to this problem is provided by fibers, or other devices, designed such that both β_2 and β_3 are compensated simultaneously [2]. The necessary conditions for designing such fibers can be obtained. For a fiber link containing two different fibers of lengths L_1 and L_2 ,

the conditions for broadband dispersion compensation are given by

$$\beta_{21} L_1 + \beta_{22} L_2 = 0 \quad \text{and} \quad \beta_{31} L_1 + \beta_{32} L_2 = 0 \quad (11)$$

where β_{2j} and β_{3j} are the GVD and TOD parameters for fiber of length L_i ($i=1,2$). It is generally difficult to satisfy both conditions simultaneously over a wide wavelength range. However, for a 1-ps pulse, it is sufficient to satisfy Eq. (11) over a 4–5 nm bandwidth. This requirement is easily met for DCFs, especially designed with negative values of β_3 (sometimes called reverse-dispersion fibers). Fiber gratings, liquid-crystal modulators, and other devices can also be used for this purpose

$$\frac{\partial A}{\partial z} + \beta_1 \frac{\partial A}{\partial z} + \frac{i\beta_2}{2} \frac{\partial^2 A}{\partial t^2} = i\gamma |A|^2 A \quad (12)$$

The parameters β_1 and β_2 include the effect of dispersion to first and second orders, respectively.

Equation (12) can be normalized in the form

$$i \frac{\partial u}{\partial z} - \frac{s}{2} \frac{\partial^2 u}{\partial \tau^2} \pm |u|^2 u = 0 \quad (13)$$

By using simple conversion

$$\tau = (t - \beta_1 Z) / T_0, \quad z = Z / L_D, \quad u = \sqrt{|Y|L_D} A \quad (14)$$

Where T_0 is pulse width and $L_D = T_0^2 / |\beta_2|$ is the dispersion length.

Using inverse scattering method reveals the solution of above mentioned equation has a form:-

$$u(z, \tau) = N * 2 / (e^\tau + e^{-\tau}) * e^{iz/2} = N \operatorname{sech}(\tau) e^{iz/2} \quad (15)$$

If N is integer, it represent the order of the soliton pulse. Very interesting situation comes when $N=1$.

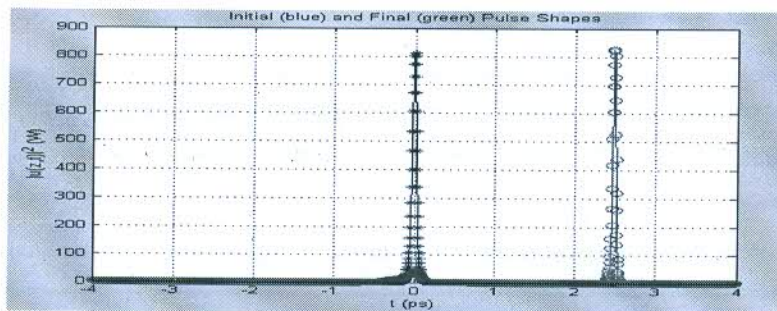


Figure 2 Pulse intensity versus propagation time

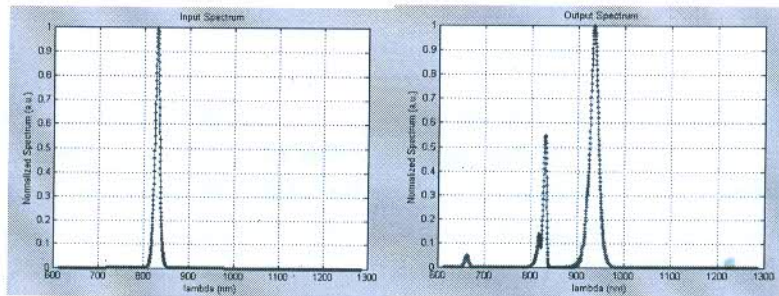


Figure: 3 Input Spectrum Vs. Output Spectrum

From figure 2 we see that pulse shape remains almost constant as it is propagated through the fiber. This is how this light pulse maintain its shape and manage the ill effects of dispersion and non linearity in PCF. Same thing can be seen in figure 3, where we compare input and output spectrum as a function of wavelength. By seeing the solitonic behavior there is a fascinating expectation of using the PCFs as dispersion compensating or dispersion managed fibers for optical communication systems.

Result and conclusions

From the above discussion it is clear that the dispersion effects can be managed by the solitonic behaviour of these fibers for the light pulse and these fibers have a strong character and possibility to behave as dispersion compensating elements in various applications in optical fiber communication

References

1. AGRAWAL, Govind P. "Applications on Nonlinear Fiber Optics". San Diego: Academic Press, 2001. 458 s. ISBN 0-12-045144-1.
2. J.C.Knight, T.A.Birks, P.St.J.Russell, and J.P.de Sandro, "Properties of photonic crystal fiber and the effective in-dex model", J.Opt.Soc.Am., Vol.15, No.3, 1998, pp.748-752.
3. PORSEZIAN, K., KURIAKOSE, V.C."Optical Solitons: Theoretical and Experimental Challenges." 1st edition.Berlin: Springer, 2003. 406 s. ISBN 3-540-00155-7.
4. Satish Khatak,G.P.Singh "Photonic Crystal Fiber –A novel medium for light propagation" IJARSE',Vol.No.3,Issue No. 8,August,2014.
5. Satish Khatak,G.P.Singh "Affects of Varying the parameters on Supercontinuum in PCF" IJAREEIE,Vol.3,Issue 9, Sepetember 2014,pp.12058-12067.
6. J.W.Fleming, "Material dispersion in lightguide glasses" Electr.Lett., Vol.14, 1978, pp.326-328.
7. Rajeev Sharma and G P Singh "Analysis of Fundamental & Higher Order Solitonic Propogation in Optical Fiber"IJRET, Vol. 2, Issue IV, July 2014, pp. 77-80.
8. Rajeev Sharma,Harish Nagar,G.P Singh "Accurate Numerical Simulation Of Higher Order Soliton Decomposition in presence of TOD and Self-Steepening" IJARET,Vol-7,Issue-1,Jan-Feb 2016,pp. 54-59 .
9. Rajeev Sharma,Harish Nagar,G.P Singh."Investigation of self frequency variation of higher order solution in optical fiber" IJSER, Vol-7, Issue-3, March 2016,pp. 997-1000.

PROPAGATION OF FEMTOSECOND PULSES IN SINGLE-MODE FIBERS WITH DISPERSION AND HIGHER-ORDER NONLINEARITY

Rajeev Sharma

Assistant Professor, The Technological Institute Of Textile & Sciences, Bhiwani

Satish Khatak

Assistant Professor, The Technological Institute Of Textile & Sciences, Bhiwani

ABSTRACT

We investigate through computer simulations the effects of higher-order dispersive and nonlinear propagation processes on the spectral and temporal evolution of ultrashort, high-intensity pulses propagating in single-mode optical fibers having normal dispersion. Our results indicate that under high power soliton splits into its constituents.

Keywords: femtosecond pulses, single-mode fibers, higher-order nonlinearity.

Cite this Article: Rajeev Sharma and Satish Khatak, Propagation of femtosecond pulses in single-mode fibers with dispersion and higher-order nonlinearity. *International Journal of Advanced Research in Engineering and Technology*, 9(3), 2018, pp. 25–28.

<http://www.iaeme.com/IJARET/issues.asp?JType=IJARET&VType=9&IType=3>

1. INTRODUCTION

The state of the art ultrafast lasers deliver usually Gaussian or secant pulse waveforms. However, many practical applications need employment of larger variety of pulse waveforms. Flat-top (rectangular-like), triangular, and parabolic pulses are used in all-optical signal processing, nonlinear optics [6-11]. Particularly, the interest on parabolic pulses over past few years was inspired by their unique properties [1]. These pulses propagate self-similarly in an active fiber in the presence of normal dispersion and nonlinearity, and therefore they are termed “similaritons”. The amplitude and width scaling in this case depends only on the amplifier parameters and the input pulse energy. Parabolic pulses have found numerous applications in pulse amplification and compression [8-10] as well as in optical communications [1, 3]. These include among others the optical regeneration [11], the pulse re-timing [11], the optimization of return-to-zero optical receivers [11], and mitigation of the linear waveform distortions [11]. In order to fulfill requirements of telecommunications, the compact fiber-based techniques for pulse shaping are preferable. Several linear- and nonlinear-optical techniques were proposed for this purpose. Linear techniques include application of specially designed superstructured fiber Bragg gratings (FBG) [11], long-period fiber grating filters, and arrayed waveguide gratings. For example, FBG is used as a linear

filter acting on an input Gaussian or secant optical pulse, and the grating coupling-strength and period profiles are designed to achieve the desired spectral transfer function. Thus, this pulse-shaping strategy is based on the proper manipulation of the spectral-domain features of the input optical pulse in order to obtain the spectral profile that corresponds to the desired temporal profile. The advantage of linear techniques is independence of the pulse reshaping from the input optical pulse power. Nonlinear techniques utilize complex dynamics of pulse evolution during ultrashort pulse propagation in a fiber with Kerr nonlinearity. The intensity dependence of the refractive index of a fiber leads either to self-phase modulation (SPM) or cross-phase modulation (XPM), depending on the peak power and shape of the input signal. The interplay of group-velocity (second-order) dispersion (GVD) and SPM gives rise to the various scenarios of pulse evolution in the fiber when both pulse shape and spectrum can be drastically changed [7-11]. Here we consider fibers with normal dispersion; in this case it is likely to obtain a parabolic waveform in the fiber due to the interaction of SPM and GVD. Particularly the application of dispersion decreasing fiber [1-6] and conventional normally dispersive fiber [11] for obtaining parabolic pulses was reported. In the first case the pulse reshaping is based on the longitudinal decreasing of the normal dispersion in the tapered fibers that is equivalent to presence of linear gain. In the second case the pulse reshaping is based on the interplay of the fixed normal dispersion and SPM; thus conventional single mode fibers can be used for pulse reshaping. The advantage of nonlinear shaping techniques is additional capabilities due to the changing of spectral content, such as spectral broadening or spectral narrowing. All mentioned approaches however, preliminary deal with picosecond pulses, whereas femtosecond pulses would be more attractive in many telecommunication applications as well as for amplification and compression purposes.

2. SIMULATION AND RESULT

For femtosecond pulses having widths $T_0 < 1$ ps, it becomes necessary to include all the higher-order terms in Equation

$$i \frac{\partial u}{\partial \xi} + \frac{1}{2} \frac{\partial^2 u}{\partial \tau^2} + |u|^2 u = \delta_3 \frac{\partial^3 u}{\partial \tau^3} - i s \frac{\partial}{\partial \tau} (|u|^2 u) + \tau_R u \frac{\partial |u|^2}{\partial \tau} \quad (1)$$

Because all three parameters δ_3 , s , and τ_R become non-negligible. Evolution of such ultrashort pulses in optical fibers is studied by solving Equation. (1) Numerically [1-11] As an illustration, Figure 1 & 2 shows

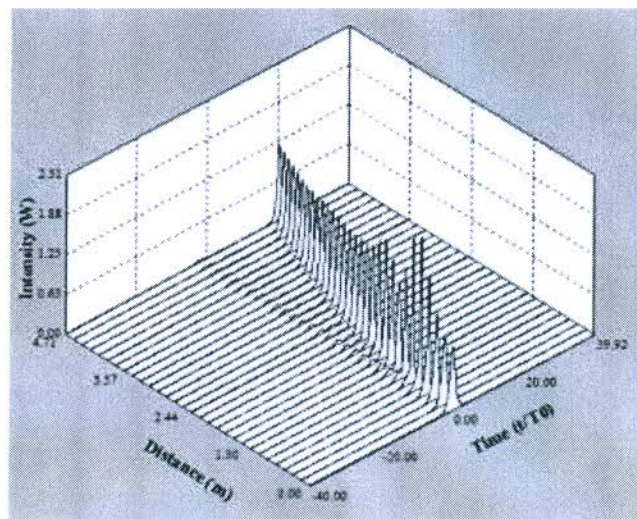


Figure 1 Evolution of pulse shapes and spectra for the case $N=2$. The other parameter values are $\delta_3 = 0.03$, $s = 0.05$, and $\tau_R = 0.1$.

Propagation of femtosecond pulses in single-mode fibers with dispersion and higher-order nonlinearity

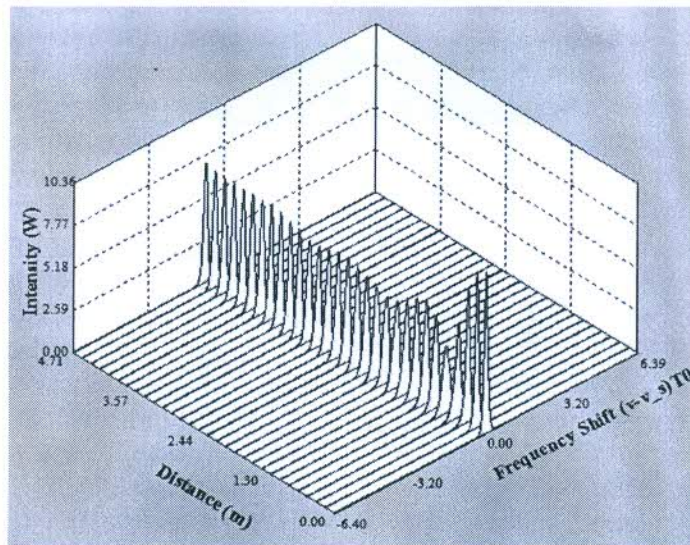


Figure 2 spectra for the case $N=2$. The other parameter values are $\delta_3=0.03$, $s=0.05$, and $\tau_R=0.1$

The pulse shapes and spectrum when a second-order soliton is fired at the input end of a fiber after choosing $\delta_3=0.03$, $s=0.05$, and $\tau_R=0.1$. These values are appropriate for a 50-fs pulse ($T_0 \approx 30$ fs) propagating in the 1.55- μm region of a standard silica fiber. Soliton decomposition occurs in a soliton period ($z_0 \approx 5$ cm), and the main crest shifts toward the trailing side at a fast rate with increasing distance. This temporal shift is due to the reduction in the group velocity v_g happening as a effect of the red shift of the soliton spectrum. A swing in the carrier frequency of the soliton changes its speed because $v_g = (d\beta/d\omega)^{-1}$ is frequency reliant. If we use $T_0=30$ fs to alter the results of Figure.2 into physical units, the 50-fs pulse has almost shifted by 40 THz or 20% of the carrier frequency after propagating a distance of only 15 cm. When the input peak power is large sufficient enough to excite a higher-order soliton such that $N \approx 1$, the pulse spectra emerges into several bands, each corresponding to separation of a fundamental soliton from the original pulse. The collective effect of TOD, self-steepening, and intrapulse Raman scattering on a higher-order soliton is to split it into its components. actually, the TOD can itself lead to soliton decomposition even in the absence of higher-order nonlinear effects when the parameter δ_3 surpass a threshold value. An fascinating question is whether Equation.1 permits shape-preserving, solitary-wave solutions under certain conditions. Several such solutions have been found using a variety of techniques [1]. In most of situation, the solution exists only for a explicit choice of parameter combinations. For example, fundamental and higher-order solitons have been found when $\tau_R=0$ $s=2\delta_3$ or $s=-6\delta_3$ [9-10]. From a practical standpoint, such solutions of Equation (1) are hardly ever useful for the reason that it is hard to find fibers whose parameters satisfy the required constraints

3. CONCLUSION

We have discussed contributions to the nonlinear chirping of ultrashort pulses in optical fibers. The dispersion in the fiber is mainly responsible for the nonlinear frequency chirp and ringing in the leading edge of the pulse, while the shock effect behaves like a damping factor. Both terms give rise to phase distortion which must be considered in pulse compression. Our results indicate that When the input peak power is large enough to excite a higher-order soliton such that $N \gg 1$ the pulse spectrum evolves into several bands, each corresponding to

splitting of a fundamental soliton from the original pulse. The spectral peak at the extreme end was associated with a soliton whose width was narrowest

REFERENCES

- [1] Satish Khatak, Mukesh Kumar, Rajeev Sharma, Kamal Sardana Signal Intensity in Optical Fiber under the Influence of Dispersion and Non-Linearity, in International Journal of Electronics Engineering, Volume 3, No.2, December 2011, pp. 293-297.
- [2] Satish Khatak, G P Singh Photonic Crystal Fiber-A Novel medium for Light Propagation in International Journal of Advanced Research in Science & Engineering, Volume 03, Issue No. 08, August 2014.
- [3] Satish Khatak, G P Singh Affects of Varying the Parameters on Supercontinuum in PCF in International Journal of Advanced Research in Electrical, Electronics and Instrumentation Engineering, Volume 03, Issue 09, September 2014.
- [4] Satish Khatak, Rajeev Sharma Governance System for Failure Anticipation in Hybrid/Optical Networks in International Journal of Advanced Research in Engineering and Technology (IJARET), pp.68-77, Volume 7, Issue 1, Jan-Feb. 2018.
- [5] Satish Khatak, G P Singh Solitons in PCF in International Journal of Latest Trends in Engineering and Technology, PP:167-171, Volume 10, Issue 2, April 2018.
- [6] Rajeev Sharma and G P Singh, Numerical Simulations of Collision Behaviors of Optical Soliton in a Kerr Law Media, International Journal Of Electronics, Communication & Instrumentation Engineering Research and Development Vol.4, Issue IV Aug2014, pp 51-54
- [7] Rajeev Sharma and G P Singh, Optical Soliton & Applications Thereof International Journal Of Electronics, Communication & Instrumentation Engineering Research and Development Vol.4, Issue IV Aug2014, pp 71-76
- [8] Rajeev Sharma and G P Singh Analysis of Fundamental & Higher Order Solitonic Propagation in Optical Fiber' IMPACT: International Journal of Research in Engineering & Technology, Vol. 2, Issue IV, July 2014, pp. 77-80
- [9] Rajeev Sharma, Harish Nagar, G.P Singh Accurate Numerical Simulation Of Higher Order Soliton Decomposition in presence of TOD and Self-Steepening International Journal of Advanced Research in Engineering and Technology, Vol-7, Issue-1, Jan-Feb 2016, pp. 54-59
- [10] Rajeev Sharma, Harish Nagar, G.P Singh Investigation of self-frequency variation of higher order soliton in optical fiber" IJSER, Vol-7, Issue-3, March 2016, pp. 997-1000
- [11] G. P. Agrawal Nonlinear Fiber Optics, Academic Press
- [12] B. Benhadou, A. Haddout, M. Benhadou, H. Bakhtari, Study and optimization of the injection molding of composites based on short hemp fibers. International Journal of Mechanical Engineering and Technology, 7(4), 2016, pp. 38-47.
- [13] Elham Jasim Mohammad, Gaillan H. Abdullah, Soliton Optical Fibers Super continuum Generation near the Zero Dispersion, International Journal of Industrial Engineering Research and Development (IJIERD), Volume 4, Issue 1, January - April (2013), pp. 52-58

Numerical simulation and comparison for computing dark and bright soliton in the optical fiber

Rajeev Sharma

AP, TIT&S, Bhiwani, Haryana, INDIA

Abstract: An analytic perturbation solution to the nonlinear Schrodinger equation with loss Gamma for both normal and anomalous dispersion is developed. Clear results are obtained through third order in the perturbation Gamma. The fallout show that the dark pulse spreads with less speed than the bright. Comparisons are made with a zeroth-order perturbation theory and with numerical simulations.

Introduction

Dark solitons denotes to the solutions of Eq.

$$\frac{i\partial U}{\partial \xi} = \text{sgn}(\beta_2) \frac{1}{2} \frac{\partial^2 U}{\partial \tau^2} - N^2 e^{-\alpha z} |U|^2 U$$

with $\text{sgn}\beta_2=1$ and occur in the normal-GVD region of fibers. They were discovered in 1973 and have drawn considerable attention since then [1–11]. The intensity profile connected with such solitons exhibits a dip in a uniform background, hence the name *dark* soliton The NLS equation describing dark solitons is obtained given by

$$\frac{i\partial u}{\partial \xi} = \frac{1}{2} \frac{\partial^2 u}{\partial \tau^2} - |u|^2 u = 0 \tag{1}$$

Similar to the case of bright solitons, the inverse scattering method has been used to find dark-soliton solutions of Eq. (1) by imposing the boundary condition that $|u(\xi, \tau)|$ tends toward a constant nonzero value for large values of $|\tau|$. Dark solitons can also be obtained by assuming a solution of the form $u(\xi, \tau) = V(\tau) \exp[i\phi(\xi, \tau)]$ then solving the normal differential equations satisfied by V and ϕ .

Simulation and Result

The main difference compared with the case of bright solitons[8-11] is that $V(\tau)$ becomes a constant (rather than being zero) as $|\tau| \rightarrow \infty$. The general solution can be written as

$$|u(\xi, \tau)| = V(\tau) = \eta \{1 - B^2 \text{sech}^2[\eta B(\tau - \tau_s)]\}^{1/2} \tag{2}$$

with the phase given by

$$\phi(\xi, \tau) = \frac{1}{2} \eta^2 (3 - B^2) \xi + \eta \sqrt{1 - B^2} \tau + \tan^{-1} \left(\frac{B \tan h(\eta B \tau)}{\sqrt{1 - B^2}} \right) \tag{3}$$

The parameters η and τ_s represent the soliton amplitude and the dip location, respectively. Similar to the bright-soliton case, τ_s can be chosen to be zero without loss of generality. In contrast with the bright-soliton case, the dark soliton has a new factor B . Physically, B governs the deepness of the dip ($B \leq 1$). For $|B|=1$, the intensity at the dip center falls to zero. For additional values of B , the dip does not go to zero. Dark solitons for which $|B| < 1$, are called *gray* solitons to stress this feature; the parameter B directs the blackness of such gray solitons. The $|B|=1$, case implies a *black* soliton. For a given value of η , Eq. (2) illustrates a family of dark solitons whose thickness increases inversely with B .

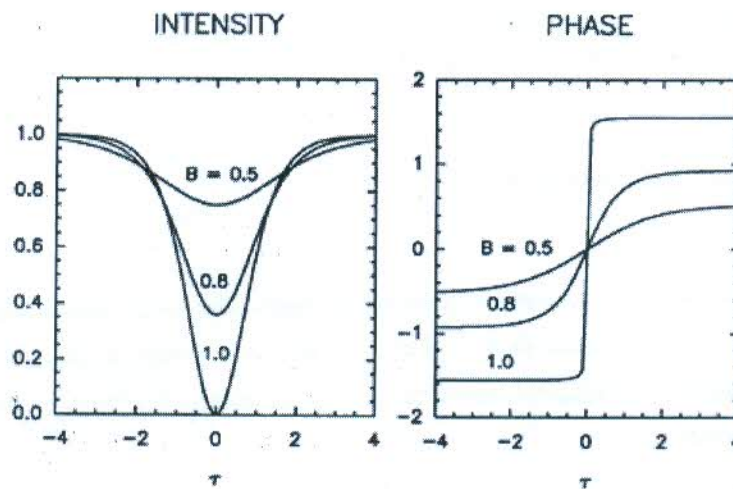


Figure 1 Intensity and phase profiles of dark solitons for several values of the blackness parameter B [12]

Figure 1 shows the intensity and phase profiles of such dark solitons for a number of values of B . While the phase of bright solitons stays constant across the entire pulse, the phase of dark soliton transforms with a total phase shift of $2\sin^{-1}B$, i.e., dark solitons are chirped. For the black soliton ($|B|=1$), due to chirp the phase changes abruptly by π in the center. The phase amendments becomes more gradual and smaller for smaller values of $|B|$. The time-dependent phase or frequency chirp of dark solitons characterize a major difference between bright and dark solitons. One outcome of this difference is that higher-order dark solitons neither form a bound state nor follow a periodic evolution pattern as in the case of bright solitons. Consider a black soliton whose canonical form is obtained from Eq. (2), choosing $\eta = 1$ and $B=1$, and given by

$$u(\xi, \tau) = \tanh(\tau) \exp(i\xi) \quad (4)$$

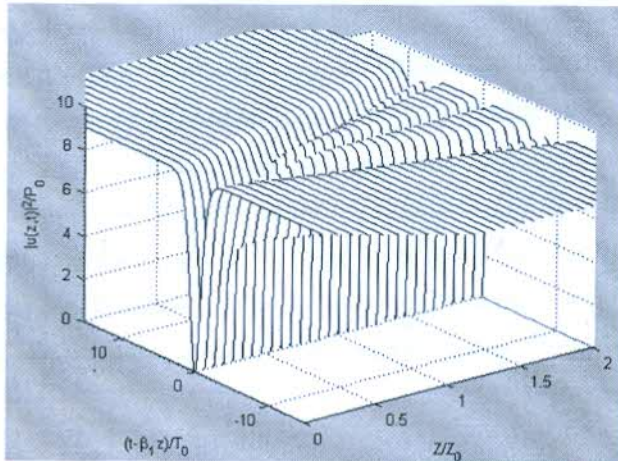


Figure.2 Evolution of a third-order dark soliton showing narrowing of the central dip and creation of two pairs of gray solitons

where the phase jump of π at $\tau = 0$ is included in the amplitude part. Thus, an input pulse with “tanh” amplitude, display an intensity “hole” at the center, would propagate without change in the normal-dispersion region of optical fibers. when the input power exceeds the $N=1$ limit. This can be answered by solving Eq. (1) numerically with an input of the form $u(\xi, \tau) = N \tanh(\tau)$

Figure 2 shows the evolution pattern for $N=3$; it should be compared with Figure 3

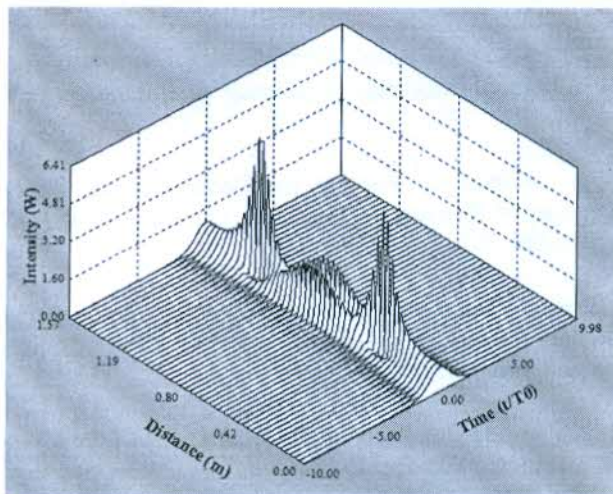


Figure 3 Temporal evolution over one soliton period for the third-order soliton. Note pulse splitting near $z_0=0.5$ and soliton recovery beyond that

where the evolution of a third-order bright soliton is displayed. Two pairs of gray solitons come into view and move away from the central black soliton as the transmission distance increases. At the same time, the width of the black soliton reduces [referene]. This nature can be understood by noting that an input pulse of the form $N \tanh(\tau)$ can form a fundamental black soliton of amplitude $N \tanh(N\tau)$ subject to its width decreases by a factor of N . It discharge part of its energy in the process that comes in the form of gray solitons. These gray solitons move away from the central black soliton since they have different group velocities. The number of pairs of gray solitons is $N=I$, where $N'=N$ for integer values of N or the next integer close to it when N is not an integer. The significant characteristic is that a fundamental dark soliton is always formed for $N>I$.

Conclusion

Dark solitons neither form a bound state nor follow a periodic evolution pattern as in the case of bright solitons. We find that Two pairs of gray solitons come into view and move away from the central black soliton as the transmission distance increases. At the same time, the width of the black soliton reduces while in case of bright soliton it retains its shape after some distance.

References

1. Satish Khatak, Mukesh Kumar, Rajeev Sharma, Kamal Sardana "Signal Intensity in Optical Fiber under the Influence of Dispersion and Non-Linearity", in International Journal of Electronics Engineering , Volume 3, No.2, December 2011, pp. 293-297
2. Satish Khatak, G P Singh "Photonic Crystal Fiber-A Novel medium for Light Propagation" in International Journal of Advanced Research in Science & Engineering , Volume 03, Issue No. 08 , August 2014.
3. Satish Khatak, G P Singh "Affects of Varying the Parameters on Supercontinuum in PCF" in International Journal of Advanced Research in Electrical, Electronics and Instrumentation Engineering , Volume 03, Issue 09, September 2014.
4. Satish Khatak, Rajeev Sharma "Governance System for Failure Anticipation in Hybrid/Optical Networks" in International Journal of Advanced Research in Engineering and Technology (IJARET), pp.68-77, Volume 7, Issue 1, Jan-Feb. 2018.
5. Satish Khatak, G P Singh "Emerging Prospects of Photonic Crystal Fibers" in International Journal of on Future Revolution in Computer Science & Communication Engineering, PP:178-181, Volume 4, Issue 3, March 2018.
6. Satish Khatak, G P Singh "Solitons in PCF" in International Journal of Latest Trends in Engineering and Technology, PP:167-171, Volume 10, Issue 2, April 2018.



7. Rajeev Sharma and G P Singh, "Numerical Simulations of Collision Behaviors of Optical Soliton in a Kerr Law Media" ,International Journal Of Electronics,Communication & Instrumentation Engineering Research and Development Vol.4,Issue IV Aug2014, pp 51-54
8. Rajeev Sharma and G P Singh, "Optical Soliton & Applications Thereof" International Journal Of Electronics,Communication & Instrumentation Engineering Research and Development Vol.4,Issue IV Aug2014, pp 71-76
9. Rajeev Sharma and G P Singh "Analysis of Fundamental & Higher Order Solitonic Propagation in Optical Fiber" IMPACT: International Journal of Research in Engineering & Technology, Vol. 2, Issue IV, July 2014, pp. 77-80
10. Rajeev Sharma,Harish Nagar,G.P Singh "Accurate Numerical Simulation Of Higher Order Soliton Decomposition in presence of TOD and Self-Steepening" International Journal of Advanced Research in Engineering and TECHNOLOGY",Vol-7,Issue-1,Jan-Feb 2016,pp. 54-59
11. Rajeev Sharma,Harish Nagar,G.P Singh "Investigation of self frequency variation of higher order soliton in optical fiber"IJSER,Vol-7,Issue-3,March 2016,pp. 997-1000
12. G. P. Agrawal Nonlinear Fiber Optics, Academic Press (2001).



Analytical Study and Simulation of TOD in Non linear Dispersive fiber

Rajeev Sharma

AP, TIT&S, Bhiwani, Haryana, INDIA

Abstract: The increasing transmission rates and link lengths of optical communication systems imply a better acquaintance of the influence of dispersion. As the transmission speed is increased, the influence of higher order dispersion is greater and must be understood. In this work we obtained a solution for a propagating pulse with third order dispersion. We could infer quantitatively the significance of third order dispersion on the pulse shape for high speed transmission systems.

Introduction

In recent years, there has been vast increase of applications in telecommunications sectors that need great amounts of bandwidth services such as interactive multimedia, video conferencing and streaming audio which has made the capacity of the existing optical fiber systems inadequate. Technologies such as Frame Relay and ATM are also requiring increased capacity. The number of Internet users is growing by many folds each year which in turn is also creating additional load and demand on the telephone access networks [11]. With the quick growth of the information industry throughout the world, more consideration is being given to optical fiber communication networks having much higher speed and larger capacity. In optical fiber communication system, dispersion is the major limiting factor as the bit rate and the transmission distance increases. Degradation of the performance of the system occurs due to increased inter-chirp interference and reduced optical power [1-11]. Dynamic dispersion compensation is becoming a concern of vital importance in high-speed optical fiber communication systems operating at 40 Gb/s and beyond as such expansion of the transmission bandwidth results in signal waveform distortion. Even if the transmission bandwidth is limited to a single channel, third-order dispersion (TOD) causes pulses to have trailing ripples which decrease the performance of the ultrahigh speed optical transmission systems [1-11]. Therefore, in such a high bit rate system, it becomes increasingly significant to exactly compensate not only the second-order dispersion, but also the TOD or dispersion slope of the fiber. There have been a number of dispersion-managed (DM) techniques to compensate for the dispersion effects. Among the different dispersion compensation techniques, there are two methods that are very useful, one using the dispersion compensation fiber (DCF) and the other, using optical fiber Bragg Grating (FBG) [11]. However, examination of TOD effect for bit rate of more than 40 Gb/s with

actual values of TOD parameters is yet to be addressed. In the present paper, we have examined the impact of TOD on the pulse shape for ultra-high speed system considering group velocity dispersion (GVD) parameter with TOD and evaluated the performance in this ultra-high speed long-haul transmission.

The qualities of optical solitons described so far are based on the NLS equation. when input pulses are so short that $T_0 < 5$ ps, it is essential to include higher-order nonlinear and dispersive effects through Eq.

$$i \frac{\partial u}{\partial \xi} + \frac{1}{2} \frac{\partial^2 u}{\partial \tau^2} + |u|^2 u = \delta_3 \frac{\partial^3 u}{\partial \tau^3} - i s \frac{\partial}{\partial \tau} (|u|^2 u) + \tau_R u \frac{\partial |u|^2}{\partial \tau} \quad (1)$$

where the pulse is assumed to propagate in the region of anomalous GVD ($\beta_2 < 0$) and fiber losses are neglected ($\alpha = 0$). The parameters δ_3, s , and τ_R administer, respectively, the effects of third-order dispersion (TOD), self-steepening, and intrapulse Raman scattering. Their explicit equations are

$$\delta_3 = \frac{\beta_3}{6|\beta_2|T_0} \quad (2)$$

$$s = 1/\omega_0 T_0 \quad (3)$$

$$\tau_R = T_R/T_0 \quad (4)$$

All three parameters changes inversely with pulse width and are insignificant for $T_0 > 1$ ps. They become substantial for femtosecond pulses. As an example, $\delta_3 \approx 0.029$, $s \approx 0.03$, $\tau_R \approx 0.1$ for a 50-fs pulse ($T_0 \approx 30$ fs) propagating at $1.55 \mu\text{m}$ in a standard silica fiber if we take $T_R = 3$ fs.

Third-Order Dispersion

When optical pulses propagate relatively far from the zero-dispersion wavelength of an optical fiber, the TOD effects on solitons is little and can be considered perturbatively. To study such effects, let us set $s = 0$ and $\tau_R = 0$ in Eq. (1) and treat the δ_3 term as a small perturbation.

Using reduced Euler-Lagrange to determine how the soliton parameter evolve with ξ . Now by putting $\epsilon(u) = \delta_3 (\partial^3 u / \partial \tau^3)$ in those equation, it is easy to show that amplitude δ , frequency η , and phase ϕ of the soliton are not susceptible to TOD. on the contrary, the peak position q changes as

$$\frac{dq}{d\xi} = -\delta + \delta_3 \eta^2 \quad (5)$$

For a fundamental soliton with $\eta = 1$ and $\delta = 0$, the soliton peak shifts linearly with ξ as $q(\xi)$. Actually, the TOD slows down the soliton and, consequently, the soliton peak is delayed by an amount that increases linearly with distance. This TOD-induced delay is insignificant in most fibers for picosecond pulses for distances as large as $\xi \sim 100$ provided that β_2 is not nearly zero. What happens if an optical pulse

propagates at or near the zero-dispersion wavelength of an optical fiber such that β_2 is nearly zero. Considerable work has been done to understand propagation behavior in this regime.

Normalizing the transmission distance to $L_D = T_0^3 / \beta_3$ through $\xi' = z/L_D$, we obtain the following equation:

$$\frac{\partial u}{\partial \xi'} - \text{sgn}(\beta_3) \frac{i \partial^3 u}{6 \partial \tau'^3} + |u|^2 u = 0 \quad (6)$$

where $u = \tilde{N}U$ with \tilde{N} is described by

$$\tilde{N}^2 = \frac{L_D}{L_{NL}} = \gamma P_0 T_0^3 / |\beta_3| \quad (7)$$

Figure 1 & Figure 2 shows the pulse shape and the spectrum at $\xi'=3$ for $\tilde{N}=2$ and compares them with those of the input pulse at $\xi'=0$. The most striking feature is splitting of the spectrum into two well-resolved spectral peaks [9-11]. These peaks denotes the outermost peaks of the SPM-broadened spectra. since the red-shifted crest exists in the anomalous-GVD regime, pulse energy within that spectral band can form a soliton. The energy in the further spectral band dissipates away easily because that part of the pulse experiences normal GVD. It is the trailing part of the pulse that dissipates away with propagation because SPM generates blue-shifted components close to the trailing edge. The pulse shape in Figure 1 display a long trailing edge with oscillations that continues to detach away from the leading part with

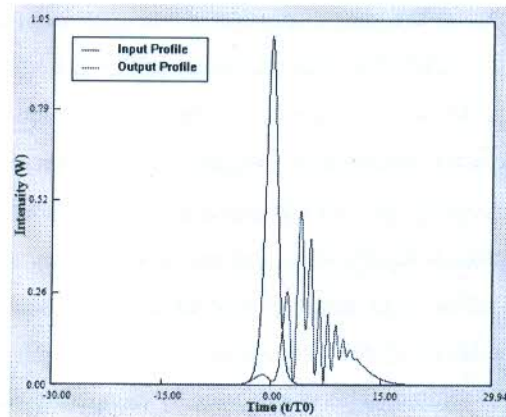


Figure 1 Pulse shape at $z/L_D=3$ of a hyperbolic secant pulse propagating at the zero-dispersion wavelength with a peak power such that $\tilde{N}=2$. Blue curves show for comparison the initial profiles at the fiber input.

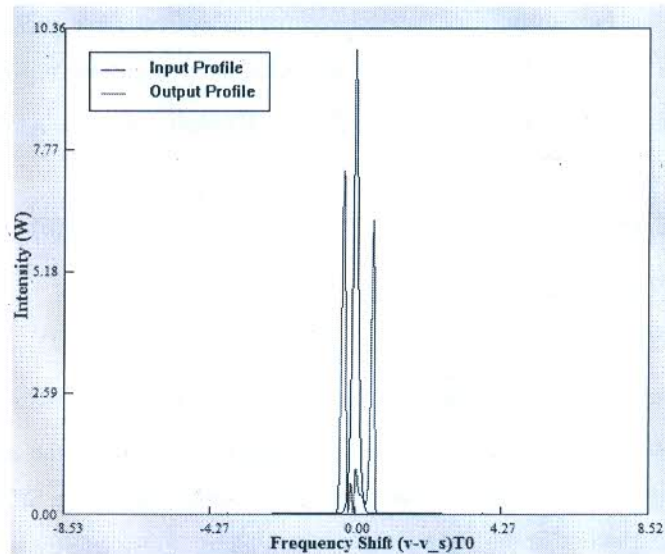


Figure 2 spectrum at $z/L'_D=3$ of a hyperbolic secant pulse propagating at the zero-dispersion wavelength with a peak power such that $\tilde{N}=2$. Blue curves show for comparison the initial profiles at the fiber input.

increasing ξ' . The significant point to note is that, owing to SPM-induced spectral broadening, the input pulse not at all actually propagate at the zero-dispersion wavelength even if $\beta_2=0$ initially. In fact, the pulse creates its own $|\beta_2|$ through SPM. The effectual value of β_2 is larger for pulses with higher peak powers. An attractive problem is whether soliton-like solutions exist at the zero dispersion wavelength of an optical fiber. Equation (6) does not appear to be integrable by the inverse scattering method. Numerical solutions show that for $\tilde{N}>1$, a “sech” pulse evolves over a length $\xi' \sim 10/\tilde{N}^2$ into a soliton that holds about half of the pulse energy. The residual energy is carried by an oscillatory structure near the trailing edge that dissipates away with propagation. This nature of solitons have also been quantified by solving Eq. (6) approximately [4]. Generally, solitons at the zero-dispersion wavelength need less power than those occurring in the anomalous-GVD regime. This can be seen by comparing Equations.

$N^2 = L_D/L_{NL} = \gamma P_0 T_0^2 / |\beta_2|$ and Equation (6). To attain the same values of N and \tilde{N} , the required power is smaller by a factor of $T_0|\beta_2/\beta_3|$ for pulses propagating at the zero-dispersion wavelength.

Conclusions

Higher order dispersion is the main factor limiting transmission length in high-speed optical single-mode fiber systems; it reduces significantly the amplitude and broadens the time width of the pulses for systems operating at high speed. From the in-depth analyses, it has been found obvious that the influence of TOD should not be ignored for ultra-high bit rate systems. The outcome of this research will be useful for designing and implementing ultra-high speed long-haul optical fiber communication system



References

1. Satish Khatak, Mukesh Kumar, Rajeev Sharma, Kamal Sardana "Signal Intensity in Optical Fiber under the Influence of Dispersion and Non-Linearity", in International Journal of Electronics Engineering , Volume 3, No.2, December 2011, pp. 293-297
2. Satish Khatak, G P Singh "Photonic Crystal Fiber-A Novel medium for Light Propagation" in International Journal of Advanced Research in Science & Engineering , Volume 03, Issue No. 08 , August 2014.
3. Satish Khatak, G P Singh "Affects of Varying the Parameters on Supercontinuum in PCF" in International Journal of Advanced Research in Electrical, Electronics and Instrumentation Engineering , Volume 03, Issue 09, September 2014.
4. Satish Khatak, Rajeev Sharma "Governance System for Failure Anticipation in Hybrid/Optical Networks" in International Journal of Advanced Research in Engineering and Technology (IJARET), pp.68-77, Volume 7, Issue 1, Jan-Feb. 2018.
5. Satish Khatak, G P Singh "Solitons in PCF" in International Journal of Latest Trends in Engineering and Technology, PP:167-171, Volume 10, Issue 2, April 2018.
6. Rajeev Sharma and G P Singh, "Numerical Simulations of Collision Behaviors of Optical Soliton in a Kerr Law Media" , International Journal Of Electronics, Communication & Instrumentation Engineering Research and Development Vol.4, Issue IV Aug 2014, pp 51-54
7. Rajeev Sharma and G P Singh, "Optical Soliton & Applications Thereof" International Journal Of Electronics, Communication & Instrumentation Engineering Research and Development Vol.4, Issue IV Aug 2014, pp 71-76
8. Rajeev Sharma and G P Singh "Analysis of Fundamental & Higher Order Solitonic Propagation in Optical Fiber" IMPACT: International Journal of Research in Engineering & Technology, Vol. 2, Issue IV, July 2014, pp. 77-80
9. Rajeev Sharma, Harish Nagar, G.P Singh "Accurate Numerical Simulation Of Higher Order Soliton Decomposition in presence of TOD and Self-Steepening" International Journal of Advanced Research in Engineering and TECHNOLOGY , Vol-7, Issue-1, Jan-Feb 2016, pp. 54-59
10. Rajeev Sharma, Harish Nagar, G.P Singh "Investigation of self frequency variation of higher order soliton in optical fiber" IJSER, Vol-7, Issue-3, March 2016, pp. 997-1000
11. G. P. Agrawal Nonlinear Fiber Optics, Academic Press (2001).

Power Analysis of ECC

Archana Singh Parmar^{#1}, Monika Sharma^{#2}, Ritu Yadav^{#3}

[#]T.I.T&S bhiwani
Haryana

Abstract—In today's world, the most important thing is data, and to keep this data safe from different types of attack we need to encrypt this data. There are various techniques for encryption, so after comparing the available techniques the most secured techniques concluded is elliptical curve. Elliptical curve cryptography is a method of encoding data files so that only specific individuals can decode them. ECC is based on the mathematics of elliptic curves and uses the location of points on an elliptic curve to encrypt and decrypt information. But in this paper we have discussed about the application of ECC with their issues if used without proper implementation.

Keywords— Elliptic curve cryptography, Security, Limitations

INTRODUCTION

With the processing power of computers increasing at such a rapid rate, it makes sense that the security of information systems will begin to falter. In response, new methods will have to be developed to counteract this trend.

Companies like IBM and Hewlett Packard are already at work testing existing methods and developing new ones. But there already exists several methods that do a good job resisting attacks. One such method is elliptic curve cryptography. Elliptic curve cryptosystems represent the state of the art for such systems.

The problem is that with today's computers getting faster and faster, there will come a point where we can't make the pseudo-prime large enough to thwart an attack. That is where elliptic curve cryptography comes in. This extension uses the properties of an elliptical curve, the same pair of keys, and some funky math, to encrypt and decrypt the target information.

The idea of elliptic curve cryptography was introduced by Victor Miller and Neal Koblitz as an alternative to public key systems that already exist such as DSA (Digital Signature Algorithm) and RSA. The advantage of ECC is that this cryptography needs shorter key compared to RSA to achieve the same level of security. The drawback is that it is slow when it is implemented in software. On the other hand, hardware implementation of this algorithm is very fast and efficient. Therefore, ECC is a primary choice of hardware implemented cryptography.

ELLIPTIC CURVE CRYPTOGRAPHY

The main attraction of ECC compared to RSA is that it offers equal security for a far smaller key size, thereby reducing processing overhead. The addition operation in ECC is the equivalent of modular multiplication in RSA, and multiple additions are the equivalent of modular exponentiation. To form a cryptographic system using elliptic curves, we need to find a "hard problem". All systems depend on the difficulty of a mathematical problem for their security. To explain the concept of difficult mathematical problem, the idea of an algorithm is required. To analyze how long an algorithm takes, computer scientists introduced the idea of polynomial time algorithms and exponential time algorithms. An algorithm runs quickly if it is polynomial time algorithm, and slowly if it is exponential time algorithm. Therefore, easy problems correspond with polynomial time algorithms, and difficult problems correspond with exponential time algorithms. When looking for a mathematical problem on which to base a public key cryptographic system, cryptographers search for a problem for which the fastest algorithm takes exponential time. The longer it takes to compute the

best algorithm for a problem, the more secure a public key cryptosystem based on that problem will be.

Three types of systems are considered secure and efficient: the Integer Factorization Systems (RSA), the Discrete Logarithm systems (DSA)[5], and the Elliptic Curve System (Elliptic Curve Discrete Logarithm System)

. In RSA, given an integer n which is the product of two large primes p and q such that, $n = pq$(1) It is easy to calculate n given p and q but it is difficult to determine p and q given n for large values of n . The U.S.

Government's Digital Signature Algorithm (DSA) is based on discrete logarithm problem modulo a prime p . Given an integer g between 0 and $p-1$, and y which is the result of exponentiation of g , we have, $y = g^x \pmod{p}$ for some x(2) The discrete logarithm problem modulo p is to determine the integer x for a given pair g and y .

The Elliptic Curve Cryptosystem (ECC), whose security rests on the discrete logarithm problem over the points on the elliptic curve. The main attraction of ECC over RSA and DSA is that the best known algorithm for solving the underlying hard mathematical problem in ECC (the elliptic curve discrete logarithm problem (ECDLP) takes full exponential time. RSA and DSA take sub-exponential time. This means that significantly smaller parameters can be used in ECC than in other systems such as RSA and DSA, but with equivalent levels of security.

Encryption / decryption using the elliptic curve

Let's look at the simplest approach to encryption / decryption using the elliptic curve. The aim is to encrypt the message M , which may be represented as a point on an elliptic curve $P_m(x, y)$.

In the encryption / decryption elliptic curve system $E_p(a, b)$ and a point G on it are considered as parameters. User B selects the private key nB and calculates the public key $PB = nB \times G$. To encrypt a message P_m the public key of the recipient B PB is used. User A selects a random positive integer k and computes an encrypted message C_m , which is a point on an elliptic curve.

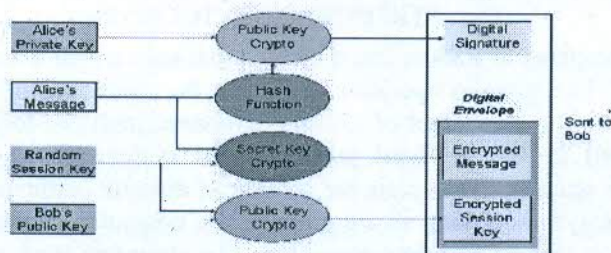
$$C_m = \{k \times G, P_m + k \times PB\}$$

To decrypt a message, a participant B multiplies the first coordinate of a point on his own private key and subtracts the result from the second coordinate:

$$P_m + k \times PB - nB \times (k \times G) = P_m + k \times (nB \times G) - nB \times (k \times G) = P_m$$

A participant encrypted message P_m by adding $k \times PB$ to it. No one knows the value of k , and so, even the PB is a public key, no one knows $k \times PB$. The enemy would have to calculate k to restore the message. It will not be easy.

The recipient also doesn't know the k , but $k \times G$ is sent to him as a hint. Multiplying $k \times G$ to a private key, the recipient receives the value that was added by the sender to the unencrypted message. Thus, the recipient, not knowing the k , but having his private key can recover the unencrypted message.



A) The main advantages:

- Much smaller length of the key that the "classical" asymmetric cryptography has got.
- The speed of the elliptic algorithms is much higher than the classic methods have.

- Due to the small length of a key and of high-speed asymmetric cryptographic algorithms based on elliptic curve can be used in smart cards and other devices with limited computing resources.

B) The main disadvantages of elliptic curve cryptography:

- All advantages of elliptic curve cryptography are derived from one particular fact: there are no subexponential algorithms for solving the discrete logarithm problem based on the elliptic curve. This reduces the length of the key increases productivity. However, if there will be such algorithms, it will mean the collapse of the elliptic curve cryptography.
- Elliptic curve cryptography - is very difficult – it has got a huge number of subtleties that must be taken into account. From the selection of the elliptic curve and ending with key generation. When there will be a mass transition to elliptic curve cryptography there will be a lot of errors and vulnerabilities that have already been coped with in the more conventional methods.

III. In Depth of ECC

here are a significant number of potential vulnerabilities to elliptic curves, such as side-channel attacks and twist-security attacks. These attacks threaten to invalidate the security ECC aims to provide to private keys.

Side-channel attacks generally occur when measurements are made on the physical implementation of a cryptosystem, resulting in leaks of information. Side-channel analysis includes a variety of attacks, such as simple timing attacks, simple power attacks, differential power attacks and fault analysis.⁵ During timing attacks, for instance, the malicious user measures the difference in time between observed peaks in power consumption with an oscilloscope. Relying on the fact that different operations or input values have a significant time variance, the attacker can deduce the secret key. Power attacks, on the other hand, are similar to timing attacks except for the fact that the actual shape and amplitude of voltage peaks is analyzed by the attacker. A variety of power attacks exist, including simple power analysis (SPA) and differential power analysis (DPA).

Simple countermeasures exist for all types of side-channel attacks. Both timing and simple-power attacks can be prevented with the implementation of the Montgomery power ladder (a scalar multiplication technique used to compute) into the ECC instead of using one of the other similar techniques (e.g., double-and-add, sliding window). Not only do Montgomery ladders have the advantage of providing fast scalar multiplication for ECC, but they also tend to behave regularly, masking the computation against timing and simple power-side-channel attacks.⁶ Unfortunately, not all existing ECC curves support the use of ladders. The number of curves that do not support this technique is vast (e.g., Anomalous, NIST P-224, BN [2,254], BrainpoolP256t1, ANSSI FRP256v1), so it is important to check if one's ECC implementation uses a curve that both implements and supports Montgomery ladders.⁷ Furthermore, simple timing attacks can be prevented by inserting dummy adds into the algorithm to act as an ignored variable; this makes the number of process operations to be performed the same regardless of the value of the secret key.⁸ DPA-type side-channel attacks can be prevented in a variety of manners, including adding significant entropy to the secret key, disguising group points and using randomized projective coordinates

IV) Conclusion

Despite the significant debate on whether there is a backdoor into elliptic curve random number generators, the algorithm, as a whole, remains fairly secure. Although there are several popular vulnerabilities in side-channel attacks, they are easily mitigated through several techniques. Quantum attacks loom over ECC, but they are yet to be widely available. Although twist-security attacks can threaten ECC, they can be militated against. Furthermore, although longer ECC keys are broken into publicly every now and then, the same is true for all other popular algorithm types. But no matter how secure ECC is theoretically, it must be properly implemented

REFERENCES

- Al-Somani, Turki F. and amin, Alaaeldin., Hardware Implementation of $GF(2^m)$ Arithmetic Using Normal Basis. Asian Network for Scientific Information, 2006.
- Kumar, Vikram V., Doraiswamy, Satish. and Jainullabudeen, Zabeer., Elliptic Curve Cryptography. Final Report Design and Analysis of Algorithms.
- Itoh, Toshiyama., Tsuji, Shigeo., A Fast Algorithm for Computing Multiplicative Inverses in $GF(2^M)$ using Normal Bases. Information and computation 78, 171-177, 1988.
- Hankerson, Darrel., Menezes, Alfred., Vanstone, Scott. Guide to Elliptic Curve Cryptography. New York: Springer-Verlag, 2004.
- Zulkifli, Muhammad. Aplikasi Timing dan Simple Power Analysis Attack Terhadap Prosesor Kriptografi Kurva Eliptik pada implementasi FPGA. Institut Teknologi Bandung, 2009.
- (2011) Pradeep_uoc on HubPages. [online]. Available: <http://hubpages.com/hub/Intorduction-to-Elliptic-Curve-Cryptography>
- Bernstein, D.; T. Lange; *et al.*; "SafeCurves: Choosing Safe Curves for Elliptic-curve Cryptography," <http://safecurves.cr.yp.to>
- Kadir, S.; A. Sasongko; *et al.*; "Simple Power Analysis Attack Against ECC Processor on FPGA Implementation," 2011,

A Comprehensive Review of Low Noise Amplifier (LNA) Topologies

Rohit Goel¹, Janak Kumar B. Patel²

¹Assistant Professor, ECE Department, TIT&S, Bhiwani, Haryana, India

²Professor, ECE Department, AUH, Gurugram, Haryana, India

¹rohit_160@rediffmail.com, ²jkpatel@ggn.amity.edu

Abstract: Communication systems operating at mm-wave frequencies take advantage of propagation effects. These are privileged frequencies for point-to-point systems and vehicular radar systems. CMOS technology has the potential for realization of RF transceiver in a single chip. In next 5-10 years wireless networks will face heavy congestion. The bridge from 4G to 5G will be having exponential growth in data rates. With this increased data rate, applications like Gbits/s file transfers, near perfect video streaming and real time gaming are feasible. It also enables wideband spread spectrum systems and high immunity to jamming and interference. With these requirements, it is required to exploit the mm-wave spectrum's increased bandwidth to provide increased data rate and better quality of received signal. The negligible absorption at 28 GHz and 38 GHz makes them ideal for 5G cellular systems. A lot of unlicensed spectrum is available at these frequencies.

This paper will investigate the system design parameters and circuit topologies for an LNA. An understanding of the functional requirements is a prerequisite for system design and synthesis. A thorough literature survey of the LNA parameters and its topologies is discussed with their circuit, advantages and disadvantages.

I. INTRODUCTION

In communication world, RF and microwave technology has a great impact. The technology mainly depends on mm wave transmission and is the most prominent research area of the current generation. It is used in satellite communication, military radar systems, and wireless technologies. SiGe and CMOS designs are evolving for designing systems for these applications.

The need for mm wave technology occurs to achieve higher bandwidth based on Shannon's theorem for maximum channel capacity. In the current world of 4G and 5G, data transmission with maximum rate is required. As the frequency increases, more bandwidth is available and hence maximum data rate. Another advantage offered by mm wave technology is higher level of integration. The fully integrated RFIC's include complete receiver, transmitter or transceiver. The blocks included are Low Noise Amplifier (LNA), mixers, Voltage Controlled Oscillators (VCO), phase lock loops (PLL), and power amplifiers. The RF design engineer works to optimize the receiver front end performance with special focus on the first active device i.e. transistor of LNA. At the front end, just after the antenna the first block required is therefore LNA. LNA consists of transistor amplifier (generally MOS), an input and output matching network, an RF

power source, and load. It is mainly used for high gain and low noise figure to minimize the impact on system G/T. It also provides stability from reflected waves which cause self oscillation at some frequencies.

LNA must have sufficient sensitivity to overcome the noise of succeeding stages. The main characteristics which are under designers control and affect the receiver sensitivity are: NF, gain, bandwidth, linearity and dynamic range. For controlling these parameters, designer must have clear understanding of the MOS device used, impedance matching, fabrication details and assembly for achieving optimal performance with fewer trade-offs.

In this paper, a detailed review of LNA is done considering its parameters of importance, topologies used with their advantages and disadvantages, design procedure. Based on this, Section II explains the important parameters; Section III gives a detail description of various LNA topologies with a specific attention on the variations done by researchers. Section IV discusses the design procedure.

II. LNA PARAMETERS

As discussed above, LNA is used to obtain low noise figure (NF) and high gain. So, here the parameters considered are NF, gain, input and output matching, linearity, 1-dB compression, third order intercept point and stability. The input and output impedances determine how the LNA interacts with the previous and next stages. These parameters trade with each other in one way or the other and are the challenges in the design of high performance LNA's. These parameters are taken one by one.

1. Noise Figure:

Noise figure affects the detection accuracy of the receiver. There are two sources of noise one is thermal noise and the other is shot noise or flicker noise [1]. Thermal noise is due to the random motion of electrons. The sources of this noise are channel and gate contacts of a MOS device, resistors, antenna radiation resistance and conducting metal contacts. The power spectral density (PSD) of thermal noise is flat and the total available power is given as:

$$P = 4KTB$$

Where K = Boltzmann's constant, T = absolute temperature and B is bandwidth.

Another component of noise is shot noise or flicker noise, where electrons flow is disturbed by trapping and release of charge carriers. In MOS device, any defects in oxide layer can be a potential candidate for trapping. The PSD of flicker noise is given by:

$$PSD = \frac{K_f}{A \times f} = \frac{K_f}{W \times L \times C_{ox} \times f}$$

Where K_f , A , f , W , L , C_{ox} represents device specific flicker noise coefficient, area of channel, frequency of operation, width of channel, length of channel and oxide capacitance respectively. It is also called $1/f$ noise.

In a receiver each block contributes noise and if an equivalent noise source is assumed at the input of the gate terminal to be added, then the receiver can be assumed as noiseless. In a MOS device, if a resistor is connected at the input, it is assumed as thermal noise in series or flicker noise in parallel. The mean square power of the noises is:

$$V_{in,R}^2 = 4KT\gamma g_{d0}f$$

$$I_{in,R}^2 = \frac{K}{WLC_{ox}f}$$

γ , g_{d0} represents the thermal noise coefficient and transconductance respectively.

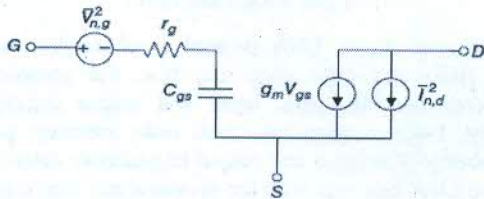


Fig. 1. Small Signal Noise Model

The noise factor (F) which is the ratio of SNR_i to SNR_o depends on the above noise power and noise figure (NF) is given by:

$$NF = 10 \log_{10} F$$

For a given power dissipation, minimum NF is obtained when the device is connected to input matching network that transforms the source impedance to optimum source impedance. So, LNA topology should be taken which has input matching network to obtain low NF.

2. Gain:

LNA is used to accept the weak signal from the small antenna and amplify it without adding noise or reducing it as much as possible. A single stage must be able to

provide sufficient gain. A conjugate match of input and output impedance can provide too much gain but it may vary and hamper both NF and bandwidth [2]. A better way is to use selective mismatching which helps in controlling gain depending on need. Typical gain lies between 10 – 20 dB and varies with frequency.

3. Input Matching:

A MOS device acting as an amplifier has ideally infinite input resistance and has C_{ox} (oxide capacitance) as input impedance. Now this capacitance should be converted to some sort of resistance to match with the optimum value $Z_{S,opt} = R_S = 50\Omega$. This input matching is discussed in detail while discussing LNA topologies as it is required to match the input impedance with optimum impedance to get high gain and low NF [3].

4. Stability:

Stability of a receiver is of prime importance. It measures the tendency of an LNA to oscillate. A lot of factors lead to LNA instability. These are: excessive parasitic inductance or ground connections, excessive in-band and out-of-band gain, insufficient isolation of RF from next stages which may provide positive feedback and make transistor oscillate instead of amplification [4] [5]. Stability compensation is implemented with RF negative feedback to filter excessive out of band gain. This can be done by using resistive feedback or using source degeneration inductive feedback. These two cases are discussed in LNA topologies.

Two port networks are characterized by their scattering (S) parameters. It allows for the calculation of potential instabilities in the LNA. A 2-port network is unconditionally stable if the reflection coefficients Γ_{in} and Γ_{out} have magnitude < 1 . Also, the impedances seen from input and output have positive real parts and are independent of load impedances at the input and output.

$$\Gamma_{in} = S_{11} + \left(\frac{S_{21}\Gamma_L S_{12}}{1 - S_{22}\Gamma_L} \right) = \frac{S_{11} - \Delta S \Gamma_L}{1 - S_{22}\Gamma_L}$$

Where $\Delta S = S_{11}S_{22} - S_{21}S_{12}$.

$$\Gamma_{in} < 1 \text{ if } \frac{|S_{21}S_{12}|}{|1 - |S_{22}|^2|} \leq 1 \text{ for } \Gamma_L < 1$$

The stability factor K , often called Linvill stability factor is given as:

$$K = \frac{1 - |S_{11}|^2 - |S_{22}|^2 + |\Delta S|^2}{2|S_{21}S_{12}|} \geq 1$$

If $K > 1$ or $\Delta S > 1$, then the device is unconditionally stable. If $K < 1$ or $\Delta S > 1$, source and load impedance must be carefully chosen to make the device stable. When

$|S_{11}| < 1$ and $|S_{22}| < 1$, then the LNA is unconditionally stable for any combination of source and load impedance.

To determine the source and load impedance that causes the device to be unstable can be determined by using stability circles on Smith chart. It represents the boundary between values of source and load impedance that cause instability or not. The circle has locus $K=1$.

5. Linearity, IIM3, IP3, 1-Db Compression Point:

Third order intercept point (IP3) is a measure of linearity of LNA. The integrated functions of LNA, mixer, and VCO should provide high amount of linearity throughout. When the input signal is large and the device saturates then instead of getting linear output, non-linearity occurs [6] [7]. The output does not respond correctly to any further increase in input. This phenomenon leads to 1-dB compression point [8]. When an input signal with multiple frequencies is fed to such a non-linear device multiple frequencies are obtained which may lie in the same band as the frequency of interest. The frequencies between original frequencies and mixing products leads to third order inter modulation products (IM3).

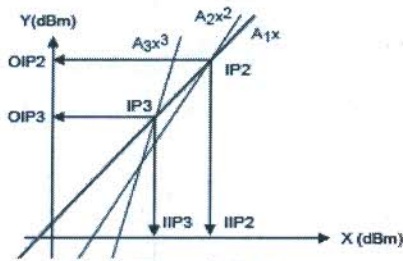


Fig. 2 IIP and OIP Curves

Once IM3 products are obtained, its value is determined using IP3. If the device is linear, a high value of IP3 is obtained and n^{th} order terms will be small. IP3 is the point where first and third order lines intercept with each other. Before saturation:

$$OIP_{dBm} = G_{dBm} + IIP_{dBm}$$

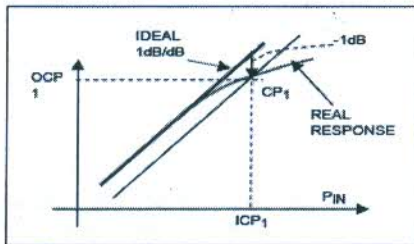


Fig. 3. 1-dB Compression Point

1-dB compression point- when after a certain level linear output is not obtained and input signal is amplified by an

amount 1-dB less than the small signal gain, it is called 1-dB compression point.

III. LNA TOPOLOGIES

Various topologies for LNA were suggested from time to time. The basic element for amplification is either BJT or MOS device. Now-a-days, MOS devices are mainly used due to lesser power dissipation. The topologies started from LNA with resistive termination to common gate LNA and finally to source degeneration LNA and its variations. These are discussed in this section one by one with their advantages and disadvantages. The general model of LNA is as shown [9]:

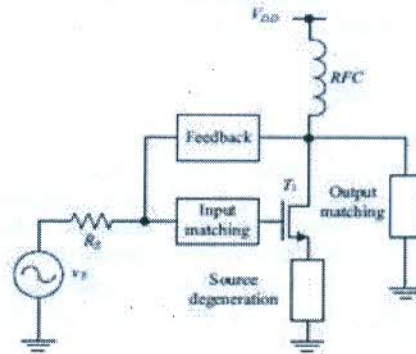


Fig. 4. General LNA Model

LNA with Shunt Resistive Termination:

This is the simplest of LNA topologies and consists of a LNA Common Source (CS) amplifier with a resistance R connected to the gate of the MOS device. Here, a broadband match is obtained, but due to the use of resistor, thermal noise is very high. It increases the noise figure from F_{min} to a larger value as R is not equal to $Z_{S, opt}$. The noise factor is given by:

$$F = 2 + \frac{4\gamma}{\alpha g_m R_S}$$

Assuming α , and $\gamma=1$, the noise factor is of the order of 8-10 and NF as 8dB which is very high.

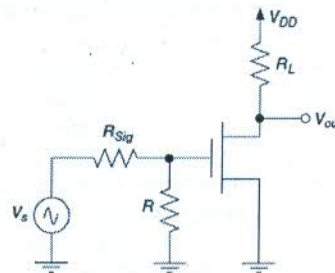


Fig. 5. LNA with Shunt Resistive Termination

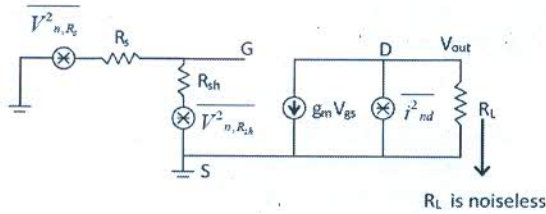


Fig. 6. Small Signal Model

As said earlier, in case of impedance match $R_s = R_{sh}$. This leads to poor NF as extra noise is added by shunt resistance. Moreover, input signal is attenuated by voltage divider resistances, so the overall gain is reduced. At high frequencies shunt L is required to tune out C_{gs} . So this topology is not used.

Shunt Series Feedback LNA:

This topology uses a feedback resistor of large value to reduce the value of input resistance to 50Ω by using Miller effect. This provides a wideband conjugate match [9]. This higher value of feedback resistance reduces the noise current at the output reducing the noise figure. But as stated earlier, any resistance added to the LNA causes thermal noise which is the main source of noise and reducing gain.

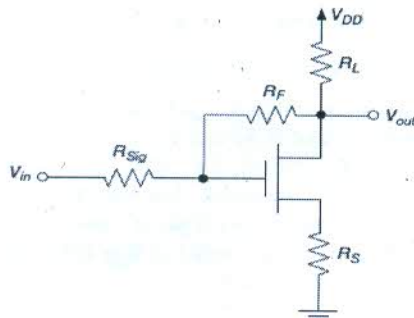


Fig. 7. LNA with Shunt Series Feedback

Common Gate LNA:

In common source amplifiers, input signal is applied to the gate of MOS. In this topology input signal from the antenna is applied to the source terminal and the gate is connected to a DC voltage for proper operating conditions. A common gate LNA provides low resistive impedance with simple input matching. The input resistance is inversely proportional to g_m which results into wideband matching of the system [10]. This impedance can be achieved by proper choice of bias current, overdrive voltage ($V_{GS} - V_{th}$) and aspect ratio (W/L). In the wideband match, performance of the LNA is analyzed at the centre frequency and 3-dB frequency is then

considered for bandwidth. The circuit does not suffer from Miller effect and provides good reverse isolation.

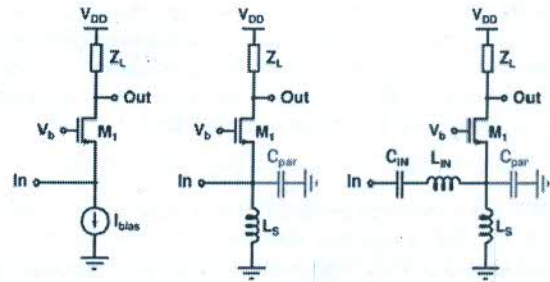


Fig. 8. Common Gate Topologies

Above figure shows various configurations of common gate LNA [11-16]. Initially a bias current is included in the signal ground to increase the impedance but it leads to more noise. To achieve better noise performance a parallel L-C resonator is used. The small signal model of the circuit is as shown:

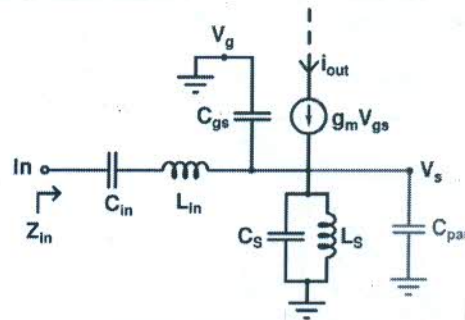


Fig. 9. Small Signal Equivalent of Common Gate Topology

Here the MOS is replaced by a gate source capacitor C_{gs} and transconductance g_m . g_m also includes the substrate transconductance. The parasitic capacitance C_{par} consists of substrate capacitance of L_s , source-body junction capacitance. The total capacitance is given by

$$C_T = C_{gs} + C_{par} + C_S$$

The center frequency is given by

$$\omega_0 = \frac{1}{\sqrt{L_S C_T}}$$

The figure of merit for wideband LNA is insertion gain which is defined as the ratio of output signal voltage to half of voltage of source driving the LNA input. Common Gate LNA uses shunt peak load for extending the bandwidth. Both input and source resonators affect I_{out} as a function of frequency. The highest operational

frequency is limited by shunt peak load and parasitic capacitance at the output node.

The noise figure of a common gate LNA is given as

$$NF = 1 + \frac{\gamma g_{d0}}{g_m} + \frac{1 + g_m R_S}{g_m R_L}$$

As g_m increases NF decreases, but g_m cannot be increased above a certain limit because it determines input matching. The main drawbacks of this topology are less gain, high NF. But it provides a low power stable circuit and is robust against parasitic capacitances. Even though it does not use any resistor at the input still its NF is very high. This is due to the noisy resistance of the channel. It is also independent of power consumption.

Common Source with Inductive Degeneration Topology:

This topology consists of an inductor at the source terminal. MOS is used in Common source configuration and provides good input matching [11]. The circuit with small signal equivalent model is as shown:

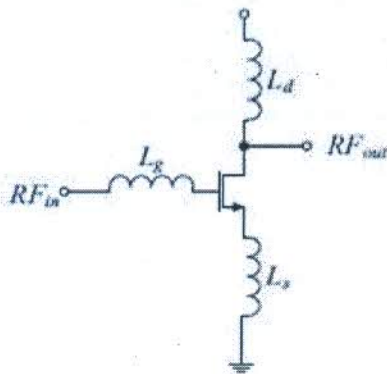


Fig. 10. Inductive Source Degeneration LNA

$$V_{in} = I_{in} S L_g + I_{in} \frac{1}{S C_{gs}} + (I_{in} + g_m V_{gs}) S L_s$$

$$= I_{in} S L_g + I_{in} \frac{1}{S C_{gs}} + \left(I_{in} + g_m \frac{I_{in}}{S C_{gs}} \right) S L_s = I_{in} Z_{in}$$

$$Z_{in} = S(L_g + L_s) + \frac{1}{S C_{gs}} + \frac{g_m L_s}{C_{gs}}$$

For $Z_{in} = R_s$, $Img(Z_{in}) = 0$ and $Re(Z_{in}) = R_s$

$$\omega_0^2 = \frac{1}{(L_g + L_s) C_{gs}} \text{ and } R_s = \frac{g_m L_s}{C_{gs}}$$

The inductor adds a resistive component to the input impedance. At resonance, reactive terms cancel out each other and Z_{in} is purely resistive. To obtain the desired resonant frequency, input inductance L_g was added. This

series resonant circuit provides higher effective transconductance and matched at center frequency [16]. The system has narrow bandwidth and only reactive components are added. Noise Figure is minimum if inductance and capacitance are lossless. Use of degenerated inductance takes Z_{in} closer to Z_{opt} and return loss is minimized. The topology provides amplifier stability and linearity.

Inductive Source Degeneration Cascode LNA Topology:

This topology is achieved by adding a common gate stage to common source inductive degeneration topology. Cascode is mainly used to provide isolation between input and output. Phase of the output signal may change which may turn negative feedback into positive feedback and hence stability of the circuit decreases. The MOS M1 of first stage sees the low input impedance from common gate stage [17-18]. At low GHz frequencies, noise from upper transistor of cascode stage is degenerated to lower transistor input impedance which causes enhanced noise performance. It replaces r_{o1} (output resistance of first stage) which is much larger. This result in a low voltage gain of M1 and Miller effect is low. In this topology, input impedance can be matched to 50Ω over a small frequency of interest. For correct frequency operation drain inductor L_d can be replaced by resonant tank circuit. For better tuning, capacitance of tank circuit can be replaced by MOS varactor. Gain, input matching and input impedance are determined by the first MOS stage. The effect of C_{gd} is less due to Miller multiplication effect, but increases with the increase in frequency. At Ka-band and millimeter waves these effects are very large.

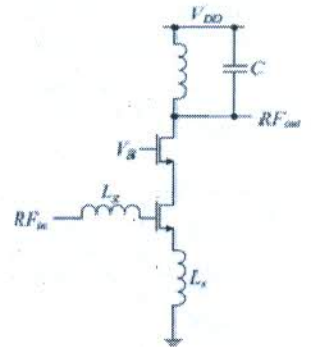


Fig. 11. Inductive Source Degeneration Cascode LNA

The advantages of this topology are low NF, high gain, good stability, low power dissipation, improved reverse isolation and decreased miller capacitance.

Differential Cascode LNA:

In a differential cascode LNA, two MOS are connected in differential mode. Due to the formation of virtual ground,

parasitic capacitances on the gate side of input MOS are removed. 2nd order terms also get cancelled due to CMRR [18-22]. Differential configuration acts as a f_T doubler, which allows wider frequency operation. This configuration suits best for wideband amplifiers. This topology works well for inductorless LNA's having feedback which allows high linearity.

The main drawbacks are that it occupy large space and requires baluns to connect to the antenna. It has 3rd and higher order intermodulation distortion. No off-chips can be used in this design. Also it has decreased noise performance but at the expense of increased power consumption.

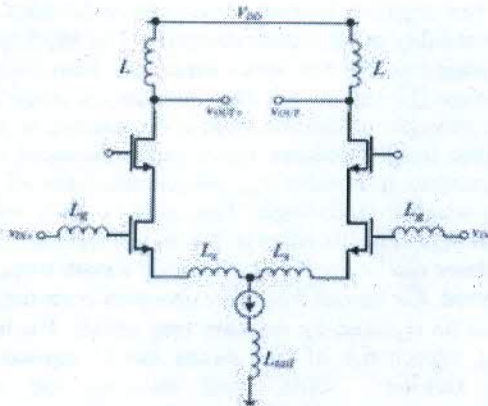


Fig. 12. Differential LNA

Table 1. Comparison of Topologies

Characteristics	Common Gate (CG)	Common Source (CS)	Cascode
Gain	Lowest	Moderate	Highest
Noise Figure	Increases with frequency	Lowest	Higher than CS
Stability	High	Low	High
Linearity	High	Moderate	Highest
Reverse Isolation	High	Low	High
Supply Voltage	Low	Low	Higher
Input Matching	Very easy	Easy	Easy

IV. DESIGN PROCEDURE

The design procedure consists of following steps:

1. Decide the LNA topology for wideband or narrowband operation. Determine the frequency of operation.

2. Determine optimum width.
3. Choose bias current I_{bias} based on power constraint.
4. Determine L_s for input matching as $w_T L_s = 50 \Omega$.
5. Calculate minimum NF.
6. Calculate L_g based on resonant frequency f_0 .
7. Add cascode MOS of same size as common source stage.
8. Choose L_d and C_d for maximum gain.

V. CONCLUSION

Low Noise Amplifier (LNA) is the most critical part of a receiver as it has to provide the overall system gain and minimize the Noise Figure (NF) as much as possible. This paper discusses the various important parameters required while designing a LNA. The importance of these parameters with their effect on each other is discussed. Different topologies with their design, advantages, disadvantages and applications are discussed in detail. Main focus is on CS, CG and cascode topologies which are used in narrowband and wideband LNA design respectively. Their mathematical derivations are also considered. A comparison of widely used LNA topologies depending on parameters is given. Depending on the best characteristics of each topology, a circuit can be picked and used for an application. Finally design procedure required for LNA is given. This paper can be considered as a starting point for new researchers working on RF front end and receiver systems.

VI. REFERENCES

- [1] P. R. Gray, P. J. Hurst, R. G. Meyer, S. H. Lewis, Analysis and design of analog integrated circuits, 5th ed., Wiley, Hoboken, 2009.
- [2] R. R. Tummala, M. Swaminathan, System-on-package: miniaturization of the entire system, 1st ed., McGraw-Hill Professional, New York, 2008.
- [3] D. Fritsche, G. Tretter, C. Carta, F. Ellinger, "Millimeter-wave low-noise amplifier design in 28-nm low-power digital CMOS," IEEE Transactions Microwave Theory Technology, Vol. 63, no. 6, pp. 1910-1922, 2015.
- [4] A. Y. K. Chen, Y. Baeyens, Y. K. Chen, J. Lin, "A low-power linear SiGe BiCMOS low-noise amplifier for millimeter-wave active imaging," Microwave Wireless Component Letters, Vol. 20, no. 2, pp. 103-105, 2010.
- [5] G. Szczepkowski, R. Farrell, "Study of linearity and power consumption requirements of CMOS low noise amplifiers in context of LTE systems and beyond," ISRN Electronics, pp. 1-11, 2014.

- [6] R. Kumar, A. Devi, A. Sarkar, F. A. Talukdar, "Design of 5.5 GHz linear low noise amplifier using post distortion technique with body biasing," *Microsystems Technology*, Vol. 22, no. 11, pp. 2681–2690, 2016.
- [7] Ludwig Bretchko, *RF circuit design: theory and applications*, 1st ed. Prentice Hall, Upper Saddle River, 2000.
- [8] G. Gonzalez, *Microwave transistor amplifiers: analysis and design*, 2nd ed., Prentice Hall, New Jersey, 1997.
- [9] Y. Soliman, L. MacEachern, L. Roy, "A CMOS ultra-wideband LNA utilizing a frequency-controlled feedback technique," 2005 IEEE international conference on ultra-wideband, pp. 530–535, Zurich, January 2005.
- [10] A. Grebennikov, N. Kumar, B. S. Yarman, *Broadband RF and microwave amplifiers*, CRC Press, Boca Raton, 2015.
- [11] Sudip Shekhar, Jeffery S. Walling, Sankaran Aniruddhan and David J. Allstot, "CMOS VCO and LNA using tuned-input tuned-output circuits," *IEEE Journal of Solid-State Circuits*, Vol. 43, no. 5, pp.1177- 1186, May 2008.
- [12] Asad A. Abidi, "RF CMOS comes of age," *IEEE Journal of Solid-State Circuits*, Vol. 39, no. 4, pp. 549- 561, April 2004.
- [13] Xiaohua Fan, Heng Zhang, and Edgar Sánchez-Sinencio, "A noise reduction and linearity improvement technique for a differential cascode LNA", *IEEE Journal of Solid-State Circuits*, Vol. 43, no. 3, pp. 588-599, March 2008.
- [14] W. Zhuo, S. H. K. Embabi, J. Pineda de Gyvez, and E. Sánchez-Sinencio, "Using capacitive crosscoupling technique in RF low-noise amplifiers and down-conversion mixer design," In *Proceedings of the European Solid-State Circuits Conference (ESSCIRC)*, pp. 116–119, Sept. 2000.
- [15] X. Li, S. Shekhar, and D. J. Allstot, "Gm-boosted common-gate LNA and differential Colpitts VCO/QVCO in 0.18- μ m CMOS," *IEEE Journal of Solid-State Circuits*, Vol. 40, no. 12, pp. 2609–2619, Dec. 2005.
- [16] W. Zhuo, X. Li, S. Shekhar, S. H. K. Embabi, J. Pineda de Gyvez, D. J. Allstot, and E. Sánchez-Sinencio, "A capacitor cross-coupled common-gate low noise amplifier," *IEEE Transaction on Circuits and Systems II: Express Briefs*, Vol. 52, no. 12, pp. 875–879, Dec. 2005.
- [17] R. D. Ortega, S. L. Khemchandani, H. G. Viquez, F. J. Del Pino Surez, *Design of low-noise amplifiers for ultra-wideband communications*, 1st ed., McGraw-Hill Professional, New-York, 2014.
- [18] T. S. Rappaport, J. N. Murdock, F. Gutierrez, "State of the art in 60 GHz integrated circuits and systems for wireless communications," *Proceedings of IEEE*, Vol. 99, no. 8, pp. 1390–1436, August 2011.
- [19] Andrea Bevilacqua, Christoph Sandner, Andrea Gerosa, and Andrea Neviani, "A fully integrated differential CMOS LNA for 3–5-GHz ultra-wideband wireless receivers," *IEEE Microwave and Wireless Components Letters*, Vol. 16, no. 3, pp. 134-136, March 2006.
- [20] Christopher Weyers, Pierre Mayr, Johannes W. Kunze, "A 22.3dB voltage gain 6.1dB NF 60GHz LNA in 65nm CMOS with differential output," *IEEE International Solid-State Circuits Conference (ISSCC 2008)*, Digest of Technical Papers, pp. 192-606, Feb. 2008.
- [21] Hong Zhang, Guican Chen, Xiao Yang, "Fully differential CMOS LNA and down-conversion mixer for 3-5 GHz MB/OFDM UWB receivers," In *Proceedings of the IEEE International Workshop on Radio- Frequency Integration Technology*, pp. 54-57, Dec. 2007.
- [22] M. H. Tsai, S. S. Hsu, F. L. Hsueh, C. P. Jou, T. J. Yeh, "Design of 60-GHz low-noise amplifiers with low NF and robust ESD protection in 65-nm CMOS," *IEEE Transactions Microwave Theory Technology*, Vol. 61, no. 1, pp. 553–561, 2013.

said that DNA computation offers copious advantages and is here to stay.

VII. REFERENCES

- [1] L.M. Adleman, Molecular computation of solutions to combinatorial problems. *Science* 266, pp. 1021–1024, 1994.
- [2] R. J. Lipton, Using DNA to solve NP-complete problems. *Science*, 268: pp. 542 – 545, 1995.
- [3] D. Boneh, C. Dunworth & R. Lipton, Breaking DES Using a Molecular Computer, Princeton, CS Tech-Report CS-TR, pp. 489-95, 1996.
- [4] M. Amos, S. Wilson, D.A. Hodgson, G. Owenson & A. Gibbons, "Practical implementation of DNA computations", *Unconventional Models of Computation*, Springer, Singapore, pp. 1–18, 1998.
- [5] C.T. Clelland, V. Risca & C. Bancroft, Hiding messages in DNA microdots. *Nature* 399, pp. 533–534, 1999.
- [6] A. Leier, C. Richter, W. Banzhaf & H. Rauhe, "Cryptography with DNA Binary Strands", *Elsevier Biosystems*, Vol. 57, Iss. 1, pp. 13-22, 2000.
- [7] G. Condon, & E. Rozenberg, "DNA Computing", *Proceedings of 6th International Workshop on DNA-Based Computers*, Leiden, The Netherlands, 2000.
- [8] T. Bajenescu & M. Borda, "Securitatea in informatica si telecomunicatii", *Editura Dacia*, 2001.
- [9] A. Gehani, T. LaBean, and J. Reif, "DNA-Based Cryptography", *Lecture Notes in Computer Science* 2950, Springer, pp. 167-188, 2004.
- [10] N.N. Rao, "A Cryptosystem Based on Recombinant DNA Technique", *Acta Electronica Sinica*, Vol. 32, Iss. 7, pp. 1216-1218, 2004.
- [11] P. Isasi, J.A. Hern, "Introduction to the applications of evolutionary computation in computer security and cryptography", *Computational Intelligence*, Vol. 20, Iss. 3, pp. 445–449, 2004.
- [12] K. Tanaka, A. Okamoto & I. Saito, "Public-Key System Using DNA as a One-Way Function for Public Key Distribution", *Elsevier Biosystems*, Vol. 81, Iss. 1, pp. 25-29, 2005.
- [13] G. Z. Xiao, "New field of cryptography: DNA cryptography," *Chinese Science Bulletin*, Vol. 51, Iss. 1, pp. 1139-1144, 2006.
- [14] S.T. Amin, M. Saeb, S. El-Gindi, "A DNA-Based Implementation of YAEA Encryption Algorithm", *Computational Intelligence*, pp. 120-125, 2006.
- [15] M. Kantarcioglu, W. Jiang, Y. Liu and B. Malin, A Cryptographic Approach to Securely Share and Query Genomic Sequences, *IEEE Transactions on Information Technology In Biomedicine*, Vol. 12, No. 5, pp.606-617, 2008.
- [16] M. Borda, O. Tornea and T. Hodoroaga, "Secret Writing by DNA Hybridization", *Acta Technica Napocensis Electronics and Telecommunications*, Vol. 50, Iss. 2, pp. 21-24, 2009.
- [17] S. Jeevidha, M.S.S. Basha & P. Dhavachelvan, "Analysis on DNA based Cryptography to Secure Data Transmission", *International Journal of Computer Applications*, Vol. 29, Iss. 8, 2011.
- [18] Q. Gao, "A Few DNA Based Security Techniques", *IEEE Long Island Systems Applications and Technology Conference (LiSAT)*, Farmingdale, NY, pp. 1-5, 2011.
- [19] R. Terec, M.F. Vaida, L. Alboaie & L. Chiorean, "DNA Security using Symmetric and Asymmetric Cryptography", *International Journal of New Computer Architecture and their Applications*, Vol. 1, Iss. 1, pp. 34-51, 2011.
- [20] A. Kahate, "Cryptography and Network Security", *Tata McGraw Hill*, New Delhi, India, 2012.
- [21] "DNA Structure" - An online article available at <http://ijarovic.wordpress.com>, 2012.
- [22] "Genetic Home Reference", A Service of the U.S. National Library of Medicine, available online at <http://ghr.nlm.nih.gov/handbook/basics/dna>, 2012.
- [23] M.I. Youssef, A.E. Emam and M. A. Elghany, "Multi-Layer Data Encryption using Residue Number System in DNA Sequences", *International Journal of Computer Applications*, Vol. 45, Iss. 10, 2012.
- [24] R. Soni, V. Soni & S.K. Mathariya, "Innovative Field of Cryptography", *Computer Science Conference Proceeding, CSIT2115*, pp. 161-179, 2012.
- [25] Y. Zhang, B. Fu & X. Zhang, "DNA Cryptography Based on DNA Fragment Assembly", *8th International Conference on Information Science and Digital Content Technology, Jeju*, Vol. 1, pp. 179-182, 2012.
- [26] H. Liu, D. Lin & A. Kadir, "A Novel Data Hiding Method Based on Deoxyribonucleic Acid Coding", *Computers and Electrical Engineering*, Vol. 39, Iss. 4, 2013.
- [27] O. Tornea & M.E. Borda, "Security and Complexity of DNA-based Cipher", *IEEE International Conference ReEduNet, Romania*, 2013.

- [28] T. Mandage, "A DNA Encryption Technique Based on Matrix Manipulation and Secure Key Generation Scheme", International Conference on Information Communication and Embedded Systems, Chennai, pp. 47-52, 2013.
- [29] A.U. Rehman, X. Liao, A. Kulsoom & S.A. Abbas, "Selective Encryption for Gray Images based on Chaos and DNA Complementary Rules", Multimedia Tools and Applications, 2014.
- [30] D.S. Chouhan & R.P. Mahajan, "An Architectural Framework for Encryption and Generation of Digital Signature Using DNA Cryptography", IEEE International Conference on Computing for Sustainable Global Development, pp. 743-748, 2014.
- [31] J. Yang, J. Ma, S. Liu & C. Zhang, "A Molecular Cryptography Model based on structures of DNA self-assembly", Chinese Science Bulletin, Vol. 59, Iss. II, pp. 1192-1198, 2014.
- [32] R.K. Jangid, N. Mohmmad, A. Didel & S. Taterh, "Hybrid Approach of Image Encryption using DNA Cryptography and TF Hill Cipher Algorithm", IEEE International Conference on Communication and Signal Processing, pp. 934-938, 2014.
- [33] S. Jain & V. Bhatnagar, "A Novel DNA Sequence Dictionary Method for Securing Data using Spiral Approach and Framework for DNA Cryptography", IEEE International Conference on Advances in Engineering and Technology Research, 2014.
- [34] G. Cui, Y. Wang, D. Han. Y. Wang, Z. Wang & Y. Yu, "An Encryption Scheme Based on DNA Microdots Technology", Journal of Computational and Theoretical Nanoscience, Vol. 12, Iss. 7, pp. 1434-1439, 2015.
- [35] Shweta & S. Indora, "Cascaded DNA cryptography and steganography", IEEE International Conference on Green Computing and Internet of Things, pp. 104-107, 2015.
- [36] A. F. Khadim, G.H.A. Majeed & R. S. Ali, "Proposal New S-Box Depending on DNA computing and Mathematical Operations", IEEE Al-Sadeq International Conference on Multidisciplinary in IT and Communication Science and Applications (AIC-MITCSA), Iraq, May 2016.
- [37] "Scytale" – An online article available on Wikipedia
<https://en.m.wikipedia.org/wiki/Scytale>.
- [38] "Bombe" – An online article available on Wikipedia
<https://en.m.wikipedia.org/wiki/Bombe>.
- [39] "DNA structure" – An Image available online on <https://media1.britannica.com/eb-media/64/47664-004-7088EE3D.jpg>
- [40] "PCR Process" – An Image available online on <http://cdn.thinglink.me/api/image/601788287824166912/1240/10/scaletowidth.jpg>.

asymmetric). The key point of consideration is that DNA ciphers work on strings, while the conventional approaches work on binary data[24].

The combination of DNA cryptography with Residue number system is proposed as the novel encryption algorithm in this 2012 paper by M. I. Youssef. It is a multi-layer encoding scheme which offers more flexibility, reliability and security with lesser intricacy. The experimental results shows its efficacy with digital image encryption as the suggested cryptosystem is tested on several parameters and proved prolific[23].

This scholarly article by Y. Zhang (2012) addresses the most important aspect of DNA cryptography design that is identifying the key to be used in the symmetric encryption. The paper also states the related softwares to be used with this new approach. Finally, taking idea from the DNA fragment assembly and digital coding, the author proposes a new symmetric encryption technique that will provide higher robustness[25].

H. Liu did an exclusive DNA-based steganographic research in 2013 which offers great strength. The authors recommend that prior to steganography, DNA encoding is applied to the plaintext, which converts it into a cipher sequence. Then, simple binary operations are performed on it like adding a random sequence and circular shifting. At last, each character of the plaintext is converted to a corresponding color and saved finally on a MS-Word document, which act as a carrier. The experimental results prove the system's strength against the brute-force attacks[26].

In 2013, O. Tornea & M. E. Borda did some comparison between the widely available cryptosystems and novel DNA-based cryptosystems. They also cartel the traditional cryptography with the BMC ideas to replace the good old classic One-Time Pads symmetric cryptograms. This research work also evaluates a cryptographic cipher based on genome databases, which provides an alternate to OTPs. The strength of the new-driven algorithm is also tested theoretically and practically according to various parameters[27].

T. Mandage published a research article in 2013 which addresses the vital question of data security from the attackers and proposes a contemporary encryption DNA scheme. This particular cipher mixes the matrix manipulation and secure key-generation to generate a vigorous encoding algorithm that exploits the immense parallelism, extraordinary storing capability and energy proficiency of DNA[28].

This exceptional research done by A. U. Rehman et. al. (2014) suggests how the DNA can be made to work for encryption of grey images. Here, the encoding is done pixel by pixel using different DNA computations. The 128-bit key is modified each time to encode the next block of the image, hence strengthening the algorithm, Prior to encryption, permutation is applied to the image

and varied ways of encryption are employed for each block coding. The investigational results prove that the proposed work offers great advantage for encryption of grey images of even larger size[29].

The brainy authors J. Yang et. al. present a contemporary concept that makes use of self-assembled arrangement of the DNA molecules in 2014. Afterwards, binary XOR operation is done in parallel at each byte for encoding and decoding it; this special feature makes this cipher work as a one-time pad. As each DNA molecule is unique, the power of the cipher is its security against the cyber-attacks. The experimental results show that DNA cryptography offers more advantages than traditional encryption methods[31].

In 2014, D. S Chouhan & R. P. Mahajan did some exhaustive research to discover that most of the ciphers available in the modern world are partially or fully broke, which puts the adversaries in charge and calls for a new unbreakable cipher. Authors suggest that the DNA computation is the answer to all the stalling security questions. They provide an architectural framework for encoding of data and also for the Digital Signatures generation using DNA technology. Through experiments, it is also observed that not only these DNA-based encoders are more secure, but also their execution time is quite low even for longer plaintexts[30].

In 2014, R. K. Jangid et.al. laid emphasis on Hill Cipher cryptanalysis and discuss how the legendary Hill Cipher and all its variants has a pitfall; nevertheless, it maybe fixed by the upcoming DNA technology. The authors propose a hybrid hill cipher- RDHill for digital images where image is first changed into binary, then into DNA and finally into amino acid on which the proposed algorithm is applied. The scrutiny of its robustness is done mainly using entropy and correlation between neighboring pixels. The outcomes of experiments demonstrated better quality and security than all variations of the Hill cipher[32].

DNA computing went to the next level when Shweta & S. Indora determined the effectiveness of DNA cryptography in case of multimedia especially videos in 2015. The authors explain a major shortcoming of English language based cryptosystems i.e. the character redundancy, which may be eliminated by use of the DNA cryptography. The paper reveals how DNA can be used for encryption of plaintexts and how it can be embedded undetectably inside a video frame[35].

The research article by G. Cui et. al. (2015) rotates around the idea of implementing microdots technology and DNA computation together. The simulation domino effect show enhanced robustness when compared to the conventional cryptosystems, as the new encryption scheme has twofold hiding of data, thus making the new DNA-based steganography system the best option for encryption[34].

A. F. Khadim et. al. focused his research on the usage of Substitution Boxes in DNA Computation and published an article regarding the same in 2016. As S-boxes are vital in the implementation of traditional ciphers, DNA cryptology can also benefit from them, hence an innovative method is proposed by authors using basic mathematical operations, XOR operations and encrypting plaintext into DNA codons. The experimental results demonstrate that the new method is not only secure but also faster than their genetic counterparts[36].

V. RESULTS AND DISCUSSION

DNA computation has brought a fresh air in the arena of encryption and it is gaining new heights with every experiment conducted and with every research paper written on the topic. The applications of DNA in cryptology are many and varied with huge benefits; moreover it has made the encryption more efficient, reliable, secure and faster than before[28]. The following table summarizes some of the exceptional research work carried out by the elite academicians (listed in the chronological order):

Table 4.1: Summary of Research work

Authors	Year	Major Contributions
A. Leier et. al	2001	DNA strands for steganography
A. Gehani et. al.	2004	Chip-based DNA for cryptography and steganography
N. N. Rao	2004	Recombinant DNA technique for cryptology
K. Tanaka et. al.	2005	One-way hash function for asymmetric encryption
S. T. Amin et. al.	2006	YAEA cipher reinvented using DNA computation
M. Kantarcioglu et. al.	2008	Data Mining techniques based on genomic sequences
M. E. Borda et. al.	2009	Self-assembling DNAs used for cryptography (OTPs) and steganography
R. Terec et. al	2011	Public-key cipher (using MATLAB) based on DNA stronger than OTPs
Q. Gao	2011	Creation of DNA-based communication Protocol, Key-exchange Scheme and Steganography
R. Soni et.	2012	Theoretical and practical

al.		aspects (BioJava & MATLAB) of DNA cryptography
M. I. Youssef et. al.	2012	Multi-layer encryption scheme using Residue Number System and DNA cryptography
Y. Zhang et. al.	2012	New cipher based on DNA fragment assembly; deduction of the secret DNA key; softwares related to DNA
H. Liu et. al.	2013	DNA steganography using MS-Word as the carrier
O. Tornea & M. E. Borda	2013	DNA Cryptosystems based on genome databases
T. Mandage	2013	DNA cryptology using matrix manipulation and secure key generation
A. U. Rehman et. al	2014	Encryption of grey images using DNA techniques
J. Yang et. al	2014	DNA self-assembly structure used for bitwise cryptography
D. S. Chouhan & R. P. Mahajan	2014	Digital signature generation using DNA
R. K. Jangid et.al	2014	Modified Hill cipher for image encryption
Shweta & S. Indora	2015	DNA encoding of data and embedding it inside a video frame
G. Cui et. al.	2015	DNA cryptography based on Microdot technology
A. F. Khadim	2016	S-Boxes for DNA cryptology

VI. CONCLUSION

The past few years have brought so much change in technology that it has transformed our world completely. In the similar fashion, DNA cryptography also sufficed from Bio-Molecular Computation and it is also take the information security world with the wind. DNA computation has myriad amazing features like great parallelism, colossal storage capacity and extraordinary confidential forte, which make it a suitable choice for steganography, secure-key generation, digital signature and cryptography (both symmetric and asymmetric). DNA cryptology paves the way for alteration of conventional ciphers using DNA, which prove to be faster, more reliable and efficient than their traditional counterparts. Overall, it can be

This shortlisting gives a rare insight on the core areas where the researchers are focusing and mining out which area has got maximum coverage and which are has gone unexplored. The following table shows the year-wise tabulation of methodologies and also the author details to gain clarity:

Table 3.3. Year-wise Methodology Result

Year	Author	Methodology
2000	A. Leier et. al	Steganography
2004	A. Gehani et. al	Steganography and Cryptography
2004	N.N. Rao	Cryptography
2005	K. Tanaka et. al	Public-Key Cryptography
2006	S. T. Amin et. al	Cryptography
2008	M. Kantarcioglu	Data mining and storage
2009	M. E. Borda et. al	OTP, Steganography and Cryptography
2011	R. Teree et.al	Cryptography
2011	Q. Gao	Key-sharing & Steganography
2012	R. Soni et. al and Y. Zhang	Cryptography
2012	M.I. Youssef	Image Encryption
2013	H. Liu	Cryptography and Steganography
2013	O. Tornea et. all and T. Mandage	Cryptography
2014	A. U. Rehman et. al & R.K. Jangid et al	Image Encryption
2014	J. Yang et. al	Cryptography
2014	D.S. Chouhan et. al	Cryptography and Digital Signature
2015	Shweta et. al	Multimedia Encryption
2015	G. Cui et. al	Cryptography and Steganography
2016	A. F. Khadim et. al	Cryptography

As depicted in the table, DNA has been widely used for the cryptography technique and elite academicians have given their vital energy and time for the betterment of enhancing security using Bio-molecular computing.

IV. LITERATURE REVIEW

DNA has been a challenging topic and exhaustive research has been done to explore it. Although a lot has been said and written about numerous techniques and methodologies to exploit the DNA and thus to find out the endless amount of applications of it. However, the idea of this contemporary research area was given by Leonard Adleman in 1994, where he solved the NP-Complete problem namely Directed Hamilton Path Problem with seven nodes by basically manipulating the DNA strands[1]. In fact, it was the first ever practical work i.e. DNA computation in the wet lab that displayed the real power of Bio-molecular computing.

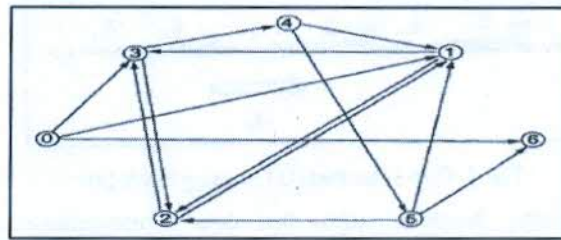


Fig. 4. Directed Hamilton Path Problem taken by Leonard Adleman [1]

This tremendous idea caused a storm in the research areas of Computing, and Biology like the solving the Satisfaction Problem - another NP-Complete problem by Lipton in 1995[2]. Further elegant studies was by Boneh et. al. in 1996, which carried out the cryptanalysis of DES algorithm using Bio-molecular computing in about 4 months for an arbitrary pair of plaintext and ciphertext and just one day in case of a chosen plaintext attack[3]. Similarly in 1999, Clelland et. al. proposed that the DNA computing can be further introduced to the Steganographic area of secret messaging by first converting the original message into DNA form and then hiding it between random DNA strands[5]. All above mentioned candid research work revolutionized the bio-molecular computation and some of the prominent scholarly work is explained as follow:

In 2000, A. Leier et. al presented how DNA binary strands can be used in conjunction with cryptography. Here, two different tactics are described: one by using an innovative encryption technique by hiding information and other by implementing steganography and assortment of binary-gel images. The steganographic techniques are based on a simple assumption that both the parties possess equivalent technological capabilities. The authors also propose some novel techniques that maybe benefitted from the DNA computing like barcoding of materials[6].

A. Gehani et. al. published a brilliant paper on DNA computing in 2004. It is one of the pioneering papers that explores the applications of DNA in cryptography and steganography. The authors suggest that DNA could prove the best option for one-time pads as a small

quantity of DNA is adequate for massive one-time pads. A new application area of two-dimensional data encryption is also suggested using chip-based DNA. Finally, few novel steganographic techniques are also discussed for improved refuge and its pros and cons are thoroughly evaluated[9].

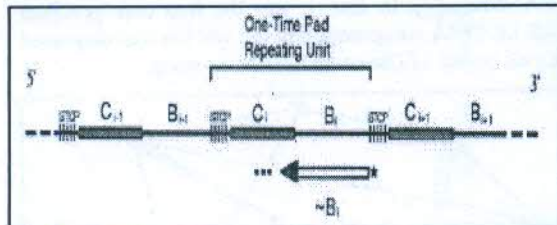


Fig. 5. One-Time Pad (OTP) using DNA [9]

Another inventive article that does comprehensive exploration in the DNA cryptography field was written by N. N. Rao in 2004. It uses the recombinant DNA technique i.e. mixing DNAs of two dissimilar species into another entity to form new genetic blend that is invaluable for cryptology. Using this superior technique, a robust cryptosystem is also designed and its safety is also scrutinized. Alongwith DNA coding is also performed, which is an added bonus to safeguard the data[10].

The research paper by K. Tanaka et. al. from the year 2005 shares a new working sphere of DNA i.e. public-key cryptosystem. It is a brilliant alternative to the key sharing quandary faced by symmetric key encryption. Here, the message-coded hidden DNA are first restored and then amplified and finally sequenced. This modified DNA act as a one-way hash function for asymmetric encryption [12].

S. T. Amin et. al.(2006) described how the storing capacity and vast parallelism inherent in the DNA can be exploited for creating conventional cryptographic algorithms like the renowned YAEA cryptosystem. The plaintext's each character here is denoted by the DNA nucleotides and then with the help of pointers, a single random position is nominated. The authors also suggested that similar technique may be employed for encoding of the digital images as well. Experimental results show that this unconventional way of cryptography offers far more refuge rather than conventional encoders

[14].

In 2008, M. Kantarcioglu et. al. developed a unique approach towards secure storage and quick querying of genomic sequences. The focal idea here is to instrument data mining on genomic databases without unveiling the original genomic sequences. The experiments showed that the proposed framework can be carried out using existing technologies and environment. Hence, Bio-molecular computing can act as a big boon for the safeguarding of medical information[15].

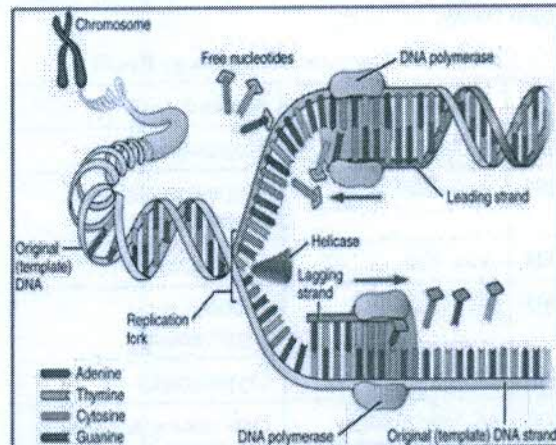


Fig 6. Polymerase Chain Reaction Process of DNA [40]

An original algorithm proposed by M. E. Borda et. al. (2009) uses DNA hybridization- a self-assembling process to enhance DNA structures. Here, Polymerase Chain Reaction (PCR) is used to amplify some portions of DNA and thus the modified DNA is used for myriad purposes like using One-Time Pads (OTPs), data encryption and even data hiding. The authors propose that initially encryption is performed followed by the hiding this encoded data. The decryption procedure is also discussed in detail and MATLAB is the implementation language for both encryption and decryption[16].

This alternative research work from 2011 by R. Tere et. al goes beyond the usual exploration and implements both symmetric and asymmetric ciphers. The authors recommended two algorithms that use private-key cryptography but use diverse platforms for the implementation i.e. Java for former algorithm and BioJava in conjunction with Matlab for the latter. The elite academicians also suggested how DNA can be used for designing a public-key cryptogram and also detailed that it will be far more safe and steadfast than the OTP-based DNA private-key cipher[19].

In this 2011 article, Q. Gao stated numerous applications of DNA cryptology for security-phobic users and their security is also examined. One area where genetic codes can be used is designing a communication protocol for secure transmission of data. Another domain mentioned here is the key-sharing between trusted parties which takes in account the base sequence of DNA. Last but not the least, two steganographic methodologies by DNA are also proposed by the author based on the intronization and LSB-based image[18].

In 2012, R. Soni et. al. presented a theoretical work that explains each and every aspect of the DNA cryptosystems. Firstly, the cryptography is described and then the notions of the DNA. Later on, researchers also explained the practical characteristics i.e. plentiful options in Java and BioJava that can be beneficial to work with the BMC (whether symmetric of

The Evolution of DNA Cryptology - A Review

Akhil Kaushik¹, Dr. Vikas Thada²

¹Ph. D Scholar, ²Associate Professor, CSE Deptt. Amity University, Gurgaon, India

¹akhilkaushik05@gmail.com, ²vthada@amity.ggn.edu

Abstract: The Cryptography has been the elite's topmost priority since the genesis of civilization and has undergone copious changes since then. A plentiful methodologies have come and gone to cater the security needs of myriad men. One novel technique that has made its mark over the horizon is the DNA Cryptography, which ensures safety by conjoining the advanced properties of DNA and Computing. This paper throws some light on the brilliant scholarly work written on the DNA Cryptography and the applications related to it.

Keywords: DNA Cryptography; Bio-Molecular Computation (BMC); Polymerase Chain Reaction (PCR)

I. INTRODUCTION

The modern era is the age of information and hence anyone who acquires current and correct information has a sure-shot key to success. The Internet and World Wide Web has provided profuse possibilities for the personal and professional benefit; and it requires a significant amount of security mechanism to make sure these wide application communication tools are used for the right purpose. Security attacks ranging from herculean financial scams to identity theft make the security issue inevitable and it must be addressed in the right amount and at the right time.

Although a lot of methodologies are available for this need, yet cryptology stands aloof from the mob. Ever since the dawn of communication, secret messaging has been the lovechild of religious men, politicians, artists and lovers. According to celebrated historians this art of secret writing was vastly prevalent and famous in ancient Greece, Sparta and Egypt[8]. A lot of cinematographic films like Da-Vinci Code also show this ancient art used heavily in the religion. Even the Arabic world contributed profoundly and so did Indians and Romans.



Fig. 1. The Spartan Scytale - An ancient Encryption Tool [37]

During the renaissance, European countries like Germany, France, Italy, etc. evolved this science through extensive research and the trend continued till the 19th century. Nevertheless, the modern form of cryptology progressed hugely during the dark ages of both World Wars, which performed as the game-changer for the

Allied Powers (especially during the Second World War). The contributions made by the Enigma machine (German rotor machine for encoding) and its counterparts BOMBE and Colossus (UK's computers to break Enigma's code) are gigantic[11]. This epoch also marked the practice of electro-mechanical devices for both cryptography and cryptanalysis. Another major inventions that simulated the cryptographic growth are "Radio" and "Telegraph" during the early 1990s and later on carried on the shoulders of an exceptional creation "Computer". Nowadays, immense opportunities and colossal challenges are present because of Internet, where securing the information is by far the most vital need of common man today[20].

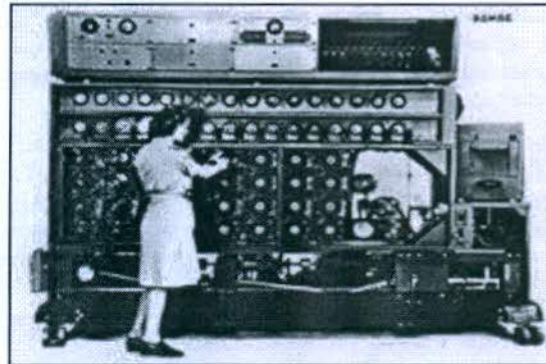


Fig. 2. BOMBE: The First Computer Made for Cryptanalysis [38]

Cryptography is defined as the art or science of deforming a message into a random appearing junk that seems meaningless. However, with proper technique and knowledge, this useless piece of junk can be retransformed into an eloquent message. Cryptanalysis on the other hand is the science which analysis the coded message and tries to recover the original message. Cryptology is the amalgamation of both cryptography and cryptanalysis, which covers the bigger picture.

II. BIO-MOLECULAR COMPUTATION

As discussed earlier, cryptography has evolved with mankind and over last fifty years, it has undergone tremendous change. Firstly the conventional cryptography of symbols and letters transformed with the help of mechanical machines and later on by computers. Then, Elliptic Curve Cryptography (ECC) came into picture which offered immense strength and secrecy due to its proximity to public key cryptosystem[20]; which was later on surpassed by the physics-based Quantum Cryptography. The latest

innovation in this very arena is the DNA Cryptography that is based on the Bio-Molecular Computation (BMC) - a hybrid research area grounded on the Biology and Computer science[13]. BMC uses recombinant RNA and DNA for innumerable applications like data storage. It is a known fact that 1 gram of DNA can accumulate approximately 10^8 tera-bytes of data. Thus, the whole storage problem of entire globe can be solved with little number of DNA grams[22][7]. DNA cryptography also roots from BMC and uses it for the betterment of cryptology.

Deoxyribonucleic Acid, also known as DNA is primarily a genetic carrier used vastly among all the living creatures and it defines their characteristics and functionality. Every DNA strand comprises of two molecules arranged in a “double-helix” arrangement similar to a twisted ladder[21]. Each molecule comprises of copious subparts- “nucleotides” and further each nucleotide contains a Phosphate group, Pentose sugar and a Nitrogenous base.

There are majorly for nitrogenous bases paired together: Adenine (A) and Thymine (T) i.e. Purines (A-T); Cytosine (C) and Guanine (G) i.e. Pyrimidines (C-G). The organization of these bases are responsible to shape unique genes, which inturn distinguishes every living being from one-another[7].

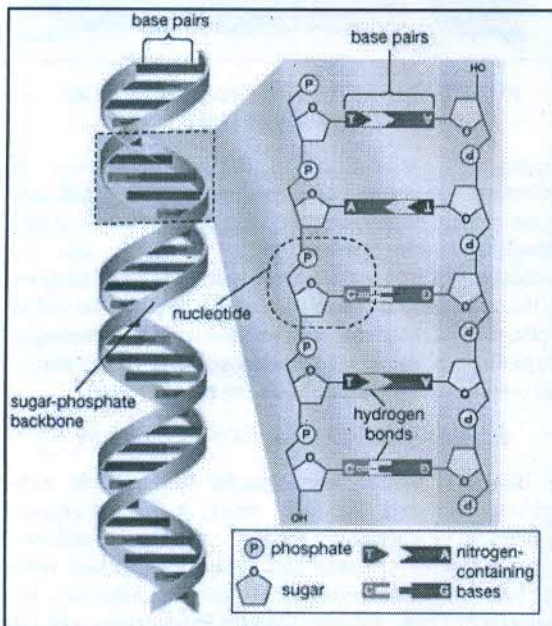


Fig. 3. A DNA Molecule Structure [39]

DNA Cryptography basically encrypts the provided data built on the concepts of Biology exploiting the DNA’s feature of carrying information securely and computational perplexity. Most of the DNA-based encryption standards firstly converts the plaintext into binary form and then encode it. The next usual step is the DNA conversion from binary digits to achieve a

stronger, proficient and elegant ciphertext, which is almost impossible to crack using conventional approaches[4][17].

During the past twenty years, countless effort has been put in the DNA computing research and the results have been extremely fruitful. The next section discusses some of the leading research work carried out by worthy scholars over the span of last twenty year. This article covers some of the vivid investigative work by some exclusive scholars in the zone of DNA cryptology.

III. RESEARCH METHODOLOGY

The first step in any research is reviewing the existing literature to understand how much work has already been done in the specified area and thus helps the researcher to proceed further in the right direction. Hence, to guide the research on proper path, a review protocol has been developed for reviewing the existing work, which is shown by the following table:

Table 3.1. Review Protocol

Year	Sources	Keywords
2001 to 2016	IEEE Explore, Science Direct, Springer Library, ACM Digital Library and Google Scholar	DNA Cryptography, DNA Steganography, Bio-Molecular Computing, etc.

After defining the review protocol, the next phase is searching the academic sources mentioned above for relevant content and categorizing them year wise, which is shown in the next table:

Table 3.2. Year-wise Search Result

Year	No. of Publications
2001	1
2004	2
2005	1
2006	1
2008	1
2009	1
2011	2
2012	3
2013	3
2014	4
2015	2
2016	1

The next phase is using a divide-&-conquer approach to identify the methodological approaches used by the revered authors in the Bio-Molecular Computing area.

2017-18

[Download full issue](#)

Discrete Mathematics

Volume 340, Issue 4, April 2017, Pages 713-721

On traceability property of equidistant codes

Anu Kathuria ^a ✉, S.K. Arora ^b, Sudhir Batra ^c ✉

Show more

Outline | Share Cite

<https://doi.org/10.1016/j.disc.2016.12.009>

Under an Elsevier user license

Get rights and content

open archive

Abstract

Necessary and Sufficient conditions for an equidistant code to be a 2-TA code are obtained. An explicit construction method is proposed to obtain linear MDS $[p + 1, 2, p]$ codes over the finite field F_p , where p is a prime. These codes can be used as 2-TA codes for $p > 2$. In particular, for $p = 3$, it is observed that the linear $[4, 2, 3]$ MDS code contradicts a result of Jin and Blaum (2007). The correct version of this result and its proof is given. Existence of some infinite families of equidistant 2-TA codes is shown by using Jacobsthal and Hadamard matrices. Some of these codes are also observed to be good equidistant code (Sinha et al., 2008).

Next

Keywords

FEEDBACK

Maximum Distance Separable (MDS) code; Equidistant code; Traceable (TA) code;
Jacobsthal matrix; Hadamard matrix; RS code

1. Introduction

Chor, Fiat and Naor [3] introduced the concept of traitor tracing as a means to limit piracy. Traitor tracing schemes may prove quite useful in protecting copyrighted digital data. When a pirated copy created by a group of authorized users of the copyrighted data is traced, traitor tracing schemes allow to trace it back to at least one producer of it. In recent years several codes have been studied for the purpose of their usefulness in traceability schemes. In general, these codes are called fingerprinting codes. The weak forms of these codes, called frameproof codes were introduced by Bonch and Shaw [2]. Strong form of codes, called identifiable parent property (IPP) codes have been introduced by Hollman, Van Lint, Linnartz and Tolhuizen [6]. Other form of codes, called traceability codes were introduced by Chor, Fiat and Naor in [3]. TA codes are stronger than IPP codes and is a subclass of IPP codes and generally have efficient traitor tracer algorithms. IPP codes on the other hand are capable of identifying traitors requiring less restrictive conditions than TA codes at the expense of not having efficient traitor tracing algorithm. Combinatorial properties of traceability schemes and frameproof codes have been studied by Staddon, Stinson and Wei [10]. Sufficient conditions for an equidistant code to be an IPP code have been derived in [6]. Some constructions of equidistant frameproof codes have been suggested in [5]. In [7], Jin and Blaum have obtained the necessary and sufficient conditions for a linear MDS $[n, k, d]$ code over F_q with $n \leq q + 1$ to be a c -TA code. In the present paper, we obtain necessary and sufficient conditions under which an equidistant code can be used as a 2-TA code (see Theorem 3.4, Theorem 3.5). We also derive a condition under which an equidistant code cannot be a m -TA code, where $m \geq 3$ (see Theorem 3.6).

In Section 4, we propose a method to construct linear MDS $[p + 1, 2, p]$ codes over the finite field F_p , where p is an odd prime. These codes are extended RS codes and can be used as 2-TA codes. In particular, for $p = 3$, the ternary Hamming code $[4, 2, 3]$ turns out to be a 2-TA code, contradicting Theorem 2.2 of [7] (see Example 2 in Section 4). At the end of this section we provide the correct version of this theorem and its proof (see Theorem 4.11).

In Section 5, we show that Jacobsthal matrices [4]; [11] for primes of the form $4m + 3$ generate equidistant 2-TA codes of length n with distance $d < 2n / 3$. Further, using the results of [1], [9] the existence of two infinite classes of non-linear equidistant 2-TA codes of length n and distance d such that $2n / 3 < d \leq 3n / 4$ is shown. Here it is also observed that some of these are good equidistant codes.

The following section is devoted to some preliminaries required for the discussion in the subsequent sections.

2. Some preliminaries

Throughout this paper, the following basic definitions and terminology from [5], [6], [7], [8], [11] will be used and F_q denotes a finite field with q elements.

2.1. Here we recall some basic definitions related to error correcting codes.

- (i) Let Q be a finite set of alphabets. Then a subset $C \subseteq Q^n$ is called a code of length n over Q . The elements of Q^n are called words and the elements of C are called codewords of length n .
- (ii) Let a and b be two words, then the hamming distance $d(a, b)$ between a and b is the number of coordinates in which they differ and the number of non-zero coordinates of a word c is called the weight of c . The minimum distance d of C is $d = \min \{d(a, b) \mid a, b \in C\}$.
- (iii) $I(x, y) = \{i : x_i = y_i\}$ for $x = (x_1, x_2, \dots, x_n), y = (y_1, y_2, \dots, y_n) \in Q^n$. Similarly, we can define $I(x, y, z, \dots)$ for any finite number of words x, y, z, \dots .
- (iv) A subspace C of F_q^n is called a linear code over F_q . The dimension of the code is defined as the dimension of the subspace. A linear code with length n , dimension k and minimum distance d is denoted as $[n, k, d]$ code. A linear code $C [n, k, d]$ is an MDS code if $d = n - k + 1$.
- (v) A code C with same distance between every pair of its codewords is called an equidistant code. If all the codewords of a code C carry same weight then code C is called constant weight code. A code C with both of these properties is known as equidistant constant weight code.
- (vi) Let $\alpha = \{\alpha_1, \alpha_2, \dots, \alpha_n\}$, where the α_i are distinct elements of F_q , and let $v = \{v_1, v_2, \dots, v_n\}$, where the v_i are non-zero (but not necessarily distinct) elements of F_q . Then the Reed-Solomon(RS) code of length n and dimension k , consists of all vectors $(v_1 f(\alpha_1), v_2 f(\alpha_2), \dots, v_n f(\alpha_n))$, where $f(x)$ ranges over all polynomials of degree less than k with coefficients from F_q .

Choose the particular polynomial basis $1, x, x^2, \dots, x^{k-1}$. In this basis the generator matrix of the above defined code is given by

$$\begin{bmatrix} v_1 & v_2 & \cdots & v_n \\ v_1 \alpha_1 & v_2 \alpha_2 & \cdots & v_n \alpha_n \\ \vdots & \vdots & \cdots & \vdots \\ v_1 \alpha_1^{k-1} & v_2 \alpha_2^{k-1} & \cdots & v_n \alpha_n^{k-1} \end{bmatrix}$$

A code whose generator matrix is given by adding a new column $(0, 0, \dots, 1)^T$ to the above matrix is called extended RS code of length $n + 1$.

2.2. Now let us define some terms related to fingerprinting codes.

(i) Detectable and Undetectable Positions. Let $X \subseteq Q^n$. Then we say that the position $i \in \{1, 2, \dots, n\}$ is undetectable for X if i th position of each word $x \in X$ is occupied with the same alphabet, otherwise the position i is detectable.

(ii) Coalition. It means two or more users meet for the purpose of creating an illegal copy of a digital object (see marking assumption (iv) also) by comparing their copies. A member of the coalition is called a pirate.

(iii) Descendant Set. For any two words $a = (a_1, a_2, \dots, a_n)$ and $b = (b_1, b_2, \dots, b_n)$ in Q^n , the set of descendants $Desc(a, b) = D(a, b)$ is defined as $D(a, b) = \{x \in Q^n \mid x_i \in \{a_i, b_i\}, i = 1, 2, \dots, n\}$.

The above definition of Descendant set can be naturally extended to any finite number of words a, b, c, \dots

(iv) Marking Assumption. In the static form of finger printing scheme, each digital content is divided into multiple segments, among which n segments are chosen for marking them with symbols which correspond to alphabets in Q . Each user receives a copy of the content with differently marked symbols. If a code C over Q of length n is used to assign the symbols for each segment to each user. Then each copy can be denoted as a codeword of C and each coordinate x_i of a codeword (x_1, x_2, \dots, x_n) can be termed as a symbol. Further, assume that any coalition of c users is only capable of creating a pirated copy whose marked symbols correspond to a word of Q^n that lie in the Descendant set of these c users.

(v) Identifiable Parent Property Code. A code C is c -IPP if for any $x \in Desc(C)$ it holds that if $C_i \subseteq C$ with $|C_i| \leq c$, then $\bigcap_{\{i: x \in Desc(C_i)\}} C_i \neq \phi$.

In other words a code C has c -IPP property if no coalition of size at most c can produce an n -tuple that cannot be traced back to at least one member of the coalition.

(vi) Traceable Code. A code C is called c -traceability code (c -TA code) for $c \geq 2$, if for all subsets (coalitions) $T \subseteq C$ of at most c codewords, if $y \in Desc(T)$, then there exists at least one $t \in T$ such that $d(y, t) < d(y, w)$ for all $w \in C - T$.

(vii) A hash function is a function $h : A \rightarrow B$, where $|A| = M \geq |B| = m$, that maps keys from A into the set of integers B . A finite set H of n hash functions is called an (n, M, m) -hash family.

Perfect Hash Family. Let M, m, w be integers such that $M \geq m \geq w \geq 2$. An (n, M, m) - hash family H is called an (n, M, m, w) - perfect hash family if for any subset $X \subseteq A$ with $|X| = w$, there is at least one function $h \in H$ such that h is injective on X .

(viii) w -Separate (M, n, m) matrix. Let C be an $M \times n$ matrix on m symbols corresponding to an (n, M, m, w) - perfect hash family. Then for any fixed t rows of C , $t \leq w$, there is at least one column of C with all distinct symbols on that fixed rows. Matrix C is then called w -Separate (M, n, m) matrix.

3. Equidistant codes as traceable codes

Throughout this section we denote $|I(a, b)|$ by s and $|I(a, b, c)|$ by l for codewords a, b, c of a code C .

Lemma 3.1

An equidistant code of length n with $n - 3s + 2l > 0$ for all $a, b, c \in C$ is always a 2-TA code.

Proof

Let C denote an equidistant code of length n with $n - 3s + 2l > 0$. Then in view of definition 2.1(iii), $|I(a, b)| = s$ is equal (constant) for all $a, b \in C$. Let $I(a, b) = \{r_1, r_2, \dots, r_s\} \subseteq \{1, 2, \dots, n\}$. Now let $c \in D(a, b)$, then by definition 2.2(iii), $I(a, b) \subseteq I(a, c) \cap I(b, c)$. This shows that there is no loss of generality in assuming that $I(a, b) = \{1, 2, \dots, s\}$. In order to prove that C is a 2-TA code, it is sufficient to show that there is no codeword $x \neq a, b$ in C such that $d(x, c) < d(a, c)$ and $d(x, c) < d(b, c)$. For this let $x = (x_1, x_2, \dots, x_n) \in C$ and $|I(a, b, x)| = l$. Further suppose that $I(a, x) = \{1, 2, \dots, l, t_1, t_2, \dots, t_m\}$ and $I(b, x) = \{1, 2, \dots, l, l_1, l_2, \dots, l_m\}$ such that $\{t_1, t_2, \dots, t_m\} \cap \{l_1, l_2, \dots, l_m\} = \phi$, where $l + 1 \leq t_i, l_i \leq n$ for all $1 \leq i \leq m$. Since C is equidistant, we must have $l + m = s$, where $0 \leq l \leq s$ and $0 \leq m \leq s$. Now any $c \in D(a, b)$ is obtained by

- (i) retaining the m_1 symbols out of m symbols, $x_{t_1}, x_{t_2}, \dots, x_{t_m}$ of codeword a .
- (ii) retaining the m_2 symbols out of m symbols, $x_{l_1}, x_{l_2}, \dots, x_{l_m}$ of codeword b .
- (iii) retaining the symbols at k_1 coordinates out of the set of $n - s - m$ coordinates, i.e., $\{1, 2, \dots, n\} - \{1, 2, \dots, s, t_1, t_2, \dots, t_m\}$.
- (iv) retaining the symbols at k_2 coordinates out of the set of $n - s - m$ coordinates, i.e., $\{1, 2, \dots, n\} - \{1, 2, \dots, s, l_1, l_2, \dots, l_m\}$.

It now follows that $m_1 + m_2 + k_1 + k_2 = n - s$, $d(a, c) = n - s - (m_1 + k_1) = m_2 + k_2$, $d(b, c) = n - s - (m_2 + k_2) = m_1 + k_1$ and $d(x, c) = n - l - m_1 - m_2 = n - s + m - m_1 - m_2 = m + k_1 + k_2$.

By hypothesis, $n - 3s + 2l > 0$. Therefore $n - s - 2m > 0$ and hence $k_1 > 0$ or $k_2 > 0$. Further, $a \neq c$ and $b \neq c$, so we have $m_1 + k_1 > 0$ and $m_2 + k_2 > 0$. Now depending upon k_1 and k_2 we distinguish the following three cases:

(a) $k_1 > 0$ and $k_2 > 0$. Since $m_1 \leq m$ and $m_2 \leq m$, therefore $d(a, c) < d(x, c)$ and $d(b, c) < d(x, c)$. Hence a and b will be traced.

(b) $k_1 = 0$. Then $k_2 > 0$ and $m_1 > 0$. In this case we have $d(a, c) \leq d(x, c)$ with equality in case when $m_2 = m$ and $d(b, c) < d(x, c)$. Hence b will always be traced.

(c) $k_2 = 0$. Then as discussed in (b) it can be shown that a will always be traced in this case.

Theorem 3.2

An equidistant code of length n with distance $d > 2n/3$ is always a 2-TA code.

Proof

Let C be an equidistant code of length n with distance $d > 2n/3$. Then by definition 2.1(iii) $|I(a, b)| = s < n/3$ for all $a, b \in C$. Therefore, $n - 3s > 0$. Trivially, $0 \leq l \leq s$ and so $n - 3s + 2l > 0$ and hence by Lemma 3.1 the result follows.

The condition that $d > 2n/3$ in the above theorem is sufficient only. In Section 5, we show that there is an infinite class of 2-TA equidistant codes with $d \leq 2n/3$.

Lemma 3.3

Let C be an equidistant code of length n such that $n - 3s + 2l = 0$ for some $a, b, x \in C$, then C is not a 2-TA code.

Proof

Let $a, b, x \in C$ be fixed such that $n - 3s + 2l = 0$, where $0 \leq l \leq s$. As discussed in Lemma 3.1, we can take $I(a, b) = \{1, 2, \dots, s\}$ and $I(a, b, x) = \{1, 2, \dots, l\}$. Since $n - 3s + 2l = 0$, $n - s = (s - l) + (s - l)$, therefore we can suppose that $I(a, x) = \{1, 2, \dots, l, s + 1, s + 2, \dots, 2s - l\}$ and $I(b, x) = \{1, 2, \dots, l, 2s - l + 1, 2s - l + 2, \dots, 3s - 2l\}$. Let $c \in D(a, b)$. Then obviously $\{1, 2, \dots, s\} \subseteq I(a, c) \cap I(b, c)$. Now suppose $I(a, c) - \{1, 2, \dots, s\} = \{s + 1, s + 2, \dots, 2s - l\}$ and $I(b, c) - \{1, 2, \dots, s\} = \{2s - l + 1, 2s - l + 2, \dots, 3s - 2l\}$. Then $d(a, c) = (n - s) - (s - l) = n - 2s + l$, $d(b, c) = (n - s) - (s - l) = n - 2s + l$ and $d(x, c) = (n - l) - (s - l) - (s - l) = n - 2s + l$. Therefore C is not a 2-TA code.

For any equidistant code of length n with s and l as above, we cannot have $n - 3s + 2l < 0$. Therefore, by combining Lemma 3.1, Lemma 3.3, we have

Theorem 3.4

An equidistant code C of length n is a 2-TA code if and only if $n - 3s + 2l > 0$.

For a code C of length n and size M , the matrix of C means $M \times n$ matrix such that each row corresponds to a codeword of C .

Theorem 3.5

Let C be an equidistant code of length n and size $M \geq 3$. Then C is 2-TA code if and only if the matrix of C is 3-separate $(M, n, 3)$ matrix.

Proof

If C is a 2-TA code, then it is a 2-IPP code and therefore matrix of C is 3-separate $(M, n, 3)$ matrix (for detail see [10]). Now let matrix of C is a 3-separate matrix. Then by definition 2.2(viii) for any three rows r, s, t of the matrix, there exists a column, say, j th such that $j \in \{1, 2, \dots, n\} - I(r, s) \cup I(s, t) \cup I(r, t)$. This implies that $(n - s) - (s - l) - (s - l) = n - 3s + 2l > 0$ and hence by Lemma 3.1 C is a 2-TA code.

Theorem 3.6

Let C be an equidistant code of length n with distance $d \leq \left(1 - \frac{1}{m^2}\right)n$, $m \geq 3$. If $I(a, b, c) = \phi$ for all $a, b, c \in \{a^{(1)}, a^{(2)}, \dots, a^{(m+1)}\} \subseteq C$, then C is not a m -TA code.

Proof

Let $a^{(i)} = (a_1^{(i)}, a_2^{(i)}, \dots, a_n^{(i)}) \in C$, where $1 \leq i \leq m + 1$. Since C is equidistant with $d \leq \left(1 - \frac{1}{m^2}\right)n$, $|I(a, b)| = s \geq \frac{n}{m^2}$ for all $a, b \in C$. Then $n \leq m^2 s = \binom{m+1}{2}s + \binom{m}{2}s$. Further $I(a, b, c) = \phi$ for all $a, b, c \in C$. Therefore, we can suppose that

$$\text{for } 2 \leq i \leq m, I(a^{(1)}, a^{(i)}) = \{(i-2)s + 1, (i-2)s + 2, \dots, (i-1)s\};$$

$$\text{for } 3 \leq i \leq m, I(a^{(2)}, a^{(i)}) = \{(m-1)s + (i-3)s + 1, \dots, (m-1)s + (i-2)s\};$$

$$\begin{aligned} \text{for } 4 \leq i \leq m, I(a^{(3)}, a^{(i)}) &= \{(m-1)s + (m-2)s + (i-4)s + 1, \dots, (m-1)s + (m-2)s + (i-3)s\}; \dots; \\ &I(a^{(m-1)}, a^{(m)}) \\ &= \{(m-1)s + (m-2)s + \dots + 2s + 1, \dots, (m-1)s + (m-2)s + \dots + s\} \end{aligned}$$

$$\text{and for } 1 \leq i \leq m, I(a^{(i)}, a^{(m+1)}) = \{ks + (i-1)s + 1, \dots, ks + is\}, \text{ where } k = m(m-1)/2.$$

It is now quite evident that $n \geq \left| \bigcup_{i=1}^{m-1} \bigcup_{j=i+1}^m I(a^{(i)}, a^{(j)}) \cup \bigcup_{i=1}^m I(a^{(i)}, a^{(m+1)}) \right| = \binom{m+1}{2}s$. Let $b \in D(a^{(1)}, a^{(2)}, \dots, a^{(m)})$ such that its first $\binom{m}{2}s$ coordinates are obtained by retaining symbols at s coordinates of each of $a^{(3)}, a^{(4)}, \dots, a^{(m)}, a^{(1)}; a^{(4)}, a^{(5)}, \dots, a^{(m)}, a^{(1)}; a^{(5)}, a^{(6)}, \dots, a^{(m)}, a^{(1)}; \dots; a^{(m-1)}, a^{(m)}, a^{(1)}; a^{(m)}, a^{(1)}; a^{(1)}$ and then next ms coordinates are obtained by retaining symbols at s coordinates of each of $a^{(1)}, a^{(2)}, \dots, a^{(m)}$ in order starting from first coordinate. Such a choice of b will be possible due to our hypothesis, i.e.,

$$b = \left(a_1^{(3)}, a_2^{(3)}, \dots, a_s^{(3)}, a_{s+1}^{(4)}, \dots, a_{2s}^{(4)}, \dots, a_{(m-3)s+1}^{(m)}, \dots, a_{(m-2)s}^{(m)}, a_{(m-2)s+1}^{(1)}, \dots, a_{(m-1)s}^{(1)}, a_{(m-1)s+1}^{(4)}, \dots, a_{ms}^{(4)}, a_{ms+1}^{(5)}, \dots, a_{(m+m-4)s}^{(m)}, \dots, a_{(m+m-3)s}^{(1)}, \dots, a_{ks}^{(1)}, a_{ks+1}^{(1)}, \dots, a_{ks+ms}^{(m)} \right).$$

It is evident that $d(b, a^{(m+1)}) = n - ms$. Further, if $n = \binom{m+1}{2}s$, then $d(a^{(1)}, b) = n - ms, d(a^{(2)}, b) = n - s, d(a^{(3)}, b) = n - 2s, \dots$ and $d(a^{(m)}, b) = n - (m-1)s$. Now for achieving $d(a^{(i)}, b) = n - ms$ for all $1 \leq i \leq m$, we must have $n = \binom{m+1}{2}s + \binom{m}{2}s$. Therefore if $n \leq \binom{m+1}{2}s + \binom{m}{2}s$, then t



$b \in D(a^{(1)}, a^{(2)}, \dots, a^{(m)})$ such that $d(a^{(i)}, b) \geq n - ms$ for all $1 \leq i \leq m$ and $d(a^{(m+1)}, b) = n - ms$. Hence C is not a m -TA code.

Remark

Suppose $m = 2$. Then the form of $b \in D(a^{(1)}, a^{(2)})$ as discussed in the proof of Theorem 3.6 is not possible, since $I(a^{(1)}, a^{(2)}) = \{1, 2, \dots, s\}$, i.e., first s positions are undetected. Therefore, Theorem 3.6 is not valid for $m = 2$ and hence different treatment is required for this case and consequence is Theorem 3.4.

4. Construction of a class of 2-TA code

Throughout this section, p is a prime and $q = p^k$ for some positive integer k . In this section we describe a method to construct linear MDS code $C[p+1, 2, p]$ over F_p . For this we first prove that $C[q+1, 2, q]$ is an equidistant constant weight code over F_q which is a direct consequence of the result stated below as Theorem 4.2. At the end of this section we also provide correct version of Theorem 2.2 of [7].

Definition 4.1

Plotkin Bound [8]

Let C be a code of length n , size N and minimum distance d over Q with m elements then $d \leq \frac{nN(m-1)}{(N-1)m}$. If $d = \frac{nN(m-1)}{(N-1)m}$ then C is said to be optimal code.

Theorem 4.2

[8], [12]

The number of codewords of weight $n - k + 1$ in an MDS code $C[n, k, d]$ over F_q is $(q-1) \binom{n}{n-k+1}$.

Lemma 4.3

A linear MDS code $C[q+1, 2, q]$ is an Equidistant Constant Weight Code. Moreover C is optimal also.

Proof

By Theorem 4.2, the number of codewords of weight q in C is $q^2 - 1$. Since the code C is linear with size q^2 , each non-zero codeword of C must be of weight q and hence is an equidistant code. Further minimum distance of the code meets the Plotkin Bound [8], i.e., $d = q = \frac{(q+1)q^2(q-1)}{(q^2-1)q}$ and hence is optimal also.

Theorem 4.4

If $q > 2$, then the above code $C [q + 1, 2, q]$ is a 2-TA code.

Proof

If $q > 2$, then trivially $q = d > 2n / 3$ and hence by Theorem 3.2 the result follows.

Example 1

Let us consider Reed Solomon Code C of length 5 and minimum distance 4 over $F_4 = \{1, \alpha, \alpha^2, \alpha^3\}$, whose 16 codewords are listed as rows in the following 16×5 matrix.

$$\begin{bmatrix} 0 & 0 & 0 & 0 & 0 \\ 0 & 1 & \alpha & \alpha & 1 \\ 0 & \alpha & \alpha^2 & \alpha^2 & \alpha \\ 0 & \alpha^2 & 1 & 1 & \alpha^2 \\ 1 & \alpha & \alpha & 1 & 0 \\ 1 & \alpha^2 & 0 & \alpha^2 & 1 \\ 1 & 0 & 1 & \alpha & \alpha \\ 1 & 1 & \alpha^2 & 0 & \alpha^2 \\ \alpha & \alpha^2 & \alpha^2 & \alpha & 0 \\ \alpha & \alpha & 1 & 0 & 1 \\ \alpha & 1 & 0 & 1 & \alpha \\ \alpha & 0 & \alpha & \alpha^2 & \alpha^2 \\ \alpha^2 & 1 & 1 & \alpha^2 & 0 \\ \alpha^2 & 0 & \alpha^2 & 1 & 1 \\ \alpha^2 & \alpha^2 & \alpha & 0 & \alpha \\ \alpha^2 & \alpha & 0 & \alpha & \alpha^2 \end{bmatrix}$$

Here α is a primitive cube root of unity. One can readily verify that $C [5, 2, 4]$ is an equidistant constant weight code and hence is a 2-TA code.

Method 4.5

We now propose a method to construct the $C [p + 1, 2, p]$ code over F_p . This is comprised of the following steps:

- (i) First construct a matrix M_1 of order $p^2 \times 2$ consisting of all ordered pairs of the elements of F_p as given below:

$$\begin{bmatrix} 0 & 0 \\ 0 & 1 \\ 0 & 2 \\ \vdots & \vdots \\ 0 & (p-1) \\ 1 & 0 \\ 1 & 1 \\ \vdots & \vdots \\ 1 & (p-1) \\ \vdots & \vdots \\ (p-1) & 0 \\ (p-1) & 1 \\ \vdots & \vdots \\ (p-1) & (p-1) \end{bmatrix}$$

(ii) Now we augment the various columns sequentially to this matrix so as to get a matrix M_p with $p+1$ columns. Let C_i , $1 \leq i \leq p+1$ denote the i th column of M_p . Then $C_{i+1} = C_i + C_1$, for $2 \leq i \leq p$, i.e., each subsequent column is obtained by adding the first column to just previously obtained column.

The p^2 rows of M_p will be the codewords of $C[p+1, 2, p]$ linear equidistant constant weight code and this has been proved in the next Theorem 4.6.

Theorem 4.6

Extended RS code generated by the words $(0, 1, 1, \dots, 1)$ and $(1, 0, 1, 2, 3, \dots, p-1)$ of length $p+1$ is an equidistant constant weight code $C[p+1, 2, p]$ over F_p obtained in the Method 4.5.

Proof

Obviously the words $u = (0, 1, 1, \dots, 1)$ and $v = (1, 0, 1, 2, 3, \dots, p-1)$ of length $p+1$ are linearly independent over F_p . Let C denote the code generated by u and v . Then by definition 2.1(vi), C is an extended RS code of length $p+1$ and dimension 2. Then

$C = \{au + bv | a, b \in F_p\} = \{a(0, 1, \dots, 1) + b(1, 0, 1, \dots, p-1) | 0 \leq a, b \leq p-1\}$. It is evident that for

$= \{b, a+b, a+2b, \dots, a+(p-1)b | 0 \leq a, b \leq p-1\}$
 a arbitrary codeword $(c_1, c_2, \dots, c_{p+1})$ of C , $c_1 = b$, $c_2 = a$, $c_{i+1} = c_i + c_1$, where $2 \leq i \leq p$. Thus the codewords of C above are the rows of the matrix M_p described in Method 4.5. Since C is RS code of length $p+1$ and dimension 2 over F_p , C is a linear MDS code. Therefore by Lemma 4.3, $C[p+1, 2, p]$ is an equidistant constant weight code over F_p .

The fact that each non-zero codeword of C above is of weight p can also be established in the following manner:

(i) If $a \neq 0$ and $b = 0$ then $wt(a(0, 1, 1, \dots, 1)) = p$.

(ii) If $a = 0$ and $b \neq 0$ then $wt(b(1, 0, 1, 2, \dots, p-1)) = p$.

(iii) If $a \neq 0$ and $b \neq 0$. Then trivially the symbols present at the first two coordinates of $au + bv$ are always non-zero. Leaving first two coordinates, a coordinate of $au + bv$ is given by $a + bk$, where $k \in \{1, 2, \dots, p-1\}$. Now suppose that $a + bk = 0$ then $k = -ab^{-1} \pmod{p}$. Therefore, for a fixed value of the pair (a, b) such that $a \neq 0, b \neq 0$, we have a unique value of k such that $a + bk = 0$. Thus $wt(a + bk) = 2 + (p-1) - 1 = p$. This proves the theorem.

Similarly, we have the following theorem related to the equidistant codes over F_q , where q is a prime power.

Theorem 4.7

Let α denote a primitive element of F_q . Then the extended RS code generated by the words $(0, 1, 1, \dots, 1)$ and $(1, 0, 1, \alpha, \alpha^2, \dots, \alpha^{q-2})$ of length $(q+1)$ is an equidistant constant weight code $C[q+1, 2, q]$ over F_q .

Example 2

Let us construct the equidistant constant weight code $C[4, 2, 3]$ over F_3 using the Method 4.5.

(i) First we construct a matrix of order 9×2 consisting of all ordered pairs of F_3 , that is

$$M_1 = \begin{bmatrix} 0 & 0 \\ 0 & 1 \\ 0 & 2 \\ 1 & 0 \\ 1 & 1 \\ 1 & 2 \\ 2 & 0 \\ 2 & 1 \\ 2 & 2 \end{bmatrix}$$

(ii) Now sequentially augment third and fourth columns as explained in the method to obtain the matrix:

$$M_3 = \begin{bmatrix} 0 & 0 & 0 & 0 \\ 0 & 1 & 1 & 1 \\ 0 & 2 & 2 & 2 \\ 1 & 0 & 1 & 2 \\ 1 & 1 & 2 & 0 \\ 1 & 2 & 0 & 1 \\ 2 & 0 & 2 & 1 \\ 2 & 1 & 0 & 2 \\ 2 & 2 & 1 & 0 \end{bmatrix}$$

The rows of the M_3 are the codewords of the desired equidistant constant weight code. Let us now recall Theorem 2.2 of [7] which, in view of Corollary 2.1 of [7], is restated below in terms of Hamming distance d instead of Group distance D_m (see Definition 2.4 of [7]):

Theorem 4.8

Let $C[n, k, d]$ be a linear MDS code over F_q with $n \leq q + 1$. Then, C is an m -TA code if and only if $d > (1 - 1/m^2)n$, $m = 2, 3, \dots$

Now observe that the code obtained in Example 2 is a ternary Hamming $[4, 2, 3]$ code (cf. Example 6.2 of [12]) and is a 2-TA code due to Theorem 3.2. Moreover it is a linear MDS (extended RS) code over F_3 such that the length of the code is $n = q + 1 = 4$ and minimum distance $d = (1 - \frac{1}{2^2})n = 3$. This shows that Theorem 4.8 is not true for the above code. In fact direct part of this theorem follows in view of a result of [3], [10] stated below:

Theorem 4.9

If C is a code of length n and minimum distance d such that $d > (1 - \frac{1}{m^2})n$, where $m \geq 2$. Then C is an m -TA code.

In order to check the error in the converse part, we revisit the proof of Theorem 2.2 of [7] and we observe that the following is claimed in the proof of the converse part (see equation (3) of [7]).

Claim 4.10

Let $C[n, k, d]$ be a linear MDS code over F_q with $n \leq q + 1$ and $m \geq 2$ be an integer. Then there always exists a collection of m codewords $\underline{u}_l = (u_{l,0}, u_{l,1}, \dots, u_{l,n-1}) \in C - \{\underline{0}\}$, $1 \leq l \leq m$, such that for each \underline{u}_l , $u_{l,n-l(k-1)} = u_{l,n-l(k-1)+1} = \dots = u_{l,n-(l-1)(k-1)-1} = 0$ and $u_{1,i} \neq u_{l,i}$ for $2 \leq l \leq m$, $0 \leq i \leq n - m(k-1) - 1$. Here $\underline{0}$ is all-zero codeword.

We show that this claim is not true in the following two cases:

(i) $k = 1$ and $m \geq 2$. In this case C is $[n, 1, n]$ code and each codeword $\underline{0} \neq \underline{u}$ in C has all entries non-zero. This obviously shows that Claim 4.10 cannot hold.

(ii) $k = 2$, $m = 2$ and $q = n - 1$. In this case we consider two codewords $\underline{u}_1 = (u_{1,0}, u_{1,1}, \dots, u_{1,n-1})$, $\underline{u}_2 = (u_{2,0}, u_{2,1}, \dots, u_{2,n-1}) \in C - \{\underline{0}\}$, such that for each \underline{u}_1 and \underline{u}_2 , $u_{1,(n-1)} = 0$ and $u_{2,(n-2)} = 0$. This setting is always possible since C is an $[n, 2, n-1]$ MDS code. Since $d(\underline{u}_1, \underline{0}) \geq n-1$ and $d(\underline{u}_2, \underline{0}) \geq n-1$, so $u_{1,i} \neq 0$ for any $0 \leq i \leq n-2$ and $u_{2,j} \neq 0$ for any $0 \leq j \leq n-3$ and $j = n-1$. Therefore, the last two positions, i.e., $(n-1)$ th and n th positions contribute 2 towards Hamming distance between \underline{u}_1 and \underline{u}_2 . Now if Claim 4.10 is true, then we must have $u_{1,i} \neq u_{2,i}$ for $0 \leq i \leq n-3$. On contrary, as discussed in [7] we suppose that there is one position t (there can be at most $k-1 = 1$ such entry) such that $u_{1,t} = u_{2,t}$. Now we show that the set

$S = \left\{ 0, \frac{u_{1,0}}{u_{2,0}}, \frac{u_{1,1}}{u_{2,1}}, \dots, \frac{u_{1,n-3}}{u_{2,n-3}} \right\}$ has $n - 1$ distinct elements of F_q . On contrary, let $\frac{u_{1,i}}{u_{2,i}} = \frac{u_{1,j}}{u_{2,j}} = r$ (say) for some $i \neq j$ and $0 \leq i, j \leq n - 3$. As discussed before, $u_{1,i}, u_{1,j} \neq 0$ for $0 \leq i, j \leq n - 3$, we have $r \neq 0$. Since C is a linear code, $ru_2 \in C$ and we obviously have $d(\underline{u}_1, ru_2) \leq n - 2$, which is a contradiction. Therefore, S has $n - 1$ distinct elements. Hence $S = F_q$ because of our supposition that $q = n - 1$. This in turn implies that there does not exist any λ such that $\lambda \underline{u}_2$ together with \underline{u}_1 , make the Claim 4.10 true. The fact that Claim 4.10 is not true for $k = 2, m = 2$ and $q = n - 1$ can be established in view of the fact that $[n, 2, n - 1]$ is an equidistant code over F_q for $n = q + 1$. For, we see in the earlier discussion that when $u_{1,(n-1)} = 0$ and $u_{2,(n-2)} = 0$, then $(n - 1)$ th and n th positions contribute 2 towards Hamming distance between \underline{u}_1 and \underline{u}_2 . Since $[n, 2, n - 1]$ is an equidistant code over F_q for $n = q + 1$, so among the first $n - 2$ positions there always exists exactly one position $0 \leq k \leq n - 3$ such that $u_{1,k} = u_{2,k}$. Therefore, it is not possible to find a pair of codewords \underline{u}_1 and \underline{u}_2 such that equation (3) of [7] holds, when last two positions contribute 2 towards Hamming distance between \underline{u}_1 and \underline{u}_2 . Thus Claim 4.10 cannot hold in case $k = 2, m = 2$ and $q = n - 1$. We now see whether the codes due to cases (i) and (ii) above have traceability property or not.

(i) If $k = 1$, then $d = n > (1 - 1/m^2)n$ for all $m \geq 2$. So by Theorem 4.9, C is an m -TA code for all $2 \leq m \leq n - 1$.

(ii) If $k = 2, m = 2$ and $n = q + 1$, then $d = n - 1 = q$. Now we differentiate three cases as follows:

(a) If $q > 3$, then $n > 4$ and so $d = (n - 1) > (1 - 1/2^2)n$ and so by Theorem 4.9, C is a 2-TA code.

(b) If $q = 3$, then $d = 3 = (1 - 1/2^2)4$ and by Theorem 3.2, C is a 2-TA code.

(c) If $q = 2$, then $d = 2 < (1 - 1/2^2)3$. Here $C = \{(0, 0, 0), (1, 0, 1), (0, 1, 1), (1, 1, 0)\}$. Now observe that $n - 3s + 2l = 3 - 3 \times 1 + 2 \times 0 = 0$ for codewords $a = (0, 0, 0), b = (1, 0, 1)$ and $c = (0, 1, 1)$ of C . Therefore, by Lemma 3.3, C is not a 2-TA code. We are now in a position to provide correct statement of Theorem 4.8 and its proof as follows.

Theorem 4.11

(I) Let $C[n, k, d]$ be a linear MDS code over F_q with $n \leq q + 1$. Then, C is an m -traceability code if and only if $d > (1 - 1/m^2)n, m = 2, 3, \dots$ except the case when $n = 4, k = 2$ and $q = 3$.

(II) The code $C = [4, 2, 3]$ over F_3 is a 2-TA code.

Proof

We can prove the result by considering the following five cases.

(i) $k = 1$, (ii) $k = 2, m = 2$ and $n = q + 1$, (iii) $k = 2, m = 2$ and $n < q + 1$, (iv) $k = 2, m \geq 3$ and $n \leq q + 1$ and (v) $k \geq 3, m \geq 2$ and $n \leq q + 1$. The cases (i) and (ii) which cover (II) and some

subcases of (I), have been proved in the paragraph preceding this theorem. While in the remaining cases (iii)–(v) the proof of Theorem 2.2 of [7] will work.

5, Classes of some non-linear equidistant codes as 2-TA codes

In this section we obtain some equidistant codes as 2-TA codes to demonstrate the usefulness of results proved in Section 3. In view of Theorem 4.9, if C is a code with minimum distance $d > 3n/4$ then C is a 2-TA code. In previous section we give one example of equidistant 2-TA code, i.e., $[4, 2, 3]$ code for which $2n/3 < d \leq 3n/4$. We now show the existence of some infinite classes of non-linear equidistant codes of length n with distance d such that $2n/3 < d \leq 3n/4$ and due to Theorem 3.2 these codes are 2-TA codes. We also show the existence of a class of 2-TA equidistant codes of length n with distance $d \leq 2n/3$.

Towards this end, we denote an equidistant code of length n , distance d and size N over Q with q elements by $E_q(n, d, N)$.

(I) We first deduce a class of codes using the results of [1].

Theorem 5.1

Cf. [1, Theorem 12]

Let $E_{q_1}(n_1, d_1, N_1)$ and $E_{q_2}(n_2, d_2, N_2)$ be two equidistant codes such that $d_1 = n_1 - 1$. Let the code E_{q_2} be optimal. Then for any k , $1 \leq k \leq q_2$ there exists an equidistant code $E_q(n, d, N)$ with parameters $q = \max(kq_1, q_2)$; $n = n_1 + n_2 - 1$; $d = d_1 + d_2$; $N = kM$, where $M = \min(N_1, N_2/q_2)$.

In order to get the desired class of $E_q(n, d, N)$ equidistant codes using above theorem, many choices of E_{q_1} and E_{q_2} given in [1] qualify for the purpose. Among all these choices, we choose that pair of E_{q_1} and E_{q_2} which provides a desired class of codes with better parameters. For this, we first obtain E_{q_1} using the result stated below.

Theorem 5.2

Cf. [1, Theorem 11 Cor. 3]

An optimal equidistant code $E_{q_1}(n, d, N)$ with parameters $q_1 = (m-1)l + 1$, $n_1 = ml + 1$, $d_1 = ml$, $N_1 = m(m-1)l + m$ exists for the following values of m and l :

(1) $m = 3$, $l \geq 1$ is any natural number;

(2) $m = 4$, $l \geq 1$ is any natural number.

(3) $m = 5$, $l \geq 1$ is any natural number with the following possible exceptions: $l = 2, 17, 2$

(4) $m = 8, l \geq 1$ is any natural number with the following possible exceptions: $l = 3, 11, 13, 20, 22, 23, 25, 26, 27, 28, 31, 38, 43, 47, 52, 53, 58, 59, 61, 67, 69, 76, 79, 93, 102, 103, 111, 112, 115, 123, 124, 125, 133, 134, 139, 140, 143, 174, 182, 191, 192, 195, 197, 199, 203, 208, 209, 211, 213, 218, 220, 223, 224, 227, 229, 230, 232, 237, 243, 247, 248, 250, 253, 254, 391, 437$.

Next let $E_{q_2}(n_2, d_2, N_2)$ be the Hadamard code due to the following result.

Theorem 5.3

Cf. [1, Lemma 5]

The existence of a Hadamard matrix H_n of order n is equivalent to the existence of an optimal binary equidistant code $E_2(4k-1, 2k, 4k)$.

Now we consider the two cases. First we take $q_1 = 2l + 1; n_1 = 3l + 1; d_1 = 3l; N_1 = 6l + 3$ and $q_2 = 2; n_2 = 4k - 1; d_2 = 2k; N_2 = 4k$. By using Theorem 5.1, we obtain an equidistant code with $q = 2l + 1$ (or $4l + 2$); $n = 3l + 4k - 1; d = 3l + 2k; N = 2k$ (or $4k$). Finally imposing the condition $2n/3 < d \leq 3n/4$, we have $2k - 2 < 3l \leq 4k - 3$. For a fixed number of alphabets q , the largest value of k , for getting the largest size N , which satisfy the above condition in k and l is $\lfloor 3l/2 \rfloor$. Thus there exists an infinite class of codes which we are looking for, with the parameters $q = 2l + 1$ (or $4l + 2$); $n = 3l + 4 \lfloor 3l/2 \rfloor - 1; d = 3l + 2 \lfloor 3l/2 \rfloor; N = 2 \lfloor 3l/2 \rfloor$ (or $4 \lfloor 3l/2 \rfloor$).

Similarly, by taking $q_1 = 3l + 1; n_1 = 4l + 1; d_1 = 4l; N_1 = 12l + 4$ and $q_2 = 2; n_2 = 4k - 1; d_2 = 2k; N_2 = 4k$, we get another class of codes $E_q(n, d, N)$ with $q = 3l + 1$ (or $6l + 2$); $n = 12l - 1; d = 8l; N = 4l$ (or $8l$).

(II) We now obtain two infinite classes of good equidistant codes using the results of [9] stated below:

Theorem 5.4

(i) Let q be a prime power, $k_1 \leq q$ an integer, $k_2 > 1$ an integer such that k_2 divides k_1 . If $q = k_1 + k_2 + 1$, then there exists a good equidistant $E_{(1+k_1/k_2)}(n = q(q-1), d = 2k_1q - k_1(k_1 + k_2), N = q)$ code.

(ii) If in addition to hypothesis in (i) above, k_2 is odd, then there exists a good equidistant $E_{(1+k_1/k_2)}(q(q-1)/2, q, k_1q - k_1(k_1 + k_2)/2)$ code.

In Theorem 5.4, let $k_1 = mk_2$ for some positive integer m and $2n/3 < d \leq 3n/4$. Then by putting $n = q(q-1)$ and $d = 2k_1q - k_1(k_1 + k_2)$ we get $2k_2(m+1)^2 + 2(m+1) < 3mk_2(m+1) + 6m$ and $3k_2(m+1)^2 + 3(m+1) \geq 4mk_2(m+1) + 8m$ and these can be further simplified to $(m+1)k_2(2-m) < 4m-2$ and $(m+1)k_2(3-m) \geq 5m-3$ respectively. Now it follows that these inequalities can hold together for $m = 2$ and $k_2 \geq 3$. Thus there is a class of equidistant codes which we were looking for. Similarly in view of Theorem 5.4 (ii) stated below, we

class of equidistant codes with distance d satisfying $2n/3 < d \leq 3n/4$. In this case again $m = 2$ but $k_2 \geq 3$ is an odd integer.

(III) Encheva and Cohen [4] have proved that Jacobsthal matrices generate ternary 2-SFPC codes. We now show that Jacobsthal matrices in fact generate ternary 2-TA codes. Towards this end we take p to be a prime of the form $4m + 3$ and use the following definition and a result related to Jacobsthal matrices.

Definition 5.5

[4], [11]

The Jacobsthal matrix (a_{ij}) is a $p \times p$ matrix whose rows and columns are labeled by $0, 1, 2, \dots, (p - 1)$ and $a_{ij} = \chi(j - i)$, where $\chi(i)$ is the Legendre's symbol, i.e., 0 if p divides i , +1 if i is a quadratic residue mod p , and -1 otherwise.

Lemma 5.6

[4], [11]

Let A denote $p \times p$ Jacobsthal matrix. Then $H = \begin{bmatrix} 1 & 1 \\ 1 & A - I \end{bmatrix}$ is a normalized Hadamard matrix of order $p + 1$, called Paley type Hadamard matrix.

Theorem 5.7

The above defined Jacobsthal matrix A is a 3-separating $[p, p, 3]$ matrix and hence the rows of A form a 2-TA code.

Proof

Let $A = \begin{bmatrix} r_1 \\ r_2 \\ \vdots \\ r_p \end{bmatrix}$. Since $p = 4m + 3$, $\chi(-1) = -1$ and therefore submatrix $\begin{bmatrix} (i, i) & (i, j) \\ (j, i) & (j, j) \end{bmatrix}$ of A formed

by parts of r_i and r_j with $i < j$ is $\begin{bmatrix} 0 & 1 \\ -1 & 0 \end{bmatrix}$ or $\begin{bmatrix} 0 & -1 \\ 1 & 0 \end{bmatrix}$. This implies that in $A - I$ this matrix gets changed into $\begin{bmatrix} -1 & 1 \\ -1 & -1 \end{bmatrix}$ or $\begin{bmatrix} -1 & -1 \\ 1 & -1 \end{bmatrix}$. Now by Lemma 5.6, $\begin{bmatrix} 1 & 1 \\ 1 & A - I \end{bmatrix}$ is a Hadamard Matrix of order $(p + 1) \times (p + 1)$, so we have for any two rows r, s of $A - I$, $|I(r, s)| = (p - 1) / 2$ and $d(r, s) = (p + 1) / 2$. Therefore for two rows r_i and r_j of A , $|I(r_i, r_j)| = (p - 3) / 2$ and $d(r_i, r_j) = (p + 3) / 2$. Thus the rows of A form ternary equidistant code of length p and distance $(p + 3) / 2$. Now we show that matrix A is a 3-separating $[p, p, 3]$ matrix. For $1 \leq i < j < k \leq p$, let r_i, r_j, r_k be any three rows of A . We claim that the entries of at least one column of

$S = \begin{bmatrix} (i, i) & (i, j) & (i, k) \\ (j, i) & (j, j) & (j, k) \\ (k, i) & (k, j) & (k, k) \end{bmatrix}$ formed by parts of rows r_i, r_j, r_k , are distinct. Now by Definition 5.5, we have $S = \begin{bmatrix} 0 & \chi(j-i) & \chi(k-i) \\ \chi(i-j) & 0 & \chi(k-j) \\ \chi(i-k) & \chi(j-k) & 0 \end{bmatrix}$.

If $\chi(i-j)\chi(i-k) = -1$, then first column of S consists of 3 distinct elements of F_3 as desired. If $\chi(i-j)\chi(i-k) = 1$, then $\chi(i-j) = 1 = \chi(i-k)$ or $\chi(i-j) = -1 = \chi(i-k)$. Again using the fact that $\chi(-1) = -1$, we have $\chi(j-i) = -1 = \chi(k-i)$ or $\chi(j-i) = 1 = \chi(k-i)$. This implies that $S = \begin{bmatrix} 0 & -1 & -1 \\ 1 & 0 & \chi(k-j) \\ 1 & \chi(j-k) & 0 \end{bmatrix}$ or $\begin{bmatrix} 0 & 1 & 1 \\ -1 & 0 & \chi(k-j) \\ -1 & \chi(j-k) & 0 \end{bmatrix}$.

Finally, since $\chi(j-k)\chi(k-j) = -1$, we get that all the entries of second or third column of S are distinct, proving that A is a 3-separating $[p, p, 3]$ matrix. Hence by Theorem 3.5 rows of A form a 2-TA code.

We see that rows of A form a equidistant 2-TA code of length $p = 4m + 3$ with distance $d = (p + 3) / 2 = 2m + 3 < 2p / 3$ for $k \geq 2$.

Conclusions. (i) We prove that an equidistant code of length n with distance $d > 2n / 3$ is always a 2-TA code.

(ii) We give necessary and sufficient condition for an equidistant code to be a 2-TA code.

(iii) We give a method for constructing 2-TA codes.

(iv) We give the correct version of Theorem 2.2 of [7] and its proof.






(v) We give some infinite families of equidistant codes which can be used as 2-TA codes. It will be interesting to obtain some other infinite families of equidistant codes for using them as 2-TA codes.

(vi) We also obtain some conditions under which an equidistant code is not a m -TA code, $m \geq 3$. However, one may try some other conditions under which an equidistant code becomes m -TA code.

Acknowledgments

The authors wish to thank the anonymous referees for giving very useful suggestions.

References

- [1] Bogdanova G.T., Zinoviev V.A., Todorov T.J.
On the construction of q -ary equidistant codes
Probl. Inf. Transm., 43 (2007), pp. 280-302
[View Record in Scopus](#) [Google Scholar](#)
- [2] Boneh D., Shaw J.
Collusion-secure fingerprinting for digital data
IEEE Trans. Inform. Theory, 44 (5) (1998), pp. 1897-1905
 [View PDF](#) [View Record in Scopus](#) [Google Scholar](#)
- [3] Chor B., Fiat A., Naor M.
Tracing traitors
Advances in Cryptology- Crypto'94, LNCS, vol. 839, Springer-Verlag (1994), pp. 257-270
 [View PDF](#) [CrossRef](#) [View Record in Scopus](#) [Google Scholar](#)
- [4] Encheva S., Cohen G.
Some new p -ary two-secure frameproof codes
Appl. Math. Lett., 14 (2001), pp. 177-182
Article  [Download PDF](#) [View Record in Scopus](#) [Google Scholar](#)
- [5] Fernandez M., Cotrina J.
Equidistant binary fingerprinting codes: Existence and identification algorithms
Computational Science and its Applications, LNCS, Springer-Verlag, Berlin, Heidelberg (2005), pp. 527-536
 [View PDF](#) [CrossRef](#) [View Record in Scopus](#) [Google Scholar](#)
- [6] Hollmann H.D.L, Lint J.H. Van, Linnartz J.P., Tolhuizen L.M.G.M.
On codes with the identifiable parent property
J. Combin. Theory Ser. A, 82 (1998), pp. 121-133
Article  [Download PDF](#) [View Record in Scopus](#) [Google Scholar](#)
- [7] Jin H., Blaum M.
Combinatorial properties of traceability codes using error correcting codes
IEEE Trans. Inform. Theory, 53 (2) (2007), pp. 804-808
[View Record in Scopus](#) [Google Scholar](#)
- [8] MacWilliam F.J., Sloane N.J.A.
The Theory of Error Correcting Codes, North Holland Publishing Company (1977)
[Google Scholar](#)
- [9] Sinha K., Wang Z., Wu D.

Good equidistant codes constructed from certain combinatorial designs

Discrete Math., 308 (2008), pp. 4205-4211

Article  Download PDF View Record in Scopus Google Scholar

[10] Staddon J.N., Stinson D.R., Wei R.

Combinatorial properties of frameproof and traceable codes

IEEE Trans. Inform. Theory, 47 (3) (2001), pp. 1042-1049

View Record in Scopus Google Scholar

[11] Stinson D.R.

Combinatorial Designs: Constructions and Analysis, Springer, New York (2004)

Google Scholar

[12] Vermani L.R.

The Theory of Error Correcting Codes, Chapman and Hall, CRC (1996)

Google Scholar

© 2016 Elsevier B.V.



Copyright © 2021 Elsevier B.V. or its licensors or contributors.
ScienceDirect® is a registered trademark of Elsevier B.V.

RELX™

FEEDBACK 

Journal of
**Information &
Optimization Sciences**

ISSN 0252-2667 (Print)
ISSN 2169-0103 (Online)

A Journal Devoted to Advances in Information Sciences,
Optimization Sciences and Related Aspects

VOLUME 38

NUMBER 8

NOVEMBER 2017

Reprint of

A Class of 2-FP Codes

by

A. KATHURIA, S. BATRA AND S. K. ARORA

pp. 1311–1324

 **TARU PUBLICATIONS**



Taylor & Francis
Taylor & Francis Group

JOURNAL OF INFORMATION & OPTIMIZATION SCIENCES

ISSN: 0252-2667 (Print)
ISSN: 2169-0103 (Online)

www.tarupublications.com/jios.html
www.tandfonline.com/tios

CHIEF EDITOR

BAL KISHAN DASS

ADVISORY EDITORS

P. Corsini

Y. Singh

J. Watada

ASSOCIATE EDITORS

R. M. Ali	H. Arsham	R. Cambini	D. K. Despotis	M. M. Deza	T. Fukuda
S. Hirasawa	I. Honkala	M. Ito	E. Lasserra	J.-Y. Lee	J. E. Martinez-Legaz
P. Mazzoleni	W. Pedrycz	H. Pham	A. Rosalsky	K. P. Shum	B. Viscolani

The *Journal of Information and Optimization Sciences (JIOS)* is published in one volume per year of eight issues in the months of January, March, April, May, July, September, October and November. This is a world leading journal publishing high quality, rigorously peer-reviewed original research in all mathematically-oriented theoretical and applied topics in information sciences, optimization sciences and related areas. Subjects include but are not limited to:

- Information Sciences
- Optimization Sciences
- Database Management
- Applications to Technology
- Information Theory
- Operational Research
- Control Theory
- Information Technology
- Mathematical Programming
- Applications to Engineering Sciences

SUBSCRIPTION INFORMATION

Annual subscription rates (2018):

	INDIA	SAARC	USA
Print + Free Online	Rs. 8000.00	US\$ 200.00	US\$ 911.00

Print prices include Air-Mail postage and handling. Back issues are also available at the current rates.

Contacts for Subscription Orders:

From India and SAARC:

 **TARU – Books & Journals**
G-159, Pushkar Encalve
Pashchim Vihar
New Delhi 110 063, INDIA
Phone : +91-11-47234452, 25260534
E-mail : info@tarubooks.com
Web Site : www.tarubooks.com

From Rest of the World:

 **Taylor & Francis**
Taylor & Francis Group
Phone : +44 (0)207 017 7720
E-mail : subscriptions@tandf.co.uk
Web Site : www.tandfonline.com

© Taru Publications

Commercial use of this journal or copying or reprinting needs a specific permission from the Publishers:

 **TARU PUBLICATIONS**
G-159, Pushkar Enclave
Pashchim Vihar
New Delhi – 110063, INDIA
Phone : +91-11-25264782
E-mail : info@tarupublications.com
Web Site : www.tarupublications.com

 **Taylor & Francis**
Taylor & Francis Group
2nd Floor, 4 Park Square
Milton Park, Abingdon
OX14 4RN, UK
Web Site : www.tandfonline.com

A Class of 2-FP Codes

Anu Kathuria *

The Technological Institute of Textile & Sciences
Bhiwani 127021
Haryana
India

Sudhir Batra †

Department of Mathematics
DCR University of Science and Technology
Murthal
Sonapat 131039
Haryana
India

S. K. Arora

Department of Mathematics
M. D University
Rohtak 124001
Haryana
India

Abstract

In this paper we propose an explicit construction of a new class of binary 2-frameproof code of size $4(9+9n)$ and length $4(4+3n)$, $n \geq 1$. For this new class of 2-frameproof code, we show that the size of the code is almost three times the length of the code. By the definition of frameproof code in [2,4] for a code C being 2-frameproof, minimum distance d of the code is given by $d > \frac{n}{2}$, n is the length of the code. Moreover, as Plotkin Bound [18] relates the size of the code with minimum distance d and length of the code n for $q = 2$ defined as

*E-mail: anu_sept24@rediffmail.com

†E-mail: batrasudhir@rediffmail.com

$A_2(n, d) \leq 2^{\lfloor \frac{d}{2d-n} \rfloor}$ if $d > \frac{n}{2}$. Here for this new class of binary 2-frameproof code, we show that the size of the code is large than the size of the code as obtained in Plotkin Bound[18].

Keywords: Error Correcting Code, Frameproof Code, Plotkin Bound.

1. Introduction

Digital Fingerprinting is a technique that is used to protect intellectual rights by preventing illegal redistribution of digital data(films, software, music etc).It is facilitated by collection of codes called fingerprinting codes. These fingerprinting codes examine the interpretation of fingerprints embedded into digital objects to use it as a method of protecting intellectual rights. Before selling any digital object in the market a merchant just embeds some marks into the content .This marking, known as fingerprint allows buyer identification. Infact, a fingerprint is a string over an alphabet and a fingerprinting code is collection of fingerprints.it is embedded into digital objects such that it is not easy for a buyer to tamper with. However, if one has multiple copies of the same object with different fingerprints,he may compare the copies and detect where the marks are different and one might be able to change the marks on detected positions. In this way,pirates may not only redistribute the copies illegally by changing fingerprints but can also frame innocent users. To prevent this Boneh and Shaw introduced c-frameproof codes and c-secure codes.

1.1 Related Work

The study of objects related to frameproof codes in the literature goes back to 1960's as Renyi introduced first the concept of a separating system in his papers concerning certain information- theoretic problems [14]-[17]. After that the concept was defined again in cryptography several decades later, under different scenarios and purposes. Besides the frameproof codes suggested by Boneh and Shaw in 1998, variants of such codes have become objects of study by many researchers. In [4,5] Stinson and Wei suggested some constructions of frameproof codes by using combinatorial structures such as t-designs, error-correcting codes and perfect hash families.Several constructions of c-frameproof codes are discussed in [6,14,15,16,17,18] over non binary symbols using balanced incomplete block designs. Although the construction of frameproof codes was first addressed in [3]. In this paper they define the c-frameproof code

over binary field, which is smaller in size and results in more number of codewords by increasing the length of the code. However construction of c-frameproof code given by us leads to the new class of 2-frameproof code over binary field in which the size of the code is almost three times the length of the code.

1.2 Organization of the paper

This paper is organized as follows. In Section 2, we give Basic definitions and necessary background of frameproof codes. In Section 3, we start our discussion by defining Marking Assumption which we follow to construct this class of 2-frameproof code. The main result of the paper is presented in Section 4, in form of lemma and then a theorem stating that this construction discussed above is in general a 2-frameproof code.

2. Definitions and Basic results on Frameproof codes

Here we give definition of frameproof codes and some basic properties of frameproof codes to be used in further discussion.

2.1 Frameproof Codes

Frameproof Codes provide protection against framing attack i.e. in a c-frameproof code, a collusion of upto c colluders cannot construct a copy of the object containing the codeword of the buyer not in colluding set. The formal definition [3] is as follows-

Let Q be an alphabet of size q representing the q different sets of marks. The letters in Q will be denoted by the integers from 1 to q .

Definition 2.1:

- (i) A set $T = \{w_{(1)}, w_{(2)}, w_{(3)} \dots w_{(n)}\} \subseteq Q^l$ will be called an (l, n) code. For $i \in \{1, 2, 3, \dots, l\}$ we say that the position ' i ' undetectable for C if the words assigned to users in C match in their i^{th} position.
- (ii) If $T = \{w_{(1)}, w_{(2)}, w_{(3)} \dots w_{(n)}\}$ be an (l, n) code and C be a coalition of users. Let R be the set of undetectable positions of C . The feasible set $F(C)$ is defined as $F(C) = \{w \in (Q \cup \{?\})^l \text{ s.t. } w|_R = w_u|_R\}$ for some user ' u ' in C . In other words, the feasible set contains all words which match the coalition's undetectable position '?' (say).
- (iii) Marking Assumption: It states that any coalition of c -users is only capable of creating an object whose fingerprint lies in the feasible set of coalition.

- (iv) The distance $d(w_{(1)}, w_{(2)})$ between any two codewords $w_{(1)} = (x_1, x_2, x_3, \dots, x_l)$ and $w_{(2)} = (y_1, y_2, y_3, \dots, y_l)$ of a code of length l is the number of positions i in which $x_i \neq y_i$ for $1 \leq i \leq l$.

Definition 2.2: A (l, n) code T is c -frameproof if for every set $W \subset T$ of size at most c , satisfies $F(W) \cap T = W$.

Thus, in a c -frameproof code, the only codewords in the feasible set of a coalition of at most c users are the codewords of the members of the coalition.

2.3 Boneh and Shaw[3] obtained a sufficient condition for a c -frameproof code in the result given as follows:

"Let T be a c -frameproof (l, p) code and C be an $(n, M, d)_q$ Error Correcting Code. If T' be the composition of T and C , then T' is a c -frameproof code, provided $d > \left(1 - \frac{1}{c}\right)n$, $c = 2, 3, 4, \dots$

Remark: In the result discussed above, C is a code defined over the set $Q = \{1, 2, 3, 4, \dots, q\}$ of q symbols. In the composition, T' discussed above, we replace each ' q ' symbol of C with a codeword of T . Here T is a frameproof-code defined over binary field smaller in size. The main idea of combining is to increase the number of codewords in resulting c -frameproof code i.e. in composition of T and C by increasing the length from l to ln . Moreover it is obvious that any code C is 2-frameproof code if $d > \left(1 - \frac{1}{2}\right)n$.

2.4 Plotkin Bound[18]: Let C be an (n, M, d) code over F_q such that $d > \frac{n}{2}$, then

$$\text{in the binary case } A_2(n, d) \leq 2 \left\lfloor \frac{d}{2d-n} \right\rfloor.$$

Corollary 2.4.1: Following bounds also hold:

- (1) if d is even, $A_2(2d, d) \leq 4d$
- (2) if d is odd, $A_2(2d, d) \leq 2d + 2$

3. Construction

In this section we describe the method for construction of a new class of 2-FP codes. Moreover we show that the condition for a code being 2-FP code given by Boneh and Shaw[3] is a sufficient condition only but not necessary.

3.1 Marking Assumption

First we provide the marking assumption in view of definition of frameproof code.

- (i) Pirates can make change only at detected positions.
- (ii) Pirate can create one of the alphabet symbols matching any one of their copies in place of detected position.

3.2 A class of 2-FP Codes: Construction

To obtain this class of 2-FP codes, the procedure is described in four different phases given below.

First we construct a code over $2(4 + 3n)$ symbols, where $n \geq 1$ is an integer, in three phases and finally in the fourth phase we replace each of $2(4 + 3n)$ symbols used so far by strings of length $(4 + 3n)$ over $\{0, 1\}$ in the codewords obtained in phase III, and obtain the desired code.

Phase I. Consider the set $Q = \{1, 2, 3, 4\}$ of four symbols and obtain 9 codewords using these symbols in the manner explained below:

- (a) Choose the first codeword as 1 2 3 4.
- (b) Construct other two codewords by retaining first position of the codeword obtained in (a) fixed and giving cyclic shift to the symbols present at remaining positions.
- (c) Now obtain another codeword by shifting the codeword taken in (a) cyclically and then form other codewords by fixing the first position of codeword so obtained and giving cyclic shift to the remaining symbols of this codeword, i.e. by repeating the procedure given in (b).

In this case, cyclic shift of the codeword obtained in (a) generates the codewords (2 1 4 3), (3 1 2 4). Using these three codewords and applying steps (b) and (c) over there, there will be three arrays of codewords i.e. A_1, A_2, A_3 where each array contains three codewords (Since length of each codeword is 4). So, at the end of this phase, we can construct 9 codewords using four symbols in which the minimum distance is 3. In fact we note that for these arrays the distance between any two codewords of an array is 3 and the distance between any two codewords of two different arrays is 4.

Phase II. Now introduce ' $3n$ ' more symbols other than 1, 2, 3 or 4 and add 6 ($3n$) more codewords by stating the procedure given below. Here we illustrate this case for $n = 1$, which can be extended to any n .

Since we are considering $n = 1$, so if we take 5, 6 and 7 as three symbols then 9 codewords will be introduced such that minimum distance of 3 can be maintained. The codewords which are obtained upto Phase II are denoted with master codewords.

- (a) In the array A_1 , replace the symbol '1' with '5', '3' with '6', and '4' with '7' and retain 2 as such. Similarly in array A_2 , replace the symbol '2' with '6', '4' with '7', and '1' with '5' and retain '3' as such. Furthermore, in array A_3 , replace the symbol '3' with '7', '1' with '5', and '2' with '6' and retain '4' as such. Finally we get three more new arrays with each array consisting of three codewords. Let these arrays be denoted with A_4 , A_5 and A_6 .

Here note that if we have $n = 2$, we have three more symbols, say 8, 9 and 10 and we get the array of three codewords i.e. A_7 , A_8 , A_9 .

Phase III. In this phase, introduce $(4 + 3n)$ more symbols, corresponding to earlier $(4 + 3n)$ symbols. Now using these symbols and earlier one's, we introduce corresponding to master codeword obtained in phase I and phase II, three more codewords. We call this set of four codewords i.e. master codeword and the above three codewords as a block. Thus we have, $(4 + 3n)$ blocks and a total of $4(9 + 9n)$ codewords. These blocks are obtained using the procedure explained below:

Since we illustrate the procedure for $n = 1$ again using the master codewords obtained in phase I and II. So as already mentioned, we introduce $4 + 3 \cdot 1 = 7$ more symbols corresponding to earlier 7 symbols of phase I and II. Let the 7 symbols introduced are 8, 9, 10, 11, 12, 13, 14 corresponding to 1, 2, 3, 4, 5, 6 and 7 and these new symbols are defined as complements of earlier symbols. Although we will justify it in next phase. Now corresponding to every master codeword we define a block of four codewords by applying the following steps:

- (a) Choose a master codeword and consider this as the first codeword of the block.
- (b) To get the 2nd codeword of this block, we keep 1st and 2nd positions same and substitute the complements at 3rd and 4th positions of first codeword.

- (c) Third codeword of this block is formed by fixing 1st and 3rd position and writing down the complements of symbols existing at remaining positions.
- (d) To obtain the 4th codeword, fix 1st and 4th position and substitute the complements of symbols at the other positions.

For example, if we select the master codeword 1 4 2 3, then the block constructed by applying the rules (b), (c) and (d) above will be

1	4	2	3
1	4	9	10
1	11	2	10
1	11	9	3

Since corresponding to every master codeword we construct a block of four codewords, so there being 18 master codewords, we will have a total of 72 codewords for $n = 1$.

Here, note that if $n = 2$, then we need to introduce $4 + 3 \cdot 2 = 10$ more symbols corresponding to earlier 10 symbols of phase I and II and these 10 new symbols can be 11, 12, 13, 14, 15, 16, 17, 18, 19, 20 corresponding to 1, 2, 3, 4, 5, 6, 7, 8, 9, 10.

Phase IV. In this phase each of $(4 + 3n)$ symbols, i.e. 1, 2, 3, 4, ..., j , ... $(4 + 3n)$ are replaced with strings of length $(4 + 3n)$ over $\{0, 1\}$ such that symbol ' j ' is replaced with a string in which entry at j^{th} position is '1' and rest are zeros.

The remaining $(4 + 3n)$ symbols i.e. $(4 + 3n) + 1$, $(4 + 3n) + 2$, ... $(4 + 3n) + j$, ... $(4 + 3n) + (4 + 3n)$ are also replaced with strings of length $(4 + 3n)$ over $\{0, 1\}$ such that the symbol $(4 + 3n) + j$ is replaced with a string in which j^{th} entry is '0' and rest are 1's. This justifies that we call the symbol $(4 + 3n) + j$ as the complement of the symbol ' j ' as mentioned earlier in phase III.

Thus for $n = 1$, we replace the symbols 1, 2, 3, 4, 5, 6 and 7 with the strings of length 7 each i.e. by

1000000, 0100000, 0010000, 0001000, 0000100, 0000010, 0000001, respectively and the symbols 8, 9, 10, 11, 12, 13 and 14 by the strings

0111111, 1011111, 1101111, 1110111, 1111011, 1111101, 1111110 respectively.

Therefore, we get 72 binary codewords of length $4(4 + 3 \cdot 1) = 28$ each for $n = 1$. Here if we take $n = 2$, then the symbols 1, 2, 3, 4, 5, ..., 10 will be replaced with strings of length 10 each and rest of things are done

correspondingly to obtain a total of $4(9+9.2) = 108$ codewords of length $4(4 + 3.2) = 40$ each and in the same way it can be constructed for any n .

In general, we have constructed here a code C consisting of $4(9+9n)$ codewords with each codeword of length $4(4 + 3n)$ using the symbols '4 + 3n' in number i.e. 1, 2, 3, 4, ..., 4 + 3n.

Remark : For the case $n=1$, if length of the code is 28 and distance $d = 14$, then the result 2.4.1(1) gives the maximum number of codewords by Plotkin Bound as $A_2(2.14, 14) \leq 4.14 = 56$. But in this construction suggested by us for $n = 1$, we get 72 codewords in total.

(2) For the case $n = 2$, if length of the code is 40 and distance $d = 21$, then

by result 2.4 of Plotkin Bound, $A_2(n, d) \leq 2 \left\lfloor \frac{d}{2d-n} \right\rfloor$

Thus we can have $A_2(40, 21) \leq 2 \left\lfloor \frac{21}{2 \cdot 21 - 40} \right\rfloor = 40$ codewords. Here for this construction we get 108 codewords as discussed above.***

Now in this section we prove the results which are required to show that the code C constructed above leads to 2-FP code in general.

4. Proof of the Theorem: To prove our theorem here we give a lemma first.

Lemma 4.1: Let $a = (a_1 a_2 a_3 a_4)$ and $b = (b_1 b_2 b_3 b_4)$ be two codewords obtained in phase III of the construction. Then for $1 \leq i \leq 4$, we have

- (i) If $d(a, b) = 4$, then there is at most one position i such that b_i is a complement of a_i .
- (ii) If $d(a, b) = 3$, then there is no position 'i' such that b_i is a complement of a_i .

Proof. Let $S = \{1, 2, 3, 4, 5, 6, 7\}$ and $T = \{8, 9, 10, 11, 12, 13, 14\}$

- (i) If $d(a, b) = 4$, then a and b belong to different blocks. Now we claim that there exists at most one position i such that b_i is complement of a_i (or a_i is complement of b_i). On contrary, suppose that there are two positions i and j such that b_j and b_i are complements of a_i and a_j respectively. Now, since b_j and b_i are complements of a_j and a_i , then as discussed in the Phase III, we must have a codeword c in the block of b which have the symbols a_j and a_i at j th and i th positions. This implies that $d(c, a) \leq 2$, which is a contradiction, because a and c belong to different blocks. It proves (i).

(ii) If $d(a, b) = 3$, then a and b belong to different blocks. First we suppose that $a = a_1 a_2 a_3 a_4$ and $b = a_1 b_2 b_3 b_4$

w.l.o.g. suppose that b_2 is a complement of a_2 such that $b_2 \in T$, then $a_2 \in S$. Now since $a_1 \in S$, therefore, we have that $c = a_1 a_2 c_3 c_4$ is the master codeword of a for some symbols c_3 and c_4 . Further, we also have that $d = a_1 a_2 d_3 d_4$ is the master codeword of b for some symbols d_3 and d_4 . Now $d(c, d) \leq 2$, which is not possible because c and d being the master codewords of a and b will belong to different blocks.

Now let $a = a_1 a_2 a_3 a_4$ and $b = b_1 a_2 b_3 b_4$. Now w.l.o.g. suppose that b_3 is complement of a_3 such that $b_3 \in T$ and $a_3 \in S$. Using the form of codewords constructed in phase III we have a codeword $c = a_1 a_2 b_3 c_4$, where b_3 and c_4 are complements of a_3 and a_4 respectively. Then a and c belong to same block. Now $d(b, c) \leq 2$, which is again not possible because a and b belong to different blocks. This proves (ii) ■

Theorem 4.2: *The code C constructed above is 2-FP code.*

Proof: We prove the result for $n = 1$, i.e. the code C consisting of 72 codewords of length 28 over the binary field is 2-frameproof code. The proof can easily be extended for the general case.

Let $a = a_1 a_2 a_3 a_4$ and $b = b_1 b_2 b_3 b_4$ collude.

Now $a_i, b_i \in \{1, 2, 3, 4, 5, 6, 7, 8, 9, 10, 11, 12, 13, 14\}$

Let $S = \{1, 2, 3, 4, 5, 6, 7\}$ and $T = \{8, 9, 10, 11, 12, 13, 14\}$

if $a_i = b_i$, then in the collusion word we must have the symbol a_i (correspondingly its replacement as a string of 0's and 1's in Phase IV) present as such.

Case I: If $a_i \neq b_i$ and $a_i, b_i \in S$ (or T), then the symbols a_i and b_i cannot form a codeword other than a_i or b_i . That is even if the symbols a_i and b_i are replaced by binary strings of length 7 as discussed in phase IV and these strings are interacted, then either any of the string (either of a_i or b_i) may be retained or can be changed to another string which is not corresponding to any of the symbols of $S \cup T$. For if $a_i = 1000000$ and $b_i = 0100000$ then a_i and b_i can produce a string which is different from a_i and b_i and contains exactly two 1's or all zero's and that string is not corresponding to any of the symbols of $S \cup T$.

Similarly, if $a_i = 1111110$ and $b_i = 1111101$, then again a_i and b_i can produce a string different from a_i and b_i which contains either all 1's

or exactly two zero's and which is again not corresponding to any of the symbol in $S \cup T$.

Case II: If $a_i \neq b_i$ and $a_i \in S$, $b_i \in T$ and b_i is not a complement of a_i . Then again as discussed in case I, interaction of a_i and b_i as binary strings cannot produce a string which is corresponding to a symbol of $S \cup T$, (Different strings must contain atleast two and atmost five 1's).

Case III: If $a_i \neq b_i$ and $a_i \in S$, $b_i \in T$ and b_i is a complement of a_i . In this case, interaction of a_i and b_i as binary strings can produce a string corresponding to any of the symbol of $S \cup T$.

Now we discuss these cases one by one.

(A) $d(a, b) = 4$, (B) $d(a, b) = 3$, (C) $d(a, b) = 2$.

(A) Let $d(a, b) = 4$, then by Lemma 4.1, there is atmost one position i such that b_i is complement of a_i . Now as discussed in Case III interaction of a_i and b_i as binary strings can produce a string corresponding to any of the symbol of $S \cup T$. There are three more positions where a_j and b_j differ, but are not complements of one another.

(a) First we consider the case, when there is exactly one position i such that b_i is a complement of a_i , $1 \leq i \leq 4$ w.l.o.g. let $a = a_1 a_2 a_3 a_4$ and such that $b_1 \in T$, $a_1 \in S$ and a_1 is a complement of a_1 .

Let the collusion word of a and b be $c = c_1 c_2 c_3 c_4$. Here c_1 can be any of the symbol (or equivalently its binary string) used in the code as discussed in case III. Since b_i is not a complement of a_i , $2 \leq i \leq 4$, so there as discussed in case I and II, in the collusion word either we have

- (i) The Binary Strings which are not corresponding to any of the symbol used in phase III can be produced for $i = 2, 3, 4$ or
- (ii) The Binary strings corresponding to symbols a_2, a_3, a_4 or b_2, b_3, b_4 are retained at the respective positions.

In case (i), if a binary string is not corresponding to any of the symbol used then the collusion word cannot be a codeword and therefore this will not frame an innocent user.

In case (ii), the collusion word can be either

- (i) $c = c_1 a_2 a_3 b_4$ (ii) $c = c_1 a_2 b_3 a_4$
- (iii) $c = c_1 b_2 a_3 a_4$ (iv) $c = c_1 b_2 b_3 a_4$
- (v) $c = c_1 b_2 a_3 b_4$ or (vi) $c = c_1 a_2 b_3 b_4$

Here $a_1 \in S \cup T$ can be any of the symbol used.

Now if $c = c_1 a_2 a_3 b_4$, then because c_1 can be a_1 so $d(a, c) = 1$ or 2.

If $d(a, c) = 1$, then ' c ' is obviously not a codeword. If $d(a, c) = 2$, then a and c must belong to same block. Now, using the forms of the codes of a block (see phase II of the construction) we get that c_1 and b_4 must be the complements of a_1 and a_4 , i.e. $c_1 = b_1$ and a_4 is complement of a_4 which is a contradiction to the fact that there is atmost one position ' i ' such that b_1 is complement of a_1 . Therefore $c = c_1 a_2 a_3 b_4$ is not a codeword. Similarly we can prove that other forms of c in (ii), (iii), (iv), (v) or (vi) are also not codewords. Hence we cannot frame an innocent user by these collusion words.

- (b) Second we consider the case, when at any position $1 \leq i \leq 4$, b_i is not a complement of a_i . In this case we also prove that the collusion words obtained using $a = a_1 a_2 a_3 a_4$ and $b = b_1 b_2 b_3 b_4$ are not the codewords. The proof can be followed on similar lines as in case (a) above.

- (B) Let $d(a, b) = 3$, then by Lemma 4.1, there is no position ' i ' such that b_i is a complement of a_i , where $1 \leq i \leq 4$.

w.l.o.g. let $a = a_1 a_2 a_3 a_4$ and $b = b_1 b_2 b_3 b_4$

Let $c = c_1 c_2 c_3 c_4$ be a collusion word of a and b .

Since b_i is not the complement of a_i , for any $2 \leq i \leq 4$, then in view of case I and II, so in the collusion word, either

- (i) the binary strings which are not corresponding to any of the symbol used in phase III, i.e. belonging to $S \cup T$ can be produced for $i = 2, 3, 4$ or
- (ii) the binary strings corresponding to the symbols a_2, a_3, a_4 or b_2, b_3, b_4 are retained at these respective positions.

In case (i) being the same as in case (A) therefore this will not frame an innocent user.

In case (ii), the collusion word can be either

- (i) $c = a_1 a_2 a_3 a_4$ (ii) $c = a_1 a_2 b_3 a_4$
 (iii) $c = a_1 b_2 a_3 a_4$ (iv) $c = a_1 b_2 b_3 a_4$
 (v) $c = a_1 b_2 a_3 b_4$ (vi) $c = a_1 a_2 b_3 b_4$

Now observe that in (i), (ii), (iii) given above $d(a, c) = 1$, therefore ' c ' cannot be a codeword and hence this will not frame an innocent

user. If we consider the (iv) case, i.e. let $c = a_1 b_2 b_3 a_4$, then $d(a, c) = 2$ and $d(b, c) = 2$.

Therefore a, b and c all belong to the same block. But we have assumed that a and b are in different blocks. Hence c is not a codeword.

Similarly, other forms of c in (v) and (vi) cannot be the codewords. Hence we cannot frame an innocent user by these collusion words.

(C) $d(a, b) = 4$. This implies that a and b belong to same block. So by using the form of codes obtained in phase III we can suppose that

$$(i) \quad a = a_1 a_2 a_3 a_4$$

$$b = a_1 a_2 b_3 a_4$$

$$(ii) \quad a = a_1 a_2 a_3 a_4$$

$$b = a_1 b_2 a_3 b_4$$

$$(iii) \quad a = a_1 a_2 a_3 a_4$$

$$b = a_1 b_2 b_3 a_4$$

$$(iv) \quad a = a_1 a_2 b_3 b_4$$

$$b = a_1 b_2 a_3 a_4$$

$$(v) \quad a = a_1 a_2 b_3 b_4$$

$$b = a_1 b_2 b_3 a_4$$

$$(vi) \quad a = a_1 b_2 a_3 b_4$$

$$b = a_1 b_2 b_3 a_4$$

where $a_1, a_2, a_3, a_4 \in S$ and $b_2, b_3, b_4 \in T$.

The symbols b_2, b_3, b_4 are complements of a_2, a_3 and a_4 respectively.

Let ' c ' be a collusion word obtained by interaction of a and b in any of the above cases. Since $d(a, c) = 2 = d(b, c)$, therefore a, b and c belong to the same block but in that block there are exactly two codewords in which the symbols at two fixed positions are same, therefore c cannot belong to block a and b which is a contradiction. Hence, no any innocent user can be framed in this case. it completes the proof of the theorem ■

5. Conclusion

If $d > n/2$, then we know that a code C is n -frameproof by [3]. But in the code C discussed here $d < n/2$. it shows that the condition above for this class of 2-FP code comes out sufficient only but not necessary. Moreover if one wishes to replace the non-binary digit of this new class

of 2-frameproof code with any other string of binary digits i.e. instead of the complements of each binary string, then it may or may not be a 2-frameproof code. Although here we present a case in which this code C does not come out as 2-frameproof code.

if we replace symbol 8 with binary string 0011000, symbol 9 with 0111000, symbol 10 with 0000011, symbol 11 with 0010100, symbol 12 with 1000001, symbol 13 with 1100000 and symbol 14 with 0110000, then if these two codewords (2 4 10 8) and (5 13 14 2) collude with their representations as; 0100000, 0001000, 0000011, 0011000

0000100, 1100000, 0110000, 0100000 then they can generate a new codeword

0100000, 1100000, 0000001, 0111000 and this is the codeword (5 13 7 9). So an innocent user can be framed in this case. Hence it is obvious that in that case this code C does not become 2-frameproof code.

References

- [1] D. Boneh and J. Shaw, "Collusion-Secure Fingerprinting for Digital Data", In *Advances in Cryptology-CRYPTO'95*, (Lecturer Notes in Computer Science), Vol.963, pp.453-465, New York, 1995.
- [2] D. Boneh and J. Shaw, "Collusion-Secure Fingerprinting for Digital Data", *IEEE Transactions on Information Theory*, Vol.44, pp.1897-1905, 1998.
- [3] D.R. Stinson, "Combinatorial Designs: Construction and Analysis", Springer-Verlag, New York, Berlin, Heidelberg, 2003.
- [4] D.R. Stinson, R. Wei, "Combinatorial Properties and Constructions of traceability schemes and frameproof codes", *SIAM Journal of Discrete mathematics*, Vol.2, pp.41-53, 1998.
- [5] Gerard Cohen, Encheva Sylvia "Frameproof Codes against coalition of pirates" *Theoretical Computer Science*, Vol.273, pp.295-304, 2002
- [6] J.N. Staddon, D.R. Stinson, R. Wei, "Combinatorial Properties of Frameproof and Traceable codes", *IEEE Transactions on Information Theory*, Vol. 47, no.3, pp.1042-1049, 2001.
- [7] Lindkvist T, "Fingerprinting of Digital Documents" Dissertation 706, Linkoping University, Sweden (2001)
- [8] Lindkvist T, Lofvenberg J, Svanstrom M, "A Class of Traceability Codes" *IEEE Transactions on Information Theory*, Vol. 48, 7(2002), pp.2094-2096.

- [9] N. Alon, G. Cohen, "Generalized Hashing and Parent Identifying Codes" *Journal of Combinatorial Theory Series A* 104(2003), pp.207-215.
- [10] N.J.A. Sloane, "The Theory of Error Correcting Codes", North Holland Publishing Company (1977).
- [11] N. Wagner, "Fingerprinting Technique", in Proceedings 1983, IEEE Symposium on Security and Privacy, pp.18-22, April 1983.
- [12] P. Sarkar, D.R. Stinson, "Frameproof and IPP Codes" LNCS (INDOCRYPT 2001), Springer 2001.
- [13] Rényi A., "On randomgenerating elements of a finiteboolean algebra," *Acta Sci. Math.(Szeged)*, Vol. 22, pp. 75-81, 1961.
- [14] Rényi A., "On measures of entropy and information," in Proceedings of the Fourth Berkeley Symposium, Berkeley, 1961, Vol. 1, pp. 547-561, Univ. of California Press.
- [15] Rényi A., "On a problem of information theory," *Publ. Math. Inst. Hungar. Aead. Sci.*, Vol. 6, pp. 505-516, 1961.
- [16] Rényi A., "Statistical laws of accumulation of information," *Bull. Inst. Internat.Stat.*, Vol. 39, no. 2, pp. 311-316, 1962.
- [17] Simon R. Blackburn, "Frameproof codes", *SIAM Journal of Discrete Mathematics*, Vol. 16, no. 3, pp.499-510, 1998
- [18] Vera Pless, W. Cary Huffman, "Fundamentals of Error Correcting Codes", Cambridge University Press (U.K.) (2003).

Received July, 2016

Information for Contributors

The *Journal of Information & Optimization Sciences* (JIOS) will consider original research articles, survey articles, and book reviews. Responses to articles and correspondence will also be considered at the Chief Editor's discretion.

Special issue proposals in cutting-edge and timely areas of research in information and optimization sciences are encouraged – please contact the Chief Editor in the first instance.

Peer Review Policy:

All submitted manuscripts are subject to initial appraisal by the Chief Editor, and, if found suitable for further consideration, to rigorous and rapid peer review by independent, anonymous expert referees. All peer review is Double blind and will undergo iThenticate cross-checking for plagiarism.

Manuscripts may be submitted to any Associate Editor or directly to: Chief Editor-JIOS, Taru Publications, G-159, Pushkar Enclave, Pashchim Vihar, New Delhi 110 063, India. *E-mail*: bkdass@tarupublications.com.

Submitted manuscripts must not have been published previously nor be under consideration for publication elsewhere. Moreover submission to the journal will be deemed to imply that the manuscript has not been and will not be submitted elsewhere if accepted. Publication of paper in the journal automatically transfers the copyrights from the authors to the publishers. However, a copyright form will also be required to be signed by the author if the paper is accepted for publication.

The language of the manuscript should be English only. Authors should submit *three* copies of a manuscript, typed on one side only, double spaced throughout. A research article should comprise of the *title*, *author(s)*, *affiliation of author(s)* (with *email(s)* and *phone number(s)*), a sufficiently informative *Abstract* of about 100 words, *Keywords* and *Introduction* of the paper. 'End of proof' should be indicated by a halmos \square . References at the end of the manuscript should be arranged alphabetically; **citation of reference in the text should be indicated by bracketed numbers, i.e., [1].**

Editorial decisions on acceptance or otherwise will be taken normally within four to six months of receipt of a paper.

The corresponding author will receive *galley proofs*, which should be corrected and returned within 48 hours of receipt.

Authors must retain a copy of every contribution, as these will not be sent along with the proofs to be corrected by the authors.

Responsibility of the contents rests upon the authors and not upon the publishers.

The authors or their institutions will be requested to honour a *voluntary page charge* to help defray the cost of publication. These charges are not obligatory nor is their payment a prerequisite for publication. Detailed information will accompany the acceptance letter or the galley proofs. The corresponding author will receive 50 free reprints of the paper with colorful personalized cover alongwith printed copy(s) of the issue if the charge is honoured.

Dissertation abstracts and *books for reviews* should be submitted in *duplicate* to the Chief Editor.

The journal is Abstracted / Indexed / Reviewed in : ABI/Inform, Biostatistica, British Library Inside, CIS, ESCI (WoS Thomson), Genamics JournalSeek, Google Scholar, INSPEC, MathSciNet, NRSJP, OR/MS, Portico, ProQuest, QCAS, SciBase, Ulrich's, WorldCat Local (OCLC), ZentralblattMATH, Zetoc.

Journal of Information & Optimization Sciences

ISSN 0252-2667 (Print)

ISSN 2169-0103 (Online)

CHIEF EDITOR BAL KISHAN DASS

Former Professor of Mathematics, University of Delhi, Delhi 110 007, INDIA

Address for Correspondence:

G-159, Pushkar Enclave, Pashchim Vihar, New Delhi 110 063, INDIA E-mail: bkdass@tarupublications.com

ADVISORY EDITORS

P. CORSINI

Dept. of Civil Engg. & Arch.,
Via delle Scienze 206
33100 UDINE
ITALY
corsini2002@yahoo.com

Y. SINGH

M. S. University of Baroda
Vadodara 390 002
Gujarat
INDIA
ys66@rediffmail.com

J. WATADA

GSIPS
Waseda University
2-7 Hibikino, Wakamatsuku
Kitakyushu, Fukuoka 808-0135
JAPAN
junzo.watada@gmail.com

ASSOCIATE EDITORS

R. M. ALI

School of Mathematical Sciences
Universiti Sains Malaysia
11800 USM Penang
MALAYSIA
rosihan@cs.usm.my

H. ARSHAM

University of Baltimore
Charles at Mount Royal
Baltimore, Maryland 21201
U.S.A.
harsham@ubalt.edu

R. CAMBINI

Dept. of Stat. & Applied Math
University of Pisa
Via Cosimo Ridolfi, 10 - 56124 Pisa
ITALY
cambric@ec.unipi.it

D. K. DESPOTIS

Department of Informatics
University of Piraeus
80, Karaoli & Dimitriou Street
18534 Piraeus, GREECE
despotis@unipi.gr

M. M. DEZA

EUJC/LIGA
Ecole Normale Supérieure
45, rue d'Ulm, F-75230
Paris, Cedex 05
FRANCE
Michel.Deza@ens.fr

T. FUKUDA

Dept. of Micro-Nano Systems Engi.
Nagoya University
Furo-cho, Chikusa-ku
Nagoya 464-8603
JAPAN
fukuda@mein.nagoya-u.ac.jp

S. HIRASAWA

Rm. 66-08-02, Ohishi Lab.
Waseda Reserach Institute for
Sc. & Engg.
3-14-9, Ohkubo, Shinjuku
Tokyo 169-0072, JAPAN
hira@waseda.jp

I. HONKALA

Department of Mathematics
University of Turku
20014 Turku
FINLAND
ihiro.honkala@utu.fi

M. ITO

Faculty of Science
Kyoto Sangyo University
Kita-Ku, Kamigamo
Kyoto 603-8555, JAPAN
ito@ksu.vx0.kyoto-su.ac.jp

E. LASSERRA

Dept. of Math. & Informatics
University of Salerno
Via Ponte Don Melillo
I-84084 Fisciano (SA), ITALY
elaserra@unisa.it

J. Y. LEE

Dept. of Statistics
Yeungnam University
214-1 Dae-Dong Gyeongsan
Gyeongbuk, 712-749
REPUBLIC OF KOREA
jlee@yu.ac.kr

J. E. MARTINEZ-LEGAZ

Dept. d'Economia i d'Historia
Economica
Universitat Autònoma de Barcelona
08193 Bellaterra, SPAIN
JuanEnrique.Martinez.Legaz @uab.cat

P. MAZZOLENI

Catholic University
Largo Gemelli, 1
20123 Milan
ITALY
piera.mazzoleni@unicatt.it

W. PEDRYCZ

Dept of ECE
University of Alberta
Edmonton
Canada
wpedrycz@ualberta.ca

H. PHAM

Dept. of Industrial & Systems Engg.
Rutgers University
Piscataway, New Jersey
U.S.A.
hopham@rci.rutgers.edu

A. ROSALSKY

Department of Statistics
University of Florida
Gainesville, Florida 32611
U.S.A.
rosalsky@stat.ufl.edu

K. P. SHUM

Institute of Mathematics
Yunnan University
Kunming, 650091
PR CHINA
kpshum@math.hku.hk

B. VISCOLANI

Department of Mathematics
University of Padova
Via Trieste 63
I - 35132 Padova PD
ITALY
viscolan@math.unipd.it



ANALYSIS OF HOT STANDBY DATABASE SYSTEM WITH STANDBY UNIT UNDER CONSTANT OBSERVATION

Amit Manocha*, Sukhvir Singh** & Anil Taneja***

*Department of Mathematics, T.I.T. S., Bhiwani, Haryana, India

**Department of Computer Science, N.C.C.E. Panipat, Haryana, India

***Former Prof., JRE Group of Institution, Greater Noida, (U.P.), India

E-mail: amitmanocha80@yahoo.com, boora_s@yahoo.com, drani_tan@rediffmail.com

ABSTRACT :

A discrete state space and continuous parameter stochastic model for two unit hot standby database system with standby database under constant observation of database administrator (DBA) has been developed. The primary unit is synchronized with hot standby unit through online transfer of archive redo logs. Standby database unit is always kept under constant observation of DBA to check either its synchronization with primary unit is working properly or not. Failure of database unit either primary or standby is also dealt by of DBA. The system is analyzed by making use of semi-Markov process and regenerative point technique. Mathematical expressions for various performance indicating measures of the system has been obtained and economic analysis has been done. Numerical examples are also discussed on the basis of data collected to illustrate the behavior of model developed. Bounds for various costs pertaining to the profitability of the system have also been obtained.

Keywords : Database system, hot standby, constant observation, semi-Markov processes, regenerative point technique.

1. INTRODUCTION

Data collection, analysis and security are significant issues in today's competitive world. Database systems designed by companies like Oracle, Microsoft, IBM etc. provides solutions to such vital issues. These systems are used to preserve the data for the industries functioning in various sectors like Telecommunication, Automobile, Gas & Oil, Transportation, Education, Medical, Finance, Marketing, Banking, Textile & Garments etc. Any type of operational error in these systems may cause substantial loss of data, resources and revenue as a whole. So, reliability, availability and economic analysis of these automated database systems is really needed in the present scenario. The present paper is an attempt to analyze two unit hot standby database system wherein standby unit is kept under constant observation.

In the literature of reliability, standby systems have been discussed very comprehensively by large number of researchers. El-Said and El-Sherbeny [1] did the profit analysis of two unit cold standby system with preventive maintenance and random change in units. Parasher and Taneja [2] discussed reliability and profit evaluation of PLC hot standby system. Goyal et al. [3] studied a two unit cold standby system working in a sugar mill with operating and rest period. Mahmoud and Moshref [4] analysed two unit cold standby system considering hardware, human error failures and preventive maintenance by considering all the time distributions arbitrary. Mathews et al. [5] carried out reliability analysis of identical two unit parallel CC plant system operative with full installed capacity. Modelling of a deteriorating system with repair satisfying general distribution was done by Yuan and Xu [6]. Jain and Rani [7] discussed availability for repairable system with warm standby, switching failure and reboot

delay. Huang et al. [8] studied a reliability model of warm standby configuration with two identical set of units. Batra and Kumar [9] did the stochastic modeling of printed circuit boards manufacturing system under different conditions. Manocha et al. [10] did the stochastic analysis of two unit hot standby database system. The present study deals with two unit hot standby database system comprised of primary database unit synchronized with hot standby unit through the online transfer of redo log files. However hot standby unit is kept under the constant observation of DBA.

2. SYSTEM DESCRIPTION AND ASSUMPTIONS

Schematic functioning of proposed two unit hot standby database system is shown in Figure 1. Under normal circumstances, all redo log files created at the primary site are archived at standby site. In case of failure of primary unit, its repair is done immediately by the DBA and pre-synchronized hot standby unit act as standard production unit to assure continuous or smooth run of process. Here the cost of using hot standby unit as primary unit will be recurred by user of system itself. Further, on the failure of primary unit, it is also observed that redo files are not created as well as updated in standby unit. Hence, it may cause serious loss of data. At this juncture, to enhance the reliability of system, standby unit is kept under constant supervision of DBA. In such a situation, probability of non-creation of redo log files in standby unit is almost zero. For availing this facility, the additional incurred cost has to be meted by the user.

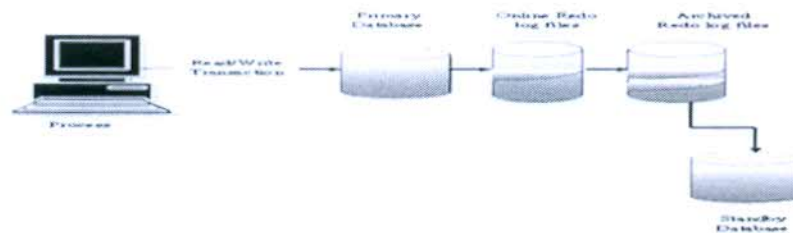


Figure 1 Two Unit Hot Standby Database System

However, non-updation of redo log files in standby unit may be faced but with lower probability. Considering these situations modelling of the system has been done. The proposed system has single DBA facility which performs dual task of repairing the failed unit as well as observing the standby unit. After each repair, the system works as good as new. Time to failure, repair, non-updation of redo log files and updation of redo log files are independent and identically distributed random variables. Time to failure of a unit and time to non-updation of redo log files follows exponential distribution whereas time for repair and updating redo log files follow general distributions.

3. MATERIALS AND METHODS

By using semi-Markov process and regenerative point technique a discrete state space and continuous time stochastic model of a two unit hot standby database system, wherein standby unit is kept under constant observation has been developed. Mathematical expressions for various performance indicating measures of the system such as Mean time to system failure, Mean time to failure of primary database unit, Availability of primary database unit, Busy period of DBA, Expected number of visits by the DBA and profit function has been obtained. Numerical examples are discussed on the basis of data collected. Bounds for various costs which affect the profitability of the system have also been obtained.

4. NOMENCLATURE

- λ / α constant failure rate of primary/ standby database unit
- β rate at which redo log files are not updated in standby database unit
- E/\bar{E} set of regenerative / non-regenerative states
- $M_i(t)$ probability that primary database unit up initially in regenerative state i is up at time t without passing through any other regenerative state or returning to itself through one or more non-regenerative state
- $g(t)/G(t)$ pdf/cdf of the time for repairing the primary database unit
- $g_1(t)/G_1(t)$ pdf/cdf of the time for repairing the standby database unit
- $h(t)/H(t)$ pdf/cdf of the time for updating the redo log files in the standby database unit
- $q_{ij}(t)/Q_{ij}(t)$ pdf /cdf of time for the system transits from regenerative state i to j
- $q_{ij}^{(k)}(t)/Q_{ij}^{(k)}(t)$ pdf / cdf of time for the system transits from regenerative state i to j via non-regenerative state k
- \otimes / \odot symbol for Stieltjes / Laplace convolution
- ** / * symbol for Laplace- Stieltjes/ Laplace Transformation

5. FORMULATION OF MATHEMATICAL MODEL

Symbols for the states of the system are

- P_0 primary database unit is operative
- $H_S / H_r / H_R$ hot standby (database)/ under repair/ repair from previous state
- S_0 hot standby database unit is used as primary database unit
- $S_r / S_w / S_R$ hot standby unit (used as primary database unit) is under repair/ waiting for repair / repair from previous state
- $F_r / F_w / F_R$ failed unit under repair / waiting for repair / repair from previous state
- $H_S \bar{A} \bar{D}$ redo log files were not updated in hot standby database unit

Based on system description and assumptions, the system may be in any of the following states :

- State 0: (P_0, H_S) State 1: $(P_0, H_S \bar{A} \bar{D})$ State 2: (P_0, H_r) State 3: (F_r, S_0) State 4: $(F_w, H_S \bar{A} \bar{D})$
- State 5: (F_w, H_R) State 6: (F_R, S_w) State 7: (P_0, S_r) State 8: (F_w, S_R)

The possible transitions between these states are shown in Figure 2.

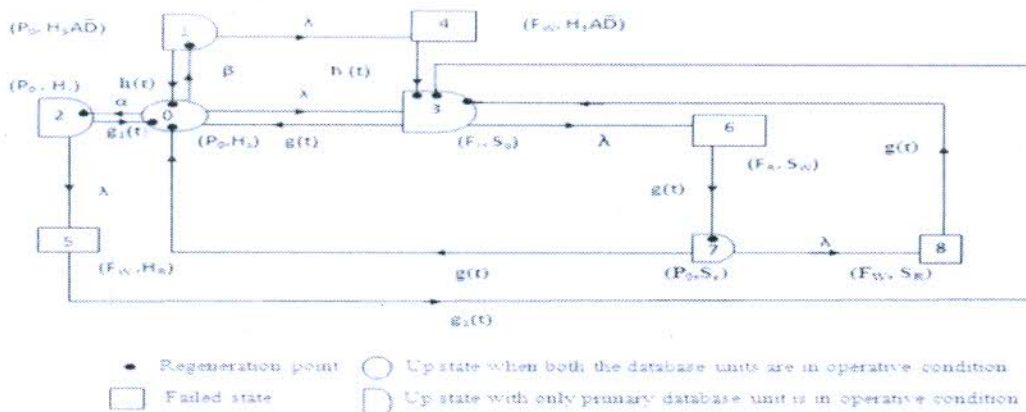


Figure 2 State transition diagram

Here, $E = \{0, 1, 2, 3, 7\}$ is a set of regenerative states whereas $\bar{E} = \{4, 5, 6, 8\}$ is a set of non-regenerative states. States 0, 1, 2, 3 and 7 are up states whereas states 4, 5, 6, and 8 are failed states.

Let $T_0 (= 0), T_1, T_2, \dots$ be the epochs at which system enters any state $i \in E$ and let X_n be the state visited at epoch in T_{n+1} i.e. just after transition at T_n . Then $\{X_n, T_n\}$ is a Markov-renewal process with state space E and $q_{ij} = P\{X_{n+1} = j, T_{n+1} - T_n \leq X_n = i\}$ is the semi-Markov kernel over E . The transition probability matrix (t.p.m.) of the embedded Markov chain is $P = (p_{ij}) = [q_{ij}(\infty) = q(\infty)]$.

By probabilistic arguments, the non-zero elements p_{ij} are,

$$\begin{aligned} p_{01} &= \int_0^\infty \beta e^{-(\lambda+\alpha+\beta)t} dt, & p_{02} &= \int_0^\infty \alpha e^{-(\lambda+\alpha+\beta)t} dt, & p_{03} &= \int_0^\infty \lambda e^{-(\lambda+\alpha+\beta)t} dt, \\ p_{10} &= \int_0^\infty e^{-\lambda t} h(t) dt, & p_{14} &= \int_0^\infty \lambda e^{-\lambda t} \bar{H}(t) dt, & p_{13}^{(4)} &= \int_0^\infty (\lambda e^{-\lambda t} \odot 1) h(t) dt, \\ p_{20} &= \int_0^\infty e^{-\lambda t} g_1(t) dt, & p_{25} &= \int_0^\infty \lambda e^{-\lambda t} \bar{G}_1(t) dt, & p_{23}^{(5)} &= \int_0^\infty (\lambda e^{-\lambda t} \odot 1) g_1(t) dt, \\ p_{30} &= p_{70} = \int_0^\infty e^{-\lambda t} g(t) dt, & p_{36} &= \int_0^\infty \lambda e^{-\lambda t} \bar{G}(t) dt, & p_{37}^{(6)} &= p_{73}^{(8)} = \int_0^\infty (\lambda e^{-\lambda t} \odot 1) g(t) dt \end{aligned}$$

It can be verified that,

$$\begin{aligned} p_{01} + p_{02} + p_{03} &= 1, & p_{10} + p_{14} &= 1, & p_{10} + p_{13}^{(4)} &= 1, & p_{20} + p_{25} &= 1, \\ p_{20} + p_{23}^{(5)} &= 1, & p_{30} + p_{36} &= 1, & p_{30} + p_{37}^{(6)} &= 1, & p_{70} + p_{73}^{(8)} &= 1, \end{aligned}$$

Mean Sojourn time in regenerative state $i \in E$ is given as :

$$\mu_0 = \int_0^\infty e^{-(\lambda+\alpha+\beta)t} dt, \quad \mu_1 = \int_0^\infty e^{-\lambda t} \bar{H}(t) dt, \quad \mu_2 = \int_0^\infty e^{-\lambda t} \bar{G}_1(t) dt, \quad \mu_3 = \mu_7 = \int_0^\infty e^{-\lambda t} \bar{G}(t) dt,$$

The contribution to mean sojourn time when system transit for any regenerative state j when it (time) is counted from the epoch of entrance into state i is given as:

$$\begin{aligned} m_{01} + m_{02} + m_{03} &= \mu_0, & m_{10} + m_{14} &= \mu_1, & m_{20} + m_{25} &= \mu_2, \\ m_{30} + m_{36} &= \mu_3, & m_{10} + m_{13}^{(4)} &= -h^*(0) = K_1 \text{ (say)}, & m_{20} + & \\ m_{23}^{(5)} &= -g_1^*(0) = K_2 \text{ (say)}, & m_{30} + m_{37}^{(6)} &= m_{70} + m_{73}^{(8)} = -g^*(0) = K_3 \text{ (say)} \end{aligned}$$

6. MEASURES OF SYSTEM EFFECTIVENESS

6.1 Mean Time to System Failure (MTSF)

Let $\pi_i(t)$ be c.d.f. of the first passage time from regenerative state $i \in E$ to a failed state. Regarding the failed state as absorbing state, the recursive relations for ' $\pi_i(t)$ ' are:

$$\pi_0(t) = Q_{01}(t) \otimes \pi_1(t) + Q_{02}(t) \otimes \pi_2(t) + Q_{03}(t) \otimes \pi_3(t)$$

$$\pi_1(t) = Q_{14}(t) + Q_{10}(t) \otimes \pi_0(t)$$

$$\pi_2(t) = Q_{25}(t) + Q_{20}(t) \otimes \pi_0(t)$$

$$\pi_3(t) = Q_{36}(t) + Q_{30}(t) \otimes \pi_0(t)$$

By taking Laplace-Stieljes transformation of the above equations and solving them for $\pi_0^{**}(s)$, We obtain $\pi_0^{**}(s) = N(s)/D(s)$

$$\text{where, } N(s) = Q_{03}^{**}(s) Q_{36}^{**}(s) + Q_{01}^{**}(s) Q_{14}^{**}(s) + Q_{02}^{**}(s) Q_{25}^{**}(s)$$

$$\text{and } D(s) = 1 - Q_{01}^{**}(s) Q_{10}^{**}(s) - Q_{02}^{**}(s) Q_{20}^{**}(s) - Q_{03}^{**}(s) Q_{30}^{**}(s)$$

The reliability of the system at time t is given by,

$$R(t) = L^{-1}[\{1 - \pi_0^{**}(s)\}/s]$$

and the mean time to system failure (MTSF) when the system starts from state '0' is

$$MTSF = \lim_{s \rightarrow 0} \{1 - \pi_0^*(s)\}/s = N/D$$

$$\text{where, } N = (\mu_0 + p_{01}\mu_1 + p_{02}\mu_2 + p_{03}\mu_3) \quad \text{and} \quad D = (1 - p_{01}p_{10} - p_{02}p_{20} - p_{03}p_{30})$$

6.2 Mean Time to Failure of Primary Database Unit (MTFP)

Let $TP_i(t)$ be the c.d.f. of the first passage time of primary database unit from regenerative state $i \in E$ to the state where it is failed. The recursive relations for ' $TP_i(t)$ ' are:

$$TP_0(t) = Q_{03}(t) + Q_{01}(t) \otimes TP_1(t) + Q_{02}(t) \otimes TP_2(t)$$

$$TP_1(t) = Q_{14}(t) + Q_{10}(t) \otimes TP_0(t)$$

$$TP_2(t) = Q_{25}(t) + Q_{20}(t) \otimes TP_0(t)$$

The mean time to failure of primary database unit when the system start from state '0' is given by

$$MTFP = \lim_{s \rightarrow 0} \{1 - TP_0^*(s)\}/s = N_1/D_1$$

$$\text{where, } N_1 = (\mu_0 + p_{01}\mu_1 + p_{02}\mu_2) \quad \text{and} \quad D_1 = (1 - p_{01}p_{10} - p_{02}p_{20})$$

6.3 Availability of Primary Database Unit (AP_0)

Let $AP_i(t)$ be the probability that the primary database unit is in upstate at instant t given that the system entered regenerative state $i \in E$ at $t = 0$. The recursive relations for ' $AP_i(t)$ ' are:

$$AP_0(t) = M_0(t) + q_{01}(t) \odot AP_1(t) + q_{02}(t) \odot AP_2(t) + q_{03}(t) \odot AP_3(t)$$

$$AP_1(t) = M_1(t) + q_{10}(t) \odot AP_0(t) + q_{13}^{(4)}(t) \odot AP_3(t)$$

$$AP_2(t) = M_2(t) + q_{20}(t) \odot AP_0(t) + q_{23}^{(5)}(t) \odot AP_3(t)$$

$$AP_3(t) = q_{30}(t) \odot AP_0(t) + q_{37}^{(6)}(t) \odot AP_7(t)$$

$$AP_7(t) = M_7(t) + q_{70}(t) \odot AP_0(t) + q_{73}^{(8)}(t) \odot AP_3(t)$$

$$\text{where, } M_0(t) = e^{-(\lambda+\alpha+\beta)t}, \quad M_1(t) = e^{-\lambda t} \bar{H}(t), \quad M_2(t) = e^{-\lambda t} \bar{G}_1(t), \quad M_7(t) = e^{-\lambda t} \bar{G}(t)$$

By taking Laplace transform of the above equations and solving them for $AP_0^*(s)$, We obtain

$$AP_0^*(s) = N_2(s)/D_2(s)$$

$$\text{where } N_2(s) = \{M_0^*(s) + q_{01}^*(s) M_1^*(s) + q_{02}^*(s) M_2^*(s)\} \{1 - q_{37}^{(6)*}(s) q_{73}^{(8)*}(s)\} \\ + q_{37}^{(6)*}(s) M_7^*(s) \{q_{01}^*(s) q_{13}^{(4)*}(s) + q_{02}^*(s) q_{23}^{(5)*}(s) + q_{03}^*(s)\}$$

$$\text{and } D_2(s) = \{1 - q_{01}^*(s) q_{10}^*(s) - q_{02}^*(s) q_{20}^*(s)\} \{1 - q_{37}^{(6)*}(s) q_{73}^{(8)*}(s)\} \\ - \{q_{30}^*(s) + q_{70}^*(s) q_{37}^{(6)*}(s)\} \{q_{01}^*(s) q_{13}^{(4)*}(s) + q_{02}^*(s) q_{23}^{(5)*}(s) + q_{03}^*(s)\}$$

In steady-state the availability of primary database unit, is given by

$$AP_0 = \lim_{t \rightarrow \infty} AP_0(t) = \lim_{s \rightarrow 0} s AP_0^*(s) = N_2/D_2$$

$$\text{where, } N_2 = (1 - p_{37}^{(6)} p_{73}^{(8)}) (\mu_0 + p_{01}\mu_1 + p_{02}\mu_2) + (1 - p_{01}p_{10} - p_{02}p_{20}) p_{37}^{(6)} \mu_7$$

$$\text{and } D_2 = (1 - p_{37}^{(6)} p_{73}^{(8)}) (\mu_0 + p_{01}K_1 + p_{02}K_2) + (1 - p_{01}p_{10} - p_{02}p_{20}) (K_3 + p_{37}^{(6)} K_3)$$

Similarly, employing the same argument discussed as above, the mathematical expressions for other performance indicating measures of the system are:

$$\text{Expected time for which standby database unit worked as primary database unit } (S_0) = N_3/D_2$$

$$\text{Expected time for updating the redo log files in standby database unit } (AU_0) = N_4/D_2$$

$$\text{Expected time for repairing primary database unit } (BP_0) = N_5/D_2$$

Expected time for repairing standby database unit $(BH_0) = N_6/D_2$

Expected number of visits by DBA $(V_0) = N_7/D_2$

where, $N_3 = (1 - p_{01}p_{10} - p_{02}p_{20})\mu_3$; $N_4 = p_{01}(1 - p_{37}^{(6)}p_{73}^{(8)})K_1$; $N_5 = (1 - p_{01}p_{10} - p_{02}p_{20})(K_1 + p_{37}^{(6)}K_1)$; $N_6 = (1 - p_{37}^{(6)}p_{73}^{(8)})p_{02}K_2$; $N_7 = (1 - p_{37}^{(6)}p_{73}^{(8)})$

7. COST-BENEFIT ANALYSIS

As the profit is defined as excess of revenue over the cost of production. So, in steady-state, the expected profit per unit time incurred to the system is given by

$$\text{Profit (P)} = C_0AP_0 - C_1S_0 - C_2AU_0 - C_3BP_0 - C_4BH_0 - C_5V_0 - 2CI - K$$

Where, C_0 = Revenue per unit uptime

C_1 = Cost per unit time for which standby database unit worked as primary database unit

C_2 = Cost per unit time for updating the redo log files in standby database unit

C_3 = Cost per unit time for which DBA is busy for repairing primary database unit

C_4 = Cost per unit time for which DBA is busy for repairing standby database unit

C_5 = Cost per visit of DBA

CI = Cost per unit time of Initial Installation

K = Cost per unit time for which standby database unit is kept under constant observation

8. NUMERICAL CALCULATIONS, RESULTS & DISCUSSION

To illustrate the mathematical expressions obtained for the above model with a numerical examples, we consider $h(t) = \gamma e^{-\gamma t}$, $g(t) = \eta e^{-\eta t}$, $g_1(t) = \alpha_1 e^{-\alpha_1 t}$. The data on various rates and costs for primary/standby database unit collected from different users are :

Constant failure rate of primary database unit $(\lambda) = 0.00205$ per hr

Constant repair rate of primary database unit $(\eta) = 0.6529$ per hr

Constant failure rate of standby database unit $(\alpha) = 0.00087$ per hr

Constant repair rate of standby database unit $(\alpha_1) = 0.8533$ per hr

Cost per unit time for which DBA is busy for repairing primary database unit $(C_3) = 7325.58$

Cost per unit time for which DBA is busy for repairing standby database unit $(C_4) = 8750$

and rest of the values are assumed values.

8.1 Effect of rates (β, γ) on MTSF and availability of primary database unit (AP_0)

MTSF and availability of primary database unit (AP_0) are calculated by varying the rate (γ) for different values of rate (β) . The results are shown in Table 1. It is observed that,

- (i). MTSF increase with the increase in the values of rate (γ) and it has higher values for lower values of rate (β) .
- (ii). Availability of primary database unit (AP_0) increase with the increase in the values of rate (γ) and it has higher values for lower values of rate (β) .

γ	MTSF (In hrs)			Availability (AP_0)		
	$\beta = 0.06$	$\beta = 0.07$	$\beta = 0.08$	$\beta = 0.06$	$\beta = 0.07$	$\beta = 0.08$
5	30707.91	27375.01	24707.3	0.996863	0.996862	0.996861
6	34980.74	31341.14	28403.07	0.996864	0.996864	0.996863
7	38851.62	34976.33	31812.98	0.996865	0.996865	0.996864
8	42377.33	38309.9	34967.79	0.996866	0.996865	0.996865
9	45602.07	41396.71	37914.56	0.996866	0.996866	0.996866
10	48571.55	44252.57	40648.3	0.996866	0.996866	0.996866

Table 1 Values of MTSF and AP_0 w.r.t. rate (γ) for different values of rate (β)

8.2 Effect of revenue (C_0) on profit (P) for different values of rate (β)

Figure 3 depicts the behavior of profit (P) with respect to revenue (C_0) for different values of rate (β) by considering other parameters as $\gamma = 12, CI = 5, K = 3, C_1 = 50, C_2 = 500, C_5 = 700$. It is interpreted that profit (P) increases with increase in the revenue (C_0) and has higher values for lower values of rate (β).

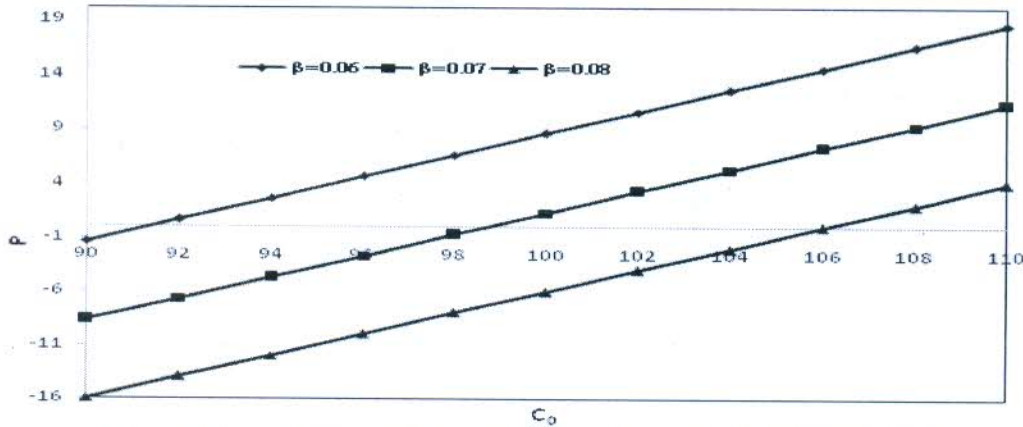


Figure 3 Profit (P) versus Revenue (C_0) for different values of rate (β)

Further,

- i. For $\beta=0.06$, the profit(P) $>$ or $=$ or $<$ 0 according as $C_0 >$ or $=$ or $<$ 91.40. Hence for $\beta=0.06$, the revenue should be more than 91.40 to get the profit.
- ii. For $\beta=0.07$, the profit(P) $>$ or $=$ or $<$ 0 according as $C_0 >$ or $=$ or $<$ 98.72. Hence for $\beta=0.07$, the revenue should be more than 98.72 to get the profit.
- iii. For $\beta=0.08$, the profit(P) $>$ or $=$ or $<$ 0 according as $C_0 >$ or $=$ or $<$ 106.03. Hence for $\beta=0.08$, the revenue should be more than 106.03 to get the profit.

8.3 Effect of Cost (C_2) on profit (P) for different values of cost (C_5)

The profit (P) of the system has been calculated with respect to cost (C_2) for different values of cost (C_5) by fixing another parameters such as $\gamma = 12, \beta = 0.01, CI = 5, K = 2, C_0 = 56, C_1 = 50$, Figure 4 reveals the behavior of profit (P) with respect to cost (C_2) for different values of cost (C_5).

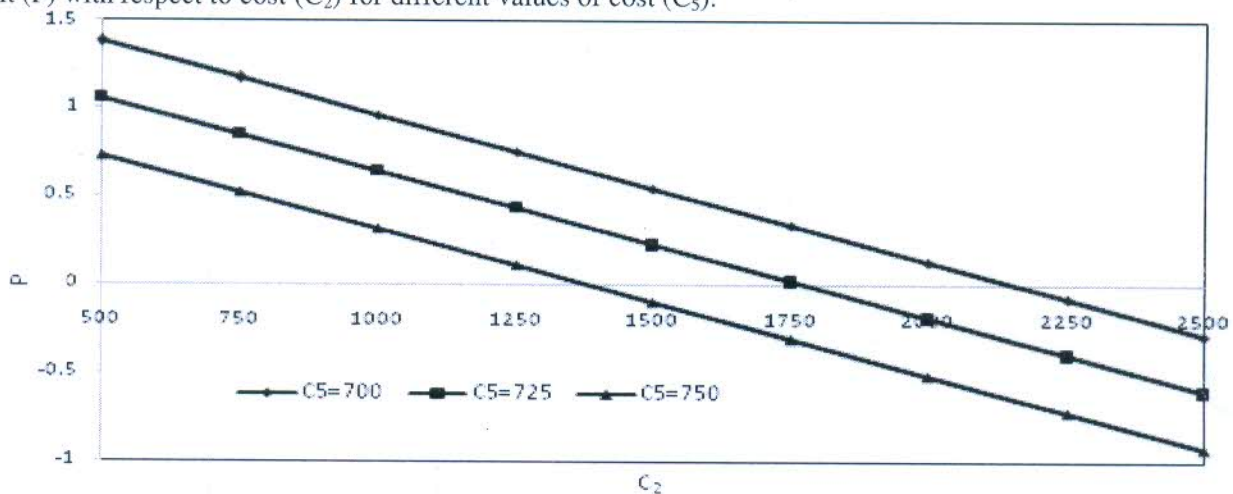


Figure 4 Profit (P) versus Cost (C_2) for different values of cost (C_5)

It can be interpreted that the

- (i). Profit (P) decreases with increase in the cost (C_2) has higher values for lower value of cost (C_5).
- (ii). For $C_5=700$, the profit(P) $>$ or $=$ or $<$ 0 according as $C_2 <$ or $=$ or $>$ 2160.85. Hence for $C_5=700$, the cost for updating the redo log files should not be more than 2160.85 to get the profit.
- (iii). For $C_5=725$, the profit(P) $>$ or $=$ or $<$ 0 according as $C_2 <=$ or $= >$ 1773.24 Hence for $C_5=725$, the cost for updating the redo log files should not be more than 1773.24 to get the profit.
- (iv). For $C_5=750$, the profit(P) $>$ or $=$ or $<$ 0 according as $C_2 <=$ or $= >$ 1385.64. Hence for $C_5=750$, the cost for updating the redo log files should not be more than 1385.64 to get the profit.

CONCLUSION

Stochastic model for a standby database system in which standby database unit always kept under constant observation of database administrator have been developed. Mathematical expressions for various performance indicating measures of the system are obtained. Numerical analysis is done on the basis of collected data. Bounds (lower/upper) for revenue and cost for updating the redo log files in standby unit have also been obtained.

REFERENCES

1. El-Said, K.M., and M.S. El-sherbeny. Profit Analysis of a Two Unit Cold Standby System with Preventive Maintenance and Random Change in Units. *Journal of Mathematics and Statistics*, 2005; 1(1) : 71-77.
2. Parashar, B., and G. Taneja. Reliability and Profit Evaluation of a Plc Hot Standby System Based on a Master- Slave Concept and Two Types of Repair Facilities. *IEEE Transactions on Reliability*, 2007; 56(3) : 534-539.
3. Goyal, A., G. Taneja , and D.V. Singh. Analysis of a two-unit cold standby system working in a sugar mill with operating and rest period . *Caledonian Journal of Engineering* 2009; 5(1): 1-5.
4. Mahmoud, M.A.W., and M.E. Mosherf. On a two- unit cold standby system considering hardware, human error failures and preventive maintenance. *Mathematical and Computer Modeling*, 2010; 51:736-745.
5. Mathews, A.G., S.M. Rizwan, M.C. Majumdar, K.P. Ramchandaran, and G Taneja. Reliability analysis of identical two unit parallel CC plant system operative with full installed capacity. *International Journal of Performability Engineering*, 2011; 7(2):179-187.
6. Yuan, W.Z., and G.Q. Xu. Modelling of a deteriorating system with repair satisfying general distribution. *Applied Mathematics and Computation*, 2012; 218 : 6340-6350.
7. Jain, M.,and S. Rani. Availability Analysis for Repairable System with warm standby, switching failure and reboot delay. *International Journal of Mathematics in Operational Research*, 2013; 5(1) : 19-39.
8. Huang W, J. Lomang, and T. Song. A reliability model of a warm standby configuration with two identical set of units. *Reliability Engineering and System Safety*, 2015; 133 :237-245.
9. Batra, S., and R. Kumar. Stochastic analysis of printed circuit boards manufacturing system considering repairs by internal/external engineers and arbitrary arrival time of external engineers. *International Journal of Pure and Applied Mathematics*, 2016; 106(1) : 59-74.
10. Manocha, A., and G.Taneja. Stochastic and cost-benefit analysis of two unit hot standby database system. *International Journal of Performability Engineering*, 2017; 13(1) : 63-72.

Stochastic and Cost-Benefit Analysis of Two Unit Hot Standby Database System

AMIT MANOCHA¹, GULSHAN TANEJA² and SUKHVIR SINGH³

¹Department of Mathematics, T.I.T. S., Bhiwani, Haryana, India

²Department of Mathematics, M.D. University Rohtak, Haryana, India

³Department of Computer Science, N.C.C.E. Panipat, Haryana, India

(Received on October 08, 2016, revised on November 30, 2016)

Abstract: A discrete state space and continuous time stochastic model for two unit hot standby database system has been developed. The system comprised of one primary unit and single hot standby unit. The primary unit is production unit synchronized with hot standby unit through online transfer of archive redo log files. Different modes of failure of primary database unit are considered. Failure of database unit either primary or standby is dealt by database administrator (DBA). Expressions for various measures of system effectiveness have been obtained by making use of semi-Markov processes and regenerative point technique. Numerical results have been drawn on the basis of data collected. Bounds pertaining the profitability of the system have also been obtained.

Keywords: Database system, hot standby, semi-Markov process, cost-benefit analysis, regenerative point technique

1. Introduction

Database system plays a pivotal role locally or globally in handling and securing data for various industries. Promising technological advancements have made enterprises absolutely dependent on automated database systems. A small operational error in these systems may lead to disastrous failures which differ in the severity of their impact depending on the operations of an organization. Few major database system provider companies to mention are Oracle corporation provides RDBMS Oracle and open source DBMS MySQL; Microsoft Corporation provides Microsoft Access and Microsoft SQL Server; IBM provides DB2. Depending upon the volume of company and significance of the data primary database unit and number of standby units are provided by the companies. Such systems maintain the data for various industries working globally in Telecommunication, Automobile, Gas & Oil, Transportation, Education, Medical, Finance, Marketing, Banking, Textile and Garments sectors, etc. Keeping that in view, reliability and availability analysis of these automated database systems is of great importance in the present scenario. The present paper is our attempt to analyze a two unit hot standby database system.

Standby systems have been discussed extensively by various researchers including [1-3]. Beith et al. [4] discussed a two-identical-cold standby system with two types of

Corresponding author's email: amitmanocha80@yahoo.com

repair persons under arbitrary life and repair times. Shakuntla et al. [5] did the reliability analysis of polytube industry by using supplementary variable technique. Reliability analysis of a seven unit desalination plant with shutdown during winter season and repair/maintenance on FCFS basis was carried out by Rizwan et al. [6]. Manocha and Taneja [7] analyzed a stochastic model for two unit cold standby system with arbitrary distribution for life, repair and waiting times. Kuo and Ke [8] did the comparative analysis of standby systems with unreliable server and switching failures. Kumar and Batra [9] developed a stochastic model for printed circuit boards (PCBs) manufacturing process.

Singh et al. [10] did the reliability and availability analysis of database system with numbers of standby units provided by system provider. Higher number of standby units eventually may lead to increased cost, which is to be paid by the user itself. Two unit hot standby database system has not being discussed so far in the literature. So, the present study deals with database system comprising of one primary production database unit synchronized with single hot standby unit through online transfer and simultaneous archiving redo logs.

Notations

λ	constant failure rate of primary database unit
α	constant failure rate of standby database unit
p_1	probability that standby unit is in synchronous with primary database unit on the failure of primary database unit
p_2	probability that redo log files are not updated in standby database unit on the failure of primary database unit
p_3	probability that redo log files are not created in standby database unit on the failure of primary database unit
$M_i(t)$	probability that primary database unit up initially in regenerative state i is up at time t without passing through any other regenerative state or returning to itself through one or more non-regenerative states
$g(t)/G(t)$	pdf/cdf of the time for repairing the primary database unit
$g_1(t)/G_1(t)$	pdf/cdf of the time for repairing the standby database unit
$h_1(t)/H_1(t)$	pdf/cdf of the time for updating the redo log files in the standby database unit
$h_2(t)/H_2(t)$	pdf/cdf of the time for creating the redo log files in the standby database unit
\otimes/\odot	symbol for Laplace-Stieljes convolution / Laplace convolution

for some standard notations one may refer to [2].

Let us now describe the system considered for modelling along with the assumptions taken for developing the same.

2. System Description and Assumptions

Figure 1 demonstrates the functioning of two unit hot standby database system. The standby database unit is kept in synchronization with primary database unit through online redo log files. Redo log files created at primary site are archived at the standby site. In case of the failure of primary unit the standby unit becomes the production unit and the failed unit goes under repair of database administrator (DBA) immediately.

The following situations, which are mutually exclusive and exhaustive, may be observed on the failure of primary unit:

- i. Standby unit working in synchronous with primary unit
- ii. Redo log files are not updated in standby unit
- iii. Redo log files are not created in standby unit

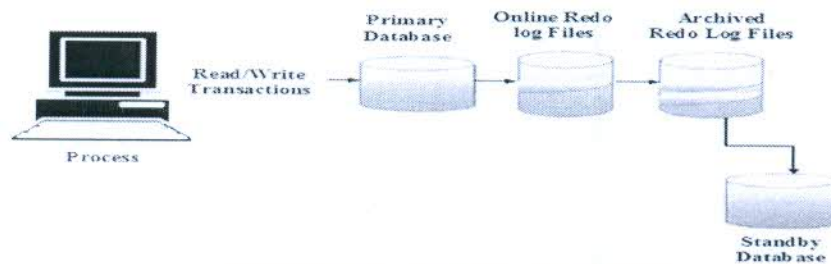


Figure 1: Two Unit Hot Standby Database System

In the situational failure of primary unit all the archived redo log files are updated/created into standby unit by the DBA, before making it production database. Cost for using standby database unit as the primary database unit is to be paid by user itself. Proposed system has a single DBA facility. After each repair, the system works as good as new. All failure times are assumed to have exponential distribution whereas repair times, time for creating and updating redo log files have general distributions. By using semi-Markov process and regenerative point technique expressions for various measures of system effectiveness such as Mean time to system failure, Mean time to failure of primary database unit, Availability of primary database unit, busy period of DBA, Expected number of visits by the DBA and profit function has obtained. Numerical analysis has been done on the basis of data collected for database systems. Bounds concerning the profitability of the system have also been obtained.

All the possibilities have been shown by states and transitions from one state to another along with transition probabilities and mean sojourn times in the following section.

3. Modelling of the System

Symbols for the states of the system are

P_0	primary database unit is operative
$H_s / H_r / H_R$	hot standby database/under repair/ repair from previous state
S_0	hot standby database unit is used as primary database unit
$S_r / S_w / S_R$	hot standby unit (used as primary database unit) is under repair/waiting for repair/ repair from previous state
$F_r / F_w / F_R$	failed unit under repair / waiting for repair / repair from previous state
$P_f H_s A \bar{D}$	primary database unit fails and redo log files are not updated in hot standby database
$P_f H_s \bar{A}$	primary database unit fails and redo log files are not created in hot standby database unit

Considering these symbols, the system can be in any one of the following states

State 0: (P_0, H_s) State 1: (F_r, S_0) State 2: (P_0, H_r) State 3: (F_w, H_R)
 State 4: $(P_f H_s A \bar{D})$ State 5: $(P_f H_s \bar{A})$ State 6: (F_R, S_w) State 7: (P_0, S_r) State 8: (F_w, S_R)

Possible transitions of the system are shown in Figure 2:

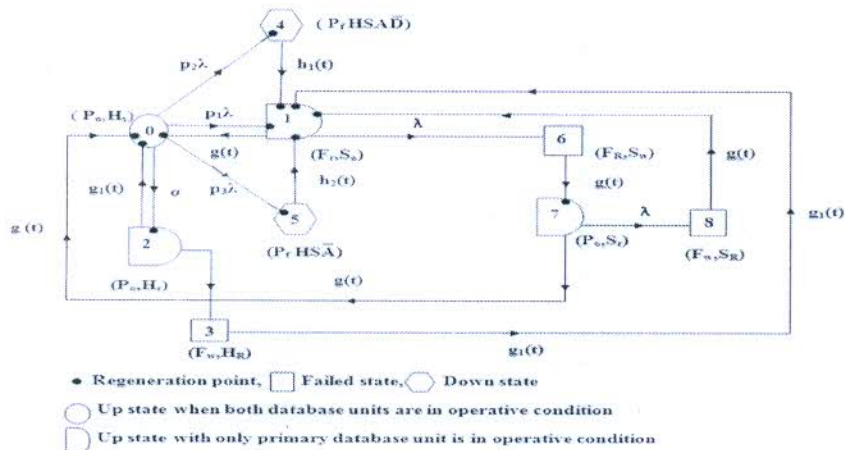


Figure 2: State Transition

Here $E = \{0, 1, 2, 4, 5, 7\}$ is set of regenerative states and $\bar{E} = \{3, 6, 8\}$ is a set of non-regenerative states. States 3, 6 and 8 are failed states, whereas 4 and 5 are down states. Let $T_0 (= 0), T_1, T_2, \dots$ be the epochs at which system enters to any state $i \in E$ and let X_n be the state visited at epoch in T_{n+1} i.e. just after transition at T_n . Then $\{X_n, T_n\}$ is a Markov-renewal process with state space E . Let

$$q_{ij} = P\{X_{n+1} = j, T_{n+1} - T_n \leq t | X_n = i\} \tag{1}$$

be the semi-Markov kernel over E . The transition probability matrix (t.p.m.) of the embedded Markov chain is, therefore, given by

$$P = (p_{ij}) = [q_{ij}(\infty) = q(\infty)] \tag{2}$$

where

$$\begin{aligned} p_{01} &= \int_0^\infty p_1 \lambda e^{-(\lambda+\alpha)t} dt, & p_{02} &= \int_0^\infty \alpha e^{-(\lambda+\alpha)t} dt, & p_{04} &= \int_0^\infty p_2 \lambda e^{-(\lambda+\alpha)t} dt, \\ p_{05} &= \int_0^\infty p_3 \lambda e^{-(\lambda+\alpha)t} dt, & p_{10} &= \int_0^\infty e^{-\lambda t} g(t) dt, & p_{20} &= \int_0^\infty e^{-\lambda t} g_1(t) dt \\ p_{23} &= \int_0^\infty \lambda e^{-\lambda t} \bar{G}_1(t) dt, & p_{41} &= \int_0^\infty h_1(t) dt, & p_{51} &= \int_0^\infty h_2(t) dt, \\ p_{70} &= \int_0^\infty e^{-\lambda t} g(t) dt, & p_{16} &= p_{78} = \int_0^\infty \lambda e^{-\lambda t} \bar{G}(t) dt, \\ p_{21}^{(3)} &= \int_0^\infty (\lambda e^{-\lambda t} \odot 1) g_1(t) dt, & p_{17}^{(6)} &= p_{71}^{(8)} = \int_0^\infty (\lambda e^{-\lambda t} \odot 1) g(t) dt. \end{aligned} \tag{3-15}$$

It can be verified that,

$$\begin{aligned} p_{01} + p_{02} + p_{04} + p_{05} &= 1, & p_{10} + p_{16} &= 1, & p_{10} + p_{17}^{(6)} &= 1, & p_{20} + p_{23} &= 1, \\ p_{20} + p_{21}^{(3)} &= 1, & p_{70} + p_{78} &= 1, & p_{41} + p_{51} &= 1, & p_{70} + p_{71}^{(8)} &= 1. \end{aligned} \tag{16-23}$$

Mean Sojourn time (μ_i) in regenerative state $i \in E$, is given as

$$\begin{aligned} \mu_0 &= \int_0^\infty e^{-(\lambda+\alpha)t} dt, & \mu_1 &= \mu_7 = \int_0^\infty e^{-\lambda t} \bar{G}(t) dt, & \mu_2 &= \int_0^\infty e^{-\lambda t} \bar{G}_1(t) dt, \\ \mu_4 &= \int_0^\infty \bar{H}_1(t) dt, & \mu_5 &= \int_0^\infty \bar{H}_2(t) dt \end{aligned} \tag{24-28}$$

The unconditional time taken by system to transit for any regenerative state j when it (time) is counted from the epoch of entrance into state i is given as

$$\begin{aligned} m_{01} + m_{02} + m_{04} + m_{05} &= \mu_0, & m_{10} + m_{16} &= \mu_1, & m_{20} + m_{23} &= \mu_2, & m_{70} + m_{78} &= \mu_7, \\ m_{41} &= \mu_4, & m_{51} &= \mu_5, & m_{10} + m_{17}^{(6)} &= m_{70} + m_{71}^{(8)} = -g''(0) = K_1 \text{ (say)}, \\ m_{20} + m_{21}^{(3)} &= -g_1''(0) = K_2 \text{ (say)}. \end{aligned} \tag{29-36}$$

Now, to find the reliability and to give cost-benefit analysis, various measures of system effectiveness are required to be obtained. The succeeding section determines all such measures.

4. Measures of System Effectiveness

4.1 Mean Time to System Failure (MTSF)

To determine mean time to system failure (MTSF) we regard the failed state as absorbing state. Let $\pi_i(t)$, where $i \in E$, be c.d.f. of the first passage time from regenerative state i to a failed state, employing the arguments used for regenerative process, we have the following recursive relations for ' $\pi_i(t)$ '

$$\begin{aligned}\pi_0(t) &= Q_{01}(t) \otimes \pi_1(t) + Q_{02}(t) \otimes \pi_2(t) + Q_{04}(t) \otimes \pi_4(t) + Q_{05}(t) \otimes \pi_5(t) \\ \pi_1(t) &= Q_{16}(t) + Q_{10}(t) \otimes \pi_0(t) \\ \pi_2(t) &= Q_{23}(t) + Q_{20}(t) \otimes \pi_0(t) \\ \pi_4(t) &= Q_{41}(t) \otimes \pi_1(t) \\ \pi_5(t) &= Q_{51}(t) \otimes \pi_1(t) \\ \pi_7(t) &= Q_{78}(t) + Q_{70}(t) \otimes \pi_0(t)\end{aligned}\quad (37-42)$$

Taking Laplace-Stieljes transformation of the above equations and solving them for $\pi_0^*(s)$, We obtain $\pi_0^*(s) = N(s)/D(s)$

$$\begin{aligned}\text{where, } N(s) &= Q_{01}^*(s) Q_{16}^*(s) + Q_{02}^*(s) Q_{23}^*(s) + Q_{04}^*(s) Q_{41}^*(s) Q_{16}^*(s) \\ &\quad + Q_{05}^*(s) Q_{51}^*(s) Q_{16}^*(s) \\ \text{and } D(s) &= 1 - Q_{01}^*(s) Q_{10}^*(s) - Q_{02}^*(s) Q_{20}^*(s) - Q_{04}^*(s) Q_{41}^*(s) Q_{10}^*(s) \\ &\quad - Q_{05}^*(s) Q_{51}^*(s) Q_{10}^*(s)\end{aligned}\quad (43-45)$$

The reliability of the system at time t is given by,

$$R(t) = L^{-1}\{[1 - \pi_0^*(s)]/s\} \quad (46)$$

Now the mean time to system failure (MTSF) when the system starts from state '0' is

$$MTSF = \int_0^\infty R(t) dt = N/D$$

where, $N = \{\mu_0 + \mu_1 (p_{01} + p_{04} + p_{05}) + p_{02}\mu_2 + p_{04}\mu_4 + p_{05}\mu_5\}$

and $D = \{p_{16} (p_{01} + p_{04} + p_{05}) + p_{02} p_{23}\}$ (47-49)

4.2 Mean Time to Failure of Primary Database Unit (MTFP)

Let $TP_i(t)$, where $i \in E$, be the c.d.f. of the first passage time of primary database unit from regenerative state i to the state where it is failed. By using arguments of theory of regenerative process, we have the following recursive relations for ' $TP_i(t)$ '

$$\begin{aligned}TP_0(t) &= Q_{01}(t) + Q_{04}(t) + Q_{05}(t) + Q_{02}(t) \otimes TP_2(t) \\ TP_2(t) &= Q_{23}(t) + Q_{20}(t) \otimes TP_0(t)\end{aligned}\quad (50-51)$$

Taking Laplace-Stieljes transformation of above equations and solving them for $TP_0^*(s)$, We obtain

$$\begin{aligned}TP_0^*(s) &= N_1(s)/D_1(s) \\ \text{where, } N_1(s) &= Q_{01}^*(s) + Q_{04}^*(s) + Q_{05}^*(s) + Q_{02}^*(s) Q_{23}^*(s) \\ \text{and } D_1(s) &= 1 - Q_{02}^*(s) Q_{20}^*(s)\end{aligned}\quad (52-54)$$

Now, the mean time to failure of primary database unit when the system start from state '0' is

$$MTFP = \lim_{s \rightarrow 0} \{1 - TP_0^*(s)\}/s = N_1/D_1$$

where, $N_1 = (\mu_0 + p_{02}\mu_2)$

and $D_1 = (1 - p_{02} p_{20})$ (55-57)

4.3 Availability of Primary Database Unit (AP₀)

Let AP_i(t), where i ∈ E, be the probability that the primary database unit is in upstate at instant t given that the system entered regenerative state i at t = 0, and using arguments the theory of regenerative process, AP_i(t) is seen to satisfy the following recursive relations

$$AP_0(t) = M_0(t) + q_{01}(t) \odot AP_1(t) + q_{02}(t) \odot AP_2(t) + q_{04}(t) \odot AP_4(t) + q_{05}(t) \odot AP_5(t)$$

$$AP_1(t) = q_{10}(t) \odot AP_0(t) + q_{17}^{(6)}(t) \odot AP_7(t)$$

$$AP_2(t) = M_2(t) + q_{20}(t) \odot AP_0(t) + q_{21}^{(3)}(t) \odot AP_1(t)$$

$$AP_4(t) = q_{41}(t) \odot AP_1(t)$$

$$AP_5(t) = q_{51}(t) \odot AP_1(t)$$

$$AP_7(t) = M_7(t) + q_{70}(t) \odot AP_0(t) + q_{71}^{(8)}(t) \odot AP_1(t)$$

$$\text{where, } M_0(t) = e^{-(\lambda+\alpha)t}, \quad M_2(t) = e^{-\lambda t} \bar{G}_1(t), \quad M_7(t) = e^{-\lambda t} \bar{G}(t) \quad (58-66)$$

Taking Laplace transform of the above equations and solving them for AP₀^{*}(s), We obtain

$$AP_0^{**}(s) = N_2(s)/D_2(s)$$

$$\text{Where, } N_2(s) = (1 - q_{17}^{(6)*}(s) q_{71}^{(8)*}(s)) (q_{02}^*(s) M_2^*(s) + M_0^*(s)) \\ + q_{17}^{(6)*}(s) (q_{01}^*(s) + q_{05}^*(s) q_{51}^*(s) + q_{04}^*(s) q_{41}^*(s) + q_{02}^*(s) q_{21}^*(s)) M_7^*(s)$$

$$\text{and } D_2(s) = (1 - q_{02}^*(s) q_{20}^*(s)) (1 - q_{17}^{(6)*}(s) q_{71}^{(8)*}(s)) - q_{04}^*(s) q_{41}^*(s) (q_{10}^*(s) \\ + q_{70}^*(s) q_{17}^{(6)*}(s)) - q_{10}^*(s) (q_{02}^*(s) q_{21}^{(3)*}(s) + q_{01}^*(s) + q_{05}^*(s) q_{51}^*(s)) \\ - q_{17}^{(6)*}(s) (q_{05}^*(s) q_{51}^*(s) q_{70}^*(s) + q_{01}^*(s) q_{70}^*(s) + q_{21}^{(3)*}(s) q_{02}^*(s) q_{70}^*(s)) \quad (67-69)$$

In steady-state the availability of primary database unit, is given by

$$AP_0 = \lim_{t \rightarrow \infty} AP_0(t) = \lim_{s \rightarrow 0} s AP_0^*(s) = N_2/D_2$$

$$\text{where, } N_2 = (1 - p_{17}^{(6)} p_{71}^{(8)}) (\mu_1 + p_{02} \mu_2) + (1 - p_{02} p_{20}) p_{17}^{(6)} \mu_7$$

$$\text{and } D_2 = (1 - p_{17}^{(6)} p_{71}^{(8)}) (\mu_0 + p_{04} \mu_4 + p_{05} \mu_5 + p_{02} K_2) + (1 - p_{02} p_{20}) (1 + p_{17}^{(6)}) K_1 \quad (70-72)$$

Proceeding in the similar manner and employing the arguments used for regenerative process, the other measures of system effectiveness are:

$$\text{Expected time for which standby database unit worked as primary database unit (S}_0\text{)} \\ = N_3/D_2$$

$$\text{Expected time for updating the redo log files in standby database unit (AU}_0\text{)} = N_4/D_2$$

$$\text{Expected time for creating redo log files in standby database unit (AC}_0\text{)} = N_5/D_2$$

$$\text{Expected time for repairing primary database unit (BP}_0\text{)} = N_6/D_2$$

$$\text{Expected time for repairing standby database unit (BH}_0\text{)} = N_7/D_2$$

$$\text{Expected number of visits by DBA (V}_0\text{)} = N_8/D_2$$

$$\text{where, } N_3 = (1 - p_{02} p_{20}) \mu_1 ; \quad N_4 = (1 - p_{17}^{(6)} p_{71}^{(8)}) p_{04} \mu_4$$

$$N_5 = (1 - p_{17}^{(6)} p_{71}^{(8)}) p_{05} \mu_5 ; \quad N_6 = (1 - p_{02} p_{20}) (K_1 + p_{17}^{(6)} K_1)$$

$$N_7 = (1 - p_{17}^{(6)} p_{71}^{(8)}) p_{02} K_2 ; \quad N_8 = (1 - p_{17}^{(6)} p_{71}^{(8)}) \quad (73-84)$$

and D₂ is already specified in equation (72).

On the basis of the above measures, the cost-benefit analysis can be carried out as in the following section.

5. Cost-Benefit Analysis

Needless to say, that the profit is most important aspect for a company/firm/organization using any type of system and hence, it is significant to carry out cost-benefit analysis for the system under consideration.

The profit is excess of revenue over the various costs involved and hence profit function takes the form

$$P(t) = \text{Expected revenue in } (0, t] - \text{Expected total cost in } (0, t] \quad (85)$$

For the model discussed in the present paper, the expected profit per unit time incurred to the system, in steady-state, is given by

Profit (P) = (Revenue generated by the system) – (Cost incurred when the secondary database is used as primary database + cost for updating the redo log files in standby database unit + cost for creating the redo log files in standby database unit + cost for which DBA is busy for repairing primary database unit + cost for which DBA is busy for repairing standby database unit + cost per visit of DBA + cost of Initial Installation)

$$\text{i.e. } P = (C_0AP_0) - (C_1S_0 + C_2AU_0 + C_3AC_0 + C_4BP_0 + C_5BH_0 + C_6V_0 + 2CI) \quad (86)$$

where, C_0 = Revenue per unit uptime

C_1 = Cost per unit time for which standby database unit worked as primary database unit

C_2 = Cost per unit time for updating the redo log files in standby database unit

C_3 = Cost per unit time for creating the redo log files in standby database unit

C_4 = Cost per unit time for which DBA is busy for repairing primary database unit

C_5 = Cost per unit time for which DBA is busy for repairing standby database unit

C_6 = Cost per visit of DBA

CI = Cost per unit time of Initial Installation

Now, one may be interested in knowing as to how the MTSF, availability of primary database unit and profit are affected with changes in various rates /cost /revenue. The authors have made an attempt to find such effects by performing various numerical calculations as done in the following section.

6. Numerical Calculations, Results and Discussion

6.1 Input Variables

For numerical calculations we consider repair times, time for updating and creating redo log files follows exponential distribution i.e.

$$g(t) = \eta e^{-\eta t}, g_1(t) = \alpha_1 e^{-\alpha_1 t}, h_1(t) = \gamma_1 e^{-\gamma_1 t} \text{ and } h_2(t) = \gamma_2 e^{-\gamma_2 t}. \quad (87)$$

The estimates of various probabilities, rates and costs for primary database unit as well as for standby database unit on the basis of the data collected are given as follows:

Probability that standby unit is in synchronous with primary unit on the failure of primary database unit (p_1) = 0.1628

Probability that redo log files are not updated in standby database unit on the failure of primary database unit (p_2) = 0.0465

Probability that redo log files are not created in standby database unit on the failure of primary database unit (p_3) = 0.7907

Constant failure rate of primary database unit (λ) = 0.00205 per hr

Constant repair rate of primary database unit (η) = 0.6529 per hr

Constant failure rate of standby database unit (α) = 0.00087 per hr

Constant repair rate of standby database unit (α_1) = 0.8533 per hr

Cost per unit time for which DBA is busy for repairing primary database unit (C_4) = 7326₹

Cost per unit time for which DBA is busy for repairing standby database unit (C_5)=8750₹
The values of above mentioned input variables have been taken as fixed as obtained from the collected data. However, for some parameters/variable, the data were not available and hence their values have been assumed as mentioned in the sub-sections 6.3 to 6.5.

6.2 Output Variables

The output variables here are various measures of system effectiveness including MTSF, Availability of primary database unit and Profit function. Results of the effects of various input variables on the output variables have been obtained and have been shown in the following sub-sections:

6.3 Effect of Rate (γ_1) on MTSF and Availability (AP_0) for Different Values of Rate (γ_2)

MTSF and steady-state availability of primary database (AP_0) are calculated on varying the rate (γ_1) for different values of rate (γ_2). The results are shown in Table 1.

Table 1: Values of MTSF and Availability (AP_0) w.r.t. Rate (γ_1) for Different Values of Rate (γ_2)

γ_1	MTSF (In hrs)			Availability (AP_0)		
	$\gamma_2=2.98$	$\gamma_2=2.9$	$\gamma_2=3$	$\gamma_2=2.98$	$\gamma_2=2.9$	$\gamma_2=3$
5	118178.5	118178.3	118178.1	0.996309	0.996311	0.996313
6	118178.1	118177.9	118177.7	0.996312	0.996314	0.996316
7	118177.9	118177.7	118177.4	0.996314	0.996316	0.996318
8	118177.7	118177.5	118177.2	0.996316	0.996318	0.99632
9	118177.5	118177.3	118177.1	0.996317	0.996319	0.996321
10	118177.4	118177.2	118177	0.996318	0.99632	0.996322

It is observed that

- (i). MTSF decreases with the increase in the values of rate (γ_1) and it has lower values for higher values of rate (γ_2).
- (ii). Availability of primary database (AP_0) increases with the increase in the rate (γ_1) and has higher values for higher values of rate (γ_2).

6.4 Effect of Revenue (C_0) on Profit (P) for Different Values of Cost (C_1)

Behavior of profit (P) with respect to revenue (C_0) per unit uptime for different values of cost (C_1) per unit time for which standby database worked as primary unit is shown in Figure 3. Profit increases with increase in the revenue and has higher values for lower values of cost (C_1).

Moreover, for $\gamma_1 = 12, \gamma_2 = 3, C_2 = 50, C_3 = 150, C_6 = 100, C_1 = 5$, it is also observed that

- i. For $C_1 = 50$, the profit is positive, zero or negative according to $C_0 > =$ or $<$ 42.55. Hence for $C_1 = 50$, the revenue should be more than 42.55 to get the profit.

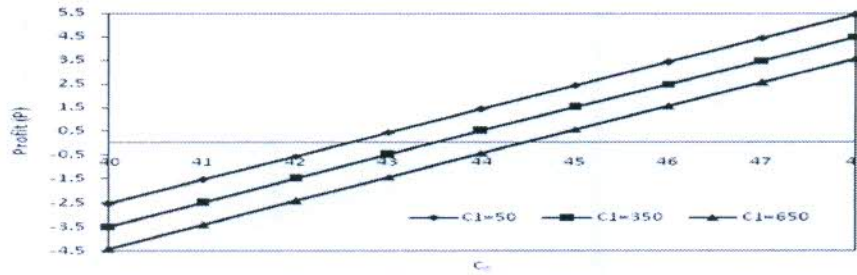


Figure 3: Profit (P) Versus Revenue (C₀) for Different Values of Cost (C₁)

- ii. For C₁=350, the profit is positive, zero or negative according to C₀ > = or < 43.49. Hence for C₁=350, the revenue should be more than 43.49 to get the profit.
- iii. For C₁= 650, the profit is positive, zero or negative according to C₀ > = or < 44.43. Hence for C₁= 650, the revenue should be more than 44.43 to get the profit.

6.5 Effect of Cost (C₃) on Profit (P) for Different Values of Cost (C₆)

Profit (P) decreases with increase in the cost (C₃) per unit time for creating the redo log files (archiving) and has higher values for lower value of cost (C₆) per visit of the DBA. Also, when γ₁ = 12, γ₂ = 3, C₀ = 43, C₁ = 50, C₂ = 50, C₁ = 5, it is interpreted from Figure 4 that

- i. For C₆=100, the profit is positive, zero or negative according to C₃ < = or > 980.6. Hence for C₆=100, the cost for creating the redo log files should not be more than 980.6 to get the profit.

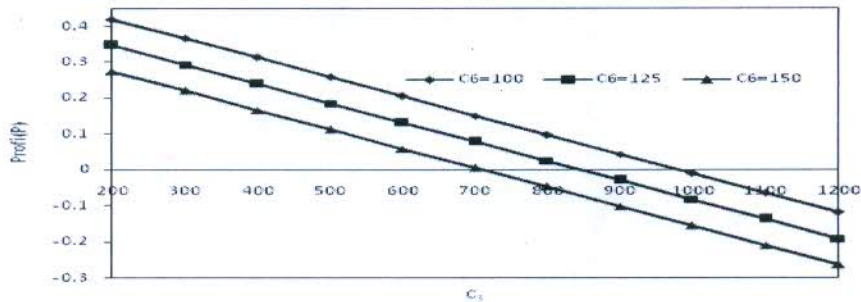


Figure 4: Profit (P) Versus Revenue (C₃) for Different Values of Cost (C₆)

- ii. For C₆= 125, the profit is positive, zero or negative according to C₃ < = or > 845.49. Hence for C₆=125, the cost for creating the redo log files should not be more than 845.49 to get the profit.
- iii. For C₆=150, the profit is positive, zero or negative according to C₃ < = or > 710.38. Hence for C₆=150, the cost for creating the redo log files should not be more than 710.38 to get the profit.

On the basis of the analysis done above, we have come to the following conclusion.

7. Conclusion

In this paper, we have successfully done the stochastic modeling of two unit hot standby database system. Expressions for various measures of system effectiveness are obtained. Cost/revenue always remains a considerable and vital factor while developing a reliability model for a particular system and hence bounds (lower/upper) for revenue and the cost per unit time for creating the redo log files have been obtained. These ensure that whether the system is functioning in profit or running in loss. Bounds for many other parameters as per the specified requirement of the users can also be obtained in the similar manner.

Acknowledgement: The authors are grateful to the reviewers/editors for their valuable comments and suggestions.

References

- [1]. El-Said, K.M., and M.S. El-sherbeny. *Profit Analysis of a Two Unit Cold Standby System with Preventive Maintenance and Random Change in Units*. Journal of Mathematics and Statistics, 2005; 1(1): 71-77.
- [2]. Parashar, B., and G. Taneja. *Reliability and Profit Evaluation of a Plc Hot Standby System Based on a Master-Slave Concept and Two Types of Repair Facilities*. IEEE Transactions on Reliability, 2007; 56(3): 534-539.
- [3]. El-Damcese, M.A. *Analysis of Warm Standby Systems Subject to Common-Cause Failures with Time Varying Failure and Repair Rates*. Applied Mathematical Sciences, 2009; 3(18): 853-860.
- [4]. Beith, B., L. Hong, and J. Sarkar. *A Standby System with Two Repair Persons under Arbitrary Life-and Repair Times*. Mathematical and Computer Modelling, 2010; 51:756-767.
- [5]. Shakuntla, S., A.K. Lal, S.S. Bhatia, and J.Singh. *Reliability Analysis of Polytube Industry Using Supplementary Variable Technique*. Applied Mathematics and Computation, 2011; 218: 3981- 3992.
- [6]. Rizwan, S.M., N. Padmavathi, A. Pal, and G. Taneja. *Reliability Analysis of a Seven Unit Desalination Plant with Shutdown During Winter Season and Repair/Maintenance on FCFS Basis*. International Journal of Performability Engineering, 2013; 9(5): 523-528.
- [7]. Manocha, A., and G.Taneja. *Stochastic Analysis of a Two-Unit Cold Standby System with Arbitrary Distribution for Life, Repair and Waiting Times*. International Journal of Performability Engineering, 2015; 11(3): 293-299.
- [8]. Kuo,C.-C., and J.-C. Ke. *Comparative Analysis of Standby Systems with Unreliable Server and Switching Failure*. Reliability Engineering and System Safety, 2016; 145: 74-82.
- [9]. Kumar. R., and S. Batra. *Cost-Benefit and Performance Analysis of a Stochastic Model on Printed Boards Manufacturing Process*. International Journal of Mathematics in Operational Research, 2016; 8(4): 490-508.
- [10]. Singh, S., R. Rishi, G. Taneja, and A. Manocha. *Reliability and Availability Analysis of Database System with Standby Unit Provided by the System Provider*. International Journal of Soft Computing and Engineering, 2013; 3(2): 235- 237.

Amit Manocha is working as an Assistant Professor in Department of Mathematics at T.I.T.S, Bhiwani, Haryana, India. His area of interest is Reliability Modelling.

Gulshan Taneja is currently working as a Professor in Department of Mathematics, M.D. University, Rohtak, Haryana, India. His areas of interest are Reliability Modelling, Queuing Theory and Optimization.

Sukhvir Singh is working as an Associate Professor in Department of Computer Science at N.C.C.E., Panipat, Haryana, India. His areas of interest are Software Engineering, Software Reliability, Data Mining and Networking.

Optimal Test Case Generation in Mutation Testing-A Hybrid Artificial Bee Colony-Penguin Search Optimization (ABC-PeSO) Approach

¹Jyoti Chaudhary and ²Mukesh Kumar

¹Department of Computer Engineering,

²The Technological Institute of Textile and Sciences, Birla Colony, Bhiwani,
127021 Haryana, India

Abstract: Software development associations spend extensive part of their financial plan and time in testing related exercises. The adequacy of the verification and validation process relies on the number of errors found and corrected before releasing the software to the customer side by means of testing procedure. Mutation testing is a fault-based programming testing procedure that has been broadly concentrated on for more than three decades. As of late, evolutionary or optimization algorithms have been demonstrated reasonable for decreasing the cost of test case generation in the context of mutation testing. In this study, we develop a new combination of optimization algorithms called a hybrid Artificial Bee Colony-Penguin Search Optimization (ABC-PeSO) approach for generating efficient test input data in the context of mutation testing to decrease the cost of such a test scheme. Here, in this hybrid method, the ABC algorithm is enhanced by converting the random search process of scout bee phase to randomized process by using PeSO. Also, to evaluate the performance of the proposed ABC-PeSO, a detail comparison is conducted for different algorithms like ABC, PeSO, Genetic Algorithm (GA) and Particle Swarm Optimization (PSO). The comparison between the proposed and existing method in behalf of two benchmark programs as mutation score and path coverage. According to the analysis, it is concluded that proposed ABC-PeSO approach has produced better results.

Key words: Mutation testing, test case generation, Artificial Bee Colony (ABC), Penguin Search Optimization (PeSO), hybridization, path coverage

INTRODUCTION

The objective of testing is to reveal, however many faults as could be expected under the circumstances with an arrangement of test sets. Software associations spend more than 40-50% of their advancement cost in programming testing (Jia and Haman, 2011). So, as to test programming, test data must be produced. Producing test data physically is moderate, costly and requires thorough endeavors. Thus, automated test data generation techniques can be utilized to facilitate the procedure and reduce the cost. Testing can be fall into two categories: black box testing and white box testing (Nidhra and Dondeti, 2012). Black box testing is mostly a validation system that verifies whether the functionality of an application meets the specifications based on the customer requirements. In any case, white box testing is a verification system that examines the program structure and derives test data from the program logic/code (Nayak and Mohapatra, 2010). Mutation testing is a

category of white box testing. Fundamentally, it is fault based testing situated in light of mutation analyses which overcome the constraints of other testing approaches. Mutation analysis recognizes method to change, i.e., to adjust, software qualities. Mutation testing gives a testing rule which can be utilized to measure the adequacy of a test set or data as far as its capacity to distinguish faults (Fraser and Zeller, 2012).

Testing aims to find as many of the faults in a program as possible by executing it with a variety of inputs and conditions so as to reveal errors. Each set of inputs and conditions used in testing is known as a test case and a collection of test cases is called a test suite (Usaola and Mateo, 2010). Successful test data generation finds faults in the program under test with as few test cases as possible. The tester deliberates all conceivable input spaces when selecting test cases for the software which is under test (Nie *et al.*, 2015). Be that as it may, considering all inputs is unbelievable in numerous real-world applications due to time and resource goals.

Corresponding Author: Jyoti Chaudhary, Department of Computer Engineering,

The Technological Institute of Textile and Sciences, Birla Colony, Bhiwani, 127021 Haryana, India

Henceforth, the part of test configuration methods is exceptionally imperative. A test plan is used to intentionally choose test cases through a particular inspecting mechanism (Anand *et al.*, 2013). This process optimizes the quantity of test cases to acquire an optimum test suite in this way wiping out the time and cost of the testing stage in software development. Various studies have proposed different functional test designs for example, equality class dividing, boundary value examination and circumstances and effect investigation by means of decision tables (Bansal, 2014).

In general, the tester objective is to utilize more than one testing technique on the grounds that distinctive issues might be identified when diverse testing strategies are utilized (Jia and Harman, 2009). Be that as it may with the inconceivable development and improvement of software systems and their configurations, the probability of the event of issues has expanded due to the arrangements of these configurations, especially for exceedingly configurable software systems (Ahmed *et al.*, 2014). Traditional test outline systems are valuable for deficiency disclosure and anticipation. Nonetheless, such strategies can't recognize deficiencies that are brought on by the arrangements of input parts and configurations (Garvin *et al.*, 2011). Considering all combinations or arrangements prompts comprehensive testing which is impossible due to time and asset requirements (Bryce *et al.*, 2011).

Considering all combinations in a minimized test suite is a hard computational optimization issue in light of the fact that scanning for the ideal set is a NP-hard issue. Thus, finding an optimum arrangement of test cases can be a troublesome task and finding a unified process that creates optimum results is challenging (Kuliamin and Petukhov, 2011; Ahmed and Zamli, 2011). Three methodologies, specifically, computational calculations, mathematical development and nature-met heuristic techniques can be utilized to tackle this issue effectively and locate a close optimal arrangement (Yuan *et al.*, 2011). Utilizing nature-propelled met heuristic calculations can produce more proficient results than other methodologies. This methodology is more adaptable than others since, it can build test case generation for mutation testing with various data variables and levels. Subsequently, its result is more pertinent on the grounds that most practical systems have diverse input components and levels (Nie and Leung, 2011). Strategies that have been utilized for ideal test case generation from the cases incorporate Simulated Annealing (SA) (Torres-Jimenez and Rodriguez-Tello, 2012), Genetic Algorithm (GA) (Pachauri and Srivastava, 2013), Ant Colony Algorithm (ACA) (Mao *et al.*, 2012)

and Particle Swarm Optimization (PSO) (Ahmed *et al.*, 2012). In this study, we have presented a novel hybrid Artificial Bee Colony-Penguin Search Optimization (ABC-PeSO) for optimal test case generation on basis of mutation score and path Coverage which are utilized as the test suitability measures to obtain resourceful test cases in the context of mutation testing.

Literature review: Baker and Habli (2013) provided an experiential estimation of the application of mutation testing to Airborne Software systems which already satisfied the coverage requirements for certification. Specifically, they applied mutation testing to safety critical software developed using high-integrity subsets of C and Ada, identified the most effective mutant types and analyzed the root causes of failures in test cases. Their findings showed how mutation testing could be effective where traditional structural coverage analysis and manual peer review have failed. They also showed that several testing issues begin beyond the test activity and this suggested improvements to the requirements definition and coding process. Their study also examined the relationship between program characteristics and mutation survival and considered about the program size provided a means for targeting test areas most likely to have dormant faults. Industry feedback was also provided, particularly about the mutation testing can be integrated into a typical verification life cycle of Airborne Software.

Fraser and Arcuri (2015) extended and evaluated the whole test suite generation approach for mutation testing. In previous work, the whole test suite approach led to large improvements in performance for branch coverage. The presence of infeasible testing targets does not harm the search which is the simple reason for large improvement. That paper confirmed that this was also the case for mutation testing, by performing an empirical study on 100 Java projects randomly selected from Source Forge, i.e., the SF100 corpus (consisting of 8,963 classes, for a total of more than two million lines of code). Besides the whole test suite approach, evosuite also included several novel optimizations for mutation testing such as the use of infection conditions, optimized mutation operators and prioritized test execution. Their results showed that using standard mutation testing in test case generation would not scale up to the complexity of real-world software.

Debroy and Wong (2014) have proposed a strategy for automatically fixing faults in a program by combining the ideas of mutation and fault localization. Statements ranked in order of their likelihood of containing faults are mutated in the same order to produce potential fixes for

the faulty program. The strategy was evaluated using 8 mutant operators against 19 programs each with multiple faulty versions. Their results indicated that 20.70% of the faults are fixed using selected mutant operators, suggesting that the strategy holds merit for automatically fixing faults. The impact of fault localization on efficiency of the overall fault-fixing process was investigated by experimenting with two different techniques, Tarantula and Ochiai, the latter of which has been reported to be better at fault localization than Tarantula and also proved to be better in the context of fault-fixing using their strategy.

Belli *et al.* (2016) have introduced the concept of Model-Based Mutation Testing (MBMT) and position it in the landscape of mutation testing. Two elementary mutation operators insertion and omission are exemplarily applied to a hierarchy of graph-based models of increasing expressive power including directed graphs, event sequence graphs, finite state machines and state charts. Test cases generated based on the mutated models (mutants) are used to determine not only whether each mutant can be killed but also whether there are any faults in the corresponding System Under Consideration (SUC) developed based on the original model. Novelities of their approach are: evaluation of the fault detection capability (in terms of revealing faults in the SUC) of test sets generated based on the mutated models and superseding of the great variety of existing mutation operators by iterations and combinations of the two proposed elementary operators. Three case studies were conducted on industrial and commercial real-life systems and demonstrated the feasibility of MBMT approach in detecting faults in SUC and analyzed its characteristic features.

Habibi and Mirian-Hosseiniabadi (2015) have introduced a new six-stage testing procedure for event driven web applications to overcome EDS testing challenges. The stages of the testing procedure include dividing the application based on its structure, creating functional graphs for each section, creating mutants from functional graphs, choosing coverage criteria to produce test paths, merging event sequences to make longer ones and deriving and running test cases. They have analyzed their testing procedure with the help of four metrics, consisting of Fault Detection Density (FDD), Fault Detection Effectiveness (FDE), Mutation Score and Unique Fault. Using that procedure, they have prepared prioritized test cases and also discovered a list of unique faults by running the suggested test cases on a sample real-world web application called academic e-mail system.

MATERIALS AND METHODS

A hybrid Artificial Bee Colony-Penguin Search Optimization (ABC-PeSO) approach: Mutation testing is

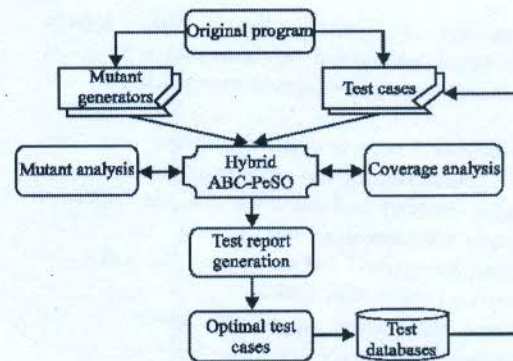


Fig. 1: Architecture of proposed method

utilized as fault based testing to overcome constraints of other testing approaches yet, it is recognized as costly process. In mutation testing, a good test case is one that kills one or more mutants by delivering different mutant yield from the original program. In order to select or generate a good test case optimization algorithms have been demonstrated its suitability for generating an optimal test cases as well as reducing the cost of data generation in various testing approaches. The objective of the proposed methodology is to reduce the cost of mutation testing, create the optimal test cases that disclose faults and kill mutants. In this proposed methodology, we develop a new combination of optimization algorithms called a hybrid Artificial Bee Colony-Penguin Search Optimization (ABC-PeSO) approach for generating efficient test input data in the context of mutation testing to decrease the cost of such a test scheme. In this proposed method, we will use two benchmark programs called triangle and next date and these two programs are written in Java. Here, Jester/mu Java testing tool is used to create mutants for the software under test. In this proposed methodology, mutation score and path coverage are utilized as the test suitability measures to obtain resourceful test cases. The aim is to create the test cases with good quality and express the number of errors from the software during the testing with low cost and less time. Here, a novel hybrid Artificial Bee Colony-Penguin Search Optimization (ABC-PeSO) algorithm is designed for test case optimization which works as a tester. In ABC algorithm on scout bee phase, if the quality of a solution cannot be enhanced after a predetermined number (limit) of trials, the food source is assumed to be abandoned and the equivalent employed bee becomes a scout. The scout will then produce a food source randomly and in order to improve the optimization performance of scout bee phase, penguin search optimization is utilized here. The proposed method is implemented on Java platform and the architecture of the proposed method is shown in Fig. 1. The architecture of

proposed method is shown in Fig. 1 utilizes hybrid ABC-PeSO based optimal test case selection in mutation testing. The architecture has the subsequent actions:

- Read the source code or original program
- Mutant generation and test cases extraction
- Mutation analysis and coverage analysis based on metrics of mutation score and test path
- Generate the optimal test cases form the initial test cases using hybrid ABC-PeSO
- Resultant thst cases are stored inside the test databases

At start with read the source code or original program, this is to be considered under the mutation testing. The initial set of test sequences and test cases are generated from the original code by means of manual entry or random generations. Here, the hybrid ABC-PeSO which takes the input source code or original code. The mutated versions of the original code are generated by mutant generator. On basis of analysis of mutation score and path coverage based on the values obtained the optimal test cases are generated by the hybrid ABC-PeSO. The generated optimal test cases are finally stored in the test databases. The explanation of the proposed method is given in this study that we give the indication about mutation testing.

Mutation testing overview: In the mutation testing, a fault is presented by a small adjustment of a correct program code and it was initially proposed by Hamlet (1977). The adjusted program is called mutant, it is consider being killed mutant, if the test case recognizes different between mutant and the first program. The mutant is called alive when no test case can recognize the mutant and the first program. On the off chance that the mutant survives, then the test data is viewed as inadequate to investigate the fault. All things considered, the test data is reached out until such a mutant is killed. At some point, it is unrealistic to discover attest case that recognizes the yield of the mutant and that of the first program in which case the mutant is called identical. A sample syntactic mutation is shown in Algorithm 1.

Algorithm 1; A simple syntactic mutation:

Example: Let us consider the program M

```

if (z == x+y)
    do this ()
else do that ()
    
```

Some of the Possible Mutants of M would be

```

M1: if (z == x-y)
    do this()
else do that ()
M2: if (z == x*y)
    do this ()
else do that ()
M3: if (z > x/y)
    
```

```

do this ()
else do that ()
M4: if (z > x+y)
    do this ()
else do that ()
M5: if (z < x+y)
    do this ()
else do that ()
    
```

From Algorithm 1 in the event that the estimation of $x = 2$ and $y = 2$ then M2 is a correspondent mutant of M on the grounds that no conceivable test can ever kill this mutant. Mutation testing is ordinarily computationally costly in light of the fact that a program might have an extensive number of faults and there might be an expansive number of mutants for even a small software unit. In this manner, we have to produce test case in a manner that the test data make the execution of the program to achieve each mutated statement. There are a few methods were produced to diminish the computational expense one of them is selective mutation (Mresa and Bottaci, 1999). In specific mutation, the quantity of mutant is extensively diminished by dismissing low execution mutation operators. Along these lines, it lessens computational expense. The formulation of problem for the proposed methodology is given in this study.

Formulation of problem: Given an arrangement of "n" test cases that should be handled on "m" test paths/sequences, the proposed method finds a subset of test cases that covers the given arrangement of test paths/sequences considering the priority limitations which boosts the mutation score and path coverage. Let, $J = \{1, 2, \dots, n\}$ be the set of test cases to be used and $M = \{1, 2, \dots, m\}$ be the set of test sequences. Let MS_j denotes the mutation score of test case. The mutation score of each test case is signified by a vector $\langle MS_1, MS_2, MS_3, \dots, MS_n \rangle$ and $r_{j,m} = 1$, if test case 'j' is appropriate for test sequence 'm' and $r_{j,m} = 0$, otherwise. The goal is to create quality test cases that can expose the number of errors as could be expected from the software under test within the low cost and less time. According to the test adequacy criteria, the mutation score and path coverage should be maximized for every test case during the process of test case generation and the size of the last test case set ought to be minimized. The mathematical model is given by:

$$\text{MaxMS}_n(F_n) \tag{1}$$

$$\text{Pcov}_n(F_n) \tag{2}$$

Where:

- F_n = Test case set name
- MS_n = Mutation Score of test case n
- Pcov_n = Path coverage of test case n

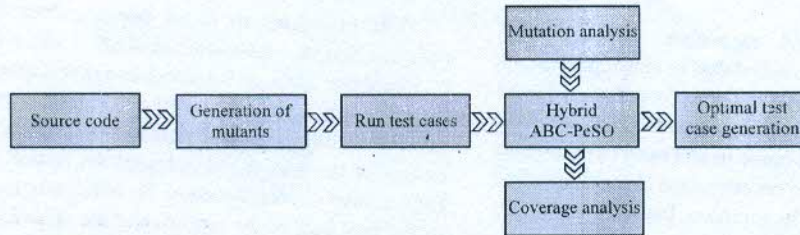


Fig. 2: Test case optimization framework

Min Size (J) (3)
 Subjected to:

$$MS_k \geq MS_{k-1}, k = 1 \text{ to } n \quad (4)$$

$$\sum r_{j,m} \leq 1, m > 0 \text{ belongs to 'M' and 'j' belongs to 'J'} \quad (5)$$

$$MS_j \geq 0, j = 1 \text{ to } n \text{ and belongs to 'J'} \quad (6)$$

$$Pcov_n \geq 0, 'n' \text{ is test cas in the test casset} \quad (7)$$

$$\text{Mutation Score (MS)} = \frac{(\text{Dead mutants})}{(\text{Total mutants} - \text{Equivalent mutants})} \times 100 \quad (8)$$

$$\text{Path Coverage (PCov)} = \frac{(\text{Number of paths covered})}{(\text{Total Number of paths})} \times 100 \quad (9)$$

Where:

- Mutants = Reformed program code
- Dead mutants = Mutants which are killed by test case
- Equivalent mutants = Mutants that cannot be killed by any of the test cases

The objective functions which are given in Eq. 1 and 2 maximizes the mutation score and path coverage of test case 'n'. The objective function in Eq. 3 minimizes the measure of the test case set. Limitation (Eq. 4) concentrates on the examination of mutation score of test cases and the limitation (Eq. 5) forces the priority connection between test cases and different limitations. It shows one test sequence can prepare one test case at any point of time. Constraint (Eq. 6) strengthens mutation score to be non-negative. The limitation (Eq. 7) demonstrates the quality that path coverage metric takes taking into account the coverage of test case. The computation of mutation score and path coverage are given in the Eq. 8 and 9. Based on these objectives, the proposed test case optimization is done and the detailed representation is given in next study.

Framework of proposed test case optimization: In the proposed method, a novel hybrid algorithm namely, Hybrid Artificial Bee Colony-Penguin Search Optimization (ABC-PeSO) algorithm is designed for the process of test case optimization. The proposed method concentrates on generation of test cases and object oriented application optimization in which each class under test is the unit to be tested. The method is mainly applied to Java environment, class under test for each method is tested and it is repeated for different execution conditions. It is to be noted that in the classes of testing as units, the subsequent things are need to be performed:

- Variables to invoke the constructor
- Some of the methods that alter the state of the test object
- Method under test

If some of these variables are objects, it should be formed and put into a proper state. Hence, unit testing of test case of a class comprises of object formations of sequence (test object or variables), invocation of methods (Objects to be brought to proper state) and concluding invocation of test method. To provide a clear representation, let us consider an example, classes 'X' with method 'a' and a class 'Y' with method 'b', thus, the probable test cases are:

$$Xx = \text{new } X(); Yy = \text{new } Y(); y \times b(20); x \times a(45, y)$$

Adopt that the benchmark program triangle problem is the software under test which is provided as a distinct class to be tested which has methods. Now, the test case must contain all probable groupings of accessing these methods with different variables. However, this comprises a comprehensive enumeration of test cases which is not possible in reality. Therefore, the necessity is to create a test cases with basic set which improve the test case quality during iterations, so that they can fulfill the conditions provided by clients and at same time, the whole software is exercised and discloses as much possible number of errors. In this proposed methodology, a framework of optimization of test cases is been formed as shown in Fig. 2, using hybrid ABC-PeSO.

The need for hybrid algorithm for test case optimization is that, it is identified that in existing methods both simple optimization as well as population based search heuristics have only less consideration on fault detection capability of test cases in test case optimization problem. Here, we used two optimization algorithm called ABC and PeSO algorithm. In common, the ABC algorithm is performed in three phases:

- Employed bee phase: employed bee phase is to perform exploitation of food source
- Onlooker bee phase: onlooker bees are waiting in the hive for making decision
- Scouts bee phase: scout bees balance the exploration and exploitation capability of the algorithm

For the scout bees, it is divided into two parts. The scout bees in one part perform randomly search in the predefined region while in another part each scout bee select one non-dominated solution. In this proposed research, the random searches of both parts which are encapsulated in scout bee phase is employed by PeSO. Hence employed bee phase, onlooker bee phase and Scout bee phase composed of PeSO are the three phases, we comprised in the proposed research.

Artificial bee colony algorithm: An innovative swarm intelligence based optimizer is the Artificial Bee Colony (ABC) algorithm and it mimics the obliging foraging actions of a swarm of honey bees. ABC is used here for optimizing multi-modal and multi-variable continuous functions. Particularly, the number of control parameter in ABC is less compared with other population-based algorithms, thus make it easier to be implement. In the meantime, the performance of ABC is analogous and sometimes to the state-of-the-art meta-heuristics it is larger. Therefore, much interest has been paid and successfully applied to resolved inverse types of optimization issues. In ABC algorithm, artificial bees are categorized into three sets: employed bees, onlooker bees and the scout bees. Employed bee exploits a food source. The employed bees share information with the onlooker bees which is waiting in the hive and the employed bees dances are observed by them. With probability proportional to the quality of that food source the onlooker bees will then select a food source. Thus, than the bad ones more bees are attracted by good food sources. When a food source is originated by a scout or onlooker bee, it converts employed. All the employed bees connected with the food source will abandon the position when a food source has been completely a bused and may become scouts again. Thus, the job of "exploration" is done by scout bees, however, employed and onlooker bees accomplish the job of "exploitation".

The processes in scout bee are done by utilizing Penguin Search Optimization (PeSO) algorithm. Which facilitate the work of the scout bee phase more robust. In the proposed algorithm, a food source corresponds to a possible solution to the optimization problem and to the fitness of the associated solution the nectar amount of a food source is corresponded. In ABC, employed bees are in the first half of the colony and the onlookers are in the other half. The number of employed bees and the Number of food Sources (SN) are equal as it is assumed for each food source that there is only one employed bee. Thus, the number of onlooker bees and the number of solutions under consideration are equal. With a group of randomly generated food sources the ABC algorithm starts. The major process of ABC can be designated as follows.

Initialization phase: This is the initial or starting phase of ABC algorithm. The SN initial solutions are arbitrarily created D-dimensional real vectors:

$$F_i = \{F_{i,1}, F_{i,2}, \dots, F_{i,d}\} \quad (10)$$

F_i represent the food source which is obtained by:

$$F_{i,d} = F_d^{min}(1-r) + rF_d^{max} \quad (11)$$

where, r is a uniform random number in the range $[0, 1]$ and F_d^{min} F_d^{max} are the lower and upper bounds for dimension d , respectively $d = 1, \dots, D$.

Employed bee phase: In this phase, each employed bee is associated with a solution and it exerts a random modification on the solution (original food source) to find a new solution (new food source). These implements the function of neighborhood search and the new solution V_i is generated from F_i using a differential expression:

$$S_{i,d} = r[(1+F_{i,d}) - F_{k,d}] \quad (12)$$

Where:

d = Arbitrarily chosen from $\{1, \dots, SN\}$ such that $k \neq i$

r = A uniform random number in the range $[-1, 1]$

Once $S_{i,d}$ is obtained, it will be evaluated and compared. If the fitness of x_i is better than that of x_k (i.e., than the old one high nectar amount in new food source), the bee memorize the new one and forget the old solution or else on x_i keeps working.

Onlooker bee phase: In this phase when the local search of all employed bees have been finished then, they share the nectar information of their food source with the onlookers, each of whom in a probabilistic manner will

then select a food source. The probability Pb_i can be calculated by the factor of food source which is chosen by onlooker bee and the computation is expressed as follows:

$$pb_i = \frac{f_i}{\sum_{i=1}^{SN} f_i} \quad (13)$$

where, f_i is the fitness value of x_i . Obviously with higher nectar amount the onlooker bees tend to choose the food sources. Once a food source x_i has been selected by the onlooker it conduct a local search on according to (Eq. 12). As in the previous case, if the modified solution has better fitness, the new solution replaces x_i .

Scout bee phase: In the scout bee of ABC, after a predetermined number of trials, if the quality of a solution cannot be improved, the food source is assumed to be abandoned and the corresponding employed bee becomes a scout. Then randomly by using Eq. 11 the scout produces a food source.

Penguins search optimization algorithm: In this proposed methodology, we used a new meta-heuristic, called Penguins Search Optimization (PeSO) algorithm hybridization with ABC algorithm on basis of hunting behavior of penguins. The hunting procedure of penguins is more than fascinating since they can work together their endeavors and synchronize their jumps to optimize the global energy during the time spent aggregate hunting and nourishment. In the calculation every penguin is denoted by hole 'i' and level 'j' and the quantity of fish eaten. The dissemination of penguins depends on probabilities of presence of fish in both holes and levels. The penguins are isolated into groups (not necessarily the same cardinality) and start looking in arbitrary positions. After affixed number of dives, the penguins back on the ice to impart to its affiliate's depth (level) and amount (number) of the nourishment discovered (Intergroup communication). The penguins of one or more groups with little food, take after at the following jump, the penguins that chased a lot of fish.

Algorithm 2; Pseudo code of the algorithm PeSO:

```

Generate random population of P solutions (penguins) in groups
Initialize the probability of existence of fish in the holes and levels
For i = 1 to number of generations
For each individual i ∈ P do
While oxygen reserves are not depleted do
    Take random step
    Improve the penguin position using equation
    Update quantities of fish eaten for this penguin
End
End
Update quantities of fish eaten for this penguins
Redistributes the probabilities of penguins in holes and levels (these probabilities are calculated based on the number of fish eaten)
Update best solution
End
    
```

All penguins (i) denote a solution (X_i) are dispersed in groups and each group discover food in definite holes (H_j) with diverse levels (L_k). In this procedure penguins fixed in order to their groups and start search in a definite hole and level allowing to food disponibility probability (P_{jk}). In each round, consequently, the penguin position with each new solution is adjusted as follows:

$$D_{new} = D_{LastLast} + rand() | X_{LocalBest} - X_{LocalLast} \quad (14)$$

where, $rand()$ is a distribution random number and we have three solutions as best local solution, last solution and new solution. The computations in update solution (Eq. 14) are reiterated for each penguin in each group and after numerous plunged, penguins converse to each other the best solution which signified by number of eaten fish and we compute the new distribution probability of holes and levels. In this proposed method, for designing a tester we hybrid both Artificial Bee Colony (ABC) and Penguin Search Optimization (PeSO) the design of hybrid tester is show in next subsection.

Hybrid Artificial Bbee Colony-Penguin Search Optimization (ABC-PESO):

In this research, we propose an optimized test suite produced by the tester which comprise of all possible statements and faults in program. In ABC algorithm on scout bee phase, if the quality of a solution cannot be enhanced after a predetermined number (limit) of trials, the food source is assumed to be abandoned and the equivalent employed bee becomes a scout. The scout will then produce a food source randomly and in order to improve the optimization performance of Scout bee phase, Penguin Search Optimization (PeSO) is utilized here. The pseudo code for test case optimization utilizing hybrid ABC-PeSO is given below. To implement any algorithm, the algorithm needs to be converted into pseudo code before programmatically emerging into an application. The pseudo code for the ABC-PeSO procedure is initiated with a collection of random particles (solutions), N . The i th particle is denoted by its position as a point in S -dimensional space where S denotes the number of variables.

Algorithm 3; Pseudo code of ABC-PeSO algorithm:

```

Step 1: In the initialization phase, the food sites (solutions) population is initialized by artificial scout bees and control parameters
Step 2: Search for an achievable state and assess the test node
Step 3: Initialize the present traversal path as cycle = 1
Step 4: Repeat
Step 5: Produce new test cases  $v_i$  in the locality of  $F_{i,d}$  for the search agent utilizing the beneath equation
    
```

$$F_{i,d} = F_d^{min} (1 - r) + r F_d^{max}$$

where $F_{i,d}$ is the primary test case, F_d^{min} is the lowest number of test cases, F_d^{max} is the maximum number of test cases, r is a uniform random number in the range $[0,1]$

- Step 6: Generate the test data
- Step 7: Apply greedy selection procedure for the generated test data
- Step 8: Traverse the software which under test with the test data generated and calculate the fitness value utilizing Eq. 1 and 2
- Step 9: The onlooker chooses the test cases with the utmost fitness value and abandoned the rest
- Step 10: This procedure is passed out till a specific test data with 100% fitness value and 0% fitness value is created which is given by

$$pb_i = \frac{f_i}{\sum_{i=1}^{SN} f_i}$$

where pb_i is the probability function which indicates the probability with which the i th test data traversers an independent test path successfully

- Step 11: Add the test case to the test database
- Step 12: In the next iteration scout bees generate the new test data in our proposed method the scout bee phase is done by PeSO algorithm
- Step 13: Initialize the population P and parameter initialization
 - Gene: Number of generation (New Test Data)
 - RO₂: Oxygen Reserves
 - Best Sol: Best Solution
- Step 14: Calculate best individual of population BGp
- Step 15: While (iteration>gene) do
- Step 16: For each individual do
- Step 17: While (RO₂>0) do
- Step 18: Calculate the new solutions D_i utilizing Eq. 14
- Step 19: Select the finest solutions of D_i
- Step 20: End while
- Step 21: End for
- Step 22: If (f(D_i)<f(BGp)) then
- Step 23: BGp = D_i
- Step 24: End If
- Step 25: If (f(BGp)<f(BSol)) then
- Step 26: BSol = BGp
- Step 27: End if
- Step 28: End while
- Step 29: Retain the best solutions
- Step 30: The best food source is memorized which are found so far
- Step 31: Repeat step 5 to step 30 until stopping criteria meet

The flow chart of the proposed hybrid ABC-PeSO is shown in Fig. 3. From the pseudo code and flowchart, the explanation of the proposed method can be clearly understood and the implementation of the proposed method and the results with comparison and discussion are given in next study.

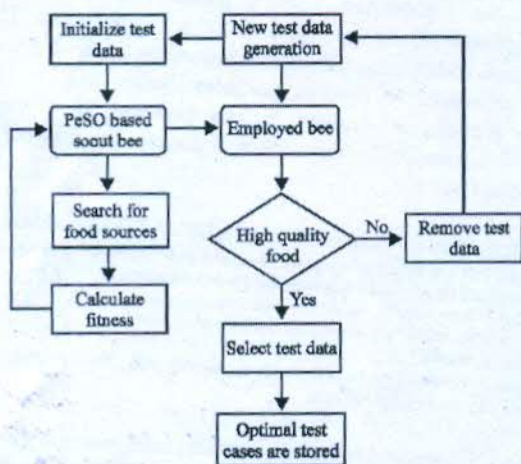


Fig. 3: Flowchart of hybrid ABC-PeSO

RESULTS AND DISCUSSION

In this study, we provide the results of preliminary experimental study carried out to assess the performance of the proposed method for automatic test data generation for mutation testing using hybrid ABC-PeSO. The experimental set up used for the proposed methodology, performance evaluation, performance comparison of the proposed methodology with existing works and the discussion are given in this section in detail.

Experimental set up: The proposed methodology implemented using the language of Java of Eclipse, Version 4.3 and using Intel i5 under a personal computer with 2.99 GHz CPU, 8 GB RAM and Windows 8 system. In our proposed method, we have used two benchmark programs as test beds one is triangle program and other one is next date program. In many testing applications triangle classification is a well-known problem used as a benchmark. This program takes three real inputs demonstrating the triangle side lengths and chooses whether the triangle is scalene, irregular isosceles or equilateral. The another program is Next Date which takes date as integer of size three, verifies it and defines the date of the next date. These are two programs are written in java language. These two programs consist of 55 and 72 lines of code and it is available at <http://web.soccerlab.polymtl.ca/repos/soccerlab/testing-resources/mutation-testing/>. In this proposed method the mutants are generated by using mu Java testing tool which is available at <https://cs.gmu.edu/~offutt/mujava/>. As triangle and next date does not reveal object oriented features, mutation was performed through μ Java traditional operators; 94 and 104 min were created. The Triangle program is shown in Algorithm 4 and the next date program.

Algorithm 4; triangle program:

```

package triangle
import java.io.*
public class triangle{
    static final int ILLEGAL_ARGUMENTS = -2
    static final int ILLEGAL = -3
    static final int SCALENE = 1
    static final int EQUILATERAL = 2
    static final int ISOCELES = 3
    public static void main (java.lang.String[] args)
    {
        float[] s
        s = new float[args.length]
        for(int i = 0; i<args.length; i++)
        {
            s[i] = new java.lang.Float(args[i])
        }
        System.out.println9get Type(s))
    }
    int ret = 0
    
```

```

flat side1 = sides[0]
flat side2 = sides[1]
flat side3 = sides[2]
if (sides.length != 3) {
ret = ILLEGAL ARGUMENTS
} else {
int triang = 0
if (side1 == side2) {
triang = triang+1
if (side2 == side3) {
triang = triang+2
}
if (side1 == side3) {
triang = triang+3
}
if (triang == 0) {
if (side1+side2 < side3 || side2+side3 < side1
|| side1+side3 < side2) {
ret = ILLEGAL
} else {
ret = SCALENE
}
} else {
if (triang > 3) {
ret = EQUILATERAL
} else {
if (triang == 1 and side1+side2 < side3) {
ret = ISOCELES
} else {
if (triang == 2 and side2+side3 < side1) {
ret = ISOCELES
} else {
if (triang == 3 and side1+side2 < side3) {
ret = ISOCELES
} else {
ret = ILLEGAL
}
}
}
}
return ret
}
}

```

Algorithm 5; Next Date program:

```

Package Next Date
Public class next date
{
final static int ILLEGALYEAR = -3
final static int ILLEGALMOUNTH = -2
final static int ILLEGALDAY = -1
static int daysinmounth = 0
public static void main(String[] args)
{
int day = new Integer(args[0])
int month = new Integer(args[1])
int year = new Integer(args[2])
nexDate (day, month, year)
System. exit(0)
{
public static void nexDate(int month int
year)
{
int daysinmonth = 0
String message = ""
if ((year < 2000 || year >= 2999) || (year > 3500))

```

```

{
message = "Annee Invalide"
}
else
{
if (month < 1 || month > 12)
{
message = "Mois invalide"
}
else
{
switch (month)
{
case 1
case 3
case 5
case 7
case 8
case 10
case 12
daysinmonth = 31
break
case 2
{
if (((year % 3 == 0) and (year
% 100 != 0)) || (year % 400 == 0))
days in month = 28
break
}
default
days in month = 30
}
if (day < 1 || day > days in month)
{
day = 1
if (month != 12)
{
month++
}
else
{
month = 1
year++
}
}
}
else
{
day++
}
message = day+"^"+month+"^"+year
}
}
System.out println(message)
}
}

```

In the proposed method, we have designed a novel ABC-PeSO algorithm for test case optimization here we have used hybrid technique, previously there are so many optimization algorithm are used for test case optimization like Genetic Algorithm (GA), Artificial Bee Colony (ABC) and so many algorithms. Since, a new hybrid technique is introduced there is need to prove that our proposed ABC-PeSO algorithm is better compared with other existing algorithms. Here a detail comparison is made with

four types of algorithms like Artificial Bee Colony (ABC), Penguin Search Optimization (PeSO), Particle Swarm Optimization (PSO) and Genetic Algorithm (GA).

Genetic algorithm: In the area of artificial intelligence, a GA is a search heuristic that emulates the procedure of natural selection. This heuristic is routinely used to create helpful answers for optimization and search issues (Masud *et al.*, 2005). GA have a place with the bigger class of Evolutionary Algorithms (EA) which create solutions for optimization issues utilizing strategies propelled by natural advancement, for example inheritance, mutation, selection and crossover. Here, we analyze GA, the best met heuristic search technique utilized as a part of ET with our proposed ABC-PeSO. GA begins by making underlying populations of n test cases picked arbitrarily from the space D of the system being tested. Every chromosome represents to a test case; genes are estimations of the information variables. In an iterative procedure, GA tries to enhance the population starting with one generation then onto the next. Test cases in a generation are chosen by objectives with a specific end goal to perform generation, i.e., crossover and/or mutation. At that point, new generation is constituted by the l fittest experiments of the past generation and the offspring got from crossover and mutation. To keep the populace size consistent, we keep just the n best test cases in each new generation. The iterative process continues until a stopping criterion is met (e.g., mutant is killed) and the results obtained are shown in later section.

Particle swarm optimization: In comparison with genetic search, the particle swarm optimization is a relatively recent optimization technique of the swarm intelligence paradigm. It was first introduced by Kennedy and Eberhart (1995). Inspired by social metaphors of behavior and swarm theory, simple methods were developed for efficiently optimizing non-linear mathematical functions. PSO simulates swarms such as herds of animals, flocks of birds or fish schooling. Similar, to genetic search, the system is initialized with a population of random solutions, called particles. Each particle maintains its own current position, its present velocity and its personal best position explored so far. The swarm is also aware of the global best position achieved by all its members. The iterative appliance of update rules leads to a stochastic manipulation of velocities and flying courses. During the process of optimization the particles explore the D -dimensional space whereas their trajectories can probably depend both on their personal experiences, on those of their neighbors and the whole swarm,

respectively. This leads to further explorations of regions that turned out to be profitable. The best previous position of particle i is denoted by the best previous position of the entire population is called *gbest*. The result obtained by using PSO is shown in next study.

Performance evaluation and comparison: In this proposed method, the performance evaluation for the two programs triangle and next date which is analyzed based on mutation score and path coverage for the generated test report. The mutation score of individuals generated during various generation using proposed ABC-PeSO, ABC, PeSO, PSO and GA for triangle program is shown in Fig. 4 and the path coverage of test cases is shown in Fig. 5.

From Fig. 4, it can see that mutation score obtained by the different method our proposed method has achieved highest mutation score of 95% whereas the mutation score of PeSO, PSO, ABC and GA are 88, 70, 72 and 54% for the particular generation. From these, the mutation score realized by proposed ABC-PeSO is clearly better than the mutation scores attained by PeSO, PSO, ABC and GA.

From Fig. 5, it can be noted that the proposed method has achieved maximum path coverage with 96% to that of path coverage achieved by PeSO, PSO, ABC and GA are 70, 72, 65 and 64% for the particular generation. Similarly the mutation score of individuals generated during various generations and the path coverage of test cases using proposed ABC-PeSO, ABC, PeSO, PSO and GA for Next Date program is shown in Fig. 6 and 7.

Similarly, for the case of the next date program, the mutation score obtained by the proposed method has achieved high value of 98% to that of mutation score obtained by PeSO, PSO, ABC and GA are 85, 71, 76 and 60% for the particular generation.

Likewise for the case of path coverage also, the proposed method has attained a high value of 98% to that of the path coverage of PeSO, PSO, ABC and GA are 86, 79, 80 and 55% for the particular generation. This result shows that the proposed hybrid ABC-PeSO has achieved better results. So, far from the results obtained from two benchmark programs we can see that our proposed method that is hybrid ABC-PeSO has attained high mutation score of 95 and 98% for triangle and nextdate program also it attained path coverage of 96 and 98% for triangle and next date program this shows the performance as well as the importance of the proposed method in the field of software testing. Our proposed method has achieved better results than previously used algorithms like ga, pso as well as abc which can be clearly seen from the results presented. Finally, from the results

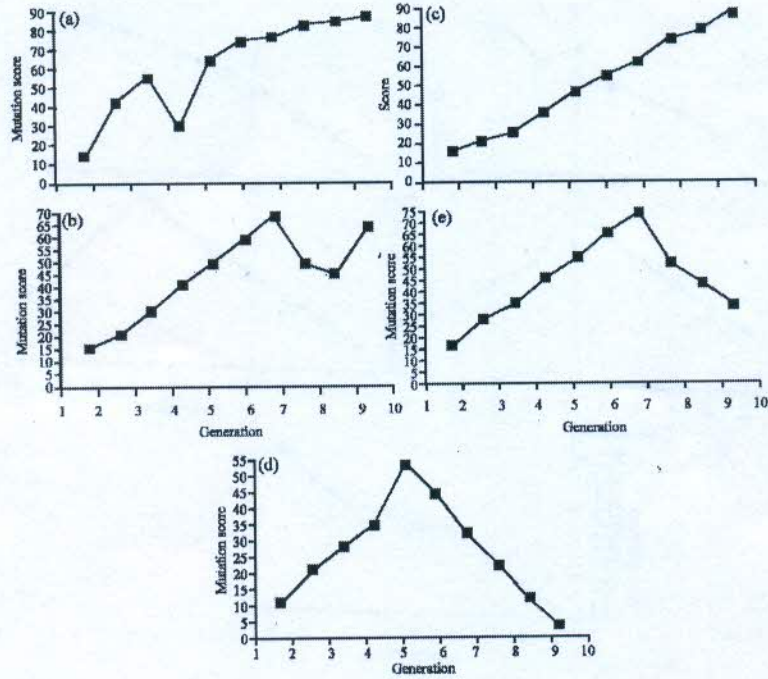


Fig. 4: Mutation score of triangle program: a) Mutation score for ABC-PeSO; b) for PeSO; c) for PSO; d) for ABC and e) for GA

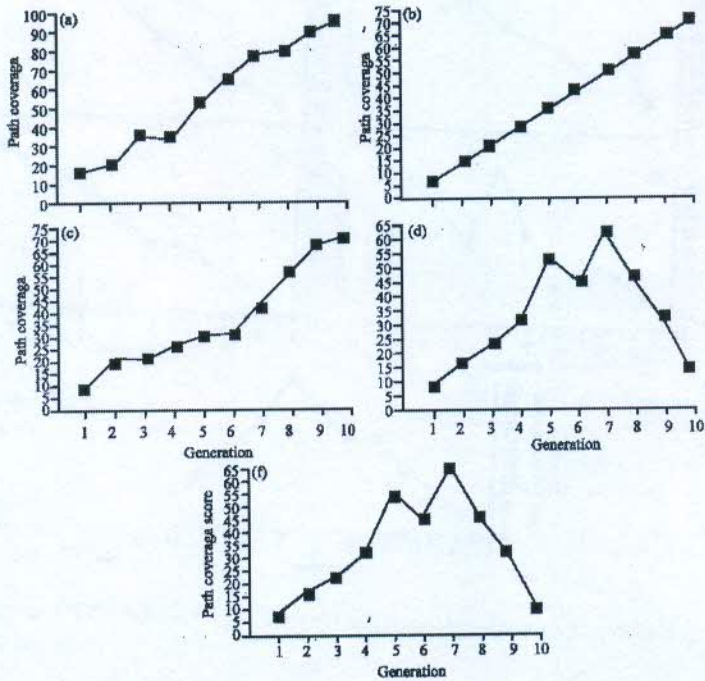


Fig. 5: Path coverage of triangle program: a) Path coverage for ABC-PeSO; b) for PeSO; c) for PSO; d) for ABC

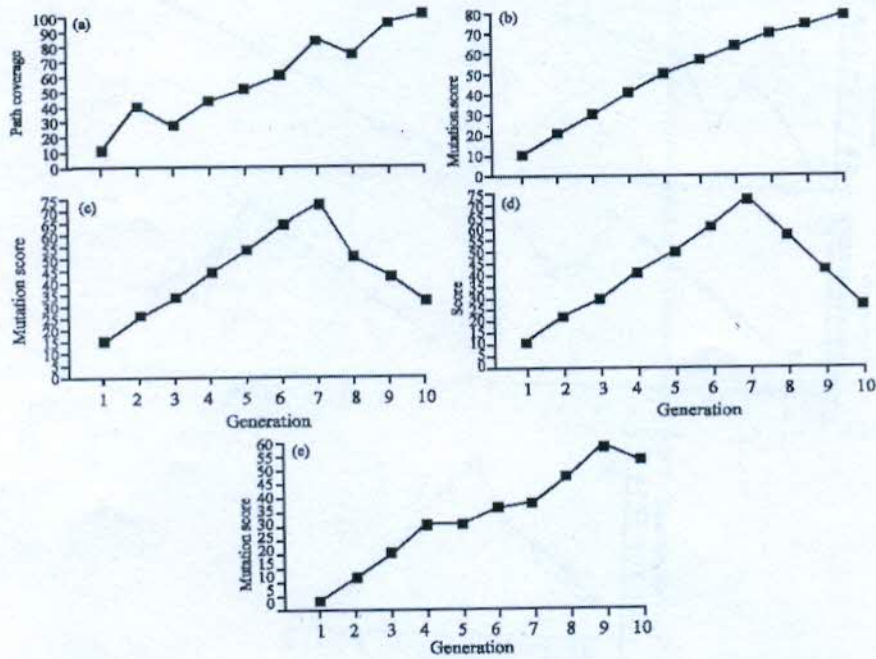


Fig. 6: Mutation score of next date program: a) Mutation score for ABC-PeSO; b) F for PeSO; c) For PSO; d) For ABC and e) For GA

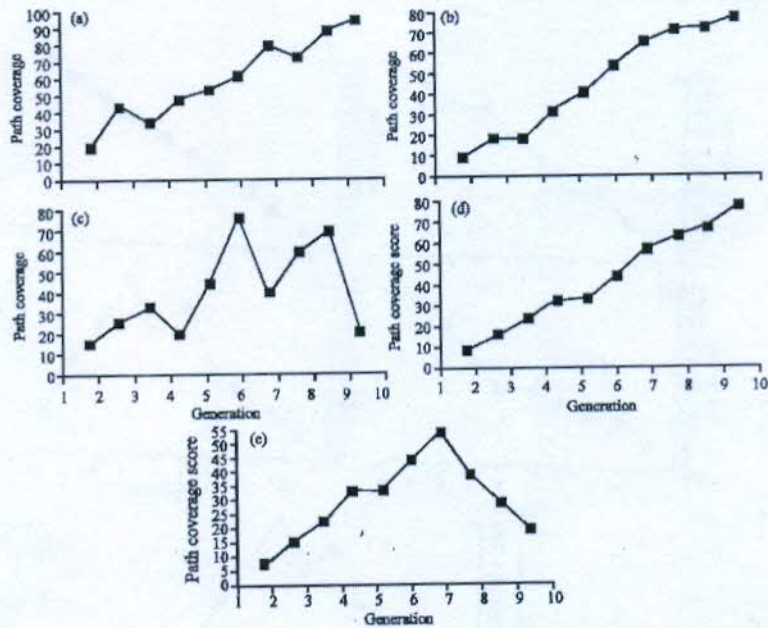


Fig. 7: Path coverage of next date program: a) Path coverage for ABC-PeSO; b) For PeSO; c) For PSO; d) For ABC and e) For GV

we can conclude that our proposed method has generated quality a test case for which clears more errors in the program with less cost. The quality of the test cases can

be easily analyzed from the mutation as well as path coverage in both these we achieved maximum results.

CONCLUSION

Testing confirms that the software sees the user circumstances and requirements. Successful generation of test cases has to be addressed in the field of software testing. Features like effort, time and cost of the testing are factors manipulating these as well. In this proposed method, we have proposed a novel hybrid ABC-PeSO to decrease the test data generation cost and time in the context of mutation testing. The proposed method is implemented on Java working platform and tested on two benchmark programs they are triangle and next date. Experimental results obtained on two programs showed that the proposed hybrid ABC-PeSO performed well and produces satisfactory results better than other algorithms like ABC, PeSO, PSO and GA this shows the importance of this newly designed method in the field of software testing.

REFERENCES

- Ahmed, B.S. and K.Z. Zamli and C.P. Lim, 2012. Application of particle swarm optimization to uniform and variable strength covering array construction. *Applied. Soft Comput. J.*, 12: 1330-1347.
- Ahmed, B.S. and K.Z. Zamli, 2011. A variable strength interaction test suites generation strategy using particle swarm optimization. *J. Syst. Software*, 84: 2171-2185.
- Ahmed, B.S., M.A. Sahib and M.Y. Potrus, 2014. Generating combinatorial test cases using Simplified Swarm Optimization (SSO) algorithm for automated GUI functional testing. *Eng. Sci. Technol. Int. J.*, 17: 218-226.
- Anand, S., E.K. Burke, T.Y. Chen, J. Clark and M.B. Cohen *et al.*, 2013. An orchestrated survey of methodologies for automated software test case generation. *J. Syst. Software*, 86: 1978-2001.
- Baker, R. and I. Habli, 2013. An empirical evaluation of mutation testing for improving the test quality of safety-critical software. *IEEE. Trans. Software Eng.*, 39: 787-805.
- Bansal, A., 2014. A comparative study of software testing techniques. *Intl. J. Comput. Sci. Mob. Comput.*, 3: 579-584.
- Belli, F., C.J. Budnik, A. Hollmann, T. Tuglular and W.E. Wong, 2016. Model-based mutation testing-approach and case studies. *Sci. Comput. Program.*, 120: 25-48.
- Bryce, R.C., S. Sampath, J.B. Pedersen and S. Manchester, 2011. Test suite prioritization by cost-based combinatorial interaction coverage. *Intl. J. Syst. Assur. Eng. Manage.*, 2: 126-134.
- Debroy, V. and W.E. Wong, 2014. Combining mutation and fault localization for automated program debugging. *J. Syst. Software*, 90: 45-60.
- Fraser, G. and A. Arcuri, 2015. Achieving scalable mutation-based generation of whole test suites. *Empirical Software Eng.*, 20: 783-812.
- Fraser, G. and A. Zeller, 2012. Mutation-driven generation of unit tests and oracles. *IEEE. Trans. Software Eng.*, 38: 278-292.
- Garvin, B.J., M.B. Cohen and M.B. Dwyer, 2011. Evaluating improvements to a meta-heuristic search for constrained interaction testing. *Empirical Software Eng.*, 16: 61-102.
- Habibi, E. and S.H. Mirian-Hosseiniabadi, 2015. Event-driven web application testing based on model-based mutation testing. *Inf. Software Technol.*, 67: 159-179.
- Hamlet, R.G., 1977. Testing programs with the aid of a compiler. *IEEE Trans. Software Eng.*, SE-3: 279-290.
- Jia, Y. and M. Harman, 2009. Higher order mutation testing. *Inf. Software Technol.*, 51: 1379-1393.
- Jia, Y. and M. Harman, 2011. An analysis and survey of the development of mutation testing. *IEEE. Trans. Software Eng.*, 37: 649-678.
- Kennedy, J. and R. Eberhart, 1995. Particle swarm optimization. *Proc. IEEE. Intl. Conf. Neural Netw.*, 1: 1942-1948.
- Kuliamin, V.V. and A.A. Petukhov, 2011. A survey of methods for constructing covering arrays. *Program. Comput. Software*, 37: 121-146.
- Mao, C., X. Yu, J. Chen and J. Chen, 2012. Generating test data for structural testing based on ant colony optimization. *Proceedings of the 12th International Conference on Quality Software (QSIC'12)*, August 27-29, 2012, IEEE Washington, USA. ISBN:978-0-7695-4833-3, pp: 98-101.
- Masud, M., A. Nayak, M. Zaman and N. Bansal, 2005. A strategy for mutation testing using genetic algorithms. *Proceedings of the Canadian Conference on Electrical and Computer Engineering*, May 1-4, 2005, Saskatoon, Sask, pp: 1049-1052.
- Mresa, E.S. and L. Bottaci, 1999. Efficiency of mutation operators and selective mutation strategies: An empirical study. *Software Test. Verif. Reliab.*, 9: 205-232.
- Nayak, N. and D.P. Mohapatra, 2010. Automatic Test Data Generation for Data Flow Testing using Particle Swarm Optimization. In: *Contemporary Computing*, Ranka, S. (Ed.). Springer, Berlin, Germany ISBN:978-3-642-14824-8, pp: 1-12.
- Nidhra, S. and J. Dondeti, 2012. Blackbox and whitebox testing techniques: A literature review. *Intl. J. Embedded Syst. Appl.*, 2: 29-50.

- Nie, C. and H. Leung, 2011. A survey of combinatorial testing. *ACM. Comput. Surv.*, 43: 11-29.
- Nie, C., H. Wu, X. Niu, F.C. Kuo and H. Leung *et al.*, 2015. Combinatorial testing, random testing and adaptive random testing for detecting interaction triggered failures. *Inf. Software Technol.*, 62: 198-213.
- Pachauri, A. and G. Srivastava, 2013. Automated test data generation for branch testing using genetic algorithm: An improved approach using branch ordering, memory and elitism. *J. Syst. Software*, 86: 1191-1208.
- Torres-Jimenez, J. and E. Rodriguez-Tello, 2012. New bounds for binary covering arrays using simulated annealing. *Inf. Sci.*, 185: 137-152.
- Usaola, M.P. and P.R. Mateo, 2010. Mutation testing cost reduction techniques: A survey. *IEEE. Software*, 27: 80-86.
- Yuan, X., M.B. Cohen and A.M. Memon, 2011. GUI interaction testing: Incorporating event context. *IEEE Trans. Software Eng.*, 37: 559-574.

2016-17



Reviewing Automatic Test Data Generation

Dr. Mukesh Kumar¹, Jyoti Chaudhary²

Associate Professor¹, Assistant Professor & Research Scholar²

Department of Computer Engineering

TIT&S, Bhiwani, India^{1,2}

UIET, MDU, Rohtak, India²

Abstract:

Automated Test Data Generation (ATDG) is an activity that in the course of software testing automatically generates test data for the software under test (SUT). It usually makes the testing more efficient and cost effective. Test Data Generation (TDG) is crucial for software testing because test data is one of the key factors for determining the quality of any software test during its execution. The multi-phased activity of ATDG involves various techniques for each of its phases. Several ATDG techniques are available, but emerging trends in computing have raised the necessity to summarize and assess the current status of this area particularly for practitioners, future researchers and students.

Keywords: Software Testing, SUT, Test Data

I. INTRODUCTION

Automated test data generation is one of the core factors that contribute towards automated testing. It is used for automatically generating test data for a SUT during software testing. Test data generation is a tedious, expensive and error prone process, if it is done manually. Automation in the test data generation process could curtail testing expenses and at the same time, increase the reliability of testing as a whole. For these reasons automated test data generation has remained a topic of interest for the past four decades. In [15]'s opinion ATDG is one of the most crucial activities of automated testing because test data is one of those key factors that determine the quality of a test during its execution. ATDG itself is a multi-phased process, which involves different techniques for every phase. For example program analysis, path generation and test data generation are the three basic phases of ATDG process, that have been mentioned by [15] while explaining the architecture of a test data generator system. Similarly random, path-oriented and goal-oriented are some of the test data generation approaches that can generally be described as data generation techniques [17]. This is the most appropriate classification in terms of test data generation, although the problem of path selection is not considered separately. The selection of a path can largely affect the whole process of test data generation. Although many techniques for automatic test data generation have been developed [Coward 1988; Gallagher and Narasimhan 1997; Gupta et al. 1998; Sthamer 1995; Korel 1990b; Lapierre et al. 1999a; Meudec 2001; Michael et al. 2001], there is no overall evaluation and comparison of these techniques. Evaluation and comparison of existing techniques are useful for choosing appropriate approaches for particular applications.

The organization of this paper is alienated as follows:

Section II describes the basic concept and notion, section III discusses the test data generator system with focus on the generator and the path selector, section IV describes various techniques for test data generation and section V depicts the conclusion.

II. BASIC CONCEPT

According to Pargas et al [13] the intelligent test-data generation approach often relies on sophisticated analysis of the code to guide the search for new test data. However in the author's opinion this approach can be extended up to the intelligent analysis of program specification as well. Figure 1 models a typical test data generator system, which consists of three parts: Program analyzer, path selector and test data generator. The source code is run through a program analyzer, which produces the necessary data used by the path selector and the test data generator. The selector inspects the program data in order to find suitable paths. Suitable path can for instance mean paths leading to high code coverage. The paths are then given as argument to the test data generator which derives input values that exercise the given paths. The generator may provide the selector with feedback such as information concerning infeasible paths.

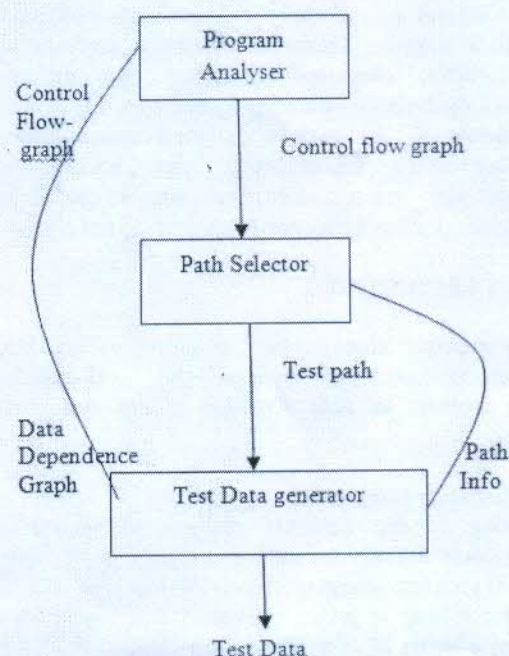


Figure.1. Architecture of a test data generator system.

Generally software is tested for its structure or functions which are supposed to be performed by its components. Testing in the prior case is commonly known as structural or white box testing, while in the later case it is called functional or black box testing [10]. For either of the cases test data is required to "traverse" through the SUT. The outcome of this traversal determines correctness, performance, or in general, the quality of the SUT. In some cases the test data is already available or given but in most cases it is required to be generated. Test data generation is a complex activity because it involves so many steps and each step has several related issues. The architecture of a test data generator can better elaborate this notion of complexity. Figure shows the architecture of an automated test data generator using the path-oriented approach in simple and easily understandable format. Important to note here is that test data generation is not a single step process rather it involves several steps. Adequate test data can never be created if performance at any of the steps is poor or the execution is incorrectly performed.

III. AN AUTOMATIC TEST DATA GENERATOR SYSTEM

A test data generator system consists of three parts: a program analyzer, a path selector, and a test data generator. In this article the focus is on selector and the generator. Therefore let us assume that the analyzer exists and works properly. At this point let us define the problem of automatic test data generation as follows: given a program P and a (unspecific) path u , generate input $x \in S$, so that x traverses u . This means that we can assume to have a program analyzer and a path selector such as in figure 1. The program analyzer provides all information concerning the program: data dependence graphs, control flow graphs etc. In turn the path selector identifies paths for which the test data generator will derive input values. Depending on the type of generator system paths could either be specific or unspecific. Our goal is to find input values that will traverse the paths received from the selector. This is achieved in two steps. First find the path predicate for the path. Second, solve the path predicate in terms of input variables. The solution will then be a system of (in) equalities describing how input data should be formed in order to traverse the path. Having such a system we can apply various search methods to come up with a solution. Examples of search methods are alternating variable, simulated annealing, and different heuristics based on equation-rewriting systems [5, 14, 3]. Due to the complexity of the derived equation systems some techniques solve one branch predicate at a time. This leads to a loss of performance since it makes it necessary to check that violations of other previously solved predicates do not occur.

IV. VARIOUS TECHNIQUES

The most appropriate classification in terms of test data generation is: random, path-oriented and goal-oriented, although the problem of path selection is not considered separately.

A. Random Test Data Generation

Random testing is the simplest method of generation techniques. It could actually be used to generate input values for any type of program since, ultimately, a data type such as integer, string, or heap is just a stream of bits. Thus, for a function taking a string as an argument we can just randomly generate a bit stream and let it represent the string. On the contrary, random testing mostly does not perform well in terms

of coverage. Since it merely relies on probability it has quite low chances in finding semantically small faults [11], and thus accomplishes high coverage. A semantically small fault is such a fault that is only revealed by a small percentage of the program input. This approach is quick and simple but might be a poor choice with complex programs and with complex adequacy criteria. A semantically small fault is a fault that is revealed only by a small percentage of the program input. However, random test data generation is used frequently as a benchmark because it is easy to implement and commonly reported in the literature.

Consider the following piece of code:

```
void foo(int a, int b) {
  if (a == b) then
    write(1);
  else
    write(2);
}
```

The probability of exercising the write(1) statement is $1/n$, where n is the maximum integer, since in order to execute this statement variables a and b must be equal. We can easily imagine that generating even more complex structures than integers will give us even worse probability. Often evaluation of search methods uses random testing as a benchmark [3, 2, 5], since it is considered to be of the lowest acceptance rate.

B. Goal-Oriented Test Data Generation

The goal-oriented approach is much stronger than random generation, in the sense of providing guidance towards a certain set of paths. Instead of letting the generator generate input that traverses from the entry to the exit of a program, it generates input that traverses a given unspecific path u . Because of this, it is sufficient for the generator to find input for any path $p \in u^*$. This in turn reduces the risk of encountering relatively infeasible paths and provides a way to direct the search for input values as well. Two methods using this technique have been found: the chaining approach and assertion-oriented approach. The latter is an interesting extension of the chaining approach. They have all been implemented in the TESTGEN system [5, 9]. Typical for the chaining approach is the use of data dependence to find solutions to branch predicates. The characteristic of chaining is to identify a chain of nodes that are vital to the execution of the goal node. This chain is built up iteratively during execution. Since this method uses the find-any-path concept it is hard to predict the coverage given a set of goals. Assertion-oriented testing truly utilizes the power of goal-oriented generation. Certain conditions, called assertions are either manually or automatically inserted in the code. When an assertion is executed it is supposed to hold, otherwise there is an error either in the program or in the assertion. For instance, with the following code:

```
Void fie (int a) {
  int b = (a+1)*(a-1);
  assert(b != 0);
  write(1/b);
}
```

we can say that before executing $1/b$ the variable b must not be zero. The goal of assertion-oriented generation is then to find any path to an assertion that does not hold. An advantage with assertion-oriented testing is that the oracle is given in the code. That is, in all the other methods the expected value of an execution of the generated test data has to be calculated from some other source than the code. With assertions this is not necessary since expected value is provided within the

assertion. In the goal-oriented approach test-data is selected from the available pool of candidate test data to execute the selected goal, such as a statement, irrespective of the path taken [13]. This approach involves two basic steps: to identify a set of statements (respective branches) the covering of which implies covering the criterion; to generate input test data that execute every selected statement (respective branch).

C. Path-Oriented Test Data Generation

Path-oriented generation is strongest among the three approaches. It does not provide the generator with a possibility of selecting among a set of paths, but just one specific. In this way it is the same as a goal-oriented test data generation, except for the use of specific paths. Successively this leads to a better prediction of coverage. On the other hand it is harder to find test data. In path-oriented test data generation the typical approach is generation of a control-flow graph. In this approach, at first a graph is generated first and subsequently, by using the graph a particular path is selected. With the help of a technique such as symbolic evaluation (in the static case otherwise it is called function minimization) test data is generated for that path in the end [13]. In symbolic execution variables are used instead of actual values while traversing the path. CASEGEN [13] and TESTGEN [8] are two systems using this technique. Since they are solely based on the control flow graph they often lead to selection of infeasible paths (both relatively and absolutely). DeMillo and Offutt [4] have proposed a constraint based test data generation method. It is focused on fault-based testing using mutants, i.e. a deliberate change in the source code. However, it is not clear how paths are selected and since this technique is somewhat similar to assertion-oriented testing it could fit under goal-oriented test data generation as well. The path-oriented approach might face the problems when generating paths/graphs, traversing test data through branches and predicates (infeasible path problem).

V. CONCLUSION

Although many techniques for automatic test data generation have been developed but there is no overall evaluation and comparison of these techniques. Evaluation and comparison of existing techniques are useful for choosing appropriate approaches for particular applications. For example, if the high quality of software is essential, a technique with the highest test coverage may be required regardless of cost. On the other hand, if execution time for the test data generation is the most important factor, a fast technique may be desirable, even though some tests that can expose faults may be omitted from the test suite. Evaluation and comparison of existing approaches also provide insights into the strengths and weaknesses of current methods. Random approach is quick and simple but might be a poor choice with complex programs and with complex adequacy criteria. The probability of selecting an adequate input by chance could be low in this case. The goal-oriented approach is much stronger than random generation, in the sense of providing guidance towards a certain set of paths. The path-oriented approach might face the problems when generating paths/graphs, traversing test data through branches and predicates (infeasible path problem), and while complexity of data types. Path-oriented generation is strongest among the three approaches. It does not provide the generator with a possibility of selecting among a set of paths, but just one specific. In this way it is the same as a goal-oriented test data generation, except for the use of specific paths. The intelligent test-data generation approach often relies on sophisticated

analysis of the code to guide the search for new test data. However in the author's opinion this approach can be extended up to the intelligent analysis of program specification as well.

VI. REFERENCES

- [1]. B. Beizer. Software Testing Techniques. Van Nostrand Reinhold, 2nd edition, 1990.
- [2]. K. Chang, W. Carlisle, J. Cross II, and D. Brown. A heuristic approach for test case generation. In Proceedings of the 1991 ACM Computer Science Conference, pages 174-180. ACM, 1991.
- [3]. W. H. Deason, D. Brown, K. Chang, and J. H. Cross II. A rule-based software test data generator. IEEE Transactions on Knowledge and Data Engineering, 3(1):108-117, March 1991.
- [4]. R.A. DeMillo and A. J. Offutt. Constraint-based automatic test data generation. IEEE Transactions on Software Engineering, 17(9):900-910, September 1991.
- [5]. R. Ferguson and B. Korel. The chaining approach for software test data generation. IEEE Transactions on Software Engineering, 5(1):63-86, January 1996.
- [6]. R. Ferguson and B. Korel. Generating test data for distributed software using the chaining approach. Information and Software Technology, 38(1):343-353, January 1996.
- [7]. N. Gupta, A. P. Mathur, and M. L. So_a. Automated test data generation using an iterative relaxation method. In Proceedings of the ACM SIGSOFT sixth international symposium on Foundations of software engineering, pages 231-244, November 1998.
- [8]. B. Korel. Automated software test data generation. IEEE Transactions on Software Engineering, 16(8):870-879, August 1990.
- [9]. B. Korel and A. M. Al-Yami. Assertion-oriented automated test data generation. In Proceedings of the 18th International Conference on Software Engineering (ICSE), pages 71-80. IEEE, 1996.
- [10]. C. Michael and G. McGraw. Automated software test data generation for complex programs. In 13th IEEE International Conference on Automated Software Engineering, pages 136-146, October 1998.
- [11]. J. Offutt and J. Hayes. A semantic model of program faults. In International Symposium on Software Testing and Analysis (ISSTA 96), pages 195-200. ACM Press, 1996.
- [12]. R. E. Prather and J. P. Myers, Jr. The path prefix software testing strategy. IEEE Transactions on Software Engineering, SE-13(7):761-765, July 1987.
- [13]. C. V. Ramamoorthy, S. F. Ho, and W. T. Chen. On the automated generation of program test data. IEEE Transactions on Software Engineering, SE-2(4):293-300, December 1976.
- [14]. N. Tracey, J. Clark, and K. Mander. Automated program flaw finding using simulated annealing. In Proceedings of ACM SIGSOFT international symposium on Software testing and analysis, volume 23, pages 73-81, March 1998.

[15]. Jon Edvardsson. A Survey on Automatic Test Data Generation. In Proceedings of the Second Conference on Computer Science and Engineering in Linkoping, pages 21-28. ECSEL, October 1999

[16]. K.K. Aggarwal, Y. Singh, "Software Engineering", New Age International Publishers, 2006.

[17].R. Torkar. Towards Automated Software Testing, Techniques, Classifications and Frameworks. Karlskrona Blekinge Institute of Technology, 2006:4. p. 235 ISBN: 91-7295-089-7, 2006.

[18]. Neelam Gupta, Aditya P. Mathur, and Mary Lou Soffa. Generating Test Data for Branch Coverage. In proceedings of 15th International conference on Automated Software Engg.

Duplicate

**International Journal of Advanced Research in Engineering and Technology
(IJARET)**

Volume 7, Issue 1, Jan-Feb 2016, pp. 54-59, Article ID: IJARET_07_01_007

Available online at

<http://www.iaeme.com/IJARET/issues.asp?JType=IJARET&VType=7&IType=1>

ISSN Print: 0976-6480 and ISSN Online: 0976-6499

© IAEME Publication

ACCURATE NUMERICAL SIMULATION OF HIGHER ORDER SOLITON DECOMPOSITION IN PRESENCE OF TOD AND SELF- STEEPENING

RAJEEV SHARMA

Research Scholar, Mewar University, Rajasthan, India

HARISH NAGAR

AP, Mewar University, Rajasthan, India

G P SINGH

Govt. Dungar College Bikaner, Rajasthan, India

ABSTRACT

Generally, one considers only the group velocity dispersion (GVD) and self-phase modulation (SPM) induced solitons in optical communication while other higher order effects such as the third-order dispersion (TOD), self-steepening, and stimulated Raman scattering are well thought-out only perturbatively. In this article, we study the existence of the TOD and self-steepening induced soliton solutions. The results have shown that, the combination of the linear with nonlinear effects escort to new qualitative feature as a shifting and the center-shift beside the deformation in the shape of the soliton. To accomplish this purpose we used, the split-step Fourier Method, in our simulations, that is broadly used to simulate numerical solutions of the nonlinear Schrodinger equation.

Key words: Group Velocity Dispersion, Stimulated Raman Scattering, TOD, Self-Steepening.

Cite this Article: Rajeev Sharma, Harish Nagar and G P Singh, Accurate Numerical Simulation of Higher Order Soliton Decomposition In Presence of TOD and Self- Steepening. *International Journal of Advanced Research in Engineering and Technology*, 7(1), 2016, pp. 54-59.

<http://www.iaeme.com/IJARET/issues.asp?JType=IJARET&VType=7&IType=1>

1. INTRODUCTION

Optical solitons are the matter of broad theoretical and experimental studies throughout the last four decades owing to their prospective applications in large distance communication and all-optical ultrafast switching devices. The revolutionary works of Hasegawa and Tappert, who predicted solitons theoretically, and Mollenauer et al. [1], who observed them experimentally, made solitons a practical instrument for this cause. The solitons, confined-in-time optical pulse, evolve from a nonlinear variation in the refractive index of the material, known as Kerr effect, stimulated by the light intensity distribution. When the collective effects of the intensity-reliant refractive index nonlinearity and the frequency-reliant pulse dispersion exactly balance for one another, the pulse propagates without any change in its shape, being self-trapped by the waveguide nonlinearity [2]. The transmission of picosecond optical pulses in mono mode optical fibers is paragon by the totally integrable nonlinear Schrodinger equation. This equation regulates the general condition of dispersion propagation of a pulse envelope with a high carrier frequency in a weakly nonlinear medium. even though the NLS equation includes only two substantial effects, group velocity dispersion (GVD) and self-phase modulation (SPM), it describes a range of nonlinear optical phenomena. Pivot on the relative signs of linear group-velocity dispersion and nonlinearity stimulated self-phase modulation, they coalesce to allow bright solitons [1], modulation instability and dark solitons. In order to boost the bit rate in fiber optic communication systems to greater than 100 Gbit/s for a single carrier frequency, it is obligatory to decrease the pulse width.

2. MODIFICATION IN NLSE

As light pulses become shorter, the standard NLS equation

$$i\frac{\partial u}{\partial \xi} + \frac{1}{2}\frac{\partial^2 u}{\partial \tau^2} + |u|^2 u = 0 \quad (1)$$

Becomes inadequate. Thus extra terms which describe the effects of third-order dispersion (TOD), self-steepening and intrapulse Raman scattering required to be added to that equation

$$i\frac{\partial u}{\partial \xi} + \frac{1}{2}\frac{\partial^2 u}{\partial \tau^2} + |u|^2 u = \delta_3 \frac{\partial^3 u}{\partial \tau^3} - is\frac{\partial}{\partial \tau}(|u|^2 u) + \tau_R u \frac{\partial |u|^2}{\partial \tau} \quad (2)$$

$$\delta_3 = \frac{\beta_3}{6|\beta_2|T_0} \quad (3)$$

$$s = 1/\omega_0 T_0 \quad (4)$$

$$\tau_R = T_R/T_0 \quad (5)$$

3. SIMULATION AND RESULT

The propagation of optical signal along an optical fiber is described by the NLSE, which has no analytical solutions except for some special cases. One can conclude that a numerical approach is often necessary for understanding nonlinear effects in dispersive media such as optical fibers [6-9]. Generally, a numerical approach is required to solve all pulse-propagation problems in optical fibers. The most commonly used method for solving these problems in nonlinear dispersive media is SSFM [3].

3.1. TOD

What happens if an optical pulse propagates at or near the zero-dispersion wavelength of an optical fiber such that β_2 is nearly zero [4]. Equation (2) cannot be used in this case because the normalization scheme used for it becomes inappropriate. Normalizing the propagation distance to $L'_D = T_0^3/\beta_3$ through $\xi' = z/L'_D$, we get

$$i \frac{\partial u}{\partial \xi'} - \text{sgn}(\beta_3) \frac{i \partial^3 u}{6 \partial \tau^3} + |u|^2 u = 0 \quad (6)$$

where $u = \tilde{N}U$ with \tilde{N} is defined by

$$\tilde{N}^2 = \frac{L'_D}{L_{NL}} = \gamma P_0 T_0^3 / \beta_3 \quad (7)$$

The effect of TOD shown in figure 1 to figure 8 where pulse shapes at $\xi = 4$ is are plotted for $\tilde{N} = 2$ and $\tilde{N} = 3$ by solving above equation with input $u(0, \tau) = \text{sech}(\tau)$

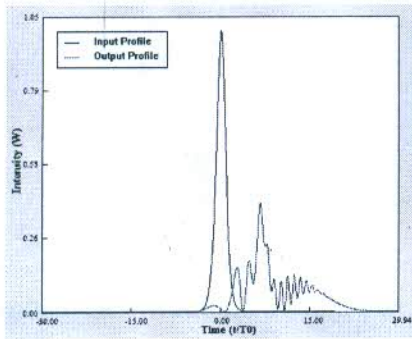


Figure.1

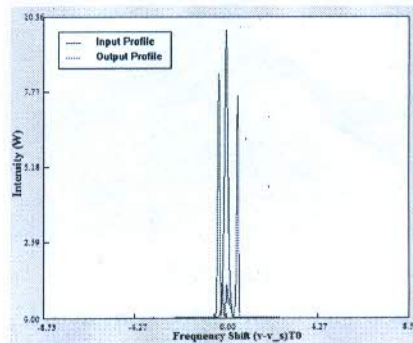


Figure.2

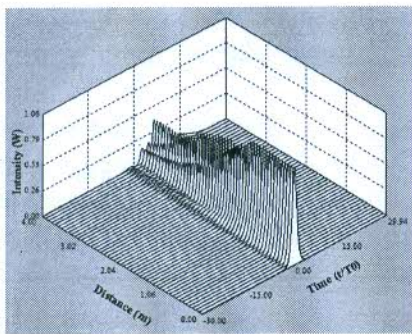


Figure.3

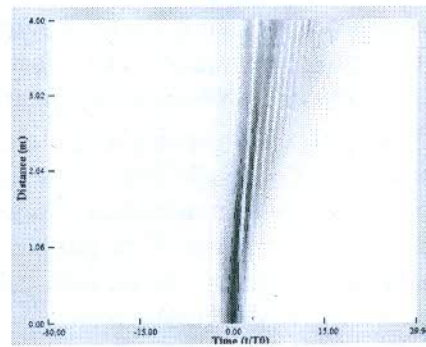


Figure.4

Pulse shape and spectrum at $z/L'_D = 4$ of a hyperbolic secant pulse propagating at the zero-dispersion wavelength with a peak power such that $\tilde{N} = 2$.

Accurate Numerical Simulation of Higher Order Soliton Decomposition in Presence of TOD and Self-Steepening

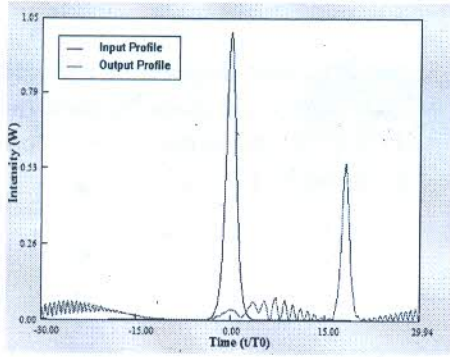


Figure.5

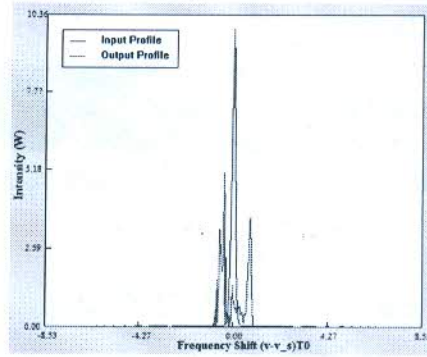


Figure.6

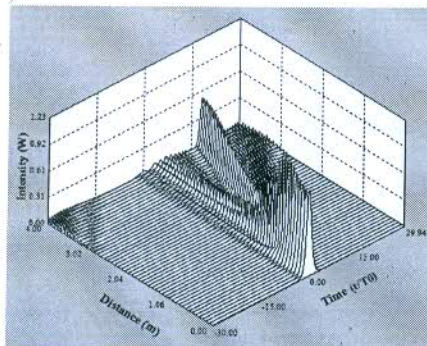


Figure.7

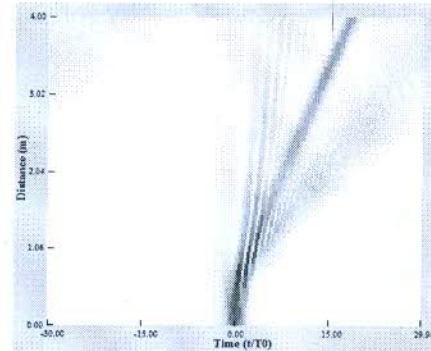


Figure.8

Pulse shape and spectrum at $z/L_D = 4$ of a hyperbolic secant pulse propagating at the zero-dispersion wavelength with a peak power such that $\tilde{N} = 3$.

Figure 1 to Figure 4 shows the pulse shape and the spectrum at $\xi' = 4$ and $\tilde{N} = 2$ and Figure 4 to Figure 8 shows the pulse shape and the spectrum at $\xi' = 4$ and $\tilde{N} = 3$ on comparing the result. The most remarkable characteristic is splitting of the spectrum into two well-resolved spectral peaks.

These peaks correspond to the outermost peaks of the SPM-broadened spectrum as the red-shifted peak lies in the anomalous-GVD regime. pulse energy in that spectral band can form a soliton. The energy in the other spectral band disperses away simply because that part of the pulse experiences normal GVD. It is the trailing part of the pulse that disperses away with propagation because SPM generates blue-shifted components near the trailing edge.

3.2. Self-Steepening

To understand the effect of self steepening we set $\delta_3 = 0$ and $\tau_R = 0$ in equation (2). Pulse advancement inside the fiber is given by

$$i \frac{\partial u}{\partial \xi} + \frac{1}{2} \frac{\partial^2 u}{\partial \tau^2} + |u|^2 u + i s \frac{\partial}{\partial \tau} (|u|^2 u) = 0 \quad (8)$$

The self-steepening-induced shift is shown in figure 9 and figure 10 where pulse shapes at $\xi = 7.5$ is plotted for $s=0.3$ and $N=1$ by solving above equation with input $u(0, \tau) = \text{sech}(\tau)$ we find that crest progress slower than the wings for $s \neq 0$. This observable fact is due to the intensity reliance of the group velocity that results in the peak of the pulse moving slower than the wings. The GVD disperse the shock and smoothes the trailing edge considerably.

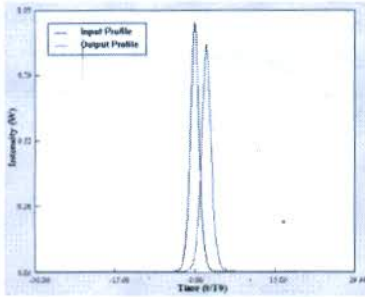


Figure.9

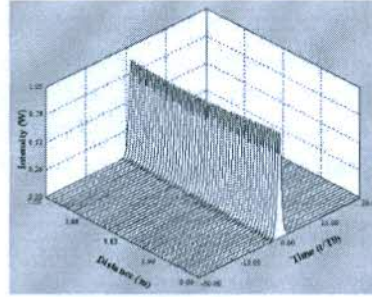


Figure.10

Pulse shapes for a fundamental soliton in the presence of self-steepening ($s=0.3$).

The result of self-steepening on higher-order solitons is leads to division of such solitons into their constituents, a fact known as soliton decay as shown in simulation results in figure.11 to figure.14

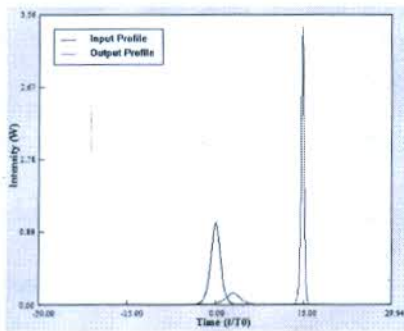


Figure.11

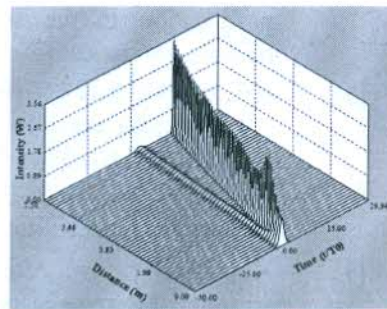


Figure.12

Decay of a second-order soliton $N=2$ induced by self-steepening ($s=0.3$).

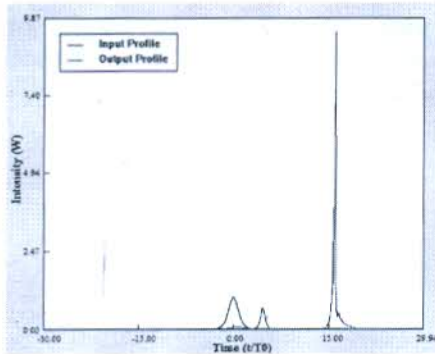


Figure.13

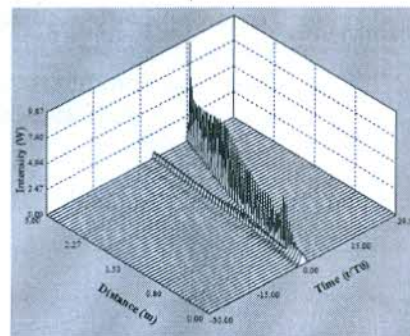


Figure.14

Decay of a third-order soliton $N=3$ induced by self-steepening ($s=0.3$).

The second order soliton $N=2$ decompose into two solitons and third-order soliton $N=3$ decompose into three solitons whose peak heights are again in agreement with inverse scattering theory.

4. CONCLUSION

In this paper, we have investigated through simulation two key phenomena's one is TOD and the other is self steepening on solitonic propagation. While studying TOD The vital point to note is that, because of SPM-induced spectral broadening, the input pulse does not actually propagate at the zero-dispersion wavelength even if $\beta_2 = 0$ initially. In effect, the pulse creates its own β_2 through SPM. Simulation result shows

that for $\tilde{N} > 1$, a “sech” pulse progress over a length $\xi' \sim 10/\tilde{N}^2$ into a soliton that contains about half of the pulse energy. The remaining energy is carried by an wavelike structure near the trailing edge that disperses away with propagation. The effect of self-steepening on higher-order solitons is significant in that it leads to disintegration of such solitons into their constituents.

REFERENCES

- [1] G. P. Agrawal Nonlinear Fiber Optics, Academic Press, 2001
- [2] K. Ohkuma, Y.H. Ichikawa, and Y. Abe, Soliton propagation along optical fibers, Opt. Lett., 12, 516–518, 1987.
- [3] S. Siddamal, R. Banakar, and B. Jinaga, Split Step Method in the Analysis and Modeling of Optical Fiber Communication System, Springer Verlag Heidelberg, 254–261, 2011.
- [4] P. K. Wai, C. R. Menyuk, Y. C. Lee, and H. H. Chen, Nonlinear pulse propagation in the neighborhood of the zero-dispersion wavelength of monomode optical fibers, Opt. Lett. 11, 464–466, 1986.
- [5] S.R. Clarke, R.H.J. Grimshaw, and B.A. Malomed, Soliton formation from a pulse passing the zero dispersion point in a nonlinear Schrödinger equation, Phys. Rev. E 61, 5794–5801, 2000.
- [6] E. A. Golovchenko, E. M. Dianov, A. M. Prokhorov, and V. N. Serkin, Decay of optical solitons, JETP Lett. 42, 87–91, 1985.
- [7] Kuo-chou Tai and Akira Hasegawa, Fission of optical solitons induced by stimulated Raman Effect, Opt. Lett. 13, 392–394, 1988.
- [8] Jing Wang, Shanshan Wang, Xiaoliang Chu, Meiling Sun, Numerical Study on Optical Solitons Transmission System with 40 Gbit/s in the Photonic Crystal Fiber, Optics and Photonics Journal, 3,141–146, 2013.
- [9] Tarnveer Kaur, Kamaljit Singh Bhatia, and Kulwinder Singh, Factors Affecting Higher Order Solitons in Soliton Transmission, International Conference on Innovations in Engineering and Technology (ICIET'2013) Dec. 25–26, 2013 Bangkok.

Introducing a New Technique for Making a Secure Steganosystem

Gopesh Sardana 1st
M.Tech scholar, Department of computer science
TIT&S, Bhiwani
Bhiwani, India
E-mail: gp.sardana@gmail.com

Nidhi Sharma 2nd
Asst. professor, Department of computer science
TIT&S, Bhiwani
Bhiwani, India
E-mail: nidhisharma1725@gmail.com

Abstract: One of the popular ways of data security is steganography. Steganography is an art of transfer hidden data or undisclosed messages over a public channel so that a third party cannot detect the presence of the secret messages. Steganography is practiced for thousands of years, but in the last two decades steganography has been introduced to digital media. Since steganography is becoming more and more common known technique, so we need to make it more secure too, i.e. even if the intruder sniffs it our information is still untraceable or secure. There are various file types related to Steganography e.g. image, audio, video, executable files. Video steganography is impressive but hard to implement, useful in hiding a quite large amount of data in smaller value and hence more secure as the size of resultant file creates no suspicion about hidden information. In this paper, we will design a new technique of steganography which is impressive, in terms of hiding and secure transmission of information. This technique does not involve stream substitution which makes this technique difficult to implement.

Keywords: Digital media, Data security, Steganography, Video stagenography.

I. INTRODUCTION

Steganography is the art and science of hiding the communication. A stenographic system embeds the hidden content in unremarkable cover media so as not to provoke an eavesdropper's suspicion. In the past, people used hidden tattoos or invisible ink to convey stenographic content. Today, computer and network technologies provide easy-to-use communication channels for steganography.

An essential part of steganography is to make sure that the stego file does not create suspicion about hidden communication. The word Steganography is of Greek origin and means "concealed writing" from the Greek words steganos means "covered or protected", and graphing meaning "to write". Steganography is the technique of hiding the message in a chosen carrier such that no one apart from the intended recipient is aware of its existence. The sender first selects the data to be sent and then chooses best way to send id by choosing the best cover file. Then the secret data is chosen and selected to be placed on the cover media. Secret file is now ready to use. The decoding process is reverse of encoding process of steganography. Block diagram of Steganography mechanism is shown in Figure 1.

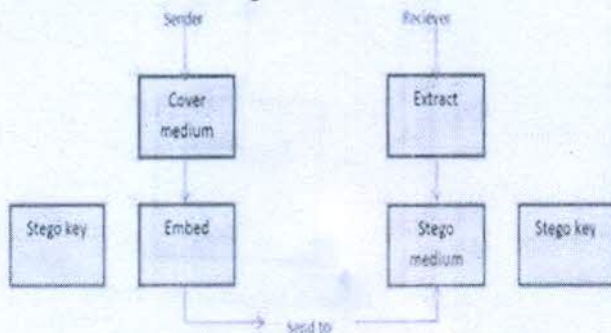


Figure 1: Block diagram showing steganography scheme.

Here a secret data is being embedded inside a cover file to produce the stego file. A key is often needed in the embedding process. The proper stego key is used by the sender for the embedding procedure. The same key is used by the recipient to extract the stego cover file in order to view the secret data. The stego file should look almost identical to the cover file.

An effective Steganography should possess the following characteristics:

Secrecy: Extraction of hidden data from the host medium should not be possible without the knowledge of the proper secret key used in the extracting procedure.

Imperceptibility: After embedding the data in the medium, it should be imperceptible from the original medium.

High capacity: The maximum length of the hidden message that can be embedded can be as long as possible.

Resistance: The hidden data should be able to survive when the host medium has been manipulated, for example lossy compression scheme.

Accurate extraction: The extraction of the hidden data from the medium should be accurate and reliable.

In this paper a hash based LSB[16] Procedure is proposed in spatial domain. An application of the algorithm is illustrated with AVI (Audio Video Interleave) file as a cover medium. The results obtained are substantial and promising. Effort has also been taken to study the steganalysis of the proposed scheme[16]. The idea behind this system is when someone know about importance of someone's data, then eavesdropper eagerly look for every sort of data going in or coming out, then how to be secure at that point of time. This proposed technique somehow secure contents of information in such situations.

II. LITERATURE SURVEY

A lot of research work has been carried out on audio and video steganography which concentrate on secret data hiding in audio and video file without image distortion. K. A. Navas, et al [13] have developed new algorithm for data embedding in

AVI videos. Two different phases are used to employ this method in cover video. In first phase, self-generating keys are used to embed data in cover video. Image is encrypted and then embedded into video in spatial and transform domains in second phase. This method requires high resolution digital video as a cover media. This method has ability to hide significant quality of information but it require large payload. In their method, the secret data are random spread over the cover file. Pseudorandom numbers are generated using key and this key is used to find out order of hidden message and location of secret data. This method withstand different attacks and very strong and secure. A. Shakir, et al [14] discussed the new method of audio steganography in which digital media can be securely transmitted over public network using internet as a distribution medium. Author has suggested new technique for hiding ciphered message into digital color bitmap image. Experimental result demonstrates that conjunction between steganography and cryptography produce immune information.

Chantana C, Karnkanak C, Jitdamrang P proposed a method in which image is hidden behind the video file. This method is based on wavelet transform. Main goal is to hide image pixels in the coefficient of frames. So video frames are transformed and then proper positions of the coefficient are selected to hide the secret image. V.Thakur, M.Saikia [7] developed a new data hiding and extraction procedure for AVI (Audio Video Interleave).The grey scale pixels values are converted to binary values and these values are then embedded in higher order coefficient value of DCT of AVI video frames. Hence intruder cannot able to unhide the image. High level of security is maintained during data transmission. Yadav P, et al [16] discussed a new video steganography method in which secret video stream is hidden in cover video stream. Secret video is divided into number of frame and each frame is broken into individual component. This component is converted into 8 bit binary values and encrypts it. This encrypted value is XORed with secret key and produce encrypted frame. Encrypted frame is hidden in least significant bit of cover video using sequential encoding method. Experimental result shows that it has better performance than traditional steganography method. Hamsathvani has developed hybrid image hiding scheme to hide image in selected video sequence. He discussed the DWT and singular value decomposition technique. In this scheme image is divided into several sub bands and secret image is embedded in singular values of cover media.SVD(Singular Value Decomposition) algorithm is applied on the cover image and then modify singular values to embed the watermark. Video is taken as input and perform some pre-processing to select video frame and then calculate MSE of each frame. Frame having low MSE is mainly selected for embedding watermark.

III. STEGANOGRAPHY SYSTEM

Steganography is the art of hiding the information in some other host object. It has been used since ancient time by the people. In ancient time, secret information is hidden in the back of wax, scalp of the slaves, in rabbits etc. With passage of time, the application of steganography and its area has become widened. With the introduction digitization era, digital steganography has emerged as the new tool to hide the information secretly. Text, digital image, digital audio and digital video has become the host object for data hiding. Below is some of the common term which is necessary to understand any steganography system.

Cover Media- It is the medium in which secret information is embedded in such a way that it is difficult to detect the presence of data.

Stego- Media- It is medium obtained after embedding the secret information.

Secret data- The data or information to be hidden in cover media.

Steganalysis- The process of detecting, presence of secret data in cover media.

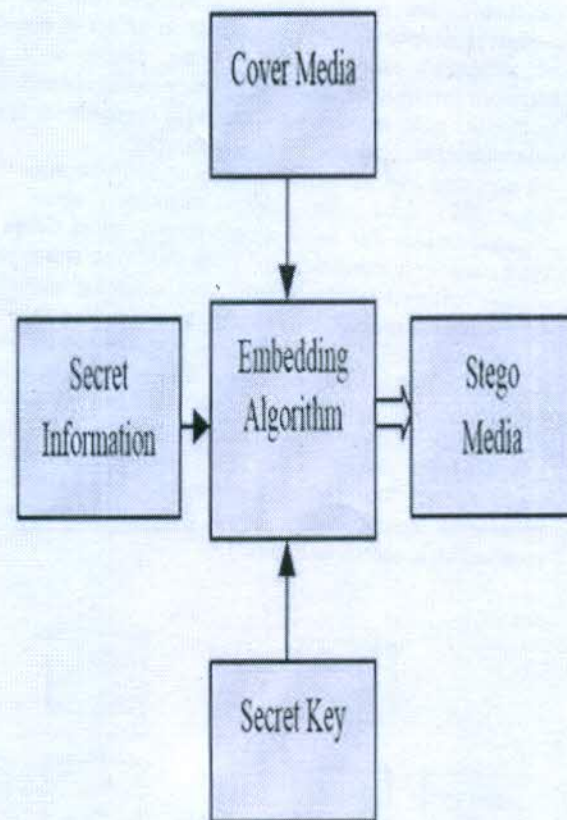


Figure 2: Steganography System

IV. PROPOSED TECHNIQUE

The technique is a new Hash based[16] technique for Video Steganography has been proposed. The flow diagram of the same is given in Figure 3 and 4.

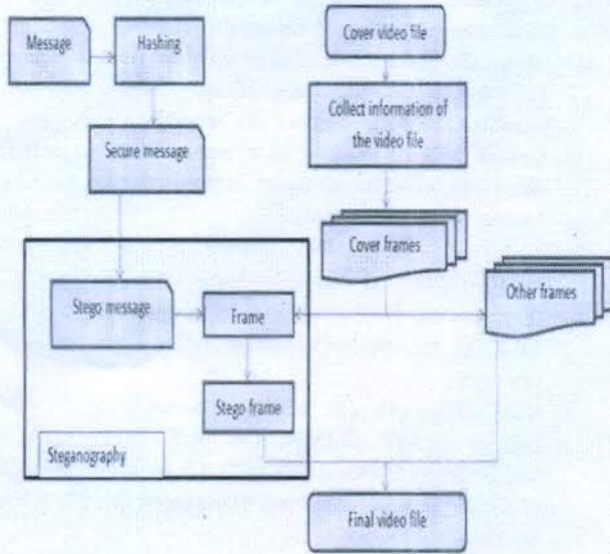


Figure 3: Proposed Encoding

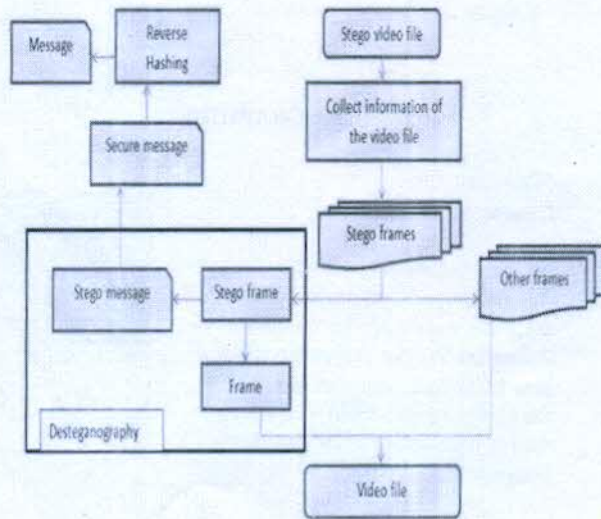


Figure 4: Proposed Decoding

A video stream (AVI) consists of collection of frames and the secret data is embedded in these frames as payload. The information of the cover video (AVI) such as number of frames (n), frame speed (fp/sec), frame height (H) and width (W) are extracted from the header. The cover video is then broken down into frames. Now the proposed LSB based technique has been applied to conceal the data in the carrier frames. The size of the message does not matter in video steganography as the message can be embedded in multiple frames[16].

In proposed system the message data is first hashed with MD5 hashing technique and then the message is embedded into the video file just as in traditional system. The work carried out is

performed using MATLAB. Here, algorithmic steps of steganography are done using MATLAB and message hash is produced using generic hash tool.

V. ALGORITHM OF NEW HASH BASED STEGANOGRAPHIC TECHNIQUE

A. Algorithm for Encoding

- Step 1: Input message to be sent.
- Step 2: Apply hashing to it.
- Step 3: Input cover video file.
- Step 4: Break video and audio part of single video file into frames.
- Step 5: Obtain the position for embedding the hashed message.
- Step 6: Embed these position values to audio part for easy decoding.
- Step 7: Embed the hashed message to cover frames to positions obtained in step 5.
- Step 8: Combine the video and audio frames.
- Step 9: Regenerate video file.

B. Algorithm for Decoding

- Step 1: Input stego video file or stream.
- Step 2: Read required information from the stego video.
- Step 3: Break the video and audio part into frames.
- Step 4: Obtain the position of embedded bits of the secret data from audio part.
- Step 5: Retrieve the bits using these positions.
- Step 6: Reconstruct the secret information.
- Step 7: Regenerate video frames.
- Step 8: Combine video and audio frames.
- Step 9: Regenerate video file.

VI. CONCLUSION

A secured hash based LSB technique for video steganography is presented in this paper. This technique utilizes cover video file in spatial domain to conceal the presence of sensitive data regardless of its format. The proposed technique is very encouraging the proposed[16] technique is applied to AVI files; however it can work with any other formats with minor procedural modification. For compressed video files like MPEG the video needs to first decompress then the technique can be applied to the uncompressed video. Whereas for Flash Video FLV files the

technique can be applied without modification. Software based Stenographic Engine for video steganography is the future scope of the technique[16].

ACKNOWLEDGMENT

It is great opportunity to write about **“Introducing a New Technique for Making a Secure Steganosystem”**, for preparing this paper I have gone through different books, research papers and websites to understand this topic easily.

I acknowledge with gratitude to Asst. Professor **Mrs. Nidhi Sharma** who has always been sincere and helpful in making me understand this research.

REFERENCES

- [1] D. Stanescu, M. Stratulat, B. Ciubotaru, D Chiciudean, R. Cioarga, M. Micea, “Embedding Data in Video Stream using Steganography”, in 4th International Symposium on Applied Computational Intelligence and Informatics, SACI-2001, pp. 241-244, IEEE, 2007.
- [2] Mritha Ramalingam, “Stego Machine Video Steganography using Modified LSB Algorithm”, in World Academy of Science, Engineering and Technology 74 2011, pp. 502-505, 2011.
- [3] A.K. Bhaumik, M. Choi, R.J. Robles, M.O. Balitanas, “Data Hiding in Video” in International Journal of Database Theory and Application Vol. 2, No. 2, pp. 9-16, June 2009.
- [4] J. J. Chae, B. S. Manjunath, “Data Hiding in Video”, in proceedings of the 6th IEEE International Conference on Image Processing, pp.311-315, 1999.
- [5] Kousik Dasgupta, J.K. Mandal, Paramartha Dutta, “HASH BASED LEAST SIGNIFICANT BIT TECHNIQUE FOR VIDEO STEGANOGRAPHY” in International Journal of Security, Privacy and Trust Management (IJSPTM), Vol. 1, No 2, April 2012.
- [6] Thakur V.Saikia, “Hiding secret image in video Intelligent Systems and Signal Processing(ISSP)”, in International Conference on 1-2 march 2013 IEEE, pp150-153.
- [7] Hardik J. Patel, Preeti K. Dave, “Least Significant Bits Based Steganography Technique”, in International Journal of Electronics Communication and Computer Engineering, Vol. 3, No. 1, pp. 97 - 103, 2012.
- [8] Shamim Ahmed Laskar, Kattamanchi Hemachandran, “Steganography Based On Random Pixel Selection For Efficient Data Hiding”, in International Journal of Computer Engineering and Technology, Vol.4, Issue 2, pp.31-44.
- [9] Mamta Juneja, Parvinder Singh Sandhu, “A New Approach for Information security using an Improved Steganography Technique”, in Journal of Info.Pro.Systems, Vol 9, and No: 3, pp.405-424.
- [10] Agniswar Dutta, Abhirup Kumar Sen, Sankar Das, Shalabh Agarwal, Asoke Nath, “New Data Hiding Algorithm in MATLAB using Encrypted secret message”, IEEE ICCSNT-201, pp.262-267.
- [11] V.S.,K.Balasuhrmaniyam,N.Murali,M.Rajakumaran, Vigneswari, “Data Hiding in Audio Signal, Video Signal, Text and JPEG Images”, in IEEE ICAESM -2012, pp. 741-746.
- [12] K.A. Navas, Vidya V., Sonia V. Dass, “High security data embedding in video”, in Recent Advances in Intelligent Computational Systems (RAICS), 2011 IEEE.
- [13] Ahmed Ch. Shakir, “Steno Encrypted Message in Any Language for Network Communication Using Quadratic Method”, in Journal of Computer Science 6 (3): 320-322.
- [14] Sutaone M.S., Khandare, M.V.”Image based steganography using LSB insertion technique”, in IEEE WMMN, pp.146-151, January 2008.
- [15] Yadav, P.; Mishra, N.; Sharma, S., “A secure video steganography with encryption based on LSB technique”, in Computational Intelligence and Computing Research (ICCR), 2013 IEEE International Conference on , vol., no., pp.1,5, 26-28 Dec. 2013.
- [16] Kousik Dasgupta, J.K. Mandal, Paramartha Dutta, “HASH BASED LEAST SIGNIFICANT BIT TECHNIQUE FOR VIDEO STEGANOGRAPHY (HLSB)”, in International Journal of Security, Privacy and Trust Management (IJSPTM), Vol. 1, No 2, April 2012.
- [17] U. Mourya Vardhan, A. Srinivasa Rao, “Imperceptible Data Transmission”, in International Journal of Technological Exploration and Learning (IJTEL) Volume 1 Issue 2 (October 2012).

BIOGRAPHIES

Gopesh Sardana

M.Tech Scholar,
Department of Computer Science,
T.I.T Bhiwani-127021
Research Work: “Introducing a new hashing technique for Steganosystem”, GCRSTS 2K16
Active member of ACM Bhiwani Chapter



Nidhi Sharma

Asst. Professor,
Department of Computer Science,
T.I.T Bhiwani-127021
Research Work: “Introducing a new hashing technique for Steganosystem”, GCRSTS 2K16





Review

Developments in application of enzymes for textile processing



Amit Madhu, J.N. Chakraborty*

Dr. B R Ambedkar National Institute of Technology Jalandhar, 144011, India

ARTICLE INFO

Article history:

Received 14 September 2016

Received in revised form

19 December 2016

Accepted 2 January 2017

Available online 6 January 2017

Keywords:

Cotton

Enzymatic processing

Immobilization

Pre-treatment

Finishing

ABSTRACT

Enzymatic treatments have gained recognition in textile industry because they are stereo specific, non-toxic, environment friendly and energy conserving alternatives. Enzymes are virtually applicable to all manufacturing steps of textile chemical processing. Amylases for textile desizing; cellulases employed for bio-polishing & denim washing; proteases for wool modifications are important to mention in this category. However in spite of lot potentials, enzymes have limited industrial acceptance due to extreme pH and temperature conditions employed in textile processing leading to their reduced properties and action. Advances in enzymology and molecular biology provide possibilities for new enzymes identification and modifications in existing enzymes as well as in enzyme-based processes suitable/to fit for environment friendly option. Enzyme immobilization is one such approach which stabilizes enzymes, extends useful life and improves action in some cases too. Additionally, recyclability & reuse of enzymes make process even more economical. This review summarizes the potential research involved in the development of enzymatic processing in textile chemical processing. The paper highlights the significance and limitations of native enzymes as well as immobilized enzymes applications in textile chemical industry.

© 2017 Elsevier Ltd. All rights reserved.

Contents

1. Introduction	115
2. Immobilization of enzymes	115
2.1. Immobilization supports	115
2.2. Methods of immobilization	116
2.3. Factors influencing the immobilization enzymes	116
2.4. Evaluation of immobilized enzymes	116
3. Enzymes in textile chemical processing	117
4. Developments in the applications of enzymes for cotton textile processing	117
4.1. Desizing	117
4.1.1. Concept of enzymatic desizing	117
4.1.2. Native amylase application	117
4.1.3. Immobilized amylase application	118
4.2. Scouring	118
4.2.1. Concept of enzymatic scouring	119
4.2.2. Native pectinases application	120
4.2.3. Immobilized pectinases application	120
4.3. Bleaching	120
4.3.1. Concept of bleaching with enzymes	120
4.3.2. Native enzyme applications in bleaching	120
4.3.3. Immobilized enzyme applications in bleaching	122

* Corresponding author. Department of Textile Technology, Dr. B R Ambedkar National Institute of Technology Jalandhar, 144011, India.
E-mail address: chakrabortyjn@hotmail.com (J.N. Chakraborty).

4.4.	Bio-polishing	122
4.4.1.	Concept of bio-polishing	122
4.4.2.	Native cellulase application	123
4.4.3.	Immobilized cellulase application	124
4.5.	Denim finishing/washing	125
4.5.1.	Concept of denim fading using cellulase	125
4.5.2.	Application of native cellulase in denim fading	125
4.5.3.	Immobilized cellulase for denim fading	125
5.	Some other potential applications of enzymes in textile processing	125
5.1.	Anti-shrinkable wool	125
5.2.	Bleach clean-up	125
5.3.	Synthetic fiber modification	126
5.4.	Biological polymer synthesis & functionalization	126
5.5.	Utilization of immobilized enzymes for textile functionalization	127
6.	New prospects in enzyme applications	127
7.	Constraints in the application of immobilized enzymes in textile industry	127
8.	Environmental impact assessment	128
9.	Conclusions	128
	References	128

1. Introduction

Enzymes as biocatalysts have been remarkably accepted in diverse sectors owing to their substrate specificity and green chemistry. Employment of enzymes specifically for textile processing is acknowledged because of their ability to replace harsh chemicals used conventionally and to conserve water & energy. However, high cost and lack of long-term stability under storage & process conditions often hampered their applications (Binod et al., 2013; Cavaco-Paulo and Gubitz, 2003).

The conventional way to catalyze the specific process using enzymes is simply to add them into the process. After completion of process it is inactivated and finally drained in effluent. Such way of enzyme application is not economical and also for the textile processing applications the enzymes should be stable against severe parameters like high temperature, pH and to the salts, alkalis, surfactants etc usually employed in the textile processing. Some improvement in process efficiency can be achieved by modifying the process conditions to suit the sensitivities of the biocatalyst (e.g., in terms of pH, temperature, and auxiliaries). The other alternative can be to use protein engineering methodologies to generate new biocatalysts to function under more ideal process conditions (thermostable and work under extreme pH). This leads to the discovery of tailored enzymes that are highly specific for numerous industrial applications but in all these instances industrial application of enzymes is still not an economical alternative (Binod et al., 2013; Diaz-Rodriguez and Davis, 2011; Gerday et al., 2000; Haki and Rakshit, 2003; Singh et al., 2013).

As enzymes are the biocatalysts, they are not consumed in reactions; hence their reusability can be the best solution for economical point. Therefore, an alternative way to use enzymes can be immobilization. Immobilization is to fix the enzymes on an adequate carrier/support material which enables simple operation, easy separation and possibility to reuse enzymes. Moreover, the effluent drain after process completion will be free from enzyme residues. Also the interest in use of immobilized enzymes in industry is due to their increased stability (to temperature, pH, solvents and auxiliaries) along with recovery & reuse (Brena et al., 2013; Busto, 1998; Mateo et al., 2007; Sheldon, 2007). Thus, the immobilization of enzymes is typically a requirement for the use of enzymes as a realistic biocatalyst. This review briefs the concept of enzyme immobilization and critically updates the potential

research referring the application of native & immobilized enzymes with focus on textile chemical processing.

2. Immobilization of enzymes

Recent developments in protein engineering have revolutionized the development of commercially available enzymes into better industrial catalysts. Immobilization of enzyme is one such approach for the improvement in enzyme properties. Immobilization of enzyme can be referred as the attachment of enzymes to support/carrier material resulting in reduction or loss of mobility with retention of their catalytic activity and which can be used repeatedly and continuously. (Brena et al., 2013; Khan and Alzohairy, 2010; Tischer and Wedekind, 1999). Immobilized enzymes have a great importance in industrial bioprocesses especially in food, nutritional and pharmaceutical technologies and in addition facilitate manufacturing of biotechnology products with application in diagnostics, bio-affinity chromatography, and biosensors (Khan and Alzohairy, 2010; Sheldon, 2007; Souza, 2002). Technological properties of immobilized enzymes or impact of immobilization on enzyme properties compared to native enzymes are illustrated in Fig. 1 (Busto, 1998; Mateo et al., 2007).

2.1. Immobilization supports

Support materials play an important role in determining the performance of the immobilized enzyme. Ideally it should have hydrophilicity, inertness towards enzymes, bio-compatibility, resistance to microbial attack, physical resistance to compression, availability at low cost and adequate large surface area together

Advantages	Disadvantages
<ul style="list-style-type: none"> • Recovery & reuse of catalyst • Continuous operation possible • Easier product separation • Easy handling • Potential of enzyme stabilization 	<ul style="list-style-type: none"> • Loss or reduction in enzyme activity • Diffusional limitation • Additional cost of support & technique

Fig. 1. Technological Properties of immobilized enzymes compared to native enzymes.

with the least diffusion limitation in the transport of substrate and product. Also in order to fully retain their biological activity enzymes should be attached to support without affecting their conformational and functional properties. Support materials for immobilization can be classified as inorganic and organic, according to their chemical composition. The organic supports can be subdivided into natural (polysaccharides-alginate, chitosan; protein-collagen etc) and synthetic polymers (polystyrene, polymethacrylates, polyacrylates, polyamides etc). While inorganic supports may include natural minerals (silica, charcoal etc) and processed minerals (glass, ceramics, activated carbon, metal oxides etc) (Brena et al., 2013; Datta et al., 2013; Krajewska, 2004; Malmiri et al., 2012; Nisha et al., 2012; Tischer and Wedekind, 1999; Wang and Caruso, 2005).

2.2. Methods of immobilization

Many methods of immobilization, coupled to a wide spectrum of supports have been revealed till date. However, even though immobilization on supports is an established technology, there are still no general rules for selecting the best support for a given application. Methods for enzyme immobilization can be classified into three basic categories compared in Fig. 2 (Brady and Jordan, 2009; Datta et al., 2013; Elnashar, 2011; Malmiri et al., 2012; Roig et al., 1986; Sheldon, 2005, 2007; Souza, 2002; Tischer and Wedekind, 1999).

2.3. Factors influencing the immobilization enzymes

The process of immobilization has profound effects on the enzyme properties as the enzyme is converted from a homogeneous catalyst to a heterogeneous catalyst. The activity, stability, pH and temperature optima, kinetic properties and substrate specificity altered by the association with a support (Brena et al., 2013). The performance of immobilized enzymes can be measured by its catalytic & non-catalytic functions (recovery & reusability). The catalytic functions are linked to activity, selectivity and stability whereas non-catalytic functions are strongly related with the physical and chemical nature of the non-catalytic part (Cao, 2005; Norouzian, 2003).

The catalytic activity of a native enzyme is principally depend on its intrinsic structure and operational conditions whereas for an immobilized enzyme it depends on many factors, including the microenvironment of carrier: the physical (shape, size, thickness) & chemical structure of the carrier, the nature of its interaction with the carrier, binding position and number of bonds, the freedom of the conformation change in the carrier, the properties of the spacer/arm linking enzyme to carrier (e.g. charged or neutral, hydrophilic or hydrophobic, size, length), and the conditions under which the enzyme molecules were immobilized (Ahmad and Sardar, 2015; Cao, 2005; Datta et al., 2013; Norouzian, 2003).

The stability of the immobilized enzymes with respect to time, temperature, other storage conditions and experimental variables might be expected to either increase or decrease on immobilization (Miletic et al., 2012; Worsfold, 1995). Quite often the operational stabilization is observed usually due to the result of loading an excess of enzyme. However, true stabilization at the molecular level may be owing to multipoint attachment. High enzyme loading during immobilization supposed to increase activity but lead to a reduction of apparent activity due to restricted diffusion (Brena et al., 2013; Mateo et al., 2007; Mohamad et al., 2015).

In the development of immobilized biocatalysts along with the selection of immobilization supports, conditions and methods of immobilization; the overall enzymatic activity, enzyme deactivation characteristics, cost of immobilization procedure, toxicity of immobilization reagents and the desired final properties of the immobilized enzymes should also be considered (Cao, 2005; Miletic et al., 2012; Powell, 1984).

2.4. Evaluation of immobilized enzymes

The immobilization factors discussed above will have a significant effect on the characteristics of the immobilized enzyme. The true immobilized enzyme should provide a well balanced overall performance, based on reasonable immobilization yields with low mass transfer limitations and high operational stability (Ahmad and Sardar, 2015; Liese and Hilterhaus, 2013; Miletic et al., 2012).

It is imperative to measure the immobilization method yield which is expressed as the combination of percentage of enzyme immobilized and the enzyme activity remaining after

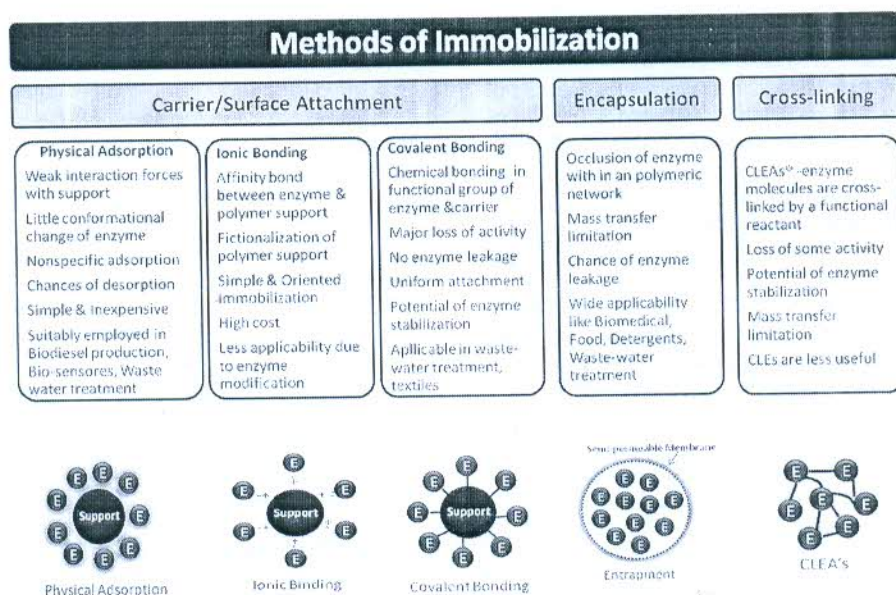


Fig. 2. Comparative study of different methods of immobilization.

immobilization with the experimental conditions. The percentage of enzyme immobilized is usually calculated in terms of bound protein by measuring the amount of enzyme remaining in the supernatant after immobilization and subtracting this from the amount originally present (Liese and Hilterhaus, 2013; Tischer and Kasche, 1999; Worsfold, 1995).

The absolute enzyme activity remaining on the support after immobilization is more difficult to determine and an apparent or specific activity is usually measured which takes into account mass transfer and diffusional restrictions in the experimental procedure. This effect arises from the fact that an immobilized enzyme bound to support and has a deliberate restricted mobility. In addition to diffusional limitation effects, the support can also exert partitioning effects due to its charge i.e. it is important when characterizing immobilized enzymes to study their activity under a variety of ionic conditions. Specific activity is usually defined as reaction rate/unit mass of the protein produced and usually expressed by the effectiveness factor which determines the effectiveness/efficiency of immobilized enzyme in relation to native enzyme under appropriate reaction conditions (Mateo et al., 2007; Miletic et al., 2012; Powell, 1984).

The other critical performance indicators are the operational and storage stability. Operational stability expressed as activity decay under working conditions like pH, temperature, solvent etc while storage stability is to monitor its activity after fixed period of time under specified storage conditions. These parameters provide the performance data, which can be expressed as productivity (product produced per unit enzyme) or enzyme consumption (enzyme consumed per unit product produced). Other quantifiable parameters for an immobilized enzyme are its pH & temperature optima (for working range), the apparent Michael's constants (K_m) for appropriate substrates (which also give an indication of immobilized enzyme selectivity) and finally the reusability cycles (Liese and Hilterhaus, 2013; Miletic et al., 2012).

3. Enzymes in textile chemical processing

Enzymes can be applied for all manufacturing steps of chemical processing as well as to the effluent treatment. (Cavaco-Paulo and Gubitz, 2003; Doshil and Shelke, 2001; Hasan et al., 2015; Jegannathan and Nielsen, 2013; Malik et al., 2010; Mojsov, 2011; Nielsen et al., 2009). In textile industry mainly hydrolases and oxidoreductases are engaged for various enzymatic applications. In terms of source the microbial enzymes are more often useful than plants or animals derived enzymes because of the great variety of catalytic activities available, the high yields possible, ease of genetic manipulation, regular supply due to absence of seasonal fluctuations and rapid growth of micro organisms on inexpensive media. Also the enzymes from microbes are more stable than their corresponding plant and animal enzymes and their production is more convenient and safer (Cavaco-Paulo and Gubitz, 2003; Mojsov, 2011; Wavhal and Balasubramanya, 2011).

Majority of the enzyme applications in textiles are confined to cotton processing: removal of impurities (desizing, scouring, bleaching); bio-finishing to improve appearance and remove of fiber fuzz from the surface; bio-stoning or 'stonewashing' of denims to produce the fashionable aged look; bleaching cleanup to remove residual H_2O_2 before dyeing (Sarkar and Etters, 2001).

In addition to that there are efforts to substitute conventional processes of anti-shrinking & anti-pilling wool (Nolte et al., 1996) & degumming of silk with protease enzyme (Ninge Gowda et al., 2007), retting of bast fibers (jute, flax, ramie) with pectinase, xylanase or hemicellulases (Patra et al., 2010), the several studies have been reported on modification of synthetics using hydrolases class of enzymes to impart hydrophilicity and antistatic properties

(Gubitz and Cavaco-Paulo, 2003; Wavhal and Balasubramanya, 2011). Moreover, detergent formulations with mixture of enzymes to remove varieties of stains in garment laundering (Galante and Cristina, 2003; Vasconcelos et al., 2006).

Furthermore, textile chemical processing is highly chemical intensive and a variety of complex chemicals & auxiliaries are employed. Hence, the effluent generated is variably pollutant and extensive toxic including acids, alkalis, detergents, grease, oils, sulphates, solvents, heavy metals, other inorganic salts, fibers and residual colorants (dyes). These pollutants not only add color to water but also cause toxicity for aquatic and other form of life. Therefore, it is necessary to treat the effluent specially the residual colorants before discharging in environment (Archana et al., 2012; Sarayu and Sandhya, 2012; Tavcer, 2011). The conventional physico-chemical processes (Yagub et al., 2014), employed for decolouration are not suitable due to high cost and low effectiveness to meet the norms stipulated by pollution control boards. Hence, several biotechnological based methods employed for the textile effluent treatment containing synthetic dyes as colorants has been discussed in many papers (Babu et al., 2007; Gupta et al., 2015; Imran et al., 2015; Khan et al., 2013; Rauf and Ashraf, 2012; Rodriguez-Couto and Herrera, 2006; Sarayu and Sandhya, 2012).

4. Developments in the applications of enzymes for cotton textile processing

A copious literature is available on the applications of enzyme technology in textile chemical processing and a lot research work is allied in this area.

The development of enzymatic textile processing can be framed into the following research strategies, depicted in Fig. 3. But the concrete efforts associated with each enzymatic treatment are different from process to process. So, the developments in enzymatic textile processing are systematically & independently discussed.

4.1. Desizing

A removable protective layer preferably of starch is applied to sustain the warp yarns. Apart from film forming material the size recipe contain other additives such as humectants, binders and lubricants. Desizing is the process to remove this surface coating to facilitate the penetration of dyes & chemicals in subsequent wet processing.

4.1.1. Concept of enzymatic desizing

Conventionally inorganic acids in mild concentrations or oxidizing agents are employed for desizing purpose. However the application of enzyme efficiently & selectively removes starch based size. The group of enzymes which catalyze chain scission in the starch molecules, the amylases, can be classified according to their biological source (bacterial, malt and pancreatic) or degradation mechanism. α -Amylases cause random cleavage of 1,4-glucosidic linkage while β -amylases liberate maltose by a stepwise hydrolysis and Amyloglucosidase split both amylase and amylopectin via stepwise hydrolysis removing D-glucose from the non-reducing end. Several reviews and researches are available which discuss their applications and biocatalytic performance in textiles as desizing agents (Hossain and Uddin, 2011; Mojsov, 2011; Regan, 1962; Sojka-Ledakowicz et al., 2006; Tzanov et al., 2001).

4.1.2. Native amylase application

Around 1900 first commercial desizing compound under name Diastafor was introduced and in 1919 Rapidase (Wallerstein & Co.) a bacterial diastase becomes available to liquefy starch (Karmakar,

1999). Developments within enzymatic desizing are discussed under different strategies in Table 1.

4.1.2.1. Economical & industrial viable amylases. Out of three amylase types, α -amylases are more suitable for degradation, dextrinization and liquification of starch while β -amylase and amyloglucosidase are quite heat sensitive would not be suitable for desizing purposes and in addition β -amylase is a saccharifying rather than a dextrinizing enzyme (Hanson and Gilbert, 1974). Initial research was oriented in obtaining inexpensive commercial amylases for industrial applications (Khan and Arif, 2006). Optimization of various types of amylases in terms of their concentration, application conditions and industrial methods was studied by many researchers. The effectiveness of amylase desizing can be enhanced by raising temperature beyond 70°, prolonging desizing time up to 60 min, adding salts as enzyme stabilizers and/or increasing agitation (Haq et al., 2010; Chimata et al., 2011, Ul-Haq and Nasir, 2012).

Assistance of salt (Chand et al., 2012) or ultrasonic waves (Wang et al., 2012; Hao et al., 2013) helps in improving effectiveness of enzyme either by reducing dosage or moderate process conditions. Various industry specific enzymes like Ca^+ independent amylase work under mild temperature range with salt stability (Chand et al., 2012); pH, temperature as well as high salt concentration stable enzyme from *Bacillus sp. SI-136* via sodic alkali soil (Sarethy et al., 2012) and low temperature acidic amylases isolated from two different *Aspergillus* species (Sreelaakshmi et al., 2014) can be better desizing agents.

4.1.2.2. Assistance with other enzymes. The assistance of other enzymes should not only improve process due to synergism but also helps in removing the other natural impurities from cellulosic materials. Incorporation of lipase helps in removing the hydrophobic part of size (tallow based lubricants especially) which are difficult to be removed even in scouring. Improved desizing with shorten process time and higher quality end product in terms of uniformity and hand (Lange, 1997). Similarly the incorporation of H_2O_2 (4 ml/L, 35%) or neutral cellulase (2% owf) along with commercial amylase gives better wet ability, higher dye uptake and lower stiffness (Ibrahim et al., 2004b).

4.1.2.3. Combined desizing with scouring. Combination of enzymatic pretreatments can be very economical and environment friendly technique. However the compatibility of enzymes is the

main constraint in combining processes. Alkali stable amylase can provide the possibility for simultaneous desizing and scouring. A fast continuous integrated desizing & scouring process was reported in (Lenting and Warmoeskerken, 2004; Aly et al., 2010) using alkaline amylase with pectate lyase, efficiently remove pectins together with hydrophobic impurities. In, 2005 Novozyme introduce an alkaline amylase with broad pH and temperature ranges (pH 5–10; 20 °C–85 °C) and studied its effectiveness in combination with pectate-lyase for simultaneous desizing & scouring (Kuilderd and Wu, 2008). Enzyme obtained from Soil rhizosphere has both amylase and pectinase activity at neutral pH and provide single step desizing & scouring (Dalvi et al., 2007).

4.1.2.4. Thermo-stable amylases. Raising the temperature desizing facilitates starch removal as well as reduces process duration therefore the thermophile amylases have gained wider acceptance. Thermophile *Bacillus licheniformis* α -amylase and many more can provide high temperature efficient starch removal with improved absorbency (Saravanan et al., 2011). Also the salt can act as enzyme stabilizer; the effect of various additives has been studied on mesophilic α -amylase to provide thermal stability for high temperature efficient desizing (Fu et al., 2015).

4.1.3. Immobilized amylase application

Despite the various forms, and many studies on immobilized amylases (Beyler-Cigil et al., 2013; Shukla and Jajpura, 2005; Talekar et al., 2013), the practical applications of immobilized amylases in textile desizing are infrequent, since they have to act upon macromolecular substrates.

Desizing of gray cotton fabric with native & immobilized α -amylase in assistance of ultrasonic energy was reported (Sahinbaskan and Kahraman, 2011). Sonification significantly improves starch removal with native and immobilized enzyme while reduced strength loss is observed with immobilized enzyme. Moreover, the immobilized α -amylase on AESO (acrylated epoxidized soyabean oil) resin retains 50% of initial activity after 5 cycles which enables its recovery and reuse. A potential for a wide range of industrial applications including textiles was claimed by Talekar et al. (2012b). He reported the immobilization of α -amylase as magnetic cross-linked enzyme aggregates having potential for industrial applications owing to easy separation under a magnetic field for repeated use.

Furthermore, an amylase from *Aspergillus Niger* was immobilized via glutaraldehyde-mediated coupling onto zirconia-coated alkylamine glass beads and used along with various detergents in removal of starch stains from cotton clothes. All the detergents gave better washing in presence of immobilized amylase (Dhingra et al., 2006). Similarly the purified and thermostable α -amylase from soybean seeds was immobilized by entrapment on agarose and agar matrices and their catalytic properties were compared. Both the agarose and agar matrix proved to be a good support with low cost for the enzyme showing more or less about 75% immobilization. Immobilized amylase improve the washing efficiency of detergents by removing starch stains from clothes thus finding potential application as detergent additives (Prakash and Jaiswal, 2011).

4.2. Scouring

Non-cellulosic impurities such as pectins, fats, waxes, proteins, natural colorants, minerals etc. are found in diverse proportions in the primary walls of cellulosic fibers which limit the dyeing and finishing due to poor wet-ability & dirty appearance. Scouring is the purifying treatment to sufficiently reduce the amount of these impurities.

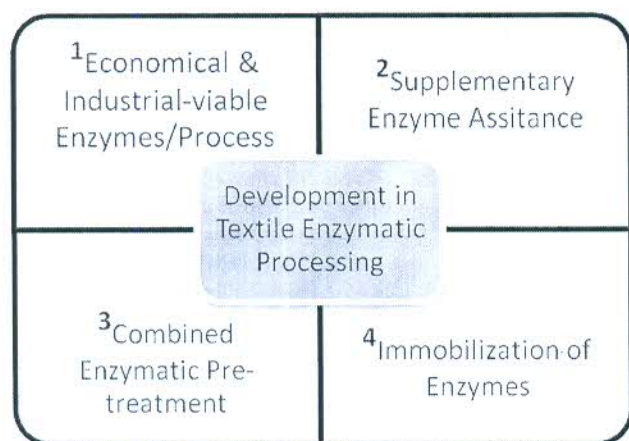


Fig. 3. Development on Enzyme applications in textile chemical processing.

Table 1
Research work involved in application of enzymes in desizing.

Research strategy	Enzyme & its source	Research description	Reference
Economical & industrial viable amylases	Rhozyme DX, Rhozyme GC, Diastafor LCD (Bacterial α -Amylases) β -Amylase (Crude Barley) Amyloglucosidase (<i>Rhizopus genus mold</i>) α -Amylase (Animal Pancreas)	α -Amylase is more suitable for desizing compared to β -amylase & amyloglucosidase	Hanson and Gilbert, 1974
	Microbial α -Amylase (<i>Bacillus amyloliquefaciens</i>) α -Amylase (<i>Aspergillus niger sp. MK 07</i>)	Amylase obtained from cheap waste animal material & efficient in desizing for exhaust and pad batch application 100% desizing achieved with 200–225 units crude enzyme, pH 6.5 & 60 °C, 1 h 300 U/ml enzyme is optimum, stable till 75 °C, pH 6.5 with 0.3 M CaCl ₂	Khan and Arif, 2006 Haq et al., 2010
	Glucoamylase (Multifect GA 10L) & α -Amylase (Optimize Next)	Industrial acid stable enzymes mixed with chelating agent in citric acid perform simultaneous acid-demineralization and desizing	Dehabadi et al., 2011
	Commercial α -amylase	Ultrasound assisted with amylase save half processing time	Wang et al., 2012 Hao et al., 2013
	α -Amylase	Winch give highest desizing quality but continuous process require sufficient time	Ul-Haq and Nasir, 2012
	Ca ²⁺ ion independent α -amylase (<i>Bacillus sp. KR8104</i>)	Moderate temperature (30–70 °C) desizing with acid-demineralization possible under acidic condition, presence of salts could decrease enzyme dosage and process time amylase obtained capable of efficient desizing (Tegewa Rating-9) at lower (50 °C) and higher (95 °C) temperature up to 12 pH	Chand et al., 2012
	α -Amylase (<i>Bacillus sp. SI-136</i>)		Sarethy et al., 2012
	Amylase (<i>Aspergillus niger</i> & <i>Aspergillus flavus</i>)	Higher desizing efficiency (<i>A. niger</i> – 96%, <i>A. flavus</i> – 90%) with significant improvement in absorbency & extractable impurities	Sreelaakshmi et al., 2014
	α -Amylase (<i>Bacillus sp. KR 8104</i>)	Simultaneous enzyme production and desizing optimized using inexpensive raw materials for α -amylase	Chand et al., 2014
	Bactosol PHC (Bacterial amylase)	Optimized desizing recipe using taguchi & GRA analysis for economy	Ishman et al., 2015
Amylase assisted with other enzymes	Aquazym amylase & Lipase	Lipase assistance improve starch removal and shorten desizing time	Lange, 1997
	α -Amylases (Aquazym)	Incorporation of H ₂ O ₂ or neutral cellulase improves desizing with whiteness and dye-ability, presence of wetting agent governed extent of desizing	Ibrahim et al., 2004a
Combined desizing with Scouring	α -Amylase Alkaline Pectate-lyase Amylase + Pectinase (Soil rhizosphere)	Fast continuous integrated desizing & scouring of 3–10 min in alkaline pH Enzyme has both amylase and pectinase activity at neutral pH, provide single step desizing & scouring with 15% at 75 °C for 90 min	Lenting and Warmoeskerken, 2004 Dalvi et al., 2007
	Alkaline amylase (Commercial enzyme Novozyme) α -Amylase Polygalacturonase (<i>Trichoderma harzianum</i>)	Combined desizing & bio-scouring in single bath being alkaline stable enzyme Optimize combined pre-treatment in terms of weight loss, residual starch %, absorbency, strength loss and copper no.	Kuilderd and Wu, 2008 Aly et al., 2010
	Thermophile α -Amylase (<i>Bacilluslicheniformis</i>) α -Amylase (<i>mesophilic</i>)	Optimize cotton desizing using taguchi design; 3 g/l acidic α -amylase with 6 pH at 85 °C for 40 min Thermal stability of α -amylase studied in various additives for high temperature desizing, chitosan saves 2/3 enzyme dosage & improve desizing effect	Saravanan et al., 2011 Fu et al., 2015
Immobilized amylase	α -Amylase (Procine pancreas)	AESO immobilized amylase efficient in starch removal with reusability & sonification improves the starch removal	Sahinbaskan and Kahraman, 2011
	CLEAs of <i>Bacillus amyloliquefaciens</i> α -amylase	CLEAs have 100% activity with enhanced thermal (up to 80 °C) and acidic condition stability and CLEAs retain 65% of its activity after 4 cycles	Talekar et al., 2012a
	Amylase (diastase) <i>Aspergillus niger</i>	Immobilized on alkylamine glass beads & efficient in removal of starch stains along with various detergents & can be reused 100 times	Ohnitra et al., 2006
	α -Amylase (soyabean seeds)	Entrapped in agarose and agar matrices with 75% & 77% activity; reused up to 5 cycles in starch stain removal	Prakash and Jaiswal, 2011

4.2.1. Concept of enzymatic scouring

Classic alkaline scouring using sodium hydroxide, removes the majority of such contaminations, essential to achieve satisfactory wet-ability. While the bio-scouring is eco-friendly, energy conserving alternative based on the idea of specially targeting the non-cellulosic impurities with appropriate enzymes without adversely affecting the substrate. Natural properties of the cotton fiber are preserved; the fabric is softer to the touch than after classic scouring. Bio-scouring can also be used for mixtures of cotton with silk, wool and cashmere, besides the severe alkaline conditions of classic scouring damage these fibers (Csiszar et al., 2001; Sojka-

Ledakowicz et al., 2006; Wang et al., 2007).

Pectin being a major non-cellulosic substance in cotton acts as cementing/adhesive material between cellulosic and non-cellulosic substances; therefore simply by removing pectin, it is easier to remove all other non-cellulosic substances. The process of bio-scouring is based on the concept of decomposition of pectin using enzyme. Pectins are complex polysaccharides comprised of α -(1,4) linked D-galacturonic acid backbone. The enzyme hydrolyzing the pectic substances into simpler molecules (galacturonic acids) are broadly known as pectinases and include polygalacturonases, pectinesterases and pectin lyases depending on their mode of

action (Tavcer et al., 2007).

4.2.2. Native pectinases application

The starting studies in bio-scouring were carried out with targeting the non-cellulosic impurities with pectinases, proteases and lipases enzymes. Favorable results were obtained with pectinases being most effective, lipase less and protease being least effective. After that many researchers work with different pectinases to optimize cotton scouring.

4.2.2.1. Industrially viable bio-scouring. The concentration of enzymes, time and temperature of treatment, pH of bath, additives and the mechanical treatment all influences the activity of enzymes. Optimum enzyme concentration varies from pectinase to pectinase but in general pectinases are effective in low concentrations 0.05–2% range. Also the optimum temperature of pectinases application is from 40°–60 °C beyond which enzyme reduces its activity (Li and Hardin, 1998). Therefore a high temperature rinsing after bio-scouring is essential for the removal of waxes (Choe et al., 2004).

The majority of pectinases are effective in pH 5–9 while the pH of bath is kept acidic or alkaline depending on the pectinase type. Alkaline and acidic pectinases both have similar scouring effects while acidic pectinase works with lower concentration. Actually the acidic medium (pH 4–6) itself degrades pectin without pectinase which assist in the pectin removal. Longer treatment time was the initial disadvantage with bio-scouring but with the developments of new pectinase enzymes and the use of additives make it industrially suitable (Ismal, 2008; Presa and Tavcer, 2008; Sahin and Gursoy, 2005; Tzanov et al., 2001).

Addition of surfactants specifically the non-ionic ones ease the enzyme penetration due to lowering surface tension of fibers and active in wax & grease removal (Buchert et al., 2000; Li and Hardin, 1997, 1998; Traore and Buschle-Diller, 2000). While weaker chelating agents assist the removal of pectin content (Csiszar et al., 2001; Losonczi et al., 2005; Presa and Tavcer, 2008). Introducing mechanical agitation and ultrasound assistance shortened the process time and reduces pectinase dosage (Hartzell-Lawon and Durrant, 2000; Yachmnev et al., 2004). A novel pectatelyase was evolved by gene mutagenesis technology for significantly better performance at a low enzyme dosage in alkaline pH & high temperature bio-scouring process (Solbak et al., 2005).

4.2.2.2. Mixed enzyme system for bio-scouring. Assistance of lipases removes natural as well as added fats & lubricants to provide better absorbency for enhanced levelness in dyeing. Bio-scouring formulations containing lipase are more effective in attaining good hydrophilicity for cellulosic textiles (Sangwatanaroj et al., 2003; Kalantzi et al., 2010). Similarly the addition of cellulases improves the impurity removal by hydrolyzing the cellulose chains (Csiszar et al., 2001b; Ismal, 2008; Li and Hardin, 1997, 1998; Saravanan et al., 2008). Use of mixed enzyme systems mainly pectinase along with lipases, proteases, cellulases, xylanases or cutinases can be very effective for this purpose (Battan et al., 2012; Csiszar et al., 2001; Hoondal et al., 2002; Tavcer et al., 2006; Thiagarajan and Selvakumar, 2008; Vigneswaran et al., 2013).

4.2.2.3. Combined scouring with bleaching. Single step scouring & bleaching can be efficiently combined to conserve energy and water. The alkaline pectinase can efficiently combined with H₂O₂ bleaching and reactive dyeing process (Ibrahim et al., 2004a) and it also provide the possibility of single bath desizing, bio-scouring and H₂O₂ bleaching of starch sized cotton fabric using glucose-oxidase enzyme (Cai et al., 2001; Li and Hinks, 2012; Hebeish et al., 2013; Shin et al., 2004; Spicka and Tavcer, 2013b; Tavcer, 2012; Tzanov

et al., 2001). Simultaneous scouring & bleaching using pectinase and Peracetic acid sufficiently removes pectin with medium whiteness (Pesa and Tavcer, 2008; Shafie et al., 2009).

A lot of research has been done with different commercial as well as specially produced pectinases alone or in mixture with other enzymes employed for bio-scouring shown in Table 2. Despite the massive research on bio-scouring, it has yet to be commercialized on industrial scale. Still there is a need of economical enzymes with higher activity & stability to high temperatures & alkaline conditions.

4.2.3. Immobilized pectinases application

Pectinases have tremendous potential to efficiently use by applying immobilization principles on them. Until now, pectinases have been immobilized by various techniques on various supports including polyacrylonitrile copolymer membrane, ion exchange resins, bone as solid support, aminated silica gel, cross linked enzyme crystals and cross linked enzyme aggregates, macroporous polyacrylamide, polygalacturonase on activated polyethylene, polymer nanocomposite microspheres, silica coated chitosan, nylon6, magnetic particles, for the application in various industries like food, paper making, medicine etc. (Dalal et al., 2007; Delcheva et al., 2007; Hiteshi et al., 2013; Li et al., 2007; Vaillant et al., 2000).

Sawada and Ueda (2001) successfully attempted to expose cotton to scouring via a pectinase immobilized in a reverse micellar system. The effectiveness of scouring was equivalent or better than that achieved by conventional alkaline processes or bio-scouring in aqueous media. The enzyme demonstrated excellent activity, even in organic media.

4.3. Bleaching

Bleaching in textiles aimed to destroying natural pigments present in the fibers account for dirty appearance before dyeing. Traditionally the whitening is achieved with chlorine and oxygen containing oxidizing agents at extreme conditions but in last two decades the H₂O₂ (hydrogen peroxide) has almost entirely replaced the conventional chlorine treatments for textile bleaching processes. Actually the radical reactions involved in the action of bleaching agents with the fibers, lead to decrease in the degree of polymerization and thus severe damage to fibers (Basto et al., 2007). Furthermore, huge amounts of water are needed to remove hydrogen peroxide from fabrics which would cause problems in dyeing.

4.3.1. Concept of bleaching with enzymes

Many of the alternative methods of bleaching have been explored for the textile industries, i.e. enzymatic bleaching using laccase/mediator systems, glucose-oxidases, peroxidases and bleaching with enzymatically in situ generated peracids. But more specific bio-bleaching process is the laccase/mediator system that only target colored substances (Pereira et al., 2005; Spicka and Tavcer, 2013 a,b). Research work involved the application of enzymes for textile bleaching is summarized in Table 3.

4.3.2. Native enzyme applications in bleaching

4.3.2.1. Laccase/mediator systems. Laccases are multi-copper-containing oxidoreductase enzymes capable of oxidizing phenols and aromatic amines, reducing molecular oxygen to water. Laccase in combination with redox mediators are used in textiles. The use of laccases in textile industry is potentially to decolorize dye effluents beside this laccases are also used to bleach textiles, modify fabric surfaces and coloration of cotton (Hadzhiyska et al., 2006; Kim S. et al., 2007; Rodriguez-Couto and Toca-Herrera, 2006). In textile bleaching first time Tzanov et al. (2003b) reported that the short-

Table 2
Research work involved in application of enzymes in scouring.

Research strategy	Enzyme & its source	Research description	Reference	
Industrially viable bio-scouring	Bioprep 3000L, Novozyme (Alkaline Pectinase)	Efficiently remove impurities, uniform dyeing consistency & equivalent color depth with different Direct dyes	Etters, 1999 Etters et al., 2001 Robert, 2002	
	Pectinase (<i>Aspergillus niger</i>) Bioprep 3000L	Agitation improve efficiency & reduce required pectinase concentration Optimized enzymatic scouring provide less damage & superior fabric quality one bath scouring & dyeing is possible save water, energy and time Both acid & alkali pectinases are equally efficient but acid pectinase works with lower concentration	Hartzell-Lawon and Durrant, 2000 Kim et al., 2005, 2006 Mangovska and Jordanov, 2006 Tzanov et al., 2001	
	Bioprep 3000L Pect062L, Biocatalyst (Acid Pectinase)	Optimize enzymatic scouring using ANOVA with acid pectinase	Calafell and Garriga, 2004	
	Acid Pectinase (Commercial Enzyme) Bioprep 3000L	Cotton knits economical scoured and FTIR study confirm 80 °C short rinsing is essential for waxes removal & higher dye uptake Optimize bio-scouring for physical, chemical & low stress mechanical properties	Choe et al., 2004 Kalantzi et al., 2008	
	Acid Pectinase (Commercial Enzyme) Pectate lyase Polygalacturonase	Combined enzyme/ultrasound offer less enzyme, shorter processing time, better treatment uniformity with substantial decrease in effluent toxicity Dyeing behavior of cotton fabric bio-scoured with pectate-lyase and polygalacturonase was examined	Yachmnev et al., 2004 Calafell et al., 2005	
	Pectinase (<i>B.macerans</i> strain V-2692)	Pectinase contain cellulase & hemi-cellulase; less efficiently remove pectin but improve fabric capillary much greater; can substitute cotton boil-off	Morozova et al., 2006	
	Pectinase assisted with other enzymes	Multifect cellulase GC (<i>Trichoderma longibrachiatum</i>) Multifect pectinase PL (<i>Aspergillus niger</i>)	Synergism of cellulase efficiently removes pectin & protein, mechanical agitation and compatible surfactants also play important role	Li and Hardin, 1997 Li and Hardin, 1998 Saravanan et al., 2008
		Celluclast 1.5L (Commercial Cellulase) Viscozyme120L (Pectinase + hemicellulase) Pulpzyme HC (Xylanase) Cellulases, hemicellulase & xylanase (Commercial Enzyme)	Enzyme treatment prior to alkaline scouring along with chelating agent at acidic pH; efficiently lightens the seed-coat fragments to improve whiteness	Csiszar et al., 2001
		Pectinase or lipase/protease & cellulase (Commercial Enzyme) Cutinase ISC-02-BE1	Agitation improves non-cellulosic impurities removal Independently not efficient but in combination provide successful scouring, dye & water absorbency with some fiber damage in presence of cellulase Cutinase able to access outer waxy cuticle layer, lead to good absorbency with pectinase	Csiszar et al., 2001b Traore and Buschle-Diller, 2000; Buchert et al., 2000; Sangwatanaroj et al., 2003; Aiy et al., 2004 Dogani et al., 2002
		Alkali Pectinase & Cellulase (Commercial enzymes) Pectinase (EC 4.2.2.2), Cellulase (EC 3.2.1.4) & Protease (<i>Bacillus</i>) Viscozyme 120L(Pectinase + hemicellulase) Pulpzyme HC (Xylanase)	Enzymatic scouring of knitted fabrics, two-step one bath process effective using combined enzymes Combination with cellulase or protease gives better results of wet-ability, pectin removal, whiteness and dyeing with 60 min treatment time Combination of enzymes efficiently removes pectins and EDTA helps in modification of pectin structure for pectin removal	Anis and Eren, 2002 Karapinar and Sariisik, 2004 Losoncz et al., 2004 Losoncz et al., 2005
Alkaline pectinase (<i>Bacillus</i>) Acidic pectinase (<i>Microorganism</i>) Neutral cellulase (<i>Aspergillus aculeatus</i>) Acidic cellulase (<i>HumicolaTrichoderma</i>)		Alkaline pectinase along with neutral cellulase best in wax removal & high absorbency	Ismal, 2008	
Bioprep 3000L Alkali Pectinase (<i>Bacillus</i> sp.) & Lipolase 100L (<i>T. lanuginosus</i>) Xylanase (<i>Bacillus pumilus</i>)		Combining lipase in one-step reduce time required & fabrics with superior properties and excellent dyeing performance obtained Thermostable xylanase provide simultaneously desizing & scouring, addition of chelating & wetting agent increase hydrolysis, removal of non-cellulosic impurities and allowed reduction of H ₂ O ₂ consumption in consecutive bleaching	Kalantzi et al., 2010 Battani et al., 2012	
Pectinase or lipase/protease, cellulase (Commercial Enzyme)		Bio-scouring using mixture of enzymes was optimized using ANN technique to achieve desired absorbency and pectin removal	Vigneswaran et al., 2013	
Combine scouring with bleaching		Alkali Pectinase	Optimized bio-scouring using alkali pectinase alone in combination with H ₂ O ₂ bleaching and reactive dyeing	Ibrahim et al., 2004a Ibrahim et al., 2005a
		Bioprep 3000L Forylase KP, Cognis (Acidic pectinase)	Single step simultaneous scouring & bleaching using pectinase & PAA sufficiently remove pectin & wax to achieve excellent absorbance with medium degree whiteness without damaging fiber Good dye-ability with less energy & water use in enzymatic and/or PAA treatments because of 60 °C & pH 6-8	Presa and Tavcer, 2008 Presa and Tavcer, 2009; Shafie et al., 2009 Tavcer, 2011

time laccase pre-treatment enhanced the whiteness of cotton fabrics and reduced significantly the hydrogen peroxide dosage in subsequent chemical bleaching. A laccase from a newly isolated strain of *T. hirsuta* was responsible for whiteness improvement of cotton most likely due to oxidation of flavonoids (Pereira et al., 2005).

Further the assistance of ultrasound technology enhances bleaching efficiency with a combination of laccase and hydrogen peroxide at mild conditions of pH-5 & 60° C for 30 min. The ultrasound provides the additional effect of de-aggregation of enzyme molecules, which could increase enzyme activity and leads to further enhancement in the diffusion of enzyme (Abou-Okeil et al., 2010; Basto et al., 2007). A 2–3 g/l peroxide combine with 2% laccase in single bath is sufficient to conventional bleaching with and causes less fiber damage with greater uniformity (Abou-Okeil et al., 2010).

4.3.2.2. Glucose-oxidase bleaching. Glucose oxidase has been considered as a possible method for producing H₂O₂ for bio-bleaching. Glucose-oxidase is a dimeric glycosylated flavoprotein – which is able to catalyze oxidation of glucose to gluconolactone, which in turn spontaneously yields gluconic acid, as well as H₂O₂ as a side product. The implementation of this enzymatic system in cotton pretreatment is also beneficial because reusing of desizing waste baths as glucose source is possible and decreases the waste water pollution and water consumption. Combined one bath desizing & bleaching or bleaching using reused desize bath was studied by many researchers (Anis et al., 2009; Buschle-Diller et al., 2001; Hebeish et al., 2013; Li and Hinks, 2012; Tzanov et al., 2002).

Generation of peroxide with glucose oxidase requires slightly acidic to neutral conditions at low temperatures while the bleaching effect of H₂O₂ under these conditions is insignificant. A high temperature 80°–90 °C & alkaline pH –11 for bleaching provide efficient results (Anis et al., 2009; Farooq et al., 2013; Ramadan, 2008; Tzanov et al., 2001) and the assistance of ultrasound energy also improve fabric whiteness due to increased enzyme reaction (Davulcu et al., 2014). While to enable bleaching with enzymatically produced H₂O₂ at low temperature in neutral media researcher also tried to transform H₂O₂ into more reactive peracids using peracid precursors which generate peracids in situ in an alkaline hydrogen peroxide solution. Tetraacetythylenediamine (TAED), nonanoyloxybenzene sulphonate (NOBS), N-[4- (triethylammoniummethyl) benzoyl] caprolactam chloride (TBCC) and various peroxidases are some bleach activators. The in-situ formation of peracid provides a potentially more efficient bleaching system at mild conditions 60 °C and pH 7–8. The formation of peracid depends on pH & temperature of bath, concentrations of peroxide & activator and type of activator in bleaching bath (Hebeish et al., 2013; Krizman et al., 2005; Li and Hinks, 2012; Opwis et al., 2004, 2008; Tavcer, 2012).

Complete one bath enzymatic pretreatment (Anis et al., 2009; Spicka and Tavcer, 2013b; Usluoglu and Arabaci, 2014, 2015) and integrated desizing-bleaching-reactive dyeing of starch-sized cotton fabric was also studied using glucose-oxidase enzymes (Ali et al., 2014; Eren et al., 2009).

4.3.2.3. Arylesterase bio-bleaching. A bio-bleaching system with arylesterases and hydrogen peroxide is also investigated and patented (Auterinen et al., 2011) which in situ generate peracetic acid and propylene glycol as bleaching agents. A commercial bio-bleaching system based on arylesterase is available from HUNTS-MAN for bleaching purpose. Researcher tried to efficiently combine bio-bleaching & bio-scouring in one bath and obtain a high degree of whiteness, good absorbency with high tenacity at mild process conditions of neutral pH and 65 °C temperature (Spicka and Tavcer,

2013a; Siddiquee et al., 2014). Combined laccase and glucose-oxidase can significantly remove lignin and effective for linen bleaching than either of the enzyme applied alone (Ren and Buschle-Diller, 2007).

4.3.3. Immobilized enzyme applications in bleaching

4.3.3.1. Immobilized laccase. Applied aspects of immobilized laccases, using a wide range of methods and substrates, have been described (Duran et al., 2002; Peralta-Zamora et al., 2003). Specifically in textiles, immobilized laccases are only involved in the decolorization of dyeing effluents. Most laccases that are efficient in decolorization are produced by white-rot fungi. Although studies have been performed with immobilized laccase at laboratory-scale with small volumes these have not addressed the large wastewater volumes generated by the textile industry (Soares et al., 2011).

4.3.3.2. Immobilized glucose-oxidase. As reported by Tzanov et al. (2001), higher quantities of enzymatically-produced peroxide were needed to accomplish the same bleaching effect as in the conventional. Probably, the added glucose acts as substrate for bleaching and oxidation, thereby consuming the peroxide, or protects the cotton from being bleached. Also increasing the bleaching temperature causes the protein to denature and deposit on the fabric surface, due to hydrophobic fabric/enzyme interactions. These problems could be overcome by using immobilized instead of native enzyme. Many researchers reported that the stability of glucose-oxidase improved via immobilization procedures on various supports (Tzanov et al., 2002).

The first textile application was reported by Opwis et al. (1999), with cyanuric chloride-mediated attachment to cotton – with subsequent release of H₂O₂ at levels, high enough to support adequate bleaching. In other research glucose-oxidase covalently immobilized on two inexpensive and commercially available supports, viz. alumina and glass. High protein immobilization yields, as well as sufficient bleaching levels were attained. Glass permitted a higher rate of generation of H₂O₂ (0.35 g/l) due to its more porous morphology and thus bound more protein; however, alumina produced a higher operational stability and permitted reuse for at least three consecutive cycles (Tzanov et al., 2002).

4.4. Bio-polishing

Bio-polishing is the process of elimination of micro, fuzzy fibrils from the fabric surfaces through the action of cellulase enzyme. It improve appearance, color brightness, hand feel, water absorbance property of fibers, strongly reduce the tendency for pill formation, and provide a cleaner surface structure with less fuzz.

4.4.1. Concept of bio-polishing

Cellulases are widely used for bio-polishing; basically cellulases constitute a group of enzymes that catalyze the hydrolysis of cellulose via degrading β-(1–4) glycosidic linkages. In nature, cellulolytic systems belong to three major classes, which are generally used in a synergistic fashion: endoglucanases or endocellulases cleave bonds along the length of cellulose chains in the middle of the amorphous region, exoglucanases or cellobiohydrolases act from the crystalline ends of cellulose chains, producing primarily cellobiose and β-glucosidases finally convert these produced cellobiose and soluble oligosaccharides to glucose. Commercially available cellulases for bio-polishing are a mixture of endoglucanases, exoglucanases & cellobiases which has the capability to modify cellulosic fibers in a controlled and desired manner (Cavaco-Paulo, 1998). A lot research work has been reported for such applications of cellulases in textiles, summarized in Table 4.

Table 3
Research work involved in application of enzymes in textile bleaching.

Research strategy	Enzyme & its source	Research description	Reference
Laccase-mediator system	Laccase	Combined laccase/peroxide bleaching either in batch & pad-dry application	Tzanov et al., 2003a,b
	Laccase (<i>Trametes hirsute</i>)	Laccase/mediator improve whiteness of cotton due to oxidation of flavonoids	Pereira et al., 2005
	Complex enzyme Laccase & Peroxidase (<i>Ph Chrysosporium</i> & <i>Trichosporon cutaneum</i> R57)	Efficiently degrade & remove lignin from flax fiber to provide whiteness	Beteheva et al., 2007
	Laccase, Novozyme (<i>Trametes villosa</i>)	Ultrasound assistance with PVA addition stabilize laccase & improve bleaching	Basto et al., 2007
Glucose-oxidase bleaching	Ecolite II (Commercial Laccase, Jeans care company)	Laccase-H ₂ O ₂ /ultrasound assisted bleaching of linen allows better dye uptake for both reactive and cationic dyes	Abou-Okeil et al., 2010
	Glucose-Oxidase	Reused desize bath to enzymatically produce peroxide for bleaching done at elevated temperature & high pH	Tzanov et al., 2001 Shin et al., 2004
	Glucose-Oxidase	Combined glucose, glucose-oxidase & peroxidase for cotton bleaching	Opwis et al., 2008
	Glucose-Oxidase (Commercial Novo Nordisk-Denmark)	Optimized bio-bleaching of cotton, linen and their blends with 25 U/ml GOE, 10 g/l D-glucose, at 85 °C & pH 10 for 90 min	Ramadan, 2008
	Glucose-Oxidase (<i>Aspergillus niger</i>) (Biozyme)	Amyloglucosidase/pullanase mixture used for sufficient (800 mg/l) H ₂ O ₂ for bleaching and maximum whiteness obtained in alkaline pH compared to neutral and acidic	Aris et al., 2009
	Glucose-Oxidase (<i>Aspergillus niger</i>)	External oxygen supply and mechanical agitation essential for H ₂ O ₂ generation Cotton bleached at room temperature & acidic pH with high enzyme concentration	Saravanan et al., 2010
	Glucose-Oxidase	6% increase in whiteness index with comparable mechanical properties using peroxide produced by glucose-oxidase	Farooq et al., 2013
	Glucose-Oxidase	Complete one bath low temperature cotton pretreatment where liberated H ₂ O ₂ converted to peracetic acid using TAED as activator	Tavcer, 2012; Spicka and Tavcer, 2013b
Complete one bath pretreatment	Glucose-Oxidase GC 199	Combined desizing, scouring with enzymes followed by bleaching with in-situ generated peracetic acid using different activators	Car et al., 2001; Li and Hinko, 2012; Hebeish et al., 2013
	Glucose-Oxidase	Assistance of ultrasound improves whiteness due to increase enzyme reaction at 90°C with pH-11	Davulcu et al., 2014
	Amyloglucosidase/pullanase (Dextrozyme DX, Novozyme)	One bath desize, bleach and reactive dyeing of starch sized cotton fabric was performed using enzymes	Eren et al., 2009 Ali et al., 2014
	Glucose-oxidase (Multifect GO 5000L, Gencor)	Similar integrated desizing-bleaching-reactive dyeing of cotton towel was performed	
Arylesterase	Catalase (Terminox Ultra 10 L)	Optimized low temperature (60 °C for 45 min) bio-bleaching for cotton/polyamide based on PAA or TAED with Sodium Perborate or H ₂ O ₂ and enzyme either lipase, protease, cellulase or pectinase shows excellent wettability and acceptable whiteness index	Usluoglu and Arabaci, 2014 Usluoglu and Arabaci, 2015
	Scourzym L		
	Lipolase 100 T		
Immobilized glucose-oxidase	Novacell BL Conc	Arylesterases and H ₂ O ₂ in situ generate peracetic acid for mild temperature 65 °C, neutral bleaching of cotton. One step bio-scouring and bio-bleaching provide high degree whiteness	Spicka and Tavcer, 2013a; Siddiquee et al., 2014
	Kimastone L H(Commercial Enzymes)		
Immobilized glucose-oxidase	Glucose-oxidase	Cheap carrier material cotton employed for glucose-oxidase immobilization; Transfer starch-desizing liquor to bleaching liquor (release H ₂ O ₂)	Opwis et al., 1999
	Glucose-oxidase (<i>Aspergillus niger</i>)	Immobilized on porous carriers - glass & alumina, low enzyme concentration provide sufficient H ₂ O ₂ release which further activated for textile bleaching	Tzanov et al., 2002

4.4.2. Native cellulase application

Firstly bio-polishing was introduced as permanent method to reduce pilling and improve softness of cellulose (Wadham, 1994). Selections of type of cellulase enzyme and process conditions are very important for bio-polishing. Various researchers optimized the bio-polishing using different commercial cellulases on varieties of cellulosic material and the optimized enzyme concentration and conditions vary from research to research. The acid cellulases enriched with endoglucanase are suited for bio-polishing of cellulose. (Bahtiyari and Duran, 2010; Bai et al., 2012; Kumar et al., 1997; Liu et al., 2000; Mojsov, 2014a; Saravanan et al., 2013; Sarkar and Eters, 2001; Schimper et al., 2006; Sreenath et al., 1996; Uddin, 2010).

Mechanical action improves the enzymatic hydrolysis of cotton while the addition of surfactant has on significant effect (Esfandiari

et al., 2014; Traore and Buschle-Diller, 1999). Bio-polishing either done before or after dyeing to the cotton fabrics influence dyeability, besides improving the appearance and handle values with various dye classes. The extent of bio-polishing is governed by the cellulose substrate, type & activity of cellulases, while dyeability and fastness of resulted bio-finished fabric depend on nature and class of dye (Ibrahim et al., 1999, 2000; Saravanan et al., 2009; Uddin, 2016). The effect of bio-polishing treatment on performance of pre or post easy care finishing treatment also has been studied by many researchers. Cellulase treatment enhances the post dyeing and resin finishing with increased softness (Ibrahim et al., 2005b; Hebeish et al., 2009). Azevedo et al. (2002) studied the desorption of cellulases from cotton using ultra-filtration for recovering and recycling of cellulases after treatment, about 62% was recovered. Bio-polishing of polyester/cotton blended textiles

was studied & optimized using cellulase (Noreen et al., 2014) & cutinase combined with cellulase (McCloskey and Jump, 2005). A novel approach of pad batch cellulase application with non-ionic wetting agent was optimized by Ibrahim et al., 2011 for smoother, clear & softer surface and improved dye-ability with minimum strength loss. Similarly the bio-treatment of cotton/wool and viscose/wool blended fabrics using cellulase and or protease, improve dye-ability with resilience and softness (Ibrahim et al., 2008).

Cellulases are also increasingly used in detergents, since they enhance their performance and improve appearance, color brightness, hand feel and dirt removal from cotton and cotton blended garments. The endoglucanase rich alkali stable cellulases are incorporated in detergent formulations, for effective stain removal and to restore brightness of colored cotton fabrics (Azevedo et al., 2002; Hossain and Uddin, 2011; Mojsov et al., 2014b; Tzanov et al., 2001).

4.4.3. Immobilized cellulase application

Since the free cellulase can easily move beyond the peripheral cellulose structure of cotton and hence associates with significant weight & strength loss which is not the objective of bio-polishing. So the immobilization i.e the attachment of cellulase to some

carrier can restrict its action to fiber surface. Various methods and supports have been reported till date for immobilization of cellulases for different purposes which improve thermal stability and reusability (Darias and Villalonga, 2001; Dourado et al., 2002; Feng et al., 2005; Hirsh et al., 2010; Jabasingh and Nachiyar, 2011; Podrepsek et al., 2012; Romo-Sanchez et al., 2014; Viet et al., 2013; Yin et al., 2013).

Specifically for textile applications Dincer and Telefoncu (2007) improved the stability of an acidic cellulase in the neutral pH range by immobilizing it on chitosan beads coated with maleic anhydride-modified polyvinyl alcohol. Acid cellulases are more popular from cost perspective and being more aggressive compared to neutral cellulases. But their application for bio-polishing or denim fading, produce more abrasion that reduces the tensile strength of the cotton fabric.

Similarly the commercial cellulase was immobilized on ion exchange and epoxy resin carriers using methanol, to conserve the cellulase after bio-polishing. Epoxy resin shows greater amount of cellulase immobilization compared to ion exchange resin. The bio-polishing effect on cotton fabric with immobilized cellulase was good for six successive cycles with a less weight & strength loss compared to free enzyme (Kumar et al., 2008). Eudragit L-100 a soluble – insoluble reversible polymer was successfully used for

Table 4
Research summary of enzyme application in bio-polishing.

Research strategy	Enzyme & its source	Research description	Reference
Commercial cellulases application	Cellulase (Denimax L) & Pectinase (Pectinex USP) Novo Nordisk V1-4 Xylanase (<i>Bacillus sp.</i>)	Optimized bio-polishing of jute/cotton blended fabrics; addition of pectinase and xylanase more efficient in fuzz removal	Sreenath et al., 1996
	Cellulase, Endo-enriched cellulase, Exo- endo mixed cellulase (Commercial Cellulases)	Whole cellulase best suited for cotton and lyocell fabric and endo-enriched suited for delicate cotton knits, linen and rayon	Kumar et al., 1997
	Cellusoft Ultra L (Acid endoglucanase) SP908 (Endo-enriched cellulase)	Optimized the process conditions for bio-polishing with commercial cellulases	Liu et al., 2000
	Cellusoft L (Traditional acid cellulase) Ecoston L 883042	Studied the desorption of cellulases from cotton using ultra-filtration for recovering and recycling, about 62% was recovered	Azevedo et al., 2002
	Denimax L (Commercial Cellulase)	Ring spun colored knitted fabrics were bio-polished for pill & fuzz removal	Ozdil et al., 2003
	G-ZYME-VGB ST (Rossari) (Commercial Cellulase)	Reported the action of cellulases on reactive dyed cotton, which have an inhibitory effect on cellulase activity	Yamada et al., 2005
	Acid Cellulase Genencor, USA	Effect of bio-polishing with cellulase on various spun yarn knitted fabrics was studied in terms of smoothness and color difference	Chinta et al., 2012
	Acid Cellulase (<i>Talaromyces emersonii</i>)	Influence of parameters of enzymatic hydrolysis on viscose, lyocell, modal & cotton fabrics was examined in terms of degradation rate and weight loss	Schimper et al., 2006
	Biopolish EC (Commercial Cellulase)	Thermo stable cellulase obtained & applied for jute-based fabrics finishing to exhibit improved lusture, handle and durable softness	Gomes et al., 2007
	Combine bio-polishing with other process	Commercial (Modified, Conventional, Endo-enriched & Concentrated acid cellulases and Neutral cellulase)	Combined scouring-bleaching followed by cellulase treatment was optimized for knit fabrics
Cellulase (<i>Trichoderma Vrde G</i>)		Six commercial cellulases employed for viscose bio-polishing in different concentrations and treatment time to statistically optimize strength loss with sufficient pilling and fuzz removal; morphological study was done by FTIR	Bahtiyari and Duran, 2010
Indiage RFW Endo rich Cellulase		Optimized cotton fabric bio-polishing to improve its smoothness with minimum weight loss	Bai et al., 2012
Indiage 44L (Gencor) Complex mixed Cellulase		Bio-scouring followed by bleaching either peroxide or per-acetic acid is efficient for towels and endoglucanase is effective instead of cellulase as additive in washing agent for terry-towel washing.	Tavoer, 2013
Cellulase (<i>Trichoderma reesei</i>)		Bio-polishing & its effect on the morphology of cotton fibers was studied with weight loss, X-ray diffraction & FTIR investigation	Saravanan et al., 2013
Commercial enzymes		A commercial & environment friendly process developed by optimizing combined desizing and bio-polishing for cotton fabrics	Esfandiari et al., 2014
Ezysoft super (Commercial Cellulase)		Comparative evaluation of cotton bio-polishing was studied w.r.t singeing in terms of breaking strength, weight loss, thickness, drape and abrasion resistance	Chinnamma and Antony, 2015
Cellulase (<i>Aspergillus niger</i>)		Immobilized on maleic anhydride modified PVA coated chitosan beads to improve stability of acidic cellulase in neutral pH range for textile applications	Dincer and Telefoncu, 2007
Biowash L (Commercial cellulase, Biocon Ltd)		Optimize the immobilization on Ceralite IRC50 & Feramer resin beads and compared the bio-polishing of cotton fabric in terms of physico-mechanical properties & reusability	Kumar et al., 2008

cellulase immobilization in many literature and could be an best alternative to apply in bio-polishing and/or bio-scouring (Dourado et al., 2002; Gozan et al., 2011; Zhang et al., 2012; Zhou, 2010).

4.5. Denim finishing/washing

Denims are very popular cotton casuals due to their special faded & aged look. Traditionally, denim garments are washed with pumice stones to achieve desirable look and increase softness & flexibility. However, the use of natural pumice stones has many unavoidable disadvantages; difficulty in removing residual pumice from processed garments, overload of stones can cause severe physical damage to garments & machines and stones dust can also clog the machine drainage passage and sewer lines (Pazarlioglu et al., 2005; Yu et al., 2013).

4.5.1. Concept of denim fading using cellulase

Cellulase enzyme cause non-homogeneous surface removal of indigo dye trapped inside the fibers creating a fading & worn look. The application of cellulases in textile processing started in the late 1980s with denim finishing. Nowadays, bio-washing with cellulase enzyme is an environment friendly alternative to achieve desirable appearance and superior quality.

4.5.2. Application of native cellulase in denim fading

There are number of cellulases with their own special properties are available to be used either alone or in combination to obtain a specific look. Cellulases are active in a wide temperature range from 30° to 60° C and based upon their application pH are classified as acid (pH 4.5–5.5), neutral (pH 6.6–7) or alkali (pH 9–10) cellulase (Araujo et al., 2008; Bhat, 2000; Sarkar and Etters, 2001).

The back-staining i.e the re-deposition of released indigo back onto the white portion of denim garments is the major problem and an ideal bio-washing would posses high abrasion with low back-staining. The high affinity between indigo and cellulase enzyme and the strong binding of cellulases to cotton cellulose is the major cause of back-staining. The authors also reported that acid cellulases have a higher affinity for indigo than neutral cellulases. Therefore, neutral and endoglucanase rich cellulase preferably suits for softening and indigo dye removal from denims. (Araujo et al., 2008; Mojsov, 2014b). The research associated in denim finishing was mainly concern on low back-staining, shown in Table 5.

Laccase can also be used for denim bleaching as an eco-friendly alternative to conventional chemical denim fading process. Various commercial solid laccase formulations are also available in market for textile wet processing (Rodríguez-Couto, 2012).

4.5.3. Immobilized cellulase for denim fading

A commercial cellulase immobilized was onto $ZrOCl_2$ activated (pumice) particles for denim washing. The immobilized enzymes could efficiently abrade indigo-dyed denim fabrics, and because strongly bound enzymes remained on the pumice, staining was detected at lower levels after the second usage with immobilized cellulase than its native counterpart (Pazarlioglu et al., 2005).

In other study investigations were made with the enzymatic treatment of the denim fabric using native and cellulase immobilized on Eudragit S-100. Covalent Eudragit–cellulase, immobilized enzyme can efficiently remove indigo dyestuffs on the surfaces of the denim fabrics without severe damage to the mechanical properties. Therefore, the immobilized cellulase has great potential in the bio-washing of denim fabrics (Yu et al., 2013).

5. Some other potential applications of enzymes in textile processing

5.1. Anti-shrinkable wool

Application of proteases for wool shrink-resistance simultaneously improve whiteness, dye-ability and handle are well recognized (Cardamone, 2002; El-sayed et al., 2002; Ibrahim et al., 2012). However, enzymatic treatment causes excessive damage to the fiber cuticle, with a consequent high degree of weight and strength losses to the wool fibers (Ge, 2009; Nolte et al., 1996; Ibrahim et al., 2012; Silva et al., 2006a,b; Vilchez et al., 2010). Transglutaminase recovers the wool and silk damages during various chemical or enzymatic treatments at different stages of processing. In addition, transglutaminase allows the grafting of amines or proteins to bring desired properties in wool fibers, studied by various researchers (Cardamone, 2007; Ge, 2009; Tesfaw and Assefa, 2014). Alternatively the immobilization of proteases typically increases their molecular size, the modified protease remained on the surface of cuticle layer region (hydrolyzing just the cuticle layer of wool), hence producing a higher tensile strength and an optimum felting of the fibers (Araujo et al., 2009; Schroeder et al., 2004).

A commercial protease (Esperase) covalently linked to Eudragit S-100 for wool shrink-resist finishing, replacing the conventional chlorine treatments. The dyeing properties of the wool fabric appeared to be unaffected with improved shrink-resistance, but with less fiber damage in terms of weight loss and tensile strength (Silva et al., 2006a,b; Shen et al., 2007).

Vasconcelos et al. (2006) also studied the stability of Esperase, immobilized on Eudragit S 100 in different detergent formulations. The immobilized Esperase was more stable than their counterpart native enzyme and efficient in removing human blood and egg yolk stains from cotton and wool fabric samples. Therefore, they can be used as a detergent additive to improve their washing performance.

Further, trypsin from bovine pancreas was covalently immobilized on sterilized cotton gauge bandages using sodium periodate for use as an anti-inflammatory agent on wound dressing. Immobilized trypsin show increased operational & storage stability with no trypsin liberated after 30 days (Sebra and Gil, 2007).

5.2. Bleach clean-up

Catalases are enzymes, which catalyze the breakdown of H_2O_2 into water and oxygen and considered as the most suitable alternative for bleach bath clean-up before reactive dyeing (Amorim et al., 2002; Gudelj et al., 2001). Catalase immobilization has been attempted by several authors using organic and inorganic materials such as porous glass, cellulose, alumina, silica gel and hydrogels. Some natural polymers – e.g. gelatin and chitosan, as well as some synthetic polymers – e.g. polyacrylamide, were found not to be appropriate for bleaching treatments. While Opwis et al. (2004, 2005, 2014) used low-cost synthetic textile fabrics as alternative carrier materials for covalent catalase immobilization by a photochemical process (UV light). The great advantage of using fabrics as carriers is that they can be removed very quickly without filtration and without protein residues.

Alumina-based supports are also suitable for catalase immobilization due to their greater mechanical stability at high pH and temperatures. Immobilized catalase (*Bacillus SF*) treated bleached bath was reused for dyeing fabrics with various dyes, resulting in acceptable color differences for all the dyes used (Costa et al., 2001). A commercial catalase (Terminox Ultra 50L) was also covalently immobilized on alumina with gultraldehyde for the recycling of textile bleaching effluents for dyeing purpose (Costa et al., 2002).

5.3. Synthetic fiber modification

Potentially a great variety of enzymes can be employed to modify the synthetic fibers. Enzymatic hydrolysis improves hydrophilicity along with some undesired properties such as weaving comfort, tendency to pilling, low dyeability, difficulties in finishing and antistatic charge generation. Enzymes are also used for the synthesis, surface functionalization and grafting of polymers that are used as textile fibers discussed in section 5.4 & 5.5.

Cutinases, lipases and esterases are the hydrolases class of enzymes suitable for polyester modification. Esterases were believed to have less potential for surface hydrolysis of polyesters than cutinases or lipases. A new esterase from *Thermobifida halotolerans* has potential for both PET and PLA surface hydrolysis, similar to cutinases (Ribitsch et al., 2012). Among cutinases, representatives from *Aspergillus oryzae*, *Humicola insolens*, *Penicillium citrinum*, *Fusarium solani*, *Thermobifida fusca*, *Thermobifida cellulolytica* and *F. oxysporum* have been described to hydrolyze polyester (Gubitz and Cavaco-Paulo, 2003; Kaneli et al., 2015; Silva and Cavaco-Paulo, 2008; Vertommen et al., 2005). Fewer lipases including from *Humicola sp.*, *Candida antarctica*, *Thermomyces lanuginosus*, *Burkholderia spp.*, *Triticum aestivum*, and *Rhizopus delemar* considered suitable (Gubitz and Cavaco-Paulo, 2003; Waslter et al., 1995). Mixture of lipase & cutinase can also be effective for this purpose (Lee and Song, 2010). Lipase treated digital printed polyester fabric shows improved color fastness of disperse inks (Ibrahim and Abd El-Salam, 2012). Oxidative enzymes such as laccases have also been shown to hydrophilize the PET without cleavage of the polymer (Miettinen-Oinonen et al., 2002).

Proteases, amidases, cutinase and peroxidases can modify polyamides. Laccases in combination with a mediator have been shown to increase the hydrophilicity of Nylon 66 fabrics (Miettinen-Oinonen et al., 2002; Silva and Cavaco-Paulo, 2008). Protease from *Beauveria Sp.*, an amidase from *Nocardia sp.* and a cutinase from *F. solani pisi* treated Nylon 66 fabrics shows improved dye bath exhaustion with reactive and acid dyes (Parvinzadeh et al., 2009). In another study it was confirmed that acid and disperse dyes showed higher exhaustion on the protease (Parvinzadeh, 2009) & lipase (Kiumarsi and Parvinzadeh, 2010) treated Nylon 6. Recent studies demonstrate that protease from a novel *Bacillus isolate* improve hydrophilicity (Begum et al., 2016), and cationic dye affinity of nylon fabric without affecting the mechanical properties (El-Bendary et al., 2012). In another work protease and lipase mixtures decreased the sample weight and the concentration of lipase enzyme had a direct influence on the darkness of dyed samples (Parvinzadeh et al., 2013). The effect of protease treatment on morphological structure, wettability and dyeability of wool/nylon blended fabric was also studied recently (Parvinzadeh, 2007; Waly et al., 2016).

Enzymatic hydrolysis of nitrile groups of polyacrylonitrile to the corresponding acids or amides by nitrilases or by an enzyme system comprising nitrile hydratase and amidase, respectively resulting in major increases in hydrophobicity. The vinyl acetate moieties in PAN can be hydrolyzed by cutinases and lipases, making this approach also applicable (Gashti et al., 2011; Gubitz and Cavaco-Paulo, 2003; Silva and Cavaco-Paulo, 2008).

5.4. Biological polymer synthesis & functionalization

Biocatalytic approach to synthesize and functionalize the polymer materials is an emerging research area with enormous scientific and technological promises. There are several potential advantages for the use of enzymes in polymer synthesis or functionalization. As the toxicity created by solvents and metal catalyst residues can be completely avoided, the enzymes specificity may

offer the potential for precisely modify polymer structure for a better control of polymer function (Gubitz and Cavaco-Paulo, 2003; Sen and Puskas, 2015; Miletic et al., 2012).

A lot research has been reviewed that give a good introduction to the field of enzymatic polymerizations. Various studies on the enzymatic synthesis of polyesters, polyamides, polycarbonates, polysaccharides, polypeptides, polyanilines, polyphenols, polystyrene, polymethyl methacrylate (Miletic et al., 2012), and cellulose (Kim S.Y. et al., 2007), chitosan (Aljawish et al., 2015) modification have been performed and some have been implemented on an industrial scale.

Hydrolases are the most explored enzymes for the in vitro polymer synthesis. This class includes lipases, which are used for fatty ester hydrolysis, glycosidases, used in polysaccharides synthesis and protease, which can be used for peptide bond formation. Cellulase, chitinase and xylanase also have immense potential in modification of natural polymers (Gubitz and Cavaco-Paulo, 2003). Lipases are widely used in polycondensation, and polytransesterification reactions, ring-opening polymerizations, and polymer modifications reactions. Particularly in the synthesis of polyester and polyamides, lipases are the most used enzymes as catalysts for their polymerization (Sen and Puskas, 2015; Stavila and Loos, 2015).

In addition to hydrolase, oxidoreductase enzymes, including peroxidase and laccase have been investigated for their ability to catalyze important polymerization reactions. Among the various radical-forming enzyme systems horseradish peroxidase (HRP) has been employed for the polymerization of vinyl monomers, such as styrene and acrylamides. Other catalysts such as soybean peroxidase, manganese peroxidase and laccases have been used to a lesser extent. Peroxidases and laccases are also able to catalyze monomer activation of phenol and aniline derivatives to produce novel polyaromatics and polyanilines (Geus, 2007; Miletic et al., 2012; Peng et al., 2009). The use of HRP as a catalyst for the synthesis of water-soluble, conducting poly (N-methylaniline) (PNMA), poly (N-ethylaniline) (PNEA), poly (N-butylaniline) (PNBA) and poly(N-phenylethanolamine) (PNPEA) are reported in Nabib and Entezami (2005) and soybean peroxidase (SBP) can catalyze the polymerization of phenols in room-temperature ionic liquids (Eker et al., 2009).

Various derivatives of chitosan can be synthesized exhibiting improved properties to enlarge the field of industrial applications. Oxidative enzymes such as polyphenol oxidases (tyrosinases, laccases) and peroxidases essentially carried out the functionalization of chitosan while other enzymes such as lipases, phosphorylases, transglutaminases confine reactions to the active site and minimize the undesired byproducts (Aljawish et al., 2015). Recently enzyme catalyzed ring open polymerization of cyclic esters in ionic liquids has been proposed as green alternative for preparation of biodegradable or bioresorbable polymers (Piotrowska and Marcin Sobczak, 2015) and enzymatic polymerization was applied to prepare functional water soluble polyesters based on dimethyl itaconate and polyethyleneglycol (Daugaard et al., 2016).

Immobilization of biocatalysts for enzymatic polymerization has a great potential; its advantages and the most important immobilization routes relevant to the field of enzymatic polymerization are reviewed in Miletic et al., 2012. Among the enzymes used successfully for polymer synthesis, *Candida antarctica* lipase B (CALB) is by far the most well-known enzyme in literature. The fundamental of enzyme mediated polymer functionalization using CALB has been explored in Sen & Puskas et al. In most reported enzymatic polymerizations it is used as an immobilized enzyme (Gokalp et al., 2016). CALB is commercially available in physically immobilized form within a macroporous resin of polymethyl methacrylate as Novozym 435. In other work graphite immobilized glucose-

Table 5
Research summary on Denim finishing using Cellulase.

Research strategy	Enzyme & its source	Research description	Reference
Industrial-viable cellulase	Endoglucanase II (<i>Trichoderma reesei</i>)	effective in removing color from denim, producing a good stonewashing effect with lowest hydrolysis level	Heikinheimo et al., 2000
	Alkali Cellulase (<i>Alkalothermophilic Thermomonospora sp.</i>)	First time alkali stable endoglucanase used for bio-polishing denims, provide abrasive effect & softness with lower backstaining & negligible weight loss	Anish et al., 2007
	Cellulases (<i>Hypocrea jecorina</i>)	Additives like nonionic surfactant & dispersing agents provide double benefits of reduction in back staining an increased cellulase activity	Zilz et al., 2012
Assistance with other enzymes	Hi-CONS (Amylase) Denimax XT (Neutral Cellulase) Denimax 992 L (Acidic Cellulase) Denilite IT (Laccase)	Lower back staining with efficient desizing and improved color fading effect observed in one step	Maryan and Montazer, 2013
Immobilized cellulase	Rogylar A (Acid cellulase)	Prevent back staining & efficient fading	Pazarlioglu et al., 2005
	Immobilized on ZrOCl ₂ activated pumice	Efficiently remove indigo from denims surface with minimum hydrolysis & possibility of cellulase reuse	Yu et al., 2013
	Suhong 989 (Acid cellulase)		
	Immobilized on Eudragit S-100		

oxidase was proposed as suitable catalyst for the oxidative polymerization of polythiophene under ambient conditions at neutral pH (Krikstolaityte et al., 2014).

5.5. Utilization of immobilized enzymes for textile functionalization

A few naturally occurring enzymes have lately been identified for their potential to be used as biological protective finishes. Hydrolase enzymes that confer antimicrobial activity also provide a potential barrier to microbial invasion through hydrolysis of cell wall polysaccharides. Lysozyme is one such & its activity against many pathogenic bacteria has been well documented and its immobilization on textiles was used to create smart material with novel properties such as self detoxifying or anti-microbial property (Shen, 2010; Paul and Genesca, 2013). Similarly the attachment of alkaline pectinase, alpha amylase or laccase on textiles lead to antimicrobial fabrics retaining full activity for at least ten consecutive wash cycles (Ibrahim et al., 2007).

Lysozyme was covalently immobilized on cotton fabrics via carbodiimide reaction using glycine or glycine dipeptide as spacer and its antimicrobial activity was proved against *Bacillus Subtilis* (Edwards et al., 2000). Cotton based wound dressing were functionalized by immobilization of various biomolecules. Lysozyme was found to have robust antimicrobial activity when conjugate to cotton and also explored the fabrics related to wound healing and neurotoxin neutralization related to decontamination (Edwards and Goheen, 2006). Immobilization of lysozyme was also performed with both carbodiimidazole and glutaraldehyde and the durability of antimicrobial activity was compared against *M. lysodeikticus* (Paul and Genesca, 2013).

Edwards et al. (2011a) also reported the attachment of lysozyme to glycine derivatized different cotton fabrics (non-woven & woven) and estimate their antimicrobial activity against *M. lysodeikticus* for potential applications in apparels, protective barrier fabrics and non-woven wipes. In another work the activity of covalently immobilized lysozyme was compared for two differently activated cotton fabrics. Linking lysozyme via carbodiimide coupling on citrate cross-linked cotton gave higher yield and activity than on aminosilanized cotton (Edwards et al., 2011b). In recent approach lysozyme was activated and covalently immobilized to glycine esterified cotton cellulose dissolved in ionic liquid solvent and lysozyme coupled cellulose fiber and film was directly regenerated using dry-wet spinning method. But no retention of lysozyme activity was observed for *M. lysodeikticus* in 6 h due to enzyme inactivation (Chen et al., 2014).

Wool based antibacterial fabrics have been produced by immobilization lysozyme using glutaraldehyde (Hu-On et al., 2008;

Wang et al., 2009) and microbial transglutaminase (Huang et al., 2009a,b) as cross-linkers. Covalently bound lysozyme was reasonably durable and the fabric shows retained activity over number of washing cycles (Shah and Halacheva, 2015). Wool fabric immobilized with lactoferin using microbial transglutaminase as biological cross-linker shows increased antibacterial properties against *S.aureus* and *E.coli* compared to native lactoferin (Han et al., 2014). This enzymatic method of wool activation provides an environment friendly antimicrobial finishing treatment (Han et al., 2014; Huang et al., 2009a,b).

Peroxidase and laccase mediated coupling of functional molecules on textiles improve technical properties. Use of laccase for grafting water insoluble phenolic compound lauryl gallate on wool for antioxidant, antibacterial and water repellent properties. Grafting of NDGA on wool using laccase develop multifunctional textiles with improved shrink resistance, tensile strength and UV protection. Similarly flame retardant properties can be imparted on natural textiles by enzymatic phosphorylation using kinases and in-situ generation of phenolic resins can be achieved by using laccase (Paul and Genesca, 2013; Wehrschutz-Sigl et al., 2010).

6. New prospects in enzyme applications

More research can be oriented towards some of the less explored areas of enzyme applications like immobilization of enzymes can be promising for synthetic fiber modification to restrict hydrolysis action on surface like bio-polishing, denim-fading and wool anti-shrinkage. Also the immobilized enzymes have great potential in textile effluent discoloration (Khan et al., 2013; Rauf and Ashraf, 2012).

Laccase can also assist the coloration of cotton textiles in many ways. The laccase assisted in-situ enzymatic coupling of dye precursors to polymeric dye, which remain fixed in fiber for cotton and protein fibers has been reported (Hadzhiyska et al., 2006). The cellulosic fibers can be colorized with in-situ formation of colored pigments on to cotton fabrics by the oxidation of flavonoids with laccase enzyme (Kim S. et al., 2007; Rodriguez-Couto and Herrera, 2006).

In recent application the alkaline catalase can be employed to generate sulphide native redox system for the reduction of sulphur dyes for cellulosic coloration (Chakraborty and Jaruhar, 2014).

7. Constraints in the application of immobilized enzymes in textile industry

As a consequence of immobilization the properties of enzymes are usually changed discussed in section 2.4. The immobilization

also associates with insolubility and increased size of enzymes. One of the major problems with the use of immobilized enzymes is the loss of specific activity, especially in textiles where enzymes are acting on macromolecular substrates. Because of poor interactions between insoluble substrates and the immobilized enzyme. But the considerable restriction is associated with the limited diffusion of immobilized enzyme inside substrate compare to the native enzymes. Furthermore, in textiles various chemicals and auxiliaries are employed which often destabilize the enzymes, and hence reduce their activity. In textiles use of nanoparticles & smart polymer as support has been suggested as a good solution to these problems. Enzymes linked to nano-size materials or smart polymers (soluble-insoluble) reduced mass transfer constraints with the advantage of increased diffusion (Brena et al., 2013; Dourado et al., 2002; Silva et al., 2006b; Soares et al., 2011; Tzanov et al., 2003a,b; Vasconcelos et al., 2006; Yu et al., 2013).

8. Environmental impact assessment

In order to assess the actual environmental benefits of enzymatic processes various researchers made LCA studies for different enzymatic processes reviewed in Jegannathan and Nielsen (2013). Life Cycle Assessment (LCA) gives a complete quantitative environmental impact assessment of enzymatic processing. An LCA study performed on scouring with pectatylases and on bleach clean-up using catalases shows that the impact of enzyme production is low compared to the impact of water, energy and chemicals that are saved (Nielsen et al., 2009). Similar LCA study on bleaching process shows that the environmental impact of enzymatic bleaching using arylesterase is small compared to environmental impact of a conventional bleaching process (Dettore, 2011).

9. Conclusions

Biocatalysts have proven to be a flexible and reliable tool in textile chemical processing and native enzymes are used in the immense numbers of processes. Often, for a given bioprocess, the native enzyme does not meet the requirements for large-scale application, and its properties thus need to be optimized or modulated. Enzyme immobilization is one of the most promising techniques for highly efficient and economical competent biotechnological processes. However, commercialization of immobilized enzymes is still at lower pace. Immobilization of enzymes is no doubt a useful technology for efficient recovery and reuse of costly enzymes, improved enzyme performance via enhance stability under both storage an operational conditions. But, the immobilization technology should provide active and stable biocatalysts, relatively using simple preparation process or an inexpensive and eco-friendly support material.

Due to wide variations in the properties of individual enzymes and due to varying requirements of reaction mechanisms, there is no thumb rule for method and support for immobilization. The final selection of support and method for immobilization depend on final practical application process. Therefore, extensive research work should be focused on immobilization techniques of various enzymes related to textile chemical processing, so as to expand their horizon for textile applications.

References

Abou-Okeil, A., El-Shafie, A., El Zawahry, M.M., 2010. Eco-friendly laccase-hydrogen peroxide/ultrasound-assisted bleaching of linen fabrics and its influence on dyeing efficiency. *Ultrason. Sonochemistry* 17, 383–390.

Ahmad, R., Sardar, M., 2015. Enzyme immobilization: an overview on nanoparticles as immobilization matrix. *Biochem. Anal. Biochem.* 4 (2), 178. <http://dx.doi.org/10.4172/2161-1009.1000178>.

Ali, S., Khatri, Z., Khatri, A., Tanwari, A., 2014. Integrated desizing-bleaching-reactive dyeing process of cotton towel using glucose oxidase enzyme. *J. Clean. Prod.* 66, 562–567. <http://dx.doi.org/10.1016/j.jclepro.2013.11.035>.

Aljawish, A., Chevalot, I., Jasniowski, J., Scher, J., Muniglia, L., 2015. Enzymatic synthesis of chitosan derivatives and their potential applications. *J. Mol. Catal. B Enzym.* 112, 25–39. <http://dx.doi.org/10.1016/j.molcatb.2014.10.014>.

Aly, A.S., Moustafa, A.B., Hebeish, A., 2004. Biotechnological treatment of cellulosic textiles. *J. Clean. Prod.* 12 (7), 697–705.

Aly, A.S., Sayed, M., Zahran, M.K., 2010. One-step process for enzymatic desizing & bio-scouring of cotton fabrics. *J. Nat. Fibers* 7 (2), 71–92.

Amorium, A.M., Gasques, M.D.G., Andreus, J., Scharf, M., 2002. The application of catalase for the elimination of hydrogen peroxide residues after bleaching of cotton fabrics. *Ann. Braz. Acad. Sci.* 74 (3), 433–436.

Anis, P., Eren, H.K., 2002. Comparison of alkaline scouring of cotton vs alkaline pectinase preparation. *AATCC Rev.* 22–26.

Anis, P., Davulcu, A., Eren, H.A., 2009. Enzymatic pre-treatment of cotton Part 2: peroxide generation in desizing liquor and bleaching. *FIBRES Text. East. Eur.* 17 (2), 87–90.

Anish, R., Rahman, M.S., Rao, M., 2007. Application of cellulases from an alkalothermophilic thermomonospora sp. in biopolishing of denims. *Biotechnol. Bioeng.* 96 (1), 48–56.

Araujo, R., Casal, M., Cavaco-Paulo, A., 2008. Application of enzymes for textile fibres processing. *Biocatal. Biotransformation* 26 (5), 332–349.

Araujo, R., Silva, C., Machado, R., Casal, M., Cunha, A.M., Rodriguez-Cabello, J.S., Cavaco-Paulo, A., 2009. Proteolytic enzyme engineering—A tool for wool. *Biomacromolecules* 10, 1655–1661.

Archana, Lokesh, K.N., Siva Kiran, R.R., 2012. Biological methods of dye removal from textile effluents – a review. *J. Biochem. Tech.* 3 (5), S177–S180.

Auterinen, A.-L., et al., 2011. Enzymatic Textile Bleaching Compositions and Methods of Use Thereof. Google Patent: EP2331668A1.

Azevedo, H., Bishop, D., Cavaco-Paulo, A., 2002. Possibilities for recycling cellulases after use in cotton processing. *Appl. Biochem. Biotechnol.* 101, 61–75.

Babu, B.R., Parande, A.K., Raghu, S., Prem Kumar, T., 2007. Cotton textile processing: waste generation and effluent treatment. *J. Cotton Sci.* 11 (3), 141–153.

Basto, C., Tzanov, T., Cavaco-Paulo, A., 2007. Combined ultrasound-laccase assisted bleaching of cotton. *Ultrason. Sonochemistry* 14, 350–354.

Bahtiyari, M.J., Duran, K., 2010. Usage of commercial cellulases in biopolishing of viscose fabrics. *TEKSTİL VE KONFEKSİYON* 1, 57–64.

Bai, G., Fu, K., Jin, N., Zhu, L., Chai, H., Lu, D., 2012. Bio-polishing of cotton fabrics with cellulase. *Adv. Material Res.* 468–471, 46–49.

Battan, B., Dhiman, S.S., Ahlawat, S., Mahajan, R., Sharma, J., 2012. Application of thermostable xylanase of *Bacillus pumilus* in textile processing. *Indian J. Microbiol.* 52 (2), 222–229.

Begum, S., Wu, J., Takawira, C.M., Wang, J., 2016. Surface modification of polyamide 66 fabrics with an alkaline protease – subtilisin. *J. Eng. Fibers Fabr.* 11 (1), 64–74.

Beteheva, R., Georgieva, N., Yotova, L., Valchev, I., Chadziska, C., 2007. Biobleaching of flax fibers by degradation of lignin with *phanerochaete chrysosporium* and *trichosporon cutaneum* R57. *J. Nat. Fibers* 4 (4), 31–40.

Beyler-Cigil, A., Cakmakci, E., Danis, O., Demir, S., Kahraman, M.V., 2013. Alpha-amylase immobilization on modified polyimide material. *Chem. Eng. Trans.* 32, 1687–1692.

Bhat, M.K., 2000. Cellulases and related enzymes in biotechnology. *Biotechnol. Adv.* 18, 355–383.

Binod, P., Paikhiwala, P., Gaikawari, R., Nampoothiri, K.M., Duggal, A., Dey, K., Pandey, A., 2013. Industrial Enzymes – present status and future perspectives for India. *J. Sci. Industrial Res.* 72, 271–286.

Brady, D., Jordan, A., 2009. Advance in enzyme immobilization. *Biotechnol. Lett.* 31 (11), 1639–1650. <http://dx.doi.org/10.1007/s10529-009-0076-4>.

Brena, B., Gonzalez-Pambo, P., Batista-Viera, F., 2013. Immobilization of enzymes: a literature survey. In: Guisan, J.M. (Ed.), *Immobilization of Enzymes and Cells*, second ed. Humana Press Inc., Totowa, NJ, pp. 15–30.

Buchert, J., Pere, J., Puolakka, A., Nousiainen, P., 2000. Scouring of cotton with pectinases, proteases, and lipases. *Text. Chem. Colorist Am. Dyest. Report.* 32 (5), 48–52.

Buschle-Diller, G., Yang, X.D., Yamamoto, R., 2001. Enzymatic bleaching of cotton fabric with glucose oxidase. *Text. Res. J.* 71 (5), 388–394.

Busto, M.D., 1998. An Experiment Illustrating the effect of immobilization on enzyme properties. *Biochem. Educ.* 26, 304–308.

Cai, J.Y., Evans, D.J., Smith, S.M., 2001. Bleaching of natural fibers with TAED and NOBS activated peroxide systems. *AATCC Rev.* 1, 31–34.

Calafell, M., Garriga, P., 2004. Effect of some process parameters in the enzymatic scouring of cotton using an acid pectinase. *Enzyme & Microb. Technol.* 34 (3–4), 326–331.

Calafell, M., KlugSanmer, B., Guebitz, G., Garriga, P., 2005. Dyeing behavior of cotton fabric bioscouring with pectate lyase and polygalacturonase. *Color. Technol.* 121 (6), 291–297.

Cao, L., 2005. *Carrier-bound Immobilized Enzymes: Principles, Applications and Design*. Wiley-Vch Verlag GmbH & Co. KGaA, Weinheim.

Cardamone, J.M., 2002. Proteolytic Activity of *aspergillus flavus* on Wool. *AATCC Review*, May, 30–35.

Cardamone, J.M., 2007. Enzyme-mediated crosslinking of wool Part-1 transglutaminase. *Text. Res. J.* 77, 214–221.

Cavaco-Paulo, A., 1998. Mechanism of cellulase action in textile processes. *Carbohydr. Polym.* 37, 273–277.

- Cavaco-Paulo, A., Gubitz, G.M., 2003. Textile Processing with Enzymes. Woodhead Publishing Ltd & CRC Press LLC.
- Chakraborty, J.N., Januar, P., 2014. Dyeing of cotton with sulphur dyes using alkaline catalase as reduction catalyst. *Indian J. Fiber & Text. Res.* 39 (3), 303–309.
- Chand, N., Natri, A.S., Sajedi, R.H., Mahadavi, A., Rassa, M., 2012. Enzymatic desizing of cotton fabric using a Ca²⁺-independent Amylase with acidic pH profile. *J. Mol. Catal. B Enzym.* 83, 46–50.
- Chand, N., Sajedi, R.H., Nateri, A.S., Khajeh, K., Mehdi, Rassa, 2014. Fermentative desizing of cotton fabric using an α -amylase-producing *Bacillus* strain: Optimization of simultaneous enzyme production and desizing. *Process Biochem.* 49 (11), 1885–1888.
- Chen, J.Y., Sun, L., Edwards, V.J., 2014. Regenerated cellulose fiber and film immobilized with lysozyme. *Bioceram. Dev. Appl.* 4 (1) <http://dx.doi.org/10.4172/2090-5025.1000078>, Chhabra M, Mishra S & Sreekrishnan T R (2008), 'Mediator-assisted Decolorization and Detoxification of Textile Dyes/Dye Mixture by *Cyathus bulleri* Laccase', *Appl Biochem Biotechnol.* 151, 587–598.
- Chimata, M.K., Chetty, C.S., Suresh, C., 2011. Fermentative production and thermo-stability characterization of α -amylase from *Aspergillus* species and its application potential evaluation in desizing of cotton cloth. *Biotechnol. Res. Int.* <http://dx.doi.org/10.4061/2011/323891>, ID 323891.
- Chinnamma, S.K., Antony, V.A.R., 2015. Production and application of cellulase enzyme for biopolishing of cotton. *Int. J. Sci. Technol. Manag.* 4 (1), 1606–1612.
- Chinta, S.K., Landage, S.M., Verma, K., 2012. Effect of biopolishing treatment on various spun yarn knitted fabrics. *Glob. J. Bio-Science Biotechnol.* 1 (2), 287–295.
- Choe, E.K., Nam, C.W., Kook, S.R., Chung, C., Cavaco-Paulo, A., 2004. Implementation of batchwise bioscouring of cotton knits. *Biocatal. Biotransformation* 22 (5/6), 375–382.
- Costa, S.A., Tzanov, T., Paar, A., Gudelj, M., Gubitz, G.M., Cavaco-Paulo, A., 2001. Immobilization of catalases from *Bacillus SF* on alumina for the treatment of textile bleaching effluents. *Enzyme Microb. Technol.* 28, 815–819.
- Costa, S.A., Tzanov, T., Paar, A., Carneiro, F., Gubitz, G.M., Cavaco-Paulo, A., 2002. Recycling of textile bleaching effluents for dyeing using immobilized catalase. *Biotechnol. Lett.* 24, 173–176.
- Csiszar, E., Losonczi, A., Szakacs, G., Rusznak, I., Bezur, L., Reicher, J., 2001. Enzymes and chelating agent in cotton pretreatment. *J. Biotechnol.* 89, 271–279.
- Csiszar, E., Urbanszki, K., Szakacs, G., 2001b. Bioremediation of desized cotton fabric by commercial cellulase and xylanase enzymes. *J. Mol. Catal. B Enzym.* 11 (4–6), 1065–1072.
- Dalal, S., Sharma, A., Gupta, M.N., 2007. A multipurpose immobilized biocatalyst with pectinase, xylanase and cellulase activities. *Chem. Central J.* 1 (1). <http://journal.chemistrycentral.com/content/1/1/16>. <http://dx.doi.org/10.1186/1752-153X-1-16>.
- Dalvi, P., Anthappan, P., Darade, N., Kanoongo, N., Adivarekar, R., 2007. Amylase & pectinase from single source for simultaneous desizing & scouring. *IJFTR* 32 (4), 459–465.
- Darias, R., Villalonga, R., 2001. Functional stabilization of cellulase by covalent modification with chitosan. *J. Chem. Technol. Biotechnol.* 76, 489–493.
- Datta, S., Christena, L.R., Rajaram, Y.R.S., 2013. Enzyme immobilization: an overview on techniques and support materials. *3 Biotech.* 3 (1), 1–9.
- Daugaard, A.E., Hoffmann, C., Andersen, C., 2016. Functional bio-based polyesters by enzymatic polymerization, abstract from nordic polymer days 2016. In: Nordic Rheology Conference, Helsinki, Finland.
- Davulcu, A., Eren, H.A., Avinc, O., Erismis, B., 2014. Ultrasound assisted biobleaching of cotton. *Cellulose* 21, 2973–2981.
- Degani, O., Gepstein, S., Dosoretz, C.G., 2002. Potential use of cutinase in enzymatic scouring of cotton fiber cuticle. *Appl. Biochem. Biotechnol.* 102–103, 277–289.
- Dehabadi, V.A., Opwis, K., Gutmann, J., 2011. Combination of acid-demineralization and enzymatic desizing of cotton fabrics by using industrial acid stable glucoamylases and α -amylases. *Starch/Stärke* 63 (1), 760–763.
- Delcheva, G., Pishtiyski, I., Dobrev, G., Krusteva, S., 2007. Immobilization of *Aspergillus Niger* pectinase on polyacrylonitrile copolymer membrane. *Trends Appl. Sci. Res.* 2 (5), 419–425.
- Dettore, C., 2011. Comparative life-cycle assessment (LCA) of textile bleaching systems: gentle power bleach vs. conventional bleaching System. In: Scientific Poster, AATCC International Conference, 22–24 March.
- Dhingra, S., Khanna, M., Pundir, C.S., 2006. Immobilization of α -amylase onto alkylamine glass beads affixed inside a plastic beaker: kinetic properties and application. *Indian J. Chem. Technol.* 13, 119–121.
- Diaz-Rodriguez, A., Davis, B.G., 2011. Chemical modification in the creation of novel biocatalysts. *Curr. Opin. Chem. Biol.* 15, 211–219.
- Dincer, A., Telefoncu, A., 2007. Improving the stability of cellulose by immobilization on modified polyvinyl alcohol-coated chitosan beads. *J. Mol. Catal. B Enzym.* 45, 10–14.
- Doshi, R., Shelke, V., 2001. Enzymes in textile industry – an environment-friendly approach. *Indian J. Fibre & Text. Res.* 26 (2), 202–205.
- Dourado, F., Bastos, M., Mota, M., Gama, F.M., 2002. Studies on the properties of Celluclast/Eudragit L-100 conjugate. *J. Biotechnol.* 99, 121–131.
- Duran, N., Rosa, M.A., Annibale, A., Gianfreda, L., 2002. Applications of laccases and tyrosinases (phenoloxidases) immobilized on different supports: a review. *Enzyme Microb. Technol.* 28, 83–99.
- Edwards, J.V., Goheen, S.C., 2006. Performance of bioactive molecules on cotton and other textiles. *RJTA* 10 (4), 19–32. <http://dx.doi.org/10.1108/RJTA10042006B003>.
- Edwards, J.V., Prevost, N., Condon, B., Sethumadhvan, K., Ullah, J., 2011a. Immobilization of Lysozyme on Cotton Fabrics: Synthesis, Characterization, and Activity. pp. 73–79. AATCC Review, May/June.
- Edwards, J.V., Prevost, N.T., Condon, B., French, A., 2011b. Covalent attachment of lysozyme to cotton/cellulose materials: protein versus solid support activation. *Cellulose* 18 (5), 1239–1249. <http://dx.doi.org/10.1007/s10570-011-9563-6>.
- Edwards, J.V., Sethumadhvan, K., Ullah, A.H.J., 2000. Conjugation and modeled structure/function analysis of lysozyme on glycine esterified cotton cellulose fibers. *Bioconjugate Chem.* 11 (4), 469–473.
- Eker, B., Zagorevski, D., Zhu, G., Linhardt, R.J., Dordick, J.S., 2009. Enzymatic polymerization of phenols in room-temperature ionic liquids. *J. Mol. Catal. B Enzym.* 59, 177–184. <http://dx.doi.org/10.1016/j.molcatb.2009.02.018>.
- El-Bendary, M.A., Abo El-Ola, S.M., Moharam, M., 2012. Enzymatic surface hydrolysis of polyamide fabric by protease enzyme and its production. *IJFTR* 37 (3), 273–279.
- El-sayed, H., Haqmed, R.R., Kantouch, A., 2002. Enzyme Based Feltproofing of Wool. AATCC Review, January, 25–28.
- Elnashar, M.M.M., 2011. The art of immobilization using biopolymers, biomaterials and nanobiotechnology. In: Elnashar, M. (Ed.), *Biotechnology of Biopolymers*. ISBN: 978-953-307-179-4. Available from: <http://www.intechopen.com/books/biotechnology-of-biopolymers/the-art-of-immobilization-using-biopolymers-biomaterials-and-nano-biotechnology>.
- Eren, H.A., Anis, P., Davulcu, A., 2009. Enzymatic one-bath desizing – bleaching – dyeing process for cotton fabrics. *Text. Res. J.* 79 (12), 1091–1098.
- Esfandiari, A., Firouzi-Pouyaei, E., Aghaei-Meibodi, P., 2014. Effect of enzymatic and mechanical treatment on combined desizing and bio-polishing of cotton fabrics. *J. Text. Inst.* 105 (11), 1193–1202.
- Etters, J.N., 1999. Cotton preparation with alkaline pectinase: an environment advance. *Text. Chem. Colorist Am. Dyest. Report.* 10 (3), 33–36.
- Etters, J.N., Sarkar, A.K., Henderson, L.A., Liu, J., 2001. The Influence of Bio-preparation of Cotton with Alkaline Pectinase on Dyeing Properties. AATCC Review, May, 22–24.
- Farooq, A., Ali, S., Abbas, N., Fatima, G.I., Ashraf, M.A., 2013. Comparative performance evaluation of conventional bleaching and enzymatic bleaching with glucose oxidase on knitted cotton fabric. *J. Clean. Prod.* 42, 167–171.
- Feng, T., Du, Y., Li, J., Sun, L., 2005. Study on the properties of immobilized cellulase for chitosan hydrolyze. *Polym. Prepr.* 46 (2), 705–706.
- Fu, K., Wang, D., Li, Y., Lu, D., 2015. Effect of additives on mesophilic α -amylase and its application in the desizing of cotton fabrics. *J. Text. Inst.* 106 (12), 1322–1327.
- Galante, Y.M., Cristina, F., 2003. Enzyme applications in detergency and in manufacturing industries. *Curr. Org. Chem.* 7 (13), 1399–1422.
- Gashti, M.P., Willoughby, J., Agrawal, P., 2011. In: Hauser, P. (Ed.), *Surface and Bulk Modification of Synthetic Textiles to Improve Dyeability, Textile Dyeing*. ISBN: 978-953-307-565-5, InTech, Available from: <http://www.intechopen.com/books/textile-dyeing/surface-and-bulk-modification-of-synthetic-textiles-to-improve-dyeability>.
- Ge, F., 2009. Transglutaminase treatment for improving wool fabric properties. *Fibers Polym.* 10 (6), 787–790.
- Gerday, C., et al., 2000. Cold-adapted enzymes: from fundamentals to biotechnology. *Trends Biotechnology* 18 (3), 103–107.
- Geus de, M., 2007. *Enzymatic Catalysis in the Synthesis of New Polymer Architectures and Materials*. Technische Universiteit Eindhoven, Eindhoven. <http://dx.doi.org/10.6100/IR617396>.
- Gokalp, N., Ulker, C., Guvenilir, Y.A., 2016. Enzymatic ring opening polymerization of caprolactone by using a novel immobilized biocatalyst. *Adv. Mater. Lett.* 7 (2), 144–149. <http://dx.doi.org/10.5185/amlett.2016.6059>.
- Gomes, I., Sarkar, P.K., Rahman, S.R., Rahim, M.A., Gomes, D.J., 2007. Production of cellulase from *Talaromyces emersonii* and evaluation of its application in eco-friendly functional finishing of jute-based fabrics. *Bangladesh J. Microbiol.* 24 (2), 109–114.
- Gozan, M., Martini, E., Park, D., Prasety, B., 2011. Cellulase immobilization using reversible soluble-insoluble polymer. *Int. J. Pharma Bio Sci.* 2 (4), 190–197.
- Gubitz, G.M., Cavaco-Paulo, A., 2003. New substrates for reliable enzymes: enzymatic modification of polymers. *Curr. Opin. Biotechnol.* 14, 577–582.
- Gudelj, M., Fruhwirth, G.O., Paar, A., Lottspeich, F., Robra, K., Cavaco-Paulo, A., Gubitz, G.M., 2001. A catalase-peroxidase from a newly isolated thermoalkaliphilic *Bacillus* sp. with potential for the treatment of textile bleaching effluents. *Extremophiles* 5, 423–429.
- Gupta, V.K., Khamparia, S., Tyagi, I., Jaspal, D., Malviya, A., 2015. Decolorization of mixture of dyes: a critical review. *Glob. J. Environ. Sci. Manage.* 1 (1), 71–94.
- Hadzhyska, H., Calafell, M., Gibert, J.M., Daga, J.M., Tzanov, T., 2006. Laccase assisted dyeing of cotton. *Biotechnol. Lett.* 28, 755–759.
- Haki, G.D., Rakshit, S.K., 2003. Developments in industrially important thermo-stable enzymes: a review. *Bioresour. Technol.* 89, 17–34.
- Han, X., Yu, Y., Wang, Q., Fan, X., Cui, L., Wang, P., 2014. Anti-bacterial properties of lactoferrin immobilized wool fabrics. *IJFTR* 29 (4), 401–405.
- Hanson, M.A., Gilbert, R.D., 1974. A new look at desizing with enzymes. *Text. Chem. Colorist Am. Dyest. Report.* 6 (12), 28–31.
- Hao, L., Wang, R., Fang, K., Liu, J., 2013. Ultrasonic effect on the desizing efficiency of α -amylase on starch-sized cotton fabrics. *Carbohydr. Polym.* 96 (2), 474–480.
- Haq, I., Ali, S., Javed, M.M., Hameed, U., Saleem, A., Adnan, F., Qadeer, M.A., 2010. Production of alpha amylase from a randomly induced mutant strain of *Bacillus amyloliquefaciens* and its application as a desizer in textile industry. *Pak. J. Bot.* 42 (1), 473–484.
- Hartzell-Lawon, M., Durrant, K., 2000. The efficiency of pectinase scouring with

- agitation to improve cotton fabric wettability. *Text. Chem. Colorist Am. Dyest. Report*. 32 (8), 86–90.
- Hasan, M.M., Nabi, E., Mahmud, R., 2015. Benefits of enzymatic process in textile wet processing. *Int. J. Fiber Text. Res. S* 5 (2), 16–19.
- Hebeish, A., Hashem, M., Shaker, N., Ramadan, M., El-Sadek, B., Hady, M.A., 2009. Effect of post- and pre-crosslinking of cotton fabrics on the efficiency of bio-finishing with cellulase enzyme. *Carbohydr. Polym.* 78, 953–960.
- Hebeish, A., Ramadan, M.A., Hashem, M., Sadek, B., Abdel-Hady, M., 2013. New development for combined bioscouring and bleaching of cotton-based fabrics. *RJTA* 17 (1), 94–103.
- Heikinheimo, L., Buchert, J., Miettinen-Oinonen, A., Suominen, P., 2000. Treating denim fabrics with *Trichoderma reesei* cellulases. *Text. Res. J.* 70 (11), 969973. <http://dx.doi.org/10.1177/004051750007001106>.
- Hirsh, S.L., Bilek, M.M.M., Nosworthy, N.J., Kondyurin, A., Remedios, C.G., McKenzie, D.R., 2010. A comparison of covalent immobilization and physical adsorption of a cellulase enzyme mixture. *Langmuir* 26 (17), 14380–14388.
- Hiteshi, K., Chauhan, S., Gupta, R., 2013. Immobilization of microbial pectinases: a review. *CIBTech J. Biotechnol.* 2 (4), 37–52.
- Hoondal, G.S., Tiwari, R.P., Tewari, R., Dahiya, N., Beg, Q.K., 2002. Microbial alkaline pectinases and their industrial applications: a review. *Appl. Microbiol. Biotechnol.* 59, 409–418.
- Hossain, S., Uddin, K., 2011. Comparative analysis between conventional pretreatment and bio-preparation. *Int. J. Eng. Technol.* 11 (3), 16–21.
- Hu-On, J.Y., Fan, X., Wang, Q., Cui, L., 2008. Immobilization of lysozyme on wool fabric. *Wool. Text. Technol.* 10, 15–18.
- Huang, D., Cui, L., Wang, Q., Wang, P., Fan, X., 2009a. Immobilization of lysozyme catalyzed by MTG on the wool and antimicrobial action. *J. Food Sci. Biotechnol.* 6, 19.
- Huang, D., Fan, X., Cui, L., Wang, Q., Wang, P., 2009b. Antibacterial action and properties of lysozyme immobilized on wool catalyzed by MTG. *Chem. Industry Engineering's Prog.* 7, 1231–1236.
- Ibrahim, D.F., Abd El-Salam, S.H., 2012. Enzymatic treatment of polyester fabrics digitally printed. *J. Text. Sci. Eng.* 2 (3) <http://dx.doi.org/10.4172/2165-8064.1000113>.
- Ibrahim, N.A., El-Zairy, M.R., Allam, E., Hassan, T.M., 1999. Dyeability of biofinished cellulosic fabrics. *Colourage* 46 (1), 47–54.
- Ibrahim, N.A., Allam, E., Morsy, M.S., Hassan, T.M., 2000. Bio-finishing of pre-dyed cotton fabrics. *Colourage* 47 (4), 29–35.
- Ibrahim, N.A., El-Hossamy, M., Morsy, M.S., Eid, B.M., 2004a. Development of new eco-friendly options for cotton wet processing. *J. Appl. Polym. Sci.* 93 (4), 1825–1836.
- Ibrahim, N.A., El-Hossamy, M., Morsy, M.S., Eid, B.M., 2004b. Optimization and modification of enzymatic desizing of starch size. *Polymer-Plastic Technol. Eng.* 43 (2), 519–538.
- Ibrahim, N.A., Abd Allah, S.Z., Borham, H.A.T., Hassan, T.M., 2005a. Economical and ecological biotreatment/half bleaching of cotton-containing knit fabrics on industrial scale. *Polymer-Plastics Technol. Eng.* 44 (5), 881–899. <http://dx.doi.org/10.1081/PTE-200060866>.
- Ibrahim, N.A., Fahmy, H.M., Hassan, T.M., Mohamed, Z.E., 2005b. Effect of cellulase treatment on the extent of post-finishing and dyeing of cotton fabrics. *J. Mater. Process. Technol.* 160, 99–106.
- Ibrahim, N.A., Gouda, M., El-Shafei, A.M., Abdel-Fatah, O.M., 2007. Antimicrobial activity of cotton fabrics containing immobilized enzymes. *J. Appl. Polym. Sci.* 104, 1754–1761. <http://dx.doi.org/10.1002/app.25821>.
- Ibrahim, N.A., Allam, E.A., El-Hossamy, M., El-Zairy, W.M., 2008. Enzymatic modification of cotton/wool and viscose/wool blended fabrics. *J. Nat. Fibers* 5 (2), 154–169. <http://dx.doi.org/10.1080/15440470801929648>.
- Ibrahim, N.A., El-Badry, K., Eid, B.M., Hassan, T.M., 2011. A new approach for bio-finishing of cellulose containing fabrics using acid cellulases. *Carbohydr. Polym.* 83 (1), 116–121. <http://dx.doi.org/10.1016/j.carbpol.2010.07.025>.
- Ibrahim, N.A., El-Shafei, H.A., Abdel-Aziz, M.S., Ghaly, M.F., Eid, B.M., Hamed, A.A., 2012. The potential use of alkaline protease from *Streptomyces albidoflavus* as an eco-friendly wool modifier. *JTI* 103 (5), 490–498. <http://dx.doi.org/10.1080/00405000.2011.588417>.
- Imran, M., Crowley, D.E., Khalid, A., Hussain, S., Mumtaz, M.W., Arshad, M., 2015. Microbial biotechnology for decolorization of textile wastewaters. *Rev. Environ. Sci. Biotechnol.* 14 (1), 73–92. <http://dx.doi.org/10.1007/s11157-014-9344-4>.
- Ismail, O.E., 2008. Influence of Wax and Pectin Removal on Cotton Absorbency. *AATCC Review*, June, 37–42.
- Jabasingh, S.A., Nachiyar, C.V., 2011. Optimization and immobilization kinetics of *Aspergillus nidulans* cellulase onto modified chitin by response surface approach. *Biotechnol. Bioinf. Bioeng.* 1 (2), 201–220.
- Jegannathan, K.R., Nielsen, P.H., 2013. Environmental assessment of enzyme use in industrial production—a literature review. *J. Clean. Prod.* 42, 228–240.
- Kalantzi, S., Mamma, D., Christakopoulos, P., Kekos, D., 2008. Effect of pectate lyase bioscouring on physical, chemical and Lowstress mechanical properties of cotton fabrics. *Bioresour. Technol.* 99 (17), 8185–8192. <http://dx.doi.org/10.1016/j.biortech.2008.03.020>.
- Kalantzi, S., Mamma, D., Kalogeris, E., Kekos, D., 2010. Improved properties of cotton fabrics treated with lipase and its combination with pectinase. *FIBRES Text. East. Eur.* 18 (5), 86–92.
- Kaneli, M., Vasilakos, S., Nikolaivits, E., Ladas, S., Christakopoulos, P., Topakas, E., 2015. Surface modification of poly(ethylene terephthalate) (PET) fibers by a cutinase from *Fusarium oxysporum*. *Process Biochem.* 50 (11), 1885–1892. <http://dx.doi.org/10.1016/j.procbio.2015.08.013>.
- Karapinar, E., Sarişik, M.O., 2004. Scouring of cotton with cellulases, pectinases and proteases. *FIBRES Text. East. Eur.* 12 (3), 79–82.
- Karnakar, S.R., 1999. Chemical Technology in the Pretreatment Processes of Textiles. Elsevier Science B.V., Amsterdam, Netherlands.
- Khan, A.A., Alzohairy, M.A., 2010. Recent advances and applications of immobilized enzyme technologies: a review. *Res. J. Biol. Sci.* 5 (8), 565–575.
- Khan, A.F., Arif, S., 2006. Development and applications of animal amylases for enzymatic desizing of woven fabric. *Pak. J. Sci. Ind. Res.* 49 (2), 103–105.
- Khan, R., Bhawana, P., Fulekar, M.H., 2013. Microbial decolorization and degradation of synthetic dyes: a review. *Rev. Environ. Sci. Biotechnol.* 12, 75–97.
- Kim, J., Kim, S.Y., Choe, E.K., 2005. The beneficial influence of enzymatic scouring on cotton properties. *J. Nat. Fibers* 2 (4), 39–52.
- Kim, J., Choe, E.K., Kim, S.Y., Nam, S.W., 2006. Optimization of the enzymatic scouring. *J. Nat. Fibers* 3 (2/3), 155–168.
- Kim, S., Moldes, D., Cavaco-Paulo, A., 2007. Laccase for enzymatic colouration of unbleached cotton. *Enzyme Microb. Technol.* 40, 1788–1793.
- Kim, S.Y., Zille, A., Murkovic, M., Guebitz, G., Cavaco-Paulo, A., 2007. Enzymatic polymerization on the surface of functionalized cellulose fibers. *Enzyme Microb. Technol.* 40, 1782–1787. <http://dx.doi.org/10.1016/j.enzmictec.2007.01.001>.
- Kiumarsi, A., Parvinzadeh, M., 2010. Enzymatic hydrolysis of nylon 6 fiber using lipolytic enzyme. *J. Appl. Polym. Sci.* 116, 3140–3147.
- Krajewska, B., 2004. Application of chitin- and chitosan-based materials for enzyme immobilizations: a review. *Enzyme Microb. Technol.* 35, 126–139.
- Krikstolaityte, V., Kuliesius, J., Ramanaviciene, A., Mikolunaite, L., Minkstiniene, A.K., Oztekin, Y., Ramanavicius, A., 2014. Enzymatic polymerization of polythiophene by immobilized glucose oxidase. *Polymer* 55 (7), 1613–1620. <http://dx.doi.org/10.1016/j.polymer.2014.02.003>.
- Krizman, P., Kovac, E., Tavcer, P.F., 2005. Bleaching of cotton fabric with peracetic acid in the presence of different bleach activators. *Color. Technol.* 121 (6), 304–309.
- Kuilderd, H., Wu, G., 2008. Simultaneous Desizing and Scouring with Enzymes. *AATCC Review*, June, 33–35.
- Kumar, A., Yoon, M., Charles, P., 1997. Optimizing the use of cellulase enzymes in finishing cellulosic fabrics. *Text. Chem. Colorist Am. Dyest. Report*. 29 (4), 37–42.
- Kumar, V.S., Meenakshisundaram, S., Selvakumar, N., 2008. Conservation of cellulase enzyme in biopolishing application of cotton fabrics. *J. Text. Inst.* 99 (4), 339–346.
- Lange, N.K., 1997. Lipase-assisted desizing of woven cotton fabrics. *Text. Chem. Colorist* 29 (6), 23–26.
- Lee, S.H., Song, W.S., 2010. Surface modification of polyester fabrics by enzyme treatment. *Fibers Polym.* 11 (1), 54–59. <http://dx.doi.org/10.1007/s12221-010-0054-4>.
- Lening, H.B.M., Warmoeskerken, M.M.C.G., 2004. A fast, continuous enzyme based pretreatment process concept for cotton containing textiles. *Biocatal. Biotransformation* 22 (5–6), 361–368.
- Li, Y., Hardin, I.R., 1997. Enzymatic scouring of cotton-effects on structure & properties. *Text. Chem. Colorist* 29 (8), 71–76.
- Li, Y., Hardin, I.R., 1998. Enzymatic scouring of cotton-surfactants, agitation & selection of enzymes. *Text. Chem. Colorist* 30 (9), 23–30.
- Li, M., Hinks, D., 2012. An Environmentally Benign Approach to Cotton Preparation: One Bath Enzymatic Desizing, Scouring & Activated Bleaching. *AATCC Review*, Sep/Oct, 46–51.
- Li, T., Wang, N., Li, S., Zhao, Q., Guo, M., Zhang, C., 2007. Optimization of covalent immobilization of pectinase on sodium alginate support. *Biotechnol. Lett.* 29, 1413–1416.
- Liese, A., Hiltnerhaus, L., 2013. Evaluation of immobilized enzymes for industrial applications. *Chem. Soc. Rev.* 42 (15), 6236–6249. <http://dx.doi.org/10.1039/C3CS35511J>.
- Liu, J., Otto, E., Lange, L., Hussain, P., Condon, B., Lund, H., 2000. Selecting cellulases for bio-polishing based on enzyme selectivity and process conditions. *Text. Chem. Colorist Am. Dyest. Report*. 32 (5), 30–36.
- Losonczy, A., Csizsar, E., Szakacs, G., Kaarela, O., 2004. Bleachability and dyeing properties of biopretreated and conventionally scoured cotton fabrics. *Text. Res. J.* 74 (6), 501–508.
- Losonczy, A., Csizsar, E., Szakacs, G., Bezur, L., 2005. Role of EDTA chelating agent in bioscouring of cotton. *Text. Res. J.* 75 (5), 411–417.
- Malik, S.K., Madhu, A., Saluja, M., 2010. Biotechnology in Today's textiles. *Man-made Text. India* 3, 81–88.
- Malmir, H.J., Jahani, M.A.G., Berenjian, A., 2012. Potential applications of chitosan nanoparticles as novel support in enzyme immobilization. *Am. J. Biochem. Biotechnol.* 8 (4), 203–219.
- Mangovska, B., Jordanov, I., 2006. Pad Roll Bioscouring Process for Cotton-woven Fabrics. *AATCC Review*, March, 33–36.
- Maryan, A.S., Montazer, M., 2013. A cleaner production of denim garment using one step treatment with amylase/cellulase/laccase. *J. Clean. Prod.* 57, 320–326.
- Mateo, C., Palomo, J.M., Fernandez-Lorente, G., Guisan, J.M., Fernandez-Lafuente, R., 2007. Improvement of enzyme activity, stability and selectivity via immobilization techniques. *Enzyme Microb. Technol.* 40, 1451–1463. <http://dx.doi.org/10.1016/j.enzmictec.2007.01.018>.
- McCoskey, S.G., Jump, J.M., 2005. Bio-polishing of polyester and polyester/cotton fabric. *Text. Res. J.* 75 (6), 480–484.
- Miettinen-Oinonen, A., Silvennoinen, M., Nousiainen, P., Buchert, J., 2002. Modification of synthetic fibres with laccase. In: *Proceedings of the Second*

- International Symposium on Biotechnology in Textile, Athens, USA, April 3–6, 13–17.
- Miletic, N., Nastasovic, A., Loos, K., 2012. Immobilization of biocatalysts for enzymatic polymerization: possibilities, advantages, applications. *Biores Tech.* 115 (Jul), 126–135. <http://dx.doi.org/10.1016/j.biortech.2011.11.054>.
- Mohamad, N.R., Marzuki, N.H.C., Buang, N.A., Huyop, F., Wahab, R.A., 2015. An overview of technologies for immobilization of enzymes and surface analysis techniques for immobilized enzymes. *Biotech Biotechnol Equip* 29 (2), 205–220. <http://dx.doi.org/10.1080/13102818.2015.1008192>.
- Mojsov, K., 2011. Application of enzymes in the Textile industry: a review. In: II International Congress 'Engineering, Ecology and Materials in the Processing Industry', Jahorina, 9th–11th March, 230–239.
- Mojsov, K.D., 2014a. Trends in bio-processing of textiles: a review. *Adv. Technol.* 3 (2), 135–138.
- Mojsov, K., 2014b. Biopolishing enzymes and their applications in textiles: a review. *Tekstilna Ind.* 61 (2), 20–24.
- Morozova, V.V., Semenova, M.V., Salanovich, T.N., Okunev, O.N., Koshelev, A.V., Bubnova, T.V., Krichevskii, G.E., Timatkov, A.G., Barysheva, N.V., Sinitsyn, A.P., 2006. Application of neutral-alkaline pectate lyases to cotton fabric boil off. *Appl. Biochem. Microbiol.* 42 (6), 603–608.
- Nabib, M.A., Entezami, A.A., 2005. Comparative study on the enzymatic polymerization of N-substituted aniline derivatives. *Polym. Adv. Technol.* <http://dx.doi.org/10.1002/pat.582>.
- Nielsen, P.H., Kuilderd, H., Zhou, W., Lu, X., 2009. Enzyme biotechnology for sustainable textiles. In: Blackburn, R.S. (Ed.), *Sustainable Textile: Life Cycle and Environment Impact*. Woodhead Publishing Limited & CRC Press, pp. 113–138.
- Ninge Gowda, K.N., Padaki, N.V., Sudhakar, R., Subramani, R., 2007. Eco-friendly Preparatory Process for Silk: Degumming by Protease Enzyme. *Man-made Textiles in India*, Jan. 28–31.
- Nisha, S., Arun Karthick, S., Gobi, N., 2012. A review on methods, application and properties of immobilized enzyme. *Chem. Sci. Rev. Lett.* 1 (3), 148–155.
- Nolle, H., Bishop, D.P., Hocker, H., 1996. Effects of proteolytic and lipolytic enzymes on untreated and shrink-resist-treated wool. *J. Text. Inst.* 87 (1), 212–226.
- Noreen, H., Zila, M.A., Ali, S., Hussain, T., 2014. Optimization of bio-polishing of polyester/cotton blended fabrics with cellulases prepared from *Aspergillus Niger*. *Indian J. Biotechnol.* 13 (1), 108–113.
- Norouziyan, D., 2003. Enzyme immobilization: the state of art in biotechnology. *Iran. J. Biotech* 1 (4), 197–206.
- Opwis, K., Knittel, D., Kele, A., Schollmeyer, E., 1999. Enzymatic recycling of starch-containing desizing liquors. *Starch* 51 (10), 348–353.
- Opwis, K., Knittel, D., Schollmeyer, E., 2004. Immobilization of Catalase on Textile Carrier Materials, vol. 4, pp. 25–28. AATCC Review.
- Opwis, K., Knittel, D., Bahners, T., Schollmeyer, E., 2005. Photochemical enzyme immobilization on textile carrier materials. *Eng. Life Sci.* 1, 63–67.
- Opwis, K., Knittel, D., Schollmeyer, E., Cordes, A., 2008. Simultaneous application of glucose oxidases and peroxidases in bleaching processes. *Eng. Life Sci.* 8 (2), 175–178.
- Opwis, K., Straube, T., Kiehl, K., Gutmann, J.S., 2014. Various strategies for the immobilization of biocatalysts on textile carrier materials. *Chem. Eng. Trans.* 38, 223–228.
- Ozdil, N., Ozdogan, E., Oktem, T., 2003. Effects of enzymatic treatment on various spun yarn fabrics. *FIBRES Text. East. Eur.* 11 4 (43), 58–61.
- Parvinzadeh, M., 2007. Effect of proteolytic enzyme on dyeing of wool with madder. *Enzyme Microb. Technol.* 40 (7), 1719–1722. <http://dx.doi.org/10.1016/j.enzmictec.2006.10.026>.
- Parvinzadeh, M., 2009. A new approach to improve dyeability of nylon 6 fibre using a subtilisin enzyme. *Colouration Technol.* 125 (4), 228–233. <http://dx.doi.org/10.1111/j.1478-4408.2009.00201.x>.
- Parvinzadeh, M., Assefipour, R., Kiumarsi, A., 2009. Biohydrolysis of nylon 66 with different proteolytic enzymes. *Polym. Degrad. Stab.* 94 (8), 1197–1205. <http://dx.doi.org/10.1016/j.polydegradstab.2009.04.017>.
- Parvinzadeh, M., Assefipour, R., Kiumarsi, A., Parvinzadeh, M., 2013. Enzymatic surface hydrolysis of polyamide 66 with mixtures of proteolytic and lipolytic Enzymes. *Prep. Biochem. Biotechnol.* 43 (8), 798–814. <http://dx.doi.org/10.1080/10826068.2013.805623>.
- Patra, A.K., Chakraborty, J.N., Madhu, A., 2010. Studies on enzymatic pre-treatment of linen. *IJFTR* 35 (4), 337–341.
- Paul, R., Genesca, E., 2013. The use of enzymatic techniques in the finishing of technical textiles. In: Gulrajni, M.L. (Ed.), *Advances in Dyeing and Finishing of Technical Textiles*. Woodhead publishing Ltd., Cambridge, pp. 177–198.
- Pazarlioglu, N.K., Sariisik, M., Telefoncu, A., 2005. Treating denim fabrics with immobilized commercial Cellulases. *Process Biochem.* 40, 767–771.
- Peng, Y., Liu, H., Zhang, X., Li, Y., Liu, S., 2009. CNT templated regioselective enzymatic polymerization of phenol in water and modification of surface of MWNT thereby. *J. Polym. Sci. Part A Polym. Chem.* 47, 1627–1635. <http://dx.doi.org/10.1002/pola>.
- Peralta-Zamora, P., Pereira, C.M., Tiburtius, E.R.L., Moraes, S.G., Rosa, M.A., Minussi, R.C., Durán, N., 2003. Decolorization of reactive dyes by immobilized laccase. *Appl. Catal. B Environ.* 42, 131–144.
- Pereira, L., Bastos, C., Tzanov, T., Cavaco-Paulo, A., Guebitz, G.M., 2005. Environmentally friendly bleaching of cotton using laccases. *Environ. Chem. Lett.* 3, 66–69.
- Piotrowska, U., Marcin Sobczak, M., 2015. Enzymatic polymerization of cyclic monomers in ionic liquids as a prospective synthesis method for polyesters used in drug delivery systems. *Molecules* 20, 1–23. <http://dx.doi.org/10.3390/molecules20010001>.
- Podrepsek, G.H., Primozi, M., Knez, Z., Habulin, M., 2012. Immobilization of cellulase for industrial production. *Chem. Eng. Trans.* 27, 235–240.
- Powell, L.W., 1984. Developments in immobilized-enzyme technology. *Biotech. Genet. Engg. Rev.* 2, 409–438 (oct.).
- Prakash, O., Jaiswal, N., 2011. Immobilization of a thermostable α -amylase on agarose and agar matrices and its application in starch stain removal. *World Appl. Sci. J.* 13 (3), 572–577.
- Presá, P., Tavčer, P.F., 2008. Bio-scouring and bleaching of cotton with pectinase enzyme and peracetic acid in one bath. *Color. Technol.* 124 (1), 36–42.
- Presá, P., Tavčer, P.F., 2009. Low water and energy saving process for cotton pre-treatment. *Text. Res. J.* 79 (1), 76–88.
- Ramadan, A.R., 2008. Characterization of biobleaching of cotton/linen fabrics. *JTATM* 6 (1), 1–12.
- Rauf, M.A., Ashraf, S.S., 2012. Survey of recent trends in biochemically assisted degradation of dyes. *Chem. Eng. J.* 209, 520–530.
- Regan, I., 1962. Enzymes and their application in textile processing, especially desizing. *J. Soc. Dye. Colour.* 78 (11), 533–542. <http://dx.doi.org/10.1111/j.14784408.1962.tb02463.x>.
- Rehman, A., Raza, Z.A., Masood, R., Hussain, M.T., Ahmad, N., 2015. Multi-respose optimization in enzymatic desizing of cotton fabric under various chemo-physical conditions using a taguchi approach. *Cellulose* 22 (3), 2107–2116.
- Ren, X., Buschle-Diller, G., 2007. Oxidoreductases for modification of linen fibers. *Colloids Surfaces A Physicochem. Eng. Aspects* 299, 15–21.
- Ribitsch, D., Acero, E.H., Greimel, K., Dellacher, A., Zitzenbacher, S., Marold, A., Rodriguez, R.D., Steinkellner, G., Gruber, K., Schwab, H., Guebitz, G.M., 2012. A new esterase from *Thermobifida halotolerans* hydrolyses polyethylene terephthalate (PET) and polylactic acid (PLA). *Polymers* 4, 617–629. <http://dx.doi.org/10.3390/polym4010617>.
- Rodriguez-Couto, S., 2012. Laccases for denim bleaching: an eco-friendly alternative. *Open Text. J.* 5, 1–7.
- Rodriguez-Couto, S., Herrera, J.L.T., 2006. Industrial and biotechnological applications of laccases: a review. *Biotechnol. Adv.* 24, 500–513.
- Rodriguez-Couto, S., Toca-Herrera, 2006. Laccase in textile industry. *Biotechnol. Mol. Biol. Rev.* 1 (4), 115–120.
- Roig, M.G., Estevez, E.B., Velasco, F.G., Ghais, N.I., Silverio, J.M.C., 1986. Methods for immobilizing enzymes. *Biochem. Educ.* 14 (4), 180–185.
- Romo-Sanchez, S., Camacho, C., Ramirez, H.L., Arevalo-Villena, M., 2014. Immobilization of commercial cellulase and xylanase by different methods using two polymeric supports. *Adv. Biosci. Biotechnol.* 5, 517–526.
- Sahin, U.K., Gursoy, N.C., 2005. Low Temperature Acidic Pectinase Scouring for Enhancing Textile Quality. AATCC Review, Jan., 27–30.
- Sahinbaskan, B.Y., Kahraman, M.V., 2011. Desizing of untreated cotton fabric with the conventional and ultrasonic bath procedures by immobilized and native α -amylase. *Starch* 63 (3), 154–159. <http://dx.doi.org/10.1002/star.201000109>.
- Sangwatanaroj, U., Choonukulpong, K., Ueda, M., 2003. Cotton Scouring with Pectinase and Lipase/Protease/Cellulase. AATCC Review, May, 17–20.
- Saravanan, D., Ramachandran, T., Rajendran, S., Rajesh, E.M., 2008. Influence of Mechanical Agitations in Enzyme Assisted Processing. *Man-made Textiles in India*, pp. 313–316. Sep.
- Saravanan, D., Vasanthi, N.S., Ramachandran, T., 2009. A review on influential behaviour of biopolishing on dyeability and certain physico-mechanical properties of cotton fabrics. *Carbohydr. Polym.* 76, 1–7.
- Saravanan, D., Vasanthi, N.S., Raja, K.S., Das, A., Ramachandran, T., 2010. Bleaching of cotton fabrics using peroxide produced by glucose oxidase. *Indian J. fibre & Text. Res.* 35 (3), 281–283.
- Saravanan, D., Prakash, A.A., Jagadeeshwaran, D., Nalankilli, G., Ramachandran, T., Prabhakaran, C., 2011. Optimization of thermophilic *Bacillus thichneriformis* α -amylase desizing of cotton fabrics. *IJFTR* 36 (3), 253–258.
- Saravanan, D., Laxmi, S.N.S., Vasanthi, N.S., Raja, K.S., 2013. Biopolishing of cotton fabric with fungal cellulase and its effect on the morphology of cotton fibres. *Indian J. fibre & Text. Res.* 38 (2), 156–160.
- Sarayu, K., Sandhya, S., 2012. Current technologies for biological treatment of textile wastewater – a review. *Appl. Biochem. Biotechnol.* 167, 645–661.
- Sarethy, I.P., Saxena, Y., Kapoor, A., Sharma, M., Seth, R., Sharma, H., Sharma, S.K., Gupta, S., 2012. Amylase produced by *Bacillus* sp. SI-136 isolated from sodic-alkaline soil for efficient starch desizing. *J. Biochem. Technol.* 4 (2), 604–609.
- Sarkar, A.K., Eters, J.N., 2001. Kinetics of the enzymatic hydrolysis of cellulose. AATCC Review, 48–52.
- Sawada, K., Ueda, M., 2001. Enzymes processing of textiles in reverse micellar solution. *J. Biotechnol.* 89, 263–269.
- Schlumper, C.B., Ibanescu, C., Bechtold, T., 2006. Technical aspects in enzymatic hydrolysis of celluloses. *Lenzing. Berichte* 85, 107–112.
- Schroeder, M., Schweitzer, M., Lenting, H.B.M., Guebitz, G.M., 2004. Chemical modification of protease for wool cuticle scale removal. *Biocatal. Biotransformation* 22 (5/6), 299–305.
- Sebra, J.L., Gil, M.H., 2007. Cotton gauze bandage: a support for protease immobilization for use in biomedical applications. *Braz. J. Pharm. Sci.* 43 (4), 535–542.
- Sen, S., Puskas, J.E., 2015. Green polymer chemistry: enzyme catalysis for polymer functionalization. *Molecules* 20, 9358–9379. <http://dx.doi.org/10.3390/molecules20059358>.
- Shafie, A.E., Fauda, M.M.G., Hashem, M., 2009. One step process for bioscouring and peracetic acid bleaching of cotton fabric. *Carbohydr. Polym.* 78 (2), 302–308.
- Shah, T., Halacheva, S., 2015. Drug-releasing textiles. In: Langenhove, L. (Ed.), *Advances in Smart Medical Textiles: Treatments and Health Monitoring*.

- Woodhead publishing Ltd., Cambridge, pp. 119–154.
- Sheldon, R.A., 2007. Enzyme immobilization: the quest for optimum performance. *Adv. Synth. Catal.* 349, 1289–1307.
- Sheldon, R.A., Schoevaert, R., Van-Langen, L.M., 2005. Cross-linked enzyme aggregates (CLEAs): a novel and versatile method for enzyme immobilization: a review. *Biocatal. Biotransform.* 23, 141–147.
- Shen, J., 2010. Enzymatic treatment of wool and silk fibres. In: Nierstrasz, V.A., Cavaco-Paulo, A. (Eds.), *Advances in Textile Biotechnology*. Woodhead publishing Ltd., Cambridge, pp. 171–192.
- Shen, J., Rushforth, M., Cavaco-Paulo, A., Guebitz, G., Lenting, H., 2007. Development and industrialization of enzymatic shrink-resist process based on modified proteases for wool machine wash-ability. *Enzyme Microb. Technol.* 34, 1–6.
- Shin, Y., Hwang, S., Ahn, I., 2004. Enzymatic bleaching of desized cotton fabrics with hydrogen peroxide produced by glucose oxidase. *J. Ind. Eng. Chem.* 10, 577–581.
- Shukla, S.R., Jajpura, L., 2005. Immobilisation of amylase by various techniques. *IJFTR* 29 (2), 75–81.
- Siddiquee, A.B., Bashar, M., Sarker, P., Tohfa, T.T., Hossain, M.A., Azad, M.I., Akhtar, N., 2014. Comparative study of conventional and enzymatic pretreatment (scouring & bleaching) of cotton knitted fabrics. *Int. J. Eng. Technol.* 3 (1), 37–43.
- Silva, C.J.S.M., Cavaco-Paulo, A., 2008. Biotransformations in synthetic fibres. *Biocatal. Biotransform.* 26 (5), 350–356. <http://dx.doi.org/10.1080/10242420802357845>.
- Silva, C.J.S.M., Guebitz, G., Cavaco-Paulo, A., 2006a. Optimization of a serine protease coupling to Eudragit S-100 by experimental design techniques. *J. Chem. Technol. Biotechnol.* 81, 8–16.
- Silva, C.J.S.M., Zhang, Q., Shen, J., Cavaco-Paulo, A., 2006b. Immobilization of proteases with a water soluble–insoluble reversible polymer for treatment of wool. *Enzyme Microb. Technol.* 39, 634–640.
- Singh, R.K., Tiwari, M.R., Singh, R., Lee, J., 2013. From protein engineering to immobilization: promising strategies for the upgrade of industrial enzymes. *Int. J. Mol. Sci.* 14, 1232–1277. <http://dx.doi.org/10.3390/ijms14011232>.
- Soares, J.C., Moreira, P.R., Queiroga, A.C., Morgado, J.E., Malcata, F.X., Pintado, M.E., 2011. Application of immobilized enzymes technologies for the textile industry: a review. *Biocatal. Biotransform.* 29 (6), 223–237.
- Sojka-Ledakowicz, J., Joanna, L., Pyc, R., 2006. Integrated enzymatic pre-treatment of cotton fabrics. *J. Nat. Fibers* 3 (2/3), 199–207.
- Solbak, A.I., et al., 2005. Discovery of pectin degrading enzymes and directed evolution of a novel pectate lyase for processing cotton fabric. *J. Biol. Chem.* 280, 9431–9438. <http://dx.doi.org/10.1074/jbc.M411838200>.
- Souza, S.F.D., 2002. Trends in immobilized enzymes and cell technology. *Indian J. Biotechnol.* 1 (4), 321–328.
- Spicka, N., Tavec, P.F., 2013a. New combined bio-scouring and bio-bleaching process of cotton fabrics. *Mater. Technol.* 47 (4), 409–412.
- Spicka, N., Tavec, P.F., 2013b. Complete enzymatic pre-treatment of cotton fabric with incorporated bleach activator. *Text. Res. J.* 83 (6), 566–573.
- Sreelakshmi, S.N., Paul, A., Vasanthi, N.S., Sarvanan, D., 2014. Low-temperature acidic amylases from *Aspergillus* for desizing of cotton fabrics. *J. Text. Inst.* 105 (1), 59–66.
- Sreenath, H.K., Shah, A.B., Yang, V.W., Gharia, M.M., Jeffries, T.W., 1996. Enzymatic polishing of jute/cotton blended fabrics. *J. Ferment. Bioeng.* 81 (1), 18–20.
- Stavila, E., Loos, K., 2015. Synthesis of polyamides and their copolymers by enzymatic polymerization. *J. Renew. Mater.* 3 (4), 268–280. <http://dx.doi.org/10.7569/JRM.2015.634102>.
- Talekar, S., Joshi, A., Joshi, G., Kamat, P., Haripurkar, R., Kambale, S., 2013. Parameters in preparation and characterization of cross linked enzyme aggregates (CLEAs). *RSC Adv.* 3, 12485–12511.
- Talekar, S., Waingade, S., Gaikwad, V., Patil, S., Nagavekar, N., 2012a. Preparation and characterization of cross linked enzyme aggregates (CLEAs) of *Bacillus amyloliquefaciens* alpha amylase. *J. Biochem. Technol.* 3 (4), 349–353.
- Talekar, S., Ghodake, V., Ghotage, T., Rathod, P., Deshmukh, P., Nadar, S., Mulla, M., Ladole, M., 2012b. Novel magnetic cross-linked enzyme aggregates (magnetic CLEAs) of alpha amylase. *Bioresour. Technol.* 123, 542–547. <http://dx.doi.org/10.1016/j.biortech.2012.07.044>.
- Tavec, P.F., 2011. Dyeing of environmentally friendly pretreated cotton fabric. In: Hauser, Peter (Ed.), *Textile Dyeing*. ISBN: 978-953-307-565-5, InTech, Available from: <http://www.intechopen.com/books/textile-dyeing/dyeing-of-environmentally-friendly-pretreated-cotton-fabric>.
- Tavec, P.F., 2012. Low-temperature bleaching of cotton induced by glucose oxidase enzymes and hydrogen peroxide activators. *Biocatal. Biotransformation* 30 (1), 20–26.
- Tavec, P.F., 2013. Effects of cellulase enzyme treatment on the properties of cotton tery fabrics. *FIBRES Text. East. Eur.* 21 (6), 100–106.
- Tavec, P.F., Krizman, P., Presa, P., 2006. Combined bio-scouring and bleaching of cotton fibres. *J. Nat. Fibers* 3 (2/3), 83–97.
- Tavec, P.F., et al., 2007. Pectinases as agents for bioscouring. *Tekstilac* 50 (1–3), 16–34.
- Teslaw, A., Assefa, F., 2014. Application of transglutaminase in textile, wool and leather processing. *Int. J. Text. Sci.* 3 (4), 64–69.
- Thiagarajan, P., Selvakumar, N., 2008. Cotton, Pectinolytic Enzymes and Enzymatic Scouring of Cotton, pp. 73–80. Colourage, May.
- Tischer, W., Kasche, V., 1999. Immobilized enzymes: crystals or carriers. *Tibtech* 17, 326–335.
- Tischer, W., Wedekind, F., 1999. Immobilized enzymes: methods and applications. *Top. Curr. Chem.* 200, 95–126.
- Traore, M.K., Buschle-Diller, G., 1999. Influence of wetting agents and agitation on enzymatic hydrolysis of cotton. *Text. Chem. Colorist Am. Dyest. Report.* 31 (4), 51–56.
- Traore, M.K., Buschle-Diller, G., 2000. Environmentally friendly scouring process. *Text. Chem. Colorist Am. Dyest. Report.* 32 (12), 40–43.
- Tzanov, T., Calafell, M., Guebitz, G.M., Cavaco-Paulo, A., 2001. Bio-preparation of cotton fabrics. *Enzyme Microbiol. Technol.* 29, 357–362.
- Tzanov, T., Costa, S.A., Guebitz, G.M., Cavaco-Paulo, A., 2002. Hydrogen peroxide generation with immobilized glucose oxidase for textile bleaching. *J. Biotechnol.* 93, 87–94.
- Tzanov, T., Andreaus, J., Guebitz, G., Cavaco-Paulo, A., 2003a. Protein interactions in enzymatic processes in textiles. *Electron. J. Biotechnol.* 6 (3), 146–154.
- Tzanov, T., Basto, C., Guebitz, G.M., Cavaco-Paulo, A., 2003b. Laccases to improve the whiteness in a conventional bleaching of cotton. *Macromol. Mater. Eng.* 288 (10), 807–810.
- Uddin, M.G., 2010. Determination of weight loss of knifabrics in combined scouring-bleaching and enzymatic treatment. *J. Innov. Dev. Strategy* 4 (1), 18–21.
- Uddin, M.G., 2016. Effect of biopolishing on dye ability of cotton fabric- a review. *Trends Green Chem.* 2 (1), 1–5. <http://dx.doi.org/10.21767/2471-9889.100011>.
- Ul-Haq, Nasir, H., 2012. Cleaner production technologies in desizing of cotton fabric. *J. Text. Inst.* 103 (3), 304–310.
- Usluoglu, A., Arabaci, G., 2014. Bleaching of Cotton/polyamide fabrics with enzymes and peracetic acid. *AsiaPacific J. Chem. Eng.* 9, 364–367. <http://dx.doi.org/10.1002/apj.1804>.
- Usluoglu, A., Arabaci, G., 2015. Bio-bleaching of Cotton/polyamide fabrics with different enzyme system at low temperature. *J. Multidiscip. Eng. Sci. Technol.* 2 (11), 3280–3284.
- Vaillant, F., Millan, A., Millan, P., Dornier, M., Decloux, M., Reynes, M., 2000. Co-immobilized pectinase and endocellulase on chitin and Nylon Supports. *Process Biochem.* 35, 989–996.
- Vasconcelos, A., Silva, C.J.S.M., Schroeder, M., Guebitz, G.M., Cavaco-Paulo, A., 2006. Detergent formulations for wool domestic washings containing immobilized enzymes. *Biotechnol. Lett.* 28, 725–731.
- Viet, T.Q., Minh, N.P., Dao, D.T.A., 2013. Immobilization of cellulase enzyme in calcium alginate gel and its immobilized stability. *Am. J. Res. Commun.* 1 (12), 254–267.
- Vigneswaran, C., Anbumani, N., Ananthasubramanian, M., Kandhavadi, P., 2013. Ecofriendly approach to improve pectinolytic reaction and process optimization of bioscouring of organic cotton textiles. *J. Eng. Fibers Fabr.* 8 (2), 121–133.
- Vilchez, S., Jovancic, P., Erra, P., 2010. Influence of chitosan on effects of proteases on wool fibres. *Fibers Polym.* 11 (1), 28–35.
- Robert, B. Waddell, 2002. Bioscouring of Cotton: Commercial Applications of Alkaline Stable Pectinase. AATCC Review, April, 28–30.
- Wadham, M., 1994. Bio-polishing of cellulosic fabrics. *J. Soc. Dye. Colour.* 110 (11), 367–368. <http://dx.doi.org/10.1111/j.14734408.1994.tb01599.x>.
- Waly, A.J., Marie, M.M., Shahin, M.F., Farouq, N.M.S., 2016. Effect of protease treatment on the physical properties and dyeability of wool/nylon blend to cutch natural dye. *IJSR* 5 (2), 1764–1770.
- Wang, Y., Caruso, F., 2005. Mesoporous silica spheres as supports for enzyme immobilization and encapsulation. *Chem. Mater.* 17 (5), 953–961.
- Wang, Q., Fan, X., Hua, Z., Gao, W., Chen, J., 2007. Degradation kinetics of pectins by an alkaline pectinase in bioscouring of cotton fabrics. *Carbohydr. Polym.* 67 (4), 572–575.
- Wang, Q., Fan, X., Hu, Y., Yuan, J., Cui, L., Wang, P., 2009. Antibacterial functionalization of wool fabric via immobilizing lysozymes. *Bioprocess Biosyst. Eng.* 32 (5), 633–639. <http://dx.doi.org/10.1007/s00449-008-0286-5>.
- Wang, W., Yu, B., Zhong, C., 2012. Use of ultrasonic energy in the enzymatic desizing of cotton fabric. *J. Clean. Prod.* 33, 179–182. <http://dx.doi.org/10.1016/j.jclepro.2012.04.010>.
- Waslter, T., Augusta, J., Muller, R.T., Widdecke, H., Klein, J., 1995. Enzymatic degradation of a model polyester by lipase from *Rhizopus delemar*. *Enzym Microbiol. Technol.* 17, 218–224.
- Wavhal, S.D., Balasubramanya, R.H., 2011. Role of biotechnology in the treatment of polyester fabric. *Indian J. Microbiol.* 51 (2), 117–123.
- Wehrschütz-Sigl, E., Hasmann, A., Guebitz, G.M., 2010. Smart textiles and biomaterials containing enzymes or enzymes substrates. In: Nierstrasz, V.A., Cavaco-Paulo, A. (Eds.), *Advances in Textile Biotechnology*. Woodhead publishing Ltd., Cambridge, pp. 171–192.
- Worsfold, P.J., 1995. Classification and chemical characteristics of immobilized enzymes. *Pure Appl. Chem.* 67 (4), 597–600.
- Yachmnev, V.G., Blanchard, E.J., Lambert, A.H., 2004. Use of ultrasonic energy for intensification of the bio-preparation of greige cotton. *Ultrasonics* 42 (1–9), 87–91.
- Yagub, M.T., Sen, T.K., Afroz, S., Ang, H.M., 2014. Dye and its removal from aqueous solution by adsorption: a review. *Adv. Colloid Interface Sci.* 209, 172–184.
- Yamada, M., Amano, Y., Horikawa, E., Nozaki, K., Kanda, T., 2005. Mode of action of cellulases on dyed cotton with a reactive dye. *Biosci. Biotechnol. Biochem.* 69 (1), 45–50. <http://dx.doi.org/10.1271/bbb.69.45>.
- Yin, H., Su, Z., Shao, H., Cai, J., Wang, X., Yin, H., 2013. Immobilization of Cellulase on modified mesoporous silica shows improved Thermal Stability and Reusability. *Afr. J. Microbiol. Res.* 7 (25), 3248–3253.
- Yu, Y., Yuan, J., Wang, Q., Fan, X., Ni, X., Wang, P., Cui, L., 2013. Cellulase immobilization onto the reversibly soluble methacrylate copolymer for denim washing. *Carbohydr. Polym.* 95 (2), 675–680.
- Zhang, Y., Xu, J., Yuan, Z., Qi, W., Liu, Y., He, M., 2012. Artificial intelligence

techniques to optimize the EDC/NHS-mediated immobilization of cellulase on Eudragit L-100. *Int. J. Mol. Sci.* 13, 7952–7962. <http://dx.doi.org/10.3390/ijms13077952>.

Zhou, J., 2010. Immobilization of cellulase on a reversibly soluble-insoluble support:

properties and application. *J. Agric. Food Chem.* 58, 6741–6746.

Zilz, L., Rao, M., Budag, N., Scharf, M., Cavaco-Paulo, A., Andraus, J., 2012. Nontoxic surfactants and dispersants for cellulase treatment of cotton textiles. *Color Technol.* 129, 49–54.

Moisture management and wicking properties of polyester- cotton plated knits

Yamini Jhanji^{1,a}, Deepti Gupta² & V K Kothari²

¹Department of Fashion & Apparel Engineering, The Technological Institute of Textiles & Sciences, Bhiwani 127 021, India

²Department of Textile Technology, Indian Institute of Technology Delhi, New Delhi 110 016, India

Received 6 February 2015; revised received and accepted 28 July 2015

Effect of yarn linear density on moisture management and wicking properties of polyester-cotton plated knit structures has been studied. Linear density of yarns used in inner and outer layer as well as the difference in the yarn linear density for the two layers have been found to affect the liquid transfer from inner to outer layer, liquid spreading in the outer layer and hence the drying ability of the designed fabrics. Wetting time increases, while decrease in absorption rate and spreading speed is observed with the increase in inner and outer layer yarn linear density. The fabrics are graded and classified based on the obtained moisture management indices. Trans planar wicking is found higher for fabrics with greater difference in linear density between inner and outer layers as a result of selection of finer yarns in inner layer.

Keywords: Knitting, Linear density, Moisture management, Plated knits, Wicking property, Polyester-cotton fabric

1 Introduction

Moisture management and wicking properties of textiles are very crucial as they control the movement of liquid moisture from skin through clothing to environment, and therefore can influence the overall wearer comfort especially in clothing intended for next to skin applications. The basic requirement of intimate wear, sportswear and active wear is rapid dissipation of moisture vapor and liquid sweat from the skin so as to provide dry feel next to skin. Plated knit structures, characterized by distinct inner (next to skin) and outer (exposed to environment) layers are fast becoming the preferred choice for next to skin applications owing to flexibility in the selection of contrastingly different fibre and yarn variables in the two layers. Yarn variables greatly determine the thermo-physiological properties and wearer comfort by the way they affect the amount of air trapped in the fabric assembly, the size of inter yarn spaces and the openness of fabric structure. Therefore, the various yarn parameters can help in controlling the extent to which a fabric transmits heat, moisture vapour and liquid moisture. Several researchers have studied the influence of yarn variables on comfort properties of different knit structures. Chidambaram *et al.*¹ studied the effect of yarn linear density on thermal comfort properties of bamboo knitted fabrics and observed

decrease in thermal resistance and an increase in air and water vapour permeability as the yarn gets finer. Similar observations were reported by Bivainyte and Mikucioniene², Bivainyte *et al.*³ and Ozdil *et al.*⁴. Ozturk *et al.*⁵ studied the influence of yarn count on wicking properties of cotton- acrylic yarns and fabrics and suggested that wicking ability of yarns and fabrics is increased with the increase in linear density of yarns. Das *et al.*⁶ studied the effect of yarn count on in-plane and vertical wicking of polyester-viscose blended fabrics and observed that wicking height and in-plane wicking of the fabrics are reduced with the increase in yarn fineness. Raja *et al.*⁷ investigated the influence of yarn linear density on liquid spreading of knitted fabrics and observed higher spreading rates for fabrics with low yarn linear density. The review of published literature suggests that the studies are primarily focused on the effect of yarn parameters on comfort properties of woven and knitted fabrics. However, there are very limited studies reporting the comfort characteristics of plated fabrics even though the structures are commercially gaining popularity as these structures can be specifically engineered with altogether different fibre and yarn components in the two distinct yet integrated layers. None of the studies report the influence of the difference in the linear density of yarns used in the two layers on liquid transfer from the inner layer and liquid spreading in the outer layer. Moreover there is lack of systematic literature available on the moisture management

^aCorresponding author.
E-mail: yjhanji@gmail.com

indices of the plated knits which give direct measure of liquid transfer from inner to outer layer and spreading of liquid in the two layers. In the view of foregoing, it is necessary to explore this field further to have clear insight into the ways in which liquid transfers and spreads in the two layers of the plated knits. The present study was, therefore undertaken to study the effect of yarn linear density on moisture management and wicking properties of polyester-cotton plated knits.

2 Materials and Methods

2.1 Materials

Cotton spun yarns of 29.5 (20s Ne), 33.3 (17.9s Ne) and 59.1 (9.9s Ne) tex and polyester filament yarns of 11.1 (100D/72), 16.6 (150D/72), 26.1 (235D/72) and 38.9 (350 D/72) tex were used for knitted sample production. Seven yarns in totality were used to knit five single jersey plated fabrics. All the five samples were knitted with cotton yarns of three varying linear density in the outer and polyester yarns of four varying linear density in the inner layer. Variation in inner and outer layer yarn linear density resulted in fabrics of different resultant yarn linear densities. Fabric cover factor for all the test samples was kept same by knitting the samples at constant machine settings.

The test samples were prepared on hand operated flatbed knitting machine (Elex, China) with machine gauge of 12, needle bed of 42 inch and 504 needles on each bed. The machine had two needle beds, namely front and rear. The front bed was utilized for sample preparation. Table 1 shows the details of prepared test samples.

2.2 Methods

2.2.1 Physical Properties

The thickness of fabrics was measured on Essdiel thickness gauge at a pressure of 20gf/cm² according to ASTM D 1777-96, 2007. Aerial density was

Table 1 — Fibre and yarn characteristics

Sample code	Fibre type		Yld, tex		Resultant Yld, tex	Outer & Inner layer Yld difference
	Outer	Inner	Outer	Inner		
PC ₁	C	PET	29.5	11.1	40.6	18.4
PC ₂	C	PET	29.5	16.6	46.1	12.9
PC ₃	C	PET	29.5	26.1	55.6	3.4
PC ₄	C	PET	59.1	26.1	85.2	33.0
PC ₅	C	PET	33.3	38.8	72.1	5.5

C — Cotton, PET — Polyester, Yld — Yarn linear density.

determined according to ASTM D-1059. A sample size of 10cm×10cm was cut and weighed on electronic weighing balance. Aerial density was obtained by dividing the weight of test sample with the area of the sample.

2.2.2 Moisture Management Properties

Moisture management tester (MMT) (SDL Atlas, Hong Kong) (AATCC Test method 195-2009) was used for testing the liquid moisture transfer properties of the fabrics. Moisture management tester is capable of determining liquid transfer through fabrics in multiple directions such as spreading of liquid outward on the inner surface of the fabric, liquid transfer through the fabric from the inner to the outer surface and spreading of liquid outward and evaporation from outer surface of fabric^{8,9,10}.

The following parameters were obtained from moisture management tester (MMT):

Wetting time WTt (top/inner) and WTb (bottom/outer) — Top and bottom wetting times are defined as time period in which inner and outer surfaces of the fabric begin to wet respectively after the test starts.

Absorption rate ARt (top/inner) and ARb (bottom/outer) — Top and bottom absorption rates are the initial slopes of the water content curves from wetting point to peak values on fabric inner and outer surfaces.

Spreading speed SSi (top/inner) and SSb (bottom/outer) — Top and bottom spreading speeds are the moisture spreading speeds on the inner and outer fabric surfaces to attain maximum wetted radius.

Accumulative one way transport index — Accumulative one way transport index (AOTI) is the difference in accumulated moisture between the inner and the outer fabric surfaces in the time period of test.

2.2.3 Wicking

Trans planar wicking (liquid absorption perpendicular to fabric plane) of test samples was determined by Gravimetric Absorbency Tester (GATS).

3 Results and Discussion

3.1 Moisture Management Properties

3.1.1 Top and Bottom Wetting Time

Top (WTt) and bottom (WTb) wetting time indicate the time taken by liquid to wet the inner (next to skin) and outer layers of the fabrics as the test commences. Figure 1 shows the top and bottom

wetting time for the test samples. It is observed that top and bottom wetting time increase with the increase in yarn linear density (PC₁ – PC₃) due to corresponding increase in fabric thickness and aerial density (Table 2). Test liquid takes longer time to traverse thicker fabrics as water has to go through more number of fibres during traversing assembly of coarse yarns and hence higher wetting time for coarser yarn fabrics. On the contrary, yarns of low linear density result in fabrics of low thickness and, in turn, low water retention capacity which would further result in fast liquid spreading behavior of fine yarn fabrics compared to their coarser yarn counterparts.

The fabrics show marginal difference in top and bottom wetting time except for PC₄ and PC₅ fabrics. PC₄ fabric is knitted with cotton of highest yarn linear density in the outer layer and PC₅ fabric with coarse

inner layer yarn and finer outer layer yarn. Top wetting time is higher than bottom wetting time for PC₅ fabric, the reason being higher linear density of inner layer yarn (polyester) compared to outer layer (cotton). Thus, the hydrophobic nature of fibre together with high yarn linear density restrict the wetting of inner layer rapidly. However, bottom wetting time is lower (2.8 s). As the inner layer of the fabric wets, the liquid transfer through capillary wicking is initiated. Hence, the wetting of inner layer is followed by liquid transfer by capillary wicking to outer layer which then immediately begins to wet and shows lower wetting time. PC₄ fabric, on the other hand shows opposite trend with bottom wetting time higher than top wetting time, and a great difference between the values of top and bottom wetting time is observed. This may be attributed to greater difference in yarn linear density of inner and outer layers (33 tex). Outer layer consists of coarse cotton yarn (59.1 tex) which takes 44.5 s to wet (Table 2) in spite of the hydrophilic nature of fibre. Grades for top wetting time ranges from medium to fast in top wetting time and slow to very fast in bottom wetting time (Table 3).

3.1.2 Top and Bottom Absorption Rate

Figure 2 shows the top (ARt) and bottom (ARb) absorption rates for the test fabrics. Top and bottom absorption rates decrease with the increase in yarn linear density due to increase in thickness and aerial density of PC₁- PC₃ fabrics. It is desirable that inner layer of fabrics intended for next to skin applications should have lower absorption rate so as to ensure dry

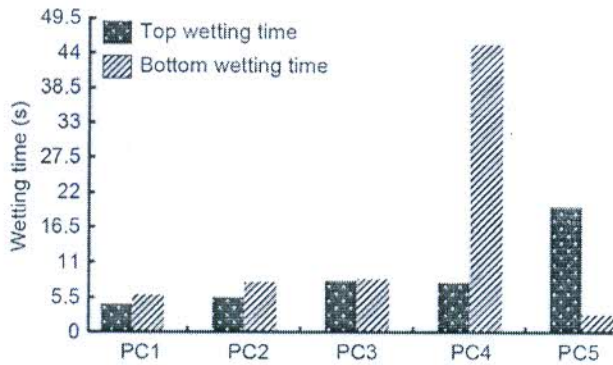


Fig. 1 —Effect of yarn linear density on top and bottom layers wetting time

Table 2 — Physical and Moisture management properties

Sample code	Aerial density g/m ²	Thickness mm	WTt s	WTb s	Art %/s	ARb %/s	SSt mm/s	SSb mm/s	AOTI
PC ₁	155	0.91	4.4	5.9	63	66.6	3.10	2.6	365.0
PC ₂	168	1.15	5.5	7.9	33	55.4	2.30	2.5	689.5
PC ₃	174	1.31	8.2	8.4	14	49.7	0.85	2.1	490.2
PC ₄	195	1.51	7.9	45.5	87.5	44.5	0.66	0.2	-15.9
PC ₅	182	1.42	19.8	2.8	197.4	53.7	0.25	1.6	964.9

WTt & WTb– Top & bottom wetting time, ART & ARb –Top & bottom absorption rate, SSt & SSb – Top & bottom spreading speed, AOTI– Accumulative one way transport index.

Table 3 — Grading of plated fabrics based on moisture management indices

Sample code	WTt s	WTb, s	Art, %/s	ARb, %/s	SSt, mm/s	SSb, mm/s	AOTI
PC ₁	Fast	Medium	Fast	Fast	Fast	Medium	Very good
PC ₂	Medium	Medium	Medium	Fast	Medium	Medium	Excellent
PC ₃	Medium	Medium	Slow	Medium	Very slow	Medium	Excellent
PC ₄	Medium	Slow	Fast	Medium	Very slow	Very slow	Poor
PC ₅	Medium	Very fast	Very fast	Fast	Very slow	Very slow	Excellent

feel next to skin. PC₅ fabric shows the highest top absorption rate followed by PC₄ fabric. Both the fabrics seem unsuitable for next to skin applications based on the findings of the study as high liquid absorption in the inner layer tend to saturate the next to skin layer with liquid slowing down the liquid transfer to outer layer and may result in feeling of skin wetness and discomfort. Bottom absorption rate is higher than top absorption rate for PC₁-PC₃ fabrics, suggesting that as these fabrics absorb less liquid in inner layer, they would remain dry next to skin. Bottom absorption rate is highest for PC₁ and lowest for PC₄ fabric. It has been reported that finer the inner layer yarn and greater the difference between inner and outer layer yarn linear density, better is the liquid transfer from the inner to the fabric's outer layer. PC₄ fabric although has greater difference in inner and outer layer yarn linear density (Table 1), it consists of coarser cotton yarn in the outer layer compared to PC₁ fabric. PC₁ fabric is knitted with finest polyester yarn in the inner layer and has the lowest resultant yarn linear density, thereby ensuring rapid liquid transfer by inner layer and high absorption in the outer layer. It can, therefore, be inferred that increasing the difference between inner and outer layer yarn linear density by use of finer yarn in inner layer rather than by increasing coarseness of outer layer yarn will result in enhanced liquid transfer properties. The test fabrics show slow to very fast grades in top absorption rate and medium to very fast grades in bottom absorption rates as shown in Table 3.

3.1.3 Top and Bottom Spreading Speed

Spreading speed of textiles is essential in determining the drying ability of textiles, as the fabric structures that can spread liquid over large areas, also facilitate liquid evaporation to the environment. Top (SS_t) and bottom (SS_b) spreading speeds are observed to decrease for PC₁ – PC₃ fabrics with the increase in

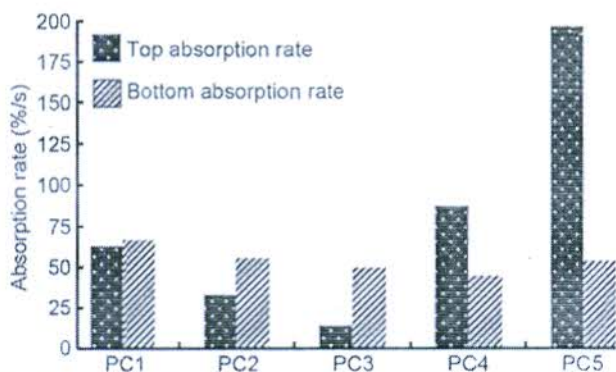


Fig. 2 — Effect of yarn linear density on top and bottom layers absorption rate

yarn linear density, as fabrics become thicker and heavier (Fig. 3). PC₁ fabric shows the highest value of top and bottom spreading speed, suggesting that the fabric provides large spreading area for liquid evaporation and hence would dry quickly. High spreading speed of PC₁ fabric may be attributed to low resultant yarn linear density and, in turn, low thickness and low wetting time, while low values of top and bottom spreading speed for PC₄ and PC₅ fabric may be attributed to high wetting time (Table 2). More time the fabric takes to wet, lesser would be its spreading speed and hence such fabric would take longer to dry. In the light of above argument, it can be said that both PC₄ and PC₅ fabrics would be slow drying fabrics.

3.1.4 Accumulative One Way Transport Index

Accumulative one way transport index (AOTI) gives a direct indication of fabric liquid transfer capability from inner to the outer layer. All the fabrics are graded very good to excellent in accumulative one way transport index except PC₄ fabric with poor grade and negative value of accumulative one way transport index, as shown in Fig. 4.

Based on the values and grades of moisture

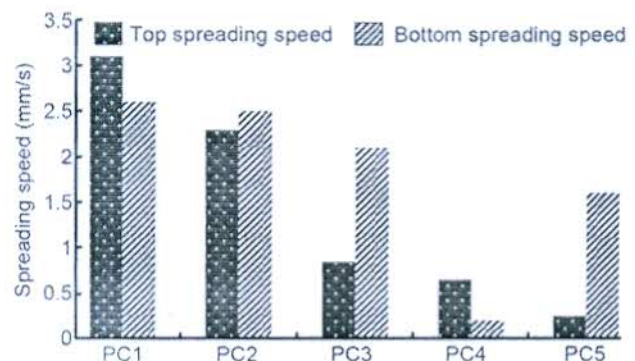


Fig. 3 — Effect of yarn linear density on top and bottom layers spreading speed

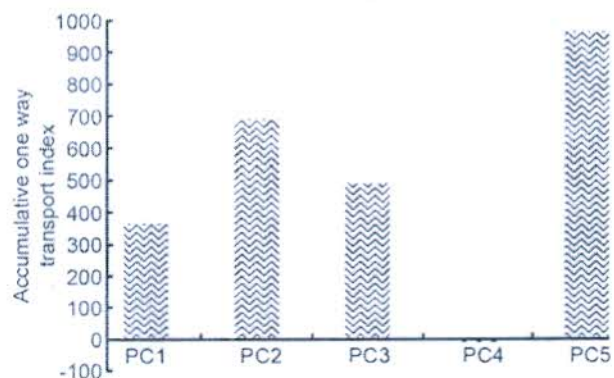


Fig. 4 — Effect of yarn linear density on accumulative one way transport index

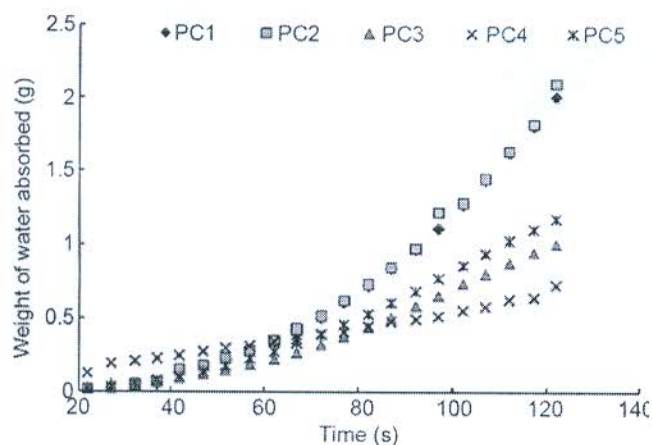


Fig. 5 — Effect of yarn linear density on trans planar wicking

management indices (Tables 2 and 3), the fabrics are classified into different categories. PC₁-PC₃ fabrics are classified as moisture management fabrics owing to high bottom spreading speed and excellent accumulative one way transport index. PC₄ fabric is classified as fast absorbing and slow drying fabric due to fast absorption in inner and outer layers, slow spreading and poor accumulative one way transport index. PC₅ fabric is classified as water penetration fabric due to small spreading area and excellent one way transport index.

3.2 Trans Planar Wicking

Figure 5 shows the trans planar wicking of the plated knits. Trans planar wicking is expected to increase with increase in yarn linear density. However, some exceptions from the trend are observed. PC₂ fabric shows the highest value of trans planar wicking which may be attributed to finer yarn in inner layer and coarser yarn in outer layer. This results in horizontal spread of liquid moisture in outer layer so that moisture is evenly distributed along this layer. Coarser yarns of outer layer increases liquid holding capacity and sinking effect, which, in turn, facilitates rapid transfer of liquid moisture from wearer's skin through inner layer to the fabric's outer layer. PC₄ fabric with greatest difference in inner and outer layer yarn linear density shows the lowest value of trans planar wicking because of coarsest cotton yarn in the outer layer; horizontal spread of liquid along the outer layer would be slow owing to more time taken to wet as suggested by high value of bottom wetting time (Table 2) even though the inner layer can pick up and transfer the moisture to outer layer. Thus, it can be inferred that there is an optimum yarn linear density and, in turn, capillary size which promote the liquid moisture transfer through wicking. Further

increase in yarn linear density may result in reduced capillary effect and hence the lower trans planar wicking.

4 Conclusion

4.1 Plated fabrics for next to skin applications can be designed with different yarn linear density in inner and outer layers. It can be inferred from the present study that fabrics knitted in plating relationship with combination of finer yarn in inner and coarser yarn in outer layer can effectively transfer liquid moisture towards outer layer owing to good moisture management and wicking properties.

4.2 Increase in inner and outer yarn linear density of plated fabrics results in increase in wetting time and decrease in absorption rate and spreading speed. Trans planar wicking increases with the increase in yarn linear density for fabrics within same range of resultant yarn linear density, although the fabrics with greater difference of linear density between inner and outer layers as a result of selection of finer yarns in inner layer show high value of trans planar wicking.

4.3 The fabrics are classified based on moisture management indices. PC₁-PC₃ fabrics are moisture management fabrics with good one way liquid transport, high absorption rate and spreading speed. The three fabrics are found suitable choice for next to skin applications owing to their ability to keep next to skin layer drier. PC₄ fabric is classified as fast absorbing and slow drying fabric while PC₅ fabric as water penetration fabric and hence both fabrics seem unsuitable in meeting the basic requirement of dry feel for next to skin clothing layer.

4.4 It is further observed that greater the difference in yarn linear density of inner and outer layer, the better is the liquid transfer from inner to outer layer by wicking, and better is the horizontal spread of transferred liquid in the outer layer. However, increasing the difference in yarn linear density by making the inner layer yarn finer rather than use of coarse yarn in outer layer results in better moisture management and wicking properties of plated fabrics.

4.5 Correct selection of inner and outer layer yarn linear density is therefore crucial for effective liquid transfer from inner to outer layers in plated fabrics intended for next to skin applications. The study therefore proposes designing of plated fabrics with fine hydrophobic yarn (polyester) preferably in the range of 11-26 tex and coarse hydrophilic yarn (cotton) preferably in the range of 29-33 tex, as such a

combination ensures dry feel next to skin by wicking of liquid moisture to outer layer without absorption in the inner (next to skin) layer. Likewise, the outer layer can absorb the transferred liquid and spread over larger area for quick evaporation to environment. It is also proposed that moisture management properties can be further improved by increasing the difference in yarn linear density of inner and outer layers preferably by increasing the fineness of inner layer yarn rather than increasing the coarseness of outer layer yarn.

References

- 1 Chidambaram P, Govindan R & Venkatraman K, *Autex Res J*, 11 (2011) 102.
- 2 Bivainyte A & Mikucioniene D, *Fibres Text East Eur*, 19 (2011) 69.
- 3 Bivainyte A, Mikucioniene D & Kerpauskas P, *Material Sci*, 18 (2012) 167.
- 4 Ozdil N, Marmarali A & Kretzschmar S, *Int J Therm Sci*, 46 (2007) 1318.
- 5 Ozturk M J, Nergis B & Candan C, *Text Res J*, 81 (2011) 324.
- 6 Das B, Das A, Kothari V K, Figueiro R & Araujo M, *J Text Inst*, 7 (2009) 588.
- 7 Raja D, Prakash C, Ramakrishnan G & Kaushik C V, *J Text Inst*, 105 (2014) 842.
- 8 Hu J Y, Li Y, Yeung K W, Wong A S & Xu W, *Text Res J*, 75 (2005) 57.
- 9 Yao B, Li Y, Hu J, Kwok Y & Yeung K, *Polym Test*, 25 (2006) 677.
- 10 Bedek G, Salaun F, Martinkouska Z, Devaux E & Dupont D, *Appl Ergon*, 42 (2011) 792.



Anthropometric Size Chart for Ethiopian Girls for Better Garment Design

Mulat Alubel, Manisha Yadav and Nagender Singh*

Abstract

Studies on anthropometric body measurements become very important because of the numerous garment fit problems the ready-to-wear industry is facing. The purpose of this paper was to create an anthropometric sizing system specifically for female Ethiopian secondary school aged 16-19 years in order to develop accurate systems for developing fitted and comfortable clothes. A total of 36 bodies measurements were taken based on international standards from various schools in Bahir Dar. Descriptive statistics has been applied to develop the sizing system by using SPSS (Statistical Packages for Social Science) and to obtain five sizes of a body measurement table. Correlations were also used to determine the relationship between the body dimensions and the selection of key dimensions for the size chart. A step by step procedure is used to generate size limits, size codes and various size charts. This pilot study has produced five main sizing systems to provide a reference for the design and production of different apparels including uniforms for Ethiopian high school girls. The study will highly benefit from the design and production of different apparels including uniforms for Ethiopian high school girls and serve as a guideline for Apparel manufacturers to generate proper sizing system.

Keywords

Anthropometric Survey; Sizing System; Garment Fit; Ethiopia

Introduction

Anthropometry is the study of the human body in both static and dynamic positions by which data are taken out from body measurement, which is very useful in various areas, such as anthropology, designing of functional garments, ergonomics, etc. Anthropometric data are important garment construction components for designing and producing high-quality garments. And garment fit is one of the main factors in the decision making of the customer. Designing garments with the right fit are related to taking accurate anthropometric data. The lack of updated anthropometric data is one of the major issues related with ill fitted garment [1].

Body size and shape, in all its variations, are very importance in ergonomic design and in improving the comfort and fit in clothing. Sizing systems are used to fit different groups of the population based on their demographic anthropometric data [2]. Different studies have been studied aimed at developing sizing standards for consumers' body shapes in the apparel industry [3].

Anthropology refers to the measurement of living human individuals for the purpose of understanding physical variation. The most notable differences in body size and shapes with respect to ethnic diversity, age, and gender. Sizing information is important to consumers, retailers, and manufacturers; poor sizing could lead to consumer dissatisfaction. Designers and manufacturers use anthropometric data to for appropriate fit dimensions in the manufacturing of. Based on the measurement of the average population, clothing manufacturers and retailers then devise and provide consumers with size code information on fit [4].

In principle, nobody proportions are standard, because as people get older, they become shorter and heavier. Ethiopian body proportions are characterized by short appendages and overly long torsos [5].

In Africa, measuring human body dimensions has been given limited attention though African body dimensions are significantly different from others. Due to this African people are being challenged with unfit garments and related products. According to one study, there is a significant difference for the same neck and waist measurement and other parts of the body measurement for Bahir Dar (Ethiopia) men as compare to European and US standard [6]. Also there is a significant difference in body measurements of Ethiopian men (age 18-26) depending on various regions and Ethnicity. According to Chan and Taylor study anthropometry is confined to width, length and girth measurements. Some anthropometric measurements are straightforward such as height or weight which is easy to gather but other parts of the body show complex geometry represent a tough challenge like faces, fingers, and feet. Anthropometry provides vital information for designing and developing of various products ranging from clothing to airplane seating [7]. It is stated that, during these surveys it was important to consider that the human body develops, grows and changes during the lifecycle by an increase in size, differentiation of structure and the alteration of shape [8]. There are a number of studies considering various parameters and countries which indicate different results in the field of sizing charts. So, clothing manufacturers and retailers should be responsible enough to study the body sizes and figure types of their consumers before they design and manufacture garments [9].

In Ethiopia, body measurements for an individual are made by Tailors, unlike western manufacturers. Therefore, an update and accurate anthropometry for Ethiopia-specific region's (like Bahir Dar) population is required to a larger extent. Nowadays people prefer readymade garments as they are easily available in different varieties and at cheaper prices. Moreover, the mass production brings the economics of scale which is very helpful for the garment industries [6]. Different countries have their own body dimensions by using that different garments are manufactured in short period of time and satisfy the demands of the customers.

Methodology

Standardization of body measurement is one of the very important aspects of the garment production for all over the world as there is a difference between countries anthropometry. So nowadays it becomes for improving garment fitness, mass production.

*Corresponding author: Nagender Singh, Lecturer, Ethiopian Institute of Textile and Fashion Technology, Bahir Dar University, P.O. Box 201, Bahir Dar, T. 42514/0944134. E-mail: angra.nagender@gmail.com

Received: March 03, 2017 Accepted: April 12, 2017 Published: April 16, 2017

Here, to determine the sample size, 95% of confidence level and 5% of margin of error were applied. Slovin's methods are used to calculate the sample size (n) given the population size (N) and margin of error (e).

It is computed as:

$$n = \frac{N}{1 + N e^2}$$

$n = 2806 / (1 + 2806 * 0.05^2)$ where margin of error is 5% and confidence level is 95%

$$n = 350$$

Only Amhara ethics were considered on the distribution of subject for the homogenous result. The distribution of the sample population for each school is shown in Table 1.

For each measurement dimension, three trials were taken, and the average value was recorded in the prepared record sheet. The subjects were barefooted, wearing thin T-shirts or uniform shirts and tights during the measurements.

Apparatus used

Among different body measurement systems, 3D body scanning technology (which is very sophisticated and expensive) and traditional measuring systems (simple and very cheap) are the most common methods. Even if the traditional measuring system is not accurate and reliable, the researcher used this body measurement method since it is simple, portable and inexpensive. The non-reliability of this method was minimized by using special equipment for different body dimensions. The body measurements were obtained with a small portable digital camera, a tripod, headboards, segmometer, and anthropometric measuring tapes to the nearest millimeter, digital caliper, portable weighing scales (0-125 kg), a meter scale, and ribbons for determining the landmarks of the body. Anthropometric tapes were calibrated periodically before use which was used to measure most of the body dimensions like height, length, width and circumference. The weighing scale also calibrated against standard weights.

Data Analysis

Data processing and analysis is carried out subsequently, by means of PC-based software which allows for the different body measurements taken to be automatically stored in a database.

The anthropometric data obtained from this study served as the basis of information for the analysis. The usefulness of anthropometric survey will depend on the extent to which these body measurements are transformed in key dimensions and used in solving design problems [10]. All the values were in centimeter except for weight

(in kg). Detailed statistical analysis of raw data was carried out using Statistical Package for the Social Sciences (SPSS). Descriptive statistics including mean, mode, median and standard deviation were calculated and utilized for the analysis of correlations. Coefficient Correlation was used in determining the relationships between the body dimensions. Multiple coefficient analyses helped in measuring the linear associations between two measurements.

Values used in the determination of correlations between the dimensions and identifying key parameters were based on BS 7231 (BSI, 1990). The standard specifies that; if the correlation coefficient is less than 0.5 then there is no relationship; if the correlation coefficient is between 0.6- 0.75 then there is a mild relationship; and if the correlation coefficient is more than 0.76 it shows a strong or high relationship.

Result and Discussions

The statistical values used for calculating the mean and standard deviation for the development of the size chart as shown in the Table 2. All the body dimensions are in inches except weight (kg) and the values of height which was measured in meters converted into inches for proper comparison. The mean is used for developing size step and it is the commonly used average value [11].

Size Range from Raw Data

The mean values and the standard deviation were used for creating size steps for the size chart. Five size steps approach was used to develop the size chart and to determine outliers. All values, which were below the values of the smallest and the largest sizes were eliminated and classified as outliers or extreme values. The five sizes were determined between the two values.

To obtain five steps for five categories of body sizes, one standard deviation (1SD) and two standard deviations (2SD) values are added to the mean to obtain two values that are higher than the mean. One standard deviation (-1SD) and two standard deviations (-2SD) values are subtracted from the mean sequentially to obtain two values that were less than the mean.

The mean value is the most widely used value for size steps and it is equivalent to the average size and the size 12 of every size chart. By subtracting one standard deviation and two standard deviation values (-1SD and -2SD) from the mean, size 8 and 10 are obtained as shown in Table 3. When one standard deviation value and two standard deviation values (+1SD and +2SD) are added, the values obtained are size 14 and size 16.

Table 1: The distribution of the sample population for each school.

No.	School Name	Owned	Total girl students	Percentage (100%)	Sample drawn
1	Bahir Dar Preparatory	Public	734	26.15	87
2	Gihon	Public	554	19.18	67
3	Tana	Public	674	24	81
4	Fasilo	Public	217	7.75	27
5	Ethio-Japan	Public	195	6.95	24
6	Bahir Dar Academy	Private	179	6.4	22
7	Catholic	Private	84	3	10
8	SoS	Private	37	1.3	5
9	Ayelech	Private	110	3.92	13
10	Horayzon	Private	22	0.8	3
	Total		2806	100%	339

Table 2: Represents the statistical values of mean, median and mode.

	Body dimensions	Mean	Median	Mode	Minimum	Maximum
1	Height	62.02	61.81	61.02	56.69	67.71
2	Neck	12.49115	12.5	12.5	1.625	14.5
3	Bust	33.31785	33	33	27.5	43
4	Waist	27.92441	28	28	12.5	37
5	Weight	50.42242	50	45	39	66
	Full length					
6	Full length (front)	15.56453	15.5	15.5	14.125	17.75
7	Full length (Back)	15.96425	16	16	1.755	18.25
	Centre length					
8	Centre front length	13.57448	13.5	13	11.5	15.125
9	Centre back length	14.94985	15	14	13.125	17
10	Shoulder length	6.206121	6.125	6	4	14
11	Bust radius	3.340118	3	3	2	4.5
12	Side length	7.913348	8	8	5.5	9.75
	Shoulder Slope (SS)					
13	Front SS	14.48532	14.5	14	11	17
14	Back SS	14.46681	14.125	14	7.75	17
	Across Shoulder					
15	Front	7.840487	7.5	7.5	5.625	10
16	Back	7.286136	7	6.5	5.375	9.5
17	Across chest	7.550516	7.375	7	5.5	9.5
18	Bust arc	7.435841	7.5	7.5	6	11.5
19	Bust span	4.123894	4	3.5	3	6
20	Across back	7.810841	7.5	7	5.25	9.5
21	Back neck	3.649336	3.5	3.5	2.875	4.5
22	Back Arc	7.549041	7.5	8	5	11.625
	Waist Arc					
23	Front	8.372788	8.5	9	6	11
24	Back	7.987094	8	9	5	12.5
	Lower Torso					
25	Abdomen circumference	30.81195	30.5	28.5	23.5	39
26	Hip circumference	35.32301	35	33	28.5	44.5
27	Side hip depth	8.145649	8	8	5.75	12
28	Waist to ankle	38.42367	38.5	38	8.625	45
	Hip Arc					
29	Front	8.391962	8.5	9	6	12.5
30	Back	9.404499	9.5	10	7	13.125
	Sleeve					
31	Biceps Circumference	10.14971	10	10	6	13
32	Elbow	10.8354	10.5	11	8.5	15.5
33	Fore arm circumference	9.03208	9	9	6	11
34	Wrist	6.519543	6.5	6	5.375	8.5
35	Sleeve length	20.51364	20.5	22	14.25	24.5
36	Under arm length	18.01024	18	18.5	11.625	21.5

Determination of Size Interval and Size Codes

The BS EN 13402-3 (2004) states that in order to accommodate variations in height by a country and company system, the 4cm or 8cm interval for women is standardized. The same standard also recommended an interval of 4cm or 6cm for both bust and waist and 4cm or 5cm for hip in order to have a flexible link between the bust, waist, and hip. there is variability of size interval some as low as 3cm and some as high as 8cm but the most logical one is an interval of 6cm and it is one which is used by most countries [12].

The size codes are based on the numeric coding method. In this

work, the size code was determined after generating five size steps values from the figure sizes. The new sizes code was termed (BD) abbreviated for Bahirdar and the code was added to establish the 5 size figures for Bahirdar preparatory school uniform. Therefore the new size codes are BD (8), BD (10), BD (12), BD (14), and BD (16). Figure 1 represents the upper and lower torso body measurement of size range from XS to XL. Figure 1(A-E) represents upper torso body measurements and figure 1(F-G) represents lower torso body measurements. Table 4(A-B) shows across shoulder and sleeve measurements of size range from XS to XL.

Table 3: Shows the size range from the raw data.

S.N.	Body Dimensions	XS (-2SD)	S (-1SD)	M	L (+1SD)	XL (+2SD)	SD
1	Height	61.67	61.74	61.81	61.88	61.95	0.07
2	Neck	10.8	11.6	12.5	13.4	14.2	0.86
3	Bust	27.3	30.4	33.3	36.3	39.3	2.98
4	Waist	23.3	25.6	27.9	30.3	32.6	2.35
5	Weight	38.66	44.54	50.42	56.3	62.18	5.88
Full Length							
6	Front	14	14.5	15.5	16.5	17	0.83
7	Back	13.7	14.8	15.964	16.8	17.9	1.14
Center Length							
8	Front	12	12.8	13.6	14.3	15.1	0.77
9	Back	13.4	14.1	14.9	15.7	16.6	0.81
10	Shoulder L	4.8	5.5	6.2	6.9	7.6	0.72
11	Bust Radius	2	2.7	3.3	3.9	4.6	0.62
12	Side Length	5.9	6.9	7.9	8.9	9.8	0.98
Shoulder Slope							
13	Front	12.9	13.7	14.5	15.3	16.1	0.86
14	Back	12.4	13.5	14.5	15.5	16.5	1.02
Across Shoulder							
15	Front	6.119	7.015	7.84	8.66	9.49	0.83
16	Back	5.198	6.242	7.286	8.33	9.374	1.04
17	Across Chest	5.71	6.63	7.55	8.47	9.39	0.92
18	Bust Arc	5.549	6.692	7.435	8.378	9.321	0.94
19	Bust Span	2.547	3.335	4.123	4.911	5.67	0.789
20	Back Arc	5.451	6.5	7.549	8.597	9.646	1.05
21	Across Back	5.914	6.862	7.81	8.758	9.706	0.95
22	Back Neck	2.9	3.3	3.6	4	4	0.40
Waist Arc							
23	Front	6.5	7.42	8.372	9.324	10.276	0.95
24	Back	5.857	6.922	7.987	9.052	10.117	1.07
Lower Torso							
25	Abdomen Cir	26	28.4	30.8	33.2	35.6	2.41
26	Hip Circum	29	32.1	35.3	38.5	41.7	3.19
27	Side Hip Depth	6.3	7.2	8.1	9	10	0.90
28	Waist To Ankle	33.6	36	38.4	40.8	43.2	2.40
Hip Arc							
29	Front	6.4	7.4	8.4	9.4	10.4	0.99
30	Back	7.516	8.46	9.407	10.348	11.292	0.94
Sleeve							
31	Sleeve Length	17.8	19.1	20.5	21.9	23.3	1.39
32	Under Arm Length	15.7	17	18.4	19.8	21.1	1.36
33	Biceps Circum.	8.2	9.2	10.14	11	12	0.96
34	Elbow Circum.	8.9	9.87	10.8	11.8	12.7	0.95
35	Fore Arm Circum.	7.25	8.14	9.03	9.93	10.8	0.89
36	Wrist	5.38	5.949	6.519	7.089	7.659	0.57

Table 4(A): - Shows upper torso body measurement (Across shoulder).

ACROSS SHOULDER	FRONT	BACK	ACROSS CHEST	BUST ARC	BUST SPAN	BACK ARC	ACROSS BACK	BACK NECK
Size 8	6.119	5.198	5.71	5.549	2.547	5.451	5.914	2.9
Size 10	7.015	6.242	6.63	6.692	3.335	6.5	6.862	3.3
Size 12	7.84	7.286	7.55	7.435	4.123	7.549	7.81	3.6
Size 14	8.66	8.33	8.47	8.378	4.911	8.597	8.758	4
Size 16	9.49	9.374	9.39	9.321	5.67	9.646	9.706	4

Determination of Lower and Upper Limits of Sizes

To establish the limit of each size and demonstrate the extent of coverage for inter size ranges, determination of lower and upper limit

is an important step. The lower and the upper limits are determined by subtracting or adding half value of the standard deviation of each body dimension to the midpoint value or mean. This procedure has

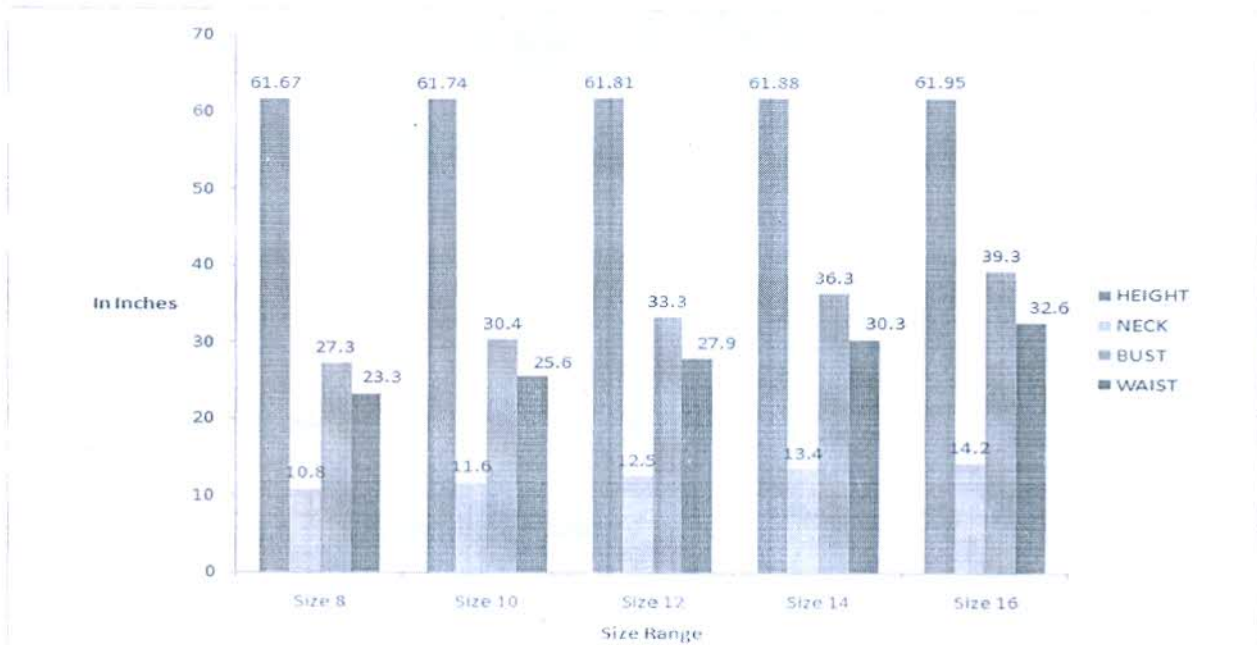


Figure 1(A): - Upper torso body measurement (Height, Neck, Bust and Waist).

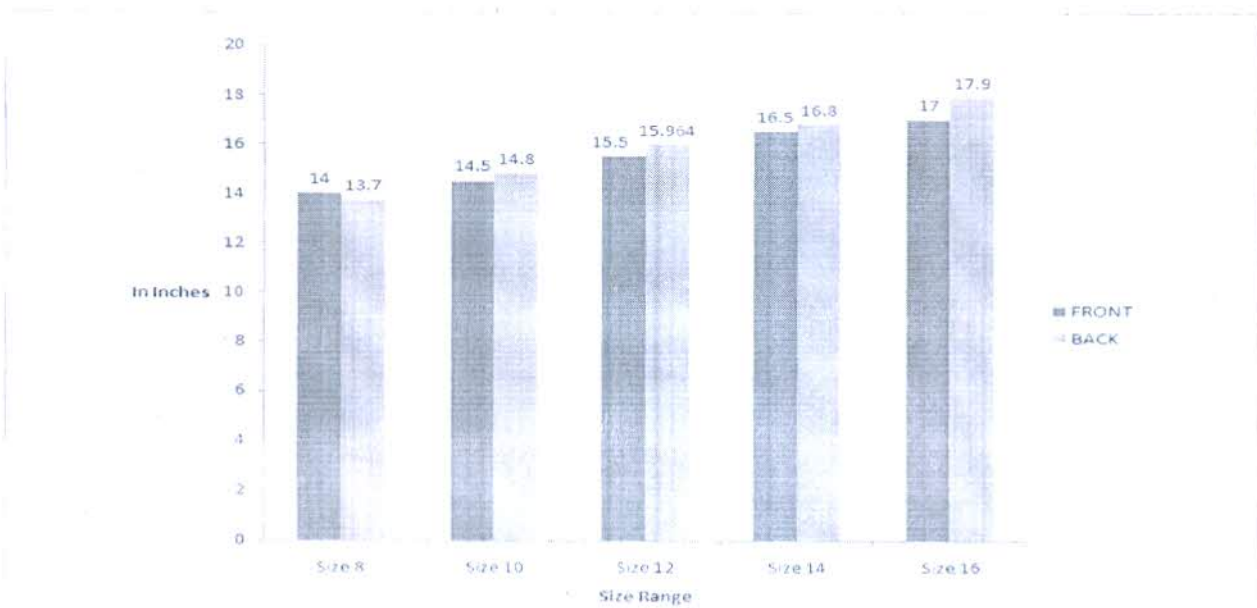
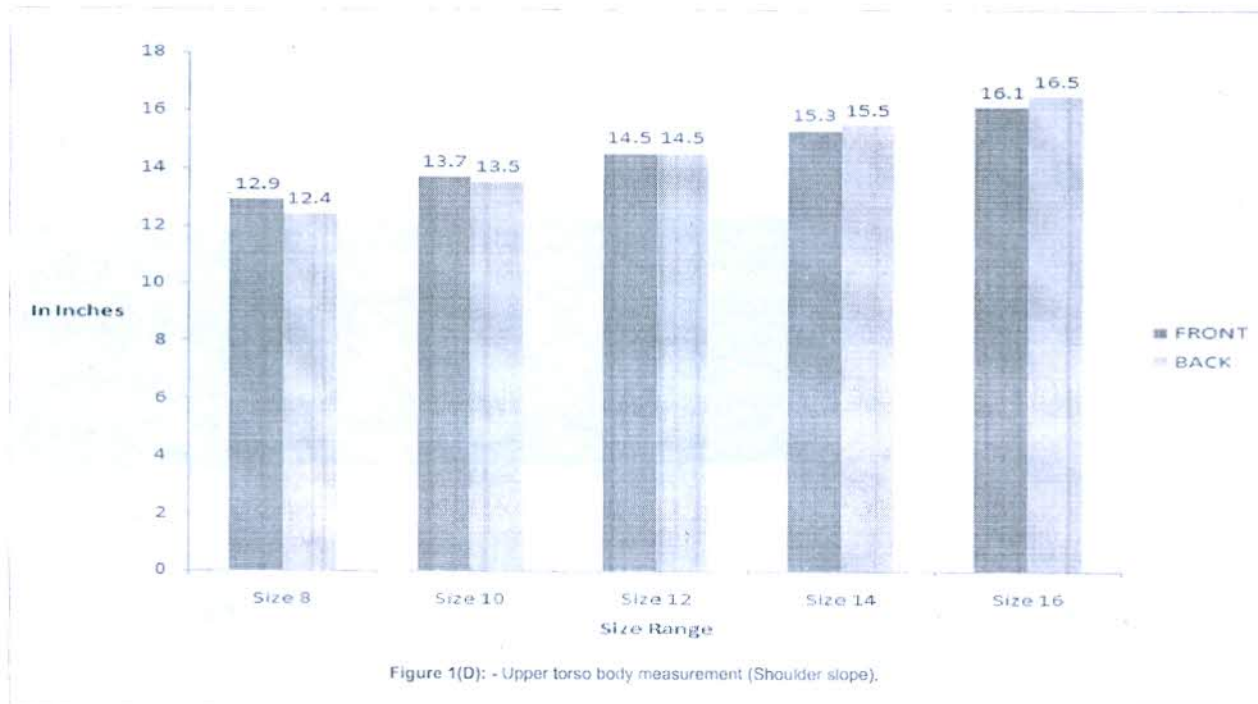
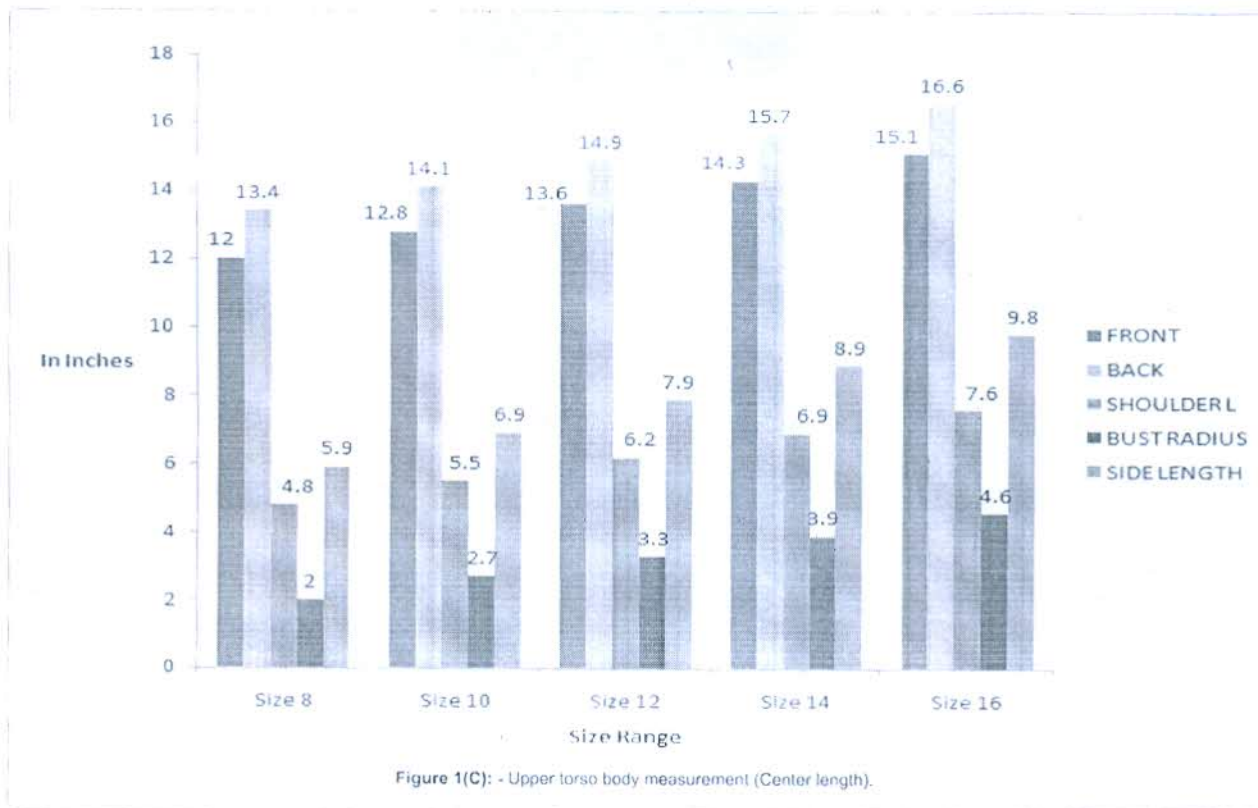
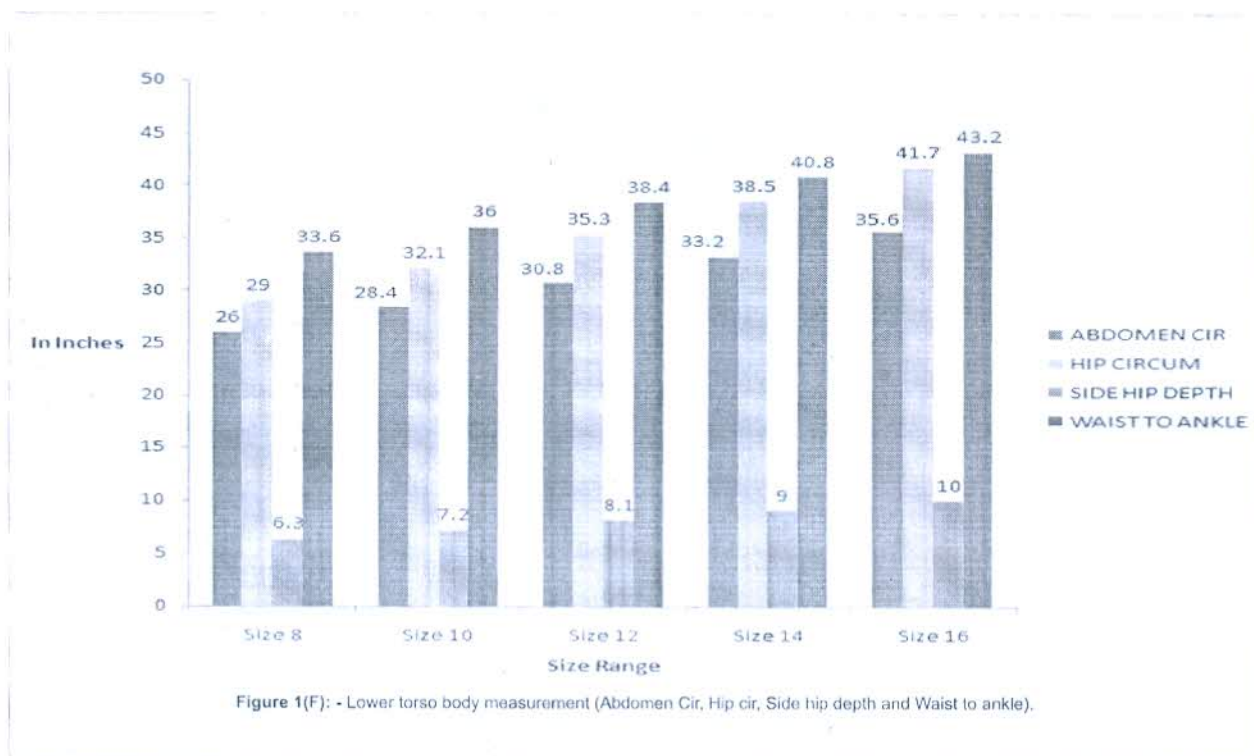
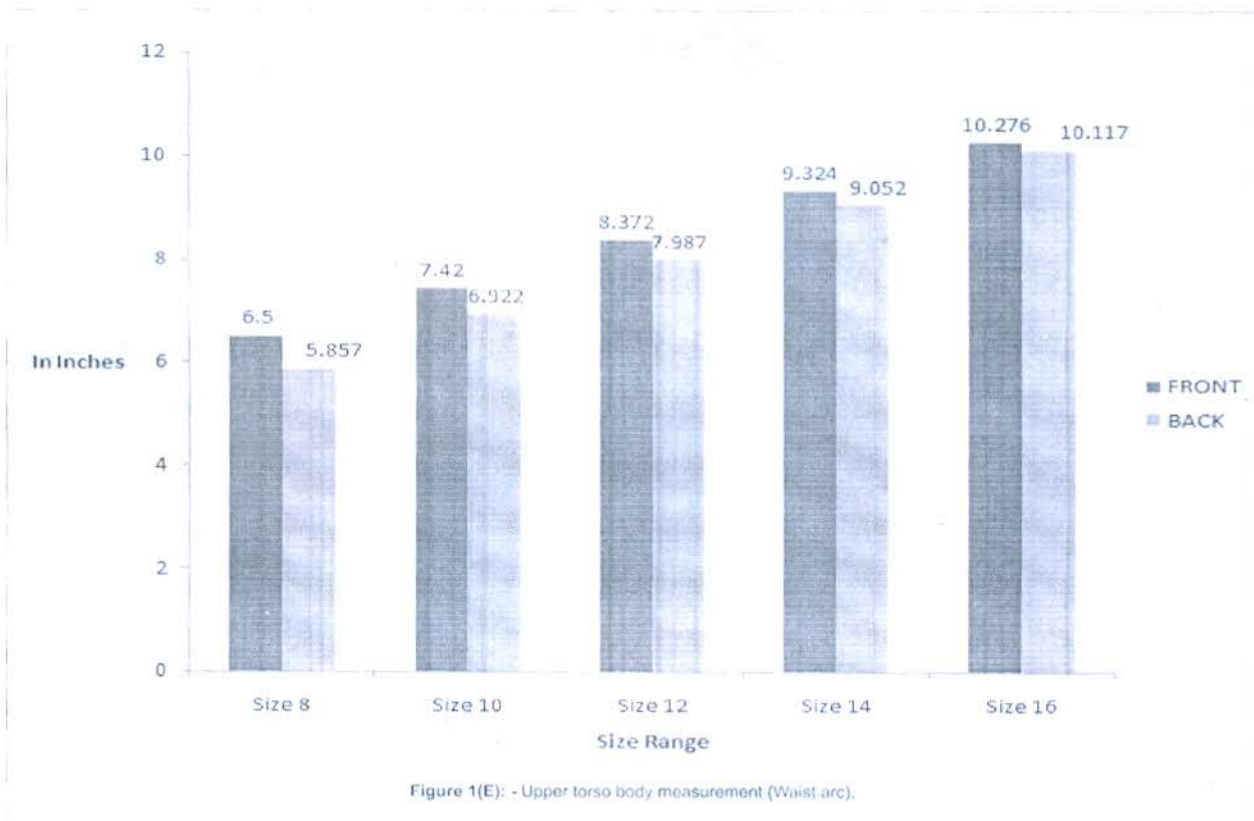


Figure 1(B): Upper torso body measurement (Full length).

Table 4(B): - Shows lower torso body measurement (Sleeve).

SLEEVE	Sleeve Length	Under Arm Length	Biceps Circum	Elbow Circum	Forearm Circu	Wrist
Size 8	17.8	15.7	8.2	8.9	7.25	5.38
Size 10	19.1	17	9.2	9.87	8.14	5.949
Size 12	20.5	18.4	10.14	10.8	9.03	6.519
Size 14	21.9	19.8	11	11.8	9.93	7.089
Size 16	23.3	21.1	12	12.7	10.8	7.659





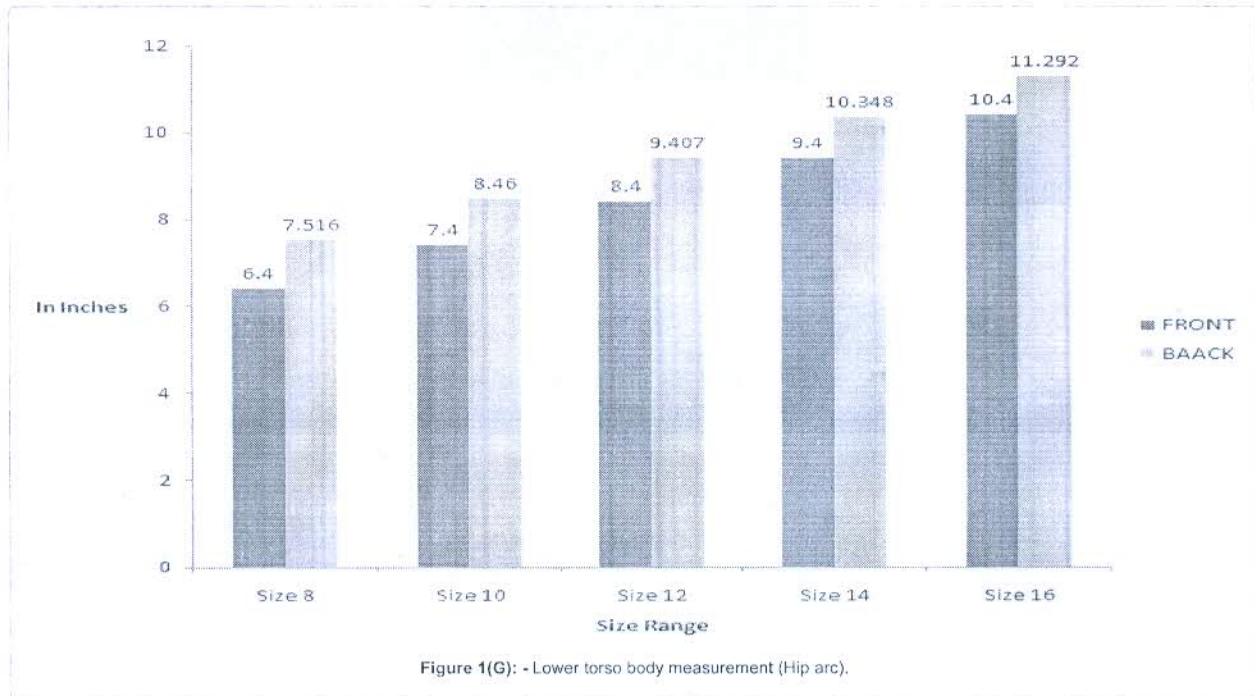


Table 5: The lower limit, midway point and upper limit of all body dimension.

S.N.	BD (size 8)	BD (Size 10)	BD (Size12)	BD (Size 14)	BD (Size 16)	SD	BD (size 8)
1	Height	61.17	61.24	61.31	61.38	61.45	0.07
		61.67	61.74	61.81	61.88	61.95	
		62.16	62.23	62.3	62.37	62.44	
2	Neck	10.37	11.17	12.07	12.97	13.77	0.86
		10.8	11.6	12.5	13.4	14.2	
		11.22	12.02	12.92	13.82	14.62	
3	Bust	25.81	28.9	31.9	34.79	37.79	2.98
		27.3	30.4	33.3	36.3	39.3	
		28.78	31.89	34.78	37.78	40.78	
4	Waist	22.13	24.47	26.77	29.07	31.47	2.348
		23.3	25.6	27.9	30.3	32.6	
		24.46	26.76	29.06	31.46	33.76	
5	Weight	35.66	41.54	47.42	53.3	59.18	5.88
		38.66	44.54	50.42	56.3	62.18	
		41.65	47.53	53.41	59.29	65.17	
6	Full Length Front	15.58	14.08	15.08	16.08	16.58	0.825
		14	14.5	15.5	16.5	17	
		14.4	14.9	15.9	16.9	17.4	
7	Back	13.13	14.23	15.34	15.93	17.33	1.135
		13.7	14.8	15.964	16.8	17.9	
		14.25	15.35	16.52	17.36	18.45	
8	Center Length Front	11.616	12.38	13.18	13.98	14.68	0.768
		12	12.8	13.6	14.3	15.1	
		12.37	13.17	13.97	14.67	15.47	
9	Back	12.99	13.69	14.49	15.29	16.19	0.808
		13.4	14.1	14.9	15.7	16.6	
		13.79	14.49	15.29	16.09	16.99	

10	Shoulder Length	4.44	5.14	5.84	6.54	7.24	0.72
		4.8	5.5	6.2	6.9	7.6	
		5.15	5.85	6.55	7.25	7.95	
11	Bust Radius	1.691	2.391	2.99	3.591	4.291	0.619
		2	2.7	3.3	3.9	4.6	
		2.299	2.99	3.59	4.19	4.89	
12	Side Length	5.41	6.41	7.41	8.41	9.31	0.977
		5.9	6.9	7.9	8.9	9.8	
		6.37	7.37	8.37	9.37	10.27	
13	Shoulder Slope Front	12.49	13.29	14.09	14.89	15.69	0.815
		12.9	13.7	14.5	15.3	16.1	
		13.29	14.09	14.89	15.69	16.49	
14	Back	11.88	12.98	13.9	14.9	15.9	1.02
		12.4	13.5	14.5	15.5	16.5	
		12.9	14	15	16	17	
15	Across Shoulder Front	5.7	6.603	7.428	8.248	9.078	0.825
		6.119	7.015	7.84	8.66	9.49	
		6.52	7.417	8.24	9.062	9.882	
16	Back	4.676	5.72	6.764	7.808	8.852	1.044
		5.198	6.242	7.286	8.33	9.374	
		5.71	6.754	7.798	8.842	9.886	
17	Across Chest	5.25	6.17	7.09	8.01	8.93	0.92
		5.71	6.63	7.55	8.47	9.39	
		6.16	7.08	8	8.92	9.84	
18	Bust Arc	5.078	6.221	6.964	7.907	8.85	0.943
		5.549	6.692	7.435	8.378	9.321	
		6.01	7.153	7.896	8.839	9.782	
19	Bust Span	2.153	2.94	3.729	4.512	5.276	0.7889
		2.547	3.335	4.123	4.911	5.67	
		2.931	3.719	4.507	5.295	6.054	
20	Back Arc	4.927	5.976	7.025	8.073	9.132	1.0486
		5.451	6.5	7.549	8.597	9.646	
		5.965	7.014	8.063	9.111	10.16	
21	Across Back	5.44	6.388	7.336	8.284	9.232	0.948
		5.914	6.862	7.81	8.758	9.706	
		6.378	7.326	8.274	9.404	10.17	
22	Back Neck	2.7	3.1	3.4	3.8	3.8	0.4
		2.9	3.3	3.6	4	4	
		3.09	0.49	3.79	4.19	4.19	
23	Waist Arc Front	6.024	6.944	7.896	8.848	9.8	0.952
		6.5	7.42	8.372	9.324	10.276	
		6.966	7.886	8.838	9.79	10.742	
24	Back	5.325	6.39	7.455	8.52	9.585	1.065
		5.857	6.922	7.987	9.052	10.117	
		6.379	7.44	8.509	9.574	10.639	
25	Lower Torso Abdomen Cir	24.798	29.602	29.598	31.998	34.398	2.405
		26	28.4	30.8	33.2	35.6	
		27.192	29.592	31.992	34.392	36.792	
26	Hip Circum.	27.41	30.59	33.69	36.91	40.11	3.185
		29	32.1	35.3	38.5	41.7	
		30.58	33.68	36.88	40.08	43.28	
27	Side Hip Depth	5.85	6.75	7.65	8.55	9.55	0.9
		6.3	7.2	8.1	9	10	
		6.74	7.64	8.54	9.44	10.44	

28	Waist To Ankle	32.4	34.8	37.2	39.6	42	2.4
		33.6	36	38.4	40.8	43.2	
		34.79	37.19	39.59	41.99	44.39	
Hip Arc							
29	Front	5.902	6.902	7.902	8.902	9.902	0.996
		6.4	7.4	8.4	9.4	10.4	
		6.888	7.888	8.888	9.888	10.888	
30	Back	7.044	7.988	8.935	9.876	10.82	0.944
		7.516	8.46	9.407	10.348	11.292	
		7.978	8.922	9.869	10.81	11.292	
Sleeve							
31	Sleeve Length	17.106	18.406	19.806	21.206	22.606	1.388
		17.8	19.1	20.5	21.9	23.3	
		18.484	19.784	19.816	22.584	23.984	
32	Under Arm Length	15.02	16.323	17.723	19.123	20.423	1.355
		15.7	17	18.4	19.8	21.1	
		16.367	17.667	19.067	20.467	21.767	
33	Biceps Circum.	7.722	8.722	9.662	10.522	11.522	0.957
		8.2	9.2	10.14	11	12	
		8.668	9.668	10.608	11.468	12.468	
34	Elbow Circum.	8.425	9.395	10.325	11.325	12.225	0.951
		8.9	9.87	10.8	11.8	12.7	
		9.365	10.335	11.265	12.265	13.165	
35	Fore Arm Circum.	6.81	7.7	8.59	9.49	10.36	0.89
		7.25	8.14	9.03	9.93	10.8	
		7.68	8.57	9.46	10.36	11.23	
36	Wrist	5.1	5.669	6.239	6.809	7.379	0.57
		5.38	5.949	6.519	7.089	7.659	
		5.65	6.219	6.789	7.359	7.929	

been used by many researchers. A value of 0.01 is subtracted from the upper limit making it less than the next value to avoid overlapping. It is important to determine the lower and the upper limit to know what percentages of the population are covered by each size [13]. The lower limit, midway point and an upper limit of all the body dimensions have been tabulated in Table 5.

Validation of Size Chart

To make it more acceptable the verification of the developed size chart is important. Validation is carried out by developing garments and by taking their trials. So, Prototype garments were constructed for the trial purpose by developing patterns using final size chart. For establishing the garment measurement ease allowance is added to each body dimension because in the developed size chart ease allowance were not added. Basic garments were prepared like skirts, trousers, shirts. The fitting trials were carried out using life models. They wore the prototype garments for 30-40 minutes. Five subjects were selected for fitting trails for each size. Height, bust, waist and hip are the key dimensions used for the study for trails. The subjects wore the trial garment over undergarments were the same as that used for the anthropometric survey for the fit evaluation.

The researcher recorded the visual observations based on the movement of the subjects and overall fit while standing, sitting and walking position. The relation between the subjects and prototype garments were justified.

Conclusion

The verification of the developed size chart demonstrated that the majority of participants had a good fit and most of the girls were falling

within 10 -14 sizes i.e. short to large sizes. The development of the size chart will facilitate manufacturing strategies for the production of ready-to-wear clothing for Ethiopian girls. The size range of the size charts covers 90-95% of girls and majority of them indicate that they were satisfied with the garment fit. This study recommends that further anthropometric studies should be conducted to cover all age categories of women/girls as well as males as they can serve as a database for sizing in the Ethiopian garment Industries.

References

- Gupta D, Gupta D, Zakaria N (2014) Anthropometry and the design and production of apparel. an overview. *Apparel Sizing and Design* 34-66.
- Ashdown SP (1998) An investigation of the structure of sizing systems: A comparison of three multidimensional optimized sizing systems generated from anthropometric data with the ASTM standard D5585-94. *Int J Cloth Sci Tech* 10: 324-341.
- Armstrong HJ (1987) *Pattern marking for fashion designer*. Harper Collins, New York, USA.
- Olieno R (2008) Approaches in researching human measurement: MMU model of utilising anthropometric data to create size charts. *EuroMed Journal of Business* 3: 63-82.
- Paquette S, Blackwell C, Hall RM, Gordon (2014) US army anthropometric survey: anthropometric models to optimize the human systems interface (ANSUR II). U11-211.C.C. (2014)
- Beshah B, Belay B, Tizazu STB, Matebu A (2014) Anthropometric data of Bahirdar Citys adult men for clothing design. *Int J Voc Tech Educ* 6: 51-57.
- Mehre A, Olieno AO, Mekonnen H, Lema O, Fera O, et al. (2016) Developing Standard Size Charts for Ethiopian Men between the ages of 18-26 through

Anthropometric Survey. *Journal of Textile and Apparel, Technology and Management* 10.


8. Harrison GA, Kuchemann CF, Moore MAS, Boyce A, Bajju T, et al. (1969). The effects of altitudinal variation in Ethiopian populations. *Philosophical Transactions of the Royal Society of London B: Biological Sciences* 256: 147-182.
9. Beazley A (1997) Size and fit: Procedures in undertaking a survey of body measurements. *Journal of Fashion Marketing and Management: An International Journal* 2: 55-85.
10. Kemsley K (1957) *Women's measurements and sizes*. HMSO, London, England.
11. Gupta D, Gangadhar BR (2004) A statistical model for developing body size charts for garments. *Int J Cloth Sci Tech* 16: 458-469.
12. Aldrich W (2008) *Metric pattern cutting*. 8th edition, Blackwell Publishing, Oxford, USA.
13. Adu-Boakye S, Power J, Wallace T, Chen Z (2012) Development of a sizing system for Ghanaian Women for the Production of Ready-to-Wear Clothing. University of Huddersfield, UK.

Author Affiliations

Top

Ethiopian Institute of Textile and Fashion Technology, Bahir Dar University, P.O. Box 26, Ethiopia

Submit your next manuscript and get advantages of SciTechnol submissions

- ❖ 80 Journals
- ❖ 21 Day rapid review process
- ❖ 3000 Editorial team
- ❖ 5 Million readers
- ❖ More than 5000 
- ❖ Quality and quick review processing through Editorial Manager System

Submit your next manuscript at www.scitechnol.com/submission

Effect of fibre, yarn and fabric variables on heat and moisture transport properties of plated knit

Y Jhanji^{1,a}, D Gupta² & V K Kothari²

¹Department of Fashion & Apparel Engineering, The Technological Institute of Textiles & Sciences, Bhiwani 127 021, India

²Department of Textile Technology, Indian Institute of Technology Delhi,
Hauz Khas, New Delhi 110 016, India

Received 6 January 2015; revised received and accepted 14 August 2015

In this study, the effect of fibre, yarn and fabric variables on heat and moisture transport properties of single jersey plated fabrics has been studied. Thermal properties, air permeability as well as moisture vapor and liquid transport properties of fabrics are found to be affected by fibre types, yarn linear density and fabric loop length. Slack fabrics knitted at longer loop length and with finer yarns in the inner layer show lower thermal insulation and are suitable choice as summer wear due to improved permeability of fabrics to air and moisture vapor. Cotton/viscose fabrics show better liquid transport properties along with the highest air and moisture vapor permeability, thereby resulting in rapid liquid dissipation and dry feel next to skin. The designed fabrics are thus suitable for use when an individual is involved in strenuous physical activity.

Keywords: Cotton, Heat transport, Moisture transport, Nylon, Permeability, Plated knit, Polyester, Single jersey fabric, Slack fabric, Thermal properties, Viscose fabric

1 Introduction

Heat and moisture transport properties of functional clothing, like active wear, sportswear and intimate wear are very crucial in providing dry skin micro climate and comfortable environment to the wearer by influencing the clothing's ability to manage heat, moisture vapor and liquid transfer. Wicking and wetting are the two main phenomena which govern the moisture transport properties of textiles. Wicking refers to displacement of a solid-air interface with a solid-liquid interface in a capillary system. Wettability is the initial behavior of a fabric, yarn, or fibre when brought into contact with a liquid and describes the interaction between the liquid and the solid surface prior to the wicking process¹.

Several fibre, yarn and fabric parameters are reported to influence the wetting and wicking behavior of textiles, as they influence the size and geometry of the capillary spaces between the fibres. The liquid transport properties of textiles are primarily influenced by the type of fibres, orientation of molecules, surface finish, cross-sectional shape, surface roughness, yarn structure, yarn tension, yarn twist, fibre shape, number of fibres in yarns, fibre

configuration, finish and surfactants. Wicking rate and liquid transported in a fabric also depend on the pore sizes and their size distribution. The capillary principle dictates that smaller pores are completely filled first and then are responsible for the liquid front movement. As the smaller pores are completely filled, the liquid then moves to the larger pores¹.

Plated knit structure is a double layered construction characterized by distinct inner (next to skin) and outer (exposed to the environment) layers. The two layers can be designed and engineered with different combinations of fibres and yarns, thereby ensuring that structures can serve different roles in providing wearer comfort. A combination of natural and synthetic fibre yarns is an optimal solution for designing plated knits intended to provide dry feel next to skin.

Natural and synthetic fibres owing to the difference in moisture absorption and liquid moisture transfer properties have the potential to influence moisture vapor as well as liquid moisture transfer through fabrics. Selection of fibre and yarn combinations in the two layers can have a great bearing on the comfort properties, performance, aesthetic appeal and end use of the knit structures.

Cotton has good permeability to water vapor and air, so it is recommended for summer garments but is

^aCorresponding author.
E-mail: yjhanji@gmail.com

not a preferred choice as next to skin layer due to skin clinginess and slow drying property²⁻⁶. On the other hand, synthetic fibres such as polyester, polypropylene and nylon being hydrophobic have an additional advantage of liquid transport and release by capillary wicking without liquid retention^{2, 7, 8}.

Several researchers have studied the effect of fibre, yarn and fabric parameters on comfort properties of knitted fabrics. Majumdar *et al.*⁹ studied the thermal properties of knitted fabrics made from natural and regenerated bamboo cellulosic fibres and observed that air and water vapor permeability increased but thermal conductivity decreased as the proportion of bamboo fibre increased. Bivainyte *et al.*³ investigated the thermal properties of double layered fabrics knitted of cotton, bamboo and four types of synthetic threads. They found that fabrics knitted from yarns of cotton and synthetic fibres have higher thermal conductivity coefficient than those knitted from bamboo and synthetic yarns. Chidambaram *et al.*¹⁰ studied the thermal comfort properties of bamboo knitted fabrics in relation to yarn linear density and observed that as the yarn gets finer, thermal resistance decreases and air and water vapor permeability increases. Similar observations were reported for double layered weft knitted fabrics by Bivainyte *et al.*³ and Ozdil *et al.*¹¹ in their studies on rib fabrics. Chidambaram *et al.*¹⁰ studied the effect of loop length on thermal comfort properties of bamboo knitted fabrics and observed an increase in air and water vapor permeability with the increase in loop length. Herath¹² observed that fabric tightness is correlated with air permeability, aerial density and fabric thickness. Fabrics knitted with lower loop length showed higher thickness & weight, and lower air permeability. Kumar and Das¹³ suggested that tightness of knitted fabric structure affected the wicking nature of fabrics with tighter fabrics showing lesser amount of vertical wicking compared to loose fabrics.

Studies are mainly focused on the effect of fibre, yarn and fabric constructional variables on comfort properties of single and double jersey structures, however there is lack of detailed and systematic studies on plated knits although the structures are fast becoming preferred choice as inner wear and intimate wear. Limited studies are devoted on the effect of inner layer fibre, yarn and fabric parameters on heat and moisture transport properties of plated fabrics even though the type of fibre and yarn used in the inner (next to skin) layer can greatly influence heat,

moisture vapor and liquid transport to the outer fabric layer. In the view of foregoing, it becomes inevitable to examine the influence of different combinations of fibre, yarn and fabric variables in the two layers of plated knits which has not been reported explicitly so far. The present study is therefore, undertaken to draw some concrete conclusions regarding the effect of fibre, yarn and fabric variables in the distinct layers of plated knits on heat and moisture transport properties.

2 Materials and Methods

2.1 Materials

Cotton spun yarn (Ne 20), and filament yarns of polyester (250D/100, 100D/100 and 200D/200), nylon (70D/20) and viscose (40D/100 and 80D/200) were used for the preparation of twelve single jersey plated knit samples (Table 1). Cotton yarn was used in the outer layer while filament yarns of three varying fibre types were used in the inner (next to skin) layer in all the test samples. Of the total twelve test samples, nine samples (CP1- CP3, CN1- CN3 and CV1-CV3) were knitted at three levels of loop length to obtain tight, medium and slack structures (Table 2).

The test samples were prepared on hand-operated flatbed knitting machine (Elex, China) with machine gauge of 12, needle bed of 42 inch and 504 needles on each bed. The machine had two needle beds – front and rear. The front bed was utilized for sample preparation.

2.2 Methods

The test samples were washed with 1% (w/v) nonionic detergent (Lisapol N) at 40°C for 30 min followed by tumble drying for 30 min.

Table 1 — Experimental Plan for sample preparation

Sample code	Fibre content in IL/OL	Yarn D in IL den	Number of filaments in IL	Yarn D in OL Ne	Resultant yarn D tex
CP ₁	PET/C	250	100	2/40	57.3
CP ₂	PET/C	250	100	2/40	57.3
CP ₃	PET/C	250	100	2/40	57.3
CP ₄	PET/C	100	100	2/40	40.6
CP ₅	PET/C	200	200	2/40	51.7
CN ₁	N/C	70	20	2/40	37.3
CN ₂	N/C	70	20	2/40	37.3
CN ₃	N/C	70	20	2/40	37.3
CV ₁	V/C	40	100	2/40	34.0
CV ₂	V/C	40	100	2/40	34.0
CV ₃	V/C	40	100	2/40	34.0
CV ₄	V/C	80	200	2/40	38.4

IL – Inner layer, OL – Outer layer, D – linear density, PET – polyester, C – Cotton, N – nylon, V – Viscose.

Table 2 — Physical properties of single jersey plated fabrics

Sample code	Aerial density g/m ²	Thickness mm	Courses/ cm	Wales/ cm	Loop length mm	Tightness factor
CP ₁	259	1.34	7.87	7.08	4.8	15.7
CP ₂	239	1.33	8.66	6.29	5.0	15.1
CP ₃	233	1.33	8.66	6.29	5.2	14.5
CP ₄	132	0.80	7.87	5.51	4.8	13.3
CP ₅	213	0.94	7.87	5.51	4.8	15.0
CN ₁	242	1.31	8.66	7.87	4.8	12.7
CN ₂	239	1.30	8.66	7.87	5.0	12.2
CN ₃	231	1.27	9.44	7.87	5.2	11.7
CV ₁	182	0.93	7.87	6.29	4.8	12.1
CV ₂	152	0.88	7.87	5.51	5.0	11.6
CV ₃	133	0.85	8.26	5.51	5.2	11.2
CV ₄	143	1.04	8.66	5.51	5.2	11.9

2.2.1 Physical Characterization of Test Samples

Aerial density, determined according to ASTM D-1059, was obtained by dividing the weight of test sample with the area of the sample. The thickness of fabrics was determined on Essdiel thickness gauge at a pressure of 20gf/cm² according to ASTM D 1777-96, 2007. Course and wale density was determined by counting the number of courses and wales per centimeter as per ASTM D3775-03 using pick glass. Tightness factor of the test fabrics was determined using the following equation:

$$\text{Tightness factor} = \frac{\sqrt{\text{Tex}}}{\text{Loop length}} \quad \dots (1)$$

where l is the loop length in cm.

2.2.2 Comfort Characteristics

Thermal Properties – Fabric samples were evaluated for their thermal properties, such as thermal resistance (TR), thermal conductivity (TC) and thermal absorptivity (TA) on Alambeta (Sensora, Czech Republic).

Air Permeability – Air permeability (AP) of the fabrics was measured on FX 3300 air permeability tester (TEXTTEST AG, Switzerland) at a pressure of 98 Pa according to ASTM D737.

Relative Water Vapor Permeability – Relative water vapor permeability (RWVP) of test samples was measured using the Permetest instrument (Sensora, Czech Republic) according to ISO 11092 standard.

Vertical Wicking – A sample of 200 mm × 25mm size was cut along course and wale directions to perform vertical wicking test. The test samples were suspended vertically with the bottom end clamped by

a weight for ensuring proper immersion in a reservoir of distilled water¹⁰.

Water Absorbency – Water absorbency of test samples was determined by gravimetric Absorbency Tester (GATS).

2.2.3 Statistical Analysis

Statistical analysis was performed by carrying out one way Anova analysis using SPSS 16 window statistical software. F and p values were obtained which enabled to conclude whether the effect of selected fibre, yarn and fabric variables has significant influence on the test properties.

3 Results and Discussion

3.1 Fabric Characterization

Table 2 shows the physical properties of test samples. Aerial density of cotton/polyester fabrics lies in the range of 132 – 259 g/m², while that for cotton/nylon and cotton/viscose fabrics varies in the range of 231 – 242 g/m² and 133 – 182 g/m² respectively. The thickness lies between 0.80 mm and 1.34 mm for cotton/polyester, 1.27 mm and 1.31 mm for cotton/nylon and 0.85 mm and 1.04 mm for cotton/viscose fabrics. Tightness factor varies from 13.3 to 15.7 for cotton/polyester, 11.7 to 12.7 for cotton/nylon and 11.2 to 12.1 for cotton/viscose fabrics.

3.2 Comfort Characteristics

3.2.1 Thermal Properties

Thermal resistance and thermal conductivity of plated fabrics knitted with polyester yarn of varying linear density in inner layer decreases as the polyester yarn becomes finer. Similar trends are observed for fabrics with viscose yarn of varying linear density in the inner layer plus cotton yarn of fixed count in the outer layer. Statistical analysis of test results show that the effect of yarn linear density has significant affect on thermal resistance (F value of 13.8 & p value of 0.06). The findings are in accordance with Chidambaram *et al.*¹⁰ on thermal properties of bamboo knitted fabrics. Decrease in thermal resistance may be attributed to the reduction in fabric thickness and aerial density with decrease in yarn linear density (Tables 2 and 3). An inverse relationship is registered between thermal resistance and thermal conductivity as given by the following equation:

$$R = \frac{h}{\lambda} \quad \dots (2)$$

where R is the thermal resistance (km^2/W); h , the fabric thickness (mm); and λ , the thermal conductivity (W/mK).

However, the test results indicate that as the thermal resistance decreases, the thermal conductivity decreases as well. This contradiction might be explained by fabric thickness. Yarn diameter and therefore fabric thickness decrease as the yarn becomes finer. If the amount of decrease in thickness is more than the amount of decrease in thermal conductivity, the thermal resistance also decreases. The average reduction in thickness with decrease in yarn linear density for cotton/polyester fabrics is found to be 22.4% as against 6.5 % decrease in thermal conductivity. Hence, the observed trend can be explained in this light.

As the fabric loop length increases, thermal resistance and thermal conductivity decrease, irrespective of the inner layer fibre type (polyester, viscose or nylon) (Table 3). The decrease in thermal resistance can be attributed to corresponding decrease in fabric thickness with the increase in loop length. Thickness by far is the greatest determinant of thermal insulation properties of textiles and hence decreases in thermal resistance with an increase in loop length (Table 3).

Cotton/polyester fabrics show the highest value while cotton/viscose fabrics show the lowest value of thermal resistance. The observed trend may be attributed to the highest fabric thickness along with low conductivity of polyester fibre compared to

viscose and nylon fibres since thermal resistance depends both on fabric thickness and thermal conductivity (Eq. 2). Likewise, the highest thermal conductivity of cotton/nylon fabric may be attributed to the highest conductivity of nylon fibre compared to other two fibres used in the study (Table 3).

Thermal Absorptivity

Figure 1 (a) shows the effect of inner layer yarn linear density on thermal absorptivity of test samples. Thermal absorptivity decreases as polyester and viscose yarns in the inner layer become finer. Results are found to be statistically significant for both cotton/polyester ($F = 7.93$ & $p = 0.02$) and cotton/viscose fabrics ($F = 8.3$ & $p = 0.04$). It can thus be inferred that these fabrics would be perceived warmer on initial brief skin contact. Plated fabrics knitted with finer yarns give slacker constructions as indicated by lower value of tightness factor (Table 2), which, in turn, leads to reduced thermal absorptivity. Similar trends were also observed by Ozdil *et al.*¹¹ in their studies on thermal comfort of knitted fabrics.

Thermal absorptivity of cotton/polyester, cotton/nylon and cotton/viscose fabrics decreases as the fabrics are knitted with longer loop lengths, as shown in Fig. 1 (b). The decrease in thermal absorptivity can be attributed to corresponding decrease in thermal conductivity and bulk density as the fabric loop length increases, owing to direct dependence of thermal absorptivity on thermal conductivity and bulk density as per following equation:

$$b = \sqrt{\lambda \rho c} \quad \dots (3)$$

where b is the thermal absorptivity; λ , the thermal conductivity; ρ , the fabric density; and c , the specific heat capacity of fabric.

Cotton/nylon fabrics show the highest value of thermal absorptivity as shown in Fig. 1(c), thereby suggesting that these fabrics would be perceived coolest on first contact with skin. The observed trend may be attributed to higher thermal conductivity of cotton/nylon fabric. However, cotton/viscose fabric with the lowest value of thermal absorptivity would give warm feeling on first contact with the skin.

3.2.2 Relative Water Vapor Permeability

Figure 2 (a) shows the effect of inner layer yarn linear density on relative water vapor permeability (RWVP). An increase in RWVP is observed for both cotton/polyester and cotton/ viscose fabrics as the

Table 3 — Thermal properties, relative water vapor permeability and air permeability

Sample code	TR $\times 10^{-3}$ km ² /W	TA W s ^{1/2} m ⁻² K ⁻¹	TC $\times 10^{-3}$ W/mK	RWVP %	AP cm ³ /cm ² /s
CP ₁	34.18	84.5	43.15	49.4	47.3
CP ₂	33.34	83.2	42.22	50.0	55.5
CP ₃	32.10	82.5	42.00	52.1	57.0
CP ₄	26.53	70.4	37.60	60.4	62.0
CP ₅	31.06	71.0	37.80	59.2	58.0
CN ₁	30.20	103.5	53.35	53.3	72.5
CN ₂	29.70	101.1	49.22	55.2	74.0
CN ₃	28.00	91.1	48.00	56.0	79.0
CV ₁	25.86	80.0	38.02	55.0	154.0
CV ₂	25.80	78.8	37.56	57.0	158.0
CV ₃	25.20	74.2	36.00	58.1	229.0
CV ₄	28.22	84.0	41.00	53.2	212.0

TR – Thermal resistance, TA – thermal absorptivity, TC – thermal conductivity, RWVP – relative water vapor permeability, AP – air permeability.

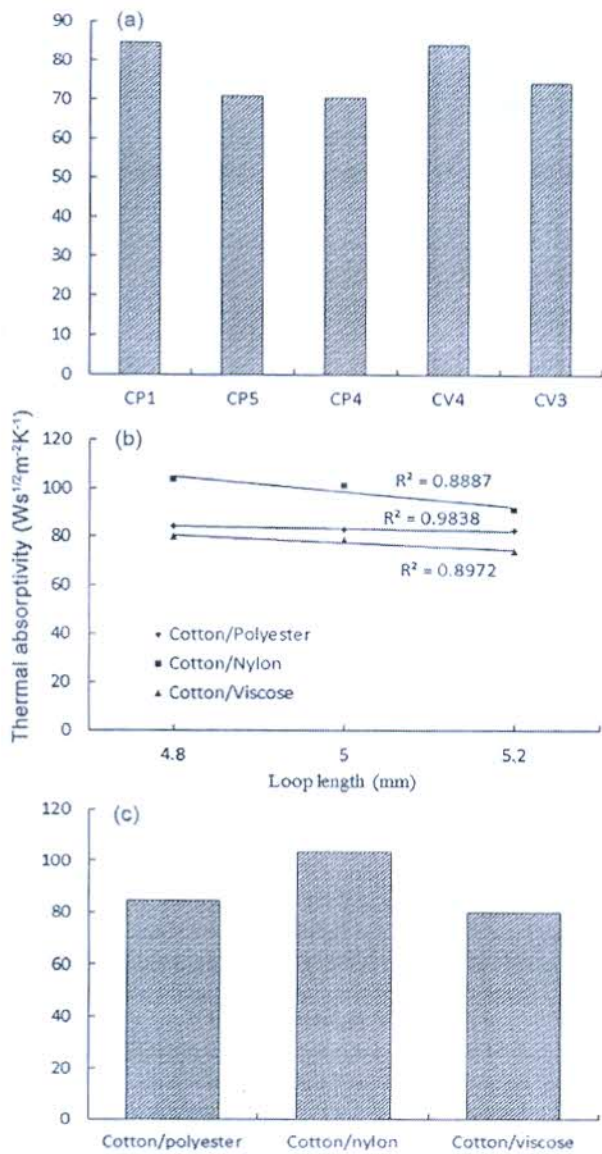


Fig. 1 — Effect of (a) inner layer yarn linear density, (b) loop length, and (c) inner layer fibre type on thermal absorptivity

polyester and viscose yarns in the inner layer become finer (Table 3). Results are found to be statistically significant at 95%. Fabrics knitted with finer yarns result in more open and porous structures, thereby allowing easier passage of water vapor through the structure. Moreover, the lower thickness and mass per square metre of finer yarn fabrics also contribute towards increased water vapor permeability as compared to their coarser yarn counterparts.

RWVP of test samples increases with the increase in loop length, irrespective of the fibre type in the inner layer, as shown in Fig. 2 (b). The reason being, the increase in loop length results in fabrics of slacker and open construction, thereby

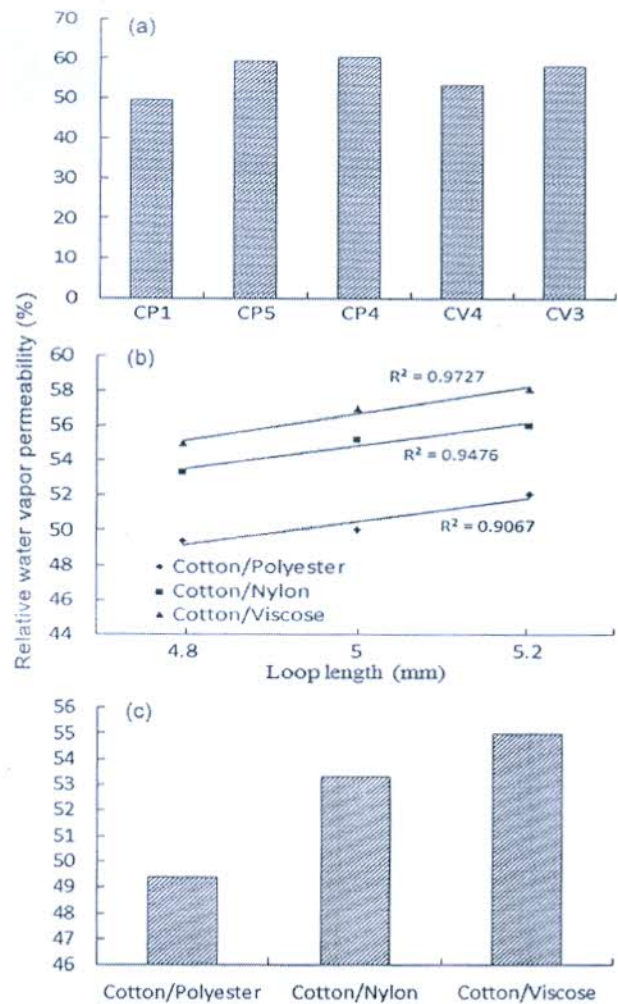


Fig. 2 — Effect of (a) inner layer yarn linear density, (b) loop length, and (c) inner layer fibre type on relative water vapor permeability

enabling easier passage of water vapor through these fabrics.

Cotton/viscose fabric shows the highest value of relative water vapor permeability while cotton/polyester fabrics are found to be the least permeable to passage of moisture vapor as shown in Fig. 2 (c). The observed trend can be explained by higher moisture regain of viscose fibre compared to polyester and nylon fibres. Moisture vapor diffusion through textiles depends on both moisture diffusivity of fibres and bulk properties of fabrics. Higher moisture regain of viscose fibre leads to higher diffusion of moisture vapor through cotton/viscose fabric. However, highest thickness and aerial density of cotton/polyester fabric inhibits easy passage of moisture vapor through fabric and hence lowest RWVP for cotton/polyester fabric.

3.2.3 Air Permeability

Figure 3 (a) shows the effect of inner layer yarn linear density on air permeability (AP) of cotton/polyester and cotton/viscose fabrics. Air permeability shows an upward trend as the polyester and viscose yarns in the inner layer become finer. Results are found to be statistically significant for both cotton/polyester ($F = 11.72$ & $p = 0.008$) and cotton/viscose ($F = 36.4$ & $p = 0$) fabrics. This may be attributed to reduction in thickness and aerial density of fabrics knitted with finer yarns.

Increase in fabric loop length results in corresponding increase in air permeability, irrespective of the inner layer fibre type, as shown in Fig. 3 (b) and Table 3. One way Anova analysis suggests that the effect of loop length on air

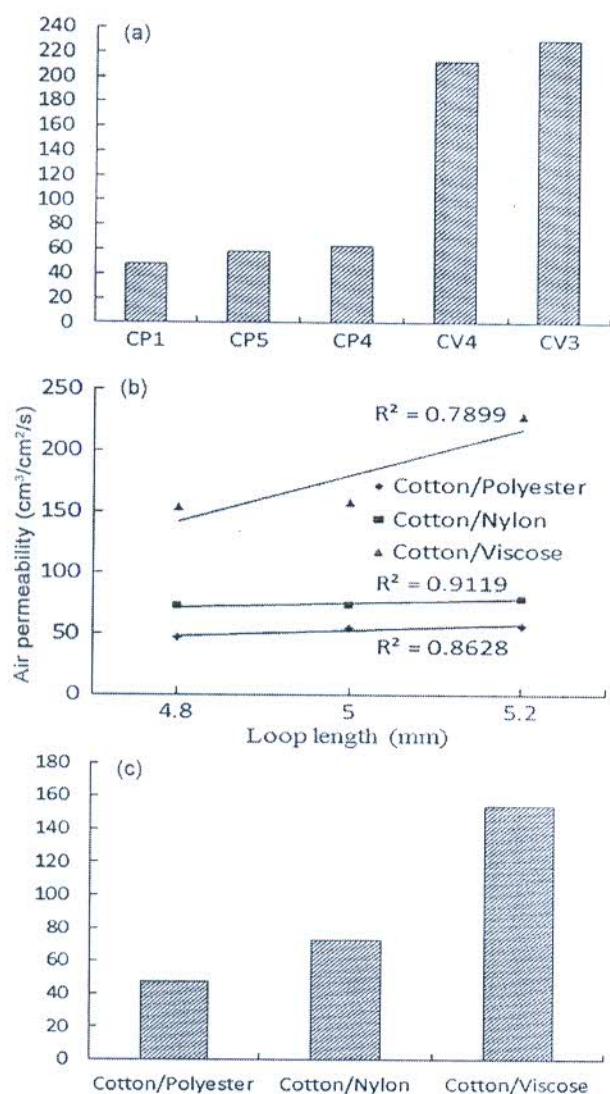


Fig. 3 — Effect of (a) inner layer yarn linear density, (b) loop length, and (c) inner layer fibre type on air permeability

permeability is found to be statistically significant. The observed trend may be attributed to increase in slackness and openness of fabric structure along with reduction in tightness factor with the increase in loop length which facilitates easy passage of air through fabrics.

Figure 3 (c) shows the effect of inner layer fibre type on air permeability of test samples. Cotton/viscose fabric shows the highest value of air permeability while cotton/polyester fabric is found to be least permeable to passage of air. Highest air permeability of cotton/viscose fabric may be attributed to highest specific gravity of viscose fibre compared to the other two fibres used in the study. The higher the specific gravity of fibre, the lesser is the volume of fibre for given weight, thus providing less fabric cover and better permeability to air through fabrics.

3.2.4 Vertical Wicking

Table 4 shows the course-wise and wale-wise vertical wicking of test samples. Cotton/polyester and cotton/viscose fabrics knitted with finer polyester and viscose yarns respectively in the inner layer show higher wicking height in both course-wise and wale-wise directions as compared to their coarser yarn counterparts (Fig. 4). The change in polyester linear density from 40.6 tex to 57.3 tex results in significant difference in wicking with respect to time. The increase in wicking height for fabrics knitted with finer yarns can be attributed to increase in the number of fine capillaries; the fibres come closer to each other introducing a greater number of capillaries with smaller diameters likely to promote enhanced liquid flow. As the radius of capillary decreases, pressure generated in the capillary increases, thereby causing faster flow through capillary and hence increased wicking height. All the test samples irrespective of fibre type in inner layer shows no particular trend with the loop length.

Vertical wicking of cotton/viscose fabrics is the highest in both course-wise and wale-wise direction, while cotton/nylon fabrics show the least wicking height after passage of 5 and 10 min both in course-wise and wale-wise directions (Fig. 5). It is expected that viscose fibre being hydrophilic would absorb moisture (as indicated by higher water absorbency of cotton/viscose fabric) and hence inhibit the liquid transfer by vertical wicking, while polyester would result in better wicking owing to its hydrophobic nature. Deviation from the trend can be explained by

Table 4 — Course-wise and wale-wise wicking height in cm

Sample code	1		2		3		4		5		6		7		8		9		10	
	C	W	C	W	C	W	C	W	C	W	C	W	C	W	C	W	C	W	C	W
CP ₁	0.3	0.7	0.7	1.7	1.2	2.3	1.7	3.3	2.4	3.6	2.7	4.0	3.1	4.5	3.5	5.1	3.7	5.5	3.9	5.9
CP ₂	1.1	0.9	2.3	2.0	4.1	3.5	5.0	4.4	5.8	5.7	6.4	6.5	7.0	7.0	7.5	7.7	8.3	8.2	8.7	8.6
CP ₃	0.9	0.5	1.8	1.7	3.0	2.5	3.8	3.5	4.5	4.2	5.8	4.7	6.3	5.4	6.7	5.8	7.2	6.3	7.5	6.6
CP ₄	2.0	2.3	3.1	3.2	3.8	3.8	4.5	4.6	5	5.5	5.3	6.2	5.7	6.8	6.0	7.2	6.2	7.6	6.4	7.9
CP ₅	1.1	1.2	2.2	2.3	3.0	3.4	3.8	4.0	4.6	4.8	5.0	5.4	5.5	6.2	5.8	6.5	6.0	6.7	6.2	7
CN ₁	0.1	0.3	0.2	1.2	0.5	1.8	0.7	2.5	1	3.1	1.2	3.7	1.6	4.2	1.9	4.5	2.3	5	2.5	5.4
CN ₂	0.1	0.2	0.7	0.7	1.0	1.5	1.5	2.1	2.0	2.4	2.4	3.0	2.9	3.4	3.3	3.7	3.6	3.9	4.0	4.5
CN ₃	0.3	0	1.1	0.2	1.7	0.4	2.2	0.8	2.8	1.2	3.2	1.7	3.5	2	4.0	2.3	4.2	2.6	4.6	2.8
CV ₁	2.5	3.3	3.9	5.2	4.6	6.0	4.9	6.7	5.3	7.4	5.7	7.9	6.1	8.2	6.5	8.5	6.7	8.7	7.0	9.0
CV ₂	2.6	3.5	3.4	5.4	3.8	5.8	4.3	6.7	4.7	7.3	5.2	8.0	5.7	8.4	5.9	8.8	6.2	9.0	6.6	9.2
CV ₃	2.8	3.3	4.0	5.2	4.9	6.1	5.5	6.9	6.1	7.5	6.7	8.0	6.9	8.4	7.2	8.6	7.4	9.0	7.5	9.4
CV ₄	3.0	2.2	3.9	3.7	4.6	4.8	5.1	5.5	5.5	5.9	5.8	6.6	6.1	7.1	6.5	7.6	6.7	8	6.9	8.4

1-10 are time in min, C- course-wise, W- wicking-wise.

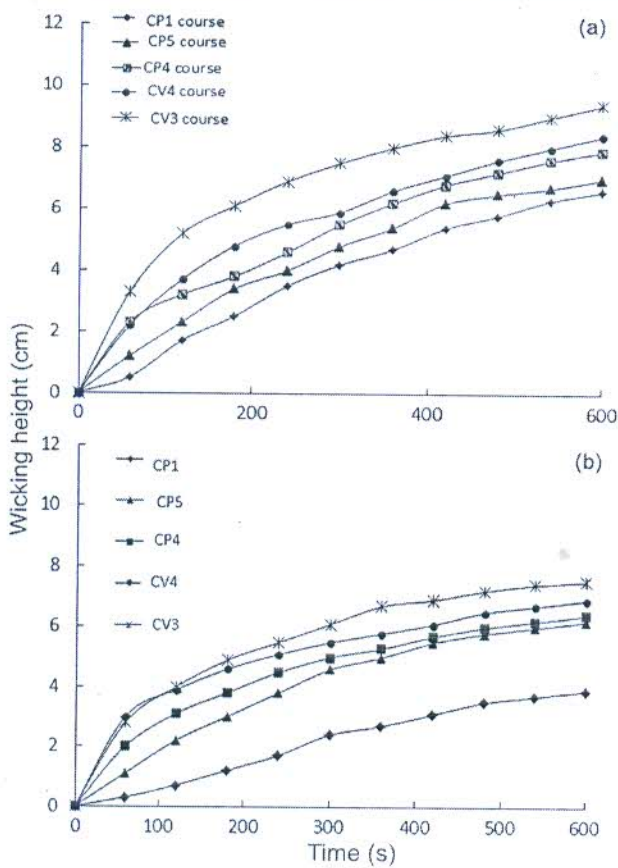


Fig.4 — Effect of inner layer yarn linear density on wicking height (a) course-wise, and (b) wale-wise

the factors that affect the vertical wicking in knitted fabrics. Wicking not only depends on the nature of fibre (hydrophobicity, hydrophilicity) but it also depends on the filament fineness. In the present study, the use of micro denier viscose filament has enabled

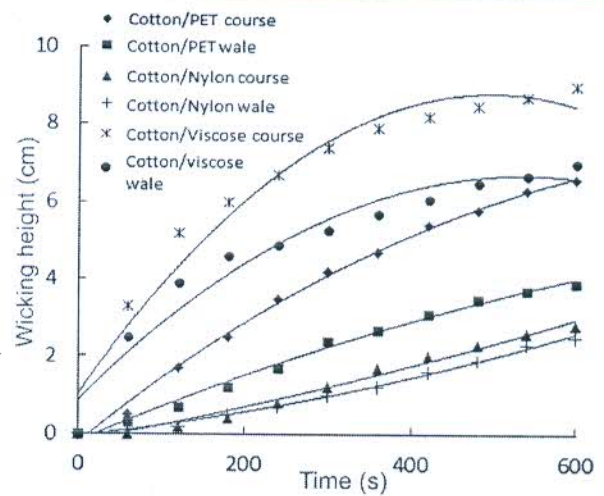


Fig.5 — Effect of inner layer fibre type on vertical wicking

to achieve higher wicking height in spite of its hydrophilic nature. Thus, it can be inferred that higher wicking can be achieved even with hydrophilic fibre in the inner layer by selection of micro denier filament.

3.2.5 Water Absorbency

Figure 6 (a) shows that water absorbency increases with the increase in inner layer yarn linear density. Amount of water absorbed by fabric depends on its bulk properties i.e. thickness and aerial density. The greater the fabric weight and thickness, the more is the amount of water absorbed by fabric. The increase in inner layer yarn linear density results in the corresponding increase in fabric weight and thickness (Table 2) and therefore, an increase in water absorbency of fabrics knitted with coarser yarns.

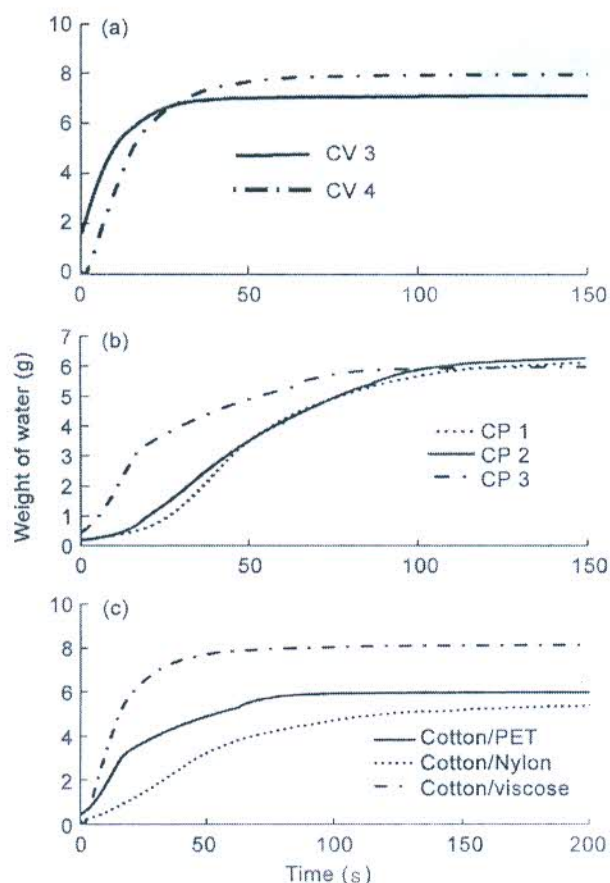


Fig. 6 — Effect of (a) inner layer yarn linear density, (b) loop length, and (c) inner layer fibre type on water absorbency

Water absorbency of fabrics knitted at longer loop length is higher compared to their shorter loop length counterparts, as shown in Fig. 6 (b). Increase in loop length results in fabrics of slack construction and high pore volume. The more the pore volume, the greater is the water entrapped by the pores and hence higher water absorbency of fabrics knitted with longer loop length.

Comparison of fabrics with varying fibre types in the inner layer shows that cotton/viscose fabric has the highest water absorbency and cotton/nylon fabric the lowest value of water absorbency as shown in Fig. 6 (c). Water absorbency of fabric depends on the moisture absorbency or regain properties of the fibres as well as with bulk properties. Higher moisture regain of viscose fibre as compared to polyester and nylon might have led to higher water absorbency for cotton/viscose fabrics. Lowest water absorbency of cotton/nylon fabric may be attributed to the lower thickness and an aerial density of cotton/nylon fabric compared to cotton/polyester fabric.

4 Conclusion

Bi-layered plated knits designed with distinct fibre, yarn and fabric combinations in the two layers can be effectively used in changing ambient conditions and at varying activity levels of individuals due to ability of fabrics to reflect varying thermal, moisture vapor and liquid transfer properties. Thermal resistance, thermal absorptivity, thermal conductivity and water absorbency decrease, while an increase in relative water vapor permeability, air permeability and wicking is observed for cotton/polyester and cotton/viscose fabrics as the yarns in the inner layer become finer. Thus, it can be concluded that plated knits designed with finer yarn in the inner/next to skin layer are suitable for use when ambience is hot and activity level of an individual is high, resulting in generation of sensible perspiration. Such fabric would be quick drying as characterized by low water absorbency and would result in rapid liquid transfer by wicking. Moreover high air and water vapor permeability further ensures wearer comfort. Decrease in thermal resistance, thermal conductivity and thermal absorptivity while an increase in relative water vapor permeability, air permeability and water absorbency are observed with the increase in loop length, irrespective of fibre type in the inner layer.

Cotton/nylon fabric would be perceived cooler on initial skin contact owing to the highest value of thermal absorptivity and thermal conductivity and can be preferred as summer wears. However, cotton/viscose fabrics owing to their better liquid transport properties as characterized by higher wicking, absorbency along with the highest permeability to moisture vapor and air seem suitable choice where rapid liquid dissipation and dry feel next to skin is the prime requirement, such as in intimate wear, sportswear, etc.

References

- 1 Patnaik A, Rangasamy R S, Kothari V K & Ghosh A, *Text Prog*, 38 (2006) 22. DOI:10.1533/jotp.2006.38.1.1
- 2 Bivainyte A & Mikucioniene D, *Fibres Text East Eur*, 19 (2011) 64.
- 3 Bivainyte A, Mikucioniene D & Kerpauskas P, *Materials Sci*, 18 (2012) 167.
- 4 Chaudhari S S, Chitnis R S & Ramakrishnan R, Water proof breathable active sports wear fabrics (2008). <http://www.sasmira.org/sportswear.pdf>.
- 5 Oglakcioglu N, Celik P, Ute B, Marmarali A & Kadoglu H, *Text Res J*, 79 (2009) 888.
- 6 Yoo S & Barker R, *Text Res J*, 75 (2005) 523.

- 7 Terliksiz S, Kalaoglu F & Eryuruk S H, *J Text Eng*, 19 (2012) 15.
- 8 Das B, Kothari V K, Fanguiero R & Araujo D, *Fiber Polym*, 9 (2008) 225.
- 9 Majumdar A, Mukhopadhyay & Yadav R, *Int J Therm Sci*, 30 (2010) 1.
- 10 Chidambaram P, Govindan R & Venkatraman K, *Autex Res J*, 11 (2011) 102.
- 11 Ozdil N, Marmarali A and Kretzschmar S, *Int J Therm Sci*, 46 (2007) 1318.
- 12 Herath C, *Fiber Polym*, 14 (2013) 1339.
- 13 Kumar B & Das A, *Fiber Polym*, 55 (2014) 625.

RESEARCH

Open Access



Optimization of monochlorotriazine β -cyclodextrin grafting on cotton and assessment of release behavior of essential oils from functionalized fabric

Shelly Khanna and J. N. Chakraborty*

*Correspondence:
chakrabortyjn@hotmail.com
National Institute
of Technology,
Jalandhar 144011, India

Abstract

Monochlorotriazinyl β -cyclodextrin (MCT β -CD) was employed for the inclusion complexation with oils of cedarwood, clove, eucalyptus and peppermint to assess their release behavior from functionalized cotton. The process of MCT β -CD grafting was optimized using response surface methodology with three independent factors including MCT β -CD concentration, pH and curing temperature and effect of their second order interactions on dependent variables as % nitrogen content, % graft yield, tensile strength and wash durability was examined. The interaction of MCT β -CD concentration and pH had the decisive effect on the investigated dependent variables. FTIR and % retained nitrogen confirmed the substantial retention of modified host on functionalized cotton after five vigorous wash cycles. ^1H NMR characterized the full entrapment of oils within MCT β -CD cavity on cotton. All the oils were substantially retained in the inclusion complexes with the MCT β -CD before and after wash than when present uncomplexed on the treated cotton. Peppermint was the slowest to fade off and cedarwood was rapid in sublimation from the cyclodextrin moieties.

Keywords: Monochlorotriazine, Grafting, % nitrogen content, % retained nitrogen, Cyclodextrin moieties

Introduction

The presence of chemical hosts in the form of native β -cyclodextrin on cotton facilitates the suppression of essential oil's release from the finished surfaces to a greater extent but their adherence to any of the treated substrates is not long lasting as only weak Vanderwaal and Hydrogen interactions prevail between cotton and β -cyclodextrin. This is due to the non existence of permanent interactions between the substrate and the anchoring host.

A temporary textile finishing of textiles is easily achieved, but is easy to wash off (Nelson 2002). It is evident that β -CD cannot form direct covalent bonds with any textile fiber but it is capable of forming only hydrogen bonds with the cellulose based materials. Their lack of durability on textile substrates severely limits their effective use as fabric finishing agents. Instead, the modified monomolecular containers are postulated

to form van der Waal bonds, ionic bonds or even covalent bonds with suitable textile surfaces such as cotton. There is currently an increasing demand for improved reactive β -CD derivatives with better stability after storage under different conditions and processes without cleavage or the production of toxic or harmful subsidiary products (Wen et al. 2010). Durable finishing is generally achieved by the slow-release method, in which the treated fabrics slowly release the oil molecules for a long duration of time (Halim et al. 2011). Monochlorotriazinyl- β -cyclodextrin (MCT- β -CD) is the first reactive cyclodextrin derivative and can be used to permanently bind β -CD to cotton with the conventional reactive dyeing method (Bhaskara-Amrit et al. 2011; Bereck 2010). The reactive chlorine atom of triazinyl group of MCT- β -CD can react with nucleophilic residues such as ^-OH to form covalent bonds (Halim et al. 2010; Sricharussin et al. 2009). It can work as a universal anchor for a wide horizon of textile materials as cotton; fabric or yarns (Halim et al. 2011; Boonsod 2007; Cabrales et al. 2012; Hauser and Jianshuo 2000; Peila et al. 2012; Shown and Murthy 2008; Marwa et al. 2013; Sricharussin et al. 2009). Mixed fiber materials like cotton/polyurethane, cotton/polyamide or even silk can be finished with MCT β -CD in good yields (Bendak et al. 2010; Ibrahim et al. 2007; Bergamasco et al. 2007; Boonsod 2007), cotton/wool, viscose/wool blends, filter papers & polyester along with its blends (Anitha et al. 2011; Shahba 2008; Popescu et al. 2011). The application of MCT- β -CD on textiles is influenced by a number of process parameters viz concentration of MCT β -CD, time of reaction of MCT β -CD with the textile substrate, temperature of curing of MCT β -CD, pH of reaction and presence of moisture in substrate (Moldenhauer and Reuscher 1999; Rehmann et al. 2003). Some studies have been carried out to assess the impact of independent process variables for the fixation of MCT β -CD on cotton to assess its antimicrobial activity (Halim et al. 2011), polyester and cotton/polyester blends for imparting antistatic property (Halim et al. 2010) and on thin polyester films after their saponification for the activation of the surface (Popescu et al. 2011). But the interactions of the process variables of MCT β -CD grafting on textile substrate holds incredible importance as physical properties of the treated substrates are immensely affected. Also, the durability of the reactive host is adjudged based upon its adherence on to the textile surfaces for the anchorage of guests as essential oils. But due to lack of scientific and systematic approach for the elucidation of impact of interactive process variables in any of the previous works, present work was carried out for the process optimization of MCT β -CD grafting on cotton with the exploitation of the key variables. The stability analysis of essential oils for aroma sustained textiles in presence of the reactive host was investigated for characterized inclusion complexes.

Methods

Materials

Thoroughly pre-treated plain woven cotton fabric possessing epi (76), ppi (70), warp (42.8 Ne^s), weft (38 Ne^s) and GSM (136) was used for finishing with four categories of essential oils, viz. clove (CO; Assay-eugenol ~85%), cedarwood (CdO; Assay-cedrol ~70%), eucalyptus (EO; Assay-cineole ~60%) and peppermint (PO; Assay-menthol ~44%). All the analytical grade chemicals, viz. β -cyclodextrin (β -CD-M.W.1134.98 and minimum assay ~98%), cyanuric chloride (M.W. 184), sodium carbonate, sodium hydroxide, ethanol, oils and phenolphthalein were supplied by SDFL (*Mumbai, India*). UV-Vis-210

spectrophotometer (*Lab India analytical UV 3000+*), FTIR-spectroscope (*Perkin Elmer, US*), Elemental Analyzer (*EuroVector EA 3000; CSIR-Central Drug Research Institute: Saif, Lucknow, India*), Bruker Avance II NMR Spectrometer (*Saif, PU, Chandigarh, India*), Thermogravimetric analyzer (*SDT Q600 V20.9 Build 20; NITRA, Gaziabad, India*), Water bath (*Laboratory glassware co., Ambala*), Electronic pH meter PH-009 (I), Electronic weighing balance (*CAS Model MW -11 series*), Drying oven (*Kaypee Udyog, Ambala, India*), Orbital shaker (*Bio-Technology Lab, M.D.U Rohtak, India*), Padding Mangle (*Electronic and Engg. Company*), Laundrometer (*RBE, Mumbai*) and Tensile tester (*Globe Tex Industries*) were the equipment used to evaluate the physical properties of the functionalized cotton and stability of the inclusion complex on cotton.

Synthesis and characterization of MCT β -CD

The synthesis of MCT β -CD was carried out according to the procedure described previously without any major process modifications with the use of reactants viz. β -cyclodextrin and cyanuric chloride in presence of alkaline medium (Khanna et al. 2015). *FTIR spectroscopy* (for micro structural analysis with FTIR-spectroscope), *elemental analysis* (for compositional analysis with elemental analyser), *Thermogravimetric Analysis* (TGA with Thermogravimetric Analyzer) and *$^1\text{H-NMR spectra}$* (for host-guest investigation with NMR spectrometer) were used for the characterization of MCT β -CD powder.

Solubility analysis of MCT β -CD in water

The solubility of MCT β -CD was analyzed in water to assess the modification in native β -CD in terms of its improvement in aqueous solubility.

Optimization of process parameters of MCT β -CD application on cotton

The process optimization of MCT β -CD grafting on cotton was carried out by the response surface methodology using 3^3 Box and Behnken factorial design i.e. MCT β -CD concentration (60, 70, 80 gpl), Temperature of curing (100, 125, 150 °C) and pH (6, 8, 10) as independent variables. Treated cotton was assessed for Graft yield%, Nitrogen content% and change in physical properties of treated cotton explicitly tensile strength and wash durability (up to five washes). Statistical analysis was done using Design Expert software version 7.1.2 (State-ease Inc., Minneapolis, USA). The statistical significance of regression co-efficient and model-fit was checked. Model equations for all responses were also determined (Fischer's test).

Graft yield% (GY) was measured by the analysis of the weight difference of the treated cotton with MCT β -CD from the untreated one according to Eq. 1. *Nitrogen content%* (N_2) was assessed for the determination of the amount of MCT β -CD fixed on cotton according to standard Kjeldahl method. *Tensile strength* was measured according to the ASTM D5034-1995 (strip method) by using digital tensile strength tester. *Wash durability* was evaluated as follows—4 cm \times 10 cm strips of MCT β -CD treated cotton and further, oil treated cotton samples were washed according to ISO 105-C03:1989 with 5 gpl of soap and 3 gpl of Na_2CO_3 with a material to liquor ratio of 50:1. The treated samples were then laundered at 60 ± 2 °C for 30 min. The washed samples were rinsed with tap water for 10 min and dried at room temperature after each wash cycle. The durability to

wash was determined with FTIR and % retained nitrogen for 5 subsequent washes. Also, the effect of wash treatments on the % retention of oils on treated fabrics was investigated for 30 vigorous washes.

$$\text{Graft yield \%} = \frac{\text{Final weight of treated cotton} - \text{Weight of untreated cotton}}{\text{Weight of untreated cotton}} \times 100 \quad (1)$$

Characterization, application and stability analysis of inclusion complexes of MCT β -CD-oils on functionalized cotton

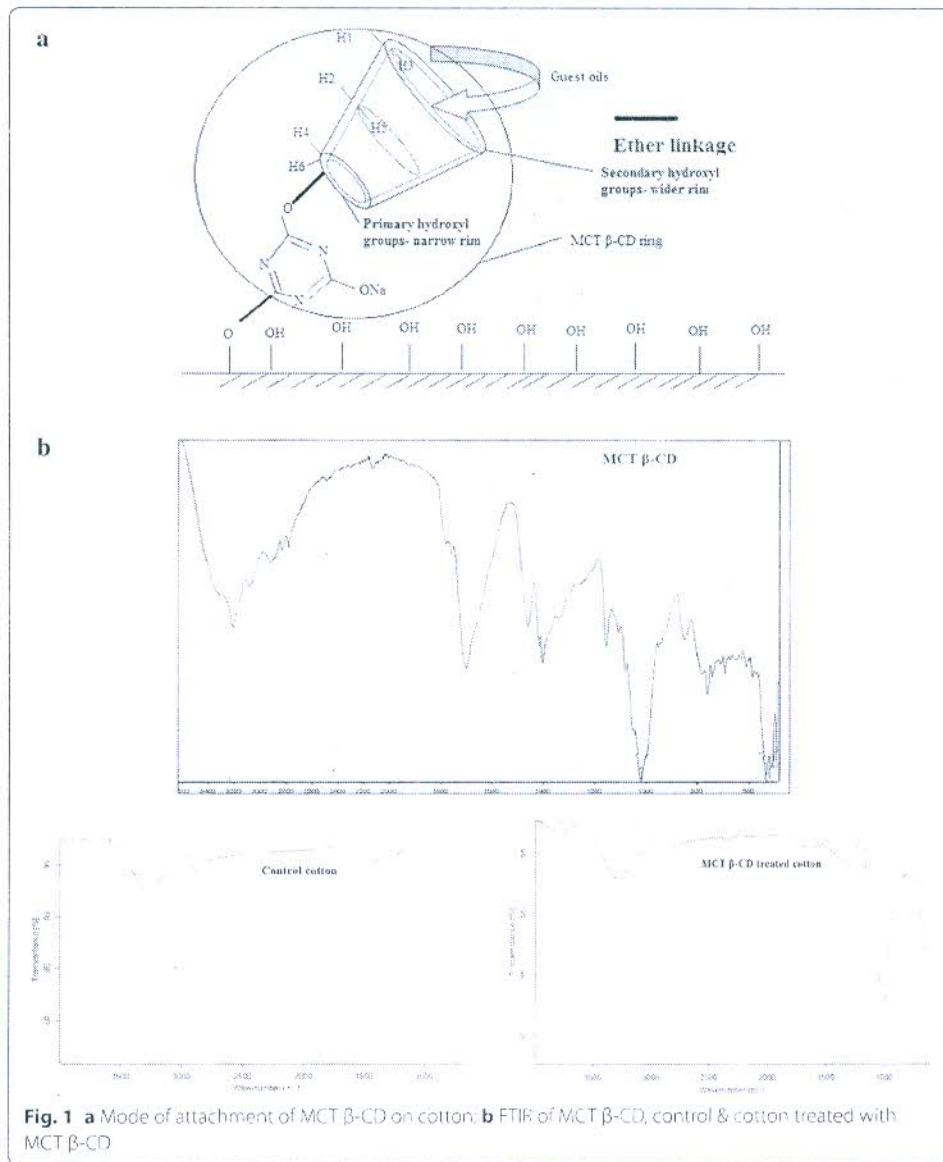
$^1\text{H-NMR}$ was used to characterize the inclusion complexes of MCT β -CD and essential oils in D_2O (solvent) at room temperature and all chemical shifts were measured relative to Trimethylsilane (TMS) as reference. The stoichiometry of MCT β -CD: oils were assumed to be 1:1. The solutions of MCT β -CD-oils were prepared at 10 mM in free state (without complex) and at 5 mM:5 mM (host: guests) for the complex. The precalculated amount of host and guest oils in uncomplexed and complexed states as 1.6 ml oil (free state), 14 g host (free state) and 0.8 ml oil and 7 g host (for inclusion complex). Dry mixing technique was used for complexation with magnetic stirring at 4000 rpm for 25 min to achieve a uniform and stable complex of MCT β -CD and oils. Further, MCT β -CD functionalized cotton was treated with essential oils at 10% concentration to achieve a dynamic yet a stable inclusion complex. Fragrance stability of oils on functionalized cotton was investigated by estimation of their release rate after extraction in ethanol solution from treated cotton at stipulated time intervals at respective λ_{max} CO (282 nm), CdO (306 nm), EO (270 nm) and PO (240 nm) according to Eq. 2. The impact of wash down treatments was analyzed by the estimation of % retained oils on cotton after 30 subsequent wash cycles as mentioned in "Optimization of process parameters of MCT β -CD application on cotton" section.

$$\begin{aligned} &\text{Rate of release of oil at stipulated time gap (\%)} \\ &= \frac{\text{Conc. at 0 h} - \text{Conc. at stipulated time interval}}{\text{Conc. at 0 h}} \times 100 \quad (2) \end{aligned}$$

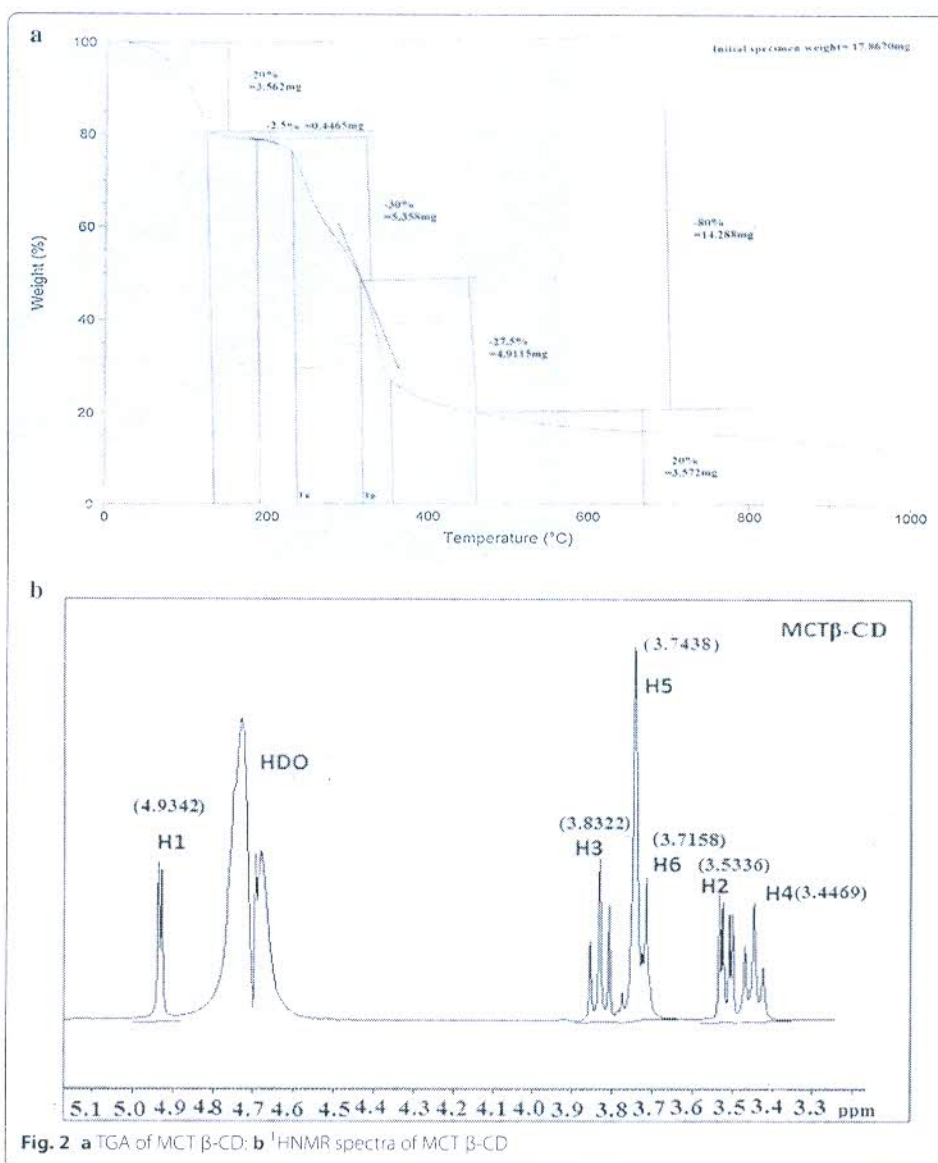
Results and discussion

Synthesis and characterization of MCT β -CD

The yield % of the reaction mechanism between β -CD and cyanuric chloride in alkaline medium was satisfactory enough at 63.34% with the peripheral structure of synthesized MCT β -CD as depicted in Fig. 1a. The degree of substitution was found to be 0.3 to 0.5 with molecular weight of 1560. *Elemental analysis* of MCT β -CD powder had shown about 3.7% N_2 present in MCT β -CD, whereas, 0% was available in native β -CD; that confirmed the modification of β -CD with monochlorotriazine group. *FTIR* revealed the appearance of bands at 2920, 2778 cm^{-1} for the presence of C-H bonds in the synthesized MCT- β -CD. The presence of strong bands at 1753, 759 and 1150 cm^{-1} characterized C=N, C-Cl and C-O groups. Further, the identification of a band at 1018 cm^{-1} accounted for carbon atoms in cyclic ring. The characteristic bands in the IR- spectra of the MCT- β -CD treated cotton were recorded at 2890 (C-H), 1745 (C=N stretching) and 1157 (C-O) in comparison to control. Also, a strong band at 759 cm^{-1} (C-Cl) was absent in the IR spectra of MCT- β -CD treated cotton that indicated the involvement



of chlorine atom in the grafting process of MCT- β -CD on cotton (Fig. 1b) as discussed in an elaborated manner in our previous publication (Khanna et al. 2015). MCT β -CD had shown thermal decomposition as a measure of % weight reduction in TGA results (Fig. 2a). At the initial stage, 20% (~3.52 mg) weight loss occurred in MCT β -CD powder as H₂O molecules are lost at 128 °C, remnant traces of moisture were lost at 195 °C resulting in about 2.5% (~0.447 mg) weight loss. The transition from solid to liquid phase took place at 310 °C resulting in about 30% fall in weight and finally, second stage thermal degradation of char resulted in about 27.5% weight loss at higher temperature of 460 °C. Figure 2b depicted ¹H-NMR spectra that characterized MCT β -CD in terms of respective chemical shifts relative to Trimethylsilane (TMS) as reference in D₂O as solvent at room temperature. The spectra had revealed that the nucleophilic substitution of β -CD takes place at the primary hydroxyl groups present at the narrower rim by the



chlorotriazine moiety (Pessine et al. 2012; Levya et al. 2001; Medronho et al. 2012). The ¹H-NMR spectra of MCT β-CD is used as a reference to adjudge the extent of chemical shifts of free and complexed states of the modified host and guests.

Solubility of MCT β-CD

MCT β-CD had shown improved solubility in water as compared to native β-CD due to the reduced ring strain of β-CD frame. The % solubility was estimated in the range of 95% (for 10 gpl) up to 65% (for 100 gpl). The scarce solubility of β-CD is due the formation of intramolecular hydrogen bonds between the hydroxyl group at carbon atom 2 (C2) and the hydroxyl group at carbon atom 3 (C3) of the adjacent glucose unit on

the cyclodextrin periphery, that prevents the β -CD from being soluble in most of the media, whereas, MCT β -CD is produced by the substitution of primary C6 -OH groups from the smaller rim of β -CD (which are the most susceptible to substitution). Thus, the substitution had helped in the relaxation of the boat-skew structure of unmodified β -cyclodextrin, and also, the intramolecular H-bond belt is prevented to form, thereby increasing its solubility in water.

Optimization of process parameters for MCT β -CD application on cotton

The desirability function (DF) = $f\{N_2, GY, TS, \text{ and } WD\}$ was formulated as:

$N_2\%$ is % nitrogen targeted to 'maximum', GY% is % Graft yield targeted to 'maximum', TS is % change in Tensile strength targeted to '1.82' (maximum on the +ve scale, experimental data), WD is wash durability in terms of % retained weight gain after 5th wash is targeted to 'maximum'. The optimum DF was achieved at 0.912 at the optimized process variables. The overall DF analysis and formulated model equations are shown in Table 1.

Nitrogen content (N_2)%

The increase in MCT β -CD concentration had shown an increase in $N_2\%$ on cotton due to the availability of more MCT β -CD molecules from the solution for attachment on the substrate. On the other hand, the increase in pH of MCT β -CD solution had resulted in $N_2\%$ increase from 0.179 to 0.56% at pH 6-8 and then decreased up to 0.263% at pH 10. MCT β -CD was unstable in acidic pH of 6 and got stabilized at pH 8 (near to neutral), finally got hydrolyzed at pH 10; thereby reducing the extent of $N_2\%$ on cotton. The minimum of N_2 (0.169%) was found at 60 gpl, 8 pH and 100 °C and maximum of N_2 was observed at 70 gpl, 8 pH and 125 °C. The interaction of concentration and pH had resulted in the achievement of the highest $N_2\%$ at 70 gpl and pH ~8 as shown in Fig. 3a. With the increase in concentration and temperature, $N_2\%$ decreased substantially due to the hydrolysis of chlorotriazine moiety that prevented its fixation on cotton as shown in Fig. 3b, c.

Graft yield (GY)%

Graft yield% is dependent on the concentration of MCT β -CD and pH as in Fig. 4a. With the increase in concentration and pH from (60 gpl and 6 pH) to (80 gpl and 10 pH), GY% had increased from 9.5% up to 13.43% due to the favorable conditions for the MCT β -CD moiety adherence on cotton; higher MCT β -CD concentration and alkaline pH ~10 had facilitated add on % for cotton but temperature had little or no impact as the interaction of concentration and pH had the decisive affect on the fixation of MCT β -CD as shown in Fig. 4b, c. The difference in the trends of $N_2\%$ and GY% was observed, attributed to the reason that $N_2\%$ on substrate is the actual indicator of the MCT β -CD presence rather, GY% is an indirect mode. The hydrolysis of chlorotriazine moiety at high temperatures directly indicated lesser adherence of cyclodextrin cavities on cotton via monochlorotriazine bridge, while higher GY% at higher temperatures could be due to free and unmodified cyclodextrin cavities present in the synthesized MCT β -CD powder attached superficially on the cotton; mostly susceptible to removal during washing.

Table 1 Experimental responses of MCT β -CD treatment on cotton

Run no.	Independent variables				Responses							Quantified MCT β -CD on cotton (g/100 g fabric)
	Concentration (gpl)	pH	Temperature of curing ($^{\circ}$ C)	GY%	N ₂ %	TS%	WD					
							1st	2nd	3rd	4th	**5th	
1	70	6	150	10.12	0.202	-3.56	10.1	10.05	10.01	9.95	9.96	2.89
2	70	8	125	12.90	0.46	-2.15	12.87	12.84	12.76	12.43	12.36	6.57
3	70	8	125	12.85	0.432	-2.19	12.81	12.78	12.67	12.56	12.34	6.17
4	60	10	125	12.56	0.263	-6.03	12.48	12.41	12.31	12.17	12.02	3.76
5	80	6	125	10.51	0.368	1.48	10.38	10.14	10.02	9.78	9.52	5.26
6	70	8	125	12.40	0.422	-2.21	12.36	12.31	12.22	12.19	12.15	6.03
7	80	8	100	13.41	0.448	1.82	13.28	13.14	13.02	12.87	12.78	6.4
8	70	10	100	13.20	0.432	-5.85	13.11	13.02	12.93	12.82	12.78	6.17
9	70	10	150	13.15	0.312	-6.45	13.07	13.01	12.97	12.89	12.82	4.46
10	70	8	125	12.81	0.441	-2.24	12.76	12.69	12.52	12.37	12.19	6.3
11	60	6	125	9.50	0.179	-2.34	9.41	9.22	9.02	8.91	8.86	2.55
12	60	8	100	11.53	0.169	-3.29	11.23	11.11	10.97	10.82	10.74	2.41
13	80	8	150	13.00	0.334	1.18	12.94	12.86	12.65	12.51	12.45	4.77
14	60	8	150	11.43	0.165	-3.11	11.25	11.08	10.78	10.65	10.44	2.36
15	70	8	125	12.54	0.422	-2.21	12.46	12.32	12.21	12.21	12.01	6.02
16	80	10	125	13.43	0.458	-0.32	13.12	13.02	12.92	12.83	12.77	6.54
17	70	6	100	10.10	0.198	-3.09	10.02	9.89	9.74	9.63	9.55	2.82

Table 1 Continued

Response	Statistical analysis of DF (model equations)	R ²	Adjusted R ²	Predicted R ²	Lack of fit (Prob > F)
Y1, GY%	Model equations -31.86 + 0.47X ₁ + 4.72X ₂ + 0.06X ₃ - 0.237X ₁ ²	0.980	0.954	0.786	0.210; not significant
Y2, N ₂ %	0.44 + 0.10 X ₁ + 0.065X ₂ - 0.03X ₃ - 0.065X ₁ ² - 0.0058 X ₂ ²	0.9773	0.9481	0.690	0.0459; not significant
Y3, T5%	50.42 - 2.849X ₁ + 4.71X ₂ + 0.37X ₃ + 0.07X ₁ ² - 0.44X ₂ ² + 0.024X ₁ * X ₂	0.999	0.998	0.991	0.011; not significant
Y4, WD	41.46 + 0.799X ₁ + 4.4X ₂ + 0.04X ₃ - 0.53X ₂ ²	0.962	0.914	0.441	0.012; not significant

GY% graft yield, N₂% nitrogen, T5% change in tensile strength, WD wash durability up to 1, 2, 3, 4. ** 5th washes (% retained weight gain), X₁ concentration of MCT β-CD solution, X₂ pH of MCT β-CD solution, X₃ temperature of curing (°C)

** WD after 5th wash considered for the analysis

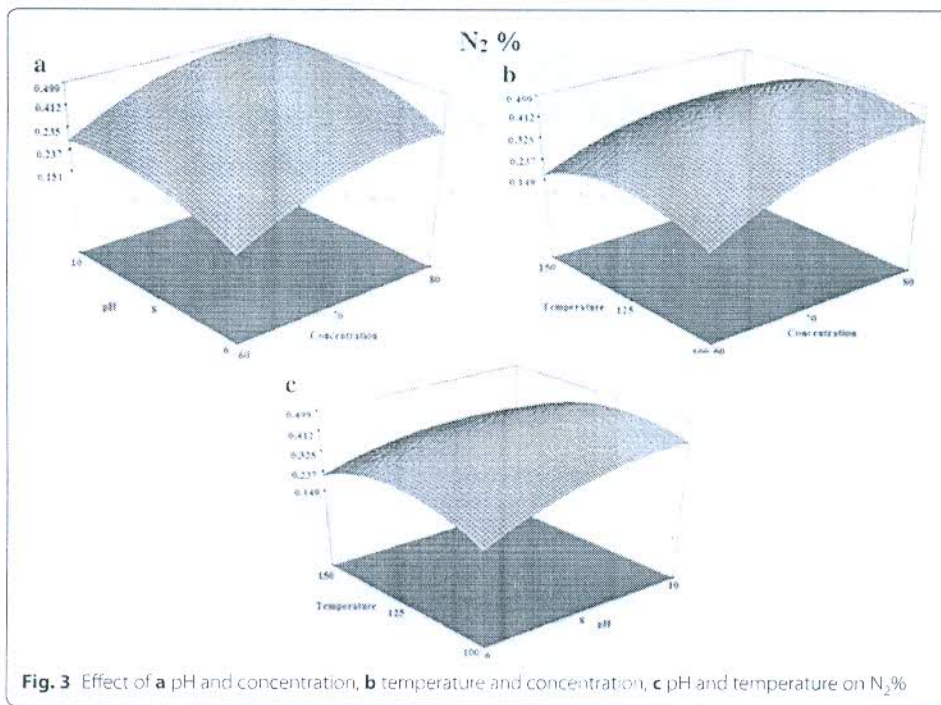


Fig. 3 Effect of **a** pH and concentration, **b** temperature and concentration, **c** pH and temperature on $N_2\%$

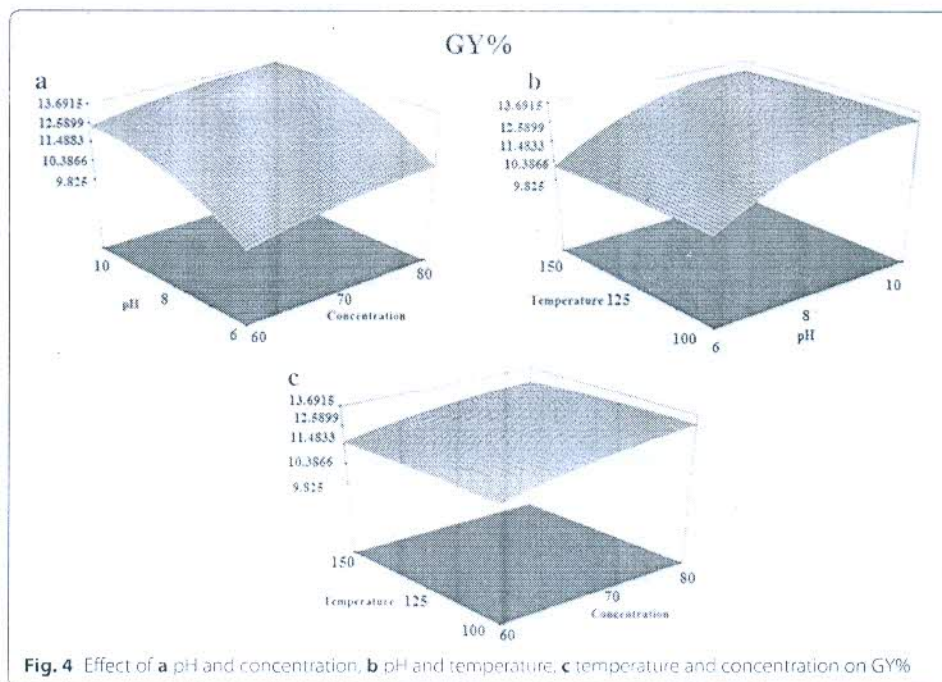


Fig. 4 Effect of **a** pH and concentration, **b** pH and temperature, **c** temperature and concentration on GY%

Change in tensile strength (TS)%

With the increase in MCT β -CD concentration from 60 to 80 gpl at pH 6 and 125 °C, the change was from -2.34 to -3.56% up to +1.48%. At pH ~10 and 125 °C, TS% was -6.03 to -5.85% up to -0.32%. This indicated that with the increase in the concentration of MCT β -CD, less loss is exhibited in TS%. But with the interaction of pH with

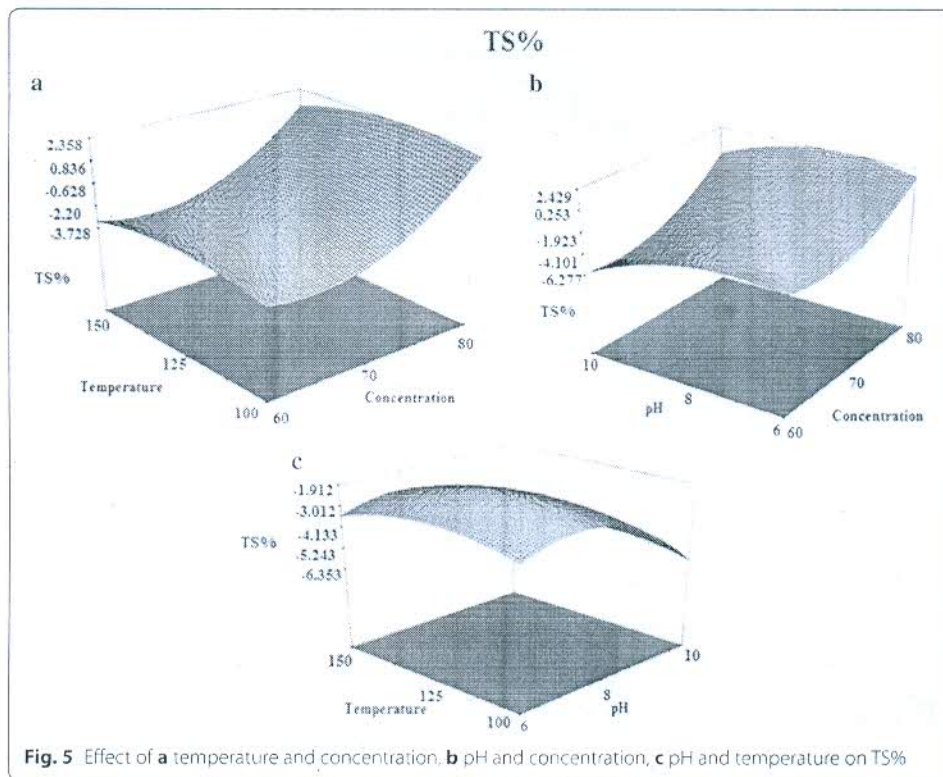
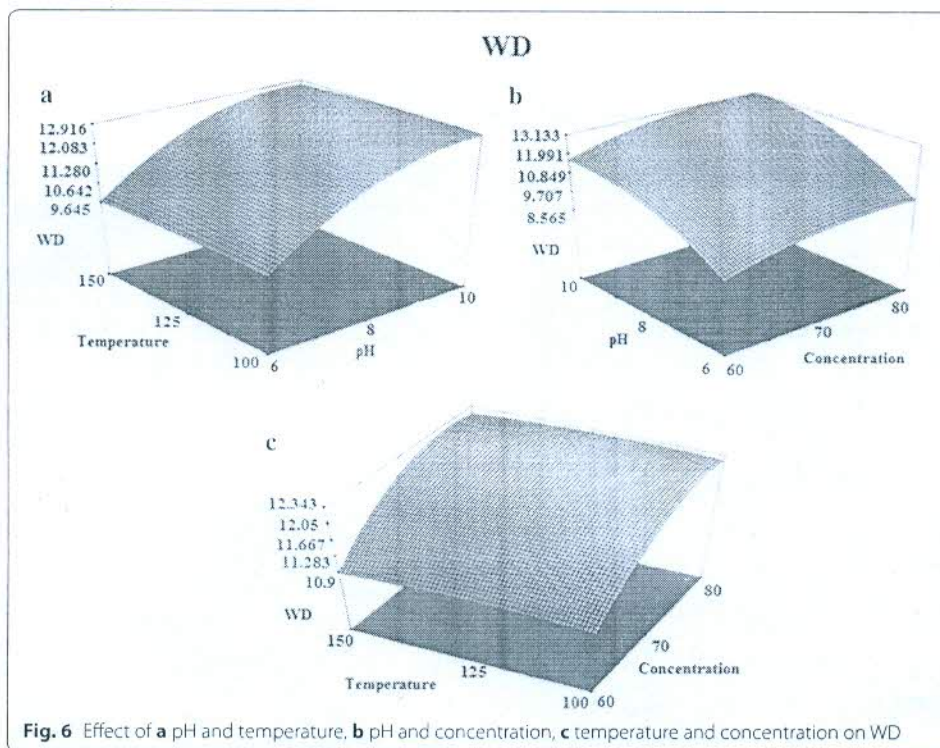


Fig. 5 Effect of **a** temperature and concentration, **b** pH and concentration, **c** pH and temperature on TS%

concentration, strength loss was encountered up to 70 gpl followed by an increase at 80 gpl; might be due to the plasticizing effect of MCT β -CD at higher concentrations that seemed to lessen the restriction of segmental movement of the cellulose chains in the cotton fibre. On the other hand, at pH 10, strength loss reduced from 60 to 80 gpl but the affect of high pH had overpowered the concentration increase to keep the variable on the negative side as shown in Fig. 5a. Thus, the interaction between pH and concentration was the main influence behind the strength loss. Degradation of cotton was observed at higher alkaline pH due to the formation of intermolecular and intramolecular crosslinks that reduces the possibility of equalizing the stress distribution, causing reduction in the capacity to withstand load. Increase in temperature from 100 to 150 °C at 70 gpl and increasing pH (6–10), –3.09 to –6.45% was the observed change (Fig. 5b). The major change was seen at pH 10 with increasing temperature from 100 to 150 °C (–5.85 to –6.85%), due to cotton tendering at higher temperatures in presence of alkaline pH (above 125 °C) (Fig. 5c).

Wash durability (WD) as % retained weight gain

The highest WD of 12.77% (with GY% of 13.43-without wash) at 80 gpl and pH ~10 with a minimum of 8.86% (with GY% of 9.5-without wash) was observed at 60 gpl and pH ~6. It followed the similar trend as GY% i.e. with the increase in the levels of both concentration and pH, WD was improved as MCT β -CD was affixed in a durable manner and thus, better retention of the host cavities on cotton (Fig. 6 b). Temperature had a little role to play as an independent factor but its interaction with either pH or concentration,



especially at their higher levels of (pH 10 and 150 °C) or (80 gpl and 150 °C) had shown a fall in WD due to the intervention of high temperature despite high initial GY% and superficial deposition of cyclodextrin cavities on cotton; which is further supported by N2%. Thus, subsequent washing had resulted in the removal of the apparent MCT moieties from the cotton surface at higher temperature (Fig. 6a, c).

The cotton was treated at optimized process variables viz. MCT β -CD concentration (79.01 gpl), pH (7.57) and curing temperature (112.37 °C). Then, this functionalized cotton was given 5 subsequent wash down treatments and comparative FTIR was recorded that assured the presence of MCT β -CD-cellulose grafting intact even after wash treatments as apparent in the unwashed treated cotton at 1157 cm^{-1} (ether group) as seen in Fig. 7. Residual % N₂ was analyzed for functionalized cotton (with and without wash) as -0.489 (Without wash), 0.252 (1st wash), 0.235 (2nd wash), 0.205 (3rd wash), 0.201 (4th wash) and 0.2 (5th wash) that evinced the presence of the reactive host even after washing of cotton. This also ascribed the initial % N₂ loss during first two washes was due to the inadequate cross linking of MCT β -CD with cotton resulting in washing off MCT β -CD but with further washes, the % retained N₂ content had stabilized.

Inclusion complexation of MCT β -CD and oils on cotton

¹H-NMR was consummated for inclusion complexation analysis of MCT β -CD-oils on cotton (Table 2; Figs. 8, 9). The chemical 'δ' and induced chemical shifts 'Δ δ' of the MCT β -CD and oils in free as well as in compounded state had revealed evident shifts ensuring the formation of dynamic complexes between anchor and guests. Δ δ (H5 > H3) had revealed significant entrapment of oil molecules into the cavities for both oils confirming

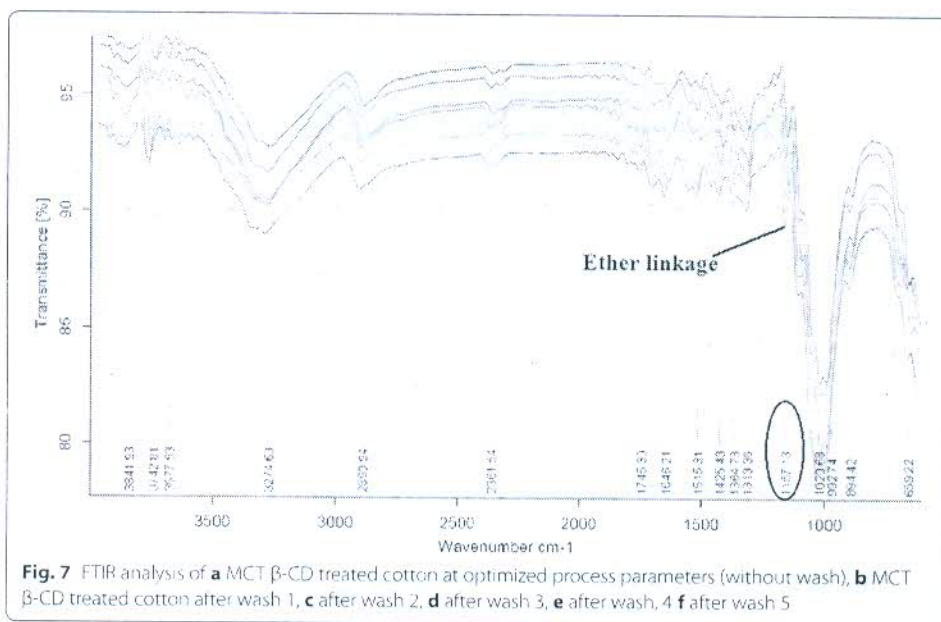
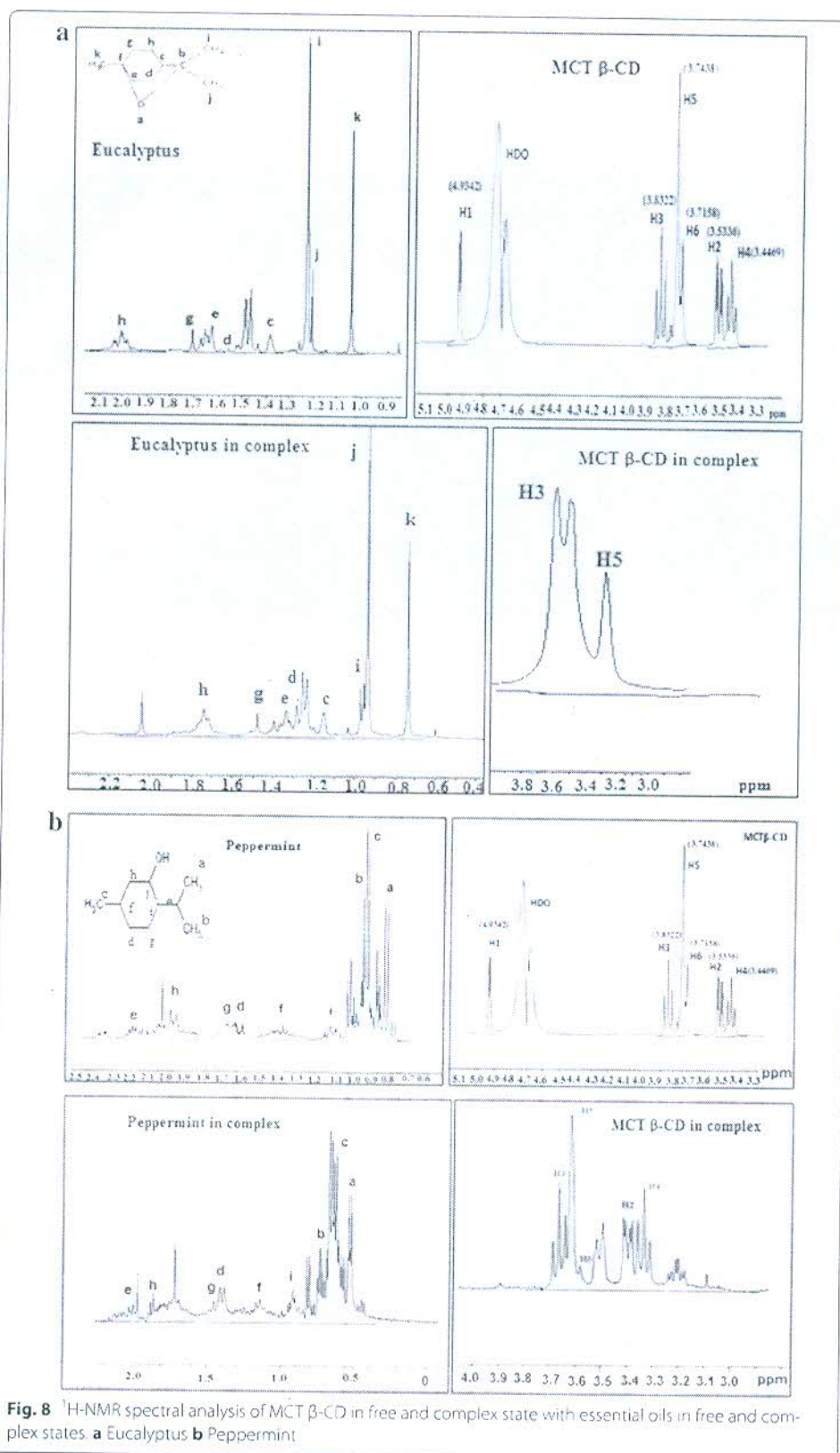


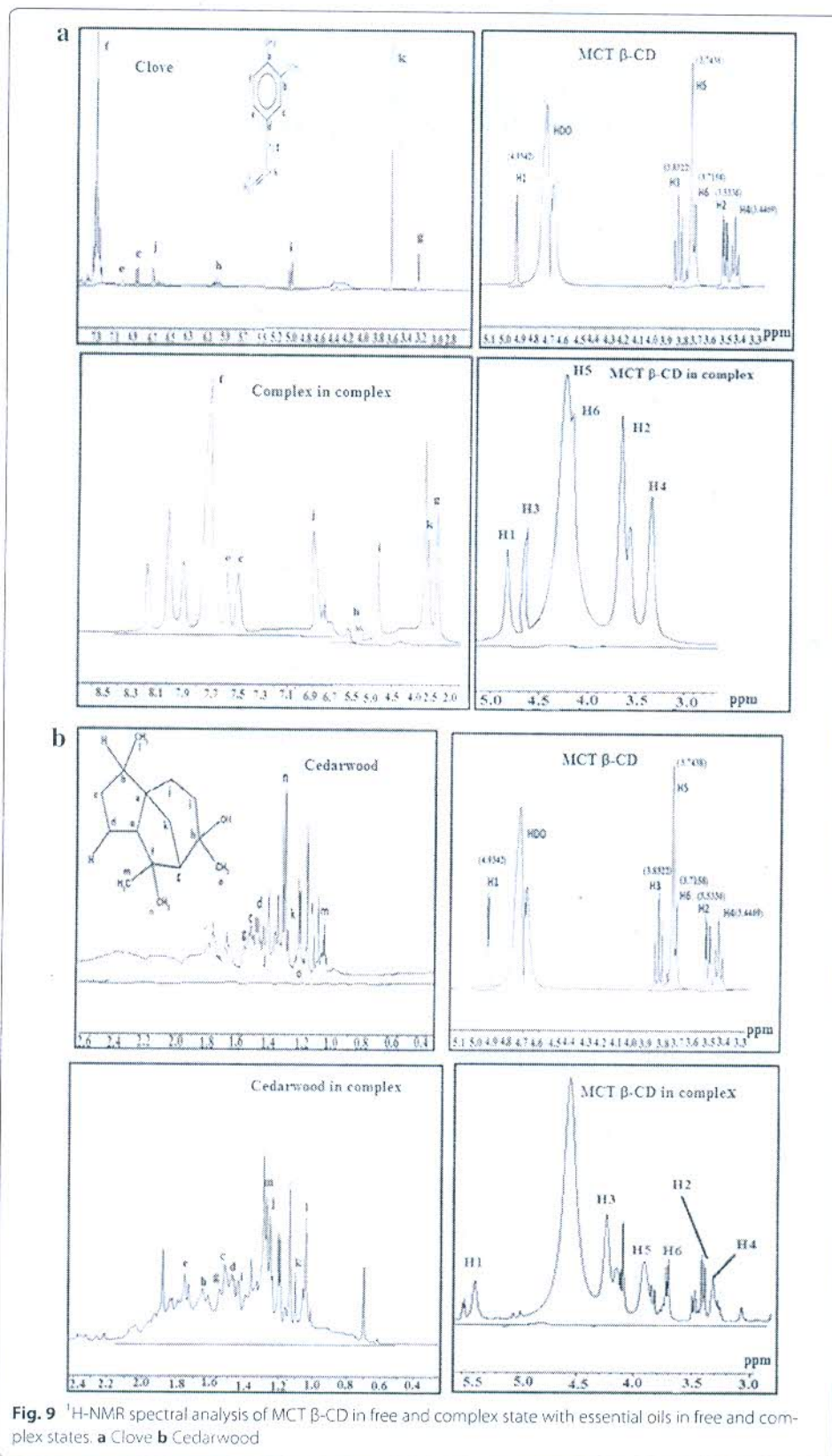
Table 2 Induced shift analysis of MCT β -CD-oil complexes in free and complex states

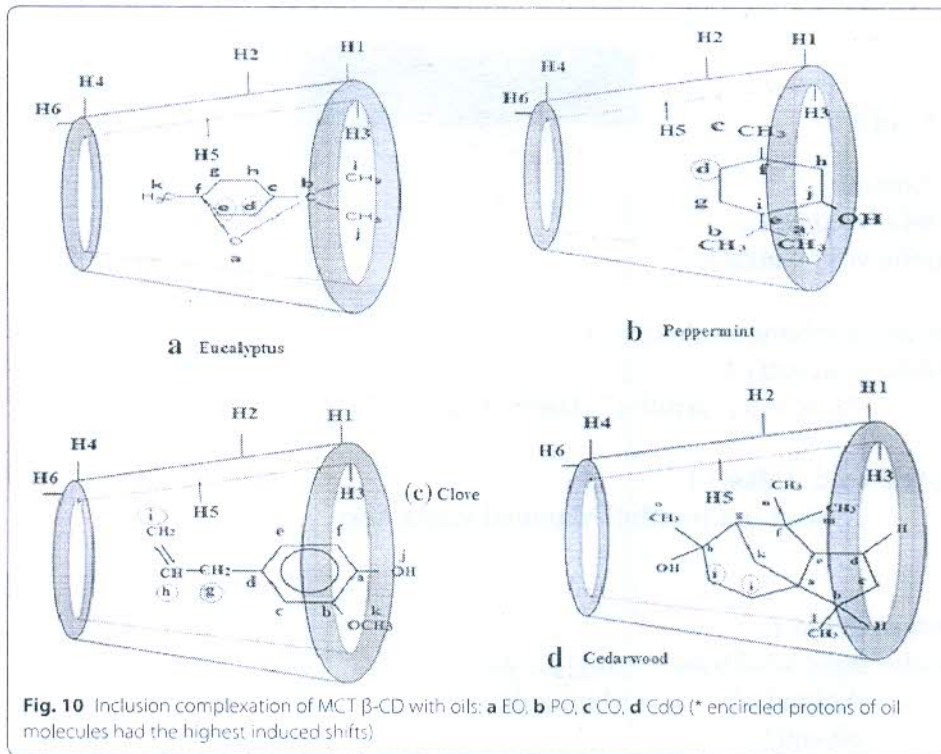
Proton (MCT β -CD)	$\delta^1_{\text{MCT } \beta\text{-CD (free)}}$	$\delta^{*2}_{\text{MCT } \beta\text{-CD (complex)}}$	$\Delta \delta^3_{\text{MCT } \beta\text{-CD}}$	$\delta^4_{\text{oil (free)}}$	$\delta^{*5}_{\text{oil (complex)}}$	$\Delta \delta^6_{\text{oil}}$	Proton (oil)	Oil type
H3	3.8322	3.7398	0.3446	3.2453	2.321	0.9243	H _g	CO
H5	3.7438	3.4124	0.3034	5.8937	5.131	0.7627	H _h	
				5.0256	4.823	0.2026	H _i	
H3	3.8322	4.659	-0.8268	1.5895	1.5123	0.0772	H _j	CdO
H5	3.7438	4.269	-0.5252	1.3601	1.2966	0.0635	H _j	
H3	3.8322	3.4873	0.3446	1.5592	1.2602	0.299	H _d	EO
H5	3.7438	3.1758	0.5681	1.6295	1.3390	0.286	H _e	
H3	3.8322	3.54	0.2922	0.7989	0.7357	0.0632	H _k	PO
H5	3.7438	3.3644	0.3794	1.6755	1.5584	0.1171	H _g	

$\delta^1_{\text{MCT } \beta\text{-CD (free)}}$ chemical shift of MCT β -CD in free state; $\delta^{*2}_{\text{MCT } \beta\text{-CD (complex)}}$ chemical shift of MCT β -CD in complex with oils; $\Delta \delta^3_{\text{MCT } \beta\text{-CD}}$ induced shift of MCT β -CD ($\delta^1_{\text{MCT } \beta\text{-CD (free)}} - \delta^{*2}_{\text{Complex}}$); $\delta^4_{\text{oil (free)}}$ chemical shift of oils in free state; $\delta^{*5}_{\text{oil (complex)}}$ chemical shift of oils in complex with MCT β -CD; $\Delta \delta^6_{\text{oil}}$ induced shift of oils ($\delta^4_{\text{oil free}} - \delta^{*5}_{\text{oil}}$)

the full inclusion of oils into the MCT β -CD cavity as H5 is more deeply embedded into MCT β -CD cavity than H3. ¹H-NMR spectra had shown generation of no newer peaks for any oil as complex formation was a dynamic process, the included oils being in a faster exchange between the free and bound states. The $\Delta \delta$ for oils had shown that in EO, Hk, Hd and He protons had shown more induced shifts than the other protons. This could be an indication that the oil had entered from the tail side into the cavity. Similarly, Hd and Hg for PO showed the inclusion of oil from the bottom side; Hi and Hj for CdO depicted segmental inclusion of the oil into the cavity and CO had shown the induced shift pattern as either Hk or Hg, Hh and Hi sided penetration into the cavity as shown in Fig. 10.

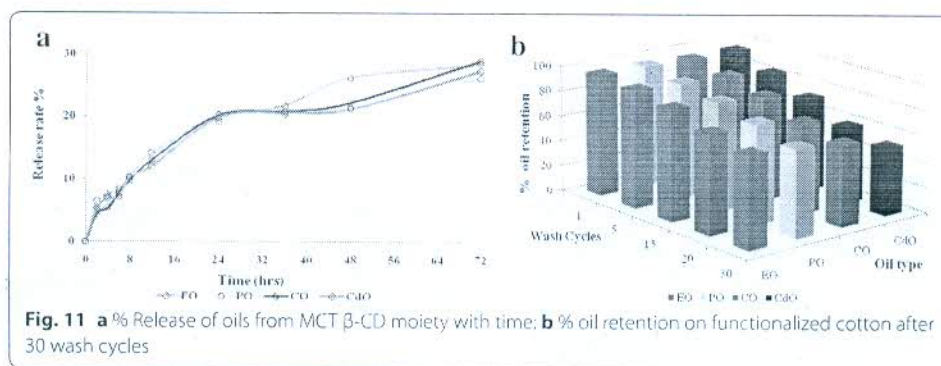






Stability analysis of oils through MCT β -CD complex—before and after wash

The application of oils on cotton was through the host compound rather than its direct application on cotton, in which, the oils are physically adsorbed on the treated surface in three subsequent phases; surface adsorption, absorption and finally the capillary action of oils into the fibrous pores of cotton that result in the development of vander-waal forces between oils and cotton at low temperature. Oils generally forms multi-molecular layer on the surface of cotton. But, covalent bonded host (MCT β -CD) tends to trap the oils into its cavities that further depends upon the compatibility between the sizes of guest and host cavity and also the thermodynamic interactions between host, guest and the solvent used (alcohol in the present case) due to the requirement of the structural conformation for either partial or full entrapment of oils into the cavities of host. The oils are hydrophobic (apolar) in nature, so these bind strongly to the hydrophobic cavities of the host. The retention of oils in the host cavities don't comply with the chemical bonding between the host and oils as the formation of inclusion complex do not exert any structural modification of the oils to be chemically bonded to the host or cotton. As if, the oils get chemically bonded to the host cavities, then to release oils on demand would require a lot of activation energy to dismantle oils from the host cavities. Thus, only non-covalent bonds (hydrophobic interactions along with vanderwaal forces) are formed in inclusion complex that allows the oils to be released on its own due to its volatile nature in a controlled manner as there is a dynamic equilibrium between the oils trapped in the host cavity and the water (moisture) present in its surroundings. Thus, all experimented oils fit well into the host cavities and had shown a curtailed release from the cotton. EO and CO were the slowest to fade off in the initial hours in comparison to the PO and CdO, with



EO being the most stable after initial 2 h, whereas, CO had shown the fastest sublimation (Fig. 11a). After the initial quick release of PO, the oil had shown a moderate release rate after 72 h. This was due to the better settlement of oil in the cyclodextrin cavities after the initial sublimation from the cotton surface during drying. This had facilitated the suppression of oil release from the cotton's surface and thus, prevented their fading off. The eugenol of CO is the middle note of the oil; on the other hand, cedrol of CdO behaves as the base note that lasted for longer time span than eugenol. In addition, monoterpenes as eugenol and thyme constitutes CO, whereas, sesquiterpenes as cedrol forms the backbone CdO. Their presence dictates the volatility of oils from cotton as monoterpenes being more volatile than the sesquiterpenes from the oil compositions.

All the oils were retained almost up to 65% even after 20 vigorous washes and substantial oil % was still present even after 30 washes. The high % aroma retention was due to the presence of anchored cavities to hold and control the release of oil from the surface of cotton. EO > PO > CO > CdO was the observed trend of % retained oils. CdO was left in the least proportion on cotton. This might be due to the reason that the retention time of cedarwood was the minimum on cotton that washed off easily after wash cycles as seen in Fig. 11 b.

Conclusions

The concentration and pH of MCT β -CD are the most influencing variables for the treated cotton as increase in concentration and pH of MCT β -CD had resulted in an increase in GY%, but TS% was tremendous ranging from low strength loss at low pH values along with some strength improvement at higher concentrations and low pH index, however, at higher pH, the strength had decreased. With the increase in concentration and temperature together, N₂% had decreased but pH played a role in the prevention of the hydrolysis of the chlorotriazine moiety for better fixation onto cotton. The inclusion complex of MCT β -CD and oils had suppressed the quicker fading off the oils from the semi-enclosed cavities.

Authors' contributions

AK and JNC planned the work, AK carried out the work and drafted the manuscript. Both authors read and approved the final manuscript.

Competing interests

The authors declare that they have no competing interests.

Received: 5 June 2016 Accepted: 24 October 2016
Published online: 28 March 2017

References

- Anitha, R., Ramachandran, T., Rajendran, R., & Mahalakshmi, M. (2011). Microencapsulation of lemon grass oil for mosquito repellent finishes in polyester textiles. *Elixir Bio Physics*, 40, 5196–5200.
- Bendak, A., Allam, O. G., & El Gabry, L. K. (2010). Treatment of polyamides fabrics with cyclodextrins to improve antimicrobial and thermal stability properties. *The Open Textile Journal*, 3, 6–13.
- Bereck, A. (2010). Cyclodextrins in textile finishing: Fixation and analysis. *Advanced Material Research*, 93–94, 1–4.
- Bergamasco, R. C., Gisella, M. Z., & Flavio, F. M. (2007). Grafting of cyclodextrins onto filter paper. *Journal of Inclusion Phenomenon and Macrocyclic Chemistry*, 57, 75–78.
- Bhaskara-Amrit, U. R., Agrawal, P. B., & Warmoeskerken, M. M. C. G. (2011). Applications of β -cyclodextrins in textiles. *Autex Research Journal*, 11(4), 94–101.
- Boonsod, T. (2007). *Finishing cotton and silk fabric with Glyoxal β -cyclodextrin complexes*. Thesis: Graduate School, Kasetsart University.
- Cabrales, L., Abidi, N., Hammond, A., & Hamood, A. (2012). Cotton fabric functionalization with cyclodextrins. *Journal of Material & Environmental Sciences*, 3(3), 561–574.
- Halim, A., El-Newehy, F. A., Abdel-Mohdy, F. A., & Al-Deyab, S. S. (2010). Chitosan and monochlorotriazinyl-beta-cyclodextrin finishes improve antistatic properties of cotton/polyester blend and polyester fabrics. *Carbohydrate Polymers*, 82(1), 202–208.
- Halim, A. E. S., Fouda, M. M. G., Sanaa, M. El-S., Hamdy, I., & Al-D., Salem S. (2011). Antimicrobial activity of monochlorotriazinyl- β -cyclodextrin/chlorohexidin diacetate finished cotton fabrics. *Carbohydrate Polymers*, 86, 1389–1394.
- Hauser, P. J., & Jianshuo, N. (2000). Covalently bound cyclodextrin: a new functional finish for celluloses. *Proceedings of the Annual International Conference & Exhibition of AATCC*, 1, 1–8.
- Ibrahim, N. A., Allam, E. A., El-Hossainy, M. B., & El-Zairy, W. M. (2007). UV-protective finishing of cellulose/wool blended fabrics. *Polymer-Plastic Technology and Engineering*, 46(9), 905–911.
- Khanna, S., Sharma, S., & Chakraborty, J. N. (2015). Performance assessment of fragrance finished cotton with cyclodextrin assisted anchoring hosts. *Fashion & Textiles*. doi:10.1186/s40691-015-0042-9, 1–17.
- Leyva, E., Moctezuma, E., Strouse, J., & Agaribay, M. A. G. (2001). Spectrometric and 2D NMR Studies on the complexation of chlorophenols with cyclodextrins. *Journal of Inclusion Phenomenon and Macrocyclic Chemistry*, 39, 41–46.
- Marwa, A. A., Amr, A., Abou-Okeil, A., & Nermin, M. A. (2013). Comfort properties of the inner padding layer for motorcycle helmet. *Life Sciences Journal*, 10(4), 1386–1399.
- Medronho, B., Andrade, R., Vivod, V., Ostlund, A., Miguel, M. G., Lindman, B., et al. (2012). Cyclodextrin-grafted cellulose: Physico-chemical characterization. *Carbohydrate Polymers*, 30, 1–7.
- Moldenhauer, J. P. & Reuscher, H. (1999). Textile finishing with MCT- β -cyclodextrin. In J. J. Torres Labandeira, J. L. Vila-Jato (Eds.), *Proceedings of the 9th International Symposium on Cyclodextrins* (pp. 161–165). Dordrecht: Kluwer Academic Publishers.
- Nelson, G. (2002). Application of microencapsulation in textiles. *International Journal of Pharmaceutics*, 242, 55–62.
- Peila, G. R., Migliavacca, F. A., & Sicardi, A. F. S. (2012). A comparison of analytical methods for the quantification of a reactive β -cyclodextrin fixed onto cotton yarns. *Cellulose*, 19, 1097–1105.
- Pessine, F. B. T., Calderini, A., & Alexandrino, G. L. (2012). Review: Cyclodextrin Inclusion Complexes Probed by NMR Techniques. *Magnetic Resonance Spectroscopy*, Prof. Dong-Hyun Kim (Ed.), ISBN: 978-953-51-0065-2, InTech, Available from: <http://www.intechopen.com/books/magneticresonance-spectroscopy/review-study-of-inclusion-complexes-with-cyclodextrins-by-mrs>, pp. 237–264.
- Popescu, V., Muresan, E. I., & Grigoriu, Ana-M. (2011). Monochlorotriazinyl- β -cyclodextrin grafting onto polyester fabrics and films. *Carbohydrate Polymers*, 86, 600–611.
- Rehmann, L., Yoshii, H., & Furuta, T. (2003). Characteristics of modified β -cyclodextrin bound to cellulose powder. *Starch/Stärke*, 55(1), 313–318.
- Shahba, F. A. (2008). Production and characterization of novel perfumed curtain fabrics. *Research Journal of Textiles & Apparels*, 12(4), 31–40.
- Shown, I., & Murthy, C. N. (2008). Grafting of cotton fiber by water-soluble cyclodextrin-based polymer. *Journal of Applied Polymer Science*, 111(4), 2056–2061.
- Sricharussin, W., Sopajaree, C., Maneerung, T., & Sangsuriya, N. (2009). Modification of cotton fabrics with β -cyclodextrin derivative for aroma finishing. *Journal of Textile Institute*, 100(8), 682–687.
- Wen, J., Liu, B., Yuan, E., Ma, Y., & Zhu, Y. (2010). Preparation and physicochemical properties of the complex of narangenin with hydroxypropyl- β -cyclodextrin. *Molecules*, 15, 4401–4407.



Sustainable fragrance cum antimicrobial finishing on cotton: Indigenous essential oil

Nagender Singh^a, Manisha Yadav^b, Shelly Khanna^c, Omprakash Sahu^{d,*}

^a Ethiopian Institute of Textile and Fashion Technology, Bahir Dar University, Ethiopia

^b Department of Textile Technology, Indian Institute of Technology Delhi, India

^c Dept. of Fashion and Apparel Engg. The Technological Institute of Textile and Sciences, India

^d Faculty of Chemical and Food Engineering, BIT, Bahir Dar University, Ethiopia

ARTICLE INFO

Keywords:

Cotton fabric
Fragrance finishing
Lavender
Microencapsulation
Textile testing

ABSTRACT

Fragrance finishing of textile has been enormously increased and used in domestic and industrial application. Fragrance can be synthesis chemically but available in natural and inorganic. The investigation of this research is to study the combined effect of fragrance and antimicrobial finishing on cotton fabric by lavender essential oil with the use of β -Cyclodextrin, Chitosan citrate and β -Cyclodextrin/Grafted Chitosan through pad-dry method. Fourier Transform Infrared spectroscopy (FTIR) was used to study the formation of ester bonds between β -cyclodextrin/grafted chitosan and cotton celluloses. For all the finished fabric samples fragrance release rate performance and antimicrobial properties were measure by standard test methods. The results revealed that β -CD was highly soluble in 0.6 gpl NaOH solution and 80 gpl β -CD and 6% essential lavender oil solutions were found to be a most suitable combination for fragrance and antimicrobial finishing. FTIR studies reveal about the formation of a carboxylic ester between cotton and β -Cyclodextrin/Grafted Chitosan at 1730 cm^{-1} ester peak.

1. Introduction

The fragrance is the word, which represents indulgence, pleasure, and luxury (Toda and Morimoto, 2008). Fragrances have been used widely in different engineering fields includes textile, medicine, food, tobacco, leather, papermaking, cosmetics etc. due to their antibacterial effect, sedative effect and tranquillization (Kyle, 2006; Nelson, 2001). Nowadays, finishing a textile with fragrance is an important commercial target and an engineering challenge. Pure fragrance compounds and essential oils have been used traditionally in folk medicine for a long time (Chandrasekaran et al., 2015). The term aromatherapy was a coin in the late 1920s by the French cosmetic chemist R.M. Gattefosse, who noticed the excellent antiseptic properties and skin permeability of essential oils (Butcher, 1998). A fragrance is a mixture of individual chemicals and has its own unique properties. Each fragrance component is interacted differently, according to chemical and structural nature (Herman, 2009).

In aromatherapy textiles, herbs essential oil is use for antimicrobial, fragrance and medical properties (Ghavamipour and Montazer, 2016). Over the last 50 years, plants utilized as a potential source of natural aromas in the form of essential oils (Cheng et al., 2008). In literature, it has been reported that the essential oils with high aromatic index are

used as insect repellency and antimicrobial growth agent (Matsushiki-Shikiso Chemical Co Ltd., 1994). Lavenders are one of the aromatic plants, which has been used medical application and fragrance industry, including soaps, colognes, perfumes, skin lotions and other cosmetics purpose (Hamada et al., 2001). It belongs to the mint family and found in the Mediterranean region of Africa and some part of Asia (Piccaglia et al., 1993). Lavender fragrance oil is believed to be of benefit for numbers of ailments, including stress, anxiety, exhaustion, irritability, headaches, migraines, depression, colds, digestion (Cheng et al., 2008). Presently, sustainability and making eco-friendly product are the focus of the textile and apparel industry. Microencapsulation can be an important tool to protect unstable or non-substantive biodegradable fragrance (Samanta et al., 2014).

During the preparation of aromatherapy textile, the most difficult task is to prolong the lifetime of fragrance. Micro-encapsulation technique found to be an effective solution of this difficulty (Samanta et al., 2016; Yin and Luk, 2016). Although there are many effective approaches of micro-encapsulation for decreasing fragrance-release, cyclodextrins are the best among them (Buschmann et al., 1991). β -CD can be incorporated onto textile by means of spraying, printing, padding, grafting, surface coating, impregnation, ink jet printing and via sol-gel (Agrawal and Warmoeskerken, 2008; Martel, 2002a,

* Corresponding author.

E-mail address: opst0121@gmail.com (O. Sahu).

2002b). In the textile area, cyclodextrin has been used for imparting properties i.e., UV protection, slow release of fragrances, insecticide delivery, and antibacterial activity (Andreas et al., 2010). The most notable feature of CDs is their ability to form solid inclusion complexes (host–guest complexes) with a very wide range of solid, liquid and gaseous compounds by molecular complexation (Meo et al., 2003). They have a high level of biocompatibility and are approved by FDA (Food and Drug Administration), thus CDs are friendly to humans. Furthermore, CDs are now readily available, and their price and production costs have declined in recent years (Jug et al., 2008).

The Chitosan is N-deacetylated form of chitin that is obtained by alkaline treatment of chitin (50% of aqueous NaOH) at high temperature (Kurita, 1998). Chitosan and its derivatives have become useful polysaccharides in the biomedical area because of its biocompatible, biodegradable, and non-toxic properties (Leo et al., 1997). It is utilized in the textile industry as an antimicrobial agent due to its ability to provide protection against allergies and infection diseases, coupled with moisture retention and wound healing capabilities (Dutta et al., 2004).

Although, the chemicals and processes used in this research are environment friendly and highly compatible. β -CD, Chitosan and lavender oil are drives form natural resources and readily available including least prices. This work has been done by focusing the triple bottom line of suitability i.e. economic, society and environment.

The aim of this research was to explore the lavender oil as an excellent value addition to home furnishings. The characterization of lavender essential oil with β -Cyclodextrin, chitosan citrate and β -Cyclodextrin/Grafted Chitosan were studied by FTIR spectra of cotton. On finished textile, the effects of fragrance, antimicrobial finishing of treated fabrics were done through pad-dry method.

2. Material and methods

2.1. Material

A 100% cotton fabric procured from 'Vardhman Fabrics', Ludhiana was used for experiment work. The specifications and properties of cotton mentioned in Tables 1 and 2 respectively. All analytical grades chemicals purchased from SDFCL Fine-Chem Limited Mumbai.

2.2. Experimental procedure

The analysis of solubility of β -CD in different mediums such as water, ethanol, and NaOH was determined by dissolving different concentrations of β -CD (10–100 gpl) in water, 50% ethanol and 6gpl NaOH for 30 min (Joshi et al., 2009). Calibration of lavender oil for fragrance analysis was done by measuring the absorbance of different concentrations of lavender as (1–10%) in 100% ethanol through UV/Visible spectrophotometer at λ_{max} (344 nm). A calibration curve thus obtained to detection of the unknown concentration of fragrance in the solution. Optimization of β -CD concentration for finishing was analyzed by weight gain and phenolphthalein titration. For phenolphthalein titration a 1% phenolphthalein solution was prepared in 80% ethanol and pH of the solution was adjusted to 10.5 by using electronic pH meter and 0.5 M sodium hydroxide solution followed by wave-

length of phenolphthalein solution was obtained as λ_{max} 558 nm through UV/Visible spectrophotometer, β -cyclodextrin treated fabric samples with different concentration were cut to a dimension of 1×1 cm and immersed independently in 30 ml phenolphthalein solution as prepared above and shaken at 35 °C for 1 h in orbital shaker at 100 rpm, then fabric was removed from the solution and absorbance of phenolphthalein solution was measured with a dilution factor of 4 at λ_{max} 558 nm. After calibration of lavender oil, different concentrations of lavender oil (1–10%) with 100% ethanol were prepared and immersed 0.1g fabric samples in each concentration followed by measurement of absorbance of remaining solution. Inclusion complex formation between β -CD and lavender was analyzed by using their optimized concentrations. Four sets of fragrance finished samples were prepared namely Lavender alone (L), β -CD and lavender (β -CD-L), Chitosan citrate and lavender (CC-L) and β -CD/ grafted chitosan and lavender (β -CD-CS-L). Characterization of β -CD-C and β -CD-CS was done in the experimental process to synthesized β -CD-CS, which were a two-step process: esterification of β -CD with citric acid and then it's grafting with chitosan. In general, the incorporation of a guest molecule involves the wider (secondary hydroxyl groups) towards rim side of β -CD. Therefore, the primary hydroxyl group side of β -CD has been suitable for conjugating with citric acid. In addition, FTIR comparative spectra of cotton, cotton with β -CD, cotton with β -CD-C and cotton with β -CD-CS were obtained to examine the esterification of β -CD with citric acid and chitosan.

2.3. Analytical methods

The fragrance release rates (qualitatively and quantitatively), laundering durability (ISO 105-C01:1989 and physical properties i.e. Tensile Strength (IS 1969-1968), Bending Length (IS: 6490-1971). Crease recovery (IS: 4681-1968), Drape (BS 5058:1973), Air permeability (IS: 11056-1984), Tear strength (ASTM D1424-09) and antimicrobial properties (AATCC Test Method 147–2004) of finished fabric samples were evaluated and investigated through international testing standard methods. Different apparatus and equipment like water bath (Laboratory glassware co. Ambala), Electronic pH meter (PH-009(I)), Electronic weighing balance (CAS Model MW-11 series), UV/Visible spectrophotometer (Lab India analytical UV 3000*), Orbital shaker (Bio-Technology Lab, M.D.U Rohtak), Padding mangles (Electronic & Engg. Company), Drying oven (Kaypee Udyog, Ambala), Laundrometer (RBE, Mumbai), Tensile tester (Globe-Tex Industries), Shirley Stiffness tester, Tearing strength tester (Elmatear), Drape tester (Curisk), Crease recovery tester (Shirley), Air permeability tester (Prolific) and FTIR (Perkin Elimer) were used for experimental and analysis.

3. Results and discussion

3.1. Characterization and optimization

3.1.1. Solubility analysis of β -CD

The β -CD solubility percentage in different mediums i.e. water, NaOH, ethanol is shown in Fig. 1. It was found that the β -CD highly soluble in 0.6gpl NaOH solution almost 100 percentages as compared with 50% ethanol and water. This may be due to the reduction of hydrophobic nature of β -CD, resulting in the breakdown of intermolecular hydrogen bond of β -CD when reacting with NaOH solution (Faruk et al., 2012).

3.1.2. Calibration of lavender

The absorbance of lavender oil with different concentrations (1–10%) were measured against blank sample at λ_{max} (344 nm) by using UV/Visible spectrophotometer. Fig. 2 shows the concentrations versus absorbance curve. The slope of the linear line was calculated from the equation to evaluate the unknown concentration of lavender oil in the cotton samples.

Table 1
Fabric structural details.

S.No	Features	Details
1	G.S.M	236
2	Weave	2/1 Twill weave
3	Warp Count	2/40 s
4	Wefit Count	2/20 s
5	E.P.I	64
6	P.P.I	78

Table 2
Fabric properties.

Crease recovery (%)		Tensile strength (kgf)		Tear strength (gmf)		Bending length (cm)		Air permeability (lph)	Drape (Drape Coefficient)
Warp	Weft	Warp	Weft	Warp	Weft	Warp	Weft		
99.1	96.4	50.1	49.4	1433.6	1670.4	2.275	2.025	39.175	0.774

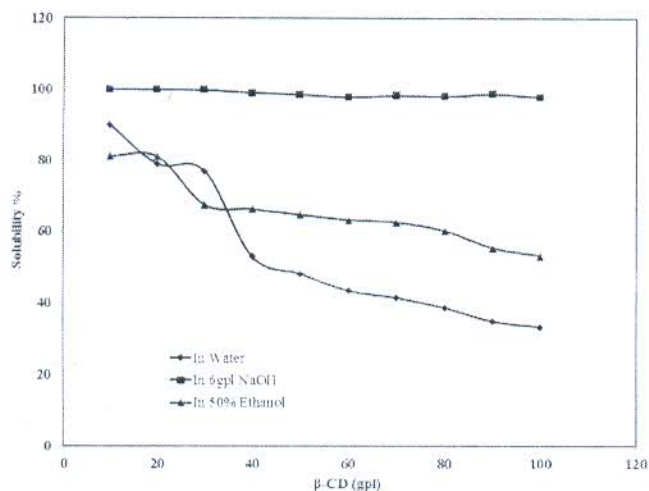


Fig. 1. Solubility Percentage of β -CD.

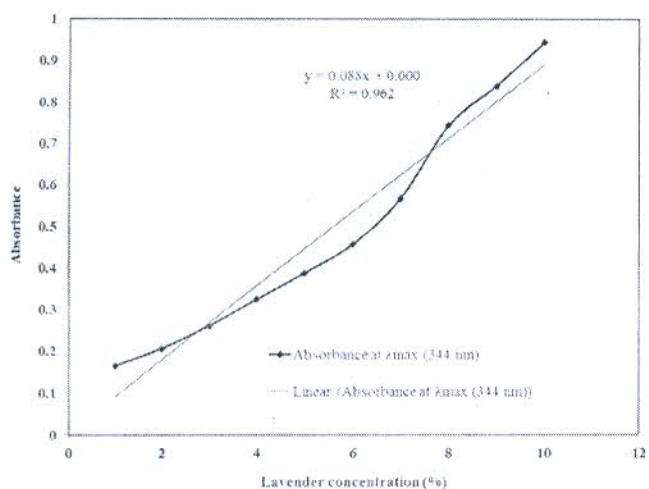


Fig. 2. Calibration curve of lavender at $\lambda_{max} = 344$ nm.

$$y = mx + b \quad (1)$$

$$\begin{aligned} \text{Abs} &= (\text{Slope} \times \text{Conc.}) + 0 \\ &= 0.088 \times \text{Conc.} \end{aligned} \quad (2)$$

3.1.3. Optimization of β -CD concentration

Optimization of β -CD concentration for finishing were carried out with two methods i.e. weight gain (percentage) and phenolphthalein titration, result represented in Fig. 3(a) and (b). As it can be seen from Fig. 3(a), the weight gain (%) of cotton were constantly increasing with a concentration of β -cyclodextrin from 20 gpl up to 80 gpl, at 100 gpl the percentage weight gain reaches the maximum limit. The optimization of β -CD was examined with phenolphthalein indicator, due to the formation of complex and participates in color change with β -CD. From Fig. 3(b), the minimum phenolphthalein absorbance observed at 80 gpl β -CD. This might be because at 80 gpl β -CD saturation point achieved and fabric fully exhausted with β -CD. This indicates that at 80 gpl

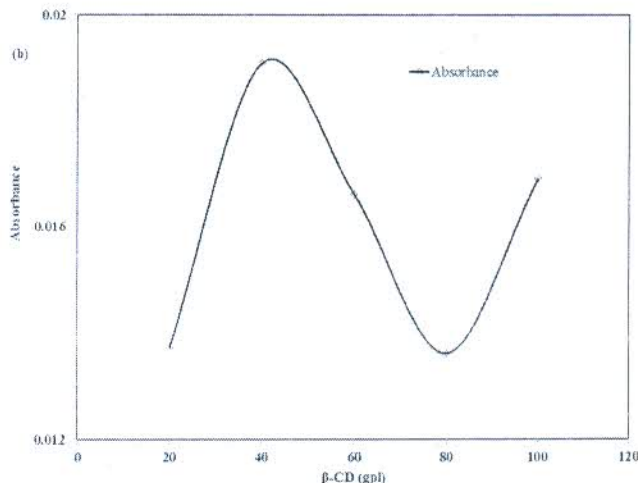
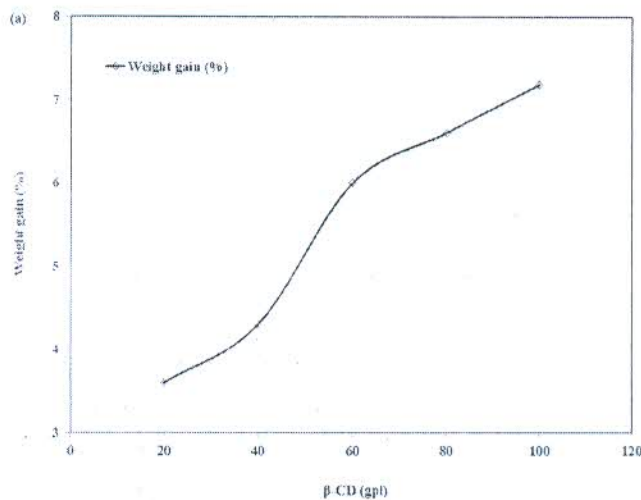


Fig. 3. (a) Effect of β -CD concentration on weight gain % of cotton and (b) Effect of increasing concentration of β -CD on absorbance of Ph-OH.

concentration maximum cyclodextrin moieties with cavities were available for complexation. From the above findings, 80 gpl has been select as the optimum concentration for the application of β -CD.

3.1.4. Optimization of lavender concentration with absorbance index

The absorbance of extracted lavender from treated fabric samples obtained at the maximum wavelength (λ_{max} 344 nm) and different time range (2–72 h). The results presented in Fig. 4. It has been observing that at 6% lavender shows maximum absorbance. Higher absorbance indicated more quantity of lavender extracted from the solution and hence confirmed the presence of more lavender on the fabric. Further increase in concentration (more than 6%) may attribute to the saturation of fabric. Interpretation of graphical representation shows that 6% lavender oil makes more complex with the fabric, which leads to selected as an optimum concentration for the application.

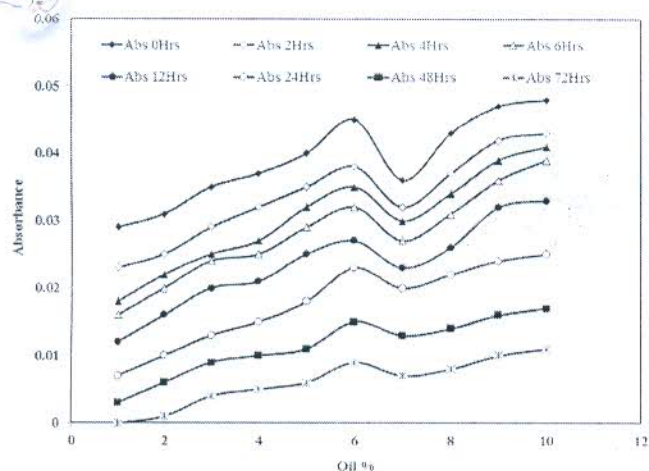


Fig. 4. Lavender absorbance index.

3.1.5. Stability analysis of Inclusion complex between β -CD and lavender

The concentrations of inclusion complex of lavender –80 gpl β -CD are shown in Fig. 5. It can be seen that minimum absorbance could be 6% lavender oil with β -CD, which indicated the maximum inclusion of lavender in β -CD cavities. This may be due to maximum deposition of lavender molecules in the β -CD cavities.

3.1.6. Characterization of β -CD-C and β -CD-CS

The FTIR spectra of cotton treated with β -CD-CS, comparative spectra of β -CD, β -CD-C and β -CD-CS and comparative spectra of cotton, cotton with β -CD, cotton with β -CD-C and cotton with β -CD-CS is shown Fig. 6(a) and (b). In Fig. 6(a), the spectrum of cotton treated with β -CD-CS presented the strong absorption band at 3411 cm^{-1} assigned to O–H and N–H stretching. Fig. 6(b) shows that when comparing the transmittance spectra of β -CD and β -CD-C and β -CD-CS, an additional absorption peak of β -CD-C at 1715 cm^{-1} attributed to C=O stretching of citrate moieties clearly observed and β -CD-CS shows a broad peak at 3404 cm^{-1} , which has been attributed to O–H stretching and N–H stretching. The absorption bands at 1114 cm^{-1} (C–O stretching) and 1628 and 1457 cm^{-1} (C=O of amide I and II) were characteristic peaks of β -CD-CS. β -CD-CS demonstrated the carbonyl absorption peak at 1628 cm^{-1} , associated with citrate moieties at the spacer. FTIR-spectra of cotton treated with β -CD-C shows strong additional ester peak at 1730 cm^{-1} Fig. 6(c). This peak indicates the formation of a carboxylic ester of β -CD-C with cellulosic hydroxyl

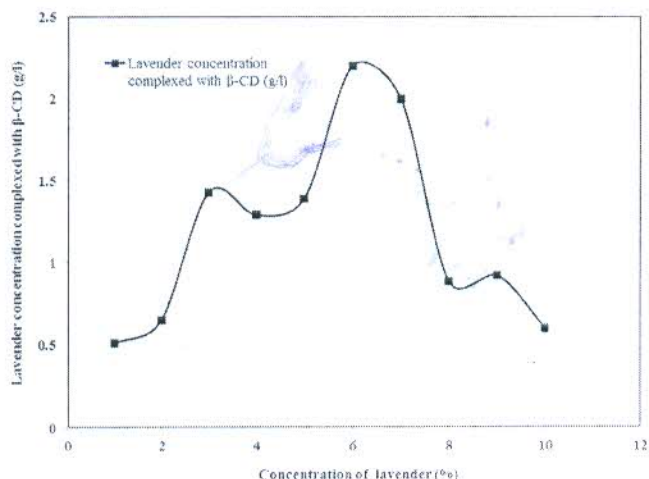


Fig. 5. Concentration of Inclusion complex of lavender – 80gpl β -CD.

groups of cotton (Abdel-Halim et al., 2010; Sricharussin et al., 2009).

3.2. Performance evaluation of finished cotton with finishing treatments

3.2.1. Fragrance release

The qualitatively fragrance evaluation for scent intensity by a panel of judgment are mention Table 3. Cotton finished with β -CD-CS-L show maximum rating even after 72 h. This may be due to the cavities of β -CD that are capable of holding fragrance of lavender and ester linkages between cotton and β -CD-C, which stabilizes as well as suppresses the release of lavender (Sun et al., 2014). Fragrance release rate (percentage) as shown in Fig. 7, the quantitative evaluation by using UV/ Visible spectrophotometer. A noticeable increase in fragrance release rate observed with a span of time. The minimum fragrance release rate investigated in cotton with β -CD-CS-L. This is because of cotton hydrogen linkage with β -CD chitosan resulting, in long last fragrance (Abdel-Halim et al., 2010).

3.2.2. Laundering durability

The Laundering durability of fragrance finish cotton is present in Fig. 8. After three washing cycles, a significant release of fragrance up to 25.8% observed when lavender applied alone on the fabric. Further, when cotton finished with β -CD-CS-L, a significant improvement in fragrance release rate was observed. This attributed to the cavities of β -CD, which were capable of forming an inclusion complex with guest molecules and lavender molecules dimensionally fitted into the cavities of β -CD (Jahed et al., 2014).

3.2.3. Tensile strength

The change in the tensile strength of finished cotton is shown in Fig. 9. It has been observed that when fabric samples finished with different techniques there is an increase in tensile strength, but its cotton finished with β -CD-CS-L shows maximum tensile strength as compared to other techniques. This increase in the strength attributed to the ester linkage between β -CD-CS-L and hydroxyl groups of cotton, which lessened the restriction of segmental movement of cellulosic chains in fiber and prevented the fiber from being tender severely (Wang et al., 2015).

3.2.4. Bending lengths

The bending length of finished samples with different techniques is present in Fig. 10. The graphical representation shows the maximum change in bending length of cotton finished with β -CD-CS-L. This might be cross-linking between cellulosic molecules of cotton fiber and β -CD-CS-L, due to extra cross-linking chains developed between fibers segments increase the abrasion resistance of fiber segments, which restrict fibers bending (Azwa et al., 2013).

3.2.5. Crease recovery

Crease recovery angle of cotton when treated with different techniques are shown in Fig. 11. As cotton treated with the β -CD-CS-L shows minimum recovery angle as compared to other techniques. This might be the deposition of finishing chemicals in pores of cotton fabric, physical bonding between adjacent molecular chains and chitosan and citrate promote less inter-fiber slippage results in lesser fabric crease resistance.

3.2.6. Drape

Drape coefficient of fragranced finished cotton fabrics presented in Fig. 12. The drape coefficient of cotton finished with β -CD-CS-L has a minimum as compared to other techniques. This may be probably due to modified host (i.e. β -CD-CS-L) as a binder for the retention of aroma on cotton fabric (Khanna and Kaur, 2016).

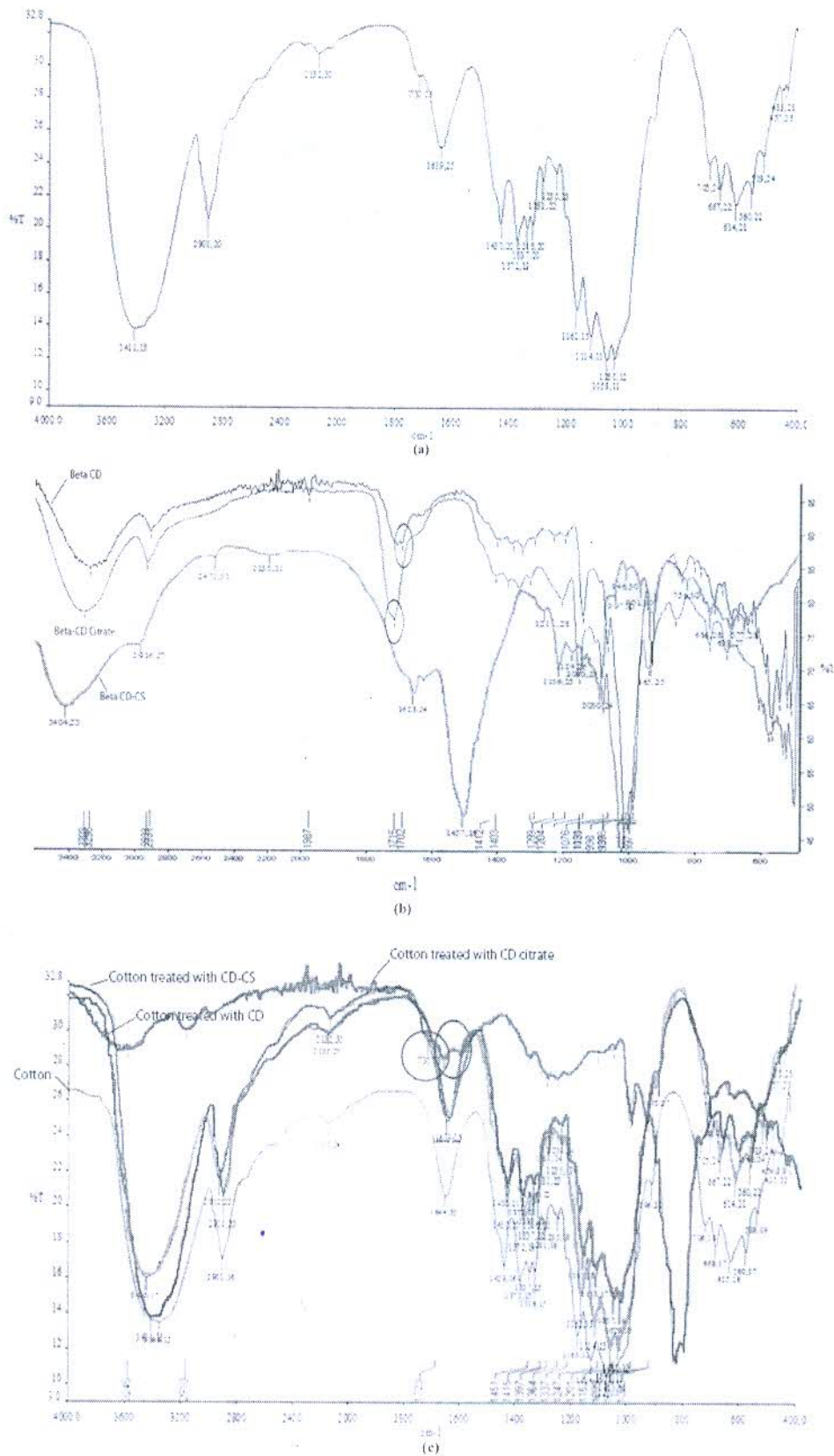


Fig. 6. (a) FTIR spectra of cotton treated with β -CD-CS, (b) FTIR comparative spectra of β -CD, β -CD-C and β -CD-CS, (c) FTIR comparative spectra of cotton, cotton with β -CD, cotton with β -CD-C and cotton with β -CD-CS.

Table 3
Scent intensity rating of finished cotton.

Techniques	0 h	2 h	4 h	6 h	12 h	24 h	48 h	72 h
C	0	0	0	0	0	0	0	0
L	4	3	3	3	2	1	0	0
β -CD-L	4	4	3	3	3	2	1	0
CC-L	4	3	3	2	2	1	0	0
β -CD-CS-L	4	4	4	4	4	3	2	1

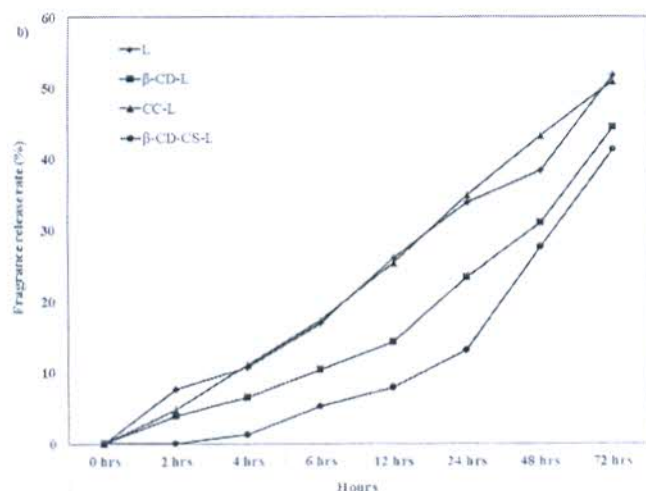


Fig. 7. Fragrance release rate of finished cotton.

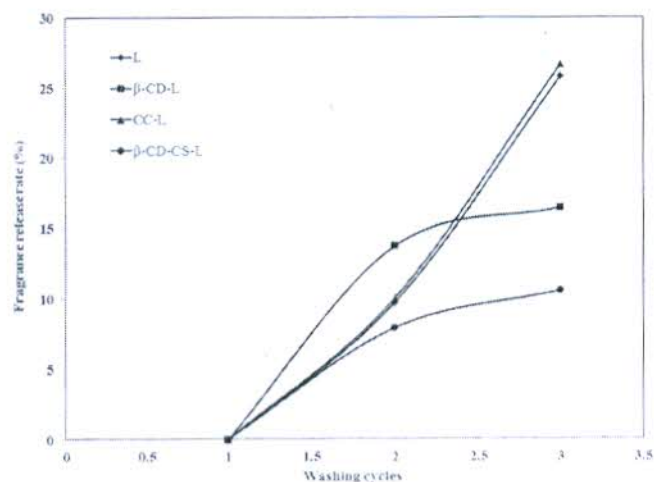


Fig. 8. Effect of washing cycles on fragrance release rate of treated cotton.

3.2.7. Air permeability

The air permeability of fragrance finish cotton shown in Fig. 13. It was observed that finishing affects the air permeability of the cotton fabric. When cotton finished with β -CD-CS-L shows maximum air permeability, which affects the passage of air through fabric. This attributes to mechanical deposition of β -CD-CS-L as a film (close fabric interstices). In addition swelling of hydrophilic cotton would change the fabric porosity and thickness that resulted in a decrease of air permeability of the fabric for all the techniques (Afzal et al., 2014).

3.2.8. Tearing strength

The tensile strength of fabric samples is shown in Fig. 14. It has been seen from Fig. 14 that there was a pronounced improvement in tearing strength of cotton when finished with fragrance compounds. Also, the force required to tear the cotton was maximum when finished

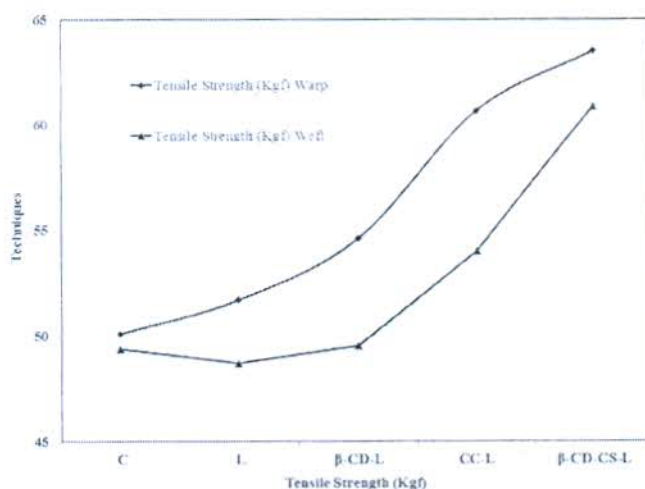


Fig. 9. Tensile strength of fragrance finished cotton.

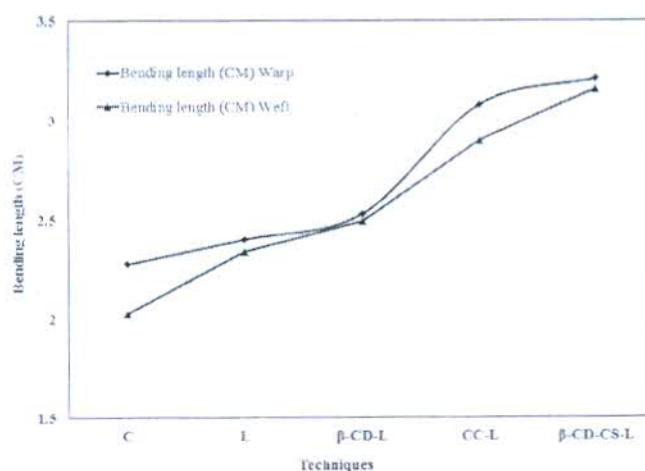


Fig. 10. Bending length of fragrance finished cotton.

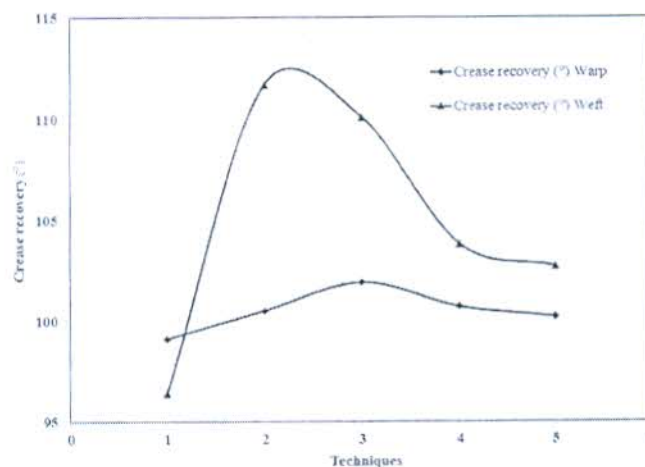


Fig. 11. Effect of fragrance finishing on crease recovery of cotton.

with β -CD-CS-L. This improved tear strength ascribed to plasticizing effect and ester linkage of β -CD-CS-L with cellulose that lessens the restriction of segmental movement of cellulose chains in the fiber and prevented the fiber from being tendered easily under load (Choi et al., 2013).

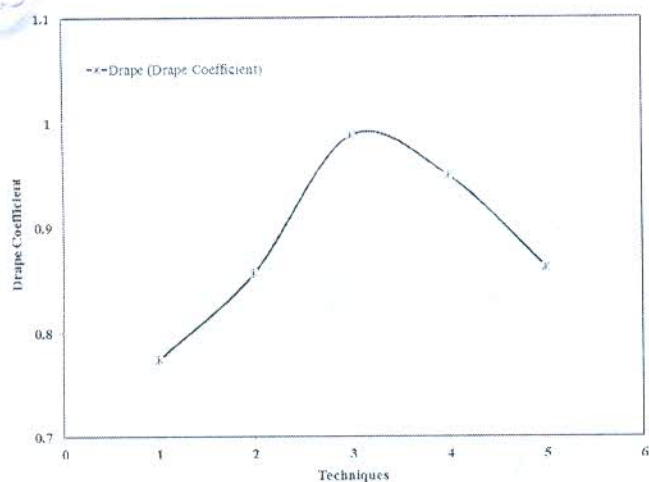


Fig. 12. Effect of fragrance finishing on drape coefficient of cotton.

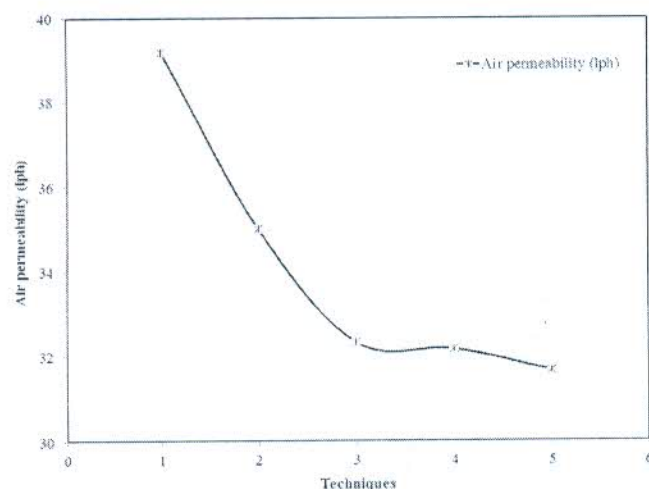


Fig. 13. Effect of fragrance finishing on air permeability of cotton.

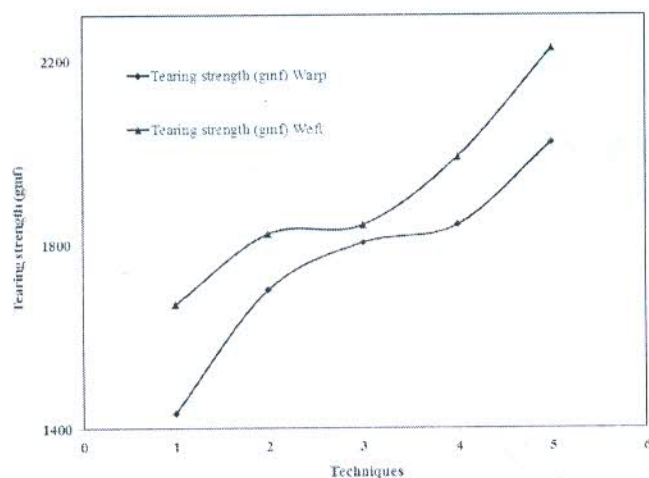


Fig. 14. Tearing Strength of finished cotton.

3.3. Antimicrobial activity

The inhibition zone of finished cotton with different techniques is present in Fig. 15. The results show that there was no inhibition zone of cotton finished with L, β -CD-L and CC-L but some inhibition zone have also been observed for cotton finished with β -CD-CS-L. The presence

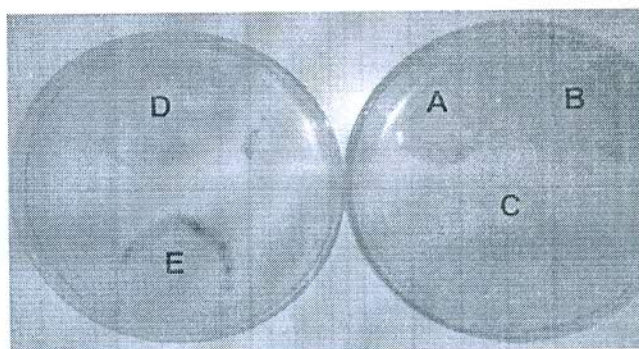


Fig. 15. Inhibition zone of finished cotton, (A) Control, (B) Lavender alone, (C) β -CD-lavender, (D) Chitosan Citrate- lavender, (E) β -CD/ grafted chitosan and lavender.

of chitosan act as it is a cationic antimicrobial agent, particularly for external disinfection and the target site of the cationic biocides, is the cell envelope of bacteria.

The mechanism behind the antimicrobial activity of chitosan can be described as follows: (1) the cationic nature of chitosan binds with sialic acid in phospholipids, consequently restraining the movement of a microbiological substance. (2) Chitosan molecules penetrate into the cells of microorganisms and prevent the growth of the cells by prohibiting the transforming of DNA to RNA. Based on the above knowledge, the antimicrobial activity was generated from the free amino groups in chitosan in an aqueous acidic environment. From the above finding, the enhancement in the antimicrobial activity of chitosan might be attributing to the penetration ability of chitosan to the cell wall of microorganisms and consequently enhancing the accessibility of the amino groups of chitosan to prohibit the growth of the microorganism (Tan et al., 2013).

On the other hand, chemical modification of chitosan via its coupling with β -CD citrate improved its antimicrobial activity. This behavior could be attributing to (1) enhancing the dissolution of chitosan and (2) the creation of carboxyl groups along with chitosan molecules serve in the dissolution of phospholipids area and causing leakage the intercellular components and finally the death of the microorganisms. The presence of lavender as an anti-microbial agent was not able to present any inhibition zone, might be due to its low used concentration (Wang et al., 2008).

3.4. Comparison of "new" and already existing procedure

Although a number of fragrance finishing techniques such as exhaustion method, etc are available but these are not providing combined effect of fragrance and antimicrobial properties. β -Cyclodextrin/Grafted Chitosan novel technique provides both fragrance and antimicrobial properties because of the use of lavender oil and chitosan. Lavender contains pleasant aroma smell and antimicrobial property, patients suffering high blood pressure feel sedation when they use a pillow made of fabric treated with lavender microcapsules. Chitosan is a natural biopolymer, antibacterial, antifungal, antiviral, non-toxic, non-allergic and biocompatible (Dutta et al., 2004). Other advantages of novel techniques are controlled fragrance release rate, improved physical properties such as tensile strength of substrates due to cross-linking of β -Cyclodextrin and cotton through citric acid and effective antimicrobial properties.

β -Cyclodextrin as a microencapsulate offers many advantages as compared to conventional processes, in terms of economy, energy saving, eco-friendliness and controlled release of substance.

4. Conclusion

The β -CD had been highly soluble in 0.6 gpl NaOH solution and least soluble in water. Stability analysis of inclusion complex between

β -CD and lavender index shows 6% lavender can make a maximum inclusion complex formation with 80 gpl β -CD. FTIR studies reveal about the formation of a carboxylic ester between cotton and β -Cyclodextrin/Grafted Chitosan at 1730 cm^{-1} ester peak. Application of β -Cyclodextrin/Grafted Chitosan and lavender oil had shown significant improvement in fragrance durability, performance properties i.e. tensile strength, bending length, etc and antimicrobial properties as compared to other conventional techniques. The pleasant smells can be created by the essential oils, which have pharmacological effects like antibacterial, and antiviral, etc., and fragrance of lavender proves a good way to meet important psychological and emotional needs. Since the durability and other properties of cotton fabric treated with β -Cyclodextrin/Grafted Chitosan are having better results. Finally, it concluding that cotton treated with β -Cyclodextrin/Grafted Chitosan is better alternative to conventional finishing. The fragrance finish fabric can be use for developing home textile applications such as curtains, wall hangings, and table covers. The outcome of this research work is that, this novel technique can be use for design and development of customized aroma fabric and give new idea on textile fragrance finishing, microbiology, pharmaceutical, chemical research etc.

References

- Abdel-Halim, E.S., Abdel-Mohdy, F.A., Al-Deeb, S.S., El-Newehy, M.H., 2010. Chitosan and mono-chlorotriazinyl- β -cyclodextrin finishes improve antibatic properties of cotton/polyester blend and polyester fabrics. *Carbohydr. Polym.* 82 (1), 202–208.
- Ahza, Z.N., Hussain, F., Malik, M.H., Javed, Z., 2014. Statistical model for predicting the air permeability of polyester/cotton-blended interlock knitted fabrics. *J. Tex. Inst.* 105 (2), 214–222.
- Agrawal, P.B., Warmoeskerken, M.M.C.G., 2008. A β -cyclodextrin based slow and controlled release system for digital finishing of cotton. In *Autex Textile World Conference 2008*. 2008. Biella, Italy.
- Andreans, J., Dalmolin, M.C., Junior, O., Barcellos, L.O., 2010. Application of cyclodextrins in textile processes. *Quim. Nova* 33 (4), 929–937.
- Azwa, Z.N., Yousif, B.F., Manalo, A.C., Karunasekar, W., 2013. A review on the degradability of polymeric composites based on natural fibres. *Mat. Des.* 47, 424–442.
- Buschmann, H.J., Knittel, D., Schollmeyer, E., 1991. Cyclodextrins and dextrans as new auxiliaries in dyeing. *Melliand Textil* 72 (12), 1012–1014.
- Butcher, D., 1998. Aromatherapy: its past and future. *Drug Cosmet. Ind.* 162 (3), 22–24.
- Chandrasekaran, K., Auhannani, N., Priyal, V.V., 2015. Analysis of eco-friendly medicinal herb extracts and essential oil applications on textile products for healthcare applications. *Indian J. Tradit. Knowl.* 14 (3), 481–487.
- Cheng, S.Y., Yuen, C.W.M., Kan, C.W., Cheuk, K.R.L., 2008. Imparting cosmetic effects on textiles. *Colourage* 55 (8), 68–74.
- Choi, K.M., Choi, M.C., Han, D.H., Park, T.S., Ha, C.S., 2013. Plasticization of poly (lactic acid)(PLA) through chemical grafting of poly (ethylene glycol)(PEG) via in situ reactive blending. *Eur. Pol. J.* 49 (8), 2336–2364.
- Dutta, P.K., Dutta, J., Tripathi, V.S., 2004. Chitin and chitosan: chemistry, properties and applications. *J. Sci. Ind. Res.* 63 (1), 20–31.
- Faruk, O., Pledzki, A.K., Fink, H.P., Sun, M., 2011. Biocomposites reinforced with natural fibers: 2000–2010. *Prog. Polym. Sci.* 37 (11), 1552–1596.
- Ghayeripour, S., Montazer, M., 2016. Micro/nanoencapsulation of essential oils and fragrances: focus on perfumed, antimicrobial, mosquito-repellent and medical textiles. *J. Microencapsul.* 33 (6), 497–510.
- Hanogda, T., Yamaguchi, M., 2001. Evoked and oscillatory neuromagnetic responses to sniffing odor in human subjects. *Behav. Brain Res.* 123 (2), 219–223.
- Herman, S.J., 2009. Applications II: Fragrance. *Chem. Technol. Flavours Fragrances* 12, 305–320.
- Jahed, V., Zarrabi, A., Bordbar, A.K., Halezi, M.S., 2014. NMR (1 H, ROESY) spectroscopic and molecular modelling investigations of supramolecular complex of β -cyclodextrin and curcumin. *Food Chem.* 165, 241–246.
- Joshi, M., Wazed Ali, S., Purwar, R., Rajendran, S., 2000. Ecofriendly antimicrobial finishing of textiles using bioactive agents based on natural products. *Indian J. Fib. Text. Res.* 34 (3), 295–304.
- Jug, M., Bećiravić, Č., Laćan, M., Bećiravić-Jagan, M., 2008. Cyclodextrin-based pharmaceuticals. *Rad. Med. Sci.* 499 (32), 9–26.
- Khanna, S., Kaur, A., 2016. Study on Aroma Finish Using Vanillin on Cotton Based Home Textiles.
- Kucula, K., 1998. Chemistry and application of chitin and chitosan. *Polym. Degrad. Stab.* 59 (1–3), 117–120.
- Kyle, G., 2006. Evaluating the effectiveness of aromatherapy in reducing levels of anxiety in palliative care patients: results of a pilot study. *Complement. Ther. Clin. Pract.* 12 (2), 148–155.
- Lee, K.Y., Park, W.H., Ha, W.S., 1997. Polyelectrolyte complexes of sodium alginate with chitosan or its derivatives for microcapsules. *J. Appl. Polym. Sci.* 63 (4), 425–432.
- Martel, B., Morellet, M., Ruffin, D., Ymet, F., Weltrowski, L., 2002a. Capture and controlled release of fragrances by CD finished textiles. *J. Incl. Phenom. Macrocycl. Chem.* 44 (1–4), 439–442.
- Martel, B., Weltrowski, M., Ruffin, D., Morellet, M., 2002b. Polycarboxylic acids as crosslinking agents for grafting cyclodextrins onto cotton and wool fabrics: study of the process parameters. *J. Appl. Polym. Sci.* 83 (7), 1449–1456.
- Matsushi-Shikiso Chemical Co. Ltd, 1994. Fixing Odorous to Textiles, High Performance Textile. 8 No author 2000.
- Meo, P.L., P'Anna, P., Riela, S., Cruttadaluia, M., Noto, R., 2003. Spectrophotometric study on the thermodynamics of binding of α - and β -cyclodextrin towards some p-nitrobenzene derivatives. *Org. Biomol. Chem.* 1 (9), 584–1590.
- Nelson, G., 2001. Microencapsulation in textile finishing. *Review of progress in coloration and related topics*, 31(1), 57–64.
- Picciaglia, R., Marotti, M., Giovanelli, E., Deans, S.G., Eaglesham, E., 1995. Antibacterial and antioxidant properties of Mediterranean aromatic plants. *Ind. Crops Prod.* 2 (1), 47–50.
- Samanata, A.K., Kar, T.R., Mukhopadhyay, A., Shome, D., Konar, A., 2016. Eco-friendly salt-free reactive dyeing of cotton (muslin) fabric after cationization with amino acid from soya. *Text. Res. J.*, (p.0040517515621135).
- Samanta, K. K., Basak, S., and Chattopadhyay, S. K., 2014. Eco-friendly coloration and functionalization of textile using plant extracts. In *Roadmap to Sustainable Textiles and Clothing* (pp. 263–287). Springer Singapore.
- Sricharussin, W., Sopajaree, C., Manornung, T., Sangsuriya, N., 2009. Modification of cotton fabrics with β -cyclodextrin derivative for aroma finishing. *J. Text. Inst.* 100 (8), 682–687.
- Sun, X., Sui, S., Fevence, C., Zhang, Y., Sui, S., Zhou, N., Zhu, W., Zhou, K., 2014. Antimicrobial and mechanical properties of β -cyclodextrin inclusion with essential oils in chitosan films. *J. Agric. Food Chem.* 62 (35), 8914–8918.
- Tan, H., Ma, R., Lin, C., Liu, Z., Tang, T., 2013. Quaternized chitosan as an antimicrobial agent: antimicrobial activity, mechanism of action and biomedical applications in orthopedics. *Int. J. Mol. Sci.* 14 (1), 1854–1869.
- Toda, M., Morimoto, K., 2008. Effect of lavender aroma on salivary endocrinological stress markers. *Arch. Oral. Biol.* 53 (10), 964–968.
- Wang, H., Wei, D., Zhao, Z., Xiao, H., Zheng, A., Zhao, Y., 2015. Preparation and properties of nonleaching antimicrobial linear low-density polyethylene films. *Ind. Eng. Chem. Res.* 54 (6), 1824–1831.
- Yip, J., Loh, M.Y.A., 2016. Microencapsulation technologies for antimicrobial textiles. *Antimicrob. Text.*, 19.